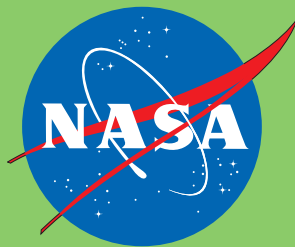


World Meteorological Organization
Global Ozone Research and Monitoring Project—Report No. 52

SCIENTIFIC ASSESSMENT OF OZONE DEPLETION: 2010



National Oceanic and Atmospheric Administration
National Aeronautics and Space Administration
United Nations Environment Programme
World Meteorological Organization
European Commission

World Meteorological Organization

7bis, avenue de la Paix
Case postale 2300
CH-1211, Geneva 2
Switzerland

United Nations Environment Programme

Ozone Secretariat

P.O. Box 30552
Nairobi, 00100
Kenya

U.S. Department of Commerce

National Oceanic and Atmospheric Administration

14th Street and Constitution Avenue NW
Herbert C. Hoover Building, Room 5128
Washington, D.C. 20230

National Aeronautics and Space Administration

Earth Science Division

NASA Headquarters
300 E Street SW
Washington, D.C. 20546-0001

European Commission

Directorate-General for Research

B-1049 Bruxelles
Belgium

Published March 2011

ISBN: 9966-7319-6-2

Hardcopies of this report are available from WMO (address above; CRenaudot@wmo.int).

This report is available on the Internet at the following locations:

<http://www.wmo.int/pages/prog/arep/gaw/ozone/>

http://ozone.unep.org/Assessment_Panels/SAP/Scientific_Assessment_2010/index.asp

<http://esrl.noaa.gov/csd/assessments>

Note: Figures from this report are in the public domain and may be used with proper attribution to source.

Citation for the whole report:

WMO (World Meteorological Organization), *Scientific Assessment of Ozone Depletion: 2010*, Global Ozone Research and Monitoring Project–Report No. 52, 516 pp., Geneva, Switzerland, 2011.

Example Chapter citation:

Forster, P.M., and D.W.J. Thompson (Coordinating Lead Authors), M.P. Baldwin, M.P. Chipperfield, M. Dameris, J.D. Haigh, D.J. Karoly, P.J. Kushner, W.J. Randel, K.H. Rosenlof, D.J. Seidel, S. Solomon, G. Beig, P. Braesicke, N. Butchart, N.P. Gillett, K.M. Grise, D.R. Marsh, C. McLandress, T.N. Rao, S.-W. Son, G.L. Stenchikov, and S. Yoden, Stratospheric changes and climate, Chapter 4 in *Scientific Assessment of Ozone Depletion: 2010*, Global Ozone Research and Monitoring Project–Report No. 52, 516 pp., World Meteorological Organization, Geneva, Switzerland, 2011.

World Meteorological Organization
Global Ozone Research and Monitoring Project—Report No. 52

SCIENTIFIC ASSESSMENT OF OZONE DEPLETION: 2010

Pursuant to Article 6 of the Montreal Protocol
on Substances that Deplete the Ozone Layer

National Oceanic and Atmospheric Administration
National Aeronautics and Space Administration
United Nations Environment Programme
World Meteorological Organization
European Commission

LIST OF INTERNATIONAL AUTHORS, CONTRIBUTORS, AND REVIEWERS

Assessment Cochairs

Ayité-Lô Nohende Ajavon
Paul A. Newman
John A. Pyle
A.R. Ravishankara

Chapters and Coordinating Lead Authors

Chapter 1: Ozone-Depleting Substances (ODSs) and Related Chemicals (*Stephen A. Montzka and Stefan Reimann*)
Chapter 2: Stratospheric Ozone and Surface Ultraviolet Radiation (*Anne Douglass and Vitali Fioletov*)
Chapter 3: Future Ozone and Its Impact on Surface UV (*Slimane Bekki and Gregory E. Bodeker*)
Chapter 4: Stratospheric Changes and Climate (*Piers M. Forster and David W.J. Thompson*)
Chapter 5: A Focus on Information and Options for Policymakers (*John S. Daniel and Guus J.M. Velders*)
Twenty Questions and Answers About the Ozone Layer: 2010 Update (*David W. Fahey and Michaela I. Hegglin*)

Scientific Review and Advisory Group

Malcolm K.W. Ko
Theodore G. Shepherd
Susan Solomon

Coordinating Editor

Christine A. Ennis

Authors, Contributors, and Reviewers

Patricio Aceituno	Chile	Donald R. Blake	USA
Ayité-Lô Nohende Ajavon	Togo	Thomas Blumenstock	Germany
Hideharu Akiyoshi	Japan	Gregory E. Bodeker	New Zealand
Daniel L. Albritton	USA	Rumen D. Bojkov	Germany
Taofiki Aminou	Benin	Janet F. Bornman	New Zealand
Stephen O. Andersen	USA	Geir O. Braathen	WMO
Julie M. Arblaster	Australia/USA	Peter Braesicke	UK
Antti Arola	Finland	Christoph Brühl	Germany
Ghassem Asrar	WMO	Claus Brünig	Belgium
Elliot Atlas	USA	Dominik Brunner	Switzerland
Pieter J. Aucamp	South Africa	James B. Burkholder	USA
John Austin	USA	John P. Burrows	Germany/UK
Alkiviadis F. Bais	Greece	Neal Butchart	UK
Mark P. Baldwin	USA	James H. Butler	USA
Dimitris Balis	Greece	André Butz	The Netherlands
Gufran Beig	India	Timothy Canty	USA
Slimane Bekki	France	Pablo O. Canziani	Argentina
Peter F. Bernath	UK	Bruno Carli	Italy

Lucy Carpenter	UK	Andrew Gettelman	USA
Ken Carslaw	UK	Manuel Gil	Spain
Marie-Lise Chanin	France	Nathan P. Gillett	Canada
Andrew J. Charlton-Perez	UK	Marco A. Giorgetta	Germany
Martyn P. Chipperfield	UK	Sophie Godin-Beekmann	France
Natalia E. Chubarova	Russia	Marco González	UNEP
Irene Cionni	Germany	Hans-F Graf	UK
Hans Claude	Germany	Lesley Gray	UK
Cathy Clerbaux	France	Kevin M. Grise	USA
Gerrie Coetzee	South Africa	Jens-Uwe Grooß	Germany
William J. Collins	UK	Joanna D. Haigh	UK
Brian J. Connor	New Zealand	Ebrahim Hajizadeh	Iran
Raul Cordero	Chile	Steven C. Hardiman	UK
Eugene C. Cordero	USA	Neil R.P. Harris	UK
Derek M. Cunnold	USA	Dennis L. Hartmann	USA
Martin Dameris	Germany	Frank Hase	Germany
John S. Daniel	USA	Birgit Hassler	USA
Christine David	France	Michaela I. Hegglin	Canada
Hugo De Backer	Belgium	François Hendrick	Belgium
Martine De Mazière	Belgium	Jay R. Herman	USA
Philippe Demoulin	Belgium	Ernest Hilsenrath	USA
Peter N. den Outer	The Netherlands	David J. Hofmann	USA
Dick Derwent	UK	Paul Horwitz	UNEP
Panuganti Devara	India	Petra Huck	New Zealand
Sandip Dhomse	UK	Robert D. Hudson	USA
Roseanne Diab	South Africa	Mohammad Ilyas	Malaysia
Susana B. Diaz	Argentina	Takashi Imamura	Japan
Marcel Dorf	Germany	Ivar S.A. Isaksen	Norway
Anne R. Douglass	USA	Charles H. Jackman	USA
Pierre Duchatelet	Belgium	Serm Janjai	Thailand
Geoffrey S. Dutton	USA	Imre M. Jánosi	Hungary
Ellsworth G. Dutton	USA	Patrick Jöckel	Germany
Kalju Eerme	Estonia	Andreas I. Jonsson	Canada
James William Elkins	USA	Kenneth Jucks	USA
Andreas Engel	Germany	David J. Karoly	Australia
Christine A. Ennis	USA	Andreas Kazantzidis	Greece
Veronika Eyring	Germany	Philippe Keckhut	France
David W. Fahey	USA	Douglas E. Kinnison	USA
Uwe Feister	Germany	Jon Klyft	Sweden
Vitali E. Fioletov	Canada	Malcolm K.W. Ko	USA
Eric L. Fleming	USA	Kunihiko Kodera	Japan
Lawrence E. Flynn	USA	Takashi Koide	Japan
Ian Folkins	Canada	Ninong Komala	Indonesia
Piers M. Forster	UK	Yutaka Kondo	Japan
James Franklin	Belgium	Karin Kreher	New Zealand
Paul J. Fraser	Australia	Mark Kroon	The Netherlands
Melissa P. Free	USA	Kirstin Krüger	Germany
Stacey M. Frith	USA	Paul B. Krummel	Australia
Lucien Froidevaux	USA	Janusz W. Krzyściń	Poland
John C. Fyfe	Canada	Anne Kubin	Germany
Annie Gabriel	Australia	Lambert Kuijpers	The Netherlands
Rolando R. Garcia	USA	Michael J. Kurylo	USA
Hella Garny	Germany	Paul J. Kushner	Canada
Marvin A. Geller	USA	Esko Kyrö	Finland

Shyam Lal	India	Dimitrios Papanastasiou	USA
Jean-François Lamarque	USA	Edward A. Parson	USA
Tom Land	USA	Nigel D. Paul	UK
Ulrike Langematz	Germany	Steven Pawson	USA
Igor Larin	Russia	Stuart A. Penkett	UK
Katharine Law	France	Judith Perlwitz	USA
Franck Lefèvre	France	Thomas Peter	Switzerland
Jos Lelieveld	Germany	Irina Petropavlovskikh	USA
Yi Liu	China	Klaus Pfeilsticker	Germany
Jennifer Logan	USA	Giovanni Pitari	Italy
Diego Loyola	Germany	Michael Pitts	USA
Cathrine Lund Myhre	Norway	R. Alan Plumb	USA
Sasha Madronich	USA	David Plummer	Canada
Emmanuel Mahieu	Belgium	Jean-Pierre Pommereau	France
Eva Mancini	Italy	Michael Ponater	Germany
Gloria L. Manney	USA	Lamont R. Poole	USA
Alistair J. Manning	UK	Robert W. Portmann	USA
Elisa Manzini	Germany	Michael J. Prather	USA
Marion Marchand	France	Ronald G. Prinn	USA
Daniel R. Marsh	USA	John A. Pyle	UK
Katja Matthes	Germany	Birgit Quack	Germany
Bernhard Mayer	Germany	S. Ramachandran	India
John C. McConnell	Canada	V. Ramaswamy	USA
C. Thomas McElroy	Canada	William J. Randel	USA
Mack McFarland	USA	T. Narayan Rao	India
Norman McFarlane	Canada	A.R. Ravishankara	USA
Danny McKenna	USA	Claire E. Reeves	UK
Richard L. McKenzie	New Zealand	Stefan Reimann	Switzerland
Charles McLandress	Canada	Markus Rex	Germany
Chris A. McLinden	Canada	Robert Rhew	USA
Inna A. Megretskaia	USA	Martin Riese	Germany
Abdelwahid Mellouki	France	Vincenzo Rizi	Italy
Martine Michou	France	Alan Robock	USA
Pauline M. Midgley	Switzerland	Howard K. Roscoe	UK
John Miller	USA	Karen H. Rosenlof	USA
Mario J. Molina	USA/Mexico	Martin N. Ross	USA
Stephen A. Montzka	USA	Eugene Rozanov	Switzerland
Olaf Morgenstern	New Zealand	Vladimir Ryabinin	WMO
Jens Mühle	USA	David Saint-Martin	France
Rolf Müller	Germany	Ross J. Salawitch	USA
Nzioka John Muthama	Kenya	Michelle L. Santee	USA
Prijitha J. Nair	France	K. Madhava Sarma	India
Hideaki Nakane	Japan	Robert Sausen	Germany
Eric R. Nash	USA	Adam A. Scaife	UK
Cindy Newberg	USA	Sue Schaufler	USA
Mike Newchurch	USA	Ulrich Schmidt	Germany
Paul A. Newman	USA	Matthias Schneider	Germany
Ole John Nielsen	Denmark	Robyn Schofield	Germany
Simon O'Doherty	UK	Ulrich Schumann	Germany
Alan O'Neill	UK	John F. Scinocca	Canada
Samuel J. Oltmans	USA	Dian J. Seidel	USA
Luke D. Oman	USA	Megumi Seki	UNEP
Vladimir L. Orkin	USA	Jonathan Shanklin	UK
Mathias Palm	Germany	Wafik M. Sharobiem	Egypt

Theodore G. Shepherd	Canada	Simone Tilmes	USA
Kiyotaka Shibata	Japan	Darin W. Toohey	USA
Keith P. Shine	UK	Kleareti Tourpali	Greece
Masato Shiotani	Japan	Matthew B. Tully	Australia
Michael Sigmond	Canada	Jéssica Valverde-Canossa	Costa Rica
Peter Simmonds	UK	Ronald Van der A	The Netherlands
Isobel J. Simpson	USA	Karel Vanicek	Czech Republic
Björn-Martin Sinnhuber	Germany	Guus J.M. Velders	The Netherlands
Harry Slaper	The Netherlands	Daniel P. Verdonik	USA
Dan Smale	New Zealand	Corinne Vigouroux	Belgium
Anne Smith	USA	Martin K. Vollmer	Switzerland
Susan Solomon	USA	Marc von Hobe	Germany
Seok-Woo Son	Canada	Dmitry I. Vyushin	Canada
Johannes Staehelin	Switzerland	Timothy J. Wallington	USA
Wolfgang Steinbrecht	Germany	Hsiang J. (Ray) Wang	USA
Georgiy L. Stenchikov	Saudi Arabia	Darryn W. Waugh	USA
David Stevenson	UK	Elizabeth C. Weatherhead	USA
Andreas Stohl	Norway	Ann R. Webb	UK
Richard S. Stolarski	USA	Mark Weber	Germany
Frode Stordal	Norway	Ray F. Weiss	USA
Susan Strahan	USA	Donald J. Wuebbles	USA
Fred Stroh	Germany	Masaaki Yamabe	Japan
William T. Sturges	UK	Eun-Su Yang	USA
Kenshi Takahashi	Japan	Shigeo Yoden	Japan
David W. Tarasick	Canada	Yoko Yokouchi	Japan
Susann Tegtmeier	Germany	Shari A. Yvon-Lewis	USA
Yukio Terao	Japan	Durwood Zaelke	USA
Hubert Teysse�re	France	Rodolphe Zander	Belgium
Said Ali Thaoubane	Comores	Christos S. Zerefos	Greece
David W.J. Thompson	USA	Lingxi Zhou	China

Remembrances

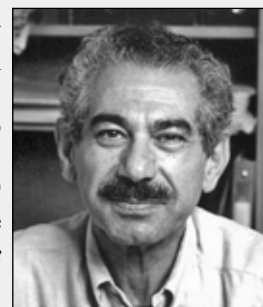
It is with sadness that we note the passing of the following scientists who have played leading roles in the international scientific assessments of the ozone layer.

Derek Cunnold (1940–2009). Derek Martin Cunnold was born July 10, 1940, in Reading, England. He received his B.A. and M.A. from St. John's College in Cambridge, England, and his Ph.D. in Electrical Engineering from Cornell University in 1965. He was a Professor Emeritus at the Georgia Institute of Technology at the time of his death. He was an author and/or contributor in all of the Ozone Assessments since 1988, and was a Lead Author of Chapter 1 (“Long-Lived Compounds”) of the 2006 Assessment.



David Hofmann (1937–2009). David J. Hofmann was born January 3, 1937. He received his Ph.D. in Physics from the University of Minnesota in 1965. He was a scientist at the University of Wyoming for 25 years and then in NOAA for 17 years, directing the Global Monitoring Division of NOAA's Earth System Research Laboratory for a decade. Over a period of 30 years, he traveled to Antarctica 19 times for research and as director of NOAA's South Pole Station. He was a reviewer for four Ozone Assessments and Lead Author of Chapter 12 (“Predicting Future Ozone Changes and Detection of Recovery”) of the 1998 Assessment.

Julius London (1917–2009). Julius London was born on March 26, 1917, in Newark, New Jersey. He received his Ph.D. in Meteorology and Oceanography from New York University in 1951. After working for several years at NYU, he moved to the University of Colorado in 1961 and remained there for his entire career, chairing the Department of Astro-Geophysics from 1966 to 1969. He was an author in NASA and WMO Assessments that predated the Montreal Protocol, including leading the chapter on “Long Period Changes in Stratospheric Parameters” in the 1979 Assessment, *The Stratosphere: Present and Future*, and chairing the Trends working group of the chapter on “Model Predictions and Trend Analysis” in the 1981 Assessment, *The Stratosphere 1981: Theory and Measurements*.



CONTENTS

SCIENTIFIC ASSESSMENT OF OZONE DEPLETION: 2010

PREFACE	xi
PROLOGUE	xv
EXECUTIVE SUMMARY CONTENTS	xxv
EXECUTIVE SUMMARY.....	ES.1
CHAPTER 1: OZONE-DEPLETING SUBSTANCES (ODSs) AND RELATED CHEMICALS <i>Coordinating Lead Authors: Stephen A. Montzka and Stefan Reimann</i>	
Scientific Summary.....	1.1
1.1 Summary of the Previous Ozone Assessment.....	1.7
1.2 Longer-Lived Halogenated Source Gases.....	1.7
1.3 Very Short-Lived Halogenated Substances (VSLS).....	1.37
1.4 Changes in Atmospheric Halogen.....	1.63
1.5 Changes in Other Trace Gases that Influence Ozone and Climate.....	1.75
References.....	1.86
CHAPTER 2: STRATOSPHERIC OZONE AND SURFACE ULTRAVIOLET RADIATION <i>Coordinating Lead Authors: Anne Douglass and Vitali Fioletov</i>	
Scientific Summary.....	2.1
Introduction.....	2.5
2.1 Ozone Observations	2.5
2.2 Polar Ozone.....	2.17
2.3 Surface Ultraviolet Radiation.....	2.31
2.4 Interpretation of Observed Ozone Changes	2.41
References.....	2.59
CHAPTER 3: FUTURE OZONE AND ITS IMPACT ON SURFACE UV <i>Coordinating Lead Authors: Slimane Bekki and Gregory E. Bodeker</i>	
Scientific Summary.....	3.1
3.1 Introduction.....	3.5
3.2 Factors Affecting Future Ozone and Surface UV	3.7
3.3 Projections of Ozone through the 21 st Century	3.18
3.4 Projections of UV Changes Related to Ozone Changes through the 21 st Century	3.42
3.5 Conclusions	3.46
References.....	3.49
Appendix 3A: Constructing Correlative Time Series Plots.....	3.59

CHAPTER 4: STRATOSPHERIC CHANGES AND CLIMATE	
<i>Coordinating Lead Authors: Piers M. Forster and David W.J. Thompson</i>	
Scientific Summary.....	4.1
4.0 Introduction and Scope	4.3
4.1 Observed Variations in Stratospheric Constituents that Relate to Climate.....	4.4
4.2 Observed Variations in Stratospheric Climate.....	4.10
4.3 Simulations of Stratospheric Climate Change	4.16
4.4 Effects of Variations in Stratospheric Climate on the Troposphere and Surface	4.25
4.5 What to Expect in the Future	4.41
References.....	4.46
CHAPTER 5: A FOCUS ON INFORMATION AND OPTIONS FOR POLICYMAKERS	
<i>Coordinating Lead Authors: John S. Daniel and Guus J.M. Velders</i>	
Scientific Summary.....	5.1
5.1 Summary of Previous Assessment and Key Issues to be Addressed in the Current Assessment.....	5.5
5.2 Metrics Used to Quantify Ozone and Climate Impacts	5.5
5.3 Future Baseline Scenarios.....	5.14
5.4 Impacts of Human Activities Relevant to Ozone Policy	5.19
5.5 The World Avoided by Ozone Policy.....	5.33
References.....	5.38
Appendix 5A	
Table 5A-1: Direct Global Warming Potentials for selected gases.....	5.47
Table 5A-2: Assumptions made in obtaining production and emission estimates for the baseline (A1) scenario.....	5.50
Table 5A-3: Mixing ratios (ppt) of the ODSs considered in the baseline (A1) scenario	5.54
Table 5A-4: Halocarbon indirect GWPs from ozone depletion using the EESC-based method described in Daniel et al. (1995).....	5.56
TWENTY QUESTIONS AND ANSWERS ABOUT THE OZONE LAYER: 2010 UPDATE	
<i>Coordinating Lead Authors: David W. Fahey and Michaela I. Hegglin</i>	
I. Ozone in Our Atmosphere	Q.4
II. The Ozone Depletion Process.....	Q.14
III. Stratospheric Ozone Depletion	Q.31
IV. Controlling Ozone-Depleting Substances.....	Q.45
V. Implications of Ozone Depletion and the Montreal Protocol	Q.52
VI. Stratospheric Ozone in the Future.....	Q.64
APPENDICES	
A LIST OF INTERNATIONAL AUTHORS, CONTRIBUTORS, AND REVIEWERS.....	A.1
B MAJOR ACRONYMS AND ABBREVIATIONS.....	B.1
C MAJOR CHEMICAL FORMULAE AND NOMENCLATURE FROM THIS ASSESSMENT.....	C.1

PREFACE

The present document will be part of the information upon which the Parties to the United Nations Montreal Protocol will base their future decisions regarding protection of the stratospheric ozone layer.

The Charge to the Assessment Panels

Specifically, the Montreal Protocol on Substances that Deplete the Ozone Layer states (Article 6): “. . . the Parties shall assess the control measures . . . on the basis of available scientific, environmental, technical, and economic information.” To provide the mechanisms whereby these assessments are conducted, the Protocol further states: “. . . the Parties shall convene appropriate panels of experts” and “the panels will report their conclusions . . . to the Parties.”

To meet this request, the Scientific Assessment Panel, the Environmental Effects Assessment Panel, and the Technology and Economic Assessment Panel have each prepared, about every 3-4 years, major assessment reports that updated the state of understanding in their purviews. These reports have been scheduled so as to be available to the Parties in advance of their meetings at which they will consider the need to amend or adjust the Protocol.

The Sequence of Scientific Assessments

The present 2010 report is the latest in a series of eleven scientific assessments prepared by the world’s leading experts in the atmospheric sciences and under the international auspices of the World Meteorological Organization (WMO) and/or the United Nations Environment Programme (UNEP). This report is the seventh in the set of major assessments that have been prepared by the Scientific Assessment Panel directly as input to the Montreal Protocol process. The chronology of all the scientific assessments on the understanding of ozone depletion and their relation to the international policy process is summarized as follows:

<u>Year</u>	<u>Policy Process</u>	<u>Scientific Assessment</u>
1981		<i>The Stratosphere 1981: Theory and Measurements</i> . WMO No. 11.
1985	Vienna Convention	<i>Atmospheric Ozone 1985</i> . Three volumes. WMO No. 16.
1987	Montreal Protocol	
1988		<i>International Ozone Trends Panel Report 1988</i> . Two volumes. WMO No. 18.
1989		<i>Scientific Assessment of Stratospheric Ozone: 1989</i> . Two volumes. WMO No. 20.
1990	London Adjustment and Amendment	
1991		<i>Scientific Assessment of Ozone Depletion: 1991</i> . WMO No. 25.
1992		<i>Methyl Bromide: Its Atmospheric Science, Technology, and Economics (Montreal Protocol Assessment Supplement)</i> . UNEP (1992).
1992	Copenhagen Adjustment and Amendment	
1994		<i>Scientific Assessment of Ozone Depletion: 1994</i> . WMO No. 37.
1995	Vienna Adjustment	
1997	Montreal Adjustment and Amendment	
1998		<i>Scientific Assessment of Ozone Depletion: 1998</i> . WMO No. 44.

1999	Beijing Adjustment and Amendment	
2002		<i>Scientific Assessment of Ozone Depletion: 2002.</i> WMO No. 47.
2006		<i>Scientific Assessment of Ozone Depletion: 2006.</i> WMO No. 50.
2007	Montreal Adjustment	
2010		<i>Scientific Assessment of Ozone Depletion: 2010.</i> WMO No. 52.
2011	23 rd Meeting of the Parties	

The Current Information Needs of the Parties

The genesis of *Scientific Assessment of Ozone Depletion: 2010* occurred at the 19th Meeting of the Parties to the Montreal Protocol in Montreal, Canada, at which the scope of the scientific needs of the Parties was defined in their Decision XIX/20 (4), which stated that "...for the 2010 report, the Scientific Assessment Panel should consider issues including:

- (a) Assessment of the state of the ozone layer and its future evolution;
- (b) Evaluation of the Antarctic ozone hole and Arctic ozone depletion and the predicted changes in these phenomena;
- (c) Evaluation of the trends in the concentration of ozone-depleting substances in the atmosphere and their consistency with reported production and consumption of ozone-depleting substances and the likely implications for the state of the ozone layer;
- (d) Assessment of the interaction between climate change and changes on the ozone-layer;
- (e) Assessment of the interaction between tropospheric and stratospheric ozone;
- (f) Description and interpretation of the observed changes in global and polar ozone and in ultraviolet radiation, as well as set future projections and scenarios for those variables, taking into account among other things the expected impacts of climate change;
- (g) Assessment of consistent approaches to evaluating the impact of very short-lived substances, including potential replacements, on the ozone layer;
- (h) Identification and reporting, as appropriate, on any other threats to the ozone layer..."

The 2010 assessment has addressed all the issues that were feasible to address to the best possible extent.

The Assessment Process

The formal planning of the current assessment was started early in 2009. The Cochairs considered suggestions from the Parties regarding experts from their countries who could participate in the process. Furthermore, an ad hoc international scientific advisory group also suggested participants from the world scientific community. In addition, this advisory group contributed to crafting the outline of the assessment report. As in previous assessments, the participants represented experts from the developed and developing world. The developing country experts bring a special perspective to the process, and their involvement in the process has also contributed to capacity building.

The information of the 2010 assessment is contained in five chapters associated with ozone-layer topics, which are preceded by a Prologue:

- Prologue. State of the Science through the 2006 WMO/UNEP Assessment
- Chapter 1. Ozone-Depleting Substances (ODSs) and Related Chemicals
- Chapter 2. Stratospheric Ozone and Surface Ultraviolet Radiation
- Chapter 3. Future Ozone and Its Impact on Surface UV
- Chapter 4. Stratospheric Changes and Climate
- Chapter 5. A Focus on Information and Options for Policymakers

The initial plans for the chapters of the 2010 Scientific Assessment Panel's report were examined at a meeting that occurred on 24–25 June 2009 in London, England. The Coordinating Lead Authors and Coauthors focused on the content of the draft chapters and on the need for coordination among the chapters.

The first drafts of the chapters were examined at a meeting that occurred on 17–19 November 2009 in Fairfax, Virginia, United States, at which the Coordinating Lead Authors, Coauthors, and a small group of international experts focused on the scientific content of the draft chapters.

The second drafts of the chapters were reviewed by 122 scientists worldwide in a mail peer review. Those comments were considered by the authors. At a Panel Review Meeting in Les Diablerets, Switzerland, held on 28 June–2 July 2010, the responses to these mail review comments were proposed by the authors and discussed by the 74 participants. Final changes to the chapters were decided upon at this meeting. The Executive Summary contained herein (and posted on the UNEP web site on 16 September 2010) was prepared and completed by the attendees of the Les Diablerets meeting. A small science advisory group assisted the Coauthors during those Les Diablerets discussions of the Executive Summary, and also helped with advance preparations during a meeting in Toronto on 17–18 May 2010.

The 2010 State-of-Understanding Report

In addition to the scientific chapters and the Executive Summary, the assessment also updates the 2006 assessment report's answers to a set of questions that are frequently asked about the ozone layer. Based upon the scientific understanding represented by the assessments, answers to these frequently asked questions were prepared, with different readerships in mind, e.g., students and the general public. These updated questions and answers are included in this report and published separately in a companion booklet to this report.

The final result of this two-year endeavor is the present assessment report. As the accompanying list indicates, the *Scientific Assessment of Ozone Depletion: 2010* is the product of 312 scientists from 39 countries of the developed and developing world who contributed to its preparation and review¹ (191 scientists prepared the report and 196 scientists participated in the peer review process).

What follows is a summary of their current understanding of the stratospheric ozone layer and its relation to humankind.

¹ Participating were Argentina, Australia, Belgium, Benin, Canada, Chile, Comoros, Costa Rica, Czech Republic, Denmark, Egypt, Estonia, Finland, France, Germany, Greece, Hungary, India, Indonesia, Iran, Italy, Japan, Kenya, Malaysia, Mexico, New Zealand, Norway, Poland, Russia, Saudi Arabia, South Africa, Spain, Sweden, Switzerland, The Netherlands, The People's Republic of China, Togo, United Kingdom, and United States of America.

PROLOGUE

PROLOGUE: STATE OF THE SCIENCE THROUGH THE 2006 WMO/UNEP ASSESSMENT

A.R. Ravishankara, Paul A. Newman, John A. Pyle, and Ayité-Lô Ajavon

Scientists have known for many decades that the stratospheric ozone layer screens harmful ultraviolet radiation (UV) from the Earth's surface. Therefore, it has also been known that the ozone layer protects against adverse effects on humans (e.g., skin cancer and cataracts), the biosphere (e.g., inhibiting plant growth and damaging ecosystems), and physical infrastructure of the modern era (e.g., degradation of materials). In the early 1970s, scientists recognized that human actions could deplete this protective layer in connection with nitrogen oxide emissions from a proposed fleet of supersonic aircraft flying in the stratosphere. Around that time, it was shown that human-produced chlorofluorocarbons (CFCs) that had been manufactured (and emitted to the atmosphere) had remained in the atmosphere because of their stability. Soon afterward, scientists warned that these CFCs that are stable in the lower atmosphere would get to the stratosphere, where they could deplete the ozone layer. They also warned that the depletion would be large if CFC emissions continued unabated. Various national and international assessments that estimated the impact of CFCs on the ozone layer were carried out. For example, using the then-state-of-the-art models of the atmosphere, a 1981 Assessment sponsored by the World Meteorological Organization (WMO) and agencies of the United States of America estimated that up to ~15% of the column ozone would be depleted by the middle of the 21st century if the CFC emissions went unabated at 1974 emission levels under certain assumptions about other emissions and changes (WMO, 1982). Studies also predicted a decrease in ozone of 5–10% if a fleet of 500 supersonic aircraft emitting nitrogen oxides were to fly routinely in the stratosphere.

In 1985, massive ozone losses in measured column abundances during the Antarctic spring (the ozone hole) were reported and CFCs were implicated for the loss. Extensive research efforts showed that CFCs and other ozone-depleting substances (ODSs) containing chlorine and bromine were the cause. Further, measured global ozone abundances showed a decrease between 0.5% and 1.5% by 1980. Thus, ozone depletion was not just a phenomenon expected by the middle of the 21st century, but was already occurring. As a result of these findings on ozone depletion, stratospheric science rapidly evolved during the latter part of the 20th century, allowing understanding, diagnosis, and prediction of the evolution of the ozone layer; these rapid scientific developments provided a sound basis for the critical policy decisions that followed.

Faced with the potential impact of human-produced long-lived halogenated chemicals on stratospheric ozone, the Vienna Convention for the Protection of the Ozone Layer was enacted in 1985 to protect human health and the environment against adverse effects resulting from modification of the ozone layer. The recognition that CFC use was increasing, and scientific evidence that this increase would cause large ozone depletions, led in 1987 to the Montreal Protocol on Substances that Deplete the Ozone Layer, a protocol that regulated and slowed the production of designated ODSs. As new scientific knowledge became available over the next two decades, the Protocol has been amended and adjusted to provide additional protection for the ozone layer. The Montreal Protocol is now more than 20 years old and has been ratified by all of the world's nations.

The Montreal Protocol, at its inception, established three expert panels—the Scientific Assessment Panel (SAP), the Environmental Effects Assessment Panel (EEAP), and the Technology and Economic Assessment Panel (TEAP). These panels provide the basis for science-based decision making via periodic assessment reports. The SAP's primary focus is to provide an assessment of ozone layer science, including information about the abundances and emissions of ozone-depleting substances, ultraviolet radiation changes, along with additional information concerning policy options for consideration by the Parties to the Protocol. In addition, the SAP reports also aid other customers: various nations, by providing information needed for their decision making; industry, by providing a basis for technology choices; the broad science community, the EEAP, and the TEAP, with the latest information about the ozone layer science; the ozone research community, with information on the current science and gaps in knowledge; and the general public, including students and educators, with key information about this complex issue. The "Twenty Questions and Answers About the Ozone Layer" and its predecessors, which are companions to the SAP assessment reports, also help by providing clear, easy-to-understand communication of the ozone layer issues to the Parties and the general public. Further, every four years, the

Cochairs of the three Assessment Panels compile a Synthesis Report based on the findings of their individual Assessment reports. These Assessments—individual Assessments and the Synthesis Report—together provide the latest information to the Parties to the Protocol.

Over the past two decades, the ozone depletion assessments have provided information updates roughly every four years and have been interspersed with a few brief reports on special topics that addressed urgent needs of the Parties to the Protocol. As knowledge of ozone layer science has increased, the assessments have built a vast amount of knowledge. Now, the SAP is addressing some key remaining issues regarding the ozone layer and its future development. They include the following:

- First, the Protocol has regulated human-produced ozone-depleting substances, resulting in the reduction of their abundances in the atmosphere. This effort has brought ozone depletion science into a period of accountability. The crucial questions now have become: Does the Montreal Protocol continue to work as envisioned? Were the specific actions effective in meeting the Protocol's goals? Are the goals of the Vienna Convention also being met? How important are additional actions in returning ozone to its natural level? When will ozone levels return to preindustrial values? When will ozone levels return to the levels seen in 1980, a level that has become a benchmark for policymakers and the public? When will the ozone hole disappear? As ozone levels increase, will we observe decreases in surface ultraviolet radiation? What is our level of understanding of the workings of the stratosphere and how confident are we in our predictions for the future?
- Second, since the ozone layer is an integral part of the Earth system, other important questions have emerged: What is the influence of climate change on the stratospheric ozone layer and its future development? Specifically, how will the cooling of the stratosphere due to anthropogenic carbon dioxide (CO₂) increases and the warming of the troposphere due to the increasing abundance of greenhouse gases influence the stratospheric ozone layer? How can we disentangle the influences of climate change on stratospheric ozone levels from the influences of ozone-depleting substances?
- Third, the changes in stratospheric ozone are but one component of stratospheric climate change, and this poses questions such as: What are the effects of changes in stratospheric climate on the global-climate system? In addition, how will decreasing concentrations of ODSs impact climate?
- Fourth, ODSs and many substitutes for the ODSs are also potent greenhouse gases. Therefore, as ODSs are phased out and new chemicals take their place, questions emerge on the suitability of the replacements. They include: How will they impact the ozone layer? Do they have appreciable effects on climate? Do they have any other unwanted effects on the environment?

The SAP's goal is to provide clear scientific answers to these questions. These questions provide the major thrust of the research in this area and are at the center of the current Assessment.

This current document provides the latest assessment of the science of the ozone layer. Below, we very briefly summarize our understanding of the science going into this Assessment. We summarize the findings of the most recent previous report of 2006 and note the key issues for the present Assessment.

Ozone-Depleting Substances (ODSs)

Emissions of ODSs were increasing at a substantial rate before the Montreal Protocol was enacted in 1987. As a result of the Protocol, emissions of most of the major ODSs—the chlorofluorocarbons (CFCs) and methyl chloroform (CH₃CCl₃)—began decreasing soon thereafter. Because of the long lifetimes of CFCs, their atmospheric abundances continued to increase in the early 1990s even as their emissions were decreasing. However the abundance of the short-lived methyl chloroform responded quickly, as expected, and started to decrease in the atmosphere. Originally, some of the CFC replacements were the so-called transition substitutes (hydrochlorofluorocarbons, HCFCs); they contained chlorine but were shorter lived than the CFCs they replaced. This substitution led to a lower accumulation of the HCFCs and a smaller fraction of their emissions being transported to the stratosphere. Subsequently, the HCFCs were also selected for phase-out, and non-chlorine containing substitutes are now being phased in. Because of these changes, the sum of the abundances of chlorine and bromine ODS species in the troposphere, as measured by equivalent chlorine (ECl), reached a peak in the 1994–1995 time period and has continued to decrease thereafter. The majority of the decrease in the ECl is attributed to the rapid decline of emissions of the short-lived methyl chloroform and, to a lesser extent, methyl bromide.

Prologue Box 1. A Clarification of the Lexicon: Ozone Destruction, Ozone Depletion, Ozone-Depleting Substances, and Montreal Gases

Ozone Destruction and Ozone Depletion

The abundance of ozone at a particular point in the stratosphere, the column abundance of ozone above a given geographical location, and the total amount of ozone in the stratosphere are controlled by a combination of production, destruction, and transport (of ozone and other chemicals into and out of the region of interest). The major mechanism for the production of ozone in the stratosphere is the breaking up of molecular oxygen (O_2) by solar UV of wavelengths less than 242 nanometers (photolysis) to make oxygen atoms (O), followed by the reaction of oxygen atoms with molecular oxygen to make ozone. The destruction of ozone occurs via the reactions of oxygen atoms (O) with ozone (O_3) (the Chapman Mechanism), as well as through cyclic chemical reactions involving naturally occurring species such the odd-hydrogen radicals (HO_x : OH and HO_2), nitrogen oxide radicals (NO_x : mostly NO and NO_2), and/or halogen radicals. The radicals are produced in the stratosphere by photolysis and oxidation of source gases (N_2O , H_2O , CH_4 , and a variety of chlorine- and bromine-containing compounds). In the absence of interference from the human emissions influencing the abundance of catalysts, there is a natural balance and this balance determines the ozone abundance in a location, the column amount over a region, and the total amount of ozone in the stratosphere. The natural amounts vary on a variety of timescales: daily variations in the ozone column are driven by meteorological variability (“weather”); seasonal variations are driven by changes in stratospheric temperature and winds; multiannual variations are driven by changes in solar input, by natural variations in the emissions of the source gases, and by interannual variability in stratospheric winds.

The natural abundance of stratospheric ozone can be changed by human influence. This change can be brought about by changes in production, destruction, and transport. The ozone abundance arises from a balance between these terms. Human emissions, for the most part, have led to an enhancement in the destruction term, shifting the balance to lower ozone abundance. Thus, any human emission of chemicals (gases or particles) that contributes to the enhancement of the ozone destruction term in the balance leads to a lowering of ozone, i.e., ozone layer depletion, and is evidenced by changes in the amount at a location, in the column amount above a location, or the total amount in the stratosphere. Because the destruction occurs through catalytic cycles that regenerate the ozone-destroying radicals multiple times, small changes in the source gases (and hence in radical concentrations) can have a large impact on ozone.

Ozone-Depleting Substances and Montreal Gases

If there is an increase in concentrations of any of these source gases that contribute nitrogen, hydrogen, or halogen radicals to the stratosphere, there will be an increase in ozone-destroying radicals and hence in stratospheric ozone destruction. Changes in the source gases could occur either naturally (e.g., by biogenic processes at the surface) or anthropogenically (by increased industrial emissions); some source gases are emitted both naturally and anthropogenically. The response of the stratosphere does not depend on whether the changes are natural or anthropogenic; the stratosphere does not “care.” However, scientists and policymakers do care and in some circumstances it is useful to have a terminology that distinguishes the different origins of the source compounds. Therefore, ozone-depleting substances (ODSs) are those whose emissions come from human activities.

It will be important in the Assessment also to consider specifically gases that have been regulated (and which traditionally we have called ODSs). Thus, the Montreal Protocol has controlled the production (and hence their emissions into the atmosphere) of certain chemicals that are listed as controlled substances in Annexes A, B, C, and E of the Protocol. **We will continue to call the controlled substances of the Montreal Protocol as ozone-depleting substances, or ODSs for short.** This definition keeps the continuity in usage and will be clear to the Parties to the Montreal Protocol.

The above description yields a few key points. First, the ozone abundance can be changed not only by destruction but also via influence on production, transport, and stratospheric climate. There are long-standing examples of such production enhancements by hydrocarbons, in particular methane, via what is usually called smog chemistry (i.e., the chemistry that leads to the tropospheric pollutant ozone production). Second, ozone abundances can be changed by both changes in the concentrations of active agents, as well as by changes in the rates at which these chemical reactions occur. The most noteworthy way is by changes in the stratospheric climate (i.e., temperature), such as that caused by the enhancements in carbon dioxide in the atmosphere. Third, the ozone abundance can be influenced by changes in transport, such as that arising from a changing climate. And fourth, while the Montreal Protocol controls many substances that deplete ozone, not all such substances are currently controlled and, for clarity, they are not called ODSs here. Reference to such substances are clearly noted in this Assessment.

The tropospheric abundance of ECl by the end of 2005 was shown in the previous Assessment to have decreased to roughly 92% of its maximum value seen during the period between 1992 and 1994 (i.e., about a 8% decline in roughly 14 years); these values will be updated in this report.

Balloon, aircraft, and satellite observations, and the interpretation of those observational data, show clearly that stratospheric abundances of chlorine and bromine are also decreasing. The vertical and temporal variations of the ODS species are generally consistent with our understanding of atmospheric dynamics and stratospheric chemical processes, though there are some quantitative differences between observations and calculations. Improvements in quantification of these variations are expected. These improvements will enable an even better definition of the stratospheric distribution and trends of the ODSs as well as their degradation products, which will enable a better quantification of their individual role in ozone layer depletion.

The CFCs, as well as some halons (which are sources of bromine to the stratosphere), have lifetimes ranging from several decades to a few centuries. Hence, the decline of stratospheric chlorine and bromine levels to values observed before 1980 will take decades.

As noted above, CFCs have been replaced by non-ozone depleting technologies, by substitutes that deplete less ozone (e.g., hydrochlorofluorocarbons or HCFCs), and by non-ozone depleting substances (e.g., hydrofluorocarbons or HFCs). The atmospheric levels of these less-depleting and non-depleting substitutes have grown rapidly over the last decade. HCFCs typically have shorter atmospheric lifetimes and lower Global Warming Potentials (GWPs) than CFCs, but HFC substitutes for HCFCs typically have comparable, and in a few cases even longer, atmospheric lifetimes and comparable or larger GWPs; but they have Ozone Depletion Potential (ODP) values of essentially zero. The increases observed for HCFCs and HFCs reflect their widespread use as ODS replacements and our understanding of their atmospheric lifetimes.

Global Stratospheric Ozone and Its Temporal and Spatial Trends

Global atmospheric column ozone amounts decreased over the decades from the 1970s to the 1990s, with a decrease amounting to 3.5% between average 1964–1980 and 2002–2005 values. Springtime Antarctic ozone levels slowly decreased in the 1970s and exhibited rapid decreases in the 1980s and early 1990s. In the 14–20 km layer of the Antarctic stratosphere, where most of the ozone resides, virtually all of the ozone is now destroyed every year in the late August to early October period. Large Arctic ozone depletions have also been observed in the spring in some years during the last two decades, but Arctic ozone depletion is modulated strongly by variability in atmospheric dynamics, transport, and temperature. The very high levels of chlorine and bromine from ODSs directly cause the observed large polar ozone depletions (both over the Antarctic and the Arctic).

Atmospheric ozone levels (often measured as a column amount) exhibit well-known and understood variations in space and time. Ozone amounts are influenced not only by the concentrations of ODSs but also by atmospheric transport (winds), incoming solar radiation, aerosols (fine particles suspended in the air), and other natural compounds. Given natural variability, methods used to measure stratospheric ozone must be consistent and very stable over decades if they are to be used to detect the changes expected over these long periods due to the changes in ODS abundances. Based on observations from ground-based instruments and satellites, it is clear that global ozone levels reached a minimum in the mid-1990s. Since then the levels have not decreased further nor have they increased substantially. Similarly, the Antarctic ozone hole continues to be no worse than in the mid-1990s but there also has been no discernible improvement, consistent with predictions from previous assessments. Both annual global ozone and the springtime Antarctic ozone levels continue to vary from year to year because of meteorological variability. There is no discernible ozone depletion over the tropics outside of the natural background variations. Vertically, ozone depletion is most evident in the lower and upper stratosphere, with minimal changes in the mid-stratosphere.

In the last few decades, ozone levels in the stratosphere have responded to volcanic eruptions that have injected large amounts of sulfur dioxide into the stratosphere, which then forms sulfate aerosols in this region. These sulfate aerosols enhance the ozone depletion by chlorine from ODSs. The very large ozone depletions induced by the presence of aerosols following the eruptions of Mt. Pinatubo (1991) and El Chichón (1982) are very clearly seen in the records in the Northern Hemisphere. The influence of these eruptions persisted for several years. As the stratosphere recovered from the volcanic emissions, there were corresponding changes in ozone. The ozone response depends on the effective abundances of chlorine and bromine in the stratosphere. Thus, response to future volcanic eruptions will likely be smaller because

chlorine/bromine concentrations will be smaller (see Figure P-1). The mechanisms for these changes are qualitatively understood, but some uncertainties remain in their quantification.

The observed levels of ozone described above and the vertical, latitudinal, and seasonal structure of their temporal trends, as well as the spatial and temporal variability, are consistent with our combined understanding of the atmospheric motions (transport), the chemistry, and the level of ODSs in the atmosphere. Even though some details of chemical and dynamical processes are uncertain, atmospheric models have been largely successful in reproducing observed ozone levels and their temporal and spatial variations. The link between ODSs and ozone depletion was clearly established in the 1989 Ozone Assessment (WMO, 1991) and that conclusion has only been strengthened since then.

Surface UV Changes

Ultraviolet radiation (UV) from the Sun is divided into wavelength bands. UV-B is the band that leads to serious medical problems. Fortunately, the majority of the UV-B is absorbed by ozone. The surface UV-B and UV-A levels (expressed as the UV Index) are directly related to the amount of overhead ozone. Other factors such as clouds, aerosols, ground reflectivity, and other tropospheric pollutants also influence surface UV-B. The data outside of the polar regions shows that, consistent with the observed small ozone depletion, there have not been large increases in surface UV-B over the last few decades. The relatively small increases of surface UV-B in the midlatitudes, which are expected based on the observed ozone decline, are responsible for small changes in the UV background level, which are superposed by other strong effects, such as changes in cloudiness. However, since medical impacts are UV-dose related, the UV changes due to ozone depletion are nonetheless important. In contrast, over Antarctica, and on occasion in other parts of the high latitudes in the Southern Hemisphere, large increases in UV-B have been seen; they are clearly associated with the ozone hole or the remnants of the ozone hole passing over the measurement sites.

The changes in UV-B levels are consistent with our understanding of UV transmission and the other factors that influence UV-B at the surface.

Factors that Influence Stratospheric Ozone and Its Future

The change in the atmospheric ODS concentrations is the most important factor in the ozone layer changes that have occurred over the past half a century and also in the predicted return of the ozone layer to levels that existed prior to 1980. However, many other aspects of the Earth system are also changing. These include changes in climate and tropospheric composition.

Climate change influences the stratosphere in many ways. The primary influence is a cooling of the mid- to upper stratosphere due to increases in carbon dioxide (CO₂) via radiation to space, which is a well-understood process. This cooling has been clearly seen in measured temperatures. The cooling influences the ozone loss rates in the stratosphere—increasing it in the lower stratosphere and decreasing it in upper stratosphere. At the same time the warming in the troposphere accelerates processes of ozone formation. Further, climate change has an effect on transport between the stratosphere and the troposphere and within the stratosphere, and in turn, climate will influence the recovery of ozone layer from the effects of ODSs.

Tropospheric changes also influence stratospheric ozone levels. For example, an increased abundance of methane (CH₄) in the troposphere will result in more methane being transported to the stratosphere, where methane interacts with chlorine compounds, converting active chlorine that destroys ozone to inactive hydrogen chloride (HCl) that does not destroy ozone. Changes in methane also lead to changes in water vapor in the stratosphere, with important consequences. Similarly, changes in nitrous oxide (N₂O) also influence ozone destruction. Other tropospheric changes of interest include processes leading to increases in sulfur in the stratosphere. In some cases, changes of these tropospheric processes may be related to climate change. For instance, climate change may affect biogeochemical cycles and cause an increase in tropospheric concentrations of certain species as well as the transport rate between the troposphere and the stratosphere. The latter may be particularly important for the very short-lived species.

The timeline of the ozone evolution from the pre-ODS era to roughly 2100 was presented in the 2006 Assessment to facilitate discussion on recognition and attribution of the recovery of the ozone layer. This approach provided a pathway for interim conclusions on this issue, but many issues remained unresolved. They include: How should recovery be defined? What time period is appropriate as a baseline against which we can measure recovery? How do we separate ozone changes

due to ODSs from those due to changes in climate and tropospheric composition? How do we describe and attribute future changes in levels of ozone? Given the natural variability, at which point will one be confident of the recovery from ODS effects? This Assessment addresses some of these issues and concepts (see Prologue Box 2 on Recovery Issues).

Influence of Stratospheric Ozone and ODS Changes on Climate

As noted above, increases in CO₂ in the atmosphere have led to a clear decrease in upper stratospheric temperature. This temperature trend is a very clear signature of the radiative influence of increasing CO₂ abundances. Changes in the stratosphere—be it the temperature decrease due to CO₂ increases or ozone layer depletion due to ODSs—are an integral part of the changes to the Earth system. Further, these changes in the stratosphere influence what happens at the surface. Therefore, the influence of stratospheric changes on surface climate is an important issue.

Ozone is a greenhouse gas that greatly influences the Earth's energy budget. Therefore, ozone changes—depletion in the stratosphere due to ODSs, recovery from the depleted state as ODSs decline, and tropospheric ozone changes—also influence climate. Further, many of these ODSs that deplete the ozone layer are also greenhouse gases. Consequently, they influenced Earth's climate in the past as their abundances increased and will continue to do so, albeit to a lesser extent, as their abundances decrease in response to compliance with the Montreal Protocol. Furthermore, many of the substitutes for CFCs and HCFCs are also potent greenhouse gases and their contribution to climate change will depend on their potency for warming and their emission rates.

These are some of the emerging issues that have been covered only briefly in the past due to a primary focus on ozone depletion issues. As research on the influence of stratospheric changes on the overall climate has emerged, the current Assessment is devoting more attention to this topic.

Major Findings of the Previous Assessment in 2006

The major findings of the 2010 Assessment are given in the Executive Summary that follows this Prologue. To place these findings in context and show the changes in our knowledge over the past four years, we provide below the summary of the 2006 Assessment (WMO, 2007). Further, for ease of comparison, the findings from the 2006 Assessment are grouped according to where they are covered in the 2010 Assessment; i.e., the 2006 Assessment is mapped on to the 2010 Assessment's structure.

A major finding of the previous Assessment in 2006, the tenth in a series of Assessments dating back to 1981, was that the Montreal Protocol was working as intended. Some specific findings of the 2006 Assessment are summarized in the schematic shown as Figure P-1.

The high-level findings of the previous Assessment (WMO, 2007) include the following.

*Findings of the 2006 Assessment that are related to “Ozone-Depleting Substances (ODSs) and Related Chemicals” covered in **Chapter 1 of the 2010 Assessment**:*

1. The total combined abundances of anthropogenic ozone-depleting gases in the troposphere continue to decline from the peak values reached in the 1992–1994 time period.
2. The combined stratospheric abundances of the ozone-depleting gases show a downward trend from their peak values of the 1990s, which is consistent with surface observations of these gases and a time lag for transport to the stratosphere.
3. Our quantitative understanding of how halogenated very short-lived substances contribute to halogen levels in the stratosphere has improved significantly since the 2002 Assessment (WMO, 2003), with brominated very short-lived substances believed to make a significant contribution to total stratospheric bromine and its effect on stratospheric ozone.

*Findings of the 2006 Assessment that are related to “Stratospheric Ozone and Surface Ultraviolet Radiation” in the past and our understanding of its changes covered in **Chapter 2 of the 2010 Assessment**:*

1. Our basic understanding that anthropogenic ozone-depleting substances have been the principal cause of the ozone depletion over the past few decades has been strengthened. During the recent period of near-constant abundances of ozone-depleting gases, variations in meteorology have been particularly important in influencing the behavior of ozone over much of the polar and extrapolar (60°S–60°N) regions.

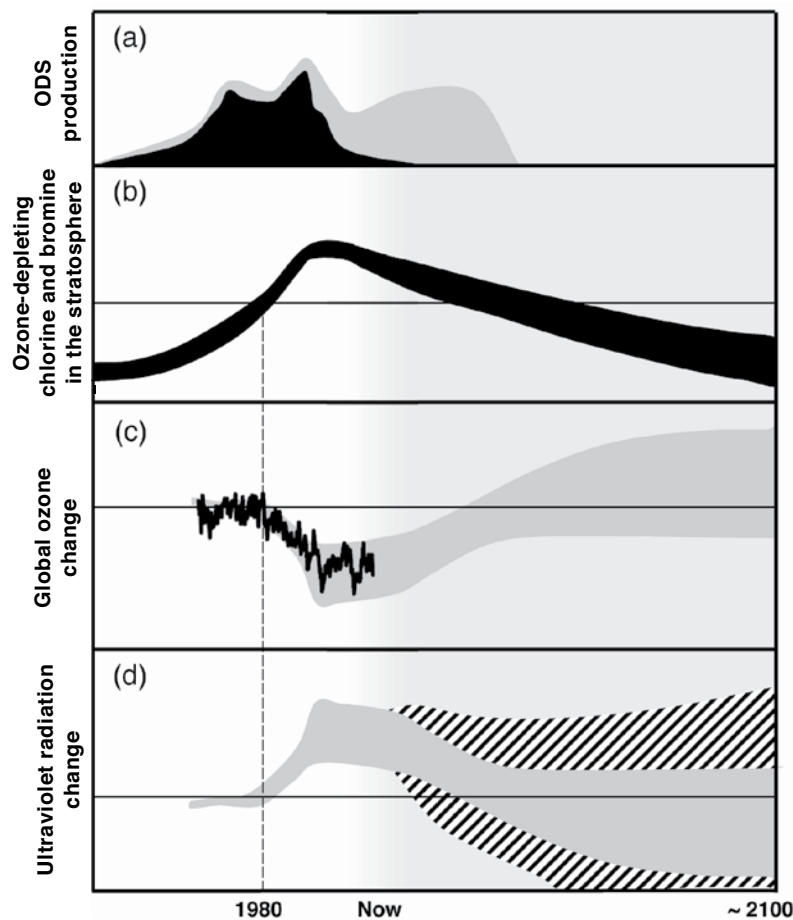


[Figure reproduced from the 2006 Ozone Assessment (WMO, 2007).]

Figure P-1. Ozone-Depleting Substances, the Ozone Layer, and UV Radiation: Past, Present, and Future.

(a) Production of ozone-depleting substances (ODSs) before and after the 1987 Montreal Protocol and its Amendments, from baseline scenario A1. Chlorofluorocarbons (CFCs) are shown in black; additional ODSs from hydrochlorofluorocarbons (HCFCs) are in gray. Note: HCFCs, which have been used as CFC replacements under the Protocol, lead to less ozone destruction than CFCs.

(b) Combined effective abundances of ozone-depleting chlorine and bromine in the stratosphere. The range reflects uncertainties due to the lag time between emission at the surface and the stratosphere, as well as different hypothetical ODS emission scenarios.

(c) Total global ozone change (outside of the polar regions; 60°S–60°N). Seasonal, quasi-biennial oscillation (QBO), volcanic, and solar effects have been removed. The black line shows measurements. The gray region broadly represents the evolution of ozone predicted by models that encompass the range of future potential climate conditions. Pre-1980 values, to the left of the vertical dashed line, are often used as a benchmark for ozone and UV recovery.

(d) Estimated change in UV erythemal (“sunburning”) irradiance for high sun. The gray area shows the calculated response to the ozone changes shown in (c). The hatched area shows rough estimates of what might occur due to climate-related changes in clouds and atmospheric fine particles (aerosols).

2. Springtime polar ozone depletion continues to be severe in cold stratospheric winters. Meteorological variability has played a larger role in the observed variability in ozone, over both poles, in the past few years.
3. The decline in abundances of extrapolar stratospheric ozone seen in the 1990s has not continued.
4. Observations together with model studies suggest that the essentially unchanged column ozone abundances averaged over 60°S–60°N over roughly the 1995–2005 period are related to the near constancy of stratospheric ozone-depleting gases during this period.
5. Measurements from some stations in unpolluted locations indicate that UV irradiance (radiation levels) has been decreasing since the late 1990s. However, at some Northern Hemisphere stations UV irradiance is still increasing, as a consequence of long-term changes in other factors that also affect UV radiation.
6. In polar regions, high UV irradiances lasting for a few days have been observed in association with episodes of low total ozone.

Findings of the 2006 Assessment that are related to “Future Ozone and Its Impact on Surface UV” covered in Chapter 3 of the 2010 Assessment:

1. It is unlikely that total ozone averaged over the region 60°S–60°N will decrease significantly below the low values of the 1990s, because the abundances of ozone-depleting substances have peaked and are in decline.

2. The decrease in ozone-depleting substances is the dominant factor in the expected return of ozone levels to pre-1980 values. Changes in climate will influence if, when, and to what extent ozone will return to pre-1980 values in different regions.
3. The Antarctic ozone hole is expected to continue for decades. Antarctic ozone abundances are projected to return to pre-1980 levels around 2060–2075, roughly 10–25 years later than estimated in the 2002 Assessment.
4. Large ozone losses will likely continue to occur in cold Arctic winters during the next 15 years.
5. Chemical reaction rates in the atmosphere are dependent on temperature, and thus the concentration of ozone is sensitive to temperature changes caused by climate change.

Findings of the 2006 Assessment that are related to the influence of “Stratospheric Changes and Climate” covered in Chapter 4 of the 2010 Assessment:

1. The stratospheric cooling observed during the past two decades has slowed in the recent years up to 2005.
2. Changes to temperature and circulation of the stratosphere affect climate and weather in the troposphere.
3. Updated datasets of stratospheric water vapor concentrations show differences in long-term behavior.
4. Future increases in greenhouse gas concentrations will contribute to the average cooling in the stratosphere.
5. Climate change will also influence surface UV radiation through changes induced mainly to clouds and the ability of the Earth’s surface to reflect light.

Findings of the 2006 Assessment that are related to “A Focus on Options and Information for Policymakers” covered in Chapter 5 of the 2010 Assessment:

1. The Montreal Protocol is working: There is clear evidence of a decrease in the atmospheric burden of ozone-depleting substances and some early signs of stratospheric ozone recovery.
2. The dates for the return of the global ozone layer and the Antarctic ozone hole to 1980 levels were provided based on the best available information to be around, respectively, 2049 and 2065.
3. Many potential options for accelerating the recovery of the ozone layer were evaluated and presented.

Organization of the Current Assessment

Much new information has been generated since the 2006 Assessment. Further, the information needs of the Parties to the Protocol have also changed. The specific requests of the Parties to the SAP are given in the Preface of this Assessment. Of particular note are the questions related to the influence of stratospheric changes on Earth’s climate. This is somewhat of a new issue to the SAP and thus demands a chapter of its own.

This Assessment is an update to previous Assessments, and in particular the 2006 Assessment. However, as noted above, the changes in ozone and UV are not rapid and there are no new major findings in this area. To reflect this updating approach and consolidation of information, the structure of this Assessment differs from the most recent reports. In this Assessment, Chapter 1 deals with all issues related to ODSs; they include long-lived and very short-lived halocarbons as well as the replacements for the ODSs. In particular, it covers the trends and abundances of the replacements for ODSs that are greenhouse gases (but not ODSs), such as HFCs that are being discussed by the Parties to the Protocol for regulation. Chapter 2 deals with all observations of ozone and surface UV to date and our understanding of these observations, including a discussion of the current state of polar ozone. Chapter 3 focuses primarily on the future response of the ozone layer and UV-B radiation to reduced halocarbon emissions and other changes in an effort to focus on the question: What should one anticipate for ozone layer depletion and its consequences? It also picks up the issue of the definition and recognition of the recovery of the ozone layer first discussed in the 2006 Assessment. Of particular note are the issues related to the influence of stratospheric changes on climate. This issue was briefly described in the 2006 Assessment, which mostly focused on the influence of climate change on the recovery of the ozone layer. Because of the emergence of information on the influence of the stratospheric changes on Earth’s climate, we have added a new chapter—Chapter 4—to address this topic. Chapter 4 focuses on the two-way connection between stratospheric changes and climate changes. This places the effects of halocarbon-induced ozone depletion on climate in the broader context of other stratospheric changes. Chapter 5 is expanded to include not only the policy options, often posed in hypothetical terms, available for further action but also other information relevant to the Parties to the Protocol.

Prologue Box 2. Recovery of the Ozone Layer: Concepts and Practical Issues

A conceptual diagram of the behavior of stratospheric ozone between 1960 and 2100 was presented in Chapter 6 of the 2006 Assessment (Bodeker and Waugh et al., 2007: “The Ozone Layer in the 21st Century”). A slightly modified version of this diagram is shown below.

As noted in the 2006 Assessment, stratospheric ozone abundances should change in response to decreases of ODSs and in response to other factors that influence ozone levels in the stratosphere. The other major factors are changes in temperature of the stratosphere because of increases in CO₂, changes in transport associated with climate change, and changes in tropospheric composition.

The ODS increases in the past few decades depleted the ozone layer. In the future, as ODSs decrease, the atmosphere in general—and the stratosphere in particular—should have decreasing amounts of ozone-destroying halogen catalysts. This decrease will follow the emissions of ODSs but will be shifted to later times because ODSs generally have long atmospheric lifetimes.

The past and future timeline of ozone behavior has been categorized as: stage I—slowing of ozone decline; stage II—onset of ozone increases; and stage III—full recovery of ozone from ODSs. In this idealization it is assumed that ozone production is not altered significantly, and that the climate and tropospheric changes are sufficiently small that the influence of ODSs is the predominant factor that controls the rate of depletion of the ozone layer. Of course, because of natural interannual variability, the ozone abundances do not show sufficiently clear changes to allow precise identification of these timeline stages. (*Continued on following page.*)

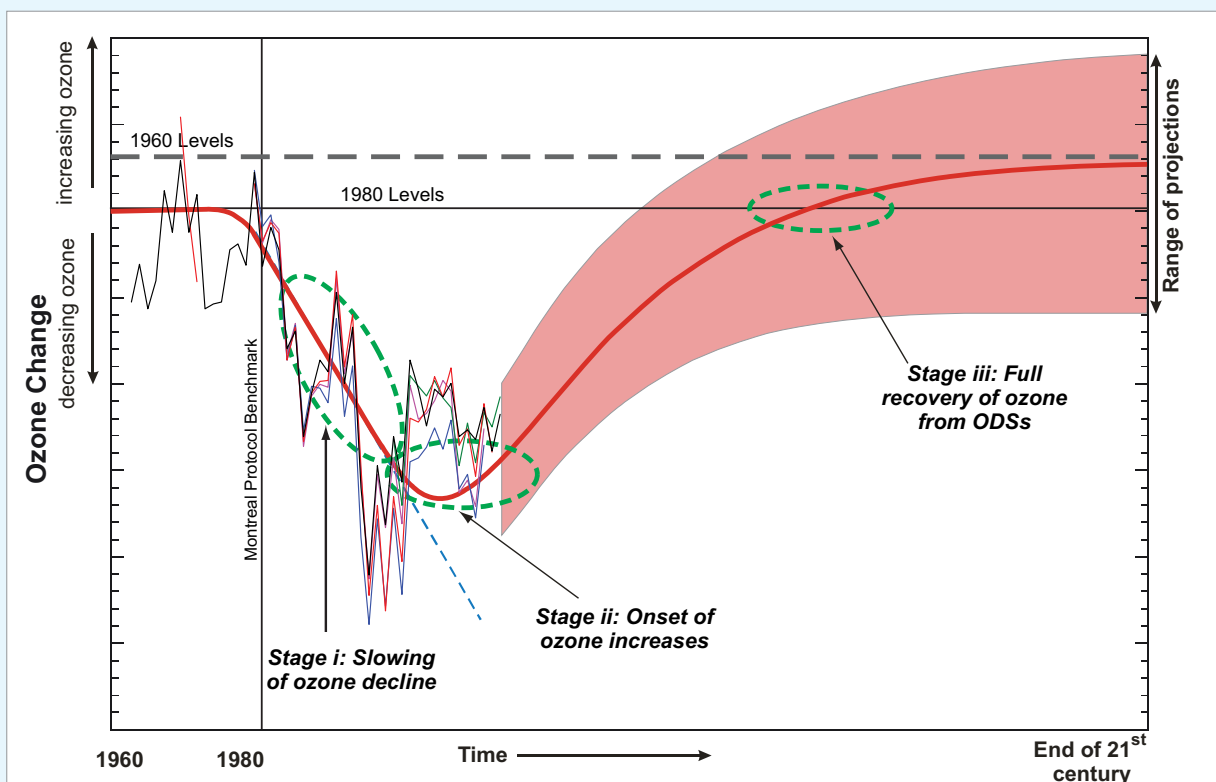


Figure P-2. A conceptual diagram of the evolution of column ozone between 60°N and 60°S between 1960 and 2100 (the x-axis is not to scale) adapted from Fig. 6-1 in the 2006 Assessment. The observations are discussed in Chapter 2. The thick red line is a representation of the ozone amounts observed to date and projected for the future. The red-shaded region represents the model results predicted for the future. The Montreal Protocol 1980 ozone level benchmark is shown as the horizontal line. The dashed thick gray line represents the somewhat uncertain 1960 levels. The three recovery stages are shown by green dashed ellipses.

Prologue Box 2, continued.

This three-stage timeline is a very useful conceptual picture for understanding ozone changes, diagnosing the current and future trends, and attempting to predict future ozone levels. However, as noted above, the ozone timeline is also influenced by other changes—climate change, volcanic eruptions that introduce sulfate aerosols in the stratosphere, and tropospheric composition changes. Further, the natural (and forced) variability in the Earth system will lead to difficulties in identifying as well as attributing these changes. These variabilities occur not only in the ozone abundances but also in the ODS levels, as climate change and other changes will alter when the ODS levels will reach values seen prior to 1980.

For all practical purposes, the Montreal Protocol has used 1980 levels as the time when there was little perturbation of the ozone layer by ODSs. This does not mean that there was no ozone depletion in 1980. Indeed, retroactive analyses of observations show that the ozone hole was growing prior to 1980. Yet we use 1980 levels of ODSs as the level when the ozone layer was not significantly influenced by ODSs and we will continue to use this date as a benchmark in this Assessment.

Because of factors other than ODSs, the ozone levels in the future could easily go above the values that were present either in the 1980s or even the 1960s. This situation was described in the previous Assessment as a “super-recovery.” Of course, this is not recovery from the influence of ODSs but due to other factors, primarily CO₂. Therefore, the use of the term “super-recovery” differs from references to recovery from ODS-forced ozone depletion.

References

- Bodeker, G.E., and D.W. Waugh (Lead Authors), H. Akiyoshi, P. Braesicke, V. Eyring, D.W. Fahey, E. Manzini, M.J. Newchurch, R.W. Portmann, A. Robock, K.P. Shine, W. Steinbrecht, and E.C. Weatherhead, The ozone layer in the 21st century, Chapter 6 in *Scientific Assessment of Ozone Depletion: 2006*, Global Ozone Research and Monitoring Project—Report No. 50, 572 pp., World Meteorological Organization, Geneva, Switzerland, 2007.
- WMO (World Meteorological Organization), *The Stratosphere 1981: Theory and Measurements*, Global Ozone Research and Monitoring Project—Report No. 11, 516 pp., Geneva, Switzerland, 1982.
- WMO (World Meteorological Organization), *Scientific Assessment of Stratospheric Ozone: 1989*, Global Ozone Research and Monitoring Project—Report No. 20, Geneva, Switzerland, 1991. [Referred to as the 1989 Assessment.]
- WMO (World Meteorological Organization), *Scientific Assessment of Ozone Depletion: 2002*, Global Ozone Research and Monitoring Project—Report No. 47, Geneva, Switzerland, 2003. [Referred to as the 2002 Assessment.]
- WMO (World Meteorological Organization), *Scientific Assessment of Ozone Depletion: 2006*, Global Ozone Research and Monitoring Project—Report No. 50, 572 pp., Geneva, Switzerland, 2007. [Referred to as the 2006 Assessment.]

SCIENTIFIC ASSESSMENT OF OZONE DEPLETION: 2010

Executive Summary



National Oceanic and Atmospheric Administration
National Aeronautics and Space Administration
United Nations Environment Programme
World Meteorological Organization
European Commission

EXECUTIVE SUMMARY

Contents

OVERVIEW	ES.1
CHANGES IN GASES THAT AFFECT STRATOSPHERIC OZONE AND CLIMATE	ES.1
Ozone-Depleting Substances and Substitutes: Tropospheric Abundances and Emissions	ES.1
CFCs, HCFCs, HFCs, and Climate Change	ES.2
Total Chlorine and Bromine and Implications for Ozone Depletion	ES.3
Figure ES-1: Emissions of ODSs and Their Substitutes	ES.3
OZONE AND CLIMATE: ANTARCTIC	ES.4
OZONE AND CLIMATE: GLOBAL AND ARCTIC	ES.4
Figure ES-2: Schematic of the Influence of Ozone-Depleting Substances and Climate Change on the Stratospheric Ozone Layer, and the Influence of Ozone Changes on Surface Ultraviolet Radiation	ES.5
INFORMATION FOR POLICYMAKERS AND OPTIONS FOR POLICY FORMULATION	ES.7
Information for Policymakers	ES.7
Options for Policy Formulation	ES.8
Table ES-1: Hypothetical Cases	ES.9
APPENDIX: SCIENTIFIC SUMMARIES OF THE CHAPTERS (included in the individual chapters)	
Chapter 1: Ozone-Depleting Substances (ODSs) and Related Chemicals	
Figure S1-1: Stratospheric EESC Relative to Peak Abundances Versus Time	
Table S1-1: Radiative Forcings of ODSs and Other Gases and Their Recent Changes	
Chapter 2: Stratospheric Ozone and Surface Ultraviolet Radiation	
Table S2-1: Summary of Ozone Changes Estimated from Observations	
Chapter 3: Future Ozone and Its Impact on Surface UV	
Chapter 4: Stratospheric Changes and Climate	
Chapter 5: A Focus on Information and Options for Policymakers	
Table S5-1: Summary of Hypothetical Cases for Accelerating the Recovery of the Ozone Layer and Reducing Carbon-Equivalent Emissions	

EXECUTIVE SUMMARY

OVERVIEW

It has been recognized since the 1970s that a number of compounds emitted by human activities deplete stratospheric ozone. The Montreal Protocol on Substances that Deplete the Ozone Layer was adopted in 1987 to protect global ozone and, consequently, protect life from increased ultraviolet (UV) radiation at Earth's surface. Chlorine- and bromine-containing substances that are controlled by the Montreal Protocol are known as ozone-depleting substances (ODSs). ODSs are responsible for the depletion of stratospheric ozone observed in polar regions (for example, the "ozone hole" above Antarctica) and in middle latitudes. The severe depletion of stratospheric ozone observed in the Antarctic has increased UV at the surface and affected climate at southern high latitudes.

The Montreal Protocol and its Amendments and Adjustments have successfully controlled the global production and consumption of ODSs over the last two decades, and the atmospheric abundances of nearly all major ODSs that were initially controlled are declining. Nevertheless, ozone depletion will continue for many more decades because several key ODSs last a long time in the atmosphere after emissions end.

In contrast to the diminishing role of ODSs, changes in climate are expected to have an increasing influence on stratospheric ozone abundances in the coming decades. These changes derive principally from the emissions of long-lived greenhouse gases, mainly carbon dioxide (CO₂), associated with human activities. An important remaining scientific challenge is to project future ozone abundances based on an understanding of the complex linkages between ozone and climate change.

Most ODSs are potent greenhouse gases. The buildup of ODS abundances over the last decades contributes to global warming. The actions taken under the Montreal Protocol have reduced the substantial contributions these gases would have made to global warming.

There is now new and stronger evidence of the effect of stratospheric ozone changes on Earth's surface climate, and of the effects of climate change on stratospheric ozone. These results are an important part of the new assessment of the depletion of the ozone layer presented here.

CHANGES IN GASES THAT AFFECT STRATOSPHERIC OZONE AND CLIMATE

Changes in the global atmospheric abundance of a substance are determined by the balance between its emissions and removals from the atmosphere. Declines observed for ozone-depleting substances controlled under the Montreal Protocol are due to global emission reductions that have made emissions smaller than removals. Most ODSs are potent greenhouse gases. As the majority of ODSs have been phased out, demand for hydrochlorofluorocarbon (HCFC) and hydrofluorocarbon (HFC) substitutes for the substances controlled under the Montreal Protocol has increased; these are also greenhouse gases. HCFCs deplete much less ozone per kilogram emitted than chlorofluorocarbons (CFCs), while HFCs are essentially non-ozone depleting gases.

Ozone-Depleting Substances and Substitutes: Tropospheric Abundances and Emissions

- **The amended and adjusted Montreal Protocol continues to be successful at reducing emissions (Figure ES-1) and thereby abundances of most controlled ozone-depleting substances in the lower atmosphere (troposphere), as well as abundances of total chlorine and total bromine from these ozone-depleting substances.** By 2008, the total tropospheric abundance of chlorine from ODSs and methyl chloride had declined to 3.4 parts per billion (ppb) from its peak of 3.7 ppb. However, the rate of decline in total tropospheric chlorine by 2008 was only two-thirds as fast as was expected. This is because HCFC abundances increased more rapidly than expected, while CFCs decreased more slowly than expected. The discrepancy in CFC decreases is most likely because of emissions from "banks" in existing applications such as refrigerators, air conditioners, and foams. The rapid HCFC increases are coincident

with increased production in developing countries, particularly in East Asia. The rate of decline of total tropospheric bromine from controlled ODSs was close to that expected and was driven by changes in methyl bromide.

- **Declines in CFCs made the largest contribution to the observed decrease in total tropospheric chlorine during the past few years and are expected to continue to do so through the rest of this century.** Observations show that CFC-12 tropospheric abundances have decreased for the first time. The decline of methyl chloroform (CH_3CCl_3) abundances made a smaller contribution to the decrease in total chlorine than described in past Assessments, because this short-lived substance has already been largely removed from the atmosphere.
- **Carbon tetrachloride (CCl_4) tropospheric abundances have declined less rapidly than expected.** Emissions derived from data reported to the United Nations Environment Programme (UNEP) are highly variable and on average appear smaller than those inferred from observed abundance trends. Although the size of this discrepancy is sensitive to uncertainties in our knowledge of how long CCl_4 persists in the atmosphere (its “lifetime”), the variability cannot be explained by lifetime uncertainties. Errors in reporting, errors in the analysis of reported data, and/or unknown sources are likely responsible for the year-to-year discrepancies.
- **Observations near the tropical tropopause suggest that several very short-lived industrial chlorinated chemicals, not presently controlled under the Montreal Protocol (e.g., methylene chloride, CH_2Cl_2 ; chloroform, CHCl_3 ; 1,2 dichloroethane, $\text{CH}_2\text{ClCH}_2\text{Cl}$; perchloroethylene, CCl_2CCl_2), reach the stratosphere.** However, their contribution to stratospheric chlorine loading is not well quantified.
- **Bromine from halons stopped increasing in the troposphere during 2005–2008.** As expected, abundances of halon-1211 decreased for the first time during 2005–2008, while halon-1301 continued to increase but at a slower rate than in the previous Assessment.
- **Tropospheric methyl bromide abundances continued to decline during 2005–2008, as expected due to reductions in industrial production, consumption, and emission.** About half of the remaining methyl bromide consumption was for uses not controlled by the Montreal Protocol (quarantine and pre-shipment applications).
- **Tropospheric abundances and emissions of some HCFCs are increasing faster now than four years ago.** Abundances of HCFC-22, the most abundant HCFC, increased more than 50% faster in 2007–2008 than in 2003–2004, while HCFC-142b abundances increased about twice as fast as in 2003–2004. HCFC-141b abundances increased at a similar rate to that observed in 2003–2004. Total emissions of HCFCs are projected to begin to decline during the coming decade due to measures already agreed to under the Montreal Protocol (Figure ES-1).
- **Tropospheric abundances and emissions of HFCs, used mainly as substitutes for CFCs and HCFCs, continue to increase.** For example, abundances of HFC-134a, the most abundant HFC, have been increasing by about 10% per year in recent years. Abundances of other HFCs, including HFC-125, -143a, -32, and -152a, have also been increasing. Regional studies suggest significant HFC emissions from Europe, Asia, and North America.

CFCs, HCFCs, HFCs, and Climate Change

- **The Montreal Protocol and its Amendments and Adjustments have made large contributions toward reducing global greenhouse gas emissions (Figure ES-1).** In 2010, the decrease of annual ODS emissions under the Montreal Protocol is estimated to be about 10 gigatonnes of avoided CO_2 -equivalent¹ emissions per year, which is about five times larger than the annual emissions reduction target for the first commitment period (2008–2012) of the Kyoto Protocol.
- **The sum of the HFCs currently used as ODS replacements contributes about 0.4 gigatonnes of CO_2 -equivalent per year to total global CO_2 -equivalent emissions, while the HCFCs contribute about 0.7 gigatonnes.** CO_2 -equivalent emissions of HFCs are increasing by about 8% per year and this rate is expected to continue to grow, while the contribution from HCFCs is expected to start decreasing in the next decade.
- **Emissions of HFC-23, a by-product of HCFC-22 production, contributed about 0.2 gigatonnes of CO_2 -equivalent**

¹ GWP-weighted emissions, also known as CO_2 -equivalent emissions, are defined as the amount of gas emitted multiplied by its 100-year Global Warming Potential (GWP).

per year in 2006–2008. HFC-23 is a particularly potent greenhouse gas with a lifetime of about 220 years. Its emissions have increased in the past decade despite global emissions reduction measures, including those covered by the Kyoto Protocol's Clean Development Mechanism projects.

Total Chlorine and Bromine and Implications for Ozone Depletion

- **Total chlorine has continued to decline from its 1990s peak values in both the troposphere and the stratosphere. Total tropospheric bromine is decreasing from its peak values, which occurred comparatively recently, while stratospheric bromine is no longer increasing.**
- **Relative declines in the sum of stratospheric chlorine and bromine from peak values are largest in midlatitudes and smallest in Antarctica** (refer to Figure S1-1 in the Scientific Summary of Chapter 1 of this Assessment). These declines are not as pronounced as observed in their tropospheric abundances. Differences between declines in the troposphere and different regions of the stratosphere are primarily associated with the time required for air to move from the troposphere to those regions. The relative declines are smallest in Antarctica primarily because the transport times to polar regions are the largest.

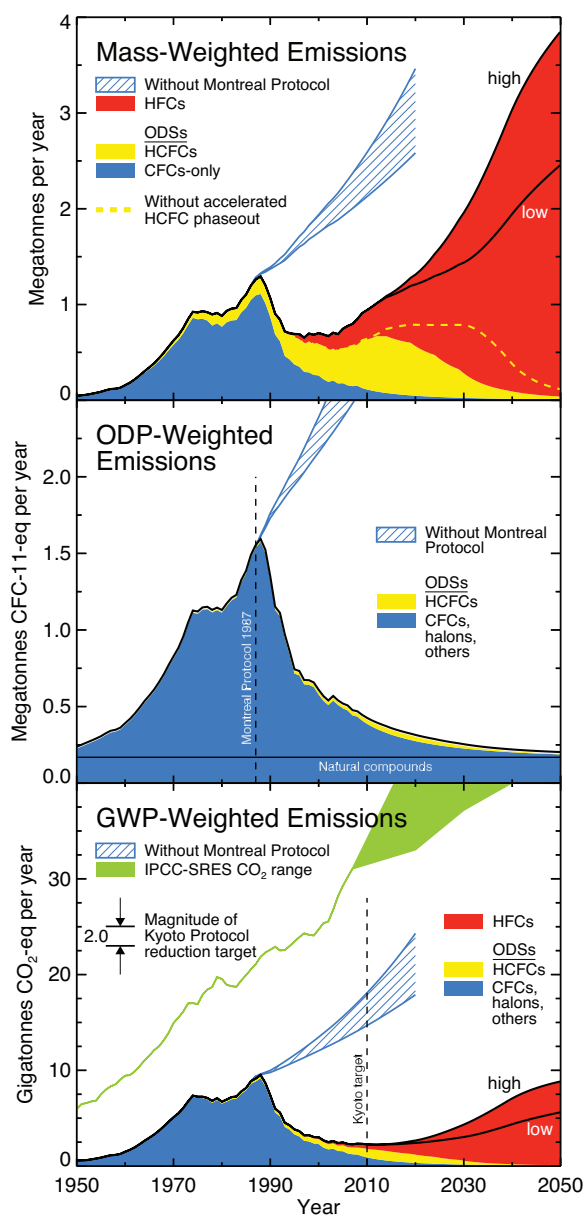


Figure ES-1. Emissions of ODSs and their substitutes. Global emissions of ODSs (CFCs, halons, HCFCs, and others) and their non-ozone depleting substitutes (HFCs) from 1950 to 2050. Emissions are the total from developing and developed countries. The legends identify the specific groups of substances included in each panel. The high and low HFC labels identify the upper and lower limits, respectively, in global baseline scenarios. The blue hatched regions indicate the emissions that would have occurred, in the absence of the Montreal Protocol, with 2–3% annual production increases in all ODSs.

Top panel: Global mass-weighted emissions expressed as megatonnes per year. The yellow dashed line shows HCFC emissions calculated without the provisions of the 2007 accelerated HCFC phase-out under the Montreal Protocol.

Middle panel: Global Ozone Depletion Potential-weighted emissions expressed as megatonnes of CFC-11-equivalent per year. The emissions of individual gases are multiplied by their respective ODPs (CFC-11 = 1) to obtain aggregate, equivalent CFC-11 emissions. The dashed line marks 1987, the year of the Montreal Protocol signing.

Bottom panel: Global GWP-weighted emissions expressed as gigatonnes of CO₂-equivalent per year. The emissions of individual gases are multiplied by their respective GWPs (direct, 100-year time horizon; CO₂ = 1) to obtain aggregate, equivalent CO₂ emissions. Shown for reference are emissions for the range of CO₂ scenarios from the Intergovernmental Panel on Climate Change (IPCC) *Special Report on Emission Scenarios* (SRES). The CO₂ emissions for 1950–2007 are from global fossil fuel use and cement production. Beyond 2007, the shaded region for CO₂ reflects the maximum (A1B) and minimum (B2) SRES scenarios. The dashed line marks 2010, the middle year of the first commitment period of the Kyoto Protocol. Also shown is the magnitude of the reduction target of the first commitment period of the Kyoto Protocol, which is based on a 1990–2010 projection of global greenhouse gas emission increases and the reduction target for participating countries.

OZONE AND CLIMATE: ANTARCTIC

The Antarctic ozone hole is the clearest manifestation of the effect of ODSs on the ozone layer. The depletion far exceeds natural variability and has occurred without exception since 1980. The ozone hole also provides the most visible example of how ozone depletion affects surface climate.

- **Springtime Antarctic total column ozone losses (the ozone hole), first recognizable around 1980, continue to occur every year (Figure ES-2c).** Although the ozone losses exhibit year-to-year variations that are primarily driven by year-to-year changes in meteorology, October mean column ozone within the vortex has been about 40% below 1980 values for the past fifteen years. The average erythemal (“sunburning”) UV measured at the South Pole between 1991 and 2006 was 55–85% larger than the estimated values for the years 1963–1980.
- **Doubts raised since the previous Assessment regarding our understanding of the cause of the Antarctic ozone hole have been dispelled.** New laboratory measurements on the key chemistry involved in polar ozone depletion have reaffirmed that past changes in ODSs are indeed the cause of the ozone hole. This is also supported by quantification of the chemicals responsible for the ozone hole via field observations.
- **There is increased evidence that the Antarctic ozone hole has affected the surface climate in the Southern Hemisphere.** Climate models demonstrate that the ozone hole is the dominant driver of the observed changes in surface winds over the Southern Hemisphere mid and high latitudes during austral summer. These changes have contributed to the observed warming over the Antarctic Peninsula and cooling over the high plateau. The changes in the winds have also been linked to regional changes in precipitation, increases in sea ice around Antarctica, warming of the Southern Ocean, and a local decrease in the ocean sink of CO₂.
- **The trends in the summertime winds in the Southern Hemisphere are not expected to persist over the next few decades.** This is because of the expected offsetting influences on the surface winds of increasing greenhouse gases and the recovering ozone hole.
- **Observed Antarctic springtime column ozone does not yet show a statistically significant increasing trend (Figure ES-2c).** Year-to-year variability, due to meteorology, is much larger than the expected response to the small ODS decreases in the Antarctic vortex to date. This is consistent with simulations using chemistry-climate models (CCMs).
- **The evolution of Antarctic springtime column ozone over the rest of the century is expected to be dominated by the decline in ODS abundance (Figure ES-2c).** CCM simulations show that greenhouse gas changes have had, and will continue to have, a small impact on the ozone hole compared to the effects of the ODS changes. There are some indications that small episodic Antarctic ozone holes may occur even through the end of the century. In spring and early summer, Antarctica will continue to experience excess surface UV.

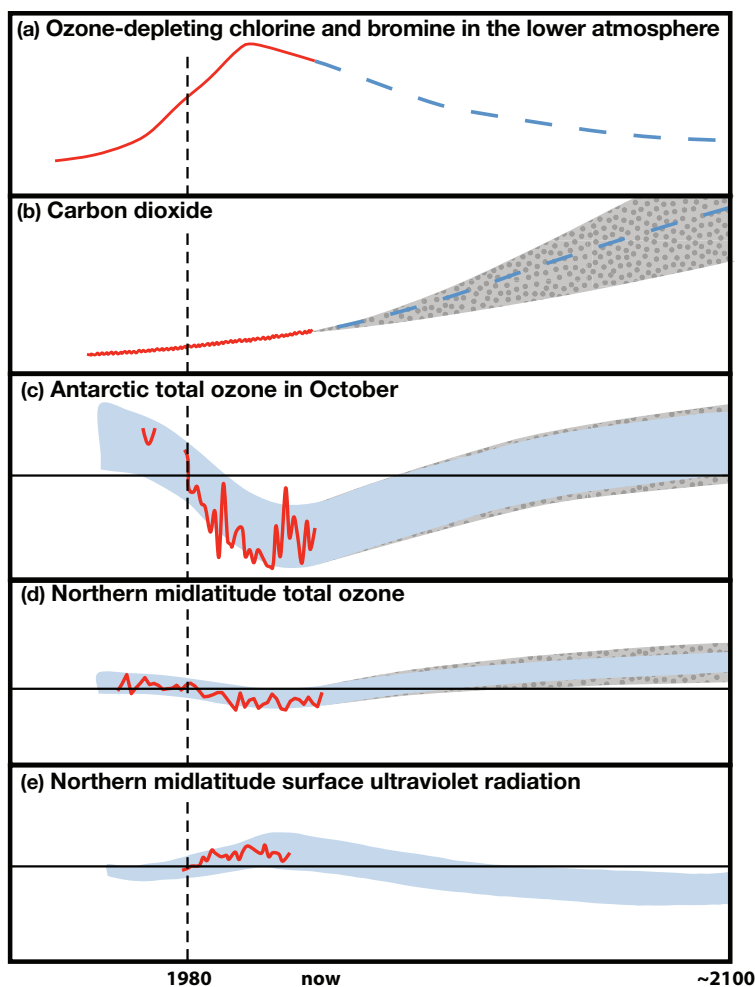
OZONE AND CLIMATE: GLOBAL AND ARCTIC

As a result of the controls introduced by the Montreal Protocol and its Amendments and Adjustments, it is expected that the decline in ODSs will lead to an increase in stratospheric ozone abundances. However, it will be challenging to attribute ozone increases to the decreases in ODSs during the next few years because of natural variability, observational uncertainty, and confounding factors, such as changes in stratospheric temperature or water vapor. A feature of this Assessment is the coordinated use by the community of chemistry-climate models (CCMs) with integrations covering the period from 1960–2100, which has allowed more detailed study of the long-term changes in the stratosphere and of the relative contributions of ODSs and greenhouse gases (GHGs).

- **Average total ozone values in 2006–2009 remain at the same level as the previous Assessment, at roughly 3.5% and 2.5% below the 1964–1980 averages respectively for 90°S–90°N and 60°S–60°N.** Midlatitude (35°–60°) annual mean total column ozone amounts in the Southern Hemisphere [Northern Hemisphere] over the period 2006–2009 have remained at the same level as observed during 1996–2005, at ~6% [~3.5%] below the 1964–1980 average.
- **The ozone loss in Arctic winter and spring between 2007 and 2010 has been variable, but has remained in a range comparable to the values prevailing since the early 1990s.** Substantial chemical loss continues to occur during cold Arctic winters.

Figure ES-2. Schematic of the influence of ozone-depleting substances (ODSs) and climate change on the stratospheric ozone layer, and the influence of ozone changes on surface ultraviolet radiation.

The red lines are based on observations to date. The blue dashed lines represent one commonly accepted scenario for the future. Shaded areas represent year-to-year variability and uncertainties in simulations of the past and future. The dashed vertical line at 1980, a year used as a benchmark for ozone and UV recovery, demarcates the situation before and after significant changes to the ozone layer. The curve for carbon dioxide (CO_2), a greenhouse gas important to Earth's climate, is shown because its changes can affect stratospheric temperatures as well as wind patterns, both of which affect stratospheric ozone.



- (a) Combined effective abundance of ozone-depleting chlorine and bromine in the lower atmosphere (troposphere). The red line is a representation of the measured atmospheric abundances. The blue dashed line is the expected combined effective abundance of chlorine and bromine based on the most likely ODS scenario used in this report and current understanding of the workings of the atmosphere. Because of the Montreal Protocol, a continued decline is expected through the end of this century, with a return to the 1980 benchmark value occurring around the middle of this century. A similar curve for the stratosphere would be shifted to the right (later dates) by a few years because of the time lag in the transport of substances from the surface to the stratosphere.
- (b) The atmospheric abundance of carbon dioxide, the major anthropogenic greenhouse gas that changes Earth's climate, including in the stratosphere; CO_2 abundance is a proxy for climate change. The gray dotted/shaded area represents expectations of increasing future CO_2 abundance based on different scenarios used in this Assessment.
- (c) The extent of the Antarctic ozone hole, as measured by the amount of ozone in the total overhead column averaged for the month of October. The ozone hole is the clearest indicator of ozone layer depletion by ODSs, and the ODSs in the atmosphere have been and are expected to continue to be the primary control on the extent and duration of the ozone hole. Antarctic ozone is expected to return to pre-1980 benchmark values in the late 21st century. The blue shaded area shows the estimated year-to-year variability of ozone for one scenario that includes changes in ODSs (panel a), CO_2 (panel b, blue dashed line), and changes in nitrous oxide and methane (not shown), but does not capture all uncertainties. The gray dotted/shaded area shows the uncertainty due to different climate scenarios, but again does not capture all uncertainties.
- (d) The extent of northern midlatitude ozone depletion, as measured by the amount of ozone in the total overhead column between 30°N and 60°N averaged over each year; blue and gray shaded areas as in panel c. Panels c and d show the approximate relative magnitudes of the northern midlatitude ozone depletion and the Antarctic ozone hole. Influences of the quasi-biennial oscillation (QBO), volcanoes, and solar cycle have been removed from the observational data. The future projections do not include the influence of any volcanic eruptions or solar cycle variations. Natural variability makes it difficult to identify the projected return of northern midlatitude ozone levels to pre-1980 levels, but the expectation is that climate change will hasten this return by several decades, such that it will occur before the middle of the 21st century (before the return of stratospheric chlorine and bromine to the 1980 benchmark value, and before the return of Antarctic ozone, panel c).
- (e) Changes in clear-sky surface UV radiation at northern midlatitudes that accompany the ozone changes of the ODS scenario above. Because the ozone depletion in the northern midlatitudes has been small, the UV changes also have been small. The blue shaded area shows the year-to-year variability of surface UV for the ozone changes of panel d. Clouds, aerosols, and air pollution significantly affect surface UV, but it is difficult to project their future changes. The uncertainties in these changes, which are larger than the uncertainties due to ozone changes, are not represented in the figure. The expectation is that climate change will result in northern midlatitude clear-sky surface UV radiation levels well below 1980 values by the second half of this century.

- **Robust linkages between Arctic stratospheric ozone depletion and tropospheric and surface climate trends have not been established, as expected from the smaller ozone depletion compared with the Antarctic.**
- **Chemistry-climate models reproduce both the latitudinal and vertical structure of the observed ozone trends in both northern and southern midlatitudes during the past periods of increase of the ODSs, confirming our basic understanding of ozone change.** Simulations agree with observations that the last decade has shown flattening of the time series of global total ozone.
- **Analyses based on surface and satellite measurements show that erythemal UV irradiance over midlatitudes has increased since the late 1970s (Figure ES-2e).** This is in qualitative agreement with the observed decrease in column ozone, although other factors (mainly clouds and aerosols) have influenced long-term changes in erythemal irradiance. Clear-sky UV observations from unpolluted sites in midlatitudes show that since the late 1990s, UV irradiance levels have been approximately constant, consistent with ozone column observations over this period.
- **New analyses of both satellite and radiosonde data give increased confidence in changes in stratospheric temperatures between 1980 and 2009.** The global-mean lower stratosphere cooled by 1–2 K and the upper stratosphere cooled by 4–6 K between 1980 and 1995. There have been no significant long-term trends in global-mean lower stratospheric temperatures since about 1995. The global-mean lower-stratospheric cooling did not occur linearly but was manifested as downward steps in temperature in the early 1980s and the early 1990s. The cooling of the lower stratosphere includes the tropics and is not limited to extratropical regions as previously thought.
- **The evolution of lower stratospheric temperature is influenced by a combination of natural and human factors that has varied over time.** Ozone decreases dominate the lower stratospheric cooling since 1980. Major volcanic eruptions and solar activity have clear shorter-term effects. Models that consider all of these factors are able to reproduce this temperature time history.
- **Changes in stratospheric ozone, water vapor, and aerosols all radiatively affect surface temperature.** The radiative forcing² of climate in 2008 due to stratospheric ozone depletion (-0.05 ± 0.1 Watts per square meter, W/m^2) is much smaller than the positive radiative forcing due to the CFCs and HCFCs largely responsible for that depletion (about $+0.3 \text{ W/m}^2$). For context, the current forcing by CO_2 is approximately $+1.7 \text{ W/m}^2$. Radiative calculations and climate modeling studies suggest that the radiative effects of variability in stratospheric water vapor ($\pm \sim 0.1 \text{ W/m}^2$ per decade) can contribute to decadal variability in globally averaged surface temperature. Climate models and observations show that major volcanic eruptions (e.g., Mt. Pinatubo in 1991, roughly -3 W/m^2) can cool the surface for several years.
- **The global middle and upper stratosphere are expected to cool in the coming century, mainly due to CO_2 increases.** Stratospheric ozone recovery will slightly offset the cooling. HFCs could warm the tropical lower stratosphere and tropopause region by about 0.3°C if stratospheric abundances reach the 1 ppb level.
- **Emerging evidence from model simulations suggests that increasing greenhouse gases lead to an acceleration of the stratospheric circulation usually referred to as the Brewer-Dobson circulation.** Such an acceleration could have important consequences, particularly decreases in column ozone in the tropics and increases in column ozone elsewhere. However, responsible mechanisms remain unclear and observational evidence for the circulation increase is lacking.
- **Global ozone is projected to increase approximately in line with the ODS decline, and the increase is accelerated by cooling of the upper stratosphere.** Global ozone is not very sensitive to circulation changes, so high confidence can be placed in this projection.
- **The evolution of ozone in the Arctic is projected to be more sensitive to climate change than in the Antarctic.** The projected strengthening of the stratospheric Brewer-Dobson circulation is expected to significantly increase lower stratospheric ozone in the Arctic, augmenting the GHG-induced ozone increase from upper stratospheric cooling and hastening the return to 1980 levels.

² Positive radiative forcings generally warm the surface; negative radiative forcings generally cool the surface.

- **GHG-induced temperature and circulation changes are projected to hasten the return of midlatitude total column ozone to 1980 levels by several decades, rising well above 1980 levels by the end of the century.** The effect is most pronounced in northern midlatitudes (Figure ES-2d), where it would result in clear-sky surface UV radiation levels well below 1980 values by the second half of the century (Figure ES-2e). In southern midlatitudes, the effect of circulation changes is projected to be weaker and ozone is also influenced by depletion in the Antarctic, where the return to 1980 levels occurs much later.

INFORMATION FOR POLICYMAKERS AND OPTIONS FOR POLICY FORMULATION

Cases related to the elimination of future emissions, production, and banks for various ozone-depleting substances (ODSs) can be formulated starting from a baseline future emission scenario. The baseline scenario here has been developed to account for past and present levels of ODSs along with emission projections. This scenario projects that stratospheric chlorine and bromine levels are likely to return to 1980 levels in midcentury for the midlatitudes and about 25 years later in the Antarctic vortex. These additional cases are used to evaluate the impact of various hypothetical policy options.

Information for Policymakers

- **The Montreal Protocol has both protected the ozone layer and provided substantial co-benefits by reducing climate change** (see Figure ES-1, bottom two panels). It has protected the stratospheric ozone layer by phasing out production and consumption of ozone-depleting substances. Simulations show that unchecked growth in the emissions of ODSs would have led to global ozone depletion in the coming decades very much larger than current levels. Solar UV radiation at the surface would also have increased substantially.
- **Projections of hydrofluorocarbon (HFC) growth in scenarios that assume no controls suggest that by 2050, Global Warming Potential–weighted emissions from these substances could be comparable to the GWP-weighted emissions of chlorofluorocarbons (CFCs) at their peak in 1988** (see Figure ES-1, bottom panel). The highest projection assumes that developing countries use HFCs with GWPs comparable to those currently in use.
- **The accelerated hydrochlorofluorocarbon (HCFC) phase-out agreed to by the Parties to the Montreal Protocol in 2007 is projected to reduce ozone depletion and to help reduce climate forcing** (see Figure ES-1). This acceleration is expected to reduce cumulative HCFC emissions by about 0.7 million Ozone Depletion Potential–tonnes between 2011 and 2050 and would bring forward the year equivalent effective stratospheric chlorine (EESC) returns to 1980 levels by 4–5 years. The accelerated HCFC phasedown is projected to reduce greenhouse gas emissions by about 0.5 gigatonnes of carbon dioxide (CO₂)-equivalent per year averaged over 2011 through 2050. The projected benefit would be determined by the climate impact of the replacements. In comparison, global anthropogenic emissions of CO₂ were greater than 30 gigatonnes per year in 2008.
- **Since the previous Assessment, new fluorocarbons have been suggested as possible replacements for potent HCFC and HFC greenhouse gases.** For example, HFC-1234yf (Ozone Depletion Potential (ODP) = 0; 100-year GWP = 4) is proposed to replace HFC-134a (ODP = 0; 100-year GWP = 1370) in mobile air conditioning. To fully assess the environmental impacts, each proposed substance would need to be evaluated for its ODP, GWP, atmospheric fate, safety, and toxicity. Preliminary analyses indicate that global replacement of HFC-134a with HFC-1234yf at today's level of use is not expected to contribute significantly to tropospheric ozone formation or produce harmful levels of the degradation product TFA (trifluoroacetic acid). It is well established that TFA is a ubiquitous component of the environment, but uncertainties remain regarding its natural and anthropogenic sources, long-term fate, and abundances.

Due to the success of the Montreal Protocol and its Amendments and Adjustments in reducing the production, emissions, and abundances of controlled ODSs, emissions from other compounds and activities not controlled by the Montreal Protocol have become relatively more important to stratospheric ozone.

- **Increasing abundances of radiatively important gases, especially carbon dioxide (CO₂) and methane (CH₄), are expected to significantly affect future stratospheric ozone through effects on temperature, winds, and chemistry.** CO₂ increased in the atmosphere at 2.1 parts per million per year from 2005–2008, while CH₄ increased by about 6.7 parts per billion per year from 2006–2008.
- **Nitrous oxide (N₂O) is known to both deplete global ozone and warm the climate. The current ODP-weighted anthropogenic emission is larger than that of any ODS.**
- **Deliberate large injections of sulfur-containing compounds into the stratosphere, which have been suggested as a climate intervention approach (geoengineering), would alter the radiative, dynamical, and chemical state of the stratosphere and could be expected to have substantial unintended effects on stratospheric ozone levels.**

Options for Policy Formulation

Additional cases have been developed to show the impact of further control measures on various substances. Table ES-1 shows the percentage reductions in integrated chlorine and bromine levels and integrated GWP-weighted emissions, relative to the baseline scenario, that can be achieved in these hypothetical cases.

- **Halons and CFCs: Leakage from banks is the largest source of current ODP-weighted emissions of ODSs.** A delay in the capture and destruction of estimated CFC banks from 2011 to 2015 is currently thought to reduce the possible ozone and climate benefits that could be achieved by about 30%.
- **Carbon tetrachloride (CCl₄):** Elimination of future CCl₄ emissions after 2010 would have an EESC impact comparable to the capture and destruction of CFC and halon banks. This is a much larger effect than was estimated in the previous Assessment because of a revision in the estimated emissions.
- **HCFCs:** The recent growth in reported HCFC production in developing countries was larger than projected in the previous Assessment. This alone would have resulted in a larger projected HCFC production in the new baseline scenario compared to the previous Assessment, but is expected to be more than compensated for by the accelerated HCFC phasedown agreed to by the Parties to the Montreal Protocol in 2007.
- **Elimination of all emissions of chlorine- and bromine-containing ODSs after 2010:** This would bring forward the return of EESC to 1980 levels by about 13 years. The elimination of these ODS emissions would have a climate impact equivalent to about a 0.7 gigatonnes of CO₂-equivalent per year reduction from 2011 through 2050, on average. The sum of current banks of CFCs plus HCFCs contributes about the same amount to these CO₂-equivalent emissions as future HCFC production.
- **Methyl bromide:** Two methyl bromide cases were examined. Case 1: A phase-out of quarantine and pre-shipment emissions beginning in 2011 would accelerate the return of EESC to 1980 levels by 1.5 years, relative to a case of maintaining emissions at 2004–2008 average levels. Case 2: Continuing critical-use exemptions at the approved 2011 level indefinitely would delay the return of EESC to 1980 levels by 0.2 year.

Table ES-1. Hypothetical cases. Reductions in integrated chlorine and bromine levels (as measured by equivalent effective stratospheric chlorine, EESC) and integrated GWP-weighted emissions, relative to the baseline scenario, that can be achieved in hypothetical cases developed to show the impact of further control measures on various substances.

Substance or Group of Substances	Reductions (%) in Integrated EESC (equivalent effective stratospheric chlorine)		Reduction in Cumulative GWP-Weighted Emissions from 2011 to 2050 (gigatonnes of CO ₂ -equivalent)	
	2011	2015	2011	2015
<i>Bank capture and destruction in 2011 and 2015:</i>				
CFCs	11	7.0	7.9	5.5
Halons	14	9.1	0.4	0.3
HCFCs	4.8	5.3 ¹	4.9	5.5 ¹
<i>Production elimination after 2010:</i>				
HCFCs		8.8		13.2
CH ₃ Br for quarantine and pre-shipment		6.7		0.002
<i>Total emissions elimination after 2010:</i>				
CCl ₄ ²		7.6		0.9
CH ₃ CCl ₃		0.1		0.004
HFCs		0.0		Up to 170 ³

¹ The impact of a 2015 HCFC bank recovery is larger than a 2011 bank recovery because this calculation assumes destruction of the bank in only a single year, and because the bank in 2015 is larger than the bank in 2011 owing to continued annual production that is larger than the annual bank release.

² Banks are assumed to be zero. Emissions include uncertain sources such as possible fugitive emissions and unintended by-product emissions.

³ Strongly dependent on future projections and does not consider HFC-23 emissions. Currently HFCs are not controlled by the Montreal Protocol, but are included in the basket of gases of the Kyoto Protocol.

CHAPTER 1

Ozone-Depleting Substances (ODSs) and Related Chemicals

Coordinating Lead Authors:

S.A. Montzka
S. Reimann

Lead Authors:

A. Engel
K. Krüger
S. O'Doherty
W.T. Sturges

Coauthors:

D. Blake
M. Dorf
P. Fraser
L. Froidevaux
K. Jucks
K. Kreher
M.J. Kurylo
A. Mellouki
J. Miller
O.-J. Nielsen
V.L. Orkin
R.G. Prinn
R. Rhew
M.L. Santee
A. Stohl
D. Verdonik

Contributors:

E. Atlas
P. Bernath
T. Blumenstock
J.H. Butler
A. Butz
B. Connor
P. Duchatelet
G. Dutton
F. Hendrick
P.B. Krummel
L.J.M. Kuijpers
E. Mahieu
A. Manning
J. Mühle
K. Pfeilsticker
B. Quack
M. Ross
R.J. Salawitch
S. Schauffler
I.J. Simpson
D. Toohey
M.K. Vollmer
T.J. Wallington
H.J.R. Wang
R.F. Weiss
M. Yamabe
Y. Yokouchi
S. Yvon-Lewis

CHAPTER 1

OZONE-DEPLETING SUBSTANCES (ODSs) AND RELATED CHEMICALS

Contents

SCIENTIFIC SUMMARY	1
1.1 SUMMARY OF THE PREVIOUS OZONE ASSESSMENT	7
1.2 LONGER-LIVED HALOGENATED SOURCE GASES	7
1.2.1 Updated Observations, Trends, and Emissions	7
1.2.1.1 Chlorofluorocarbons (CFCs)	7
Box 1-1. Methods for Deriving Trace Gas Emissions	14
1.2.1.2 Halons	15
1.2.1.3 Carbon Tetrachloride (CCl ₄)	16
Box 1-2. CCl ₄ Lifetime Estimates	18
1.2.1.4 Methyl Chloroform (CH ₃ CCl ₃)	19
1.2.1.5 Hydrochlorofluorocarbons (HCFCs)	20
1.2.1.6 Methyl Bromide (CH ₃ Br)	23
1.2.1.7 Methyl Chloride (CH ₃ Cl)	27
Box 1-3. Atmospheric Lifetimes and Removal Processes	34
1.2.2 Loss Processes	35
1.3 VERY SHORT-LIVED HALOGENATED SUBSTANCES (VSLS)	37
1.3.1 Emissions, Atmospheric Distributions, and Abundance Trends of Very Short-Lived Source Gases	37
1.3.1.1 Chlorine-Containing Very Short-Lived Source Gases	37
Box 1-4. Definition of Acronyms Related to Short-Lived Gases	39
1.3.1.2 Bromine-Containing Very Short-Lived Source Gases	41
1.3.1.3 Iodine-Containing Very Short-Lived Source Gases	44
1.3.1.4 Halogen-Containing Aerosols	44
1.3.2 Transport of Very Short-Lived Substances into the Stratosphere	44
1.3.2.1 VSLS Transport from the Surface in the Tropics to the Tropical Tropopause Layer (TTL)	45
1.3.2.2 VSLS Transport from the TTL to the Stratosphere	46
1.3.2.3 VSLS Transport from the Surface to the Extratropical Stratosphere	46
1.3.3 VSLS and Inorganic Halogen Input to the Stratosphere	47
1.3.3.1 Source Gas Injection (SGI)	47
1.3.3.2 Product Gas Injection (PGI)	49
1.3.3.3 Total Halogen Input into the Stratosphere from VSLS and Their Degradation Products	51
1.3.4 Potential Influence of VSLS on Ozone	53
1.3.5 The Potential for Changes in Stratospheric Halogen from Naturally Emitted VSLS	54
1.3.6 Environmental Impacts of Anthropogenic VSLS, Substitutes for Long-Lived ODSs, and HFCs	54
1.3.6.1 Evaluation of the Impact of Intensified Natural Processes on Stratospheric Ozone	55
1.3.6.2 Very Short-Lived New ODSs and Their Potential Influence on Stratospheric Halogen	55
1.3.6.3 Evaluation of Potential and In-Use Substitutes for Long-Lived ODSs	55
1.4 CHANGES IN ATMOSPHERIC HALOGEN	63
1.4.1 Chlorine in the Troposphere and Stratosphere	63
1.4.1.1 Tropospheric Chlorine Changes	63
1.4.1.2 Stratospheric Chlorine Changes	64
1.4.2 Bromine in the Troposphere and Stratosphere	66
1.4.2.1 Tropospheric Bromine Changes	66

1.4.2.2	Stratospheric Bromine Changes.....	67
1.4.3	Iodine in the Upper Troposphere and Stratosphere.....	73
1.4.4	Equivalent Effective Chlorine (EECl) and Equivalent Effective Stratospheric Chlorine (EESC)	73
1.4.5	Fluorine in the Troposphere and Stratosphere	75
1.5	CHANGES IN OTHER TRACE GASES THAT INFLUENCE OZONE AND CLIMATE	75
1.5.1	Changes in Radiatively Active Trace Gases that Directly Influence Ozone.....	76
1.5.1.1	Methane (CH ₄).....	76
1.5.1.2	Nitrous Oxide (N ₂ O).....	79
1.5.1.3	COS, SO ₂ , and Sulfate Aerosols.....	80
1.5.2	Changes in Radiative Trace Gases that Indirectly Influence Ozone.....	81
1.5.2.1	Carbon Dioxide (CO ₂)	81
1.5.2.2	Fluorinated Greenhouse Gases	82
1.5.3	Emissions of Rockets and Their Impact on Stratospheric Ozone	85
	REFERENCES	86

SCIENTIFIC SUMMARY

The amended and adjusted Montreal Protocol continues to be successful at reducing emissions and atmospheric abundances of most controlled ozone-depleting substances (ODSs).

Tropospheric Chlorine

- **Total tropospheric chlorine from long-lived chemicals (~3.4 parts per billion (ppb) in 2008) continued to decrease between 2005 and 2008.** Recent decreases in tropospheric chlorine (Cl) have been at a slower rate than in earlier years (decreasing at 14 parts per trillion per year (ppt/yr) during 2007–2008 compared to a decline of 21 ppt/yr during 2003–2004) and were slower than the decline of 23 ppt/yr projected in the A1 (most likely, or baseline) scenario of the 2006 Assessment. The tropospheric Cl decline has recently been slower than projected in the A1 scenario because chlorofluorocarbon-11 (CFC-11) and CFC-12 did not decline as rapidly as projected and because increases in hydrochlorofluorocarbons (HCFCs) were larger than projected.
- **The contributions of specific substances or groups of substances to the decline in tropospheric Cl have changed since the previous Assessment.** Compared to 2004, by 2008 observed declines in Cl from methyl chloroform (CH_3CCl_3) had become smaller, declines in Cl from CFCs had become larger (particularly CFC-12), and increases in Cl from HCFCs had accelerated. Thus, the observed change in total tropospheric Cl of -14 ppt/yr during 2007–2008 arose from:
 - -13.2 ppt Cl/yr from changes observed for CFCs
 - -6.2 ppt Cl/yr from changes observed for methyl chloroform
 - -5.1 ppt Cl/yr from changes observed for carbon tetrachloride
 - -0.1 ppt Cl/yr from changes observed for halon-1211
 - $+10.6$ ppt Cl/yr from changes observed for HCFCs
- **Chlorofluorocarbons (CFCs), consisting primarily of CFC-11, -12, and -113, accounted for 2.08 ppb (about 62%) of total tropospheric Cl in 2008.** The global atmospheric mixing ratio of CFC-12, which accounts for about one-third of the current atmospheric chlorine loading, decreased for the first time during 2005–2008 and by mid-2008 had declined by 1.3% (7.1 ± 0.2 parts per trillion, ppt) from peak levels observed during 2000–2004.
- **Hydrochlorofluorocarbons (HCFCs), which are substitutes for long-lived ozone-depleting substances, accounted for 251 ppt (7.5%) of total tropospheric Cl in 2008.** HCFC-22, the most abundant of the HCFCs, increased at a rate of about 8 ppt/yr (4.3%/yr) during 2007–2008, more than 50% faster than observed in 2003–2004 but comparable to the 7 ppt/yr projected in the A1 scenario of the 2006 Assessment for 2007–2008. HCFC-142b mixing ratios increased by 1.1 ppt/yr (6%/yr) during 2007–2008, about twice as fast as was observed during 2003–2004 and substantially faster than the 0.2 ppt/yr projected in the 2006 Assessment A1 scenario for 2007–2008. HCFC-141b mixing ratios increased by 0.6 ppt/yr (3%/yr) during 2007–2008, which is a similar rate observed in 2003–2004 and projected in the 2006 Assessment A1 scenario.
- **Methyl chloroform (CH_3CCl_3) accounted for only 32 ppt (1%) of total tropospheric Cl in 2008, down from a mean contribution of about 10% during the 1980s.**
- **Carbon tetrachloride (CCl_4) accounted for 359 ppt (about 11%) of total tropospheric Cl in 2008.** Mixing ratios of CCl_4 declined slightly less than projected in the A1 scenario of the 2006 Assessment during 2005–2008.

Stratospheric Chlorine and Fluorine

- **The stratospheric chlorine burden derived by ground-based total column and space-based measurements of inorganic chlorine continued to decline during 2005–2008.** This burden agrees within ± 0.3 ppb ($\pm 8\%$) with the amounts expected from surface data when the delay due to transport is considered. The uncertainty in this burden is large relative to the expected chlorine contributions from shorter-lived source gases and product gases of 80 (40–130)

ppt. Declines since 1996 in total column and stratospheric abundances of inorganic chlorine compounds are reasonably consistent with the observed trends in long-lived source gases over this period.

- **Measured column abundances of hydrogen fluoride increased during 2005–2008 at a smaller rate than in earlier years.** This is qualitatively consistent with observed changes in tropospheric fluorine (F) from CFCs, HCFCs, hydrofluorocarbons (HFCs), and perfluorocarbons (PFCs) that increased at a mean annual rate of 40 ± 4 ppt/yr ($1.6 \pm 0.1\%/yr$) since late 1996, which is reduced from 60–100 ppt/yr observed during the 1980s and early 1990s.

Tropospheric Bromine

- **Total organic bromine from controlled ODSs continued to decrease in the troposphere and by mid-2008 was 15.7 ± 0.2 ppt, approximately 1 ppt below peak levels observed in 1998.** This decrease was close to that expected in the A1 scenario of the 2006 Assessment and was driven by declines observed for methyl bromide (CH_3Br) that more than offset increased bromine (Br) from halons.
- **Bromine from halons stopped increasing during 2005–2008.** Mixing ratios of halon-1211 decreased for the first time during 2005–2008 and by mid-2008 were 0.1 ppt below levels observed in 2004. Halon-1301 continued to increase in the atmosphere during 2005–2008 but at a slower rate than observed during 2003–2004. The mean rate of increase was 0.03–0.04 ppt/yr during 2007–2008. A decrease of 0.01 ppt/yr was observed for halon-2402 in the global troposphere during 2007–2008.
- **Tropospheric methyl bromide (CH_3Br) mixing ratios continued to decline during 2005–2008, and by 2008 had declined by 1.9 ppt (about 20%) from peak levels measured during 1996–1998.** Evidence continues to suggest that this decline is the result of reduced industrial production, consumption, and emission. This industry-derived emission is estimated to have accounted for 25–35% of total global CH_3Br emissions during 1996–1998, before industrial production and consumption were reduced. Uncertainties in the variability of natural emissions and in the magnitude of methyl bromide stockpiles in recent years limit our understanding of this anthropogenic emissions fraction, which is derived by comparing the observed atmospheric changes to emission changes derived from reported production and consumption.
- **By 2008, nearly 50% of total methyl bromide consumption was for uses not controlled by the Montreal Protocol (quarantine and pre-shipment applications).** From peak levels in 1996–1998, industrial consumption in 2008 for controlled and non-controlled uses of CH_3Br had declined by about 70%. Sulfuryl fluoride (SO_2F_2) is used increasingly as a fumigant to replace methyl bromide for controlled uses because it does not directly cause ozone depletion, but it has a calculated direct, 100-year Global Warming Potential (GWP_{100}) of 4740. The SO_2F_2 global background mixing ratio increased during recent decades and had reached about 1.5 ppt by 2008.

Stratospheric Bromine

- **Total bromine in the stratosphere was 22.5 (19.5–24.5) ppt in 2008. It is no longer increasing and by some measures has decreased slightly during recent years.** Multiple measures of stratospheric bromine monoxide (BrO) show changes consistent with tropospheric Br trends derived from observed atmospheric changes in CH_3Br and the halons. Slightly less than half of the stratospheric bromine derived from these BrO observations is from controlled uses of halons and methyl bromide. The remainder comes from natural sources of methyl bromide and other bromocarbons, and from quarantine and pre-shipment uses of methyl bromide not controlled by the Montreal Protocol.

Very Short-Lived Halogenated Substances (VSLs)

VSLs are defined as trace gases whose local lifetimes are comparable to, or shorter than, tropospheric transport timescales and that have non-uniform tropospheric abundances. In practice, VSLs are considered to be those compounds having atmospheric lifetimes of less than 6 months.

- **The amount of halogen from a very short-lived source substance that reaches the stratosphere depends on the location of the VSLS emissions, as well as atmospheric removal and transport processes.** Substantial uncertainties remain in quantifying the full impact of chlorine- and bromine-containing VSLS on stratospheric ozone. Updated results continue to suggest that brominated VSLS contribute to stratospheric ozone depletion, particularly under enhanced aerosol loading. It is unlikely that iodinated gases are important for stratospheric ozone loss in the present-day atmosphere.
- **Based on a limited number of observations, very short-lived source gases account for 55 (38–80) ppt chlorine in the middle of the tropical tropopause layer (TTL).** From observations of hydrogen chloride (HCl) and carbonyl chloride (COCl₂) in this region, an additional ~25 (0–50) ppt chlorine is estimated to arise from VSLS degradation. The sum of contributions from source gases and these product gases amounts to ~80 (40–130) ppt chlorine from VSLS that potentially reaches the stratosphere. About 40 ppt of the 55 ppt of chlorine in the TTL from source gases is from anthropogenic VSLS emissions (e.g., methylene chloride, CH₂Cl₂; chloroform, CHCl₃; 1,2 dichloroethane, CH₂ClCH₂Cl; perchloroethylene, CCl₂CCl₂), but their contribution to stratospheric chlorine loading is not well quantified.
- **Two independent approaches suggest that VSLS contribute significantly to stratospheric bromine.** Stratospheric bromine derived from observations of BrO implies a contribution of 6 (3–8) ppt of bromine from VSLS. Observed, very short-lived source gases account for 2.7 (1.4–4.6) ppt Br in the middle of the tropical tropopause layer. By including modeled estimates of product gas injection into the stratosphere, the total contribution of VSLS to stratospheric bromine is estimated to be 1–8 ppt.
- **Future climate changes could affect the contribution of VSLS to stratospheric halogen and its influence on stratospheric ozone.** Future potential use of anthropogenic halogenated VSLS may contribute to stratospheric halogen in a similar way as do present-day natural VSLS. Future environmental changes could influence both anthropogenic and natural VSLS contributions to stratospheric halogens.

Equivalent Effective Stratospheric Chlorine (EESC)

EESC is a sum of chlorine and bromine derived from ODS tropospheric abundances weighted to reflect their potential influence on ozone in different parts of the stratosphere. The growth and decline in EESC varies in different regions of the atmosphere because a given tropospheric abundance propagates to the stratosphere with varying time lags associated with transport. Thus the EESC abundance, when it peaks, and how much it has declined from its peak vary in different regions of the atmosphere.

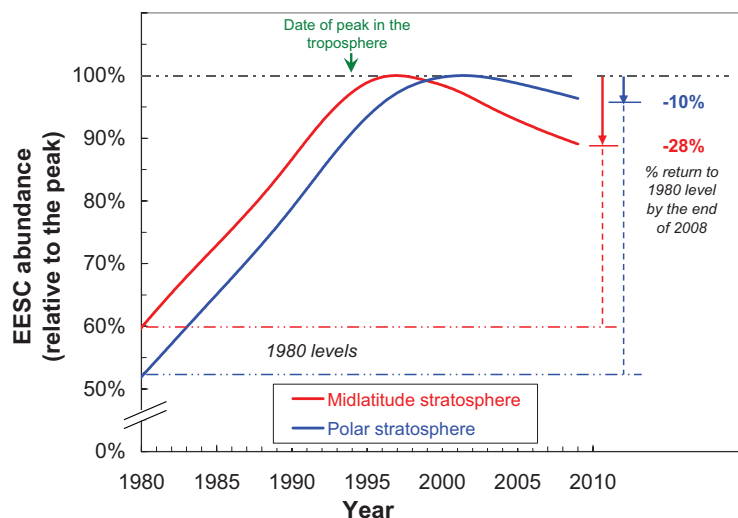


Figure S1-1. Stratospheric EESC derived for the midlatitude and polar stratospheric regions relative to peak abundances, plotted as a function of time. Peak abundances are ~1950 ppt for the midlatitude stratosphere and ~4200 ppt for the polar stratosphere. Percentages shown to the right indicate the observed change in EESC by the end of 2008 relative to the change needed for EESC to return to its 1980 abundance. A significant portion of the 1980 EESC level is from natural emissions.

- **EESC has decreased throughout the stratosphere.**
 - By the end of 2008, midlatitude EESC had decreased by about 11% from its peak value in 1997. This drop is 28% of the decrease required for EESC in midlatitudes (red curve in figure) to return to the 1980 benchmark level.
 - By the end of 2008, polar EESC had decreased by about 5% from its peak value in 2002. This drop is 10% of the decrease required for EESC in polar regions (blue curve in figure) to return to the 1980 benchmark level.
- **During the past four years, no specific substance or group of substances dominated the decline in the total combined abundance of ozone-depleting halogen in the troposphere.** In contrast to earlier years, the long-lived CFCs now contribute similarly to the decline as do the short-lived CH_3CCl_3 and CH_3Br . Other substances contributed less to this decline, and HCFCs added to this halogen burden over this period.

Emission Estimates and Lifetimes

- **While global emissions of CFC-12 derived from atmospheric observations decreased during 2005–2008, those for CFC-11 did not change significantly over this period.** Emissions from banks account for a substantial fraction of current emissions of the CFCs, halons, and HCFCs. Emissions inferred for CFCs from global observed changes did not decline during 2005–2008 as rapidly as projected in the A1 scenario of the 2006 Assessment, most likely because of underestimates of bank emissions.
- **Global emissions of CCl_4 have declined only slowly over the past decade.**
 - These emissions, when inferred from observed global trends, were between 40 and 80 gigagrams per year (Gg/yr) during 2005–2008 given a range for the global CCl_4 lifetime of 33–23 years. By contrast, CCl_4 emissions derived with a number of assumptions from data reported to the United Nations Environment Programme (UNEP) ranged from 0–30 Gg/yr over this same period.
 - In addition, there is a large variability in CCl_4 emissions derived from data reported to UNEP that is not reflected in emissions derived from measured global mixing ratio changes. This additional discrepancy cannot be explained by scaling the lifetime or by uncertainties in the atmospheric trends. If the analysis of data reported to UNEP is correct, unknown anthropogenic sources may be partly responsible for these observed discrepancies.
- **Global emissions of HCFC-22 and HCFC-142b derived from observed atmospheric trends increased during 2005–2008.** HCFC-142b global emissions increased appreciably over this period, compared to a projected emissions decline of 23% from 2004 to 2008. By 2008, emissions for HCFC-142b were two times larger than had been projected in the A1 scenario of the 2006 Assessment. These emission increases were coincident with increasing production of HCFCs in developing countries in general and in East Asia particularly. It is too soon to discern any influence of the 2007 Adjustments to the Montreal Protocol on the abundance and emissions of HCFCs.
- **The sum of CFC emissions (weighted by direct, 100-year GWPs) has decreased on average by $8 \pm 1\%$ /yr from 2004 to 2008, and by 2008 amounted to 1.1 ± 0.3 gigatonnes of carbon dioxide-equivalent per year ($\text{GtCO}_2\text{-eq/yr}$).** The sum of GWP-weighted emissions of HCFCs increased by $5 \pm 2\%$ /yr from 2004 to 2008, and by 2008 amounted to 0.74 ± 0.05 $\text{GtCO}_2\text{-eq/yr}$.
- **Evidence is emerging that lifetimes for some important ODSs (e.g., CFC-11) may be somewhat longer than reported in past assessments.** In the absence of corroborative studies, however, the CFC-11 lifetime reported in this Assessment remains unchanged at 45 years. Revisions in the CFC-11 lifetime would affect estimates of its global emission derived from atmospheric changes and calculated values for Ozone Depletion Potentials (ODPs) and best-estimate lifetimes for some other halocarbons.

Other Trace Gases That Directly Affect Ozone and Climate

- **The methane (CH₄) global growth rate was small, averaging 0.9 ± 3.3 ppb/yr between 1998–2006, but increased to 6.7 ± 0.6 ppb/yr from 2006–2008.** Analysis of atmospheric data suggests that this increase is due to wetland sources in both the high northern latitudes and the tropics. The growth rate variability observed during 2006–2008 is similar in magnitude to that observed over the last two decades.
- **In 2005–2008 the average growth rate of nitrous oxide (N₂O) was 0.8 ppb/yr, with a global average tropospheric mixing ratio of 322 ppb in 2008.** A recent study has suggested that at the present time, Ozone Depletion Potential-weighted anthropogenic emissions of N₂O are the most significant emissions of a substance that depletes ozone.
- **Long-term changes in carbonyl sulfide (COS) measured as total columns above the Jungfrauoch (46.5°N) and from surface flasks sampled in the Northern Hemisphere show that atmospheric mixing ratios have increased slightly during recent years concurrently with increases in “bottom-up” inventory-based emissions of global sulfur.** Results from surface measurements show a mean global surface mixing ratio of 493 ppt in 2008 and a mean rate of increase of 1.8 ppt/yr during 2000–2008. New laboratory, observational, and modeling studies indicate that vegetative uptake of COS is significantly larger than considered in the past.

Other Trace Gases with an Indirect Influence on Ozone

- **The carbon dioxide (CO₂) global average mixing ratio was 385 parts per million (ppm) in 2008 and had increased during 2005–2008 at an average rate of 2.1 ppm/yr.** This rate is higher than the average growth rate during the 1990s of 1.5 ppm/yr and corresponds with increased rates of fossil fuel combustion.
- **Hydrofluorocarbons (HFCs) used as ODS substitutes continued to increase in the global atmosphere.** HFC-134a is the most abundant HFC; its global mixing ratio reached about 48 ppt in 2008 and was increasing at 4.7 ppt/yr. Other HFCs have been identified in the global atmosphere at <10 ppt (e.g., HFC-125, -143a, -32, and -152a) and were increasing at ≤ 1 ppt/yr in 2008.
- **Emissions of HFC-23, a by-product of HCFC-22 production, have increased over the past decade even as efforts at minimizing these emissions were implemented in both developed and developing countries.** These emission increases are concurrent with rapidly increasing HCFC-22 production in developing countries and are likely due to increasing production of HCFC-22 in facilities not covered by the Kyoto Protocol’s Clean Development Mechanism projects. Globally averaged HFC-23 mixing ratios reached 21.8 ppt in 2008, with a yearly increase of 0.8 ppt/yr (3.9%/yr).
- **The sum of emissions (weighted by direct, 100-year GWPs) of HFCs used as ODS replacements has increased by 8–9%/yr from 2004 to 2008, and by 2008 amounted to 0.39 ± 0.03 GtCO₂-eq/yr.** Regional studies suggest significant contributions of HFC-134a and -152a emissions during 2005–2006 from Europe, North America, and Asia. Emissions of HFC-23, most of which do not arise from use of this substance as an ODS replacement, added an additional 0.2 Gt CO₂-eq/yr, on average, during 2006–2008.
- **Sulfur hexafluoride (SF₆) and nitrogen trifluoride (NF₃):** Global averaged mixing ratios of SF₆ reached 6.4 ppt in 2008, with a yearly increase of 0.2 ppt/yr. NF₃ was detected in the atmosphere for the first time, with a global mean mixing ratio in 2008 of 0.45 ppt and a growth rate of 0.05 ppt/yr, or 11%/yr.

Direct Radiative Forcing

The abundances of ODSs as well as many of their replacements contribute to radiative forcing of the atmosphere. These climate-related forcings have been updated using the current observations of atmospheric abundances and are summarized in Table S1-1. This table also contains the primary Kyoto Protocol gases as reference.

- Over these 5 years, radiative forcing from the sum of ODSs and HFCs has increased but, by 2008, remained small relative to the forcing changes from CO₂ (see Table S1-1).

Table S1-1. Direct radiative forcings of ODSs and other gases, and their recent changes.

Specific Substance or Group of Substances	Direct Radiative Forcing (2008), milliWatts per square meter (mW/m ²)	Change in Direct Radiative Forcing (2003.5–2008.5), mW/m ²
CFCs *	262	-6
Other ODSs *	15	-2
HCFCs *	45	8
HFCs #,a	12	5
HFC-23 #	4	0.9
CO ₂ #	1740	139
CH ₄ #	500	4
N ₂ O #	170	12
PFCs #	5.4	0.5
SF ₆ #	3.4	0.7
<i>Sum of Montreal Protocol gases</i> *	322	0
<i>Sum of Kyoto Protocol gases</i> #	2434	163

* Montreal Protocol Gases refers to CFCs, other ODSs (CCl₄, CH₃CCl₃, halons, CH₃Br), and HCFCs.

Kyoto Protocol Gases (CO₂, CH₄, N₂O, HFCs, PFCs, and SF₆).

^a Only those HFCs for which emissions arise primarily through use as ODS replacements (i.e., not HFC-23).

1.1 SUMMARY OF THE PREVIOUS OZONE ASSESSMENT

The 2006 Assessment report (WMO, 2007) documented the continued success of the Montreal Protocol in reducing the atmospheric abundance of ozone-depleting substances (ODSs). Tropospheric abundances and emissions of most ODSs were decreasing by 2004, and tropospheric chlorine (Cl) and bromine (Br) from ODSs were decreasing as a result. Methyl chloroform contributed more to the decline in tropospheric chlorine than other controlled gases. ODS substitute chemicals containing chlorine, the hydrofluorochlorocarbons (HCFCs), were still increasing during 2000–2004, but at reduced rates compared to earlier years.

A significant mismatch between expected and atmosphere-derived emissions of carbon tetrachloride (CCl₄) was identified. For the first time a decline was observed in the stratospheric burden of inorganic Cl as measured both by ground- and space-based instrumentation. The amount and the trend observed for stratospheric chlorine was consistent with abundances and trends of long-lived ODSs observed in the troposphere, though lag times and mixing complicated direct comparisons.

Tropospheric bromine from methyl bromide and halons was determined in the previous Assessment to be decreasing. Changes derived for stratospheric inorganic bromine (Br_y) from observations of BrO were consistent with tropospheric trends measured from methyl bromide and the halons, but it was too early to detect a decline in stratospheric Br_y. Amounts of stratospheric Br_y were higher than expected from the longer-lived, controlled gases (methyl bromide and halons). This suggested a significant contribution of 5 (3–8) parts per trillion (ppt) of Br potentially from very short-lived substances (VSLS) with predominantly natural sources. Large emissions of very short-lived brominated substances were found in tropical regions, where rapid transport from Earth's surface to the stratosphere is possible. Quantitatively accounting for this extra Br was not straightforward given our understanding at that time of timescales and heterogeneity of VSLS emissions and oxidation product losses as these compounds become transported from Earth's surface to the stratosphere. It was concluded that this additional Br has likely affected stratospheric ozone levels, and the amount of Br from these sources would likely be sensitive to changes in climate that affect ocean conditions, atmospheric loss processes, and atmospheric circulation.

By 2004, equivalent effective chlorine (EECl), a simple metric to express the overall effect of these changes on ozone-depleting halogen abundance, continued to decrease. When based on measured tropospheric changes through 2004, EECl had declined then by an amount that was 20% of what would be needed to return EECl val-

ues to those in 1980 (i.e., before the ozone hole was observed).

In the past, the discussions of long-lived and short-lived compounds were presented in separate chapters but are combined in this 2010 Assessment. Terms used to describe measured values throughout Chapter 1 are mixing ratios (for example parts per trillion, ppt, pmol/mol), mole fractions, and concentrations. These terms have been used interchangeably and, as used here, are all considered to be equivalent.

1.2 LONGER-LIVED HALOGENATED SOURCE GASES

1.2.1 Updated Observations, Trends, and Emissions

1.2.1.1 CHLOROFLUOROCARBONS (CFCs)

The global surface mean mixing ratios of the three most abundant chlorofluorocarbons (CFCs) declined significantly during 2005–2008 (Figure 1-1 and Table 1-1). After reaching its peak abundance during 2000–2004, the global annual surface mean mixing ratio of CFC-12 (CCl₂F₂) had declined by 7.1 ± 0.2 ppt (1.3%) by mid-2008. Surface means reported for CFC-12 in 2008 by the three independent global sampling networks (532.6–537.4 ppt) agreed to within 5 ppt (0.9%). The consistency for CFC-12 among these networks has improved since the previous Assessment and stems in part from a calibration revision in the National Oceanic and Atmospheric Administration (NOAA) data. The 2008 annual mean mixing ratio of CFC-11 (CCl₃F) from the three global sampling networks (243.4–244.8 ppt) agreed to within 1.4 ppt (0.6%) and decreased at a rate of -2.0 ± 0.6 ppt/yr from 2007 to 2008. Global surface means observed by these networks for CFC-113 (CCl₂FCClF₂) during 2008 were between 76.4 and 78.3 ppt and had decreased from 2007 to 2008 at a rate of -0.7 ppt/yr.

Long-term CFC-11 and CFC-12 data obtained from ground-based infrared solar absorption spectroscopy are available from the Jungfraujoch station (Figure 1-2; an update of Zander et al., 2005). Measured trends in total vertical column abundances during 2001 to 2008 indicate decreases in the atmospheric burdens of these gases that are similar to the declines derived from the global sampling networks over this period. For example, the mean decline in CFC-11 from the Jungfraujoch station column data is $-0.83(\pm 0.06)\%/yr$ during 2001–2009 (relative to 2001), and global and Northern Hemisphere (NH) surface trends range from -0.78 to $-0.88\%/yr$ over this same period (range of trends from different networks). For CFC-

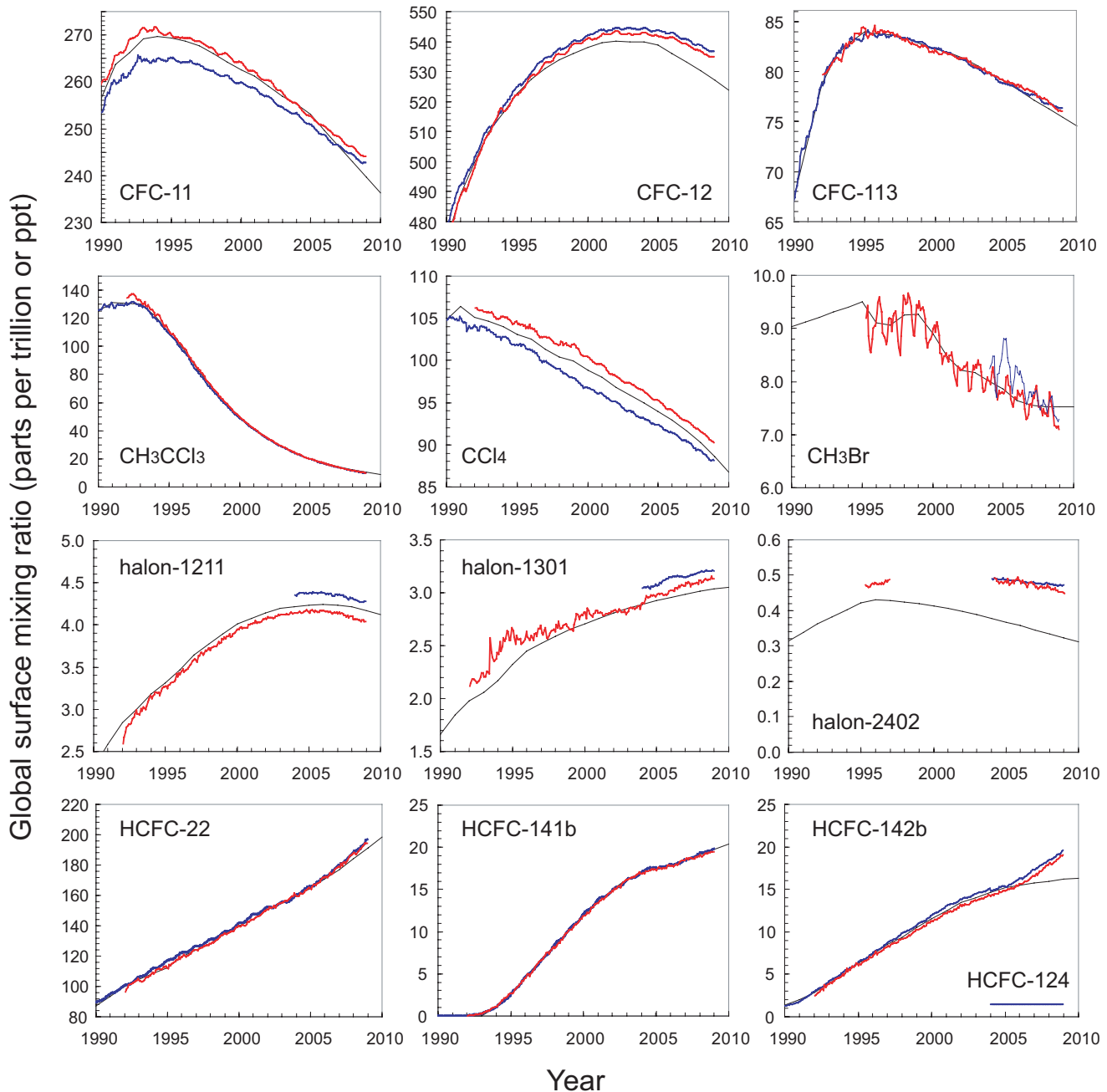


Figure 1-1. Mean global surface mixing ratios (expressed as dry air mole fractions in parts per trillion or ppt) of ozone-depleting substances from independent sampling networks and from scenario A1 of the previous Ozone Assessment (Daniel and Velders et al., 2007) over the past 18 years. Measured global surface monthly means are shown as red lines (NOAA data) and blue lines (AGAGE data). Mixing ratios from scenario A1 from the previous Assessment (black lines) were derived to match observations in years before 2005 as they existed in 2005 (Daniel and Velders et al., 2007). The scenario A1 results shown in years after 2004 are projections made in 2005.

12, the rate of change observed at the Jungfraujoch station was $-0.1(\pm 0.05)\%$ during 2001–2008 (relative to 2001), while observed changes at the surface were slightly larger at $-0.2\%/yr$ over this same period.

Additional measurements of CFC-11 in the upper troposphere and stratosphere with near-global coverage have been made from multiple satellite-borne instruments (Kuell et al., 2005; Hoffmann et al., 2008; Fu et al., 2009).

Table 1-1. Measured mole fractions and growth rates of ozone-depleting gases from ground-based sampling.

Chemical Formula	Common or Industrial Name	Annual Mean Mole Fraction (ppt)			Growth (2007–2008)		Network, Method
		2004	2007	2008	(ppt/yr)	(%/yr)	
CFCs							
CCl ₂ F ₂	CFC-12	543.8	539.6	537.4	-2.2	-0.4	AGAGE, in situ (Global)
		542.3	537.8	535.5	-2.3	-0.4	NOAA, flask & in situ (Global)
		539.7	535.1	532.6	-2.5	-0.5	UCI, flask (Global)
		541.5	541.2	541.0	-0.3	-0.05	NIES, in situ (Japan)
		-	542.9	540.1	-2.9	-0.5	SOGE-A, in situ (China)
CCl ₃ F	CFC-11	251.8	245.4	243.4	-2.0	-0.8	AGAGE, in situ (Global)
		253.8	247.0	244.8	-2.2	-0.9	NOAA, flask & in situ (Global)
		253.7	246.1	244.2	-1.9	-0.8	UCI, flask (Global)
		253.6	247.7	247.6	-0.1	0.0	NIES, in situ (Japan)
		254.7	247.4	244.9	-2.6	-1.1	SOGE, in situ (Europe)
CCl ₂ FCClF ₂	CFC-113	79.1	77.2	76.5	-0.6	-0.8	AGAGE, in situ (Global)
		81.1	78.9	78.3	-0.6	-0.8	NOAA, in situ (Global)
		79.3	77.4	76.4	-1.0	-1.3	NOAA, flask (Global)
		79.1	77.8	77.1	-0.7	-0.9	UCI, flask (Global)
		79.7	78.1	78.0	-0.1	-0.1	NIES, in situ (Japan)
CClF ₂ CClF ₂	CFC-114	16.6	16.5	16.4	-0.04	-0.2	AGAGE, in situ (Global)
		16.2	16.4	16.2	-0.2	-1.3	UCI, flask (Global)
		16.0	15.9	16.0	0.05	0.3	NIES, in situ (Japan)
		-	16.7	-	-	-	SOGE, in situ (Europe)
		8.3	8.3	8.4	0.02	0.3	AGAGE, in situ (Global)
CClF ₂ CF ₃	CFC-115	8.6	8.3	8.3	0.05	0.6	NIES, in situ (Japan)
		8.3	8.5	8.5	0.0	0.0	SOGE, in situ (Europe)
HCFCs							
CHClF ₂	HCFC-22	163.4	183.6	192.1	8.6	4.6	AGAGE, in situ (Global)
		162.1	182.9	190.8	7.9	4.2	NOAA, flask (Global)
		160.0	180.7	188.3	7.6	4.2	UCI, flask (Global)
		-	190.7	200.6	9.9	5.2	NIES, in situ (Japan)
		-	197.3	207.3	10.0	5.0	SOGE-A, in situ (China)
CH ₃ CCl ₂ F	HCFC-141b	17.5	18.8	19.5	0.7	3.6	AGAGE, in situ (Global)
		17.2	18.7	19.2	0.5	2.6	NOAA, flask (Global)
		-	18.2	18.8	0.6	3.2	UCI, flask (Global)
		-	20.2	21.2	0.9	4.6	NIES, in situ (Japan)
		-	20.8	21.2	0.5	2.2	SOGE, in situ (Europe)
CH ₃ CClF ₂	HCFC-142b	15.1	17.9	18.9	1.1	5.9	AGAGE, in situ (Global)
		14.5	17.3	18.5	1.2	6.7	NOAA, flask (Global)
		-	17.0	18.0	1.0	5.7	UCI, flask (Global)

Table 1-1, continued.

Chemical Formula	Common or Industrial Name	Annual Mean Mole Fraction (ppt)			Growth (2007–2008)		Network, Method
		2004	2007	2008	(ppt/yr)	(%/yr)	
CH ₃ CClF ₂	HCFC-142b	-	18.9	20.2	1.3	6.5	NIES, in situ (Japan)
		-	19.7	21.0	1.4	6.8	SOGE, in situ (Europe)
		-	20.9	21.8	0.9	4.1	SOGE-A, in situ (China)
CHClFCF ₃	HCFC-124	1.43	1.48	1.47	-0.01	-0.8	AGAGE, in situ (Global)
		-	0.81	0.80	-0.01	-1.2	NIES, in situ (Japan)
Halons							
CB ₂ F ₂	halon-1202	0.038	0.029	0.027	-0.002	-7.0	UEA, flasks (Cape Grim only)
CBrClF ₂	halon-1211	4.37	4.34	4.30	-0.04	-0.9	AGAGE, in situ (Global)
		4.15	4.12	4.06	-0.06	-1.4	NOAA, flasks (Global)
		4.31	4.29	4.25	-0.04	-0.8	NOAA, in situ (Global)
		-	4.30	4.23	-0.06	-1.4	UCI, flasks (Global)
		4.62	4.50	4.40	-0.1	-2.0	SOGE, in situ (Europe)
		-	4.40	4.31	-0.1	-2.0	SOGE-A, in situ (China)
		4.77	4.82	4.80	-0.02	-0.4	UEA, flasks (Cape Grim only)
CBrF ₃	halon-1301	3.07	3.17	3.21	0.04	1.3	AGAGE, in situ (Global)
		2.95	3.09	3.12	0.03	1.1	NOAA, flasks (Global)
		3.16	3.26	3.29	0.03	1.2	SOGE, in situ (Europe)
		-	3.15	3.28	0.1	3.8	SOGE-A, in situ (China)
		2.45	2.48	2.52	0.03	1.3	UEA, flasks (Cape Grim only)
CBrF ₂ CBrF ₂	halon-2402	0.48	0.48	0.47	-0.01	-1.2	AGAGE, in situ (Global)
		0.48	0.47	0.46	-0.01	-2.0	NOAA, flasks (Global)
		0.43	0.41	0.40	-0.01	-1.2	UEA, flasks (Cape Grim only)
Chlorocarbons							
CH ₃ Cl	methyl chloride	533.7	541.7	545.0	3.3	0.6	AGAGE, in situ (Global)
		545	550	-	-	-	NOAA, in situ (Global)
		537	548	547	-0.7	-0.1	NOAA, flasks (Global)
		526	541	547	5.9	1.1	SOGE, in situ (Europe)
CCl ₄	carbon tetrachloride	92.7	89.8	88.7	-1.1	-1.3	AGAGE, in situ (Global)
		95.7	92.3	90.9	-1.4	-1.5	NOAA, in situ (Global)
		95.1	92.6	91.5	-1.1	-1.2	UCI, flask (Global)
		-	90.2	88.9	-1.3	-1.5	SOGE-A, in situ (China)
CH ₃ CCl ₃	methyl chloroform	21.8	12.7	10.7	-2.0	-17.6	AGAGE, in situ (Global)
		22.5	13.2	11.4	-1.9	-15.1	NOAA, in situ (Global)
		22.0	12.9	10.8	-2.1	-17.8	NOAA, flasks (Global)
		23.9	13.7	11.5	-2.2	-17.5	UCI, flask (Global)
		22.2	13.1	11.0	-2.2	-18.0	SOGE, in situ (Europe)
-	13.3	11.7	-1.6	-12.8	SOGE-A, in situ (China)		

Table 1-1, continued.

Chemical Formula	Common or Industrial Name	Annual Mean Mole Fraction (ppt)			Growth (2007–2008)		Network, Method
		2004	2007	2008	(ppt/yr)	(%/yr)	
Bromocarbons							
CH ₃ Br	methyl	8.2	7.7	7.5	-0.2	-2.7	AGAGE, in situ (Global)
	bromide	7.9	7.6	7.3	-0.3	-3.6	NOAA, flasks (Global)
	-		<i>8.5</i>	<i>8.1</i>	<i>-0.4</i>	<i>-5.2</i>	SOGE, in situ (Europe)

Notes:

Rates are calculated as the difference in annual means; relative rates are this same difference divided by the average over the two-year period. Results given in bold text and indicated as “Global” are estimates of annual mean global surface mixing ratios. Those indicated with italics are from a single site or subset of sites that do not provide a global surface mean mixing ratio estimate. Measurements of CFC-114 are a combination of CFC-114 and the CFC-114a isomer. The CFC-114a mixing ratio has been independently estimated as being ~10% of the CFC-114 mixing ratio (Oram, 1999) and has been subtracted from the results presented here assuming it has been constant over time.

These observations are updated from the following sources:

Butler et al. (1998), Clerbaux and Cunnold et al. (2007), Fraser et al. (1999), Maione et al. (2004), Makide and Rowland (1981), Montzka et al. (1999, 2000, 2003, 2009), O’Doherty et al. (2004), Oram (1999), Prinn et al. (2000, 2005), Reimann et al. (2008), Rowland et al. (1982), Stohl et al. (2010), Sturrock et al. (2001), Reeves et al. (2005), Simmonds et al. (2004), Simpson et al. (2007), Xiao et al. (2010a, 2010b), and Yokouchi et al. (2006).

AGAGE, Advanced Global Atmospheric Gases Experiment; NOAA, National Oceanic and Atmospheric Administration; SOGE, System for Observation of halogenated Greenhouse gases in Europe; SOGE-A, System for Observation of halogenated Greenhouse gases in Europe and Asia; NIES, National Institute for Environmental Studies; UEA, University of East Anglia; UCI, University of California-Irvine.

These results uniquely characterize the interhemispheric, interannual, and seasonal variations in the CFC-11 upper-atmosphere distribution, though an analysis of the consistency in trends derived from these platforms and from surface data has not been performed.

The global mixing ratios of the two less abundant CFCs, CFC-114 (CClF₂CClF₂) and CFC-115 (CClF₂CF₃), have not changed appreciably from 2000 to 2008 (Table 1-1) (Clerbaux and Cunnold et al., 2007). During 2008, global mixing ratios of CFC-114 were between 16.2 and 16.4 ppt based on results from the Advanced Global Atmospheric Gases Experiment (AGAGE) and University

of California-Irvine (UCI) networks, and AGAGE measurements show a mean global mixing ratio of 8.4 ppt for CFC-115 (Table 1-1). For these measurements, CFC-114 measurements are actually a combination of CFC-114 and CFC-114a (see notes to Table 1-1).

Observed mixing ratio declines of the three most abundant CFCs during 2005–2008 were slightly slower than projected in scenario A1 (baseline scenario) from the 2006 WMO Ozone Assessment (Daniel and Velders et al., 2007) (Figure 1-1). The observed declines were smaller than projected during 2005–2008 in part because release rates from banks were underestimated in the A1 scenario

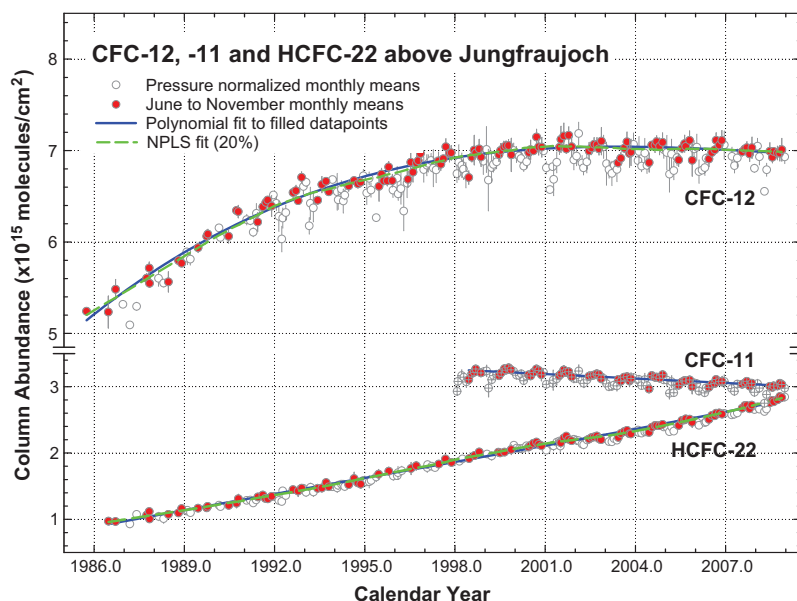


Figure 1-2. The time evolution of the monthly-mean total vertical column abundances (in molecules per square centimeter) of CFC-12, CFC-11, and HCFC-22 above the Jungfraujoch station, Switzerland, through 2008 (update of Zander et al., 2005). Note discontinuity in the vertical scale. Solid blue lines show polynomial fits to the columns measured only in June to November so as to mitigate the influence of variability caused by atmospheric transport and tropopause subsidence during winter and spring (open circles) on derived trends. Dashed green lines show non-parametric least-squares fits (NPLS) to the June to November data.

during this period (Daniel and Velders et al., 2007). For CFC-12, some of the discrepancy is due to revisions to the NOAA calibration scale. In the A1 scenario, CFC-11 and CFC-12 release rates from banks were projected to decrease over time based on anticipated changes in bank sizes from 2002–2015 (IPCC/TEAP 2005). The updated observations of these CFCs, however, are more consistent with emissions from banks having been fairly constant during 2005–2008, or with declines in bank emissions being offset by enhanced emissions from non-bank-related applications. Implications of these findings are further discussed in Chapter 5 of this Assessment.

The slight underestimate of CFC-113 mixing ratios during 2005–2008, however, is not likely the result of inaccuracies related to losses from banks, since banks of CFC-113 are thought to be negligible (Figure 1-1). The measured mean hemispheric difference (North minus South) was ~ 0.2 ppt during 2005–2008, suggesting the potential presence of only small residual emissions (see Figure 1-4). The mean exponential decay time for CFC-113 over this period is 100–120 years, slightly longer than the steady-state CFC-113 lifetime of 85 years. This observation is consistent with continuing small emissions (≤ 10 gigagrams (Gg) per year). Small lifetime changes are expected as atmospheric distributions of CFCs respond to emissions becoming negligible, but changes in the atmospheric distribution of CFC-113 relative to loss regions (the stratosphere) suggest that the CFC-113 lifetime should become slightly shorter, not longer, as emissions decline to zero (e.g., Prather, 1997).

CFC Emissions and Banks

Releases from banks account for a large fraction of current emissions for some ODSs and will have an important influence on mixing ratios of many ODSs in the future. Banks of CFCs were 7 to 16 times larger than amounts emitted in 2005 (Montzka et al., 2008). Implications of bank sizes, emissions from them, and their influence on future ODS mixing ratios are discussed further in Chapter 5.

Global, “top-down” emissions of CFCs derived from global surface observations and box models show rapid declines during the early 1990s but only slower changes in more recent years (Figure 1-3) (see Box 1-1 for a description of terms and techniques related to deriving emissions). Emission changes derived for CFC-11, for example, are small enough so that different model approaches (1-box versus 12-box) suggest either slight increases or slight decreases in emissions during 2005–2008. Considering the magnitude of uncertainties on these emissions, changes in CFC-11 emissions are not distinguishable from zero over this four-year period. “Bottom-up” estimates of emissions derived from production and use data have not

been updated past 2003 (UNEP/TEAP, 2006), but projections made in 2005 indicated that CFC-11 emissions from banks of ~ 25 Gg/yr were not expected to decrease substantially from 2002 to 2008 (IPCC/TEAP, 2005) (Figure 1-3).

“Top-down” emissions derived for CFC-11 during 2005–2008 averaged 80 Gg/yr. These emissions are larger than derived from “bottom-up” estimates by an average of 45 (37–60) Gg/yr over this same period. The discrepancy between the atmosphere-derived and “bottom-up” emissions for CFC-11 is not fully understood but could suggest an underestimation of releases from banks or fast-release applications (e.g., solvents, propellants, or open-cell foams). Emissions from such short-term uses were estimated at 15–26 Gg/yr during 2000–2003 (UNEP/TEAP, 2006; Figure 1-3) and these accounted for a substantial fraction of total CFC-11 emissions during those years. The discrepancy may also arise from errors in the CFC-11 lifetime used to derive “top-down” emissions. New results from models that more accurately simulate air transport rates through the stratosphere suggest a steady-state lifetime for CFC-11 of 56–64 years (Douglass et al., 2008), notably longer than 45 years. A relatively longer lifetime for CFC-12 was not suggested in this study. A longer CFC-11 lifetime of 64 years would bring the atmosphere-derived and “bottom-up” emissions into much better agreement (see light blue line in Figure 1-3).

Global emissions of CFC-12 derived from observed atmospheric changes decreased from ~ 90 to ~ 65 Gg/yr during 2005–2008 (Figure 1-3). These emissions and their decline from 2002–2008 are well accounted for by leakage from banks as projected in a 2005 report (IPCC/TEAP, 2005). Global emissions of CFC-113 derived from observed global trends and 1-box or 12-box models and a global lifetime of 85 years were small compared to earlier years, and averaged <10 Gg/yr during 2005–2008 (Figure 1-3).

Summed emissions from CFCs have declined during 2005–2008. When weighted by semi-empirical Ozone Depletion Potentials (ODPs) (Chapter 5), the sum of emissions from CFCs totaled 134 ± 30 ODP-Kt in 2008 (where 1 kilotonne (Kt) = 1 Gg = 1×10^9 g). The sum of emissions of CFCs weighted by direct, 100-yr Global Warming Potentials (GWPs) has decreased on average by $8 \pm 1\%$ /yr from 2004 to 2008, and by 2008 amounted to 1.1 ± 0.3 gigatonnes of CO₂-equivalents per year (Gt CO₂-eq/yr).

Emission trends and magnitudes can also be inferred from measured hemispheric mixing ratio differences. This approach is valid when emissions are predominantly from the Northern Hemisphere and sink processes are symmetric between the hemispheres. Hemispheric mixing ratio differences for CFC-11 and CFC-12 averaged between 10 and 20 ppt during the 1980s when emissions were large, but since then as emissions declined, hemispheric differences also became smaller. United Nations

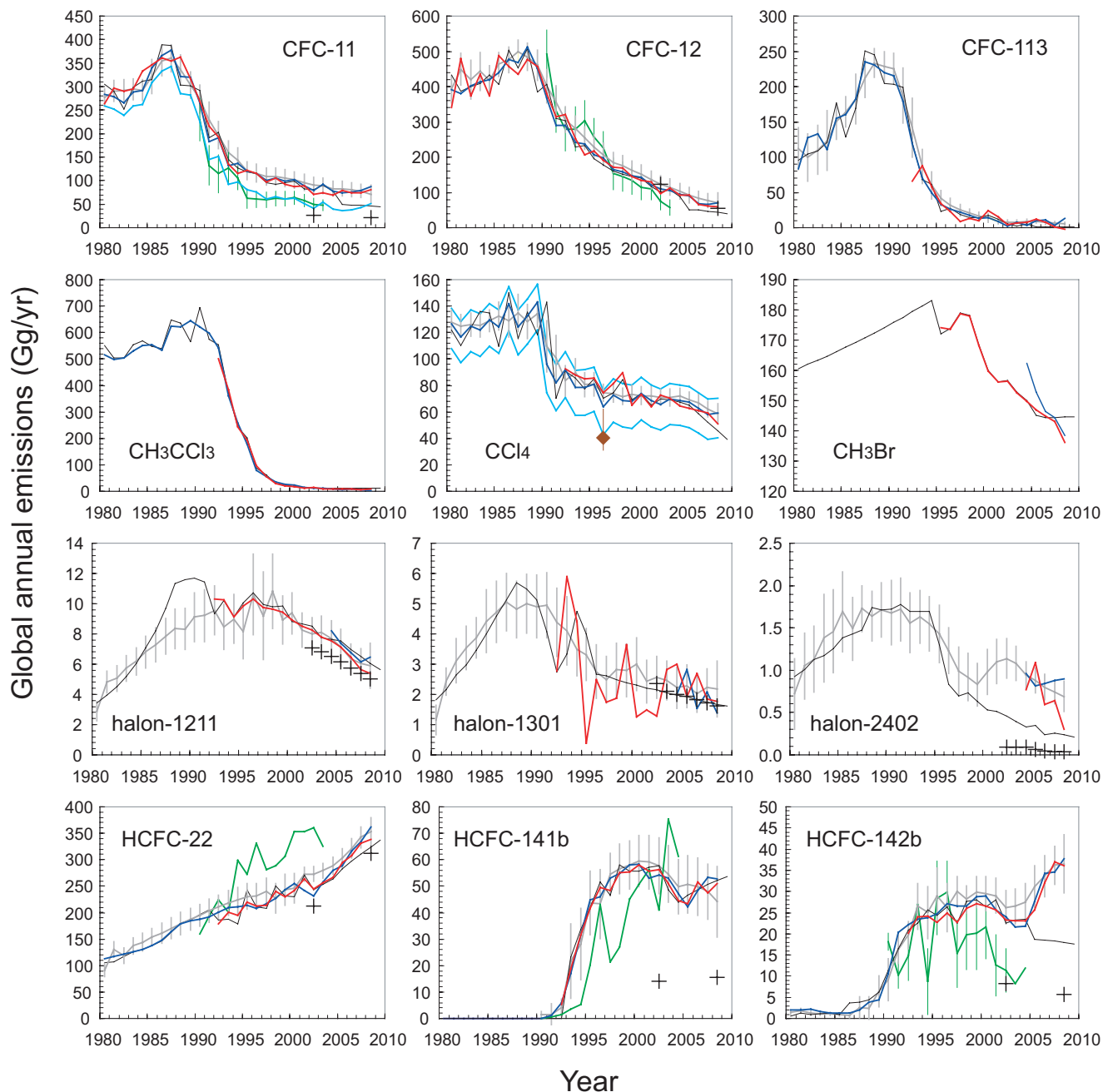


Figure 1-3. “Top-down” and “bottom-up” global emission estimates for ozone-depleting substances (in Gg/yr). “Top-down” emissions are derived with NOAA (red lines) and AGAGE (blue lines) global data and a 1-box model. These emissions are also derived with a 12-box model and AGAGE data (gray lines with uncertainties indicated) (see Box 1-1). Halon and HCFC emissions derived with the 12-box model in years before 2004 are based on an analysis of the Cape Grim Air Archive only (Fraser et al., 1999). A1 scenario emissions from the 2006 Assessment are black lines (Daniel and Velders et al., 2007). “Bottom-up” emissions from banks (refrigeration, air conditioning, foams, and fire protection uses) are given as black plus symbols (IPCC/TEAP, 2005; UNEP, 2007a), and total, “bottom-up” emissions (green lines) including fast-release applications are shown for comparison (UNEP/TEAP, 2006). A previous bottom-up emission estimate for CCl₄ is shown as a brown point for 1996 (UNEP/TEAP, 1998). The influence of a range of lifetimes for CCl₄ (23–33 years) and a lifetime of 64 years for CFC-11 are given as light blue lines.

Box 1-1. Methods for Deriving Trace Gas Emissions

- a) Emissions derived from production, sales, and usage (the “bottom-up” method).** Global and national emissions of trace gases can be derived from ODS global production and sales magnitudes for different applications and estimates of application-specific leakage rates. For most ODSs in recent years, production is small or insignificant compared to historical levels and most emission is from material in use. Leakage and releases from this “bank” of material (produced but not yet emitted) currently dominate emissions for many ozone-depleting substances (ODSs). Uncertainties in these estimates arise from uncertainty in the amount of material in the bank reservoir and the rate at which material is released or leaks from the bank. Separate estimates of bank magnitudes and loss rates from these banks have been derived from an accounting of devices and appliances in use (IPCC/TEAP, 2005). Emissions from banks alone account for most, if not all, of the “top-down,” atmosphere-derived estimates of total global emission for some ODSs (CFC-12, halon-1211, halon-1301, HCFC-22; see Figure 1-3).
- b) Global emissions derived from observed global trends (the “top-down” method).** Mass balance considerations allow estimates of global emissions for long-lived trace gases based on their global abundance, changes in their global abundance, and their global lifetime. Uncertainties associated with this “top-down” approach stem from measurement calibration uncertainty, imperfect characterization of global burdens and their change from surface observations alone, uncertain lifetimes, and modeling errors. The influence of sampling-related biases and calibration-related biases on derived emissions is small for most ODSs, given the fairly good agreement observed for emissions derived from different measurement networks (Figure 1-3). Hydroxyl radical (OH)-derived lifetimes are believed to have uncertainties on the order of $\pm 20\%$ for hydrochlorofluorocarbons (HCFCs), for example (Clerbaux and Cunnold et al., 2007). Stratospheric lifetimes also have considerable uncertainty despite being based on model calculations (Prinn and Zander et al., 1999) and observational studies (Volk et al., 1997). Recent improvements in model-simulated stratospheric transport suggest that the lifetime of CFC-11, for example, is 56–64 years instead of the current best estimate of 45 years (Douglass et al., 2008).
- Global emissions derived for long-lived gases with different models (1-box and 12-box) show small differences in most years (Figure 1-3) (UNEP/TEAP, 2006). Though a simple 1-box approach has been used extensively in past Assessment reports, emissions derived with a 12-box model have also been presented. The 12-box model emissions estimates made here are derived with a Massachusetts Institute of Technology-Advanced Global Atmospheric Gases Experiment (MIT-AGAGE) code that incorporates observed mole fractions and a Kalman filter applying sensitivities of model mole fractions to 12-month semi-hemispheric emission pulses (Chen and Prinn, 2006; Rigby et al., 2008). This code utilizes the information contained in both the global average mole fractions and their latitudinal gradients. Uncertainties computed for these annual emissions enable an assessment of the statistical significance of interannual emission variations.
- c) Continental and global-scale emissions derived from measured global distributions.** Measured mixing ratios (hourly through monthly averages) can be interpreted using inverse methods with global Eulerian three-dimensional (3-D) chemical transport models (CTMs) to derive source magnitudes for long-lived trace gases such as methane (CH_4), methyl chloride (CH_3Cl), and carbon dioxide (CO_2) on continental scales (e.g., Chen and Prinn, 2006; Xiao, 2008; Xiao et al., 2010a; Peylin et al., 2002; Rödenbeck et al., 2003; Meirink et al., 2008; Peters et al., 2007; Bergamaschi et al., 2009). Although much progress has been made with these techniques in recent years, some important obstacles limit their ability to retrieve unbiased fluxes. The first is the issue that the underdetermined nature of the problem (many fewer observations than unknowns) means that extra information, in the form of predetermined and prior constraints, is typically required to perform an inversion but can potentially impose biases on the retrieved fluxes (Kaminski et al., 2001). Second, all of these methods are only as good as the atmospheric transport models and underpinning meteorology they use. As Stephens et al. (2007) showed for CO_2 , biases in large-scale flux optimization can correlate directly with transport biases.
- d) Regional-scale emissions derived from high-frequency data at sites near emission regions.** High-frequency measurements (e.g., once per hour) near source regions can be used to derive regional-scale ($\sim 10^4$ – 10^6 km^2) trace gas emission magnitudes. The method typically involves interpreting measured mixing ratio enhancements above a background as an emissive flux using Lagrangian modeling concepts.

Qualitative indications of emission source regions or “hotspots” are provided by correlating observed mixing ratio enhancements with back trajectories (typically 4- to 10-day) calculated for the sampling time and location (e.g., Maione et al., 2008; Reimann et al., 2004; Reimann et al., 2008).

Quantitative emission magnitudes have been derived with the “ratio-method” (e.g., Dunse et al., 2005; Yokouchi et al., 2006; Millet et al., 2009; Guo et al., 2009). In this straightforward approach, trace-gas emissions are derived from correlations between observed enhancements above background for a trace gas of interest and a second trace gas (e.g., carbon monoxide or radon) whose emissions are independently known. Uncertainties in this approach are reduced when the emissions of the reference substance are well known, co-located, and temporally covarying with the halocarbon of interest, and when the mixing ratio enhancements of both chemicals are well correlated and large relative to uncertainties in the background levels.

More complex and powerful tools combine Lagrangian 3-D models and inverse methods to estimate regional emission fluxes (e.g., Manning et al., 2003; Stohl et al., 2009). As with larger-scale inversions, the challenge with these methods is that the inversion problem is underdetermined and results are dependent on transport accuracy. Furthermore, each station is sensitive to emissions only from a restricted region in its vicinity. To obtain global coverage of emissions from regional measurements, global transport models are used. Stohl et al. (2009) have recently developed a formal analytical method that takes into account a priori information for halocarbon emissions, which allows for regional-scale inversions with a global coverage.

Environment Programme consumption data suggest that CFC emissions continue to be dominated by releases in the Northern Hemisphere (UNEP, 2010). Furthermore, the small (0.2 ppt) hemispheric difference (North minus South) measured for CFC-113 since 2004—when emissions derived from atmospheric trends of this compound were very small (<10 Gg/yr)—indicates at most only a small contribution of loss processes to hemispheric differences for long-lived CFCs (Figure 1-4). By contrast, mean annual hemispheric differences for CFC-11 and CFC-12 have remained between 1.5 and 3 ppt since 2005 and suggest the presence of continued substantial Northern Hemispheric emissions of these chemicals. For CFC-11, the hemispheric difference (North minus South) measured in both global networks has not declined appreciably since 2005 (Figure 1-4), consistent with fairly constant emissions over that period (Figure 1-3).

Polar Firm and Volcano Observations

New CFC observations in firn air collected from the Arctic (two sites) and Antarctic (three sites) show small but detectable CFC-11, -12, and -114 levels increasing after ~1940 and CFC-113 and -115 appearing and increasing after ~1970 (Martinerie et al., 2009). These results add to conclusions from earlier firn-air studies (Butler et al., 1999; Sturrock et al., 2002) indicating that natural sources of CFCs, CCl₄, CH₃CCl₃, halons, and HCFCs, if they exist, must be very small. Such conclusions rely on these compounds being stable in firn. Consistent with this result, studies of fumarole discharges from three Central American volcanoes over two years show that volcanic emissions are not a significant natural source of CFCs (Frische et al., 2006).

1.2.1.2 HALONS

Updated observations show that the annual global surface mean mixing ratio of halon-1301 (CBrF₃) increased at a rate of 0.03–0.04 ppt/yr during 2007–2008 and reached 3.1–3.2 ppt in mid-2008 (Figure 1-1; Table 1-1). Revised calibration procedures and reliance on gas chromatography with mass spectrometric detection analyses of flasks within NOAA have improved the consistency (within 5% in 2008) among results from independent laboratories compared to past reports (Clerbaux and Cunnold et al., 2007).

The global surface mean mixing ratio of halon-1211 (CBrClF₂) began to decrease during 2004–2005 and changed by -0.05 ± 0.01 ppt/yr during 2007–2008 (Figure 1-1; Table 1-1). The global surface mean in 2008 was only about 0.1 ppt lower than peak levels measured in 2004.

Updated halon-2402 (CBrF₂CBrF₂) observations indicate that global surface mixing ratios declined from 0.48 ppt in 2004 to 0.46–0.47 ppt in 2008 at a rate of -0.01 ppt/yr in 2007–2008 (Table 1-1).

Updated halon-1202 (CBr₂F₂) measurements (Fraser et al., 1999; Reeves et al., 2005) show a substantial decrease in mixing ratios of this chemical since 2000. Southern Hemispheric mixing ratios decreased from 0.038 ppt in 2004 to 0.027 ppt in 2008 at a rate of -0.002 ppt/yr in 2007–2008.

The observed changes in halon-1211 mixing ratios during 2005–2008 are similar to those projected in the A1 scenario of the previous Assessment (Daniel and Velders et al., 2007); halon-1301 has increased at a slightly higher rate than projected. Observed surface mixing ratios of halon-2402 are notably higher than scenarios from past

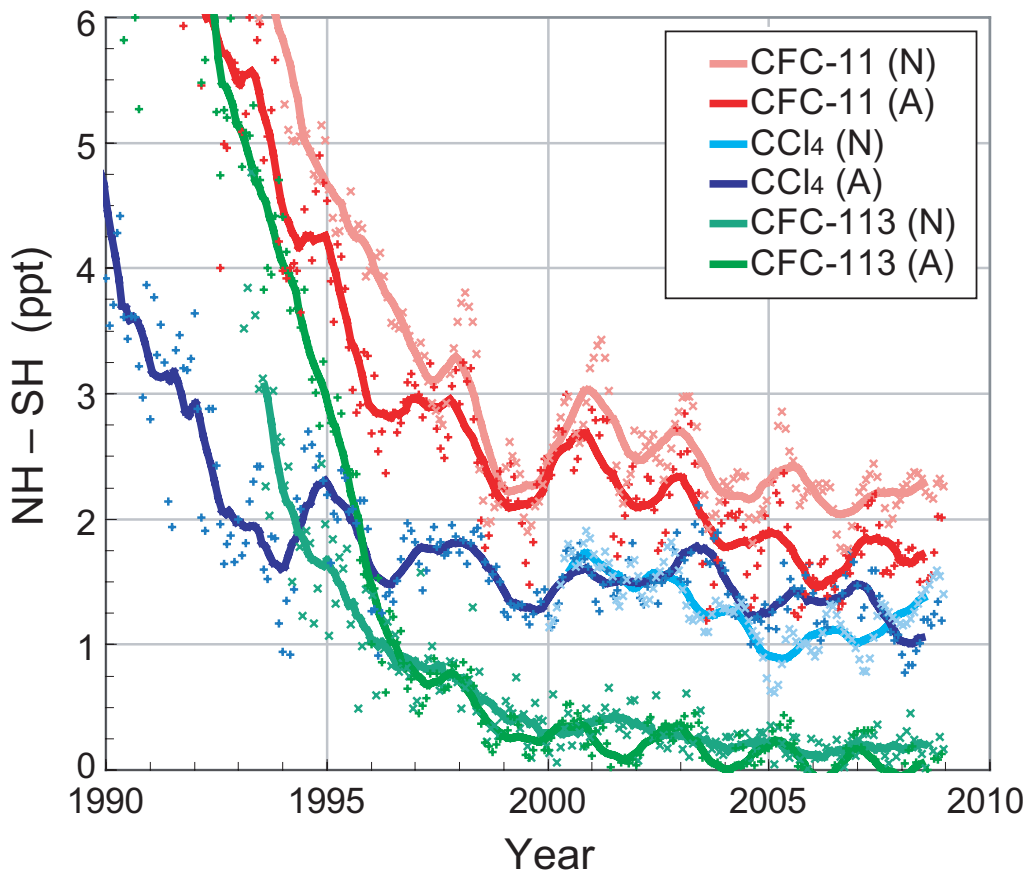


Figure 1-4. Mean hemispheric mixing ratio differences (North minus South, in parts per trillion) measured for some ODSs in recent years from independent sampling networks (AGAGE data (A) as plusses, Prinn et al., 2000; and NOAA data (N) as crosses, Montzka et al., 1999). Points are monthly-mean differences; lines are running 12-month means of the monthly differences.

Assessments because those scenarios were not based on actual measurement data (Figure 1-1).

Halon Emissions, Stockpiles, and Banks

Stockpiles and banks of halons, which are used primarily as fire extinguishing agents, represent a substantial reservoir of these chemicals. The amounts of halons present in stockpiles or banks are not well quantified, but were estimated to be 15–33 times larger than emissions of halon-1211 and halon-1301 in 2008 (UNEP, 2007a). “Bottom-up” estimates of halon emissions derived from production and use data were recently revised based on a reconsideration of historic release rates and the implications of this reanalysis on current bank sizes (UNEP, 2007a). The magnitude and trends in these emission estimates compare well with those derived from global atmospheric data and best-estimate lifetimes for halon-1211 and halon-1301 (Figure 1-3).

“Bottom-up” emission estimates of halon-2402 are significantly lower than those derived from global atmospheric trends. Bank-related emissions are thought to account for nearly all halon emissions (plusses in Figure 1-3). Halons are also used in small amounts in non-fire suppressant applications and as chemical feedstocks, but these amounts are not included in the “bottom-up” emissions estimates included in Figure 1-3.

Summed emissions of halons, weighted by semi-empirical ODPs, totaled 90 ± 19 ODP-Kt in 2008. When weighted by 100-yr direct GWPs, summed halon emissions totaled 0.03 Gt CO₂-eq in 2008.

1.2.1.3 CARBON TETRACHLORIDE (CCl₄)

The global mean surface mixing ratio of CCl₄ continued to decrease during 2005–2008 (Figure 1-1). By 2008, the surface mean from the three global surface networks was approximately 90 ± 1.5 ppt and had de-

creased during 2007–2008 at a rate of -1.1 to -1.4 ppt/yr (Table 1-1).

Global CCl₄ Emissions

Though the global surface CCl₄ mixing ratio decreased slightly faster during 2005–2008 than during 2000–2004 (Figure 1-1), the observations imply only a slight decrease in CCl₄ emissions over time (Figure 1-3). The measured global CCl₄ mixing ratio changes suggest “top-down,” global emissions between 40 and 80 Gg/yr during 2005–2008 for a lifetime of 33–23 years (see Box 1-2). Similar emission magnitudes and trends are derived for recent years from the independent global sampling networks and with different modeling approaches (Figure 1-3). The decline observed for CCl₄ mixing ratios during 2005–2008 was slightly less rapid than that projected in the A1 scenario of the previous Assessment (Daniel and Velders et al., 2007), which was derived assuming a linear decline in emissions from 65 Gg/yr in 2004 to 0 Gg/yr in 2015 and a 26-year lifetime (Daniel and Velders et al., 2007).

As with other compounds, “top-down” emissions for CCl₄ are sensitive to errors in global lifetimes. A lifetime at the upper (or lower) end of the current uncertainty range yields a smaller (larger) emission than when calculated with the current best-estimate lifetime of 26 years (Figure 1-5). The magnitude of uncertainties that remain in the quantification of CCl₄ sinks (i.e., stratosphere, ocean, and soil), however, do not preclude revisions to the CCl₄ lifetime in the future that could significantly change the magnitude of “top-down” emissions.

Global CCl₄ emission magnitudes and their trends also can be qualitatively assessed from measured hemispheric differences, which are roughly proportional to emissions for long-lived trace gases emitted primarily in the Northern Hemisphere (see Section 1.2.1.1). This difference has remained fairly constant for CCl₄ at 1.25–1.5 ppt over the past decade (Figure 1-4). These differences are independent of measured year-to-year changes in atmospheric mixing ratios and so provide a first-order consistency check on emission magnitudes and trends. Though the hemispheric difference (NH minus SH) expected for CCl₄ in the absence of emissions is not well defined, it is expected to be small because the asymmetry in loss fluxes between the hemispheres due to oceans and soils is likely small (<10 Gg/yr) and offsetting. This analysis suggests, based on the considerations discussed above for CFCs, that the significant and sustained NH minus SH difference observed for CCl₄ mixing ratios arises from substantial NH CCl₄ emissions that have not changed substantially over the past decade (Figure 1-3).

In contrast to the CCl₄ emissions derived from “top-down” methods, those derived with “bottom-up”

techniques suggest substantially smaller emissions in most years. In the past two Assessment reports, for example, the “bottom-up” emissions estimate for CCl₄ during 1996 was 41 (31–62) Gg/yr (UNEP/TEAP 1998), or 20–50 Gg/yr lower than the “top-down,” atmosphere-derived estimate for that year (Montzka and Fraser et al., 2003; Clerbaux and Cunnold et al., 2007). Because similar estimates have not been made for subsequent years, we derive here “potential emissions” from the difference between CCl₄ production magnitudes in excess of amounts used as feedstock and amounts destroyed that are reported to UNEP (UNEP, 2010) (for the European Union (EU), feedstock magnitudes were determined from numbers reported by the individual EU countries and not from the EU as a whole). An upper limit to these “potential emissions” was also derived from this same data by filling apparent gaps in production and feedstock data reported to UNEP, including a 2% fugitive emissions rate from quantities used as feedstock, and incorporating an efficiency for reported CCl₄ destruction of only 75% (Figure 1-5). This approach yields emissions of 0–30 Gg/yr during 2005–2008. As is apparent from this figure, CCl₄ continues to be produced in substantial quantities (reported production in 2008 was 156 Gg), but the primary use of this production is for feedstocks (e.g., in the production of some hydrofluorocarbons (HFCs), see Table 1-11, and other chemicals) that should yield only small emissions.

This “bottom-up” “potential emission” history derived from reported production, feedstock, and destruction data is inconsistent with the magnitude and variability in the “top-down,” atmosphere-derived emissions. Importantly, these differences cannot be reconciled by a simple scaling of the CCl₄ atmospheric lifetime (Figure 1-5). This is particularly true during 2003–2008, when large declines are derived for “bottom-up” “potential emissions” but are not suggested by the atmosphere-derived “top-down” estimates or by the relatively constant NH minus SH difference measured during these years. The discrepancies during 2005–2008 between the “top-down” and “potential emission” estimates are between 30 and 50 Gg/yr. Even when the upper limits to “potential emissions” are compared to the lower range of “top-down” emissions (lifetime = 33 years), a discrepancy during 2005–2008 of 15–30 Gg/yr remains (Figure 1-5). Though the magnitude of this discrepancy is sensitive to the uncertain CCl₄ lifetime (Box 1-2), the different time-dependent changes implied for emissions particularly during 2003–2008 with the different estimation methods are not sensitive to this lifetime.

Regional Studies

Observational studies can potentially provide information about regional source distributions and magnitudes (Box 1-1). Recently, Xiao et al. (2010b) have inversely

Box 1-2. CCl₄ Lifetime Estimates

The loss of carbon tetrachloride (CCl₄) in the global atmosphere is dominated by photolytic destruction in the stratosphere but also occurs by surface ocean uptake and uptake by soils. The atmospheric lifetime due to photolysis is estimated to be 35 years based on older modeling data and measured gradients in the lower stratosphere (Prinn and Zander et al., 1999; Volk et al., 1997). This number is based in part on the atmospheric lifetime of CFC-11. For example, in an analysis of global CCl₄ distributions measured by satellite, Allen et al. (2009) derived a lifetime for CCl₄ of 34 ± 5 years relative to a lifetime for CFC-11 of 45 years. An updated analysis of model-derived lifetimes, however, indicates that current models that more accurately simulate different stratospheric metrics (age of air, for example) calculate a substantially longer stratospheric lifetime for CFC-11 of 56–64 years (Douglass et al., 2008). Although CCl₄ was not explicitly considered in the Douglass et al. study, the results could suggest a longer CCl₄ partial lifetime with respect to stratospheric loss of ~44–50 yr. A recent independent analysis provides further evidence that the CCl₄ stratospheric lifetime may be as long as 50 years (Rontu Carlon et al., 2010).

Undersaturations of CCl₄ have been observed in many different regions of the world's ocean waters and are indicative of a CCl₄ sink (Wallace et al., 1994; Lee et al., 1999; Huhn et al., 2001; Yvon-Lewis and Butler, 2002; Tanhua and Olsson, 2005). These undersaturations are larger than can be explained from laboratory-determined hydrolysis rates and the responsible loss mechanism is not known. In the absence of new results, the partial lifetime with respect to oceanic loss of 94 (82–191) years (Yvon-Lewis and Butler, 2002) remains unchanged.

Losses of atmospheric CCl₄ to a subset of terrestrial biomes have been observed in independent studies published since the previous Assessment (Liu, 2006; Rhew et al., 2008). These results confirm that terrestrial biomes can act as a sink for CCl₄, but the magnitude of this loss remains uncertain. Losses to tropical soils account for most of the calculated soil sink (62%), but are based primarily on results from one tropical forest (Happell and Roche, 2003) and have yet to be remeasured. The new flux estimates reported for temperate forest and temperate grassland areas were derived with soil gas gradient methods and, in semi-arid and arid shrublands, with flux chamber methods. In these re-measured biomes, Liu (2006) and Rhew et al. (2008) found a mean sink about half as strong as in the original Happell and Roche (2003) study. When a range of partial lifetimes with respect to soil losses and other losses is considered, a mid-range estimate for CCl₄ lifetime remains at 26 (23–33) years (see Table 1).

Box 1-2 Table 1. Sensitivity of total global CCl₄ lifetime to component sink magnitudes.

Partial Lifetimes (years) with Respect to Loss to:				
Stratosphere	Ocean	Soil	Total Lifetime	Description and Notes
35	∞	∞	35	pre-2003 Ozone Assessments
35	94	∞	26	post-2003 Ozone Assessments ¹
35	94	90	20	a
35	94	101	20	b
35	94	195	23	c
44–50	94	∞	30–33	d
44–50	94	195	26–28	c & d
44–50	94	101	23–25	b & d

Notes:

¹ Montzka and Fraser et al. (2003); Clerbaux and Cunnold et al. (2007).

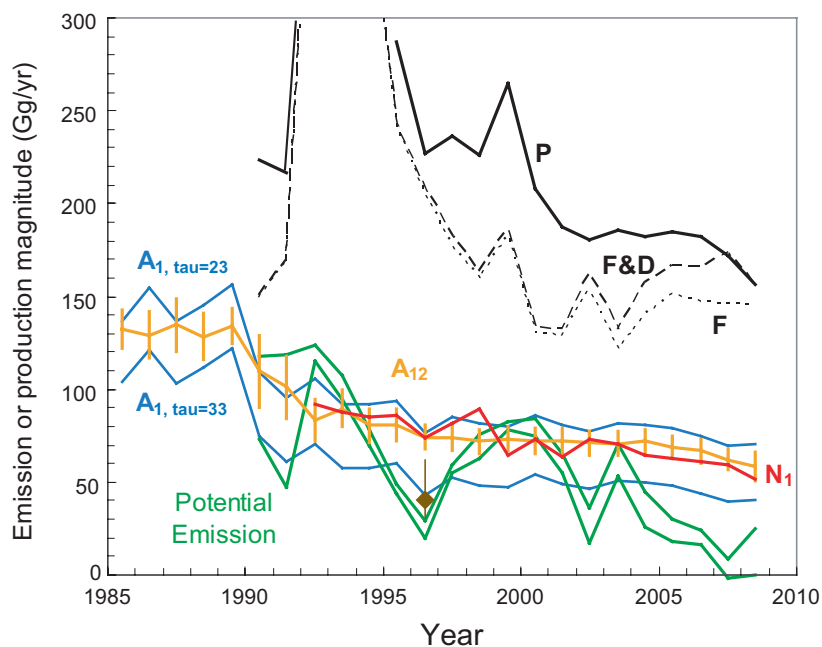
(a) Partial lifetime from loss to soils derived from Happell and Roche (2003) from measurements in seven different biomes.

(b) Rhew et al. (2008) and Liu (2006) estimates of loss to arid land, temperate forest, and temperate grasslands soils used instead of those estimated by Happell and Roche (2003), and Happell and Roche (2003) loss estimates for soils in the other four biomes.

(c) All soil losses in Happell and Roche (2003) were scaled by 0.5 to account for updated results (Rhew et al. (2008) and Liu (2006)) in three of the seven biomes originally studied being only half as large, on average, as originally found.

(d) A longer stratospheric CCl₄ lifetime (of 50 years) is considered based on a CFC-11 lifetime of 56–64 years rather than 45 years (Douglass et al., 2008) (44 yr = 35×56/45; 50 yr = 35×64/45), consistent with the recent work of Rontu Carlon et al. (2010).

Figure 1-5. Atmospheric (“top-down”) global CCl_4 emissions (Gg/yr) derived from observations (blue, red, and orange lines, some of which are shown in Figure 1-3) compared to “potential emissions” derived from UNEP production data (green lines). The lower “potential emissions” green line is derived from the difference between total CCl_4 production (solid black line labeled “P”) reported to UNEP and the sum of feedstock and amounts destroyed (dashed line labeled “F&D”) (production magnitudes to feedstock alone are indicated with the dotted line labeled “F”). The upper “potential emission” green line was derived similarly as the lower line but was augmented by additional amounts to fill apparent gaps in UNEP reporting, plus an allotment for fugitive emissions of 2% of reported CCl_4 feedstock use, plus an efficiency of only 75% for reported destruction. Top-down emission estimates are derived from a 1-box model of NOAA atmospheric data (red line labeled N_1) and a 12-box analysis of the AGAGE data (orange line labeled A_{12}) with a lifetime of 26 years (see Box 1-1). The influence of lifetimes between 23 and 33 years on emissions derived with the 1-box model from AGAGE data are also indicated (blue lines labeled $A_{1, \tau=23}$ and $A_{1, \tau=33}$). The TEAP “bottom-up” emission estimate for 1996 is shown as a brown diamond (UNEP/TEAP, 1998).



estimated regional and global annual CCl_4 emissions and sinks using the three-dimensional Model of Atmospheric Transport and Chemistry (3D-MATCH) model, a monthly applied Kalman filter, a priori industrial emission patterns for 8 regions in the world, and observed monthly-mean mixing ratios from 1996–2004 at multiple, globally distributed AGAGE and NOAA/Earth System Research Laboratory (ESRL) sites. The average 1996–2004 East Asian (including China) emissions accounted for $53.3 \pm 3.6\%$ of the global total industrial emissions during this period. The fraction of global emissions inferred from South Asia (including India) were estimated at $22.5 \pm 3.0\%$, those from Africa at $9.0 \pm 1.2\%$, those from North America at $6.6 \pm 1.9\%$, and those from Europe at $4.0 \pm 2.2\%$.

Regional emissions of CCl_4 have also been estimated from measured mixing ratio enhancements in pollution events near source regions. These studies have suggested small or no detectable (ND) emissions from North America during 2003–2006 (Millet et al., 2009: ND; Hurst et al., 2006: <0.6 Gg/yr), Australia (Dunse et al., 2005: none detected in most years during 1995–2000), and Japan (Yokouchi et al., 2005: 1.8 Gg/yr in 2001 decreasing to 0.27 Gg/yr in 2003). Larger emissions have been inferred as coming from China (Vollmer et al., 2009: 15 (10–22) Gg/yr for the period Oct 2006–

March 2008). While these studies and those of Xiao et al. (2010b) point to countries in South East Asia (including China) as providing a large fraction of CCl_4 emissions in the past, it is not possible to gauge their consistency relative to one another or relative to “top-down” global emission magnitudes owing to the different time periods included and incomplete geographic coverage addressed by these studies.

1.2.1.4 METHYL CHLOROFORM (CH_3CCl_3)

Surface mixing ratios of methyl chloroform (CH_3CCl_3) continued to decrease at a near-constant exponential rate in the remote global atmosphere during 2005–2008. By mid-2008 the global surface mean mixing ratio had decreased to about 11 ppt (Figure 1-1). This decline represents more than a factor of 10 decrease in global surface mixing ratios of this chemical since the early 1990s. As CH_3CCl_3 mixing ratios have declined in response to reduced emissions, hemispheric differences have also diminished. The mean annual hemispheric difference (NH minus SH) was a few percent of the global mean during 2005–2008, much smaller than during the 1980s when emissions were substantial. Measured abundances and rates of change in 2008 agree to within about

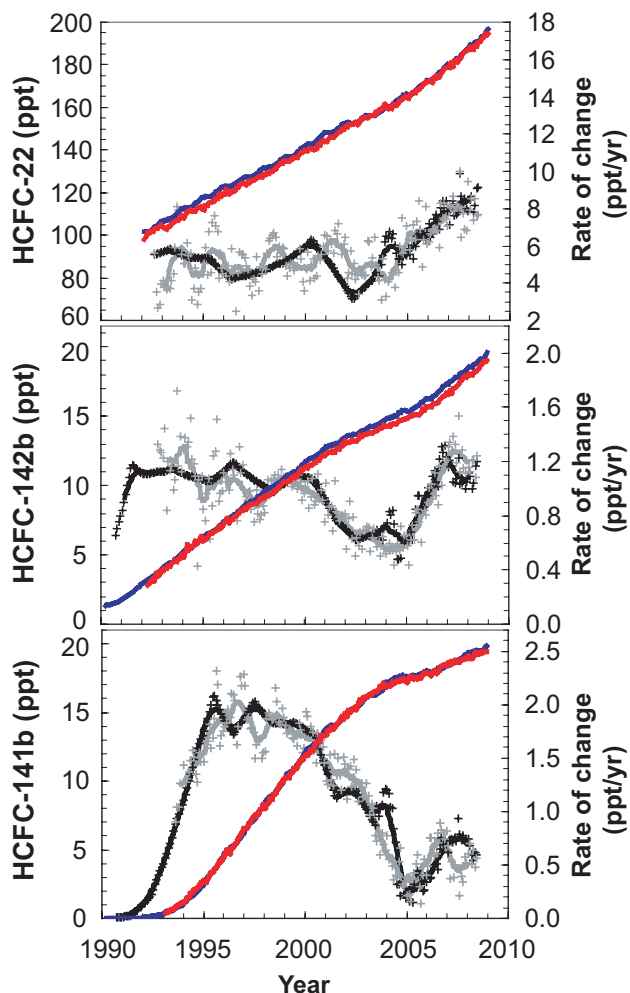


Figure 1-6. Global surface monthly-mean mixing ratios (parts per trillion) measured by NOAA (red) and AGAGE (blue) for the three most abundant HCFCs (left-hand scale) (Montzka et al., 2009; O’Doherty et al., 2004). Growth rates (ppt/yr) estimated as 12-month differences from AGAGE (black points) and NOAA (gray points) are shown relative to the right-hand scale and are plotted relative to the midpoint of the 12-month interval. Growth rates smoothed over 12-month periods appear as black and gray lines. Tic marks correspond to the beginning of each year.

12% among the different ground-based measurement networks (Table 1-1).

Losses of CH_3CCl_3 are dominated by oxidation by the hydroxyl radical (OH). Other processes such as photolysis and oceanic removal also are significant sinks for CH_3CCl_3 (Clerbaux and Cunnold et al., 2007; Yvon-Lewis and Butler, 2002). Accurate quantification of all CH_3CCl_3 loss processes is particularly important because budget analyses of this chemical (e.g., Prinn et al., 2005) provide

estimates of global abundance of the hydroxyl radical, an important oxidant for many reduced atmospheric gases.

The potential for significant terrestrial losses of CH_3CCl_3 has been further explored since the previous Assessment. Aerobic soils had been previously identified as a sink for CH_3CCl_3 , accounting for $5 \pm 4\%$ (26 ± 19 Gg/yr) of global removal rates in 1995 (Happell and Wallace, 1998). This estimate was based on soil gas profiles measured in Long Island, New York. A more recent study using flux chamber methods in southern California salt marshes and shrublands showed average net fluxes for CH_3CCl_3 that were $<10\%$ of uptake rates in the Long Island study, suggesting a less significant role for soils as a sink for this compound (Rhew et al., 2008). No new studies related to oceanic losses have been published since 2006; the estimated partial atmospheric lifetime for CH_3CCl_3 with respect to ocean loss remains 94 (81–145) years.

CH_3CCl_3 Emissions and Banks

Emissions of CH_3CCl_3 have declined substantially since the early 1990s. When derived from atmospheric changes and a 5-year lifetime, inferred emissions of CH_3CCl_3 during 2005–2008 are calculated to be less than 10 Gg/yr (Figure 1-3). Banks for CH_3CCl_3 are thought to be negligible owing to its dominant past use in applications resulting in rapid release to the atmosphere.

CH_3CCl_3 emissions arise primarily from industrial production, though some fugitive emissions may arise from its use as a feedstock in the production of HCFC-141b and HCFC-142b. Previous laboratory-based studies of biomass combustion combined with limited field sampling of biomass burning plumes suggested the potential for nonindustrial emissions of 2.5–11.5 Gg/yr CH_3CCl_3 from biomass burning (Rudolph et al., 1995; Rudolph et al., 2000). A recent study of many ambient air samples significantly affected by biomass burning suggests very small or negligible CH_3CCl_3 emissions from this source ($\ll 1$ Gg/yr) (Simpson et al., 2007).

1.2.1.5 HYDROCHLOROFLUOROCARBONS (HCFCs)

HCFCs are regularly measured in three global ground-based networks and at a number of additional sites around the world using grab-sampling techniques (Montzka et al., 2009; O’Doherty et al., 2004; Stemmler et al., 2007; Yokouchi et al., 2006). Results from all three networks indicate that global mean surface mixing ratios of the three most abundant HCFCs (i.e., HCFC-22, -142b, and -141b) continued to increase during 2005–2008 (Figure 1-6). Mixing ratios have also been determined for HCFC-22 and HCFC-142b from Fourier transform infrared (FTIR) instruments onboard the Envisat (the Michelson Interferometer for Passive Atmospheric Sounding, or

MIPAS-E) and Atmospheric Chemistry Experiment (the ACE-Fourier Transform Spectrometer or ACE-FTS instrument) satellites, respectively (Moore and Remedios, 2008; Rinsland et al., 2009).

The global mean surface mixing ratio of HCFC-22 (CHClF_2) was 188–192 ppt in 2008, with an averaged annual growth rate of 8.0 ± 0.5 ppt/yr ($4.3 \pm 0.3\%$ /yr) during 2007–2008 (Table 1-1; Figure 1-6). This increase is approximately 60% larger than the mean rate of change during 1992–2004 or the rate of change reported from global surface sampling networks during 2003–2004 (Clerbaux and Cunnold et al., 2007). Though the rate of HCFC-22 increase from 2007–2008 was comparable to that projected in the A1 scenario of the previous Assessment report (7 ppt/yr; Daniel and Velders et al., 2007), the mixing ratio increase during the entire 2005–2008 period was notably larger than in the scenario projection (Figure 1-1).

Moore and Remedios (2008) report a 2003 global mean HCFC-22 mixing ratio from MIPAS-E at 300 hPa of 177 ± 18 ppt (uncertainty includes 0.5 ppt of random error on the mean and an additional systematic uncertainty); this value is in fairly good agreement with the 2003 global mean surface mixing ratio of 160 ± 2 ppt (Clerbaux and Cunnold et al., 2007). They also deduce an average HCFC-22 growth rate of $3.5 \pm 0.4\%$ /yr (5.4 ± 0.7 ppt/yr) in the northern midlatitude (20°N – 50°N) lower stratosphere (50–300 hPa) between November 1994 and October 2003 from the Atmospheric Trace Molecule Spectroscopy (ATMOS) (Atmospheric Laboratory for Applications and Science, ATLAS-3) based on measured HCFC-22/nitrous oxide (N_2O) correlations. This rate is similar to the $3.92 \pm 2.08\%$ /yr derived using a similar approach with ATMOS and ACE-FTS (from 2004) HCFC-22 data near 30°N (Rinsland et al., 2005). A slightly larger mean growth rate ($4.3 \pm 0.5\%$ /yr or 6.0 ± 0.7 ppt/yr) is estimated for the lower stratosphere from the MIPAS-E HCFC-22 data at southern high latitudes (60°S – 80°S) (Moore and Remedios, 2008). This averaged rate is comparable to global mean HCFC-22 trends at the surface during this period (~ 5.2 ppt/yr).

Total vertical column abundances of HCFC-22 above the Jungfraujoch station (Figure 1-2, an update of Zander et al., 2005) also indicate an increase of $4.31 \pm 0.17\%$ /yr with respect to 2005 values over the 2005–2008 period, which is comparable with NH trends from surface networks (4.2 – 4.5% /yr calculated similarly). Moreover, Gardiner et al. (2008) applied a bootstrap resampling method to aggregated total and partial column data sets from six European remote sensing sites to quantify long-term trends across the measurement network; they found a mean tropospheric increase for HCFC-22 at these sites of $3.18 \pm 0.24\%$ /yr, which is slightly smaller than determined from ground-level grab samples at surface sites in high northern latitudes such as Mace Head, Barrow, or Alert during the analyzed period (1999–2003 rates of 3.7 – 3.9% /yr).

The global mean surface mixing ratio of HCFC-142b (CH_3CClF_2) increased to 18.0–18.9 ppt in 2008 with an averaged annual growth rate of about 1.0–1.2 ppt/yr ($6.1 \pm 0.6\%$ /yr) during 2007–2008 (Table 1-1; Figure 1-6). After declining from the late 1990s to 2003, the growth rate of HCFC-142b increased substantially during 2004–2008. During 2007–2008 this rate was approximately two times faster than reported for 2003–2004 (Montzka et al., 2009). This accelerated accumulation of HCFC-142b was not projected in the A1 scenario of the 2006 Assessment (the projected 2007–2008 rate was 0.2 ppt/yr); a substantial divergence occurred between projected and observed mixing ratios after 2004 (Figure 1-1). The mean difference in reported mixing ratios from AGAGE and NOAA of 3.3% (with AGAGE being higher) is primarily related to calibration differences of $\sim 2.9\%$ reported previously (O'Doherty et al., 2004). Global means from UCI are approximately 2% lower than NOAA (Table 1-1).

The first satellite measurements of HCFC-142b have been made from the ACE-FTS instrument (Rinsland et al., 2009). Monthly-mean ACE-FTS HCFC-142b mixing ratios over 13–16 kilometers (km) altitude, with an estimated total (random and systematic) error of $\sim 20\%$, were used to derive trends at northern (25 – 35°N) and southern (25 – 35°S) midlatitudes of $4.94 \pm 1.51\%$ /yr and $6.63 \pm 1.23\%$ /yr, respectively, over the interval from February 2004 to August 2008. The ACE-FTS trends are consistent with those computed from flask sampling measurements over a similar time period ($5.73 \pm 0.14\%$ /yr at Niwot Ridge (40°N) and $5.46 \pm 0.08\%$ /yr at Cape Grim (40°S) over the interval from July 2003 to July 2008) (Rinsland et al., 2009).

The global mean surface mixing ratio of HCFC-141b ($\text{CH}_3\text{CCl}_2\text{F}$) continued to increase during 2005–2008. By 2008, mean, global surface mixing ratios were 18.8–19.5 ppt (Table 1-1). The growth rate of HCFC-141b decreased from approximately 2 ppt/yr in the mid-1990s to <0.5 ppt/yr in 2004–2005 (Figure 1-6). Since 2005 the growth rate has varied between 0.2–0.8 ppt/yr, similar to the mean 0.5 ppt/yr increase projected in the A1 scenario over this period (Daniel and Velders et al., 2007). The mean increase during 2007–2008 was 0.6 (± 0.1) ppt/yr (or $3.2 \pm 0.5\%$ /yr).

The annual global surface mean mixing ratio of HCFC-124 (CHClFCF_3) has been updated from AGAGE measurements (Prinn et al., 2000) and has decreased to 1.5 ± 0.1 ppt in 2008, with an averaged annual growth rate of -0.01 ± 0.01 ppt/yr ($-0.8 \pm 0.8\%$ /yr) for 2007–2008. No updated HCFC-123 (CHCl_2CF_3) measurements are available.

Recent changes in atmospheric growth rates of the three most abundant HCFCs can be explained qualitatively with UNEP (2010) production and consumption data (Figure 1-7). Global HCFC production for dispersive uses increased rapidly in developed countries during the

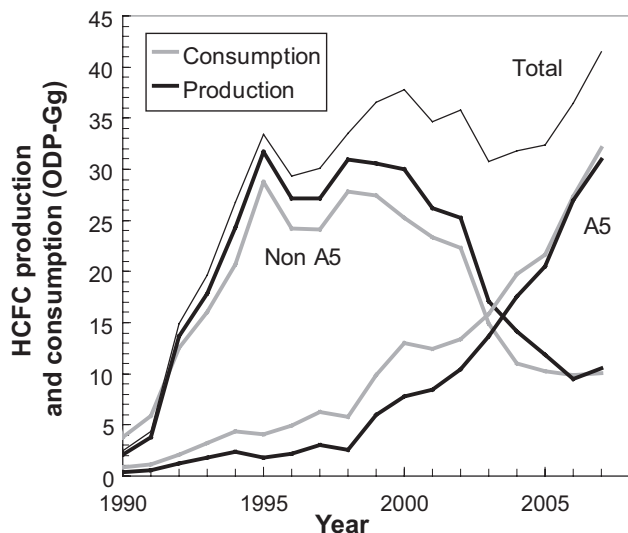


Figure 1-7. Production and consumption (in ODP-Gg) of HCFCs in developed (Non A5) and developing (A5) countries as reported to UNEP for dispersive uses only. Also shown (thin line) is the global total reported production (UNEP, 2010). Note that 1 ODP-Gg = 1 ODP-Kt.

1990s. But as this production was being phased out in developed countries, global totals decreased slightly from 2000–2003. This trend reversed during 2003–2008 as production and consumption grew substantially in developing countries (those operating under Article 5 of the Montreal Protocol, also referred to as A5 countries). In 2008 HCFC data reported to UNEP, developing (A5) countries accounted for 74% and 73% of total, ODP-weighted HCFC consumption and production, respectively (UNEP, 2010).

HCFC Emissions and Banks

Global emissions of HCFC-22 continued to increase during 2005–2008. By 2008, “top-down” emissions inferred from global atmospheric changes totaled 320–380 Gg/yr, up from approximately 280 Gg/yr in 2004. These emissions are reasonably consistent with the emissions derived from banks for 2002 and projected for 2008 in a 2005 study (IPCC/TEAP, 2005) (Figure 1-3). These results suggest that the dominant emission for HCFC-22 is from banks contained in current, in-use applications. Total “bottom-up” emissions derived for past years (UNEP/TEAP, 2006; estimates available through 2003 only) show a similar trend to emissions derived from atmospheric data, but are larger in most years (Figure 1-3).

While atmosphere-derived global emissions for HCFC-141b and HCFC-142b decreased slightly during the 2000–2004 period as production in developed countries was diminishing (Montzka et al., 2009), emissions of

both of these HCFCs increased during 2005–2008 (Figure 1-3). The substantial increase in HCFC-142b emissions was not projected in the A1 scenario of the previous Assessment (Daniel and Velders, 2007). In that scenario, a 23% emissions decline was projected during 2004 to 2008 (relative to 2004 levels). Instead, HCFC-142b emissions in 2008 derived from observed global mixing ratio changes (37 ± 7 Gg/yr) were approximately two times larger than had been projected for that year. Changes in HCFC-141b emissions during 2005–2008 were quite consistent with those projected in the A1 scenario (Daniel and Velders, 2007).

“Bottom-up” estimates of HCFC-141b emissions (UNEP/TEAP, 2006) have captured the overall increase in emissions of this compound derived from “top-down” calculations, but with a slightly different time lag. Similar “bottom-up” estimates of HCFC-142b have also captured the rough changes implied from atmospheric data, but in this case, the “bottom-up” estimates are substantially lower than implied from year-to-year atmospheric observations during 2000–2004 (Figure 1-3). For both HCFCs, it is apparent that emissions from banks estimated for 2002 and projected for 2008 (IPCC/TEAP, 2005) account for <50% of total emissions for these compounds. About 10–20% of annual production of HCFC-141b is for solvent uses that result in release to the atmosphere shortly after production (UNEP/TEAP, 2006). Based on production data this would yield emissions of 10–20 Gg/yr and explain some of the difference between atmosphere-derived emissions and bank-related emissions (UNEP/TEAP, 2006). Rapid losses of HCFC-142b during or shortly after production would also provide an explanation for only some of the shortfall in emissions not explained by bank releases. HCFC bank magnitudes have increased in recent years given that reported production in recent years has substantially exceeded emissions (Montzka et al., 2009).

Summed, “top-down” emissions from HCFCs have increased during 2005–2008. When weighted by semi-empirical ODPs (Chapter 5), the sum of emissions from HCFCs totaled 22 ± 2 ODP-Kt in 2008. The sum of emissions of HCFCs weighted by direct, 100-yr GWPs has increased on average by $5 \pm 2\%$ /yr from 2004 to 2008, and by 2008 amounted to 0.74 ± 0.05 Gt CO₂-eq/yr.

The 2007 Adjustments to the Montreal Protocol are expected to have a discernable influence on HCFC emissions in the coming decade (see Chapter 5). But because those Adjustments are scheduled to affect HCFC production and consumption only after 2009, it is too soon to discern any influence of these Protocol adjustments in the mixing ratios or emissions derived for 2008 or earlier years reported in this Assessment.

Regional emissions for HCFCs from atmospheric measurements (Box 1-1) have been derived in different studies since the previous Assessment report. Compari-

sions with “bottom-up” estimates provide useful information on the accuracy of individual country accounting of their emissions of ODSs and regional estimates derived from atmospheric measurements. In an analysis of United States (U.S.) HCFC emissions, HCFC-22 mean emissions during 2004–2006 were estimated from aircraft measurements to be 46 (21–69) Gg/yr, or substantially lower than amounts derived from “bottom-up” estimates (Millet et al., 2009). U.S. HCFC-22 emissions estimated with “bottom-up” inventory methods by the U.S. Environmental Protection Agency (EPA) were estimated at between 89 and 97 Gg/yr during 2004–2008 and have been used to derive a U.S. contribution to global HCFC-22 atmospheric mixing ratios of between 21 and 45% during 2006 (Montzka et al., 2008).

Detailed analyses of HCFC emissions have also been reported for China in recent years, concurrent with a substantial increase in reported HCFC production and consumption in this country. Inventory-based, “bottom-up” estimates suggest HCFC-22 emissions increasing from 34 to 69 Gg/yr during 2004–2007 (Wan et al., 2009), or 12–20% of total global emissions during these years. Atmosphere-derived emissions attributed to China based on correlations to carbon monoxide (CO) and inversion modeling of elevated mixing ratios at down-wind sampling locations suggest slightly larger emissions than the inventory approach (52 ± 34 Gg/yr as the average of 2004–2005 from Yokouchi et al., 2006; 60 and 71 Gg/yr for 2005 and 2006 from Stohl et al. (2009); and 165 (140–213) Gg/yr in 2007 from Vollmer et al. (2009), though the Vollmer et al. (2009) estimate may be biased high because of relatively higher per-capita HCFC-22 emissions near Beijing than in other regions of China (Stohl et al., 2009)).

1.2.1.6 METHYL BROMIDE (CH₃Br)

The global, annual mean surface mixing ratio of methyl bromide (CH₃Br) had reached 7.3 to 7.5 ppt in 2008 (Figure 1-8; Table 1-1), down from the 9.2 ppt measured during the three years (1996–1998) before industrial production declined as a result of the Montreal Protocol (Yvon-Lewis et al., 2009). Global mixing ratios declined during 2005–2008 at a rate of -0.14 ppt/yr, which is slightly slower than the mean decline observed since 1999 when industrial production was first reduced. Since 1999, the annual mean hemispheric difference (NH minus SH) has decreased by nearly 50%: this measured difference was 1.2 ppt in 2008 compared to 2.3 ± 0.1 ppt during 1996–1998 (Figure 1-8).

Declines in the global tropospheric abundance and hemispheric difference of CH₃Br have coincided with decreases in global industrial production and subsequent emission. Reported global methyl bromide consumption in 2008 for all uses including uncontrolled quarantine and

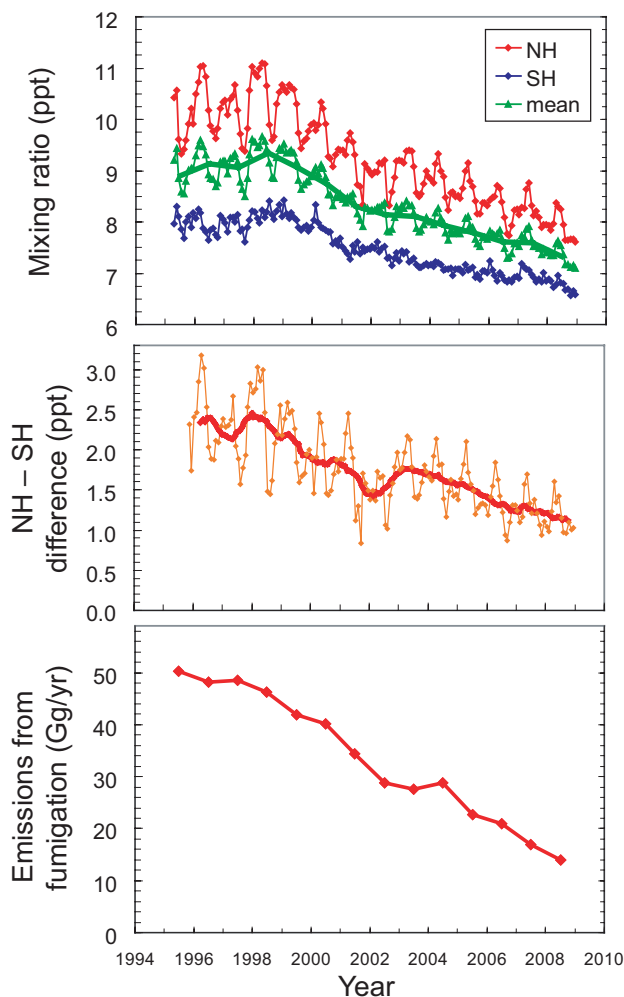


Figure 1-8. Top panel: Monthly hemispheric means for CH₃Br mixing ratios (ppt) (Montzka et al., 2003 updated). Middle panel: NH - SH difference by month (points) and smoothed over 12-month periods (bold red line). Bottom panel: Fumigation-related emissions (Gg/yr) of CH₃Br derived from reported regulated consumption $\times 0.65$ plus reported quarantine and pre-shipment consumption $\times 0.84$ (UNEP 2007b), where 0.65 and 0.84 are the estimated mean fractions of reported production to these different uses that ultimately become emitted to the atmosphere (UNEP 2007b).

pre-shipment (QPS) uses was 73% below peak amounts reported in the late 1990s. An emission history derived from these reported data suggests a reduction in total fumigation-related CH₃Br emissions of 71% by the end of 2008 (see Figure 1-8).

The concurrent decline in the measured hemispheric difference and industrially derived emissions suggests a mean hemispheric mixing ratio difference close to 0 ppt

Table 1-2. Summary of the estimated source and sink strengths (Gg/yr) of methyl bromide (CH₃Br) for periods 1996–1998 and 2008.

	1996–1998	Range	2008	Range	Reference	Note
SOURCES						
Fumigation- dispersive (soils)	41.5	(28.1 to 55.6)	6.7	(4.6 to 9.0)	1, 2	a
Fumigation- quarantine/ pre-shipment	7.9	(7.4 to 8.5)	7.6	(7.1 to 8.1)	1, 2	b
Ocean	42	(34 to 49)	42	(34 to 49)	3, 4	c
Biomass Burning	29	(10 to 40)	29	(10 to 40)	5, 6	d
Leaded gasoline	5.7	(4.0 to 7.4)	< 5.7		7	e
Temperate peatlands*	0.6	(–0.1 to 1.3)	0.6	(–0.1 to 1.3)	8, 9, 10	f
Rice paddies*	0.7	(0.1 to 1.7)	0.7	(0.1 to 1.7)	11, 12	g
Coastal salt marshes*	7	(0.6 to 14)	7	(0.6 to 14)		h
<i>based on California saltmarshes</i>	14	(7 to 29)	14	(7 to 29)	13, 14	i
<i>based on Scottish saltmarsh</i>	1	(0.5 to 3.0)	1	(0.5 to 3.0)	15	j
<i>based on Tasmania saltmarsh</i>	0.6	(0.2 to 1.0)	0.6	(0.2 to 1.0)	16	k
Mangroves	1.3	(1.2 to 1.3)	1.3	(1.2 to 1.3)	17	l
Shrublands*	0.2	(0 to 1)	0.2	(0 to 1)	18	m
Rapeseed	4.9	(3.8 to 5.8)	5.1	(4.0 to 6.1)	19	n
Fungus (litter decay)	1.7	(0.5 to 5.2)	1.7	(0.5 to 5.2)	20	o
Fungus (leaf-cutter ants)	0.5		0.5		21	p
Potential terrestrial sources						q
Tropical trees	n.q.		n.q.		22, 23	r
Temperate woodlands	n.q.		n.q.		24, 25	s
Tropical ferns	n.q.		n.q.		26	
Abiotic decomposition	n.q.		n.q.		27	t
Subtotal (Sources)	143		111.5			
SINKS						
Ocean	56	(49 to 64)	49	(45 to 52)	3	u
OH and photolysis	77		63.6		3	v
Soils	40	(23 to 56)	32	(19 to 44)	28–33	w
Subtotal (Sinks)	177		147.6			
Total (SOURCES–SINKS)	–34		–36.1			

* All asterisked items were estimated from measurements of net fluxes and may be influenced by sinks within them, thus they represent minimum gross fluxes. n.q. = not quantified.

Notes:

- Soil fumigation emission rates estimated as 65% (46–91%) of reported consumption rates (ref 2).
- QPS emission rates estimated as 84% (78–90%) of reported consumption rates (ref 2).
- Oceanic production rate calculated based on saturation state of pre-phase-out ocean: production = net oceanic flux – ocean sink, where net flux is –14 (–7 to –22) Gg/yr.
- Biomass burning estimates unchanged from the previous Assessment (Clerbaux and Cunnold et al., 2007), which is slightly higher than the 18–23 Gg/yr estimate in ref (3).
- 2006–2008 values are not separately quantified but expected to be lower with the phase-out of leaded gasoline use.
- Temperate peatlands net flux calculated by updating (ref 7) with 3-year average fluxes at same New Hampshire sites (ref 8). Range includes median estimate of 0.9 Gg/yr from Irish peatland study (ref 10).

Table 1-2, continued (notes).

- g. Re-evaluation of global emission rates that were previously estimated as 3.5 Gg/yr in ref (11).
- h. Salt marsh net flux estimated as the mid-range of the best estimates provided from four different studies.
- i. Estimates were 14 (7–29) Gg/yr (from ref 13) and 8 to 24 Gg/yr (ref 14) depending on whether extrapolation incorporated or excluded mudflats, respectively.
- j. Low and high range based on lowest and highest emitting of eight sites in ref (15).
- k. Extrapolations calculated using mean fluxes reported in ref (16).
- l. Based on study of two mangrove species, with range as results of two different methods of extrapolation.
- m. Shrublands range as reported in Montzka and Fraser et al. (2003).
- n. Rapeseed flux as reported in ref (19) with year-by-year data from author. 2007–2008 data uses results for 2003, the last year estimated.
- o. These emission rates may possibly incorporate emission rates reported for woodlands and forest soils.
- p. No range provided.
- q. Terrestrial sources are poorly quantified and based on very limited studies so are not included in the tabulated sources.
- r. Global extrapolations based on measurements of Malaysian trees (18 Gg/yr in ref 22) exceed the upper limit on net flux estimated in a study of a tropical South American rainforest (17 Gg/yr in ref 23), so no discrete estimate is included here.
- s. Range of temperate woodland fluxes of 0.4 to 3.1 Gg/yr can be estimated by extrapolating net fluxes in ref (24) and gross production rates in ref (25) to global area of 13×10^{12} m². Eucalyptus forest floor shows no net emissions (ref 16).
- t. The largest abiotic production rates, observed from the decomposition of saltwort leaves (ref 27), are roughly 2% of the emission rates from the live saltwort plant (ref 14).
- u. Oceanic consumption calculated assuming production rates constant, with a decrease in saturation anomaly because of decreasing atmospheric concentrations, with global average net flux in 2007 predicted to be -6.6 (-3.3 to -10.4) Gg/yr. Range assumes the same net flux error range as 1996–1998 (as percent of flux).
- v. A range has not been provided here.
- w. Soil sink (refs. 28, 29) scaled to updated background Northern Hemisphere concentrations of 10.3 ppt (1996–1998) and 8.2 ppt (2006–2008), and includes a new tundra sink (refs. 30, 31) and a revised average temperate grasslands flux (refs. 28, 32, 33).

References:

1. UNEP, 2010. 2. UNEP, 2007b. 3. Yvon-Lewis et al., 2009. 4. King et al., 2002. 5. Clerbaux and Cunnold et al., 2007. 6. Andreae and Merlet, 2001. 7. Thomas et al., 1997. 8. Varner et al., 1999a. 9. White et al., 2005. 10. Dimmer et al., 2001. 11. Redeker and Cicerone, 2004. 12. Lee-Taylor and Redeker, 2005. 13. Rhew et al., 2000. 14. Manley et al., 2006. 15. Drewer et al., 2006. 16. Cox et al., 2004. 17. Manley et al., 2007. 18. Rhew et al., 2001. 19. Mead et al., 2008b. 20. Lee-Taylor and Holland, 2000. 21. Mead et al., 2008a. 22. Blei et al., 2010. 23. Gebhardt et al., 2008. 24. Drewer et al., 2008. 25. Rhew et al., 2010. 26. Saito and Yokouchi, 2006. 27. Wishkerman et al., 2008. 28. Shorter et al., 1995. 29. Varner et al., 1999b. 30. Rhew et al., 2007. 31. Hardacre et al., 2009. 32. Rhew and Abel, 2007. 33. Teh et al., 2008.

for CH₃Br in preindustrial times. Accordingly, the pre-1990 global mixing ratio trend used in creating scenario A1 for CH₃Br in Chapter 5 was derived from Southern Hemisphere firm data by including a time-varying hemispheric ratio that increased linearly from 1.0 in 1940 to 1.3 in 1995.

In the past, much research related to methyl bromide focused on refining our understanding of source and sink magnitudes in order to understand the relative contribution of anthropogenic methyl bromide emissions to methyl bromide atmospheric abundance and, therefore, provide more accurate projections of the atmospheric response to reduced industrial production. For example, the global measured decline since 1996–1998 of ~2 ppt in response to a decline in fumigation emissions of 60–70% suggests a total contribution from fumigation-related production before the phase-out (i.e., during 1996–1998) of 2.8–3.2 ppt (provided other sources or loss frequencies did not change appreciably). Considering that peak global mixing ratios were 9.2 ppt during 1996–1998, this suggests that industrially derived emissions accounted for 31–36% of total CH₃Br emissions in the three years before the phase-out began.

A recent modeling analysis of global atmospheric CH₃Br observations provided additional constraints to our

understanding (Yvon-Lewis et al., 2009). It suggested that the observed global declines are well explained given our understanding of CH₃Br sources and sinks and the known changes in anthropogenic emissions, though a substantial source (~35 Gg/yr) is still unaccounted for in current budget compilations (Yvon-Lewis et al., 2009) (Table 1-2). The best-estimate budget derived in this work (based on observed global and hemispheric mixing ratio trends and seasonal variations together with time-varying sources and sinks) suggested a pre-phase-out anthropogenic fumigation contribution of ~28%. Though uncertainties in the variability of natural emissions and in the magnitude of methyl bromide stockpiles in recent years add uncertainty to our understanding of this ratio, when these new model results are considered together with the more simple analysis of methyl bromide mixing ratio changes since 1999 (see previous paragraph), a pre-phase-out anthropogenic contribution of 25–35% is estimated.

Our understanding of preindustrial mixing ratios of methyl bromide in the Southern Hemisphere has improved since the 2006 Assessment. A 2000-year record derived for methyl bromide from an ice core collected at South Pole (Saltzman et al., 2008) shows no systematic trend and a mean mixing ratio in samples with mean ages from 160 Before the Common Era (BCE) to 1860 CE of 5.39 ± 0.06

ppt (uncertainty represents 1 standard error here). This preindustrial mixing ratio is similar to the 5.1–5.5 ppt observed in the deepest firn-air samples at South Pole and Law Dome, Antarctica (Butler et al., 1999; Trudinger et al., 2004) and previous ice-core results at a different site in Antarctica in samples dated 1671–1942 CE (5.8 ppt; Saltzman et al., 2004). Based on these preindustrial SH mixing ratio results, the observed decline in SH mixing ratios from their peak (8.0 ppt) through the end of 2008 (6.7 ppt) suggests that SH mixing ratios have declined 50–60% of the way back to preindustrial levels as industrial production declined by a similar magnitude (60–70%).

The concurrence between global atmospheric changes relative to expected emissions declines, the decreased NH–SH differences, and the decline in the mean SH mixing ratio much of the way back to its preindustrial value, all suggest that production restrictions on CH₃Br have been successful at substantially reducing the global atmospheric abundance of CH₃Br. It is worth noting that this benefit was achieved despite substantial emissions from natural sources and an incomplete understanding of the global budget of CH₃Br.

Budget

Significant uncertainties remain in the detailed atmospheric budget of methyl bromide despite additional research since the previous Assessment. As indicated above, known sinks still outweigh best estimates of known sources by about 35 Gg/yr or roughly 20% of the total annual flux. This discrepancy remains even though the tropospheric burden, known sources, and known sinks have quantifiably changed in the last decade.

In light of the changing atmospheric concentrations of CH₃Br, separate budgets are created for pre-phase-out (1996–1998) and the 2008 atmospheres (Table 1-2). Reported consumption of CH₃Br from fumigation (dispersive and quarantine/pre-shipment uses) declined 73% between these periods, from 70.5 Gg/yr to 18.9 Gg/yr (UNEP, 2010). Before phase-out, pre-plant soil fumigation was the major use for CH₃Br, but this use had declined by 84% by 2008. Over the same period, CH₃Br consumption for quarantine and pre-shipment (QPS) applications has ranged between 7.5 and 12.5 Gg/yr, as this particular application is an exempted use (UNEP, 2010). As a result, consumption for QPS use accounted for nearly 50% of total global CH₃Br uses during 2007 and 2008 (UNEP, 2010). These values do not include production for use as a chemical feedstock, which is assumed to be completely consumed and which averaged 3.9 Gg/yr from 1995–1997 and 6.6 Gg/yr from 2003–2005 (the last three years reported in UNEP, 2007b).

Other anthropogenically influenced sources of CH₃Br include leaded gasoline combustion, biomass

burning, and growth of certain methyl bromide-emitting crops. Our understanding of the amount of methyl bromide emitted from biomass burning remains unchanged from the previous Assessment report as 29 (10 to 40) Gg/yr. Biomass burning emissions, however, vary substantially from year to year and peaked in 1998 during the strong El Niño event and enhanced burning then (van der Werf et al., 2004; Yvon-Lewis et al., 2009). Emissions from biofuel burning in the developing world are included in the above estimate, although they have been derived separately to be 6.1 ± 3.1 Gg/yr (Yvon-Lewis et al., 2009). Crop production levels of rapeseed (canola) and rice, two known crop sources of methyl bromide, have been increasing steadily due to demand for food supply and biofuel (FAO, 2009). A recent extrapolation of rapeseed CH₃Br emissions using crop harvest, growth rate, and global production data suggest a three- to four-fold increase from 1980 to 2003 (Mead et al., 2008a). In this new study, estimated average emission rates ranged from 4.3 to 6.2 Gg/yr between 1996 and 2003 (the final year estimated). These values are slightly less than the previous estimate of 6.6 Gg/yr (Clerbaux and Cunnold et al., 2007; Gan et al., 1998). While cabbage and mustard production also are increasing, total emission from these crops is estimated at <0.1 Gg/yr. A re-evaluation of CH₃Br emission from rice crops using a model incorporating temperature, seasonality, and soil moisture effects yields a lower source estimate (0.5 to 0.9 Gg/yr) than derived previously (3.5 Gg/yr) (Lee-Taylor and Redeker, 2005; Redeker and Cicerone, 2004).

Emission rates from the three known major natural sources (oceans, freshwater wetlands, and coastal salt marshes) have been revised downward since the 2002 Assessment (compare Table 1-2 to Table 1-9 in Montzka and Fraser et al., 2003). Ocean production rates have been revised from 63 (23–119) Gg/yr down to 42 (34–49) Gg/yr (Yvon-Lewis et al., 2009). Freshwater wetlands were previously estimated as a 4.6 (2.3 to 9.2) Gg/yr net source based on a partial season of measurements from two New Hampshire peatlands (Varner et al., 1999a). This source, specified in Table 1-2 as temperate peatlands, has been revised downward to 0.6 (–0.1 to 1.3) Gg/yr based on a 3-year study at the same New Hampshire sites, which showed much lower average net fluxes (White et al., 2005). Coastal salt marshes were previously estimated as a 14 (7–29) Gg/yr source based on a study of two southern California salt marshes (33°N) (Rhew et al., 2000). While a separate, nearby study (34°N) found similar net fluxes, the global extrapolations varied from 8 Gg/yr (assuming salt marsh areas included low-producing mudflats) to 24 Gg/yr (assuming surface areas were entirely vegetated) (Manley et al., 2006). However, much smaller CH₃Br net emission rates were observed from coastal salt marshes in Scotland (56°N) (Drewer et al., 2006) and Tasmania, Aus-

tralia (41°S) (Cox et al., 2004), which suggested global emission rates of 1 (0.5–3.0) Gg/yr and 0.6 (0.2–1.0) Gg/yr, respectively. Because emissions are strongly related to plant species and climatic conditions, the quantification of this source requires a more detailed understanding of salt marsh distributions and vegetation types. The updated value in Table 1-2 (7 Gg/yr) represents the mid-range of globally extrapolated fluxes, with the full range representing the various study mean values.

Since the previous Assessment report, several additional natural CH₃Br sources have been identified (see Table 1-2), although the addition of these sources does not yet resolve the budget imbalance between sources and sinks. Mangroves (Manley et al., 2007) and fungus cultivated by leaf-cutter ants (Mead et al., 2008b) are newly identified sources, although they are estimated to be relatively minor sources globally. Measurements from tropical trees (Blei et al., 2010) and ferns (Saito and Yokouchi, 2006) in SE Asia suggest that these may be large sources, up to 18 Gg/yr if results from these studies are globally representative. Aircraft measurements over a South American rainforest revealed no significant net emissions, however, and suggest an upper limit of 17 Gg/yr for the global tropical forest flux (Gebhardt et al., 2008). Because of this disparity, this source is not included in Table 1-2. In addition to the previously identified mechanism to produce methyl halides abiotically from the degradation of organic matter (Keppler et al., 2000), the abiotic production of methyl bromide in plant material has also been shown (Wishkerman et al., 2008); it is not clear how important these mechanisms are in relation to biotic production rates.

Natural terrestrial ecosystems can be both sources (e.g., from fungi, litter decomposition, certain plant species) and sinks (biological degradation in soils) for CH₃Br. Both emissions and uptake have been observed in temperate grasslands (Cox et al., 2004; Rhew and Abel, 2007; Teh et al., 2008), temperate forest (Dimmer et al., 2001; Varner et al., 2003), temperate shrubland (Rhew et al., 2001), and Arctic tundra (Rhew et al., 2007; Teh et al., 2009). Temperate woodland soils in Scotland are a net source for CH₃Br (Drewer et al., 2008) while oak-savanna woodland soils in California are a net sink (Rhew et al., 2010). To better understand the highly variable net fluxes found in many of these ecosystems, measurements of gross production and consumption rates have been derived by clearing vegetation from some sites (White et al., 2005; Drewer et al., 2006), using a stable isotope tracer method (Rhew and Abel, 2007; Teh et al., 2008; Teh et al., 2009; Rhew et al., 2010), or modeling soil uptake separately (Varner et al., 2003).

Known sinks of CH₃Br (oceans, OH, photolysis, and soil microbial uptake) have uptake rates that scale to tropospheric concentrations and, therefore, have declined in the current decade, as indicated in Table 1-2 (Yvon-Lewis et al., 2009). The partial lifetime of atmospheric

CH₃Br with respect to ocean loss has been updated to 2.2–2.4 years based on new model results (Yvon-Lewis et al., 2009). The partial lifetime with respect to loss by oxidation by OH and photolysis remains unchanged at 1.7 years. The partial lifetime with respect to soil loss has increased from 3.1 years to 3.3 to 3.4 years, as described below. The best estimate lifetime for atmospheric CH₃Br has therefore increased slightly from 0.7 years to 0.8 years.

In the last two Assessment reports (Clerbaux and Cunnold et al., 2007; Montzka and Fraser et al., 2003), the soil sink was estimated to be 47 Gg/yr based on earlier studies that assumed Northern Hemisphere tropospheric concentrations of 11 ppt. The soil sink was recalculated for 1996–1998 and 2008 using background Northern Hemisphere concentrations of 10.3 ppt and 8.2 ppt, respectively, to yield uptake rates of 44 ± 15 and 35 ± 12 Gg/yr, respectively. The addition of the tundra sink (0.31 ± 0.06 Gg/yr) does not significantly change these results (Rhew et al., 2007; Hardacre et al., 2009). However, recent field studies in temperate grasslands in California (Rhew and Abel, 2007) and Colorado (Teh et al., 2008) show gross uptake rates that are one-fourth and one-eighth of the previous temperate grassland uptake rates. The average growing season uptake rate incorporating these new studies is half of the previously reported flux for temperate grasslands, which implies a 15% reduction of the soil sink to 40 ± 16 Gg/yr for 1996–1998 and 32 ± 13 Gg/yr for 2008. While still within the range of errors, the best estimate for partial atmospheric lifetime for CH₃Br with respect to the soil sink would be increased from 3.0–3.1 years to 3.3–3.4 years. New results from a temperate woodland also suggest lower soil uptake rates (Rhew et al., 2010), but these were not included in the revised soil uptake rate here.

1.2.1.7 METHYL CHLORIDE (CH₃Cl)

Methyl chloride is the most abundant chlorine-containing organic compound in the atmosphere and contributes 16% to the total chlorine from long-lived gases in the troposphere (see, for example, Table 1-12). Although it is not a controlled substance, CH₃Cl has several natural sources and sinks in common with CH₃Br, which is a controlled substance. Thus, atmospheric changes in CH₃Cl and an updated knowledge of its global budgets can provide a context for understanding a large amount of atmospheric Cl that is not controlled by the Montreal Protocol, as well as insights into changes in the natural CH₃Br budget.

Global mixing ratios of CH₃Cl increased by small amounts during 2004–2008 (2.3 to 2.7 ± 1.2 ppt/yr, or 0.4 – $0.5 \pm 0.2\%$ /yr), though these changes follow larger decreases reported for 1998–2001 of -1.5% /yr (Simmonds et al., 2004). Changes observed from 2007 to 2008 are small,

though both increases and decreases are reported by different measurements networks. The cause of these differences is not well documented, but the differences may be insignificant relative to measurement errors, or may reflect regional variations in rates of change for this compound.

Incorporating CH₃Cl observations from global and regional networks (AGAGE, NOAA, System for Observation of halogenated Greenhouse gases in Europe (SOGE), National Institute for Environmental Studies (NIES)) into a 3-D global chemical transport model, Xiao et al. (2010a) estimated global emissions for 2000–2004 to be 4.10 ± 0.47 Tg/yr, which is comparable to emissions reported in the previous Assessment (4.1 to 4.4 Tg/yr, Clerbaux and Cunnold et al., 2007). Model results indicate that about 55%, or 2.3 ± 0.3 Tg/yr, of CH₃Cl comes from tropical terrestrial sources that vary with global temperature changes (Xiao et al., 2010a). This is also comparable to prior model study estimates of 2.4 to 2.9 Tg/yr from tropical ecosystems, as reported in the previous Assessment.

Since the previous Assessment, several studies on South American and Asian rainforests have reinforced the importance of the tropical terrestrial CH₃Cl source. Air samples obtained by aircraft over South American tropical rainforests (Suriname, French Guyana) in 2005 indicated net emissions of CH₃Cl (Gebhardt et al., 2008). A survey of 197 plants from the subtropical island of Iriomote (Japan) found that 18% produced significant amounts of CH₃Cl (Yokouchi et al., 2007), while a survey of 119 tree species from tropical Malaysia found that 21% produced significant amounts of CH₃Cl (Saito et al., 2008). A separate study in Malaysian Borneo showed large emissions from live plants, though much smaller emissions were found from leaf litter (Blei et al., 2010). Global tropical source estimates based on extrapolations of the above studies ranged from 0.9 to 2.5 Tg/yr (Blei et al., 2010; Gebhardt et al., 2008; Saito et al., 2008; Yokouchi et al., 2007). These values are on the lower side of estimates of tropical emission magnitudes provided in the previous Assessment. Additional minor tropical sources of CH₃Cl have been identified, including mangroves (~ 0.011 Tg/yr) (Manley et al., 2007; Yokouchi et al., 2007) and fungus cultivated by leaf cutter ants (< 0.001 Tg/yr) (Mead et al., 2008b).

Emissions of CH₃Cl can originate from biogenic production by vascular plants (Yokouchi et al., 2002), abiotic release from dead or senescent plant material (Hamilton et al., 2003), and emissions from tropical wood-rot fungi (Moore et al., 2005). Mass balance approaches have been used to estimate emission magnitudes from sources that have distinct stable carbon isotope ratios ($\delta^{13}\text{C}$). Methyl chloride produced from the abiotic methylation of chloride has an exceptionally depleted $\delta^{13}\text{C}$ value (Keppler et al., 2004), and a mass balance approach suggests that this mechanism is a dominant source of atmospheric CH₃Cl in terrestrial tropical and subtropical ecosystems at

1.8 to 2.5 Tg/yr (Keppler et al., 2005). Saito and Yokouchi (2008) also use an isotopic mass balance approach, incorporating more recent isotopic measurements of CH₃Cl from tropical plants, and estimate the total tropical source to be 2.9 to 4.2 Tg/yr, with 1.5 to 3.0 Tg/yr coming from live vegetation and the remainder from abiotic production from senescent leaves.

Biomass burning, oceans, and anthropogenic activities are major sources of atmospheric CH₃Cl. A mechanism to produce CH₃Cl through the photochemical reaction of dissolved organic matter in saline waters has been reported (Moore, 2008). Supersaturations of CH₃Cl have been observed in coastal waters off of the United States (Hu et al., 2010) and China (Lu et al., 2010), and global coastal emissions may increase the global oceanic emission estimate by 0.02 to 0.10 Tg/yr (Hu et al., 2010). The inversion analysis of Xiao et al. (2010a) suggests emissions of 0.43 ± 0.1 Tg/yr from the global ocean, consistent with the estimate of 0.38–0.51 Tg/yr in the previous Assessment. Though there are no updates to the biomass burning and anthropogenic source terms, the Xiao et al. (2010a) inversion analysis suggests global biomass burning emissions of 0.92 ± 0.2 Tg/yr.

Coastal salt marshes were previously estimated to be a large CH₃Cl source, up to 0.17 (0.07 to 0.44) Tg/yr, based on measurements in southern California (Rhew et al., 2000). Recent studies, however, show large geographic variability in this source and high sensitivity to methods of extrapolation. Measurements at a different southern California salt marsh scale up to 0.05 to 0.16 Tg/yr, depending on whether or not the areal averaging incorporates low-producing mudflats along with vegetated areas (Manley et al., 2006). Much smaller emission rates observed at a salt marsh in Tasmania scale to < 0.01 Tg/yr (Cox et al., 2004). A salt marsh in China appeared to be a net sink during the growing season, though these results were derived under unusually high ambient concentrations (1–60 parts per billion (ppb)) (Wang et al., 2006).

The major sinks of tropospheric CH₃Cl include oxidation by hydroxyl radicals, loss to the stratosphere, reaction with chlorine radicals, loss to polar ocean waters, and uptake by soils. These sink estimates remain largely unmodified since the previous Assessment so the CH₃Cl lifetime remains unchanged (Table 1-3), although a study using stable isotope ratios suggests that the soil sink may be much larger than previously estimated (Keppler et al., 2005). The Arctic tundra appears to be a net sink for CH₃Cl, with uptake rates increasing under drier conditions (Rhew et al., 2007; Teh et al., 2009). However, measurements at a sub-Arctic wetland show a small net source for CH₃Cl (Hardacre et al., 2009). The causes of such geographic differences are not currently understood, although there are significant temperature, vegetation, and hydrological differences between the two regions.

Table 1-3. Global trace gas lifetimes for selected halocarbons with lifetimes longer than 0.5 years.
(See Table 1-4 for estimates of local lifetimes for short-lived gases).

Industrial Designation or Common Name	Chemical Formula	Total Lifetime from Previous Assessments ^a (years)	New Total Lifetime ^a (years)	OH Lifetime ^d (years)	Stratospheric Lifetime (years)	Notes
Halogenated Methanes						
HFC-41	CH ₃ F	2.4	2.8	2.9	64	2, 5, 6
HFC-32	CH ₂ F ₂	4.9	5.2	5.5	89	1, 4
HFC-23	CHF ₃	270	222	245	2347	2, 4
PFC-14 (Carbon tetrafluoride)	CF ₄	50,000	> 50,000		> 50,000	7
Methyl chloride	CH ₃ Cl	1.0	1.0	1.5		1, 8
Carbon tetrachloride	CCl ₄	26	26		35	see text and Box 1-2
HCFC-31	CH ₂ ClF	1.3	1.3	1.3	38	1, 5, 9
HCFC-22	CHClF ₂	12.0	11.9	12.8	186	1, 4
HCFC-21	CHCl ₂ F	1.7	1.7	1.8	33	1, 5, 6, 9
CFC-11	CCl ₃ F	45	45		45	8
CFC-12	CCl ₂ F ₂	100	100		100	8
CFC-13	CClF ₃	640	640		640	7
Methyl bromide	CH ₃ Br	0.7	0.8	1.9		1, see text
Bromodifluoromethane	CHBrF ₂	5.8	5.2	6.0	39	1, 5, 9
Halon-1301	CBrF ₃	65	65		65	8
Halon-1211	CBrClF ₂	16	16			8, 10
Halon-1202	CBr ₂ F ₂	2.9	2.9			8, 11
Halogenated Ethanes						
HFC-152a	CH ₃ CHF ₂	1.4	1.5	1.6	45.4	2, 4, 6
HFC-143	CH ₂ FCHF ₂	3.5	3.5	3.7	73	1, 5
HFC-143a	CH ₃ CF ₃	52	47.1	55	327	1, 4
HFC-134	CHF ₂ CHF ₂	9.6	9.7	10.5	134	1, 5
HFC-134a	CH ₂ FCF ₃	14.0	13.4	14.3	232	1, 4, 6
HFC-125	CHF ₂ CF ₃	29	28.2	32	246	1, 4, 6
PFC-116 (Perfluoroethane)	CF ₃ CF ₃	10,000	> 10,000		> 10,000	7
Methyl chloroform	CH ₃ CCl ₃	5.0	5.0	6.1 ^e	39	1, 8
HCFC-141b	CH ₃ CCl ₂ F	9.3	9.2	10.7	64.9	1, 4, 6
HCFC-142b	CH ₃ CClF ₂	17.9	17.2	19.3	160	1, 4, 6
HCFC-133a	CH ₂ ClCF ₃		4.3	4.5	72	2, 5, 9
HCFC-123	CHCl ₂ CF ₃	1.3	1.3	1.4	35.6	1, 4, 6
HCFC-123a	CHClF ₂ CF ₂ Cl		4.0	4.3	63	1, 5, 9

Table 1-3, continued.

Industrial Designation or Common Name	Chemical Formula	Total Lifetime from Previous Assessments ^a (years)	New Total Lifetime ^a (years)	OH Lifetime ^d (years)	Stratospheric Lifetime (years)	Notes
HCFC-123b	CHF ₂ CCl ₂ F		6.2	~7	52	5, 9, 12
HCFC-124	CHClFCF ₃	5.8	5.9	6.3	111	1, 4, 6
HCFC-124a	CHF ₂ CClF ₂		9.1	~10	107	5, 9, 12
CFC-113	CCl ₂ FCClF ₂	85	85		85	8
CFC-113a	CCl ₃ CF ₃		~45		~45	13
CFC-114	CClF ₂ CClF ₂	300	190		190	34
CFC-114a	CCl ₂ FCF ₃		~100		~100	14
CFC-115	CClF ₂ CF ₃	1,700	1020		1020	34
Halon-2311 (Halothane)	CHBrClCF ₃		1.0	1.1	11	1, 5, 9
Halon-2402	CBrF ₂ CBBrF ₂	20	20			8, 10
Halogenated Propanes						
HFC-263fb	CH ₃ CH ₂ CF ₃	1.6	1.2	1.2	38	2, 5
HFC-245ca	CH ₂ FCF ₂ CHF ₂	6.2	6.5	6.9	105	1, 5
HFC-245ea	CHF ₂ CHFCHF ₂	4.0	3.2	3.4	70	2, 5
HFC-245eb	CH ₂ FCHFCF ₃	4.0	3.1	3.3	69	2, 5
HFC-245fa	CHF ₂ CH ₂ CF ₃	7.6	7.7	8.2	116	1, 5
HFC-236cb	CH ₂ FCF ₂ CF ₃	13.6	13.1	14.3	160	2, 5
HFC-236ea	CHF ₂ CHFCF ₃	10.7	11.0	11.9	144	1, 5
HFC-236fa	CF ₃ CH ₂ CF ₃	240	242	253	5676	1, 4
HFC-227ea	CF ₃ CHFCF ₃	34.2	38.9	44.5	310	2, 5
PFC-218 (Perfluoropropane)	CF ₃ CF ₂ CF ₃	2,600	2,600		2,600	8
PFC-c216 (Perfluorocyclopropane)	c-C ₃ F ₆	>1,000	~3,000		~3,000	15
HCFC-243cc	CH ₃ CF ₂ CCl ₂ F	26.4	19.5	27.1	70	1, 5, 9
HCFC-234fb	CF ₃ CH ₂ CCl ₂ F		49	117	84	2, 5, 9
HCFC-225ca	CHCl ₂ CF ₂ CF ₃	1.9	1.9	2.0	43.7	1, 4
HCFC-225cb	CHClFCF ₂ CClF ₂	5.8	5.9	6.3	101	1, 4
Halogenated Higher Alkanes						
HFC-365mfc	CH ₃ CF ₂ CH ₂ CF ₃	8.6	8.7	9.3	125	1, 5
HFC-356mcf	CH ₂ FCH ₂ CF ₂ CF ₃	1.2	1.3	1.3	40	1, 5
HFC-356mff	CF ₃ CH ₂ CH ₂ CF ₃	8.1	8.3	8.9	122	1, 5
HFC-338pcc	CHF ₂ CF ₂ CF ₂ CHF ₂	12.3	12.9	14.0	159	1, 5
HFC-329p	CHF ₂ CF ₂ CF ₂ CF ₃		28.4	32	256	5, 16
PFC-C318 (Perfluorocyclobutane)	c-C ₄ F ₈	3,200	3,200		3,200	7

Table 1-3, continued.

Industrial Designation or Common Name	Chemical Formula	Total Lifetime from Previous Assessments ^a (years)	New Total Lifetime ^a (years)	OH Lifetime ^d (years)	Stratospheric Lifetime (years)	Notes
PFC-31-10 (Perfluorobutane)	C ₄ F ₁₀	2,600	2,600		2,600	7
HFC-43-10mee	CF ₃ CHFCHFCF ₂ CF ₃	15.9	16.1	17.9	157	1, 4
HFC-458mfcf	CF ₃ CH ₂ CF ₂ CH ₂ CF ₃	23.2	22.9	25.5	224	1, 5
PFC-41-12 (Perfluoropentane)	C ₅ F ₁₂	4,100	4,100		4,100	7
HFC-55-10mccf	CF ₃ CF ₂ CH ₂ CH ₂ CF ₂ CF ₃	7.7	7.5	8.0	115	1, 5
HFC-52-13p	CHF ₂ CF ₂ CF ₂ CF ₂ CF ₂ CF ₃		32.2	36.4	275	3, 5
PFC-51-14 (Perfluorohexane)	C ₆ F ₁₄	3,200	3,100		3,100	7
PFC-61-16 (Perfluoroheptane)	C ₇ F ₁₆		~3,000		~3,000	17
Perfluorodecalin	C ₁₀ F ₁₈	2,000	~2,000		~2,000	18
Fluorinated Alcohols						
1,1,1,3,3,3-hexafluoroisopropanol	(CF ₃) ₂ CHOH	2.0	1.9	2.0	51	1, 5
Halogenated Ethers						
HFE-143a	CH ₃ OCF ₃	4.3	4.8	5.1	88	1, 5
HFE-134	CHF ₂ OCHF ₂	26	24.4	28.4	240	1, 5
HFE-125	CHF ₂ OCF ₃	136	119	147	620	1, 5
HFE-227ea	CF ₃ OCHFCF ₃	11 ^b	51.6	60	370	2, 5
HCFE-235da2 (Isoflurane)	CHF ₂ OCHClCF ₃	2.6	3.5	3.7	65	2, 5, 9
HFE-236ea2 (Desflurane)	CHF ₂ OCHF ₂ CF ₃	5.8 ^b	10.8	11.7	143	2, 5
HFE-236fa	CF ₃ OCH ₂ CF ₃	3.7 ^b	7.5	~8	115	5, 19
HFE-245fa1	CF ₃ OCH ₂ CHF ₂	2.2 ^b	6.6	~7	106	5, 20
HFE-245fa2	CHF ₂ OCH ₂ CF ₃	4.9	5.5	5.8	95	2, 5
HFE-245cb2	CH ₃ OCF ₂ CF ₃	5.1	4.9	5.2	89	1, 5
HFE-254cb2	CH ₃ OCF ₂ CHF ₂	2.6	2.5	2.6	60	1, 5
HFE-236ca	CHF ₂ OCF ₂ CHF ₂	26.5	20.8	23.1	212	2, 5
HCFE-235ca2 (Enflurane)	CHF ₂ OCF ₂ CHFCI		4.3	4.6	62	5, 9, 21
	CF ₃ CF ₂ OCF ₂ CHF ₂	6.8 ^b	22.5	20–30	222	5, 22
	CF ₃ CF ₂ OCH ₂ CF ₃	4.3 ^b	7.5	~8	115	5, 23
	CH ₃ OCF ₂ CF ₂ CF ₃	5.2	5.0	5.3	90	1, 5
	CF ₃ CF ₂ OCH ₂ CHF ₂	2.8 ^b	6.6	~7	106	5, 24
	CHF ₂ OCH ₂ CF ₂ CF ₃	5.9	5.7	6.0	97	1, 5

Table 1-3, continued.

Industrial Designation or Common Name	Chemical Formula	Total Lifetime from Previous Assessments ^a (years)	New Total Lifetime ^a (years)	OH Lifetime ^d (years)	Stratospheric Lifetime (years)	Notes
	CF ₃ CH ₂ OCF ₂ CHF ₂	7.1	6.0	6.4	100	5, 25
	CH ₃ OCF ₂ CHF ₂ CF ₃	0.94 ^b	~3	~3	77	5, 26
	CH ₃ OCF ₂ CF ₂ CHF ₂	0.93 ^b	~3	~3	77	5, 26
	CHF ₂ CH ₂ OCF ₂ CHF ₂	2.0 ^b	5.7	~6	97	5, 27
	CHF ₂ OCH ₂ CF ₂ CHF ₂	3.6	3.5	3.7	73	1, 5
HFE-347 isomer (Sevoflurane)	(CF ₃) ₂ CHOCH ₂ F		2.2	2.3	56	5, 28
HFE-338 isomer	(CF ₃) ₂ CHOCHF ₂	3.1 ^b	21.2	23.5	214	2, 5
	(CF ₃) ₂ CFOCH ₃	3.4	3.7	3.9	75	2, 5
	CH ₃ O(CF ₂) ₃ CF ₃	5	4.7	5.0	87	2, 5
HFE-54-11 isomer	CF ₃ CHF ₂ CF ₂ OCH ₂ CF ₂ CF ₃	9.1	8.8	9.5	127	5, 29
	CH ₃ CH ₂ O(CF ₂) ₃ CF ₃	0.77	0.8	0.8	30	5, 30
	CHF ₂ OCF ₂ OCHF ₂	12.1 ^c	25.0	28.0	237	2, 5
	CHF ₂ OCF ₂ CF ₂ OCHF ₂	6.2 ^c	12.9	14.0	159	2, 5
	CHF ₂ OCF ₂ OCF ₂ CF ₂ OCHF ₂	6.3 ^c	13.5	14.7	163	2, 5
	CF ₃ OC(O)H	3.6	<3.5	3.7	73	5, 31, 33
	C ₂ F ₅ OC(O)H	3.6	<3.5	3.7	73	5, 32, 33
	n-C ₃ F ₇ OC(O)H	2.6	<2.6	2.7	61	5, 32, 33
Other Fluorinated Compounds						
Trifluoromethyl-sulfurpentafluoride	SF ₅ CF ₃	650–950	650–950		650–950	8
Sulfur hexafluoride	SF ₆	3,200	3,200		3,200	7
Nitrogen trifluoride	NF ₃	740	500		500	34
Sulfuryl fluoride	SO ₂ F ₂		36	> 300	630	35

^a Includes OH reaction, ocean loss, and stratospheric loss (reactive and photolytic) as appropriate.

^b Lifetime estimated from theoretically calculated reaction rate constants.

^c Lifetime estimated using room temperature data.

^d Lifetime with respect to reaction with tropospheric OH calculated relative to 6.1 years for CH₃CCl₃, assuming an average temperature of 272 K (Spivakovsky et al., 2000; Prather and Ehhalt et al., 2001).

^e The value of τ_{OH} of 6.1 years for methyl chloroform was derived from its measured overall lifetime of 5.0 years (Clerbaux and Cunnold et al., 2007; Prinn et al., 2005) taking into account an ocean loss of 89 years and stratospheric loss of 39 years.

Notes:

- OH rate constants taken from JPL 06-2.
- OH rate constants taken from JPL 10-6. JPL 10-6 is cited here whenever there is a change in a rate constant recommendation or the accompanying note. It does not necessarily mean that a major change was recommended for a rate constant. Nevertheless, updates in JPL 10-6 reflect improved kinetic understanding.

Table 1-3, continued (notes).

3. OH rate constants taken from Atkinson et al. (2008).
4. Stratospheric lifetime taken from Naik et al. (2000).
5. Stratospheric reaction lifetime estimated from an empirical correlation between the tropospheric and stratospheric lifetimes that were reported by Naik et al. (2000) for HFCs for which OH and O(¹D) reaction rate constants were available.
6. Total lifetime includes a very minor contribution for ocean loss derived in Yvon-Lewis and Butler (2002).
7. Total lifetime from Ravishankara et al. (1993). The lifetimes for CF₄, CF₃CF₃, and C₄F₁₀ were reported as lower limits.
8. Total lifetime taken from Table 1-4 in Clerbaux and Cunnold et al. (2007).
9. Stratospheric lifetime includes a photolysis lifetime estimated from that of a fully halogenated compound containing equivalent Cl and/or Br groupings.
10. Lifetime is due to a combination of tropospheric and stratospheric photolysis.
11. Lifetime is due primarily to tropospheric photolysis with a smaller contribution associated with the stratospheric photolysis.
12. OH rate constant estimated relative to CHF₂CF₃ using available data on the effects of Cl substitution.
13. Total lifetime assumed to be the same as CFC-11.
14. Total lifetime assumed to be the same as CFC-12.
15. Total lifetime assumed to be comparable to those for perfluoropropane, perfluorobutane, and perfluorocyclobutane.
16. OH rate constants taken from Young et al. (2009).
17. Total lifetime assumed to be the same as perfluorohexane.
18. Total lifetime estimated by Shine et al. (2005).
19. OH lifetime estimated by adjusting the lifetime of CF₃CH₂OCF₂CHF₂ for the contribution of -CF₂CHF₂.
20. OH lifetime estimated relative to CF₃OCH₃ and CHF₂CH₂CF₃.
21. OH rate constants taken from Tokuhashi et al. (1999).
22. OH lifetime estimated as greater than CHF₂CF₂OCHF₂ and less than CHF₂CF₂CF₂CF₃.
23. OH lifetime assumed to be the same as CF₃OCH₂CF₃.
24. OH lifetime assumed to be the same as CHF₂CH₂OCF₃.
25. OH rate constants taken from Wilson et al. (2007).
26. OH and total lifetimes estimated as approximately the same as for CH₃OCF₂CHF₂.
27. OH lifetime estimated relative to CF₃CF₂OCF₂CHF₂ and CF₃CF₂OCH₂CHF₂.
28. OH rate constant taken from Langbein et al. (1999) using an estimated temperature dependence.
29. OH rate constants taken from Chen et al. (2005a).
30. OH rate constants taken from Christensen et al. (1998) using an estimated temperature dependence.
31. OH rate constants taken from Chen et al. (2004a).
32. OH rate constants taken from Chen et al. (2004b).
33. Ocean loss for perfluoro esters has been estimated from hydrolysis and solubility data for non-fluorinated and partially fluorinated esters by Kutsuna et al. (2005). These authors suggest that the ocean sink can be comparable to the tropospheric reaction sink for perfluoro ethers, thereby reducing the total lifetimes given in this table by as much as a factor of 2.
34. From Prather and Hsu (2008) with the lifetimes recalculated using the JPL 06-2 recommended rate constants for the O(¹D) reactions corrected for the deactivation channel (see also Section 1.2.2).
35. From Papadimitriou et al. (2008b) and Mühle et al. (2009). The total lifetime is primarily due to ocean uptake.

Box 1-3. Atmospheric Lifetimes and Removal Processes

The total atmospheric lifetime or turnover time (τ_{total}) of a trace gas is the time required to remove or chemically transform approximately 63% (i.e., $1-1/e$) of its global atmospheric burden (C_{global}). τ_{total} can be defined as the ratio of the burden to the total removal rate (L_{total}) from the atmosphere:

$$\tau_{\text{total}} = C_{\text{global}} / L_{\text{total}}$$

L_{total} can be broken down into the sum of loss rates associated with various removal processes

$$L_{\text{total}} = L_{\text{atm}} + L_{\text{soil}} + L_{\text{ocean}} + \dots L_X$$

where L_{atm} is the loss rate for processes occurring in the atmosphere, L_{soil} is the loss rate for soil uptake, L_{ocean} is the rate for loss to the oceans, and L_X is the loss rate for any other removal process, X . Each of these loss rates is associated with a characteristic lifetime such that

$$L_i = C_{\text{global}} / \tau_i$$

Therefore,

$$L_{\text{total}} = C_{\text{global}} / \tau_{\text{total}} = C_{\text{global}} / \tau_{\text{atm}} + C_{\text{global}} / \tau_{\text{soil}} + C_{\text{global}} / \tau_{\text{ocean}} + \dots C_{\text{global}} / \tau_X$$

and τ_{total} can be expressed as

$$(\tau_{\text{total}})^{-1} = (\tau_{\text{atm}})^{-1} + (\tau_{\text{soil}})^{-1} + (\tau_{\text{ocean}})^{-1} + \dots (\tau_X)^{-1}$$

The atmospheric loss rate is typically broken down into separate loss rates associated with processes occurring in the troposphere and in the stratosphere

$$L_{\text{atm}} = L_{\text{trop}} + L_{\text{strat}} = C_{\text{global}} / \tau_{\text{trop}} + C_{\text{global}} / \tau_{\text{strat}}$$

such that

$$(\tau_{\text{atm}})^{-1} = (\tau_{\text{trop}})^{-1} + (\tau_{\text{strat}})^{-1}$$

The tropospheric lifetimes for most trace gases are primarily controlled by reactions with hydroxyl radicals (OH), although reactions with ozone (O_3), nitrate radical (NO_3), and chlorine radicals (Cl) can also play limited roles. UV photolysis in the troposphere, designated by the characteristic lifetime τ_j , is the dominant sink for iodine-containing compounds and can also be important for some bromine-containing compounds. Hydrolysis-related removal processes (such as wet deposition, rainout, or washout), characterized collectively by τ_{hydrol} , can also contribute. Thus,

$$(\tau_{\text{trop}})^{-1} = (\tau_{\text{OH}})^{-1} + (\tau_{\text{O}_3})^{-1} + (\tau_{\text{Cl}})^{-1} + (\tau_{\text{NO}_3})^{-1} + (\tau_{\text{hydrol}})^{-1} + (\tau_j)^{-1}$$

Compounds whose tropospheric lifetimes are longer than the characteristic mixing time in the troposphere are designated as “long lived” in this chapter. For such well-mixed compounds, lifetimes due to reaction with tropospheric hydroxyl radicals can be estimated relative to the corresponding lifetime of methyl chloroform (Spivakovsky et al., 2000)

$$\tau_{\text{OH}}^{\text{RH}} = \frac{k_{\text{MCF}}(272 \text{ K})}{k_{\text{RH}}(272 \text{ K})} \cdot \tau_{\text{OH}}^{\text{MCF}}$$

where $\tau_{\text{OH}}^{\text{RH}}$ is the partial OH lifetime for the compound of interest (RH), $k_{\text{RH}}(272 \text{ K})$ and $k_{\text{MCF}}(272 \text{ K})$ are the rate constants for the reactions of OH with RH and with methyl chloroform (MCF) at $T = 272 \text{ K}$, and $\tau_{\text{OH}}^{\text{MCF}} = 6.1 \text{ years}$ (see Table 1-3, footnote “e”).

Stratospheric loss processes, such as reactions with OH, O_3 , and excited state oxygen atoms ($\text{O}(^1\text{D})$), and UV

photolysis can also play important roles in dictating the lifetime of a long-lived compound. The contribution from photolysis at Lyman- α (121.6 nm), which is important only for very long-lived compounds, can be included here, although it occurs at altitudes above the stratosphere (≥ 70 km). UV and Lyman- α photolysis are the most important loss processes for nonreactive compounds:

$$(\tau_{\text{strat}})^{-1} = (\tau_{\text{OH}})^{-1} + (\tau_{\text{O}_3})^{-1} + (\tau_{\text{O}({}^1\text{D})})^{-1} + (\tau_J)^{-1} + (\tau_{\text{Lyman-}\alpha})^{-1}$$

For long-lived compounds, τ_{total} can be considered to be a global lifetime that is representative of the compound's persistence in Earth's atmosphere.

In the context of this chapter, very short-lived substances (VSLS) are compounds with lifetimes less than or equal to 0.5 years (i.e., shorter than the characteristic time of mixing processes in the troposphere) (see Section 1.3). The actual atmospheric lifetimes of VSLS depend on the emission location and season as well as on local atmospheric conditions. Consistent with past Assessments, $\tau_{\text{OH}}^{\text{RH}}$ for VSLS was estimated with hydroxyl radical concentrations $[\text{OH}] = 1 \times 10^6$ molecule/cm³ and an OH reaction rate constant at $T = 275$ K:

$$\tau_{\text{OH}}^{\text{RH}} = 1/(k_{\text{RH}}(275 \text{ K}) \times [\text{OH}])$$

The use of a mean global tropospheric OH concentration in such calculations provides only approximate "local lifetimes." The concept of a single global lifetime, Ozone Depletion Potential (ODP), or Global Warming Potential (GWP) is inappropriate for such short-lived gases (see Section 1.3).

1.2.2 Loss Processes

Halocarbons are removed from the atmosphere by a number of processes including oxidation by hydroxyl radicals, photolysis, uptake by the ocean, and uptake by terrestrial ecosystems. The combined influence of these processes can be expressed as a lifetime (see Box 1-3). Lifetimes for ODSs are generally based on a combination of modeling studies and analysis of observations, particularly stratospheric observations. Updates to our understanding of the persistence, expressed as lifetimes, of halocarbons in the environment are based on the consideration of updated kinetic information (see Table 1-3). Uncertainties associated with these lifetimes stem from uncertain hydroxyl radical concentrations and distributions, and uncertain reaction rate constants. Modeling uncertainties related to absorption cross sections and stratospheric air transport rates also affect the calculation of lifetimes. This is particularly important for CFCs, for example, as this represents their primary sink.

New results from models that more accurately simulate air transport rates through the stratosphere than older models suggest a steady-state lifetime for CFC-11 of 56–64 years (Douglass et al., 2008), notably longer than the 45 years used in recent past Assessments. This finding has the potential to affect lifetimes, ODPs, and emissions derived from global measured trends for some other ODSs. For example, while the CFC-12 lifetime calculated in this same study was not substantially different from its current, best-estimate lifetime of 100 years, the stratospheric lifetime of CCl₄ is calculated as ~50 years

in this same model (Rontu Carlon et al., 2010), which is notably longer than the current best estimate of 35 years. A revision to the CFC-11 or CCl₄ lifetime is not recommended in this Assessment, pending a comprehensive analysis by the atmospheric observation and modeling communities.

New modeling calculations by Prather and Hsu (2008) have yielded significantly shorter lifetimes for CFC-114 and CFC-115. The O(¹D) (excited-state oxygen atoms) reaction rate coefficients used in their calculation, however, included both the chemical oxidation of the CFCs as well as the nonreactive, physical quenching of O(¹D). This resulted in an overestimation of loss for these CFCs from O(¹D). When the O(¹D) rates for only reactive channels are considered (Sander et al., 2006, hereafter referred to as JPL 06-2), lifetimes of 190 years for CFC-114 and 1020 years for CFC-115 are calculated (Table 1-3; Prather and Hsu, 2010), which are still significantly shorter than considered in past Assessments (300 years for CFC-114 and 1700 years for CFC-115; Clerbaux and Cunnold et al., 2007).

A significantly shorter lifetime for nitrogen trifluoride (NF₃) was also calculated by Prather and Hsu (2008) using an older O(¹D) reaction rate constant (Sorokin et al., 1998). The NF₃ lifetime given in this Assessment (500 years compared to 740 years in Clerbaux and Cunnold et al., 2007) is based on the Prather and Hsu (2008) results revised using the O(¹D) + NF₃ rate constant recommended in JPL 06-2. A new study of this rate constant has been published by Zhao et al. (2010). Use of the rate constant reported by these authors would reduce the life-

time for NF_3 by about 7% from the 500 years reported in this chapter.

The principal differences between these new (revised) CFC-114 and CFC-115 lifetimes and those recommended in earlier Assessments (based on Ravishankara et al., 1993) are primarily due to improved photolysis models (see Chapter 6 in SPARC CCMVal, 2010) that include updated solar fluxes in the Herzberg continuum (200–220 nanometers (nm)) and in the Schumann-Runge bands (<205 nm). Note that the more rapidly photolyzed CFCs (-11, -12, and -113) are destroyed in the lower stratosphere at wavelengths whose opacities are dominated by the molecular oxygen (O_2) Herzberg continuum, while the much longer-lived gases (CFC-114, -115, and NF_3) are lost primarily between altitudes of 32 to 40 km and in the wavelength region where the opacity is controlled by the O_2 Schumann-Runge bands. This is why the CFC-11, CFC-12, and CFC-113 lifetimes are not appreciably influenced by use of the improved photolysis model.

The Prather and Hsu (2008) model did not include losses above 70 km, where photolysis at Lyman-alpha (121.6 nm) wavelengths occurs. This loss is likely important for some very long-lived chemicals, particularly CFC-115. The lifetime for CFC-13 derived by Ravishankara et al. (1993) remains unchanged here (640 years) despite these considerations because atmospheric loss of this chemical is primarily associated with reactive removal by $\text{O}(^1\text{D})$ atoms in the stratosphere. For NF_3 , the Prather and Hsu (2008) calculations revise earlier lifetime estimates that were based on a one-dimensional (1-D) photolysis calculation (not including $\text{O}(^1\text{D})$ reactions) referenced as a private communication in Molina et al. (1995).

Other considerations also affect the usefulness of the stratospheric lifetimes calculated in Table 1-3. These lifetimes are derived for steady-state conditions, yet global atmospheric mixing ratios of most ODSs are not at steady state. For CFCs and other compounds destroyed primarily by photolysis in the stratosphere, steady-state lifetimes are generally longer than lifetimes in the absence of significant emissions (e.g., Prather, 1997). Finally, many models suggest that future changes in stratospheric circulation expected from enhanced greenhouse gas concentrations will enhance photolytic loss rates for the long-lived halocarbons. This influence is predicted to result in shorter stratospheric lifetimes than those listed in Table 1-3.

Since the previous Assessment, considerably more kinetic data have become available for the reactions of OH with a wide variety of CFC and halon substitutes, especially fluorinated alkenes, ethers, and alcohols for which limited or no data previously existed. A comprehensive analysis of available kinetic data since the last Assessment has revealed a number of compounds for which our understanding of losses has improved.

Most notably, lifetimes of three hydrofluoroethers (HFEs) are now based on experimentally measured OH reaction rate constants (HFE-227ea, HFE-236ea2, and $(\text{CF}_3)_2\text{CHOCHF}_2$) (Sander et al., 2010; hereafter referred to as JPL 10-6). Previous estimates were based on theoretically calculated OH reaction rate constants that significantly overestimated the loss rates for these gases, leading to unrealistically short lifetimes.

Rate constants for eight other HFEs (HFE-236fa, HFE-245fa1, $\text{CF}_3\text{CF}_2\text{OCF}_2\text{CHF}_2$, $\text{CF}_3\text{CF}_2\text{OCH}_2\text{CF}_3$, $\text{CF}_3\text{CF}_2\text{OCH}_2\text{CHF}_2$, $\text{CH}_3\text{OCF}_2\text{CHF}_2$, $\text{CH}_3\text{OCF}_2\text{CF}_2\text{CHF}_2$, $\text{CHF}_2\text{CH}_2\text{OCF}_2\text{CHF}_2$) that had also been derived from theoretical considerations can now be better estimated from the kinetic data on fluoroethers that are now available (Table 1-3). The revised lifetimes for these HFEs are considerably longer than recommended in the previous Assessment.

Updated lifetimes for three additional HFEs ($\text{CHF}_2\text{OCF}_2\text{OCF}_2\text{CF}_2\text{OCHF}_2$, $\text{CHF}_2\text{OCF}_2\text{OCHF}_2$, and $\text{CHF}_2\text{OCF}_2\text{CF}_2\text{OCHF}_2$) have been derived using the temperature dependencies of the OH reaction rate constants estimated in JPL 10-6 (which are based on existing data for other fluoroethers) and evaluated at 272 K (see Box 1-3). Previously assessed lifetime estimates for these three HFEs were based on rate constants at 298 K (Ramaswamy et al., 2001), which are ~80% faster.

Significant revisions have also been made to the lifetimes of three HFCs:

- The updated total lifetime for HFC-23 (CHF_3) of 222 years is ~20% shorter than the 270 years recommended in the previous Assessment (Clerbaux and Cunnold et al., 2007). This change in total lifetime results from a shorter tropospheric lifetime due to the OH rate constant recommended in JPL 10-6 being ~15% larger than given in JPL 06-2 and a stratospheric lifetime of 2347 years based on the model calculation of Naik et al. (2000).
- The new total lifetime of HFC-227ea ($\text{CF}_3\text{CHF}_2\text{CF}_3$) is longer than given in the previous Assessment (38.9 years vs. 34.2 years) primarily because the updated rate constant (JPL 10-6) is smaller than previously recommended due to the inclusion of new temperature-dependent kinetic data (Tokuhashi et al., 2004).
- The revised total lifetime of HFC-41 (CH_3F) is 2.8 years. The revision is based on the current recommendation for the OH reaction rate constant (JPL 10-6) and an estimation of stratospheric loss (64 years derived from Naik et al. (2000); Table 1-3).

1.3 VERY SHORT-LIVED HALOGENATED SUBSTANCES (VSLS)

While the longer-lived ODSs account for the majority of the halogen loading in the present-day stratosphere, there is evidence suggesting that halogenated very short-lived substances (VSLS) with lifetimes of 0.5 years or less and their degradation products contribute to halogen in the stratosphere (Ko and Poulet et al., 2003; Law and Sturges et al., 2007). In Table 1-4, some of the halogenated VSLS considered in this section are listed together with their lifetimes. The abbreviations for chemical and meteorological parameters used in this section are explained in Box 1-4).

While some VSLS originate from anthropogenic sources, others are of partly or wholly natural origins. We include discussions of naturally emitted VSLS here for two reasons. First, much of our current understanding of the mode and rate of delivery of the VSLS—whether natural or anthropogenic—to the stratosphere arises from studies of naturally occurring halocarbons. Second, the emission and the stratospheric injection of natural halocarbons might not be constant in a changing climate.

1.3.1 Emissions, Atmospheric Distributions, and Abundance Trends of Very Short-Lived Source Gases

Since the 2006 Assessment (Law and Sturges et al., 2007) new findings on emissions of anthropogenic and natural VSLS have been made as well as on trends of anthropogenic chlorinated VSLS. New data are also available on very short-lived (VSL) source gases (SGs) in the upper troposphere and the importance of product gases (PGs) is assessed.

1.3.1.1 CHLORINE-CONTAINING VERY SHORT-LIVED SOURCE GASES

A number of chlorinated VSLS from anthropogenic and natural sources have been measured in the background atmosphere. Industrial sources of these gases are discussed in McCulloch et al. (1999), Simmonds et al. (2006), Worton et al. (2006), and on the web site of the U.S. Environmental Protection Agency (www.epa.gov; Toxic Air Pollutants). Dichloromethane (methylene chloride, CH_2Cl_2) is principally used as a paint remover, and also in foam production and foam blowing applications, as a solvent and degreaser, and in fumigation. Trichloromethane (chloroform, CHCl_3) is used almost exclusively in the production of HCFC-22 and fluoropolymers, but is also released as a by-product from chlorine bleaching in the paper and pulp industry,

and from water chlorination. Tetrachloroethene (perchloroethylene, CCl_2CCl_2) is used in the textile industry, in dry-cleaning applications, and in vapor degreasing of metals, as is trichloroethene (trichloroethylene, CHClCCl_2). 1,2-Dichloroethane ($\text{CH}_2\text{ClCH}_2\text{Cl}$) is principally used in the production of polymers and rubbers, and is also used as a solvent, as a fumigant, and was historically used widely as an additive to leaded gasoline. Chloroethane ($\text{C}_2\text{H}_5\text{Cl}$) is mostly used in the manufacture of ethyl cellulose, dyes, and pharmaceuticals and was formerly used in the manufacture of tetraalkyl lead additives for gasoline. Other related compounds include a number of mixed-halogenated compounds, notably the bromochloromethanes. These latter compounds are believed to originate largely from natural sources and are generally present at lower abundances than the aforementioned chlorinated compounds. They are discussed in Section 1.3.1.2 in the context of brominated source gases.

Estimates of total global and industrial emissions of chlorinated VSLS are shown in Table 1-5 for those gases for which such estimates exist. From this table it can be seen that total CCl_2CCl_2 and CH_2Cl_2 emissions derived from a “top-down” analysis of atmospheric observations are similar to independently estimated industrial emissions derived from inventories. Although not all of the estimates coincide in time (e.g., industry inventories are mostly from the early or mid-1990s, whereas the atmospheric measurements used in the emissions models are mostly from several years later), the results suggest that most emissions of CCl_2CCl_2 and CH_2Cl_2 arise from anthropogenic activity. A model analysis of the atmospheric data (Simmonds et al., 2006) also indicates that more than 90% of the emissions for these two compounds emanate from the Northern Hemisphere (NH), further indicative of their predominantly industrial origins. The industrial inventories, however, indicate that only 1% of industrial emissions are in the Southern Hemisphere (SH) (McCulloch et al., 1999), suggesting that other sources such as biomass burning might contribute. An earlier estimate of the biomass burning contribution to global atmospheric CH_2Cl_2 (7% according to Keene et al., 1999) is supported by Xiao (2008), but both are based largely on the same underlying data. These high values have been questioned by Simmonds et al. (2006) on the basis of the lower (by two orders of magnitude) biomass burning emission factors they observed from Australian wild fires.

Industrial emissions of chloroform were estimated to contribute 25 to 29% of total emissions in 2001 by modeling atmospheric measurements (Worton et al., 2006). This is less than that modeled in earlier years due to a rapid decline in emissions attributed to the paper and pulp industry. The absolute emissions estimate from this study for 2001 is, however, higher than an earlier industry inventory figure given by McCulloch et al. (2003) (see

Table 1-4. Lifetimes for very short-lived halogenated source gases.

Compound	Local Lifetime from Previous Assessments (τ_{local}), days	OH Lifetime ¹ (τ_{OH}), days	Photolysis Lifetime from Previous Assessments (τ_{local}), days	New Local Lifetime, (τ_{local}), days	Notes
Chlorocarbons					
CH ₂ Cl ₂	140	144	> 15000	144	2, 8
CHCl ₃	150	149	> 15000	149	2, 8
CH ₃ CH ₂ Cl	30	39		39	2
CH ₂ ClCH ₂ Cl	70	65		65	4
CH ₃ CH ₂ CH ₂ Cl		14		14	5
CHClCCl ₂		4.9	> 15000	4.9	3, 8
CCl ₂ CCl ₂	99	90		90	3
CH ₃ CHClCH ₃		18		18	5
Bromocarbons					
CH ₂ Br ₂	120	123	5000	123	2, 8
CHBr ₃	26	76	36	24	2, 8
CH ₂ BrCl	150	137	15000	137	2, 8
CHBrCl ₂	78	121	222	78	6, 8
CHBr ₂ Cl	69	94	161	59	7, 8
CH ₃ CH ₂ Br	34	41		41	2
CH ₂ BrCH ₂ Br	55	70		70	4
n-C ₃ H ₇ Br	13	12.8	> 1200	12.8	3, 8
iso-C ₃ H ₇ Br		16.7		16.7	3
Iodocarbons					
CH ₃ I	7	158	7 (4–12)	7	4, 8
CF ₃ I	4	860	not determined	4	2
CH ₂ CI	0.1		0.1	0.1	8
CH ₂ BrI	0.04		0.04	0.04	8
CH ₂ I ₂	0.003		0.003	0.003	8
CH ₃ CH ₂ I	4	17.5	5 (2–8)	4	4, 8
CH ₃ CH ₂ CH ₂ I	0.5	7.7	0.6 (0.5–1.5)	0.5	4, 8
CH ₃ CHICH ₃	1.2	9.7	1.4 (1–3)	1.2	4, 8
CF ₃ CF ₂ CF ₂ I			< 2	< 2	9

Notes:

- These local OH lifetimes are calculated using an average tropospheric OH concentration of 1×10^6 molecule/cm³ and the OH reaction rate constant at T = 275 K. Local lifetimes quoted here are not meant to be estimates of global lifetimes, which for short-lived gases depend on the emission location and season as well as local atmospheric conditions. The concept of a single global lifetime, ODP, or GWP is inappropriate for such short-lived gases.
- OH reaction rate constant taken from JPL 06-2.
- OH reaction rate constant taken from JPL 10-6. JPL 10-6 is cited here whenever there is a change in a rate constant recommendation or the accompanying note. It does not necessarily mean that a major change was recommended for a rate constant. Nevertheless, updates in JPL 10-6 reflect improved kinetic understanding.
- OH reaction rate constant taken from Atkinson et al. (2008).
- OH reaction rate constant taken from Yujing and Mellouki (2001).
- Room temperature OH reaction rate constant taken from Bilde et al. (1998). The temperature dependence of the OH reaction rate constant was estimated from the reactivity of CHCl₃, CHCl₂Br, and CHBr₃.
- OH reaction rate constant estimated from the OH reactivity of CHCl₃, CHCl₂Br, and CHBr₃.
- Photolysis lifetime taken from Table 2-4 in Ko and Poulet et al. (2003).
- Photolysis lifetime estimated from comparison of UV spectra and lifetimes for CF₃I and CF₃CF₂CF₂I.

Box 1-4. Definition of Acronyms Related to Short-Lived Gases

Chemical Parameters

VSL	very short-lived substances—organic and inorganic gases with lifetimes of less than 0.5 years
VSL	very short-lived
SG/SGI	source gas / source gas injection—refers to a halogenated organic source gas and its injection into the stratosphere
PG/PGI	product gas / product gas injection—refers to halogenated organic and inorganic degradation products and their injection into the stratosphere
Br _y	total inorganic stratospheric bromine (e.g., HBr, BrO, 2×Br ₂) resulting from degradation of bromine-containing organic source gases (halons, methyl bromide, VSLs), and natural inorganic bromine sources (e.g., volcanoes, sea salt, and other aerosols)
Cl _y	total inorganic stratospheric chlorine (e.g., HCl, ClO) resulting from degradation of chlorine-containing source gases (CFCs, HCFCs, organic VSLs), and natural inorganic chlorine sources (e.g., sea salt and other aerosols)
I _y	total inorganic stratospheric iodine (e.g., IO, OIO, HOI) resulting from degradation of iodine-containing source gases (VSLs), and natural inorganic sources (e.g., sea salt and other aerosols)
Br _y ^{VSL}	the component of stratospheric Br _y from the degradation of organic brominated VSL SGs and tropospheric inorganic bromine sources (also called “additional” stratospheric Br _y)

Meteorological Parameters

BDC	Brewer-Dobson circulation
LMS	lowermost stratosphere
TTL	tropical tropopause layer—a layer exhibiting properties of both the stratosphere and troposphere. In this Assessment we follow the definition of the TTL as used in Law and Sturges et al. (2007). The bottom of TTL is taken as the region of maximum convective outflow (about 12 km altitude, or 345K potential temperature) and the upper end is identical to the tropical cold point tropopause (about 17 km or 380 K potential temperature).
z ₀	altitude of clear-sky zero radiative heating. As in the previous Assessment (Law and Sturges et al., 2007) we define the level at about 15 km or 360K, where there is a transition from clear-sky radiative cooling to clear-sky radiative heating. In general, air masses above this level are expected to enter the stratosphere.
CPT	cold point tropopause—defined by the minimum atmospheric temperature and gives the position of the tropical tropopause. At this altitude air parcels enter the stratospheric overworld.
Washout	the removal of trace gases from the gas phase, including subsequent falling of rain or ice particles

Table 1-5). Biomass burning is thought to contribute 1% or less to emissions of CHCl₃, CCl₂CCl₂, and CHClCCl₂ (Table 1-5).

Annual mean mole fractions and trends of some of these chlorinated VSL source gases at Earth’s surface during recent years are given in Table 1-6. CH₂Cl₂ has increased significantly in recent years in both hemispheres, having previously fallen from 1995 (when records began) to about 2000 (updated from Simmonds et al., 2006). In the NH, mean surface mixing ratios in 2008 were similar to those previously observed in the mid-1990s. CHCl₃ concentrations have remained approximately constant since 2000 suggesting little change in the fraction arising from industrial emissions. CCl₂CCl₂ has decreased almost monotonically since the late 1980s (updated from Simpson et al., 2004). Data in Table 1-6 indicate that this trend may have reversed in the most recently reported year, but

this may be within the scatter of the interannual variability of the measurements. Global long-term measurements are available for CHClCCl₂ for the first time (Table 1-6). The large standard deviation reflects the very large seasonal cycle of this very reactive gas. The short record and large annual variability do not yet allow a trend to be established for this compound.

There are very few reported lower tropospheric measurements of the other chlorinated VSLs since the last Assessment, and likewise no industrial emission estimates are available for these species. In the last Assessment (Law and Sturges et al., 2007) one citation (Low et al., 2003) gave mean NH and SH C₂H₅Cl mixing ratios of 2.6 and 1.6 ppt, respectively, which, given the short lifetime of this gas (39 days; Table 1-4), requires a significant, presumably nonindustrial, source to sustain the observed SH abundances. Higher values were noted in the tropical

Table 1-5. Annual emissions of chlorinated VSLS.

Compound	Fraction of Global Emissions in the NH (%)	“Top-Down” Average Annual Global Emissions (Gg/yr)	Estimated Industrial Emissions (Gg/yr)	Estimated Biomass Burning Emissions (Gg/yr)	Origin
CH ₂ Cl ₂	93	515 ± 22	519 ± 32	59	1
	-	629 ± 44	430 ± 12	75 ± 18	2
CHCl ₃	-	-	-	2	1
	62	370 ± 120	-	2 ± 2	2
	-	315–373	79–108	-	3
	-	-	66 ± 23	-	4
CCl ₂ CCl ₂	94	250–205	278 ± 20	0	1
CHClCCl ₂	-	-	246 ± 13	0	1

Notes:

1. Simmonds et al. (2006) global and hemispheric emissions 1999–2003; McCulloch et al. (1999) industrial emission estimates (using the factors given in McCulloch et al. (1999) to estimate values appropriate for 1995); Keene et al. (1999) biomass burning emissions.
2. Xiao (2008) (values shown are for 2000–2004).
3. Worton et al. (2006) (values shown are for 2001).
4. McCulloch et al. (2003) (reference year not given).

marine boundary layer, also indicative of a natural origin. The mixing ratios given in the last two Assessments for CH₂ClCH₂Cl (20–40 ppt in the NH and 5–7 ppt in the SH) appear to have been incorrectly cited from an original paper (Class and Ballschmiter, 1987). The values given in this latter paper are <1 to 24 ppt for the NH and <1 ppt for the SH. We do not know of any globally distributed or long-term measurements of this species since this date, however, the large interhemispheric ratio suggests predominantly anthropogenic uses at that time. There are no emis-

sion estimates or inventories for this compound, making it a significant uncertainty in the chlorinated VSLS budget.

It is likely that significant calibration differences exist between measurements of chlorinated VSLS by different laboratories. This is particularly evident in the case of CCl₂CCl₂ (Table 1-6) but is equally true for all of the chlorocarbons discussed here (e.g., Simmonds et al., 2006; Butler et al., 2010). Simmonds et al. (2006) mention a 10% difference between NOAA and AGAGE measurements for CCl₂CCl₂, but no intercomparison exercises

Table 1-6. Measured mole fractions and growth rates of chlorinated very short-lived source gases.

Chemical Formula	Common or Industrial Name	Annual Mean Mole Fraction (ppt)			Growth (2007–2008)		Laboratory ^a
		2004	2007	2008	(ppt/yr)	(%/yr)	
CH ₂ Cl ₂	dichloromethane	17.3 ± 5.7	20.3 ± 6.7	22.1 ± 6.7	1.8 ± 0.5	8.1 ± 2.3	AGAGE, in situ (Global)
CHCl ₃	chloroform	6.8 ± 1.2	7.0 ± 1.5	7.0 ± 1.5	-0.02 ± 0.09	-0.3 ± 1.3	AGAGE, in situ (Global)
CCl ₂ CCl ₂	tetrachloroethene	1.9 ± 0.9	1.7 ± 0.7	1.7 ± 0.7	0.01 ± 0.00	0.6 ± 0.1	AGAGE, in situ (Global)
		3.0	2.5	2.7	0.2	7	UCI, flask (Global)
CHClCCl ₂ ^b	trichloroethene	-	0.19 ± 0.19	0.28 ± 0.28	-	-	AGAGE, in situ (Global)

^a AGAGE global mixing ratios updated from Simmonds et al. (2006). UCI global mixing ratios updated from Simpson et al. (2004).

^b Because of the short lifetime (4.9 days) the global mole fraction of CHClCCl₂ should be seen rather as an approximation than a defined global value.

have yet been published for CCl_2CCl_2 or any other chlorinated VSLS.

The anthropogenic contribution to the tropospheric abundances of chlorine from VSLS can be estimated by assuming that the anthropogenic fraction (industrial plus biomass burning) of individual gases is 90% for CH_2Cl_2 (average of 100% and 80% from modeled global emissions from Table 1-5); 100% for CCl_2CCl_2 , CHClCCl_2 , and $\text{CH}_2\text{ClCH}_2\text{Cl}$; and 25% for CHCl_3 . All other chlorinated gases are assumed to be of solely natural origin. Taking the averaged 2008 molar ratios in Table 1-6 and an average value of approximately 6 ± 6 ppt for $\text{CH}_2\text{ClCH}_2\text{Cl}$ (see above), yields a global average surface abundance of Cl from anthropogenic VSLS in 2008 of 67 ± 30 ppt.

In Table 1-7, observations of a range of various VSLS in the marine boundary layer, the upper troposphere, and the tropical tropopause layer are compiled from a number of measurement campaigns (see also Section 1.3.3.1). These measurement campaigns cover a range of dates and locations and, therefore, are not directly comparable with one another or the surface values in Table 1-6. Nevertheless, mixing ratios in the upper troposphere are on average less than those measured in the marine boundary layer, as would be expected for measurements of VSLS at some distance from their sources.

Updated mixing ratios of organic chlorine from VSLS of 59 (36–70) ppt in the tropical upper troposphere (10–12 km) (Table 1-7) are similar to the value of 55 (52–60) ppt at 10 km reported in the last Assessment, although with a wider spread. The main contributors to organic chlorine from VSLS at this altitude are CH_2Cl_2 and CHCl_3 .

Abundances at about 15 km in the tropics can be considered to represent the lower limit of source gas injection into the stratosphere (see Section 1.3.3.1). Taking this observed total of 55 (38–80) ppt Cl from all chlorinated VSLS at this height and the same anthropogenic fractions as discussed above, a minimum stratospheric injection of 39 (27–59) ppt Cl from anthropogenic VSLS is estimated (Table 1-7).

These anthropogenic totals do not include the product gases hydrogen chloride (HCl) and phosgene (COCl_2), which can be formed during atmospheric decomposition from both VSL SGs (primarily CHCl_3 and CCl_2CCl_2) and long-lived SGs (e.g., CCl_4 and CH_3CCl_3) and together could contribute an additional 0–50 ppt Cl to the stratosphere (see Section 1.3.3.3).

1.3.1.2 BROMINE-CONTAINING VERY SHORT-LIVED SOURCE GASES

In contrast to chlorinated VSLS, anthropogenic sources of brominated VSLS are small in comparison to natural sources. The most notable anthropogenic brominated VSLS are 1-bromopropane (n-propyl bromide,

$\text{C}_3\text{H}_7\text{Br}$), which is used as a substitute for CFC-113 and CH_3CCl_3 in metal and electronic part cleaning; and 1,2-dibromoethane (ethylene dibromide, $\text{CH}_2\text{BrCH}_2\text{Br}$), which is used as a fumigant and chemical intermediate and was formerly widely used as an additive to leaded gasoline (U.S. EPA web site at www.epa.gov; Toxic Air Pollutants). Small emissions of trihalomethanes, notably CHBr_3 , occur from chlorination of drinking water and power plant cooling water (Worton et al., 2006). There have been very few studies of long-term trends in atmospheric abundances of brominated VSLS. In the last Assessment one study was reported indicating small increases in brominated trihalomethanes since the early 20th century from Arctic firn air, but no significant trends in dibromomethane (CH_2Br_2) and bromochloromethane (CH_2BrCl) (Worton et al., 2006), which leads to the conclusion that the latter are of entirely natural origin. Atmospheric concentrations of brominated VSLS are highly variable due to the heterogeneous distribution and time-varying nature of sources; notably natural sources. Natural sources include marine phytoplankton, coastal macrophytes (seaweeds), and possibly terrestrial vegetation such as rice (Law and Sturges et al., 2007). Surface mixing ratios (predominantly from the marine boundary layer) reported in the last Assessment are summarized in Table 1-7. Mixing ratios of other bromocarbons tend to be lower than any of the aforementioned substances.

Most progress since the last Assessment has been with regard to estimating natural oceanic emissions of bromocarbons (see Table 1-8), notably bromoform (CHBr_3) and CH_2Br_2 . These range from 430–1400 Gg Br/yr for CHBr_3 , and 57–280 Gg Br/yr for CH_2Br_2 and are mostly larger than the estimates given in the previous Assessment report (Table 2-3 in Law and Sturges et al., 2007). There are large uncertainties associated with these estimates, notably due to the large variability in emissions from coastal zones (Butler et al., 2007). Some of the studies included in Table 1-8 emphasize the potential importance of coastal oceans (e.g., Butler et al., 2007; Carpenter et al., 2009; Liang et al., 2010). In contrast, Palmer and Reason (2009) considered tropical coastal sources to be unimportant based on a supposition that seaweeds are largely absent from the tropics. Yokouchi et al. (2005), however, reported very high mixing ratios of CHBr_3 , dibromochloromethane (CHBr_2Cl), and CH_2Br_2 associated with algal-colonized tropical shores. While numerous studies have identified coastal macroalgae as sources of halocarbons, and CHBr_3 in particular (Law and Sturges et al., 2007), there have been relatively few studies in the tropics compared to the extratropics. Furthermore, it has not been unequivocally proven that macroalgae account for all such coastal emissions. Close to shore in Cape Verde in the tropical Atlantic, O'Brien et al. (2009) detected elevated mixing ratios of CHBr_3 and CH_2Br_2 without evidence of

Table 1-7. Summary of available observations of VSLS source gases from the marine boundary layer (MBL) to the tropical tropopause layer (TTL). Abundances measured in the MBL are taken from the last Assessment (Law and Sturges et al., 2007). Data in and above the upper troposphere have been compiled from observations during the PEM-West A and B, TC4, Pre-AVE, and CR-AVE aircraft campaigns (see Schauffler et al., 1999) and from Teresina balloon observations (Laube et al., 2008 and updates). All table entries are mixing ratios, with units of parts per trillion (ppt).

Height Range	Marine Boundary Layer (MBL) ^a		Upper Troposphere (UT) ^b		Lower TTL ^c		LZRH (z_0) ^{c,d}		Upper TTL ^c		Tropical Tropopause ^c	
	Median (ppt)	Range ^e (ppt)	Mean (ppt)	Range ^e (ppt)	Mean (ppt)	Range ^e (ppt)	Mean (ppt)	Range ^e (ppt)	Mean (ppt)	Range ^e (ppt)	Mean (ppt)	Range ^e (ppt)
Potential Temperature Range					340–355 K		355–365 K		365–375 K		375–385 K	
CH ₂ Cl ₂	17.5	9–39	13.9	8.6–20.9	14.9	11.7–18.4	14.3	10.8–20.6	13.2	9.8–21.2	12.6	7.2–22.5
CHCl ₃	7.8	5.2–13.1	5.8	3.9–7.5	7.1	5.9–9.2	5.7	3.5–7.9	4.8	3.5–6.6	4.9	3.3–6.4
CH ₂ ClCH ₂ Cl	3.7	0.7–14.5	3.7 ^f	1.9–5.4	2.9 ^g	1.9–4.1	2.7 ^g	1.6–4.9	2.2 ^g	1.2–4.0	2.0	0.6–4.3
CHClCCl ₂	0.5	0.05–2	0.36 ^f	0–2.02	0.05 ^g	0.00–0.16	0.03 ^g	0.00–0.17	0.02 ^g	0.00–0.05	0.03	0.00–0.17
CCl ₂ CCl ₂	1.8	1.2–3.8	1.3	0.7–1.8	1.1	0.8–1.5	0.9	0.4–1.3	0.6	0.3–0.9	0.5	0.1–1.0
CH ₂ Br ₂	1.1	0.7–1.5	0.86	0.63–1.21	0.92	0.77–1.15	0.74	0.59–0.99	0.66	0.43–0.83	0.51	0.3–0.86
CHBr ₃	1.6	0.5–2.4	0.50	0.12–1.21	0.61	0.3–1.11	0.22	0.00–0.63	0.14	0.01–0.29	0.09	0.00–0.31
CH ₂ BrCl	0.5	0.4–0.6	0.09 ^h	0.03–0.16	0.14 ⁱ	0.13–0.16	0.10 ⁱ	0.08–0.13	0.11 ⁱ	0.1–0.12	0.08	0.05–0.11
CHBr ₂ Cl	0.3	0.1–0.8	0.11	0.01–0.36	0.10 ⁱ	0.06–0.15	0.06 ⁱ	0.03–0.11	0.05 ⁱ	0.01–0.11	0.03	0.00–0.14
CHBrCl ₂	0.3	0.1–0.9	0.11	0.02–0.28	0.20	0.18–0.22	0.10	0.12–0.18	0.12	0.11–0.14	0.06	0.03–0.12
Other brominated SG ^j							< 0.2 ^j		< 0.2 ^j		< 0.2 ^j	
CH ₃ I	0.80	0.3–1.9	0.13	0.03–0.42	0.12 ^k	0.00–0.23	0.04 ^k	0.00–0.10	0.00 ^k	0.00–0.01	0.01	0.00–0.06
Total Cl	76	41–171	59	36–70	62	48–78	55	38–80	48	38–74	46	26–77
Anthrop. Cl ^l	55	27–136	43	26–51	43	32–55	39	27–59	34	25–55	32	17–58
Total Br	8.40	3.6–13.3	3.5	1.7–7.4	4.3	2.8–6.5	2.7	1.4–4.6	2.0	1.1–3.2	1.5	0.7–3.4
Total I	0.80	0.3–1.9	0.13	0.03–0.42	0.12	0.00–0.23	0.04	0.00–0.10	0.00	0.00–0.01	0.01	0.00–0.06

PEM-West = Pacific Exploratory Mission-West; TC4 = Tropical Composition, Cloud, and Climate Coupling mission; Pre-AVE = Pre-Aura Validation Experiment; CR-AVE = Costa Rica Aura Validation Experiment.

Notes:

^a Marine boundary layer mixing ratios are identical to those in Table 2-2 of the previous Assessment (Law and Sturges et al., 2007).

^b UT data are from DC-8 aircraft observations during PEM-West A, PEM-West B, and TC4.

^c TTL and tropopause data are from WB-57 aircraft observations during TC4, Pre-AVE, and CR-AVE (see Aschmann et al., 2009, Hossaini et al., 2010 and Liang et al., 2010) and balloon observations from Teresina, Brazil, in June 2005 (Laube et al. 2008) and June 2008 (update of Laube et al., 2008).

^d LZRH(z_0) corresponds to the level of zero clear-sky radiative heating (z_0) (see Box 1-4). As in the previous assessment (Law and Sturges et al., 2007), we define this level at about 15 km or 360K, where there is a transition from clear-sky radiative cooling to clear-sky radiative heating. In general, air masses above this level are expected to enter the stratosphere.

^e The stated observed range represents the smallest mean minus 1 standard deviation and the largest mean plus 1 standard deviation

Table 1-7, continued (notes).

- among all measurement campaigns.
- ^f CH₂ClCH₂Cl (dichloroethane) and CHClCCl₂ (trichloroethene) in the UT only from TC4.
- ^g CH₂ClCH₂Cl and CHClCCl₂ in the TTL, including the LZRH, only from TC4, Pre-AVE, and CRAVE.
- ^h CH₂BrCl in the UT only from PEM-West B.
- ⁱ CH₂BrCl and CHBrCl₂ in the TTL, including the LZRH, only from TC4 and Teresina balloon measurements.
- ^j Estimated maximum contribution from species like C₂H₅Br, C₂H₄Br₂, C₃H₇Br.
- ^k CH₃I in the TTL, including the LZRH, only from TC4 and Pre-AVE.
- ^l The anthropogenic fraction of chlorinated VSLS (Anthrop. Cl) has been calculated by adding 90% of CH₂Cl₂, 25% of CHCl₃, and 100% of CCl₂CCl₂, CHClCCl₂, and CH₂ClCH₂Cl (see also Section 1.3.1.1).

significant macroalgae on the local shore. Peak concentrations were observed at solar noon (2–44 ppt CHBr₃ and 1–9 ppt CH₂Br₂), rather than low tide as would be expected for emissions from intertidal macroalgae.

In a case study off the West coast of Africa, Quack et al. (2007) suggest that CH₂Br₂ might originate partly from biologically mediated reductive hydrogenolysis of CHBr₃. Some studies (e.g., Palmer and Reason, 2009; Kerkweg et al., 2008) suggest significant regional “hotspots” in the tropics and subtropics especially in the west Pacific Ocean near Indonesia, but with large seasonal and temporal variations. This point is also in accord with Butler et al. (2007), who estimated that 64% of bromoform emissions originated from the Pacific (47% from the tropical Pacific, and 70% in total from the tropics), compared with just 3% from the Atlantic. For CH₂Br₂ the corresponding figures were 40% (24%, 40%) and 20%, respectively. In the last Assessment (Law and

Sturges et al., 2007) it was proposed that regions of oceanic upwelling could be important sources of bromocarbon emissions. Since then Quack et al. (2007) and Carpenter et al. (2009) have shown, based on measurements in the Mauritanian upwelling, that such regions may be collectively relatively minor contributors to global emissions (e.g., around 1% of CHBr₃ and CH₂Br₂ global emissions).

It should also be noted that discrepancies between observation-based studies arise from the “snapshot” picture they supply of a highly heterogeneous and variable system, as well as possible substantial differences between calibration scales (Butler et al., 2010) and methods of estimating fluxes and extrapolating them to larger areas (e.g., Carpenter et al., 2009 and O’Brien et al., 2009). The picture of global bromocarbon emissions is therefore highly complex with substantial uncertainties. Understanding the regional and seasonal variability of emissions is, however,

Table 1-8. Fluxes of bromine from bromoform (CHBr₃) and dibromomethane (CH₂Br₂) in Gg Br/yr, and iodine from methyl iodide (CH₃I) in Gg I/yr.

Reference	CHBr ₃ Flux (Gg Br/yr)			CH ₂ Br ₂ Flux (Gg Br/yr)			CH ₃ I Flux (Gg I/yr)		
	Global	Open Ocean	Coastal	Global	Open Ocean	Coastal	Global	Open Ocean	Coastal
Butler et al. (2007)	800	150	650	280	50	230	550	270	280
Carpenter et al. (2009)			200						
Liang et al. (2010) ^c	430	260	170	57	34	23			
O’Brien et al. (2009)	820 ^a 1400 ^b								
Palmer and Reason (2009)		120 ^c							
Yokouchi et al. (2005)	820 ^a								
Warwick et al. (2006)	560 ^d	280 ^d	280 ^d	100					

^a Scaled to CH₂Br₂ emissions from Ko and Poulet et al. (2003), based on global loss rates and an estimated global burden.

^b Scaled to CH₂Br₂ emissions from Warwick et al. (2006).

^c Tropical ocean only.

^d Modeling study: “Scenario 5”: 70% of emissions in the tropics; August/September.

^e Emissions from Liang et al. (2010) are from modeling of airborne measurements in the Pacific and North American troposphere and lower stratosphere.

vital in assessing their likely impact on the stratosphere, since it is the coincidence in both space and time of VSL SG emissions with surface to tropical tropopause layer (TTL) transport that will largely dictate the efficiency with which these emissions reach the stratosphere.

Updated mixing ratios of organic bromine from VSLS of 3.5 (1.7–7.4) ppt in the tropical upper troposphere (10–12 km) (Table 1-7) confirm reported figures from the last Assessment of 3.5 (3.1–4.0) ppt at 10 km. This organic bromine from VSLS consists mostly of CH_2Br_2 and CHBr_3 with smaller amounts of bromochloromethanes and is discussed further in Section 1.3.3.1.

1.3.1.3 IODINE-CONTAINING VERY SHORT-LIVED SOURCE GASES

The occurrence and chemistry of iodinated compounds, all of which are VSLS, were discussed extensively in previous Assessments due to their potentially very high ODPs should they reach the stratosphere (the “alpha” factor for iodine in the stratosphere is higher than bromine). Iodinated gases are predominantly of natural origin, but have been considered for use as fire suppressants as a halon replacement on aircraft (e.g., CF_3I) or to reduce flammability in refrigerant mixtures. CH_3I is also currently being licensed in the U.S. and Japan as a replacement for CH_3Br as a fumigant (UNEP/TEAP, 2010). Domestic biomass burning in Africa reportedly contributes a small flux of CH_3I to the atmosphere (Mead et al., 2008c).

The dominant source of iodinated VSLS is from the ocean. Butler et al. (2007) estimated approximately equal global fluxes of CH_3I from the open ocean and coastal regions (Table 1-8) and a higher total flux than given in the previous Assessment by about a factor of two. Yokouchi et al. (2008) observed an increase in CH_3I with sea surface temperature at midlatitudes, which might be of significance in a warming climate, and a corresponding seasonality with higher concentrations in summer. An intriguing observation is that of Williams et al. (2007), who presented evidence for enhanced emissions of CH_3I from the ocean, apparently from an abiotic chemical mechanism stimulated by dust deposition. A corollary of this is that a similar mechanism might operate in atmospheric aerosols. Sive et al. (2007) conclude that terrestrial biomes contribute a small but significant flux to the atmosphere.

Several recent studies have measured a range of iodinated species in the marine boundary layer (MBL) and considered the active iodine-mediated chemistry therein. It is unlikely, however, that either the shortest-lived iodinated species (those with lifetimes of minutes or hours), or inorganic iodinated gases (e.g., I_2 , IO, and OIO; Read et al., 2008), would escape the MBL in appreciable quantities (see also Section 1.4.3).

1.3.1.4 HALOGEN-CONTAINING AEROSOLS

In addition to organic VSLS, inorganic sources, notably halogen-containing aerosols, may be precursors of reactive halogens in the atmosphere. Although aerosols are subject to gravitational and wet depositional processes, they can have significant atmospheric residence times under the dry conditions prevalent in the free troposphere (e.g., several days for sea salt aerosol; Yang et al., 2005). Yang et al. (2005) suggested that 0.1–1.0 ppt of bromine monoxide (BrO) in the troposphere arises from a combination of Br release from sea salt and decomposition of bromomethanes. Support for such a mechanism comes from the model described by O’Brien et al. (2009) where additional release of halogens from halide-containing aerosol (over and above that from degradation of bromocarbons) was required to explain BrO abundances measured within the tropical marine boundary layer (Read et al., 2008). Pyle et al. (2007) note that sea salt production rates are highly uncertain and that using two separate formulations results in a factor of two difference in sea salt aerosol production rates. Bromine and iodine have been detected in aerosols of tropospheric origin in the stratosphere several kilometers above the local tropopause height (Murphy et al., 2007). The influence of these aerosols on lower stratospheric halogen abundances is likely small but is poorly quantified. We conclude that the contribution from sea salt aerosol to stratospheric Br_y is likely to be substantially less than 1 ppt.

1.3.2 Transport of Very Short-Lived Substances into the Stratosphere

The efficiency of VSLS transport into the stratosphere results from the competition between fast vertical transport and chemical destruction or removal via washout of the source gases (SGs) and product gases (PGs). Conversion of SG to PG reduces the efficiency of halogen transport to the stratosphere if the PG is taken up by aerosols and becomes washed out before reaching the stratosphere. The probability of washout decreases with increasing height within the troposphere and becomes small in the TTL. In general, SG and PG reach the “tropical stratosphere” above the cold point tropopause (CPT), which is climatologically located at 380 K (~17 km altitude). Therefore, timescales for transport through the TTL are especially important for determining the efficiency of VSLS transport through this layer. For a detailed TTL schematic see Figure 1-9 (adapted from Fueglistaler et al. (2009a) and modified to provide definitions of the TTL consistent with past Assessments).

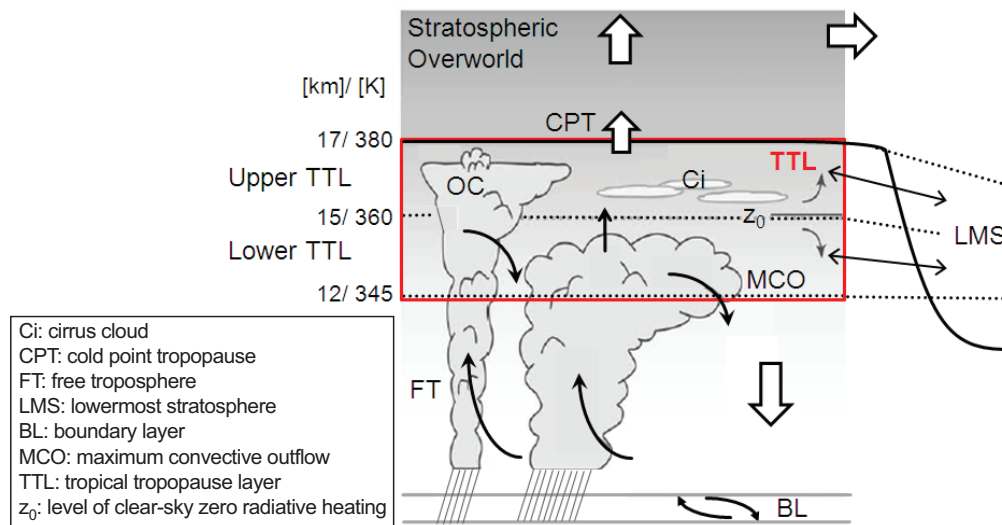


Figure 1-9. Schematic showing principal dynamical pathways in the tropics transporting VSL source gases (SG) and product gases (PGs) into the stratosphere (modified from Fueglistaler, 2009a). The position of the tropopause is designated by the bold black line.

1.3.2.1 VLSL TRANSPORT FROM THE SURFACE IN THE TROPICS TO THE TROPICAL TROPOPAUSE LAYER (TTL)

While shorter-lived VLSL with lifetimes of only hours to days are unlikely to reach the TTL unless emitted directly into the active cell of tropical deep convection, VLSL with lifetimes of weeks to months can reach the TTL via a range of transport pathways described in Figure 1-9.

Additional evidence has become available since the previous Assessment supporting the tropical Western Pa-

cific as a region where VLSL emissions can be efficiently transported to the TTL (Aschmann et al., 2009) (Figure 1-10). New results also suggest that the efficiency of this TTL transport varies with season. Higher VLSL concentrations in the TTL are predicted in NH winter compared to the rest of the year (Aschmann et al., 2009; Gettelman et al., 2009) due to a combination of higher convective cloud tops reaching the TTL and higher vertical velocities within the TTL (Gettelman et al., 2009).

In NH summer, air masses can cross the TTL and enter the stratosphere, but with a reduced and more zonally uniform distributed flux compared to NH winter (Fueg-

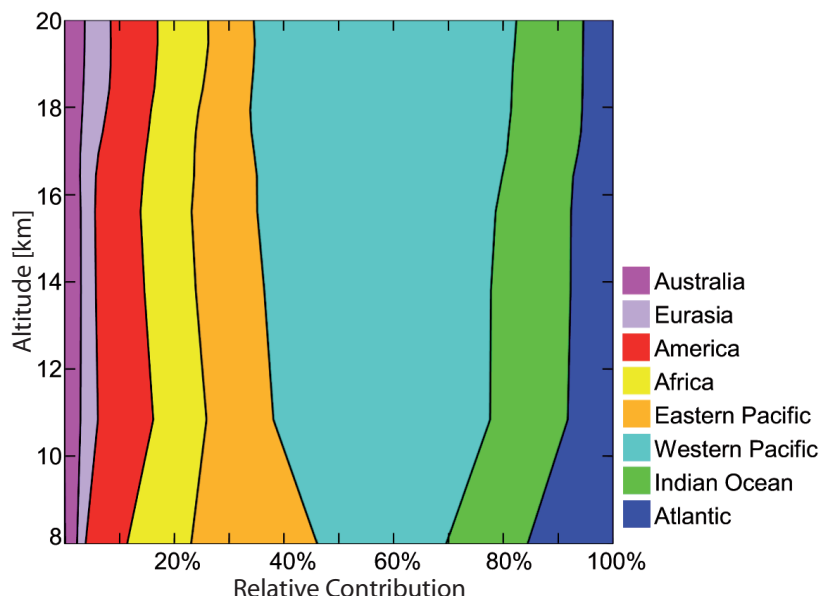


Figure 1-10. The relative contribution (%) of individual source regions to the total amount of an idealized CHBr_3 tracer (with a 20-day lifetime) between 8 and 20 km in the tropics, averaged over 2000–2005. Australia includes Maritime Continent and Africa includes Arabian Peninsula. The relative contribution from the Mediterranean region was also diagnosed but is too small to be visible in this figure (modified from Aschmann et al., 2009).

listaler et al., 2005). However, the northward shift of the deepest convection with the Indian summer monsoon linked with the anticyclonic circulation in the upper troposphere/lower stratosphere could lead to more efficient transport of surface emissions in certain regions of the world (e.g., Bay of Bengal and Sea of China) to the TTL and potentially to the stratospheric overworld (e.g., James et al., 2008; Randel et al., 2010). For instance, Stohl et al. (2002) have estimated that in NH summer, Asian surface emissions can be transported into the TTL with average timescales of a week or less instead of three weeks in NH winter. Consistent with these findings, Donner et al. (2007) simulate enhanced methyl iodide (CH_3I) concentrations over the Tibetan plateau and the Himalaya during NH summer in the free troposphere and above the cold-point tropopause due to overshooting convection. Thus tropical overshooting convection can directly inject surface air into the upper TTL and to the stratosphere as is observed (e.g., Ricaud et al., 2007) and simulated by different models (Donner et al., 2007; James et al., 2008). Due to the very rare and localized occurrence of such events (Liu and Zipser, 2005; Liu et al., 2007), the amount of VLSL halogen reaching the stratosphere via these events is expected to be small on a global basis, as has been discussed analogously for the stratospheric water vapor budget (Fueglistaler et al., 2009b; Schiller et al., 2009; Homan et al., 2010). Besides, Hossaini et al. (2010) suggest that especially for longer-lived VLSL (e.g., CH_2Br_2), large-scale transport and mixing of planetary boundary layer (PBL) air to the TTL could also be important transport processes in addition to overshooting convection.

Because observational evidence for direct VLSL transport from the surface to the TTL and to the stratosphere is scarce, the relative roles of boundary layer mixing, convection, and overshooting convection are still a matter of debate. In addition to the uncertainties in convective parameterizations in models discussed in the last Assessment (Law and Sturges et al., 2007), washout of VLSL influences the amount of VLSL actually reaching the stratosphere (Section 1.3.3).

1.3.2.2 VLSL TRANSPORT FROM THE TTL TO THE STRATOSPHERE

Transport through the upper TTL primarily takes place as large-scale horizontal and slow vertical motions (weeks to ascend through this region of the TTL) accompanied by infrequent localized and rapid (hours) overshooting convection into the stratosphere (Law and Sturges et al., 2007; Fueglistaler et al., 2009a; Figure 1-9). Furthermore, the transport of VLSL through the TTL is also dependent on the region and season of VLSL emissions and varies interannually (Aschmann et al., 2009; Gettelman et al., 2009; Krüger et al., 2009).

In the last Assessment a large uncertainty was reported for the residence time in the TTL, with a range of 20 to 80 days in the upper TTL. The understanding of residence times in the TTL has since improved to some extent. In particular, the residence time depends strongly on vertical velocities, on the particular layer being considered within the TTL, and on the temporal and horizontal variability used for calculating the transport. New approaches and improved data assimilation have become available. This has led to a reduced uncertainty range of 25 to 45 days for transport through the upper TTL (Krüger et al., 2009; Ploeger et al., 2010).

Of particular relevance for the VLSL fraction reaching the stratosphere is the slow, radiatively driven transport through the upper TTL (from the level of clear-sky zero radiative heating (z_0) at 360 K to the CPT at 380 K) (see Figure 1-9). The annual cycle of air mass transport from the TTL to the stratosphere peaks over the tropical Western Pacific during NH winter and over the Indian monsoon regions during NH summer (Fueglistaler et al., 2005; Law and Sturges et al., 2007). In addition, the TTL residence time close to the CPT is lower by 25% in NH winter compared to NH summer (Kremser et al., 2009; Ploeger et al., 2009) and this also influences the efficiency of VLSL transport to the stratosphere.

At the CPT and above, large-scale vertical motion dominates the air mass transport (Krüger et al., 2008; Fueglistaler et al., 2009a; Gettelman et al., 2009) and readily brings air to regions of the stratosphere where ozone is depleted. Above the tropical Western Pacific, Krüger et al. (2009) found that most air parcels are transported in less than 25 days through the 360 K to 380 K layers during NH winters 1962–2001, which is at the lower end of the averaged residence time of 25–45 days stated above. They derived a long-term interannual variability of the averaged residence time for air parcels in the upper TTL during NH winter of up to 20% (± 2 sigma); with shorter residence times being significantly correlated with periods of enhanced extratropical and subtropical wave driving. General changes in tropical upwelling rates and of the Brewer-Dobson circulation (BDC) are discussed in more detail in later Chapters (Sections 3.2.4 and 4.2.2). These considerations lead to a higher potential of halogens from VLSL entering the stratosphere within these regions and seasons during periods of enhanced wave driving and/or convective overshoot.

1.3.2.3 VLSL TRANSPORT FROM THE SURFACE TO THE EXTRATROPICAL STRATOSPHERE

The extratropical lowermost stratosphere (LMS) is the region between the extratropical tropopause and approximately the 380 K isentropic surface (see Figure 1-9). While the contribution of VLSL to halogen in the extratropical

stratosphere is mainly controlled by upwelling into the tropical stratosphere and quasi-horizontal isentropic transport into the extratropics, it has been perceived in recent years that vertical transport by convection into the extratropical stratosphere can also be of importance (Section 2.4.2 of Law and Sturges et al., 2007). Furthermore, new evidence suggests that a larger fraction of tropical air masses in the TTL are transported into the extratropical stratosphere than into the stratospheric overworld, as detailed below.

Levine et al. (2008) simulate that up to 5 times more air mass is transported from the bottom of the TTL into the LMS than from the bottom of the TTL into the tropical stratospheric overworld throughout the year. However, the amount of transport into the extratropical LMS is largest toward the SH and shows, for both transport pathways, a seasonal dependence with a maximum during NH winter and a minimum during NH summer.

In contrast, the studies by Bönisch et al. (2009) and Berthet et al. (2007), which concentrated on the NH only, analyzed a stronger transport from the tropical troposphere to the extratropical LMS during NH summer. Bönisch et al. (2009) estimate a strong seasonality of the origin of tropical air masses in the LMS of the NH, with a maximum tropospheric influence during October. The authors conclude that the seasonality is influenced by the transit times from the tropical troposphere into the LMS, which are shortest (<0.3 years) during summer and longest (>0.8 years) during late spring. From this it can be concluded that the strength of the subtropical jet and the lower branch of the BDC strongly influence the transport of VSLS in the LMS (i.e., the subtropical jet is weaker from summer to mid-autumn, and the residual transport timescales within the lower branch of the BDC are shorter in summer than in winter and dominate the tropospheric influence in the LMS). Berthet et al. (2007) also find that during NH summer, the extratropical LMS layer between 370 K and 410 K is well ventilated with tropospheric air from the tropics compared to the layer below 340 K, which is mainly influenced by extratropical air. During NH winter this distinction holds but with weaker tropical troposphere-to-stratosphere transport (TST) due to a more impermeable barrier.

Convective overshooting of air across the tropopause into the LMS is quite frequent in the extratropics. These injections, together with transport from the TTL, form a mixed layer extending about 25 K above the tropopause (Hoor et al., 2004). Sometimes, injections even deeper into the stratosphere can occur and influence the chemical composition of the lower stratosphere (Hegglin et al., 2004). The deepest injections are produced by the high instability and breaking of gravity waves excited by strong convection inside super-cell thunderstorms (Wang, 2007; Wang et al., 2009). While water vapor enrichments have been documented by this mechanism, no studies

related to VSLS transport via this mechanism have been published. Another possibility for surface air to be injected directly into the extratropical stratosphere (even into the stratospheric overworld) is by pyro-convection associated with strong forest fires. Single pyro-convection events can double the zonally averaged aerosol optical depth in the LMS and these aerosol layers can persist in the stratosphere for months (Fromm et al., 2008). While this process is not captured by global models, special high-resolution models have recently shown skill in simulating pyro-convection (Trentmann et al., 2006; Luderer et al., 2007). So far, no observations of halogenated VSLS in pyro-convective outflows have been reported.

1.3.3 VSLS and Inorganic Halogen Input to the Stratosphere

In the previous Assessment (Law and Sturges et al., 2007) the contribution of VSLS species to the stratospheric halogen loading was discussed in detail. Since this last Assessment new observations of VSLS SGs in the tropical upper troposphere and TTL have become available, as well as modeling studies of the possible input of product gases (PGs) from these VSLS. However, for brominated PGs still no observations are available from the upper tropical troposphere and from the TTL that would enable us to identify the contribution of PGs to stratospheric bromine loading.

1.3.3.1 SOURCE GAS INJECTION (SGI)

Source gases deliver halogen into the stratosphere in the same form as they are emitted at the surface. Some recent modeling studies (Donner et al., 2007; Aschmann et al., 2009; Liang et al., 2010; Hossaini et al., 2010) have used observational data of the most important bromine- and iodine-containing VSLS species (CH_2Br_2 , CHBr_3 , and CH_3I) to compare with their modeling results. These new observational data on VSLS species in the TTL have become available from the Aura Validation Experiment (AVE; http://espoarchive.nasa.gov/archive/arcs/pre_ave/ and <http://www.espo.nasa.gov/ave-costarica2/>) and TC4 (Tropical Composition, Cloud and Climate Coupling, <http://www.espo.nasa.gov/tc4/>) missions, and from balloonborne observations (Laube et al., 2008). In addition, available data from the Pacific Exploratory Mission (PEM) West A and B campaigns have been used. New balloonborne observations of chlorinated VSLS and of additional brominated VSLS have also been reported by Laube et al. (2008). The averages and the ranges of these observations are compiled in Table 1-7 for the upper tropical troposphere (10 km altitude range), the bottom of the TTL (340–355 K), z_0 (taken as about 355–365 K), the upper

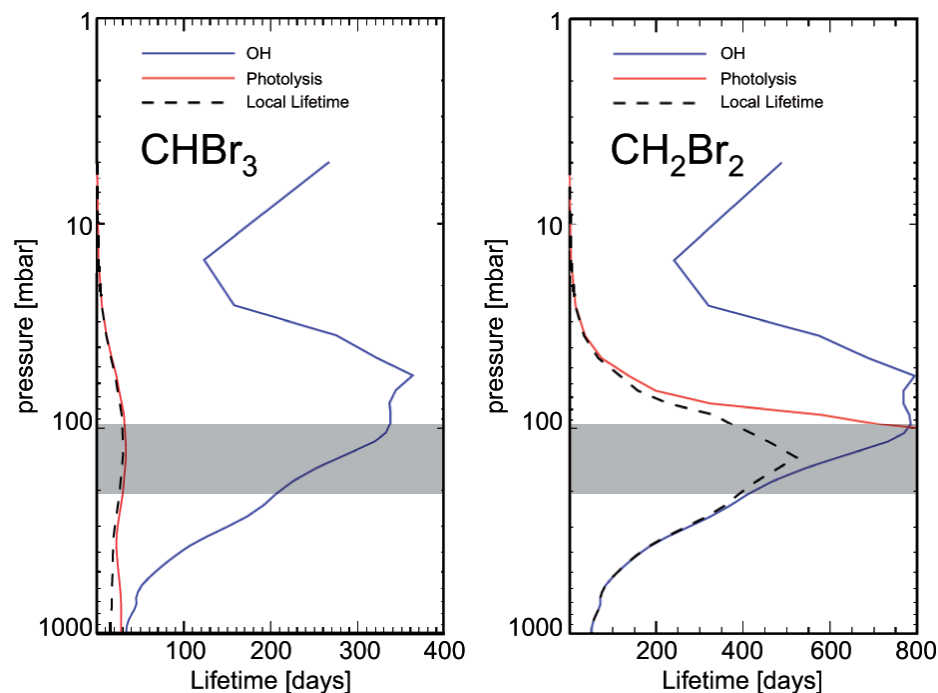


Figure 1-11. The modeled vertical distribution of the annual mean lifetime (days) of CHBr_3 and CH_2Br_2 in the tropics ($\pm 20^\circ$ latitude) with respect to the two main loss processes: photolysis (solid red line) and reaction with OH (solid blue line), as well as the overall lifetime (dashed black line). The region between the base of the TTL and the cold-point tropopause (CPT) is indicated as the gray bar. Modified from Hossaini et al. (2010).

TTL (365–375 K), and the tropical cold point tropopause (375–385 K) (Figure 1-9). In the following discussion of uncertainties, we do not take into account uncertainties in absolute calibrations (e.g., Butler et al., 2010). Rather we use data from different sources and take the ranges of the reported mixing ratios. Uncertainties in the absolute calibrations will thus be reflected in the range of uncertainties due to the use of data from different sources. Furthermore, the data coverage is still sparse (e.g., not all possible input areas and seasons have been sampled) and it is unclear how far the available observations reflect the complete range of possible input values.

SGI from Chlorinated VSLs

Law and Sturges et al. (2007) concluded on the basis of multiple airborne campaigns that the chlorine content from VSL SGs in the tropical upper troposphere was about 50 ppt, representing about 1 to 2% of the inorganic stratospheric chlorine (Cl_y) input from long-lived source gases. Recent airborne and balloonborne observations in the tropics have confirmed and refined these conclusions (Laube et al., 2008) (see Table 1-7). The major loss process for most chlorine-containing VSLs is the reaction with OH. As the rate constants for these reactions decrease at the low temperatures in the upper tropical troposphere and TTL, vertical mixing ratio gradients are rather small. The total chlorine contained in VSL source gases decreases from about 60 ppt in the upper tropical troposphere and lower TTL to about 50 ppt near the tropical tropopause. $\text{C}_2\text{H}_5\text{Cl}$ was not quantified, but was estimated to be on the

order of 1.5 ppt in the upper tropical troposphere (Law and Sturges et al., 2007).

Our best estimate of chlorine injected as SG from VSLs into the stratosphere is 55 (38–80) ppt and largely confirms the estimate of 50 (± 10) ppt given in the previous Assessment (Law and Sturges et al., 2007).

SGI from Brominated VSLs

The two main brominated VSLs (CHBr_3 and CH_2Br_2) show different vertical gradients in the transition region between the troposphere and the stratosphere (see Table 1-7). Whereas mixing ratios of CH_2Br_2 decrease from about 0.9 ppt in the upper tropical troposphere and the lower TTL to about 0.5 ppt near the tropical tropopause, mixing ratios of CHBr_3 decrease more substantially in this region, declining from 0.5 ppt in the upper troposphere and lower TTL to 0.1 ppt near the tropical tropopause.

These observed differences are explained by the different local lifetimes of these gases within the TTL. While photolysis dominates the destruction of CHBr_3 and leads to a modeled local lifetime that is similar to transport times for air through the TTL, the lifetime of CH_2Br_2 (set mainly by $[\text{OH}]$) is much longer than transport timescales (Figure 1-11).

Lifetime differences are also noted in the troposphere for these gases, and this influences the efficiency of surface emissions reaching the upper troposphere. The tropospheric local lifetime of 23 days for CHBr_3 is mainly determined by photolysis (36-day partial lifetime) and to a lesser degree by its reaction with the OH radical (76-day

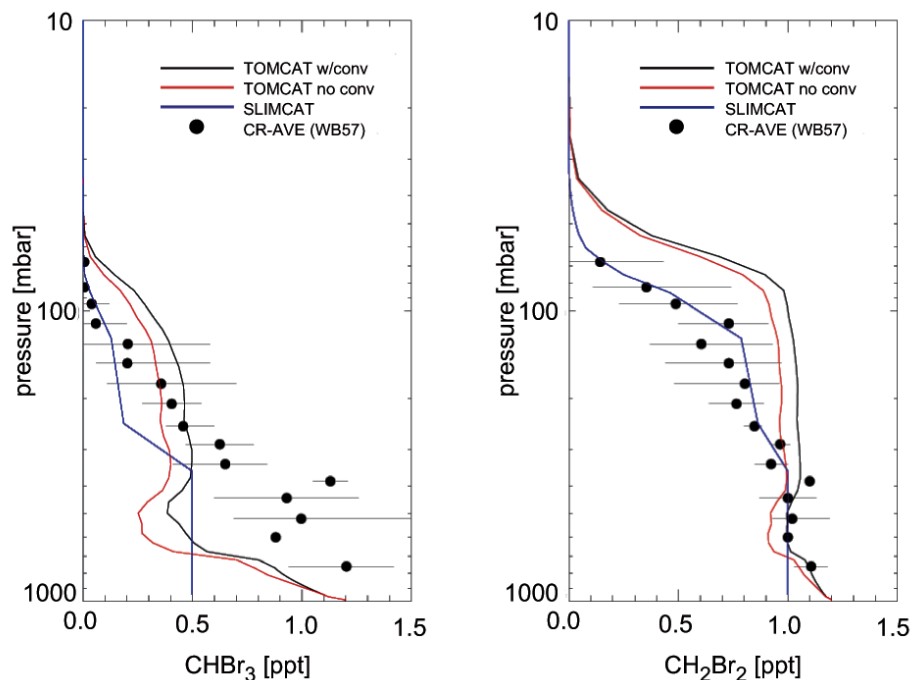


Figure 1-12. A comparison between observed and modeled vertical distributions of CHBr_3 (left panel) and CH_2Br_2 (right panel) mixing ratios (ppt) at tropical latitudes (Hossaini et al., 2010). The red and black lines are from TOMCAT model runs using ECMWF vertical velocities, without and with parameterized convection, respectively, while the SLIMCAT model run (blue lines) is based on calculated diabatic heating rates. Black dots are measurements from the CR-AVE campaign. Modified from Hossaini et al. (2010).

partial lifetime). In contrast, the considerably longer tropospheric local lifetime of CH_2Br_2 of 123 days is nearly completely governed by its reaction with the OH radical (Table 1-4 and Figure 1-11).

As a result of these influences, a 1-D model calculation suggests that 70% and 28% of the specified surface concentrations of CH_2Br_2 and CHBr_3 , respectively, reach 18 km altitude (top of the TTL), when operational European Centre for Medium-Range Weather Forecasts (ECMWF) velocity fields, a convective source, and a VSLS sink are taken into account (Gettelman et al., 2009). Hossaini et al. (2010) also discuss the breakdown of CH_2Br_2 and CHBr_3 in the atmosphere and compare their three-dimensional (3-D) model results with observational data (Figure 1-12). In the upper tropical troposphere and the TTL, Hossaini et al. (2010) achieved an overall better agreement of simulated and observed CH_2Br_2 and CHBr_3 profiles when using the slower (climatological) diabatic heating rates in the Single Layer Isentropic Model of Chemistry and Transport (SLIMCAT) model compared to using the faster analyzed vertical velocities in the Toulouse Off-line Model of Chemistry and Transport (TOMCAT)-chemical transport model. Assuming uniform mixing ratios of 1.2 ppt of CH_2Br_2 and CHBr_3 in the tropical lower troposphere, they derive a SGI of about 2 ppt Br into the stratosphere. Additionally, the sum of CH_2BrCl , CHBr_2Cl , and CHBrCl_2 contributes about 0.5 ppt of bromine to the upper troposphere and lower TTL. Near the tropical tropopause the total contribution of these source gases declines to about 0.2 ppt. Additional bromine from species not quantified, like $\text{C}_2\text{H}_5\text{Br}$ and n-propyl bromide ($\text{C}_3\text{H}_7\text{Br}$), is expected to

be presently less than 0.2 ppt in the TTL. In summary, we estimate VSLS bromine source gases, including unmeasured species, to account for about 2.7 (1.4–4.6) ppt of bromine at about 15 km altitude in the tropics and about 1.5 (0.7–3.4) ppt at the tropical CPT at around 17 km altitude.

SGI from Iodinated VSLS

Newly available data for CH_3I in the TTL from the Pre-AVE and TC4 experiments (see Table 1-7) (Aschmann et al., 2009) as well as data from Bell et al. (2002), which are compared to modeling results in Donner et al. (2007), indicate that the mixing ratios of this most important iodine source gas in the TTL at 15 km altitude are generally below 0.1 ppt and drop below 0.05 ppt at the cold point tropopause. This is consistent with the estimate of 0.08 ppt from the previous Assessment for CH_3I in the upper tropical troposphere (Law and Sturges et al., 2007). Three recent studies have also investigated the transport of methyl iodide into the TTL (Donner et al., 2007; Gettelman et al., 2009; Aschmann et al., 2009). These studies confirm that due to its short lifetime, only a very small fraction of CH_3I from the boundary layer reaches the TTL and the stratosphere.

1.3.3.2 PRODUCT GAS INJECTION (PGI)

In addition to the input of halogen from VSLS source gases, their chemical degradation products (so-called product gases or PGs) are also likely to contribute halogens to the stratosphere. Due to their solubility in water

and the significant uptake coefficients on ice of many of these PGs (see Law and Sturges et al., 2007, for a detailed discussion) their fate is less clear than that of source gases and depends critically on the physical and chemical conditions in the area where they are formed. This leads to a strong coupling between chemistry, removal processes, and atmospheric transport processes relevant for VSLS species. While observations of source gases discussed in Section 1.3.3.1 have become available, observations of PGs are sparse for chlorine and no observations of PGs above detection limits of the respective instruments have been reported for bromine and iodine in the upper tropical troposphere and the TTL. An assessment of plausible values of PGI for these two halogens therefore relies largely on modeling results that are not currently constrained by observations.

PGI from Chlorinated VSLS

In the previous Assessment there were large uncertainties regarding the contribution of chlorinated PGs, notably COCl_2 (phosgene) and HCl, arising from degradation of chlorinated VSLS (and longer-lived SGs) to Cl_y . The picture is complicated due to possible “double counting” of chlorinated PGs recirculated from the stratosphere and thus already taken into account in the budget of source gases entering the stratosphere. Fu et al. (2007) reported satellite measurements of COCl_2 , albeit with large uncertainty limits, between February 2004 and May 2006. Chlorine from COCl_2 between 15 and 20°N was 43 ± 27 ppt Cl at 8.5 km (upper troposphere), 31 ± 22 ppt Cl at 14.5 km, and **36 ± 26 ppt Cl at 17.5 km, i.e., approximately 32 ± 22 ppt of chlorine at z_0 (~15 km).** These values are at the lower end of the range (40 – 50 ppt Cl) estimated in the previous Assessment (Law and Sturges et al., 2007). As it is unclear how much of the chlorine in COCl_2 is already included in the budgets from the SGs, we follow the same approach as in the previous Assessment by considering a range of values, or 0–32 ppt of additional chlorine. A best estimate of 16 ppt results as possible additional chlorine input to the stratosphere in the form of COCl_2 , which is not accounted for in the very short-lived source gas budgets.

Marcy et al. (2007) reported HCl to be below their detection limit of 5 ppt in upper tropospheric air over the tropical east Pacific. In the lower TTL over the east Pacific in January 2004, however, Marcy et al. (2007) reported HCl to be mostly non-zero with values ranging to almost 40 ppt around 15 km altitude, and increasing to about 20–80 ppt in the upper TTL, with the increase being mainly attributed to in-mixing of lowermost extratropical stratospheric air. Mébarki et al. (2010), using a less sensitive long-path instrument, placed an upper limit of 30 and 20 ppt HCl in the upper TTL (~15–17 km) from two flights over Brazil

in June 2005 and June 2008, respectively. Marcy et al. (2007) estimated that at most only 3–8 ppt of the HCl that they observed in the TTL could have originated from in situ degradation of CH_3Cl . Park et al. (2008) report that profiles of HCl concentration reached minimum values of about 10 to 30 ppt at around 13 km above the Asian continent, consistent with the measurements reported by Marcy et al. (2007). In summary, we conclude that HCl values in the TTL are typically on the order of 20 (0–40) ppt. As it is unclear how much of this chlorine will eventually reach the stratosphere or has already been accounted for by source gases, we estimate that somewhere between 0 and 100% of this HCl (i.e., 0–20 ppt of chlorine) could represent an additional source of chlorine from VSLS to the stratosphere, with a best estimate value being the midpoint (10 ppt).

PGI from Brominated VSLS

The only bromine PG that has been measured in the TTL is bromine monoxide (BrO) (Dorf et al., 2008; see also Section 1.4). The observed values were reported to be below detection (i.e., below 1 ppt BrO) in the TTL, though a value of 2 ± 1.5 ppt BrO was derived around the local tropopause at about 17 km. Because this sparse observational information does not tightly constrain the average input of brominated PG into the stratosphere, a range of plausible values is derived here based on modeling studies.

Most modeling studies rely on the assumption that bromine from photo-oxidized VSLS is immediately transformed to inorganic bromine (mainly as hydrogen bromide (HBr), hypobromous acid (HOBr), and BrO). This is supported by Hossaini et al. (2010), who concluded that all intermediate organic products of the oxidation of bromocarbons are short lived, with COBr_2 being the longest-lived organic intermediate with an atmospheric lifetime of 7 days.

The assumption that the degradation of organic bromine-containing VSLS yields inorganic bromine is thus fairly well established. The subsequent fate, however, of this inorganic bromine (Br_y) is less clear. Most inorganic bromine gases, especially HOBr and HBr, are highly soluble in water and have high uptake coefficients on ice (see Section 2.3.4 of Law and Sturges et al., 2007). The removal of Br_y from the gas phase and the subsequent washout is parameterized in models. This parameterization has a strong influence on the fraction of product gases reaching the stratosphere. Furthermore, as already emphasized in the last Assessment, heterogeneous reactions of HOBr and HBr with sulfuric acid producing photolabile dibromine monoxide (Br_2O) and molecular bromine (Br_2) further complicate the modeling of this process.

Model studies presented in the previous Assessment used prescribed removal timescales for Br_y in the TTL (e.g., Warwick et al., 2006; Sinnhuber and Folkins,

2006), i.e., the removal processes (wet deposition, uptake on ice, and dehydration) have not been calculated explicitly. Hossaini et al. (2010) follow a similar approach and test the sensitivity of the amount of bromine reaching the stratosphere on different washout times for Br_y , ranging from 10 days to infinity. Depending on the assumed time constants for washout times, the PGI bromine from CH_2Br_2 and CHBr_3 varies between 0.4 ppt (10 days washout) and 1.7 ppt (40 days washout time) and can be as high as 3.9 ppt of bromine if an infinite washout time is assumed. This range of values is consistent with the ranges presented in the previous Assessment (Law and Sturges et al., 2007). Two other recent studies (Aschmann et al., 2009; Liang et al., 2010) have attempted to explicitly calculate the removal processes, based on dehydration processes in the model. Aschmann et al. (2009) used an idealized tracer that has properties similar to CHBr_3 . The inorganic bromine is either completely removed if dehydration occurs in a grid box or it is not removed at all. They derive a bromine input from this tracer that is between 1.6 and 3 ppt, of which 0.3 ppt is in the form of the SGs. The range in PGI from bromoform is thus between 1.3 and 2.7 ppt. Therefore, even with the assumption of complete solubility and instantaneous washout, only about 50% of the PGs are removed in the TTL in this study. Using the Goddard Earth Observing System (GEOS) chemistry-climate model (version 2) with a detailed wet deposition scheme, Liang et al. (2010) suggest that washout is mainly effective below 500 hectoPascals (hPa) and that virtually all inorganic bromine that is released from the SGs above that level reaches the stratosphere.

These large differences in the effect of washout predicted by models show the high degree of uncertainty in the physical understanding of the removal of inorganic bromine during the transport into the tropical stratosphere. Due to this high level of uncertainty and due to the lack of observations of bromine PG in the TTL, it is not possible to derive a best estimate of the amount of bromine entering the stratosphere in the form of PG. Based on the studies presented above and in previous Assessments, the range of PGI from CHBr_3 and CH_2Br_2 is estimated to be between 0.4 and 3.9 ppt. Based on the vertical profiles of other minor bromine source gases, an additional product gases injection from these could range between 0 and 0.3 ppt. Total PGI could thus be somewhere in the range between 0.4 and 4.2 ppt Br.

PGI from Iodinated VSLS

Consistent with the observations presented in the previous Assessment (Law and Sturges et al., 2007), balloonborne measurements using the Differential Optical Absorption Spectroscopy (DOAS) technique have revealed no measurable amount of iodine monoxide (IO) or

iodine dioxide (OIO) in the TTL above detection limits of 0.1 ppt (Butz et al., 2009).

1.3.3.3 TOTAL HALOGEN INPUT INTO THE STRATOSPHERE FROM VSLS AND THEIR DEGRADATION PRODUCTS

As discussed above, both PGI and SGI can contribute halogen to the stratosphere. Here we consider only amounts transported into the stratosphere above the CPT as estimated from the mixing ratios of SGs and PGs at that level and at 15 km (z_0). Since the previous Assessment, additional observations of bromine VSL SGs in the TTL have become available. The halogen contribution from PGs, however, remains much more uncertain. We summarize the available estimates of SGI and PGI for the individual halogens (chlorine, bromine, iodine) in Table 1-9. PG observations are available for chlorine but not for bromine. Therefore, a best estimate of total chlorine input to the stratosphere is derived, based on SG values observed at z_0 and typical values of chlorine PG observed in the TTL. In contrast only a range of possible values is derived for bromine, based on observations at the CPT and modeled PGI. Only upper limits are available for iodine from observations.

Total Input from Chlorinated VSLS

Adding up the entire range of SG and PG observations discussed in Sections 1.3.3.1 and 1.3.3.2 yields a range between 25 and 170 ppt of chlorine from VSLS. For a best estimate of chlorine input into the stratosphere from this range, we use SG observations in the middle of the TTL (at z_0), where VSLS chlorine is 55 (38–80) ppt. It is difficult to assess if chlorine from the PGs HCl and COCl_2 represents an additional source or is already taken into account in the source gas budgets. The best estimate is 16 (0–32) ppt of chlorine from COCl_2 and 10 (0–20) ppt of HCl (see Section 1.3.3.2). The best estimate values for total VSLS chlorine is thus 80 (40–130) ppt, largely in agreement with the estimate given in the previous Assessment of about 50 ppt of chlorine from SGs and about 40 to 50 ppt chlorine from PGs (taken then to include COCl_2 only).

Total Input from Brominated VSLS

In order to avoid double counting, two approaches are used to derive total bromine input from VSLS: (i) the range of possible values of VSLS bromine entering the stratosphere is derived from the range of SG observations at the CPT and the range of modeled PG injections, and (ii) a probable input is derived based on SG observations at z_0 , and assuming that PGs produced above that level

Table 1-9. Summary of source gas (SG) and product gas (PG) observations and modeling results to constrain input of halogens from VLSLs into the stratosphere. Note that only observations of chlorine-containing PGs exist; estimates of PG amounts for bromine are based solely on modeling studies and only upper limits of iodine-containing PGs are available. For bromine and iodine only ranges can be estimated from this. Details on the way that these numbers have been derived can be found in the Sections 1.3.3.1 (SG), 1.3.3.2 (PG), and 1.3.3.3 (total). All values are given in ppt.

Halogen or Compound	Measured TTL to CPT Abundance (ppt Cl, Br, or I)	“Best Estimate” TTL Abundance (ppt Cl, Br, or I)	“Best Estimate” Contribution from VLSLs (ppt Cl, Br, or I)
<i>Chlorine</i>			
VSL SGs	26–80 ^{a, b}	55 (38–80) ^c	55 (38–80)
HCl PG	0–40 ^d	20 (0–40)	10 (0–20)
COCl ₂ PG	31 ± 22 to 36 ± 26 ^e	32 (± 22)	16 (0–32)
Total chlorine	25–170 ^f		80 (40–130) ^f
<i>Bromine</i>			
VSL SGs	0.7–6.5 ^{a, b}	2.7 (1.4–4.6) ^{a, c}	0.7–3.4 ^{a, g}
PG sum			0.4–4.2 ^h
Total bromine			1–8 ^{i, f}
<i>Iodine</i>			
CH ₃ I SG	< 0.05 ^a	< 0.05 ^a	< 0.05 ^a
IO, OIO PG	< 0.1 ^j	< 0.1 ^j	< 0.1 ^j
Total iodine			< 0.15 ^k

^a Based on observations compiled in Table 1-7.

^b Entire range of values observed in TTL and at the CPT, based on Table 1-7.

^c Value and range at the level of zero clear-sky heating (z_0).

^d Range of observed values from Marcy et al. (2007), Mebarki et al. (2010), Park et al. (2008).

^e Fu et al. (2007).

^f Rounded from the range of sums of PG and SG.

^g For the best estimate of bromine, only the SG range at the CPT has been used, as modeled PGI would include contributions from all SG broken down at lower altitudes.

^h Based on modeling work of Hossaini et al. (2010), Aschmann et al. (2009), and Liang et al. (2010); see Section 1.3.3.2.

ⁱ Calculated from the range of SG observations at the tropical tropopause and the PG modeling range.

^j Upper limits reported by Butz et al. (2009) for IO and OIO, respectively.

^k Rounded from Butz et al. (2009), based on observed upper limits of IO and OIO in the lower stratosphere and photochemical modeling.

are transported into the stratosphere, while PGs produced lower in the TTL and upper tropical troposphere have been washed out. Following the first approach, we estimate that a lower limit of 1.1 (0.7 SG and 0.4 PG) ppt of bromine from VLSLs is transported into the stratosphere, while our upper limit estimate is 7.6 (3.4 ppt SG and 4.2 ppt PG). Based on the SG observations at z_0 (15 km) (the second method of estimation), it is probable that 2.7 (1.4–4.6) ppt reaches the stratosphere. In summary, by taking into account PGI and SGI the total contribution is estimated to

be between 1 and 8 ppt (values rounded). This estimated range is slightly lower than given in the previous Assessment (Law and Sturges et al., 2007), where a contribution of 5 ppt (range 3 to 8 ppt) was estimated, but is well within the respective ranges of uncertainty.

Total Input from Iodinated VLSLs

Both SG and PG observations suggest that no significant amount of iodine enters the stratosphere. Butz et

al. (2009) derived an upper limit of 0.09–0.16 ppt of total iodine in the stratosphere from photochemical modeling and the upper limits of IO and OIO from their observations in the tropical lower stratosphere. The total amount of inorganic stratospheric iodine (I_y) is thus estimated to be below 0.15 ppt (Table 1-9).

1.3.4 Potential Influence of VSLS on Ozone

In the previous Assessment (Law and Sturges et al., 2007) a modeling study (Salawitch et al., 2005) was discussed that suggested that 4 to 8 ppt of “additional” stratospheric bromine from VSLS caused enhanced ozone depletion primarily during periods of elevated aerosol loading. Halogens are released efficiently from VSL SGs in the lowermost stratosphere, leading to ozone loss at these altitudes by $BrO + ClO$ catalytic cycles. This process is enhanced in the presence of co-located high aerosol loading of volcanic origin. Law and Sturges et al. (2007) also indicated that iodine-mediated ozone loss due to 0.1 ppt of I_y could only account for at most a few percent of ozone loss and only below about 17 km, depending on the efficiency of catalytic cycles. The associated chemistry remains a matter of significant uncertainty.

More recently Feng et al. (2007) and Sinnhuber et al. (2009) have reported qualitative agreement with the above studies in the sense that additional bromine from VSLS decreased modeled column ozone, but only by a small amount, except during volcanic aerosol events. The two studies, however, produced divergent quantitative column ozone amounts that do not fit all features of the trends at all times, nor do they reproduce absolute column ozone amounts simultaneously in both hemispheres. A detailed discussion of possible reasons for these discrepancies in terms of the respective model setups is beyond the scope of this Assessment, but serves to highlight the uncertainties of such modeling studies.

Sinnhuber et al. (2009) showed better agreement between their modeled trends in column ozone and satellite observations (1980–2005) in the midlatitude SH than in the NH using a two-dimensional (2-D) transport, chemistry, and radiation model. Without additional Br from VSLS, the model follows the larger features of the ozone trend in NH midlatitudes but generally underpredicts the observed declines in column ozone, particularly between 1991 and 1998, which includes a period of high aerosol loading from the 1991 eruption of Mt. Pinatubo. Modeled and measured midlatitude NH ozone depletion for this period of time are, however, in closer agreement when an additional 4 ppt of stratospheric bromine from VSLS are included in the calculations. The addition of 4 ppt of bromine from VSLS enhances modeled ozone loss above that due to all other ODSs by as much as 40% at altitudes below 20 km during the period of peak aerosol

loading following the eruption of Mt. Pinatubo (see Figure 1-13). The effect of Br_y from VSLS (Br_y^{VSLS}) on calculated ozone during times of background aerosol loading is quite small, in agreement with the results of Salawitch et al. (2005).

Sinnhuber et al. (2009) also discussed altitudinal profiles of the modeled ozone changes. Figure 1-13 compares calculated ozone abundances during NH spring during a year with high stratospheric aerosol (1993 with 1980 as a reference year). The significant modeled impact of bromine from VSLS is evident and is confined between the tropopause and about 20 km, which is in qualitative agreement with the calculations by Salawitch et al. (2005).

We conclude from these various studies that the addition of 4–6 ppt of inorganic bromine to the stratosphere (i.e., 240–360 ppt of equivalent chlorine using $\alpha = 60$) from VSLS results in a considerable increase in midlatitude column ozone loss during times of elevated aerosol

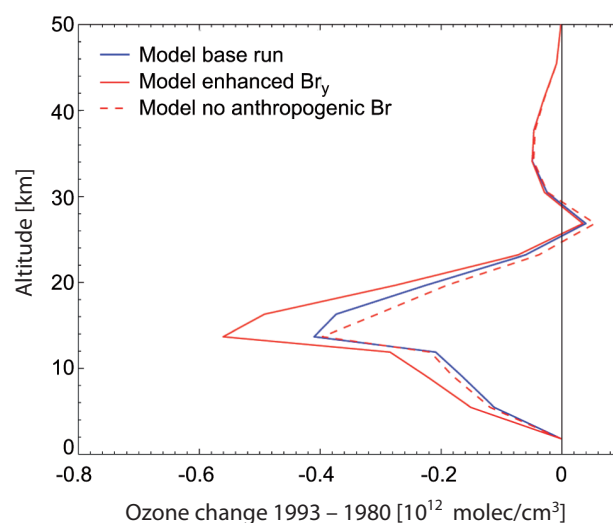


Figure 1-13. Modeled differences between annual mean ozone concentration (molecules per cubic centimeter) calculated for March 1980 and March 1993 at 47°N, illustrating the effect of additional bromine from very short-lived source gases during a period of enhanced stratospheric aerosol (i.e., influenced by the eruption of Mt. Pinatubo in 1991) (Sinnhuber et al., 2009). The base model run (blue line) includes contributions to stratospheric Br_y from CH_3Br , halon-1301, and halon-1211; the solid red model line includes 4 ppt of additional bromine from CH_2Br_2 and $CHBr_3$; and the dashed red line results from the same model run as shown by the solid red line, but with total bromine loading fixed at 1959 levels. Modified from Sinnhuber et al. (2009).

loading, with the largest effect in the lowermost stratosphere (altitudes below ~20 km). To date no analogous study has been undertaken to quantify the effects on ozone of additional chlorine from VSLS, which may amplify the effect on ozone of bromine from VSLS.

1.3.5 The Potential for Changes in Stratospheric Halogens from Naturally Emitted VSLS

As discussed in Section 1.3.4, the current emissions of natural halogenated VSLS have a small but non-negligible impact on the halogen loading in the stratosphere. This situation could change in the future, resulting in a larger role for VSLS in response to factors connected to climate change.

Natural oceanic emissions of VSLS might change in the future in response to changes in climate, as might the efficiency with which VSLS either as SGs or as PGs are transported to the stratosphere. Future oceanic emissions of VSLS will potentially be influenced by changes in seawater temperature, pH, wind speed, mixed layer depth, light penetration, nutrient supply, and depth of biotic production/degradation of trace gases in a potentially more stratified ocean (e.g., Kloster et al., 2007; Schmittner et al., 2008). Hense and Quack (2009) modeled higher CHBr_3 emissions in NH winter for the tropical Atlantic Ocean concurrent with a deepening of the mixed layer depth (MLD), enhancing the connection between the zone of subsurface net production and ocean-air transition. For nutrients, diverging effects have been found for different bromocarbons around the Mauritanian Upwelling of West Africa (Quack et al., 2007). Measurements in this region showed that while CH_2Br_2 concentrations were enhanced in colder, nitrogen-enriched and deeper waters, CHBr_3 productivity was higher in warmer nutrient-poor waters, with little relationship to chlorophyll *a* abundance. Palmer and Reason (2009), however, found a correlation of elevated CHBr_3 concentrations with chlorophyll *a* from the tropical oceans and more surface CHBr_3 from waters with a larger MLD. Zhou et al. (2008) found a linear relationship between bromocarbon emissions and wind speeds above 4 meters per second over the ocean, and strong enhancements in air masses recently affected by a tropical storm. Taken together, seasonal MLD deepening and greater wind-driven surface evasion may account for an order of magnitude higher emissions of CHBr_3 in winter than summer in tropical oceans (Hense and Quack, 2009; Palmer and Reason, 2009). This leads to the conclusion that if climate change would result in greater amplitudes of MLDs and stronger average wind velocities above the oceans, then future emissions of CH_2Br_2 and CHBr_3 could possibly be enhanced, although other factors could either

mitigate or enhance such effects (such as deepening of the subsurface production zone).

When assessing the fate of naturally emitted halocarbons in a future atmosphere, two concurring effects have been discussed to be relevant (i.e., changes in transport and in atmospheric degradation). Pyle et al. (2007) and Dessens et al. (2009) modeled higher Br_y in the tropical troposphere and stratosphere by 2100 due to enhanced convection resulting from increased greenhouse gases and sea surface temperatures. This effect, which is mainly attributed to CH_2Br_2 (>90%), and secondarily to CHBr_3 was, however, only obtained if VSLS were allowed to be emitted in the tropics (20°N–20°S). Placing the emissions outside the tropics resulted in no enhancement of stratospheric Br_y , as the VSLS species were largely oxidized before injection into the stratosphere. This underlines the crucial influence of the geographic location of sources of VSLS on their impact on the stratosphere.

These projections for atmospheric transport in a warmer climate are, however, still under discussion, as other models simulate a weakening of the tropospheric circulation and convective updrafts in the tropics in the future (e.g., Vecchi and Soden, 2007). Furthermore, Zeng et al. (2008) indicate OH increases in a simulation of 2100 conditions, with the largest increases of 20–30% in the tropics between 3 and 8 km (although some decreases occurred in the boundary layer and upper troposphere due to decreased ozone in these regions). This would likely affect those VSLS species with predominantly OH-oxidation sinks (including CH_2Br_2) but would have little effect on those with predominantly photolysis-limited lifetimes (i.e., CHBr_3).

1.3.6 Environmental Impacts of Anthropogenic VSLS, Substitutes for Long-Lived ODSs, and HFCs

Anthropogenic emissions of VSLS can either occur by intensifying natural processes (e.g., agriculture, biomass burning) or by release after industrial production of VSLS. This section covers the potential future influence of both types of emissions. Furthermore, environmental impacts of non-ozone depleting VSLS being considered as substitutes for long-lived HFCs are also discussed in this section.

1.3.6.1 EVALUATION OF THE IMPACT OF INTENSIFIED NATURAL PROCESSES ON STRATOSPHERIC OZONE

There are a number of ways in which human activity might intensify emissions of otherwise naturally

occurring VSLS. An area of high potential impact is changes in agriculture practices. It is noted in Section 1.2.1.5 that some crops are capable of producing methyl halides. For VSLS, anticipated increases of future rice production in the tropics (Bhatia et al., 2010) could be important, as rice cultivation is known to emit considerable amounts of CH_3I (e.g., Lee-Taylor and Redeker, 2005). Furthermore, Gan et al. (1998) and Rhew et al. (2003) reported that emissions of methyl halides from halogen-methylating plants are strongly linked to the halide content of the growth substrate. With increasing salinization of soils through irrigation, coastal inundation, or deliberate cultivation of poorer soils, emissions might increase in the future. This issue is emphasized by the finding of Sive et al. (2007) that fluxes of CH_3I from terrestrial biomes over the eastern U.S. are presently comparable with oceanic sources over the Atlantic. Another possible impact from future agriculture would be the aquaculture of marine algae for food, chemicals, biofuel, and for sequestering atmospheric carbon (Packer, 2009; Aizawa et al., 2007). Furthermore, water chlorination, both of drinking water and domestic wastewater, and also seawater coolant in coastal power plants may contribute small amounts of halogen to the stratosphere and this contribution could change in the future, but no new information has become available since the previous Assessment concerning these potential contributions.

1.3.6.2 VERY SHORT-LIVED NEW ODSs AND THEIR POTENTIAL INFLUENCE ON STRATOSPHERIC HALOGEN

Chlorocarbons such as CCl_2CCl_2 (perchloroethene) and CHClCCl_2 (trichloroethene) have been used for many decades in large quantities as industrial solvents. Additionally, new very short-lived chlorocarbons, bromocarbons, and iodocarbons (with lifetimes <0.5 years) have recently been introduced or are proposed as potential substitutes for long-lived ODSs. The pathways and reactions by which halogens from these anthropogenic VSLS reach the stratosphere are similar to those of natural compounds, such as CH_2Br_2 and CHBr_3 , as discussed in Sections 1.3.2–1.3.3. These anthropogenic VSLS are considered separately from the long-lived ODS, as the traditional concept of a single, geographical-independent Ozone Depletion Potential (ODP) does not apply and their impact depends on the location and season of emissions.

The issue of ODPs for short-lived ODSs has already been discussed for *n*-propyl bromide and CF_3I in the previous two Assessments (Ko and Poulet et al., 2003; Law and Sturges et al., 2007). For CHCl_3 , CCl_2CCl_2 , and CHClCCl_2 , Kindler et al. (1995) have derived mean, semi-empirical ODPs of 0.008–0.01, 0.006–0.007, and 0.0005–0.0007, respectively, based on a 2-D modeling analysis

and source gas atmospheric distributions that are similar to those observed. Furthermore, in Law and Sturges et al. (2007) it was estimated that 1% of uniformly distributed land mass emissions of a theoretical VSLS with a tropospheric lifetime of 25 days would reach the stratosphere. Consequently the ODP of such a compound with one chlorine atom and similar molecular weight to CFC-11 has been calculated as being about 0.003. This approach, however, neglects the issue of the ODP being sensitive to the location and seasonality of emission.

Wuebbles et al. (2009) updated an earlier 2-D model approach of Li et al. (2006) to calculate the ODPs for CF_3I by using a 3-D global chemical transport model (CTM). An ODP of 0.016 and 0.008 is calculated for CF_3I surface emissions in the tropics and in the midlatitudes, respectively, which compares well with the earlier ODP values from Li et al. (2006) of 0.018 and 0.011 for CF_3I released in the tropics and in the midlatitudes, respectively. These new figures confirm the higher probability of VSLS released in the tropics reaching the stratosphere, which results in higher ODPs for VSLS released near the equator. In the last Assessment (Law and Sturges et al., 2007) it was also noted that ODPs are dependent upon the altitude of emission, which would be relevant if CF_3I were used on aircraft as a replacement for halons. However, no update on this is available.

1.3.6.3 EVALUATION OF POTENTIAL AND IN-USE SUBSTITUTES FOR LONG-LIVED ODSs

A wide range of chemicals with zero or near-zero ODPs and low GWPs are currently being considered as substitutes for ODSs and long-lived HFCs. In Table 1-10, atmospheric lifetimes of substitutes that are already in use or potentially could be used in applications such as refrigeration, foam blowing, fire control, propellants, and solvents are listed. The list is not restricted to VSLS because many longer-lived HFCs are in use or are being considered as ODS replacements.

In Table 1-11, substitutes that are already in use or have been identified as most likely to be used in the near future are listed together with their applications, potential feedstocks, and atmospheric lifetime. Furthermore, metrics of environmental effects such as GWP, Photochemical Ozone Creation Potential (POCP), and trifluoroacetic acid (TFA) formation are specified. For reasons of completeness and to link with the issue of global warming and climate change, fluorinated substances are also listed that are not ODS substitutes in the strictest sense (i.e., NF_3 , hexafluorobutadiene, COF_2).

Hydrocarbons receive use as ODS substitutes in refrigeration and foam-blowing applications. They do not deplete stratospheric ozone and they have very small GWPs. However, the oxidation of hydrocarbons

Table 1-10. Local and partial lifetimes of in-use and potential replacement compounds for long-lived ODSs (long-lived substitutes in italics).

Compound	Local Lifetime from Previous Assessment (days)	OH Lifetime (days)	Photolysis Lifetime (days)	New Local Lifetime (days)	Notes
Hydrocarbons					
CH ₂ =CHCH ₃ (propene)	0.37	0.35		0.35	1, 5
(CH ₃) ₂ C=CH ₂ (isobutene)		0.20		0.20	1, 5
CH ₃ CH ₂ CH ₃ (propane, R-290)		12.5		12.5	1, 3
(CH ₃) ₂ CHCH ₃ (isobutane, R-600a)		6.0		6.0	1, 5
CH ₃ CH ₂ CH ₂ CH ₂ CH ₃ (n-pentane)	3.7	3.4		3.4	1, 6
c-CH ₂ CH ₂ CH ₂ CH ₂ CH ₂ (cyclopentane)	2.9	2.7		2.7	1, 6
(CH ₃) ₂ CHCH ₂ CH ₃ (isopentane)	3.7	3.4		3.4	1, 6
CH ₃ OCHO (methyl formate)	58	72		72	1, 7
(CH ₃) ₂ CHOH (isopropanol)	4.8	2.0		2.0	1, 3
CH ₃ OCH ₂ OCH ₃ (methylal)		2.2		2.2	1, 8
Hydrofluorocarbons					
CH ₃ CH ₂ F (HFC-161)	77	66		66	1, 3
CH ₂ FCH ₂ F (HFC-152)	219	146		146	1, 4
CH ₃ CHFCH ₃ (HFC-281ea)	22	23		23	1, 3
<i>CHF₂CH₂CF₃ (HFC-245fa)</i>	<i>7.6 years</i>	<i>8.2 years</i>	<i>116 years</i>	<i>7.7 years</i>	<i>2, 3, 9</i>
<i>CH₃CF₂CH₂CF₃ (HFC-365mfc)</i>	<i>8.6 years</i>	<i>9.3 years</i>	<i>125 years</i>	<i>8.7 years</i>	<i>2, 3, 9</i>
<i>CHF₂CHF₂ (HFC-134)</i>	<i>9.6 years</i>	<i>10.5 years</i>	<i>134 years</i>	<i>9.7 years</i>	<i>2, 3, 9</i>
<i>CF₃CHF₂CF₃ (HFC-227ea)</i>	<i>34.2 years</i>	<i>44.5 years</i>	<i>310 years</i>	<i>38.9 years</i>	<i>2, 4, 9</i>
<i>CF₃CH₂CF₃ (HFC-236fa)</i>	<i>240 years</i>	<i>253 years</i>	<i>5676 years</i>	<i>242 years</i>	<i>2, 3, 9</i>
Unsaturated Fluorocarbons					
CH ₂ =CHF		2.1		2.1	1, 4
CH ₂ =CF ₂		4.0		4.0	1, 4
CF ₂ =CF ₂		1.1		1.1	1, 4
CH ₂ =CHCH ₂ F		0.7		0.7	1, 4
CH ₂ =CHCF ₃		7.6		7.6	1, 4
CH ₂ =CF ₂ CF ₃		10.5		10.5	1, 4
<i>E</i> -CF ₃ CH=CHF		16.4		16.4	1, 4
<i>E</i> -CF ₃ CF=CHF		4.9		4.9	1, 4
<i>Z</i> -CF ₃ CF=CHF		8.5		8.5	1, 4
CF ₂ =CF ₂ CF ₃		4.9		4.9	1, 4
CH ₂ =CHCF ₂ CF ₃		7.9		7.9	1, 4
CF ₂ =CF ₂ CF=CF ₂		1.1		1.1	1, 10
Unsaturated Chlorocarbons					
<i>E</i> -CF ₃ CH=CHCl		26		26	1, 11
CH ₂ =CHCl		1.5		1.5	1, 4

Table 1-10, continued.

Compound	Local Lifetime from Previous Assessment (days)	OH Lifetime (days)	Photolysis Lifetime (days)	New Local Lifetime (days)	Notes
CH ₂ =CCl ₂		0.9		0.9	1, 4
CHCl=CCl ₂	4.6	4.9	> 15000	4.9	1, 4, 21
CCl ₂ =CCl ₂	99	90		90	1, 4
CF ₂ =CFCl		1.4		1.4	1, 12
CF ₂ =CFCF ₂ Cl		~ 5		~ 5	1, 13
CF ₂ =CFCF ₂ CFCl ₂		~ 5		~ 5	1, 13
Unsaturated Bromocarbons					
CFBr=CF ₂		1.4		1.4	1, 14
CHBr=CF ₂		2.3		2.3	1, 14
CH ₂ =CBrCF ₃		2.7		2.7	1, 14
CH ₂ =CBrCF ₂ CF ₃		3.1		3.1	1, 14
CH ₂ =CHCF ₂ CF ₂ Br		6.5		6.5	1, 14
Fluorinated Ethers, HFE					
CH ₃ OCH ₂ CF ₃ (HFE-263fb2)	37	23		23	1, 15, 17
CH ₃ OCHF ₂ CF ₃ (HFE-254eb2)		88		88	1, 4
CH ₃ OCH ₂ CF ₂ CF ₃	40	21		21	1, 16, 17
CH ₃ CH ₂ OCF ₂ CHF ₂	1826 (error)	64		64	1, 4
CF ₃ CH ₂ OCH ₂ CF ₃	146	105		105	1, 4
CH ₃ OCH(CF ₃) ₂		61		61	1, 18
Fluorinated Ketones					
CF ₃ CF ₂ C(O)CF(CF ₃) ₂ (FK-5-1-12)	< 14	> 63 years	7–14	7–14	19
Fluorinated Alcohols					
CH ₂ FCH ₂ OH	15	12.9		12.9	1, 4
CHF ₂ CH ₂ OH		51		51	1, 4
CF ₃ CH ₂ OH	150	142		142	1, 4
C ₂ F ₅ CH ₂ OH	142	143		143	1, 4
C ₄ F ₉ CH ₂ OH	164	142		142	1, 4
CF ₃ CHF ₂ CH ₂ OH	124	112		112	1, 5
Special Compounds					
CF ₃ CF ₂ CF ₂ I (1-iodo-heptafluoropropane)			< 2	< 2	20
CH ₃ I (methyl iodide)	7	158	7 (4–12)	7	1, 5, 21, 22
COF ₂ (carbonyl fluoride)				5–10	27
PBr ₃	< 0.01	0.14		< 0.01	22, 23
NH ₃	Few days	93		Few days	1, 3, 24
SO ₂ F ₂ (sulfuryl fluoride)		> 300 years	630 years	36 years	9, 25
NF ₃	740 years			500 years	26
CH ₃ CH ₂ Br (bromoethane)	34	41		41	1, 3

Table 1-10, continued (notes).

Notes:

1. These local OH lifetimes are calculated using an average tropospheric OH concentration of 1×10^6 molecule/cm³ and the OH reaction rate constant at $T = 275$ K. Local lifetimes quoted here are not meant to be estimates of global lifetimes, which, for short-lived gases depend on the emission location and season as well as local atmospheric conditions. The concept of a single global lifetime, ODP, or GWP is inappropriate for such short-lived gases.
2. Lifetimes for long-lived compounds with respect to reaction with tropospheric OH calculated relative to 6.1 years for CH₃CCl₃, assuming an average temperature of 272 K (Spivakovsky et al., 2000; Prather and Ehhalt et al., 2001).
3. OH reaction rate constant taken from JPL 06-2.
4. OH reaction rate constant taken from JPL 10-6. JPL 10-6 is cited here whenever there is a change in a rate constant recommendation or the accompanying note. It does not necessarily mean that a major change was recommended for a rate constant. Nevertheless, updates in JPL 10-6 reflect improved kinetic understanding.
5. OH reaction rate constant taken from Atkinson et al. (2008).
6. OH reaction rate constant taken from Calvert et al. (2008).
7. OH reaction rate constant taken from Le Calvé et al. (1997).
8. OH reaction rate constant taken from Porter et al. (1997).
9. Lifetime shown in “Photolysis Lifetime” column corresponds to the overall stratospheric lifetime. See Table 1-3.
10. OH reaction rate constant taken from Acerboni et al. (2001).
11. OH reaction rate constant taken from Sulbaek Andersen et al. (2008).
12. OH reaction rate constant taken from Abbatt and Anderson (1991).
13. Local lifetime estimated as similar to that of CF₃CF=CF₂.
14. OH reaction rate constant taken from Orkin et al. (2002).
15. OH reaction rate constant taken from Oyaro et al. (2005).
16. OH reaction rate constant taken from Oyaro et al. (2004).
17. Room temperature data only; OH reaction lifetime calculated assuming a temperature dependence (E/R) of 500 K.
18. OH reaction rate constant from Chen et al. (2005b).
19. Lifetimes taken from Taniguchi et al. (2003).
20. Photolysis lifetime estimated from comparison of UV spectra and lifetimes for CF₃I and CF₃CF₂CF₂I.
21. Photolysis lifetime taken from Table 2-4 in Ko and Poulet et al. (2003).
22. Local lifetime taken from Table 2-1 in Law and Sturges et al. (2007).
23. OH reaction rate constant taken from Jourdain et al. (1982). Local lifetime is probably dictated by photolysis.
24. Local lifetime taken from IPCC/TEAP (2005); it is dictated by washout rates (see Box 1-4).
25. From Papadimitriou et al. (2008b) and Mühle et al. (2009). The total lifetime is primarily due to ocean uptake.
26. From Prather and Hsu (2008) with the lifetimes recalculated using the JPL 06-2 recommended rate constants for the O(¹D) reactions corrected for the deactivation channel (see also Section 1.2.2).
27. Local lifetime taken from Wallington et al. (1994).

Table 1-11. Applications, feedstocks, and environmental impact of in-use and likely potential future ODS-substitutes (long-lived substitutes in italics).

Compound	Application	Feedstock	Lifetime ¹	POCP ^{2,3,4}	GWP ₁₀₀ ⁵	TFA molar yield
Hydrocarbons						
propene, CH ₃ CH=CH ₂ (HC1270)	refrigerant	petroleum	0.35 d	117 ²	5 ^{6,7}	0%
isopentane, (CH ₃) ₂ CHCH ₂ CH ₃	foams (replacing CFC-11 and HCFC-141b)	petroleum/ natural gas	3.4 d	34 ²		0%
cyclopentane, c-CH ₂ CH ₂ C ₂ CH ₂ CH ₂	foams (replacing CFC-11 and HCFC-141b)	natural gas	2.7 d	51 ³		0%
n-pentane, CH ₃ CH ₂ CH ₂ CH ₂ CH ₃	foams (replacing CFC-11 and HCFC-141b)	petroleum/ natural gas	3.4 d	40 ²		0%
isobutene, (CH ₃) ₂ C=CH ₂	foams (replacing CFC-12)	petroleum	0.2 d	75 ²		0%
methylal, CH ₃ OCH ₂ OCH ₃	foams (replacing CFC-11 and HCFC-141b)	methanol	2.2 d	32 ³		0%
methyl formate, CH ₃ OCHO	foams (replacing HCFCs)	methanol/ formic acid	72 d	3 ²		0%
Hydrofluorocarbons						
<i>HFC-245fa,</i> <i>CHF₂CH₂CF₃</i>	<i>foams (replacing</i> <i>HCFCs)</i>	<i>HF + CCl₄ +</i> <i>CH₂=CHCl</i>	7.7 y	0.1 ³	1050	< 10% ^{8,9}
<i>HFC-365mfc,</i> <i>CH₃CF₂CH₂CF₃</i>	<i>foams (replacing</i> <i>HCFCs)</i>	<i>HF + CCl₄ +</i> <i>CH₂=CClCH₃</i>	8.7 y	0.1 ³	842	< 10% ^{9,10}
<i>HFC-227ea,</i> <i>CF₃CHF₂CF₃</i>	<i>propellant for CFC-12</i> <i>and firefighting for</i> <i>halon-1301</i>	<i>HF + CHCl₃ →</i> <i>CHClF₂ →</i> <i>CF₃CF=CF₂</i>	39 y	< 0.1 ³	3580	100% ¹¹
<i>HFC-236fa,</i> <i>CF₃CH₂CF₃</i>	<i>firefighting for</i> <i>halon-1211/1301 (civil</i> <i>aviation); refrigerant</i>	<i>HF + CCl₄ +</i> <i>CH₂=CCl₂</i>	242 y	< 0.1 ³	9820	< 10% ¹²
Unsaturated Fluorocarbons						
trans-HFC-1234ze, trans-CF ₃ CH=CHF	foams (for CFC-12)	a) CHCl ₃ + HF → CHClF ₂ → CF ₃ CF=CF ₂ → CF ₃ CHFCH ₂ F or b) HFC-245fa	16.4 d	6.4 ⁴	7 ^{6,13}	< 10% ^{14,9}
HFC-1234yf, CF ₃ CF=CH ₂	refrigerant potentially for replacing HFC-134a	CHCl ₃ + HF → CHClF ₂ → CF ₃ CF=CF ₂ → CF ₃ CHFCH ₂ F	10.5 d	7.0 ⁴	4 ^{6,15}	100% ^{16,17}
Fluorinated Ketones						
FK-5-1-12, CF ₃ CF ₂ C(O)CF(CF ₃) ₂	halon-1301 replacement	C ₃ F ₆ C ₂ F ₅ COF	7-14 d			< 10% ¹⁸

Table 1-11, continued.

Compound	Application	Feedstock	Lifetime ¹	POCP ^{2,3,4}	GWP ₁₀₀ ⁵	TFA molar yield
Special Compounds						
ammonia, NH ₃	CFC replacement in refrigeration	N ₂ + H ₂	few days	NA		0%
1-iodo-heptafluoropropane, CF ₃ CF ₂ CF ₂ I	halon replacement (in Russia: -2402 and/or -1301)	CF ₃ I + C ₂ F ₄	< 2 d	NA		< 10% ¹⁸
bromoethane, CH ₃ CH ₂ Br	solvent and part of halon-2402 blend	a) HBr + C ₂ H ₄ or b) HBr + CH ₃ CH ₂ OH	41 d	4.2 ³		0%
2-bromo-3,3,3-trifluoroprop-1-ene, CH ₂ =CBrCF ₃	halon-1211 replacement	CH ₂ =CHCF ₃	2.7 d	9.3 ³		< 10% ^{19,9}
methyl iodide, CH ₃ I	CH ₃ Br replacement	CH ₃ OH / I ₂	7 d	1.0 ³		0%
<i>sulfuryl fluoride</i> , SO ₂ F ₂	<i>CH₃Br replacement</i>	<i>KF + SO₂F₂</i>	<i>36 y</i> ²⁰	<i>NA</i>	<i>4740</i> ²¹	<i>0%</i>
<i>NF₃</i>	<i>etchant to replace C₂F₆</i>	<i>a) NH₃ + F₂ or b) (NH₄)HF₂</i>	<i>500 y</i> ²²	<i>NA</i>	<i>17,500</i>	<i>0%</i>
hexafluorobutadiene	etchant		1.1 d	10 ³		0%
carbonyl fluoride, COF ₂	etchant	a) CO ₂ + F ₂ or b) Oxidation of C ₂ F ₄	5–10 d	NA		0%

Notes:

- See Table 1-10 for notes on lifetime derivations.
- Derwent et al. (2007).
- No value for the POCP (Photochemical Ozone Creation Potential) of this substance has been published by full trajectory analyses. This value was calculated based on information from Derwent et al. (1998) and Jenkin (1998), using the method that Wallington et al. (2010) used for unsaturated HFCs. The derived POCP is an approximation and is related to the molecular structure of the compound and its OH-reactivity. The calculations were only conducted for species lost mainly through OH-radical reactions; others are declared as NA (not available).
- Wallington et al. (2010).
- GWPs from Chapter 5 Appendix (Table 5A.1) if not specified differently.
- GWPs are generally calculated assuming a uniform global distribution of the trace gas. Hence, such methods are in principle not accurate for short-lived gases (i.e., gases with atmospheric lifetime shorter than about 0.5 years) because the atmospheric distribution of short-lived gases will likely be non-uniform and will also depend upon the location and season of emission. Thus, GWPs calculated in this way for short-lived gases provide only a very rough measure of the time-integrated radiative effect of these gases.
- This value represents an indirect GWP (100-year), derived with a global three-dimensional Lagrangian model (Collins et al., 2002) and an emission distribution related to fossil-fuel use. The indirect GWP includes influences on the abundance of methane (through changes in OH), tropospheric ozone, and on CO₂.
- The oxidation of HFC-245fa gives CF₃CHO as a major product (Chen et al., 1997).
- Photolysis is the main fate of CF₃CHO (lifetime of approximately 19 hours in lower troposphere for overhead Sun; Calvert et al., 2008) and this does not give TFA. Reactions with water (Sulbaek Andersen et al., 2006) or OH radicals are minor losses of CF₃CHO and can lead to TFA (Hurley et al., 2006). The yield of TFA is estimated to be <10%.
- The oxidation of HFC-365mfc gives CF₃CHO and COF₂ as major products (Inoue et al., 2008).
- Zellner et al. (1994).
- The oxidation of HFC-236fa gives CF₃C(O)CF₃ (Møgelberg et al., 1995). Photolysis is the main fate of CF₃C(O)CF₃ (lifetime of approximately 6.2 days in lower troposphere for overhead Sun; Calvert et al., 2008). The photolysis of CF₃C(O)CF₃ will give CF₃CO radicals, a small fraction of which

Table 1-11, continued.

- can react further to give TFA (Hurley et al., 2006). The molar yield of TFA from the atmospheric oxidation of HFC-236fa is estimated to be <10%.
13. This direct GWP (Orkin et al., 2010) was calculated using a semi-empirical approach with the revised lifetime of 16.4 days given in Table 1-10 but without accounting for inhomogeneous emission and atmospheric mixing ratio distributions.
 14. Søndergaard et al. (2007); Javadi et al. (2008).
 15. This direct GWP is from Papadimitriou et al. (2008a) and Orkin et al. (2010) and was calculated with the revised lifetime of 10.5 days given in Table 1-10 but without accounting for inhomogeneous emission and atmospheric mixing ratio distributions.
 16. Nielsen et al., 2007.
 17. Hurley et al., 2008.
 18. Photolysis will lead to the formation of C_2F_5 radicals. Approximately 1–10% of C_xF_{2x+1} radicals are converted in the atmosphere into $C_{x-1}F_{2x-1}C(O)F$ (Wallington et al., 2006). The sole atmospheric fate of the 1–10% $CF_3C(O)F$ produced is hydrolysis to give TFA.
 19. The atmospheric oxidation of $CF_3CBr=CH_2$ is believed to give $CF_3C(OH)=CH_2$ and/or $CF_3C(O)CH_2OH$ (Orkin et al., 2002; Sulbaek Andersen et al., 2009a). Further oxidation will likely give CF_3CHO .
 20. Mühle et al. (2009).
 21. Derived from Papadimitriou et al. (2008b) with a radiative efficiency rounded to two decimal places (0.22 W/m^2ppb versus 0.222 W/m^2ppb) used in Papadimitriou et al. (2008b) (see Chapter 5).
 22. See Table 1-10, footnote 26.

in the presence of elevated nitrogen oxides (NO_x) leads to the formation of carbon dioxide (CO_2) (e.g., Collins et al., 2002) and can contribute to the production of tropospheric ozone, which indirectly affects atmospheric levels of methane (CH_4). POCPs are used to assess the relative efficiency of hydrocarbon species for forming tropospheric ozone. POCPs, expressed relatively to ethene (POCP = 100), are shown in Table 1-11 and have either been taken from Derwent et al. (2007) or Wallington et al. (2010) or have been calculated using the method of Derwent et al. (1998) and Jenkin (1998) (specified for unsaturated HFCs by Wallington et al., 2010). While this methodology provides a rough estimate of POCPs for trace gases that are predominately destroyed by atmospheric oxidation, its application to species for which photolysis and hydrolysis are dominant loss processes is not valid.

POCPs are lower for saturated hydrocarbons, typically used as refrigerants and for foam blowing (i.e., propane, isobutane, pentanes), but higher for the alkenes (propene, isobutene). Although releases associated with refrigeration are minor in comparison to hydrocarbon emissions from traffic and solvent usage, the combined impact of these hydrocarbons could be non-negligible, especially in already polluted regions. For the HFCs and other compounds discussed as substitutes in Table 1-11, the POCP values are generally smaller than 10 and hence their relevance for the formation of tropospheric ozone will be very small.

The unsaturated halocarbons (halogenated alkenes) contain a $C=C$ double bond that makes them readily susceptible to degradation by OH (and ozone (O_3)). As a result, their atmospheric lifetimes are typically days to weeks. This group of compounds can be further divided into unsaturated HFCs (sometimes referred to as hydrofluoro-olefins, HFOs) and chloro- and bromoalkenes. Unsaturated HFCs are being considered as

potential replacements for ODSs and HFCs in mobile air conditioners and for foam blowing, as they typically have smaller GWPs than saturated (long-lived) HFCs. These smaller GWPs are partially offset for these unsaturated compounds by the production of tropospheric ozone, a strong greenhouse gas.

Chlorinated and brominated alkenes also have short lifetimes but still can have non-negligible ODPs (e.g., Kindler et al., 1995). Chlorinated alkenes such as CCl_2CCl_2 (perchloroethene) and $CHClCCl_2$ (trichloroethene) have been used in large quantities for decades as industrial solvents and a certain amount of this chlorine reaches the stratosphere as a result of use of these gases (see Section 1.3.3.1).

Oxygenated fluorocarbons are another group of ODS replacement compounds with lifetimes typically spanning days to months (Table 1-10 and Table 1-11). In fact a number of fluorinated ethers (e.g., HFE-7100, HFE-7200) have been already used as first-generation ODS substitutes in niche applications such as refrigerants, as solvents, and as heat transfer fluids, but no information about their atmospheric abundance is available.

The atmospheric degradation of (saturated and unsaturated) HFCs and oxygenated fluorocarbons is initiated by their reaction with OH radicals or O_3 , (important only for unsaturated HFCs). The oxygenated products from these reactions are removed from the atmosphere via deposition and washout processes and may accumulate in oceans, lakes, and other reservoirs. A potential toxic by-product of the atmospheric degradation of fluorocarbons with CF_3 groups is trifluoroacetic acid (TFA; $CF_3C(O)OH$). Yields of TFA from the degradation of different HFCs are included in Table 1-11. TFA is removed from the atmosphere by wet deposition but is known to accumulate in certain ecosystems. However, much uncertainty remains

in understanding the processes involved in maintaining measured abundances of TFA in today's aquatic environments. Whereas average TFA concentrations of 200 nanograms per liter in deep ocean waters suggest natural sources in the ocean (Frank et al., 2002), TFA levels were below detection in old ice core and groundwater samples (Nielsen et al., 2001).

At present HFC-134a ($\text{CF}_3\text{CH}_2\text{F}$) is the HFC that contributes the most TFA to the environment among ODS replacement gases. With global emissions of 149 ± 27 Gg/yr in 2008 (Section 1.5) and a TFA yield of 7–20% (Figure 1-14; Wallington, 1996), a current yearly global input of 9–35 Gg/yr of TFA can be derived from HFC-134a. The unsaturated HFC-1234yf ($\text{CF}_3\text{CF}=\text{CH}_2$) is being considered as a replacement for HFC-134a in mobile air conditioners (Hurley et al., 2008). The TFA

production yield of the atmospheric degradation of HFC-1234yf is 100% (Hurley et al., 2008; Figure 1-14; Table 1-11). The use of HFC-1234yf has the potential to influence TFA concentrations near the source regions to a greater extent than HFC-134a, owing to its shorter lifetime and its higher efficiency to produce TFA. A recent modeling study has shown that deposition of TFA could average $0.16\text{--}0.24$ kg/km² by 2017 in the continental U.S. from the full adoption of HFC-1234yf in mobile air conditioners, and that concentrations of TFA in Eastern U.S. rainfall would more than double as a result in comparison to today's values (Luecken et al., 2010).

Apart from TFA, monofluoroacetic acid (MFA) and difluoroacetic acid (DFA) could potentially be produced in the degradation of HFCs. MFA and DFA have been measured in the atmosphere and their environmental occurrence has been discussed, for example by Römpf et al. (2001) and Martin et al. (2003).

Replacements for halons (firefighting) and CH_3Br (agriculture) are also being sought. Whereas for halons various substitutes are being considered for different applications, SO_2F_2 is specifically considered as an important replacement for CH_3Br (see also Section 1.5.2.2). This compound is, however, toxic to humans and has a longer atmospheric lifetime (36 years) than CH_3Br (Papadimitriou et al., 2008b).

Ammonia (NH_3) used as a replacement in refrigeration could potentially influence the tropospheric particle loading via its reaction with nitric acid (HNO_3) to form ammonium nitrate (NH_4NO_3). However, emissions from in-use systems are negligible compared to NH_3 emitted from agriculture and natural sources.

Nitrogen trifluoride (NF_3), hexafluorobutadiene, and carbonyl fluoride (COF_2) can be used as substitutes for the extremely long-lived perfluorocarbons (PFCs) as etchants in the electronics industry. In fact, NF_3 has already become an important chemical for silicon etching, e.g., in the production of flat computer and television screens (see also Section 1.5), though it has a long lifetime of 500 years and a high GWP_{100} of 17,500 (Chapter 5).

Finally, information on feedstock for the production of many substitutes is provided in Table 1-11. As different production methods exist for specific molecules, this list is not exhaustive, but it is meant to serve as a starting point for a discussion of emission that could potentially arise during production of substitute chemicals. Although emissions to the atmosphere during production are believed to be generally small, a possible pathway of ODSs to the atmosphere could be the production of HFCs, which can include the reaction of carbon tetrachloride (CCl_4) with chlorinated alkenes and subsequent replacement of the Cl-atoms with fluorine (see also the discussion on CCl_4 in Section 1.2.1.3).

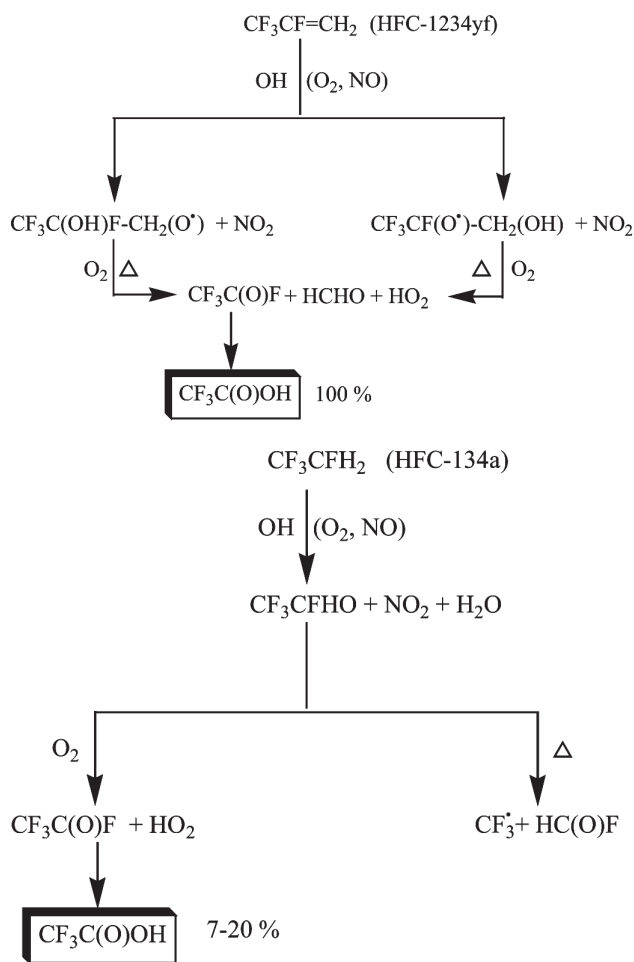


Figure 1-14. Degradation scheme of HFC-1234yf (yielding 100% TFA; $\text{CF}_3\text{C}(\text{O})\text{OH}$) and of HFC-134a (yielding 7–20% TFA) (Wallington et al., 1996; Hurley et al., 2008).

1.4 CHANGES IN ATMOSPHERIC HALOGEN

1.4.1 Chlorine in the Troposphere and Stratosphere

1.4.1.1 TROPOSPHERIC CHLORINE CHANGES

Total organic chlorine from long-lived gases reached its peak in the troposphere at 3660 ± 23 ppt between 1992 and 1994 and has since declined. While this peak value includes 80 ppt from VSLS, the quoted error encompasses only the difference in total Cl determined from two different sampling networks and not uncertainties related to the contribution of Cl from VSLS (see Section 1.3). By mid-2008, tropospheric organic Cl from long-lived gases had declined by 8.4% from its peak to a value of 3352 ± 4 ppt (Table 1-12 and Figure 1-15). The main drivers behind this decline have changed over time. Methyl chloroform (CH_3CCl_3) now contributes much less to the decline in total Cl than it did in the mid-1990s and early 2000s. This is because the global tropospheric mixing ratio of CH_3CCl_3 has declined substantially: by 2008 it accounted for 32 ± 1 ppt of Cl, or only 1%, of tropospheric

Cl (Table 1-12). As a result, declines in Cl from CH_3CCl_3 have become less important to total Cl changes and this influence will continue to diminish in the future.

As the influence of CH_3CCl_3 on tropospheric Cl changes has diminished, declines in tropospheric Cl have slowed. Tropospheric chlorine from long-lived gases changed at a rate of -14 ppt Cl/yr ($-0.42\%/yr$) during 2007–2008, compared to -21 ppt/yr during 2003–2004, and was slower than the change of -23 ppt/yr projected for 2007–2008 in the A1 (most likely, or baseline) scenario of the previous Assessment. The decline observed during 2007–2008 was also about half as rapid as measured in 1995–1996 (-28 ppt Cl/yr or $-0.8\%/yr$; Clerbaux and Cunnold et al., 2007) (Table 1-12). For reference, the mean annual rate of change in tropospheric Cl from long-lived gases averaged over 1996–2008 was $-0.6(\pm 0.05)\%/yr$ in data from the NOAA or AGAGE global sampling networks.

The decline in tropospheric Cl has also slowed recently because of increases observed in the accumulation rate of hydrochlorofluorocarbons (HCFCs) since 2004 (Table 1-12). By 2008, Cl from HCFCs was increasing at a faster rate (10.6 ppt Cl/yr) than had been observed in 2000 and 2004 and Cl from HCFCs accounted for 251 ± 3 ppt Cl, or 7.5% of total tropospheric chlorine.

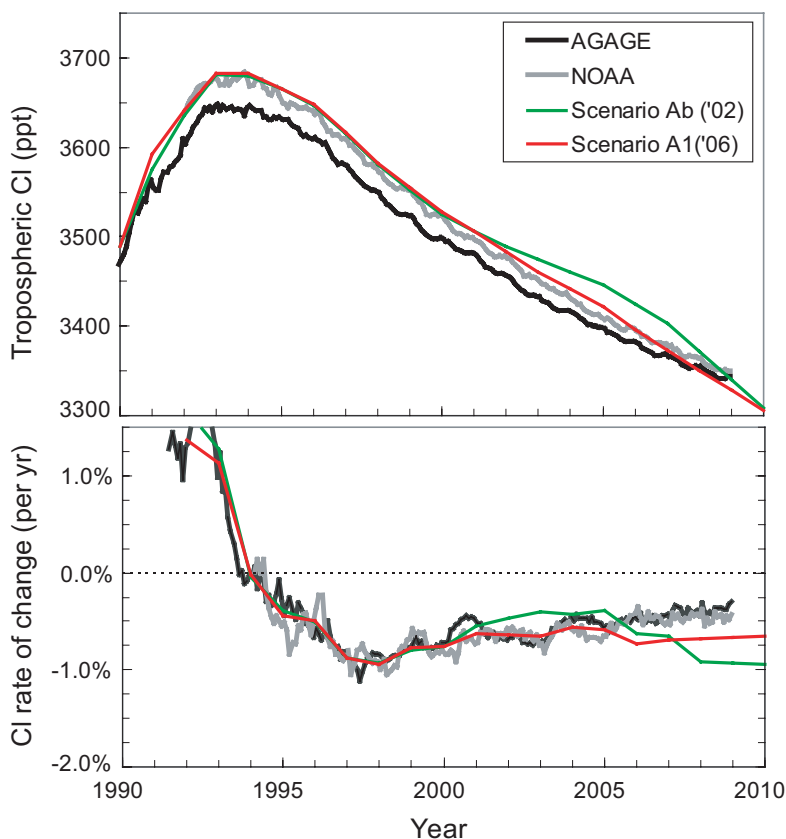


Figure 1-15. Top panel: The tropospheric abundance (ppt) of organic chlorine (CCl_y) from the NOAA (gray) and AGAGE (black) global measurement networks (updates of Montzka et al., 2003, and O'Doherty et al., 2004). Quantities are based upon independently measured mixing ratios of CFC-11, CFC-12, CFC-113, HCFC-22, HCFC-141b, HCFC-142b, methyl chloroform, carbon tetrachloride, and halon-1211. Results for CFC-114 and CFC-115 from Prinn et al. (2000) are used in both aggregations. An additional constant 550 ppt was added for CH_3Cl and 80 ppt was added for short-lived gases such as CH_2Cl_2 , CHCl_3 , CCl_2CCl_2 , and COCl_2 (consistent with 40–130 ppt discussed in Section 1.3). Bottom panel: Annual rates of change (% per year) determined from 12-month differences. In both panels, observations are compared with the baseline scenario (Ab) from WMO 2002 (green line; Montzka and Fraser et al., 2003) and the baseline scenario A1 from WMO 2006 (red line; Daniel and Velders et al., 2007).

Table 1-12. Contributions of halocarbons to total chlorine in the troposphere.

	Total Cl * (ppt Cl)			Contribution to Total Cl (%)			Rate of Change in Total Cl ** (ppt Cl / yr)		
	Mid-2000	Mid-2004	Mid-2008	Mid-2000	Mid-2004	Mid-2008	2000	2004	2008
All CFCs	2154	2123	2076 (3)	61%	62%	62%	-1.9 (1.9)	-9.4 (2.0)	-13.2 (0.8)
CCl ₄	392	377	359 (6)	11.2%	11.0%	10.7%	-4.0 (0.7)	-4.0 (0.6)	-5.1 (0.7)
HCFCs	182	214	251 (3)	5.2%	6.3%	7.5%	9.2 (0.8)	6.0 (1.3)	10.6 (0.5)
CH ₃ CCl ₃	136	66	32 (1)	3.9%	1.9%	1.0%	-26.8 (1.0)	-13.4 (2.1)	-6.2 (0.3)
Halon-1211	4.02	4.26	4.17 (0.1)	0.1%	0.1%	0.1%	0.1 (0.00)	0.0 (0.08)	-0.1 (0.01)
Total Cl	3499	3414	3352 (4)				-23 (2.4)	-21 (3.2)	-14 (1.2)
							-0.67%	-0.61%	-0.42%

* An average of AGAGE and NOAA/ESRL global means was used to derive these mid-year mixing ratios. Uncertainties are given in parentheses and represent 1 standard deviation of the results reported by different global networks. They do not include an additional amount for potential systematic calibration errors, errors associated with deriving tropospheric means from surface measurements, or uncertainties in Cl contributed from VSLS.

** Total Cl changes and relative rates of change are calculated assuming a constant 550 ppt Cl from CH₃Cl and a constant 80 ppt from VSLS (see Section 1.3). Rates of change were calculated as the difference between the indicated year and the previous year and relative rates were normalized by the mean mixing ratio over these two-year periods. Numbers for past years differ slightly from previous Assessments because of updated calibration information (see text).

But while increases in Cl from HCFCs have accelerated, declines in Cl from CFCs have become more rapid. The 2004–2008 period was the first time that declines derived for tropospheric Cl from long-lived CFCs as a class were larger than the decline from CH₃CCl₃ (Table 1-12). CFCs accounted for 2076 ± 3 ppt Cl during 2008. Chlorine from CFCs (as a class) declined by just over 13 ppt (0.6%) from 2007–2008 and this Cl decrease was comparable to the summed influence of other decreasing compounds (CCl₄, CH₃CCl₃, and halon-1211). The fraction of total organic chlorine attributable to CFCs has remained fairly constant at about 62% over the past decade even as Cl from CFCs has decreased by 4% from its 1998 peak.

As mentioned above, the decline in tropospheric Cl since 2004 was slower than anticipated in scenario A1 of the 2006 Ozone Assessment (Daniel and Velders et al., 2007) (Figure 1-15). Measured tropospheric Cl from long-lived gases in 2008 was ~40 ppt higher than projected in the A1 scenario. This slower decline in tropospheric Cl resulted mostly from CFC-11 and CFC-12. Although global mixing ratios of CFC-11 and CFC-12 declined more rapidly during 2005–2008 than in earlier years, Cl from these CFCs in 2008 was ~28 ppt Cl higher than had been projected. HCFCs also played a role in the slower than anticipated Cl decline. By 2008, mixing ratios observed for HCFC-22 and HCFC-142b contributed ~8 ppt more Cl than had been projected (see Figure 1-1). Some of the discrepancy for CFC abundances arises because the calibration of CFC-12 measurements by the NOAA group

has been revised with improved standards since the last Assessment. Observed changes for other Cl-containing compounds during 2005–2008 were similar to those projected in the A1 scenario.

1.4.1.2 STRATOSPHERIC CHLORINE CHANGES

As discussed in previous Assessments, the stratospheric burden of chlorine is controlled by input from the troposphere and by transport and mixing processes. Time-scales for air to be transported to higher altitudes in the midlatitude and polar stratosphere after crossing the tropopause range from 3 to 6 years. As a result, changes in stratospheric chlorine and bromine abundances lag behind tropospheric changes and, furthermore, are smoothed and flattened because of mixing (Waugh and Hall, 2002). Changes in total stratospheric Cl calculated from tropospheric observations allow this lag to be visualized for the midlatitude stratosphere (Figure 1-16) (update of Engel et al., 2002). They also show how the magnitude of the decline in stratospheric Cl is expected to be altitude dependent.

Most chlorine enters the stratosphere chemically bound to carbon (organic Cl) in long-lived source gases and undergoes photochemical oxidation to inorganic forms as air is transported to higher altitudes within the stratosphere. Long-term changes in stratospheric inorganic Cl abundances are derived from ground-based and satellite-based instruments measuring total column abundances or

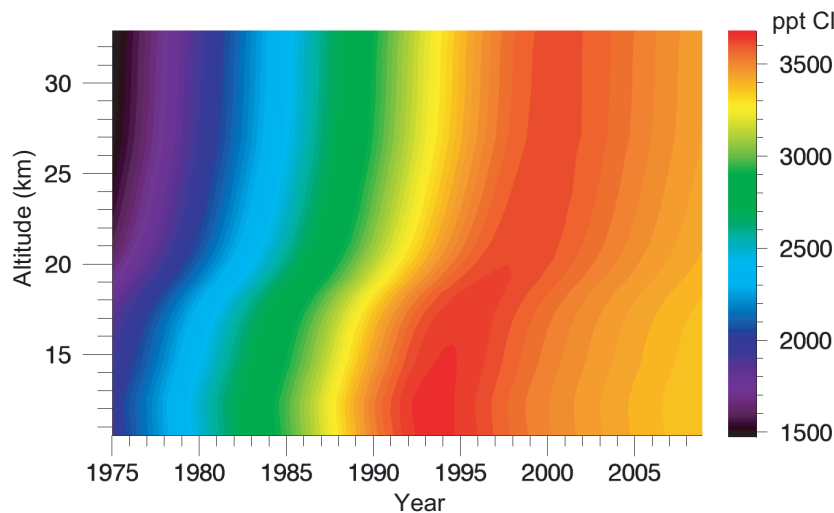


Figure 1-16. The evolution of total chlorine abundance (ppt) in the stratosphere, calculated based on the tropospheric chlorine time series shown in Figure 1-15, and including a constant contribution of 80 ppt of chlorine from VLSL species (consistent with 40–130 ppt estimated in Section 1.3). Typical profiles of mean age in the stratosphere (derived from observations of SF₆ and CO₂) and a parameterization of the age spectrum are used for the calculation of the effects of mixing and transport in the stratosphere (updated from Engel et al., 2002).

mixing ratio profiles of hydrogen chloride (HCl) and chlorine nitrate (ClONO₂), the two main inorganic reservoir chemicals for Cl in the stratosphere. Total column measurements from ground-based Fourier transform infrared (FTIR) instrumentation above the Jungfraujoch and Lauder show changes in inorganic Cl compound abundances that are fairly consistent with the amounts and changes in Cl being delivered to the stratosphere from long-lived source gases (Figure 1-17, Table 1-13) (update to Mahieu et al., 2004 and Rinsland et al., 2003). These findings are consistent with only a fairly small contribution of VLSL to stratospheric Cl. The mean fraction of stratospheric Cl attributable to VLSL, 80 (40–130) ppt (see Section 1.3), is approximately 1.5–3%. The relative contribution of VLSL to reactive Cl, however, can be substantially higher in the lower stratosphere for VLSL that have local lifetimes shorter than the longer-lived ODSs.

Average rates of change observed by ground-based FTIR measurements of total stratospheric chlorine (HCl + ClONO₂) since 1996 were $-0.9 \pm 0.2\%/yr$ to $-1.5 \pm 0.2\%/yr$ (Table 1-13). The faster declines are apparent in the column measurements above Kiruna, but this may reflect greater meteorological variability at polar sites than above lower latitude sites. Comparable or slightly slower rates of change (-0.6 ± 0.1 to $-0.9 \pm 0.2\%/yr$) have been measured since 2004 for upper stratospheric HCl measured over much of the globe from ACE-FTS and the Aura Microwave Limb Sounder (MLS) instruments (see Figure 1-18 and Table 1-13). These observed trends are reasonably consistent with the observed changes in total tropospheric Cl since 1996, though uncertainties related to chemical partitioning, mixing processes, and time lags associated with transport make a direct comparison between these different measures difficult.

Satellite data for upper stratospheric and lower mesospheric HCl from two different instruments (MLS and the ACE-FTS) agree to within ~ 0.15 ppb in recent years. This small difference is not significant given the systematic uncertainties on the ACE-FTS and MLS HCl measurements of 0.15 to 0.3 ppb (Figure 1-18) (Froidevaux et al., 2008; Mahieu et al., 2008). These satellite results agree to within ± 0.3 ppb ($\pm 8\%$) with total Cl amounts derived from long-lived chlorinated source gases, once mixing and lag times associated with transport are considered (Figure 1-18). The uncertainty in this measured stratospheric Cl burden is large relative to the expected chlorine contributions from shorter-lived source gases and product gases (80, 40–130 ppt), and so these stratospheric data do not provide additional constraints to Cl contributions from chlorinated VLSL gases. HCl is estimated to account for $>95\%$ of total stratospheric Cl at altitudes above ~ 50 km.

Though the Cl contained in HCl and ClONO₂ is not directly involved in the chemical reactions depleting stratospheric ozone, their summed abundance in the upper stratosphere is approximately proportional to the amount of reactive Cl present in the stratosphere. Chlorine monoxide (ClO), however, is directly involved in reactions that deplete stratospheric ozone. Updated measurements of upper stratospheric ClO (near 4 hPa) show an overall trend that is consistent with the declines observed for HCl and ClONO₂ (Figure 1-19) (update of Solomon et al., 2006). Short-term variability is observed, however, suggesting that other factors influence the proportion of stratospheric Cl present in reactive (e.g., ClO) versus unreactive (e.g., HCl and ClONO₂) forms, as discussed previously (e.g., Siskind et al., 1998; Froidevaux et al., 2000). Such influences also imply that measured ClO trends are not directly comparable to changes in total stratospheric chlorine.

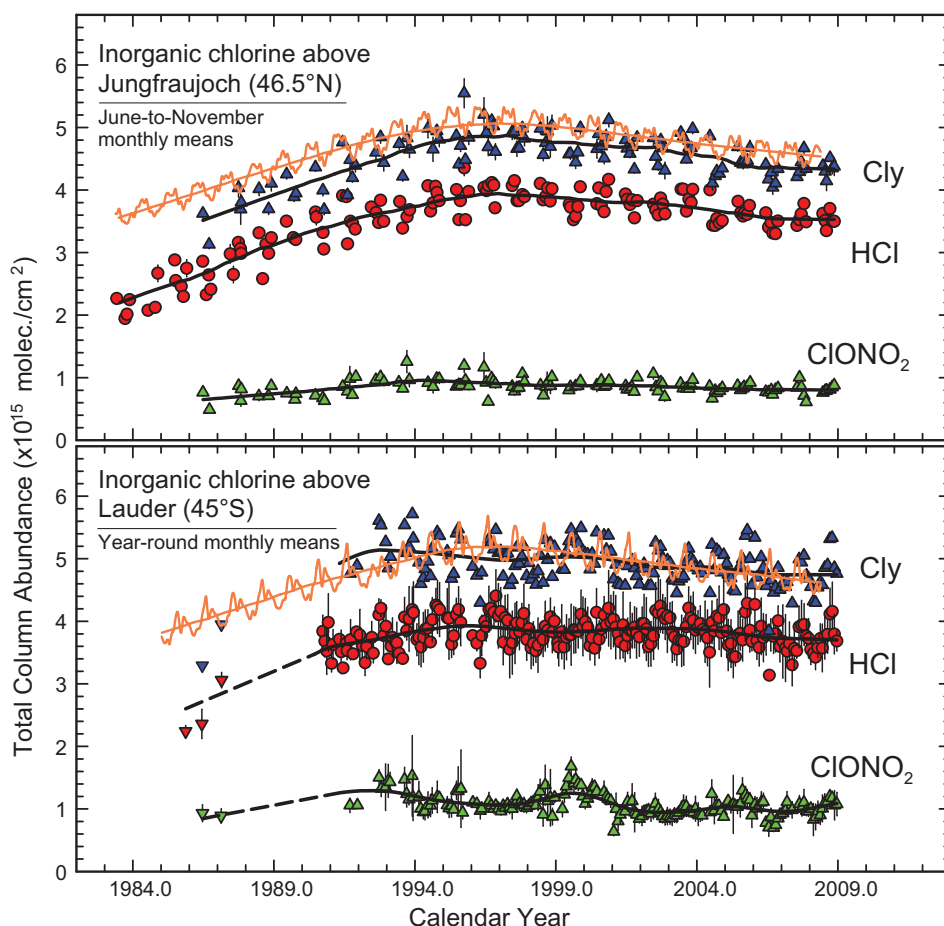


Figure 1-17. Time series of monthly-mean total column HCl (red circles) and ClONO₂ (green triangles) abundance (molecules per square centimeter), as measured above the Jungfraujoch (46.5°N) and Lauder (45°S) (updated from Mahieu et al., 2004 and Rinsland et al., 2003). Cl_y column estimates (blue triangles) are the sum of HCl and ClONO₂ columns. Jungfraujoch data are shown only for June to November of each year; results from all months are displayed for Lauder. Fits to the data sets are given by the black curves. The orange curves and corresponding fits represent Cl_y (HCl + ClONO₂) from the University of Leeds 2-D model, as in the previous Assessment report (Clerbaux and Cunnold et al., 2007).

Given observed changes in methane, a compound that affects this proportion, the measured decline of $-0.9 \pm 0.2\%/yr$ in ClO for 1995–2007 (Table 1-13) is consistent with a somewhat slower rate of change in total chlorine (about $-0.7\%/yr$) (see Solomon et al., 2006).

New observations of chlorofluorocarbonyl (COFCl) have been reported for the TTL and in the stratosphere (Fu et al., 2009; Rinsland et al., 2007). The contribution of this compound to total Cl above 35 km is expected to be small (<10 ppt) and accounts for only a small portion of total inorganic Cl in the upper stratosphere. Furthermore, COFCl is believed to result almost entirely from degradation of long-lived compounds containing Cl and F in the stratosphere, and so its abundance is not included as an additional term in sums of total organic Cl from long- and short-lived source gases.

1.4.2 Bromine in the Troposphere and Stratosphere

1.4.2.1 TROPOSPHERIC BROMINE CHANGES

Bromine in the troposphere from halons and methyl bromide continued to decline during 2005–2008. By 2008, 15.7 ± 0.2 ppt of tropospheric Br was measured at Earth's surface from these long-lived chemicals by two independent networks (annual mean). These results indicate that total Br from these substances has declined by about 1 ppt in the troposphere from peak levels measured in 1998 (Figure 1-20) (Montzka et al., 2003), similar to that expected in the A1 scenario of the last Assessment (Daniel and Velders et al., 2007). This decline has been

Table 1-13. Measured chlorine-related changes in the upper atmosphere.

Instrumentation Technique / Location	Species and Altitude Region	Time Period	Rate of Change (percent/yr) (2-sigma error)
ground-based microwave ¹ Hawaii	ClO upper stratosphere	1995–2007	–0.9 (0.2)
spaceborne ACE-FTS ² IR solar occultation	HCl upper stratosphere	Jan. 2004–Sept. 2009	–0.9 (0.2)
spaceborne Aura MLS ³ Microwave emission	HCl upper stratosphere	Aug. 2004–Jan. 2010	–0.6 (0.1)
ground-based FTIR Jungfraujoch ⁴	HCl column	1996–2009	–0.9 (0.1)
Kirunawvq ⁵		1996–2009	–0.8 (0.2)
ground-based FTIR Jungfraujoch ⁴	ClONO ₂ column	1996–2009	–0.9 (0.3)
Kiruna ⁵		1996–2009	–2.9 (0.4)
ground-based FTIR Jungfraujoch ⁴	HCl + ClONO ₂ column	1996–2009	–0.9 (0.2)
Kiruna ⁵		1996–2009	–1.5 (0.2)

1. *Ground-based microwave ClO data (Hawaii, 20°N)*: Updated data and results following Solomon et al. (2006). Rate of change (%/yr) is referenced to 1995 (January). See Figure 1-19.
2. *ACE-FTS HCl data (60°S–60°N average)*: Updated data and results following Froidevaux et al. (2006). Rate of change (%/yr) is referenced to the average abundance during the data time period. See Figure 1-18.
3. *Aura MLS HCl data (60°S–60°N average)*: Updated data and results following Froidevaux et al. (2006). Rate of change (%/yr) is referenced to the average abundance during the data time period. See Figure 1-18.
4. *Ground-based FTIR column data (Jungfraujoch, 46.5°N)*: Updated data and results following Mahieu et al. (2004) and Clerbaux and Cunnold et al. (2007). Rates of change (%/yr) are referenced to 1996. See Figure 1-17.
5. *Ground-based FTIR column data (Kiruna, 67.8°N)*: Updated data and results following Mikuteit (2008). Rates of change (%/yr) are referenced to 1996.

primarily a result of decreasing mixing ratios of CH₃Br in response to reduced industrial production and emission after 1998. Though Br from halons increased throughout most of the 1998–2008 period, during 2005–2008 Br from halons peaked in air at Earth’s surface at 8.2–8.5 ppt and was no longer increasing (see Table 1-1). Surface-based data suggest that global surface Br from halons may have decreased slightly from 2007 to 2008 (at –0.3 to –0.5%/yr).

1.4.2.2 STRATOSPHERIC BROMINE CHANGES

New results from ongoing ground-based DOAS (Differential Optical Absorption Spectroscopy) measurements of stratospheric BrO at both Lauder (45°S) and Harestua (60°N) show changes over time in inorganic bromine (Br_y) that are highly consistent with the observed tropospheric Br changes measured for halons and CH₃Br (Hendrick et al., 2008) (Figure 1-21). Updated stratospheric balloon measurements (Dorf et al., 2006) (Figure 1-21) do not provide as tight a constraint on Br_y changes since 2000, but the available results are consistent with

the tropospheric trends measured for Br from long-lived gases and the UV-visible measurements of Hendrick et al. (2008). Despite the significant contribution of non-controlled, very short-lived Br source gases to inorganic Br_y in the stratosphere (Section 1.3.3), temporal changes in stratospheric inorganic Br abundance appear to follow the measured changes in tropospheric Br from controlled substances (i.e., CH₃Br and the halons) (Figure 1-21).

Table 1-14 is an update from the previous Assessment (Table 2-8 in Law and Sturges et al., 2007) and lists estimates of Br_y from VSLS (Br_y^{VSLS}) and their uncertainty ranges for 12 studies. The contribution of VSLS to Br_y is derived in these studies by calculating Br_y from measured BrO using a photochemical model and then subtracting the contribution of long-lived gases (halons and CH₃Br). Seven of these studies were discussed previously, though one preliminary study in the previous Assessment is no longer considered. The estimate based on an analysis of MLS measurements of BrO by Livesey et al. (2006) shown in the previous Assessment has been updated with a newer study of the same data set by Kovalenko et al. (2007), who infer a VSLS contribution of 6.5 ± 5.5 ppt to stratospheric

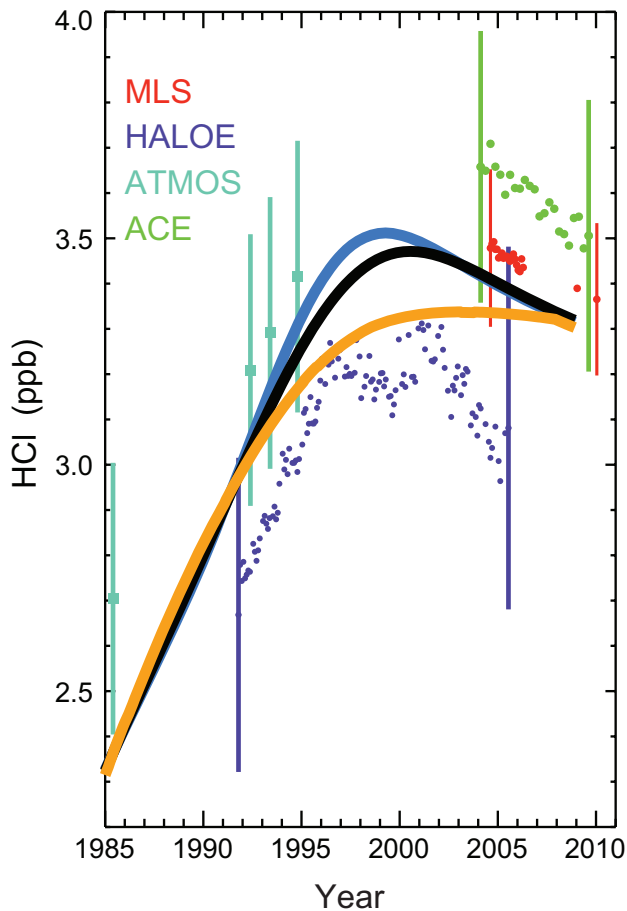


Figure 1-18. Time series of near-global HCl abundances (ppb) at about 53 km (near 0.5 hPa) (updated from Froidevaux et al. (2006) and the previous Assessment report (Clerbaux and Cunnold et al., 2007)). The satellite data sets have been updated for ACE-FTS (version 2.2 data, quarterly averages for 60°S–60°N, green dots) and for Aura MLS (version 2.2 monthly averages for same latitude range, red dots); both these data sets are for averages over 0.46 and 0.68 hPa (about 50 to 54 km). The solid curves are expectations for HCl (total Cl × 0.96) near 55 km based on the ground-based total tropospheric chlorine, and include a range of air-age spectrum widths (blue, black, and orange curves are for widths of 0, 2, and 4 years). The MLS data are interrupted after early 2006, because of a lifetime issue that affects the main HCl band's retrievals so it has been turned on only sparingly since; the MLS points in early 2009 and 2010 represent averages from 3–4 days in early January of each year. The Halogen Occultation Experiment (HALOE) data set (monthly averages, purple) ended in November 2005 and no updated results are available from the Atmospheric Trace Molecule Spectroscopy (ATMOS) instrument. Error bars (2-sigma estimates of systematic uncertainties) are given for the various time series and are shown typically only for the first and last points in the series (for clarity).

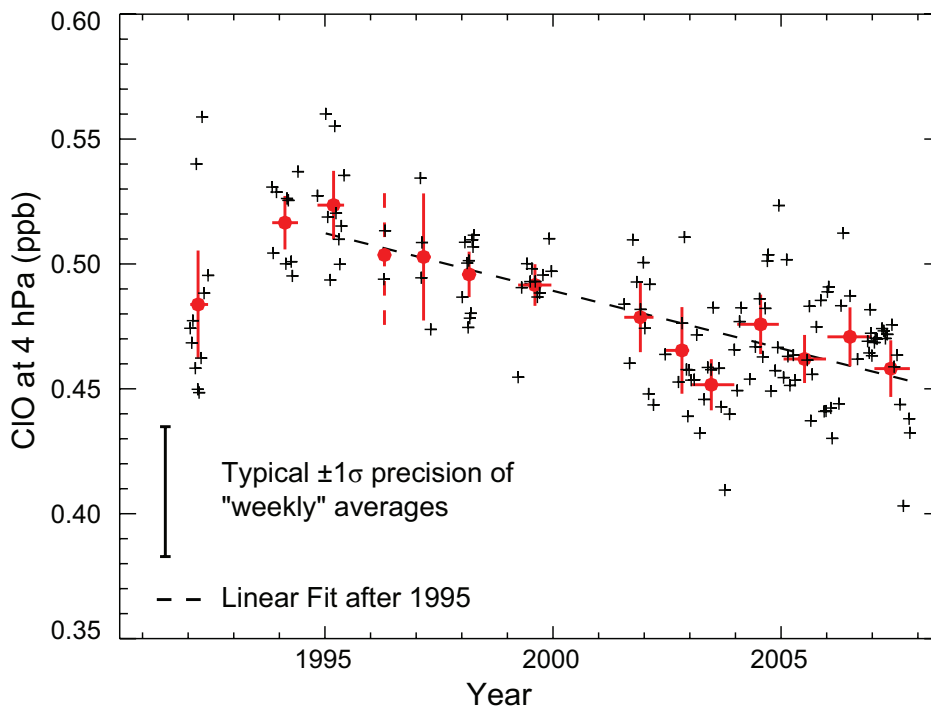


Figure 1-19. Time series of ClO abundances (ppb) above Hawaii (at 35–39 km or about 4 hPa) derived from ground-based millimeter-wave measurements since 1992 (update of Solomon et al., 2006). Black and red symbols are “weekly” and “yearly” averages of deseasonalized data, and error bars typically show two standard deviations about the means (see above reference). Dashed line gives a linear fit to the observations after 1995 (see also Table 1-13).

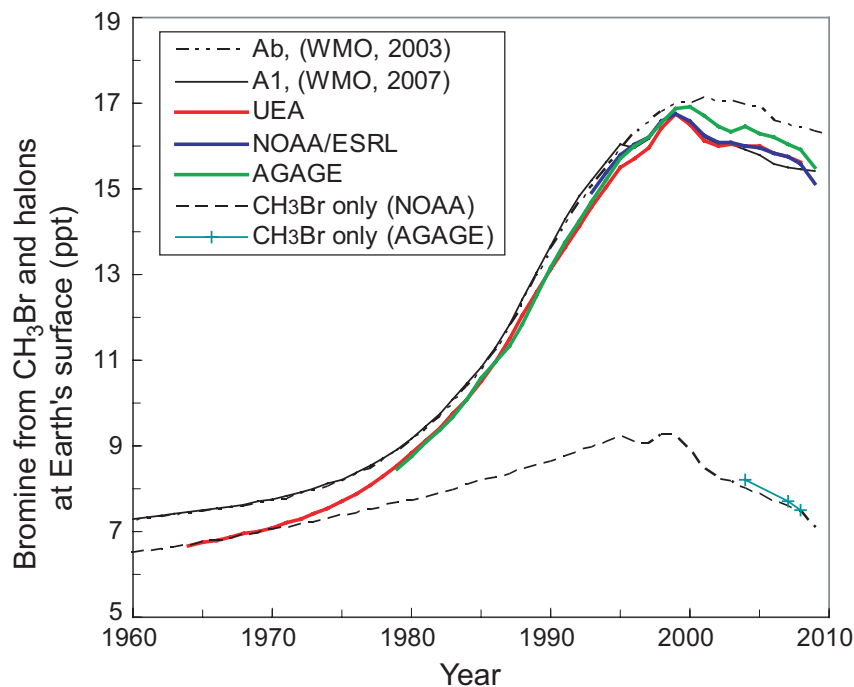


Figure 1-20. Tropospheric Br (ppt) from CH₃Br and halons over time. Halons measured by AGAGE (green line; Prinn et al., 2000; Sturrock et al., 2002), UEA (red line; Reeves et al., 2005), and NOAA (blue line) are added to CH₃Br data from NOAA (dashed black line; Montzka et al., 2003) or AGAGE (plus symbols; Simmonds et al., 2004). Ab (dot-dot-dashed line indicated as WMO, 2003 (Montzka and Fraser et al., 2003)) and A1 (solid black line indicated as WMO, 2007 (Clerbaux and Cunnold et al., 2007)) baseline scenarios are shown for comparison. Updated considerations of preindustrial mixing ratios in the current Assessment cause the differences in earlier years (see Section 1.2.1.6 and Chapter 5).

bromine. Two of the other four new estimates introduced in Table 1-14 are based on ground-based DOAS BrO measurements (Theys et al., 2007 and Hendrick et al., 2008) and suggest that a contribution of 7 ± 4 ppt and 6 ± 4 ppt of bromine, respectively, is needed from VLSL to account for the total measured bromine loading. McLinden et al. (2010) calculate a contribution from VLSL of 5 ± 5 ppt based on stratospheric BrO profiles measured by OSIRIS (Optical Spectrograph and InfraRed Imager System) during 2001–2008. Salawitch et al. (2010) inferred a value for Br_y^{VLSL} of 7 (5 to 10) ppt from OMI (Ozone Monitoring Instrument) measurements of total column BrO and tropospheric partial column BrO calculated from aircraft profiles (Neuman et al., 2010) obtained during Arctic spring.

These new results support the conclusion, made in the last Assessment (Law and Sturges et al., 2007), that substantially more Br_y is measured in the stratosphere than can be accounted for by CH₃Br and the halons alone; the new “ensemble” value reported in Table 1-14 is 1 ppt higher than the 5 ppt previously derived, while the range has stayed the same with 3 to 8 ppt. In other words, the majority of studies available to date continue to suggest a non-zero, positive value for Br_y^{VLSL} of 6 (3–8) ppt, which is large enough to affect ozone photochemistry in the lower middle stratosphere (see Section 1.3.4). Only 2 out of the 12 studies reported in Table 1-14 include a zero contribution from Br_y^{VLSL} in their uncertainty range. Taking this ensemble value for Br_y^{VLSL} of 6 (3–8) ppt derived from consideration of all available stratospheric Br_y estimates,

and adding tropospheric Br from CH₃Br and the halons from 2003–2004 in order to account for lags due to transport, a 2008 total stratospheric bromine mixing ratio of 22.5 (19.5–24.5) ppt can be derived. This result is comparable, given the range in results reported by different techniques, to the Br_y abundance derived from stratospheric measurements of BrO made in 2008. Annual mean Br_y derived from the NH Harestua site (60°N) during 2008 averaged 22.5 ± 4 ppt (an update of Hendrick et al., 2008), and 19.5 ± 2.5 ppt Br_y was derived from a single balloon profile made on 27 June 2008 in the tropics (5°S, 43°W; update of Dorf et al., 2006) (Figure 1-21).

These results imply that slightly less than half (40–45%) of the 2008 stratospheric Br_y burden is derived from controlled uses of halons (~8.3 ppt Br) and methyl bromide (0.4–0.9 ppt Br). As a result, more than half of the 2008 stratospheric Br_y burden is accounted for by natural sources of methyl bromide and other bromocarbons, and from quarantine and pre-shipment uses of methyl bromide not controlled by the Montreal Protocol. The total contribution of VLSL to stratospheric Br is estimated to be 1–8 ppt Br from measurements of VLSL source gases and modeling of their chemistry and transport (Table 1-9; Section 1.3.3.3). This magnitude is derived from the observed abundances of brominated source gases (SG) at the tropopause plus the modeled contributions of product gases (PG) in this region of the atmosphere (Hossaini et al., 2010; Aschmann et al., 2009; Liang et al., 2010).

The potential difference between Br_y from SGs and Br_y from BrO is also influenced by uncertainties in

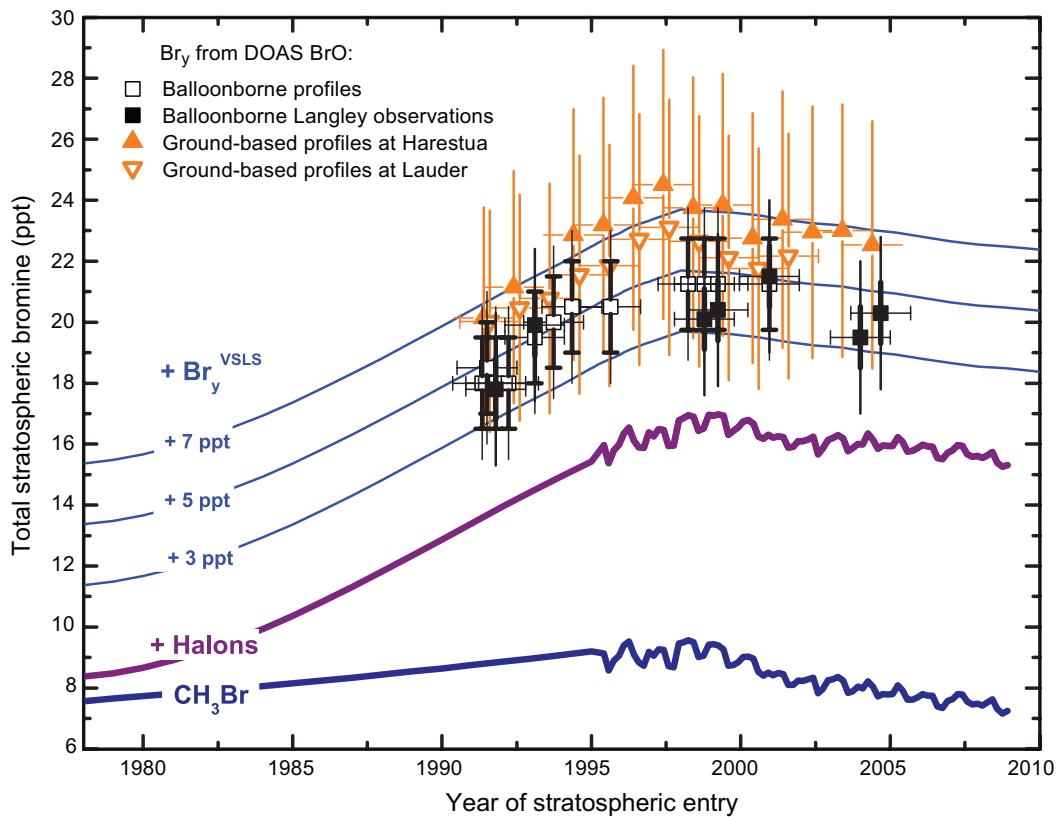


Figure 1-21. Changes in total stratospheric Br_y (ppt) derived from balloonborne BrO observations (squares) (update of Dorf et al., 2006) and annual mean mixing ratios calculated from ground-based UV-visible measurements of stratospheric BrO made at Harestua (60°N) and Lauder (45°S) (filled and open orange triangles, respectively) (adapted from Hendrick et al., 2008). These stratospheric trends are compared to trends in measured bromine (ppt) at Earth's surface with additional constant amounts of Br_y added (thin lines). Lines show global tropospheric bromine from methyl bromide as measured in ambient air and firn air with no correction for tropospheric CH_3Br loss (dark blue line; Butler et al. (1999) through 1998 including a changing interhemispheric gradient—see Chapter 5; Montzka et al. (2003) thereafter); global tropospheric bromine from the sum of methyl bromide plus halons (purple line; Butler et al. (1999) and Fraser et al. (1999) through 1995; Montzka et al. (2003) thereafter); and bromine from CH_3Br , halons, plus additional constant amounts of 3, 5, and 7 ppt Br (thin blue lines). Squares show total inorganic bromine derived from stratospheric measurements of BrO and photochemical modeling that accounts for BrO/Br_y partitioning from slopes of Langley BrO observations above balloon float altitude (filled squares) and lowermost stratospheric BrO measurements (open squares). For the balloonborne observations, bold/faint error bars correspond to the precision/accuracy of the estimates, respectively. For the ground-based measurements (triangles), the error bars correspond to the total uncertainties in the Br_y estimates. For stratospheric data, the date corresponds to the time when the air was last in the troposphere, i.e., sampling date minus estimated mean age of the stratospheric air parcel. For tropospheric data, the date corresponds to the sampling time, i.e., no corrections are applied for the time required to transport air from Earth's surface to the tropopause. Preindustrial levels were 5.8 ± 0.3 ppt for CH_3Br (Saltzman et al., 2004) and 0 ppt for the halons (Reeves et al., 2005). This figure is an update to Figure 2-3 from the previous Assessment (Law and Sturges et al., 2007).

Table 1-14. Estimates of inorganic bromine from very short-lived substances ($\text{Br}_y^{\text{VLSL}}$) contribution to stratospheric bromine derived from BrO measurements. Update of Table 2-8 from the previous Assessment (Law and Sturges et al., 2007), extended with new results.

Data Source	$\text{Br}_y^{\text{VLSL}}$ Central Value (ppt)	$\text{Br}_y^{\text{VLSL}}$ Range (ppt)	Reference
Ground-based BrO 11 sites, 78°S–79°N	5	1–9 ^a	Sinnhuber et al. (2002)
Ground-based BrO Lauder, New Zealand, 45°S	6	3–9	Schofield et al. (2004)
Ground-based BrO Arrival Heights, Antarctica, 78°S	6	3–9	Schofield et al. (2006)
DOAS balloon BrO profiles 5°S–68°N, 0–35 km	4.1	1.6–6.6	Dorf et al. (2006)
Aircraft & balloon BrO profiles, 22°S–35°N, 17–32 km and GOME satellite column BrO, 60°S–60°N	7	4–10 ^a	Salawitch et al. (2005)
SCIAMACHY satellite BrO profiles 80°S–80°N, 15–28 km	8.4	6.4–10.4	Sioris et al. (2006)
SCIAMACHY satellite BrO profiles 80°S–80°N, 15–28 km	3	0–6	Sinnhuber et al. (2005)
Ground-based BrO Harestua (60°N) and Lauder (45°S)	6	2–10	Hendrick et al. (2008)
Ground-based BrO Reunion Island (21°S, 56°E)	7	3–11 ^b	Theys et al. (2007)
MLS satellite BrO profiles 55°S–55°N, 10–4.6 hPa	6.5	1–12	Kovalenko et al. (2007)
OSIRIS satellite BrO profiles 80°S–80°N, 20–34 km	5	0–10	McLinden et al. (2010)
OMI total column BrO and aircraft tropo- spheric BrO profiles, Arctic spring	7 ^c	5–10	Salawitch et al. (2010)
Ensemble	6 (3–8)^d		

DOAS, Differential Optical Absorption Spectroscopy; GOME, Global Ozone Monitoring Experiment; SCIAMACHY, Scanning Imaging Absorption Spectrometer for Atmospheric Cartography; MLS, Microwave Limb Sounder; OSIRIS, Optical Spectrograph and InfraRed Imager System; OMI, Ozone Monitoring Instrument.

^a Range estimated by previous Assessment (Law and Sturges et al., 2007), based on the uncertainty in stratospheric Br_y inferred from BrO that was stated in the reference.

^b Range estimated based on the Hendrick et al. (2008) study that uses the same method.

^c Salawitch et al. (2010) has a different treatment of CH_2Br_2 than the other studies listed here. Their estimate for $\text{Br}_y^{\text{VLSL}}$ would be slightly higher (~ 1 ppt) if CH_2Br_2 were treated in the same manner as in the other studies.

^d Average and range of the central values of the 12 estimates of $\text{Br}_y^{\text{VLSL}}$.

absolute calibration scales for measurements of brominated organic SGs (Butler et al., 2010) and product gases. Furthermore, concentrations of VSLs sampled by a whole-air sampler represent only local influences for a small region over a short time in the tropical tropopause layer. In contrast, Br_y from BrO is measured in an air parcel in which the Br content represents a weighted average of Br in air parcels with a distribution of mean ages and that has been influenced by stratospheric mixing processes.

In addition to observations of BrO, measurements of stratospheric bromine nitrate (BrONO_2) have been analyzed from the Michelson Interferometer for Passive Atmospheric Sounding (MIPAS-E) instrument onboard the Envisat satellite for September 2002 and September 2003 (Höpfner et al., 2009). The authors report that the maximum values of BrONO_2 observed during night are always in the range of 20–25 ppt (with an uncertainty of 20–25% depending upon altitude). Large uncertainties remain, however, in the absorption cross section and its temperature dependence, so reliable estimates of Br_y from these measurements are not currently possible.

The contribution of tropospheric BrO to ground- and satellite-based measurements of stratospheric Br_y has been discussed in recent years. As in the last Ozone Assessment (Law and Sturges et al., 2007), it remains unclear whether BrO is distributed throughout the global troposphere with a background abundance of up to 3 ppt. Such a BrO background is supported by several studies (e.g., Richter et al., 2002; Van Roozendaal et al., 2002; Theys et al., 2007), where comparisons of Global Ozone Monitoring Experiment (GOME) BrO vertical columns with model results, balloonborne observations, and ground-based measurements have led to the conclusion that a significant background of several ppt BrO is present in the free troposphere. However, other observations support much lower values that include a contribution of zero ppt Br (e.g., Schofield et al., 2004; Dorf et al., 2008). Tropospheric BrO levels of less than 1 ppt imply larger stratospheric BrO columns than can be accounted for by CH_3Br and halons alone, and, as a result, an important contribution of VSLs to stratospheric Br_y is necessary to explain the total column observations (e.g., Salawitch et al., 2005).

Similarly, two independent studies (also discussed in detail in the previous Assessment) show BrO profiles retrieved from Scanning Imaging Absorption Spectrometer for Atmospheric Cartography (SCIAMACHY) radiances that lead to different results. While Sioris et al. (2006) derive large BrO abundances in the tropical tropopause layer and lowermost stratosphere (LMS), consistent with $\text{Br}_y^{\text{VSLs}}$ of 8.4 ± 2 ppt, Sinnhuber et al. (2005) imply a much smaller value for $\text{Br}_y^{\text{VSLs}}$ of 3 ± 3 ppt. One cause for this discrepancy is that Sinnhuber et al. (2005) suggest the presence of 1 ± 0.5 ppt of tropospheric BrO while Sioris et al. (2006) suggest a much smaller level of global

tropospheric BrO. Balloonborne DOAS observations of a BrO profile made in the tropics in 2005 found that BrO in the lower and middle troposphere is <1 ppt and compatible with zero within the uncertainties (Dorf et al., 2008). The authors derive a total contribution of 5.2 ± 2.5 ppt from brominated VSL SGs and inorganic PGs to stratospheric Br_y and so suggest a $\text{Br}_y^{\text{VSLs}}$ magnitude in between the earlier results derived from SCIAMACHY.

The recent ARCTAS (Arctic Research of the Composition of the Troposphere from Aircraft and Satellites) and ARCPAC (Aerosol, Radiation, and Cloud Processes affecting Arctic Climate) campaigns included airborne in situ measurements of BrO and O_3 (Neuman et al., 2010), placed in the footprint of satellite observations, to quantify the relative contribution of tropospheric and stratospheric partial columns to total column BrO and the relation between BrO hotspots (regions where column BrO is enhanced by 2 to 3×10^{13} radicals cm^{-2} relative to the zonal mean) and surface ozone depletion events. Salawitch et al. (2010) reported that aircraft in situ measurements of BrO and O_3 near the surface often bear little relation to OMI BrO “hotspots.” The geographic location of numerous BrO hotspots was shown to be consistent with the location of high total column ozone and a low-altitude (~ 5 km) tropopause, suggesting a stratospheric origin to the BrO enhancements that implied, on average, $\text{Br}_y^{\text{VSLs}}$ equal to 7 (5–10) ppt. It has been noted that the largest source of uncertainty in deriving Br_y from measurements of total column BrO is the rate constant of $\text{BrO} + \text{NO}_2 + \text{M} \rightarrow \text{BrNO}_3 + \text{M}$ (Sioris et al., 2006; Hendrick et al., 2008; Salawitch et al., 2010). Salawitch et al. (2010) suggest that the preponderance of prior observations of elevated BrO over Hudson Bay during spring may be related to a synoptic weather pattern known as the Hudson Bay low that is responsible for the very low-altitude tropopause (e.g., Liu and Moore, 2004). They stress that proper understanding of BrO “hotspots” requires accurate treatment of perturbations originating from both the stratosphere and troposphere, which generally has not been the focus of prior studies (i.e., many prior studies erroneously treat the stratospheric signal as spatially constant, ascribing all contributions to BrO hotspots as originating from below the tropopause).

In addition to the previously reported observations of BrO in the midlatitude marine boundary layer (Leser et al., 2003; Saiz-Lopez et al., 2004), BrO has now also been observed directly in the tropical and subtropical marine boundary layer. Mean daytime maxima of 2.5 ± 1.1 ppt were reported for observations made from November 2006 until June 2007 at Cape Verde (Read et al., 2008) and peak mixing ratios of 10.2 ± 3.7 ppt were measured during a ship cruise along the African coast during February 2007 (Martin et al., 2009). It is not clear to what extent this BrO influences Br abundances above the marine boundary layer.

1.4.3 Iodine in the Upper Troposphere and Stratosphere

Updated results since the last Assessment continue to suggest that gaseous iodine-bearing compounds contribute very little iodine to the current lower stratosphere. Balloonborne solar occultation spectra of IO and OIO in the tropical upper troposphere/lower stratosphere (UT/LS) obtained during balloon flights in 2005 and 2008 confirm the low values of IO and OIO for the tropical upper troposphere and lower stratosphere (Butz et al., 2009). A photochemical model of these results yields corresponding upper limits for the total gaseous inorganic iodine burden (I_y) of 0.17 to 0.35 (+0.20/−0.08) ppt in the tropical upper troposphere (13.5 km to 16.5 km) and 0.09 to 0.16 (+0.10/−0.04) ppt in the tropical lower stratosphere (16.5 km to 21.0 km).

These observations do not preclude iodine reaching the lower stratosphere in chemical forms other than commonly considered in photochemical models, or in particulate matter. There is evidence that iodine that may have originated in the lower troposphere can be found in lower stratospheric aerosol (Murphy et al., 2007). But if present in the TTL or stratosphere in forms other than IO and OIO, the extent to which this iodine might become available for ozone-depleting reactions in other parts of the stratosphere is not known.

The inferred upper limits for IO and OIO concentrations in the lower stratosphere suggest that catalytic cycles involving iodine have only a minor contribution to total ozone loss, but it remains unclear whether reactive iodine contributes—possibly through coupling with chlorine or bromine—to the observed trend of declining ozone in the lower stratosphere (e.g., Butz et al., 2009).

1.4.4 Equivalent Effective Chlorine (EECI) and Equivalent Effective Stratospheric Chlorine (EESC)

Changes in the stratospheric burden of total inorganic halogen (Cl and Br) are estimated from measured tropospheric changes in ODS abundances with a number of different metrics such as equivalent effective stratospheric chlorine (EESC), EESC-Antarctica, and EESC-Midlatitudes; changes in total tropospheric halogen (Cl and Br) are addressed with the equivalent effective chlorine (EECI), and equivalent chlorine (ECI) metrics (Clerbaux and Cunbold et al., 2007). By accounting for transport times, the efficiency for different halogens to deplete ozone, mixing processes, and age-of-air-dependent ODS decomposition rates (i.e., fractional release values), inorganic halogen abundances and changes can be estimated with EESC for different regions of the stratosphere from tropospheric

ODS measurements. As discussed in the last report and in recent publications, new approaches have been explored that enhance the usefulness of EESC for more accurately estimating halogen abundances and changes in specific stratospheric regions by considering that the extent of degradation of an ODS in the stratosphere is fairly well described by the mean stratospheric age of an air parcel (Newman et al., 2007). This new approach incorporates revised fractional release values for some compounds that are based primarily on observations (Schauffler et al., 2003) but that are also consistent with models (Douglass et al., 2008; Daniel and Velders et al., 2007). New fractional releases have not been considered for HCFC-142b and HCFC-141b owing to large discrepancies between the values derived by observations (e.g., Schauffler et al., 2003) and those based on model calculations that have been used in past Ozone Assessments.

New methods have been devised to more readily convey the magnitude of decline in EESC over time by referencing the changes in EESC to peak levels observed in the mid-1990s and amounts inferred for 1980 (Hofmann and Montzka, 2009). Though ozone depletion was likely non-negligible in 1980 (see Chapter 2 and Chapter 5), the EESC value in 1980 is still used in this report as an important benchmark for ozone recovery, as in past reports.

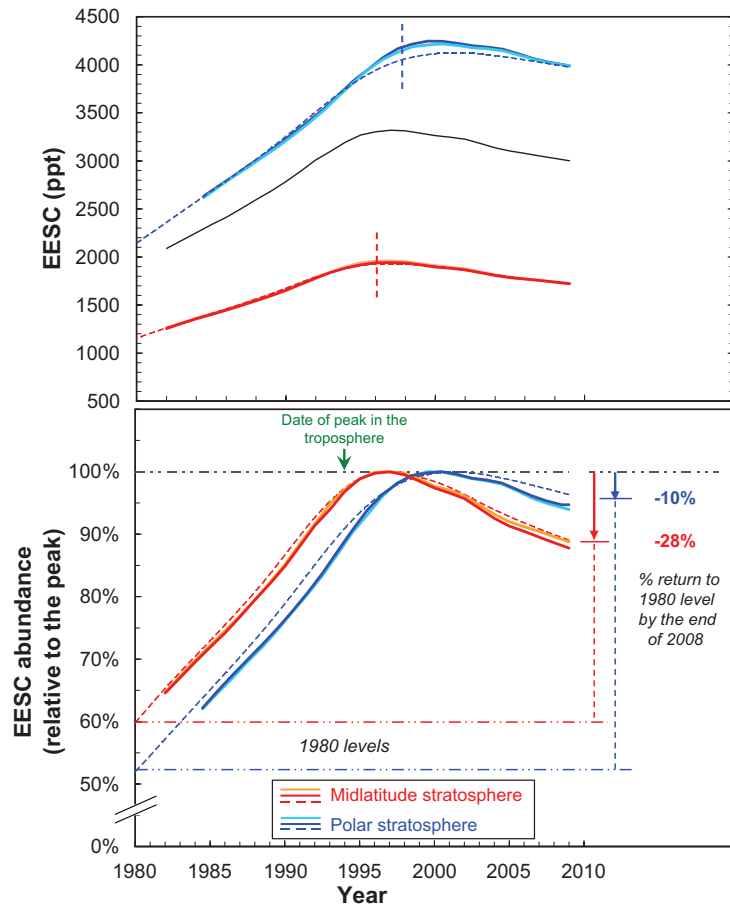
Stratospheric air parcels in midlatitudes having a mean age of 3 years have substantially less inorganic halogen as EESC than an air parcel with a mean age of 5.5 years typical of the Antarctic spring vortex (Figure 1-22, top panel) (Newman et al., 2007). Older air has larger EESC values because as air ages in the stratosphere, ODSs photochemically decompose so that a higher fraction of available halogen is present in inorganic forms.

As discussed in the last Assessment report (Daniel and Velders et al., 2007), calculating EESC in this way also demonstrates that EESC peaks at different times in different regions of the stratosphere. With the shorter transit times and higher relative contribution of rapidly declining short-lived ODSs in midlatitudes (e.g., CH_3CCl_3), EESC peaks earlier in midlatitudes than in polar regions (Figure 1-22, lower panel).

The date when the second derivative in EESC reaches a minimum also varies with stratospheric region. This date has been proposed as the time when a significant reduction in the rate of ozone decline might be expected, i.e., the “first stage” of ozone recovery (Yang et al., 2008). The second derivative in EESC reaches a minimum in early 1996 in midlatitudes (mean age = 3 years and age-of-air spectrum width = 1.5 years) and in late 1997 in the Antarctic stratosphere (mean age = 5.5 years and age-of-air spectrum width = 2.75 years) (Figure 1-22).

The similarity between global surface means derived for ODSs from independent surface sampling

Figure 1-22. Top panel: Equivalent effective stratospheric chlorine (EESC) (ppt) calculated for the midlatitude stratosphere from surface measurements (see Figure 1-1) and absolute fractional release values from Clerbaux and Cunnold et al. (2007) (black line) or with age-of-air-dependent fractional release values for the midlatitude stratosphere (red lines; mean age = 3 years) and the Antarctic springtime stratosphere (blue lines; mean age = 5.5 years). EESC calculated with stratospheric mixing processes included are shown as dashed colored lines for the different stratospheric regions (i.e., an air-age spectrum width equal to one-half the mean age; Newman et al., 2007). Different shades of the same colors represent EESC calculated with tropospheric halocarbon data from the different surface networks (NOAA and AGAGE, not always distinguishable from one another) without consideration of air-age spectra. Vertical dashed lines represent the date when the second derivative of EESC reaches a minimum (see text). Bottom panel: EESC derived for the midlatitude and polar stratospheric regions as a function of time plotted relative to peak abundances of 1950 ppt for the midlatitude stratosphere and 4150 ppt for the polar stratosphere. Percentages shown on right of this panel indicate the observed change in EESC relative to the change needed for EESC to return to its 1980 abundance (note that a significant portion of the 1980 EESC level is from natural emissions of CH_3Cl and CH_3Br). Colors and line styles represent the same quantities as in the top panel.



networks (Table 1-1) suggests only small uncertainties in our estimate of EESC abundance and trend in recent years related to measurement errors. Larger uncertainties are associated with using tropospheric data to derive actual inorganic halogen abundances in different regions of the stratosphere. These additional uncertainties stem from an imperfect understanding of ODS decomposition rates in the stratosphere (fractional release factors), stratospheric mixing processes, and stratospheric air-age spectra (Newman et al., 2007).

Results from all three global surface sampling networks indicate that EESC and tropospheric EECl continued to decline during 2005–2008. By 2008, tropospheric EECl (weighted with fractional release factors appropriate for the midlatitude stratosphere) had dropped 14% from its peak value measured in 1993–1994. Note that the magnitude of this decline is somewhat sensitive to the fractional release factors used. While a 14% drop is calculated with the updated fractional release factors discussed above, a drop in EECl of only 11% would be

calculated with the fractional release factors used in the previous Assessment report.

Changes in stratospheric inorganic halogen abundance (EESC) through 2008 can also be estimated from tropospheric measurements of ODSs. By 2008, midlatitude EESC had decreased by about 11% from its peak value in 1997. This stratospheric decline is smaller than derived for tropospheric EECl because of the time lag associated with transporting air from the troposphere to the stratosphere. When referenced to EESC in 1980, this drop is 28% of the decrease required for EESC in midlatitudes to return to that benchmark level (Figure 1-22, bottom panel). These EESC declines calculated for midlatitudes are similar whether or not mixing processes are accounted for with an air-age spectrum.

An even smaller decline is derived for the inorganic halogen abundance in the Antarctic polar vortex. By 2008, polar EESC had decreased by about 5% from its peak value in 2002. The much smaller decline over Antarctica stems from less time having elapsed since peak

abundances were observed in this older air and the dampening of changes by mixing air with a wider age spectrum across the maximum in EESC. This drop is approximately 10% of the decrease required for EESC in polar regions to return to the 1980 benchmark level (Figure 1-22, bottom panel). The EESC declines calculated for polar regions are more sensitive to mixing processes than in midlatitudes (see Figure). Slightly smaller declines are calculated for polar regions when an air-age-spectrum width of 2.75 years (one-half of the mean age of 5.5 years) is considered (a total decline of ~4% compared to 5% when mixing processes are not included in the EESC calculation).

In previous Assessment reports, it was noted that declines in the shorter-lived gases CH_3CCl_3 and CH_3Br were the main reason for the observed declines in EECL and EESC. During the past four years, however, no single chemical class has dominated the decline in the total combined abundance of ozone-depleting halogen in the troposphere. From 2005 through 2008, the long-lived CFCs (-17 ppt EESC) contributed similarly to the EESC decline as did the short-lived CH_3CCl_3 (-20 ppt EESC) and CH_3Br (-24 ppt EESC). Other compounds and compound classes contributed less to this decline (CCl_4 : -10 ppt EESC; halons: -4 ppt EESC), and HCFCs (+6 ppt EESC) added to this halogen burden over this period.

1.4.5 Fluorine in the Troposphere and Stratosphere

In contrast to the declines observed for tropospheric Cl and Br in recent years, the tropospheric abundance of fluorine (F) increased at a mean annual rate of $1.6 \pm 0.1\%/yr$ (40 ± 4 ppt/yr) since 1996 (fluorine from CFCs -11, -12, -113, -114, -115; HCFCs -22, -141b, -142b, -124; halons -1211, -1301, -2402; HFCs -23, -152a, -134a, -143a, -125; PFCs -14, -116, -218; and SF_6). This rate is substantially less than the annual increases of 60–100 ppt/yr (annually $5.9 \pm 0.3\%/yr$) observed for tropospheric F during the 1980s as CFC abundances were rapidly increasing. Many replacement compounds (HCFCs, HFCs, and PFCs) and other gases contributing F to the atmosphere degrade very slowly in the stratosphere and, therefore, do not affect stratospheric hydrogen fluoride (HF) changes as much as shorter-lived gases. Tropospheric F from compounds having stratospheric lifetimes <100 yrs (CFCs, halons, HCFC-141b, and HFC-152a; see Table 1-3) peaked in 2001 and was decreasing slowly during 2005–2008 (trend of $-0.4 \pm 0.1\%/yr$). Stratospheric changes in HF are likely to be between these two ranges ($-0.4\%/yr$ to $+1.6\%/yr$).

Stratospheric column FTIR measurements of HF, carbonyl fluoride (COF_2), and F_y^* (where $F_y^* = \text{HF} + 2 \times \text{COF}_2$) also suggest a decrease in accumulation rate

for atmospheric F beginning in 1999 (Figure 1-23). During 2005–2008 the rate of increase was $0.4\%/yr$, which is smaller than observed during the late 1980s–early 1990s. This change in rate is consistent with tropospheric changes in F-containing gases propagating to the stratosphere and a lag associated with transport. While the abundance and rates of change observed for stratospheric F_y^* are fairly well calculated with a 2-D model (Chipperfield et al., 1997) in which tropospheric changes for a subset of F-containing gases were considered, the calculated F abundance is likely a lower limit for F as some less abundant fluorine source gases were not included in the model. Data from other FTIR sites have also shown continued increases in HF column abundances. The measurements from Kiruna, Sweden, for example, indicate that an average increase in HF column of $1\%/yr$ ($\pm 0.3\%/yr$) occurred during 1996–2008 (relative to 2000; updates to Mikuteit (2008)). The rates of increase in stratospheric HF columns derived from these ground-based observations are within the expected range derived from surface observations ($-0.4\%/yr$ to $+1.6\%/yr$).

1.5 CHANGES IN OTHER TRACE GASES THAT INFLUENCE OZONE AND CLIMATE

In addition to the Cl- and Br-containing ODSs, other trace substances can affect stratospheric ozone. The most important substances in this group are the greenhouse gases. As greenhouse gases have been recently assessed by the Working Group I of the IPCC Fourth Assessment Report (AR4) (Forster et al., 2007; Denman et al., 2007) only updates on recent trends of mole fractions (Table 1-15), and information on sources and sinks are provided. Furthermore, in Figure 1-24 the development of the radiative forcing of the greenhouse gases discussed in this section is shown. In Section 1.5.1, CH_4 , N_2O , and sulfur compounds are discussed, which, apart from their direct influence on the abundance of the stratospheric ozone, also have an effect on the radiative forcing. A special focus in this section is the renewed increase of atmospheric CH_4 mixing ratios (Rigby et al., 2008; Dlugokencky et al., 2009) and the re-evaluated influence of N_2O on stratospheric ozone (Ravishankara et al., 2009). Sulfur trace gases and SO_2 as their main degradation product can potentially reach the stratosphere and can influence stratospheric ozone by enhancing its degradation through heterogeneous reactions. In Section 1.5.2, fluorinated greenhouse gases, which only indirectly influence stratospheric ozone via the greenhouse effect, are discussed.

The influence of rockets on stratospheric ozone will be discussed in Section 1.5.3, as their emissions could be highly relevant because they are emitted either in or near the stratospheric ozone layer.

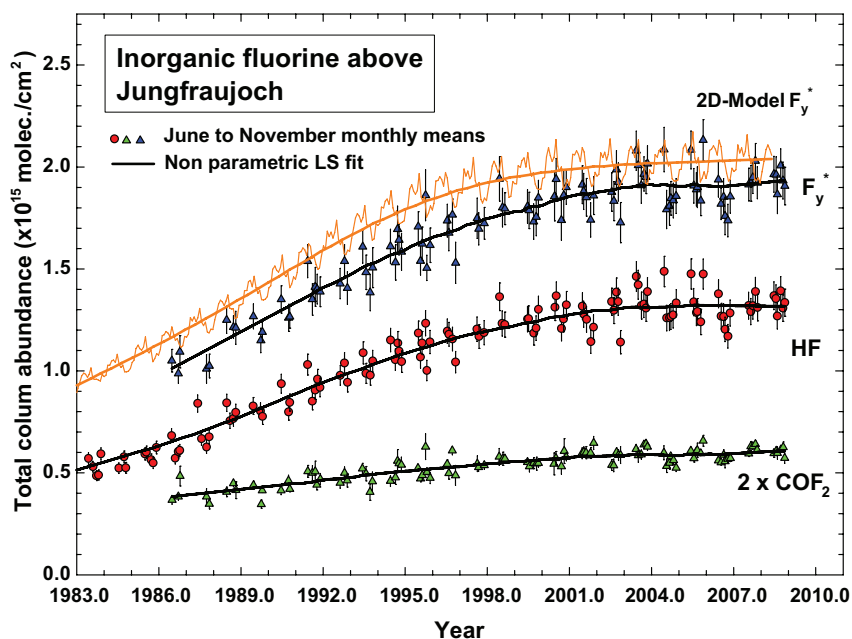


Figure 1-23. Time series of monthly-mean total column HF (red circles) and COF_2 (green triangles) (molecules per square centimeter), as derived from the Jungfraujoch (46.5°N) database, updated from the previous Assessment (Clerbaux and Cunnold et al., 2007). Duchatelet et al. (2009) have provided an updated analysis for the COF_2 results shown here, using a multispectral, multi-window approach. Data values are limited to June to November months to reduce variability. Fits to the data sets are given by the black curves. F_y^+ estimates (blue triangles) are calculated from $\text{HF} + 2 \times \text{COF}_2$. Also shown are column F_y^+ estimates from a 2-D model (based on Chipperfield et al., 1997) shown by the orange curve, with corresponding fit, that are derived from surface observations of CFC-11, CFC-12, CFC-113, and HCFC-22.

1.5.1 Changes in Radiatively Active Trace Gases that Directly Influence Ozone

In this section substances that are not controlled by the Montreal Protocol but that nevertheless have an influence on stratospheric ozone are discussed.

1.5.1.1 METHANE (CH_4)

Apart from its well-established influence on radiative forcing, methane (CH_4) is both a sink of reactive chlorine and a source of water vapor in the stratosphere and, therefore, influences the availability of inorganic halogen for depleting stratospheric ozone (see Section 1.4.1). Furthermore, CH_4 is a significant sink of tropospheric OH radicals and, hence, changes in its abundance can lead to changes in the lifetimes of ozone-depleting substances removed by OH (e.g., CH_3CCl_3 , HCFCs, VSLS).

A detailed description of the global methane budget and its uncertainties through 2005 is given in the IPCC AR4 (Forster et al., 2007). They reported that the global average CH_4 mole fraction in 2005 was 1774 ppb, which far exceeds the natural range during the last 650,000 years, and that the observed increase since preindustrial times is very likely due to anthropogenic activities (agriculture, fossil fuel use, etc.). Here we focus on important results

published afterwards and any similarities and differences between these recent and earlier studies.

For the IPCC A2 scenario, Portmann and Solomon (2007) compute methane-induced ozone increases over the 21st century of 2–12% below 20 km, and 0–4% between 20 and 40 km. On the other hand, they compute ozone decreases of 0–12% between 40 and 60 km. By 2008, the radiative forcing of CH_4 arising from mixing ratio changes since 1750 had reached about 0.5 W/m^2 , second only to CO_2 . Indirect effects of atmospheric methane related to changes in stratospheric H_2O and tropospheric ozone suggest that the present-day net radiative forcing of CH_4 could be as large as 0.7 W/m^2 (Forster et al., 2007).

After eight years of minimal net change, the mole fractions of CH_4 began to increase in 2007 in both hemispheres (Rigby et al., 2008; Dlugokencky et al., 2009). The growth rate was about 0.9 ± 3.3 ppb/yr from 1998–2006, while the global growth rate for 2007–2008 averaged 5.9 ppb/yr (NOAA) or 8.4 ppb/yr (AGAGE) (Table 1-15). The growth rate anomalies during 2006–2008 have been similar in magnitude to those observed in some years since 1990. The inverse analysis of Rigby et al. (2008) suggests that the renewed increase in growth rate was attributable either to increasing tropical and high latitude emissions or to a smaller high-latitude emissions increase along with a few percent low-latitude OH decrease (or to some combination of the two). A second analysis of spatial gradients

Table 1-15. Mole fractions of CO₂, CH₄, N₂O, SF₆, SO₂F₂, COS, and selected HFCs and PFCs.

	Mole Fraction				Annual Change in Mole Fraction		
	2005	2006	2007	2008	2005/06	2006/07	2007/08
CO ₂ [ppm] N	378.8	381.0	382.7	384.8	2.2	1.7	2.1
CH ₄ [ppb] N	1774.7	1775.4	1781.7	1787.6	0.7	6.3	5.9
CH ₄ [ppb] A	1774.2	1774.6	1780.8	1789.2	0.4	6.2	8.4
N ₂ O [ppb] N	319.0	319.8	320.5	321.5	0.8	0.7	1.0
N ₂ O [ppb] A	319.2	319.9	320.6	321.6	0.7	0.7	1.0
SF ₆ [ppt] N	5.6	5.9	6.2	6.4	0.3	0.3	0.2
SF ₆ [ppt] A	5.6	5.9	6.2	6.4	0.3	0.3	0.2
HFC-134a [ppt] N	34.4	38.8	43.2	47.6	4.4	4.4	4.4
HFC-134a [ppt] A	34.6	38.9	43.3	48.2	4.3	4.4	4.9
HFC-23 [ppt] A *	19.0	20.0	21.0	21.8	1.1	1.0	0.8
HFC-152a [ppt] A	4.1	4.5	5.3	5.9	0.4	0.8	0.6
HFC-143a [ppt] A	5.8	6.6	7.5	8.5	0.8	0.9	1.0
HFC-32 [ppt] A	1.3	1.6	2.1	2.7	0.3	0.5	0.6
HFC-125 [ppt] A	3.9	4.5	5.2	6.1	0.6	0.7	0.9
HFC-365mfc [ppt] A	0.1	0.3	0.4	0.4	0.2	0.1	0.1
HFC-245fa [ppt] **	0.4	0.6	0.7	1.0	0.2	0.1	0.4
PFC-14 [ppt] A	75.1	75.7	76.4	77.1	0.6	0.7	0.7
PFC-116 [ppt] A	3.7	3.8	3.8	3.9	0.1	0.0	0.1
PFC-218 [ppt] A	0.4	0.4	0.5	0.5	0.0	0.1	0.0
SO ₂ F ₂ [ppt] A	1.35	1.42	1.47	1.51	0.07	0.05	0.04
COS [ppt] N	488	491	494	491	2.2	2.9	-2.1

Data are global surface means.

These observations are updated from the following sources: Conway et al. (1994), Dlugokencky et al. (2009), Geller et al. (1997), Grealley et al. (2005, 2007), Hall et al. (2007), Miller et al. (2010), Montzka et al. (1996, 2007), Mühle et al. (2009, 2010), O'Doherty et al. (2004, 2009), Prinn et al. (2000), Rigby et al. (2008), Stemmler et al. (2007), and Vollmer et al. (2006).

Annual changes in mole fraction are derived from the difference between year x and $x-1$.

N denotes data from NOAA.

A denotes data from AGAGE.

* Global averaged mixing ratios for HFC-23 before 2007 have been modeled using archived air data from the SH (Miller et al., 2010).

** Data are an average of measurements from the Jungfraujoch, Switzerland (47°N) and Cape Grim, Australia (40°S) (updated from Vollmer et al., 2006).

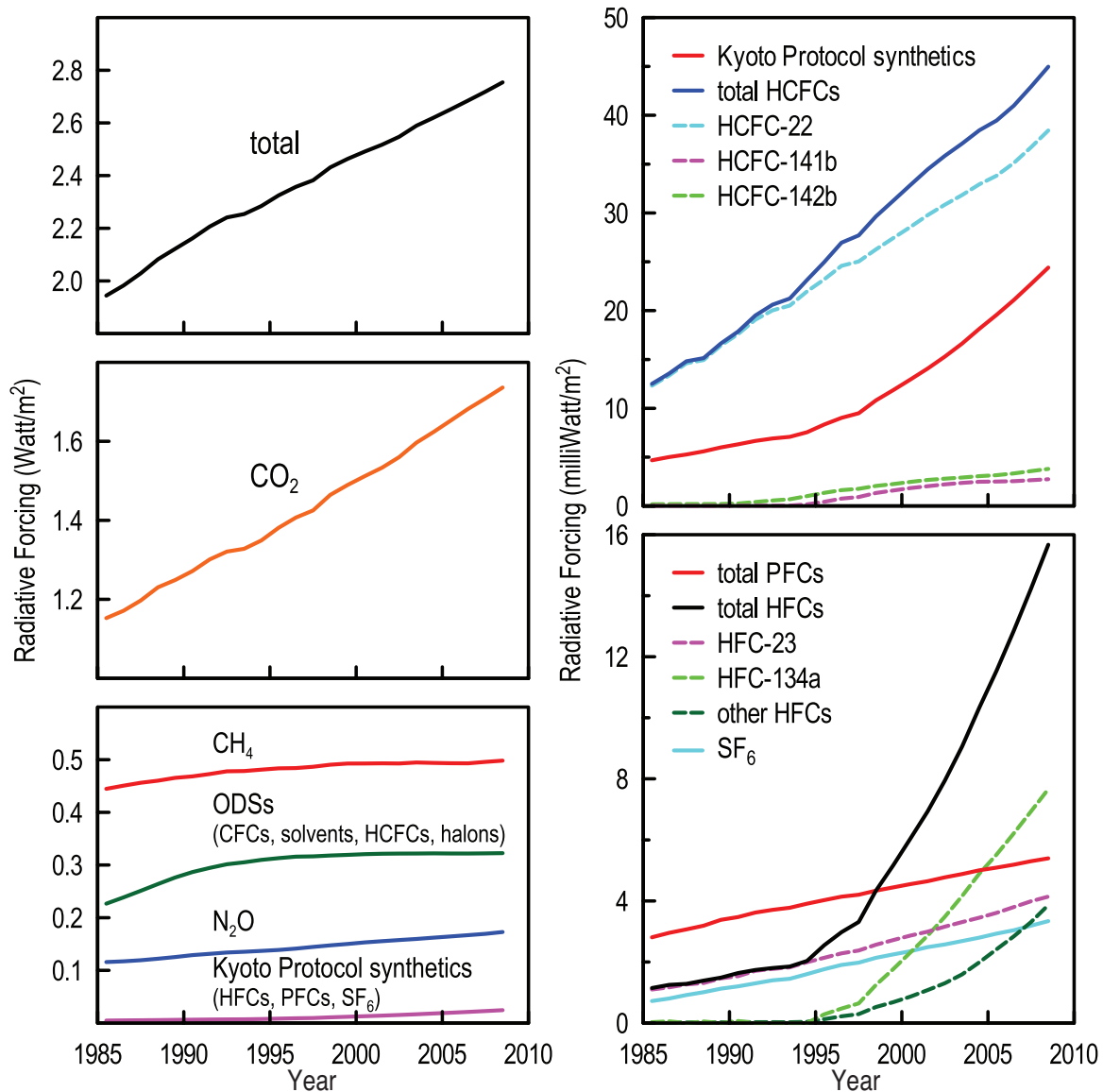


Figure 1-24. Left panels: The evolution of radiative forcings from the sum of the major greenhouse gases (CO_2 , CH_4 , N_2O), the ODSs (CFCs, HCFCs, halons, CH_3CCl_3 , CCl_4), and the Kyoto Protocol synthetic gases (HFCs, PFCs, SF_6) in W/m^2 . Right panels: The upper panel shows the evolution of radiative forcings (note change in scale) from individual HCFCs and their sum, and from the sum of Kyoto Protocol synthetic gases (HFCs, PFCs, and SF_6), which appear individually or grouped together in the lower right panel (in mW/m^2). Forcings are calculated from background mixing ratios in Table 1-1 and Table 1-15 and radiative efficiencies given in Chapter 5.

and Arctic isotopic signals by Dlugokencky et al. (2009) suggests primarily an increased wetland source in both the high latitudes and tropics for 2007, while the 2008 increase was predominantly seen at tropical latitudes. They argued for little influence from OH variations. Furthermore, an increase in interhemispheric exchange during the cool phase of the El Niño-Southern Oscillation (ENSO) (consistent with observed changes in the SF_6 mean inter-

hemispheric difference), could have contributed, in part, to changes in Southern Hemisphere growth rates. Bousquet et al. (2006) suggested that the relatively stable period for CH_4 mixing ratios between 1999 and 2006 was a fortuitous combination of a decreasing wetland source masking an increasing anthropogenic energy-related source, with the chemical loss of CH_4 due to OH playing a potential role in the observed atmospheric variability. In compari-

son, Chen and Prinn (2006) evaluated growth rates and distributions of CH₄ during 1996–2001 relative to earlier years and found decreased energy-related emissions and increased emissions from rice, with the 1998 anomaly due to increased global wetland and wildfire emissions. Chen and Prinn (2006) note that their inferred increased rice emissions (about 25 Tg CH₄/yr) could also be attributed to surrounding non-rice wetland emissions.

While the possibility of very large methane emissions from plants (as proposed by Keppler et al., 2006) has been ruled out (Ferretti et al., 2007; Beerling et al., 2008; Bloom et al., 2010a), laboratory experiments have shown that UV-irradiated plant pectin produces CH₄ (Vigano et al., 2008). While not ascribed to aerobic methanogenesis, Carmo et al. (2006) presented evidence for a canopy source of CH₄ from upland forest and Rice et al. (2010) reported a “bottom-up” estimate of global CH₄ emissions of 60 ± 20 Tg/year from trees in flooded soils.

In the last decade, satellite observations have become available that fill an important gap in the global coverage of the temporal and spatial variations of CH₄ (e.g., Frankenberg et al., 2005; Frankenberg et al., 2008). Furthermore, satellite observations have also detected an increase in global mixing ratios in recent years (Bloom et al., 2010b) and identified increased wetland emissions as a potential cause, consistent with in situ measurements.

Future trends in atmospheric CH₄ are highly uncertain and depend to a large extent on the proportion of the carbon stored in Arctic permafrost that emanates as CH₄ following permafrost thaw and the extent of permafrost thawing. Tarnocai et al. (2009) estimate that frozen Arctic soils contain about 1670 petagrams (Pg) of carbon. While current observations do not imply a large role for thawing permafrost, this could change with large future Arctic warming. Additionally, large stores of CH₄ exist in the form of frozen CH₄ hydrates on the sea floor (Buffett, 2004). These potentially could be liberated either by warming induced by ocean circulation changes or via attempted extraction for fuel usage. Changes in wetland extent, agricultural practice, and fossil fuel extraction (excluding hydrates) could also affect future atmospheric CH₄ levels, but have much smaller potential for impact than the large frozen soil-carbon reservoirs mentioned above.

1.5.1.2 NITROUS OXIDE (N₂O)

The photochemical degradation of nitrous oxide (N₂O) in the stratosphere leads to ozone-depleting nitric oxide (NO) and nitrogen dioxide (NO₂) and to important free radical reservoir species (e.g., HNO₃, ClONO₂). In addition, N₂O is an important greenhouse gas.

Forster et al. (2007) reported that the global average mole fraction of N₂O in 2005 was 319 ppb compared to a preindustrial value of 270 ppb. The growth rate has been

approximately constant since 1980 with more than one-third of its emissions being anthropogenic (agriculture, etc.). In 2005–2008 the average growth rate of N₂O was 0.8 ppb/yr (NOAA and AGAGE), with an average global mixing ratio in 2008 of 321.5 ppb (NOAA) and 321.6 ppb (AGAGE) (Table 1-15). N₂O is an important ozone-depleting and greenhouse gas. For the A2 IPCC scenario, Portmann and Solomon (2007) compute 21st century ozone decreases up to 8% in the 20–40 km altitude region from changes in N₂O alone. By comparing the Ozone Depletion Potential-weighted anthropogenic emissions of N₂O with those of ozone-depleting substances, Ravishankara et al. (2009) show that N₂O emissions currently are the single most important emissions of a chemical that depletes ozone. Yet, N₂O is not controlled by the Montreal Protocol. The findings of Ravishankara et al. (2009) are discussed in more depth in Sections 5.2 and 5.4 of Chapter 5. Future anthropogenic emissions of N₂O may increase if nitrogen-containing fertilizer use is enhanced for the production of biofuels, as discussed by Crutzen et al. (2008). Limiting or reducing future N₂O emissions, one target of the Kyoto Protocol, would enhance the recovery of the ozone layer from its depleted state and would also reduce anthropogenic forcing of the climate system.

Recently, Huang et al. (2008) used AGAGE, NOAA/ESRL, and Commonwealth Scientific and Industrial Research Organisation (CSIRO) observations, the 3-D MATCH model (1.8° × 1.8°), and a Kalman filter to deduce regional N₂O emissions. The effects of model errors were assessed using a large ensemble of 2-D model inversions. They concluded that global N₂O emissions with 66% probability errors are $16.3^{+1.5}_{-1.2}$ and $15.4^{+1.7}_{-1.3}$ Tg N (N₂O)/yr, for 1997–2001 and 2001–2005, respectively. Emissions from the equator to 30°N increased significantly from the earlier Bouwman et al. (1995) estimates, while emissions from the southern oceans (30°S–90°S) decreased significantly. Relative to Bouwman et al. (1995), Huang et al. (2008) found that land emissions from South America, Africa, and China/Japan/South East Asia are larger, while land emissions from Australia/New Zealand are smaller. Their study also showed a shift of the oceanic sources from the extratropical to the tropical oceans relative to Bouwman et al. (1995). Between the periods 1996–2001 and 2002–2006, emissions increased in China/Japan/South East Asia, 0°–30°N oceans, and North West Asia; emissions decreased in Australia/New Zealand, 30°S–90°S oceans, 30°N–90°N oceans, and Africa. The lower tropical ocean emissions in 1997–2001 relative to 2002–2005 could result from the effects of the 1997–1998 El Niño in the earlier period.

The N₂O fluxes from the equator to 30°N region reported by Hirsch et al. (2006) and Huang et al. (2008) are significantly larger than estimated by Bouwman et al. (1995) and Prinn et al. (1990), while the emissions

from the southern oceans (30°S–90°S) are significantly smaller. The differences between the two recent and two earlier studies may be due to either real long-term variations or different modeling and methodological approaches. Huang et al. (2008) found that $23 \pm 4\%$ of the global total N₂O emissions come from the oceans, which is at the low range of the Hirsch et al. (2006) and Bouwman et al. (1995) estimates. Overall, the Hirsch et al. (2006) and Huang et al. (2008) studies show reasonably good agreement. Considering the fact that Hirsch et al. (2006) only used N₂O measurements from NOAA/ESRL for the 1998 to 2001 time period and the inversion techniques and transport models used in the two studies differ as well, these good agreements may indicate that the relative contributions of regional N₂O surface fluxes to the global total may indeed have changed significantly from the Bouwman et al. (1995) estimates for 1990 and the Prinn et al. (1990) estimates for 1978–1988. In comparison with Prinn et al. (1990), the Huang et al. (2008) study shows smaller surface emissions in the 30°S–90°S and 30°N–90°N regions, significantly higher fluxes in the 0°–30°N region, and similar fluxes in the 0°–30°S region. Huang et al. (2008) concluded that uncertainty in modeling troposphere and stratosphere exchange is the most significant source of uncertainty in deriving regional N₂O emissions.

High-precision measurements of atmospheric N₂O over the last decade reveal subtle signals of interannual variability (IAV) superimposed upon the more prominent growth trend. Nevison et al. (2007) explored the causes of both seasonal and interannual variability using comparisons of a 1993–2004 3-D model simulation to observations of N₂O at five AGAGE stations. The model does not include a stratospheric sink and thus isolates the effects of surface sources and tropospheric transport. Both model and observations yield correlations in seasonal and interannual variability among species, but only in a few cases are model and observed variability correlated to each other. The results suggest that tropospheric transport contributes significantly to observed variability, especially at the Samoa station. However, some features of observed variability (e.g., at Mace Head, Ireland) are not explained by the model simulation and appear more consistent with the effects of downward mixing of N₂O-poor stratospheric air.

Finally, Jiang et al. (2007) carried out a systematic study of the N₂O seasonal cycle and its latitudinal variation using AGAGE and NOAA/ESRL data. The seasonal cycles were statistically significant at Alert (82°N, 62°W), Barrow (71°N, 157°W), Mace Head (53°N, 10°W), Cape Kumukahi (19°N, 155°W), Cape Matatula (14°S, 171°W), Cape Grim (41°S, 145°E), and South Pole (90°S, 102°W). The amplitude (peak to peak) of the seasonal cycle varies from 0.29 ppb at the South Pole to 1.15 ppb at Alert. The month at which the seasonal cycle is at a minimum var-

ies monotonically from April (South Pole) to September (Alert). The seasonal cycle in the Northern Hemisphere shows the influence of the stratosphere, owing to seasonal variations in exchange between the stratosphere and troposphere in the Arctic; the seasonal cycle in the Southern Hemisphere suggests greater influence from surface sources.

1.5.1.3 COS, SO₂, AND SULFATE AEROSOLS

Carbonyl sulfide (COS) and other sulfur-containing gases such as sulfur dioxide (SO₂) are important precursors of sulfate aerosols in the stratosphere (Notholt et al., 2005; SPARC, 2006), which catalyze ozone depletion by ODSs (e.g., Newman and Pyle et al., 2003; Danilin and McConnell, 1995) and affect the radiative balance of the atmosphere (e.g., Forster et al., 2007). The relative contributions of the sulfate aerosol precursors are difficult to quantify because SO₂ has a short lifetime, and the nonvolcanic stratospheric sulfur (S) burden is not well determined.

COS is the most abundant sulfur-containing trace gas in the atmosphere. Long-term trends in COS mixing ratios suggest that global changes during the past decade have been fairly small (Aydin et al., 2008; Montzka et al., 2004; Montzka et al., 2007; Zander et al., 2005). Updated data show a mean global surface mixing ratio of 491 ppt in 2008 and a mean rate of increase of 1.8 ppt/yr during 2000–2008 (Table 1-15). The current background concentration is more than 60% higher than preindustrial values of ~300 ppt (Montzka et al., 2004; Aydin et al., 2008). Long-term COS trends from long-path infrared solar absorption measurements above Jungfraujoch (Switzerland) (updated from Zander et al., 2005) show an annual increase in the total vertical column of $0.79 \pm 0.09\%$ over 2000–2008 (relative to January 2000 values) and an increased growth rate of $1.26 \pm 0.29\%/yr$ over 2005–2008 (relative to January 2005 values). Over decadal-to-centennial periods, COS mixing ratios appear correlated to anthropogenic sulfur emissions (Montzka et al., 2004). The updated Jungfraujoch data also show this behavior, exhibiting decreases in total column COS during the late 1980s to early 1990s. Both ground-based flask sampling and Jungfraujoch remote sensing results then show a reversal, with increases since the mid-2000s, concurrent with 5%/yr increases in global coal combustion since then (BP, 2009).

Global flask measurements show large seasonal changes across broad geographic scales (Montzka et al., 2007). The observed variations suggest an important role for the oceans in determining the seasonality in the SH and uptake by the terrestrial biosphere during the growing season in the NH. The amplitude of observed seasonal changes in the NH suggests significantly larger vegetative

uptake of COS and, as a result, a shorter global lifetime of 2–4 years (Montzka et al., 2007; Suntharalingam et al., 2008) than derived in earlier studies.

COS mixing ratio distributions derived from satellites have provided an estimate of COS stratospheric loss. From correlations to measured CFC abundances, a stratospheric lifetime of 64 ± 21 years can be derived. This lifetime suggests that COS contributes 34–66 Gg S/yr to the stratosphere (Barkley et al., 2008). Given the wide range in estimates of sulfur emissions necessary to maintain the stratospheric sulfate aerosol layer, it is difficult to accurately estimate the contribution of sulfur from COS to this layer. Some estimates from midlatitude data suggest that COS could contribute ~50% of aerosol sulfur mass being transported to the midlatitude lower stratosphere (Martinsson et al., 2005). Other results implying 300–400 Gg S/yr to explain observed seasonal changes above some NH sites would suggest a much smaller relative contribution of COS to stratospheric sulfur (Hofmann et al., 2009). This latter study also provided evidence for large changes in stratospheric aerosol during recent years. Because COS mixing ratios in the background atmosphere have not increased by more than a few percent since 2000, the cause for this aerosol increase is not likely attributable entirely to the observed COS changes (Hofmann et al., 2009).

Sources of atmospheric SO₂ have been reviewed by Stern (2005) and Fisher et al. (2007). Anthropogenic emissions of SO₂ are mainly due to fossil fuel burning and metal smelting. Natural sources consist of the oxidation of COS, dimethyl sulfide (DMS), carbon disulfide (CS₂), and hydrogen sulfide (H₂S), as well as emissions from volcanic activities. Based on “bottom-up” estimates (see Box 1-1), anthropogenic sulfur emissions reached a maximum of ~75 Tg S/yr in the 1980s (Stern, 2005). Emissions subsequently decreased as a consequence of legislation addressing enhanced acidification (in industrialized countries) and because of reduced industrial activity in Eastern Europe (Stern, 2005). In 2000, global emissions were estimated to be 55–62 Tg S/yr (Fisher et al., 2007), of which ~17 Tg S/yr was emitted from Asia (Stern, 2005; Klimont et al., 2009). In some projections future emissions from Asia are expected to increase substantially (e.g., 40 Tg S/yr by 2030; Klimont et al., 2009), with the main increase expected to occur either in China (Fisher et al., 2007) or in India (Klimont et al., 2009). SO₂ mixing ratios decline rapidly with height and distance from the source regions to a few tens of ppt (SPARC, 2006), and therefore the same limitations for its transport into the stratosphere apply as for VSLS discussed in Section 1.3.

Natural sources of atmospheric SO₂, which consist of volcanic eruptions and the oxidation of primarily oceanic substances (COS, DMS, and H₂S), are estimated to account for 17–41 Tg S/yr (Haywood and Boucher, 2000). Infrequent explosive volcanic eruptions do temporarily enhance

the sulfate aerosol burden of the stratosphere dramatically. For example, in 1991 the eruption of Mt. Pinatubo added ~10 Tg S into the atmosphere (Read et al., 1993; Guo et al., 2004), which partly reached the stratosphere and significantly affected the atmospheric radiative balance. Deliberately enhancing S in the stratosphere is being discussed as a geoengineering option for mitigating the heating influence from greenhouse gases (see Chapter 5).

1.5.2 Changes in Radiative Trace Gases that Indirectly Influence Ozone

Carbon dioxide and fluorinated compounds are greenhouse gases and have no direct effect on stratospheric ozone. Nevertheless, they are discussed in this section, as their impact on global warming can indirectly lead to changes in stratospheric ozone, as discussed in Chapter 4 of this Assessment.

1.5.2.1 CARBON DIOXIDE (CO₂)

Since 1750 CO₂ has been the most important anthropogenic greenhouse gas and it still continues to dominate atmospheric radiative forcing at 1.74 W/m² in 2008 (Hofmann et al., 2006) (Figure 1-24). The 2003.5–2008.5 increase in CO₂ radiative forcing (0.14 W/m²) was six times greater than the total direct forcing increase from all other radiatively active, long-lived gases in this same period.

In 2008, the global average CO₂ mole fraction was 384.8 ppm (Table 1-15). The global growth rate of CO₂ averaged 2.1 ppm/yr between 2005 and 2008, when derived with results from all 37 marine boundary layer sites in the NOAA/ESRL surface air sampling network. This is similar to the average growth rate for the previous four-year period (2.0 ppm/yr), but significantly higher than the average growth rate in the 1990s (1.5 ppm/yr). The increase in atmospheric growth rate in the last 8 years corresponds closely with acceleration in the combustion of fossil fuels (Boden et al., 2009; BP, 2009). The increase in global fossil fuel-based CO₂ emissions averaged 0.8%/yr in the 1990s and 3.2%/yr between 2000 and 2008 (with estimated emissions of 8.7 Pg C/yr in 2008).

The fraction of fossil carbon remaining in the atmosphere (airborne fraction) shows no discernible trend over the past 20 years, with 5-year means stable at about 50% (Knorr et al., 2009). There is significant interannual variability in the atmospheric growth (and airborne fraction), of which about 50% can be explained by ENSO and volcanism (Bacastow, 1976; Reichenau and Esser, 2003) and their effect on carbon balance of the land biosphere.

Although the number of coupled climate carbon cycle models and their mechanistic sophistication has increased, there is still no consensus as to the centennial-

scale fate of the airborne fraction and the 50% radiative forcing discount that it has provided in recent decades. Most models predict a declining efficiency in the uptake of atmospheric carbon by the oceans by the middle of the century (Friedlingstein et al., 2006). Whether or not this decline can be observed already in the Southern Ocean is a matter of scientific debate and is discussed in detail in Chapter 4. The fate of the land biosphere sink of CO₂ is also uncertain, with some models predicting increased uptake due to boreal forest expansion and general CO₂ fertilization, while others predict drought-stress related die back of forests and losses in productivity (Friedlingstein et al., 2006). The coupling of the carbon cycle to climate variability remains a first-order uncertainty in the prediction of future climate. This is especially true considering the uncertain fate of an estimated 1000 Pg C of carbon frozen in the top 3 meters of Arctic soils (Tarnocai et al., 2009), which have not been considered in coupled climate carbon cycle models.

1.5.2.2 FLUORINATED GREENHOUSE GASES

With the exception of carbon tetrafluoride (CF₄), the fluorinated compounds discussed in this section are virtually entirely of anthropogenic origin. Hydrofluorocarbons (HFCs) are replacement chemicals for the long-lived ODSs in various applications such as refrigeration, fire extinguishers, propellants, and foam blowing (IPCC/TEAP, 2005). The very long-lived perfluorocarbons (PFCs) and sulfur hexafluoride (SF₆) have been emitted over past decades from established industrial processes and, in the case of PFCs, recently from newer applications largely in the electronics sector. The newest compounds detected in the atmosphere are sulfonyl fluoride (SO₂F₂) (used as a replacement for CH₃Br) and nitrogen trifluoride (NF₃) used in the electronic sector.

By mid-2008, the contribution of the fluorinated substances (HFCs, PFCs, SF₆) to radiative forcing had increased to ~24 mW/m². Contributions were 16 mW/m² for HFCs (including HFC-23), 3.4 mW/m² for SF₆, and 5.4 mW/m² from the sum of CF₄, C₂F₆, and C₃F₈ (Mühle et al., 2010), assuming a natural background for CF₄ of 34.7 ppt (Figure 1-24). These contributions to total radiative forcing by 2008 are small compared to CO₂ (1740 mW/m²), CH₄ (500 mW/m²), CFCs (262 mW/m²), and N₂O (170 mW/m²), but amount to about half of the radiative forcing from HCFCs (45 mW/m²) (Figure 1-24). However, these values are radiative forcings since preindustrial times. Considering changes only over the past 5 years (2003.5–2008.5), CO₂ direct radiative forcing increased by 139 mW/m², that from N₂O increased by 12 mW/m², and that from CH₄ increased by 4 mW/m². Radiative forcing from the sum of HFCs, PFCs, and SF₆ increased by 8 mW/m² over this same period, whereas the ODSs con-

trolled under the Montreal Protocol have positive and negative contributions (CFCs, CI-solvents, and halons: -8 mW/m²; HCFCs: +8 mW/m²). This means that during 2003.5–2008.5, the change in direct radiative forcing from the sum of HFCs, PFCs, and SF₆ was comparable to the change in direct radiative forcing from either CH₄ or N₂O. Further impacts of the potential large future increase of fluorinated greenhouse gases are discussed in Chapter 5 of this Assessment.

Summed emissions from HFCs used primarily as replacements for ODSs (i.e., not HFC-23) have increased since 2004. The sum of emissions (weighted by GWP) of HFCs used as ODS replacements increased by 8–9%/yr from 2004 to 2008, and by 2008 amounted to 0.39 ± 0.03 gigatonnes of CO₂ equivalents per year (Gt CO₂-eq/yr). Emissions of HFC-23, predominantly the result of HCFC-22 production, contributed an additional ~0.2 Gt CO₂-eq/yr emission during 2006–2008 (Montzka et al., 2010). Recently published data with higher time resolution suggest that the 2008 HFC-23 emission may be slightly less than this 3-year average (~0.17 Gt CO₂-eq/yr in 2008; Miller et al., 2010).

The following paragraphs are an update on the abundance and the sources of different types of fluorinated greenhouse gases (GHGs).

HFC-134a (CH₂FCF₃)

HFC-134a has replaced CFC-12 as the preferred refrigerant in refrigeration and mobile air conditioning (MAC), and it also has a minor usage in foam-blowing applications. Observed global abundances and rates of change estimated by two independent global sampling networks (NOAA and AGAGE) are in good agreement. HFC-134a has been growing steadily and reached a global mean mole fraction of ~48 ppt in 2008 (Table 1-15), with an average trend of 4.6 ppt/yr (or ~10%/yr) in 2007–2008. HFC-134a contributed ~8 mW/m² to atmospheric radiative forcing in 2008.

A 12-box model analysis of measured changes in the global atmospheric abundance of HFC-134a was used to derive global emissions of 149 ± 27 Gg/yr during 2008 (approximately 125 ± 16 Gg/yr was derived for 2005–2006). Stohl et al. (2009) used regional-scale inversions with a global coverage to derive global HFC-134a emissions in 2005–2006 of 130–140 Gg/yr, similar to the 12-box model result for these years once uncertainties are considered. Analyses of pollution events observed by high-frequency measurements and other regional studies provide insights into regional contributions to these global emissions. In the Stohl et al. (2009) study for the period 2005–2006, about 40 Gg/yr was attributed to North America, 25 Gg/yr to Europe, 43 Gg/yr to Asia, and lesser amounts were derived for other regions of the globe. For the United States alone, Stohl et al. (2009) derived 28–35

Gg/yr of HFC-134a emission in 2005 and 2006, which is similar to the 27 (12–39) Gg/yr HFC-134a emissions from the United States estimated from aircraft measurement campaigns in 2004 and 2006 (Millet et al., 2009). In a separate study in which high-frequency data from three stations in Eastern Asia were considered, East Asian emissions of HFC-134a were estimated at 19.2 Gg/yr in 2008, of which 12.9 ± 1.7 Gg/yr was attributed to China (Stohl et al., 2010). This is only slightly higher than the HFC-134a emission estimate for China of 8.7 (6.5–12) Gg/yr in 2008 derived from high-frequency atmospheric measurements in South Korea (Kim et al., 2010).

Because of the long lifetime of HFC-134a (13.4 years, Table 1-3) and a relatively high GWP₁₀₀ (1370, Chapter 5), the use of HFC-134a will eventually be phased out in Europe. This will lead to a very gradual phase-down of the use of HFC-134a in cars, which is expected to also take place outside Europe because of the global nature of the car industry. However, in developing countries the potential for growth of HFC-134a is potentially large (Velders et al., 2009).

HFC-23 (CHF₃)

HFC-23 is primarily emitted to the atmosphere from over-fluorination of chloroform during the production of HCFC-22. Other minor emissions of HFC-23 arise from the electronics industry, refrigeration, and fire extinguishers (Oram et al., 1998). Due to its long lifetime of 222 years (Table 1-3) and continued emissions, HFC-23 global mixing ratios reached 22 ppt in 2008, with a growth rate of 0.83 ppt/yr (Miller et al., 2010). At this global abundance, HFC-23 contributed ~ 4 mW/m² to the atmospheric radiative forcing in 2008 (Figure 1-24).

A study of Antarctic firn air suggested a 50% increase in global HFC-23 emissions from 8.7 ± 2 Gg/yr during the 1990s to a mean of 13.5 ± 2 Gg/yr during 2006–2008 (Montzka et al., 2010). HFC-23 emissions increased even though emissions reported by developed countries declined from 6–8 Gg/yr in the late 1990s to 2.8 Gg/yr in 2007 and despite the destruction by incineration of 5–7 Gg of HFC-23 in developing countries in 2007–2008 through United Nations Framework Convention on Climate Change (UNFCCC) Clean Development Mechanism (CDM) projects (Montzka et al., 2010). The increase inferred for global HFC-23 emissions is coincident with a substantial increase in HCFC-22 production in developing countries, which accounted for 60% of global HCFC-22 production in 2007. The mean yield of HFC-23 emission from global HCFC-22 production during 2006–2008 was estimated at $1.7 \pm 0.3\%$, which is slightly lower than the mean of 2.3% derived for the early 1990s (Montzka et al., 2010).

These firn-air-derived global emission estimates for HFC-23 are largely consistent with a recent analysis

of archived air (back to 1978) and ongoing remote atmospheric measurements at multiple sites since late 2007 (Miller et al., 2010). These ongoing data provide higher time resolution during 2006–2008 than the analysis of firn measurements, however, and suggest that global HFC-23 emissions declined after 2006 and were 12.0 (+0.6/–0.7) Gg/yr in 2008.

East Asian HFC-23 emission magnitudes and distributions have been derived using inversion modeling of in situ measurements at three locations (Stohl et al., 2010). Emissions from this region during 2008 were dominated by 6.2 ± 0.7 Gg/yr from China. This analysis yielded enhanced emissions from locations where HCFC-22 production facilities are known to be located, both in China and Japan (Stohl et al., 2010). The uncertainties (1 standard deviation) quoted in Stohl et al. (2010) do not include any systematic errors in their dispersion model or in the meteorological input data used in their inversion analysis. A higher HFC-23 emission of 12 (8.6–15 Gg/yr) was derived in 2008 for China recently from a combined inversion/ratio method based on data from the Korean Gosan station (Kim et al., 2010). This is similar to the 10 ± 5 Gg/yr inferred from China for 2004 and 2005 in an earlier study (Yokouchi et al., 2005). Substantial HFC-23 emissions from China are likely ongoing in 2008 because less than half of HCFC-22 production in developing countries during this time was associated with the UNFCCC CDM projects (Montzka et al., 2010).

HFC-152a (CH₃CHF₂)

HFC-152a is used as a foam-blowing agent and as an aerosol propellant (Greally et al., 2007). In 2008 its globally averaged mole fraction was 5.9 ppt and its radiative forcing 0.5 mW/m². It has a relatively short lifetime of 1.5 years (Table 1-3), due to efficient removal by OH oxidation. HFC-152a has the smallest GWP₁₀₀ (133; Chapter 5) of all major HFCs. Given its short lifetime, the increase in background concentrations (0.6 ppt/yr (+11%/yr) in 2007–2008) implies a substantial increase of emissions in recent years. Emissions derived from the observed atmospheric change were 50 Gg/yr in 2008 (AGAGE data), compared to 28 Gg/yr in 2004 (Greally et al., 2007).

As was found for HFC-134a, an analysis of mixing ratio enhancements above background levels from high-frequency measurements suggest substantial emissions of HFC-152a from North America (12.3–15.1 Gg/yr), Asia (9.6–9.8 Gg/yr), and Europe (3.5–3.9 Gg/yr) during 2005–2006 (Stohl et al., 2009). The total global emissions derived from this regional study (29 Gg/yr in 2005 and 33 Gg/yr in 2006) are similar to the global emission totals derived from the 12-box analysis of mean global mixing ratio changes (34 ± 4 in 2005 and 41 ± 4 Gg in 2005 and 2006, respectively) once uncertainties are considered.

HFC-143a (CH₃CF₃)

Mixing ratios of HFC-143a, which is used mainly in refrigerant blends, of 1.8 ppt have been reported in 1997 by Culbertson et al. (2004), with a strong increase (25%/yr) in the second half of the 1990s. Recent independent measurements from the AGAGE network show that HFC-143a increased to 8.5 ppt in 2008, increasing by 1.0 ppt/yr (13%/yr) in 2007–2008 (updated from Grealley et al., 2005), resulting in a radiative forcing of 1 mW/m² and global emissions of 17 Gg/yr in 2008.

HFC-32 (CH₂F₂)

Mixing ratios of HFC-32, which is mainly used in refrigerant blends, were reported by Grealley et al. (2005) to be 0.7 ppt in 2004 at Mace Head (Ireland). Updated measurements from the AGAGE network show that mixing ratios have increased to 2.7 ppt in 2008 with a yearly increase of 0.6 ppt (26%) in 2007–2008. In 2008, emissions of 8.9 Gg/yr have been derived by applying the 12-box model to AGAGE measurements.

HFC-125 (CHF₂CF₃)

HFC-125 is used in refrigeration blends and for fire suppression (IPCC/TEAP, 2005). Background mixing ratios have grown to 6.1 ppt in 2008, which results in a direct radiative forcing contribution of 1.7 mW/m². The interhemispheric gradient (2008) and growth rate (2007–2008) were 1.4 ppt and 0.9 ppt/yr (16%/yr), respectively (O'Doherty et al., 2009; Table 1-15), from which global emissions increasing from 7.5 Gg in 2000 to 22 Gg in 2008 are derived. European emissions in 2007 have been estimated at 3.7–5.5 Gg/yr (O'Doherty et al., 2009).

HFC-365mfc (CF₃CH₂CF₂CH₃) and HFC-245fa (CF₃CH₂CHF₂)

HFC-365mfc and HFC-245fa are replacements for HCFC-141b in foam-blowing applications (Vollmer et al., 2006). HFC-365mfc showed low mixing ratios of 0.05 ppt in early 2003 at Jungfraujoch (Switzerland) (Stemmler et al., 2007). An update, using AGAGE and SOGE measurements, shows a global mixing ratio of 0.44 ppt in 2008, with a mixing ratio increase of 0.05 ppt (11%/yr) in 2007–2008, and global emissions of 3 Gg/yr in 2008. Vollmer et al. (2006) reported HFC-245fa mixing ratios of 0.3 ppt at Jungfraujoch in 2004 and estimated global emissions of 5.1–5.9 Gg/yr during 2005. The remote-atmosphere mixing ratio of HFC-245fa (results from one site in each hemisphere) reached 1.0 ppt in 2008 and had increased by 0.4 ppt (32%) from 2007 to 2008 (Vollmer et al., 2006).

HFC-227ea (CF₃CHF₂CF₃)

HFC-227ea is mainly used for fire suppression and to a lesser extent in metered dose inhalers, refrigeration, and foam blowing. Laube et al. (2010) have recently reported the use of firn air measurements from Greenland to reconstruct the atmospheric history of HFC-227ea in the Northern Hemisphere. These results indicated the mixing ratio has grown from less than 0.1 ppt in the 1990s to 0.59 ppt in 2007. The rate of growth increased from 0.026 ppt/yr in 2000 to 0.057 ppt/yr in 2007. Global emissions were estimated to be ~1.8 Gg/yr in 2007.

Perfluorocarbons (PFCs)

Perfluorocarbons (PFCs) have very large radiative efficiencies and lifetimes in the range of 2,000 to 50,000 years (Table 1-3). PFC-14 (CF₄) is largely emitted as a by-product of aluminium production and to a smaller degree from the electronics industry (plasma etching), while for PFC-116 (C₂F₆) both sources are significant. PFC-218 (C₃F₈) is largely emitted by the electronics industry, with very small contributions from aluminium smelting and increasing contributions from refrigeration use. The origin of PFC-c-318 (c-C₄F₈) is uncertain but possibly due to a combination of electronics (plasma etching) and plastics (PTFE) thermal decomposition (Harnisch, 1999; Harnisch, 2000).

Recently developed gas chromatography-mass spectrometry (GC-MS) instrumentation has been deployed at AGAGE sites, achieving significantly improved precisions on annual means for CF₄ (~0.1%), C₂F₆ (~0.8%), and C₃F₈ (~3%) (Grealley et al., 2005; Miller et al., 2008; Mühle et al., 2010). Global mixing ratios (2008) and annual growth rates (2007–2008) for CF₄, C₂F₆, and C₃F₈ of 77.1 ppt and 0.9%/yr, 3.9 ppt and 2.6%/yr, and 0.5 and 5.2%/yr, respectively, were measured in the AGAGE network. The radiative forcing contributions by 2008 for CF₄, C₂F₆, and C₃F₈ were 4, 1, and 0.1 mW/m², respectively.

The preindustrial CF₄ level has been re-estimated at 34.7 ± 0.2 ppt (Mühle et al., 2010), based on analysis of Greenland and Antarctic firn air samples, slightly less than the 39 ± 6 ppt estimated previously (Harnisch et al., 1996). Direct evidence of a natural source (crustal degassing) of CF₄ sufficient to maintain preindustrial CF₄ abundances (34 ppt) has been found in desert groundwaters (Deeds et al., 2008).

From the early 1970s to the late 1990s, Greenland and Antarctic firn data suggest a small decline in CF₄ emissions from 13 Gg/yr to 11–12 Gg/yr (Worton et al., 2007). Mühle et al. (2010) report that emissions were ~15 Gg/yr in 1975, rising to ~18 Gg/yr around 1980, generally declining to ~11 Gg/yr in 2000, and stabilizing at ~11 Gg/yr thereafter. They derive a growing difference between

emissions reported by the global aluminium industry and emissions derived from atmospheric measurements in the last years. They suggest that either nonmetallic CF₄ emissions (possibly from the electronics sector) are growing or that the “bottom-up” approach to estimating CF₄ emissions from the aluminium industry is underestimating emissions, or a combination of both. The influence of the semiconductor industry on global C₂F₆ emissions can be seen in both “bottom-up” and “top-down” estimates of emissions, increasing from about 0.5 Gg/yr to 1.8 Gg/yr between 1990 and 2001 (Worton et al., 2007).

Sulfur Hexafluoride (SF₆)

Sulfur hexafluoride (SF₆) is an important greenhouse gas because it combines a high radiative efficiency with a very long lifetime and a considerable annual increase. Global average (NOAA, AGAGE) mixing ratios of SF₆ reached 6.4 ppt in 2008, with a yearly (2007–2008) increase of 0.2 ppt/yr (3%), resulting in a contribution to radiative forcing of 3.4 mW/m² by 2008. Levin et al. (2010) found a similar mixing ratio of 6.7 ppt in 2008 and inferred a global emission of 7.16 Gg/yr in 2008. Comparable global SF₆ growth rates (0.2–0.3 ppt/yr) have been derived from the MIPAS satellite data in 2002–2004 (Stiller et al., 2008), and solar spectroscopy at Jungfraujoch has been used to derive long-term trends in the total column of SF₆ (Zander et al., 2008).

Nitrogen Trifluoride (NF₃)

NF₃, which is used as a replacement for PFCs in plasma etching, in the semiconductor industry, and in the production of flat panel displays, has recently been discovered in the atmosphere by Weiss et al. (2008). Although NF₃ has a high GWP it is not currently included in the Kyoto Protocol (Prather and Hsu, 2008). In 2008 the mean global tropospheric concentration was 0.45 ppt, increasing at 0.05 ppt/yr, or 11%/yr (Weiss et al., 2008). “Bottom-up” emissions in 2006 were estimated at 0.14 Gg/yr (Robson et al., 2006). This emission figure was corrected to be 0.62 Gg/yr in 2008, based on the measured global background abundance and trend by Weiss et al. (2008).

The lifetime and GWP of NF₃ have been revised since the previous Assessment by Prather and Hsu (2008). As a result the NF₃ lifetime (740 years) and GWP₁₀₀ (17,200) given in IPCC’s 4th Assessment (Forster et al., 2007) have now been revised to 500 years and 17,500, respectively (see Section 1.2.2 and Chapter 5).

Sulfuryl Fluoride (SO₂F₂)

Sulfuryl fluoride (SO₂F₂) is used as a fumigant to replace methyl bromide (except for quarantine/pre-

shipment uses). The global total atmospheric lifetime of SO₂F₂ has been recently assessed to be 36 ± 11 years (Mühle et al., 2009), which is significantly longer than previous estimates (<5 years) (Table 1-3). Oceanic hydrolysis is the major sink with the global oceanic uptake atmospheric lifetime being 40 ± 13 years. Compared to hydrolysis, gas-phase tropospheric and stratospheric loss processes are only marginally important (Papadimitriou et al., 2008b; Dillon et al., 2008). The global tropospheric background concentration of SO₂F₂ has increased from ~0.3 ppt in 1978 to 1.51 ppt in 2008, with a yearly increase (2007–2008) of 0.04 ppt (3%). Papadimitriou et al. (2008b) calculated that the GWP₁₀₀ of SO₂F₂ is 4780, similar to that of CFC-11, using newly measured infrared absorption cross sections and the lifetime reported by Mühle et al. (2009). A slightly lower GWP₁₀₀ of 4740 is reported for SO₂F₂ in Table 1-11 owing to a slightly different radiative efficiency being used in the calculations appearing in Chapter 5 (see note 19 to Table 1-11). Sulbaek Anderson et al. (2009b) list a GWP₁₀₀ range of 120–7600 for SO₂F₂ lifetimes from 1–100 years. The emissions calculated from atmospheric observations increased from ~0.6 Gg in 1978 to ~1.9 Gg in 2007. Global production magnitudes of SO₂F₂ are on average 1.5 times emissions deduced from global atmospheric measurements. This suggests that about one-third of SO₂F₂ may be destroyed during application (like CH₃Br) or the presence of additional losses.

1.5.3 Emissions of Rockets and Their Impact on Stratospheric Ozone

In this section the historic and actual emissions of rockets and their potential to impact stratospheric ozone are discussed. The future emissions and their impacts will be discussed in Section 5.4.2.5 of Chapter 5 of this Assessment.

A variety of propellant combinations contribute to the global emissions of rockets. All produce gases and particles that affect ozone chemistry in the stratosphere and mesosphere to varying degrees. The emissions from solid rocket motors (SRM) are much better understood than the emissions from the three liquid propellant types—liquid oxygen/kerosene (O₂/HC), cryogenic (O₂/H₂), hypergolic (N₂O₄/hydrazine), and hybrid (N₂O/HC).

It is thought that chlorine and aluminum oxide (“alumina”) from SRMs account for most of the global ozone loss associated with worldwide rocket launches. Global, annually averaged ozone losses due to these emissions are estimated to be of the order of 0.1% or less (Ross et al., 2009), though this still has not been confirmed with observations or models.

Since the last Assessment of rocket impacts on stratospheric ozone (Newman and Pyle et al., 2003), there

have been some important developments that impact projections of ozone losses due to rockets. First, the decreasing trend in rocket launches at the start of the 21st century has reversed, with the global annual launch rate increasing by 20% since 2005 (<http://planet4589.org/space/log/launchlog.txt>). Second, recent studies of the mass fraction of SRM sub-micron alumina emissions call into question the assumptions that have gone into previous model estimates of the contribution of heterogeneous chlorine reactions on alumina to global ozone loss. Values for that sub-micron mass ranging from 2% (Danilin et al., 2001), 8% (Schmid et al., 2003), 12% (Brady and Martin, 1997), and 50% (Gossé et al., 2006) have now been reported. These sub-micron particles have a disproportionately large impact on ozone abundances, not only because of their high surface-to-mass ratios, but also because of their relatively long lifetimes above the tropopause compared to larger particles. In addition, the previously assumed heterogeneous reaction rates may be low compared to the actual reactivity in stratospheric plumes (Danilin et al., 2003). If the larger values of these parameters are confirmed, previous studies will have significantly underestimated ozone losses from SRMs by as much as a factor of ten. It will also be the case that rocket emissions of alumina will have a greater impact on ozone than rocket emissions of chlorine, in which case much larger impacts could be expected in cold, low-UV regions of the stratosphere (e.g., lowermost stratosphere and polar vortices in springtime). The

geographic variations in ozone loss due to rockets have yet to be studied in detail.

There have been few studies of the role of rocket emissions of nitrogen oxides (NO_x). An estimate of global ozone loss from a hypergolic propellant (N₂O₄/hydrazine) rocket did show that it caused approximately 2% of the ozone loss from an SRM rocket of approximately the same payload (Ross et al., 2004). However, there are no measurements of NO_x emissions from these rockets to validate the NO_x emissions assumed in the model.

The impacts on ozone by rocket emissions other than alumina and chlorine remain unclear (e.g., water vapor, NO_x, HCs, and soot). Given the tendency for heterogeneous reactions to enhance ozone destruction, it is likely that all H₂O-containing particles produced by rockets, directly or as ice nucleation sources (e.g., alumina and soot), will be net-destroyers of ozone. Since rockets emit exhaust throughout the stratosphere, the net impact of NO_x emissions is most-likely ozone destruction via catalytic NO_x reactions and increased aerosol surface area with subsequent halogen activation. Rocket emissions of H₂O into the winter polar stratosphere and summer mesosphere can also increase occurrence frequencies of polar stratospheric and mesospheric clouds (Stevens et al., 2005; Meier, et al., 2010). At current launch rates, the impacts of non-SRM rocket emissions are thought to be less important than SRM emissions of alumina and chlorine (Ross et al., 2009).

REFERENCES

- Abbatt, J.P.D., and J.G. Anderson, High-pressure discharge flow kinetics and frontier orbital mechanistic analysis for OH + CH₂CCl₂, *cis*-CHClCHCl, *trans*-CHClCHCl, CFCICF₂, and CF₂CCl₂ → products, *J. Phys. Chem.*, *95* (6), 2382-2390, doi: 10.1021/j100159a049, 1991.
- Acerboni, G., J.A. Beukes, N.R. Jensen, J. Hjorth, G. Myhre, C.J. Nielsen, and J.K. Sundet, Atmospheric degradation and global warming potentials of three perfluoroalkenes, *Atmos. Environ.*, *35*, 4113-4123, 2001.
- Aizawa, M., K. Asaoka, M. Atsumi, and T. Sakou, Seaweed bioethanol production in Japan – The Ocean Sunrise Project, *Oceans 2007*, 1-5, doi: 10.1109/OCEANS.2007.4449162, 2007.
- Allen, N.D.C., P.F. Bernath, C.D. Boone, M.P. Chipperfield, D. Fu, G.L. Manney, D.E. Oram, G.C. Toon, and D.K. Weisenstein, Global carbon tetrachloride distributions obtained from the Atmospheric Chemistry Experiment (ACE), *Atmos. Chem. Phys.*, *9* (19), 7449-7459, doi: 10.5194/acp-9-7449-2009, 2009.
- Andreae, M.O., and P. Merlet, Emission of trace gases and aerosols from biomass burning, *Global Biogeochem. Cycles*, *15* (4), 955-966, doi: 10.1029/2000GB001382, 2001.
- Aschmann, J., B.-M. Sinnhuber, E.L. Atlas, and S.M. Schauffler, Modeling the transport of very short-lived substances into the tropical upper troposphere and lower stratosphere, *Atmos. Chem. Phys.*, *9* (23), 9237-9247, doi: 10.5194/acp-9-9237-2009, 2009.
- Atkinson, R., D.L. Baulch, R.A. Cox, J.N. Crowley, R.F. Hampson, R.G. Hynes, M.E. Jenkin, M.J. Rossi, J. Troe, and T.J. Wallington, *Atmos. Chem. Phys.*, *8*, 4141-4496, 2008. Updates at: IUPAC Subcommittee for Gas Kinetic Data Evaluation: <http://www.iupac-kinetic.ch.cam.ac.uk>.
- Aydin, M., M.B. Williams, C. Tatum, and E.S. Saltzman, Carbonyl sulfide in air extracted from a South Pole ice core: A 2000 year record, *Atmos. Chem. Phys.*, *8* (24), 7533-7542, doi: 10.5194/acp-8-7533-2008, 2008.
- Bacastow, R.B., Modulation of atmospheric carbon dioxide by the Southern Oscillation, *Nature*, *261*, 116-118, doi: 10.1038/261116a0, 1976.
- Barkley, M.P., P.I. Palmer, C.D. Boone, P.F. Bernath, and P. Suntharalingam, Global distributions of carbonyl sulfide in the upper troposphere and stratosphere, *Geophys. Res. Lett.*, *35*, L14810, doi:

- 10.1029/2008GL034270, 2008.
- Beerling, D.J., T. Gardiner, G. Leggett, A. McLeod, and W.P. Quick, Missing methane emissions from leaves of terrestrial plants, *Global Change Biol.*, *14* (8), 1821-1826, doi: 10.1111/j.1365-2486.2008.01607.x, 2008.
- Bell, N., L. Hsu, D.J. Jacob, M.G. Schultz, D.R. Blake, J.H. Butler, D.B. King, J.M. Lobert, and E. Mair-Reimer, Methyl iodide: Atmospheric budget and use as a tracer of marine convection in global models, *J. Geophys. Res.*, *107* (D17), 4340, doi: 10.1029/2001JD001151, 2002.
- Bergamaschi, P., C. Frankenberg, J.F. Meirink, M. Krol, M.G. Villani, S. Houweling, F. Dentener, E.J. Dlugokencky, J.B. Miller, L.V. Gatti, A. Engel, and I. Levin, Inverse modeling of global and regional CH₄ emissions using SCIAMACHY satellite retrievals, *J. Geophys. Res.*, *114*, D22301, 28, doi: 10.1029/2009JD012287, 2009.
- Berthet, G., J.G. Esler, and P.H. Haynes, A Lagrangian perspective of the tropopause and the ventilation of the lowermost stratosphere, *J. Geophys. Res.*, *112*, D18102, doi: 10.1029/2006JD008295, 2007.
- Bhatia, A., H. Pathak, P.K. Aggarwal, and N. Jain, Trade-off between productivity enhancement and global warming potential of rice and wheat in India, *Nutr. Cycl. Agroecosyst.*, *86* (3), 413-424, doi: 10.1007/s10705-009-9304-5, 2010.
- Bilde, M., T.J. Wallington, C. Ferronato, J.J. Orlando, G.S. Tyndall, E. Estupiñan, and S. Haberkorn, Atmospheric chemistry of CH₂BrCl, CHBrCl₂, CHBr₂Cl, CF₃CHBrCl, and CBr₂Cl₂, *J. Phys. Chem. A*, *102* (11), 1976-1986, doi: 10.1021/jp9733375, 1998.
- Blei, E., C.J. Hardacre, G.P. Mills, K.V. Heal, and M.R. Heal, Identification and quantification of methyl halide sources in a lowland tropical rainforest, *Atmos. Environ.*, *44* (8), 1005-1010, doi: 10.1016/j.atmosenv.2009.12.023, 2010.
- Bloom, A.A., J. Lee-Taylor, S. Madronich, D.J. Messenger, P.I. Palmer, D.S. Reay, and A.R. McLeod, Global methane emission estimates from ultraviolet irradiation of terrestrial plant foliage, *New Phytologist*, *187*, 417-425, doi: 10.1111/j.1469-8137.2010.03259.x, 2010a.
- Bloom, A.A., P.I. Palmer, A. Fraser, D.S. Reay, and C. Frankenberg, Large-scale controls of methanogenesis inferred from methane and gravity spaceborne data, *Science*, *327* (5963), 322-325, doi: 10.1126/science.1175176, 2010b.
- Boden, T.A., G. Marland, and R.J. Andres, Global, regional, and national fossil-fuel CO₂ emissions, Carbon Dioxide Information Analysis Center, Oak Ridge National Laboratory, U.S. Department of Energy, Oak Ridge, TN, U.S.A., doi: 10.3334/CDIAC/00001, 2009.
- Bönisch, H., A. Engel, J. Curtius, Th. Birner, and P. Hoor, Quantifying transport into the lowermost stratosphere using simultaneous in-situ measurements of SF₆ and CO₂, *Atmos. Chem. Phys.*, *9* (16), 5905-5919, doi: 10.5194/acp-9-5905-2009, 2009.
- Bousquet, P., P. Ciais, J.B. Miller, E.J. Dlugokencky, D.A. Hauglustaine, C. Prigent, G.R. Van der Werf, P. Peylin, E.-G. Brunke, C. Carouge, R.L. Langenfelds, J. Lathière, F. Papa, M. Ramonet, M. Schmidt, L.P. Steele, S.C. Tyler, and J. White, Contribution of anthropogenic and natural sources to atmospheric methane variability, *Nature*, *443*, 439-443, doi: 10.1038/nature05132, 2006.
- Bouwman, A.F., K.W. Van der Hoek, and J.G.J. Olivier, Uncertainties in the global source distribution of nitrous oxide, *J. Geophys. Res.*, *100* (D2), 2785-2800, 1995.
- BP (British Petroleum), *BP Statistical Review of World Energy 2009*, available: http://www.bp.com/live-assets/bp_internet/globalbp/globalbp_uk_english/reports_and_publications/statistical_energy_review_2008/STAGING/local_assets/2009_downloads/statistical_review_of_world_energy_full_report_2009.pdf, 2009.
- Brady, B.B., and L.R. Martin, Modeling the multiphase atmospheric chemistry of launch clouds, *J. Space. Rockets*, *34* (6), 780-784, 1997.
- Buffett, B., and D. Archer, Global inventory of methane clathrate: Sensitivity to changes in the deep ocean, *Earth Planet. Sci. Lett.*, *227* (3-4), 185-199, doi: 10.1016/j.espl.2004.09.005, 2004.
- Butler, J.H., S.A. Montzka, A.D. Clarke, J.M. Lobert, and J.W. Elkins, Growth and distribution of halons in the atmosphere, *J. Geophys. Res.*, *103* (D1), 1503-1511, doi: 10.1029/97JD02853, 1998.
- Butler, J.H., M. Battle, M.L. Bender, S.A. Montzka, A.D. Clarke, E.S. Saltzman, C.M. Sucher, J.P. Severinghaus, and J.W. Elkins, A record of atmospheric halocarbons during the twentieth century from polar firn air, *Nature*, *399* (6738), 749-755, doi: 10.1038/21586, 1999.
- Butler, J.H., D.B. King, J.M. Lobert, S.A. Montzka, S.A. Yvon-Lewis, B.D. Hall, N.J. Warwick, D.J. Moneel, M. Aydin, and J.W. Elkins, Oceanic distributions and emissions of short-lived halocarbons, *Global Biogeochem. Cycles*, *21*, GB1023, doi: 10.1029/2006GB002732, 2007.
- Butler, J.H., T.G. Bell, B.D. Hall, B. Quack, L.J. Carpenter, and J. Williams, Technical Note: Ensuring consistent, global measurements of very short-lived halocarbon gases in the ocean and atmosphere, *Atmos. Chem. Phys.*, *10* (2), 327-330, doi: 10.5194/acp-10-327-2010, 2010.
- Butz, A., H. Bösch, C. Camy-Peyret, M.P. Chipperfield,

- M. Dorf, S. Kreycky, L. Kritten, C. Prados-Roman, J. Schwärzle, and K. Pfeilsticker, Constraints on inorganic gaseous iodine in the tropical upper troposphere and stratosphere inferred from balloon-borne solar occultation observations, *Atmos. Chem. Phys.*, *9* (18), 7229-7242, doi: 10.5194/acp-9-7229-2009, 2009.
- Calvert, J.G., R.G. Derwent, J.J. Orlando, G.S. Tyndall, and T.J. Wallington, *Mechanisms of Atmospheric Oxidation of the Alkanes*, 1008 pp., Oxford University Press, New York, NY, 2008.
- Carmo, J.B., M. Keller, J.D. Dias, P.B. Camargo, and P. Crill, A source of methane from upland forests in the Brazilian Amazon, *Geophys. Res. Lett.*, *33*, L04809, doi: 10.1029/2005GL025436, 2006.
- Carpenter, L.J., C.E. Jones, R.M. Dunk, K.E. Hornsby, and J. Woeltjen, Air-sea fluxes of biogenic bromine from the tropical and North Atlantic Ocean, *Atmos. Chem. Phys.*, *9* (5), 1805-1816, doi: 10.5194/acp-9-1805-2009, 2009.
- Chen, J., V. Young, H. Niki, and H. Magid, Kinetic and mechanistic studies for reactions of $\text{CF}_3\text{CH}_2\text{CHF}_2$ (HFC-245fa) initiated by H-atom abstraction using atomic chlorine, *J. Phys. Chem. A*, *101* (14), 2648-2653, doi: 10.1021/jp963735s, 1997.
- Chen, L., S. Kutsuna, K. Tokuhashi, and A. Sekiya, Kinetics of the gas-phase reaction of $\text{CF}_3\text{OC}(\text{O})\text{H}$ with OH radicals at 242-328 K, *Int. J. Chem. Kinet.*, *36* (6), 337-344, doi: 10.1002/kin.20004, 2004a.
- Chen, L., S. Kutsuna, K. Tokuhashi, and A. Sekiya, Kinetics study of the gas-phase reactions of $\text{C}_2\text{F}_5\text{OC}(\text{O})\text{H}$ and $n\text{-C}_3\text{F}_7\text{OC}(\text{O})\text{H}$ with OH radicals at 253-328 K, *Chem. Phys. Lett.*, *400* (4-6), 563-568, 2004b.
- Chen, L., S. Kutsuna, K. Tokuhashi, and A. Sekiya, Kinetics study of the gas-phase reactions of $\text{CHF}_2\text{CF}_2\text{OCHF}_2$ and $\text{CF}_3\text{CHF}_2\text{CF}_2\text{OCH}_2\text{CF}_2\text{CF}_3$ with OH radicals at 253-328 K, *Chem. Phys. Lett.*, *403* (1-3), 180-184, 2005a.
- Chen, L., S. Kutsuna, K. Tokuhashi, A. Sekiya, R. Tamaï, and Y. Hibino, Kinetics and mechanism of $(\text{CF}_3)_2\text{CHOCH}_3$ reaction with OH radicals in an environmental reaction chamber, *J. Phys. Chem. A*, *109* (21), 4766-4771, doi: 10.1021/jp050491f, 2005b.
- Chen, Y.-H., and R.G. Prinn, Estimation of atmospheric methane emissions between 1996 and 2001 using a three-dimensional global chemical transport model, *J. Geophys. Res.*, *111*, D10307, 25, doi: 10.1029/2005JD006058, 2006.
- Chipperfield, M.P., M. Burton, W. Bell, C.P. Walsh, T. Blumenstock, M.T. Coffey, J.W. Hannigan, W.G. Mankin, B. Galle, J. Mellqvist, E. Mahieu, R. Zander, J. Notholt, B. Sen, and G.C. Toon, On the use of HF as a reference for the comparison of stratospheric observations and models, *J. Geophys. Res.*, *102* (D11), 12901-12919, doi: 10.1029/96JD03964, 1997.
- Christensen, L.K., J. Sehested, O.J. Nielsen, M. Bilde, T.J. Wallington, A. Guschin, L.T. Molina, and M.J. Molina, Atmospheric chemistry of HFE-7200 ($\text{C}_4\text{F}_9\text{OC}_2\text{H}_5$): Reaction with OH radicals and fate of $\text{C}_4\text{F}_9\text{OCH}_2\text{CH}_2\text{O}(\cdot)$ and $\text{C}_4\text{F}_9\text{OCHO}(\cdot)\text{CH}_3$ radicals, *J. Phys. Chem. A*, *102* (25), 4839-4845, doi: 10.1021/jp981128u, 1998.
- Class, Th., and K. Ballschmiter, Global baseline pollution studies, X. Atmospheric halocarbons: Global budget estimations for tetrachloroethene, 1,2-dichloroethane, 1,1,1,2-tetrachloroethane, hexachloroethane and hexachlorobutadiene. Estimation of the hydroxyl radical concentrations in the troposphere of the northern and southern hemisphere, *Fresenius' Z. Anal. Chem.*, *327* (2), 198-204, doi: 10.1007/BF00469817, 1987.
- Clerbaux, C., and D.M. Cunnold (Lead Authors), J. Anderson, A. Engel, P.J. Fraser, E. Mahieu, A. Manning, J. Miller, S.A. Montzka, R. Nassar, R. Prinn, S. Reimann, C.P. Rinsland, P. Simmonds, D. Verdonik, R. Weiss, D. Wuebbles, and Y. Yokouchi, Long-lived compounds, Chapter 1 in *Scientific Assessment of Ozone Depletion: 2006*, Global Ozone Research and Monitoring Project—Report No. 50, 572 pp., World Meteorological Organization, Geneva, Switzerland, 2007.
- Collins, W.J., R.G. Derwent, C.E. Johnson, and D.S. Stevenson, The oxidation of organic compounds in the troposphere and their global warming potentials, *Clim. Change*, *52* (4), 453-479, doi: 10.1023/A:1014221225434, 2002.
- Conway, T.J., P.P. Tans, L.S. Waterman, K.W. Thoning, D.R. Kitzis, K.A. Masarie, and N. Zhang, Evidence for interannual variability of the carbon cycle from the National Oceanic and Atmospheric Administration/Climate Monitoring and Diagnostics Laboratory Global Air Sampling Network, *J. Geophys. Res.*, *99* (D11), 22831-22855, doi: 10.1029/94JD01951, 1994.
- Cox, M.L., P.J. Fraser, G.A. Sturrock, S.T. Siems, and L.W. Porter, Terrestrial sources and sinks of halomethanes near Cape Grim, Tasmania, *Atmos. Environ.*, *38* (23), 3839-3852, doi: 10.1016/j.atmosenv.2004.03.050, 2004.
- Crutzen, P.J., A.R. Mosier, K.A. Smith, and W. Winwarter, N_2O release from agro-biofuel production negates global warming reduction by replacing fossil fuels, *Atmos. Chem. Phys.*, *8* (2), 389-395, doi: 10.5194/acp-8-389-2008, 2008.
- Culbertson, J.A., J.M. Prins, E.P. Grimsrud, R.A. Rasmussen, M.A.K. Khalil, and M.J. Shearer, Observed trends for CF_3 -containing compounds in background air at Cape Meares, Oregon, Point Barrow, Alaska, and Palmer Station, Antarctica, *Chemo-*

- sphere*, 55 (8), 1109-1119, doi: 10.1016/j.chemosphere.2003.11.002, 2004.
- Daniel, J.S., and G.J.M. Velders (Lead Authors), A.R. Douglass, P.M.D. Forster, D.A. Hauglustaine, I.S.A. Isaksen, L.J.M. Kuijpers, A. McCulloch, and T.J. Wallington, Halocarbon scenarios, ozone depletion potentials, and global warming potentials, Chapter 8 in *Scientific Assessment of Ozone Depletion: 2006*, Global Ozone Research and Monitoring Project—Report No. 50, 572 pp., World Meteorological Organization, Geneva, Switzerland, 2007.
- Danilin, M.Y., and J.C. McConnell, Stratospheric effects of bromine activation on/in sulfate aerosol, *J. Geophys. Res.*, 100 (D6), 11237-11243, doi: 10.1029/95JD00999, 1995.
- Danilin, M.Y., R.-L. Shia, M.K.W. Ko, D.K. Weisenstein, N.D. Sze, J.J. Lamb, T.W. Smith, P.D. Lohn, and M.J. Prather, Global stratospheric effects of the alumina emissions by solid-fueled rocket motors, *J. Geophys. Res.*, 106 (D12), 12727-12738, doi: 10.1029/2001JD900022, 2001.
- Danilin, M.Y., P.J. Popp, R.L. Herman, M.K.W. Ko, M.N. Ross, C.E. Kolb, D.W. Fahey, L.M. Avallone, D.W. Toohey, B.A. Ridley, O. Schmid, J.C. Wilson, D.G. Baumgardner, R.R. Friedl, T.L. Thompson, and J.M. Reeves, Quantifying uptake of HNO₃ and H₂O by alumina particles in Athena-2 rocket plume, *J. Geophys. Res.*, 108 (D4), 4141, doi: 10.1029/2002JD002601, 2003.
- Deeds, D.A., M.K. Vollmer, J.T. Kulongoski, B.R. Miller, J. Mühle, C.M. Harth, J.A. Izbicki, D.R. Hilton, and R.F. Weiss, Evidence for crustal degassing of CF₄ and SF₆ in Mojave Desert groundwaters, *Geochim. Cosmochim. Acta*, 72 (4), 999-1013, doi: 10.1016/j.gca.2007.11.027, 2008.
- Denman, K.L., G. Brasseur, A. Chidthaisong, P. Ciais, P.M. Cox, R.E. Dickinson, D. Hauglustaine, C. Heinze, E. Holland, D. Jacob, U. Lohmann, S. Ramachandran, P.L. da Silva Dias, S.C. Wofsy, and X. Zhang, Couplings between changes in the climate system and biogeochemistry, Chapter 7 in *Climate Change 2007: The Physical Science Basis. Contribution of Working Group I to the Fourth Assessment Report of the Intergovernmental Panel on Climate Change*, edited by S. Solomon, D. Qin, M. Manning, Z. Chen, M. Marquis, K.B. Averyt, M. Tignor, and H.L. Miller, 996 pp., Cambridge University Press, Cambridge, U.K., and New York, NY, U.S.A., 2007.
- Derwent, R.G., M.E. Jenkin, S.M. Saunders, and M.J. Pilling, Photochemical ozone creation potentials for organic compounds in Northwest Europe calculated with a master chemical mechanism, *Atmos. Environ.*, 32 (14-15), 2429-2441, doi: 10.1016/S1352-2310(98)00053-3, 1998.
- Derwent, R.G., M.E. Jenkin, N.R. Passant, and M.J. Pilling, Reactivity-based strategies for photochemical ozone control in Europe, *Environ. Sci. Policy*, 10 (5), 445-453, doi: 10.1016/j.envsci.2007.01.005, 2007.
- Dessens, O., G. Zeng, N. Warwick, and J. Pyle, Short-lived bromine compounds in the lower stratosphere; impact of climate change on ozone, *Atmos. Sci. Lett.*, 10 (3), 201-206, doi: 10.1002/asl.236, 2009.
- Dillon, T.J., A. Horowitz, and J.N. Crowley, The atmospheric chemistry of sulphuryl fluoride, SO₂F₂, *Atmos. Chem. Phys.*, 8 (6), 1547-1557, doi: 10.5194/acp-8-1547-2008, 2008.
- Dimmer, C.H., P.G. Simmonds, G. Nickless, and M.R. Bassford, Biogenic fluxes of halomethanes from Irish peatland ecosystems, *Atmos. Environ.*, 35 (2), 321-330, doi: 10.1016/S1352-2310(00)00151-5, 2001.
- Dlugokencky, E.J., L. Bruhwiler, J.W.C. White, L.K. Emons, P.C. Novelli, S.A. Montzka, K.A. Masarie, P.M. Lang, A.M. Croswell, J.B. Miller, and L.V. Gatti, Observational constraints on recent increases in the atmospheric CH₄ burden, *Geophys. Res. Lett.*, 36, L18803, doi: 10.1029/2009GL039780, 2009.
- Donner, L.J., L.W. Horowitz, A.M. Fiore, C.J. Seman, D.R. Blake, and N.J. Blake, Transport of radon-222 and methyl iodide by deep convection in the GFDL Global Atmospheric Model AM2, *J. Geophys. Res.*, 112, D17303, doi: 10.1029/2006JD007548, 2007.
- Dorf, M., J.H. Butler, A. Butz, C. Camy-Peyret, M.P. Chipperfield, L. Kritten, S.A. Montzka, B. Simmes, F. Weidner, and K. Pfeilsticker, Long-term observations of stratospheric bromine reveal slow down in growth, *Geophys. Res. Lett.*, 33, L24803, doi: 10.1029/2006GL027714, 2006.
- Dorf, M., A. Butz, C. Camy-Peyret, M.P. Chipperfield, L. Kritten, and K. Pfeilsticker, Bromine in the tropical troposphere and stratosphere as derived from balloonborne BrO observations, *Atmos. Chem. Phys.*, 8 (23), 7265-7271, doi: 10.5194/acp-8-7265-2008, 2008.
- Douglass, A.R., R.S. Stolarski, M.R. Schoeberl, C.H. Jackman, M.L. Gupta, P.A. Newman, J.E. Nielsen, and E.L. Fleming, Relationship of loss, mean age of air and the distribution of CFCs to stratospheric circulation and implications for atmospheric lifetimes, *J. Geophys. Res.*, 113, D14309, doi: 10.1029/2007JD009575, 2008.
- Drewer, J., M.R. Heal, K.V. Heal, and K.A. Smith, Temporal and spatial variation in methyl bromide flux from a salt marsh, *Geophys. Res. Lett.*, 33, L16808, doi: 10.1029/2006GL026814, 2006.
- Drewer, J., K.V. Heal, K.A. Smith, and M.R. Heal, Methyl bromide emissions to the atmosphere from temperate woodland ecosystems, *Global Change*

- Biol.*, 14 (11), 2539-2547, doi: 10.1111/j.1365-2486.2008.01676.x, 2008.
- Duchatelet, P., E. Mahieu, R. Ruhnke, W. Feng, M. Chipperfield, P. Demoulin, P. Bernath, C.D. Boone, K.A. Walker, C. Servais, and O. Flock, An approach to retrieve information on the carbonyl fluoride (COF₂) vertical distributions above Jungfraujoch by FTIR multi-spectrum multi-window fitting, *Atmos. Chem. Phys.*, 9 (22), 9027-9042, doi: 10.5194/acp-9-9027-2009, 2009.
- Dunse, B.L., L.P. Steele, S.R. Wilson, P.J. Fraser, and P.B. Krummel, Trace gas emissions from Melbourne, Australia, based on AGAGE observations at Cape Grim, Tasmania, 1995–2000, *Atmos. Environ.*, 39 (34), 6334-6344, doi: 10.1016/j.atmosenv.2005.07.014, 2005.
- Engel, A., M. Strunk, M. Müller, H.-P. Haase, C. Poss, I. Levin, and U. Schmidt, Temporal development of total chlorine in the high-latitude stratosphere based on reference distributions of mean age derived from CO₂ and SF₆, *J. Geophys. Res.*, 107 (D12), 4136, doi: 10.1029/2001JD000584, 2002.
- FAO (Food and Agriculture Organization of the United Nations), FAOSTAT database, available at: faostat.fao.org, 2009.
- Feng, W., M.P. Chipperfield, M. Dorf, K. Pfeilsticker, and P. Ricaud, Mid-latitude ozone changes: Studies with a 3-D CTM forced by ERA-40 analyses, *Atmos. Chem. Phys.*, 7 (9), 2357-2369, doi: 10.5194/acp-7-2357-2007, 2007.
- Ferretti, D.F., J.B. Miller, J.W.C. White, K.R. Lassey, D.C. Lowe, and D.M. Etheridge, Stable isotopes provide revised global limits of aerobic methane emissions from plants, *Atmos. Chem. Phys.*, 7 (1), 237-241, doi: 10.5194/acp-7-237-2007, 2007.
- Fisher, B., and N. Nakicenovic, (Co-ordinating Lead Authors), K. Alfsen, J. Corfee Morlot, F. de la Chesnaye, J.-Ch. Hourcade, K. Jiang, M. Kainuma, E. La Rovere, A. Matysek, A. Rana, K. Riahi, R. Richels, S. Rose, D. van Vuuren, and R. Warren, Issues related to mitigation in the long term context, Chapter 3 in *Climate Change 2007: Mitigation. Contribution of Working Group III to the Fourth Assessment Report of the Intergovernmental Panel on Climate Change*, edited by B. Metz, O.R. Davidson, P.R. Bosch, R. Dave, and L.A. Meyer, Cambridge University Press, Cambridge, U.K. and New York, NY, U.S.A., 2007.
- Forster, P., V. Ramaswamy, (Coordinating Lead Authors), P. Artaxo, T. Berntsen, R. Betts, D.W. Fahey, J. Haywood, J. Lean, D.C. Lowe, G. Myhre, J. Nganga, R. Prinn, G. Raga, M. Schulz, and R. Van Dorland, Changes in atmospheric constituents and in radiative forcing, Chapter 2 in *Climate Change 2007: The Physical Science Basis. Contribution of Working Group I to the Fourth Assessment Report of the Intergovernmental Panel on Climate Change*, edited by S. Solomon, D. Qin, M. Manning, Z. Chen, M. Marquis, K.B. Averyt, M. Tignor, and H.L. Miller, 996 pp., Cambridge University Press, Cambridge, U.K., and New York, NY, U.S.A., 2007.
- Frank, H., E.H. Christoph, O. Holm-Hansen, and J.L. Bullister, Trifluoroacetate in ocean waters, *Environ. Sci. Technol.*, 36 (1), 12-15, doi: 10.1021/es0101532, 2002.
- Frankenberg, C., J.F. Meirink, M. van Weele, U. Platt, and T. Wagner, Assessing methane emissions from global space-borne observations, *Science*, 308 (5724), 1010-1014, doi: 10.1126/science.1106644, 2005.
- Frankenberg, C., P. Bergamaschi, A. Butz, S. Houweling, J.F. Meirink, J. Notholt, A.K. Petersen, H. Schrijver, T. Warneke, and I. Aben, Tropical methane emissions: A revised view from SCIAMACHY onboard ENVISAT, *Geophys. Res. Lett.*, 35, L15811, doi: 10.1029/2008GL034300, 2008.
- Fraser, P.J., D.E. Oram, C.E. Reeves, S.A. Penkett, and A. McCulloch, Southern Hemispheric halon trends (1978–1998) and global halon emissions, *J. Geophys. Res.*, 104 (D13), 15985-15999, doi: 10.1029/1999JD900113, 1999.
- Friedlingstein, P., P. Cox, R. Betts, L. Bopp, W. von Bloh, V. Brovkin, P. Cadule, S. Doney, M. Eby, I. Fung, G. Bala, J. John, C. Jones, F. Joos, T. Kato, M. Kawamiya, W. Knorr, K. Lindsay, H.D. Matthews, T. Raddatz, P. Rayner, C. Reick, E. Roeckner, K.-G. Schnitzler, R. Schnur, K. Strassmann, A.J. Weaver, C. Yoshikawa, and N. Zeng, Climate–carbon cycle feedback analysis: Results from the (C⁴MIP) model intercomparison, *J. Clim.*, 19 (14), 3337-3353, doi: 10.1175/JCLI3800.1, 2006.
- Frische, M., K. Garofalo, T.H. Hansteen, R. Borchers, and J. Harnisch, The origin of stable halogenated compounds in volcanic gases, *Environ. Sci. Pollut. Res.*, 13 (6), 406-413, doi: 10.1065/espr2006.01.291, 2006.
- Froidevaux, L., J.W. Waters, W.G. Read, P.S. Connell, D.E. Kinnison, and J.M. Russell III, Variations in the free chlorine content of the stratosphere (1991–1997): Anthropogenic, volcanic, and methane influences, *J. Geophys. Res.*, 105 (D4), 4471-4481, 2000.
- Froidevaux, L., N.J. Livesey, W.G. Read, R.J. Salawitch, J.W. Waters, B. Drouin, I.A. MacKenzie, H.C. Pumphrey, P. Bernath, C. Boone, R. Nassar, S. Montzka, J. Elkins, D. Cunnold, and D. Waugh, Temporal decrease in upper atmospheric chlorine, *Geophys. Res. Lett.*, 33, L23812, doi: 10.1029/2006GL027600, 2006.
- Froidevaux, L., Y.B. Jiang, A. Lambert, N.J. Livesey,

- W.G. Read, J.W. Waters, R.A. Fuller, T.P. Marcy, P.J. Popp, R.S. Gao, D.W. Fahey, K.W. Jucks, R.A. Stachnik, G.C. Toon, L.E. Christensen, C.R. Webster, P.F. Bernath, C.D. Boone, K.A. Walker, H.C. Pumphrey, R.S. Harwood, G.L. Manney, M.J. Schwartz, W.H. Daffer, B.J. Drouin, R.E. Cofield, D.T. Cuddy, R.F. Jarnot, B.W. Knosp, V.S. Perun, W.V. Snyder, P.C. Stek, R.P. Thurstans, and P.A. Wagner, Validation of Aura Microwave Limb Sounder HCl measurements, *J. Geophys. Res.*, *113*, D15S25, doi: 10.1029/2007JD009025, 2008.
- Fromm, M., E.P. Shettle, K.H. Fricke, C. Ritter, T. Trickl, H. Giehl, M. Gerding, J.E. Barnes, M. O'Neill, S.T. Massie, U. Blum, I.S. McDermid, T. Leblanc, and T. Deshler, Stratospheric impact of the Chisholm pyrocumulonimbus eruption: 2. Vertical profile perspective, *J. Geophys. Res.*, *113*, D08203, doi: 10.1029/2007JD009147, 2008.
- Fu, D., C.D. Boone, P.F. Bernath, K.A. Walker, R. Nassar, G.L. Manney, and S.D. McLeod, Global phosgene observations from the Atmospheric Chemistry Experiment (ACE) mission, *Geophys. Res. Lett.*, *34* (17), L17815, doi: 10.1029/2007GL029942, 2007.
- Fu, D., C.D. Boone, P.F. Bernath, D.K. Weisenstein, C.P. Rinsland, G.L. Manney, and K.A. Walker, First global observations of atmospheric COClF from the Atmospheric Chemistry Experiment mission, *J. Quant. Spectrosc. Radiat. Transfer*, *110* (12), 974-985, doi: 10.1016/j.jqsrt.2009.02.018, 2009.
- Fueglistaler, S., M. Bonazzola, P.H. Haynes, and T. Peter, Stratospheric water vapor predicted from the Lagrangian temperature history of air entering the stratosphere in the tropics, *J. Geophys. Res.*, *110*, D08107, doi: 10.1029/2004JD005516, 2005.
- Fueglistaler, S., A.E. Dessler, T.J. Dunkerton, I. Folkins, Q. Fu, and P.W. Mote, Tropical tropopause layer, *Rev. Geophys.*, *47*, RG1004, doi: 10.1029/2008RG000267, 2009a.
- Fueglistaler, S., B. Legras, A. Beljaars, J.-J. Morcrette, A. Simmons, A.M. Tompkins, and S. Uppala, The diabatic heat budget of the upper troposphere and lower/mid stratosphere in ECMWF reanalyses, *Quart. J. Roy. Meteorol. Soc.*, *135* (638), 21-37, doi: 10.1002/qj.361, 2009b.
- Gan, J., S.R. Yates, H.D. Ohr, and J.J. Sims, Production of methyl bromide by terrestrial higher plants, *Geophys. Res. Lett.*, *25* (19), 3595-3598, doi: 10.1029/98GL52697, 1998.
- Gardiner, T., A. Forbes, M. de Mazière, C. Vigouroux, E. Mahieu, P. Demoulin, V. Velasco, J. Notholt, T. Blumenstock, F. Hase, I. Kramer, R. Sussmann, W. Stremme, J. Mellqvist, A. Strandberg, K. Ellingsen, and M. Gauss, Trend analysis of greenhouse gases over Europe measured by a network of ground-based remote FTIR instruments, *Atmos. Chem. Phys.*, *8* (22), 6719-6727, doi: 10.5194/acp-8-6719-2008, 2008.
- Gebhardt, S., A. Colomb, R. Hofmann, J. Williams, and J. Lelieveld, Halogenated organic species over the tropical South American rainforest, *Atmos. Chem. Phys.*, *8* (12), 3185-3197, doi: 10.5194/acp-8-3185-2008, 2008.
- Geller, L.S., J.W. Elkins, J.M. Lobert, A.D. Clarke, D.F. Hurst, J.H. Butler, and R.C. Meyer, Tropospheric SF₆: Observed latitudinal distribution and trends, derived emissions and interhemispheric exchange time, *Geophys. Res. Lett.*, *24* (6), 675-678, doi: 10.1029/97GL00523, 1997.
- Gottelman, A., P.H. Lauritzen, M. Park, and J.E. Kay, Processes regulating short-lived species in the tropical tropopause layer, *J. Geophys. Res.*, *114*, D13303, doi: 10.1029/2009JD011785, 2009.
- Gossé, S., L. Hespel, P. Gossart, and A. Delfour, Morphological characterization and particle sizing of alumina particles in solid rocket motor, *J. Propul. Power*, *22* (1), 127-135, 2006.
- Greally, B.R., P.G. Simmonds, S. O'Doherty, A. McCulloch, B.R. Miller, P.K. Salameh, J. Mühle, T. Tanhua, C. Harth, R.F. Weiss, P.J. Fraser, P.B. Krummel, B.L. Dunse, L.W. Porter, and R.G. Prinn, Improved continuous in situ measurements of C₁-C₃ PFCs, HFCs, HCFCs, CFCs and SF₆ in Europe and Australia, *J. Integr. Environ. Sci.*, *2* (2-3), 253-261, doi: 10.1080/15693430500402614, 2005.
- Greally, B.R., A.J. Manning, S. Reimann, A. McCulloch, J. Huang, B.L. Dunse, P.G. Simmonds, R.G. Prinn, P.J. Fraser, D.M. Cunnold, S. O'Doherty, L.W. Porter, K. Stemmler, M.K. Vollmer, C.R. Lunder, N. Schmidbauer, O. Hermansen, J. Arduini, P.K. Salameh, P.B. Krummel, R.H.J. Wang, D. Folini, R.F. Weiss, M. Maione, G. Nickless, F. Stordal, and R.G. Derwent, Observations of 1,1-difluoroethane (HFC-152a) at AGAGE and SOGE monitoring stations in 1994-2004 and derived global and regional emission estimates, *J. Geophys. Res.*, *112*, D06308, doi: 10.1029/2006JD007527, 2007.
- Guo, H., A.J. Ding, T. Wang, I.J. Simpson, D.R. Blake, B. Barletta, S. Meinardi, F.S. Rowland, S.M. Saunders, T.M. Fu, W.T. Hung, and Y.S. Li, Source origins, modeled profiles, and apportionments of halogenated hydrocarbons in the greater Pearl River Delta region, southern China, *J. Geophys. Res.*, *114*, D11302, doi: 10.1029/2008JD011448, 2009.
- Guo, S., G.J.S. Bluth, W.I. Rose, I.M. Watson, and A.J. Prata, Re-evaluation of SO₂ release of the 15 June 1991 Pinatubo eruption using ultraviolet and infrared satellite sensors, *Geochem. Geophys. Geosyst.*, *5*, Q04001, doi: 10.1029/2003GC000654, 2004.

- Hall, B.D., G.S. Dutton, and J.W. Elkins, The NOAA nitrous oxide standard scale for atmospheric observations, *J. Geophys. Res.*, *112*, D09305, doi: 10.1029/2006JD007954, 2007.
- Hamilton, J.T.G., W.C. McRoberts, F. Keppler, R.M. Kalin, and D.B. Harper, Chloride methylation by plant pectin: An efficient environmentally significant process, *Science*, *301* (5630), 206-209, doi: 10.1126/science.105036, 2003.
- Happell, J.D., and D.W.R. Wallace, Removal of atmospheric CCl₄ under bulk aerobic conditions in groundwater and soils, *Environ. Sci. Technol.*, *32* (9), 1244-1252, doi: 10.1021/es970653o, 1998.
- Happell, J.D., and M.P. Roche, Soils: A global sink of atmospheric carbon tetrachloride, *Geophys. Res. Lett.*, *30* (2), 1088, doi: 10.1029/2002GL015957, 2003.
- Hardacre, C.J., E. Blei, and M.R. Heal, Growing season methyl bromide and methyl chloride fluxes at a sub-arctic wetland in Sweden, *Geophys. Res. Lett.*, *36*, L12401, doi: 10.1029/2009GL038277, 2009.
- Harnisch, J., Reactive fluorine compounds, Chapter 3 in *The Handbook of Environmental Chemistry, Volume 4E: Reactive Halogen Compounds in the Atmosphere*, edited by P. Fabian, and O.N. Singh, 81-111, Springer-Verlag, Berlin Heidelberg, 1999.
- Harnisch, J., Atmospheric perfluorocarbons: Sources and concentrations, in *Non-CO₂ Greenhouse Gases: Scientific Understanding, Control and Implementation*, edited by J. van Ham, A.P.M. Baede, L.A. Meyer, and R. Ybema, 205-210, Kluwer Academic Publishers, Dordrecht, Netherlands, 2000.
- Harnisch, J., R. Borchers, P. Fabian, H.W. Gäggeler, and U. Schotterer, Effect of natural tetrafluoromethane, *Nature*, *384* (6604), 32, doi: 10.1038/384032a0, 1996.
- Haywood, J., and O. Boucher, Estimates of the direct and indirect radiative forcing due to tropospheric aerosols: A review, *Rev. Geophys.*, *38* (4), 513-543, 2000.
- Hegglin, M.I., D. Brunner, H. Wernli, C. Schwierz, O. Martius, P. Hoor, H. Fischer, U. Parchatka, N. Spelten, C. Schiller, M. Krebsbach, U. Weers, J. Staehelin, and Th. Peter, Tracing troposphere-to-stratosphere transport above a mid-latitude deep convective system, *Atmos. Chem. Phys.*, *4* (3), 741-756, doi: 10.5194/acp-4-741-2004, 2004.
- Hendrick, F., P.V. Johnston, M. De Mazière, C. Fayt, C. Hermans, K. Kreher, N. Theys, A. Thomas, and M. Van Roozendael, One-decade trend analysis of stratospheric BrO over Harestua (60°N) and Lauder (45°S) reveals a decline, *Geophys. Res. Lett.*, *35*, L14801, doi: 10.1029/2008GL034154, 2008.
- Hense, I., and B. Quack, Modelling the vertical distribution of bromoform in the upper water column of the tropical Atlantic Ocean, *Biogeosciences*, *6* (4), 535-544, doi: 10.5194/bg-6-535-2009, 2009.
- Hirsch, A.I., A.M. Michalak, L.M. Bruhwiler, W. Peters, E.J. Dlugokencky, and P.P. Tans, Inverse modeling estimates of the global nitrous oxide surface flux from 1998–2001, *Global Biogeochem. Cycles*, *20*, GB1008, doi: 10.1029/2004GB002443, 2006.
- Hoffmann, L., M. Kaufmann, R. Spang, R. Müller, J.J. Remedios, D.P. Moore, C.M. Volk, T. von Clarmann, and M. Riese, Envisat MIPAS measurements of CFC-11: Retrieval, validation, and climatology, *Atmos. Chem. Phys.*, *8* (13), 3671-3688, doi: 10.5194/acp-8-3671-2008, 2008.
- Hofmann, D.J., and S.A. Montzka, Recovery of the ozone layer: The Ozone Depleting Gas Index, *EOS Transactions*, *90* (1), 1-2, doi: 10.1029/2009EO010001, 2009.
- Hofmann, D.J., J.H. Butler, E.J. Dlugokencky, J.W. Elkins, K. Masarie, S.A. Montzka, and P. Tans, The role of carbon dioxide in climate forcing from 1979 to 2004: Introduction of the Annual Greenhouse Gas Index, *Tellus*, *58B*, 614-619, doi: 10.1111/j.1600-0889.2006.00201.x, 2006.
- Hofmann, D., J. Barnes, M. O'Neill, M. Trudeau, and R. Neely, Increase in background stratospheric aerosol observed with lidar at Mauna Loa Observatory and Boulder, Colorado, *Geophys. Res. Lett.*, *36*, L15808, doi: 10.1029/2009GL039008, 2009.
- Homan, C.D., C.M. Volk, A.C. Kuhn, A. Werner, J. Baehr, S. Viciani, A. Ulanovski, and F. Ravegnani, Tracer measurements in the tropical tropopause layer during the AMMA/SCOUT-O3 aircraft campaign, *Atmos. Chem. Phys.*, *10* (8), 3615-3627, doi: 10.5194/acp-10-3615-2010, 2010.
- Hoor, P., C. Gurk, D. Brunner, M.I. Hegglin, H. Wernli, and H. Fischer, Seasonality and extent of extratropical TST derived from in-situ CO measurements during SPURT, *Atmos. Chem. Phys.*, *4* (5), 1427-1442, doi: 10.5194/acp-4-1427-2004, 2004.
- Höpfner, M., J. Orphal, T. von Clarmann, G. Stiller, and H. Fischer, Stratospheric BrONO₂ observed by MIPAS, *Atmos. Chem. Phys.*, *9* (5), 1735-1746, doi: 10.5194/acp-9-1735-2009, 2009.
- Hossaini, R., M.P. Chipperfield, B.M. Monge-Sanz, N.A.D. Richards, E. Atlas, and D.R. Blake, Bromoform and dibromomethane in the tropics: A 3-D model study of chemistry and transport, *Atmos. Chem. Phys.*, *10* (2), 719-735, doi: 10.5194/acp-10-719-2010, 2010.
- Hu, L., S.A. Yvon-Lewis, Y. Liu, J.E. Salisbury, and J.E. O'Hern, Coastal emissions of methyl bromide and methyl chloride along the eastern Gulf of Mexico and the east coast of the United States, *Global Biogeochem. Cycles*, *24*, GB1007, doi: 10.1029/2009GB003514, 2010.
- Huang, J., A. Golombek, R. Prinn, R. Weiss, P. Fraser, P. Simmonds, E.J. Dlugokencky, B. Hall, J. Elkins,

- P. Steele, R. Langenfelds, P. Krummel, G. Dutton, and L. Porter, Estimation of regional emissions of nitrous oxide from 1997 to 2005 using multinet-work measurements, a chemical transport model, and an inverse method, *J. Geophys. Res.*, *113*, D17313, doi: 10.1029/2007JD009381, 2008.
- Huhn, O., W. Roether, P. Beining, and H. Rose, Validity limits of carbon tetrachloride as an ocean tracer, *Deep-Sea Res.*, *1*, 48 (9), 2025-2049, doi: 10.1016/S0967-0637(01)00004-8, 2001.
- Hurley, M.D., J.C. Ball, T.J. Wallington, M.P. Sulbaek Andersen, O.J. Nielsen, D.A. Ellis, J.W. Martin, and S.A. Mabury, Atmospheric chemistry of n - $C_xF_{2x+1}CHO$ ($x = 1, 2, 3, 4$): Fate of n - $C_xF_{2x+1}C(O)$ radicals, *J. Phys. Chem. A*, *110* (45), 12443-12447, doi: 10.1021/jp064029m, 2006.
- Hurley, M.D., T.J. Wallington, M.S. Javadi, and O.J. Nielsen, Atmospheric chemistry of $CF_3CF=CH_2$: Products and mechanisms of Cl atom and OH radical initiated oxidation, *Chem. Phys. Lett.*, *450* (4-6), 263-267, doi: 10.1016/j.cplett.2007.11.051, 2008.
- Hurst, D.F., J.C. Lin, P.A. Romashkin, B.C. Daube, C. Gerbig, D.M. Matross, S.C. Wofsy, B.D. Hall, and J.W. Elkins, Continuing global significance of emissions of Montreal Protocol-restricted halocarbons in the United States and Canada, *J. Geophys. Res.*, *111*, D15302, doi: 10.1029/2005JD006785, 2006.
- Inoue, Y., M. Kawasaki, T.J. Wallington, and M.D. Hurley, Atmospheric chemistry of $CF_3CH_2CF_2CH_3$ (HFC-365mfc): Kinetics and mechanism of chlorine atom initiated oxidation, infrared spectrum, and global warming potential, *Chem. Phys. Lett.*, *462*, 4-6, 164-168, doi: 10.1016/j.cplett.2008.07.054, 2008.
- IPCC/TEAP (Intergovernmental Panel on Climate Change/Technology and Economic Assessment Panel), *IPCC/TEAP Special Report on Safeguarding the Ozone Layer and the Global Climate System: Issues Related to Hydrofluorocarbons and Perfluorocarbons*, prepared by Working Groups I and III of the Intergovernmental Panel on Climate Change, and the Technical and Economic Assessment Panel, Cambridge University Press, Cambridge, U.K. and New York, NY, U.S.A., 2005.
- James, R., M. Bonazzola, B. Legras, K. Surbled, and S. Fueglistaler, Water vapor transport and dehydration above convective outflow during Asian monsoon, *Geophys. Res. Lett.*, *35*, L20810, doi: 10.1029/2008GL035441, 2008.
- Javadi, M.S., R. Søndergaard, O.J. Nielsen, M.D. Hurley, and T.J. Wallington, Atmospheric chemistry of trans- $CF_3CH=CHF$: Products and mechanisms of hydroxyl radical and chlorine atom initiated oxidation, *Atmos. Chem. Phys.*, *8* (12), 3141-3147, doi: 10.5194/acp-8-3141-2008, 2008.
- Jenkin, M.E., *Photochemical Ozone and PAN Creation Potentials: Rationalisation and Methods of Estimation*, AEA Technology plc, AEAT Report 4182/20150/003, Issue 1, National Environmental Technology Centre, U.K., 1998.
- Jiang, X., W.L. Ku, R.-L. Shia, Q. Li, J.W. Elkins, R.G. Prinn, and Y.L. Yung, Seasonal cycle of N_2O : Analysis of data, *Global Biogeochem. Cycles*, *21*, GB1006, doi: 10.1029/2006GB002691, 2007.
- Jourdain, J.L., G. Le Bras, and J. Combourieu, Kinetic study by electron paramagnetic resonance and mass spectrometry of the elementary reactions of phosphorus tribromide with H, O, and OH radicals, *J. Phys. Chem.*, *86* (21), 4170-4175, doi: 10.1021/j100218a016, 1982.
- JPL 06-2: see Sander et al., 2006.
- JPL 10-6: see Sander et al., 2010.
- Kaminski, T., P.J. Rayner, M. Heimann, and I.G. Enting, On aggregation errors in atmospheric transport inversions, *J. Geophys. Res.*, *106* (D5), 4703-4715, doi: 10.1029/2000JD900581, 2001.
- Keene, W.C., M.A.K. Khalil, D.J. Erickson, A. McCulloch, T.E. Graedel, J.M. Lobert, M.L. Aucott, S.L. Gong, D.B. Harper, G. Kleiman, P. Midgley, R.M. Moore, C. Seuzaret, W.T. Sturges, C.M. Benkovitz, V. Koropalov, L.A. Barrie, and Y.F. Li, Composite global emissions of reactive chlorine from anthropogenic and natural sources: Reactive Chlorine Emissions Inventory, *J. Geophys. Res.*, *104* (D7), 8429-8440, doi: 10.1029/1998JD100084, 1999.
- Keppler, F., R. Eiden, V. Niedan, J. Pracht, and H.F. Schöler, Halocarbons produced by natural oxidation processes during degradation of organic matter, *Nature*, *403*, 298-301, doi: 10.1038/35002055, 2000.
- Keppler, F., R.M. Kalin, D.B. Harper, W.C. McRoberts, and J.T.G. Hamilton, Carbon isotope anomaly in the major plant C_1 pool and its global biogeochemical implications, *Biogeosciences*, *1* (2), 123-131, doi: 10.5194/bg-1-123-2004, 2004.
- Keppler, F., D.B. Harper, T. Röckmann, R.M. Moore, and J.T.G. Hamilton, New insight into the atmospheric chloromethane budget gained using stable carbon isotope ratios, *Atmos. Chem. Phys.*, *5* (9), 2403-2411, doi: 10.5194/acp-5-2403-2005, 2005.
- Keppler, F., J.T.G. Hamilton, M. Braß, and T. Röckmann, Methane emissions from terrestrial plants under aerobic conditions, *Nature*, *439*, 187-191, doi: 10.1038/nature04420, 2006.
- Kerkweg, A., P. Jöckel, N. Warwick, S. Gebhardt, C.A.M. Brenninkmeijer, and J. Lelieveld, Consistent simulation of bromine chemistry from the marine boundary layer to the stratosphere – Part 2: Bromocarbons, *Atmos. Chem. Phys.*, *8* (19), 5919-5939, doi: 10.5194/acp-8-5919-2008, 2008.

- Kim, J., S. Li, K.-R. Kim, A. Stohl, J. Mühle, S.-K. Kim, M.-K. Park, D.-J. Kang, G. Lee, C.M. Harth, P.K. Salameh, and R.F. Weiss, Regional atmospheric emissions determined from measurements at Jeju Island, Korea: Halogenated compounds from China, *Geophys. Res. Lett.*, *37*, L12801, doi: 10.1029/2010GL043263, 2010.
- Kindler, T.P., W.L. Chameides, P.H. Wine, D.M. Cunnold, F.N. Alyea, and J.A. Franklin, The fate of atmospheric phosgene and the stratospheric loadings of its parent compounds: CCl₄, C₂Cl₄, C₂HCl₃, CH₃CCl₃, and CHCl₃, *J. Geophys. Res.*, *100* (D1), 1235-1251, doi: 10.1029/94JD02518, 1995.
- King, D.B., J.H. Butler, S.A. Yvon-Lewis, and S.A. Cotton, Predicting oceanic methyl bromide saturation from SST, *Geophys. Res. Lett.*, *29* (24), 2199, doi: 10.1029/2002GL016091, 2002.
- Klimont, Z., J. Cofala, J. Xing, W. Wei, C. Zhang, S. Wang, J. Kejun, P. Bhandari, R. Mathur, P. Purohit, P. Rafaj, A. Chambers, M. Amann, and J. Hao, Projections of SO₂, NO_x and carbonaceous aerosols emissions in Asia, *Tellus*, *61B* (4), 602-617, doi: 10.1111/j.1600-0889.2009.00428.x, 2009.
- Kloster, S., K.D. Six, J. Feichter, E. Maier-Reimer, E. Roeckner, P. Wetzela, P. Stier, and M. Esch, Response of dimethylsulfide (DMS) in the ocean and atmosphere to global warming, *J. Geophys. Res.*, *112*, G03005, doi: 10.1029/2006JG000224, 2007.
- Knorr, W., Is the airborne fraction of anthropogenic CO₂ emissions increasing?, *Geophys. Res. Lett.*, *36*, L21710, doi: 10.1029/2009GL040613, 2009.
- Ko, M.K.W., and G. Poulet (Lead Authors), D.R. Blake, O. Boucher, J.H. Burkholder, M. Chin, R.A. Cox, C. George, H.-F. Graf, J.R. Holton, D.J. Jacob, K.S. Law, M.G. Lawrence, P.M. Midgley, P.W. Seakins, D.E. Shallcross, S.E. Strahan, D.J. Wuebbles, and Y. Yokouchi, Very short-lived halogen and sulfur substances, Chapter 2 in *Scientific Assessment of Ozone Depletion: 2002*, Global Ozone Research and Monitoring Project—Report No. 47, World Meteorological Organization, Geneva, Switzerland, 2003.
- Kovalenko, L.J., N.L. Livesey, R.J. Salawitch, C. Camy-Peyret, M.P. Chipperfield, R.E. Cofield, M. Dorf, B.J. Drouin, L. Froidevaux, R.A. Fuller, F. Goutail, R.F. Jarnot, K. Jucks, B.W. Knosp, A. Lambert, I.A. MacKenzie, K. Pfeilsticker, J.-P. Pommereau, W.G. Read, M.L. Santee, M.J. Schwartz, W.V. Snyder, R. Stachnik, P.C. Stek, P.A. Wagner, and J.W. Waters, Validation of Aura Microwave Limb Sounder BrO observations in the stratosphere, *J. Geophys. Res.*, *112*, D24S41, doi: 10.1029/2007JD008817, 2007.
- Kremser, S., I. Wohltmann, M. Rex, U. Langematz, M. Dameris, and I. Wohltmann, Water vapour transport in the tropical tropopause region in coupled Chemistry-Climate Models and ERA-40 reanalysis data, *Atmos. Chem. Phys.*, *9* (8), 2679-2694, doi: 10.5194/acp-9-2679-2009, 2009.
- Krüger, K., S. Tegtmeier, and M. Rex, Long-term climatology of air mass transport through the Tropical Tropopause Layer (TTL) during NH winter, *Atmos. Chem. Phys.*, *8* (4), 813-823, doi: 10.5194/acp-8-813-2008, 2008.
- Krüger, K., S. Tegtmeier, and M. Rex, Variability of residence time in the Tropical Tropopause Layer during Northern Hemisphere winter, *Atmos. Chem. Phys.*, *9* (18), 6717-6725, doi: 10.5194/acp-9-6717-2009, 2009.
- Kuell, V., D. Offermann, M. Jarisch, B. Schaeler, A. Engel, H. Claude, H.G.J. Smit, A. Ebel, and H. Feldmann, Tropopause region temperatures and CFC 11 mixing ratios from CRISTA 2, *J. Geophys. Res.*, *110*, D16104, doi: 10.1029/2004JD005592, 2005.
- Kutsuna, S., L. Chen, T. Abe, J. Mizukado, T. Uchimaru, K. Tokuhashi, and A. Sekiya, Henry's law constants of 2,2,2-trifluoroethyl formate, ethyl trifluoroacetate, and non-fluorinated analogous esters, *Atmos. Environ.*, *39* (32), 5884-5892, doi: 10.1016/j.atmosenv.2005.06.021, 2005.
- Langbein, T., H. Sonntag, D. Trapp, A. Hoffmann, W. Malms, E.P. Roth, V. Mors, and R. Zellner, Volatile anaesthetics and the atmosphere: Atmospheric lifetimes and atmospheric effects of halothane, enflurane, isoflurane, desflurane and sevoflurane, *British J. Anaesthesia*, *82* (1), 66-73, 1999.
- Laube, J.C., A. Engel, H. Bönisch, T. Möbius, D.R. Worton, W.T. Sturges, K. Grunow, and U. Schmidt, Contribution of very short-lived organic substances to stratospheric chlorine and bromine in the tropics—a case study, *Atmos. Chem. Phys.*, *8* (23), 7325-7334, doi: 10.5194/acp-8-7325-2008, 2008.
- Laube, J.C., P. Martinerie, E. Witrant, T. Blunier, J. Schwander, C.A.M. Brenninkmeijer, T.J. Schuck, M. Bolder, T. Röckmann, C. van der Veen, H. Bönisch, A. Engel, G.P. Mills, M.J. Newland, D.E. Oram, C.E. Reeves, and W.T. Sturges, Accelerating growth of HFC-227ea (1,1,1,2,3,3,3-heptafluoropropane) in the atmosphere, *Atmos. Chem. Phys.*, *10* (13), 5903-5910, doi: 10.5194/acp-10-5903-2010, 2010.
- Law, K.S., and W.T. Sturges (Lead Authors), D.R. Blake, N.J. Blake, J.B. Burkholder, J.H. Butler, R.A. Cox, P.H. Haynes, M.K.W. Ko, K. Kreher, C. Mari, K. Pfeilsticker, J.M.C. Plane, R.J. Salawitch, C. Schiller, B.-M. Sinnhuber, R. von Glasow, N.J. Warwick, D.J. Wuebbles, and S.A. Yvon-Lewis, Halogenated very short-lived substances, Chapter 2 in *Scientific Assessment of Ozone Depletion: 2006*, Global Ozone Research and Monitoring Project—

- Report No.50, World Meteorological Organization, Geneva, Switzerland, 2007.
- Le Calvé, S., G. Le Bras, and A. Mellouki, Temperature dependence for the rate coefficients of the reactions of the OH radical with a series of formates, *J. Phys. Chem. A*, *101* (30), 5489-5493, doi: 10.1021/jp970554x, 1997.
- Lee, B.-S., J.L. Bullister, and F.A. Whitney, Chlorofluorocarbon CFC-11 and carbon tetrachloride removal in Saanich Inlet, an intermittently anoxic basin, *Mar. Chem.*, *66* (3-4), 171-185, doi: 10.1016/S0304-4203(99)00039-0, 1999.
- Lee-Taylor, J.M., and E.A. Holland, Litter decomposition as a potential natural source of methyl bromide, *J. Geophys. Res.*, *105* (D7), 8857-8864, doi: 10.1029/1999JD901112, 2000.
- Lee-Taylor, J., and K.R. Redeker, Reevaluation of global emissions from rice paddies of methyl iodide and other species, *Geophys. Res. Lett.*, *32*, L15801, doi: 10.1029/2005GL022918, 2005.
- Leser, H., G. Hönniger, and U. Platt, MAX-DOAS measurements of BrO and NO₂ in the marine boundary layer, *Geophys. Res. Lett.*, *30* (10), 1537, doi: 10.1029/2002GL015811, 2003.
- Levin, I., T. Naegler, R. Heinz, D. Osusko, E. Cuevas, A. Engel, J. Ilmberger, R.L. Langenfelds, B. Neisinger, C. v. Rohden, L.P. Steele, R. Weller, D.E. Worthy, and S.A. Zimov, The global SF₆ source inferred from long-term high precision atmospheric measurements and its comparison with emission inventories, *Atmos. Chem. Phys.*, *10* (6), 2655-2662, doi: 10.5194/acp-10-2655-2010, 2010.
- Levine, J.G., P. Braesicke, N.R.P. Harris, and J.A. Pyle, Seasonal and inter-annual variations in troposphere-to-stratosphere transport from the tropical tropopause layer, *Atmos. Chem. Phys.*, *8* (13), 3689-3703, doi: 10.5194/acp-8-3689-2008, 2008.
- Li, Y., K.O. Patten, D. Youn, and D.J. Wuebbles, Potential impacts of CF₃I on ozone as a replacement for CF₃Br in aircraft applications, *Atmos. Chem. Phys.*, *6* (12), 4559-4568, doi: 10.5194/acp-6-4559-2006, 2006.
- Liang, Q., R.S. Stolarski, S.R. Kawa, J.E. Nielsen, J.M. Rodriguez, A.R. Douglass, J.M. Rodriguez, D.R. Blake, E.L. Atlas, and L.E. Ott, Finding the missing stratospheric Br_y: A global modeling study of CHBr₃ and CH₂Br₂, *Atmos. Chem. Phys.*, *10* (5), 2269-2286, doi: 10.5194/acp-10-2269-2010, 2010.
- Liu, A.Q., and G.W.K. Moore, Lake-effect snowstorms over southern Ontario, Canada, and their associated synoptic-scale environment, *Mon. Wea. Rev.*, *132* (11), 2595-2609, doi: 10.1175/MWR2796.1, 2004.
- Liu, C., and E.J. Zipser, Global distribution of convection penetrating the tropical tropopause, *J. Geophys. Res.*, *110*, D23104, doi: 10.1029/2005JD006063, 2005.
- Liu, C., E.J. Zipser, and S.W. Nesbitt, Global distribution of tropical deep convection: Different perspectives from TRMM infrared and radar data, *J. Clim.*, *20* (3), 489-503, doi: 10.1175/JCLI4023.1, 2007.
- Liu, X.-F., Evidence of Biodegradation of Atmospheric Carbon Tetrachloride in Soils: Field and Microcosm Studies, Ph.D. thesis, 139 pp., Columbia University, New York, NY, U.S.A., 2006.
- Livesey, N.J., L.J. Kovalenko, R.J. Salawitch, I.A. MacKenzie, M.P. Chipperfield, W.G. Read, R.F. Jarnot, and J.W. Waters, EOS Microwave Limb Sounder observations of upper stratospheric BrO: Implications for total bromine, *Geophys. Res. Lett.*, *33*, L20817, doi: 10.1029/2006GL026930, 2006.
- Low, J.C., N.Y. Wang, J. Williams, and R.J. Cicerone, Measurements of ambient atmospheric C₂H₅Cl and other ethyl and methyl halides at coastal California sites and over the Pacific Ocean, *J. Geophys. Res.*, *108* (D19), 4608, doi: 10.1029/2003JD003620, 2003.
- Lu, X.-L., G.-P. Yang, G.-S. Song, and L. Zhang, Distributions and fluxes of methyl chloride and methyl bromide in the East China Sea and the Southern Yellow Sea in autumn, *Mar. Chem.*, *118* (1-2), 75-84, doi: 10.1016/j.marchem.2009.11.002, 2010.
- Luderer, G., J. Trentmann, K. Hungershofer, M. Herzog, M. Fromm, and M.O. Andreae, Small-scale mixing processes enhancing troposphere-to-stratosphere transport by pyro-cumulonimbus storms, *Atmos. Chem. Phys.*, *7* (23), 5945-5957, doi: 10.5194/acp-7-5945-2007, 2007.
- Luecken, D.J., R.L. Waterland, S. Papasavva, K.N. Tadonio, W.T. Hutzell, J.P. Rugh, and S.O. Andersen, Ozone and TFA impacts in North America from degradation of 2,3,3,3-tetrafluoropropene (HFO-1234yf), a potential greenhouse gas replacement, *Environ. Sci. Technol.*, *44* (1), 343-348, doi: 10.1021/es902481f, 2010.
- Mahieu, E., P. Duchatelet, R. Zander, P. Demoulin, C. Servais, C.P. Rinsland, M.P. Chipperfield, and M. De Mazière, The evolution of inorganic chlorine above the Jungfraujoch station: An update, in *Ozone Vol. II, Proceedings of the XX Quadrennial Ozone Symposium*, 1-8 June 2004, Kos, Greece, edited by C.S. Zerefos, 997-998, Int. Ozone Comm., Athens, Greece, 2004.
- Mahieu, E., P. Duchatelet, P. Demoulin, K.A. Walker, E. Dupuy, L. Froidevaux, C. Randall, V. Catoire, K. Strong, C.D. Boone, P.F. Bernath, J.-F. Blavier, T. Blumenstock, M. Coffey, M. De Mazière, D. Griffith, J. Hannigan, F. Hase, N. Jones, K.W. Jucks, A. Kagawa, Y. Kasai, Y. Mebarki, S. Miku-teit, R. Nassar, J. Notholt, C.P. Rinsland, C. Robert, O. Schrems, C. Senten, D. Smale, J. Taylor, C. Té-tard, G.C. Toon, T. Warneke, S.W. Wood, R. Zan-

- der, and C. Servais, Validation of ACE-FTS v2.2 measurements of HCl, HF, CCl₃F and CCl₂F₂ using space-, balloon- and ground-based instrument observations, *Atmos. Chem. Phys.*, *8* (20), 6199-6221, doi: 10.5194/acp-8-6199-2008, 2008.
- Maione, M., J. Arduini, G. Mangani, and A. Geniali, Evaluation of an automatic sampling gas chromatographic-mass spectrometric instrument for continuous monitoring of trace anthropogenic gases, *Int. J. Environ. Anal. Chem.*, *84* (4), 241-253, doi: 10.1080/03067310310001626740, 2004.
- Maione, M., U. Giostra, J. Arduini, L. Belfiore, F. Furlani, A. Geniali, G. Mangani, M.K. Vollmer, and S. Reimann, Localization of source regions of selected hydrofluorocarbons combining data collected at two European mountain stations, *Sci. Total Environ.*, *391* (2-3), 232-240, doi: 10.1016/j.scitotenv.2007.10.023, 2008.
- Makide, Y., and F.S. Rowland, Tropospheric concentrations of methylchloroform, CH₃CCl₃, in January 1978 and estimates of the atmospheric residence times for hydrohalocarbons, *Proc. Natl. Acad. Sci.*, *78* (10), 5933-5937, 1981.
- Manley, S.L., N.-Y. Wang, M.L. Walser, and R.J. Ciccone, Coastal salt marshes as global methyl halide sources from determinations of intrinsic production by marsh plants, *Global Biogeochem. Cycles*, *20*, GB3015, doi: 10.1029/2005GB002578, 2006.
- Manley, S.L., N.-Y. Wang, M.L. Walser, and R.J. Ciccone, Methyl halide emissions from greenhouse-grown mangroves, *Geophys. Res. Lett.*, *34*, L01806, doi: 10.1029/2006GL027777, 2007.
- Manning, A.J., D.B. Ryall, R.G. Derwent, P.G. Simmonds, and S. O'Doherty, Estimating European emissions of ozone-depleting and greenhouse gases using observations and a modeling back-attribution technique, *J. Geophys. Res.*, *108* (D14), 4405, doi: 10.1029/2002JD002312, 2003.
- Marcy, T.P., P.J. Popp, R.S. Gao, D.W. Fahey, E.A. Ray, E.C. Richard, T.L. Thompson, E.L. Atlas, M. Loewenstein, S.C. Wofsy, S. Park, E.M. Weinstock, W.H. Swartz, and M.J. Mahoney, Measurements of trace gases in the tropical tropopause layer, *Atmos. Environ.*, *41* (34), 7253-7261, doi: 10.1016/j.atmosenv.2007.05.032, 2007.
- Martin, J.W., S.A. Mabury, C.S. Wong, F. Noventa, K.R. Solomon, M. Alaei, and D.C.G. Muir, Airborne haloacetic acids, *Environ. Sci. Technol.*, *37* (13), 2889-2897, doi: 10.1021/es026345u, 2003.
- Martin, M., D. Pöhler, K. Seitz, R. Sinreich, and U. Platt, BrO measurements over the Eastern North-Atlantic, *Atmos. Chem. Phys.*, *9* (24), 9545-9554, doi: 10.5194/acp-9-9545-2009, 2009.
- Martinerie, P., E. Nourtier-Mazauric, J.-M. Barnola, W.T. Sturges, D.R. Worton, E. Atlas, L.K. Gohar, K.P. Shine, and G.P. Brasseur, Long-lived halocarbon trends and budgets from atmospheric chemistry modelling constrained with measurements in polar firn, *Atmos. Chem. Phys.*, *9* (12), 3911-3934, doi: 10.5194/acp-9-3911-2009, 2009.
- Martinsson, B.G., H.N. Nguyen, C.A.M. Brenninkmeijer, A. Zahn, J. Heintzenberg, M. Hermann, and P.F.J. van Velthoven, Characteristics and origin of lowermost stratospheric aerosol at northern midlatitudes under volcanically quiescent conditions based on CARIBIC observations, *J. Geophys. Res.*, *110*, D12201, doi: 10.1029/2004JD005644, 2005.
- McCulloch, A., M.L. Aucott, T.E. Graedel, G. Kleiman, P.M. Midgley, and Y.-F. Li, Industrial emissions of trichloroethene, tetrachloroethene, and dichloromethane: Reactive Chlorine Emissions Inventory, *J. Geophys. Res.*, *104* (D7), 8417-8427, doi: 10.1029/1999JD900011, 1999.
- McCulloch, A., Chloroform in the environment: Occurrence, sources, sinks and effects, *Chemosphere*, *50* (10), 1291-1308, doi: 10.1016/S0045-6535(02)00697-5, 2003.
- McLinden, C.A., C.S. Haley, N.D. Lloyd, F. Hendrick, A. Rozanov, B.-M. Sinnhuber, F. Goutail, D.A. Degenstein, E.J. Llewellyn, C.E. Sioris, M. Van Roozendaal, J.P. Pommereau, W. Lotz, and J.P. Burrows, Odin/OSIRIS observations of stratospheric BrO: Retrieval methodology, climatology, and inferred Br_y, *J. Geophys. Res.*, *115*, D15308, doi: 10.1029/2009JD012488, 2010.
- Mead, M.I., I.R. White, G. Nickless, K.-Y. Wang, and D.E. Shallcross, An estimation of the global emission of methyl bromide from rapeseed (*Brassica napus*) from 1961 to 2003, *Atmos. Environ.*, *42* (2), 337-345, doi: 10.1016/j.atmosenv.2007.09.020, 2008a.
- Mead, M.I., M.A.H. Khan, G. Nickless, B.R. Grealley, D. Tainton, T. Pitman, and D.E. Shallcross, Leaf cutter ants: A possible missing source of biogenic halocarbons, *Environ. Chem.*, *5* (1), 5-10, doi: 10.1071/EN07068, 2008b.
- Mead, M.I., M.A.H. Khan, I.R. White, G. Nickless, and D.E. Shallcross, Methyl halide emission estimates from domestic biomass burning in Africa, *Atmos. Environ.*, *42* (21), 5241-5250, doi: 10.1016/j.atmosenv.2008.02.066, 2008c.
- Mébariki, Y., V. Catoire, N. Huret, G. Berthet, C. Robert, and G. Poulet, More evidence for very short-lived substance contribution to stratospheric chlorine inferred from HCl balloon-borne in situ measurements in the tropics, *Atmos. Chem. Phys.*, *10* (2), 397-409, doi: 10.5194/acp-10-397-2010, 2010.
- Meier, R.R., J.M.C. Plane, M.H. Stevens, L.J. Paxton, A.B. Christensen, and G. Crowley, Can mo-

- lecular diffusion explain Space Shuttle plume spreading?, *Geophys. Res. Lett.*, *37*, L08101, doi: 10.1029/2010GL042868, 2010.
- Meirink, J.F., P. Bergamaschi, C. Frankenberg, M.T.S. d'Amelio, E.J. Dlugokencky, L.V. Gatti, S. Houweling, J.B. Miller, T. Röckmann, M.G. Villani, and M.C. Krol, Four-dimensional variational data assimilation for inverse modelling of atmospheric methane emissions: Analysis of SCIAMACHY observations, *J. Geophys. Res.*, *113*, D17301, doi: 10.1029/2007JD009740, 2008.
- Mikuteit, S., Trendbestimmung stratosphärischer Spurengase mit Hilfe bodengebundener FTIR-Messungen, dissertation, FZK Report No. 7385, Forschungszentrum Karlsruhe, Germany, available: <http://www-imk.fzk.de/asf/ftir/refs.htm>, 2008.
- Miller, B.R., R.F. Weiss, P.K. Salameh, T. Tanhua, B.R. Grealley, J. Mühle, and P.G. Simmonds, Medusa: A sample preconcentration and GC/MS detector system for in situ measurements of atmospheric trace halocarbons, hydrocarbons, and sulfur compounds, *Anal. Chem.*, *80* (5), 1536-1545, doi: 10.1021/ac702084k, 2008.
- Miller, B.R., M. Rigby, L.J.M. Kuijpers, P.B. Krummel, L.P. Steele, M. Leist, P.J. Fraser, A. McCulloch, C. Harth, P. Salameh, J. Mühle, R.F. Weiss, R.G. Prinn, R.H.J. Wang, S. O'Doherty, B.R. Grealley, and P.G. Simmonds, HFC-23 (CHF₃) emission trend response to HCFC-22 (CHClF₂) production and recent HFC-23 emission abatement measures, *Atmos. Chem. Phys.*, *10* (16), 7875-7890, doi: 10.5194/acp-10-7875-2010, 2010.
- Millet, D.B., E.L. Atlas, D.R. Blake, N.J. Blake, G.S. Diskin, J.S. Holloway, R.C. Hudman, S. Meinardi, T.B. Ryerson, and G.W. Sachse, Halocarbon emissions from the United States and Mexico and their global warming potential, *Environ. Sci. Technol.*, *43* (4), 1055-1060, doi: 10.1021/es802146j, 2009.
- Møgelberg, T.E., J. Platz, O.J. Nielsen, J. Sehested, and T.J. Wallington, Atmospheric chemistry of HFC-236fa: Spectrokinetic investigation of the CF₃CHO₂·CF₃ radical, its reactions with NO, and the fate of the CF₃CHO·CF₃ radical, *J. Phys. Chem.*, *99* (15), 5373-5378, doi: 10.1021/j100015a021, 1995.
- Molina, L.T., P.J. Wooldridge, and M.J. Molina, Atmospheric reactions and ultraviolet and infrared absorptivities of nitrogen trifluoride, *Geophys. Res. Lett.*, *22* (14), 1873-1876, doi: 10.1029/95GL01669, 1995.
- Montzka, S.A., and P.J. Fraser (Lead Authors), J.H. Butler, P.S. Connell, D.M. Cunnold, J.S. Daniel, R.G. Derwent, S. Lal, A. McCulloch, D.E. Oram, C.E. Reeves, E. Sanhueza, L.P. Steele, G.J.M. Velders, R.F. Weiss, and R.J. Zander, Controlled substances and other source gases, Chapter 1 in *Scientific Assessment of Ozone Depletion: 2002*, Global Ozone Research and Monitoring Project—Report No. 47, Geneva, Switzerland, 2003.
- Montzka, S.A., R.C. Myers, J.H. Butler, J.W. Elkins, L.T. Lock, A.D. Clarke, and A.H. Goldstein, Observations of HFC-134a in the remote troposphere, *Geophys. Res. Lett.*, *23* (2), 169-172, doi: 10.1029/95GL03590, 1996.
- Montzka, S.A., J.H. Butler, J.W. Elkins, T.M. Thompson, A.D. Clarke, and L.T. Lock, Present and future trends in the atmospheric burden of ozone-depleting halogens, *Nature*, *398*, 690-694, doi: 10.1038/19499, 1999.
- Montzka, S.A., C.M. Spivakovsky, J.H. Butler, J.W. Elkins, L.T. Lock, and D.J. Mondeel, New observational constraints for atmospheric hydroxyl on global and hemispheric scales, *Science*, *288* (5465), 500-503, doi: 10.1126/science.288.5465.500, 2000.
- Montzka, S.A., J.H. Butler, B.D. Hall, D.J. Mondeel, and J.W. Elkins, A decline in tropospheric organic bromine, *Geophys. Res. Lett.*, *30* (15), 1826, doi: 10.1029/2003GL017745, 2003.
- Montzka, S.A., M. Aydin, M. Battle, J.H. Butler, E.S. Saltzman, B.D. Hall, A.D. Clarke, D. Mondeel, and J.W. Elkins, A 350-year atmospheric history for carbonyl sulfide inferred from Antarctic firn air and air trapped in ice, *J. Geophys. Res.*, *109*, D22302, doi: 10.1029/2004JD004686, 2004.
- Montzka, S.A., P. Calvert, B.D. Hall, J.W. Elkins, T.J. Conway, P.P. Tans, and C. Sweeney, On the global distribution, seasonality, and budget of atmospheric carbonyl sulfide (COS) and some similarities to CO₂, *J. Geophys. Res.*, *112*, D09302, doi: 10.1029/2006JD007665, 2007.
- Montzka, S.A., J.S. Daniel, J. Cohen, and K. Vick, Current trends, mixing ratios, and emissions of ozone-depleting substances and their substitutes, in *Trends in Emissions of Ozone-Depleting Substances, Ozone Layer Recovery, and Implications for Ultraviolet Radiation Exposure*, Synthesis and Assessment Product 2.4, report by the U.S. Climate Change Science Program and the Subcommittee on Global Change Research, edited by A.R. Ravishankara, M.J. Kurylo, and C.A. Ennis, 29-78, Department of Commerce, NOAA National Climatic Data Center, Asheville, NC, 2008.
- Montzka, S.A., B.D. Hall, and J.W. Elkins, Accelerated increases observed for hydrochlorofluorocarbons since 2004 in the global atmosphere, *Geophys. Res. Lett.*, *36*, L03804, doi: 10.1029/2008GL036475, 2009.
- Montzka, S.A., L. Kuijpers, M.O. Battle, M. Aydin, K.R. Verhulst, E.S. Saltzman, and D.W. Fahey, Recent increases in global HFC-23 emissions, *Geophys. Res. Lett.*, *37*, L02808, doi: 10.1029/

- 2009GL041195, 2010.
- Moore, D.P., and J.J. Remedios, Growth rates of stratospheric HCFC-22, *Atmos. Chem. Phys.*, *8* (1), 73-82, doi: 10.5194/acp-8-73-2008, 2008.
- Moore, R.M., A photochemical source of methyl chloride in saline waters, *Environ. Sci. Technol.*, *42* (6), 1933-1937, doi: 10.1021/es0719201, 2008.
- Moore, R.M., A. Gut, and M.O. Andreae, A pilot study of methyl chloride emissions from tropical woodrot fungi, *Chemosphere*, *58* (2), 221-225, doi: 10.1016/j.chemosphere.2004.03.011, 2005.
- Mühle, J., J. Huang, R.F. Weiss, R.G. Prinn, B.R. Miller, P.K. Salameh, C.M. Harth, P.J. Fraser, L.W. Porter, B.R. Grealley, S. O'Doherty, and P.G. Simmonds, Sulfuryl fluoride in the global atmosphere, *J. Geophys. Res.*, *114*, D05306, doi: 10.1029/2008JD011162, 2009.
- Mühle, J., A.L. Ganesan, B.R. Miller, P.K. Salameh, C.M. Harth, B.R. Grealley, M. Rigby, L.W. Porter, L.P. Steele, C.M. Trudinger, P.B. Krummel, S. O'Doherty, P.J. Fraser, P.G. Simmonds, R.G. Prinn, and R.F. Weiss, Perfluorocarbons in the global atmosphere: Tetrafluoromethane, hexafluoroethane, and octafluoropropane, *Atmos. Chem. Phys.*, *10* (11), 5145-5164, doi: 10.5194/acp-10-5145-2010, 2010.
- Murphy, D.M., D.J. Cziczo, P.K. Hudson, and D.S. Thomson, Carbonaceous material in aerosol particles in the lower stratosphere and tropopause region, *J. Geophys. Res.*, *112*, D04203, doi: 10.1029/2006JD007297, 2007.
- Naik, V., A.K. Jain, K.O. Patten, and D.J. Wuebbles, Consistent sets of atmospheric lifetimes and radiative forcings on climate for CFC replacements: HCFCs and HFCs, *J. Geophys. Res.*, *105* (D5), 6903-6914, doi: 10.1029/1999JD901128, 2000.
- Neuman, J.A., J.B. Nowak, L.G. Huey, J.B. Burkholder, J.E. Dibb, J.S. Holloway, J. Liao, J. Peischl, J.M. Roberts, T.B. Ryerson, E. Scheuer, H. Stark, R.E. Stickel, D.J. Tanner, and A. Weinheimer, Bromine measurements in ozone depleted air over the Arctic Ocean, *Atmos. Chem. Phys.*, *10* (14), 6503-6514, doi: 10.5194/acp-10-6503-2010, 2010.
- Nevison, C.D., N.M. Mahowald, R.F. Weiss, and R.G. Prinn, Interannual and seasonal variability in atmospheric N₂O, *Global Biogeochem. Cycles*, *21*, GB3017, doi: 10.1029/2006GB002755, 2007.
- Newman, P.A. and J.A. Pyle (Lead Authors), J. Austin, G.O. Braathen, P.O. Canziani, K.S. Carslaw, P.M. de F. Forster, S. Godin-Beekmann, B.M. Knudsen, K. Kreher, H. Nakane, S. Pawson, V. Ramaswamy, M. Rex, R.J. Salawitch, D.T. Shindell, A. Tabazadeh, and D.W. Toohey, Polar stratospheric ozone: Past and future, Chapter 3 in *Scientific Assessment of Ozone Depletion: 2002*, Global Ozone Research and Monitoring Project—Report No. 47, Geneva, Switzerland, 2003.
- Newman, P.A., J.S. Daniel, D.W. Waugh, and E.R. Nash, A new formulation of equivalent effective stratospheric chlorine (EESC), *Atmos. Chem. Phys.*, *7* (17), 4537-4522, doi: 10.5194/acp-7-4537-2007, 2007.
- Nielsen, O.J., B.F. Scott, C. Spencer, T.J. Wallington, and J.C. Ball, Trifluoroacetic acid in ancient freshwater, *Atmos. Environ.*, *35* (16), 2799-2801, doi: 10.1016/S1352-2310(01)00148-0, 2001.
- Nielsen, O.J., M.S. Javadi, M.P. Sulbaek Andersen, M.D. Hurley, T.J. Wallington, and R. Singh, Atmospheric chemistry of CF₃CF=CH₂: Kinetics and mechanisms of gas-phase reactions with Cl atoms, OH radicals, and O₃, *Chem. Phys. Lett.*, *439* (1-3), 18-22, doi: 10.1016/j.cplett.2007.03.053, 2007.
- Notholt, J., B.P. Luo, S. Fueglistaler, D. Weisenstein, M. Rex, M.G. Lawrence, H. Bingemer, I. Wohltmann, T. Corti, T. Warneke, R. von Kuhlmann, and T. Peter, Influence of tropospheric SO₂ emissions on particle formation and the stratospheric humidity, *Geophys. Res. Lett.*, *32*, L07810, doi: 10.1029/2004GL022159, 2005.
- O'Brien, L.M., N.R.P. Harris, A.D. Robinson, B. Gostlow, N. Warwick, X. Yang, and J.A. Pyle, Bromocarbons in the tropical marine boundary layer at the Cape Verde Observatory – measurements and modelling, *Atmos. Chem. Phys.*, *9* (22), 9083-9099, doi: 10.5194/acp-9-9083-2009, 2009.
- O'Doherty, S., D.M. Cunnold, A. Manning, B.R. Miller, R.H.J. Wang, P.B. Krummel, P.J. Fraser, P.G. Simmonds, A. McCulloch, R.F. Weiss, P. Salameh, L.W. Porter, R.G. Prinn, J. Huang, G. Sturrock, D. Ryall, R.G. Derwent, and S.A. Montzka, Rapid growth of hydrofluorocarbon 134a and hydrochlorofluorocarbons 141b, 142b, and 22 from Advanced Global Atmospheric Gases Experiment (AGAGE) observations at Cape Grim, Tasmania, and Mace Head, Ireland, *J. Geophys. Res.*, *109*, D06310, doi: 10.1029/2003JD004277, 2004.
- O'Doherty, S., D.M. Cunnold, B.R. Miller, J. Mühle, A. McCulloch, P.G. Simmonds, A.J. Manning, S. Reimann, M.K. Vollmer, B.R. Grealley, R.G. Prinn, P.J. Fraser, L.P. Steele, P.B. Krummel, B.L. Dunse, L.W. Porter, C.R. Lunder, N. Schmidbauer, O. Hermansen, P.K. Salameh, C.M. Harth, R.H.J. Wang, and R.F. Weiss, Global and regional emissions of HFC-125 (CHF₂CF₃) from in situ and air archive atmospheric observations at AGAGE and SOGE observatories, *J. Geophys. Res.*, *114*, D23304, doi: 10.1029/2009JD012184, 2009.
- Oram, D.E., Trends of Long-Lived Anthropogenic Halocarbons in the Southern Hemisphere and Model

- Calculations of Global Emissions, Ph.D. thesis, Univ. of E. Anglia, Norwich, U.K., 249 pp., 1999.
- Oram, D.E., W.T. Sturges, S.A. Penkett, A. McCulloch, and P.J. Fraser, Growth of fluorofom (CHF_3 , HFC-23) in the background atmosphere, *Geophys. Res. Lett.*, 25 (1), 35-38, doi: 10.1029/97GL03483, 1998.
- Orkin, V.L., F. Louis, R.E. Huie, and M.J. Kurylo, Photochemistry of bromine-containing fluorinated alkenes: Reactivity toward OH and UV spectra, *J. Phys. Chem. A*, 106 (43), 10195-10199, doi: 10.1021/jp014436s, 2002.
- Orkin, V.L., L.E. Martynova, and A.N. Ilichev, High-accuracy measurements of OH reaction rate constants and IR absorption spectra: $\text{CH}_2=\text{CF}-\text{CF}_3$ and *trans*- $\text{CHF}=\text{CH}-\text{CF}_3$, *J. Phys. Chem. A*, 114 (19), 5967-5979, doi: 10.1021/jp9092817, 2010.
- Oyaro, N., S.R. Sellevåg, and C.J. Nielsen, Study of the OH and Cl-initiated oxidation, IR absorption cross-section, radiative forcing, and global warming potential of four C_4 -hydrofluoroethers, *Environ. Sci. Technol.*, 38 (21), 5567-5576, doi: 10.1021/es0497330, 2004.
- Oyaro, N., S.R. Sellevåg, and C.J. Nielsen, Atmospheric chemistry of hydrofluoroethers: Reaction of a series of hydrofluoroethers with OH radicals and Cl atoms, atmospheric lifetimes, and global warming potentials, *J. Phys. Chem. A*, 109 (2), 337-346, doi: 10.1021/jp047860c, 2005.
- Packer, M., Algal capture of carbon dioxide; biomass generation as a tool for greenhouse gas mitigation with reference to New Zealand energy strategy and policy, *Energy Policy*, 37 (9), 3428-3437, doi: 10.1016/j.enpol.2008.12.025, 2009.
- Palmer, C.J., and C.J. Reason, Relationships of surface bromoform concentrations with mixed layer depth and salinity in the tropical oceans, *Global Biogeochem. Cycles*, 23, GB2014, doi: 10.1029/2008GB003338, 2009.
- Papadimitriou, V.C., R.K. Talukdar, R.W. Portmann, A.R. Ravishankara, and J.B. Burkholder, $\text{CF}_3\text{CF}=\text{CH}_2$ and (*Z*)- $\text{CF}_3\text{CF}=\text{CHF}$: Temperature dependent OH rate coefficients and global warming potentials, *Phys. Chem. Chem. Phys.*, 10, 808-820, doi: 10.1039/B714382F, 2008a.
- Papadimitriou, V.C., R.W. Portmann, D.W. Fahey, J. Mühle, R.F. Weiss, and J.B. Burkholder, Experimental and theoretical study of the atmospheric chemistry and global warming potential of SO_2F_2 , *J. Phys. Chem. A*, 112 (49), 12657-12666, doi: 10.1021/jp806368u, 2008b.
- Park, M., W.J. Randel, L.K. Emmons, P.F. Bernath, K.A. Walker, and C.D. Boone, Chemical isolation in the Asian monsoon anticyclone observed in Atmospheric Chemistry Experiment (ACE-FTS) data, *Atmos. Chem. Phys.*, 8 (3), 757-764, doi: 10.5194/acp-8-757-2008, 2008.
- Peters, W., A.R. Jacobson, C. Sweeney, A.E. Andrews, T.J. Conway, K. Masarie, J.B. Miller, L.M.P. Bruhwiler, G. Pétron, A.I. Hirsch, D.E.J. Worthy, G.R. van der Werf, J.T. Randerson, P.O. Wennberg, M.C. Krol, and P.P. Tans, An atmospheric perspective on North American carbon dioxide exchange: Carbon-Tracker, *Proc. Natl. Acad. Sci.*, 104 (48), 18925-18930, doi: 10.1073/pnas.0708986104, 2007.
- Peylin, P., D. Baker, J. Sarmiento, P. Ciais, and P. Bousquet, Influence of transport uncertainty on annual mean and seasonal inversions of atmospheric CO_2 data, *J. Geophys. Res.*, 107 (D19), 4385, doi: 10.1029/2001JD000857, 2002.
- Ploeger, F., P. Konopka, G. Günther, J.-U. Groß, and R. Müller, Impact of the vertical velocity scheme on modeling transport in the tropical tropopause layer, *J. Geophys. Res.*, 115, D03301, doi: 10.1029/2009JD012023, 2010.
- Porter, E., J. Wenger, J. Treacy, H. Sidebottom, A. Melouki, S. Téton, and G. LeBras, Kinetic studies on the reactions of hydroxyl radicals with diethers and hydroxyethers, *J. Phys. Chem. A*, 101 (32), 5770-5775, doi: 10.1021/jp971254i, 1997.
- Portmann, R.W., and S. Solomon, Indirect radiative forcing of the ozone layer during the 21st century, *Geophys. Res. Lett.*, 34, L02813, doi: 10.1029/2006GL028252, 2007.
- Prather, M.J., Timescales in atmospheric chemistry: CH_3Br , the ocean, and ozone depletion potentials, *Global Biogeochem. Cycles*, 11 (3), 393-400, doi: 10.1029/97GB01055, 1997.
- Prather, M., and D. Ehhalt (Co-ordinating Lead Authors), F. Dentener, R. Derwent, E. Dlugokencky, E. Holland, I. Isaksen, J. Katima, V. Kirchhoff, P. Matson, P. Midgley, and M. Wang (Lead Authors), Atmospheric chemistry and greenhouse gases, Chapter 4 in *Climate Change 2001: The Scientific Basis. Contribution of Working Group I to the Third Assessment Report of the Intergovernmental Panel on Climate Change*, edited by J.T. Houghton, Y. Ding, D.J. Griggs, M. Noguer, P.J. van der Linden, X. Dai, K. Maskell, and C.A. Johnson, 881 pp., Cambridge University Press, Cambridge, U.K., 2001.
- Prather, M.J., and J. Hsu, NF_3 , the greenhouse gas missing from Kyoto, *Geophys. Res. Lett.*, 35, L12810, doi: 10.1029/2008GL034542, 2008.
- Prather, M.J., and J. Hsu, Correction to "NF₃, the greenhouse gas missing from Kyoto," *Geophys. Res. Lett.*, 37, L11807, doi: 10.1029/2010GL043831, 2010.
- Prinn, R.G., and R. Zander (Lead Authors), D.M. Cunnold, J.W. Elkins, A. Engel, P.J. Fraser, M.R. Gunson, M.K.W. Ko, E. Mahieu, P.M. Midgley, J.M.

- Russell III, C.M. Volk, and R.F. Weiss, Long-lived ozone-related compounds, Chapter 1 in *Scientific Assessment of Ozone Depletion: 1998*, Global Ozone Research and Monitoring Project–Report No. 44, World Meteorological Organization, Geneva, Switzerland, 1999.
- Prinn, R., D. Cunnold, R. Rasmussen, P. Simmonds, F. Alyea, A. Crawford, P. Fraser, and R. Rosen, Atmospheric emissions and trends of nitrous oxide deduced from 10 years of ALE-GAGE data, *J. Geophys. Res.*, *95* (D11), 18369-18385, doi: 10.1029/JD095iD11p18369, 1990.
- Prinn, R.G., R.F. Weiss, P.J. Fraser, P.G. Simmonds, D.M. Cunnold, F.N. Alyea, S. O'Doherty, P. Salameh, B.R. Miller, J. Huang, R.H.J. Wang, D.E. Hartley, C. Harth, L.P. Steele, G. Sturrock, P.M. Midgley, and A. McCulloch, A history of chemically and radiatively important gases in air deduced from ALE/GAGE/AGAGE, *J. Geophys. Res.*, *105* (D14), 17751-17792, doi: 10.1029/2000JD900141, 2000.
- Prinn, R.G., J. Huang, R.F. Weiss, D.M. Cunnold, P.J. Fraser, P.G. Simmonds, A. McCulloch, C. Harth, S. Reimann, P. Salameh, S. O'Doherty, R.H.J. Wang, L.W. Porter, B.R. Miller, and P.B. Krummel, Evidence for variability of atmospheric hydroxyl radicals over the past quarter century, *Geophys. Res. Lett.*, *32*, L07809, doi: 10.1029/2004GL022228, 2005.
- Pyle, J.A., N. Warwick, X. Yang, P.J. Young, and G. Zeng, Climate/chemistry feedbacks and biogenic emissions, *Phil. Trans. R. Soc. A*, *365* (1856), 1727-1740, doi: 10.1098/rsta.2007.2041, 2007.
- Quack, B., E. Atlas, G. Petrick, and D.W.R. Wallace, Bromoform and dibromomethane above the Mauritanian upwelling: Atmospheric distributions and oceanic emissions, *J. Geophys. Res.*, *112*, D09312, doi: 10.1029/2006JD007614, 2007.
- Ramaswamy, V. (Co-ordinating Lead Author), O. Boucher, J. Haigh, D. Hauglustaine, J. Haywood, G. Myhre, T. Nakajima, G.Y. Shi, and S. Solomon (Lead Authors), Radiative forcing of climate change, Chapter 6 in *Climate Change 2001: The Scientific Basis. Contribution of Working Group I to the Third Assessment Report of the Intergovernmental Panel on Climate Change*, edited by J.T. Houghton, Y. Ding, D.J. Griggs, M. Noguer, P.J. van der Linden, X. Dai, K. Maskell, and C.A. Johnson, 881 pp., Cambridge University Press, Cambridge, U.K., 2001.
- Randel, W.J., M. Park, L. Emmons, D. Kinnison, P. Bernath, K.A. Walker, C. Boone, and H. Pumphrey, Asian monsoon transport of pollution to the stratosphere, *Science*, *328* (5978), 611-613, doi: 10.1126/science.1182274, 2010.
- Ravishankara, A.R., S. Solomon, A.A. Turnipseed, and R.F. Warren, Atmospheric lifetimes of long-lived halogenated species, *Science*, *259* (5092), 194-199, doi: 10.1126/science.259.5092.194, 1993.
- Ravishankara, A.R., J.S. Daniel, and R.W. Portmann, Nitrous oxide (N₂O): The dominant ozone-depleting substance emitted in the 21st century, *Science*, *326* (5949), 123-125, doi: 10.1126/science.1176985, 2009.
- Read, K.A., A.S. Mahajan, L.J. Carpenter, M.J. Evans, B.V.E. Faria, D.E. Heard, J.R. Hopkins, J.D. Lee, S.J. Moller, A.C. Lewis, L. Mendes, J.B. McQuaid, H. Oetjen, A. Saiz-Lopez, M.J. Pilling, and J.M.C. Plane, Extensive halogen-mediated ozone destruction over the tropical Atlantic Ocean, *Nature*, *453*, 1232-1235, doi: 10.1038/nature07035, 2008.
- Read, W.G., L. Froidevaux, and J.W. Waters, Microwave limb sounder measurement of stratospheric SO₂ from the Mt. Pinatubo Volcano, *Geophys. Res. Lett.*, *20* (12), 1299-1302, doi: 10.1029/93GL00831, 1993.
- Redeker, K.R., and R.J. Cicerone, Environmental controls over methyl halide emissions from rice paddies, *Global Biogeochem. Cycles*, *18*, GB1027, doi: 10.1029/2003GB002092, 2004.
- Reeves, C.E., W.T. Sturges, G.A. Sturrock, K. Preston, D.E. Oram, J. Schwander, R. Mulvaney, J.-M. Barnola, and J. Chappellaz, Trends of halon gases in polar firn air: Implications for their emission distributions, *Atmos. Chem. Phys.*, *5* (8), 2055-2064, doi: 10.5194/acp-5-2055-2005, 2005.
- Reichenau, T.G., and G. Esser, Is interannual fluctuation of atmospheric CO₂ dominated by combined effects of ENSO and volcanic aerosols?, *Global Biogeochem. Cycles*, *17* (4), 1094, doi: 10.1029/2002GB002025, 2003.
- Reimann, S., D. Schaub, K. Stemmler, D. Folini, M. Hill, P. Hofer, B. Buchmann, P.G. Simmonds, B.R. Grealley, and S. O'Doherty, Halogenated greenhouse gases at the Swiss high alpine site of Jungfrauoch (3580 m asl): Continuous measurements and their use for regional European source allocation, *J. Geophys. Res.*, *109*, D05307, doi: 10.1029/2003JD003923, 2004.
- Reimann, S., M.K. Vollmer, D. Folini, M. Steinbacher, M. Hill, B. Buchmann, R. Zander, and E. Mahieu, Observations of long-lived anthropogenic halocarbons at the high-Alpine site of Jungfrauoch (Switzerland) for assessment of trends and European sources, *Sci. Total Environ.*, *391* (2-3), 224-231, doi: 10.1016/j.scitotenv.2007.10.022, 2008.
- Rhew, R.C., and T. Abel, Measuring simultaneous production and consumption fluxes of methyl chloride and methyl bromide in annual temperate grasslands, *Environ. Sci. Technol.*, *41* (22), 7837-7843, doi: 10.1021/es0711011, 2007.

- Rhew, R.C., B.R. Miller, and R.F. Weiss, Natural methyl bromide and methyl chloride emissions from coastal salt marshes, *Nature*, *403*, 292-295, doi: 10.1038/35002043, 2000.
- Rhew, R.C., B.R. Miller, M.K. Vollmer, and R.F. Weiss, Shrubland fluxes of methyl bromide and methyl chloride, *J. Geophys. Res.*, *106* (D18), 20875-20882, doi: 10.1029/2001JD000413, 2001.
- Rhew, R.C., L. Østergaard, E.S. Saltzman, and M.F. Yanofsky, Genetic control of methyl halide production in Arabidopsis, *Current Biology*, *13* (20), 1809-1813, doi: 10.1016/j.cub.2003.09.055, 2003.
- Rhew, R.C., Y.A. Teh, and T. Abel, Methyl halide and methane fluxes in the northern Alaskan coastal tundra, *J. Geophys. Res.*, *112*, G02009, doi: 10.1029/2006JG000314, 2007.
- Rhew, R.C., B.R. Miller, and R.F. Weiss, Chloroform, carbon tetrachloride and methyl chloroform fluxes in southern California ecosystems, *Atmos. Environ.*, *42* (30), 7135-7140, doi: 10.1016/j.atmosenv.2008.05.038, 2008.
- Rhew, R.C., C. Chen, Y.A. Teh, and D. Baldocchi, Gross fluxes of methyl chloride and methyl bromide in a California oak-savanna woodland, *Atmos. Environ.*, *44* (16), 2054-2061, doi: 10.1016/j.atmosenv.2009.12.014, 2010.
- Ricaud, P., B. Barret, J.-L. Attié, E. Motte, E. Le Flochmoën, H. Teyssède, V.-H. Peuch, N. Livesey, A. Lambert, and J.-P. Pommereau, Impact of land convection on troposphere-stratosphere exchange in the tropics, *Atmos. Chem. Phys.*, *7* (21), 5639-5657, doi: 10.5194/acp-7-5639-2007, 2007.
- Rice, A.L., C.L. Butenhoff, M.J. Shearer, D. Teama, T.N. Rosenstiel, and M.A.K. Khalil, Emissions of anaerobically produced methane by trees, *Geophys. Res. Lett.*, *37*, L03807, doi: 10.1029/2009GL041565, 2010.
- Richter, A., F. Wittrock, A. Ladstätter-Weißmayer, and J.P. Burrows, GOME measurements of stratospheric and tropospheric BrO, *Adv. Space Res.*, *29* (11), 1667-1672, doi: 10.1016/S0273-1177(02)00123-0, 2002.
- Rigby, M., R.G. Prinn, P.J. Fraser, P.G. Simmonds, R.L. Langenfelds, J. Huang, D.M. Cunnold, L.P. Steele, P.B. Krummel, R.F. Weiss, S. O'Doherty, P.K. Salameh, H.J. Wang, C.M. Harth, J. Mühle, and L.W. Porter, Renewed growth of atmospheric methane, *Geophys. Res. Lett.*, *35*, L22805, doi: 10.1029/2008GL036037, 2008.
- Rinsland, C.P., E. Mahieu, R. Zander, N.B. Jones, M.P. Chipperfield, A. Goldman, J. Anderson, J.M. Russell III, P. Demoulin, J. Notholt, G.C. Toon, J.-F. Blavier, B. Sen, R. Sussmann, S.W. Wood, A. Meier, D.W.T. Griffith, L.S. Chiou, F.J. Murcray, T.M. Stephen, F. Hase, S. Mikuteit, A. Schulz, and T. Blumenstock, Long-term trends of inorganic chlorine from ground-based infrared solar spectra: Past increases and evidence for stabilization, *J. Geophys. Res.*, *108* (D8), 4252, doi: 10.1029/2002JD003001, 2003.
- Rinsland, C.P., C. Boone, R. Nassar, K. Walker, P. Bernath, E. Mahieu, R. Zander, J.C. McConnell, and L. Chiou, Trends of HF, HCl, CCl₂F₂, CCl₃F, CHClF₂ (HCFC-22), and SF₆ in the lower stratosphere from Atmospheric Chemistry Experiment (ACE) and Atmospheric Trace Molecule Spectroscopy (ATMOS) measurement near 30°N latitude, *Geophys. Res. Lett.*, *32* (16), L16S03, doi: 10.1029/2005GL022415, 2005.
- Rinsland, C.P., R. Nassar, C.D. Boone, P. Bernath, L. Chiou, D.K. Weisenstein, E. Mahieu, and R. Zander, Spectroscopic detection of COClF in the tropical and mid-latitude lower stratosphere, *J. Quant. Spectrosc. Radiat. Transfer*, *105* (3), 467-475, doi: 10.1016/j.jqsrt.2006.11.013, 2007.
- Rinsland, C.P., L. Chiou, C. Boone, P. Bernath, and E. Mahieu, First measurements of the HCFC-142b trend from atmospheric chemistry experiment (ACE) solar occultation spectra, *J. Quant. Spectrosc. Radiat. Transfer*, *110* (18), 2127-2134, doi: 10.1016/j.jqsrt.2009.05.011, 2009.
- Robson, J.I., L.K. Gohar, M.D. Hurley, K.P. Shine, and T.J. Wallington, Revised IR spectrum, radiative efficiency and global warming potential of nitrogen trifluoride, *Geophys. Res. Lett.*, *33*, L10817, doi: 10.1029/2006GL026210, 2006.
- Rödenbeck, C., S. Houweling, M. Gloor, and M. Heimann, CO₂ flux history 1982–2001 inferred from atmospheric data using a global inversion of atmospheric transport, *Atmos. Chem. Phys.*, *3* (6), 1919-1964, doi: 10.5194/acp-3-1919-2003, 2003.
- Römpf, A., O. Klemm, W. Fricke, and H. Frank, Haloacetates in fog and rain, *Environ. Sci. Technol.*, *35* (7), 1294-1298, doi: 10.1021/es0012220, 2001.
- Rontu Carlon, N., D.K. Papanastasiou, E.L. Fleming, C.H. Jackman, P.A. Newman, and J.B. Burkholder, UV absorption cross sections of nitrous oxide (N₂O) and carbon tetrachloride (CCl₄) between 210 and 350 K and the atmospheric implications, *Atmos. Chem. Phys.*, *10* (13), 6137-6149, doi: 10.5194/acp-10-6137-2010, 2010.
- Ross, M.N., M.Y. Danilin, D.K. Weisenstein, and M.K.W. Ko, Ozone depletion caused by NO and H₂O emissions from hydrazine-fueled rockets, *J. Geophys. Res.*, *109*, D21305, doi: 10.1029/2003JD004370, 2004.
- Ross, M., D. Toohey, M. Peinemann, and P. Ross, Limits on the space launch market related to stratospheric

- ozone depletion, *Astropolitics*, 7 (1), 50-82, doi: 10.1080/14777620902768867, 2009.
- Rowland, F.S., S.C. Tyler, D.C. Montague, and Y. Makide, Dichlorodifluoromethane, CCl_2F_2 , in the Earth's atmosphere, *Geophys. Res. Lett.*, 9 (4), 481-484, doi: 10.1029/GL009i004p00481, 1982.
- Rudolph, J., A. Khedim, R. Koppmann, and B. Bonsang, Field study of the emissions of methyl chloride and other halocarbons from biomass burning in Western Africa, *J. Atmos. Chem.*, 22 (1-2), 67-80, doi: 10.1007/BF00708182, 1995.
- Rudolph, J., K. von Czapiewski, and R. Koppmann, Emissions of methyl chloroform (CH_3CCl_3) from biomass burning and the tropospheric methyl chloroform budget, *Geophys. Res. Lett.*, 27 (13), 1887-1890, doi: 10.1029/1999GL011178, 2000.
- Saito, T., and Y. Yokouchi, Diurnal variation in methyl halide emission rates from tropical ferns, *Atmos. Environ.*, 40 (16), 2806-2811, doi: 10.1016/j.atmosenv.2006.01.016, 2006.
- Saito, T., and Y. Yokouchi, Stable carbon isotope ratio of methyl chloride emitted from glasshouse-grown tropical plants and its implication for the global methyl chloride budget, *Geophys. Res. Lett.*, 35, L08807, doi: 10.1029/2007GL032736, 2008.
- Saito, T., Y. Yokouchi, Y. Kosugi, M. Tani, E. Philip, and T. Okuda, Methyl chloride and isoprene emissions from tropical rain forest in Southeast Asia, *Geophys. Res. Lett.*, 35, L19812, doi: 10.1029/2008GL035241, 2008.
- Saiz-Lopez, A., J.M.C. Plane, and J.A. Shillito, Bromine oxide in the mid-latitude marine boundary layer, *Geophys. Res. Lett.*, 31, L03111, doi: 10.1029/2003GL018956, 2004.
- Salawitch, R.J., D.K. Weisenstein, L.J. Kovalenko, C.E. Sioris, P.O. Wennberg, K. Chance, M.K.W. Ko, and C.A. McLinden, Sensitivity of ozone to bromine in the lower stratosphere, *Geophys. Res. Lett.*, 32, L05811, doi: 10.1029/2004GL021504, 2005.
- Salawitch, R.J., T. Canty, T. Kurosu, K. Chance, Q. Liang, A. da Silva, S. Pawson, J.E. Nielsen, J.M. Rodriguez, P.K. Bhartia, X. Liu, L.G. Huey, J. Liao, R.E. Stickel, D.J. Tanner, J.E. Dibb, W.R. Simpson, D. Donohoue, A. Weinheimer, F. Flocke, D. Knapp, D. Montzka, J.A. Neuman, J.B. Nowak, T.B. Ryerson, S. Oltmans, D.R. Blake, E.L. Atlas, D.E. Kinnison, S. Tilmes, L.L. Pan, F. Hendrick, M. Van Roozendael, K. Kreher, P.V. Johnston, R.S. Gao, B. Johnson, T.P. Bui, G. Chen, R.B. Pierce, J.H. Crawford, and D.J. Jacob, A new interpretation of total column BrO during Arctic spring, *Geophys. Res. Lett.*, 37, L21805, doi: 10.1029/2010GL043798, 2010.
- Saltzman, E.S., M. Aydin, W.J. De Bruyn, D.B. King, and S.A. Yvon-Lewis, Methyl bromide in pre-industrial air: Measurements from an Antarctic ice core, *J. Geophys. Res.*, 109, D05301, doi: 10.1029/2003JD004157, 2004.
- Saltzman, E.S., M. Aydin, C. Tatum, and M.B. Williams, 2,000-year record of atmospheric methyl bromide from a South Pole ice core, *J. Geophys. Res.*, 113, D05304, doi: 10.1029/2007JD008919, 2008.
- Sander, S.P., R.R. Friedl, D.M. Golden, M.J. Kurylo, G.K. Moortgat, H. Keller-Rudek, P.H. Wine, A.R. Ravishankara, C.E. Kolb, M.J. Molina, B.J. Finlayson-Pitts, R.E. Huie, and V.L. Orkin, *Chemical Kinetics and Photochemical Data for Use in Atmospheric Studies*, Evaluation Number 15, JPL Publication 06-02, Jet Propulsion Laboratory, Pasadena, Calif., 2006.
- Sander, S.P., J. Abbatt, J.R. Barker, J.B. Burkholder, R.R. Friedl, D.M. Golden, R.E. Huie, C.E. Kolb, M.J. Kurylo, G.K. Moortgat, V.L. Orkin, and P.H. Wine, *Chemical Kinetics and Photochemical Data for Use in Atmospheric Studies*, Evaluation Number 17, JPL Publication 10-6, Jet Propulsion Laboratory, Pasadena, Calif., available: <http://jpldataeval.jpl.nasa.gov/>, 2010.
- Schauffler, S.M., E.L. Atlas, D.R. Blake, F. Flocke, R.A. Lueb, J.M. Lee-Taylor, V. Stroud, and W. Travnicek, Distributions of brominated organic compounds in the troposphere and lower stratosphere, *J. Geophys. Res.*, 104 (D17), 21513-21536, 1999.
- Schauffler, S.M., E.L. Atlas, S.G. Donnelly, A. Andrews, S.A. Montzka, J.W. Elkins, D.F. Hurst, P.A. Romashkin, G.S. Dutton, and V. Stroud, Chlorine budget and partitioning during the Stratospheric Aerosol and Gas Experiment (SAGE) III Ozone Loss and Validation Experiment (SOLVE), *J. Geophys. Res.*, 108, 4173, doi: 10.1029/2001JD002040, 2003.
- Schiller, C., J.-U. Grooß, P. Konopka, F. Plöger, F.H. Silva dos Santos, and N. Spelten, Hydration and dehydration at the tropical tropopause, *Atmos. Chem. Phys.*, 9 (24), 9647-9660, doi: 10.5194/acp-9-9647-2009, 2009.
- Schmid, O., J.M. Reeves, J.C. Wilson, C. Wiedinmyer, C.A. Brock, D.W. Toohey, L.M. Avallone, A.M. Gates, and M.N. Ross, Size-resolved particle emission indices in the stratospheric plume of an Athena II rocket, *J. Geophys. Res.*, 108, 4250, doi: 10.1029/2002JD002486, 2003.
- Schmittner, A., A. Oschlies, H.D. Matthews, and E.D. Galbraith, Future changes in climate, ocean circulation, ecosystems, and biogeochemical cycling simulated for a business-as-usual CO_2 emission scenario until year 4000 AD, *Global Biogeochem. Cycles*, 22, GB1013, doi: 10.1029/2007GB002953, 2008.
- Schofield, R., K. Kreher, B.J. Connor, P.V. Johnston, A. Thomas, D. Shooter, M.P. Chipperfield, C.D.

- Rodgers, and G.H. Mount, Retrieved tropospheric and stratospheric BrO columns over Lauder, New Zealand, *J. Geophys. Res.*, *109*, D14304, doi: 10.1029/2003JD004463, 2004.
- Schofield, R., P.V. Johnston, A. Thomas, K. Kreher, B.J. Connor, S. Wood, D. Shooter, M.P. Chipperfield, A. Richter, R. von Glasow, and C.D. Rodgers, Tropospheric and stratospheric BrO columns over Arrival Heights, Antarctica, 2002, *J. Geophys. Res.*, *111*, D22310, doi: 10.1029/2005JD007022, 2006.
- Shine, K.P., L.K. Gohar, M.D. Hurley, G. Marston, D. Martin, P.G. Simmonds, T.J. Wallington, and M. Watkins, Perfluorodecalin: Global warming potential and first detection in the atmosphere, *Atmos. Environ.*, *39* (9), 1759-1763, doi: 10.1016/j.atmosenv.2005.01.001, 2005.
- Shorter, J.H., C.E. Kolb, P.M. Crill, R.A. Kerwin, R.W. Talbot, M.E. Hines, and R.C. Harriss, Rapid degradation of atmospheric methyl bromide in soils, *Nature*, *377*, 717-719, doi: 10.1038/377717ao, 1995.
- Simmonds, P.G., R.G. Derwent, A.J. Manning, P.J. Fraser, P.B. Krummel, S. O'Doherty, R.G. Prinn, D.M. Cunnold, B.R. Miller, H.J. Wang, D.B. Ryall, L.W. Porter, R.F. Weiss, and P.K. Salameh, AGAGE Observations of methyl bromide and methyl chloride at Mace Head, Ireland, and Cape Grim, Tasmania, 1998-2001, *J. Atmos. Chem.*, *47* (3), 243-269, doi: 10.1023/B:JOCH.0000021136.52340.9c, 2004.
- Simmonds, P.G., A.J. Manning, D.M. Cunnold, A. McCulloch, S. O'Doherty, R.G. Derwent, P.B. Krummel, P.J. Fraser, B. Dunse, L.W. Porter, R.H.J. Wang, B.R. Grealley, B.R. Miller, P. Salameh, R.F. Weiss, and R.G. Prinn, Global trends, seasonal cycles, and European emissions of dichloromethane, trichloroethene, and tetrachloroethene from the AGAGE observations at Mace Head, Ireland, and Cape Grim, Tasmania, *J. Geophys. Res.*, *111*, D18304, doi: 10.1029/2006JD007082, 2006.
- Simpson, I.J., S. Meinardi, N.J. Blake, F.S. Rowland, and D.R. Blake, Long-term decrease in the global atmospheric burden of tetrachloroethene (C₂Cl₄), *Geophys. Res. Lett.*, *31*, L08108, doi: 10.1029/2003GL019351, 2004.
- Simpson, I.J., N.J. Blake, D.R. Blake, S. Meinardi, M.P.S. Andersen, and F.S. Rowland, Strong evidence for negligible methyl chloroform (CH₃CCl₃) emissions from biomass burning, *Geophys. Res. Lett.*, *34*, L10805, doi: 10.1029/2007GL029383, 2007.
- Sinnhuber, B.-M., and I. Folkins, Estimating the contribution of bromoform to stratospheric bromine and its relation to dehydration in the tropical tropopause layer, *Atmos. Chem. Phys.*, *6* (12), 4755-4761, doi: 10.5194/acp-6-4755-2006, 2006.
- Sinnhuber, B.-M., D.W. Arlander, H. Bovensmann, J.P. Burrows, M.P. Chipperfield, C.-F. Enell, U. Frieß, F. Hendrick, P.V. Johnston, R.L. Jones, K. Kreher, N. Mohamed-Tahrin, R. Müller, K. Pfeilsticker, U. Platt, J.-P. Pommereau, I. Pundt, A. Richter, A.M. South, K.K. Tørnkvist, M. Van Roozendaal, T. Wagner, and F. Wittrock, Comparison of measurements and model calculations of stratospheric bromine monoxide, *J. Geophys. Res.*, *107*, 4398, doi: 10.1029/2001JD000940, 2002.
- Sinnhuber, B.-M., A. Rozanov, N. Sheode, O.T. Afe, A. Richter, M. Sinnhuber, F. Wittrock, J.P. Burrows, G.P. Stiller, T. von Clarmann, and A. Linden, Global observations of stratospheric bromine monoxide from SCIAMACHY, *Geophys. Res. Lett.*, *32*, L20810, doi: 10.1029/2005GL023839, 2005.
- Sinnhuber, B.-M., N. Sheode, M. Sinnhuber, M.P. Chipperfield, and W. Feng, The contribution of anthropogenic bromine emissions to past stratospheric ozone trends: A modelling study, *Atmos. Chem. Phys.*, *9* (8), 2863-2871, doi: 10.5194/acp-9-2863-2009, 2009.
- Sioris, C.E., L.J. Kovalenko, C.A. McLinden, R.J. Salawitch, M. Van Roozendaal, F. Goutail, M. Dorf, K. Pfeilsticker, K. Chance, C. von Savigny, X. Liu, T.P. Kurosu, J.-P. Pommereau, H. Bösch, and J. Frerick, Latitudinal and vertical distribution of bromine monoxide in the lower stratosphere from Scanning Imaging Absorption Spectrometer for Atmospheric Chartography limb scattering measurements, *J. Geophys. Res.*, *111*, D14301, doi: 10.1029/2005JD006479, 2006.
- Siskind, D.E., L. Froidevaux, J.M. Russell, and J. Lean, Implications of upper stratospheric trace constituent changes observed by HALOE for O₃ and ClO from 1992 to 1995, *Geophys. Res. Lett.*, *25* (18), 3513-3516, 1998.
- Sive, B.C., R.K. Varner, H. Mao, D.R. Blake, O.W. Wingenter, and R. Talbot, A large terrestrial source of methyl iodide, *Geophys. Res. Lett.*, *34*, L17808, doi: 10.1029/2007GL030528, 2007.
- Solomon, P., J. Barrett, T. Mooney, B. Connor, A. Parrish, and D.E. Siskind, Rise and decline of active chlorine in the stratosphere, *Geophys. Res. Lett.*, *33*, L18807, doi: 10.1029/2006GL027029, 2006.
- Søndergaard, R., O.J. Nielsen, M.D. Hurley, T.J. Wallington, and R. Singh, Atmospheric chemistry of *trans*-CF₃CH=CHF: Kinetics of the gas-phase reactions with Cl atoms, OH radicals, and O₃, *Chem. Phys. Lett.*, *443* (4-6), 199-204, doi: 10.1016/j.cplett.2007.06.084, 2007.
- Sorokin, V.I., N.P. Gritsan, and A.I. Chichinin, Collisions of O(¹D) with HF, F₂, XeF₂, NF₃, and CF₄: Deactivation and reaction, *J. Chem. Phys.*, *108* (21), 8995-9003, doi: 10.1063/1.476346, 1998.

- SPARC (Stratospheric Processes And their Role in Climate), *SPARC Assessment of Stratospheric Aerosol Properties*, edited by L. Thomason and Th. Peter, World Climate Research Program Report 124, SPARC Report 4, WMO/TD- No. 1295, 346 pp., Verrières le Buisson, France, 2006.
- SPARC CCMVal (Stratospheric Processes And their Role in Climate), *SPARC Report on the Evaluation of Chemistry-Climate Models*, edited by V. Eyring, T.G. Shepherd, and D.W. Waugh, SPARC Report No. 5, WCRP-132, WMO/TD-No. 1526, 478 pp., available: http://www.atmosph.physics.utoronto.ca/SPARC/ccmval_final/index.php, 2010.
- Spivakovsky, C.M., J.A. Logan, S.A. Montzka, Y.J. Balkanski, M. Foreman-Fowler, D.B.A. Jones, L.W. Horowitz, A.C. Fusco, C.A.M. Brenninkmeijer, M.J. Prather, S.C. Wofsy, and M.B. McElroy, Three-dimensional climatological distribution of tropospheric OH: Update and evaluation, *J. Geophys. Res.*, *105* (D7), 8931-8980, 2000.
- Stemmler, K., D. Folini, S. Uhl, M.K. Vollmer, S. Reimann, S. O'Doherty, B.R. Grealley, P.G. Simmonds, and A.J. Manning, European emissions of HFC-365mfc, a chlorine-free substitute for the foam blowing agents HCFC-141b and CFC-11, *Environ. Sci. Technol.*, *41* (4), 1145-1151, doi: 10.1021/es061298h, 2007.
- Stephens, B.B., K.R. Gurney, P.P. Tans, C. Sweeney, W. Peters, L. Bruhwiler, P. Ciais, M. Ramonet, P. Bousquet, T. Nakazawa, S. Aoki, T. Machida, G. Inoue, N. Vinnichenko, J. Lloyd, A. Jordan, M. Heimann, O. Shibistova, R.L. Langenfelds, L.P. Steele, R.J. Francey, and A.S. Denning, Weak northern and strong tropical land carbon uptake from vertical profiles of atmospheric CO₂, *Science*, *316*, 1732-1735, doi: 10.1126/science.1137004, 2007.
- Stern, D.I., Global sulfur emissions from 1850 to 2000, *Chemosphere*, *58* (2), 163-175, doi: 10.1016/j.chemosphere.2004.08.022, 2005.
- Stevens, M.H., R.R. Meier, X. Chu, M.T. DeLand, and J.M.C. Plane, Antarctic mesospheric clouds formed from space shuttle exhaust, *Geophys. Res. Lett.*, *32*, L13810, doi: 10.1029/2005GL023054, 2005.
- Stiller, G.P., T. von Clarmann, M. Höpfner, N. Glatthor, U. Grabowski, S. Kellmann, A. Kleinert, A. Linden, M. Milz, T. Reddmann, T. Steck, H. Fischer, B. Funke, M. López-Puertas, and A. Engel, Global distribution of mean age of stratospheric air from MIPAS SF₆ measurements, *Atmos. Chem. Phys.*, *8* (3), 677-695, doi: 10.5194/acp-8-677-2008, 2008.
- Stohl, A., S. Eckhardt, C. Forster, P. James, and N. Spichtinger, On the pathways and timescales of intercontinental air pollution transport, *J. Geophys. Res.*, *107*, 4684, doi: 10.1029/2001JD001396, 2002.
- Stohl, A., P. Seibert, J. Arduini, S. Eckhardt, P. Fraser, B.R. Grealley, C. Lunder, M. Maione, J. Mühle, S. O'Doherty, R.G. Prinn, S. Reimann, T. Saito, N. Schmidbauer, P.G. Simmonds, M.K. Vollmer, R.F. Weiss, and Y. Yokouchi, An analytical inversion method for determining regional and global emissions of greenhouse gases: Sensitivity studies and application to halocarbons, *Atmos. Chem. Phys.*, *9* (5), 1597-1620, doi: 10.5194/acp-9-1597-2009, 2009.
- Stohl, A., J. Kim, S. Li, S. O'Doherty, J. Mühle, P.K. Salameh, T. Saito, M.K. Vollmer, D. Wan, R.F. Weiss, B. Yao, Y. Yokouchi, and L.X. Zhou, Hydrochlorofluorocarbon and hydrofluorocarbon emissions in East Asia determined by inverse modeling, *Atmos. Chem. Phys.*, *10* (8), 3545-3560, doi: 10.5194/acp-10-3545-2010, 2010.
- Sturrock, G.A., L.W. Porter, P.J. Fraser, *In situ* measurement of CFC replacement chemicals and other halocarbons at Cape Grim: The AGAGE CG-MS program, in *Baseline Atmospheric Program Australia 1997-98*, edited by N.W. Tindale, N. Derek, and R.J. Francey, Bureau of Meteorology and CSIRO Atmospheric Research, Melbourne, 2001.
- Sturrock, G.A., D.M. Etheridge, C.M. Trudinger, P.J. Fraser, and A.M. Smith, Atmospheric histories of halocarbons from analysis of Antarctic firn air: Major Montreal Protocol species, *J. Geophys. Res.*, *107*, 4765, doi: 10.1029/2002JD002548, 2002.
- Sulbaek Andersen, M.P., A. Toft, O.J. Nielsen, M.D. Hurley, T.J. Wallington, H. Chishima, K. Tonokura, S.A. Mabury, J.W. Martin, and D.A. Ellis, Atmospheric chemistry of perfluorinated aldehyde hydrates (n -C_xF_{2x+1}CH(OH)₂, $x = 1, 3, 4$): Hydration, dehydration, and kinetics and mechanism of Cl atom and OH radical initiated oxidation, *J. Phys. Chem. A*, *110* (32), 9854-9860, doi: 10.1021/jp060404z, 2006.
- Sulbaek Andersen, M.P., E.J.K. Nilsson, O.J. Nielsen, M.S. Johnson, M.D. Hurley, and T.J. Wallington, Atmospheric chemistry of *trans*-CF₃CH=CHCl: Kinetics of the gas-phase reactions with Cl atoms, OH radicals, and O₃, *J. Photochem. Photobiol. A: Chemistry*, *199* (1), 92-97, doi: 10.1016/j.jphotochem.2008.05.013, 2008.
- Sulbaek Andersen, M.P., M.D. Hurley, and T.J. Wallington, Kinetics of the gas phase reactions of chlorine atoms and OH radicals with CF₃CBr=CH₂ and CF₃CF₂CBr=CH₂, *Chem. Phys. Lett.*, *482* (1-3), 20-23, doi: 10.1016/j.cplett.2009.09.056, 2009a.
- Sulbaek Andersen, M.P., D.R. Blake, F.S. Rowland, M.D. Hurley, and T.J. Wallington, Atmospheric chemistry of sulfuranyl fluoride: Reaction with OH radicals, Cl atoms and O₃, atmospheric lifetime, IR spectrum, and global warming potential, *Environ.*

- Sci. Technol.*, 43 (4), 1067-1070, doi: 10.1021/es802439f, 2009b.
- Suntharalingam, P., A.J. Kettle, S.M. Montzka, and D.J. Jacob, Global 3-D model analysis of the seasonal cycle of atmospheric carbonyl sulfide: Implications for terrestrial vegetation uptake, *Geophys. Res. Lett.*, 35, L19801, doi: 10.1029/2008GL034332, 2008.
- Tanhua, T., and K.A. Olsson, Removal and bioaccumulation of anthropogenic, halogenated transient tracers in an anoxic fjord, *Mar. Chem.*, 94 (1-4), 27-41, doi: 10.1016/j.marchem.2004.07.009, 2005.
- Taniguchi, N., T.J. Wallington, M.D. Hurley, A.G. Guschin, L.T. Molina, and M.J. Molina, Atmospheric chemistry of $C_2F_5C(O)CF(CF_3)_2$: Photolysis and reaction with Cl atoms, OH radicals, and ozone, *J. Phys. Chem. A*, 107 (15), 2674-2679, doi: 10.1021/jp0220332, 2003.
- Tarnocai, C., J.G. Canadell, E.A.G. Schuur, P. Kuhry, G. Mazhitova, and S. Zimov, Soil organic carbon pools in the northern circumpolar permafrost region, *Global Biogeochem. Cycles*, 23, GB2023, doi: 10.1029/2008GB003327, 2009.
- Teh, Y.A., R.C. Rhew, A. Atwood, and T. Abel, Water, temperature, and vegetation regulation of methyl chloride and methyl bromide fluxes from a shortgrass steppe ecosystem, *Global Change Biol.*, 14 (1), 77-91, doi: 10.1111/j.1365-2486.2007.01480.x, 2008.
- Teh, Y.A., O. Mazéas, A.R. Atwood, T. Abel, and R.C. Rhew, Hydrologic regulation of gross methyl chloride and methyl bromide uptake from Alaskan Arctic tundra, *Global Change Biol.*, 15 (2), 330-345, doi: 10.1111/j.1365-2486.2008.01749.x, 2009.
- Theys, N., M. Van Roozendaal, F. Hendrick, C. Fayt, C. Hermans, J.-L. Barray, F. Goutail, J.-P. Pommereau, and M. De Mazière, Retrieval of stratospheric and tropospheric BrO columns from multi-axis DOAS measurements at Reunion Island (21°S, 56°E), *Atmos. Chem. Phys.*, 7 (18), 4733-4749, doi: 10.5194/acp-7-4733-2007, 2007.
- Thomas, V.M., J.A. Bedford, and R.J. Cicerone, Bromine emissions from leaded gasoline, *Geophys. Res. Lett.*, 24 (11), 1371-1374, 1997.
- Tokuhashi, K., A. Takahashi, M. Kaise, and S. Kondo, Rate constants for the reactions of OH radicals with $CH_3OCF_2CH_2F$, $CHF_2OCF_2CH_2F$, $CHF_2OCH_2CF_3$, and $CH_3CH_2OCF_2CH_2F$, *J. Geophys. Res.*, 104 (D15), 18681-18688, doi: 10.1029/1999JD900278, 1999.
- Tokuhashi, K., L. Chen, S. Kutsuna, T. Uchimaru, M. Sugie, and A. Sekiya, Environmental assessment of CFC alternatives: Rate constants for the reactions of OH radicals with fluorinated compounds, *J. Fluor. Chem.*, 125 (11), 1801-1807, doi: 10.1016/j.jfluchem.2004.09.013, 2004.
- Trentmann, J., G. Luderer, T. Winterrath, M.D. Fromm, R. Servranckx, C. Textor, M. Herzog, H.-F. Graf, and M.O. Andreae, Modeling of biomass smoke injection into the lower stratosphere by a large forest fire (Part I): Reference simulation, *Atmos. Chem. Phys.*, 6 (12), 5247-5260, doi: 10.5194/acp-6-5247-2006, 2006.
- Trudinger, C.M., D.M. Etheridge, G.A. Sturrock, P.J. Fraser, P.B. Krummel, and A. McCulloch, Atmospheric histories of halocarbons from analysis of Antarctic firn air: Methyl bromide, methyl chloride, chloroform, and dichloromethane, *J. Geophys. Res.*, 109, D22310, doi: 10.1029/2004JD004932, 2004.
- UNEP (United Nations Environment Programme), 2006 *Report of the Halons Technical Options Committee 2006 Assessment*, edited by D. Catchpole and D. Verdonik, Nairobi, Kenya, 2007a.
- UNEP (United Nations Environment Programme), 2006 *Report of the Methyl Bromide Technical Options Committee 2006 Assessment*, coordinated by M. Pizano, I. Porter, M. Marcotte, M. Besri, and J. Banks, Nairobi, Kenya, 2007b.
- UNEP (United Nations Environment Programme), data reported to the ozone secretariat, available online at: http://ozone.unep.org/Data_Reporting/, 2010.
- UNEP/TEAP (United Nations Environment Programme/Technology and Economic Assessment Panel), 1998 *Assessment Report of the Technology and Economic Assessment Panel (TEAP)*, 286 pp., Nairobi, Kenya, available at: http://ozone.unep.org/teap/Reports/TEAP_Reports/TEAPAS98.pdf, 1998.
- UNEP/TEAP (United Nations Environment Programme/Technology and Economic Assessment Panel), *Task Force on Emissions Discrepancies Report*, co-chaired by P. Ashford, L. Kuijpers, and S. Montzka, Nairobi, Kenya, 2006.
- UNEP/TEAP (United Nations Environment Programme/Technology and Economic Assessment Panel), *Report of the Technology and Economic Assessment Panel (TEAP), Progress report, Volume 2*, coordinated by L. Kuipers and M. Seki, Nairobi, Kenya, 2010.
- van der Werf, G.R., J.T. Randerson, G.J. Collatz, L. Giglio, P.S. Kasibhatla, A.F. Arellano Jr., S.C. Olsen, and E.S. Kasischke, Continental-scale partitioning of fire emissions during the 1997 to 2001 El Niño/La Niña period, *Science*, 303 (5654), 73-76, doi: 10.1126/science.1090753, 2004.
- Van Roozendaal, M., T. Wagner, A. Richter, I. Pundt, D.W. Arlander, J.P. Burrows, M. Chipperfield, C. Fayt, P.V. Johnston, J.-C. Lambert, K. Kreher, K. Pfeilsticker, U. Platt, J.-P. Pommereau, B.-M. Sinnhuber, K.K. Tørnkvist, and F. Wittrock, In-

- tercomparison of BrO measurements from ERS-2 GOME, ground-based and balloon platforms, *Adv. Space Res.*, 29 (11), 1661-1666, 2002.
- Varner, R.K., P.M. Crill, and R.W. Talbot, Wetlands: A potentially significant source of atmospheric methyl bromide and methyl chloride, *Geophys. Res. Lett.*, 26 (16), 2433-2436, 1999a.
- Varner, R.K., P.M. Crill, R.W. Talbot, and J.H. Shorter, An estimate of the uptake of atmospheric methyl bromide by agricultural soils, *Geophys. Res. Lett.*, 26 (6), 727-730, 1999b.
- Varner, R.K., M.L. White, C.H. Mosedale, and P.M. Crill, Production of methyl bromide in a temperate forest soil, *Geophys. Res. Lett.*, 30, 1521, doi: 10.1029/2002GL016592, 2003.
- Vecchi, G.A., and B.J. Soden, Global warming and the weakening of the tropical circulation, *J. Climate*, 20 (17), 4316-4340, 2007.
- Velders, G.J.M., D.W. Fahey, J.S. Daniel, M. McFarland, and S.O. Andersen, The large contribution of projected HFC emissions to future climate forcing, *Proc. Natl. Acad. Sci.*, 106 (27), 10949-10954, 2009.
- Vigano, I., H. van Weelden, R. Holzinger, F. Keppler, A. McLeod, and T. Röckmann, Effect of UV radiation and temperature on the emission of methane from plant biomass and structural components, *Biogeosciences*, 5 (3), 937-947, doi: 10.5194/bg-5-937-2008, 2008.
- Volk, C.M., J.W. Elkins, D.W. Fahey, G.S. Dutton, J.M. Gilligan, M. Loewenstein, J.R. Podolske, K.R. Chan, and M.R. Gunson, Evaluation of source gas lifetimes from stratospheric observations, *J. Geophys. Res.*, 102 (D21), 25543-25564, 1997.
- Vollmer, M.K., S. Reimann, D. Folini, L.W. Porter, and L.P. Steele, First appearance and rapid growth of anthropogenic HFC-245fa ($\text{CHF}_2\text{CH}_2\text{CF}_3$) in the atmosphere, *Geophys. Res. Lett.*, 33, L20806, doi: 10.1029/2006GL026763, 2006.
- Vollmer, M.K., L.X. Zhou, B.R. Grealley, S. Henne, B. Yao, S. Reimann, F. Stordal, D.M. Cunnold, X.C. Zhang, M. Maione, F. Zhang, J. Huang, and P.G. Simmonds, Emissions of ozone-depleting halocarbons from China, *Geophys. Res. Lett.*, 36, L15823, doi: 10.1029/2009GL038659, 2009.
- Wallace, D.W.R., P. Beining, and A. Putzka, Carbon tetrachloride and chlorofluorocarbons in the South Atlantic Ocean, 19°S, *J. Geophys. Res.*, 99 (C4), 7803-7819, 1994.
- Wallington, T.J., W.F. Schneider, D.R. Worsnop, O.J. Nielsen, J. Sehested, W.J. DeBruyn, and J.A. Shorter, The environmental impact of CFC replacements – HFCs and HCFCs, *Environ. Sci. Technol.*, 28 (7), 320A-326A, doi: 10.1021/es00056a002, 1994.
- Wallington, T.J., M.D. Hurley, J.M. Fracheboud, J.J. Orlando, G.S. Tyndall, J. Sehested, T.E. Møgelberg, and O.J. Nielsen, Role of excited CF_3CFHO radicals in the atmospheric chemistry of HFC-134a, *J. Phys. Chem.*, 100 (46), 18116-18121, doi: 10.1021/jp9624764, 1996.
- Wallington, T.J., M.D. Hurley, J. Xia, D.J. Wuebbles, S. Sillman, A. Ito, J.E. Penner, D.A. Ellis, J. Martin, S.A. Mabury, O.J. Nielsen, and M.P. Sulbaek Andersen, Formation of $\text{C}_7\text{F}_{15}\text{COOH}$ (PFOA) and other perfluorocarboxylic acids during the atmospheric oxidation of 8:2 fluorotelomer alcohol, *Environ. Sci. Technol.*, 40 (3), 924-930, doi: 10.1021/es051858x, 2006.
- Wallington, T.J., M.P. Sulbaek Andersen, and O.J. Nielsen, Estimated photochemical ozone creation potentials (POCPs) of $\text{CF}_3\text{CF}=\text{CH}_2$ (HFO-1234yf) and related hydrofluoroolefins (HFOs), *Atmos. Environ.*, 44 (11), 1478-1481, doi: 10.1016/j.atmosenv.2010.01.040, 2010.
- Wan, D., J. Xu, J. Zhang, X. Tong, and J. Hu, Historical and projected emissions of major halocarbons in China, *Atmos. Environ.*, 43 (36), 5822-5829, doi: 10.1016/j.atmosenv.2009.07.052, 2009.
- Wang, J., R. Li, Y. Guo, P. Qin, and S. Sun, The flux of methyl chloride along an elevational gradient of a coastal salt marsh, Eastern China, *Atmos. Environ.*, 40 (34), 6592-6605, doi: 10.1016/j.atmosenv.2006.05.065, 2006.
- Wang, P.K., The thermodynamic structure atop a penetrating convective thunderstorm, *Atmos. Res.*, 83, 254-262, doi: 10.1016/j.atmosres.2005.08.010, 2007.
- Wang, P.K., M. Setvák, W. Lyons, W. Schmid, and H.-M. Lin, Further evidences of deep convective vertical transport of water vapor through the tropopause, *Atmos. Res.*, 94 (3), 400-408, doi: 10.1016/j.atmosres.2009.06.018, 2009.
- Warwick, N.J., J.A. Pyle, G.D. Carver, X. Yang, N.H. Savage, F.M. O'Connor, and R.A. Cox, Global modeling of biogenic bromocarbons, *J. Geophys. Res.*, 111, D24305, doi: 10.1029/2006JD007264, 2006.
- Waugh, D., and T. Hall, Age of stratospheric air: Theory, observations, and models, *Rev. Geophys.*, 40, 1010, doi: 10.1029/2000RG000101, 2002.
- Weiss, R.F., J. Mühle, P.K. Salameh, and C.M. Harth, Nitrogen trifluoride in the global atmosphere, *Geophys. Res. Lett.*, 35, L20821, doi: 10.1029/2008GL035913, 2008.
- White, M.L., R.K. Varner, P.M. Crill, and C.H. Mosedale, Controls on the seasonal exchange of CH_3Br in temperate peatlands, *Global Biogeochem. Cycles*, 19, GB4009, doi: 10.1029/2004GB002343, 2005.
- Williams, J., V. Gros, E. Atlas, K. Maciejczyk, A. Batsaikhan, H.F. Schöler, C. Forster, B. Quack, N.

- Yassaa, R. Sander, and R. Van Dingenen, Possible evidence for a connection between methyl iodide emissions and Saharan dust, *J. Geophys. Res.*, *112*, D07302, doi: 10.1029/2005JD0006702, 2007.
- Wilson, E.W., Jr., W.A. Hamilton, and H.R. Mount, Rate constants for the reactions of hydroxyl radical with several fluoroethers by the relative rate method, *J. Phys. Chem. A*, *111* (9), 1610-1617, doi: 10.1021/jp068355d, 2007.
- Wishkerman, A., S. Gebhardt, C.W. McRoberts, J.T.G. Hamilton, J. Williams, and F. Keppler, Abiotic methyl bromide formation from vegetation, and its strong dependence on temperature, *Environ. Sci. Tech.*, *42* (18), 6837-6842, doi: 10.1021/es800411j, 2008.
- WMO (World Meteorological Organization), *Scientific Assessment of Ozone Depletion: 2006*, Global Ozone Research and Monitoring Project-Report No. 50, 572 pp., Geneva, Switzerland, 2007.
- Worton, D.R., W.T. Sturges, J. Schwander, R. Mulvaney, J.-M. Barnola, and J. Chappellaz, 20th century trends and budget implications of chloroform and related tri- and dihalomethanes inferred from firn air, *Atmos. Chem. Phys.*, *6* (10), 2847-2863, doi: 10.5194/acp-6-2847-2006, 2006.
- Worton, D.R., W.T. Sturges, L.K. Gohar, K.P. Shine, P. Martinerie, D.E. Oram, S.P. Humphrey, P. Begley, L. Gunn, J.-M. Barnola, J. Schwander, and R. Mulvaney, Atmospheric trends and radiative forcings of CF₄ and C₂F₆ inferred from firn air, *Environ. Sci. Technol.*, *41* (7), 2184-2189, doi: 10.1021/es061710t, 2007.
- Wuebbles, D.J., D. Youn, K. Patten, D. Wang, and M. Martinez-Aviles, Metrics for ozone and climate: Three-dimensional modeling studies of ozone depletion potentials and indirect global warming potentials, in *Twenty Years of Ozone Decline, Proceedings of the Symposium for the 20th Anniversary of the Montreal Protocol*, edited by C. Zerefos, G. Contopoulos, and G. Skalkas, 297-326, Springer, Netherlands, doi: 10.1007/978-90-481-2469-5_23, 2009.
- Xiao, X., Optimal Estimation of the Surface Fluxes of Chloromethanes Using a 3-D Global Atmospheric Chemical Transport Model, Ph.D. thesis, Massachusetts Institute of Technology, Cambridge, MA, U.S.A., 210 pp., 2008.
- Xiao, X., R.G. Prinn, P.J. Fraser, P.G. Simmonds, R.F. Weiss, S. O'Doherty, B.R. Miller, P.K. Salameh, C.M. Harth, P.B. Krummel, L.W. Porter, J. Mühle, B.R. Grealley, D. Cunnold, R. Wang, S.A. Montzka, J.W. Elkins, G.S. Dutton, T.M. Thompson, J.H. Butler, B.D. Hall, S. Reimann, M.K. Vollmer, F. Stordal, C. Lunder, M. Maione, J. Arduini, and Y. Yokouchi, Optimal estimation of the surface fluxes of methyl chloride using a 3-D global chemical transport model, *Atmos. Chem. Phys.*, *10* (12), 5515-5533, doi: 10.5194/acp-10-5515-2010, 2010a.
- Xiao, X., R.G. Prinn, P.J. Fraser, R.F. Weiss, P.G. Simmonds, S. O'Doherty, B.R. Miller, P.K. Salameh, C.M. Harth, P.B. Krummel, A. Golombek, L.W. Porter, J.W. Elkins, G.S. Dutton, B.D. Hall, L.P. Steele, R.H.J. Wang, and D.M. Cunnold, Atmospheric three-dimensional inverse modeling of regional industrial emissions and global oceanic uptake of carbon tetrachloride, *Atmos. Chem. Phys.*, *10* (21), 10421-10434, doi:10.5194/acp-10-10421-2010, 2010b.
- Yang, E.-S., D.M. Cunnold, M.J. Newchurch, R.J. Salawitch, M.P. McCormick, J.M. Russell, J.M. Zawodny, and S.J. Oltmans, First stage of Antarctic ozone recovery, *J. Geophys. Res.*, *113*, D20308, doi: 10.1029/2007JD009675, 2008.
- Yang, X., R.A. Cox, N.J. Warwick, J.A. Pyle, G.D. Carver, F.M. O'Connor, and N.H. Savage, Tropospheric bromine chemistry and its impacts on ozone: A model study, *J. Geophys. Res.*, *110*, D23311, doi: 10.1029/2005JD006244, 2005.
- Yokouchi, Y., M. Ikeda, Y. Inuzuka, and T. Yukawa, Strong emission of methyl chloride from tropical plants, *Nature*, *416*, 163-165, doi: 10.1038/416163a, 2002.
- Yokouchi, Y., F. Hasebe, M. Fujiwara, H. Takashima, M. Shiotani, N. Nishi, Y. Kanaya, S. Hashimoto, P. Fraser, D. Toom-Sauntry, H. Mukai, and Y. Nojiri, Correlations and emission ratios among bromoform, dibromochloromethane, and dibromomethane in the atmosphere, *J. Geophys. Res.*, *110*, D23309, doi: 10.1029/2005JD006303, 2005.
- Yokouchi, Y., S. Taguchi, T. Saito, Y. Tohjima, H. Tanimoto, and H. Mukai, High frequency measurements of HFCs at a remote site in east Asia and their implications for Chinese emissions, *Geophys. Res. Lett.*, *33*, L21814, doi: 10.1029/2006GL026403, 2006.
- Yokouchi, Y., T. Saito, C. Ishigaki, and M. Aramoto, Identification of methyl chloride-emitting plants and atmospheric measurements on a subtropical island, *Chemosphere*, *69* (4), 549-553, doi: 10.1016/j.chemosphere.2007.03.028, 2007.
- Yokouchi, Y., K. Osada, M. Wada, F. Hasebe, M. Agama, R. Murakami, H. Mukai, Y. Nojiri, Y. Inuzuka, D. Toom-Sauntry, and P. Fraser, Global distribution and seasonal concentration change of methyl iodide in the atmosphere, *J. Geophys. Res.*, *113*, D18311, doi: 10.1029/2008JD009861, 2008.
- Young, C.J., M.D. Hurley, T.J. Wallington, and S.A. Mabury, Atmospheric chemistry of CF₃CF₂H and CF₃CF₂CF₂CF₂H: Kinetics and products of gas-phase reactions with Cl atoms and OH radicals, infrared spectra, and formation of perfluorocar-

- boxylic acids, *Chem. Phys. Lett.*, *473* (4-6), 251-256, doi: 10.1016/j.cplett.2009.04.001, 2009.
- Yujing, M., and A. Mellouki, Rate constants for the reactions of OH with chlorinated propanes, *Phys. Chem. Chem. Phys.*, *3*, 2614-2617, doi: 10.1039/b102971c, 2001.
- Yvon-Lewis, S.A., and J.H. Butler, Effect of oceanic uptake on atmospheric lifetimes of selected trace gases, *J. Geophys. Res.*, *107*, 4414, doi: 10.1029/2001JD001267, 2002.
- Yvon-Lewis, S.A., E.S. Saltzman, and S.A. Montzka, Recent trends in atmospheric methyl bromide: Analysis of post-Montreal Protocol variability, *Atmos. Chem. Phys.*, *9* (16), 5963-5974, doi: 10.5194/acp-9-5963-2009, 2009.
- Zander, R., E. Mahieu, P. Demoulin, P. Duchatelet, G. Roland, C. Servais, M. De Mazière, and C.P. Rinsland, Evolution of a dozen non-CO₂ greenhouse gases above central Europe since the mid-1980s, *Environ. Sci.*, *2* (2-3), 295-303, 2005.
- Zander, R., E. Mahieu, P. Demoulin, P. Duchatelet, G. Roland, C. Servais, M. De Mazière, S. Reimann, and C.P. Rinsland, Our changing atmosphere: Evidence based on long-term infrared solar observations at the Jungfraujoch since 1950, *Sci. Tot. Environ.*, *391* (2-3), 184-195, doi: 10.1016/j.scitotenv.2007.10.018, 2008.
- Zellner, R., G. Bednarek, A. Hoffmann, J.P. Kohlmann, V. Mörs, and H. Saathoff, Rate and mechanism of the atmospheric degradation of 2H-heptafluoropropane (HFC-227), *Ber. Bunsenges. Phys. Chem.*, *98* (2), 141-146, doi: 10.1002/bbpc.19940980202, 1994.
- Zeng, G., J.A. Pyle, and P.J. Young, Impact of climate change on tropospheric ozone and its global budgets, *Atmos. Chem. Phys.*, *8* (2), 369-387, doi: 10.5194/acp-8-369-2008, 2008.
- Zhao, Z., P.L. Laine, J.M. Nicovich, and P.H. Wine, Reactive and nonreactive quenching of O(¹D) by the potent greenhouse gases SO₂F₂, NF₃, and SF₅CF₃, *Proc. Natl. Acad. Sci.*, *107* (15), 6610-6615, doi: 10.1073/pnas.0911228107, 2010.
- Zhou, Y., H. Mao, R.S. Russo, D.R. Blake, O.W. Wingenter, K.B. Haase, J. Ambrose, R.K. Varner, R. Talbot, and B.C. Sive, Bromoform and dibromomethane measurements in the seacoast region of New Hampshire, 2002–2004, *J. Geophys. Res.*, *113*, D08305, doi: 10.1029/2007JD009103, 2008.

CHAPTER 2

Stratospheric Ozone and Surface Ultraviolet Radiation

Coordinating Lead Authors:

A. Douglass
V. Fioletov

Lead Authors:

S. Godin-Beekmann
R. Müller
R.S. Stolarski
A. Webb

Coauthors:

A. Arola
J.B. Burkholder
J.P. Burrows
M.P. Chipperfield
R. Cordero
C. David
P.N. den Outer
S.B. Diaz
L.E. Flynn
M. Hegglin
J.R. Herman
P. Huck
S. Janjai
I.M. Jánosi
J.W. Krzyścin
Y. Liu
J. Logan
K. Matthes
R.L. McKenzie
N.J. Muthama
I. Petropavlovskikh
M. Pitts
S. Ramachandran
M. Rex
R.J. Salawitch
B.-M. Sinnhuber
J. Staehelin
S. Strahan
K. Tourpali
J. Valverde-Canossa
C. Vigouroux

Contributors:

G.E. Bodeker
T. Canty
H. De Backer
P. Demoulin
U. Feister
S.M. Frith
J.-U. Grooß
F. Hase
J. Klyft
T. Koide
M.J. Kurylo
D. Loyola
C.A. McLinden
I.A. Megretskaja
P.J. Nair
M. Palm
D. Papanastasiou
L.R. Poole
M. Schneider
R. Schofield
H. Slaper
W. Steinbrecht
S. Tegtmeier
Y. Terao
S. Tilmes
D.I. Vyushin
M. Weber
E.-S. Yang

CHAPTER 2

STRATOSPHERIC OZONE AND SURFACE ULTRAVIOLET RADIATION

Contents

SCIENTIFIC SUMMARY	1
INTRODUCTION	5
2.1 OZONE OBSERVATIONS	5
2.1.1 State of Science in 2006	5
2.1.2 Update on Methods Used to Evaluate the Effect of ODSs on Ozone	5
2.1.3 Update on Total Ozone Changes	6
2.1.3.1 Measurements	6
2.1.3.2 Total Ozone Changes and Trends	8
2.1.4 Update on Ozone Profile Changes	10
2.1.4.1 Measurements	10
2.1.4.2 Ozone Profile Changes	12
2.2 POLAR OZONE	17
2.2.1 State of Science in 2006	17
2.2.2 Polar Ozone Chemistry	18
2.2.2.1 Laboratory Studies of the ClOOCI UV Absorption Spectrum	19
2.2.2.2 Field Observations of Chlorine Partitioning	21
2.2.2.3 Other Issues Related to Polar Ozone Chemistry	25
2.2.3 Polar Stratospheric Cloud Processes	25
2.2.3.1 New Observational Data Sets	26
2.2.3.2 PSC Composition	27
2.2.3.3 PSC Forcing Mechanisms	27
2.2.3.4 Use of Proxies to Represent PSC Processes	28
2.2.4 Arctic Polar Temperatures and Ozone	29
2.2.5 Antarctic Polar Temperatures and Ozone	30
2.2.6 The Onset of Antarctic Ozone Depletion	31
2.3 SURFACE ULTRAVIOLET RADIATION	31
2.3.1 State of Science in 2006	31
Box 2-1 Radiation Amplification Factor for Erythral Irradiance	32
2.3.2 Update on Factors Affecting UV Radiation	33
2.3.2.1 Ozone Effects	33
2.3.2.2 Other Influences on UV	34
2.3.3 Ground-Based and Satellite UV Data	35
2.3.3.1 Ground-Based UV Measurements	35
2.3.3.2 Ground-Based UV Reconstruction	35
2.3.3.3 UV Estimates from Satellite Observations	36
2.3.4 Long-Term Changes in UV	37
2.3.4.1 Ground-Based Observations	37
2.3.4.2 Reconstructed UV Data	38
2.3.4.3 Satellite Estimates of Irradiance Changes	40
2.3.4.4 Consistency of UV Estimates from Observations, Reconstructions, and Satellite Data	41
2.4 INTERPRETATION OF OBSERVED OZONE CHANGES	41
2.4.1 State of Science in 2006	41

2.4.2	Updates to Kinetic and Photochemical Data.....	43
2.4.2.1	Update from JPL 2002 to JPL 2006.....	43
2.4.2.2	Updates since JPL 2006.....	43
2.4.3	The Distribution and Variability of Stratospheric Ozone and Their Representation in Models.....	44
2.4.3.1	Annual Cycle and Natural Variability.....	44
2.4.3.2	Solar Cycle.....	44
2.4.3.3	Volcanic and Aerosol Effects.....	46
2.4.3.4	Evaluation of Simulated Transport.....	47
2.4.3.5	Evaluation of the Chemical Mechanism and Its Implementation.....	49
2.4.3.6	Evaluation of Simulations of the Upper Troposphere/Lower Stratosphere.....	49
2.4.4	Recovery Detection and Attribution.....	50
2.4.4.1	Dynamical Contributions to Apparent Trend.....	50
2.4.4.2	Greenhouse Gas Effects on Ozone Trends.....	50
2.4.4.3	Polar Loss and Dilution to Midlatitudes.....	51
2.4.5	Simulation of Ozone Changes for the Last Three Decades.....	51
2.4.5.1	Total Ozone Trends.....	51
2.4.5.2	Midlatitude Profile Trends.....	53
2.4.5.3	Tropical Profile Trends.....	55
2.4.5.4	Polar Trends.....	55
2.4.5.5	Trends and Recovery in the Upper Troposphere and Lower Stratosphere.....	58
REFERENCES.....		59

SCIENTIFIC SUMMARY

Global Ozone Observations and Interpretation

As a result of the Montreal Protocol, ozone is expected to recover from the effect of ozone-depleting substances (ODSs) as their abundances decline in the coming decades. The 2006 Assessment showed that globally averaged column ozone ceased to decline around 1996, meeting the criterion for the first stage of recovery. Ozone is expected to increase as a result of continued decrease in ODSs (second stage of recovery). This chapter discusses recent observations of ozone and ultraviolet radiation in the context of their historical records. Natural variability, observational uncertainty, and stratospheric cooling necessitate a long record in order to attribute an ozone increase to decreases in ODSs. Table S2-1 summarizes ozone changes since 1980.

The primary tools used in this Assessment for prediction of ozone are chemistry-climate models (CCMs). These CCMs are designed to represent the processes determining the amount of stratospheric ozone and its response to changes in ODSs and greenhouse gases. Eighteen CCMs have been recently evaluated using a variety of process-based comparisons to measurements. The CCMs are further evaluated here by comparison of trends calculated from measurements with trends calculated from simulations designed to reproduce ozone behavior during an observing period.

Total Column Ozone

- **Average total ozone values in 2006–2009 have remained at the same level for the past decade, about 3.5% and 2.5% below the 1964–1980 averages respectively for 90°S–90°N and 60°S–60°N.** Average total ozone from CCM simulations behaves in a manner similar to observations between 1980 and 2009. The average column ozone for 1964–1980 is chosen as a reference for observed changes for two reasons: 1) reliable ground-based observations sufficient to produce a global average are available in this period; 2) a significant trend is not discernible in the observations during this period.
- **Southern Hemisphere midlatitude (35°S–60°S) annual mean total column ozone amounts over the period 2006–2009 have remained at the same level as observed during 1996–2005, approximately 6% below the 1964–1980 average.** Simulations by CCMs also show declines of the same magnitude between 1980 and 1996, and minimal change after 1996, thus both observations and simulations are consistent with the expectations of the impact of ODSs on southern midlatitude ozone.
- **Northern Hemisphere midlatitude (35°N–60°N) annual mean total column ozone amounts over the period 2006–2009 have remained at the same level as observed during 1998–2005, approximately 3.5% below the 1964–1980 average.** A minimum about 5.5% below the 1964–1980 average was reached in the mid-1990s. Simulations by CCMs agree with these measurements, again showing the consistency of data with the expected impact of ODSs. The simulations also indicate that the minimum in the mid-1990s was primarily caused by the ozone response to effects of volcanic aerosols from the 1991 eruption of Mt. Pinatubo.
- **The latitude dependence of simulated total column ozone trends generally agrees with that derived from measurements, showing large negative trends at Southern Hemisphere mid and high latitudes and Northern Hemisphere midlatitudes for the period of ODS increase.** However, in the tropics the statistically significant range of trends produced by CCMs (–1.5 to –4 Dobson units per decade (DU/decade)) does not agree with the trend obtained from measurements (+0.3 ± 1 DU/decade).

Ozone Profiles

- **Northern Hemisphere midlatitude (35°N–60°N) ozone between 12 and 15 km decreased between 1979 and 1995, and increased between 1996 and 2009.** The increase since the mid-1990s is larger than the changes expected from the decline in ODS abundances.

- **Northern Hemisphere midlatitude (35°N–60°N) ozone between 20 and 25 km declined during 1979–1995 and has since ceased to decline.** Observed increases between 1996 and 2008 are statistically significant at some locations but not globally.
- **Northern Hemisphere midlatitude (35°N–60°N) ozone between 35 and 45 km measured using a broad range of ground-based and satellite instruments ceased to decline after the mid-1990s, consistent with the leveling off of ODS abundances.** All data sets show a small ozone increase since that time, with varying degrees of statistical significance but this increase cannot presently be attributed to ODS decrease because of observational uncertainty, natural ozone variability, and stratospheric cooling. CCMs simulate the ozone response to changes in ODSs and increases in greenhouse gases; analysis of CCM results suggests that longer observational records are required to separate these effects from each other and from natural variability.
- **In the midlatitude upper stratosphere (35–45 km) of both hemispheres, the profile ozone trends derived from most CCMs from 1980 to 1996 agree well with trends deduced from measurements.** The agreement in both magnitude and shape of the ozone trends provides evidence that increases in ODSs between 1980 and 1996 are primarily responsible for the observed behavior.
- **In the tropical lower stratosphere, all simulations show a negative ozone trend just above the tropopause, centered at about 18–19 km (70–80 hPa), due to an increase in upwelling.** The simulated trends in the lower tropical stratosphere are consistent with trends deduced for 1985–2005 from Stratospheric Aerosol and Gas Experiment (SAGE II) satellite data, although uncertainties in the SAGE II trends are large. The near-zero trend in tropical total ozone measurements is inconsistent with the negative trend found in the integrated SAGE I + SAGE II stratospheric profiles. The tropospheric ozone column does not increase enough to resolve this discrepancy.

Table S2-1. Summary of ozone changes estimated from observations.

	Column Ozone	12–15 km	20–25 km	35–45 km	Comment
Data Sources	Ground-based, satellite	Ozonesondes	Ozonesondes, satellites, FTIR	Satellites, Umkehrs, FTIR	
Northern midlatitudes 1980–1996	Declined by about 6%	Declined by about 9%	Declined by about 7%	Declined by about 10%	1992–1996 column and lower stratosphere data affected by Mt. Pinatubo
Northern midlatitudes 1996–2009	Increased from the minimum values by about 2% by 1998 and remained at the same level thereafter	Increased by about 6%	Increased by about 2.5%	Increased by 1 to 2%, but uncertainties are large	
Southern midlatitudes 1980–1996	Declined by 6%	No information	Declined by about 7%	Declined by about 10%	
Southern midlatitudes 1996–2009	Remained at approximately the same level	No statistically significant changes	No statistically significant changes	Increased by 1 to 3%, but uncertainties are large	

Polar Ozone Observations and Interpretation

- **The Antarctic ozone hole continued to appear each spring from 2006 to 2009.** This is expected because decreases in stratospheric chlorine and bromine have been moderate over the last few years. Analysis shows that since 1979 the abundance of total column ozone in the Antarctic ozone hole has evolved in a manner consistent with the time evolution of ODSs. Since about 1997 the ODS amounts have been nearly constant and the depth and magnitude of the ozone hole have been controlled by variations in temperature and dynamics. The October mean column ozone within the vortex has been about 40% below 1980 values for the past fifteen years.
- **Arctic winter and spring ozone loss has varied between 2007 and 2010, but remained in a range comparable to the values that have prevailed since the early 1990s.** Chemical loss of about 80% of the losses observed in the record cold winters of 1999/2000 and 2004/2005 has occurred in recent cold winters.
- **Recent laboratory measurements of the chlorine monoxide dimer (ClOCl) dissociation cross section and analyses of observations from aircraft and satellites have reaffirmed the fundamental understanding that polar springtime ozone depletion is caused primarily by the ClO + ClO catalytic ozone destruction cycle, with significant contributions from the BrO + ClO cycle.**
- **Polar stratospheric clouds (PSCs) over Antarctica occur more frequently in early June and less frequently in September than expected based on the previous satellite PSC climatology.** This result is obtained from measurements by a new class of satellite instruments that provide daily vortex-wide information concerning PSC composition and occurrence in both hemispheres. The previous satellite PSC climatology was developed from solar occultation instruments that have limited daily coverage.
- **Calculations constrained to match observed temperatures and halogen levels produce Antarctic ozone losses that are close to those derived from data.** Without constraints, CCMs simulate many aspects of the Antarctic ozone hole, however they do not simultaneously produce the cold temperatures, isolation from middle latitudes, deep descent, and high amounts of halogens in the polar vortex. Furthermore, most CCMs underestimate the Arctic ozone loss that is derived from observations, primarily because the simulated northern winter vortices are too warm.

Ultraviolet Radiation

Ground-based measurements of solar ultraviolet (UV) radiation (wavelength 280–400 nanometers) remain limited both spatially and in duration. However, there have been advances both in reconstructing longer-term UV records from other types of ground-based measurements and in satellite UV retrievals. Where these UV data sets coincide, long-term changes agree, even though there may be differences in instantaneous, absolute levels of UV.

- **Ground-based UV reconstructions and satellite UV retrievals, supported in the later years by direct ground-based UV measurements, show that erythemal (“sunburning”) irradiance over midlatitudes has increased since the late 1970s, in qualitative agreement with the observed decrease in column ozone.** The increase in satellite-derived erythemal irradiance over midlatitudes during 1979–2008 is statistically significant, while there are no significant changes in the tropics. Satellite estimates of UV are difficult to interpret over the polar regions.
- **In the Antarctic, large ozone losses produce a clear increase in surface UV radiation.** Ground-based measurements show that the average spring erythemal irradiance for 1990–2006 is up to 85% greater than the modeled irradiance for 1963–1980, depending on site. The Antarctic spring erythemal irradiance is approximately twice that measured in the Arctic for the same season.
- **Clear-sky UV observations from unpolluted sites in midlatitudes show that since the late 1990s, UV irradiance levels have been approximately constant, consistent with ozone column observations over this period.**

- **Surface UV levels and trends have also been significantly influenced by clouds and aerosols, in addition to stratospheric ozone.** Daily measurements under all atmospheric conditions at sites in Europe and Japan show that erythemal irradiance has continued to increase in recent years due to net reductions in the effects of clouds and aerosols. In contrast, in southern midlatitudes, zonal and annual average erythemal irradiance increases due to ozone decreases since 1979 have been offset by almost a half due to net increases in the effects of clouds and aerosols.

INTRODUCTION

This chapter presents information on several topics but is conceptually organized around a single question: is the Montreal Protocol working? This chapter is focused on the observational record and interpretation thereof up to the present, and consolidates information found in three separate chapters in the previous Assessment (WMO, 2007): Chapter 3 (“Global Ozone: Past and Present,” Chipperfield and Fioletov et al., 2007), Chapter 4 (“Polar Ozone: Past and Present,” Newman and Rex et al., 2007), and Chapter 7 (“Surface Ultraviolet Radiation: Past, Present and Future,” Bais and Lubin et al., 2007). There are four sections in this chapter: Ozone Observations, Polar Ozone, Surface Ultraviolet Radiation, and Interpretation of Observed Ozone Changes. Each section begins with a summary of WMO (2007) followed by a combination of updates to the observational records and longer discussion of new discoveries and observations.

2.1 OZONE OBSERVATIONS

2.1.1 State of Science in 2006

The long-term changes in global ozone were reviewed in Chapter 3 of WMO (2007). From the analysis of data from multiple sources, it was shown that the global mean total column ozone values for the period 2002–2005 had stabilized to values similar to those observed in 1998–2001, at approximately 3.5% below the 1964–1980 average values. Differences between the Northern and Southern Hemispheres (NH and SH) were noted, with ozone average values respectively 3% and 5.5% below their pre-1980 average values. The time series behavior of total ozone column was also shown to be different in both hemispheres during the 1990s. Ozone showed a minimum in the NH around 1993 followed by an increase, while it decreased through the late 1990s in the SH and leveled off in about 2000. Seasonal differences between ozone changes over midlatitude regions in both hemispheres were also noticed. The changes with respect to the pre-1980 values were larger in spring in the NH, while no seasonal dependence was found in the SH. Over the tropics, no change in column ozone values was found, which was consistent with the findings of WMO (2003).

Because total ozone column was no longer decreasing in most observations, several methods were discussed in WMO (2003) and WMO (2007) for the evaluation of ozone trends. Previous Assessments had described long-term ozone changes due to chemical destruction by ozone-depleting substances (ODSs) in terms of linear trends estimated using multiple regression analysis. Because the change in ODSs after the mid-1990s was no longer linear

with time, other methods were proposed, e.g., the piecewise linear trend model in which different linear fits are used before and after a turning point, and the fit to the equivalent effective stratospheric chlorine (EESC) function (see Chapter 1 of this Assessment). Such methods have been used in most recent studies on ozone trends and are also discussed in the present Assessment.

Regarding changes in the vertical ozone distribution, satellite and ground-based measurements showed that in the upper stratosphere, the ozone decrease had stopped and ozone values were relatively constant since 1995. Similar stabilization was found in the lower stratosphere between 20 and 25 kilometers (km) altitude. In the lowermost stratosphere below 15 km altitude in the NH, a significant increase was found from 1996, after the strong decrease observed between 1979 and 1995. This change in the lowermost stratosphere had a substantial impact on the total ozone column. Such an ozone increase was not observed in the SH. The lowermost stratosphere is defined and discussed in more detail in Section 2.4 below.

All studies in WMO (2007) pointed out the stabilization of ozone both in total column and in the vertical distribution at various levels, various locations, and at the global scale. They concurred that the first stage of recovery (i.e., slowing of ozone decline attributable to ODS changes) had already occurred and that the second stage (i.e., onset of ozone increase) was expected to become evident within the next two decades.

2.1.2 Update on Methods Used to Evaluate the Effect of ODSs on Ozone

As discussed in previous Assessments, the long-term and short-term variability of ozone in the stratosphere is generally estimated using multi-regression statistical models that quantify the relationship between ozone and different explanatory variables describing natural or anthropogenic forcings (e.g., SPARC, 1998). The long-term trend components representing the effect of ODSs are extracted simultaneously with other regression terms and autocorrelated noise.

To describe the long-term trend in ozone that is related to ODSs, the equivalent effective stratospheric chlorine (EESC) (see Section 1.4.4 of Chapter 1) is commonly used as a proxy in statistical models (Stolarski et al., 2006; Dhomse et al., 2006; Brunner et al., 2006; Randel and Wu, 2007; Wohltmann et al., 2007; Mäder et al., 2007; Vyushin et al., 2007; Harris et al., 2008). Statistical methods are used to quantify the relationship between ozone changes and EESC, and verify whether the EESC-related term is statistically significant. Analysis of the residuals, for example, by the Cumulative Sum of Residuals (CUSUM) technique (Reinsel et al., 2002;

Newchurch et al., 2003) then can be used to check that a statistical model with the EESC term adequately describes the observed ozone changes.

The EESC depends on latitude and altitude. Moreover, the present estimates of EESC are different from those used, for example, in WMO (2003), as discussed in Section 1.4.4 of Chapter 1. As a result, all of the ozone trend studies mentioned above did not use the same EESC function. While a particular shape of the EESC curve has little effect on the EESC-based trend estimates in the past (they all represent a linear decline during the 1980s and early 1990s with leveling off thereafter), the shape of an EESC function will have more impact on the estimated trend value as time moves from the EESC turning point. The shape of the EESC curve is particularly important for the detectability of future trends (Vyushin et al., 2010). On the other hand, once the EESC shape is specified, the sensitivity of ozone to EESC obtained from this type of statistical analysis varies little as a result of small differences in the length of record.

A statistically significant EESC-related term can be used as evidence of the ODS-related destruction of ozone. The EESC was a linear function of time in the 1980s and thus the EESC fit to ozone can be expressed in terms of linear changes at that time, with results reported in ozone changes (% or Dobson units (DU)) per decade. WMO (2007, Section 3.2.1) discussed ozone trends in terms of EESC. Adding four more years to 25-year-long observation records discussed in WMO (2007) does not change the trend estimates for that period significantly. Similarly, the EESC is nearly a linear function in the 2000s and therefore the expected rate of ozone increase during the declining phase of the EESC can be expressed in % or DU per decade.

WMO (2007) concluded that the first stage of the ozone recovery, i.e., the slowing of ozone decline, identified as the occurrence of a statistically significant reduction in the rate of decline in ozone due to changing EESC, had already occurred. The second stage of the ozone recovery or the onset of ozone increases (turnaround) is identified as the occurrence of statistically significant increases in ozone above previous minimum values due to declining EESC.

The ozone increase after the minimum can be estimated by fitting the data with a linear function or by calculating a piecewise linear trend (PWLT) with a turning point near the EESC maximum (Reinsel et al., 2005; Miller et al., 2006; Vyushin et al., 2007; S.-K. Yang et al., 2009). The slope estimated from ozone data during the declining phase of EESC should agree with the slope expected from the EESC fit if the ozone increase is indeed related to the EESC decline.

As discussed by WMO (2007, Section 3.4.2) a sizable fraction of the long-term ozone changes, particularly

over northern mid and high latitudes, can be related to dynamical processes. Estimation of ozone trends requires a proper accounting for the effect of these processes on ozone. One approach is to add more terms to the statistical model used for trend calculations using a purely statistical approach and letting the regression model find the best proxies (e.g., Mäder et al., 2007) or by adding proxies based on possible physical processes that cause the ozone changes (e.g., Wohltmann et al., 2007). However the physical mechanisms underlying these additional terms are often not well understood, and therefore it is difficult to account for them properly in a statistical model. This issue is addressed in detail in Section 2.4. Another approach is to consider the contribution from dynamical processes as noise. This results in a larger uncertainty in the trend estimates and also requires an additional analysis of the autocorrelation function of the residuals (Vyushin et al., 2007). In both approaches, the eleven-year solar activity cycle and the quasi-biennial oscillation (QBO) are typically included in the statistical model because these oscillations are located in a narrow frequency range.

2.1.3 Update on Total Ozone Changes

2.1.3.1 MEASUREMENTS

Ground-Based Measurements

Dobson, Brewer, and filter instruments provide long-term ground-based total ozone time series. The instrumental precision of well maintained Dobson and Brewer instruments was recently estimated by Scarnato et al. (2010) to be respectively 0.5% and 0.15% (1-sigma). When comparing ground-based total ozone measurements with satellite overpass data, the standard deviation of monthly differences was on average about 1.5% and within 0.6–2.6% for 90% of Dobson and Brewer network stations and on average about 2% and within 1.5–3.5% for 90% of stations equipped with filter instruments M-124 (Fioletov et al., 2008). The agreement between various instruments can be further improved as new ozone absorption cross sections are adopted (Scarnato et al., 2009). A recently established committee is presently addressing the issue of ozone cross sections used in ground-based and satellite measurements (see <http://igaco-o3.fmi.fi/ACSO/>). Since the end of the 1980s, other instruments have been implemented for the monitoring of total ozone. Long-term and regular ground-based Fourier transform infrared (FTIR) measurements are performed at many stations around the world and these data were used to assess ozone trends over Western Europe from 79°N to 28°N (Vigouroux et al., 2008). The precision of FTIR ozone total columns

is about 4%, but it has been demonstrated that it can reach 1 DU in some conditions (Schneider et al., 2008). No calibration is needed, but the instrumental line shape must be known in order to avoid introducing a bias in the ozone retrievals. UV-Visible spectrophotometers such as the System d'Analyse par Observation Zenitale (SAOZ) instruments (Pommereau and Goutail, 1988) retrieve total ozone as well as nitrogen dioxide (NO₂) column amounts from zenith sky measurements using Differential Optical Absorption Spectroscopy (DOAS). A new version of the zenith-sky retrieval algorithm using improved air mass factors was recently introduced. SAOZ observations were used here in addition to Dobson, Brewer, and filter instrument data to form the ground-based zonal mean data set as described by Fioletov et al. (2002). This data set with the list of contributed stations is available from http://woudc.org/data_e.html.

Satellite Measurements

Satellite instruments have observed the total ozone distributions at the global scale since 1970, when the Nimbus 4 satellite was launched with the Backscatter Ultraviolet (BUV) instrument onboard. To date, the longest total ozone records are provided by the series of Total Ozone Mapping Spectrometer (TOMS) and Solar Backscatter Ultraviolet 2 (SBUV/2) instruments. Since 2004, the TOMS total ozone record has been taken over by the Ozone Monitoring Instrument (OMI), an instrument on the Aura satellite. TOMS, BUV, and SBUV/2 data presented here are retrieved with the version 8 algorithm (Bhartia et al., 2004; Flynn, 2007). There are two operationally available OMI satellite total ozone column data products, based on the OMI-TOMS and the OMI-DOAS retrieval algorithms, but outputs of the OMI-TOMS algorithm agree better with the most accurate ground-based measurements than those for the OMI-DOAS algorithm (Balis et al., 2007). The TOMS algorithm uses only two wavelengths (317.5 and 331.2 nanometers (nm)) to derive total ozone (four other wavelengths are used for diagnostics and error correction). The version 8.5 OMI algorithm is similar to the TOMS version 8 algorithm and is used to process OMI data presented here.

In order to obtain long-term total ozone records, several data sets merging various satellite ozone records have been constructed. The TOMS+OMI+SBUV(2) merged ozone data set (MOD) (Stolarski and Frith, 2006), used in WMO (2007), has been updated through December of 2009. The input now includes version 8.5 data from OMI and version 8.0 data from NOAA-17 SBUV/2. Data from 1970 through 1972 have also been added from the Nimbus 4 BUV experiment in 1970–1977. The merged

ozone data set (MOD) can be obtained at http://acdb-ext.gsfc.nasa.gov/Data_services/merged/.

Version 8 ozone retrievals from Nimbus 7 SBUV, and NOAA-9, -11, -14, -16, -17, and -18 SBUV/2 instruments were used in a NOAA cohesive SBUV(2) total ozone data set (S.K. Yang et al., 2009) available at ftp://ftp.cpc.ncep.noaa.gov/long/SBUV_v8_Cohesive.

The European instruments Global Ozone Monitoring Experiment (GOME) on the European Remote Sensing Satellite (ERS-2) (1995–2003, global coverage), Scanning Imaging Absorption Spectrometer for Atmospheric Cartography (SCIAMACHY) on the Environmental Satellite (Envisat; 2002–present), and GOME-2 on Meteorological Operational satellite (MetOp)-A (2006–present) apply the DOAS algorithm technique in the continuous 325–335 nm wavelength range (Burrows et al., 1999) to retrieve total ozone estimates. Different types of DOAS algorithms have been developed: WFDOAS (Coldewey-Egbers et al., 2005), TOGOMI/TOSOMI (Eskes et al., 2005), and SDOAS/GDOAS/GDP (Van Roozendaal et al., 2006). By comparing to Brewer/Dobsons and other satellite data, all algorithms applied to GOME were shown to be in good agreement (Weber et al., 2005; Balis et al., 2007; Fioletov et al., 2008). Overall good agreement was also found in the comparison of SCIAMACHY total ozone to ground data and other satellite data over more than six years (Lerot et al., 2009). However, a downward drift of total ozone from SCIAMACHY with respect to GOME and other correlative data has been identified that is independent of the algorithm used (Lerot et al., 2009; Loyola et al., 2009a). GOME-2 has almost three years of total ozone data. First validation results have been reported (Antón et al., 2009). A merged data set from GOME, SCIAMACHY, and GOME-2 by successive scaling of SCIAMACHY and GOME-2 monthly-mean zonal mean data to GOME is described in Loyola et al. (2009a). They report that a scaling of +2 to +3% was required to match GOME-2 to the GOME data record.

The GOME-SCIAMACHY data is based on combined GOME, SCIAMACHY, and GOME-2 records, with SCIAMACHY and GOME-2 records adjusted using a stable record of the GOME instrument (although with a limited coverage after 2003). While multiple versions of the data processing algorithm and merged data sets exist (Weber et al., 2007; Loyola et al., 2009a), they produce nearly identical records of zonal monthly-mean ozone values.

Measurements from four TOMS instruments, GOME, four SBUV(2) instruments, and OMI are used to produce the New Zealand National Institute of Water and Atmospheric Research (NIWA) combined total ozone data set (Bodeker et al., 2005; Müller et al., 2008). Offsets and drifts between all of the satellite-based data sets are removed through intercomparisons with the

Dobson and Brewer ground-based network. The NIWA data set is available from <http://www.bodekerscientific.com/data/ozone>.

2.1.3.2 TOTAL OZONE CHANGES AND TRENDS

The quasi-global (60°S–60°N) ozone record from the MOD is shown in Figure 2-1. The annual variation and an 11-year periodical component are evident from the plot and are discussed in detail in WMO, 2007 (Chipperfield and Fioletov et al., 2007). The total ozone deviations for the 60°S–60°N, 90°S–90°N, 25°S–25°N, 35°N–60°N, and 35°S–60°S latitude belts are shown in Figure 2-2. The approach used in Fioletov et al. (2002) and WMO (2007) is again used here. Five data sets of 5°-wide zonal averages of total ozone values are analyzed in this Assessment. Area-weighted annual averages are calculated for different latitude belts and for the globe. All panels of Figure 2-2 indicate that average total ozone deviations in 2006–2009 display very little change as compared to the 2002–2005 values reported in WMO (2007). The global and 60°S–60°N averages were about 3.5% and 2.5% below the 1964–1980 average values, respectively. The total column ozone for 1964–1980 is chosen as a reference for observed changes for two reasons: (1) reliable ground-based observations sufficient to produce a global average are available in this period; and (2) a significant trend is not discernible in the observations during this period. In midlatitude regions of both hemispheres, ozone values in the NH and SH stabilized at respectively about 3.5% and 6% lower than the 1964–1980 average, with little sign of increase in recent years.

Several authors have examined the zonally averaged total ozone data and find statistically significant positive trends since the second half of the 1990s. S.-K. Yang et al. (2009) find a positive trend of about $1.2 \pm 0.8\%$ /decade for the period 1996–2007 in the averaged 50°S–50°N SBUV(2) satellite data using the PWLT model. Using Dobson total ozone measurements, Angell and Free (2009) find positive trends in the same regions after application of 5-year running linear trends to the smoothed individual station ground-based data. They used 11-year running means to minimize the 11-year solar and QBO effects in the ozone time series. It should be mentioned however, that the positive trend in 50°S–50°N region is largely associated with an ozone increase in the tropical belt related to relatively low ozone values there in the mid-1990s and relatively high values during the recent solar activity minimum. Loyola et al. (2009b) analyzed the merged GOME(2)+SCIAMACHY data set as well the MOD set for the period from June 1995 to April 2009. They report a statistically significant positive linear trend between 5°S and 30°N for both satellite data sets. All these findings seem to contradict previous estimates of the number of

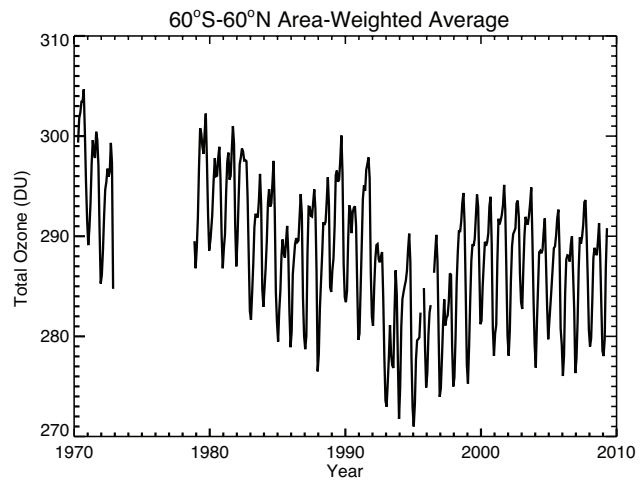


Figure 2-1. Quasi-global (60°N–60°S) average of total ozone distribution (Dobson units) for the period 1970–2009 from the BUV/TOMS/SBUV(2) merged ozone data set.

years required to detect statistically significant ozone trend expected from the decline of ODSs (Weatherhead et al., 2000; Vyushin et al., 2007). These studies predicted that statistically significant ozone trends will be detectable first at southern midlatitudes but that this will not be possible earlier than 2015–2020.

Comparison of the PWLT (or linear trend) estimates with results based on the EESC fit, shows that these recent positive ozone trends are larger than those expected from the decline in ODSs. As mentioned above, knowing the EESC decreasing rate after the turning point in the late 1990s, the corresponding linear term in total ozone regression can be compared to positive trends in PWLT models. Figure 2-3 (updated Figures 8 and 9 of Vyushin et al., 2007) illustrates the ozone zonal trends by PWLT and EESC models with the solar and QBO terms applied to the MOD set for the periods 1979–2008, with the turning point for the PWLT in 1996. Figure 2-3 shows the rate of ozone increase based on the EESC fit for the period corresponding to the declining phase of EESC and the estimates for the linear trend after the turning point of the PWLT. The gray areas indicate 95% confidence intervals for the PWLT estimate. The two trends are fairly similar in southern middle and high latitudes, although the uncertainties on the observed trends encompass zero. In northern middle and high latitudes, however, the observed linear trend is roughly four times the EESC-predicted trend and is actually statistically significant over northern middle and low latitudes according to the PWLT estimate of the noise. In these regions, the ODS decrease induces a positive trend but it is overwhelmed by large dynamically driven variations. This result is confirmed by several

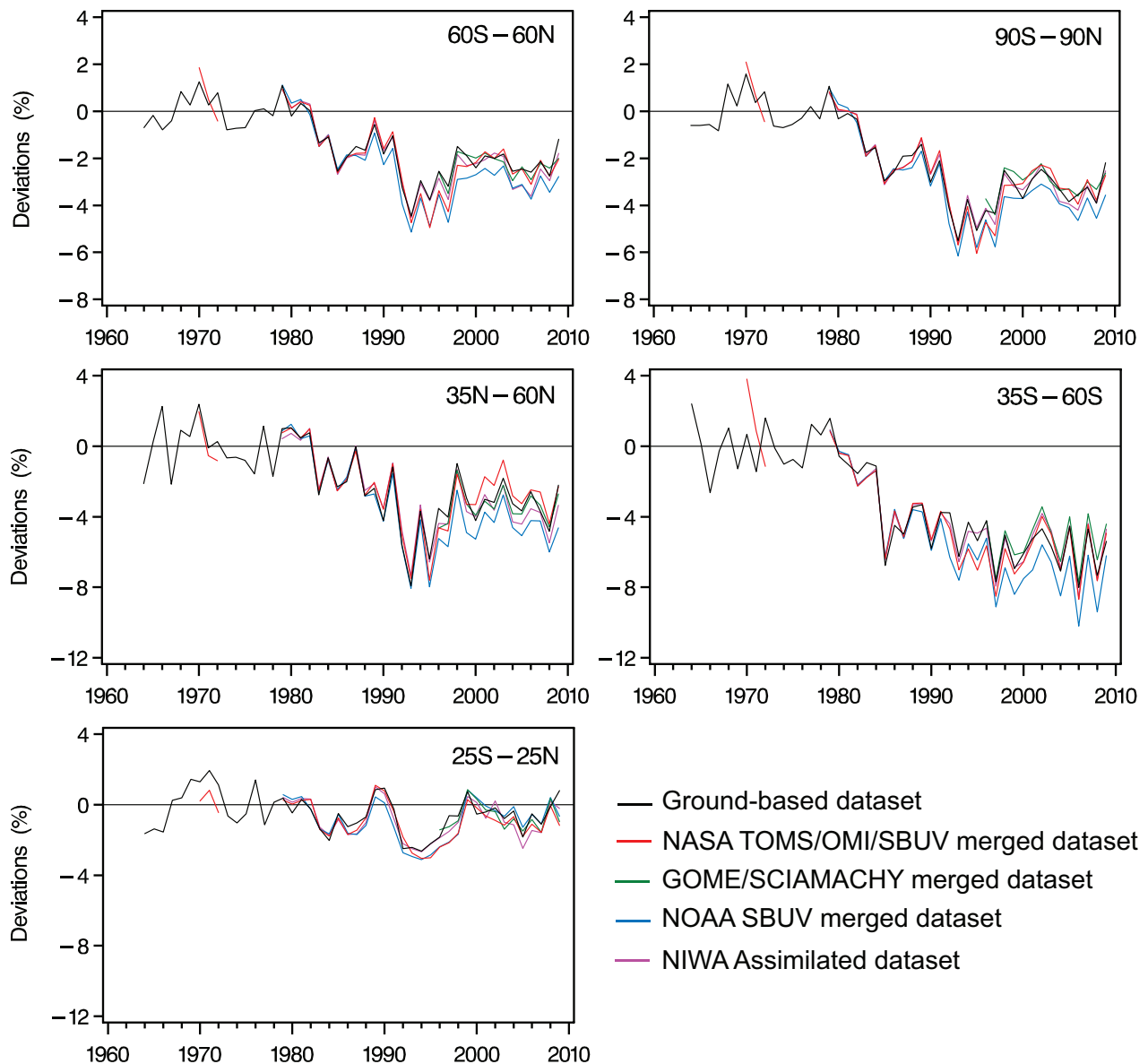


Figure 2-2. Annual mean area-weighted total ozone deviations from the 1964–1980 means for the latitude bands 90°S–90°N, 60°S–60°N, 25°S–25°N, 35°N–60°N, and 35°S–60°S, estimated from different global data sets: ground-based (black), NASA TOMS/OMI/SBUV(/2) merged satellite data set (red), National Institute of Water and Atmospheric Research (NIWA) assimilated data set (magenta), NOAA SBUV(/2) (blue), and GOME/SCIAMACHY merged total ozone data (green). Each data set was deseasonalized with respect to the period 1979–1987. The average of the monthly-mean anomalies for 1964–1980 estimated from ground-based data was then subtracted from each anomaly time series. Deviations are expressed as percentages of the ground-based time average for the period 1964–1980. Figure updated from Chapter 3 of WMO, 2007.

authors, who indicate that the EESC decrease since the mid-1990s is not a major contributor to the recent increase in ozone (Reinsel et al., 2005; Dhomse et al., 2006; Wohltmann et al., 2007; Harris et al., 2008).

On a regional scale, Krzyścin and Borkowski (2008) evaluate the ozone trend variability over Europe using 10-year blocks of reconstructed total ozone time

series since 1950. Statistically significant negative trends of 1 to 5%/decade are found almost over the whole of Europe only in the period 1985–1994. Trends up to –3%/decade appeared over small areas in earlier periods when the anthropogenic forcing on the ozone layer was weak. Vigouroux et al. (2008) provide total ozone trends from homogenized FTIR measurements in European stations,

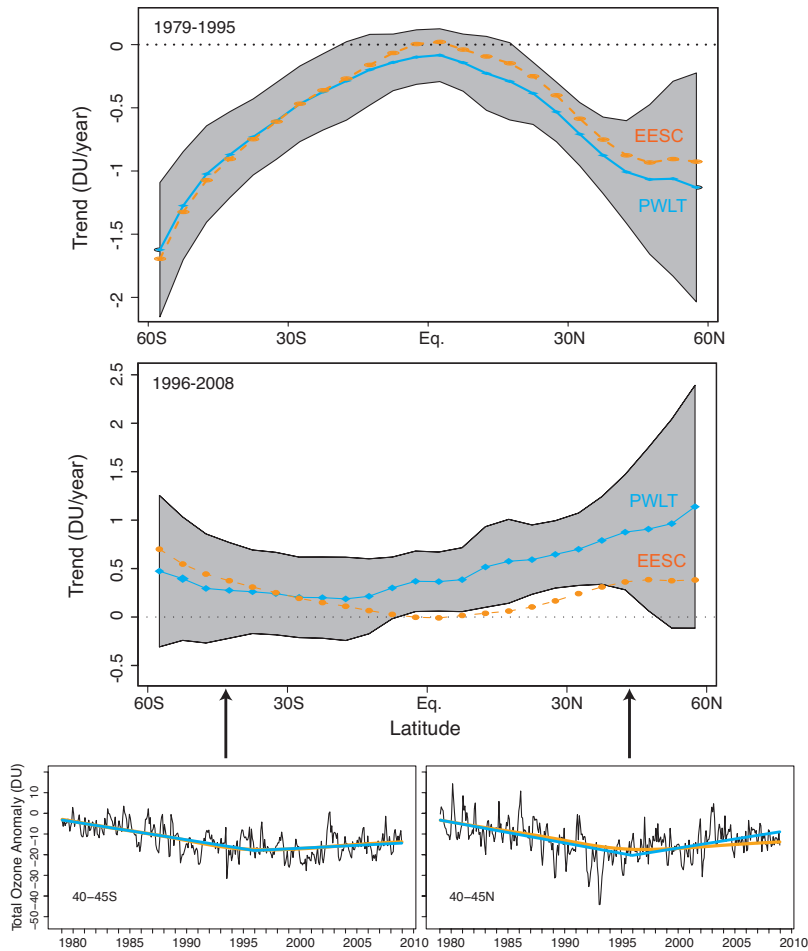


Figure 2-3. (top) The EESC-based linear trend in ozone (Dobson units/year) calculated for the increasing part of EESC (yellow solid circles connected by the yellow line) is compared to the first (declining) slope of the PWLT fit for the period 1979–1995 (blue diamonds connected by the solid blue line) with 95% confidence intervals (gray shading) for the PWLT fit. (middle) The EESC-based linear trend in ozone (DU/year) calculated for the declining part of EESC (yellow solid circles connected by the yellow line) is compared to the second (increasing) slope of the PWLT fit for the period 1996–2008 (blue diamonds connected by the solid blue line) with 95% confidence intervals (gray shading) for the PWLT fit. (bottom) Monthly and zonal mean total ozone anomalies for the 40°S–45°S and 40°N–45°N latitude bands obtained by filtering out the seasonal cycle, QBO, and solar flux, together with the EESC (yellow) and PWLT (blue) fits. Updated from Vyushin et al. (2007). The MOD set was used.

over the 1995–2004 period. These trends have been updated for the 1995–2009 period for the present Assessment and are summarized in Table 2-1. Because the time series are too short to employ the multi-regression models described in Section 2.1.2, a bootstrap resampling method was used, which allows for non-normally distributed data and gives an independent evaluation of the uncertainty in the trend value (Gardiner et al., 2008). The total column trends are close to zero and not significant at all stations except at Kiruna, where the trend is significantly positive.

2.1.4 Update on Ozone Profile Changes

2.1.4.1 MEASUREMENTS

Ground-Based Measurements

Ozonesondes, Dobson and Brewer spectrometers using the Umkehr method, lidars, and microwave instruments provide long-term measurements of ozone vertical distribution. Various recent studies have focused on

assessing the quality and stability of ozonesonde data. Differences ranging from 5 to 10% were found between data obtained with sondes produced from different manufacturers or with different sensing solutions (Thompson et al., 2007; Smit et al., 2007; Kivi et al., 2007; Deshler et al., 2008; Stübi et al., 2008). The Umkehr method retrieves ozone profiles from Dobson and Brewer measurements with a vertical resolution of about 5 km in the stratosphere. Current Umkehr data are retrieved using the UMK04 algorithm already released for the previous Assessment (Petropavlovskikh et al., 2005a, 2005b). Lidars and microwave spectrometers provide range-resolved measurements from the lower stratosphere to about 50 km for the lidar and higher for the microwave. Lidar measurements are characterized by a higher vertical resolution than microwave measurements, but they require clear skies so fewer measurements are obtained. A detailed description of the characteristics of ozonesondes, Umkehr, lidar, and microwave measurements in terms of accuracy and vertical resolution can be found in WMO (2007) and SPARC (1998).

A new ozone profile data source has been introduced for this Assessment, based on the inversion of FTIR measurements (Hase, 2000; Pougatchev et al., 1995). The

Table 2-1. Annual ozone trends and uncertainties (95% confidence limits), in %/decade, for partial and total columns. The measurements at Ny-Ålesund and Kiruna are restricted to the March–September and January–November period, respectively. Updated from Vigouroux et al. (2008).

FTIR Station	Latitude	Period	Ozone Trend (%/decade)			Total Column
			10–18 km	18–27 km	27–42 km	
Ny-Ålesund	79°N	1995–2009	0.0 ± 5.4	−0.8 ± 2.8	5.7 ± 2.7	0.0 ± 2.6
Kiruna	68°N	1996–2009	−1.0 ± 3.9	4.2 ± 2.3	11.4 ± 2.5	2.8 ± 2.2
Harestua	60°N	1995–2009	−11.4 ± 6.2	4.9 ± 2.3	7.2 ± 2.6	0.3 ± 2.7
Jungfraujoch	47°N	1995–2009	−1.9 ± 3.6	0.4 ± 0.9	0.8 ± 0.9	−0.1 ± 1.1
Izaña	28°N	1999–2009	−3.6 ± 4.2	1.8 ± 1.1	1.0 ± 1.2	0.5 ± 1.1

inversion is based on the optimal estimation method (Rodgers, 2000) and leads to 4–5 degrees of freedom in the whole column (Barret et al., 2002). Therefore, in addition to total column ozone, FTIR measurements can provide ozone profile data in 4 vertical layers (approximately ground–10 km; 10–18 km; 18–27 km; and 27–42 km). The precision of these four ozone partial columns is about 9.5%, 6.5%, 8.5%, and 6.0%, respectively (Vigouroux et al., 2008).

Satellite Measurements and Merged Data Sets

The second Stratospheric Aerosol and Gas Experiment (SAGE II) and Halogen Occultation Experiment (HALOE) satellite instruments that provided long and stable global observations of the ozone vertical distribution using the solar occultation technique ceased operation in 2005. Their long observational records, which were used in the previous Assessments, cover the periods 1984–2005 and 1991–2005 respectively. The longest ozone profile record based on a single instrument type still in operation is now provided by the series of SBUV and SBUV/2 instruments in operation since 1978. Retrieved profiles however have much lower vertical resolution than SAGE II or HALOE. The data are retrieved with the version 8 algorithm also used for total ozone retrieval (Bhartia et al., 2004; Flynn, 2007).

Data availability and quality remain the key issues in assessing changes in ozone profiles from satellite data. Jones et al. (2009) estimated that the smallest detectable linear trend in the midlatitude upper stratosphere from accurate but sparse SAGE occultation data was ~2.9%/decade (for the 1979–1997 period), while a trend of 1.5%/decade could be detected if the SAGE time series are combined with HALOE and much more frequent SBUV(/2) nadir observations. The SBUV(/2) record is comprised of data from multiple instruments. Biases between some of these instruments are comparable with

long-term ozone changes (e.g., Terao and Logan, 2007; Fioletov, 2009) that make the combined record difficult to use for the trend estimates.

In the last decade, several satellite instruments providing ozone profile measurements according to various measuring techniques have been launched onboard various satellite platforms, e.g., Odin (launched in 2001), Envisat (2002), SCISAT (2003), Aura (2004), and MetOp-A (2006), but their records are too short to contribute to this analysis on their own. Evaluation of the impact of the stabilization and subsequent decrease of ODS abundances in the stratosphere thus requires the merging of multiple data sets.

Merging the various satellite ozone profile data sets into a single, homogeneous data record suitable for trend studies is a challenge since each record is subject to its own instrument effects (noise, systematic errors, degradation, aging) and sampling issues (vertical and horizontal sampling, resolution, repeat time). Several such data sets have been introduced, based on single instrument type, such as SBUV and SBUV(/2) (Frith et al., 2004) or multiple instruments, e.g., sondes and solar occultation instruments (Randel and Wu, 2007; Hassler et al., 2008), or satellite instruments using different measurement techniques (Jones et al., 2009). McLinden et al. (2009) provide another data set based on SAGE and SBUV(/2) data spanning 1979–2005 where drifts in individual SBUV instruments and inter-SBUV biases are corrected using SAGE I and II by calculating differences between coincident SAGE-SBUV(/2) measurements. In this way the daily, near-global coverage of SBUV(/2) is combined with the stability and precision of SAGE to provide a homogeneous ozone record. Another approach is used by Jones et al. (2009): in order to remove biases between individual instrument records, ozone anomalies (deviations from the annual cycle) in overlapping periods are compared and then corrected for the difference. The data quality issue for trend estimates has become particularly important after

August 2005, when the SAGE II instrument stopped its operation, ending its long and stable data record. Because both SAGE II and HALOE ceased operations in 2005, few trend analyses using satellite ozone profile data were performed since the WMO (2007) report.

2.1.4.2 OZONE PROFILE CHANGES

Profile Trends in Altitude and Pressure Coordinates

As discussed in the previous Ozone Assessments, care must be taken when comparing trends in ozone derived from data in different geophysical units and/or different vertical coordinate systems (WMO, 2007). This is due to simultaneous trends in temperature that impact the air density directly and the altitude of a pressure surface indirectly. Rosenfield et al. (2005) demonstrated using a two-dimensional model that trends in upper stratospheric ozone may differ by 1 to 2%/decade depending on the units and vertical coordinate of the time series. Terao and Logan (2007) show differences up to 4%/decade between SAGE trends in altitude and pressure coordinates if National Centers for Environmental Prediction (NCEP) temperature reanalysis data are used for the conversion. An analysis of SBUV(2) and SAGE ozone time series suggests that this difference can be as much as 4% in the upper stratosphere if SAGE trends calculated in number density versus altitude are compared to SBUV(2) partial pressure versus pressure trends (Figure 2-4). However, if SAGE data are converted to the same units as SBUV(2) using temperature data with proper temperature trends (Randel et al., 2009) and are adjusted to match SBUV(2) vertical resolution as was done in the SAGE-corrected SBUV data set (McLinden et al., 2009), the ozone trends derived from SAGE and SBUV(2) are consistent at the 1–2%/decade level, roughly that of the trend uncertainties.

Ozone Changes in the Upper Stratosphere

The upper stratosphere (35–45 km) is the region where the effects of ODSs are expected to be the easiest to quantify, since the destruction of ozone there is mainly due to processes linked to homogeneous chemistry (WMO, 1999). Most studies performed in that region show a strong and statistically significant decline (6–8% per decade) for the period up to the mid-1990s and a near-zero or slightly positive trend thereafter (e.g., Randel and Wu, 2007; Steinbrecht et al., 2009; Jones et al., 2009; McLinden et al., 2009).

The ozone variability in the upper stratosphere (35–45 km) was examined by Steinbrecht et al. (2009) from various satellites and five ground-based lidar stations located in northern midlatitudes, tropical latitudes, and

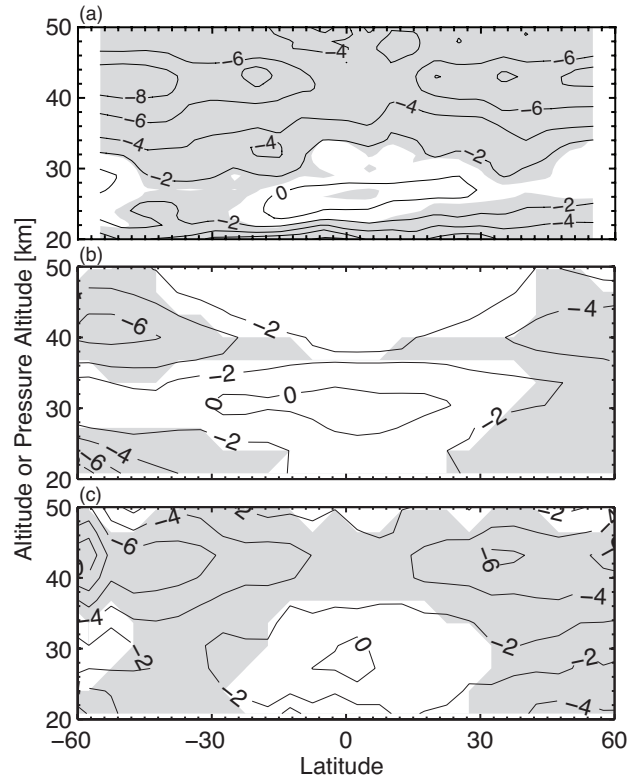
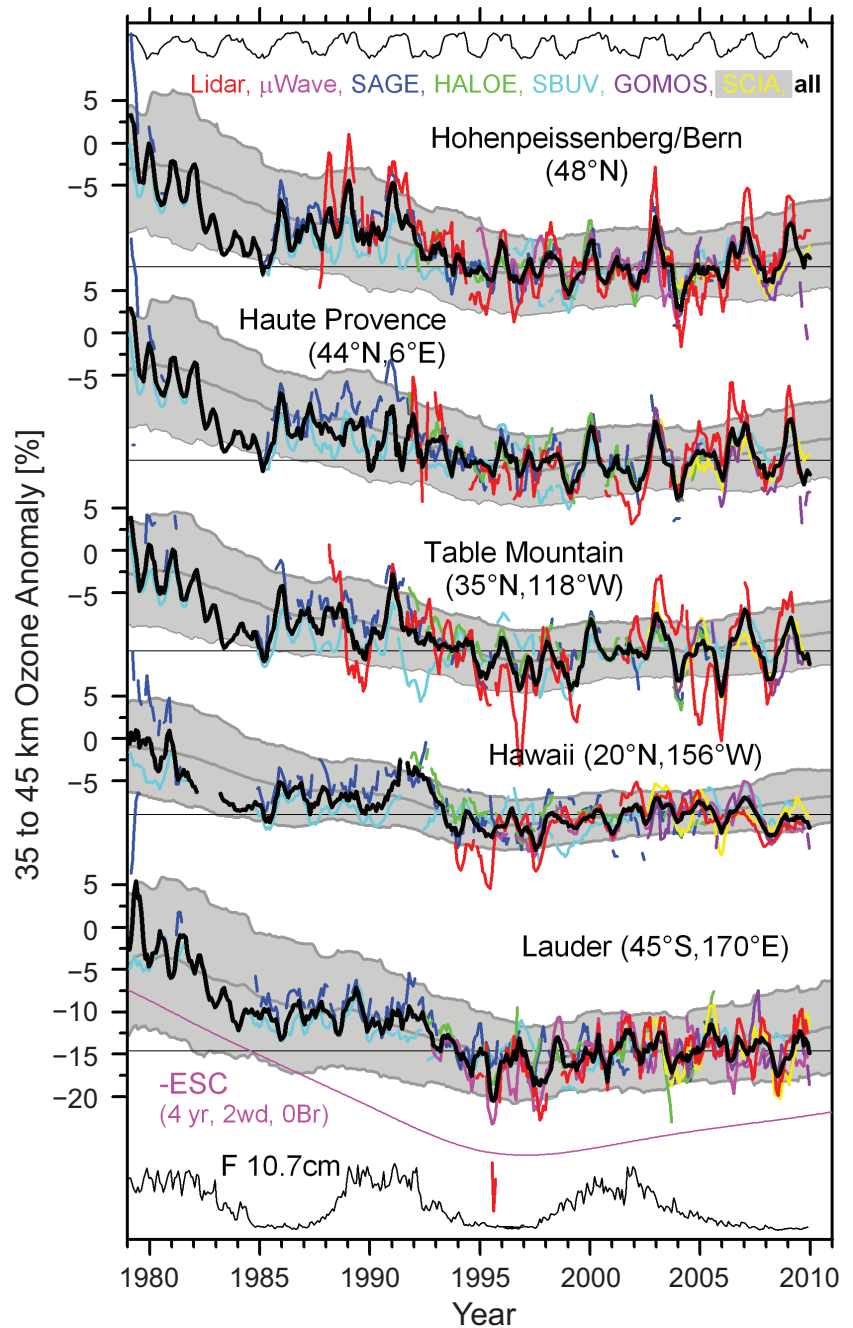


Figure 2-4. Stratospheric ozone trends as functions of latitude and altitude or pressure altitude from various data sources. The trends were estimated using regression to an EESC curve and converted to % per decade using the variation of EESC with time in the 1980s. The plots display trend estimates from various published data sets: (a) SAGE I+II (adapted from Randel and Wu, 2007), (b) the NASA merged SBUV(2) data set, (c) SAGE-corrected SBUV(2) (McLinden et al., 2009). For panel (c) SAGE I+II data are converted onto a pressure using a temperature trend from Randel et al. (2009) and then vertically smoothed to match the SBUV vertical resolution. Shading indicates the trends are significant at the 2σ level. Panel (a) is plotted in altitude, the remaining panels in pressure-altitude. Pressure-altitude is defined as $z^* = -16 \log_{10}(p/1000)$, where p is in hPa and z^* is km. Trend contours are every 2% per decade.

southern midlatitudes (Figure 2-5). This study extends results mentioned in WMO (2007) and includes an evaluation of temperature variability over the same locations. The new analysis confirms that the upper stratospheric ozone decline apparent from 1979 until the mid-1990s has stopped and ozone has stabilized since 1995–1996, depending on the latitude. Tatarov et al. (2009) analyzed 20 years (1988–2008) of stratospheric ozone and temperature

Figure 2-5. Ozone anomalies over the 1979 to early 2010 period from different data sets at five NDACC stations. Anomalies are averaged over the 35–45 km range. Light blue: SBUV(/2)-MOD version 8. Dark blue: SAGE I and II version 6.20. Green: HALOE version 19.0. Red: Lidar. Magenta: Microwave. Yellow: SCIAMACHY IUP–Bremen version 2.0. Violet: GOMOS ESA IPF 5.00. Black: Average of all available instruments. Gray underlay: CCMVal model simulations, 24-month running average ± 2 standard deviations. Observed data are smoothed by a five-month running mean. Lidar and microwave data are station means; all other data are zonal means. The thin black lines at the top and bottom show negative 10 hPa zonal wind at the equator as a proxy for the QBO, and 10.7 cm solar flux as a proxy for the 11-year solar cycle, respectively. The thin magenta line near the bottom shows inverted effective stratospheric chlorine as a proxy for ozone destruction by chlorine (ESC, 4 years mean age, 2 years spectral width, no bromine; see Newman et al., 2006). Updated from Steinbrecht et al. (2009).



profiles measured by differential absorption lidar (DIAL) data at the National Institute for Environmental Studies in Tsukuba (36°N, 140°E), Japan. Ozone data in the upper stratosphere exhibit a strong negative trend from 1988 to 1997 and a statistically insignificant trend after 1998.

Similar results were obtained for SAGE II coincident data over the station.

The lack of a significant ozone trend during the recent period (since 1996) in the upper stratosphere has also been found in the Arosa Umkehr data (Zanis et al., 2006).

In contrast, analyses of the homogenized Umkehr record for Belsk yielded a statistically significant upward trend in the upper stratosphere in the period 1996–2007 but not a decisive trend at other altitudes (Krzyścin and Rajewska-Wiech, 2009). From FTIR measurements, trends in the upper stratospheric layer of the ozone profile retrieval (27–42 km) range from an insignificant 0.8% per decade trend at Jungfraujoch (47°N) to a significant positive trend of up to 11% per decade at high latitude stations (see Table 2-1). Trend results from relatively short time series in the Arctic should be considered with caution due to the high variability of ozone in this region, especially during wintertime.

Jones et al. (2009) provide a global estimate of ozone trends from the average of various satellite ozone anomaly records. Using the PWLT statistical model with a turning point in 1997, they find that the largest statistically significant ozone declines in 1979–1997 are found in the midlatitude regions between 35 and 45 km altitude in both hemispheres, with trend values of approximately -7% /decade. For the period 1997 to 2008, they derive trends of 1.4 and 0.8%/decade in the NH and SH respectively, but these are not statistically significant (see Table 2-2).

Ozone Changes in the Lower Stratosphere

The lower stratosphere between 20 and 25 km over middle latitudes is another region where a statistically significant decline of about 4 to 5%/decade (or 7–8% total decline) occurred between 1979 and the mid-1990s, followed by stabilization or a slight (2–3%) ozone increase thereafter.

Angell and Free (2009) analyzed long-term ozone profile time series from four Northern Hemisphere Dobson Umkehr and 9 ozonesonde stations for trend analysis between 1970 and 2007. The 5-year trends were derived

from the 11-year running mean of the time series to minimize the impact of the 11-year solar cycle and QBO signals in the data. Both Umkehr and sonde data showed that nearly half of the increase in north temperate total-ozone trend between 1989 and 2000 was due to an increase in the 10–19 km layer in the lower stratosphere, with the troposphere contributing only about 5% of the change. Nonsignificant positive ozone trends at the end of the record in 2000 were found at four Umkehr layers in the middle and high stratosphere, as well as between 10 and 32 km altitude in sonde data.

Murata et al. (2009) could not detect any trend from a 14-year data set of ozone profiles measured with a balloonborne optical ozone sensor beginning in 1994 at Sanriku, Japan. This lack of trend was attributed to the leveling off of ODSs in the stratosphere. The extension of the FTIR trend analysis up to 2009 shows no significant trend at the midlatitudes station for the 18–27 km layer (Table 2-1). Similarly, the global trend analysis of Jones et al. (2009) shows no significant trend for the 20–25 km altitude range in the NH and SH midlatitudes for the period 1997–2008.

Figures 2-6a and 2-6b show the temporal evolution of deseasonalized ozone monthly means in three pressure ranges (upper, lower, and lowermost stratosphere) based on ozonesondes, Umkehr, and SBUV(2) observations over Europe and Lauder in the SH, respectively (adapted from Terao and Logan, 2007). The various time series show very similar interannual variation, although some biases are apparent between the measurements. In the upper and lower stratosphere, ozone levels have stabilized after a decrease from the early 1980s to the mid-1990s. In the lower stratosphere, the decrease was more pronounced over Europe than in the SH. In the lowermost stratosphere, no significant long-term variation is observed at

Table 2-2. Average ozone trends and uncertainties (95% confidence limits) in %/decade in the lower and upper stratosphere in the NH and SH midlatitudes, from various data sources for the period 1996–2008. The ozonesondes and Umkehr results correspond to the PWLT trends in Figure 2-7. The FTIR results are for the Jungfraujoch station only, for the 1995–2009 period, and correspond to respectively the 18–27 km and the 27–42 km altitude ranges for the lower and upper stratosphere.

Data Source	Ozone Trend 30°S–60°S (%/decade)		Ozone Trend 30°N–60°N (%/decade)	
	20–25 km	35–45 km	20–25 km	35–45 km
Satellite (from Jones et al., 2009)	-1.0 ± 2.0	0.8 ± 2.1	0.2 ± 1.9	1.4 ± 2.3
Umkehr	0.2 ± 2.6	2.0 ± 1.5	3.2 ± 2.1	1.5 ± 1.3
Ozonesondes			1.5 ± 0.6	
FTIR (updated from Vigouroux et al., 2008)			0.4 ± 0.9	0.8 ± 0.9

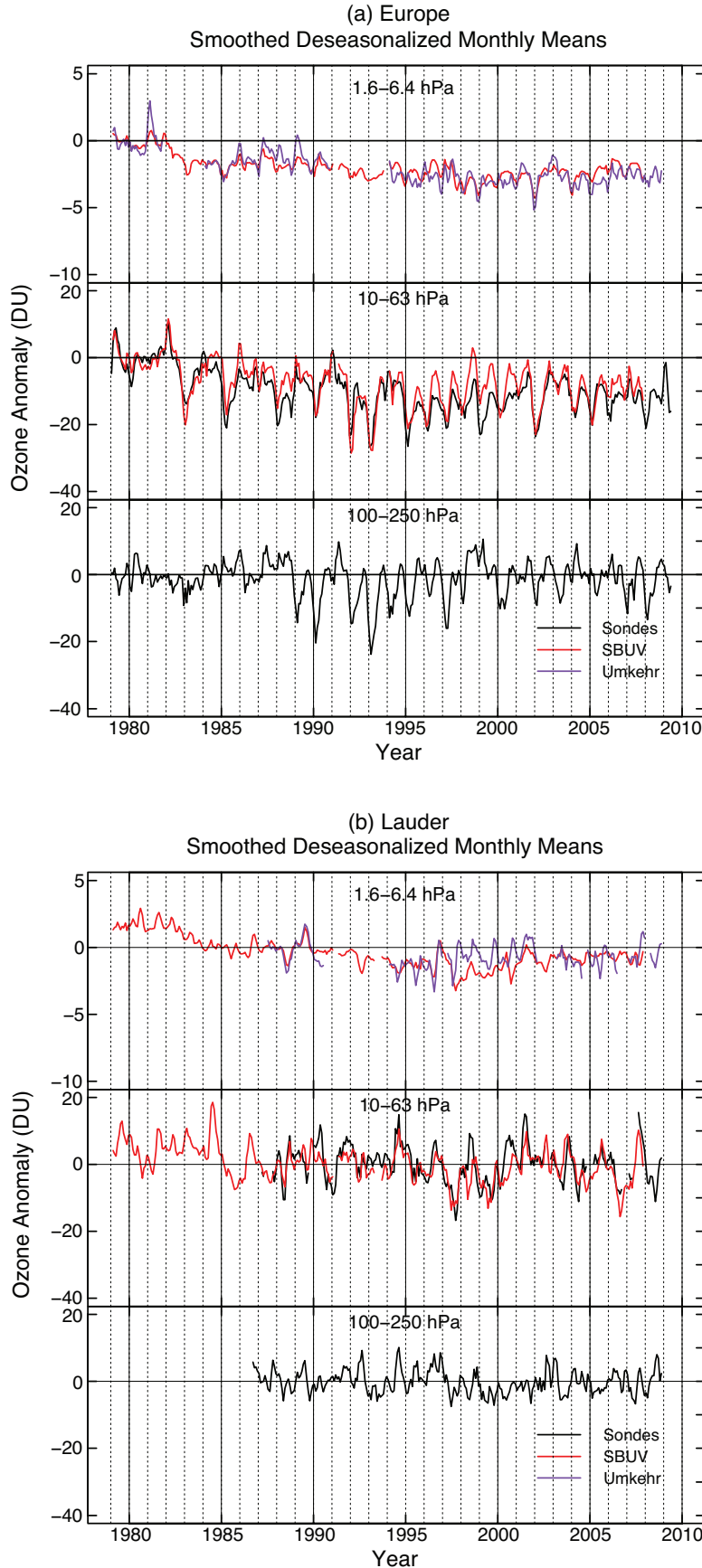


Figure 2-6. (a) Monthly ozone anomalies in Dobson units for Europe as measured by ozonesondes (black line), SBUV(/2) (red line), and Umkehr (blue line) at three pressure layers. The monthly anomalies were computed as the difference between a given monthly mean and the average of monthly means for 1979–1987 for each data set. The average of the monthly-mean anomalies for 1979–1981 was then subtracted from each anomaly time series to set the zero level in each panel. A three-month running mean was applied to the anomalies. The SBUV(/2) data were selected within a grid box of 45°N–55°N and 10°W–30°E. The ozonesonde data are the average of measurements at three European stations: Hohenpeissenberg, Payerne, and Uccle. The Umkehr data are from Arosa, Belsk, and Haute-Provence Observatory. The sonde and SBUV(/2) analysis is updated from Terao and Logan (2007). (b) Same as for (a) but for the Southern Hemisphere. The sonde data are from Lauder, New Zealand. The SBUV(/2) data were selected within a grid box of 40°S–50°S and 150°E–170°W. The monthly anomalies were computed using the monthly means for 1987–1991.

either location over the whole period, but higher short-term variability was seen during the nineties in Europe.

The vertical profile of ozone trends computed from SBUV(/2), Umkehr, and ozonesonde data over Northern midlatitudes stations is displayed in Figure 2-7 for both the increasing and decreasing periods of EESC (e.g., 1979–1995 and 1996–2008). The trends were derived using EESC as a regression term accounting for the variation of mean age of air as a function of altitude (see Waugh and Hall (2000) for a discussion of age of air and its spatial dependence). In the case of ozonesondes, trends were computed as the average of trends derived for nine northern midlatitude stations, as in the previous Ozone Assessment (Chapter 3). For Umkehr, the trend was derived from the average of ozone anomalies at four northern midlatitude stations and for SBUV(/2), the 40°N–50°N zonal mean data were used. Piecewise linear trends with inflection

point in January 1996 derived from ozonesonde and Umkehr data are also represented in the figure. As shown in WMO (2007), ozone trends during the first increasing period of EESC display two maxima in the upper and lower stratosphere, reaching -5 to -7% /decade and -4 to -5% /decade respectively (total decline of about 10% and 7% respectively), with generally good agreement between the various observations, except for Umkehr in the lower stratosphere. In both cases, the EESC and PWLT trend models give similar results for this period. For the decreasing EESC period, positive ozone trends are derived. In the upper and lower stratosphere, EESC and PWLT models provide similar trends of about 2%/decade. The PWLT trends are significant in the lower stratosphere and barely significant in the upper stratosphere. These results indicate that while the decrease of ODSs is indeed causing an increase of ozone over these midlatitude stations, this in-

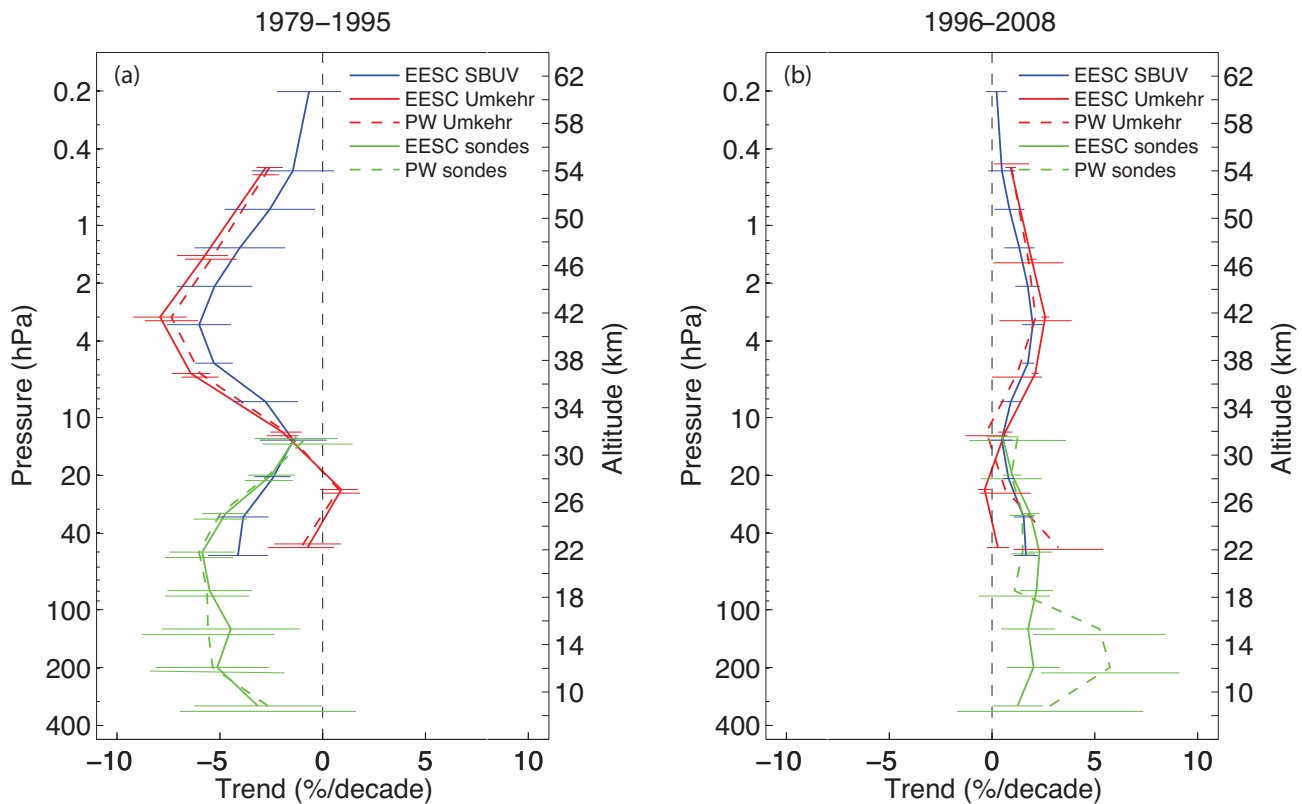


Figure 2-7. Vertical profile of ozone trends over Northern midlatitudes estimated from ozonesondes, Umkehr, and SBUV(/2) measurements for the period 1979–2008. The trends were estimated using regression to an EESC curve and converted to % per decade using the variation of EESC with time from 1979 to 1995 in panel (a) and from 1996 to 2008 in panel (b). Piecewise linear trends with inflection point in January 1996 derived from ozonesonde and Umkehr data are also shown. The trend models also include QBO and solar cycle terms. The sonde results are an average of trends for Churchill, Goose Bay, Boulder, Wallops Island, Hohenpeissenberg, Payerne, Uccle, Sapporo, and Tateno, along with two standard errors of the nine trends. The Umkehr trends were derived from averaged ozone anomalies at Belsk, Arosa, OHP, and Boulder. For SBUV(/2), the 40°N–50°N zonal mean data were used. The altitude scale is from the standard atmosphere. The error bars correspond to 95% confidence interval.

crease is still barely significant, especially in the upper stratosphere where trends derived from PWLT and EESC models are expected to show the best agreement. In contrast, in the lowermost stratosphere, EESC and PWLT trends derived from sondes data differ significantly, with large positive trend values in the latter case, suggesting that the ozone increase is due to factors other than chlorine decline, for example dynamical processes (see Section 2.4).

Table 2-2 summarizes the average trends found from various data sources using the PWLT model in the NH and SH midlatitudes in the lower (20–25 km) and upper (35–45 km) stratosphere. Most results show positive ozone trends (1–3% increase) since 1996 in the various regions. These trends are significant at some locations (e.g., over Northern midlatitudes) but the results from global satellite data are still not significant at the 95% confidence level (Jones et al., 2009).

Northern Hemisphere midlatitude (35°N–60°N) ozone between 12 and 15 km decreased by about 9% between 1979 and 1995, and increased by about 6% between 1996 and 2009 (Figure 2-7). The increase since the mid-1990s is larger than the changes expected from the decline in ODS abundances.

2.2 POLAR OZONE

Chapter 4 of WMO (2007) (“Polar Ozone: Past and Present”, Newman and Rex et al., 2007) builds upon the sequence of polar ozone chapters in the WMO Assessment series. The present discussion updates WMO (2007), highlighting changes over the past four years. Discussion of polar ozone recovery is found in Chapter 3 of this Assessment, and interactions of polar chemistry and climate are found in Chapter 4.

2.2.1 State of Science in 2006

The discovery of the Antarctic ozone hole by Farman et al. (1985) prompted considerable effort to develop the scientific basis necessary to model and predict polar ozone loss. As noted in the previous chapter, the stratospheric chlorine burden reached its peak in the late 1990s and has since begun to decrease. During the period of increasing chlorine concentrations, the springtime polar ozone values decreased in both hemispheres. Consistently low values in springtime ozone have been observed since the mid-1980s in the Southern Hemisphere. A unique dynamical situation, the first major sudden stratospheric warming in the Southern Hemisphere, led to the anomalously high ozone levels in 2002; this situation is discussed in detail in Chapter 4 of WMO (2007). The Arctic polar ozone loss is much more variable, depending not just on the stratospheric chlorine level but also on whether or not the winter is cold enough and of sufficient

length for chlorine-catalyzed ozone loss to occur. Because chlorofluorocarbons are long-lived, atmospheric chlorine loading is declining slowly.

The springtime averages of total ozone poleward of 63° latitude in the Arctic and Antarctic are shown in Figure 2-8 (an update of Figure 4-7 from WMO, 2007). Inter-annual variability in polar stratospheric ozone abundance and chemistry is driven by variability in temperature and transport due to year-to-year differences in dynamics. The horizontal gray lines in Figure 2-8 are the averages of ozone values obtained between 1970 and 1982, and the shading emphasizes the differences between these averages and subsequent years.

WMO (2007) outlined the processes important to polar ozone loss. The rate-limiting step of the dominant cycle for polar ozone destruction is the photolysis of chlorine peroxide (ClOOCl, also known as the chlorine monoxide dimer). Since the previous Assessment, a laboratory study suggesting a much lower photolysis rate of ClOOCl than previously recommended (Pope et al., 2007) prompted a number of subsequent laboratory studies on the subject. The implications of the laboratory studies since WMO (2007) for the interpretation of the observations of chlorine monoxide (ClO) and ClOOCl and for the assessment of the uncertainty in computation of ozone loss rates are discussed below along with other updates to the photochemical data in Section 2.2.2.

WMO (2007) concluded that Antarctic ozone loss had stabilized over the time period 1995–2005, with higher ozone levels in 2002 and 2004 that were dynamically

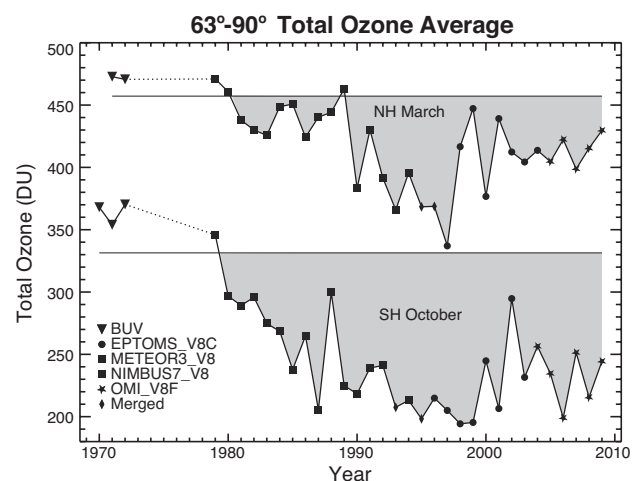


Figure 2-8. Total ozone average (Dobson units) of 63°–90° latitude in March (NH) and October (SH). Symbols indicate the satellite data that have been used in different years. The horizontal gray lines represent the average total ozone for the years prior to 1983 in March for the NH and in October in the SH. Updated from Figure 4-7, WMO (2007).

driven and not related to reductions in the stratospheric halogen load. For the Arctic it was concluded that for the coldest Arctic winters, the volume of air cold enough to support polar stratospheric clouds (PSCs) had increased significantly since the late 1960s. Arctic spring total ozone was reported to be lower than in the 1980s and was also noted to be highly variable from year to year depending on dynamical conditions. This is discussed further in Sections 2.2.4 and 2.2.5.

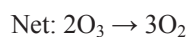
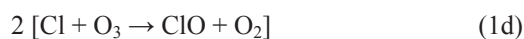
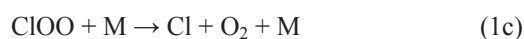
Transport and mixing both affect high-latitude winter ozone, making it challenging to diagnose the chemical loss rate from observations. WMO (2003) presented an overview of various methods that have been used to separate these effects, mainly for the Arctic winter. WMO (2007) included a comparison of the methods, focusing on the 2002/2003 winter. This colder-than-average winter was chosen because aircraft and ground field campaigns provided the data needed to assess our understanding of polar ozone loss, particularly for the large solar zenith angle-conditions of early winter. WMO (2007) noted that the various methods had been refined since WMO (2003) and produced consistent results.

WMO (2007) included evidence that nitric acid trihydrate (NAT) polar stratospheric cloud particles nucleate above the ice frost point and are widespread. Improved NAT mechanisms in chemistry-transport models (CTMs) produce more realistic denitrification, but fail to capture observed interannual variability for the northern winters. Issues concerning polar stratospheric clouds and their representation in models are discussed in Section 2.2.3. This section emphasizes new measurements from the Cloud-Aerosol Lidar and Infrared Pathfinder Satellite Observation (CALIPSO) satellite launched in 2006.

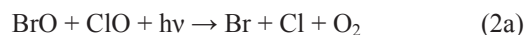
2.2.2 Polar Ozone Chemistry

Chemical loss of polar ozone during winter and spring occurs primarily by two gas-phase catalytic cycles that involve chlorine oxide radicals (Molina and Molina, 1987) and bromine and chlorine oxides (McElroy et al., 1986).

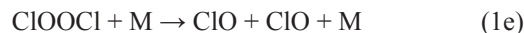
Cycle 1



Cycle 2



Loss of ClOOC by thermal decomposition



or chemical processes that recycle ClO without the formation of O_2 do not cause ozone depletion. Production of $\text{Br} + \text{OC}(\text{O})$ by $\text{BrO} + \text{ClO}$ also leads to a null cycle. Small contributions to polar ozone loss occur due to cycles involving the reactions $\text{ClO} + \text{O}$ and $\text{ClO} + \text{HO}_2$.

Since WMO (2007), attention has focused on resolving uncertainties in the photolysis cross sections and quantum yields for the ClO dimer, ClOOC. Pope et al. (2007) reported a ClOOC absorption spectrum with cross sections at wavelengths between 300 and 350 nm much lower than recommended and than reported in prior studies (e.g., Sander et al., 2006 (referred to in this chapter as JPL 06-2) and references therein), challenging the fundamental understanding of polar ozone depletion (i.e., Schiermeier, 2007; von Hobe, 2007). Photochemical models using the cross sections reported in Pope et al. (2007), with all other kinetic parameters from JPL 06-2, underestimate the ozone loss rate (von Hobe et al., 2007) as well as observed abundances of ClO (von Hobe et al., 2007; Santee et al., 2008; Schofield et al., 2008). A workshop entitled “The Role of Halogen Chemistry in Polar Stratospheric Ozone Depletion” was convened in summer 2008 to assess the fundamental understanding of polar ozone depletion in light of the Pope et al. (2007) measurements. The following material incorporates findings from this workshop (SPARC, 2009).

The small ClOOC cross sections reported by Pope et al. (2007) have been contradicted by all subsequent laboratory studies, as detailed below. There is now consensus in the community that photolysis of ClOOC occurs much faster than implied by Pope et al. (2007). Further, no credible “missing chemical process” has been proposed that can be included in models that use the Pope et al. (2007) cross section values to adequately account for observed levels of $[\text{ClO}]$ (or in some cases $[\text{ClO}]$ and $[\text{ClOOC}]$; brackets denote concentration of the species) as well as ozone loss derived from observations. The fundamental understanding that polar ozone depletion is caused primarily by reactions involving $\text{ClO} + \text{ClO}$, with significant contribution from reactions involving $\text{BrO} + \text{ClO}$, has been strengthened since WMO (2007), based on new laboratory

studies and analyses of field observations. The renewed focus on ClOOCl photolysis has improved knowledge of the UV absorption spectrum and cross sections such that a better quantitative understanding of polar ozone depletion and the relation to halogens has been achieved in the past few years. Present uncertainties in the ClOOCl absorption cross section, as recommended in Sander et al., 2009 (referred to in this chapter as JPL 09-31), are consistent with our fundamental understanding that halogens cause depletion of polar ozone. The following discussion supports the statements given above.

2.2.2.1 LABORATORY STUDIES OF THE ClOOCl UV ABSORPTION SPECTRUM

Figure 2-9 shows the ClOOCl ultraviolet-visible (UV/vis) absorption spectrum, $\sigma_{\text{ClOOCl}}(\lambda)$, reported in the laboratory studies of Burkholder et al. (1990) and Pope et al. (2007) combined with the spectra recommended by Atkinson et al., 2007 (hereafter referenced as IUPAC, 2007) (based on Huder and DeMore, 1995) and JPL 06-2 (Sander et al., 2006) (based on Cox and Hayman, 1988; DeMore and Tschuikow-Roux, 1990; Permien et al., 1988; and Burkholder et al., 1990), which represents the state of knowledge in 2007. The laboratory measurements published after 2007 and the recent NASA JPL Panel for Data Evaluation recommendation (JPL 09-31, Sander et al., 2009) are also shown in Figure 2-9. The JPL Panel revised the recommendations for a number of kinetic parameters for processes important in modeling stratospheric ozone depletion. The recommended ClOOCl cross sections in JPL 09-31 were unchanged from JPL 06-2, since the recommendation was formulated prior to the appearance of several more recent studies, but the recommended uncertainty limits were decreased. The estimated uncertainty limits from JPL 06-2 and JPL 09-31 are included in Figure 2-9, which also illustrates the most critical wavelength region for the calculated photolysis rate constant of ClOOCl (J_{1b}) in polar regions. The uncertainty in the calculated photolysis rate constant stems primarily from the uncertainty in the absorption cross sections and increases considerably for wavelengths (λ) greater than 350 nm, where there is more limited experimental data. At the time of WMO (2007), only Burkholder et al. (1990) and DeMore and Tschuikow-Roux (1990) had reported measured cross section data for $\lambda > 360$ nm, while several other studies provided extrapolated values. The recent studies of von Hobe et al. (2009) and Papanastasiou et al. (2009) confirm substantial contributions to J_{1b} from this spectral region. The uncertainty in the calculated photolysis rate constant is much less using the JPL 09-31 recommendation than using the JPL 06-2 recommendation.

Pope et al. (2007) reported a ClOOCl absorption spectrum at 195 K that was normalized at 245 nm to the

absolute cross section value recommended in JPL 06-2. The ClOOCl spectrum was obtained using a fitting procedure of measured spectra, which contained significant contributions from molecular chlorine (Cl_2). For the photolytically active region $\lambda > 300$ nm, their inferred cross sections are significantly lower than reported in all earlier studies, prompting investigations of the impact of the cross sections reported by Pope et al. (2007) on observations of stratospheric ClO and polar ozone loss (von Hobe et al., 2007; Santee et al., 2008; Schofield et al., 2008; see also Section 2.2.2.2).

Laboratory studies of $\sigma_{\text{ClOOCl}}(\lambda)$ (Papanastasiou et al., 2009), the relative absorption spectrum (von Hobe et al., 2009), and the product of the cross section and quantum yield, $\sigma_{\text{ClOOCl}}(\lambda)\Phi(\lambda)$ (Chen et al., 2009; Lien et al., 2009; Jin et al., 2010; Wilmouth et al., 2009) have been published subsequent to Pope et al. (2007). These studies used complementary experimental techniques designed to reduce the uncertainty in the photochemistry of ClOOCl and to address the discrepancy between Pope et al. (2007) and earlier studies. The more recent laboratory studies either included a method for quantification of Cl_2 (von Hobe et al., 2009; Papanastasiou et al., 2009; Wilmouth et al., 2009) or used a mass-selected detection method independent of interference from Cl_2 and other impurities (Chen et al., 2009; Lien et al., 2009; Jin et al., 2010). Indeed, one of the salient points from the Stratospheric Processes and their Role in Climate (SPARC) initiative was the need for laboratory studies to address the sensitivity of $\sigma_{\text{ClOOCl}}(\lambda)$ to the presence of Cl_2 (e.g., Figure 2.2 of SPARC, 2009). All of these studies indicate that ClOOCl photolyzes much more rapidly than suggested by Pope et al. (2007). These studies have led to a reduction in the overall uncertainty in $\sigma_{\text{ClOOCl}}(\lambda)$ relative to the state of knowledge at the time of WMO (2007). However, only one of the new gas-phase studies (Papanastasiou et al., 2009) extended cross section measurements to $\lambda > 352$ nm and, thus, a higher level of uncertainty remains for the longer wavelengths.

von Hobe et al. (2009) measured a ClOOCl UV absorption spectrum, for λ between 220 and 400 nm, in a neon (Ne) matrix at ~ 10 K. Absolute cross sections were not measured, but cross sections were determined by scaling the measured spectrum to the peak value of the gas-phase cross section reported by JPL 06-2. When interpreting the von Hobe et al. (2009) spectrum it needs to be considered that a spectrum measured in a Ne matrix at 10 K is not directly comparable to a gas-phase spectrum at atmospheric temperatures (> 190 K). For the photolytically active region ($\lambda > 300$ nm), the matrix cross sections are significantly greater than the Pope et al. (2007) cross sections when both spectra are normalized to the same peak cross section. The cross sections reported by von Hobe et al. (2009) are somewhat less than the JPL 06-2

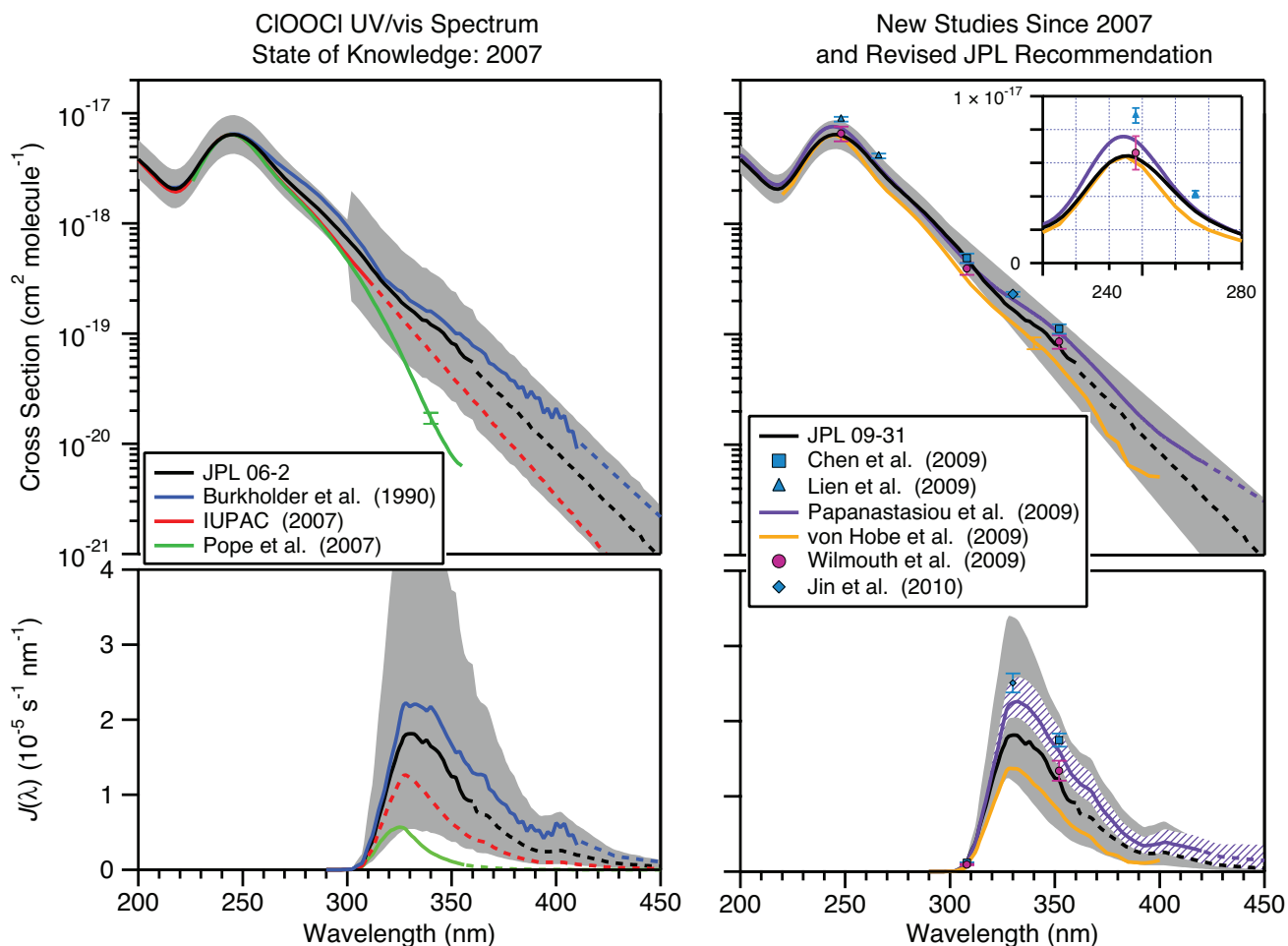


Figure 2-9. The left column summarizes the CIOOCI photochemical state of knowledge (UV/vis absorption spectra, $\sigma(\lambda)$, and representative photolysis rates, $J(\lambda)$, for the polar region) in 2007 and the right column gives the advancements since 2007 (as indicated in the legends). The cross sections for Chen et al. (2009), Lien et al. (2009), and Jin et al. (2010) at 200 K and Wilmouth et al. (2009) at 240 K were calculated from their reported values of $\sigma(\lambda)\Phi(\lambda)$ assuming $\Phi(\lambda) = 1$. The Pope et al. (2007) and Papanastasiou et al. (2009) spectra were recorded at ~ 200 K. Included for comparison is the von Hobe et al. (2009) spectrum recorded in a Ne matrix at ~ 10 K. The dashed lines represent wavelength regions where extrapolated cross section data rather than measured values were reported. The error bars shown were taken from the individual studies. The gray shaded regions in the upper panels are the error limits in $\sigma(\lambda)$ reported in JPL 06-2 and JPL 09-31. $J(\lambda)$ values were obtained for a solar zenith angle of 86 degrees at 20 km and the gray shaded regions are derived from the estimated uncertainties in $\sigma(\lambda)$ from JPL 06-2 and JPL 09-31. The hashed region was derived from the reported 2σ uncertainty in the Papanastasiou et al. (2009) absorption cross section data. Inset in the top right panel shows the absorption spectrum of CIOOCI in the wavelength region 220–280 nm. The choice of a linear y-axis allows a better visual assessment of the uncertainties in the peak absorption.

recommendation in the range 300–350 nm (Figure 2-9). However, significantly greater cross sections would result by scaling the von Hobe et al. (2009) absorption spectrum to a larger value of the peak cross section, as suggested by new observations (see below).

Chen et al. (2009) (308 and 351 nm), Lien et al. (2009) (248 and 266 nm), Jin et al. (2010) (330 nm), and Wilmouth et al. (2009) (248, 308, and 352 nm) have re-

ported values of $\sigma_{\text{CIOOCI}}(\lambda)\Phi(\lambda)$ at the wavelengths given in parentheses (Figure 2-9). The first three of these studies measured the loss of CIOOCI following photolysis in an effusive molecular beam. Assuming $\Phi(\lambda) = 1$, the derived cross sections are greater than those given in JPL 09-31 and agree most closely with those of Burkholder et al. (1990) and Papanastasiou et al. (2009). These three studies also report a weak temperature dependence to the

cross sections at 308, 330, and 352 nm. Wilmouth et al. (2009) used a discharge flow apparatus combined with Cl atom resonance fluorescence detection of photolysis products. Their reported values of $\sigma_{\text{ClOOCl}}(352 \text{ nm})$ at 240 K, assuming $\Phi(352 \text{ nm}) = 1$, are in good agreement with JPL 09-31. These values are a factor of 12 greater than Pope et al. (2007), a factor of 2.3 greater than the IUPAC (2007) recommendation, and $\sim 30\%$ lower than the value reported by Chen et al. (2009). The cross section measurements at several wavelengths from the effusive beam studies (e.g., Figure 5 of Lien et al., 2009) are in agreement with the spectrum reported by von Hobe et al. (2009).

Papanastasiou et al. (2009) reported $\sigma_{\text{ClOOCl}}(\lambda)$ from 200 to 420 nm at $\sim 200 \text{ K}$. The ClOOCl cross sections obtained at $\lambda > 300 \text{ nm}$ are in agreement with values reported by Burkholder et al. (1990). Their measurements agree with the results of Lin and co-workers and Wilmouth et al. (2009), assuming $\Phi(\lambda) = 1$, within the combined estimated measurement uncertainties (Figure 2-9). Their $\sigma_{\text{ClOOCl}}(\lambda > 300 \text{ nm})$ values are significantly greater than those of Pope et al. (2007) and are also somewhat greater than the values recommended in JPL 09-31.

The studies of Papanastasiou et al. (2009) and Lien et al. (2009) report ClOOCl absorption cross sections near the peak of the spectrum of $7.6^{+0.8}_{-0.5} \times 10^{-18} \text{ cm}^2 \text{ molecule}^{-1}$ at 244.25 nm and $(8.85 \pm 0.42) \times 10^{-18} \text{ cm}^2 \text{ molecule}^{-1}$ at 248.4 nm, respectively. These are greater than the JPL 09-31 recommended cross section of $6.4 \times 10^{-18} \text{ cm}^2 \text{ molecule}^{-1}$ at 244 nm. Wilmouth et al. (2009) report a value of $(6.6 \pm 1.0) \times 10^{-18} \text{ cm}^2 \text{ molecule}^{-1}$ at 248 nm, in close agreement with JPL 09-31. The spread in recent measurements of the peak absorption cross section is greater than the estimated uncertainty given by JPL 06-2 and many prior evaluations. Furthermore, the uncertainty limit of the Lien et al. (2009) peak cross section does not overlap with the uncertainty limits reported by Wilmouth et al. (2009) and Papanastasiou et al. (2009) (Figure 2-9). Scaling the absorption spectrum for ClOOCl to the peak cross section reported by Lien et al. (2009) would result in larger values for the ClOOCl cross section, leading to greater photolysis rates for ClOOCl as reported by various prior studies. However, even if the Pope et al. (2007) spectrum was scaled to the maximum cross section compatible with current measurements and the reported error bars, the resulting cross sections for $\lambda > 300 \text{ nm}$ would still be significantly less than reported in all other studies.

Papanastasiou et al. (2009) also reported estimated 2σ uncertainties in the photolysis rate constant of ClOOCl, J_{1b} , based on their cross section data (Figure 2-9). The uncertainty is a function of solar zenith angle (SZA) (i.e., the wavelength dependence of the ClOOCl spectrum) and was estimated to be $+40\%/-15\%$, $+50\%/-20\%$, and $+80\%/-25\%$ at SZAs of 80° , 86° , and 90° , respectively.

Better quantification of σ_{ClOOCl} for $\lambda > 350 \text{ nm}$ would reduce this level of uncertainty.

There is a consensus in the community that photolysis of ClOOCl occurs much faster than implied by the measured spectrum and the determined cross sections reported by Pope et al. (2007). The weight of new laboratory evidence suggests that values of the ClOOCl absorption cross section (σ_{ClOOCl}) in the atmospherically important region of wavelengths greater than 300 nm reported by Pope et al. (2007) are erroneous due to overcorrection of their measured spectra for the contribution of a Cl_2 impurity. The study by von Hobe et al. (2009) showed that ClOOCl exhibits an absorption feature similar to the spectral shape of the Cl_2 . Papanastasiou et al. (2009) demonstrated that the spectral interference by Cl_2 in the Pope et al. (2007) experiment led to an underestimate of σ_{ClOOCl} at $\lambda > 300 \text{ nm}$. The JPL 09-31 recommended value of Φ ($\lambda > 308 \text{ nm}$) is 0.9, although only limited experimental studies are available (Moore et al., 1999; Plenge et al., 2004). The understanding that polar ozone depletion is caused by reactions involving halogens has been reaffirmed by the numerous laboratory studies conducted since the publication of the paper by Pope et al. (2007).

2.2.2.2 FIELD OBSERVATIONS OF CHLORINE PARTITIONING

A large number of field studies over the past several decades have focused on the quantitative understanding of the partitioning of ClO and ClOOCl. The chemistry linking ClO and ClOOCl is thought to be especially simple. During daytime when temperatures are low enough that loss of ClOOCl occurs mainly by photolysis, the ratio $[\text{ClO}]^2/[\text{ClOOCl}]$ essentially equals J_{1b}/k_{1a} (e.g., Stimpfle et al., 2004) (brackets denote concentration of the species). During night after hours of darkness, when loss of ClOOCl occurs exclusively by thermal decomposition, this ratio equals k_{1c}/k_{1a} , which is the equilibrium constant (K_{EQ}) between ClO and ClOOCl. Since the rate of ozone loss by Cycle 1 is controlled by the parameters J_{1b} and k_{1a} , comparisons of measured and modeled daytime values of $[\text{ClO}]$ and $[\text{ClOOCl}]$ provide a quantitative measure of the speed of this cycle in the atmosphere. Thermal decomposition of ClOOCl completes a null cycle. Precise knowledge of K_{EQ} and an accurate measurement of nighttime $[\text{ClO}]$ enable $[\text{ClO}_x]$ ($[\text{ClO}_x] = [\text{ClO}] + 2 \times [\text{ClOOCl}]$) to be estimated in a manner that is independent of σ_{ClOOCl} .

Stimpfle et al. (2004) introduced a quantitative basis for comparison of modeled $[\text{ClO}]^2/[\text{ClOOCl}]$ to the measured value of this quantity at various SZAs during daytime, termed β , to quantify how well models represent the true value of J_{1b}/k_{1a} . The notion that β represents the value of J_{1b}/k_{1a} assumes that the partitioning of ClO and ClOOCl is dominated by the self-reaction of ClO and the

photolysis of ClOOCl (i.e., the temperature is low enough that thermal dissociation of ClOOCl is much slower than photolysis of ClOOCl). The Stimpfle et al. (2004) data were obtained at sufficiently low temperature that this assumption is valid given known chemistry. This data set is also notable for having achieved quantitative closure of the chlorine budget (Wilmouth et al., 2006).

Figure 2-10 (left) shows β , as a function of SZA, for the laboratory studies and recommendations of $\sigma_{\text{ClOOCl}}(\lambda)$

that existed in 2007 and provided enough spectral information for calculation of J_{1b} . The black dotted lines indicate the 1σ uncertainty in β based on measured [ClO] and [ClOOCl], whereas the error bars indicate the uncertainty in the modeled value of β (see caption). The β ratio indicates that the partitioning of ClO and ClOOCl is not consistent with J_{1b}/k_{1a} based on the Pope et al. (2007) measurement of $\sigma_{\text{ClOOCl}}(\lambda)$. The slight change in k_{1a} in JPL 09-31 does not affect this or any other conclusion of this

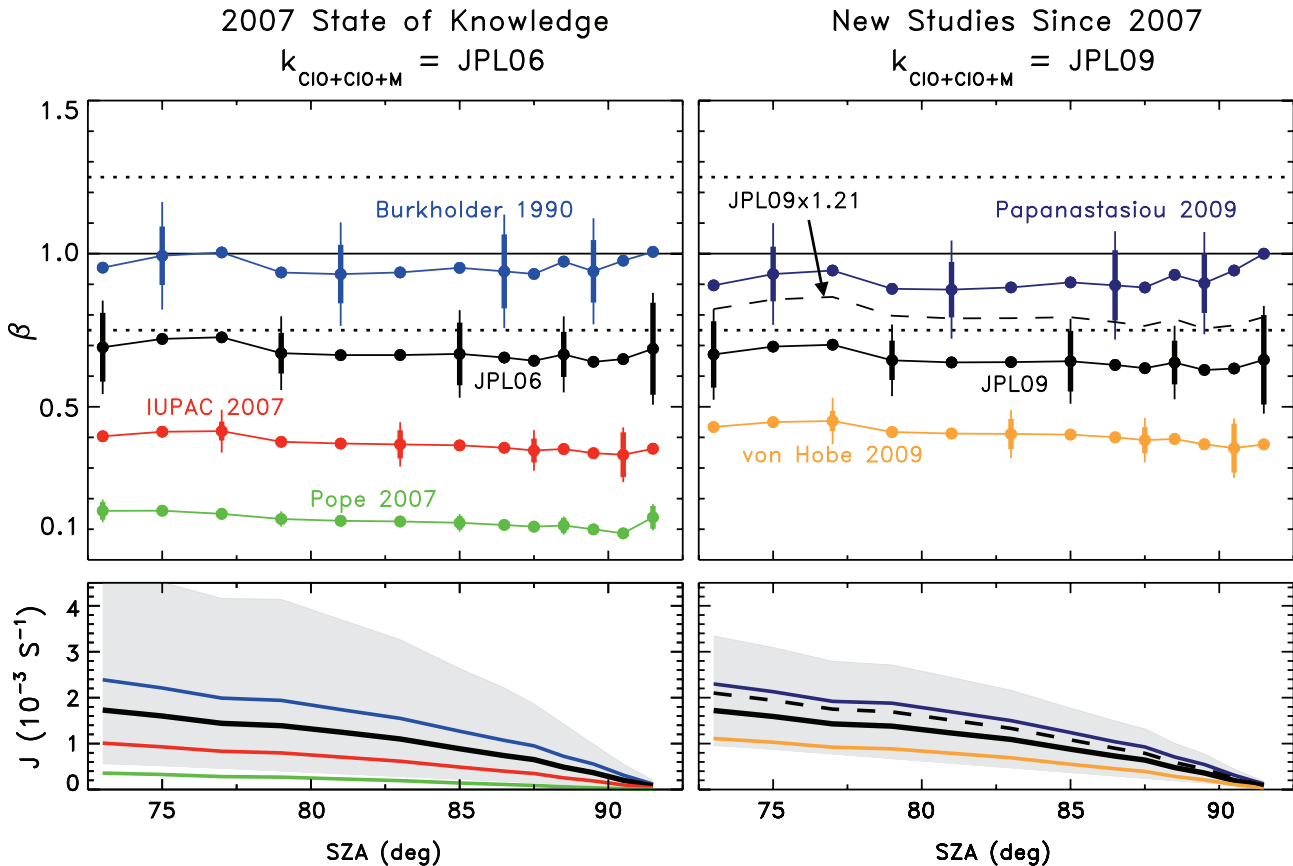


Figure 2-10. Analysis of β versus SZA, for all daytime measurements obtained during the SAGE III Ozone Loss and Validation Experiment (SOLVE), where $\beta = \{([\text{ClO}]^2 / [\text{ClOOCl}])_{\text{MODEL}}\} / \{([\text{ClO}]^2 / [\text{ClOOCl}])_{\text{OBSERVATION}}\}$. The left panel shows results for J_{1b} using values of $\sigma_{\text{ClOOCl}}(\lambda)$ available as of 2007 (same colors and studies as used in Figure 2-9). The right-hand side shows results for J_{1b} using values of $\sigma_{\text{ClOOCl}}(\lambda)$ available after 2007. The black dotted lines depict the $\pm 25\%$ uncertainty (1σ) in β attributable to uncertainties in observations of [ClO] and [ClOOCl]. The thick colored error bars denote the standard deviation about the mean for all of the individual determinations of β within a particular SZA bin. The thin error bar represents total uncertainty in the modeled component of β , found by combining the JPL 06-2 (left panel) or JPL 09-31 (right panel) uncertainty in k_{1a} in a root-sum-square fashion with the standard deviations. If the thin error bar falls within the range of the dotted lines, this is agreement of model and measurements to within combined 1σ uncertainties. The black dashed line on the right hand side depicts results of an illustrative calculation, the scaling of the JPL 09-31 value of $\sigma_{\text{ClOOCl}}(\lambda)$, which minimizes the distance between the scaled cross section and determinations of the peak cross section near 244 nm reported by Lien et al. (2009), Papanastasiou et al. (2009), and Wilmouth et al. (2009). The bottom panel compares J_{1b} as a function of SZA, for the altitude and surface albedo of the observations, for the various values of $\sigma_{\text{ClOOCl}}(\lambda)$ shown in the upper panels. After Stimpfle et al. (2004) and Figure 4-15 of WMO (2007).

section. As noted by Stimpfle et al. (2004), the cross section recommended by IUPAC (2007), based solely on the laboratory study of Huder and DeMore (1995), also yields a value of β inconsistent with field observations. The JPL 06-2 cross section is consistent with the field observations (overlap of error bars) and the Burkholder et al. (1990) value is most consistent (β near unity).

Figure 2-10 (right) shows a similar comparison for the laboratory measurements of $\sigma_{\text{ClOOCl}}(\lambda)$ published since 2007. Here, the JPL 09-31 value of k_{1a} is used. As noted above, von Hobe et al. (2009) normalized their spectrum to the JPL 06-2 peak cross section. Use of this cross section leads to values of β that are outside of the 1σ uncertainty on the measured value of $[\text{ClO}]^2/[\text{ClOOCl}]$. Clearly, if the von Hobe et al. (2009) spectrum were normalized to a higher peak, as perhaps is warranted by more recent measurements of the peak cross section, then β would lie closer to unity (β scales in an approximately linear fashion with the peak cross section). The JPL 09-31 spectrum and cross sections (unchanged since JPL 06-2, except for the uncertainty limits) is consistent with the field observations (overlap of error bars). The Papanastasiou et al. (2009) spectrum and cross sections results in the best agreement (value of β close to unity).

Many of the ClOOCl laboratory studies to date report the wavelength dependence of the ClOOCl spectrum normalized to an absolute value of the cross section near the peak. Typically, the JPL 09-31 peak value of $6.4 \times 10^{-18} \text{ cm}^2$ at 244 nm has been used (e.g., Huder and DeMore, 1995; Pope et al., 2007; von Hobe et al., 2009). The analysis presented in Figure 2-10 is complicated by the fact that three laboratory studies published in 2009 report peak absolute cross sections greater than the JPL 09-31 value (see Figure 2-9). To illustrate the importance of this scaling, the black dashed line in Figure 2-10 (right) shows the result of a calculation where the JPL 09-31 cross section has been multiplied by a factor of 1.21, which scales the peak cross section of JPL 09-31 to the mean of the cross section values near 244 nm reported by Lien et al. (2009), Papanastasiou et al. (2009), and Wilmouth et al. (2009). The JPL 09-31 cross section, scaled in this manner, provides a better representation of field data than found using the recommended cross section. We highlight this sensitivity to illustrate the importance of this laboratory parameter for quantitative understanding of halogen photochemistry in the polar vortex. The Pope et al. (2007) absorption spectrum for ClOOCl is entirely inconsistent with field data, for any reasonable amount of scaling.

The bottom panels of Figure 2-10 show the photolysis first-order rate constant (J_{1b}) as a function of SZA, for various cross section data sets. The shaded region shows propagation of the JPL 06-2 uncertainty (left) and the JPL 09-31 uncertainty (right). This figure reveals consistency

between laboratory studies of $\sigma_{\text{ClOOCl}}(\lambda)$ published after 2007 and the uncertainty given by JPL 09-31, which was not based on these studies. Absorption cross sections derived from the measurements of Lin and co-workers and Wilmouth et al. (2009) at specific wavelengths in the photolytically active region are, as shown in Figure 2-9, generally consistent with the values reported by Papanastasiou et al. (2009). Therefore, all new laboratory studies of $\sigma_{\text{ClOOCl}}(\lambda)$ conducted since 2007 lead to a consistent picture of good understanding of polar ozone chemistry, in contrast to the state of knowledge that existed upon the 2007 publication of the Pope et al. results.

Figure 2-11 extends Figure 2-10 by summarizing the high level findings for J_{1b}/k_{1a} from Stimpfle et al. (2004) as well as seven other studies, relative to the value of J_{1b}/k_{1a} recommended by JPL 06-2. Similar to the conclusions noted above, the seven other studies also suggest the value of J_{1b}/k_{1a} is as large as, or larger than, the value found using $\sigma_{\text{ClOOCl}}(\lambda)$ from JPL 06-2 and JPL 09-31. The field observations are most consistent with values of J_{1b}/k_{1a} found using the cross sections from Burkholder et al. (1990) and Papanastasiou et al. (2009) (the central portion of most of the blue bars lies closest to the arrow denoting J_{1b}/k_{1a} from these two laboratory studies). Both of these laboratory studies measured absolute values of the ClOOCl cross section.

Figure 2-11 shows that field data are not consistent with J_{1b}/k_{1a} found using the recommendation for $\sigma_{\text{ClOOCl}}(\lambda)$ from IUPAC (2007) (based on Huder and DeMore, 1995) or von Hobe et al. (2009) (both spectra scaled to JPL 06-2). As described above, three 2009 studies report values of the peak absolute cross section greater than given in JPL 06-2. The value of J_{1b}/k_{1a} found using the spectra reported by von Hobe et al. (2009) and Huder and DeMore (1995) will exhibit closer agreement with the field data if these spectra are scaled to peak cross section values reported in the new laboratory measurements, as was illustrated by scaling the JPL 09-31 recommended spectrum in Figure 2-10. At present the peak cross section and thus scaling factor has an uncertainty in the 20 to 30% range. Most of the literature is based on the JPL 06-2 estimate (identical to the JPL 09-31 value), which is at the low end of this range. If the peak cross section is revised by future evaluations, these revisions will likely indicate a greater role for ClO in polar ozone loss, since $d\text{O}_3/dt$ is roughly proportional to J_{1b} .

Finally, Figure 2-11 shows that the field data are not consistent with J_{1b}/k_{1a} found using $\sigma_{\text{ClOOCl}}(\lambda)$ from Pope et al. (2007). The range of uncertainty in k_{1a} (red bar) does not come close to encompassing the value of J_{1b}/k_{1a} found using $\sigma_{\text{ClOOCl}}(\lambda)$ from Pope et al. (2007) and the slight revision in k_{1a} in JPL 09-31 is inconsequential. No reasonable scaling of the Pope et al. (2007) spectrum will resolve the inconsistency with field data. An analysis of satellite observations reported by Santee et al. (2008) supports the

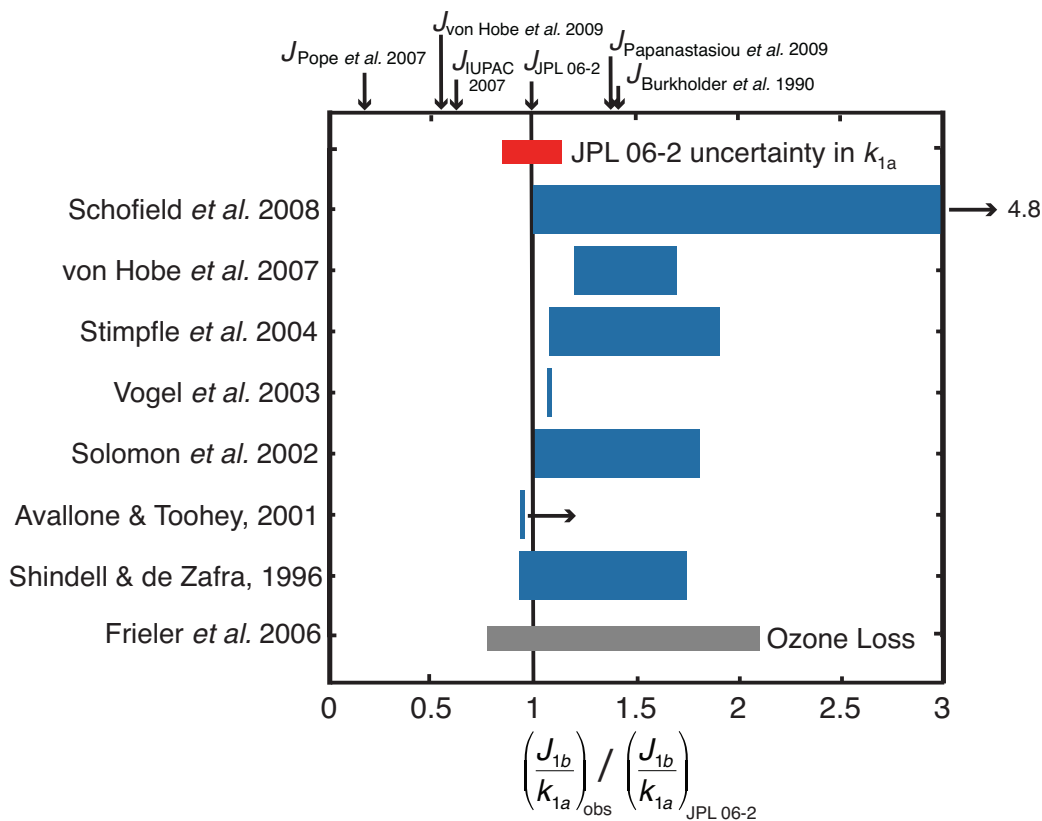


Figure 2-11. The ratio J_{1b}/k_{1a} inferred from analysis of daytime measurements of [ClO] or [ClO] and [ClOOCl] divided by the value of J_{1b}/k_{1a} from JPL 06-2, from various studies (blue bars; length of each bar represents range of uncertainty, generally 1σ). Horizontal black arrows denote lower limits for the ratio determined by two of the studies. The red bar shows the 1σ uncertainty in k_{1a} from JPL 06-2, evaluated at 190 K. The gray bar shows the value of J_{1b}/k_{1a} needed to match observed ozone loss in the Arctic and Antarctic vortices. The value of J_{1b}/k_{1a} using absorption cross sections of ClOOCl from various laboratory studies and data evaluations, relative to the JPL 06-2 value, is indicated by downward pointing arrows. The JPL 06-2 value of k_{1a} was used throughout the analysis because most of the cited papers relied on k_{1a} from JPL 06-2. The slight change in the high-pressure limit of this rate constant recommended by JPL 09-31 has a barely discernable effect on the appearance of this plot. Schofield et al. (2008) analyzed airborne in situ observations of [ClO] during the “self Match flight” of the European Polar Stratospheric Cloud and Lee Wave Experiment (EUPLEX) in the Arctic; von Hobe et al. (2007) examined airborne in situ observations of [ClO] and [ClOOCl] in the Arctic obtained during the SOLVE, EUPLEX, and Envisat Validation campaigns; Stimpfle et al. (2004) analyzed airborne in situ observations of [ClO] and [ClOOCl] in the Arctic obtained during the SOLVE campaign; Vogel et al. (2003) examined balloonborne in situ observations of [ClO] obtained in the Arctic during the Third European Stratospheric Experiment on Ozone (THESEO) 2000; Solomon et al. (2002) and Shindell and de Zafra (1996) analyzed ground-based observations of [ClO] over Antarctica; and Avallone and Toohey (2001) examined airborne in situ observations of [ClO] obtained in the Arctic during Airborne Arctic Stratospheric Expedition (AASE) I and II. Figure first published as Figure 3.1 of SPARC (2009).

conclusion that the Pope et al. (2007) spectrum cannot be reconciled with atmospheric measurements of [ClO].

Section 4.2.1.3 of WMO (2007) examined our understanding of calculated and observed polar ozone loss rates. A major advance is recognition that calculated polar ozone loss rates using values for $\sigma_{\text{ClOOC1}}(\lambda)$ from Pope et al. (2007) are not consistent with ozone loss rates derived from observations (von Hobe et al., 2007; Santee et al., 2008; Schofield et al., 2008; Kawa et al., 2009; SPARC, 2009). A detailed summary is given in SPARC (2009). The gray bar in Figure 2-11 summarizes the understanding articulated in these studies: ozone loss rates derived from observations are consistent with values of J_{1b}/k_{1a} ranging from slightly less than that obtained using the JPL 06-2 recommended cross sections to about a factor of 2 larger than that found using JPL 06-2, with best agreement found for the Burkholder et al. (1990) and Papanastasiou et al. (2009) spectrum and cross sections.

2.2.2.3 OTHER ISSUES RELATED TO POLAR OZONE CHEMISTRY

Kawa et al. (2009) used Monte Carlo model calculations to evaluate the impact and significance of the estimated uncertainties in the kinetic parameters given in JPL 06-2 on polar stratospheric ozone loss. The simulations indicate that the most of the uncertainty in the calculated ozone loss and the rate of ozone loss is due to the uncertainty in the ClOOC1 photolysis reaction. Uncertainties in the BrO + ClO reaction rate coefficient and its product branching ratio were also found to be important. Canty et al. (2005) note an inconsistency between theory and observation of nighttime chlorine dioxide (OCIO) that could be resolved by higher yields of the branches of BrO + ClO that lead to ozone loss. Uncertainties in the rate coefficients for the reactions $\text{ClO} + \text{OH} \rightarrow \text{HCl} + \text{O}_2$ and $\text{Br} + \text{H}_2\text{CO} \rightarrow \text{HBr} + \text{HCO}$ were found to be significant, but to have a smaller overall impact on the calculated polar ozone loss. The uncertainties in these processes were re-evaluated by the NASA JPL Data Panel and reductions in the uncertainties were made in JPL 09-31.

Theoretical calculations by Matus et al. (2008) found the ClClO₂ isomer was more stable than ClOOC1 by 3.1 kcal mol⁻¹ at 298 K. However, as described in SPARC (2009), observational evidence suggests ClClO₂ is not present in appreciable quantities during times of chlorine activation in the Arctic vortex. SPARC (2009) concluded that if unknown chemistry plays a role for the polar ozone loss mechanism, it can only be a minor modification of known mechanisms.

Analyses of field observations by von Hobe et al. (2007), Wetzal et al. (2010), and Santee et al. (2010) are somewhat more consistent with the revised JPL 09-31 recommendation for K_{EQ} at temperatures below ~210 K

than with the JPL 06-2 recommendation. Observations obtained during nighttime conditions when photolysis is negligible all point to higher abundances of ClO and lower abundances of ClOOC1 than found in models using JPL 06-2 kinetics. However, uncertainty in K_{EQ} , which is believed to drive nighttime chemistry, has no bearing on the rate of polar ozone depletion (e.g., Kawa et al. (2009) and references therein). Nevertheless, there is interest in reducing the uncertainty in K_{EQ} because accurate knowledge of this quantity will improve estimates of [ClO_x] from nighttime observations of [ClO]. Such improvement is needed, for example, because representation of polar ozone chemistry in chemistry and transport models (CTMs) and chemistry-climate models (CCMs) is better evaluated by comparing modeled and measured [ClO_x] rather than comparing modeled and measured [ClO]. If [ClO] is used, one must factor in SZA and temperature, which greatly complicates the comparison (Chapter 6 of SPARC CCMVal, 2010).

2.2.3 Polar Stratospheric Cloud Processes

As discussed in previous WMO reports, heterogeneous reactions on the surfaces of stratospheric particles at cold temperatures convert chlorine reservoir species that do not react with ozone, such as hydrogen chloride (HCl) and chlorine nitrate (ClONO₂), to chlorine radical species that lead to catalytic ozone destruction (Solomon et al., 1986). Liquid-phase binary sulfuric acid/water (H₂SO₄/H₂O) droplets, commonly known as background stratospheric aerosols, are ubiquitous throughout the stratosphere. Under cold conditions, these background aerosols take up nitric acid (HNO₃) and H₂O (Carslaw et al., 1994; Tabazadeh et al., 1994) and evolve into ternary HNO₃/H₂SO₄/H₂O droplets, commonly referred to as supercooled ternary solution (STS) polar stratospheric clouds (PSCs). PSC particles may also take the form of H₂O ice and solid hydrates of nitric acid, likely nitric acid trihydrate, or NAT (Voigt et al., 2000). Particle ensembles in the polar winter stratosphere are primarily mixtures of liquid (binary or ternary) droplets and solid particles (NAT and H₂O ice) in varying sizes and number densities (e.g., Toon et al., 2000; Biele et al., 2001; Drdla et al., 2003). Chlorine activation rates on stratospheric particles are dependent on the uptake coefficient of the particle and the particulate surface area density (SAD) (Lowe and MacKenzie, 2008). Both the uptake coefficients and the available surface area of the liquid particles are generally much higher than that of NAT PSC particles, making liquid particles much more efficient in chlorine activation (Portmann et al., 1996; Lowe and MacKenzie, 2008). Liquid particles also increase ozone loss by extending both the height range (Hofmann and Oltmans, 1993) and the season over which heterogeneous chemistry can occur (Portmann et

al., 1996). Solid particles play an important indirect role in ozone depletion by their influence on the abundance of gas-phase nitrogen. Formation and sedimentation of large NAT particles (Waibel et al., 1999; Fahey et al., 2001) can irreversibly redistribute HNO_3 (denitrify) in the polar stratosphere, allowing the ozone depletion process to continue for a longer period by delaying the reformation of the chlorine reservoir ClONO_2 .

2.2.3.1 NEW OBSERVATIONAL DATA SETS

Since the previous Assessment, the PSC observational database has been greatly expanded by measurements from the Cloud-Aerosol Lidar and Infrared Pathfinder Satellite Observation (CALIPSO) satellite that was launched in 2006. Measurements from the polarization-sensitive lidar on CALIPSO (Pitts et al., 2007; Noel et al., 2008) provide comprehensive daily information on the occurrence of PSCs in both the Arctic and Antarctic over the

entire polar region, including the polar night that cannot be sampled by solar occultation instruments. The general climatology of PSCs included in previous Ozone Assessments (e.g., WMO, 1995; WMO, 1999) was established from long-term solar occultation data records (e.g., Poole and Pitts, 1994; Fromm et al., 2003), which were the only available data source at that time. Pitts et al. (2007) compared the PSC frequency observed by CALIPSO in 2006 over the entire Antarctic region (50°S – 82°S) with the PSC frequency derived by subsampling the CALIPSO database only at the time-varying latitudes observed by the SAM II (Stratospheric Aerosol Measurement II) solar occultation sensor, which ranged from 65°S in June to 80°S in September. As shown in Figure 2-12, the temporal distribution of PSCs derived from solar occultation data is not representative of the polar region as a whole. For example, in early June the solar occultation sensor samples only near the edge of the vortex ($\sim 65^\circ\text{S}$) and underestimates the PSC frequency of the vortex as a whole. In September the

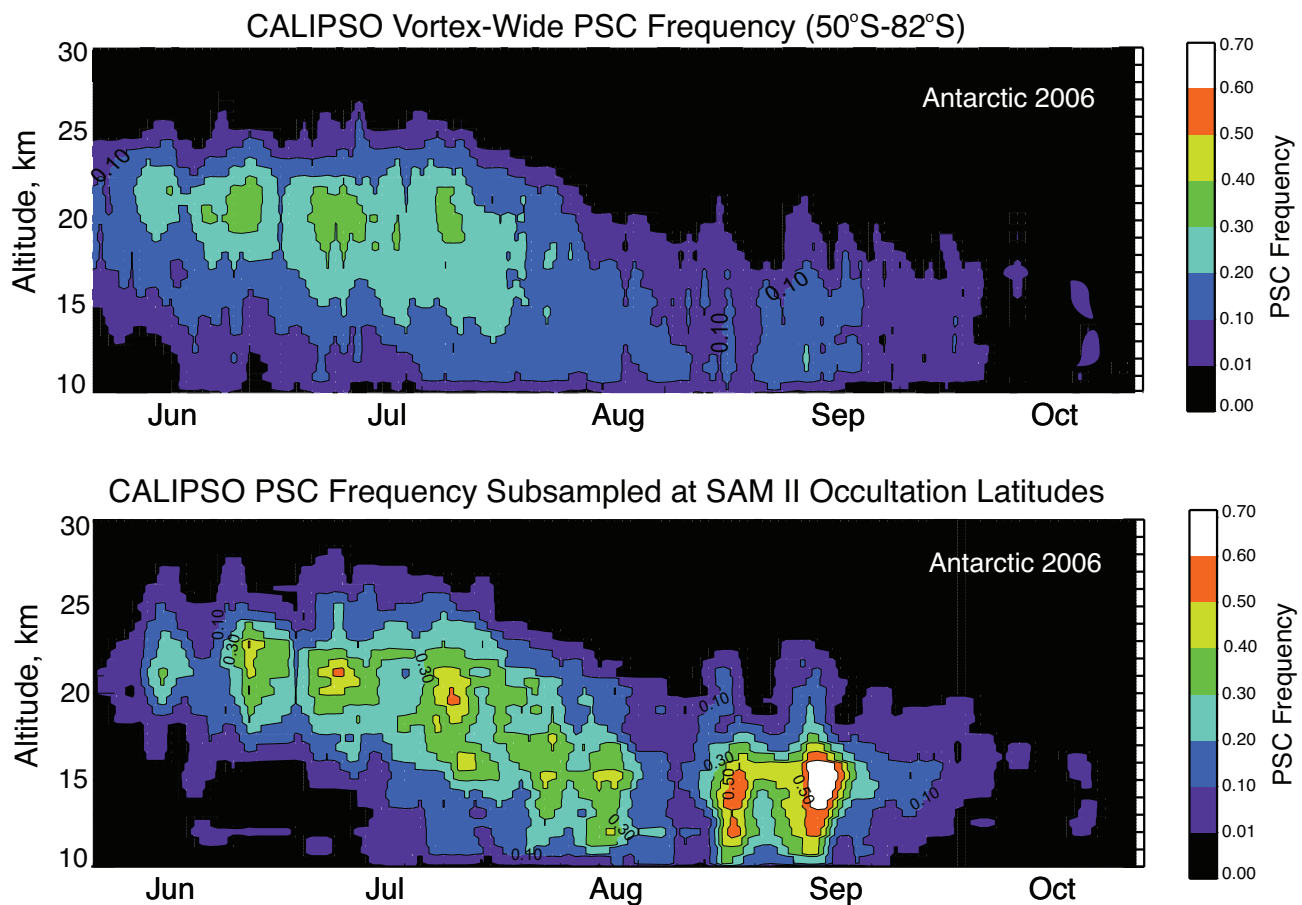


Figure 2-12. PSC frequency for the 2006 Antarctic season (adapted from Pitts et al., 2007). Top panel: PSC frequency as observed by CALIPSO over the entire polar region (50°S – 82°S). Bottom panel: PSC frequency that is deduced by subsampling the CALIPSO data set at measurement latitudes seen by a solar occultation instrument (e.g., SAM II).

occultation sensor samples only near the core of the vortex (80°S) and hence overestimates the PSC frequency of the vortex as a whole. CALIPSO provides a more accurate representation of PSC occurrence on a day-by-day basis over the entire polar region than the historical solar occultation-based observations. But on a season-long basis, both CALIPSO and the historical solar occultation data show that PSCs occur much more frequently and over a longer time period in the Antarctic than in the Arctic.

Optical modeling results (Pitts et al., 2009) suggest that from an ensemble point of view, CALIPSO PSC detection limits are as good as or better than those of historic solar occultation sensors. The ensemble detection limits are also comparable to those of ground-based and airborne lidars, except that CALIPSO cannot resolve very tenuous PSCs with the optical characteristics of a mixture of binary liquid aerosols and very low number densities ($<3-5 \times 10^{-4} \text{ cm}^{-3}$) of NAT particles. For reference, NAT particle surface areas in these PSCs are $<0.1 \mu\text{m}^2 \text{ cm}^{-3}$, which is about 10% of the surface area of the liquid binary aerosols and $<1\%$ of the surface area of a fully developed STS PSC.

2.2.3.2 PSC COMPOSITION

A more complete picture of PSC occurrence and composition has emerged since the previous Assessment. Pitts et al. (2009) examined the seasonal evolution of PSC composition utilizing CALIPSO lidar observations and found that the vast majority of PSC observations over the Antarctic from mid-June until mid-September consisted of liquid/NAT mixtures, while liquid STS clouds were predominant in the Antarctic in late May through early June and again in late September and October. Ice PSCs were much more episodic in nature and accounted for only about 10% of all CALIPSO PSC observations in the Antarctic. Pitts et al. (2009) found that mixtures containing NAT particles in higher number densities/volumes (similar to the so-called type 1a enhanced PSCs) are much more common in the Antarctic than in the Arctic, while the relative frequency of liquid STS clouds is higher in the Arctic than in the Antarctic. These results are generally consistent with the climatologies from ground-based lidars (Adriani et al., 2004; Maturilli et al., 2005; Blum et al., 2005; Massoli et al., 2006).

The spaceborne Michelson Interferometer for Passive Atmospheric Sounding (MIPAS) on Envisat, a limb-sounding infrared spectrometer with full coverage of the Arctic and Antarctic regions, also provides information on PSC composition. Höpfner et al. (2006a) analyzed MIPAS measurements of mid-IR emissions by PSCs during the 2003 Antarctic winter and found evidence of NAT, STS, and water ice clouds. Information on PSC composition is derived from CALIPSO and MIPAS data using

fundamentally different approaches, yet the results are consistent (Höpfner et al., 2009).

2.2.3.3 PSC FORCING MECHANISMS

Several studies have examined formation mechanisms for PSCs. In the NH, Felton et al. (2007) showed that wave-induced temperature perturbations account for about 11% of PSC detections in the Arctic during the SOLVE-THESEO campaign. In the Antarctic, recent studies provide evidence that mountain wave PSCs may be a significant source of NAT particles that can be transported throughout the Antarctic polar vortex. Höpfner et al. (2006b) attribute the large-scale outbreak of NAT particles observed by MIPAS during June 2003 to heterogeneous nucleation on ice in the cooling-phases of large-amplitude mountain waves over the Antarctic Peninsula and Ellsworth Mountains. Eckermann et al. (2009) corroborate this hypothesis, showing that a small region of mountain wave activity over the Antarctic Peninsula on 10–14 June likely served as the source of this circumpolar NAT outbreak. Eckermann et al. (2009) conclude that this is observational evidence of the “mother cloud” theory, which posits that vortex-wide NAT formation and growth are driven by ice formed in mountain wave activity. Noel et al. (2009) used CALIPSO data to examine wave-induced PSCs with near-unity optical depths, concluding that this relatively rare class of PSC can lead to widespread NAT and ice particles downstream from the mountain wave. Based on a combination of Polar Ozone and Aerosol Measurement (POAM) III aerosol extinction measurements and Challenging Minisatellite Payload GPS Radio Occultation (CHAMP GPS/RO) temperature measurements, McDonald et al. (2009) found that gravity wave-induced temperature perturbations may explain enhanced PSC incidence over the Antarctic Peninsula in June, while they contribute to only about 15% of the PSC observations later in the winter at higher latitudes. Innis and Klekociuk (2006), using lidar observations over Davis, Antarctica, also found that gravity wave perturbations influence PSC formation about 15% of the time. Wang et al. (2008) propose a different Antarctic PSC formation mechanism based on their analysis of observations by the NASA A-train satellites that showed two thirds of PSCs over west Antarctica and one half of PSCs over east Antarctica can be related to deep tropospheric cloud systems.

PSCs both influence and are influenced by climate change. Randel et al. (2009) report large trends in temperature in the lower stratosphere in spring. David et al. (2010) show that trends in the mean temperature and also trends in extreme temperatures are important for prediction of PSC occurrence. The long-term trend in global-mean lower stratospheric temperatures reported by Randel et al. (2009) is strongly driven by changes in stratospheric

ozone. Thus, both stratospheric cooling and the increase in PSC occurrence may reverse substantially as ozone will recover in the future. This conclusion is supported by model predictions by Hitchcock et al. (2009).

2.2.3.4 USE OF PROXIES TO REPRESENT PSC PROCESSES

PSC occurrence is often represented in modeling and diagnostic studies of polar ozone loss by simple thermodynamic proxies. A proxy used frequently in the past is that PSCs are present if the ambient temperature is below T_{NAT} , the theoretical threshold temperature for NAT existence. CALIPSO provides the first observational estimates of vortex-wide PSC areal coverage that can be used to directly assess the validity of simple thermo-

dynamic proxies for PSC occurrence. Pitts et al. (2007) showed that the use of T_{NAT} alone is a poor quantitative proxy for PSC occurrence and significantly overestimates the PSC areal extent; Figure 2-13 illustrates this point for the 2007 Antarctic season. The observation that T_{NAT} is not an accurate proxy for PSC occurrence is not surprising since analyses of CALIPSO and MIPAS data, as well as earlier studies, suggest that PSCs are primarily mixtures of liquid droplets and solid particles. However, as discussed below in Section 2.2.4, the empirical relationship between ozone loss and the volume of vortex air below T_{NAT} indicates that T_{NAT} is a useful gauge of low stratospheric temperatures that trigger chlorine activation and ozone loss, even though the activation is primarily occurring on liquid particles.

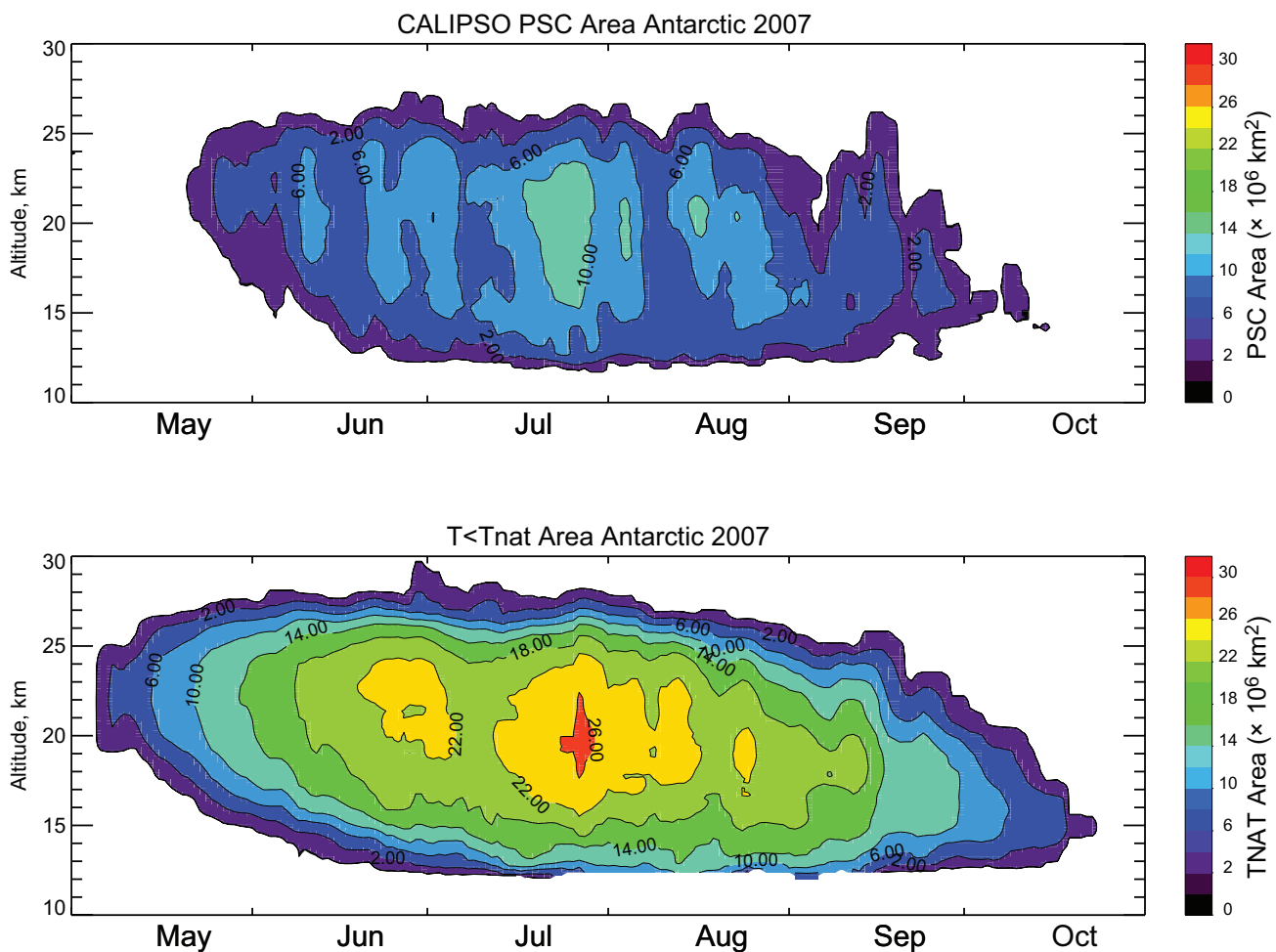


Figure 2-13. Daily time series of CALIPSO PSC area (km^2) versus area with $T < T_{\text{NAT}}$ for the 2007 Antarctic season (adapted from Pitts et al., 2007, and Pitts et al., 2009). Note that very tenuous PSCs containing a mixture of binary liquid aerosols and very low number densities ($<3\text{--}5 \times 10^{-4} \text{ cm}^{-3}$) of NAT particles are below the CALIPSO ensemble detection threshold. NAT particle surface areas in these PSCs are $<0.1 \mu\text{m}^2 \text{ cm}^{-3}$, or about 10% of the surface area of the liquid binary aerosols and $<1\%$ of the surface area of a fully developed STS PSC.

2.2.4 Arctic Polar Temperatures and Ozone

The annual cycle and variability for the minimum temperature poleward of 50° latitude in the Northern Hemisphere for 1979–2004 was shown in WMO (2007) (Newman and Rex et al., 2007, their Figure 4-1, top panel). The temperatures at 50 hPa for recent years fall within this range of variability. Temperatures in the Arctic winter stratosphere exhibit a high degree of natural variability. The winters 2006/2007 and 2007/2008 were among the ten coldest winters from 1965 to present. The 2008/2009 winter was very cold in midwinter but PSC conditions were terminated by a strong warming in late January.

Polar ozone during recent Arctic winters remains low compared with values observed during the 1980s and continues to strongly vary interannually (Figure 2-14, top panel). The figure shows the minimum total ozone over the polar cap for March (calculated as the minimum of the daily average column ozone poleward of 63° equivalent latitude). This is an indicator of polar ozone loss that shows a reasonable correlation with observed chemical ozone depletion (Müller et al., 2008). In the years since WMO (2007), the minimum spring ozone values over the Arctic polar cap remained in a range comparable with values prevailing since the early 1990s (Figure 2-14, top panel). This indicates that substantial chemical loss continues to occur in cold Arctic winters.

Arctic winter and spring ozone loss has varied between 2007 and 2010, but remained in a range comparable to the values that have prevailed since the early

1990s. Chemical ozone destruction on the order of 100 DU (about 80% of the values derived for the record cold winters of 1999/2000 and 2004/2005) is deduced for both Arctic winters 2006/2007 and 2007/2008 (derived from ozonesonde measurements following the approach described by Rex et al., 2006). A strong reduction in column ozone during these winters is in accordance with strong chemical destruction at 475 K in mid-March reported for 2006/2007 based on Odin data (Rösevall et al., 2007) and 2007/2008 based on Microwave Limb Sounder (MLS) data (Kuttippurath et al., 2009). Reliable ozone loss estimates are not possible for the Arctic winter 2008/2009 because a strong midwinter warming in late January led to extensive mixing of air from low latitudes with the polar vortex air.

Tegtmeier et al. (2008) showed that the variability of (1) chemical loss of ozone in the Arctic and (2) the amount of ozone transported into the Arctic during winter each contribute about half of the observed variability of high latitude total ozone during spring (Figure 2-15). The supply of ozone due to transport has so far usually been larger than the chemical loss (with possibly very small net loss only in 1995, 1996, and 2000) such that the total ozone column has not declined in the course of Arctic winters and the extreme ozone anomalies associated with the Antarctic ozone hole are not observed in any long-term Arctic record (Solomon et al., 2007). Tegtmeier et al. (2008) also showed that these terms are correlated and variability in both is driven by variability in wave driving from the troposphere, making both terms sensitive to potential changes in wave driving due to climate change.

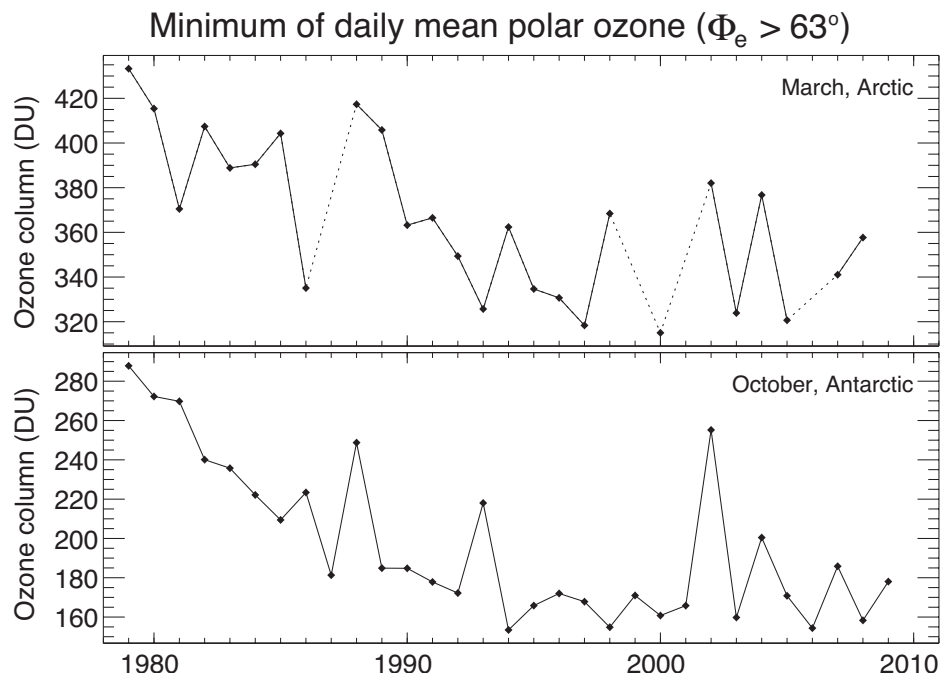


Figure 2-14. Time series of minimum total ozone (Dobson units) over the polar cap, for March in the Arctic (top panel) and October in the Antarctic (bottom panel), calculated as the minimum of daily average column ozone poleward of 63° equivalent latitude. Winters in which the vortex broke up before March (1987, 1999, 2001, and 2006) are not shown for the Arctic time series. Figure adapted from Müller et al. (2008), updated using the NIWA combined total column ozone database (version 2.7).

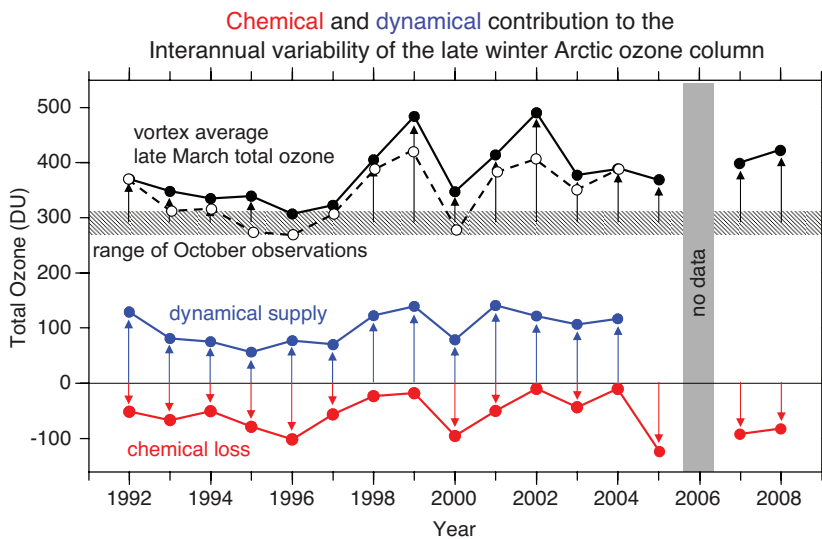


Figure 2-15. Interannual variability of the observed late winter (March) total ozone column (Dobson units) averaged over the polar vortex (black), the dynamical supply of ozone to the polar vortex (blue) and the chemical loss of ozone over the winter inside the vortex (red). The hashed range around 290 DU illustrates the very limited range of early winter (October) variability. The dashed black line close to the late winter observations is the sum of early winter ozone, dynamical supply and chemical loss (updated from Tegtmeier et al., 2008; based on ozonesonde data combined with meteorological data and transport modeling).

Several diagnostics use volume of vortex air below T_{NAT} , the theoretical threshold temperature for NAT existence for typical values of stratospheric water and nitric acid mixing ratios (Rex et al., 2004; Rex et al., 2006; Tilmes et al., 2004). This volume has commonly been referred to as V_{PSC} . Because V_{PSC} calculated in this way is not a good proxy for the existence of NAT particles (see Section 2.2.3.4 above), other proxies for the onset of polar heterogeneous chlorine activation have been considered that involve also the surface area density of binary sulfate aerosol particles, e.g., Tilmes et al. (2008a) consider the potential for activation of chlorine (PACl). However, observations show that T_{NAT} may still be a useful proxy because the onset of chlorine activation does not necessarily occur on NAT particles (Toohey et al., 1993; SPARC, 2009). Therefore, it is meaningful to consider a relation between ozone loss and such calculated values of V_{PSC} . The ozone loss observed in Arctic winters since the previous Assessment falls along the relation between chemical ozone loss and V_{PSC} that was discussed in the previous Assessment (WMO 2007, Figure 4-13).

Rex et al. (2006) noted a tendency toward higher extreme values in the overall volume of air at temperatures below the PSC threshold (V_{PSC}) over the past four decades, i.e., a cooling of the “cold” Arctic winters. An update of this relation is shown in Figure 2-16. Values of V_{PSC} since WMO (2007) were all less than that computed for NH winter 2004/05, but on a statistical basis established over the past four decades, a new maximum occurs about only once in five-year intervals. Therefore, it is not possible to draw a conclusion about the continuation of the changes in the severity of extreme values based on absence of a new record V_{PSC} in the past four years. It is notable that

three of the past four winters had V_{PSC} values in the upper 25% of the long-term distribution even though a midwinter major warming occurred in all of the winters since the previous Assessment.

2.2.5 Antarctic Polar Temperatures and Ozone

Winters remain very cold in the Antarctic, and the seasonal cycles for the minimum temperatures poleward of 50°S for recent years fall within the range of variability for 1979–2005 that is shown in the bottom panel of Figure 4-1 of WMO (2007). Exceptional dynamical activity and associated warming, like that in Antarctic winters 2002 and 2004, has not occurred since the previous Assessment, but in 2006 the springtime increase in the minimum temperature took place slightly later than usual.

The minimum of total ozone over the polar cap for October (calculated as the minimum of the daily average column ozone poleward of 63° equivalent latitude) has remained approximately at the low levels observed in the mid-1990s until 2009 (Figure 2-14 bottom panel). Chemical ozone loss in the Antarctic since the previous Assessment remained stable at the level of the mid-1990s. Ozonesonde observations at South Pole (Hofmann et al., 2009a) consistently indicate that, with the exception of the years 2002 and 2004, more than 90% of the ozone is removed each year since the mid-1990s, at about 18 km (~ 70 hPa). Maximum ozone losses at this altitude reach 99% (Solomon et al., 2005; Solomon et al., 2007). The lowest ozone partial column (2 DU) in the altitude range 14–21 km observed at South Pole (in the time period 1986–2007)

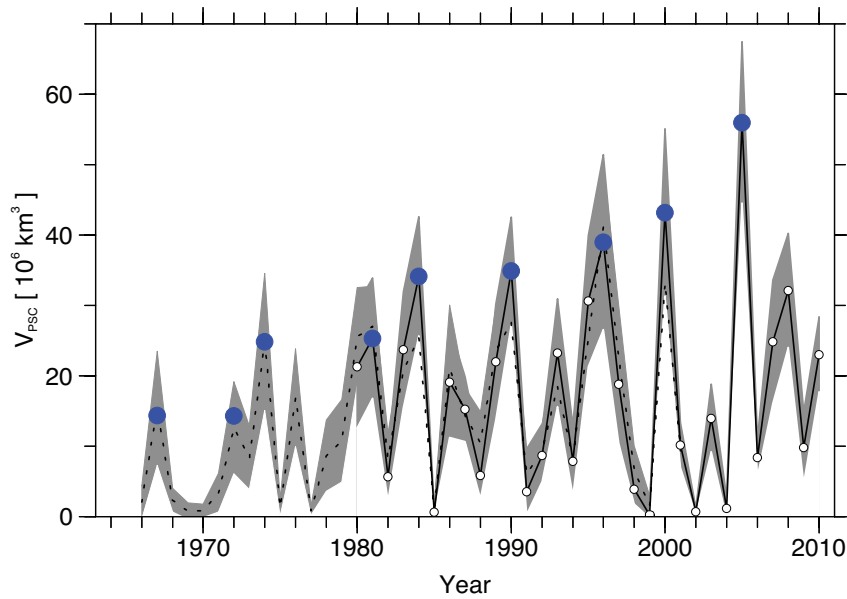


Figure 2-16. Evolution of V_{PSC} (km^3) for the Arctic over the past four decades obtained from European Centre for Medium-Range Weather Forecasts (ECMWF) and Free University of Berlin (FUB) data. The blue dots represent the maximum values of V_{PSC} during five-year intervals. The dotted line is based on radiosonde analyses of the FUB, and the solid line is ECMWF ERA-15 data extended by operational analyses. The gray shading represents the uncertainty of V_{PSC} assuming a 1-K uncertainty of the long-term stability of radiosonde temperatures. Updated from Figure 4-3 of WMO (2007) and Rex et al. (2004).

occurred in 2006 (Hofmann et al., 2009a). The chemical ozone loss in the Antarctic vortex core for the altitude range 350–550 K deduced from satellite data for the period 1992–2005 is ~ 130 DU, more than found for even the coldest Arctic winters (Tilmes et al., 2006).

In summary, ozone loss during Antarctic winters remained stable with little year-to-year variability since the previous Assessment. This is expected since moderate changes in EESC are not expected to have a detectable effect on measures of Antarctic ozone loss (WMO 2007; Newman et al., 2006; see also Section 2.4.5 for further discussion). Since about 1997 the ODS amounts have been nearly constant and the depth and magnitude of the ozone hole have been controlled by variations in temperature and dynamics. The October mean column ozone within the vortex has been about 40% below 1980 values for the past fifteen years.

2.2.6 The Onset of Antarctic Ozone Depletion

The average total ozone poleward of 63° latitude in March (NH) and October (SH) is compared to an average of the observations between 1970 and 1982 to provide an indication of the amount of ozone lost each year due to polar processes (Figure 2-8). This choice of reference level is somewhat arbitrary. The 1970–1982 average includes observations from 1970–1972 and 1979–1982 in the SH and from 1971–1972 and 1979–1982 in the NH. These observations and data from ground-based instruments at several locations suggest that ozone de-

creased between the early 1970s and the early 1980s in both hemispheres, but computing a trend from the satellite observations is not meaningful because of the data gaps. The ground-based data records have smaller gaps but exhibit year-to-year variations and are not representative of the entire polar region. A near-continuous, near-global record of satellite observations of total ozone has been available only since the Nimbus 7 Total Ozone Mapping Spectrometer (TOMS) instrument began taking data late in 1978.

2.3 SURFACE ULTRAVIOLET RADIATION

2.3.1 State of Science in 2006

Chapter 7 of the 2006 Assessment (Bais and Lubin et al., 2007) explored factors that affect surface UV irradiance, examined the methods of assessing this irradiance (ground-based measurements, satellite retrievals, and radiative transfer modeling), and reviewed measurement series, reconstructions, and numerical models of future scenarios to identify past and potential future changes in surface UV irradiance. Much of our understanding of UV radiative transfer remains valid today, while updates since 2006 follow later in the section.

The influence of stratospheric ozone on the transmission of short wavelength UV radiation through the atmosphere is well understood. Since the ozone-related change in UV radiation is wavelength dependent (becoming negligible at wavelengths greater than 340 nm), the way in which UV radiation is defined or measured (e.g.,

spectral, UV-B (280–315 nm) waveband, UV-B + UV-A (315–400 nm), or biologically weighted UV) determines its sensitivity to ozone. Broadband erythemal radiometers are the most widespread instruments for measuring surface UV irradiance, but they cannot identify the contribution of individual wavelengths to the observed change in erythemal irradiance and so cannot separate ozone-induced changes from other influences on UV radiation.

For UV effects for which there is a known action spectrum, e.g., erythemally weighted UV, the sensitivity

to ozone changes is often expressed as a radiation amplification factor (RAF) (see Box 2-1), which differs from the monochromatic RAF.

Clouds, aerosol, surface albedo, and ozone all affect surface UV radiation. For many locations, the observed changes in UV radiation are influenced by changes in all of these. The importance of each varies with latitude, climate, and the amount of atmospheric pollution at each site. Cloud transmission is the greatest and most changeable atmospheric determinant of UV variability at

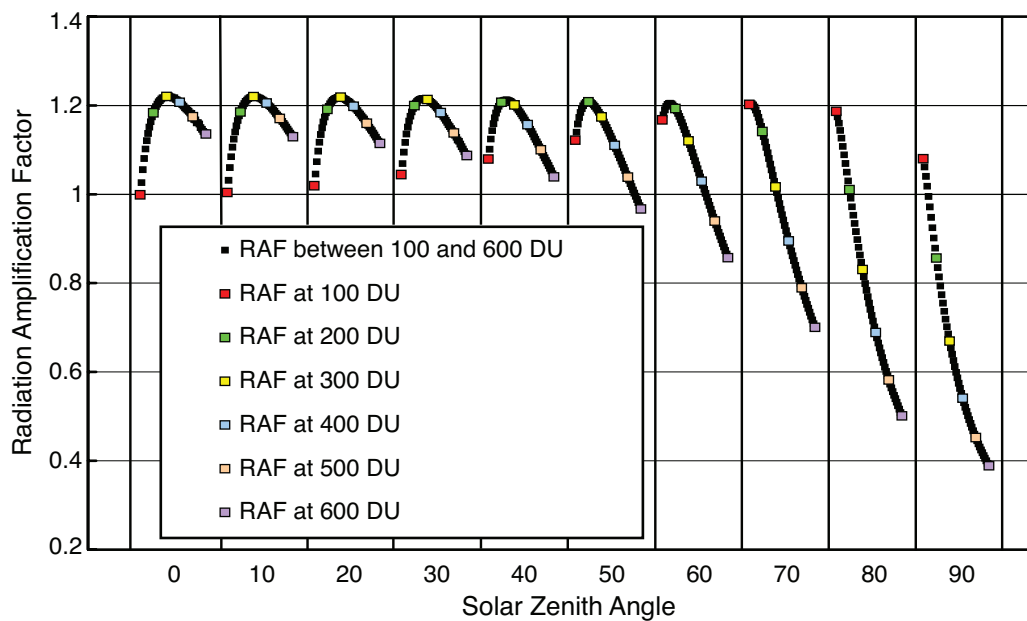
Box 2-1. Radiation Amplification Factor for Erythemal Irradiance

The relationship between change in total column ozone (O_3) and change in biologically effective radiation, e.g., erythemal irradiance (E), can be quantified using the radiation amplification factor (RAF) (Booth and Madronich, 1994). For example, $RAF = 1.5$ means that a 1% decrease in ozone will lead to a 1.5% increase in the biologically effective radiation. For small fractional changes in ozone (of the order of 10%) the RAF for erythema can be defined as

$$RAF = -\left(\frac{\Delta E}{E}\right) / \left(\frac{\Delta O_3}{O_3}\right)$$

where ΔE and ΔO_3 are the respective changes of erythemal irradiance and column ozone.

As the relationship between ozone and erythemal irradiance is nonlinear, the RAF is not a constant in all conditions but depends on factors that change the shape of the solar spectrum, primarily solar zenith angle and ozone column, as illustrated in Figure 1. While for solar zenith angles (SZAs) from 0° to 50° and typical midlatitude ozone the RAF for erythema is 1.1 ± 0.1 , for larger SZAs and large total ozone values the RAF gradually decreases.



Box 2-1, Figure 1. Radiation amplification factor for erythemal irradiance as a function of SZA, for several total column ozone amounts. RAF values were calculated in SZA-steps of 10° and steps of 10 DU in ozone column. The first value in each SZA-bin refers to 100 DU; the last value refers to 600 DU (from WMO, 2008).

the surface. Although UV radiation is reduced slightly less than visible radiation by clouds, heavily overcast conditions can still reduce surface UV irradiance by 90%. Broken-cloud conditions can produce short-term enhancements in UV irradiance up to 25% over clear-sky conditions. Clouds vary on many timescales and thus hinder attempts to identify small ozone-induced changes in UV irradiance from ground-based measurements at locations where ozone depletion has been modest.

Pollutants in the lower troposphere, notably ozone, nitrogen dioxide, and sulfur dioxide, are strong attenuators of UV radiation. Ozone and sulfur dioxide (SO₂) attenuate at UV-B wavelengths, while nitrogen dioxide (NO₂) attenuates most strongly in the range from 330 to 400 nm, with a smaller influence in the UV-B waveband. The UV response to changes in these gaseous pollutants, and UV-absorbing aerosols such as organic carbon from motor vehicles or biomass burning, may be larger than the UV response to changes in stratospheric ozone. In some locations increased pollution and aerosols may have masked an increase in UV irradiance due to ozone decrease in the 1980s and 1990s, and present cleaner air policies may hide the effect of ozone recovery on UV irradiance.

High surface albedo (reflectivity) greatly enhances surface UV irradiance where there is extensive snow and/or ice cover. Enhancements of erythemal irradiance of ~20% have been reported in regions with snow cover; even greater enhancements are seen in Antarctica due to very clean, high-albedo snow over a large area.

In the previous Assessment, ground-based UV measurement records that began in the 1990s covered a period with no significant ozone trends except at high latitudes, and reducing the uncertainties in quantifying surface UV irradiance remained a challenging task. Ozone-related changes in UV irradiance were apparent in unpolluted regions of the SH where previous increases in surface UV irradiance had ceased or reversed along with observed increases in ozone. At polluted midlatitudes in the NH, UV surface irradiance was generally still increasing by small amounts (a few percent per decade) at the time of the previous Assessment, but at unpolluted sites any increase had ceased. Short events with low column ozone and high UV irradiance had also been recorded at a variety of locations.

Satellite-derived erythemal irradiance estimates from 1979, based on ozone, aerosol, and cloud measurements, were being evaluated against ground-based data at the time of WMO (2007). Satellite data have the advantage of providing global coverage, but the retrieved products must be validated. TOMS (Total Ozone Mapping Spectrometer) data, and since July 2004 data from Ozone Monitoring Instrument (OMI) on the Aura spacecraft, had been analyzed. Satellite-estimated UV irradiance compares well with ground-based measurements in clean conditions, but at polluted sites the satellite retrievals failed to

adequately account for tropospheric pollution, leading to overestimates of about 10% and up to 40%.

Both ground-based measured and satellite-estimated UV radiation data have increased in availability since WMO (2007). In addition to improved and reanalyzed ground-based data, there has been substantial progress in development of both satellite-derived UV products and ground-based reconstructed UV time series, and the climatologies and trend estimates derived from them. The following sections detail the advances in our knowledge and understanding since WMO (2007).

2.3.2 Update on Factors Affecting UV Radiation

The main factors affecting UV radiation are well established and recent studies were mostly focused on quantification of the effect of different factors on UV irradiance. In particular, better estimates of the effects of air pollution on UV irradiance, including their magnitude and wavelength dependence, were the subject of many recent studies.

2.3.2.1 OZONE EFFECTS

Where ozone changes are large, e.g., in the Antarctic, they produce a clear signature in the surface UV radiation. Measurements from Summit Station, Greenland (72°N, established in 2004), show that for comparable solar zenith angles, the spring erythemal irradiance at the South Pole is 50–130% larger than at Summit Station, despite the similar location of the two sites on vast high-altitude ice sheets (Bernhard et al., 2008). Bernhard et al. (2008) also show that these differences are almost entirely caused by the difference in spring total ozone at South Pole and Summit.

Due to the ozone decline, the average erythemal irradiance measured at the Pole between 1991 and 2006 was up to 85% larger than the estimate for the years 1963–1980 (Bernhard et al., 2010). At McMurdo, the average erythemal irradiance for October and November is estimated to be about 30–60% higher than historically.

The ozone-related influence on UV radiation can be identified from the spectral dependence of the changes, because ozone absorption increases strongly toward the shorter wavelengths in the UV-B region. Seckmeyer et al. (2008a) demonstrated that the ratio between UV values at Garmisch, Germany, and Lauder, New Zealand, as a function of wavelength clearly shows features related to the ozone absorption spectrum. Monthly erythemal UV radiation is up to 50% lower in the European summer compared to sites with comparable latitudes in New Zealand. These large differences are caused mainly by differences in total ozone (~15%), cloudiness, aerosol loading, and Sun–

Earth separation. At similar SZAs, the ratio between UV irradiance values at Garmisch and Lauder as a function of wavelength clearly shows features related to the ozone absorption spectrum.

2.3.2.2 OTHER INFLUENCES ON UV

Since ozone is not the only influence on surface UV, and may not be the only parameter to change in the future, or to have done so in recent years, we update and further quantify our knowledge of these other influences.

Clouds can cause large and rapid changes (increases as well as decreases) in surface UV radiation and in total radiation (i.e., radiation integrated over the entire spectrum from about 300 nm to 3000 nm). On average, clouds have an attenuating effect of 15–32% in the UV waveband (Seckmeyer et al., 2008a; den Outer et al., 2005), but for any given situation the cloud effect will depend on the cloud type, depth, and distribution across the sky. Thus, cloud transmission of UV irradiance is difficult to quantify in sufficient detail to provide an exact determination of its effect at a given time and place (Thiel et al., 2008). This latter statement becomes important when considering satellite UV retrievals, detailed in Section 2.3.3.3, where cloud effects are averaged over a large field of view.

Another localized influence on surface UV radiation is air pollution, i.e., scattering and absorption by aerosols (black and organic carbon, hydrocarbons, dust, and smoke) as well as absorption by tropospheric O₃, NO₂, and other gases. Such pollution can reduce UV radiation by up to 15% at polluted sites, with reductions greater than 25% in highly polluted cities, e.g., occasionally in Los Angeles and frequently in Beijing. McKenzie et al. (2008) show that tropospheric extinctions in Tokyo account for much of the 40% reduction in UV-B radiation when compared to the clean atmosphere of New Zealand, and that UV-A radiation could occasionally be affected by high levels of tropospheric NO₂.

Black carbon is the main absorbing component present in atmospheric aerosols. In addition, soil dust absorbs radiation in the UV and visible wavebands, and some organic materials absorb at UV wavelengths. Recently there have been several studies including measurements of enhanced UV absorption due to organic carbon. The sources and formation of these compounds and their temporal variability, however, are currently not well understood (Andreae and Gelencsér, 2006; Bergstrom et al., 2007).

The wavelength dependence of aerosol absorption optical depth is often expressed as an Absorption Angstrom Exponent (AAE). The theoretical AAE value for black carbon, assuming spectrally constant refractive index, is one. The higher values (spectrally steeper absorption) are usually attributed to dust and absorbing organic

components. Recent studies that include UV wavelengths show large values of AAE for organic species (Bergstrom et al., 2010; Barnard et al., 2008; Martins et al., 2009; M. Yang et al., 2009).

Corr et al. (2009) analyzed measurements at UV wavelengths from Mexico City and found that there is no significant single scattering albedo (SSA, i.e., the ratio of scattering optical depth to the total optical depth (scattering + extinction) of the atmosphere) variability between 332 and 368 nm. Barnard et al. (2008) analyzed data from the same Megacity Initiative: Local and Global Research Observations (MILAGRO) campaigns and also concluded there was little SSA wavelength dependence between about 300 and 400 nm for aerosols in the Mexico City area. However, Barnard et al. (2008) found a steep increase in SSA between ~400 and 500 nm and attributed the enhanced absorption at UV wavelengths to organic matter. Marley et al. (2009) also concluded that enhanced UV absorption was due to organic aerosols.

Surface reflectivity in the UV is usually less than 0.1, unless the surface is snow covered. The albedo for snow-covered surfaces varies with snow type and age, and can approach unity for fresh, pure snow (Wuttke et al., 2006a; Meinander et al., 2008). The UV irradiance over a high-albedo surface is greater than that above a snow-free surface, and this effect can be further enhanced by cloudiness and the multiple reflections between snow and cloud surfaces (Wuttke et al., 2006a). Changes in the extent and seasonality of snow cover due to climate change could thus change surface UV.

Surface UV radiation is a response to the combination of all influences on UV radiative transfer. Thus, while latitudinal and seasonal variations for UV radiation are firstly determined by the solar zenith angle, instantaneous UV irradiance values at high-latitude sites may sometimes significantly exceed those at lower latitudes due to the effect of clouds, aerosols, or ozone, particularly at sites affected by the ozone hole (Diaz et al., 2006; Vernet et al., 2009). Under similar solar zenith angles, there can still be large differences in UV irradiance between urban and rural locations, or between sites in the NH and generally cleaner sites in the SH. McKenzie et al. (2006), using measurements from the United States Department of Agriculture UV network, show that peak UV Index values at 45°S in New Zealand are approximately 40% greater than those at 45°N in North America. Subsequently, it has been shown that cloud effects are also less severe at SH sites in the South Pacific region compared with similar latitudes in Europe (Seckmeyer et al., 2008a).

Seasonal differences in surface UV irradiance are highly dependent on latitude, moderated by local cloud and aerosol climatologies. They also depend on the UV wavelength/waveband, or biological weighting, of the irradiance being considered or measured. For erythemally

weighted UV, the ratio between summer and winter mean noon erythral irradiance is in the range 17–24 around 55°N (24 in Moscow at 57°N (Chubarova, 2008), and 17 at 53°N, representative of, e.g., Liverpool, U.K., or Berlin, Germany (Seckmeyer et al., 2008b)), while it is 5 at 35°N. These seasonal contrasts tend to be greater, latitude for latitude, in the SH (McKenzie et al., 2009).

2.3.3 Ground-Based and Satellite UV Data

The majority of sites making direct measurements of UV radiation became active in the 1990s. With rare exceptions, ground-based data prior to this are reconstructions. To estimate the long-term evolution of UV radiation at the surface they use proxy data. While the approach is not new, recent studies used it for the first time to reconstruct UV over a large area (Europe) and study regional effects of ozone and clouds on UV irradiance. Satellite retrievals of UV irradiance have the advantage of a nearly global coverage and are available since 1979, the beginning of the almost continuous record of total column ozone and surface reflectivity from satellite instruments. While total ozone data merged from several satellite instruments have long been available (see Section 2.1.3.1), it is only recently that satellite reflectivity measurements have been merged together into a uniform data set (Herman et al., 2009), making it possible to study long-term trends in satellite-derived erythral irradiance over a long period.

2.3.3.1 GROUND-BASED UV MEASUREMENTS

The main classes of instruments presently in use for measuring solar UV irradiance reaching the ground have been described in previous Assessments (WMO 2003; WMO, 2007). Broadband instruments provide a measurement across a specified waveband, most commonly designed to mimic the erythral action spectrum (Hülse et al., 2008; Webb et al., 2006). Multispectral filter instruments measure several narrow wavelength bands (usually less than 10 bands from 1 nm to 10 nm wide) at the same time or sequentially (e.g., Petkov et al., 2006), thus providing some spectral information. Spectroradiometer systems measure the spectrally resolved solar irradiance, ideally at a resolution of 1 nm or better. No instrument is perfect, with uncertainties in the data coming from a variety of instrument-dependent sources (see, e.g., Johnsen et al., 2008; Cordero et al., 2008a; Cordero et al., 2008b). It follows that instruments must be carefully characterized and regularly calibrated (Webb et al., 1998; Wuttke et al., 2006b). Since standards of spectral irradiance have uncertainties in the UV-B of ~3%, Cordero et al. (2008a) estimate uncertainties between 4 and 6% in the absolute calibration of double monochromator-based spectroradi-

ometers. Additional uncertainties (e.g., imperfect cosine response) result in an overall uncertainty for solar measurements of 7–9%. This accords well with the work of Gröbner et al. (2006), who show results of an intercomparison of 25 European spectroradiometers relative to a transportable reference spectroradiometer. Almost half of the instruments had absolute agreement with the reference spectroradiometer to within $\pm 4\%$ for UV-B and UV-A wavelengths. Broadband instruments, usually calibrated by a spectroradiometer, have uncertainties in the range 7–16% (Gröbner et al., 2007), with imperfections in the cosine response being a major source of error.

While absolute calibration is important for comparing measurements at different locations, or between different techniques (e.g., ground versus satellite), the most important requirement for trend detection is good long-term stability in instrument sensitivity. Stability can be determined by repeated checks against standard lamps in the laboratory or by various techniques applied to the data obtained in the field, i.e., the Langley method (Slusser et al., 2000). Some instruments are known to be very stable against standard lamps and can produce radiance stability near 1% (Cede et al., 2006).

Despite the need for geographical comparison between traceable quality-controlled UV measurements, ground-based monitoring stations provide sparse coverage. Most UV measuring stations are located in the NH in Europe and North America, with gradually increasing numbers in Asia. There are a few stations in South America, New Zealand, Australia, and Africa. A well calibrated polar network of seven stations has been maintained by the U.S. National Science Foundation, while the international Network for the Detection of Atmospheric Composition Change (NDACC) also maintains a long-term database of quality-assured UV data from a small number of observation sites. The World Ozone and Ultraviolet Data Center (WOUDC), the repository for Global Atmospheric Watch (GAW) and GAW-related station data, holds both spectral and broadband data.

Given the limited time series of UV measurements at most ground-based sites, there have been recent attempts to extend some of the data sets back in time using other data sets available for the sites, as detailed in the next section.

2.3.3.2 GROUND-BASED UV RECONSTRUCTION

Consistent records of reliable UV data covering more than 15–20 years are generally not available. Recent studies show the possibility of calculating the surface UV irradiance using variables directly affecting UV radiation, e.g., total ozone and cloud characteristics from standard weather station observations. The reconstructed data sets, which can extend backward to the beginning of the UV

proxy observations, are valuable for examining the UV variability in periods without UV measurements.

Radiative transfer calculations and statistical models are additional tools used to reconstruct the UV irradiance reaching the Earth's surface for data-poor periods. These calculations provide hypothetical irradiance that would be measured if input parameters (ozone, aerosols, and ground albedo) were known for selected measuring sites. However, uncertainties in the model input parameters yield uncertainties in the model outputs of about 6% for clean sites, and up to 20% for sites with very large aerosol load (Cordero et al., 2007; Badosa et al., 2007).

The most common hybrid algorithm calculates all-sky UV irradiance by multiplying the radiative transfer model output for clear-sky conditions by an empirical cloud modification factor (CMF) to account for cloud attenuation effects. CMF represents a ratio between measured shortwave radiation and its potential clear-sky value. The UV-relevant CMF is usually derived via model calculations from an empirical formula based on total irradiance, which is measured routinely on many meteorological stations (Staiger et al., 2008; den Outer et al., 2005; den Outer et al., 2010). Comparison of 16 European UV reconstruction models (COST 726, 2010) shows that the models using total irradiance for the CMF calculation prevail over models based on other parameterizations of the cloud effects, since total irradiance represents all the influences on radiation transmission through the atmosphere.

Ultraviolet irradiance data have been reconstructed by merging five different UV reconstruction models and ground-based measurements for eight European sites from Finland to Greece (den Outer et al., 2010) for the period 1963–2004. Reconstruction techniques are based on neural networks (Junk et al., 2007; Janouch and Metelka, 2007), and radiative transfer modeling (Lindfors et al., 2007) or combine radiative transfer modeling with empirical relationships (den Outer et al., 2005; Kazantzidis et al., 2006). Besides total column ozone, all models use pyranometer data (total radiation) to determine the cloud impact on the UV irradiance. The five different models have been validated against ground-based measurements on a range of timescales using daily to yearly sums of erythemally weighted irradiance. Good correspondence between reconstructed and measured data was found for all-sky conditions at sites with concurrent observations of total radiation and total ozone used as input of the reconstruction model. The study by den Outer et al. (2010) compares the output of the models with erythemal doses measured at the eight European stations. Standard deviations in the ratios of modeled to measured daily sums vary between 10 and 30% depending on site and model, and for yearly totals are less than 5%.

While no single model is able to fully represent all sites (each performs best at its site of origin), the combined (best estimate) approach based on all models has resulted in significant reduction in uncertainties in the reconstructed data: the range of deviations compared to measurements is at least halved for the best estimate when compared to the individual models.

Fixed aerosol properties are usually assumed in the UV reconstruction model. Simulations over Europe have used gridded climatological values of aerosol optical depth in the UV range that are calculated on a monthly basis by combining AERONET (AEROSOL ROBOTIC NETWORK) and MODIS (MODERATE RESOLUTION IMAGING SPECTRORADIOMETER) aerosol data (COST 726, 2010). Variable aerosol properties appear as input to the reconstruction model at a few sites (e.g., Moscow; Chubarova, 2008) and are important where there has been a significant change in aerosols (e.g., in Thessaloniki due to reduction of urban pollution). Kazadzis et al. (2007) found the decrease of aerosol optical depth to be $2.9\% \pm 0.9\%$ per year at 320 nm between 1997 and 2006. den Outer et al. (2010) discuss the dramatic effect of this on the positive trend in the erythemal UV daily sums, up to $1.4\% \pm 0.1\%$ per year, whereas without the aerosol change the trend would be around $0.3\% \pm 0.1\%$ per year. Several authors demonstrate that local pollution (aerosols and trace gases) over urban regions significantly affects surface UV irradiance levels (Chubarova, 2008; McKenzie et al., 2008; Panicker et al., 2009).

A further important input to reconstructions in some climates is elevated ground-albedo during the snow-covered season, which can be incorporated if snow data are available (Rieder et al., 2008; Pribullová and Chmelík, 2008; COST 726, 2010).

While reconstructions provide a historical view of UV irradiance for as long as the required ancillary data are available, recent reconstruction data intended for trend analysis exist only for a small number of sites, concentrated in Europe and Canada (Fioletov et al., 2001).

2.3.3.3 UV ESTIMATES FROM SATELLITE OBSERVATIONS

Global estimates of long-term UV records from satellite ozone and reflectivity data were previously discussed using observations from Nimbus 7 Total Ozone Mapping Spectrometer (N7-TOMS), and have now been updated and extended up to 2008 by Herman (2010). The updated time series, 1979–2008, uses ozone data obtained from the NASA merged satellite data set of monthly and 5° zonal average band values (Stolarski and Frith, 2006). The UV estimates are obtained from measurements of backscattered UV by using radiative transfer calculations

that include ozone, surface reflectivity, and aerosol estimates embedded in a Rayleigh scattering atmosphere adjusted for the local terrain height within a satellite field of view. Another TOMS-based global climatology was published recently (Lee-Taylor et al., 2009). This study also discusses changes in UV irradiance in the 1990s relative to the 1980s and separates contributions from ozone and cloud changes.

Recent validation studies of satellite estimates have focused on OMI data using comparisons to ground-based measurements (Tanskanen et al., 2006; Tanskanen et al., 2007; Ialongo et al., 2008; Buchard et al., 2008; Weihs et al., 2008; Kazadzis et al., 2009a). All find that the OMI UV estimates are biased high, particularly at more polluted sites. In snow-free conditions, they are biased high by 10% compared with ground-based measurements; the high bias is up to 40% in some highly polluted environments. This bias is similar to that for TOMS-based estimates: analysis of Belsk (Poland) data shows that the ratio between satellite-derived and measured erythemally weighted doses calculated for the snowless period (April–October) is stable over the period 1979–2008 (Krzyścin et al., 2011). The ratio for the earliest part of the satellite UV data (from TOMS measurements onboard of the Nimbus 7 satellite in the period 1979–1993) is 1.23 ± 0.06 , only slightly larger than that obtained from the measurements by the TOMS onboard the Earth Probe satellite (1.19 ± 0.07 for the period 1996–2003) and from the measurements by OMI onboard the Aura satellite (1.19 ± 0.05 for the period 2004–2008).

One of the sources of differences is that satellite measurements represent a much larger region (OMI minimum pixel at nadir: $13 \times 24 \text{ km}^2$) than ground-based measurements. Ground-based measurement of erythemal dose at various sites within one OMI satellite pixel showed deviations of $\pm 5\%$ in cloud-free conditions, or 20% if urban areas were included (Weihs et al., 2008; Kazadzis et al., 2009b). For partly cloudy conditions and overcast conditions the discrepancy of instantaneous values between the stations can exceed 200%. If 3-hourly averages are considered, the agreement is better than 20% within a distance of 10 km (Weihs et al., 2008). This spatial discrepancy can explain much of the random variation between ground-based and satellite data but does not generally explain a strong systematic bias. The largest relative differences between the satellite-derived and the measured irradiance are observed in urban areas, where UV-absorbing aerosols play an important role. The OMI overestimate of ground-based UV measurements may be partly explained by the lack of sensitivity of satellite instruments to the boundary layer (Tanskanen et al., 2007; Ialongo et al., 2008; Weihs et al., 2008; Kazadzis et al., 2009a; Buchard et al., 2008). The bias between OMI and ground-based measurements increases with increasing

aerosol absorption optical thickness (Arola et al., 2005; Kazadzis et al., 2009b; Ialongo et al., 2010). The largest positive OMI biases were found at 305 nm (the lowest common wavelength routinely available), reaching 32% and 27% for cloudy and cloudless measurements (Kazadzis et al., 2009b), indicative of ozone variability in addition to aerosol variability.

Additionally, over snow-covered surfaces the OMI-derived daily erythemal dose is generally lower than the ground-based measurement because the OMI surface UV algorithm uses climatological surface albedo that may then be lower than the actual effective surface albedo. Part of the problem is that a portion of the observed reflectivity may be incorrectly interpreted as cloud cover, which reduces the estimated irradiance. All-conditions data and snow-free data have been compared separately to evaluate the effect of albedo. For example, a recent comparison by Buchard et al. (2008) demonstrated that OMI overestimates erythemal daily doses by 14% for days without snow on the surface and only by 8% if days with snow are included in the comparison.

UV irradiance is also derived by using column ozone in conjunction with cloud fraction data from geostationary satellites in combination with polar-orbiting satellites (Verdebout, 2004a and 2004b; Wuttke et al., 2003; Gadhavi et al., 2008; Janjai et al., 2010). The difference of about 10% between satellite and ground-based measurements is due to the limited information from the boundary layer (Arola et al., 2009; Kazadzis et al., 2009a). Schallhart et al. (2008) developed a method to generate near real time UV-index maps from Meteosat Second Generation (MSG) for Austria. The method is similar to that developed by Verdebout (2000) but with an additional input from ground-based UV measurements.

2.3.4 Long-Term Changes in UV

2.3.4.1 GROUND-BASED OBSERVATIONS

Over much of the Earth's surface, long-term increases in UV radiation due to decreases in ozone derived from records of ground-based instruments are small and difficult to separate from the sometimes larger effects of changes in clouds, aerosols, and pollutants. Spectral instruments at clean sites in regions with significant ozone change are in the best position to identify ozone-related changes in UV radiation, either from ozone depletion or recovery. Elsewhere, with small ozone changes, changes in climate (clouds/albedo) and human activities (pollution, gaseous and aerosols) may have greater importance for UV radiation than the ozone.

At clean-air sites such as Lauder, New Zealand, the increase in summertime UV irradiance reported previously

has not continued, and in recent years, the peak summertime UV amounts have been lower than in the late 1990s. Ozone is no longer decreasing at this site, with lowest values occurring in the summer of 1998/1999. However, year-to-year differences are comparable with the measurement uncertainty.

One of the longest series of UV measurements has been taken at Belsk (Poland). The erythemally weighted daily doses have been homogenized for the period 1976–2008 to account for instrument differences and time drift. Figure 2-17 shows that the mean erythemal irradiance level at Belsk in the warm subperiods of the year (April–October) in the 2000s has been ~10% larger than the overall mean level for the whole period of observations 1976–2008 (Krzyściński et al., 2011). The increase for clear-sky days is inferred from a simple model taking into account only ozone anomalies multiplied by the radiation amplification factor (RAF) of 1.1 (see Box 2-1). However, for data measured under all atmospheric conditions, the erythemal irradiance continues to increase when ozone reduction ceases. Borkowski (2008) shows an increase of 2.3% per decade in annual dose during the period 1976–2006 using Belsk’s monthly data.

Similarly, but for a shorter time period, increasing trends in erythemal irradiance have been seen at Sapporo,

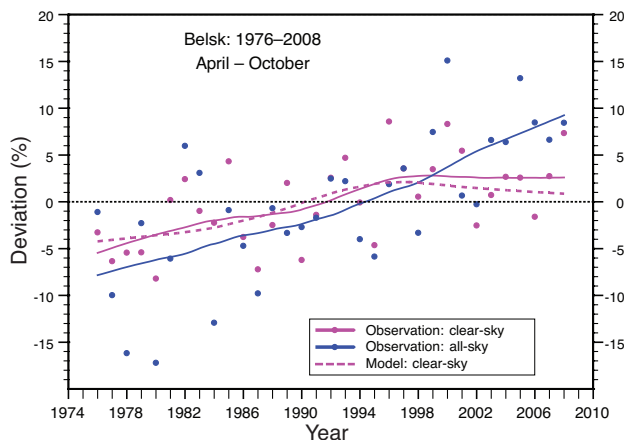


Figure 2-17. Deviations (%) of the monthly mean erythemal dose relative to the long-term (1976–2008) monthly means averaged over the warm subperiod of the year (April–October). The homogenized results of measurements by various broadband instruments at Belsk, Poland, for the period 1976–2008 are shown for all-sky conditions (blue dots) and clear-sky conditions (magenta dots). Curves illustrate the smoothed data. The dashed magenta line shows the modeled ozone signal in the UV series (corresponding total ozone deviations are multiplied by $RAF = 1.1$, see Box 2-1). Adapted from Krzyściński et al. (2011).

Tsukuba, and Naha since the early 1990s. At these sites total ozone was at its lowest around the early 1990s and since then there has been little increase in ozone. The increasing trends in erythemal irradiance since the early 1990s cannot be attributed only to changing ozone (JMA, 2009). Changes in aerosol and weather conditions at the Japanese sites are suggested as reasons for the observed increases in UV radiation.

Analysis of surface 280–320 nm UV irradiance measured by Multi-Filter Rotating Shadowband Radiometer (UV-MFRSR) from the U.S. Department of Agriculture (USDA) network shows annual irradiance changes from -5% per decade to $+2\%$ per decade at eight stations with approximately 10-year records (Hicke et al., 2008). Interannual variability of surface UV-B radiation was 2 to 5% of the mean. Trends at each site were calculated for individual months, but during most months trends were not statistically different from zero.

2.3.4.2 RECONSTRUCTED UV DATA

Using the erythemally weighted yearly doses reconstructed by various models (see Section 2.3.3.2), den Outer et al. (2010) find statistically significant UV trends for eight European sites. The trends vary between 3–6% per decade between 1980 and 2006. Upward trends were observed from 1980 to the mid-1990s for most sites, with levels in the 1980s being lower than the long-term average. Thereafter the rate of change altered at some sites and certainly cannot be extrapolated into the future. Ozone change accounts for $\sim 1\text{--}2\%$ of the increase per decade and clouds account for about 2–3% per decade. Observed increases in surface UV radiation are partly attributed to the decreased pollution since the late 1980s (e.g., Wang et al., 2009). The European continent has “brightened,” possibly due to air pollution abatement policies (e.g., Kazadzis et al., 2007; Ruckstuhl et al., 2008).

Lindfors et al. (2007) reconstructed erythemally weighted irradiance back to the early 1980s at four Northern European stations based on measured total ozone and total irradiance. The reconstructed time series show an increase in erythemal irradiance (3–4% per decade) for the stations having a clear increase in total radiation. Feister et al. (2008) found a similar long-term pattern for Central European stations, with a decrease between the 1950s and 1980 followed by an increase, resulting in UV irradiances $\sim 5\text{--}10\%$ higher than the overall (1950–2004) mean level at the end of the time series. Sites in Finland show similar long-term behavior since the early 1980s, but an increase is found between 1951 and the end of the 1960s, opposite to the Central European sites.

Junk et al. (2007) and Feister et al. (2008) reconstructed series of erythemal irradiance (see Feister et al., 2008, Figure 12) since 1893 based on sunshine duration

measurements at Potsdam. Additional measurements of global and diffuse irradiation were included since 1937, and variability of total ozone was included since 1964. The analysis indicates a few percent decrease in erythemal dose between 1893 and about 1910, a slight increase in the 1950s, followed by a gradual decrease of a few percent until 1980 and a subsequent increase after 1980 of a few percent to the highest levels in the time series. Chubarova (2008) discusses the long-term UV changes over Moscow using reconstructed time series since 1968. The overall trend for 1968–2006 is not statistically significant because of a significant decline (–11% per decade) in cloud transmission at the beginning of time series (1968–1980). Since 1980, the growth of ~6% per decade in the yearly sums of erythemally weighted doses has been caused by a decrease in total ozone (2.5% per decade), cloud (2.1% per decade), and aerosol effects (1.1% per decade). In Austria (Vienna and Sonnblick), changes in erythemally weighted doses relative to a reference decade (1976–1985) showed that changes in total ozone had a larger influence on erythemally weighted doses than changes in cloudiness; here ozone accounted for about 66% of the annually averaged change. However, in recent years the relative influence of changes in cloudiness on UV-doses became larger (reaching 50%) over Vienna (Rieder et al., 2008). Curylo et al. (2007) used reconstructed erythemally weighted data for Poland since 1964 for four stations, finding positive trends in the yearly data (with a maximum trend of about 4% per decade in Warsaw). The trends disappeared over some stations in summer due to increasing cloud attenuation.

Kvalevåg et al. (2009), addressing an extended period, found an extensive reduction of erythemally weighted irradiance of up to 15–20% over most land areas since 1750. An increase is suggested only in polar regions, most strongly in the SH and associated with the appearance of the Antarctic ozone hole. The estimate is based on a UV reconstruction taking into account preindustrial (1750) and present (2000) atmospheric conditions including changes in the stratospheric and tropospheric ozone (within the last 2–3 decades) and centennial changes in SO₂, NO₂, the direct and indirect effects of aerosol changes, and albedo changes. The long-term changes in pollutants could mask an increase of surface UV radiation due to stratospheric ozone decline in recent decades. It seems that the increase of UV extinction by carbonaceous aerosols is mostly responsible for such compensation.

Figure 2-18 presents a summary of estimated changes in UV radiation based on the reconstructions at eight European locations (den Outer et al., 2010). The 10-year running means of the yearly sums of erythemal irradiance are shown separately for all-sky and clear-sky conditions. To make the results of these eight different sites

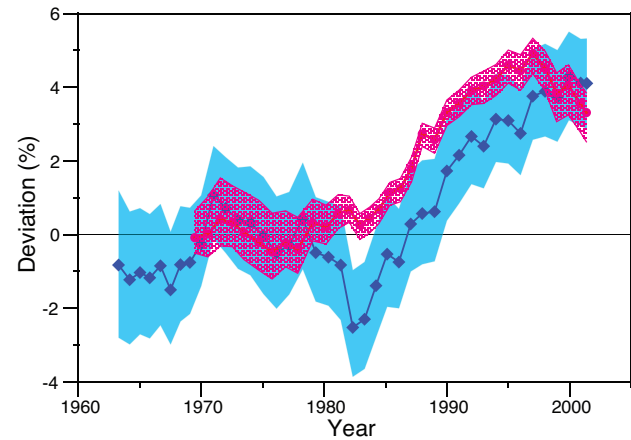


Figure 2-18. The 10-year running means of the yearly sums of erythemal irradiance at eight European sites for all-sky conditions (blue diamonds) and clear sky-only conditions (red dots). Prior to averaging, each reconstructed time series is normalized with respect to the 1970–1980 average. The light blue and red areas depict the uncertainty envelope for all-sky and clear sky-only conditions, respectively. Adapted from den Outer et al. (2010).

comparable, each reconstruction was first normalized with respect to the average level in 1983–2004, which is the overlap period of available data. The uncertainty bands shown in Figure 2-18 stem from the uncertainties in the reconstructed yearly erythemal sums. These uncertainties, assigned to each year separately, were derived from the long-term stability and underlying agreement of the models, and the agreement with actual UV measurements. The uncertainties to higher and lower values than the estimate are independent, and generally differ in magnitude. The high (low) limit of the final uncertainty band is based on the high (low) limits for the individual yearly sums. Summations and averaging in these processes were always carried out with statistical weights assigned to the individual data points. The final running means, as presented in Figure 2-18, are normalized again with respect to the period 1970–1980. Note the divergence between the trends for clear-sky and all-sky data since the mid-1990s, similar to the observations in Figure 2-17.

In conclusion, reconstructed trends, like those observed from direct UV measurement, are a superposition of the ozone, cloud, and aerosol effects on UV radiation. The magnitude of the trend depends very much on the period selected for the trend analyses, and on local characteristics of the cloud and aerosol changes as well as ozone. The statistically significant positive trends in erythemally weighted irradiance identified at many stations in the last half-century are due to reduced attenuation of radiation by

clouds since the beginning of the 1980s, and the general tendency of declining ozone until the mid-1990s.

2.3.4.3 SATELLITE ESTIMATES OF IRRADIANCE CHANGES

Herman (2010) analyzed satellite data (total ozone from multiple satellites) to estimate zonal average percent changes in UV irradiance from 290 to 400 nm and percent changes in biologically weighted irradiance reaching

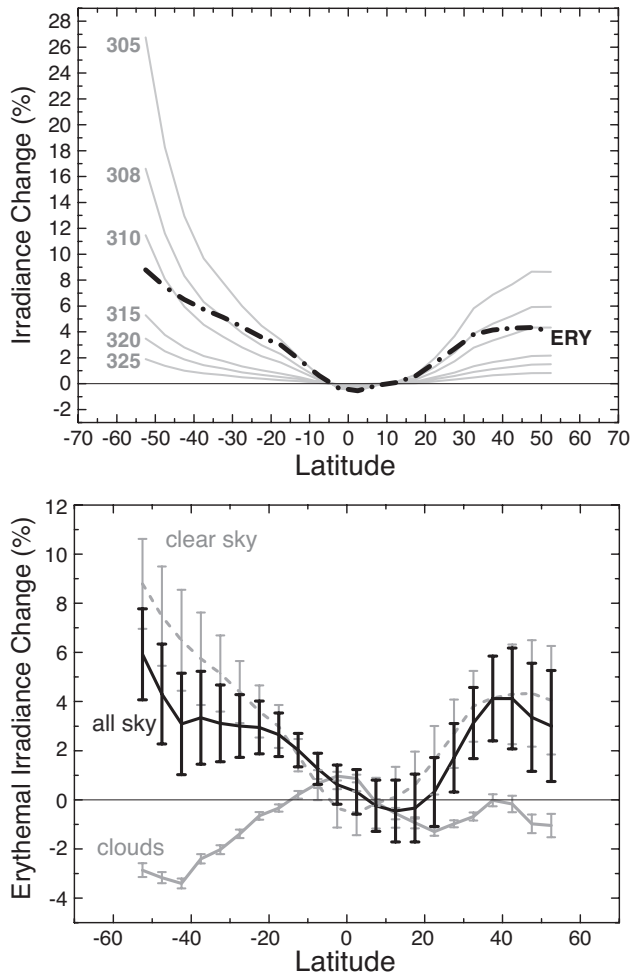


Figure 2-19. (top) Percent changes in erythemal irradiance from total change in ozone amount for 30 years (1979 to 2008). Also shown for comparison are six monochromatic irradiance changes. (bottom) The change in erythemal irradiance (solid black line) caused by changes in reflectivity and cloud transmission (solid gray line) and the changes in ozone amount represented by the clear-sky changes in erythemal irradiance (dashed gray line). Error bars are estimated from the linear least squares fitting procedure. Adapted from Herman (2010).

the Earth's surface (using the concept of RAFs and Beer's Law) for the period 1979 to 2008.

As shown in Figure 2-19 (top), clear-sky biologically weighted UV irradiance increased significantly except in the tropics. The increase was caused by decreases in ozone amount from 1979 to 1998. Since 1998, ozone amounts and UV irradiance levels have been approximately constant. Also shown for comparison are the percent changes in irradiance at six wavelengths (305, 308, 310, 315, 320, and 325 nm), which have different responses to ozone and contribute in different ways to biological effects. The annual estimates of zonal average UV irradiance changes are restricted to latitudes between 53°S and 53°N to avoid SZA > 80° during winter solstice, where spherical geometry effects become significant.

When all atmospheric conditions are considered, changes in cloud and aerosol transmission have a significant effect on UV irradiance in both hemispheres. In the SH the annual average UV increase is partially offset by a decrease in cloud and aerosol transmission (hemispherical dimming), while in the NH the effect was minimal (Figure 2-19, bottom).

For clear skies, the largest increases were at the higher latitudes and in the SH (about 8.5% for erythemally weighted irradiance at 50°S compared to 4% at 50°N). At 30°S the increase was about 5%, which is comparable to the increase at 30–40°N. As mentioned earlier, the weakness in this method is that the satellite sensors do not adequately probe the lowermost regions of the atmosphere, so the method is insensitive to changes in UV-absorbing pollution in the boundary layer of the atmosphere.

The average all-sky changes in erythemally weighted irradiance are more similar at higher latitudes in both hemispheres: 3.1% at 50°N, near the Canadian border, and 5.2% at 50°S latitude near the southern tip of South America. In the SH, changes in cloud transmission partially offset the clear-sky increase. The zonal average irradiance increases vary locally and regionally because of different amounts of local cloud and aerosol cover.

Figure 2-20 shows the monthly percent change in erythemally weighted irradiance, caused by ozone, from 1979 to 2008. Erythemally weighted irradiance has increased dramatically at higher latitudes in the SH and moderately elsewhere. In the SH spring (October and November) the increases are similar to the NH spring (April and May) changes and are about 5% to 7% at 40° to 45° latitude. However the SH summer changes in December to February are much larger than in the NH (June to August) at latitudes >40°. The major population centers in middle and southern South America, Southern Africa, Australia, and New Zealand experience significant increases in erythemally weighted irradiance compared to 30 years ago. The increases have occurred during most of the spring and summer when the solar UV irradiance

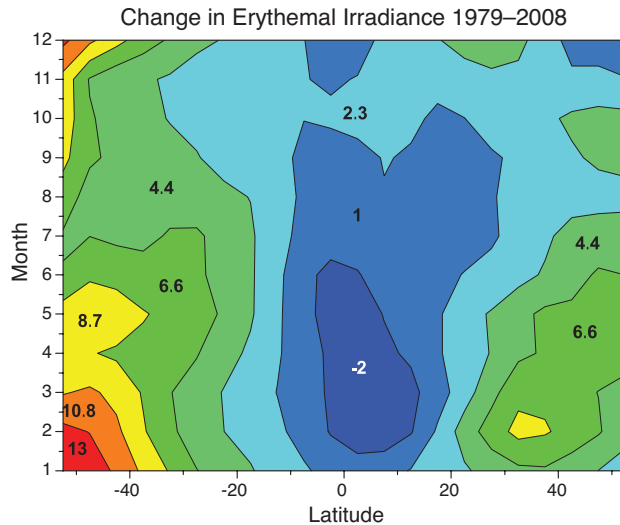


Figure 2-20. Percent change for erythemally weighted irradiance caused by changes in ozone amount for the period 1979 to 2008 as a function of latitude and month. From Herman (2010).

exposure is at a maximum (more clear days as well as seasonally declining ozone going into the summer).

2.3.4.4 CONSISTENCY OF UV ESTIMATES FROM OBSERVATIONS, RECONSTRUCTIONS, AND SATELLITE DATA

Since most of the ground-based UV measurement records are relatively short, they are not suitable for validation of long-term UV trends derived from satellite data. Long-term records of reconstructed data have to be used instead. Figure 2-21 shows summertime daily erythemally weighted doses estimated from ground-based UV measurements, ground-based reconstructions, and satellite estimates for the Northern Hemisphere (May–August) and the Southern Hemisphere (November–February). The comparison was limited to the summertime to avoid conditions with snow on the ground, when satellite estimates are unreliable. In general, satellite estimates are able to reproduce year-to-year variability, although there is a substantial bias between them and ground-based measurements and reconstructions (discussed in Section 2.3.3.3). Linear trend estimates for the period 1980–2003 from ground-based reconstructions and TOMS satellite estimates show a substantial difference between individual sites that reflects the importance of local conditions, and is well captured by both data sets. The average of four linear trend values for seven European sites shown in Figure 2-21 is $4.8\% \pm 1.7\%$ per decade for the reconstructed data and $5.0\% \pm 1.4\%$ per decade for satellite estimates (the uncertainties represent the 95% confidence level of the average of trend values at

individual sites). While satellite estimated irradiance data has a positive bias compared to ground-based data, this does not influence trend detection if the bias is consistent over time. The agreement between independent methods of measurement and trend analysis in Figure 2-21, and discussed in Section 2.3.3.3, implies that at least for the European sites explored, this is the case.

It should be noted that summertime trends over seven European sites with reconstructed data from Figure 2-21 are noticeably larger than those over Toronto, Lauder, and two Japanese stations and substantially larger than trends in zonal mean UV radiation over northern midlatitudes shown in Figure 2-19 (about 4% over the 1979–2008 period). This is likely due to long-term changes in the cloud cover over Europe. The mean trend over the same seven stations (Sodankyla is excluded to avoid snow influence on satellite estimates) is $4.3\% \pm 0.9\%$ per decade for all atmospheric conditions, but the UV trend due to ozone is only $1.5\% \pm 0.4\%$ per decade or about 4% over the entire period (see den Outer et al., 2010, their Table 6, for the trend values at individual sites), which is in line with satellite estimates from Figure 2-20.

2.4 INTERPRETATION OF OBSERVED OZONE CHANGES

The focus of this section is to interpret the observed ozone changes reported earlier in the chapter. This is accomplished primarily through comparisons of observations with simulations produced by chemistry-climate models (CCMs). These models couple the general circulation of the atmosphere with a photochemical mechanism using the latest available evaluation of chemical reaction rates and photolysis cross sections (e.g., JPL 06-2). Eighteen of these models were extensively compared with each other and with data in the second Chemistry-Climate Model Validation (CCMVal) exercise documented in SPARC CCMVal (2010). The models all produced simulations of the past, the future, and a present-day time slice. One of the models included a coupled ocean and some had interactive tropospheric chemistry. Most, but not all, simulated the 11-year solar cycle. Most also simulated the response to large enhancements of aerosol surface area following the eruptions of the El Chichón and Mt. Pinatubo volcanoes.

2.4.1 State of Science in 2006

WMO (2003) concluded that chemistry-transport models (CTMs) including observed changes in halocarbons, other source gases, and aerosols captured the long-term behavior of ozone in the midlatitudes. This conclusion, repeated in WMO (2007) following examination of

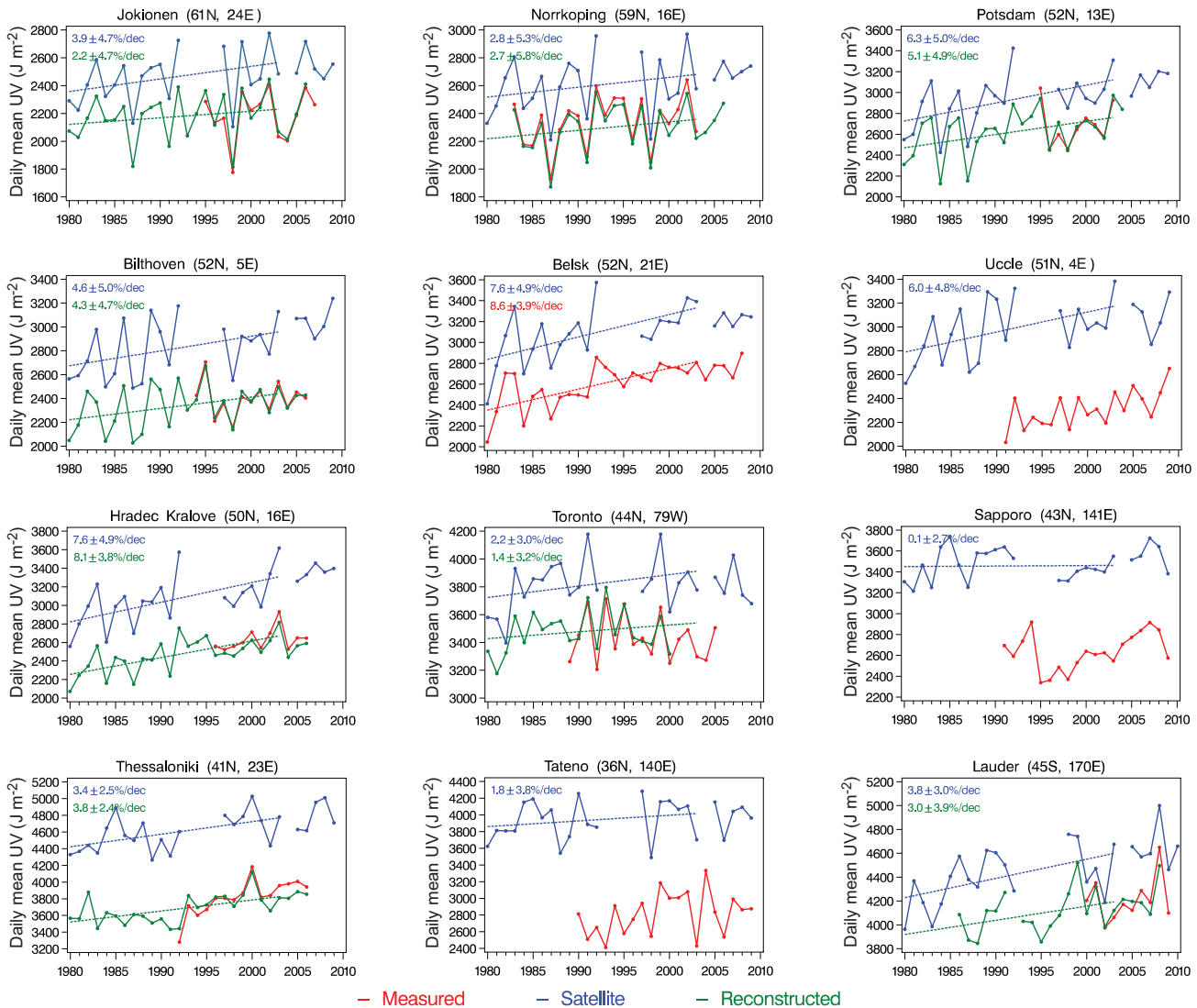


Figure 2-21. Summertime (May–August for NH and November–February for SH) mean daily erythemal UV doses (joules per square meter) from ground-based UV measurements (red), ground-based reconstructions (green), and satellite estimates (blue). The dashed lines show the linear trends for 1980–2004 calculated from reconstructions (green) and satellite estimates (blue). The derived trend values in percent per decade are also shown.

four additional years of measurements and analyses, was based on the faithful representation of general features of the observed ozone changes as functions of latitude, altitude, and season obtained from a suite of models (both CTMs and CCMs).

WMO (2007) pointed out unresolved issues relating to deficiencies of then-current models. These include (1) the failure of models to reproduce the difference between observed southern and northern middle latitude ozone trends; (2) the consistent simulation of a Southern Hemisphere effect of the Mt. Pinatubo aerosols on ozone contrary to observed ozone behavior; and (3) worse comparisons of upper atmospheric ozone trend derived from observations with trends produced by models with tem-

perature feedback than from models without this important process. The models used in WMO (2007) did not include a contribution from short-lived bromine compounds, perhaps leading to an underestimate of the decline in ozone following injection of volcanic aerosols into the stratosphere. Finally, although reproduction of the vertical structure of the solar cycle variation of ozone could be an important critical test of models, observational uncertainties made this test of limited value.

WMO (2007) noted increased evidence that changes in atmospheric dynamics had a significant influence on ozone over the northern midlatitudes on decadal time-scales. WMO (2007) concluded that changes in tropospheric and stratospheric dynamics were partially respon-

sible for both the ozone decline up to the mid-1990s and for the increase after that time.

2.4.2 Updates to Kinetic and Photochemical Data

There have been many revisions to JPL 02-25 (Sander et al., 2003) in chemical rate coefficients, photochemical parameters, and estimated uncertainties reported in JPL 06-2 (Sander et al., 2006) and JPL 09-31 (Sander et al., 2009). These do not result in major changes in our understanding of the response of stratospheric ozone to release of ozone-depleting substances. Recent developments in kinetic parameters of importance to polar ozone chemistry are discussed in Section 2.2.2.

2.4.2.1 UPDATE FROM JPL 2002 TO JPL 2006

An important difference between JPL 02-25 and JPL 06-2 is revision of the recommended rates for reactions of excited-state oxygen atoms $O(^1D)$ with molecular nitrogen (N_2), nitrous oxide (N_2O), H_2O , and methane (CH_4) based on several laboratory studies. Dunlea and Ravishankara (2004) show that the revised rate coefficient for $O(^1D) + H_2O$ reduces the production rate of hydrogen radicals in the stratosphere by 10–15% compared to the 2002 rate coefficient recommendation.

JPL 06-2 introduced the reaction of $O + BrONO_2$ for the first time in the NASA evaluation using data from Soller et al. (2001). Sinnhuber et al. (2002) and Salawitch et al. (2005) showed that including this reaction in chemical models increases the daytime bromine monoxide/total inorganic bromine (BrO/Br_y) ratio by about 20%. The presence of a greater fraction of inorganic bromine in radical form increases the sensitivity of ozone to halogens as well as the contribution of bromine to EESC (Section 1.4.4). The CCMVal-2 comparison (Section 2.4.3.5) shows that many CCM groups did not add this reaction when adopting JPL 06-2 kinetics (Chapter 6 of SPARC CCMVal, 2010). Including this reaction also impacts the amount of Br_y inferred from measured BrO , one method for estimating the impact of very short-lived bromocarbons on the stratospheric bromine budget. The photochemical models used in this Assessment to estimate Br_y from BrO have all included this reaction (Chapter 1, Table 1-14).

The most notable impact of kinetics changes between JPL 02-25 and JPL 06-2 is likely to be the increase in the computed BrO/Br_y ratio. Other reaction rates constants updated in JPL 06-2 include reactions of chlorine atoms (Cl) with hydrochlorofluorocarbons (HCFCs) and hydrofluorocarbons (HFCs); the hydroperoxyl radical (HO_2) self-reaction; OH reactions with oxygenated organics; the yield of pernitrous acid ($HOONO$) from $OH + NO_2$

+ M and $HO_2 + NO_2 + M$; and the photochemistry for a number of organic carbonyl compounds. WMO (2007) used the kinetic evaluations from JPL 02-25 with a few updates. To our knowledge there are no published estimates of the impact on global ozone of the change from JPL 02-25 kinetics to JPL 06-2 kinetics.

2.4.2.2 UPDATES SINCE JPL 2006

$O(^1D)$ Reactions

Additional studies (Carl, 2005; Takahashi et al., 2005; Dillon et al., 2008; Vranckx et al., 2008) have led to a further revision in the recommended $O(^1D) + N_2O$ and CH_4 reaction rate coefficients in JPL 09-31. Recent simulations using the NASA Goddard two-dimensional (2-D) model described by Fleming et al. (2007) show a 1 part per billion by volume (ppbv) increase in NO_y (~8%) due to the increase in the recommended rate coefficient for $O(^1D) + N_2O \rightarrow 2NO$. Atmospheric measurements do not differentiate between these results. The same 2-D model also produces a 10–12% deeper minimum in the Antarctic springtime ozone with the JPL 09-31 rates versus JPL 06-2, with about half of the difference due to the change in the $O(^1D) + N_2O$ reaction rate coefficient.

$HO_2 + NO$

Laboratory studies by Butkovskaya et al. (2007, 2009) examined the reaction product yields of the $HO_2 + NO$ reaction, reporting that the yield of the HNO_3 product increased at lower temperature (223–323 K) and higher pressure, 72–660 Torr (96–880 hPa), and in the presence of water vapor. Cariolle et al. (2008) tested the impact of the updated reaction rate coefficient on the HNO_3 formation from the $HO_2 + NO$ reaction using 2-D and 3-D models and found a significant impact on nitrogen oxides (NO_x) and odd hydrogen (HO_x) in the free troposphere and O_3 abundance in the troposphere at low latitudes. They found only small changes in minor species distributions in the stratosphere.

$ClO + HO_2$

JPL 09-31 revised the recommendation for the rate constant for the reaction $ClO + HO_2$ based on the new laboratory study by Hickson et al. (2007). The revised rate constant has been increased by 25% at room temperature and by 37% at 200 K. Kovalenko et al. (2007) showed that atmospheric measurements of hypochlorous acid ($HOCl$) obtained by several balloonborne instruments are consistent with a value for the $ClO + HO_2$ rate constant considerably larger than values recommended by JPL 06-2 or reported by Hickson et al. (2007). Kovalenko et al. (2007) also showed

good agreement between measured and modeled HOCl using the older rate constant measurement of Stimpfle et al. (1979), which was weighted more heavily in recommendations prior to JPL 02-25. Comparison of measured and modeled HOCl serves as a proxy for the rate of ozone loss by the ClO + HO₂ cycle, which is often the dominant halogen loss process in the midlatitude lower stratosphere. Kovalenko et al. (2007) suggest that models underestimate ozone loss by this process because models using this kinetic input commonly underestimate observed HOCl.

2.4.3 The Distribution and Variability of Stratospheric Ozone and Their Representation in Models

The detection and attribution of trends in ozone depend on both long-term changes in ozone and on the variability of ozone. In Section 2.1, it was noted that ozone concentrations over the last decade or so remained more or less constant. A central problem is attributing these changes to causes such as dynamical variability, long-term climate change, decreasing ODSs, or the changing phase of the solar cycle.

WMO (2007) relied on 2-D models, 3-D CTMs, and CCMs, a mix of models that included and excluded radiative feedback. The current Assessment makes near-exclusive use of 3-D CCMs because they represent the state of the art of our understanding of the physical and chemical processes controlling atmospheric composition. These models have been developed significantly over the last four years. Recently their radiative, dynamical, chemical, and transport processes have been subjected to extensive evaluation using a wide range of diagnostics derived from observations (SPARC CCMVal, 2010). Understanding the mean ozone distribution and ozone variability requires not only analyses of observations but also evaluations of the processes that control the mean distribution and variability found in models.

The following sections summarize some of the key conclusions drawn from extensive evaluations of the 18 CCMs presented in the SPARC CCMVal report (2010). Table 3-1 of Chapter 3 gives a description of the CCMs.

2.4.3.1 ANNUAL CYCLE AND NATURAL VARIABILITY

Stratospheric ozone is known to vary in response to natural factors, such as the QBO, El Niño-Southern Oscillation (ENSO), variations in transport associated with the Brewer-Dobson circulation, and dynamical variability associated with the annular modes. Ozone observations have demonstrated variations on many spatial and temporal scales. Diagnostics for each of the different sources of natural variability in stratospheric ozone have

been applied to the chemistry-climate models participating in this Assessment. The relative importance of the different sources of natural variability in stratospheric ozone has been assessed using multiple linear regression. When possible, the connection between the sources of natural variability and ozone has been addressed by analyzing the processes that determine it. Understanding and quantifying the underlying natural ozone variations are necessary to quantify the impact of anthropogenic perturbations of the ozone layer and to make reliable predictions of future ozone abundances.

The annual cycle is a forced variation of the atmosphere that is reflected in ozone concentrations. Figure 2-22 (panels a and b) shows the annual cycle in ozone concentration at 1 hPa for 40°S and 40°N derived from MLS data compared to the annual cycles calculated by CCMs. Figure 2-22 (panels c and d) shows the annual cycle also at 72°S and 72°N calculated in the lower stratosphere at 46 hPa. The vertical and latitudinal distribution of the annual cycle in stratospheric zonal monthly-mean ozone is well represented in stratosphere- and mesosphere-resolving models with a few outstanding issues. In the lower stratosphere, models tend to have a late occurrence of the polar ozone depletion (Antarctic ozone hole, Figure 2-22c). In the upper stratosphere (Figure 2-22a) the zonal mean MLS data at 40°S show an interesting peak in May and June for three of the four years that is not reproduced by models. SBUV data show a similar peak.

Model simulations reproduce many of the key features of the observed interannual variability of column ozone. All models show the expected minimum in polar variability in the summer season. However, in the NH dynamically active period, most of the models underestimate the interannual polar ozone variability. In the SH some models overestimate while others underestimate interannual variability in ozone.

Most models reproduce the connections between the dynamical processes responsible for the interannual polar ozone variations and the ozone response. Models with poor performance in interannual polar variability also tend to perform poorly in the diagnosed dynamics-ozone connections. There are various techniques that use observations to cause a model to produce a QBO. These improve simulated ozone variability. However, there are biases in the amplitude of the QBO ozone signal from these simulations that are comparable to biases for models with internally generated QBO signals.

2.4.3.2 SOLAR CYCLE

Here we update the extensive discussion of the relationship between ozone and solar radiation associated with the 11-year solar cycle and the 27-day solar rotation period given in WMO (2007). Variations of total ozone

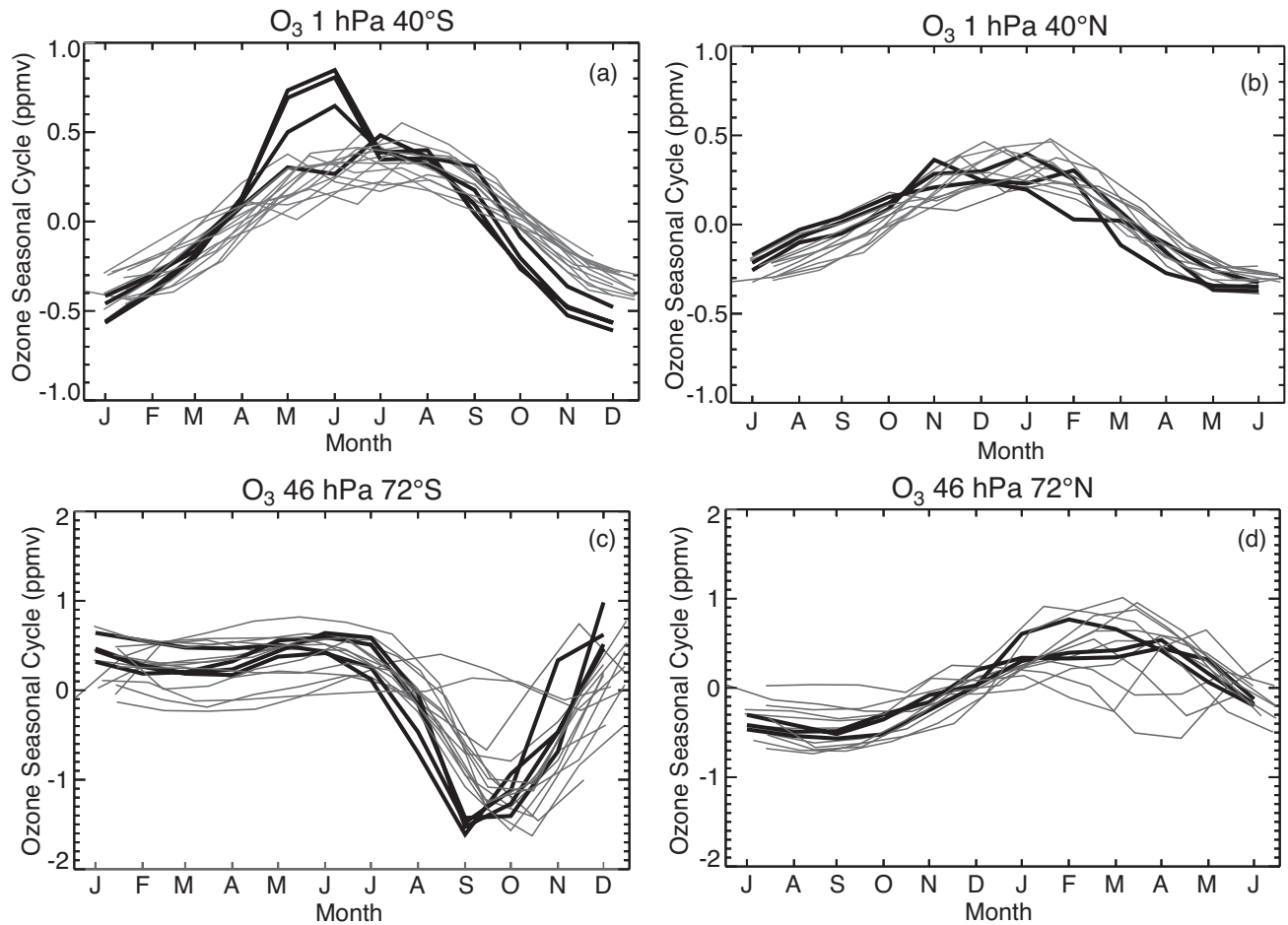


Figure 2-22. (a) and (b): Ozone seasonal cycle (in parts per million by volume) from MLS data at 1 hPa compared to models at 40°S and 40°N. (c) and (d): Same but for 46 hPa and 72°S and 72°N. Heavy lines are MLS data for each of four years (2005–2008); light lines are from models. Adapted from Figure 8.2 in Chapter 8 of SPARC CCMVal (2010).

column in phase with the solar cycle of 2–3% were reported, along with the stratospheric ozone profile response as a function of latitude. The detailed mechanism to explain the ozone response observed in the lower stratosphere remained uncertain. The following updates the discussion of the vertical structure of the tropical solar response given in WMO (2007) using additional observations and model results (see also Gray et al., 2010).

Recent analysis of the CCMVal models shows that although the 11-year solar cycle in column ozone is reproduced by the models, the amplitude of the response varies among models. Differences in radiation, photolysis, and transport all contribute to the spread in response. The latitudinal dependence of the solar response in column ozone derived from observations compares better with that derived from present models than earlier studies (Austin et al., 2008). The large spread at mid to high latitudes is due

to large interannual variability and limits the discussion of extratropical signals.

Recent observational studies using ground-based and satellite data sets agree with previous results, reporting ozone variations in phase with the 11-year and 27-day solar cycle in the upper stratosphere (e.g., Fioletov, 2009; Remsberg, 2008) and the lower stratosphere (e.g., Tourpali, et al., 2007; Sitnov, 2009). Similarly, the vertical structure of the solar signal in SAGE I and II data (Randel and Wu, 2007) shows a maximum response in the tropical upper stratosphere, a smaller (statistically insignificant) response in the middle stratosphere (~30–35 km), and a secondary maximum in the tropical lower stratosphere. This structure of the stratospheric ozone response in the tropics is supported by analysis of ground-based Umkehr measurements at the Mauna Loa station (Tourpali et al., 2007).

The QBO complicates the statistical detection of the solar signal. Smith and Matthes (2008) found that the presence of a QBO in their simulation could contaminate the detection of the solar signal when 2–4 solar cycles were included in the analysis. The near coincidence of the El Chichón and Mt. Pinatubo volcanic eruptions in 1982 and 1991 with two solar maxima also complicates the quantification of solar signals derived from data. Thus, there is still uncertainty in quantifying the solar cycle by statistical analysis from observations, particularly in the lower stratosphere. Chapter 8 of SPARC CCMVal (2010) finds that the direct solar response in temperature and ozone in the upper stratosphere is well represented, but the vertical structure in the tropics below 10 hPa varies considerably among the models and between models and observations. Chapter 8 also notes large uncertainties in the middle to lower stratosphere that are the result of short observational records, possible aliasing of signals from QBO and volcanoes, as well as possible nonlinear interactions of the solar cycle signal with QBO, ENSO, and volcanic signals.

Recent model analyses show an improved representation of the vertical distribution of the solar signal in ozone in the tropics as compared to WMO (2007). However, reasons for the better agreement in the 2-D and 3-D models are still under discussion and conflicting explanations for the tropical solar ozone response in the lower stratosphere are presented. Austin et al. (2008) noted that models participating in the first CCMVal exercise reproduced the observed vertical structure of the stratospheric tropical solar ozone signal, although the magnitude of the response was smaller than derived from observations. Climate forcings, including observed sea surface temperatures (SSTs) as well as time-dependent solar cycle forcings, were considered essential to simulating this response. Neither the QBO nor the upper atmospheric effects of energetic particles were found to be necessary to explain the observed solar cycle response of ozone or temperature. Large discrepancies among the models and a small (insignificant) solar signal found in the tropical lower stratosphere in models that did not include solar forcing suggest possible influences from other processes (SST variations and aliasing between the signals) or from random variability in the records (Austin et al., 2008).

Schmidt and Brasseur (2006) used the Hamburg Model of the Neutral and Ionized Atmosphere (HAMMONIA) to simulate the difference between solar maximum and solar minimum. They produced a solar signal in the tropical lower stratosphere using climatological sea surface temperatures and a repeating solar cycle. This solar signal is independent of the presence of a self-consistently produced QBO (Schmidt et al., 2010). Tsutsui et al. (2009) found a small, not significant (0.6%) solar cycle response of ozone in the tropical lower strato-

sphere in a simulation using the Whole-Atmosphere Community Climate Model (WACCM) forced with climatological SSTs and a time-varying solar cycle. However, McCormack et al. (2007) highlight the importance of the presence of a QBO for the solar signal in tropical ozone in their 2-D model simulations. Their internally generated QBO is itself modified by the solar cycle. Additional complications arise from aliasing between ENSO and the solar cycle in the tropical lower stratosphere (Marsh and Garcia, 2007). Recent statistical analysis applied to observations and model simulations includes a proxy term that accounts for ENSO variations (Randel et al., 2009; Chapter 8 of SPARC CCMVal, 2010).

In summary, the upper stratospheric ozone response (2–3% between solar minimum and solar maximum) is reproduced by the CCMVal models and is a direct radiative effect of heating and photochemistry. The lower stratospheric solar cycle in tropical ozone appears to be caused indirectly through a dynamical response to solar ultraviolet variations. The origin of such a dynamical response to the solar cycle is not fully understood.

2.4.3.3 VOLCANIC AND AEROSOL EFFECTS

Sulfate volcanic aerosols affect stratospheric circulation and temperature, provide surfaces for chemical heterogeneous reactions, and lead to ozone depletion (Hofmann and Solomon, 1989). The aerosols produced by Mt. Pinatubo, which erupted in June 1991, decayed by 1996. No major volcanic eruptions have occurred between 1996 and present, but efforts to quantify fully the effects of volcanic aerosols on stratospheric ozone continue, in part due to the importance of quantifying potential effects of continuous injection of sulfur into the stratosphere that has been discussed as a “geoengineering” approach to counteract global warming from increased greenhouse gases (e.g., Crutzen, 2006; Rasch et al., 2008). Geoengineering is discussed further in Section 3.2.6 of Chapter 3.

1-D, 2-D, and 3-D models have been used to determine the chemical and dynamical effects of volcanic aerosols (e.g., Zhao et al., 1995; Tie et al., 1994; Stolarski et al., 2006). The polar vortex strengthens in NH after a volcanic eruption because of the changes in the equator-to-pole temperature gradient in the lower stratosphere (Stenchikov et al., 2002). A stronger polar vortex increases the probability of formation of polar stratospheric clouds, thereby enhancing the rate of heterogeneous chemical destruction of stratospheric ozone (Tabazadeh et al., 2002). The effects on stratospheric ozone depletion in the wake of a volcanic eruption are largest when chlorine and bromine levels are largest (Tie and Brasseur, 1995). The surface area density (SAD) of sulfate aerosols in models, the crucial input parameter to simulate this aspect of ozone depletion,

is usually prescribed based on observations. Comparisons of simulations with observations suggest that there are no significant missing processes or greatly inaccurate reaction rates (e.g., Fahey et al., 1993; Dessler et al., 1997).

Analysis of CCMVal-2 models (SPARC CCMVal, 2010) shows that the simulated post-eruption changes in total column ozone are well correlated with changes in lower stratospheric chlorine monoxide. Although most models use the same aerosol SAD data set to drive the anomalous post-eruption chemistry, the sensitivity to aerosols and the background SAD values differ among models, leading to different amounts of chlorine activation and associated ozone loss. Mäder et al. (2007) used statistical analysis of total ozone data from 158 ground stations to show that the SAD had the largest impact on the decrease of total ozone in the Northern Hemisphere. This is consistent with the conclusions in WMO (2007) that the Mt. Pinatubo aerosols appeared to have a stronger effect on ozone in the Northern Hemisphere than in the Southern Hemisphere.

Telford et al. (2009), using a nudged CCM (UK Chemistry and Aerosols (UKCA)) simulation, concluded that the depletion of stratospheric ozone was produced mainly as a result of photochemical changes due to heterogeneous reactions, but there was some evidence for dynamically induced ozone reduction, especially in the NH midlatitudes. Fleming et al. (2007) found that the interannual dynamical variability in two-dimensional model simulations acts to reinforce the ozone perturbation in the NH midlatitudes, while in the SH the observationally derived circulation mitigates or even cancels the aerosol-induced chemical ozone reactions. Robock et al. (2007), using National Centers for Environmental Prediction (NCEP) and European Centre for Medium-Range Weather Forecasts (ECMWF) analyses and Goddard Institute for Space Studies (GISS) Model E, and Feng et al. (2007), using a 3-D CTM, did not find a clear signal of chemical ozone loss in the SH midlatitudes after the eruption of Mt. Pinatubo. In contrast Brunner et al. (2006), using Candido Assilated Three-dimensional Ozone (CATO), demonstrated a significant effect of volcanic aerosols on ozone in SH mid (south of about 45°) and high latitudes. In summary, observations and model simulations found a significant effect of Mt. Pinatubo volcanic aerosols on stratospheric ozone in the NH compared to the SH. The absence of a stronger observation of ozone loss in the SH is not yet understood.

Polar ozone is also sensitive to volcanic enhancement of stratospheric aerosols. There have been no new findings on this subject since WMO (2007), but results are summarized here due to the potential importance of an increase in stratospheric aerosols through geoengineering as discussed above and in Section 3.2.6. Studies of the Arctic winter 1991/1992 consistently find enhanced polar ozone loss due to the presence of Mt. Pinatubo aerosol

(Rex et al., 2004; Tilmes et al., 2008b) although the quantitative estimates of the volcanically induced signal differ. Further, Portmann et al. (1996) showed that Antarctic ozone depletion in the 1980s and early 1990s was influenced by enhanced sulfate aerosol SAD, and speculated that the ozone hole might have been detected later than the mid-1980s if there had been no increase in aerosol loading from El Chichón and several earlier minor eruptions. Portmann et al. (1996) also suggested that future Arctic ozone depletion could be severe in unusually cold winters with large volcanic aerosol SAD present. Several studies attempt to discern the effects of volcanic aerosol perturbations on PSC characteristics (Deshler et al., 1994; David et al., 1998; Fromm et al., 2003). These studies are inconclusive, largely because it is much more difficult to distinguish PSCs – especially STS – when the background (non-PSC) sulfate aerosol level is elevated and varies temporally.

As noted above, there have been no recent major volcanic eruptions, but there is evidence that the background stratospheric aerosol layer is changing. Hofmann et al. (2009b) analyzed ground-based measurements to show that stratospheric aerosol amount exhibits an increasing trend since 2000, attributing the background stratospheric aerosol since 2002 to an increase in the SO₂ emissions caused by an increase in global coal consumption, mainly in China. Hofmann et al. (2009b) estimate the contributions to the increase in the stratospheric aerosol from major volcanic activity and from increased tropical upwelling due to change in the Brewer-Dobson circulation, concluding that these are not significant. However, analysis of observations from the Cloud-Aerosol Lidar with Orthogonal Polarization (CALIOP) suggests that small volcanic eruptions may play a role. CALIOP data show significant changes in aerosol concentration in the tropical stratosphere between 2006 and 2008 (Vernier et al., 2009). CALIOP data showed slow ascent of the Soufriere plume in 2006 from 20 to 25 km, consistent with the Brewer-Dobson circulation and remnants of aerosols from minor volcanic eruptions such as Manam in 2005. Quantitative attribution of the sources of the observed change in background aerosols has not been accomplished.

2.4.3.4 EVALUATION OF SIMULATED TRANSPORT

The evaluation of transport emphasizes the model ability to reproduce observations that are directly related to large-scale physical processes affecting ozone distribution, such as tropical ascent and Antarctic vortex isolation. The reader is referred to Chapter 5 of the SPARC CCMVal (2010) report for detailed evaluation of individual models.

The distributions of long-lived trace gases in the stratosphere are controlled by transport processes, mainly

by the balance between the diabatic circulation and quasi-horizontal mixing (e.g., Holton, 1986). Transport affects the ozone distribution directly and indirectly. In the lower stratosphere ozone is long lived, and large-scale transport from source regions is important to its spatial and temporal distribution. Transport affects ozone indirectly by determining the mixture of chemicals that affect ozone loss at a given location. In Chapter 5 of SPARC CCMVal (2010), diagnostics for circulation and mixing were developed from observations and applied to CCMs. These evaluations identified key processes essential for realistic transport. Chapter 5 concluded that for the credible prediction of future stratospheric composition, the following transport requirements are essential: (1) realistic tropical ascent in the lower stratosphere; (2) realistic mixing between the tropics and extratropics in the lower and middle stratosphere; (3) generation of an isolated lower stratospheric Antarctic vortex in spring; (4) local conservation of chemical family mixing ratios (e.g., Cl_y); and (5) good agreement on all mean-age diagnostics. A summary of the performance of participating CCMs on these criteria is given below.

An adequate tracer advection scheme must conserve chemical families such as total inorganic chlorine (Cl_y) for credible predictions of future ozone levels. Conservation of Cl_y means that models should not produce higher levels of Cl_y in the upper stratosphere than released in the form of organic chlorine at the surface. Three CCMs failed to conserve total chlorine, undermining their credibility for assessment of ozone trends due to chlorine. A fourth model had excess stratospheric chlorine due to insufficient tropospheric removal of hydrogen chloride (HCl).

For more than a decade, model transport has been evaluated using comparisons of simulated and observationally derived mean age at 50 hPa in the midlatitudes and tropics (e.g., Hall et al., 1999; Eyring et al., 2006). These comparisons revealed several issues with model transport. However, at 50 hPa, age distributions computed by many models participating in CCMVal-2 compare well with those derived from observations even though other diagnostics reveal persistent transport issues. The average mean age diagnostic (AMA) was developed in the SPARC CCMVal (2010) report to broaden the comparisons with observationally derived ages in order to assess a model's overall transport fidelity. AMA is based on mean age comparisons at seven locations in the lower and middle stratosphere between 60°S and 60°N. The mean age is a sensitive function of both the circulation and mixing, and the distribution of mean ages throughout the stratosphere reflects the balance between them, which varies as a function of height. While compensating errors in ascent and quasi-horizontal mixing can result in good mean age in some altitudes, it is unlikely that a model will have perfectly balanced compensating errors in both

the lower and middle stratosphere, making the AMA diagnostic a more stringent test of transport than mean age at 50 hPa alone.

Although AMA is a strict diagnostic, fortuitous agreement with mean ages derived from observations is possible because excessive recirculation increases mean age while a fast circulation decreases it. Together they can produce compensating transport errors. It is therefore important to independently assess both the circulation and mixing in models. Significant problems with tropical stratospheric transport have been identified in half of the 18 participating CCMs. Tropical ascent and tropical-midlatitude (T-M) mixing across the subtropics are crucial to distributing ODSs in the stratosphere, and deficiencies in the transport of ODSs affect modeled abundances of the products of ODS destruction (Cl_y) everywhere. Ten of the 18 CCMs were found to have realistic ascent in the tropical lower stratosphere. Of the remaining eight, two models showed a very slow circulation, while six had faster-than-observed ascent rates. T-M mixing, essentially a measure of the degree of isolation of the tropics, was evaluated using as many as four diagnostics in the lower and middle stratosphere. Nine of the ten CCMs with realistic ascent rates also showed reasonable mixing across the subtropics. Of the other nine models, the two models with slow circulations had too little T-M mixing while the other seven showed too much mixing between the tropics and midlatitudes. Strong T-M mixing increases the simulated mean age by allowing older midlatitude air to re-enter the tropics and recirculate through the stratosphere, increasing mean age everywhere. The wide range of independent observations from which the diagnostics are derived strengthens the usefulness and credibility of these evaluations.

Other essential transport processes for simulation of the ozone response to changing chlorine levels are strong descent in the southern winter vortex and the presence of a barrier to mixing between the vortex and midlatitudes in early spring in the Antarctic. Chapter 5 of SPARC CCMVal (2010) showed that vortex isolation is uncorrelated with the AMA, tropical ascent, and T-M mixing and therefore must be evaluated in addition to the other circulation and mixing diagnostics. Of the nine models showing both good tropical ascent and T-M mixing, seven also showed realistic, isolated descent at the end of austral winter. Lower stratospheric vortex isolation in spring, which is crucial to maintaining the high levels of Cl_y necessary for a credible ozone hole, was found to be sufficient in only eight of 18 CCMs. Of the eight CCMs producing an isolated vortex, only four also showed realistic tropical ascent, T-M mixing, average mean age, and polar descent. Those models are CMAM, GEOSCCM, UM-SLIMCAT, and WACCM. (See Table 3-1 of Chapter 3 for descriptions of the CCMs.)

2.4.3.5 EVALUATION OF THE CHEMICAL MECHANISM AND ITS IMPLEMENTATION

Chapter 6 of CCMVal-2 (SPARC CCMVal, 2010) presents the first major attempt at quantifying the behavior of stratospheric chemistry modules within various global 3-D CCMs. Eight of the 18 models participating in CCMVal-2 took part in a photolysis intercomparison (PhotoComp). The chemical mechanism within CCMs was evaluated by comparison of radical species output by each CCM to calculations conducted using a benchmark photochemical steady state (PSS) model, constrained by the abundance of long-lived species and sulfate surface area density (SAD) from each CCM. This comparison was conducted for 14 of the 18 groups. Quantitative metrics were developed for both PhotoComp and PSS, based on equation (4) of Waugh and Eyring (2008). Careful attention was devoted to proper definition of uncertainties. The majority of models showed good agreement with the PhotoComp benchmark.

Models showed a range of agreement with the evaluation of fast chemistry, with some models showing very good to excellent representation of both radicals and their precursors. The radicals in some models show significant discrepancies with the PSS benchmark; in some cases the precursors disagree with a suite of atmospheric observations included in the evaluation (Chapter 6, SPARC CCMVal, 2010). The most realistic representations of fast chemistry were found to be provided by the WACCM, EMAC, GEOSCCM, CMAM, and UM-SLIMCAT models (Figure 6.11 of SPARC CCMVal, 2010). Results for these models are highlighted in subsequent figures.

The PSS evaluation provides an important new tool for quantitative evaluation of the chemical mechanism within CCMs based on analysis of archived model output. A particular CCM model has been observed to exhibit a much larger sensitivity of ozone to anthropogenic halogens than any of the other CCMs; the PSS evaluation shows that this sensitivity is the result of omission of the HCl production from $\text{ClO} + \text{OH}$ in their chemical mechanism (Chapter 6 of SPARC CCMVal, 2010). Previously, chemical mechanisms have been evaluated either by exchange of code or by various groups performing prescribed calculations, both of which are arduous tasks.

The comparisons carried out for CCMVal-2 also showed that models used widely varying distributions of sulfate SAD, even for simulations designed to simulate past behavior (Chapter 6 of SPARC CCMVal, 2010). These differences may be due to the specification of the SAD climatology as a function of geometric altitude, a coordinate not commonly used in CCMs.

One notable difference among the various CCMs was the abundance of Cl_y at the tropopause. Some models have near-zero Cl_y ($\ll 50$ parts per trillion (ppt)) while

other models have much larger values ($\gg 50$ ppt). Models with high levels of Cl_y at the tropopause tend to have excess Cl_y throughout the lowermost stratosphere. These differences in Cl_y are likely due to various representations of HCl uptake and removal in the troposphere (Chapter 6 of SPARC CCMVal, 2010). This is an important detail because models with the higher values of Cl_y in the lowermost stratosphere display greater sensitivity to future changes in stratospheric H_2O and temperature than models with near-zero Cl_y .

2.4.3.6 EVALUATION OF SIMULATIONS OF THE UPPER TROPOSPHERE/LOWER STRATOSPHERE

Chemistry-climate models are important for disentangling and quantifying the effects of halogens on ozone from those of climate change. In the upper troposphere/lower stratosphere (UTLS, approximately defined here as the region between 5 and 22 km), dynamical variability and its expected response to climate change are large. The ability of CCMs to represent the basic characteristics of the dynamical and chemical structure of the UTLS has been tested in Chapter 7 of SPARC CCMVal (2010; also see Gettelman et al., 2009; Gettelman et al., 2010). Various characteristics of the tropical and extratropical chemical and dynamical structures have been evaluated using both quantitative and qualitative diagnostics derived from robust relationships found in aircraft and satellite observations, or reanalyses data sets. The tested characteristics include the representation of the tropical tropopause layer, the tropopause inversion layer, the extratropical tropopause transition layer, and the seasonal cycles in tropical cold point temperatures, lowermost stratospheric mass, and tropical and extratropical water vapor and ozone.

Most CCMs represent the basic dynamical and chemical characteristics of both the tropics and the extratropics well. Models mostly reproduce the annual cycle of tropical cold point temperatures in the tropics, with the right amplitude and timing. However, they show some significant biases in the annual mean cold point temperature. Similar findings are found for the representation of the seasonal cycle in ozone. However, amplitude, timing, and mean value of tropical water vapor does not follow the tropical cold point temperature as expected, which indicates errors in transport and/or microphysics in the models.

In the extratropics, the dynamical structure including zonal mean winds, the seasonal cycle in the lowermost stratospheric mass, and the seasonality and latitudinal behavior of the tropopause inversion layer are well captured. This implies that both the climatological distribution of radiatively active species and the radiative transfer in the models are realistic. The models fail to reproduce the observed sharpness in the tropopause inversion layer, most likely due to limited spatial resolution. The seasonal cycles

in ozone and water vapor are generally well reproduced but indicate a too large (small) amplitude at 100 (200) hPa. The models also resolve the strong tracer gradients across the extratropical tropopause, indicating that simulation of the Brewer-Dobson and the tropospheric baroclinic circulations is at least qualitatively realistic. Models that perform particularly well in the extratropics are CMAM, E39CA, GEOSCCM, and WACCM (Chapter 7 of SPARC CCMVal, 2010). Models that perform less well have issues that include insufficient vertical and horizontal resolution or use of a diffusive numerical transport scheme.

Outstanding deficiencies in the models that affect the ozone distribution and introduce uncertainties in UTLS evaluations are the lack of comprehensive representations of tropospheric chemistry involving nonmethane carbons, of wet and dry deposition, and of lightning NO_x. CCMs include varying lightning NO_x parameterizations, however, the most common one dates back to Price and Rind (1992), which has been shown in recent chemistry transport model studies to be inadequate in generating observed NO_x levels in lightning-affected regions in the upper troposphere (Hudman et al., 2007; Sauvage et al., 2007; Parrington et al., 2008).

2.4.4 Recovery Detection and Attribution

Section 2.1 discussed the data obtained over the past decades including a time-series analysis directed toward determining the current stage of ozone recovery as defined in WMO (2007). Here we discuss the problem of attribution of changes in ozone to changes in chlorine and bromine in the stratosphere.

The past evolution of ozone has been influenced by changes in ODSs and also by changes in greenhouse gas (GHG) concentrations. GHGs influence stratospheric ozone in two ways. In the upper stratosphere, cooling due to increased GHG concentrations leads to an ozone increase by slowing the temperature-dependent catalytic loss cycles. In the lower stratosphere where ozone is long-lived, radiatively driven dynamical changes to the Brewer-Dobson circulation that result from increased GHG concentrations affect the ozone distribution through transport. Attribution of past trends is complicated by the need to untangle the effects of the increases and leveling off of ODSs from the effects of continued increases in GHGs. The implications of these processes on the future development of the ozone layer are discussed in detail in Chapter 3 of this Assessment.

2.4.4.1 DYNAMICAL CONTRIBUTIONS TO APPARENT TREND

In addition to the slow trend in ozone expected due to changing GHGs, dynamical variability in short time series of measurements or model simulations can give rise

to an apparent trend. WMO (2007) summarized a number of studies using chemistry and transport models (CTMs) driven by analyzed winds and studies using empirical relations between planetary wave activity and circulation to address the question of dynamical contribution to Northern Hemisphere midlatitude ozone trend. WMO (2007) concluded that about 30% of the observed negative trend from 1979 to the mid-1990s could be attributed to changes in the lower stratospheric circulation based on both empirical and model studies.

Numerous model and observational studies have demonstrated the importance of dynamical contributions to ozone trends. In an extension of previous studies, Feng et al. (2007) used a CTM to show how spurious trends could result from the use of analyzed winds. They concluded that their simulation with nearly constant ODSs could reproduce the increase in NH midlatitude ozone from the 1990s. Brunner et al. (2006) empirically analyzed ozone data to show that the Brewer-Dobson circulation was a dominant contributor to interannual variability at both high and low latitudes. They further showed that this variability accounted for some of the ozone increase seen in the Northern Hemisphere since the mid-1990s. Fleming et al. (2007) used a 2-D model with winds derived from planetary wave forcing derived from ERA-40 and also from NCEP. They found a good fit to the overall ozone column variability from 1979 through 2005 that appears to have a dynamical contribution to both the downward trend between 1979 and the mid-1990s and the upward trend since then. Harris et al. (2008) examined both chemical and dynamical influences on decadal ozone trends, primarily in the Northern Hemisphere. They found that recent increases in ozone were linked to dynamical processes in the lower stratosphere.

Overall, studies agree that dynamical variability contributed to both the downward trend in the NH through the mid-1990s and to the upward trend in total ozone since the mid-1990s. In addition, Fleming et al. (2007) found little impact of dynamical variability on the fit to the EESC curve for the overall time period from 1979 through 2005.

2.4.4.2 GREENHOUSE GAS EFFECTS ON OZONE TRENDS

In addition to the possible trends due to interannual variability, the change in composition due to the increasing GHGs may cause ozone trends through changes in chemistry and dynamics, as noted previously. CCMs consistently predict a strengthening of the stratospheric Brewer-Dobson circulation (BDC) due to climate change (Butchart and Scaife, 2001; Butchart et al., 2006; McLandress and Shepherd, 2009) that leads to changes in the spatial distribution of ozone (Shepherd, 2008; Li et

al., 2009; Hegglin and Shepherd, 2009). Shepherd (2008) showed that CMAM results indicated an eventual recovery to values above 1980 (or 1960) (i.e., super-recovery) in the mid and high latitudes and under-recovery in the tropics. Both Shepherd (2008) and Li et al. (2009) found nearly latitude-independent increases in upper stratospheric ozone due to temperature decreases in CMAM and GEOSCCM, respectively. Both studies also found lower stratospheric ozone decreases in the tropics and increases elsewhere due to the simulated change in the BDC. In CMAM the effects from the upper and lower stratosphere largely cancel in the 60°S–60°N mean total ozone. According to CMAM, total ozone in the tropics will remain below pre-1980 values, whereas in the midlatitudes, and in particular in the NH between 35°N and 60°N, total ozone will increase to values about 5% above pre-1980 levels in the second half of the 21st century. The GEOSCCM calculates lower stratospheric ozone changes that approximately cancel when averaged globally (Li et al., 2009), so that the resulting change in global mean total ozone is dominated by the upper stratospheric ozone increase.

The studies by Shepherd (2008) and Li et al. (2009) showed the combined effect of GHGs and ODSs on stratospheric ozone, but did not quantify past and future changes to changes in ODSs or GHGs. Shepherd and Jonsson (2008) argued that carbon dioxide (CO₂)-induced cooling had masked about 20% of the ODS-induced ozone depletion. Waugh et al. (2009), using calculations from the GEOSCCM to separate the effect of ODSs and GHGs, found that simulated stratospheric ozone changes during the past decades were clearly dominated by ODSs, except for the tropical lower stratosphere. Here the calculated ozone change during past decades due to the increased strength of the BDC (enhanced tropical upwelling) exceeded the calculated effect of ODSs.

CCMs suggest that GHG-induced changes in temperature and in the BDC may partly be responsible for past ozone changes. Therefore, it is important to assess the realism of the simulated circulation changes. Changes in the strength of the Brewer-Dobson circulation have not been unambiguously detected from observations. Engel et al. (2009) have analyzed balloonborne measurements of CO₂ and sulfur hexafluoride (SF₆) over the past 30 years to derive possible trends in stratospheric age of air. They found a small but insignificant increase of the age of air in the midlatitude middle stratosphere, in contrast to the small decrease in age of air due to the increased BDC calculated with CCMs. The results from this analysis can neither confirm nor deny the model results because of the large error bars and shortness of the record (see also Waugh, 2009). Because the simulated change in the BDC is most apparent in the tropical lower stratosphere where the ozone vertical gradient is steep, CCMs predict a change in ozone there that may be detectable in a long, stable time series of observa-

tions. There are significant issues with ozone trends in the tropical lower stratosphere due to insufficient length of the observational record as discussed below in Section 2.4.5.3.

2.4.4.3 POLAR LOSS AND DILUTION TO MIDLATITUDES

WMO (2007) discussed in detail the importance of export of ozone-depleted air from the polar vortices to mid-latitude trends, attributing about 30% (50%) of the northern (southern) midlatitude trends in total ozone for 1979 to 1995 to this process. Results from multiannual simulations are generally consistent with detailed process studies for a few specific years in both hemispheres. Andersen and Knudsen (2006) conclude that longitudinal differences in the export of ozone-depleted air accounts for the longitudinal dependence of winter and springtime ozone trends at northern midlatitudes. The simulation of polar loss and its comparison to data are discussed in Section 2.4.5.4 below.

2.4.5 Simulation of Ozone Changes for the Last Three Decades

Previous sections discussed specific perturbations of stratospheric ozone in current chemistry-climate models. The CCMVal-2 report evaluates these models with a particular emphasis on their representation of processes by comparison to measurements of the current or recent past atmosphere. In this section we consider the ability of these models to reproduce the observed ozone trends over the last three decades by comparison to the data shown in Section 2.1.

2.4.5.1 TOTAL OZONE TRENDS

Figure 2-23 shows the total ozone trend for 1979–1995 as a function of latitude computed by multiple linear regression (MLR) as described in Section 2.1.2. The sensitivity of total ozone to EESC is calculated by applying the MLR to the entire data period (1978–2009), and the trend is shown for the time period during which EESC increased linearly (1979–1995). The models are also fit with EESC from 1978 through the end of the REF-B1 simulation (usually 2004 to 2007). Note that the EESC fit obtained in this manner is more sensitive to the shape of the EESC function than to the length of record (see Section 2.1.2). The models generally reproduce the latitude dependence of the total ozone trend derived from the merged ozone data, but differ in some significant details. Most models produce a negative trend in the tropics while the data show no trend. Red lines are from three models (CMAM, GEOSCCM, WACCM) that rated highest in CCMVal-2 evaluations of transport, photochemistry, and UTLS discussed in

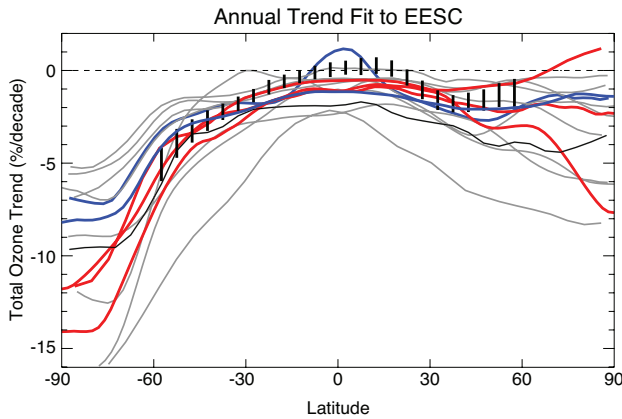


Figure 2-23. Latitude dependence of the annual total ozone trend (%/decade) from 13 of the 18 models used in CCMVal-2 and the merged ozone data set. Trends derived from measurements with 2σ uncertainties are indicated by vertical bars. Red lines are from three models (CMAM, GEOSCCM, WACCM) that rated highest in all three CCMVal-2 tests. Blue lines are from two models (UMSLIMCAT and EMAC) that rated highest in one or two of the three CCMVal-2 tests. Model trends for 1978–1996 are calculated by fitting to EESC using output from 1978 through the end of the REF-B1 simulation. Model descriptions are given in Table 3-1 of Chapter 3.

Sections 2.4.3.4–2.4.3.6 above. Blue lines are from two models (UMSLIMCAT and EMAC) that rated highest in one or two of the three CCMVal-2 tests.

In the southern midlatitudes, with one exception, the model trends vary with latitude in a manner similar to the trend derived from observations, but with significant spread in the magnitude of model trends. A similar spread is found for northern midlatitude trends. The model results show less spread when output beginning in 1960 is used to determine the fit to EESC (not shown), particularly in the north-polar region where interannual variability is large. In the tropics and midlatitudes, the models highlighted as having the best representations of transport, chemistry, or the UTLS generally are more similar to each other than the collection of all model simulations. The same is not true for polar regions. In the tropics most models show a negative trend in total column ozone that does not agree with the trend deduced from either satellite or ground-based data sets. One exception is the EMAC model that has a region of significant positive trend over a portion of the tropics due to an ozone increase in the tropical troposphere; however, the EMAC positive trend disagrees with the trend derived from measurements.

This raises the question of whether the discrepancy in the tropics could be the result of increased tropospheric ozone that is of the same magnitude as the decrease in stratospheric ozone. Most of the models in this comparison do not include tropospheric chemistry or tropospheric physical processes, such as wet and dry deposition and the production of NO_x (and O_3) by lightning. In the tropics, about 10% of the ozone column is in the troposphere. To offset the 1% per decade decrease found in model simulations would require a $\sim 10\%$ per decade increase in tropospheric ozone from the late 1970s through about the mid-1990s. Studies have searched for evidence of a tropospheric trend. Ziemke et al. (2005), using a 25-year record of tropospheric column ozone (TCO) derived from TOMS and SBUV(2) data (1979–2003), showed a zero trend ($\pm \sim 1\text{DU}$ per decade) in the tropics in the Pacific. Beig and Singh (2007) used TOMS data along with the Model for Ozone and Related Chemical Tracers (MOZART) model to derive a trend versus longitude that is negative but insignificant over most of the tropics, but positive and significant over the Indonesian region ($\sim 7\text{--}9\%$ /decade). This trend appears to be the result of large fires in that region leading to ozone increases in the last few years that dominate the change in the record. Clain et al. (2009) derive marginally positive trends from ozonesonde records at Reunion Island (20.8°S , 55.5°E) and Irene, South Africa (25.9°S , 28.2°E). In summary, observational studies to date find no conclusive evidence for a tropospheric O_3 trend large enough to explain the difference between simulated and observed trends in total column ozone, thus the reasons for model disagreement with the observed tropical trend remain a mystery.

Figure 2-24a-d shows the annual average total ozone time series from the merged ozone data set and from each of the CCMs for four regions. The quasi-global average from 60°S to 60°N is shown in Figure 2-24a. In general the models reproduce the overall behavior of the data. The four models showing the best transport representation are highlighted in red and show a smaller difference than the ensemble of all models. Some of the models include forcing due to solar cycle, volcanoes, and QBO while others do not. Although there is a spread in the magnitude of the ozone change from the beginning of the record to the last few years, the models agree with the data that the total ozone has been relatively constant over the last 7–8 years at about 2–4% below 1980 values. The midlatitude time series shown in Figure 2-24b and 2-24d show similar behavior with more variability in the data and among models. Figure 2-24c shows results for the tropics where an apparent solar cycle is prominent in the data and most of the models run below the data, consistent with the trends shown in Figure 2-23.

2.4.5.2 MIDLATITUDE PROFILE TRENDS

In previous Assessments it was noted that 2-D models without temperature feedback showed better agreement with observed ozone trends in the upper stratosphere than models that did include the feedback. The CCMs used here have improved somewhat in this regard. Figure 2-25 and Figure 2-26 show trends deduced from measurements (SAGE, SAGE adjusted SBUV(2), SBUV(2), and ozonesondes) for the northern and southern midlatitudes, respectively. The trends calculated from SAGE for the upper stratosphere have been converted to pressure coordinates and have been adjusted to account for the temperature trend and the accompanying change of altitude at a given pressure level and the conversion of number density

mixing ratio (see Section 2.1.4; Rosenfield et al., 2005). The model results presented in both figures are all from simulations including temperature feedback.

The northern midlatitude simulated trends show a spread in the maximum upper stratospheric depletion that is centered near the trend deduced from data. The red region in Figure 2-25a shows the range of the 3 models with high ratings in each of CCMVal-2 evaluations of the transport, chemistry, and UTLS. The red plus blue regions show the range of those 3 models plus the 3 that were with high ratings in at least one evaluation. The range of deduced ozone trends for these 6 models is narrower than for the entire suite of models (gray shading) and centered near the trend derived from satellite observations. The derived trends from Umkehr measurements are somewhat larger

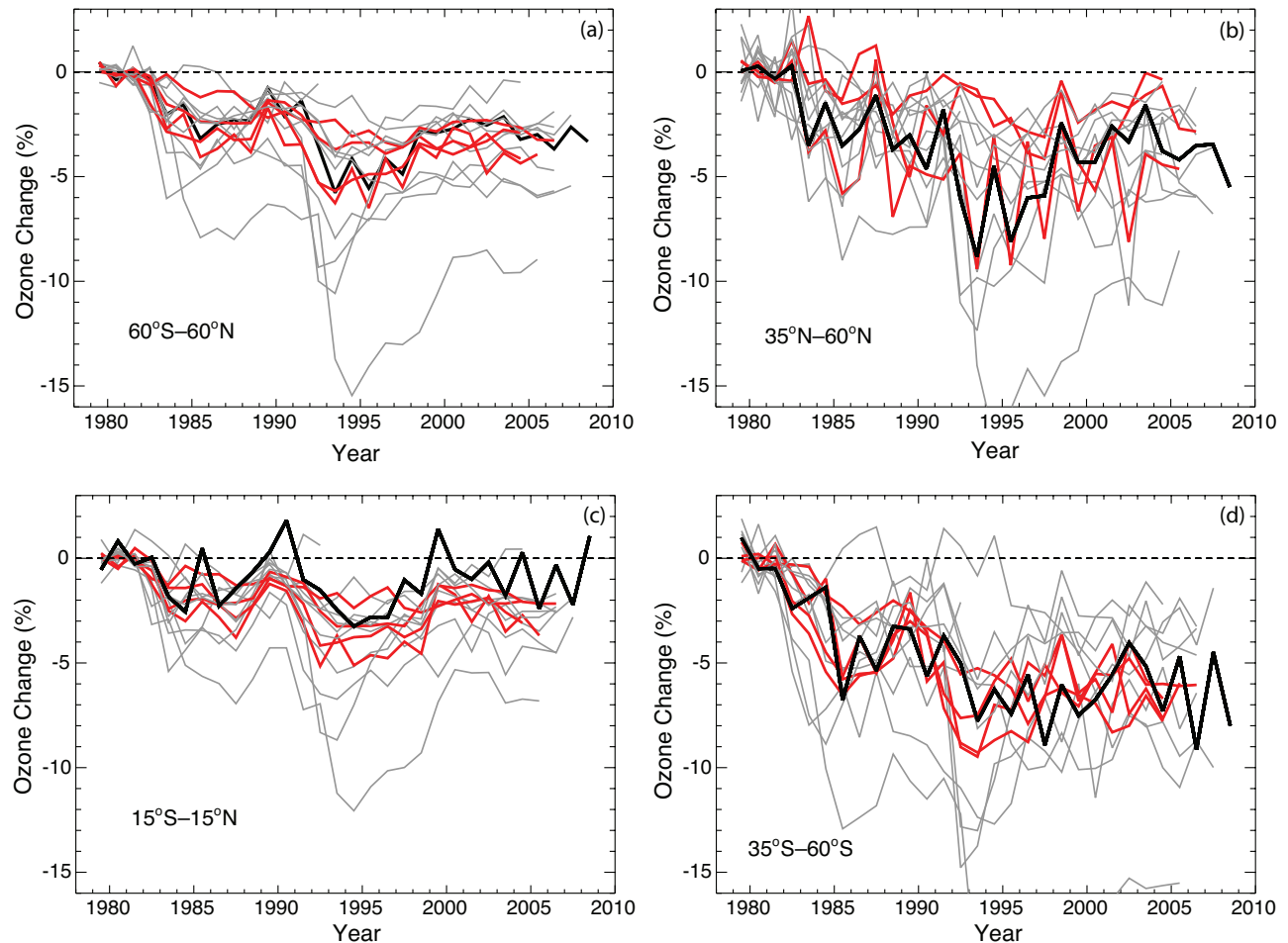


Figure 2-24. (a) Quasi-global time series of annual mean total ozone change (%) from 1980 value calculated from merged ozone data set in heavy black line and from 13 models in lighter lines. Changes in both models and observations are computed relative to the average for 1979–1981. Red lines are results from the four models that rated highest in the CCMVal-2 transport evaluation (CMAM, GEOSCCM, UMSLIMCAT, WACCM). The light gray line with large depletion appears to be an outlier to the rest of the models. (b) Same for northern midlatitudes. (c) Same for tropics. (d) Same for southern midlatitudes.

Figure 2-25. Altitude profile of calculated ozone trend (%/decade) at northern midlatitudes from 17 models. Trends derived from measurements are as defined in Figures 2-4 and 2-7. Panel (a): Trends for the period 1979–1996 are obtained by fitting to EESC. Trends derived from measurements with 2σ uncertainties are indicated by horizontal lines. The solid line is the trend derived from SAGE I + SAGE II data. The dashed line is trend derived from SAGE-corrected SBUV(2) data. The dash-dot line is the trend derived from SBUV(2) data. The dash-dot-dot line is the trend derived from sonde data. The long dashed line is the trend derived from Umkehr data. Red shading is the range of 3 models with high ratings in all 3 evaluations. Blue shading adds the range of 3 models that were highest in at least 1 evaluation. Panel (b): Altitude profile of trends calculated from model simulations for the time period 2000–2009, when the beginning of recovery is expected. Shaded regions are the same as in (a). Although the simulated upward trends and trends from measurements are broadly consistent, the observed increase cannot presently be attributed to ODS decrease because of observational uncertainty, natural ozone variability, and stratospheric cooling. Note that both stratospheric cooling and ODS decrease lead to a projected upper stratospheric ozone increase.

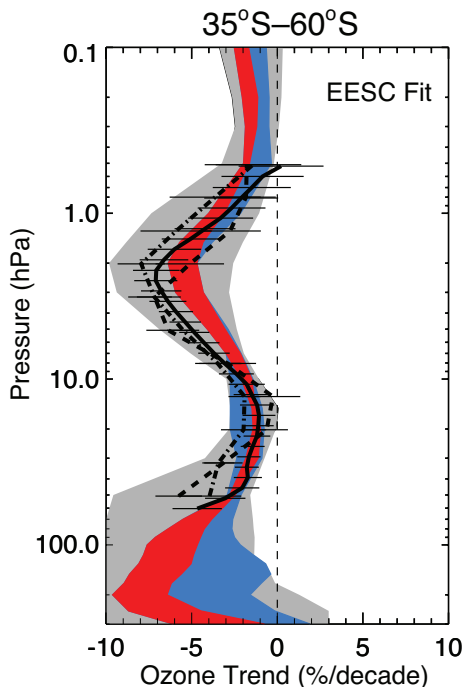
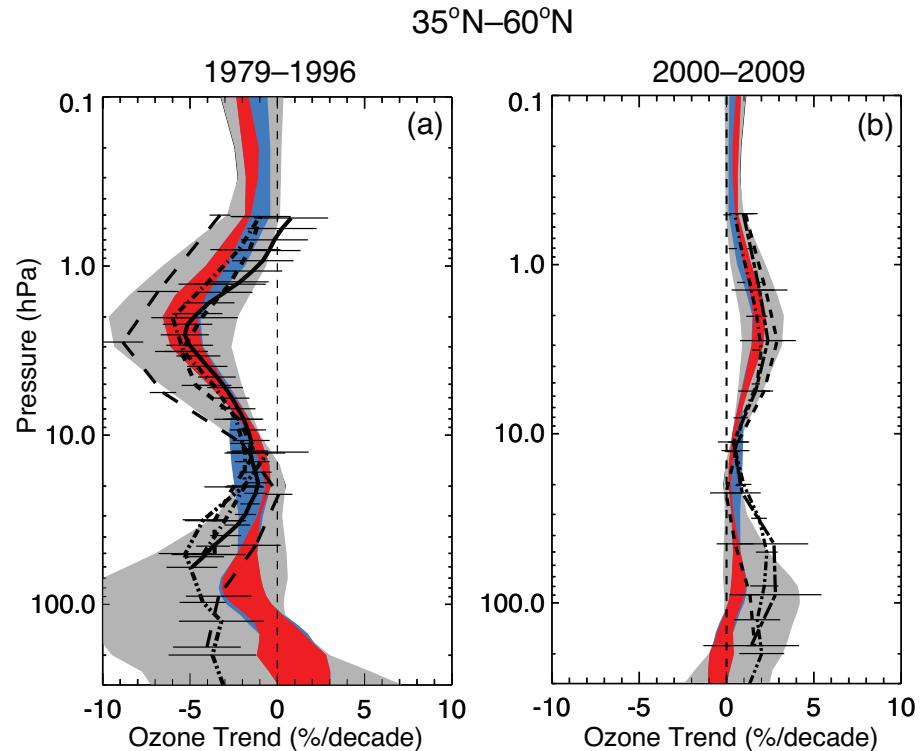


Figure 2-26. Same as 2-25a for the southern midlatitudes.

than the models and the trends derived from satellite measurements. The spread among models is larger in the lower stratosphere but is still significantly reduced by use of the diagnostics to filter results. Here the models that perform best on the diagnostics tended to have smaller trends than those deduced from ozonesonde measurements.

Figure 2-25b shows trends calculated from model simulations for the period after 2000 when the beginning of recovery is expected. Although the simulated upward trends and trends from measurements are broadly consistent, the observed increase cannot presently be attributed to ODS decrease because of observational uncertainty, natural ozone variability, and stratospheric cooling. Note that both stratospheric cooling and ODS decrease lead to a projected upper stratospheric ozone increase.

In the southern midlatitude (Figure 2-26) upper stratosphere, trends from the models that perform best on the diagnostics are somewhat smaller than those deduced from measurements. In the southern midlatitude lower stratosphere, the range of ozone trends deduced from models is somewhat more narrow for simulations that perform best on the CCMVal-2 diagnostics. In both the northern

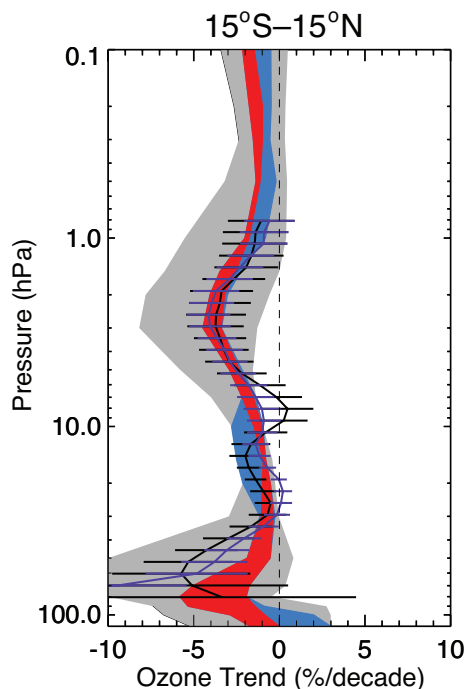


Figure 2-27. Ozone trends (%/decade) computed from CCMVal-2 simulations by 17 models as a function of altitude for the tropics. Black line: trend derived from SAGE II data alone. Purple line: trend derived from SAGE I + SAGE II data. The range of model simulations is as in Figure 2-25a.

and southern midlatitudes, the transport diagnostic selects simulations with smaller ozone depletion. Although we do not have enough sonde data to compare to southern midlatitude trends in the lower stratosphere, it appears that the simulated trends are smaller than trends derived from measurements at the northern midlatitudes.

2.4.5.3 TROPICAL PROFILE TRENDS

In the tropical lower stratosphere the models predict a decrease in column ozone due to increased upwelling (e.g., Butchart et al., 2006), in contrast to trends deduced from total column ozone measurements. The trends in the tropics computed from the simulations by 17 models are shown as a function of pressure in Figure 2-27. Almost all of the simulations show a similar pattern, with a decrease in the upper stratosphere centered at about 2–3 hPa and a smaller, narrower decrease in the lower stratosphere between the tropopause and about 60 hPa. The increase in tropical upwelling bringing up air with lower ozone amounts into the lower stratosphere and mixing of ozone-depleted air into the lower tropical stratosphere may both contribute to this trend.

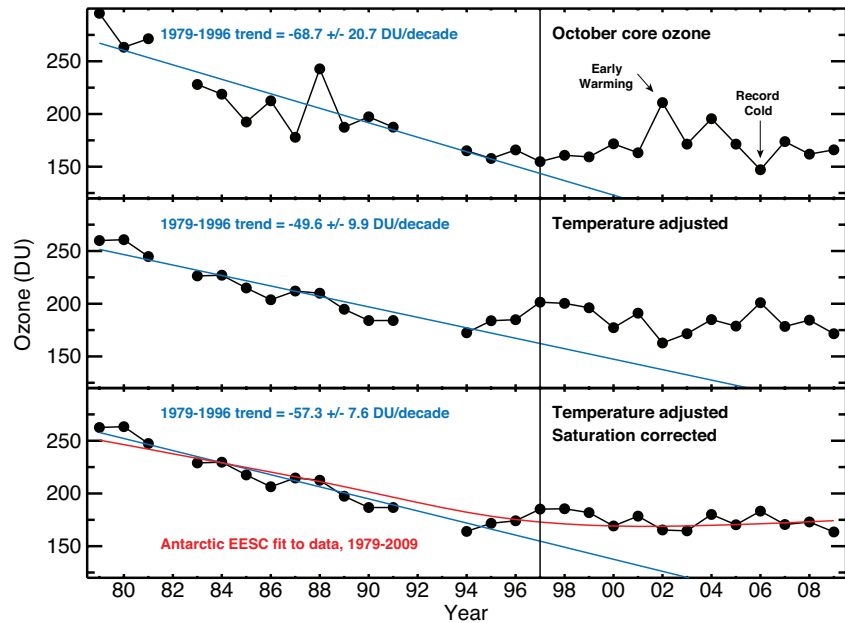
There is evidence for this lower stratospheric negative trend in data as shown by the SAGE I and SAGE I+II results in Figure 2-27. These trends are an update of Randel and Wu (2007). The results for SAGE I+II rely on the relative calibration of SAGE I to SAGE II, and are consistent with the results from SAGE II only and with the simulated trends. Brunner et al. (2006) used the CATO data set that uses measurements of total ozone and the analyses from ECMWF to infer global distributions of ozone. They found a narrow region of negative ozone trends in the tropical lower stratosphere and noted that these were consistent with those found for 1984–2000 in SAGE II data as reported in WMO (2003). As discussed in Section 2.4.5.1, the near-zero trend in tropical total ozone measurements is inconsistent with the negative trend found in the integrated SAGE I + SAGE II stratospheric profiles, and the tropospheric ozone column does not increase enough to resolve this discrepancy. The disagreement between trends obtained from vertically integrated SAGE data and trends obtained from the merged TOMS/SBUV(2) column ozone data set was discussed in WMO (2007).

2.4.5.4 POLAR TRENDS

Yang et al. (2008) report that Antarctic ozone is in the first stage of recovery. Ozone within the springtime Antarctic vortex is affected by both chemical and dynamical processes (Newman et al., 2006). Yang et al. (2008) used correlations between monthly means of total ozone column and temperatures to construct ozone anomaly time series, which reflect variations in ozone due to chemical forcing (Figure 2-28). The ozone anomaly time series reveals a statistically significant leveling off of ozone column since 1997, relative to the previous rate of decline. Yang et al. (2008) estimate ozone loss saturation by comparing the frequency distribution of measured ozone with the distribution expected from a reconstruction of ozone that hypothetically allows ozone abundances to drop below zero. This analysis indicates that the recent leveling off of the total ozone anomaly time series is due to changes in Antarctic halogen loading rather than loss saturation (bottom panel, Figure 2-28). They also identified the minimum of the second derivative of Antarctic EESC as a useful quantitative means to specify the break point for a piecewise linear fit to the data (further discussed in Chapter 1 of this Assessment).

As noted in the previous Assessment (WMO, 2007), trends in Arctic ozone are much more difficult to assess due to strong year-to-year variability of meteorological conditions and the dependence of inferred trends in temperature or ozone on start and end date. Furthermore, the trend in Arctic temperature is not sufficient to assess the impact of long-term changes on ozone (see

Figure 2-28. Time series of Dobson/Brewer measurements of total column ozone (Dobson units) in the core of the Antarctic vortex during October. Top panel: observed ozone column. Middle panel: resulting time series after removing effects of monthly mean temperature variations from the time series. Bottom panel: resulting time series after removing effects of loss saturation and monthly mean temperature variations from the time series. The blue line indicates the downward trend in column ozone for the respective time series, calculated for 1979 to 1996 and forecasted linearly afterward. Linear trends and 95% confidence intervals, DU/decade, are given. The red line in the bottom panel shows a fit of Antarctic EESC to the time series, considering data for the entire record. Years of “record cold” and of a sudden, “early warming” are indicated. Temperatures were warmer than usual in 1988, corresponding to the anomalously high levels of ozone observed that year. The vortex remained intact following the rise in temperature, hence 1988 is not classically considered to have experienced a sudden, “early warming.” From Yang et al. (2008), updated to include data for 2008 and 2009.



Years of “record cold” and of a sudden, “early warming” are indicated. Temperatures were warmer than usual in 1988, corresponding to the anomalously high levels of ozone observed that year. The vortex remained intact following the rise in temperature, hence 1988 is not classically considered to have experienced a sudden, “early warming.” From Yang et al. (2008), updated to include data for 2008 and 2009.

Section 4.1.1.1 of WMO, 2007). Since the previous Assessment, temperature conditions in the Arctic vortex have not been extremely cold for any particular ozone loss season. Chemical loss of Arctic ozone for recent years falls along the compact, near-linear relation with V_{PSC} (volume of air in the vortex exposed to temperature below the threshold for formation of PSCs) identified by Rex et al. (2004).

Much progress has been achieved in the evaluation of the representation of polar ozone loss in CCMs since the previous Assessment. The CCMVal-2 effort has provided important new insight into the chemical, dynamical, and radiative properties of CCMs (Chapter 6 of SPARC CCMVal, 2010). The chemical modules contained in CCMs are similar to the schemes used in off-line 3-D CTMs and other models known to produce good simulations of polar ozone loss under specified meteorological conditions (e.g., Chipperfield et al., 2005; Frieeler et al., 2006; von Hobe et al., 2007). However, use of a realistic and complete description of the relevant chemical (and microphysical) processes related to polar ozone depletion is only the first step toward obtaining an accurate representation of springtime polar ozone loss in coupled CCMs. The host general circulation model (GCM) must also simulate the correct descent over the pole, the correct timing and isolation of the polar vortex, and realistic temperatures that allow PSCs to form in the model.

Most CCMs include simplified schemes for PSC microphysics. Chapter 6 of SPARC CCMVal (2010) analyzed how well observed distributions of HNO_3 , H_2O , and HCl in the Antarctic were simulated by the CCMs. The models generally reproduced observed H_2O but overestimated HNO_3 . The CCMs generally use simplified equilibrium denitrification schemes and this discrepancy for HNO_3 will be affected by deficiencies in transport. Although conversion of HCl to active chlorine is essentially complete in most CCMs near 500–600 K, as expected from observations, the CCMs overestimate HCl at lower altitudes. This indicates incomplete chlorine activation in some CCMs, which would contribute to an underestimate of the simulated column ozone loss.

Figure 2-29 shows the time dependence of chemical loss of column ozone for the Arctic (top panel) and Antarctic (bottom panel) for 15 CCMs. Ozone loss derived from observations made by the Halogen Occultation Experiment (HALOE) instrument on the Upper Atmosphere Research Satellite (UARS) is also shown. The chemical loss of column ozone is calculated using analysis of the relationship between ozone and N_2O using archived records from each CCM. Chapter 6 of SPARC CCMVal (2010) shows that this method to quantify chemical ozone loss is reasonable because the simulated ozone versus N_2O relationship is well organized along isopleths, as observed. Also, Figure 2-29 shows that prior to ~1980 there

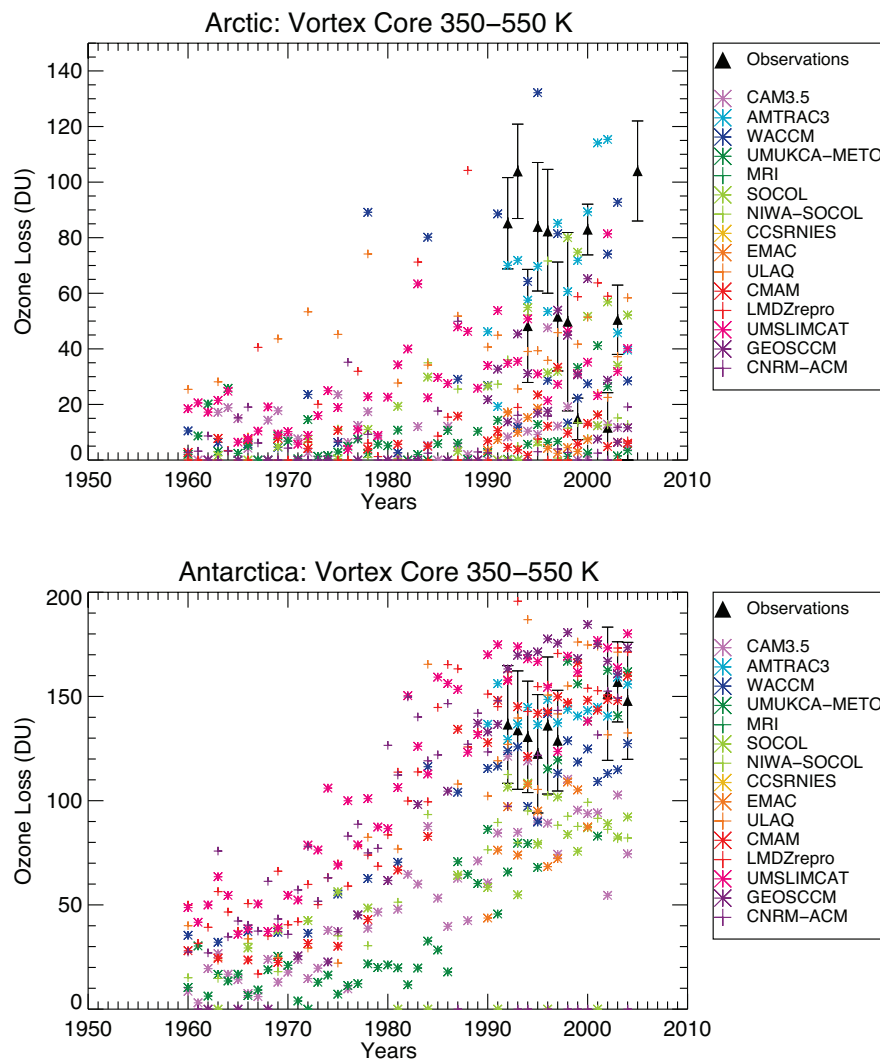


Figure 2-29. Chemical ozone depletion (Dobson units) in the polar vortex from January through April (top panel) and July through October (bottom panel) between 350 and 550 K. Results from observations (black triangles) were derived from HALOE on UARS for the polar vortex core. Model results are shown in different colors and calculated for equivalent latitudes poleward of 80°. Model descriptions are given in Table 3-1 of Chapter 3. (Reproduction of Figure 6.36, Chapter 6 of SPARC CCMVal, 2010).

is chemical loss of column ozone during the ozone loss season. Note that methyl chloride (CH_3Cl) supplies a natural background level of ~ 0.6 ppb Cl_y and anthropogenic ODSs were also increasing during this time period. Cl_y from both of these sources leads to chemical loss of ozone in the early part of the displayed time series, should meteorological conditions result in chlorine activation. Note that the loss due to CH_3Cl is natural and helps determine background levels of polar ozone prior to the buildup of Cl_y due to anthropogenic release of ODSs.

Figure 2-29 shows that modeled chemical loss of column ozone compares better with loss derived from observations in the Antarctic than in the Arctic. There are long-standing discrepancies between model behavior and observations related to the polar lower stratosphere, particularly for the Arctic (e.g., Eyring et al., 2006). CCMs tend to exhibit a cold bias in the Antarctic lower stratosphere and a concomitant westerly circulation that is too strong. The polar vortex then persists later into spring

than observed. Analysis of the CCM tracer transport shows that the different CCMs vary widely in their ability to produce an isolated lower stratospheric Antarctic vortex, with about half of them producing sufficient isolation for the altitude region and time period critical for ozone loss. In the Arctic, where observed temperatures are nearer the threshold for PSC formation, the CCMs are on average warm-biased and there is a large amount of model-to-model variation. The CCMs underestimate the observed frequency of cold Arctic winters. Because the CCMs are generally warm biased in the Arctic they tend to underestimate observed chemical loss of column ozone in the NH. In the SH CCMs are generally cold biased, and simulated column ozone loss generally scatter about the range of column loss derived from observations. In the SH ozone loss tends to saturate in the cold, isolated vortex. Another factor that may contribute to the spread in model results in Figure 2-29 is that although the standard CCMVal-2 runs only included bromine from long-lived

source gases, some models included ~6 pptv extra bromine to be more consistent with the actual stratospheric loading. This increases the loss computed for these models.

2.4.5.5 TRENDS AND RECOVERY IN THE UPPER TROPOSPHERE AND LOWER STRATOSPHERE

The upper troposphere and lower stratosphere (UTLS) are key regions where ozone changes can affect radiative forcing, and hence climate. At middle and high latitudes, up to 30% of total ozone resides in the lower stratosphere, i.e., the region between the tropopause and 100 hPa (Logan, 1999). WMO (2007) noted that apparent trends in this region were mostly the result of interannual variability and could not be ascribed to ODSs. It also concluded that changes in transport were a major contributor to the increase in midlatitude total ozone since the mid-1990s, particularly in the lowermost stratosphere (tropopause to 380K). Yang et al. (2006) showed that abundance of partial column ozone above 18 km altitude has risen slightly since 1997 in response to the decline in the atmospheric abundance of ODSs, whereas partial column ozone between the tropopause and 18 km rose much faster since 1997 than could be attributed to the decline in ODSs. The increases in total column were shown to differ significantly from the recovery in ozone expected solely from declining levels of ODS.

Vyushin et al. (2007), Mäder et al. (2007), and Harris et al. (2008) highlight the importance of accounting for dynamical variability and also volcanic aerosol in statistical models explaining observed changes in total ozone. Brunner et al. (2006) draw similar conclusions from analysis of vertically resolved ozone trends for the period 1979–2004 obtained by multiple linear regression analysis of the CATO ozone data set (see also WMO, 2007). Following the approach of Newchurch et al. (2003), Brunner et al. (2006) fitted their regression model to the reference period 1979–1995 during which EESC was increasing, but analyzed the residuals for the period 1996–2004 using different sets of explanatory variables. Their results show that a combination of EESC, QBO, and solar forcing is not sufficient to explain the recent ozone trend, as significantly positive residuals remained in the extratropical lower stratosphere for the period 1996–2004. However, most of the variations since 1996 could be explained when also accounting for volcanic aerosol and the Eliassen Palm (EP)-flux as a proxy for the wave forcing of the stratospheric circulation. This result demonstrates the importance of interannual variations in dynamics in producing the recent variations in ozone in the lower stratosphere. Brunner et al. (2006) also replaced EESC by a linear trend, assuming a continuation of the negative trend between 1979 and 1995. This resulted in an increase of the residuals that is much stronger than that resulting from

omission of aerosols or EP-flux, demonstrating the importance of the Montreal Protocol in addition to natural variability for explaining the recent observed ozone changes.

The main driver for the natural variations in UTLS ozone is climate variability, as has been extensively discussed in the WMO (2007). This includes variability in the stratospheric mean meridional circulation (e.g., Fusco and Salby, 1999) as well as variability in the tropospheric circulation through synoptic scale wave activity (e.g., Weiss et al., 2001). Recent studies explore the impact of climate variability on vertically resolved ozone in the UTLS. Thouret et al. (2006) used ozone measurements from the MOZAIC program to show that ozone in the upper troposphere is positively correlated with the North Atlantic Oscillation (NAO) index (the dominant mode of variability in surface pressure in the North Atlantic) while ozone in the lower stratosphere is anticorrelated with the extremes of the Northern Annular Mode (NAM) index (extension of the NAO to the full hemisphere) calculated at 150 hPa. Hess and Lamarque (2007), using the MOZART CTM driven by NCEP meteorological analyses, found that ozone is reduced throughout the troposphere at latitudes higher than 50°N during the positive phase of the Arctic Oscillation (AO, the surface manifestation of the NAM). This decrease can be linked to a decrease in ozone transported from the stratosphere. The El Niño-Southern Oscillation (ENSO) may also influence UTLS ozone. Fischer et al. (2008), using three different CCMs, found that ENSO forces a strengthening of the Brewer-Dobson circulation, which leads to lower total ozone in the tropics and higher total ozone at higher latitudes. While their study does not discuss the vertically resolved impact of the ENSO, the change in the Brewer-Dobson circulation is likely to have an impact on ozone in the lower stratosphere.

The question remains concerning how much the underlying long-term climate change may have contributed to the observed ozone changes. Hegglin and Shepherd (2009) use a stratosphere-resolving chemistry-climate model (CMAM) to study the effect of climate change on the stratospheric ozone distribution and derive expected trends of -1%, -3%, and +1% per decade in the SH lower stratosphere, the tropical lower stratosphere, and the NH lower stratosphere, respectively. They assumed a linear ozone response to climate change between 1960 and 2100. These numbers are consistent with those derived by Li et al. (2009) and are also confirmed in a multi-model comparison by Gettelman et al. (2010) except for the SH lower stratosphere, where the results were statistically not significant. These CCM results suggest that climate change may have masked around 30% of the ozone decrease due to EESC in the NH.

The evaluation of time series of ozone measurements at 200–100 hPa between 1960 and 2010 shows that the increase in ozone due to climate change is strongly

modulated by ozone depletion and recovery, with a larger signature in the SH than in the NH (Gettelman et al., 2010). This modulation is characterized by strong decreases in lower stratospheric ozone up to around the year 2000, followed by a strong increase, qualitatively agreeing with observations in this region (compare to Figure 2-7). However, the decline of lower stratospheric ozone in the tropics has not yet been shown unambiguously as stated earlier. WMO (2003, 2007) further pointed out the importance of decadal scale variability in dynamics that modulates the underlying slow dynamical contribution from climate change. The degree to which the decrease and increase are driven by such decadal scale variability is not known.

The changes in lower stratospheric ozone are likely to affect upper tropospheric (UT) ozone. Mid- and upper tropospheric ozone trends exhibit strong regional differences and are not yet well understood (Staehelin et al., 2001). CTMs with realistic ozone precursor emissions but without realistic stratospheric chemistry fail to reproduce either tropospheric background levels (Parrish et al., 2009) or observed trends (Fiore et al., 2009). In addition, Ordoñez et al. (2007) present observational evidence of a significant correlation between ozone at 150 hPa and tropospheric background ozone at two European mountain sites over the period 1992–2004, indicating local coupling of these air masses through stratosphere-to-troposphere exchange. At northern high latitudes, stratospheric ozone is estimated to contribute up to 40% to ozone at 500 hPa and up to 30% at northern midlatitudes (Terao et al., 2008). Hsu and Prather (2009) show the strong modulation of stratosphere-troposphere exchange (STE) ozone fluxes by the QBO, also pointing to stratospheric control of UT ozone.

It is likely that changes in the STE ozone fluxes induced by climate change need to be taken into account to understand observed UT ozone changes. Hegglin and Shepherd (2009) using the CMAM find that the simulated stratospheric ozone flux into the troposphere changes over the time period between 1960 and 2000 due to effects of both ozone depletion/recovery and climate change. Changes in the NH stratospheric ozone flux are around 6%, while changes in the SH are about –8%. A multi-model comparison of STE ozone fluxes performed during CCMVal-2 agrees with the global mean predictions (Chapter 10 of SPARC CCMVal, 2010). While the predicted STE ozone fluxes seem to be biased high by around 20% when compared to observations, the models' range of STE ozone flux is much smaller than found in previous studies used for the IPCC (2007). The impact of STE ozone flux on tropospheric chemistry is discussed further in Section 4.4.4 of Chapter 4.

In summary, evaluations of observed ozone changes show evidence of a statistically significant positive

change in ozone in the lower stratosphere; a part of this change may be attributed to decreasing ODSSs. Dynamical changes are still mainly responsible for these changes, at least in the NH. CCMs simulate increases in lower stratospheric ozone and suggest that up to 30% of the ozone depletion was masked by the dynamical changes due to climate change. While the importance of lower stratospheric ozone changes on upper tropospheric ozone has been recognized, understanding of upper tropospheric ozone trends remains incomplete.

REFERENCES

- Adriani, A., P. Massoli, G. Di Donfrancesco, F. Cairo, M.L. Moriconi, and M. Snels, Climatology of polar stratospheric clouds based on lidar observations from 1993 to 2001 over McMurdo Station, Antarctica, *J. Geophys. Res.*, *109*, D24211, doi: 10.1029/2004JD004800, 2004.
- Andersen, S.B., and B.M. Knudsen, The influence of polar vortex ozone depletion on NH mid-latitude ozone trends in spring, *Atmos. Chem. Phys.*, *6*, 2837–2845, 2006.
- Andreae, M.O., and A. Gelencsér, Black carbon or brown carbon? The nature of light-absorbing carbonaceous aerosols, *Atmos. Chem. Phys.*, *6*, 3131–3148, doi: 10.5194/acp-6-3131-2006, 2006.
- Angell, J.K., and M. Free, Ground-based observations of the slowdown in ozone decline and onset of ozone increase, *J. Geophys. Res.*, *114*, D07303, doi: 10.1029/2008JD010860, 2009.
- Antón, M., D. Loyola, M. López, J.M. Vilaplana, M. Bañón, W. Zimmer, and A. Serrano, Comparison of GOME-2/MetOp total ozone data with Brewer spectroradiometer data over the Iberian Peninsula, *Ann. Geophys.*, *27*, 1377–1386, 2009.
- Arola, A., S. Kazadzis, N. Krotkov, A. Bais, J. Gröbner, and J.R. Herman, Assessment of TOMS UV bias due to absorbing aerosols, *J. Geophys. Res.*, *110*, D23211, doi: 10.1029/2005JD005913, 2005.
- Arola, A., S. Kazadzis, A. Lindfors, N. Krotkov, J. Kujanpää, J. Tamminen, A. Bais, A. di Sarra, J.M. Villaplana, C. Brogniez, A.M. Siani, J. Janouch, P. Weihs, A. Webb, T. Koskela, N. Kouremeti, D. Meloni, V. Buchard, F. Auriol, I. Ialongo, M. Staneck, S. Simic, A. Smedley, and S. Kinne, A new approach to correct for absorbing aerosols in OMI UV, *Geophys. Res. Lett.*, *36*, L22805, doi: 10.1029/2009GL041137, 2009.
- Atkinson, R., D.L. Baulch, R.A. Cox, J.N. Crowley, R.F. Hampson, R.G. Hynes, M.E. Jenkin, M.J. Rossi, and J. Troe, Evaluated kinetic and photochemical data for atmospheric chemistry: Volume III - gas phase reactions of inorganic halogens, *Atmos.*

- Chem. Phys.*, 7 (4), 981-1191, 2007. (Cited as IUPAC, 2007.)
- Austin, J., K. Tourpali, E. Rozanov, H. Akiyoshi, S. Bekki, G. Bodeker, C. Brühl, N. Butchart, M. Chipperfield, M. Deushi, V.I. Formichev, M.A. Giorgetta, L. Gray, K. Kodera, F. Lott, E. Manzini, D. Marsh, K. Matthes, T. Nagashima, K. Shibata, R.S. Stolarski, H. Struthers, and W. Tian, Coupled chemistry climate model simulations of the solar cycle in ozone and temperature, *J. Geophys. Res.*, 113 (D11), doi: 10.1029/2007JD009391, 2008.
- Avallone, L.M., and D.W. Toohey, Tests of halogen photochemistry using in situ measurements of ClO and BrO in the lower polar stratosphere, *J. Geophys. Res.*, 106 (D10), 10411-10422, 2001.
- Badosa, J., R.L. McKenzie, M. Kotkamp, J. Calbó, J.A. González, P.V. Johnston, M. O'Neill, and D.J. Anderson, Towards closure between measured and modelled UV under clear skies at four diverse sites, *Atmos. Chem. Phys.*, 7 (11), 2817-2837, 2007.
- Bais, A.F., and D. Lubin (Lead Authors), A. Arola, G. Bernhard, M. Blumthaler, N. Chubarova, C. Erlick, H.P. Gies, N. Krotkov, K. Lantz, B. Mayer, R.L. McKenzie, R.D. Piacentini, G. Seckmeyer, J.R. Slusser, and C.S. Zerefos, Surface ultraviolet radiation: Past, present, and future, Chapter 7 in *Scientific Assessment of Ozone Depletion: 2006*, Global Ozone Research and Monitoring Project—Report No. 50, 572 pp., World Meteorological Organization, Geneva, Switzerland, 2007.
- Balis, D., J.-C. Lambert, M. Van Roozendaal, R. Spurr, D. Loyola, Y. Livschitz, P. Valks, V. Amiridis, P. Gerard, J. Granville, and C. Zehner, Ten years of GOME/ERS2 total ozone data—the new GOME data processor (GDP) version 4: 2. Ground-based validation and comparisons with TOMS V7/V8, *J. Geophys. Res.*, 112, D07307, doi: 10.1029/2005JD006376, 2007.
- Barnard, J.C., R. Volkamer, and E.I. Kassianov, Estimation of the mass absorption cross section of the organic carbon component of aerosols in the Mexico City Metropolitan Area, *Atmos. Chem. Phys.*, 8 (22), 6665-6679, 2008.
- Barret, B., M. De Mazière, and P. Demoulin, Retrieval and characterization of ozone profiles from solar infrared spectra at the Jungfraujoeh, *J. Geophys. Res.*, 107, 4788, doi: 10.1029/2001JD001298, 2002.
- Beig, G., and V. Singh, Trends in tropical tropospheric column ozone from satellite data and MOZART model, *Geophys. Res. Lett.*, 34, L17801, doi: 10.1029/2007GL030460, 2007.
- Bergstrom, R.W., P. Pilewskie, P.B. Russell, J. Redemann, T.C. Bond, P.K. Quinn, and B. Sierau, Spectral absorption properties of atmospheric aerosols, *Atmos. Chem. Phys.*, 7 (23), 5937-5943, 2007.
- Bergstrom, R.W., K.S. Schmidt, O. Coddington, P. Pilewskie, H. Guan, J.M. Livingston, J. Redemann, and P.B. Russell, Aerosol spectral absorption in the Mexico City area: Results from airborne measurements during MILAGRO/INTEX B, *Atmos. Chem. Phys.*, 10 (13), 6333-6343, doi: 10.5194/acp-10-6333-2010, 2010.
- Bernhard, G., C.R. Booth, and J.C. Eshamjian, Comparison of UV irradiance measurements at Summit, Greenland; Barrow, Alaska; and South Pole, Antarctica, *Atmos. Chem. Phys.*, 8 (16), 4799-4810, doi: 10.5194/acp-8-4799-2008, 2008.
- Bernhard, G., C.R. Booth, and J.C. Eshamjian, Climatology of ultraviolet radiation at high latitudes derived from measurements of the National Science Foundation's ultraviolet spectral irradiance monitoring network, Chapter 3 in *UV Radiation in Global Climate Change: Measurements, Modeling and Effects on Ecosystems*, edited by W. Gao, D.L. Schmoldt, and J.R. Slusser, 550 pp., Springer-Verlag and Tsinghua University Press, ISBN: 978-3-642-03312-4, 48-72, 2010.
- Bhartia, P.K., C.G. Wellemeyer, S.L. Taylor, N. Nath, and A. Gopalan, Solar Backscatter Ultraviolet (SBUV) version 8 profile algorithm, in *Ozone Vol. I, Proceedings of the XX Quadrennial Ozone Symposium*, 1-8 June 2004, Kos, Greece, edited by C.S. Zerefos, 295-296, International Ozone Commission, Athens, Greece, 2004.
- Biele, J., A. Tsias, B.P. Luo, K.S. Carslaw, R. Neuber, G. Beyerle, and T. Peter, Nonequilibrium coexistence of solid and liquid particles in Arctic stratospheric clouds, *J. Geophys. Res.*, 106 (D19), 22991-23007, doi: 10.1029/2001JD900188, 2001.
- Blum, U., K.H. Fricke, K.P. Müller, J. Siebert, and G. Baumgarten, Long-term lidar observations of polar stratospheric clouds at Esrange in northern Sweden, *Tellus*, 57B, 412-422, 2005.
- Bodeker, G.E., H. Shiona, and H. Struthers, The NIWA assimilated total column ozone data base and assimilated trace gas profile data base for validation of CCMs, paper presented at *CCMVal 2005 Workshop*, October 2005, Boulder, Colo., available: http://www.pa.op.dlr.de/workshops/CCMVal2005/CCMVal2005_abstract.html, 2005.
- Booth, C.R., and S. Madronich, Radiation amplification factors: Improved formulation accounts for large increases in ultraviolet radiation associated with Antarctic ozone depletion, in *Ultraviolet Radiation in Antarctica: Measurement and Biological Effects*, edited by C.S. Weiler and P.S. Penhale, *AGU Antarctic Res. Ser.*, 62, 39-52, 1994.
- Borkowski, J.L., Modelling UV radiation variations at

- different time scales, *Ann. Geophys.*, *26*, 441-446, 2008.
- Brunner, D., J. Staehelin, J.A. Maeder, I. Wohltmann, and G.E. Bodeker, Variability and trends in total and vertically resolved stratospheric ozone based on the CATO ozone data set, *Atmos. Chem. Phys.*, *6* (12), 4985-5008, doi: 10.5194/acp-6-4985-2006, 2006.
- Buchard, V., C. Brogniez, F. Auriol, B. Bonnel, J. Lenoble, A. Tanskanen, B. Bojkov, and P. Veefkind, Comparison of OMI ozone and UV irradiance data with ground-based measurements at two French sites, *Atmos. Chem. Phys.*, *8* (16), 4517-4528, doi: 10.5194/acp-8-4517-2008, 2008.
- Burkholder, J.B., J.J. Orlando, and C.J. Howard, Ultraviolet-absorption cross sections of Cl₂O₂ between 210 and 410 nm, *J. Phys. Chem.*, *94*, 687-695, 1990.
- Burrows, J.P., M. Weber, M. Buchwitz, V. Rozanov, A. Ladstädter-Weißmayer, A. Richter, R. de Beek, R. Hoogen, K. Bramstedt, K.-U. Eichmann, M. Eisinger, and D. Perner, The Global Ozone Monitoring Experiment (GOME): Mission concept and first scientific results, *J. Atmos. Sci.*, *56*, 151-175, 1999.
- Butchart, N., and A.A. Scaife, Removal of chlorofluorocarbons by increased mass exchange between the stratosphere and troposphere in a changing climate, *Nature*, *410* (6830), 799-802, 2001.
- Butchart, N., A.A. Scaife, M. Bourqui, J. de Grandpré, S.H.E. Hare, J. Kettleborough, U. Langematz, E. Manzini, F. Sassi, K. Shibata, D. Shindell, and M. Sigmond, Simulations of anthropogenic change in the strength of the Brewer-Dobson circulation, *Clim. Dyn.*, *27* (7-8), 727-741, doi: 10.1007/s00382-006-0162-4, 2006.
- Butkovskaya, N., A. Kukui, and G. Le Bras, HNO₃ forming channel of the HO₂ + NO reaction as a function of pressure and temperature in the ranges of 72–600 Torr and 223–323 K, *J. Phys. Chem. A*, *111*, 9047-9053, doi: 10.1021/jp074117m, 2007.
- Butkovskaya, N., M.-T. Rayez, J.-C. Rayez, A. Kukui, and G. Le Bras, Water vapor effect on the HNO₃ yield in the HO₂ + NO reaction: Experimental and theoretical evidence, *J. Phys. Chem. A*, *113*, 11327-11342, doi: 10.1021/jp811428p, 2009.
- Canty, T., E.D. Rivière, R.J. Salawitch, G. Berthet, J.-B. Renard, K. Pfeilsticker, M. Dorf, A. Butz, H. Bösch, R.M. Stimpfle, D.M. Wilmouth, E.C. Richard, D.W. Fahey, P.J. Popp, M.R. Schoeberl, L.R. Lait, and T.P. Bui, Nighttime OCIO in the winter Arctic vortex, *J. Geophys. Res.*, *110*, D01301, doi: 10.1029/2004JD005035, 2005.
- Cariolle, D., M.J. Evans, M.P. Chipperfield, N. Butkovskaya, A. Kukui, and G. Le Bras, Impact of the new HNO₃-forming channel of the HO₂ + NO reaction on tropospheric HNO₃, NO_x, HO_x and ozone, *Atmos. Chem. Phys.*, *8* (14), 4061-4068, doi: 10.5194/acp-8-4061-2008, 2008.
- Carl, S.A., A highly sensitive method for time-resolved detection of O(¹D) applied to precise determination of absolute O(¹D) reaction rate constants and O(³P) yields, *Phys. Chem. Chem. Phys.*, *7*, 4051-4053, doi: 10.1039/b513576c, 2005.
- Carslaw, K.S., B.P. Luo, S.L. Clegg, Th. Peter, P. Brimblecombe, and P.J. Crutzen, Stratospheric aerosol growth and HNO₃ gas phase depletion from coupled HNO₃ and water uptake by liquid particles, *Geophys. Res. Lett.*, *21* (23), 2479-2482, 1994.
- Cede, A., J. Herman, A. Richter, N. Krotkov, and J. Burrows, Measurements of nitrogen dioxide total column amounts using a Brewer double spectrophotometer in direct sun mode, *J. Geophys. Res.*, *111*, D05304, doi: 10.1029/2005JD006585, 2006.
- Chen, H.-Y., C.-Y. Lien, W.-Y. Lin, Y.T. Lee, and J.J. Lin, UV absorption cross sections of ClOOCl are consistent with ozone degradation models, *Science*, *324*, 781-784, doi: 10.1126/science.1171305, 2009.
- Chipperfield, M.P., and V.E. Fioletov (Lead Authors), B. Bregman, J. Burrows, B.J. Connor, J.D. Haigh, N.R.P. Harris, A. Hauchecorne, L.L. Hood, S.R. Kawa, J.W. Krzyścin, J.A. Logan, N.J. Muthama, L. Polvani, W.J. Randel, T. Sasaki, J. Stähelin, R.S. Stolarski, L.W. Thomason, and J.M. Zawodny, Global ozone: Past and present, Chapter 3 in *Scientific Assessment of Ozone Depletion: 2006*, Global Ozone Research and Monitoring Project—Report No. 50, 572 pp., World Meteorological Organization, Geneva, Switzerland, 2007.
- Chipperfield, M., W. Feng, and M. Rex, Arctic ozone loss and climate sensitivity: Updated three-dimensional model study, *Geophys. Res. Lett.*, *32*, L11813, doi: 10.1029/2005GL022674, 2005.
- Chubarova, N.Y., UV variability in Moscow according to the long-term UV measurements and reconstruction model, *Atmos. Chem. Phys.*, *8* (12), 3025-3031, doi: 10.5194/acp-8-3025-2008, 2008.
- Clain, G., J.L. Baray, R. Delmas, R. Diab, J. Leclair de Bellevue, P. Keckhut, F. Posny, J.M. Metzger, and J.P. Cammas, Tropospheric ozone climatology at two Southern Hemisphere tropical/subtropical sites, (Reunion Island and Irene, South Africa) from ozonesondes, LIDAR, and in situ aircraft measurements, *Atmos. Chem. Phys.*, *9* (5), 1723-1734, doi: 10.5194/acp-9-1723-2009, 2009.
- Coldewey-Egbers, M., M. Weber, L.N. Lamsal, R. de Beek, M. Buchwitz, and J.P. Burrows, Total ozone retrieval from GOME UV spectral data using the weighting function DOAS approach, *Atmos. Chem. Phys.*, *5* (4), 1015-1025, doi: 10.5194/acp-5-1015-2005, 2005.

- Cordero, R.R., G. Seckmeyer, D. Pissulla, L. DaSilva, F. Labbe, Uncertainty evaluation of the spectral UV irradiance evaluated by using the UVSPEC Radiative Transfer Model, *Opt. Commun.*, 276, 44-53, doi: 10.1016/j.optcom.2007.04.008, 2007.
- Cordero, R.R., G. Seckmeyer, D. Pissulla, L. DaSilva, and F. Labbe, Uncertainty evaluation of spectral UV irradiance measurements, *Meas. Sci. Technol.*, 19 (4), 045104, 1-15, doi: 10.1088/0957-0233/19/4/045104, 2008a.
- Cordero, R.R., G. Seckmeyer, D. Pissulla, and F. Labbe, Uncertainty of experimental integrals: Application to the UV index calculation, *Metrologia*, 45 (1), 1-10, doi: 10.1088/0026-1394/45/1/001, 2008b.
- Corr, C.A., N. Krotkov, S. Madronich, J.R. Slusser, B. Holben, W. Gao, J. Flynn, B. Lefer, and S.M. Kreidenweis, Retrieval of aerosol single scattering albedo at ultraviolet wavelengths at the T1 site during MILAGRO, *Atmos. Chem. Phys.*, 9 (15), 5813-5827, doi: 10.5194/acp-9-5813-2009, 2009.
- COST 726 (European Cooperation in Science and Technology), Final report of COST action 726 – *Long Term Changes and Climatology of UV Radiation over Europe*, edited by Z. Lityńska, P. Koepke, H. De Backer, J. Gröbner, A. Schmalwieser, and L. Vuilleumier, COST Earth System Science and Environmental Management, Luxembourg: Office for Official Publications of the European Communities, 137 pp., available: <http://www.cost726.org/>, in press, 2010.
- Cox, R.A., and G.D. Hayman, The stability and photochemistry of dimers of the ClO radical and implications for Antarctic ozone depletion, *Nature*, 332 (6167), 796-800, doi: 10.1038/332796a0, 1988.
- Crutzen, P.J., Albedo enhancement by stratospheric sulfur injections: A contribution to resolve a policy dilemma?, *Clim. Change*, 77 (3-4), 211-220, doi: 10.1007/s10584-006-9101-y, 2006.
- Curylo, A., J. Krzyścin, and B. Bogdańska, UV reconstruction with long time series global radiation measurements, in *Proceedings of the UV Conference "One Century of UV Radiation Research,"* 18-20 September 2007, Davos, Switzerland, edited by J. Gröbner, 211-212, 2007.
- David, C., S. Bekki, S. Godin, G. Mégie, and M.P. Chipperfield, Polar stratospheric clouds climatology over Dumont d'Urville between 1989 and 1993 and the influence of volcanic aerosols on their formation, *J. Geophys. Res.*, 103, 22163-22180, 1998.
- David, C., P. Keckhut, A. Armetta, J. Jumelet, M. Snels, M. Marchand, and S. Bekki, Radiosonde stratospheric temperatures at Dumont d'Urville (Antarctica): Trends and link with polar stratospheric clouds, *Atmos. Chem. Phys.*, 10 (8), 3813-3825, doi: 10.5194/acp-10-3813-2010, 2010.
- DeMore, W.B., and E. Tschuikow-Roux, Ultraviolet spectrum and chemical reactivity of the chlorine monoxide dimer, *J. Phys. Chem.*, 94 (15), 5856-5860, doi: 10.1021/j100378a046, 1990.
- den Outer, P.N., H. Slaper, and R.B. Tax, UV radiation in the Netherlands: Assessing long-term variability and trends in relation to ozone and clouds, *J. Geophys. Res.*, 110, D02203, 1-11, doi: 10.1029/2004JD004824, 2005.
- den Outer, P.N., H. Slaper, J. Kaurola, A. Lindfors, A. Kazantzidis, A.F. Bais, U. Feister, J. Junk, M. Janouch, and W. Josefsson, Reconstructing erythral ultraviolet radiation levels in Europe for the past 4 decades, *J. Geophys. Res.*, 115, D10102, doi: 10.1029/2009JD012827, 2010.
- Deshler, T., B.J. Johnson, and W.R. Rozier, Changes in the character of polar stratospheric clouds over Antarctica in 1992 due to the Pinatubo volcanic aerosol, *Geophys. Res. Lett.*, 21 (4), 273-276, 1994.
- Deshler, T., J.L. Mercer, H.G.J. Smit, R. Stubi, G. Levrat, B.J. Johnson, S.J. Oltmans, R. Kivi, A.M. Thompson, J. Witte, J. Davies, F.J. Schmidlin, G. Brothers, and T. Sasaki, Atmospheric comparison of electrochemical cell ozonesondes from different manufacturers, and with different cathode solution strengths: The Balloon Experiment on Standards for Ozonesondes, *J. Geophys. Res.*, 113, D04307, doi: 10.1029/2007JD008975, 2008.
- Dessler, A.E., D.B. Considine, J.E. Rosenfield, S.R. Kawa, A.R. Douglass, and J.M. Russell III, Lower stratospheric chlorine partitioning during the decay of the Mt. Pinatubo aerosol cloud, *Geophys. Res. Lett.*, 24 (13), 1623-1626, 1997.
- Dhomse, S., M. Weber, I. Wohltmann, M. Rex, and J.P. Burrows, On the possible causes of recent increases in NH total ozone from a statistical analysis of satellite data from 1979 to 2003, *Atmos. Chem. Phys.*, 6 (5), 1165-1180, doi: 10.5194/acp-6-1165-2006, 2006.
- Diaz, S., C. Camilión, G. Deferrari, H. Fuenzalida, R. Armstrong, C. Booth, A. Paladini, S. Cabrera, C. Casiccia, C. Lovengreen, J. Pedroni, A. Rosales, H. Zagarese, and M. Vernet, Ozone and UV radiation over southern South America: Climatology and anomalies, *Photochem. Photobiol.*, 82 (4), 834-843, doi: 10.1562/2005-09-26-RA-697, 2006.
- Dillon, T.J., A. Horowitz, and J.N. Crowley, The atmospheric chemistry of sulphuryl fluoride, SO₂F₂, *Atmos. Chem. Phys.*, 8 (6), 1547-1557, doi: 10.5194/acp-8-1547-2008, 2008.
- Drdla, K., B.W. Gandrud, D. Baumgardner, J.C. Wilson, T.P. Bui, D. Hurst, S.M. Schauffler, H. Jost, J.B. Greenblatt, and C.R. Webster, Evidence for the

- widespread presence of liquid-phase particles during the 1999-2000 Arctic winter, *J. Geophys. Res.*, *108* (D5), 8318, doi: 10.1029/2001JD001127, 2003.
- Dunlea, E.J., and A.R. Ravishankara, Measurement of the rate coefficient for the reaction of O(¹D) with H₂O and re-evaluation of the atmospheric OH production rate, *Phys. Chem. Chem. Phys.*, *6*, 3333-3340, doi: 10.1039/b402483d, 2004.
- Eckermann, S.D., L. Hoffmann, M. Höpfner, D.L. Wu, and M.J. Alexander, Antarctic NAT PSC belt of June 2003: Observational validation of the mountain wave seeding hypothesis, *Geophys. Res. Lett.*, *36*, L02807, doi: 10.1029/2008GL036629, 2009.
- Engel, A., T. Möbius, H. Bönisch, U. Schmidt, R. Heinz, I. Levin, E. Atlas, S. Aoki, T. Nakazawa, S. Sugawara, F. Moore, D. Hurst, J. Elkins, S. Schauffler, A. Andrews, and K. Berine, Age of stratospheric air unchanged within uncertainties over the past 30 years, *Nature Geosci.*, *2*, 28-31, doi: 10.1038/GEO388, 2009.
- Eskes, H.J., R.J. van der A, E.J. Brinksma, J.P. Veefkind, J.F. de Haan, and P.J.M. Valks, Retrieval and validation of ozone columns derived from measurements of SCIAMACHY on Envisat, *Atmos. Chem. Phys. Discuss.*, *5*, 4429-4475, doi: 10.5194/acpd-5-4429-2005, 2005.
- Eyring, V., N. Butchart, D.W. Waugh, H. Akiyoshi, J. Austin, S. Bekki, G.E. Bodeker, B.A. Boville, C. Brühl, M.P. Chipperfield, E. Cordero, M. Dameris, M. Deushi, V.E. Fioletov, S.M. Frith, R.R. Garcia, A. Gettelman, M.A. Giorgetta, V. Grewe, L. Jourdain, D.E. Kinnison, E. Mancini, E. Manzini, M. Marchand, D.R. Marsh, T. Nagashima, P.A. Newman, J.E. Nielsen, S. Pawson, G. Pitari, D.A. Plummer, E. Rozanov, M. Schraner, T.G. Shepherd, K. Shibata, R.S. Stolarski, H. Struthers, W. Tian, and M. Yoshiki, Assessment of temperature, trace species, and ozone in chemistry-climate model simulations of the recent past, *J. Geophys. Res.*, *111*, D22308, doi: 10.1029/2006JD007327, 2006.
- Fahey, D.W., S.R. Kawa, E.L. Woodbridge, P. Tin, J.C. Wilson, H.H. Jonsson, J.E. Dye, D. Baumgardner, S. Borrmann, D.W. Toohey, L.M. Avallone, M.H. Proffitt, J. Margitan, M. Loewenstein, J.R. Podolske, R.J. Salawitch, S.C. Wofsy, M.K.W. Ko, D.E. Anderson, M.R. Schoeberl, and K.R. Chan, In situ measurements constraining the role of sulfate aerosols in midlatitude ozone depletion, *Nature*, *363* (6429), 509-514, doi: 10.1038/363509a0, 1993.
- Fahey, D.W., R.S. Gao, K.S. Carslaw, J. Kettleborough, P.J. Popp, M.J. Northway, J.C. Holecek, S.C. Ciciora, R.J. McLaughlin, T.L. Thompson, R.H. Winkler, D.G. Baumgardner, B. Gandrud, P.O. Wennberg, S. Dhaniyala, K. McKinney, Th. Peter, R.J. Salawitch, T.P. Bui, J.W. Elkins, C.R. Webster, E.L. Atlas, H. Jost, J.C. Wilson, R.L. Herman, A. Kleinböhl, and M. von König, The detection of large HNO₃-containing particles in the winter Arctic stratosphere, *Science*, *291*, 1026-1031, 2001.
- Farman, J.C., B.G. Gardiner, and J.D. Shanklin, Large losses of total ozone in Antarctica reveal seasonal ClO_x/NO_x interaction, *Nature*, *315*, 207-210, 1985.
- Feister, U., J. Junk, M. Woldt, A. Bais, A. Helbig, M. Janouch, W. Josefsson, A. Kazantzidis, A. Lindfors, P.N. den Outer, and H. Slaper, Long-term solar UV radiation reconstructed by ANN modelling with emphasis on spatial characteristics of input data, *Atmos. Chem. Phys.*, *8* (12), 3107-3118, doi: 10.5194/acp-8-3107-2008, 2008.
- Felton, M.A. Jr., T.A. Kovacs, A.H. Omar, and C.A. Hostetler, *Classification of Polar Stratospheric Clouds using LIDAR Measurements from the SAGE III Ozone Loss and Validation Experiment*, Tech. Rep. ARL-TR-4154, 36 pp., U.S. Army Research Laboratory, Adelphi, Md., 2007.
- Feng, W., M.P. Chipperfield, M. Dorf, K. Pfeilsticker, and P. Ricaud, Mid-latitude ozone changes: Studies with a 3-D CTM forced by ERA-40 analyses, *Atmos. Chem. Phys.*, *7* (9), 2357-2369, doi: 10.5194/acp-7-2357-2007, 2007.
- Fioletov, V.E., Estimating the 27-day and 11-year solar cycle variations in tropical upper stratospheric ozone, *J. Geophys. Res.*, *114*, D02302, doi: 10.1029/2008JD010499, 2009.
- Fioletov, V.E., L.J.B. McArthur, J.B. Kerr, and D.I. Wardle, Long-term variations of UV-B irradiance over Canada estimated from Brewer observations and derived from ozone and pyranometer measurements, *J. Geophys. Res.*, *106* (D19), 23009-23027, 2001.
- Fioletov, V.E., G.E. Bodeker, A.J. Miller, R.D. McPeters, and R. Stolarski, Global and zonal total ozone variations estimated from ground-based and satellite measurements: 1964-2000, *J. Geophys. Res.*, *107* (D22), 4647, doi: 10.1029/2001JD001350, 2002.
- Fioletov, V.E., G. Labow, R. Evans, E.W. Hare, U. Köhler, C.T. McElroy, K. Miyagawa, A. Redondas, V. Savastiouk, A.M. Shalamyansky, J. Staehelin, K. Vanicek, and M. Weber, Performance of ground-based total ozone network assessed using satellite data, *J. Geophys. Res.*, *113*, D14313, doi: 10.1029/2008JD009809, 2008.
- Fiore, A.M., F.J. Dentener, O. Wild, C. Cuvelier, M.G. Schultz, P. Hess, C. Textor, M. Schulz, R.M. Doherty, L.W. Horowitz, I.A. MacKenzie, M.G. Sanderson, D.T. Shindell, D.S. Stevenson, S. Szopa, R. Van Dingenen, G. Zeng, C. Atherton, D. Bergmann, I. Bey, G. Carmichael, W.J. Collins, B.N. Duncan, G. Faluvegi, G. Folberth, M. Gauss, S. Gong, D. Hau-

- glustaine, T. Holloway, I.S.A. Isaksen, D.J. Jacob, J.E. Jonson, J.W. Kaminski, T.J. Keating, A. Lupu, E. Marmer, V. Montanaro, R.J. Park, G. Pitari, K.J. Pringle, J.A. Pyle, S. Schroeder, M.G. Vivanco, P. Wind, G. Wojcik, S. Wu, and A. Zuber, Multimodel estimates of intercontinental source-receptor relationships for ozone pollution, *J. Geophys. Res.*, *114*, D04301, doi: 10.1029/2008JD010816, 2009.
- Fischer, A.M., D.T. Shindell, B. Winter, M.S. Bourqui, G. Faluvegi, E. Rozanov, M. Schraner, and S. Brönnimann, Stratospheric winter climate response to ENSO in three chemistry-climate models, *Geophys. Res. Lett.*, *35*, L13819, doi: 10.1029/2008GL034289, 2008.
- Fleming, E.L., C.H. Jackman, D.K. Weisenstein, and M.K.W. Ko, The impact of interannual variability on multidecadal total ozone simulations, *J. Geophys. Res.*, *112*, D10310, doi: 10.1029/2006JD007953, 2007.
- Flynn, L.E., (editor), *Solar Backscatter Ultraviolet Instrument (SBUV/2) Version 8 Ozone Retrieval Algorithm Theoretical Basis Document (V8 ATBD)*, NOAA National Environmental, Satellite, Data, and Information Service, Center for Satellite Applications and Research, available: http://www.star.nesdis.noaa.gov/smcd/spb/calibration/icvs/sbuw/doc/SBUV2_V8_ATBD_020207.pdf, 2007.
- Frieler, K., M. Rex, R.J. Salawitch, T. Canty, M. Streibel, R.M. Stimpfle, K. Pfeilsticker, M. Dorf, D.K. Weisenstein, and S. Godin-Beekmann, Toward a better quantitative understanding of polar stratospheric ozone loss, *Geophys. Res. Lett.*, *33*, L10812, doi: 10.1029/2005GL025466, 2006.
- Frith, S., R. Stolarski, and P.K. Bhartia, Implications of Version 8 TOMS and SBUV data for long-term trend analysis, in *Ozone Vol. I, Proceedings of the XX Quadrennial Ozone Symposium*, 1-8 June 2004, Kos, Greece, edited by C.S. Zerefos, 65-66, International Ozone Commission, Athens, Greece, 2004.
- Fromm, M., J. Alfred, and M. Pitts, A unified, long-term, high-latitude stratospheric aerosol and cloud database using SAM II, SAGE II, and POAM II/III data: Algorithm description, database definition, and climatology, *J. Geophys. Res.*, *108* (D12), 4366, doi: 10.1029/2002JD002772, 2003.
- Fusco, A.C., and M.L. Salby, Interannual variations of total ozone and their relationship to variations of planetary wave activity, *J. Clim.*, *12* (6), 1619-1629, 1999.
- Gadhavi, H., R.T. Pinker, and I. Laszlo, Estimates of surface ultraviolet radiation over north America using Geostationary Operational Environmental Satellites observations, *J. Geophys. Res.*, *113*, D21205, doi: 10.1029/2007JD009308, 2008.
- Gardiner, T., A. Forbes, M. de Mazière, C. Vigouroux, E. Mahieu, P. Demoulin, V. Velazco, J. Notholt, T. Blumenstock, F. Hase, I. Kramer, R. Sussmann, W. Stremme, J. Mellqvist, A. Strandberg, K. Ellingsen, and M. Gauss, Trend analysis of greenhouse gases over Europe measured by a network of ground-based remote FTIR instruments, *Atmos. Chem. Phys.*, *8* (22), 6719-6727, doi: 10.5194/acp-8-6719-2008, 2008.
- Gottelman, A., T. Birner, V. Eyring, H. Akiyoshi, S. Bekki, C. Brühl, M. Dameris, D.E. Kinnison, F. Lefevre, F. Lott, E. Mancini, G. Pitari, D.A. Plummer, E. Rozanov, K. Shibata, A. Stenke, H. Struthers, and W. Tian, The tropical tropopause layer 1960–2100, *Atmos. Chem. Phys.*, *9* (5), 1621-1637, doi: 10.5194/acp-9-1621-2009, 2009.
- Gottelman, A., M.I. Hegglin, S.-W. Son, J. Kim, M. Fujiwara, T. Birner, S. Kremser, M. Rex, J.A. Añel, H. Akiyoshi, J. Austin, S. Bekki, P. Braesike, C. Brühl, N. Butchart, M. Chipperfield, M. Dameris, S. Dhomse, H. Garny, S.C. Hardiman, P. Jöckel, D.E. Kinnison, J.F. Lamarque, E. Mancini, M. Marchand, M. Michou, O. Morgenstern, S. Pawson, G. Pitari, D. Plummer, J.A. Pyle, E. Rozanov, J. Scinocca, T.G. Shepherd, K. Shibata, D. Smale, H. Teyssèdre, and W. Tian, Multimodel assessment of the upper troposphere and lower stratosphere: Tropics and trends, *J. Geophys. Res.*, *115*, D00M08, doi: 10.1029/2009JD013638, 2010.
- Gray, L.J., J. Beer, M. Geller, J.D. Haigh, M. Lockwood, K. Matthes, U. Cubasch, D. Fleitmann, G. Harrison, L. Hood, J. Luterbacher, G.A. Meehl, D. Shindell, B. van Geel, and W. White, Solar influence on climate, *Rev. Geophys.*, *48*, RG4001, doi: 10.1029/2009RG000282, 2010.
- Gröbner, J., M. Blumthaler, S. Kazadzis, A. Bais, A. Webb, J. Schreder, G. Seckmeyer, and D. Rembges, Quality assurance of spectral solar UV measurements: Results from 25 UV monitoring sites in Europe, 2002 to 2004, *Metrologia*, *43*, S66-S71, doi: 10.1088/0026-1394/43/2/S14, 2006.
- Gröbner, J., G. Hülsen, L. Vuilleumier, M. Blumthaler, J.M. Vilaplana, D. Walker, and J.E. Gil, *Report of the PMOD/WRC-COST Calibration and Intercomparison of Erythral Radiometers*, Davos, Switzerland, 28 July–23 August 2006, 108 pp., European Cooperation in Science and Technology (COST), available: ftp.pmodwrc.ch/pub/publications/PMOD_COST726_BBreport.pdf, 2007.
- Hall, T.M., D.W. Waugh, K.A. Boering, and R.A. Plumb, Evaluation of transport in stratospheric models, *J. Geophys. Res.*, *104* (D15), 18815-18839, 1999.
- Harris, N.R.P., E. Kyrö, J. Staehelin, D. Brunner, S.-B. Andersen, S. Godin-Beekmann, S. Dhomse, P.

- Hadjinicolaou, G. Hansen, I. Isaksen, A. Jrrar, A. Karpetchko, R. Kivi, B. Knudsen, P. Krizan, J. Lastovicka, J. Maeder, Y. Orsolini, J.A. Pyle, M. Rex, K. Vanicek, M. Weber, I. Wohltmann, P. Zanis, and C. Zerefos, Ozone trends at northern mid- and high latitudes – a European perspective, *Ann. Geophys.*, *26*, 1207-1220, 2008.
- Hase, F., Inversion von Spurengasprofilen aus Hochaufgelösten Bodengebundenen FTIR-Messungen in Absorption, Wissenschaftliche Berichte Forschungszentrum Karlsruhe, FZKA 6512; Ph.D. thesis, 156 pp., ISSN 0947-8620, available: <http://www-imk.fzk.de/asf/ftir/diss/hase.pdf>, 2000.
- Hassler, B., G.E. Bodeker, and M. Dameris, Technical Note: A new global database of trace gases and aerosols from multiple sources of high vertical resolution measurements, *Atmos. Chem. Phys.*, *8* (17), 5403-5421, doi: 10.5194/acp-8-5403-2008, 2008.
- Hegglin, M.I., and T.G. Shepherd, Large climate-induced changes in stratosphere-to-troposphere ozone flux and ultraviolet index, *Nature Geosci.*, *2*, 687-691, doi: 10.1038/NCEO604, 2009.
- Herman, J.R., Global increase in UV irradiance during the past 30 years (1979–2008) estimated from satellite data, *J. Geophys. Res.*, *115*, D04203, doi: 10.1029/2009JD012219, 2010.
- Herman, J.R., G. Labow, N.C. Hsu, and D. Larko, Changes in cloud cover derived from reflectivity time series using SeaWiFS, N7-TOMS, EP-TOMS, SBUV-2, and OMI radiance data, *J. Geophys. Res.*, *114*, D01201, doi: 10.1029/2007JD009508, 2009.
- Hess, P.G., and J.-F. Lamarque, Ozone source attribution and its modulation by the Arctic oscillation during the spring months, *J. Geophys. Res.*, *112*, D11303, doi: 10.1029/2006JD007557, 2007.
- Hicke, J.A., J. Slusser, K. Lantz, and F.G. Pascual, Trends and interannual variability in surface UVB radiation over 8 to 11 years observed across the United States, *J. Geophys. Res.*, *113*, D21302, doi: 10.1029/2008JD009826, 2008.
- Hickson, K.M., L.F. Keyser, and S.P. Sander, Temperature dependence of the HO₂ + ClO reaction. 2. Reaction kinetics using the discharge flow-resonance fluorescence technique, *J. Phys. Chem. A*, *111*, 8126-8138, doi: 10.1021/jp0689464, 2007.
- Hitchcock, P., T.G. Shepherd, and C. McLandress, Past and future conditions for polar stratospheric cloud formation simulated by the Canadian middle atmosphere model, *Atmos. Chem. Phys.*, *9* (2), 483-495, doi: 10.5194/acp-9-483-2009, 2009.
- Hofmann, D.J., and S. Solomon, Ozone destruction through heterogeneous chemistry following the eruption of El Chichón, *J. Geophys. Res.*, *94* (D4), 5029-5041, 1989.
- Hofmann, D.J., and S.J. Oltmans, Anomalous Antarctic ozone during 1992: Evidence for Pinatubo volcanic aerosol effects, *J. Geophys. Res.*, *98* (D10), 18555-18562, 1993.
- Hofmann, D.J., B.J. Johnson, and S.J. Oltmans, Twenty-two years of ozonesonde measurements at the South Pole, *Int. J. Remote Sens.*, *30* (15-16), 3995-4008, doi: 10.1080/01431160902821932, 2009a.
- Hofmann, D., J. Barnes, M. O'Neill, M. Trudeau, and R. Neely, Increase in background stratospheric aerosol observed with lidar at Mauna Loa Observatory and Boulder, Colorado, *Geophys. Res. Lett.*, *36*, L15808, doi: 10.1029/2009GL039008, 2009b.
- Holton, J.R., Meridional distribution of stratospheric trace constituents, *J. Atmos. Sci.*, *43* (12), 1238-1242, 1986.
- Höpfner, M., B.P. Luo, P. Massoli, F. Cairo, R. Spang, M. Snels, G. Di Donfrancesco, G. Stiller, T. von Clarmann, H. Fischer, and U. Biermann, Spectroscopic evidence for NAT, STS, and ice in MIPAS infrared limb emission measurements of polar stratospheric clouds, *Atmos. Chem. Phys.*, *6* (5), 1201-1219, doi: 10.5194/acp-6-1201-2006, 2006a.
- Höpfner, M., N. Larsen, R. Spang, B. Luo, J. Ma, S.H. Svendsen, S.D. Eckermann, B. Knudsen, P. Massoli, F. Cairo, G. Stiller, T. v. Clarmann, and H. Fischer, MIPAS detects Antarctic stratospheric belt of NAT PSCs caused by mountain waves, *Atmos. Chem. Phys.*, *6* (5), 1221-1230, doi: 10.5194/acp-6-1221-2006, 2006b.
- Höpfner, M., M.C. Pitts, and L.R. Poole, Comparison between CALIPSO and MIPAS observations of polar stratospheric clouds, *J. Geophys. Res.*, *114*, D00H05, doi: 10.1029/2009JD012114, 2009.
- Hsu, J., and M.J. Prather, Stratospheric variability and tropospheric ozone, *J. Geophys. Res.*, *114*, D06102, doi: 10.1029/2008JD010942, 2009.
- Huder, K.J., and W.B. DeMore, Absorption cross-sections of the ClO dimer, *J. Phys. Chem.*, *99*, 3905-3908, 1995.
- Hudman, R.C., D.J. Jacob, S. Turquety, E.M. Leibensperger, L.T. Murray, S. Wu, A.B. Gilliland, M. Avery, T.H. Bertram, W. Brune, R.C. Cohen, J.E. Dibb, F.M. Flocke, A. Fried, J. Holloway, J.A. Neuman, R. Orville, A. Perring, X. Ren, G.W. Sachse, H.B. Singh, A. Swanson, and P.J. Wooldrige, Surface and lightning sources of nitrogen oxides over the United States: Magnitudes, chemical evolution, and outflow, *J. Geophys. Res.*, *112*, D12S05, doi: 10.1029/2006JD007912, 2007.
- Hülsem, G., J. Gröbner, A. Bais, M. Blumthaler, P. Disterhoft, B. Johnsen, K.O. Lantz, C. Meleti, J. Schreder, J.M. Vilaplana Guerrero, and L. Ylianttila, Intercomparison of erythemal broadband radiometers

- calibrated by seven UV calibration facilities in Europe and the USA, *Atmos. Chem. Phys.*, *8* (16), 4865-4875, doi: 10.5194/acp-8-4865-2008, 2008.
- Ialongo, I., G.R. Casale, and A.M. Siani, Comparison of total ozone and erythral UV data from OMI with ground-based measurements at Rome station, *Atmos. Chem. Phys.*, *8* (12), 3283-3289, doi: 10.5194/acp-8-3283-2008, 2008.
- Ialongo, I., V. Buchard, C. Brogniez, G.R. Casale, and A.M. Siani, Aerosol Single Scattering Albedo retrieval in the UV range: An application to OMI satellite validation, *Atmos. Chem. Phys.*, *10* (2), 331-340, doi: 10.5194/acp-10-331-2010, 2010.
- Innis, J.L., and A.R. Klekociuk, Planetary wave and gravity wave influence on the occurrence of polar stratospheric clouds over Davis Station, Antarctica, seen in lidar and radiosonde observations, *J. Geophys. Res.*, *111*, D22102, doi: 10.1029/2006JD007629, 2006.
- IPCC (Intergovernmental Panel on Climate Change), *Climate Change 2007: Synthesis Report, Contribution of Working Groups I, II and III to the Fourth Assessment Report of the Intergovernmental Panel on Climate Change*, edited by Core Writing Team, R.K. Pachauri, and A. Reisinger, IPCC, Geneva, Switzerland, 104 pp., 2007.
- IUPAC (International Union of Pure and Applied Chemistry), 2007: see Atkinson et al., 2007.
- Janjai, S., S. Buntung, R. Wattan, and I. Masiri, Mapping solar ultraviolet radiation from satellite data in a tropical environment, *Remote Sens. Environ.*, *114* (3), 682-691, doi: 10.1016/j.rse.2009.11.008, 2010.
- Janouch, M., and L. Metelka, Modeling UV spectra with help of neural networks, in *Proceedings of the UV Conference "One Century of UV Radiation Research,"* 18-20 September 2007, Davos, Switzerland, edited by J. Gröbner, 207-208, 2007.
- Jin, B., I.-C. Chen, W.-T. Huang, C.-Y. Lien, N. Guchhait, and J.J. Lin, Photodissociation cross section of ClOOCl at 330 nm, *J. Phys. Chem. A.*, *114*, 4791-4797, doi: 10.1021/jp909374k, 2010.
- JMA (Japan Meteorological Agency), *Climate Change Monitoring Report 2008*, 87 pp., Japan Meteorological Agency, Tokyo, available: <http://ds.data.jma.go.jp/tcc/tcc/products/gwp/CCMR2008.pdf>, 2009.
- Johnsen, B., B. Kjeldstad, T.N. Aalerud, L.T. Nilsen, J. Schreder, M. Blumthaler, G. Bernhard, C. Topaloglou, O. Meinander, A. Bagheri, J.R. Slusser, and J. Davis, Intercomparison and harmonization of UV Index measurements from multiband filter radiometers, *J. Geophys. Res.*, *113*, D15206, doi: 10.1029/2007JD009731, 2008.
- Jones, A., J. Urban, D.P. Murtagh, P. Eriksson, S. Brohede, C. Haley, D. Degenstein, A. Bourassa, C. von Savigny, T. Sonkaew, A. Rozanov, H. Bovensmann, and J. Burrows, Evolution of stratospheric ozone and water vapour time series studied with satellite measurements, *Atmos. Chem. Phys.*, *9* (16), 6055-6075, doi: 10.5194/acp-9-6055-2009, 2009.
- JPL (Jet Propulsion Laboratory) 02-25: see Sander et al, 2003.
- JPL (Jet Propulsion Laboratory) 06-2: see Sander et al, 2006.
- JPL (Jet Propulsion Laboratory) 09-31: see Sander et al, 2009.
- Junk, J., U. Feister, and A. Helbig, Reconstruction of daily solar UV radiation from 1893 to 2002 in Potsdam, Germany, *Int. J. Biometeorol.*, *51* (6), 505-512, doi: 10.1007/s00484-007-0089-4, 2007.
- Kawa, S.R., R.S. Stolarski, P.A. Newman, A.R. Douglass, M. Rex, D.J. Hofmann, M.L. Santee, and K. Frieler, Sensitivity of polar stratospheric ozone loss to uncertainties in chemical reaction kinetics, *Atmos. Chem. Phys.*, *9* (22), 8651-8660, doi: 10.5194/acp-9-8651-2009, 2009.
- Kazadzis, S., A. Bais, V. Amiridis, D. Balis, C. Meleti, N. Kouremeti, C.S. Zerefos, S. Rapsomanikis, M. Petrakakis, A. Kelesis, P. Tzoumaka, and K. Kelektsoglou, Nine years of UV aerosol optical depth measurements at Thessaloniki, Greece, *Atmos. Chem. Phys.*, *7* (8), 2091-2101, doi: 10.5194/acp-7-2091-2007, 2007.
- Kazadzis, S., A. Bais, A. Arola, N. Krotkov, N. Kouremeti, and C. Meleti, Ozone Monitoring Instrument spectral UV irradiance products: comparison with ground based measurements at an urban environment, *Atmos. Chem. Phys.*, *9* (2), 585-594, doi: 10.5194/acp-9-585-2009, 2009a.
- Kazadzis, S., A. Bais, D. Balis, N. Kouremeti, M. Zempila, A. Arola, E. Giannakaki, V. Amiridis, and A. Kazantzidis, Spatial and temporal UV irradiance and aerosol variability within the area of an OMI satellite pixel, *Atmos. Chem. Phys.*, *9* (14), 4593-4601, doi: 10.5194/acp-9-4593-2009, 2009b.
- Kazantzidis, A., A. Bais, K. Garane, S. Kazadzis, and C. Meleti, Estimation of UV irradiance from ancillary data and comparison with measurements at Thessaloniki, Greece (40.5°N, 23°E), in *Remote Sensing of Clouds and the Atmosphere XI*, edited by J.R. Slusser, K. Schäfer, and A. Comerón, Proc. SPIE, 6362, 636228, doi: 10.1117/12.689813, 2006.
- Kivi, R., E. Kyrö, T. Turunen, N.R.P. Harris, P. von der Gathen, M. Rex, S.B. Andersen, and I. Wohltmann, Ozone observations in the Arctic during 1989–2003: Ozone variability and trends in the lower stratosphere and free troposphere, *J. Geophys. Res.*, *112*, D08306, doi: 10.1029/2006JD007271, 2007.

- Kovalenko, L.J., K.W. Jucks, R.J. Salawitch, G.C. Toon, J.-F. Blavier, D.G. Johnson, A. Kleinböhl, N.J. Livesey, J.J. Margitan, H.M. Pickett, M.L. Santee, B. Sen, R.A. Stachnik, and J.W. Waters, Observed and modeled HOCl profiles in the midlatitude stratosphere: Implication for ozone loss, *Geophys. Res. Lett.*, *34*, L19801, doi: 10.1029/2007GL031100, 2007.
- Krzyżcin, J.W., and J.L. Borkowski, Variability of the total ozone trend over Europe for the period 1950–2004 derived from reconstructed data, *Atmos. Chem. Phys.*, *8* (11), 2847–2857, doi: 10.5194/acp-8-2847-2008, 2008.
- Krzyżcin, J.W., and B. Rajewska-Więch, Trends in the ozone vertical distribution from the Umkehr observations at Belsk 1963–2007, *Int. J. Remote Sens.*, *30* (15), 3917–3926, doi: 10.1080/014311609002821866, 2009.
- Krzyżcin, J.W., P.S. Sobolewski, J. Jarosławski, J. Podgórski, and B. Rajewska-Więch, Erythematous UV observations at Belsk, Poland, in the period 1976–2008: Data homogenization, climatology, and trends, *Acta Geophysica*, *59* (1) 155–182, 2011.
- Kuttippurath, J., S. Godin-Beekmann, F. Lefèvre, and A. Pazmiño, Ozone depletion in the Arctic winter 2007–2008, *Int. J. Remote Sens.*, *30* (15–16), 4071–4082, doi: 10.1080/01431160902821965, 2009.
- Kvalevåg, M.M., G. Myhre, and C.E. Lund Myhre, Extensive reduction of surface UV radiation since 1750 in world's populated regions, *Atmos. Chem. Phys.*, *9* (20), 7737–7751, doi: 10.5194/acp-9-7737-2009, 2009.
- Lee-Taylor, J., S. Madronich, C. Fischer, and B. Mayer, A climatology of UV radiation, 1979–2000, 65S–65N, Chapter 1 in *UV Radiation in Global Climate Change: Measurements, Modeling and Effects on Ecosystems*, edited by W. Gao, D.L. Schmoldt, and J. Slusser, 550 pp., Springer-Verlag and Tsinghua University Press, ISBN: 978-3-642-03312-4, 1–20, 2009.
- Lerot, C., M. Van Roozendaal, J. van Geffen, J. van Gent, C. Fayt, R. Spurr, G. Lichtenberg, and A. von Barmen, Six years of total ozone column measurements from SCIAMACHY nadir observations, *Atmos. Meas. Tech.*, *2*, 87–98, doi: 10.5194/amt-2-87-2009, 2009.
- Li, F., R.S. Stolarski, and P.A. Newman, Stratospheric ozone in the post-CFC era, *Atmos. Chem. Phys.*, *9* (6), 2207–2213, doi: 10.5194/acp-9-2207-2009, 2009.
- Lien, C.Y., W.Y. Lin, H.Y. Chen, W.T. Huang, B. Jin, I.C. Chen, and J.J. Lin, Photodissociation cross sections of ClOOCl at 248.4 and 266 nm, *J. Chem. Phys.*, *131* (17), 174301, 2009.
- Lindfors, A., J. Kaurola, A. Arola, T. Koskela, K. Lakkala, W. Josefsson, J.A. Olseth, and B. Johnsen, A method for reconstruction of past UV radiation based on radiative transfer modeling: Applied to four stations in northern Europe, *J. Geophys. Res.*, *112*, D23201, doi: 10.1029/2007JD008454, 2007.
- Logan, J., An analysis of ozonesonde data for the lower stratosphere: Recommendations for testing models, *J. Geophys. Res.*, *104* (D13), 16151–16170, 1999.
- Lowe, D., and A.R. MacKenzie, Polar stratospheric cloud microphysics and chemistry, *J. Atmos. Solar-Terr. Phys.*, *70*, 13–40, doi: 10.1016/j.jastp.2007.09.011, 2008.
- Loyola, D.G., R.M. Coldewey-Egbers, M. Dameris, H. Garny, A. Stenke, M. Van Roozendaal, C. Lerot, D. Balis, and M. Koukouli, Global long-term monitoring of the ozone layer — a prerequisite for predictions, *Int. J. Remote Sens.*, *30*, 4295–4318, doi: 10.1080/01431160902825016, 2009a.
- Loyola, D.G., R.M. Coldewey-Egbers, W. Zimmer, M. Koukouli, D. Balis, C. Lerot, M. Van Roozendaal, and M. Dameris, Total ozone trends derived from the 14-years merged GOME/SCIAMACHY/GOME-2 data record, *Proc. ESA Atmospheric Science Conference*, 7–11 September 2009, Barcelona, Spain, European Space Agency, ESA SP-676, available: http://uv-vis.aeronomie.be/publications/proceedings/2009a_loyola.pdf, 2009b.
- Mäder, J.A., J. Staehelin, D. Brunner, W.A. Stahel, I. Wohltmann, and T. Peter, Statistical modeling of total ozone: Selection of appropriate explanatory variables, *J. Geophys. Res.*, *112*, D11108, doi: 10.1029/2006JD007694, 2007.
- Marley, N.A., J.S. Gaffney, M. Tackett, N.C. Sturchio, L. Heraty, N. Martinez, K.D. Hardy, A. Marchany-Rivera, T. Guilderson, A. MacMillan, and K. Steelman, The impact of biogenic carbon sources on aerosol absorption in Mexico City, *Atmos. Chem. Phys.*, *9* (5), 1537–1549, doi: 10.5194/acp-9-1537-2009, 2009.
- Marsh, D.R., and R.R. Garcia, Attribution of decadal variability in lower-stratospheric tropical ozone, *Geophys. Res. Lett.*, *34*, L21807, doi: 10.1029/2007GL030935, 2007.
- Martins, J.V., P. Artaxo, Y.J. Kaufman, A.D. Castanho, and L.A. Remer, Spectral absorption properties of aerosol particles from 350–2500 nm, *Geophys. Res. Lett.*, *36*, L13810, doi: 10.1029/2009GL037435, 2009.
- Massoli, P., M. Maturilli, and R. Neuber, Climatology of Arctic polar stratospheric clouds as measured by lidar in Ny-Ålesund, Spitsbergen (79°N, 12°E), *J. Geophys. Res.*, *111*, D09206, doi: 10.1029/2005JD005840, 2006.

- Maturilli, M., R. Nueber, P. Massoli, F. Cairo, A. Adriani, M.L. Moriconi, and G. Di Donfrancesco, Differences in Arctic and Antarctic PSC occurrence as observed by lidar in Ny-Ålesund (79°N, 12°E) and McMurdo (78°S, 167°E), *Atmos. Chem. Phys.*, 5 (8), 2081-2090, doi: 10.5194/acp-5-2081-2005, 2005.
- Matus, M.H., M.T. Nguyen, D.A. Dixon, K.A. Peterson, and J.S. Francisco, ClClO₂ is the most stable isomer of Cl₂O₂. Accurate coupled cluster energetics and electronic spectra of Cl₂O₂ isomers, *J. Phys. Chem. A*, 112, 9623-9627, doi: 10.1021/jp806220r, 2008.
- McCormack, J.P., D.E. Siskind, and L.L. Hood, Solar-QBO interaction and its impact on stratospheric ozone in a zonally averaged photochemical transport model of the middle atmosphere, *J. Geophys. Res.*, 112, D16109, doi: 10.1029/2006JD008369, 2007.
- McDonald, A.J., S.E. George, and R.M. Woollands, Can gravity waves significantly impact PSC occurrence in the Antarctic?, *Atmos. Chem. Phys.*, 9 (22), 8825-8840, doi: 10.5194/acp-9-8825-2009, 2009.
- McElroy, M.B., R.J. Salawitch, S.C. Wofsy, and J.A. Logan, Reductions of Antarctic ozone due to synergistic interactions of chlorine and bromine, *Nature*, 321, 759-762, doi: 10.1038/321759a0, 1986.
- McKenzie, R., G. Bodeker, G. Scott, J. Slusser, and K. Lantz, Geographical differences in erythemally-weighted UV measured at mid-latitude USDA sites, *Photochem. Photobiol. Sci.*, 5 (3), 343-352, doi: 10.1039/B510943D, 2006.
- McKenzie, R.L., C. Weinreis, P.V. Johnston, B. Liley, H. Shiona, M. Kotkamp, D. Smale, N. Takegawa, and Y. Kondo, Effects of urban pollution on UV spectral irradiances, *Atmos. Chem. Phys.*, 8 (18), 5683-5697, doi: 10.5194/acp-8-5683-2008, 2008.
- McKenzie, R.L., J.B. Liley, and L.O. Björn, UV radiation: Balancing risks and benefits, *Photochem. Photobiol.*, 85, 88-98, doi: 10.1111/j.1751-1097.2008.00400.x, 2009.
- McLandress, C., and T.G. Shepherd, Simulated anthropogenic changes in the Brewer-Dobson circulation, including its extension to high latitudes, *J. Clim.*, 22, 1516-1540, doi: 10.1175/2008JCLI2679.1, 2009.
- McLinden, C.A., S. Tegtmeier, and V. Fioletov, Technical note: A SAGE-corrected SBUV zonal-mean ozone data set, *Atmos. Chem. Phys.*, 9 (20), 7963-7972, doi: 10.5194/acp-9-7963-2009, 2009.
- Meinander, O., A. Kontu, K. Lakkala, A. Heikkilä, L. Ylianttila, and M. Toikka, Diurnal variations in the UV albedo of arctic snow, *Atmos. Chem. Phys.*, 8 (21), 6551-6563, doi: 10.5194/acp-8-6551-2008, 2008.
- Miller, A.J., A. Cai, G. Taio, D.J. Wuebbles, L.E. Flynn, S.-K. Yang, E.C. Weatherhead, V. Fioletov, I. Petropavlovskikh, X.-L. Meng, S. Guillas, R.M. Nagatani, and G.C. Reinsel, Examination of ozonsonde data for trends and trend changes incorporating solar and Arctic oscillation signals, *J. Geophys. Res.*, 111, D13305, doi: 10.1029/2005JD006684, 2006.
- Molina, L.T., and M.J. Molina, Production of Cl₂O₂ from the self-reaction of the ClO radical, *J. Phys. Chem.*, 91, 433-436, 1987.
- Moore, T.A., M. Okumura, J.W. Seale, and T.K. Minton, UV photolysis of ClOOCl, *J. Phys. Chem. A*, 103 (12), 1691-1695, 1999.
- Müller, R., J.-U. Groöß, C. Lemmen, D. Heinze, M. Dameris, and G. Bodeker, Simple measures of ozone depletion in the polar stratosphere, *Atmos. Chem. Phys.*, 8 (2), 251-264, doi: 10.5194/acp-8-251-2008, 2008.
- Murata, I., K. Sato, S. Okano, and Y. Tomikawa, Measurements of stratospheric ozone with a balloon-borne optical ozone sensor, *Int. J. Remote Sens.*, 30, 3961-3966, doi: 10.1080/01431160902822823, 2009.
- Newchurch, M.J., E.-S. Yang, D.M. Cunnold, G.C. Reinsel, J.M. Zawodny, and J.M. Russell III, Evidence for slowdown in stratospheric ozone loss: First stage of ozone recovery, *J. Geophys. Res.*, 108 (D16), 4507, doi: 10.1029/2003JD003471, 2003.
- Newman, P.A., and M. Rex (Lead Authors), P.O. Canziani, K.S. Carslaw, K. Drdla, S. Godin-Beekmann, D.M. Golden, C.H. Jackman, K. Kreher, U. Langematz, R. Müller, H. Nakane, Y.J. Orsolini, R.J. Salawitch, M.L. Santee, M. von Hobe, and S. Yoden, Polar ozone: Past and present, Chapter 4 in *Scientific Assessment of Ozone Depletion: 2006*, Global Ozone Research and Monitoring Project-Report No. 50, 572 pp., World Meteorological Organization, Geneva, Switzerland, 2007.
- Newman, P.A., E.R. Nash, S.R. Kawa, S.A. Montzka, and S.M. Schauffler, When will the Antarctic ozone hole recover?, *Geophys. Res. Lett.*, 33, L12814, doi: 10.1029/2005GL025232, 2006.
- Noel, V., A. Hertzog, H. Chepfer, and D.M. Winker, Polar stratospheric clouds over Antarctica from the CALIPSO spaceborne lidar, *J. Geophys. Res.*, 113, D02205, doi: 10.1029/2007JD008616, 2008.
- Noel, V., A. Hertzog, and H. Chepfer, CALIPSO observations of wave-induced PSCs with near-unity optical depth over Antarctica in 2006-2007, *J. Geophys. Res.*, 114, D05202, doi: 10.1029/2008JD010604, 2009.
- Ordóñez, C., D. Brunner, J. Staehelin, P. Hadjinicolaou, J.A. Pyle, M. Jonas, H. Wernli, and A.S.H. Prévôt, Strong influence of lowermost stratospheric ozone on lower tropospheric background ozone changes over Europe, *Geophys. Res. Lett.*, 34, L07805, doi:

- 10.1029/2006GL029113, 2007.
- Panicker, A.S., G. Pandithurai, T. Takamura, and R.T. Pinker, Aerosol effects in the UV-B spectral region over Pune, an urban site in India, *Geophys. Res. Lett.*, *36*, L10802, doi: 10.1029/2009GL037632, 2009.
- Papanastasiou, D.K., V.C. Papadimitriou, D.W. Fahey, and J.B. Burkholder, UV absorption spectrum of the ClO dimer (Cl₂O₂) between 200 and 420 nm, *J. Phys. Chem. A*, *113*, 13711-13726, doi: 10.1021/jp9065345, 2009.
- Parrington, M., D.B.A. Jones, K.W. Bowman, L.W. Horowitz, A.M. Thompson, D.W. Tarasick, and J.C. Witte, Estimating the summertime tropospheric ozone distribution over North America through assimilation of observations from the Tropospheric Emission Spectrometer, *J. Geophys. Res.*, *113*, D18307, doi: 10.1029/2007JD009341, 2008.
- Parrish, D.D., D.B. Millet, and A.H. Goldstein, Increasing ozone in marine boundary layer inflow at the west coasts of North America and Europe, *Atmos. Chem. Phys.*, *9* (4), 1303-1323, doi: 10.5194/acp-9-1303-2009, 2009.
- Permien, T., R. Vogt, and R.N. Schindler, Absorption spectra of HOCl and Cl₂O₂, in *Mechanisms of Gas Phase-Liquid Phase Chemical Transformations*, edited by R.A. Cox, *Air Pollution Report #17*, 149-153, Environmental Research Program of the CEC, EUR 12035 EN, Brussels, Belgium, 1988.
- Petkov, B., V. Vitale, C. Tomasi, U. Bonafè, S. Scaglione, D. Flori, R. Santaguida, M. Gausa, G. Hansen, and T. Colombo, Narrowband filter radiometer for ground-based measurements of global ultraviolet solar irradiance and total ozone, *Appl. Opt.*, *45* (18), 4383-4395, doi: 10.1364/AO.45.004383, 2006.
- Petropavlovskikh, I., C. Ahn, P.K. Bhartia, and L.E. Flynn, Comparison and covalidation of ozone anomalies and variability observed in SBUV(2) and Umkehr northern midlatitude ozone profile estimates, *Geophys. Res. Lett.*, *32*, L06805, doi: 10.1029/2004GL022002, 2005a.
- Petropavlovskikh, I., P.K. Bhartia, and J.J. DeLuisi, New Umkehr ozone profile retrieval algorithm optimized for climatological studies, *Geophys. Res. Lett.*, *32*, L16808, doi: 10.1029/2005GL023323, 2005b.
- Pitts, M.C., L.W. Thomason, L.R. Poole, and D.M. Winker, Characterization of Polar Stratospheric Clouds with spaceborne lidar: CALIPSO and the 2006 Antarctic season, *Atmos. Chem. Phys.*, *7* (19), 5207-5228, doi: 10.5194/acp-7-5207-2007, 2007.
- Pitts, M.C., L.R. Poole, and L.W. Thomason, CALIPSO polar stratospheric cloud observations: Second-generation detection algorithm and composition discrimination, *Atmos. Chem. Phys.*, *9* (19), 7577-7589, doi: 10.5194/acp-9-7577-2009, 2009.
- Plenge, J., R. Flesch, S. Köhl, B. Vogel, R. Müller, F. Stroh, and E. Rühl, Ultraviolet photolysis of the ClO dimer, *J. Phys. Chem. A*, *108*, 4859-4863, 2004.
- Pommereau, J.P., and F. Goutail, O₃ and NO₂ ground-based measurements by visible spectrometry during Arctic winter and spring 1988, *Geophys. Res. Lett.*, *15*, (8) 891-894, 1988.
- Poole, L.R., and M.C. Pitts, Polar stratospheric cloud climatology based on Stratospheric Aerosol Measurement II observations from 1978 to 1989, *J. Geophys. Res.*, *99* (D6), 13083-13089, 1994.
- Pope, F.D., J.C. Hansen, K.D. Bayes, R.R. Friedl, and S.P. Sander, Ultraviolet absorption spectrum of chlorine peroxide, ClOCl, *J. Phys. Chem.*, *111*, 4322-4332, 2007.
- Portmann, R.W., S. Solomon, R.R. Garcia, L.W. Thomason, L.R. Poole, and M.P. McCormick, Role of aerosol variations in anthropogenic ozone depletion in the polar regions, *J. Geophys. Res.*, *101* (D17), 22991-23006, 1996.
- Pougatchev, N.S., B.J. Connor, and C.P. Rinsland, Infrared measurements of the ozone vertical distribution above Kitt Peak, *J. Geophys. Res.*, *100* (D8), 16689-16697, 1995.
- Pribullová, A., and M. Chmelík, Typical distribution of the solar erythemal UV radiation over Slovakia, *Atmos. Chem. Phys.*, *8* (17), 5393-5401, doi: 10.5194/acp-8-5393-2008, 2008.
- Price, C., and D. Rind, A simple lightning parameterization for calculating global lightning distributions, *J. Geophys. Res.*, *97* (D9), 9919-9933, 1992.
- Randel, W.J., and F. Wu, A stratospheric ozone profile data set for 1979-2005: Variability, trends, and comparisons with column ozone data, *J. Geophys. Res.*, *112*, D06313, doi: 10.1029/2006JD007339, 2007.
- Randel, W.J., K.P. Shine, J. Austin, J. Barnett, C. Claud, N.P. Gillett, P. Keckhut, U. Langematz, R. Lin, C. Long, C. Mears, A. Miller, J. Nash, D.J. Seidel, D.W.J. Thompson, F. Wu, and S. Yoden, An update of observed stratospheric temperature trends, *J. Geophys. Res.*, *114*, D02107, doi: 10.1029/2008JD010421, 2009.
- Rasch, P.J., P.J. Crutzen, and D.B. Coleman, Exploring the geoengineering of climate using stratospheric sulfate aerosols: The role of particle size, *Geophys. Res. Lett.*, *35*, L02809, doi: 10.1029/2007GL032179, 2008.
- Reinsel, G.C., E.C. Weatherhead, G.C. Tiao, A.J. Miller, R.M. Nagatani, D.J. Wuebbles, and L.E. Flynn, On detection of turnaround and recovery in trend for ozone, *J. Geophys. Res.*, *107* (D10), 4078, doi: 10.1029/2001JD000500, 2002.
- Reinsel, G.C., A.J. Miller, E.C. Weatherhead, L.E. Flynn,

- R. Nagatani, G.C. Tiao, and D.J. Wuebbles, Trend analysis of total ozone data for turnaround and dynamical contributions, *J. Geophys. Res.*, *110*, D16306, doi: 10.1029/2004JD004662, 2005.
- Remsberg, E.E., On the response of Halogen Occultation Experiment (HALOE) stratospheric ozone and temperature to the 11-year solar cycle forcing, *J. Geophys. Res.*, *113*, D22304, doi: 10.1029/2008JD010189, 2008.
- Rex, M., R.J. Salawitch, P. von der Gathen, N.R.P. Harris, M.P. Chipperfield, and B. Naujokat, Arctic ozone loss and climate change, *Geophys. Res. Lett.*, *31*, L04116, doi: 10.1029/2003GL018844, 2004.
- Rex, M., R.J. Salawitch, H. Deckelmann, P. von der Gathen, N.R.P. Harris, M.P. Chipperfield, B. Naujokat, E. Reimer, M. Allaart, S.B. Andersen, R. Bevilacqua, G.O. Braathen, H. Claude, J. Davies, H. De Backer, H. Dier, V. Dorokhov, H. Fast, M. Gerdling, S. Godin-Beekmann, K. Hoppel, B. Johnson, E. Kyrö, Z. Litynska, D. Moore, H. Nakane, M.C. Parrondo, A.D. Risley Jr., P. Skrivankova, R. Stübi, P. Viatte, V. Yushkov, and C. Zerefos, Arctic winter 2005: Implications for stratospheric ozone loss and climate change, *Geophys. Res. Lett.*, *33*, L23808, doi: 10.1029/2006GL026731, 2006.
- Rieder, H.E., F. Holawe, S. Simic, M. Blumthaler, J.W. Krzyściński, J.E. Wagner, A.W. Schmalwieser, and P. Weihs, Reconstruction of erythemal UV-doses for two stations in Austria: A comparison between alpine and urban regions, *Atmos. Chem. Phys.*, *8* (20), 6309-6323, doi: 10.5194/acp-8-6309-2008, 2008.
- Robock, A., T. Adams, M. Moore, L. Oman, G. Stenchikov, Southern Hemisphere atmospheric circulation effects of the 1991 Mount Pinatubo eruption, *Geophys. Res. Lett.*, *34*, L23710, doi: 10.1029/2007GL031403, 2007.
- Rodgers, C.D., *Inverse Methods for Atmospheric Sounding: Theory and Practice*, 240 pp., ISBN 981-02-2740X, World Scientific Publishing Co. Ltd., London, UK, 2000.
- Rosenfield, J.E., S.M. Frith, and R.S. Stolarski, Version 8 SBUV ozone profile trends compared with trends from a zonally averaged chemical model, *J. Geophys. Res.*, *110*, D12302, doi: 10.1029/2004JD005466, 2005.
- Rösevall, J.D., D.P. Murthagh, and J. Urban, Ozone depletion in the 2006/2007 Arctic winter, *Geophys. Res. Lett.*, *34*, L21809, doi: 10.1029/2007GL030620, 2007.
- Ruckstuhl, C., R. Philipona, K. Behrens, M. Collaud Coen, B. Dürr, A. Heimo, C. Mätzler, S. Nyeki, A. Ohmura, L. Vuilleumier, M. Weller, C. Wehrli, and A. Zelenka, Aerosol and cloud effects on solar brightening and the recent rapid warming, *Geophys. Res. Lett.*, *35*, L12708, doi: 10.1029/2008GL034228, 2008.
- Salawitch, R.J., D.K. Weisenstein, L.J. Kovalenko, C.E. Sioris, P.O. Wennberg, K. Chance, M.K.W. Ko, and C.A. McLinden, Sensitivity of ozone to bromine in the lower stratosphere, *Geophys. Res. Lett.*, *32* (5), L05811, doi: 10.1029/2004GL021504, 2005.
- Sander, S.P., R.R. Friedl, D.M. Golden, M.J. Kurylo, R.E. Huie, V.L. Orkin, G.K. Moortgat, A.R. Ravishankara, C.E. Kolb, M.J. Molina, and B.J. Finlayson-Pitts, *Chemical Kinetics and Photochemical Data for Use in Atmospheric Studies: Evaluation No. 14, JPL Publication 02-25*, Jet Propulsion Laboratory, Pasadena, Calif., 2003. (Cited as JPL 02-25.)
- Sander, S.P., R.R. Friedl, D.M. Golden, M.J. Kurylo, G.K. Moortgat, H. Keller-Rudek, P.H. Wine, A.R. Ravishankara, C.E. Kolb, M.J. Molina, B.J. Finlayson-Pitts, R.E. Huie, and V.L. Orkin, *Chemical Kinetics and Photochemical Data for Use in Atmospheric Studies: Evaluation No. 15, JPL Publication 06-2*, Jet Propulsion Laboratory, Pasadena, Calif., 2006. (Cited as JPL 06-2.)
- Sander, S.P., J. Abbatt, J.R. Barker, J.B. Burkholder, R.R. Friedl, D.M. Golden, R.E. Huie, C.E. Kolb, M.J. Kurylo, G.K. Moortgat, V.L. Orkin, and P.H. Wine, *Chemical Kinetics and Photochemical Data for Use in Atmospheric Studies: Evaluation Number 16, JPL Publication 09-31*, Jet Propulsion Laboratory, Pasadena, Calif., available at <http://jpldataeval.jpl.nasa.gov>, 2009. (Cited as JPL 09-31.)
- Santee, M.L., I.A. MacKenzie, G.L. Manney, M.P. Chipperfield, P.F. Bernath, K.A. Walker, C.D. Boone, L. Froidevaux, N.J. Livesey, and J.W. Waters, A study of stratospheric chlorine partitioning based on new satellite measurements and modeling, *J. Geophys. Res.*, *113*, D12307, doi: 10.1029/2007JD009057, 2008.
- Santee, M.L., S.P. Sander, N.J. Livesey, and L. Froidevaux, Constraining the chlorine monoxide (ClO)/chlorine peroxide (ClOOCl) equilibrium constant from Aura Microwave Limb Sounder measurements of nighttime ClO, *Proc. Nat. Acad. Sci.*, *107* (15), 6588-6593, doi: 10.1073/pnas.0912659107, 2010.
- Sauvage, B., R.V. Martin, A. van Donkelaar, X. Liu, K. Chance, L. Jaeglé, P.I. Palmer, S. Wu, and T.-M. Fu, Remote sensed and in situ constraints on processes affecting tropical tropospheric ozone, *Atmos. Chem. Phys.*, *7* (3), 815-838, doi: 10.5194/acp-7-815-2007, 2007.
- Scarnato, B., J. Staehelin, T. Peter, J. Gröbner, and R. Stübi, Temperature and slant path effects in Dobson and Brewer total ozone measurements, *J. Geophys. Res.*, *114*, D24303, doi: 10.1029/2009JD012349, 2009.

- Scarnato, B., J. Staehelin, R. Stübi, and H. Schill, Long term total ozone observations at Arosa (Switzerland) with Dobson and Brewer instruments (1988–2007), *J. Geophys. Res.*, *115*, D13306, doi: 10.1029/2009JD011908, 2010.
- Schallhart, B., M. Blumthaler, J. Schreder, and J. Verdebout, A method to generate near real time UV-Index maps of Austria, *Atmos. Chem. Phys.*, *8* (24), 7483–7491, doi: 10.5194/acp-8-7483-2008, 2008.
- Schiermeier, Q., Chemists poke holes in ozone theory, *Nature*, *449*, 382–383, 2007.
- Schmidt, H., and G.P. Brasseur, The response of the middle atmosphere to solar cycle forcing in the Hamburg Model of the neutral and ionized atmosphere, *Space Sci. Rev.*, *125*, 345–356, doi: 10.1007/s11214-006-9068-z, 2006.
- Schmidt, H., G.P. Brasseur, and M.A. Giorgetta, Solar cycle signal in a general circulation and chemistry model with internally generated quasi-biennial oscillation, *J. Geophys. Res.*, *115*, D00114, doi: 10.1029/2009JD012542, 2010.
- Schneider, M., A. Redondas, F. Hase, C. Guirado, T. Blumenstock, and E. Cuevas, Comparison of ground-based Brewer and FTIR total O₃ monitoring techniques, *Atmos. Chem. Phys.*, *8* (18), 5535–5550, doi: 10.5194/acp-8-5535-2008, 2008.
- Schofield, R., K. Frieler, I. Wohltmann, M. Rex, M. von Hobe, F. Stroh, G. Koch, T. Peter, T. Canty, R. Salawitch, and C.M. Volk, Polar stratospheric chlorine kinetics from a self-match flight during SOLVE-II/EUPLEX, *Geophys. Res. Lett.*, *35*, L01807, doi: 10.1029/2007GL031740, 2008.
- Seckmeyer G., M. Glandorf, C. Wichers, R. McKenzie, D. Henriques, F. Carvalho, A. Webb, A.M. Siani, A. Bais, B. Kjeldstad, C. Brogniez, P. Werle, T. Koskela, K. Lakkala, J. Gröbner, H. Slaper, P. den Outer, and U. Feister, Europe's darker atmosphere in the UV-B, *Photochem. Photobiol. Sci.*, *7* (8), 925–930, 2008a.
- Seckmeyer, G., D. Pissulla, M. Glandorf, D. Henriques, B. Johnsen, A. Webb, A.-M. Siani, A. Bais, B. Kjeldstad, C. Brogniez, J. Lenoble, B. Gardiner, P. Kirsch, T. Koskela, J. Kaurola, B. Uhlmann, H. Slaper, P. den Outer, M. Janouch, P. Werle, J. Gröbner, B. Mayer, A. de la Casiniere, S. Simic, and F. Carvalho, Variability of UV irradiance in Europe, *Photochem. Photobiol.*, *84*, 172–179, doi: 10.1111/j.1751-1097.20007.00216.x, 2008b.
- Shepherd, T.G., Dynamics, stratospheric ozone, and climate change, *Atmos.-Ocean*, *46* (1), 117–138, doi: 10.3137/ao.460106, 2008.
- Shepherd, T.G., and A.I. Jonsson, On the attribution of stratospheric ozone and temperature changes to changes in ozone-depleting substances and well-mixed greenhouse gases, *Atmos. Chem. Phys.*, *8* (5), 1435–1444, doi: 10.5194/acp-8-1435-2008, 2008.
- Shindell, D.T., and R.L. de Zafra, Chlorine monoxide in the Antarctic spring vortex 2. A comparison of measured and modeled diurnal cycling over McMurdo Station, 1993, *J. Geophys. Res.*, *101* (D1), 1475–1487, 1996.
- Sinnhuber, B.-M., D.W. Arlander, H. Bovensmann, J.P. Burrows, M.P. Chipperfield, C.-F. Enell, U. Frieß, F. Hendrick, P.V. Johnston, R.L. Jones, K. Kreher, N. Mohamed-Tahrin, R. Müller, K. Pfeilsticker, U. Platt, J.-P. Pommereau, I. Pundt, A. Richter, A.M. South, K.K. Tørnkvist, M. Van Roozendaal, T. Wagner, and F. Wittrock, Comparison of measurements and model calculations of stratospheric bromine monoxide, *J. Geophys. Res.*, *107* (D19), 4398, doi: 10.1029/2001JD000940, 2002.
- Sitnov, S., Influence of the 11-year solar cycle on the effects of the equatorial quasi-biennial oscillation, manifesting in the extratropical northern atmosphere, *Clim. Dyn.*, *32*, 1–17, doi: 10.1007/s00382-007-0362-6, 2009.
- Slusser, J., J. Gibson, D. Bigelow, D. Kolinski, P. Disterhoft, K. Lantz, and A. Beaubien, Langley method of calibrating UV filter radiometers, *J. Geophys. Res.*, *105* (D4), 4841–4849, 2000.
- Smit, H.G.J., W. Straeter, B.J. Johnson, S.J. Oltmans, J. Davies, D.W. Tarasick, B. Goegger, R. Stubi, F.J. Schmidlin, T. Northam, A.M. Thompson, J.C. Witte, I. Boyd, and F. Posny, Assessment of the performance of ECC ozonesondes under quasi-flight conditions in the environmental simulation chamber: Insights from the Juelich Ozone Sonde Intercomparison Experiment (JOSIE), *J. Geophys. Res.*, *112*, D19306, doi: 10.1029/2006JD007308, 2007.
- Smith, A.K., and K. Matthes, Decadal-scale periodicities in the stratosphere associated with the solar cycle and the QBO, *J. Geophys. Res.*, *113*, D05311, doi: 10.1029/2007JD009051, 2008.
- Soller, R., J.M. Nicovich, and P.H. Wine, Temperature-dependent rate coefficients for the reactions of Br(²P_{3/2}), Cl(²P_{3/2}), and O(³P_J) with BrONO₂, *J. Phys. Chem. A*, *105* (9), 1416–1422, 2001.
- Solomon, P., B. Connor, J. Barrett, T. Mooney, A. Lee, and A. Parrish, Measurements of stratospheric ClO over Antarctica in 1996–2000 and implications for ClO dimer chemistry, *Geophys. Res. Lett.*, *29* (15), 1708, doi: 10.1029/2002GL015232, 2002.
- Solomon, S., R.R. Garcia, F.S. Rowland, and D.J. Wuebbles, On the depletion of Antarctic ozone, *Nature*, *321*, 755–758, doi: 10.1038/321755a0, 1986.
- Solomon, S., R.W. Portmann, T. Sasaki, D.J. Hofmann, and D.W.J. Thompson, Four decades of ozonesonde measurements over Antarctica, *J. Geophys. Res.*,

- 110, D21311, doi: 10.1029/2005JD005917, 2005.
- Solomon, S., R.W. Portmann, and D.W.J. Thompson, Contrasts between Antarctic and Arctic ozone depletion, *Proc. Nat. Acad. Sci.*, *104* (2), 445-449, doi: 10.1073/pnas.0604895104, 2007.
- SPARC (Stratospheric Processes And their Role in Climate), *SPARC/IOC/GAW Assessment of Trends in the Vertical Distribution of Ozone*, edited by N. Harris, R. Hudson, and C. Phillips, SPARC Report No. 1, WMO Global Ozone Research and Monitoring Project Report No. 43, 289 pp., Verrières le Buisson, France, 1998.
- SPARC (Stratospheric Processes And their Role in Climate), *The Role of Halogen Chemistry in Polar Stratospheric Ozone Depletion*, Report from the June 2008 Cambridge UK Workshop for an Initiative under the Stratospheric Processes and Their Role in Climate (SPARC) Project of the World Climate Research Programme, authored by M.J. Kurylo, B.-M. Sinnhuber, N.R.P. Harris, M. von Hobe, P.A. Newman, D.W. Fahey, R.S. Gao, R.J. Salawitch, M.P. Chipperfield, J.G. Anderson, M.L. Santee, T.P. Canty, R. Müller, R. Schofield, R.M. Stimpfle, F. Strohm, D.W. Toohey, J. Urban, S.R. Kawa, D.J. Hofmann, K.W. Hoppel, M. Rex, K.D. Bayes, D.A. Dixon, K.W. Jucks, S.P. Sander, J.-U. Groöb, and D.E. Kinnison, 48 pp., available: http://www.atmosp.physics.utoronto.ca/SPARC/HalogenChem_Final_20090213.pdf, 2009.
- SPARC CCMVal (Stratospheric Processes And their Role in Climate), *SPARC Report on the Evaluation of Chemistry-Climate Models*, edited by V. Eyring, T.G. Shepherd, and D.W. Waugh, SPARC Report No. 5, WCRP-132, WMO/TD-No. 1526, 478 pp., available: <http://www.atmosp.physics.utoronto.ca/SPARC>, 2010.
- Staehelin, J., N.R.P. Harris, C. Appenzeller, and J. Eberhard, Ozone trends: A review, *Rev. Geophys.*, *39*, 231-290, 2001.
- Staiger, H., P.N. den Outer, A.F. Bais, H. Feister, B. Johnsen, and L. Vuilleumier, Hourly resolved cloud modification factors in the ultraviolet, *Atmos. Chem. Phys.*, *8* (9), 2493-2508, doi: 10.5194/acp-8-2493-2008, 2008.
- Steinbrecht, W., H. Claude, F. Schöenborn, I.S. McDermid, T. Leblanc, S. Godin-Beekmann, P. Keckhut, A. Hauchecorne, J.A.E. Van Gijssel, D.P.J. Swart, G.E. Bodeker, A. Parrish, I.S. Boyd, N. Kämpfer, K. Hocke, R.S. Stolarski, S.M. Frith, L.W. Thomason, E.E. Remsberg, C. Von Savigny, A. Rozanov, and J.P. Burrows, Ozone and temperature trends in the upper stratosphere at five stations of the Network for the Detection of Atmospheric Composition Change, *Int. J. Remote Sens.*, *30*, 3875-3886, doi: 10.1080/01431160902821841, 2009.
- Stenchikov, G., A. Robock, V. Ramaswamy, M.D. Schwarzkopf, K. Hamilton, and S. Ramachandran, Arctic Oscillation response to the 1991 Mount Pinatubo eruption: Effects of volcanic aerosols and ozone depletion, *J. Geophys. Res.*, *107* (D24), 4803, doi: 10.1029/2002JD002090, 2002.
- Stimpfle, R.M., R.A. Perry, and C.J. Howard, Temperature-dependence of the reaction of ClO and HO₂ radicals, *J. Chem. Phys.*, *71* (12), 5183-5190, doi: 10.1063/1.438293, 1979.
- Stimpfle, R., D.M. Wilmouth, R.J. Salawitch, and J.G. Anderson, First measurements of ClOOC1 in the stratosphere: The coupling of ClOOC1 and ClO in the Arctic polar vortex, *J. Geophys. Res.*, *109*, D03301, doi: 10.1029/2003JD003811, 2004.
- Stolarski, R.S., and S.M. Frith, Search for evidence of trend slow-down in the long-term TOMS/SBUV total ozone data record: The importance of instrument drift uncertainty, *Atmos. Chem. Phys.*, *6*, 4057-4065, 2006.
- Stolarski, R.S., A.R. Douglass, S. Steenrod, and S. Pawson, Trends in stratospheric ozone: Lessons learned from a 3D Chemical Transport Model, *J. Atmos. Sci.*, *63* (3), 1028-1041, 2006.
- Stübi, R., G. Levrat, B. Hoegger, P. Viatte, J. Staehelin, and F. J. Schmidlin, In-flight comparison of Brewer-Mast and electrochemical concentration cell ozonesondes, *J. Geophys. Res.*, *113*, D13302, doi: 10.1029/2007JD009091, 2008.
- Tabazadeh, A., R.P. Turco, K. Drdla, M.Z. Jacobson, and O.B. Toon, A study of Type I polar stratospheric cloud formation, *Geophys. Res. Lett.*, *21* (15), 1619-1622, 1994.
- Tabazadeh, A., Y.S. Djikaev, P. Hamill, and H. Reiss, Laboratory evidence for surface nucleation of solid polar stratospheric cloud particles, *J. Phys. Chem. A*, *106*, 10238-10246, 2002.
- Takahashi, K., Y. Takeuchi, and Y. Matsumi, Rate constants of the O(¹D) reactions with N₂, O₂, N₂O, and H₂O at 295 K, *Chem. Phys. Lett.*, *410*, 196-200, 2005.
- Tanskanen, A., N.A. Krotkov, J.R. Herman, and A. Arola, Surface ultraviolet irradiance from OMI, *Geosci. Remote Sens.*, *44* (5), 1267-1271, doi: 10.1109/TGRS.2005.862203, 2006.
- Tanskanen, A., A. Lindfors, A. Määttä, N. Krotkov, J. Herman, J. Kaurola, T. Koskela, K. Lakkala, V. Fioletov, G. Bernhard, R. McKenzie, Y. Kondo, M. O'Neill, H. Slaper, P. den Outer, A.F. Bais, and J. Tamminen, Validation of daily erythemal doses from Ozone Monitoring Instrument with ground-based UV measurement data, *J. Geophys. Res.*, *112*, D24S44, doi: 10.1029/2007JD008830, 2007.

- Tatarov, B., H. Nakane, Ch. B. Park, N. Sugimoto, and I. Matsui, Lidar observation of long-term trends and variations of stratospheric ozone and temperature over Tsukuba, Japan, *Int. J. Remote Sens.*, *30* (15-16), 3951-3960, doi: 10.1080/01431160902821882, 2009.
- Tegtmeier, S., M. Rex, I. Wohltmann, and K. Krüger, Relative importance of dynamical and chemical contributions to Arctic wintertime ozone, *Geophys. Res. Lett.*, *35*, L17801, doi: 10.1029/2008GL034250, 2008.
- Telford, P., P. Braesicke, O. Morgenstern, and J. Pyle, Re-assessment of causes of ozone column variability following the eruption of Mount Pinatubo using a nudged CCM, *Atmos. Chem. Phys.*, *9* (13), 4251-4260, doi: 10.5194/acp-9-4251-2009, 2009.
- Terao, Y., and J.A. Logan, Consistency of time series and trends of stratospheric ozone as seen by ozonesonde, SAGE II, HALOE, and SBUV(2), *J. Geophys. Res.*, *112*, D06310, doi: 10.1029/2006JD007667, 2007.
- Terao, Y., J.A. Logan, A.R. Douglass, and R.S. Stolarski, Contribution of stratospheric ozone to the interannual variability of tropospheric ozone in the northern extratropics, *J. Geophys. Res.*, *113*, D18309, doi: 10.1029/2008JD009854, 2008.
- Thiel, S., L. Ammannato, A. Bais, B. Bandy, M. Blumthaler, B. Bohn, O. Engelsen, G.P. Gobbi, J. Gröbner, E. Jäkel, W. Junkermann, S. Kazadzis, R. Kift, B. Kjeldstad, N. Kouremeti, A. Kylling, B. Mayer, P.S. Monks, C.E. Reeves, B. Schallhart, R. Scheirer, S. Schmidt, R. Schmitt, J. Schreder, R. Silbernagl, C. Topaloglou, T.M. Thorseth, A.R. Webb, M. Wendisch, and P. Werle, Influence of clouds on the spectral actinic flux density in the lower troposphere (INSPECTRO): Overview of the field campaigns, *Atmos. Chem. Phys.*, *8* (6), 1789-1812, doi: 10.5194/acp-8-1789-2008, 2008.
- Thompson, A.M., J.B. Stone, J.C. Witte, S.K. Miller, R.B. Pierce, R.B. Chatfield, S.J. Oltmans, O.R. Cooper, A.L. Loucks, B.F. Taubman, B.J. Johnson, E. Joseph, T.L. Kucsera, J.T. Merrill, G.A. Morris, S. Hersey, G. Forbes, M.J. Newchurch, F.J. Schmidlin, D.W. Tarasick, V. Thouret, and J.-P. Cammas, Intercontinental Chemical Transport Experiment Ozonesonde Network Study (IONS) 2004: 1. Summertime upper troposphere/lower stratosphere ozone over northeastern North America, *J. Geophys. Res.*, *112*, D12S12, doi: 10.1029/2006JD007441, 2007.
- Thouret, V., J.-P. Cammas, B. Sauvage, G. Athier, R. Zbinden, P. Nédélec, P. Simon, and F. Karcher, Tropopause referenced ozone climatology and inter-annual variability (1994–2003) from the MOZAIC programme, *Atmos. Chem. Phys.*, *6* (4), 1033-1051, doi: 10.5194/acp-6-1033-2006, 2006.
- Tie, X.X., and G.P. Brasseur, The response of stratospheric ozone to volcanic eruptions: Sensitivity to atmospheric chlorine loading, *Geophys. Res. Lett.*, *22* (22), 3035-3038, 1995.
- Tie, X.X., G.P. Brasseur, B. Briegleb, and C. Granier, Two-dimensional simulation of Pinatubo aerosol and its effect on stratospheric ozone, *J. Geophys. Res.*, *99* (D10), 20545-20562, 1994.
- Tilmes, S., R. Müller, J.-U. Groöf, and J.M. Russell III, Ozone loss and chlorine activation in the Arctic winters 1991–2003 derived with the tracer-tracer correlations, *Atmos. Chem. Phys.*, *4* (8), 2181-2213, doi: 10.5194/acp-4-2181-2004, 2004.
- Tilmes, S., R. Müller, A. Engel, M. Rex, and J. M. Russell, Chemical ozone loss in the Arctic and Antarctic stratosphere between 1992 and 2005, *Geophys. Res. Lett.*, *33*, L20812, doi: 10.1029/2006GL026925, 2006.
- Tilmes, S., R. Müller, and R. Salawitch, The sensitivity of polar ozone depletion to proposed geoengineering schemes, *Science*, *320*, 1201-1204, 2008a.
- Tilmes, S., R. Müller, R.J. Salawitch, U. Schmidt, C.R. Webster, H. Oelhaf, C.C. Camy-Peyret, and J.M. Russell III, Chemical ozone loss in the Arctic winter 1991–1992, *Atmos. Chem. Phys.*, *8* (7), 1897-1910, doi: 10.5194/acp-8-1897-2008, 2008b.
- Toohey, D.W., L.M. Avallone, L.R. Lait, P.A. Newman, M.R. Schoeberl, D.W. Fahey, E.L. Woodbridge, and J.G. Anderson, The seasonal evolution of reactive chlorine in the northern hemisphere stratosphere, *Science*, *261* (5125), 1134-1136, doi: 10.1126/science.261-5125.1134, 1993.
- Toon, O., A. Tabazadeh, E. Browell, and J. Jordan, Analysis of lidar observations of Arctic polar stratospheric clouds during January 1989, *J. Geophys. Res.*, *105* (D16), 20589-20615, 2000.
- Tourpali, K., C.S. Zerefos, D.S. Balis, and A.F. Bais, The 11-year solar cycle in stratospheric ozone: Comparison between Umkehr and SBUVv8 and effects on surface erythemal irradiance, *J. Geophys. Res.*, *112*, D12306, doi: 10.1029/2006JD007760, 2007.
- Tsutsui, J., K. Nishizawa, and F. Sassi, Response of the middle atmosphere to the 11-year solar cycle simulated with the Whole Atmosphere Community Climate Model, *J. Geophys. Res.*, *114*, D02111, doi: 10.1029/2008JD010316, 2009.
- Van Roozendaal, M., D. Loyola, R. Spurr, D. Balis, J.-C. Lambert, Y. Livschitz, P. Valks, T. Ruppert, P. Kenter, C. Fayt, and C. Zehner, Ten years of GOME/ERS-2 total ozone data – The new GOME data processor (GDP) version 4: 1. Algorithm description, *J. Geophys. Res.*, *111*, D14311, doi: 10.1029/2005JD006375, 2006.
- Verdebout, J., A method to generate surface UV radiation

- maps over Europe using GOME, Meteosat, and ancillary geophysical data, *J. Geophys. Res.*, *105* (D4), 5049-5058, 2000.
- Verdebout, J., A European satellite-derived UV climatology available for impact studies, *Radiat. Prot. Dosim.*, *111* (4), 407-411, 2004a.
- Verdebout, J., A satellite-derived UV radiation climatology over Europe to support impact studies, *Arct. Antarct. Alp. Res.*, *36* (3), 357-363, 2004b.
- Vernet, M., S.B. Diaz, H.A. Fuenzalida, C. Camilion, C.R. Booth, S. Cabrera, C. Casiccia, G. Deferrari, C. Lovengreen, A. Paladini, J. Pedroni, A. Rosales, and H.E. Zagarese, Quality of UVR exposure for different biological systems along a latitudinal gradient, *Photochem. Photobiol.*, *8*, 1329-1345, doi: 10.1039/b904540f, 2009.
- Vernier, J.P., J.P. Pommereau, A. Garnier, J. Pelon, N. Larsen, J. Nielsen, T. Christensen, F. Cairo, L.W. Thomason, T. Leblanc, and I.S. McDermid, Tropical stratospheric aerosol layer from CALIPSO lidar observations, *J. Geophys. Res.*, *114*, D00H10, doi: 10.1029/2009JD011946, 2009.
- Vigouroux C., M. De Mazière, P. Demoulin, C. Servais, F. Hase, T. Blumenstock, I. Kramer, M. Schneider, J. Mellqvist, A. Strandberg, V. Velazco, J. Notholt, R. Sussmann, W. Stremme, A. Rockmann, T. Gardiner, M. Coleman, and P. Woods, Evaluation of tropospheric and stratospheric ozone trends over Western Europe from ground-based FTIR network observations, *Atmos. Chem. Phys.*, *8* (23), 6865-6886, doi: 10.5194/acp-8-6865-2008, 2008.
- Vogel, B., R. Müller, T. Deshler, J.-U. Grooß, J. Karhu, D.S. McKenna, M. Müller, D. Toohey, G.C. Toon, and F. Stroh, Vertical profiles of activated ClO and ozone loss in the Arctic vortex in January and March 2000: In situ observations and model simulations, *J. Geophys. Res.*, *108* (D22), 8334, doi: 10.1029/2002JD002564, 2003.
- Voigt, C., J. Schreiner, A. Kohlman, P. Zink, K. Mauersberger, N. Larsen, T. Deshler, C. Kröger, J. Rosen, A. Adriani, F. Cairo, G. Di Donfrancesco, M. Viterbini, J. Ovarlez, H. Ovarlez, C. David, and A. Dörnbrack, Nitric acid trihydrate (NAT) in polar stratospheric clouds, *Science*, *290*, 1756-1758, 2000.
- von Hobe, M., Revisiting ozone depletion, *Science*, *318*, 1878-1879, 2007.
- von Hobe, M., R.J. Salawitch, T. Canty, H. Keller-Rudek, G.K. Moortgat, J.-U. Grooß, R. Müller, and F. Stroh, Understanding the kinetics of the ClO dimer cycle, *Atmos. Chem. Phys.*, *7* (12), 3055-3069, doi: 10.5194/acp-7-3055-2007, 2007.
- von Hobe, M., F. Stroh, H. Beckers, T. Benter, and H. Willner, The UV/Vis absorption spectrum of matrix-isolated dichlorine peroxide, ClOOC1, *Phys. Chem. Chem. Phys.*, *11*, 1571-1580, doi: 10.1039/b814373k, 2009.
- Vranckx, S., J. Peeters, and S.A. Carl, Absolute rate constant and O(³P) yield for the O(¹D) + N₂O reaction in the temperature range 227 K to 719 K, *Atmos. Chem. Phys.*, *8* (20), 6261-6272, doi: 10.5194/acp-8-6261-2008, 2008.
- Vyushin, D., V.E. Fioletov, and T.G. Shepherd, Impact of long-range correlations on trend detection in total ozone, *J. Geophys. Res.*, *112*, D14307, doi: 10.1029/2006JD008168, 2007.
- Vyushin, D., T.G. Shepherd, and V.E. Fioletov, On the statistical modeling of persistence in total ozone anomalies, *J. Geophys. Res.*, *115*, D16306, doi: 10.1029/2009JD013105, 2010.
- Waibel, A.E., T. Peter, K.S. Carslaw, H. Oelhaf, G. Wetzel, P.J. Crutzen, U. Pöschl, A. Tsias, E. Reimer, and H. Fischer, Arctic ozone loss due to denitrification, *Science*, *283*, 2064-2069, 1999.
- Wang, K., R.E. Dickinson, and S. Liang, Clear sky visibility has decreased over land globally from 1973 to 2007, *Science*, *323* (5921), 1468-1470, doi: 10.1126/science.1167549, 2009.
- Wang, Z., G. Stephens, T. Deshler, C. Trepte, T. Parish, D. Vane, D. Winker, D. Liu, and L. Adhikari, Association of Antarctic polar stratospheric cloud formation on tropospheric cloud systems, *Geophys. Res. Lett.*, *35*, L13806, doi: 10.1029/2008GL034209, 2008.
- Waugh, D., Atmospheric dynamics: The age of stratospheric air, *Nature Geosci.*, *2*, 14-16, doi: 10.1038/nge0397, 2009.
- Waugh, D.W., and T.M. Hall, Age of stratospheric air: Theory, observations, and models, *Rev. Geophys.*, *40*, doi: 10.1029/2000RG000101, 2000.
- Waugh, D.W., and V. Eyring, Quantitative performance metrics for stratospheric-resolving chemistry-climate models, *Atmos. Chem. Phys.*, *8* (18), 5699-5713, doi: 10.5194/acp-8-5699-2008, 2008.
- Waugh, D.W., L. Oman, S.R. Kawa, R.S. Stolarski, S. Pawson, A.R. Douglass, P.A. Newman, and J.E. Nielsen, Impacts of climate change on stratospheric ozone recovery, *Geophys. Res. Lett.*, *36*, L03805, doi: 10.1029/2008GL036223, 2009.
- Weatherhead, E.C., G.C. Reinsel, G.C. Tiao, C.H. Jackman, L. Bishop, S.M.H. Frith, J. DeLuisi, T. Keller, S.J. Oltmans, E.L. Fleming, D.J. Wuebbles, J.B. Kerr, A.J. Miller, J. Herman, R. McPeters, R.M. Nagatani, and J.E. Frederick, Detecting the recovery of total column ozone, *J. Geophys. Res.*, *105* (D17), 22201-22210, 2000.
- Webb, A.R., B.G. Gardine, T.J. Martin, K. Leszczynsk, J. Metzendorf, and V.A. Mohnen, *Guidelines for Site Quality Control of UV Monitoring*, WMO/GAW

- No. 126, WMO TD 884, World Meteorological Organization, Geneva, 39 pp., 1998.
- Webb, A.R., J. Gröbner, and M. Blumthaler, *A Practical Guide to Operating Broadband Instruments Measuring Erythemally Weighted Irradiance*, publication of COST 726 and World Meteorological Organization, 21 pp., European Cooperation in Science and Technology (COST) Office, Luxembourg, available: <http://www.cost726.org/>, 2006.
- Weber, M., L.N. Lamsal, M. Coldewey-Egbers, K. Bramstedt, and J.P. Burrows, Pole-to-pole validation of GOME WFDOAS total ozone with ground-based data, *Atmos. Chem. Phys.*, 5 (5), 1341-1355, doi: 10.5194/acp-5-1341-2005, 2005.
- Weber, M., L.N. Lamsal, and J.P. Burrows, Improved SCIAMACHY WFDOAS total ozone retrieval: Steps towards homogenising long-term total ozone datasets from GOME, SCIAMACHY, and GOME2, in *Proceedings of the Envisat Symposium 2007*, Montreux, Switzerland, 23-27 April 2007, ESA SP-636, available: <http://envisat.esa.int/envisatsymposium/proceedings/posters/3P4/463281we.pdf>, 2007.
- Weih, P., M. Blumthaler, H.E. Rieder, A. Kreuter, S. Simic, W. Laube, A.W. Schmalwieser, J.E. Wagner, and A. Tanskanen, Measurements of UV irradiance within the area of one satellite pixel, *Atmos. Chem. Phys.*, 8 (18), 5615-5626, doi: 10.5194/acp-8-5615-2008, 2008.
- Weiss, A.K., J. Staehelin, C. Appenzeller, and N.R.P. Harris, Chemical and dynamical contributions to ozone profile trends of the Payerne (Switzerland) balloon soundings, *J. Geophys. Res.*, 106 (D19), 22685-22694, 2001.
- Wetzel, G., H. Oelhaf, O. Kirner, R. Ruhnke, F. Friedl-Vallon, A. Kleinert, G. Maucher, H. Fischer, M. Birk, G. Wagner, and A. Engel, First remote sensing measurements of ClOOCl along with ClO and ClONO₂ in activated and deactivated Arctic vortex conditions using new ClOOCl IR absorption cross sections, *Atmos. Chem. Phys.*, 10 (3), 931-945, doi: 10.5194/acp-10-931-2010, 2010.
- Wilmouth, D.M., R.M. Stimpfle, J.G. Anderson, J.W. Elkins, D.F. Hurst, R.J. Salawitch, and L.R. Lait, Evolution of inorganic chlorine partitioning in the Arctic polar vortex, *J. Geophys. Res.*, 111, D16308, doi: 10.1029/2005JD006951, 2006.
- Wilmouth, D.M., T.F. Hanisco, R.M. Stimpfle, and J.G. Anderson, Chlorine-catalyzed ozone destruction: Cl atom production from ClOOCl photolysis, *J. Phys. Chem. A*, 113, 14099-14108, doi: 10.1021/jp9053204, 2009.
- WMO (World Meteorological Organization), *Scientific Assessment of Ozone Depletion: 1994*, Global Ozone Research and Monitoring Project-Report No. 37, Geneva, Switzerland, 1995.
- WMO (World Meteorological Organization), *Scientific Assessment of Ozone Depletion: 1998*, Global Ozone Research and Monitoring Project-Report No. 44, Geneva, Switzerland, 1999.
- WMO (World Meteorological Organization), *Scientific Assessment of Ozone Depletion: 2002*, Global Ozone Research and Monitoring Project-Report No. 47, Geneva, Switzerland, 2003.
- WMO (World Meteorological Organization), *Scientific Assessment of Ozone Depletion: 2006*, Global Ozone Research and Monitoring Project-Report No. 50, 572 pp., Geneva, Switzerland, 2007.
- WMO (World Meteorological Organization), *Instruments to Measure Solar Ultraviolet Radiation – Part 2: Broadband Instruments Measuring Erythemally Weighted Solar Irradiance*, WMO TD No. 1289, G. Seckmeyer, A. Bais, G. Bernhard, M. Blumthaler, C.R. Booth, K. Lantz, and R.L. McKenzie, 55 pp., Geneva, Switzerland, available: <http://www.wmo.int/pages/prog/arep/gaw/gaw-reports.html>, 2008.
- Wohltmann, I., R. Lehmann, M. Rex, D. Brunner, and J. Mäder, A process-oriented regression model for column ozone, *J. Geophys. Res.*, 112, D12304, doi: 10.1029/2006JD007573, 2007.
- Wuttke, S., J. Verdebout, and G. Seckmeyer, An improved algorithm for satellite-derived UV radiation, *Photochem. Photobiol.*, 77 (1), 52-57, 2003.
- Wuttke, S., G. Seckmeyer, and G. König-Langlo, Measurements of spectral snow albedo at Neumayer, Antarctica, *Ann. Geophys.*, 24, 7-21, 2006a.
- Wuttke, S., G. Seckmeyer, G. Bernhard, J. Ehrhmanian, R. McKenzie, P. Johnston, and M. O'Neill, New spectroradiometers complying with the NDSC standards, *J. Atmos. Oceanic Tech.*, 23, 241-251, 2006b.
- Yang, E.-S., D.M. Cunnold, R.J. Salawitch, M.P. McCormick, J. Russell III, J.M. Zawodny, S. Oltmans, and M.J. Newchurch, Attribution of recovery in lower-stratospheric ozone, *J. Geophys. Res.*, 111, D17309, doi: 10.1029/2005JD006371, 2006.
- Yang, E.-S., D.M. Cunnold, M.J. Newchurch, R.J. Salawitch, M.P. McCormick, J.M. Russell III, J.M. Zawodny, and S.J. Oltmans, First stage of Antarctic ozone recovery, *J. Geophys. Res.*, 113, D20308, doi: 10.1029/2007JD009675, 2008.
- Yang, M., S.G. Howell, J. Zhuang, and B.J. Huebert, Attribution of aerosol light absorption to black carbon, brown carbon, and dust in China – interpretations of atmospheric measurements during EAST-AIRE, *Atmos. Chem. Phys.*, 9 (6), 2035-2050, doi: 10.5194/acp-9-2035-2009, 2009.
- Yang, S.-K., C.S. Long, A.J. Miller, X. He, Y. Yang,

- D.J. Wuebbles, and G. Tiao, Modulation of natural variability on a trend analysis of updated cohesive SBUV(2) total ozone, *Int. J. Remote Sens.*, *30*, 3975-3986, doi: 10.1080/01431160902821924, 2009.
- Zanis, P., E. Maillard, J. Staehelin, C. Zerefos, E. Kosmidis, K. Tourpali, and I. Wohltmann, On the turnaround of stratospheric ozone trends deduced from the reevaluated Umkehr record of Arosa, Switzerland, *J. Geophys. Res.*, *111*, D22307, doi: 10.1029/2005JD006886, 2006.
- Zhao, J., R.P. Turco, and O.B. Toon, A model simulation of Pinatubo volcanic aerosols in the stratosphere, *J. Geophys. Res.*, *100* (D4), 7315-7328, 1995.
- Ziemke, J.R., S. Chandra, and P.K. Bhartia, A 25-year data record of atmospheric ozone in the Pacific from Total Ozone Mapping Spectrometer (TOMS) cloud slicing: Implications for ozone trends in the stratosphere and troposphere, *J. Geophys. Res.*, *110*, D15105, doi: 10.1029/2004JD005687, 2005.

CHAPTER 3

Future Ozone and Its Impact on Surface UV

Coordinating Lead Authors:

S. Bekki
G.E. Bodeker

Lead Authors:

A.F. Bais
N. Butchart
V. Eyring
D.W. Fahey
D.E. Kinnison
U. Langematz
B. Mayer
R.W. Portmann
E. Rozanov

Coauthors:

P. Braesicke
A.J. Charlton-Perez
N.E. Chubarova
I. Cionni
S.B. Diaz
N.P. Gillett
M.A. Giorgetta
N. Komala
F. Lefèvre
C. McLandress
J. Perlwitz
T. Peter
K. Shibata

Contributors:

H. Akiyoshi
J. Austin
M.P. Chipperfield
M. Dameris
S. Dhomse
S.M. Frith
R.R. Garcia
H. Garny
A. Gettelman
S.C. Hardiman
P. Jöckel
A.I. Jonsson
A. Kazantzidis
A. Kubin
J.-F. Lamarque
E. Mancini
M. Marchand
M. Michou
O. Morgenstern
L.D. Oman
S. Pawson
G. Pitari
D. Plummer
J.A. Pyle
D. Saint-Martin
J.F. Scinocca
T.G. Shepherd
D. Smale
R.S. Stolarski
H. Teysse re
S. Tilmes

CHAPTER 3

FUTURE OZONE AND ITS IMPACT ON SURFACE UV

Contents

SCIENTIFIC SUMMARY	1
3.1 INTRODUCTION	5
Box 3-1. Measures of Atmospheric Halogens.....	5
Box 3-2. Ozone Return Dates and Full Ozone Recovery.....	7
3.2 FACTORS AFFECTING FUTURE OZONE AND SURFACE UV	7
3.2.1 Stratospheric Halogen Loading.....	8
3.2.2 Stratospheric Reactive Nitrogen and Hydrogen Levels	8
3.2.3 Stratospheric Temperatures.....	9
3.2.4 Transport and Dynamics	10
3.2.4.1 Brewer-Dobson Circulation.....	10
3.2.4.2 Vortex Integrity and Mixing.....	10
3.2.5 Background and Volcanic Stratospheric Aerosols.....	12
3.2.6 Geoengineering by Sulfate Aerosol Injection.....	13
3.2.7 Effects of Ozone on Future Surface UV	15
3.2.8 Factors Other Than Stratospheric Ozone Affecting Surface UV	16
3.2.8.1 Clouds	16
3.2.8.2 Aerosols	17
3.2.8.3 Surface Albedo and Sea Ice Cover	17
3.2.8.4 Tropospheric Gases.....	17
3.3 PROJECTIONS OF OZONE THROUGH THE 21 ST CENTURY	18
3.3.1 Model Descriptions and Scenarios.....	18
3.3.2 Model Evaluation and Multi-Model Mean Analysis.....	19
3.3.2.1 Model Evaluation.....	19
3.3.2.2 Analysis Method for Multi-Model Time Series.....	22
3.3.3 Tropical Ozone.....	22
3.3.3.1 Long-Term Projections of Tropical Ozone.....	22
3.3.3.2 Processes Determining Future Tropical Ozone	25
3.3.4 Midlatitude Ozone.....	28
3.3.4.1 Long-Term Projections of Midlatitude Ozone.....	28
3.3.4.2 Processes Determining Future Midlatitude Ozone	28
3.3.5 Polar Ozone.....	30
3.3.5.1 Long-Term Projections of Polar Ozone.....	30
3.3.5.2 Processes Determining Future Polar Ozone	34
3.3.6 Ozone Return Dates and Ozone Recovery.....	36
3.3.7 Uncertainties in Model Projections and Open Questions.....	41
3.3.7.1 Uncertainty in Future Emissions Scenarios	41
3.3.7.2 Future CCM Development.....	42
3.4 PROJECTIONS OF UV CHANGES RELATED TO OZONE CHANGES THROUGH THE 21 ST CENTURY	42
3.4.1 Midlatitude and Tropical UV	42
3.4.2 Polar UV.....	44
3.4.3 Link to UNEP Environmental Effects Panel Assessment.....	46

3.5 CONCLUSIONS	46
REFERENCES	49
APPENDIX 3A: CONSTRUCTING CORRELATIVE TIME SERIES PLOTS.....	59

SCIENTIFIC SUMMARY

Globally averaged total column ozone has declined over recent decades due to the release of ozone-depleting substances (ODSs) into the atmosphere. Now, as a result of the Montreal Protocol, ozone is expected to recover from the effects of ODSs as ODS abundances decline in the coming decades. However, a number of factors in addition to ODSs have led to and will continue to lead to changes in ozone. Discriminating between the causes of past and projected ozone changes is necessary, not only to identify the progress in ozone recovery from ODSs, but also to evaluate the effectiveness of climate and ozone protection policy options.

Factors Affecting Future Ozone and Surface Ultraviolet Radiation

- **At least for the next few decades, the decline of ODSs is expected to be the major factor affecting the anticipated increase in global total column ozone. However, several factors other than ODS will affect the future evolution of ozone in the stratosphere.** These include changes in (i) stratospheric circulation and temperature due to changes in long-lived greenhouse gas (GHG) abundances, (ii) stratospheric aerosol loading, and (iii) source gases of highly reactive stratospheric hydrogen and nitrogen compounds. Factors that amplify the effects of ODSs on ozone (e.g., stratospheric aerosols) will likely decline in importance as ODSs are gradually eliminated from the atmosphere.
- **Increases in GHG emissions can both positively and negatively affect ozone.** Carbon dioxide (CO₂)-induced stratospheric cooling elevates middle and upper stratospheric ozone and decreases the time taken for ozone to return to 1980 levels, while projected GHG-induced increases in tropical upwelling decrease ozone in the tropical lower stratosphere and increase ozone in the extratropics. Increases in nitrous oxide (N₂O) and methane (CH₄) concentrations also directly impact ozone chemistry but the effects are different in different regions.
- **The Brewer-Dobson circulation (BDC) is projected to strengthen over the 21st century and thereby affect ozone amounts.** Climate models consistently predict an acceleration of the BDC or, more specifically, of the upwelling mass flux in the tropical lower stratosphere of around 2% per decade as a consequence of GHG abundance increases. A stronger BDC would decrease the abundance of tropical lower stratospheric ozone, increase poleward transport of ozone, and could reduce the atmospheric lifetimes of long-lived ODSs and other trace gases. While simulations showing faster ascent in the tropical lower stratosphere to date are a robust feature of chemistry-climate models (CCMs), this has not been confirmed by observations and the responsible mechanisms remain unclear.
- **Substantial ozone losses could occur if stratospheric aerosol loading were to increase in the next few decades, while halogen levels are high.** Stratospheric aerosol increases may be caused by sulfur contained in volcanic plumes entering the stratosphere or from human activities. The latter might include attempts to geoengineer the climate system by enhancing the stratospheric aerosol layer. The ozone losses mostly result from enhanced heterogeneous chemistry on stratospheric aerosols. Enhanced aerosol heating within the stratosphere also leads to changes in temperature and circulation that affect ozone.
- **Surface ultraviolet (UV) levels will not be affected solely by ozone changes but also by the effects of climate change and by air quality change in the troposphere.** These tropospheric effects include changes in clouds, tropospheric aerosols, surface reflectivity, and tropospheric sulfur dioxide (SO₂) and nitrogen dioxide (NO₂). The uncertainties in projections of these factors are large. Projected increases in tropospheric ozone are more certain and may lead to reductions in surface erythemal (“sunburning”) irradiance of up to 10% by 2100. Changes in clouds may lead to decreases or increases in surface erythemal irradiance of up to 15% depending on latitude.

Expected Future Changes in Ozone

Full ozone recovery from the effects of ODSs and return of ozone to historical levels are not synonymous. In this chapter a key target date is chosen to be 1980, in part to retain the connection to previous Ozone Assessments. Noting, however, that decreases in ozone may have occurred in some regions of the atmosphere prior to 1980, 1960 return dates are also reported.

The projections reported on in this chapter are taken from a recent compilation of CCM simulations. The ozone projections, which also form the basis for the UV projections, are limited in their representativeness of possible futures since they mostly come from CCM simulations based on a single GHG emissions scenario (scenario A1B of *Emissions Scenarios. A Special Report of Working Group III of the Intergovernmental Panel on Climate Change*, Cambridge University Press, 2000) and a single ODS emissions scenario (adjusted A1 of the previous (2006) Ozone Assessment).

Throughout this century, the vertical, latitudinal, and seasonal structure of the ozone distribution will be different from what it was in 1980. For this reason, ozone changes in different regions of the atmosphere are considered separately.

- **The projections of changes in ozone and surface clear-sky UV are broadly consistent with those reported on in the 2006 Assessment.**
- **The capability of making projections and attribution of future ozone changes has been improved since the 2006 Assessment.** Use of CCM simulations from an increased number of models extending through the entire period of ozone depletion and recovery from ODSs (1960–2100) as well as sensitivity simulations have allowed more robust projections of long-term changes in the stratosphere and of the relative contributions of ODSs and GHGs to those changes.
- **Global annually averaged total column ozone is projected to return to 1980 levels before the middle of the century and earlier than when stratospheric halogen loading returns to 1980 levels.** CCM projections suggest that this early return is primarily a result of GHG-induced cooling of the upper stratosphere because the effects of circulation changes on tropical and extratropical ozone largely cancel. Global (90°S–90°N) annually averaged total column ozone will likely return to 1980 levels between 2025 and 2040, well before the return of stratospheric halogens to 1980 levels between 2045 and 2060.
- **Simulated changes in tropical total column ozone from 1960 to 2100 are generally small.** The evolution of tropical total column ozone in models depends on the balance between upper stratospheric increases and lower stratospheric decreases. The upper stratospheric increases result from declining ODSs and a slowing of ozone destruction resulting from GHG-induced cooling. Ozone decreases in the lower stratosphere mainly result from an increase in tropical upwelling. From 1960 until around 2000, a general decline is simulated, followed by a gradual increase to values typical of 1980 by midcentury. Thereafter, although total column ozone amounts decline slightly again toward the end of the century, by 2080 they are no longer expected to be affected by ODSs. Confidence in tropical ozone projections is compromised by the fact that simulated decreases in column ozone to date are not supported by observations, suggesting that significant uncertainties remain.
- **Midlatitude total column ozone is simulated to evolve differently in the two hemispheres.** Over northern midlatitudes, annually averaged total column ozone is projected to return to 1980 values between 2015 and 2030, while for southern midlatitudes the return to 1980 values is projected to occur between 2030 and 2040. The more rapid return to 1980 values in northern midlatitudes is linked to a more pronounced strengthening of the poleward transport of ozone due to the effects of increased GHG levels, and effects of Antarctic ozone depletion on southern midlatitudes. By 2100, midlatitude total column ozone is projected to be above 1980 values in both hemispheres.
- **October-mean Antarctic total column ozone is projected to return to 1980 levels after midcentury, later than in any other region, and yet earlier than when stratospheric halogen loading is projected to return to 1980 levels.** The slightly earlier return of ozone to 1980 levels (2045–2060) results primarily from upper stratospheric cooling and resultant increases in ozone. The return of polar halogen loading to 1980 levels (2050–2070)

in CCMs is earlier than in empirical models that exclude the effects of GHG-induced changes in circulation. Our confidence in the drivers of changes in Antarctic ozone is higher than for other regions because (i) ODSs exert a strong influence on Antarctic ozone, (ii) the effects of changes in GHG abundances are comparatively small, and (iii) projections of ODS emissions are more certain than those for GHGs. Small Antarctic ozone holes (areas of ozone <220 Dobson units, DU) could persist to the end of the 21st century.

- **March-mean Arctic total column ozone is projected to return to 1980 levels two to three decades before polar halogen loading returns to 1980 levels, and to exceed 1980 levels thereafter.** While CCM simulations project a return to 1980 levels between 2020 and 2035, most models tend not to capture observed low temperatures and thus underestimate present-day Arctic ozone loss such that it is possible that this return date is biased early. Since the strengthening of the Brewer-Dobson circulation through the 21st century leads to increases in springtime Arctic column ozone, by 2100 Arctic ozone is projected to lie well above 1960 levels.

Uncertainties in Projections

- **Conclusions dependent on future GHG levels are less certain than those dependent on future ODS levels since ODS emissions are controlled by the Montreal Protocol.** For the six GHG scenarios considered by a few CCMs, the simulated differences in stratospheric column ozone over the second half of the 21st century are largest in the northern midlatitudes and the Arctic, with maximum differences of 20–40 DU between the six scenarios in 2100.
- **There remain sources of uncertainty in the CCM simulations.** These include the use of prescribed ODS mixing ratios instead of emission fluxes as lower boundary conditions, the range of sea surface temperatures and sea ice concentrations, missing tropospheric chemistry, model parameterizations, and model climate sensitivity.
- **Geoengineering schemes for mitigating climate change by continuous injections of sulfur-containing compounds into the stratosphere, if implemented, would substantially affect stratospheric ozone, particularly in polar regions.** Ozone losses observed following large volcanic eruptions support this prediction. However, sporadic volcanic eruptions provide limited analogs to the effects of continuous sulfur emissions. Preliminary model simulations reveal large uncertainties in assessing the effects of continuous sulfur injections.

Expected Future Changes in Surface UV

While a number of factors, in addition to ozone, affect surface UV irradiance, the focus in this chapter is on the effects of changes in stratospheric ozone on surface UV. For this reason, clear-sky surface UV irradiance is calculated from ozone projections from CCMs.

- **Projected increases in midlatitude ozone abundances during the 21st century, in the absence of changes in other factors, in particular clouds, tropospheric aerosols, and air pollutants, will result in decreases in surface UV irradiance.** Clear-sky erythemal irradiance is projected to return to 1980 levels on average in 2025 for the northern midlatitudes, and in 2035 for the southern midlatitudes, and to fall well below 1980 values by the second half of the century. However, actual changes in surface UV will be affected by a number of factors other than ozone.
- **In the absence of changes in other factors, changes in tropical surface UV will be small because changes in tropical total column ozone are projected to be small.** By the middle of the 21st century, the model projections suggest surface UV to be slightly higher than in the 1960s, very close to values in 1980, and slightly lower than in 2000. The projected decrease in tropical total column ozone through the latter half of the century will likely result in clear-sky surface UV remaining above 1960 levels. Average UV irradiance is already high in the tropics due to naturally occurring low total ozone columns and high solar elevations.

- **The magnitude of UV changes in the polar regions is larger than elsewhere because ozone changes in polar regions are larger.** For the next decades, surface clear-sky UV irradiance, particularly in the Antarctic, will continue to be higher than in 1980. Future increases in ozone and decreases in clear-sky UV will occur at slower rates than those associated with the ozone decreases and UV increases that occurred before 2000. In Antarctica, surface clear-sky UV is projected to return to 1980 levels between 2040 and 2060, while in the Arctic this is projected to occur between 2020 and 2030. By 2100, October surface clear-sky erythemal irradiance in Antarctica is likely to be between 5% below to 25% above 1960 levels, with considerable uncertainty. This is consistent with multi-model-mean October Antarctic total column ozone not returning to 1960 levels by 2100. In contrast, by 2100, surface clear-sky UV in the Arctic is projected to be 0–10% below 1960 levels.

3.1 INTRODUCTION

The primary goal of the Montreal Protocol and its Amendments and Adjustments is to avoid depletion of the ozone layer. Ozone depletion elevates surface ultraviolet (UV) radiation, thereby posing a threat to Earth's biosphere. The mechanism used to achieve this goal is the control of the production and consumption of anthropogenic ozone-depleting substances (ODSs; see Box 3-1). Chapter 5 in this Assessment describes the Montreal Protocol mechanism in more detail while Chapters 1, 2 and 5 summarize the success of the Montreal Protocol to date. At present, throughout most of the stratosphere, equivalent stratospheric chlorine (ESC; see Box 3-1) is significantly elevated above natural levels due to the cumulative effect

of historical emissions of ODSs. Elevated ESC remains the most important anthropogenic perturbation to stratospheric ozone. However, as halogen loading declines in the future, other factors are expected to displace ODSs as the dominant influence on ozone. Perhaps the most important of these are continued and increasing emissions of long-lived greenhouse gases (GHGs). For example, GHGs affect ozone directly because they act as stratospheric source gases for ozone-destroying radicals (e.g., methane (CH₄) and nitrous oxide (N₂O)) and indirectly because they change temperatures (predominantly carbon dioxide (CO₂)).

This chapter builds on and extends Chapter 5 of the 2006 Ozone Assessment ("Climate-Ozone Connections," Baldwin and Dameris et al., 2007) by assessing the most

Box 3-1. Measures of Atmospheric Halogens

In this chapter, as in the 2006 Ozone Assessment (hereafter also cited as WMO (2007)), ozone-depleting substances (ODSs) are defined as those gases of anthropogenic origin controlled under the Montreal Protocol. Principal ODSs are chlorofluorocarbons (CFCs), hydrochlorofluorocarbons (HCFCs), halons, carbon tetrachloride, 1,1,1-trichloroethane (methyl chloroform), and methyl bromide. These gases are useful in meeting global application demands, for example, in refrigeration, air conditioning, insulating foams, and fumigation, but contain the halogens (chlorine and/or bromine atoms) which, when released, react to destroy stratospheric ozone. Other gases emitted in human activities (e.g., methane (CH₄) and nitrous oxide (N₂O)) also influence ozone (Section 3.2.2), but have not been considered ODSs under the Montreal Protocol.

When chlorine and bromine atoms are released from the degradation of ODSs in the stratosphere, they combine to form the inorganic chlorine- and bromine-containing compounds that belong to the chemical groups called total inorganic chlorine (Cl_y) and inorganic bromine (Br_y). The combination of Cl_y and Br_y amounts represents the potential for halogens to destroy ozone in a stratospheric air mass. A measure of this potential is defined as equivalent stratospheric chlorine (ESC; Eyring et al., 2007), "equivalent" since it weights Br_y with respect to Cl_y, according to

$$\text{ESC} = \text{Cl}_y + \alpha \times \text{Br}_y \quad (1)$$

where the units are stratospheric mixing ratio and α is the weighting factor that accounts for the greater effectiveness of bromine in ozone destruction compared to the effectiveness of chlorine on a per-atom basis. In general, α varies with altitude, latitude, and time, following changes in Cl_y and Br_y which in turn follow total emissions of organic halogen gases at Earth's surface. In 2010, α is estimated to be ~60 in the lower stratosphere and ~5 in the upper stratosphere (Sinnhuber et al., 2009). ESC can be calculated as a function of latitude, longitude, altitude, and time from distributions of Cl_y and Br_y simulated with a chemistry-climate model (CCM). Some ODSs, such as methyl chloride and methyl bromide, and a number of other halogen-containing gases, have natural sources. These natural emissions are responsible for the low background level of ESC.

Deriving ESC directly from observations is hindered by the lack of direct measurements of Cl_y and Br_y. As an alternative, the spatial and temporal distributions of Cl_y and Br_y can be approximated from time series measurements of ODS surface concentrations combined with estimated rates at which individual gases release their halogens into the stratosphere (so-called fractional release rates) and estimates of the age of air parcels (i.e., the time elapsed since air parcels entered the stratosphere at the tropical tropopause; see Box 8-1 of WMO (2007)). Using these estimates in equation (1) yields equivalent effective stratospheric chlorine (EESC; see Section 1.4.4 of Chapter 1), which has been widely used before the availability of ESC from CCM outputs. ESC and EESC are similar in that they both represent aggregate quantities that quantify the combined potential of Cl_y and Br_y in a particular air mass to destroy ozone. They differ in the way in which the Cl_y and Br_y inputs are obtained. For CCMs, ESC is calculated directly from the simulated fields of chlorine- and bromine-containing species. In contrast, EESC is estimated from measured source gas surface concentrations and assumptions about their transport and conversion to Cl_y and Br_y in the stratosphere.

recent literature on the likely effects of increasing GHG emissions on future ozone amounts and resultant changes in climate parameters. This chapter also builds on and extends Chapter 6 of the 2006 Ozone Assessment (“The Ozone Layer in the 21st Century,” Bodeker and Waugh et al., 2007) by assessing chemistry-climate model (CCM) projections of the evolution of ozone through the 21st century. The number of available CCMs and CCM sensitivity simulations has significantly increased since the previous Assessment. In contrast to WMO (2007), which assessed two- and three-dimensional model simulations of future ozone, this chapter assesses ozone projections from the current generation of three-dimensional CCMs. The simulations used in this chapter are based on those from 17 CCMs that participated in the second round of a coordinated model intercomparison organized by the Chemistry-Climate Model Validation (CCMVal) Activity (Eyring et al., 2005) of WCRP’s (World Climate Research Programme) SPARC (Stratospheric Processes And their Role in Climate) project (hereafter referred to as CCMVal-2). The participating CCMs are listed in Table 3-1 (see Section 3.3.1) and described in detail in the cited literature, in Chapter 2 of SPARC CCMVal (2010), and in Morgenstern et al. (2010). An extensive assessment of these CCMs was made in the SPARC CCMVal Report (2010), which provides a strong foundation for this chapter. Results presented in that report are augmented here by including additional reference model simulations, as well as sensitivity simulations in which either greenhouse gas (GHG) or ODS levels are kept fixed at 1960 values or in which alternative GHG scenarios are used. The reference simulations include the most important forcings of the long-term evolution of ozone and provide the primary data set of ozone projections used here. The sensitivity simulations, by fixing a single forcing at a constant baseline level, permit a quantitative separation of the effects of different factors on future ozone. Thus details of the full recovery of ozone from the effects of ODSs (see Box 3-2) were determined by quantifying the contribution of ESC to future ozone changes and contrasting it with that from climate change.

Although interest in the factors affecting surface UV has focused primarily on ozone to date, other factors, some related to changes in climate, will play an increasingly important role in modulating future surface UV levels as the ozone layer recovers. This chapter builds on and extends the prognostic aspects of Chapter 7 of the 2006 Ozone Assessment (“Surface Ultraviolet Radiation: Past, Present, and Future,” Bais and Lubin et al., 2007), with a primary focus on the role of ozone in affecting the future evolution of UV. While a brief discussion of the non-ozone factors affecting surface UV is included in this chapter, it primarily serves as a link to the UNEP (United

Nations Environment Programme) Environmental Effects Assessment Panel report (UNEP, 2010).

While ESC is projected to return close to historical levels during the 21st century, global ozone amounts are not necessarily expected to return close to their respective historical levels over the same period because factors other than ESC will increasingly affect future ozone amounts. Therefore, this chapter reports both the dates when ESC, ozone, and UV return to some respective historical values, and the dates when ozone is no longer expected to be influenced by ODSs (Box 3-2). Annual mean total column ozone and surface UV may not necessarily return to historical levels at the same time. Summertime ozone exerts a greater influence on annual mean surface UV than ozone in other seasons, and so it is the return of summertime ozone to historical levels that is more relevant for surface UV.

The scope of this chapter includes providing a discussion framework that accommodates a wide variety of factors beyond ODSs that affect ozone. In some regions of the atmosphere, for example in the Antarctic lower stratosphere, the steep decline in springtime ozone until ~2000 is projected to be followed by a slow increase back to 1980 levels during the latter half of the 21st century, mirroring what is expected from changes in ESC over that period. In the tropical upper stratosphere, where the effects of GHG-induced cooling are significant, ozone concentrations could significantly exceed 1960 or 1980 values by the end of the 21st century. These changes are necessarily larger than what would be expected from ESC declines alone. In contrast, in the tropical lower stratosphere, ozone shows little sensitivity to stratospheric halogen loading and is more strongly influenced by long-term changes in atmospheric circulation. This chapter, in addition to addressing the full recovery of ozone from ODSs, explores a suite of scenarios for future ozone in different regions of the atmosphere, and the impact of projected ozone changes on surface UV.

Section 3.2 details how future changes in stratospheric halogen loading will affect the future evolution of ozone (the primary focus in this chapter), describes other factors that will affect future ozone, and discusses how ozone and other factors will affect future surface UV. Section 3.3 begins by noting the recent improvements in ozone projections compared to those presented in WMO (2007) and by describing the CCMs, the emissions scenarios to which they were applied, and their evaluation. Section 3.3 focuses mainly on long-term CCM projections of stratospheric ozone based primarily on a common reference scenario. In addition to this reference scenario, a number of sensitivity simulations allow the two most important factors affecting future ozone (i.e., ODSs and GHGs) to be quantitatively disentangled. These results form the basis for statements regarding the milestones of

Box 3-2. Ozone Return Dates and Full Ozone Recovery

The context for the discussion of future ozone in this chapter is provided by defining two distinct milestones in the future evolution of ozone. These quantitative milestones are motivated by the need to answer questions often put forth by policymakers and the public, viz.:

1. When do we expect ozone to return to levels typical of some earlier time?
2. When do we expect ozone to no longer be significantly affected by ozone-depleting substances (ODSs)?

Identifying the first milestone requires *no attribution* to the separate factors affecting ozone and, hence, can be evaluated directly from time series of observed or simulated ozone. If ozone has already returned to levels typical of some target year, measurements alone can be used to address this milestone and answer the related question. Since this is not the case for the target years considered here (i.e., 1960 and 1980), the expected return of ozone to these historical levels is evaluated here instead from multi-model mean chemistry-climate model (CCM) projections. The selection of a target year, and its associated ozone level, should not be interpreted as selecting past states defined by the absence of significant ozone depletion from ODSs.

In this chapter a key target date is chosen to be 1980 in order to retain a connection to previous Ozone Assessments. Noting, however, that decreases in ozone may have occurred in some regions of the atmosphere prior to 1980, 1960 return dates are also presented and discussed. Evaluating return dates is relevant for gauging when the adverse impacts of enhanced surface ultraviolet radiation on human health and ecosystems caused by ozone depletion are likely to become negligible. In addition, the return dates of ozone to historical levels in some regions are also valuable in demonstrating the effectiveness of policies that have abated anthropogenic ODS emissions if ODSs have been the dominant driver of ozone changes in those regions.

Identifying the second milestone is equivalent to assessing when the third stage of ozone recovery, so-called “full ozone recovery from ODSs” as defined in WMO (2007), has or is expected to occur. This, by definition, requires an *attribution* of projected changes in ozone to different factors, since ozone is not affected by ODSs alone. The required attribution can be obtained using idealized CCM simulations that hold certain model forcings fixed in conjunction with reference simulations that include the most important forcings for the long-term evolution of ozone. The reference and idealized simulations also provide a method, based on a subjective statistical test, for quantifying what is meant by “no longer significantly affected by ODSs” (Section 3.3.6). When analyzing CCM simulations for full ozone recovery from ODSs as defined here, the choice of 1960 as the start date implicitly assumes that the contribution of anthropogenic emissions of ODSs to equivalent stratospheric chlorine (ESC) prior to 1960 was negligible. However, ESC in 1960 was not zero because of the contribution of natural sources of halogens (see Box 3-1). If the sensitivity of ozone destruction to stratospheric halogen loading does not change with time, this milestone is equivalent to a return of ESC to 1960 levels. This definition has the advantage that it directly assesses the effectiveness of the Montreal Protocol in model projections of ozone but requires the additional step of attributing observed or modeled changes in ozone to ODS and other factors.

Both milestones defined above can be evaluated for total column ozone or vertically resolved ozone, averaged globally or averaged over some region of the atmosphere.

full ozone recovery from the effects of ODSs. Section 3.4 builds on the ozone projections in Section 3.3 to detail how future surface UV radiation will be affected by changes in ozone and provides a point of connection between this Ozone Assessment and the UNEP Environmental Effects Assessment Panel report (UNEP, 2010).

3.2 FACTORS AFFECTING FUTURE OZONE AND SURFACE UV

This section discusses the factors that will affect the future evolution of stratospheric ozone and consequently UV reaching the surface. While the primary focus remains on ODS emissions and the associated increase in stratospheric halogen loading (Section 3.2.1), developments

since WMO (2007) have highlighted the potentially important roles of nitrous oxide (N₂O) emissions (Section 3.2.2) and anthropogenic enhancements of the stratospheric sulfate aerosol layer, from both increased surface sulfur emissions (Section 3.2.5) and possible geoengineering actions (Section 3.2.6). New research has also advanced our understanding of how the Brewer-Dobson circulation (BDC) is likely to change (Section 4.2.2 of Chapter 4 of this Assessment) and affect future ozone (Section 3.2.4.1). The increase in GHG emissions and subsequent changes in climate, including cooling of the stratosphere (Section 3.2.3), is an overarching theme linking many of the factors likely to affect ozone in the future. Evaluating the recovery of ozone from ODSs involves all of these factors, in addition to ODSs. As ESC levels decline in the future, the factors that act to amplify the effects of ESC on ozone

(e.g., stratospheric aerosols) will decline in importance, while other factors, especially those related to GHGs and climate change, will emerge to dominate the long-term evolution of ozone. Attributing past and future changes in ozone to these different factors is essential to identify the stages of ozone recovery. Furthermore, because ozone protection policy governs only ESC (by limiting emissions of ODSs), evaluating the effectiveness of such policy requires attributing observed and projected ozone changes to ESC and other factors. While the discussion of UV in this section is primarily focused on the effects of future changes in stratospheric ozone on surface UV (Section 3.2.7), research since WMO (2007) has mostly dealt with other factors affecting surface UV, which are summarized briefly in Section 3.2.8.

3.2.1 Stratospheric Halogen Loading

At present, and for much of the 21st century, elevated stratospheric halogen loading is expected to remain the most important factor affecting stratospheric ozone. In the model simulations of 21st century ozone made in support of WMO (2007), ODSs were prescribed at the surface according to the Ab “best guess” scenario of WMO (2003) (Eyring et al., 2007). This scenario was superseded by the “baseline” halogen scenario A1 defined in WMO (2007), which prescribes halogen loadings higher than in Ab. There are notable differences between the two scenarios. The A1 scenario includes larger emissions of chlorofluorocarbon-11 (CFC-11) and CFC-12 after 2010 due to their larger estimated banks. Increases in projected hydrochlorofluorocarbon-22 (HCFC-22) emissions, due to expectations of greater future use in A1 than in the Ab scenario, are also important. However, at the 2007 Meeting of the Parties to the Montreal Protocol, the Parties agreed to an earlier phase-out of HCFCs, with nearly a full phase-out in developing countries (Article 5) by 2030. Scenario A1 does not include this phase-out. Hence, a new scenario has been developed that includes this phase-out. This adjusted A1 scenario has been used in the model simulations performed in support of the present Assessment. In this new scenario, only HCFCs have been adjusted, while emissions of CFCs, halons, and other non-HCFC species remain identical to the original A1 scenario.

Due to the uncertainty in their future trends, brominated very short-lived substances (VSLS, atmospheric lifetime <0.5 year) are not considered in the standard scenarios. As a result, the bromine loading in most CCMs used in support of the previous and current Assessments is only determined by the projected evolution of long-lived organic source gases methyl bromide (CH₃Br) and halons (halon-1211, halon-1202, halon-1301, and halon-2402). However, observations suggest that the stratospheric bromine loading is 5⁺³ parts per trillion (ppt) higher than can

be explained by tropospheric levels of CH₃Br and the halons. This additional bromine (~5 ppt out of the current total of ~20 ppt) may likely come from short-lived bromine-containing compounds (see Chapter 1; WMO, 2007). The degradation of those species could release a substantial amount of bromine into the tropical tropopause layer (TTL) and lowermost stratosphere. The average photochemical lifetime of VSLS is comparable with, or shorter than, the average transport timescales in the TTL, which vary from rapid in deep convection to slow outside of regions of deep convection. This may lead to a highly variable distribution of bromine injections in the form of VSLS into the tropical lower stratosphere, as some surface and balloon observations suggest (see Section 1.3.1 and references therein). There is also uncertainty in how dehydration and wet removal of degradation products of VSLS occur (Sinnhuber and Folkins, 2006). Current and future trends in brominated VSLS are difficult to determine. VSLS, and their rapid vertical transport through the troposphere, are also very difficult to describe in global models and are not explicitly treated in the CCMs used here. Together, these gaps in our understanding of the stratospheric bromine budget are a source of uncertainty in long-term projections of stratospheric halogen loading and hence ozone.

3.2.2 Stratospheric Reactive Nitrogen and Hydrogen Levels

Natural ozone loss in the absence of chlorine is primarily due to the chemical effects of nitrogen (NO_x) and hydrogen (HO_x) radicals. NO_x and HO_x levels are controlled by the amount of the long-lived source gases N₂O, H₂O, and CH₄, which are also GHGs. Since the levels of these source gases are affected by anthropogenic emissions and/or climate change, their future evolution will influence ozone through changes in NO_x and HO_x.

The amount of NO_x in the stratosphere is largely controlled by the amount of N₂O entering at the tropical tropopause (of which approximately 10% is converted to NO_x). The preindustrial level of N₂O was ~270 parts per billion (ppb) and the present level is ~320 ppb. Future changes in ozone due to NO_x increases have been evaluated using model simulations based on scenarios for the 21st century that include projected N₂O emissions (Randeniya et al., 2002; Chipperfield and Feng, 2003; Portmann and Solomon, 2007). It was shown that several percent of global total ozone loss is possible by 2100 due to increases in anthropogenic N₂O. The effects of increasing N₂O levels on ozone depend on altitude. The resulting NO_x increase causes ozone losses in the middle stratosphere, centered just above the ozone concentration maximum, while chlorine and hydrogen radicals destroy ozone predominately

in both the lower and upper stratosphere (see Figure 3-1). Interactions between halogen and nitrogen species cause nitrogen species to be less effective at destroying ozone in the lower stratosphere while halogen levels remain elevated. In contrast, temperature decreases cause a faster chemical loss of total reactive nitrogen (NO_y) and hence NO_x (nitrogen oxides, $\text{NO} + \text{NO}_2$) in the upper stratosphere (Rosenfield and Douglass, 1998). Because of these effects, the changes in active nitrogen species levels and in the amount of ozone destroyed by those species are not expected to follow the change in N_2O levels.

The efficiency of N_2O emissions in destroying stratospheric ozone can also be compared to that of ODSs. Ravishankara et al. (2009) computed the Ozone Depletion Potential (ODP, see Chapter 5) of N_2O in the same way that it is computed for halogen source gases. Surprisingly, they found that the ODP-weighted anthropogenic emissions of N_2O were larger than those of any chlorine-containing source gas emitted in 2008. Moreover, they also found that the ODP-weighted anthropogenic emissions of N_2O were already significant in 1987 when CFC emissions were peaking. This result is partly due to the long lifetime of N_2O (approximately 125 years) since the ODP is weighted by the ozone depletion over the lifetime of the gas. Further study is needed to characterize the

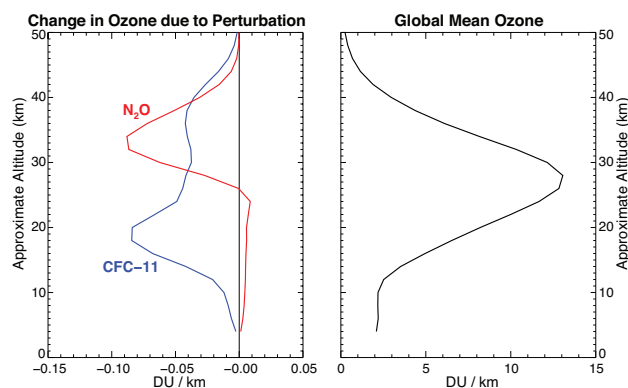


Figure 3-1. The change in global average ozone concentrations (Dobson units per kilometer) due to a 100 ppt increase in CFC-11 and a 20 ppb increase in N_2O for year 2000 levels of source gases and background aerosol conditions computed with the NOCAR 2-D model (Portmann et al., 1999). The global average ozone profile for the same conditions is also shown. Note that in order to illustrate differences in the ozone loss profiles, the relative sizes of the CFC-11 and N_2O perturbations were chosen to achieve ozone loss peaks of the same magnitude. Adapted from Figure S1 of the supplementary material from Ravishankara et al. (2009).

effects of N_2O emissions and carefully examine the tradeoffs with ODSs (see also Section 5.4.2.2).

Future levels of HO_x will be mostly determined by changes in CH_4 emissions and by the amount of H_2O entering the tropical stratosphere. In terms of ozone depletion, these two sources of HO_x have differing effects on ozone. Increasing H_2O tends to enhance the chemical ozone loss in the upper stratosphere where H_2O is converted to HO_x (HO_x is the dominant ozone loss cycle in the upper stratosphere and mesosphere), whereas increasing H_2O leads to a reduction in ozone loss in the middle stratosphere because H_2O enhances conversion of nitrogen dioxide (NO_2), the ozone-destroying nitrogen radical, into HNO_3 . However, when all the radiative and dynamical feedbacks associated with the H_2O increase are accounted for in a CCM, the effects on column ozone exhibit a strong hemispheric asymmetry, especially at high latitudes (Tian et al., 2009). Changes in the abundance of H_2O also have the potential to affect the sulfuric acid aerosol size distribution. However, these H_2O -driven aerosol changes have been estimated to be negligible (SPARC, 2006). Polar stratospheric cloud (PSC) formation and the heterogeneous reaction rates on liquid ternary aerosol are more sensitive to H_2O changes. H_2O increases may be expected to enhance PSC formation and hence accelerate chemical polar ozone destruction as long as chlorine levels are high enough. CH_4 increases also enhance H_2O in the stratosphere but additionally cause ozone increases in the troposphere and lowermost stratosphere due to direct ozone production from methane oxidation. The net effect of increases in CH_4 levels on global ozone is expected to be ozone production (Randeniya et al., 2002). Thus it is important to assess the sources of H_2O changes in the stratosphere to predict the net effect on ozone.

H_2O increased in the stratosphere in the latter part of the 20th century but showed a sustained decrease after 2000 (Randel et al., 2006). Increases in CH_4 levels have caused part of this H_2O increase in the middle and upper stratosphere but not in the lower stratosphere (Rohs et al., 2006). In addition, the separation of the climate change signal from natural variability has proved difficult (Garcia et al., 2007; Austin et al., 2007; Oman et al., 2008).

3.2.3 Stratospheric Temperatures

Because of the temperature dependence of gas-phase chemical reaction rates and the formation of PSCs, stratospheric temperatures have a large impact on ozone abundances. A cooling of the middle and upper stratosphere increases ozone by slowing gas-phase destruction rates. In contrast, a cooling of the polar lower stratosphere is expected to enhance PSC formation which, when halogen levels are elevated, favors ozone destruction. In the Antarctic, where temperatures are already well below the

thresholds of PSC formation, additional cooling is likely to have less of an effect than in the Arctic, where stratospheric temperatures are closer to the thresholds of PSC formation. Predictions of future changes in ozone must therefore account for future changes in temperature.

Stratospheric temperatures are controlled by a combination of radiative and dynamical processes (see also Section 4.3.1). Since regional heating and cooling by dynamical processes tend to cancel out in the global mean, the global mean temperature is in radiative equilibrium to a good approximation (e.g., Fomichev et al., 2002). Dynamical processes, on the other hand, lead to latitudinal variations in heating and cooling. For example, the projected strengthening of the BDC in response to increasing GHG levels (Section 4.3.2) causes adiabatic cooling of the tropical lower and middle stratosphere, and adiabatic warming at high latitudes (Section 3.2.4).

Current CCMs are reasonably good at reproducing the Stratospheric Sounding Unit/Mesosospheric Sounding Unit (SSU/MSU) record of observed changes in stratospheric temperature since 1979 (Figure 4-10, and Section 4.3; Gillett et al., 2010). The multi-model ensemble approximately captures the magnitude of observed global mean cooling in the upper and lower stratosphere, as well as the volcanic warming and the recent leveling off of lower stratospheric temperatures (Section 4.3.1). Nonetheless, discrepancies between individual models and the observations may still be significant, and there are some clear areas of disagreement between the models and observations, such as in SSU channel 26 after 1995. However, the uncertainties in the observations remain poorly quantified (Randel et al., 2009). Thus it is possible that this discrepancy results from observational errors rather than from a common bias in the CCMVal models. Over the 21st century CCMVal-2 models simulate a continued strong cooling of the middle to upper stratosphere of 4–10 K in the tropics, due to increasing GHG concentrations (Figure 3-2(e)). Weaker cooling is simulated lower down in the stratosphere, and little change in temperature is simulated in the lowermost stratosphere due to the competing effects of ozone recovery and continued GHG increases.

3.2.4 Transport and Dynamics

3.2.4.1 BREWER-DOBSON CIRCULATION

As described in Section 4.2.2, the BDC is the stratospheric overturning circulation that transports air upward in the tropics, poleward at midlatitudes, and downward at middle and high latitudes, and so plays a crucial role in determining the meridional distribution of ozone and long-lived trace gases. Climate models and CCMs consistently predict an acceleration of the BDC in response

to climate change, producing a trend of ~2% per decade in net upward mass flux in the tropical lower stratosphere in the multi-model mean (Section 4.3.2). An acceleration of the BDC would increase the rate at which ODSs are removed from the stratosphere (Butchart and Scaife, 2001), thus advancing ozone recovery. However, this removal mechanism is not represented in current CCMs as a consequence of the lower boundary condition for ODSs where mixing ratios, not fluxes, are specified (Section 3.3.7). An accelerated BDC would also increase the rate at which other gases such as N₂O and CH₄ get into the stratosphere, which would in turn affect the lifetimes of these gases and the evolution of ozone. In addition, the projected increase in the strength of the BDC would decrease ozone in the tropical lower stratosphere where ozone-poor air of tropospheric origin enters and rises slowly in relative isolation within this region. During the transit through the tropical lower stratosphere, ozone is continuously produced by molecular oxygen (O₂) photolysis within the rising air. As a result, tropical lower stratospheric ozone content is mostly determined by a balance between the rate of ozone production (i.e., from photolysis of O₂) and the rate at which the air is transported through and out of the tropical lower stratosphere (essentially the rate of ascent and, to a lesser extent, mixing with the subtropics) (Avallone and Prather, 1996). A faster transit of air through the tropical lower stratosphere from an enhanced BDC would ultimately lead to less time for production of ozone and hence lower ozone levels in this region. In contrast, ozone levels would increase in the extratropical lower stratosphere due to increased downward transport of ozone-rich air from above. This latitudinal dependence is illustrated in Figure 3-3, which shows 1970 to 2090 changes in the residual vertical velocity \bar{w}^* at 70 hPa and the corresponding changes in total column ozone from an ensemble of simulations using one CCM, the Canadian Middle Atmosphere Model (CMAM) (McLandress and Shepherd, 2009a). The close correspondence between changes in \bar{w}^* and ozone (a negative correlation) highlights the potential importance of future changes in the strength of the BDC on ozone. However, the fact that the modest modeled increases in the strength of the BDC to date are difficult to detect in the currently available measurements (Section 4.2.2) suggests that some caution should be exercised when diagnosing projected future changes in ozone in the light of expected changes in the BDC.

3.2.4.2 VORTEX INTEGRITY AND MIXING

Future changes in the shape and strength of the polar vortex and in the frequency and strength of sudden stratospheric warmings (SSWs) will likely alter meridional transport which will in turn affect polar ozone. Charlton-Perez et al. (2008) diagnose a significant increase in major SSW

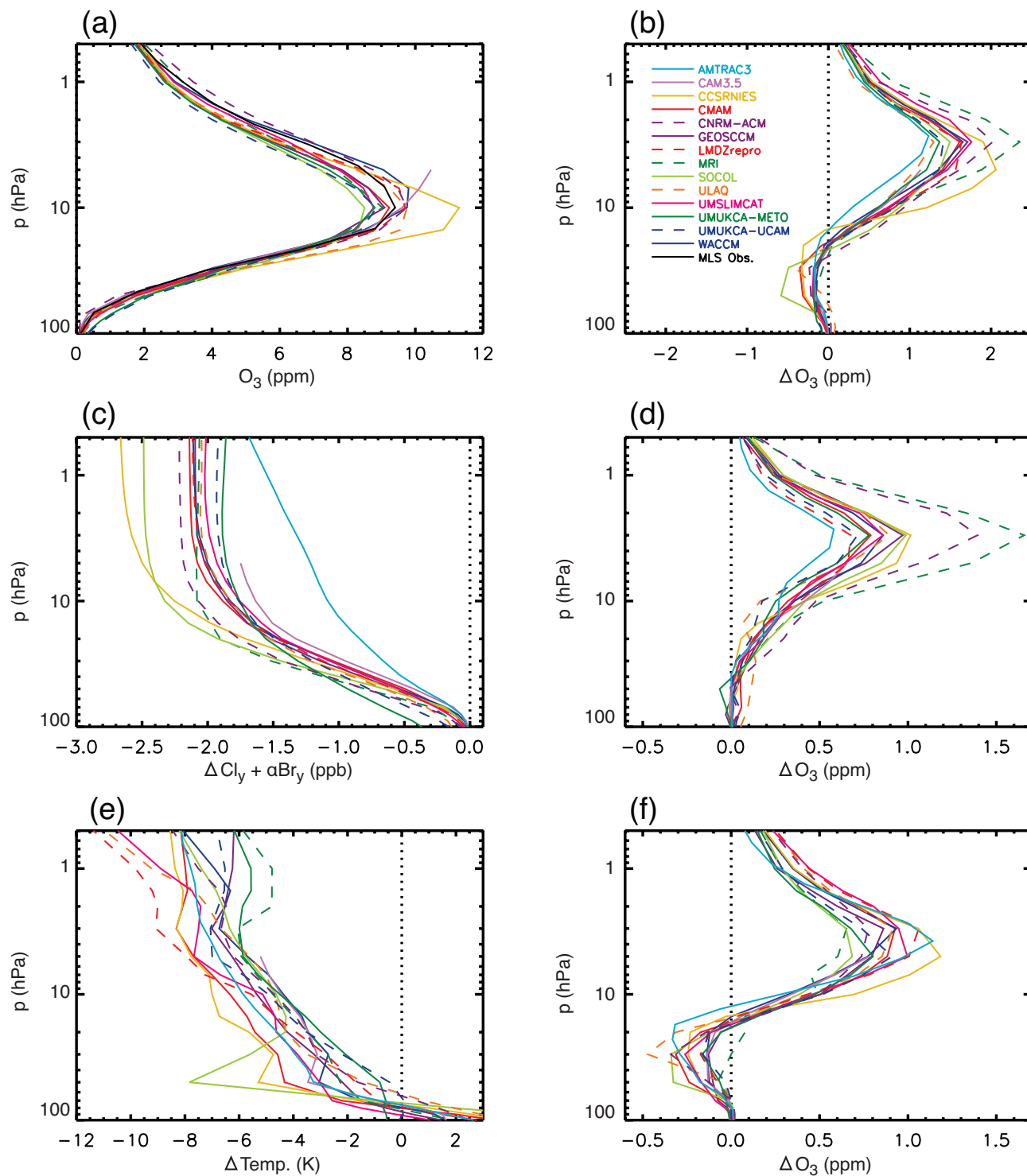
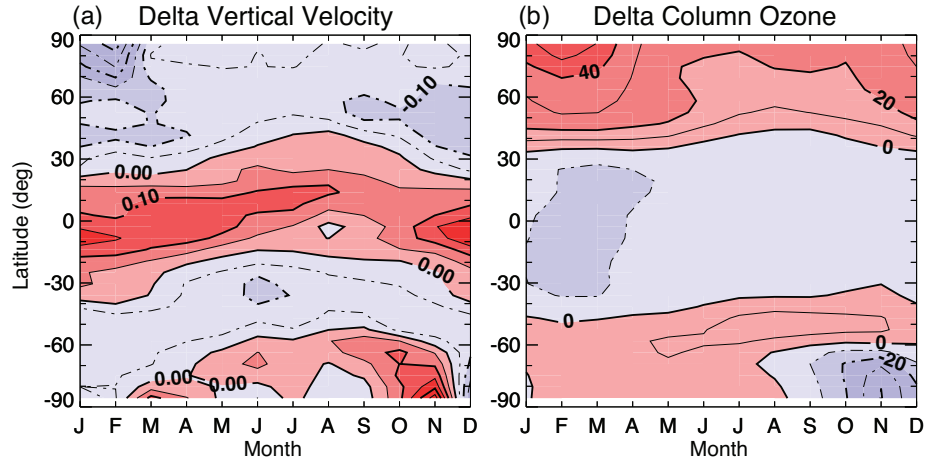


Figure 3-2. Vertical profile results of the Multiple Linear Regression (MLR) analysis for the CCMVal-2 models (described in Table 3-1) in the latitude band 10°S–10°N. (a) Ozone in the year 2000 (parts per million) versus pressure (hectoPascals), (b) Ozone change from 2000 to 2100, (c) ESC change (parts per billion) from 2000 to 2100, (d) ESC-congruent ozone change. (e) temperature change and (f) temperature-congruent ozone change. From Chapter 9 of SPARC CCMVal (2010), their Figure 9.5.

Figure 3-3. Difference between future and past (a) residual vertical velocity at 70 hPa and (b) total column ozone (deviation about global mean). Contour intervals are 0.05 mm/s and 10 DU. Future and past time periods are computed using 20-year means centered about 2090 and 1970, respectively. From McLandress and Shepherd (2009a), adapted from panels (b) and (f) of their Figure 6.



frequency of 1 event per decade between 1960 and 2099 in the Atmospheric Model with TRansport and Chemistry (AMTRAC) using a crossing method based on transition from westerlies to easterlies to detect major SSWs. However, using a criterion for major SSW occurrence based on the amplitude of the Northern Annular Mode and simulations from the CMAM, McLandress and Shepherd (2009b) showed that the future increase in the frequency of major SSWs in that model was a consequence of changes in the underlying climatology (i.e., mean vortex strength) and did not mean an increase in stratospheric variability. A recent study by Bell et al. (2010), however, found an increase in both stratospheric variability and major SSW frequency in simulations using enhanced GHG concentrations. Clearly, a consensus on the impact of stratospheric climate changes on vortex variability has not yet been reached, and cleanly separating changes in vortex variability from changes in the mean vortex strength remains a challenge.

The isolation of the polar vortex in conjunction with mixing across the vortex edge is an important dynamical regulator for ozone amounts at high latitudes (e.g., Strahan and Polansky, 2006) and midlatitudes (Braesicke and Pyle, 2003; Hadjinicolaou and Pyle, 2004; Wohltmann et al., 2007). Assessments of observed and modeled changes in stratospheric mixing are sparse. Garny et al. (2007) diagnosed recent trends in stratospheric mixing on selected isentropic surfaces in the lower stratosphere and found substantial differences for different heights, horizontal regions, and seasons, with, for example, long-term positive trends in mixing in southern midlatitudes at 450K and negative trends in southern high latitudes at 650K from May to August. In models, the choice of vertical resolution (Rind et al., 2007) and advection algorithm (Stenke et al., 2008) plays an important role. Modeling the 2002 major warming in the Southern Hemisphere, Konopka et al. (2005) diagnosed a larger degree of isolation than for similar events in the Northern Hemisphere. Changes in Antarctic vortex isolation at the

end of the 21st century have been examined for a subset of CCMs (Chapter 5 of the SPARC CCMVal Report, 2010). Some of the models analyzed indicate increased mixing between the vortex and midlatitudes above 1000K (~35 km) in the future, suggesting that winter planetary wave activity may have increased in the models. In this model intercomparison, no consensus could be found as to how the Antarctic vortex size and depth may change toward 2100. Note that the link between the modeled strengthening of the BDC and changes in mixing is not straightforward. Therefore, based on current knowledge, we cannot judge with high confidence how mixing across vortex barriers will change in the future and how this will affect ozone.

3.2.5 Background and Volcanic Stratospheric Aerosols

A layer of sulfuric acid aerosol is present at all latitudes in the lower stratosphere. During volcanically quiescent periods (also called “background” conditions), the dominant source of this aerosol layer is thought to be carbonyl sulfide photolysis and, possibly, sulfur entering the stratosphere in the form of sulfur dioxide (SO₂) (SPARC, 2006). The other major source of sulfur to the stratosphere is volcanoes. Chapters 3 and 6 of WMO (2007) (Chipperfield and Fioletov et al., 2007; Bodeker and Waugh et al., 2007) contain an in-depth discussion of volcanic aerosols and their effects on ozone. Chapter 8 of the CCMVal report (SPARC CCMVal, 2010) contains recent modeling intercomparisons of volcanic effects on ozone.

Volcanic eruptions can inject large amounts of sulfur directly into the stratosphere. This can considerably enhance the stratospheric aerosol layer (or Junge layer) for several years. Such an effect was observed after the eruptions of El Chichón in 1982 and Mt.

Pinatubo in 1991. The enhanced stratospheric aerosol loading can lead to very significant ozone depletion on a global scale, as was both observed and modeled after these eruptions. The ozone depletion is mostly due to heterogeneous reactions on sulfuric acid aerosol particles that convert halogen reservoir species into more reactive forms. The overall chemical changes include an increase in halogen radicals at the expense of nitrogen radicals. Thus, the net effect on ozone depends primarily on the stratospheric halogen loading, changing for instance from ozone decreases when chlorine loading is high to small ozone increases when chlorine loading is low (Tie and Brasseur, 1995). As a result, the potential for ozone depletion from enhanced aerosol loading is expected to decline as ESC decays toward natural levels late in the 21st century. The future recovery of ozone would be temporarily interrupted by large volcanic eruptions, especially during the first half of the 21st century. Small volcanic eruptions can also influence ozone, as was found in aircraft measurements that probed the Hekla, Iceland, volcanic plume in the lowermost stratosphere (Millard et al., 2006). The volcanic plume contained high SO₂ levels and very low ozone levels, near zero in places, and was still 30% depleted two weeks after. Simulations using a three-dimensional (3-D) chemistry-transport model (Chipperfield, 2006) showed that increased heterogeneous activation of chlorine due to elevated H₂O and HNO₃ from the volcanic plume was the likely cause of the ozone loss. Events such as these would not be expected to cause widespread ozone loss because of both the small size of the eruption and the short residence time of volcanic aerosols in the lowermost stratosphere. The analyses of these events do, however, confirm the link between aerosols and ozone depletion.

By virtue of their optical properties, aerosols also impact the radiative balance of the atmosphere and, hence, can affect stratospheric temperatures and dynamics substantially. Since the previous Assessment, several studies have attempted to separate the chemical and dynamical signals in the ozone response following the Mt. Pinatubo eruption. Using a two-dimensional model forced with meteorological analyses, Fleming et al. (2007) showed that, while the chemical ozone destruction due to halogen chemistry on volcanic aerosols took place in the lower stratosphere in both hemispheres, dynamical effects acted to decrease (increase) total column ozone in the Northern (Southern) Hemisphere. This result was confirmed by Telford et al. (2009) using a CCM nudged toward meteorological analyses. They found that, in addition to the ~10 Dobson unit (DU) chemical ozone loss in both hemispheres following the Mt. Pinatubo eruption, the quasi-biennial oscillation (QBO) (see Chapter 2) increased ozone by ~10 DU in the Southern

Hemisphere and decreased ozone by ~10 DU in the Northern Hemisphere. These two modeling studies confirm the earlier work of Hadjinicolaou et al. (1997) that demonstrated the existence of a large dynamical effect on ozone following the eruption.

From long-term aerosol measurements, it has been suggested that background stratospheric aerosol levels have been increasing in the last decade possibly due to enhanced tropospheric SO₂ background (see Sections 2.4.3.3 and 4.1.4 in Chapters 2 and 4 of this Assessment). There are a few reasons why a change in background aerosol levels could significantly affect ozone while chlorine levels remain elevated. First, halogen radical levels (and thus ozone loss) increase more strongly with aerosol loading when the aerosol loading is small, because the halogen activation saturates at high aerosol loadings due to the reduction of dinitrogen pentoxide (N₂O₅). Second, depending on the cause of this observed aerosol increase, it is possible that the increases may be larger at lower altitudes, where halogen radicals impact ozone most strongly. Thus, the potential for significant changes in background aerosol levels remains an uncertainty in predicting ozone changes in the coming decades.

3.2.6 Geoengineering by Sulfate Aerosol Injection

Doubts regarding the effectiveness of current international agreements to restrict emissions of GHGs to the atmosphere to mitigate climate change have led to a debate about the possibility of intentionally modifying climate through large-scale geoengineering actions; see Crutzen (2006) and a series of replies in a special issue of *Climatic Change* (vol. 77, no. 3-4, 2006). Such climate engineering schemes, if ever applied, might impact stratospheric ozone (Royal Society, 2009). Proposed schemes and uncertainties in their implementation are discussed in Chapter 5 of this Assessment (Section 5.4.2.4). Present knowledge strongly suggests that the addition of sunlight-reflecting sulfuric acid aerosols into the stratosphere would have large impacts on the future evolution of stratospheric ozone and as such should be considered alongside the other factors discussed in this chapter.

As discussed in the previous section, observations show a marked decrease in global ozone following the explosive volcanic eruptions of El Chichón in 1982 and Mt. Pinatubo in 1991. The primary reason for this enhanced ozone loss is the enhanced activation of stratospheric chlorine on volcanic aerosol particles (Kinnison et al., 1994; Solomon et al., 1996; Portmann et al., 1996; Tilmes et al., 2008b). Similar effects are expected for geoengineered stratospheric aerosol enhancements. An

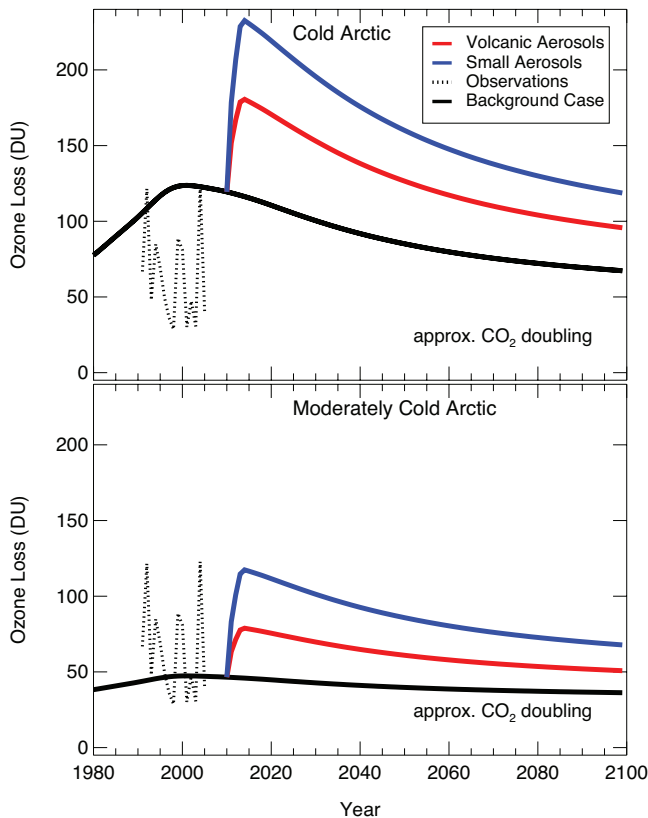


Figure 3-4. An illustration of the possible impact of geoengineering by stratospheric injection of sulfate aerosols on Arctic chemical ozone loss. The panels show estimates of the potential ozone loss (Dobson units) from chlorine activation as a function of time for different stratospheric aerosol loadings and for two types of Arctic winters. The top panel corresponds to cold Arctic winters, conditions that are expected to lead to the maximum impact of geoengineering on ozone depletion. The bottom panel is for moderately cold Arctic winters, representative of about half of the past 15 Arctic winters. In each panel, the solid and dotted black lines represent the ozone loss for a background stratospheric aerosol loading and observed stratospheric aerosol loading respectively. The red line shows the ozone loss estimated when 2 teragrams per year (Tg/yr) of stratospheric sulfur are added to the stratosphere, starting in 2010 and reaching a saturation value of 5.3 Tg of sulfur in the form of large volcanic-sized aerosol particles. The blue line corresponds to an alternative geoengineering scenario assuming the formation of smaller aerosol particles. In this scenario, a smaller injection of 1.5 Tg of sulfur per year would achieve the same radiative effect necessary to counteract the impact of a doubling of atmospheric carbon dioxide concentrations. Adapted from Tilmes et al. (2008a).

illustration of the impact of an enhanced stratospheric aerosol layer on chemical ozone loss is shown in Figure 3-4 (Tilmes et al., 2008a). For large, geoengineered, stratospheric aerosol loadings that appear to be required for significant climate change mitigation, model estimates suggest that chlorine activation could be more than doubled in the Arctic if it is implemented in the next 20 years, resulting in Arctic ozone depletion of 200–230 DU during very cold winters (comparable to the total amount of available ozone in the Arctic lower stratosphere). As stratospheric halogen levels decline over the 21st century, the impact of an enhanced aerosol layer on chlorine activation would be reduced but would still be significant. The expected recovery of the Antarctic ozone hole could be delayed by between 30 to 70 years depending on the assumed geoengineered aerosol size distribution (Tilmes et al., 2008a).

Further understanding of the consequences of geoengineering for stratospheric ozone and climate has been gained from numerical model simulations initially using global climate models (Matthews and Caldeira, 2007; Caldeira and Wood, 2008; Rasch et al., 2008; Robock et al., 2009) and, more recently, CCMs (Tilmes et al., 2009; Heckendorn et al., 2009). The CCM investigations confirm the empirical results of Tilmes et al. (2008a) that stratospheric sulfate injection could enhance stratospheric ozone depletion in both the Arctic and Antarctic while the levels of halogens remain elevated. Tilmes et al. (2009) quantified the impact of an enhanced burden of stratospheric sulfur on the ozone layer including the impacts on stratospheric dynamics and transport during the period when the stratospheric halogen loading is projected to slowly decline (Newman et al., 2007). Model calculations with a fixed enhanced sulfate aerosol loading (large enough to counteract the forcing generated by a doubling of CO₂ abundance with respect to preindustrial values) predict a one- to two-fold increase in Arctic ozone depletion due to a stronger polar vortex and lower temperatures (Rasch et al., 2008). The impact on midlatitude ozone was calculated to be smaller for 2050 chlorine levels (Tilmes et al., 2009). An additional risk is the possible occurrence of a large volcanic eruption, further increasing the amount of sulfur in the stratosphere (Tilmes et al., 2009).

Significant uncertainty remains regarding the behavior of artificially injected stratospheric aerosol, since the coagulation and settling of aerosol is strongly dependent on the injection scenario. Aerosol heating, in particular at the tropical tropopause, could also result in enhanced amounts of water vapor entering the stratosphere (Heckendorn et al., 2009), which would cause stratospheric ozone loss. According to CCM simulations of predicted 2050 conditions (Tilmes et al., 2009; Heckendorn et al., 2009), a geoengineered enhanced aerosol loading would lead to substantial and coupled changes in stratospheric dynam-

ics and ozone chemistry, especially in halogen heterogeneous chemistry. To date there have been no investigations of the impact on ozone caused by a gradual ramp-up of the amount of SO_2 injected, with the purpose of keeping global average temperature nearly constant (Wigley, 2006). Overall, we caution that these ozone projections are based on simple scenarios, idealized conditions, and on only two CCMs, including one without any aerosol microphysics. Because the ozone response depends on complex and competing interactions between chemical, aerosol microphysical, radiative, and dynamical processes that are represented differently in different models, more reliable ozone projections in a hypothetical geoengineered climate state require more realistic simulations with a range of models.

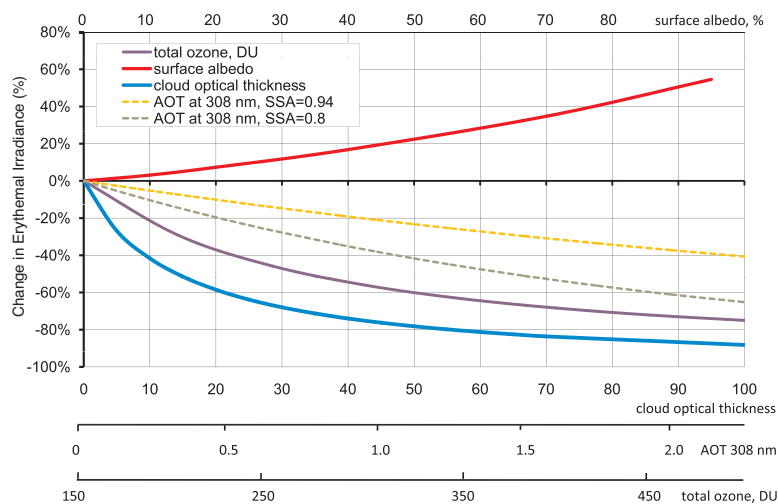
3.2.7 Effects of Ozone on Future Surface UV

In the 1980s and 1990s, a number of theoretical and experimental studies were devoted to quantifying ozone effects on UV spectral irradiance reaching the ground (e.g., Brühl and Crutzen, 1989; Schwander et al., 1997; Tsay and Stamnes, 1992; Madronich et al., 1998; Lapeta et al., 2000). Figure 3-5 shows the dependence of erythemal irradiance (CIE, 1993) on total ozone and other atmospheric parameters (cloud optical thickness, surface albedo, and aerosol optical thickness) within the range of values that can be observed in real atmospheric conditions. To quantify UV radiation, we use here the “erythemally weighted irradiance,” or simply “erythemal irradiance,” which is a

measure of the biological effectiveness of solar UV radiation incident per unit area of human skin and is commonly used for public information and awareness. The effective wavelengths of erythemal irradiance lie between 307 and 325 nm, depending mainly on solar zenith angle and total ozone. Other effects on humans and ecosystems are more sensitive to shorter or longer wavelengths of UV radiation, hence ozone-induced changes in the corresponding weighted irradiances would be either larger (e.g., for DNA damage) or smaller (e.g., for phytoplankton damage) compared to erythemal irradiance.

To estimate the response of UV radiation to ozone variations, the radiation amplification factor (RAF) approach proposed by Booth and Madronich (1994) is widely used. It provides simple but useful estimates of different biological weightings of UV irradiance response to ozone changes. For erythemal irradiance, the RAF was shown to be about -1.1 (WMO, 1999). At the same time, the influence of ozone on UV irradiance depends on solar elevation. Recently, a simple equation was proposed by Madronich (2007) enabling the calculation of erythemal irradiance (or the UV Index) under cloud-free skies and low surface-albedo conditions as a function of total ozone (in the range 200–400 DU), taking into account also the effect of solar zenith angle. The uncertainty of these estimates increases for solar zenith angles larger than $\sim 60^\circ$. However, the application of these approaches can lead to random and/or systematic uncertainties in calculating the UV response to future total ozone changes because they do not account for possible changes in ozone and temperature profiles. The influence of aerosols, clouds, and surface albedo are also neglected.

Figure 3-5. Relative changes (percent) in erythemal irradiance due to total ozone, cloud optical thickness, surface albedo, and aerosol optical thickness (AOT) at 308 nm for two values of single scattering albedo (SSA), calculated for 50° solar zenith angle with the Tropospheric Ultraviolet-Visible (TUV) v.2 model (Madronich and Flocke, 1999). All parameters vary within the range observed in real atmospheric conditions. Except for the effect of cloud optical thickness, all calculations refer to cloud-free skies. For the calculation of erythemal irradiance changes due to ozone, typical values were used for the aerosol optical thickness, $\text{AOT} = 0.31$, (Kinne et al., 2006) and the single scattering albedo, $\text{SSA} = 0.94$ (Chubarova, 2009). For estimating the effects from aerosols, surface albedo, and cloud optical thickness, an ozone column of 300 DU was used in the model simulations.



The effects of the vertical distribution of ozone in the troposphere and the stratosphere, as well as the temperature profiles (which affect the ozone cross-sections) should be taken into account when calculating the UV response to ozone changes (Brühl and Crutzen, 1989; Schwander et al., 1997; McKenzie et al., 2003). As discussed in Tsay and Starnes (1992) and Brühl and Crutzen (1989), transport of ozone from the stratosphere to the troposphere tends to decrease UV at the surface, but for low solar elevation angles an increase may occur. Changes in ozone vertical distribution and temperature profile can modify erythemal irradiance by as much as 14%, according to Lapeta et al. (2000). In Kazantzidis et al. (2005) it was emphasized that the most significant effects of changes in vertical ozone distribution on surface erythemal irradiance are observed at large solar zenith angles (up to 20% at 85° solar zenith angle). However, UV levels are usually very small for these conditions.

The future evolution of ozone will determine to a great extent future levels of surface UV radiation and the date of return to the UV levels in the 1980s or 1960s. However, in some regions UV radiation levels in the future may not return to historical levels due to influences from factors related to climate change (e.g., cloudiness, surface albedo, aerosols, UV-absorbing tropospheric gases; see Section 3.2.8). A detailed analysis of future UV levels due to ozone in different geographical areas is given in Section 3.4.

3.2.8 Factors Other Than Stratospheric Ozone Affecting Surface UV

In addition to ozone, UV radiation is affected by other atmospheric parameters, for example, changes in cloudiness, aerosols, surface albedo, and, to some extent, by other mineral and organic gas species. Since WMO (2007) a number of publications have discussed and quantified the factors other than ozone that affect surface UV irradiance (e.g., Kazadzis et al., 2007; Tanskanen and Manninen, 2007; Lindfors and Arola, 2008; Staiger et al., 2008; Badosa et al., 2007; Chubarova, 2008; Rieder et al., 2008; McKenzie et al., 2008; Chubarova et al., 2009). A comparison of the relative effects of changes in ozone and in other atmospheric parameters on surface erythemal irradiance is shown in Figure 3-5. Changes in cloud optical thickness, typically between 0 and 40, are the most important driver of day-to-day and long-term changes in surface UV irradiance, generally dominating the effect of changes in total column ozone. Aerosols, and in particular highly absorbing aerosols, also affect surface UV irradiance. However, for typical values of aerosol optical thickness (~0.3), the effect is small compared to clouds. Increases in surface albedo, for example due to changes in snow or ice cover, can significantly enhance surface UV. The

sensitivity of surface UV to the changes in atmospheric parameters shown in Figure 3-5 does not account for more complicated, nonlinear interactions in their effects (for example, the interaction of clouds and inhomogeneous surface albedo, or cloud and aerosol interactions) or for spatial inhomogeneities in the atmosphere.

Since surface UV is appreciably sensitive to a number of factors other than ozone, projections of these factors, in addition to ozone, are required to make reliable and robust projections of surface UV irradiance. However, at present, projections of atmospheric factors other than ozone have large uncertainties, making accurate projections of surface UV elusive.

3.2.8.1 CLOUDS

Because climate change is likely to affect future cloudiness, and given the sensitivity of surface UV to changes in cloudiness (Figure 3-5), understanding potential future changes in cloud cover is essential to quantifying future changes in UV. To this end, projections of changes in cloudiness obtained from the Third Coupled Model Intercomparison Project (IPCC, 2007) and indirectly from Chapter 10 of SPARC CCMVal (2010) have been used. Climate models forced according to the Special Report on Emissions Scenarios (SRES) A1B scenario from IPCC (2000) (which is the standard scenario of the stratospheric ozone projections discussed here; see Section 3.3.1) predict with some consistency that by the end of the 21st century cloud cover would have decreased over most of the low and middle latitudes, and substantially increased at high latitudes. Trenberth and Fasullo (2009) examined top-of-atmosphere radiation changes in climate model projections and also found decreases in cloudiness through the 21st century predominantly after 2040. Coverage of optically thick low-level clouds is projected to also decrease over low and middle latitudes (Trenberth and Fasullo, 2009), in agreement with the tendency for low-level clouds to dissipate as the ocean warms (Clement et al., 2009). In Chapter 10 of SPARC CCMVal (2010), cloud projections were used to estimate future changes in surface erythemal irradiance by converting shortwave cloud transmittance to erythemal UV cloud transmittance. Shortwave cloud transmittances evaluated from the IPCC (2007) climate models and from Chapter 10 of SPARC CCMVal (2010) CCMs agree reasonably well. However, these projections are highly uncertain as the cloud response to climate change appears to be the primary source of spread between climate model simulations (Dufresne and Bony, 2008).

Projections of surface UV irradiance that include the effects of cloud changes result in more complex patterns in projected UV compared to clear-sky UV projections. Increases in erythemal irradiance of 10–15% by the

end of 21st century due to changes in cloudiness are projected for the tropical regions of South-East Asia and Central America, with more moderate increases over Southern Europe in summer (Chapter 10 of SPARC CCMVal, 2010). A UV reduction of 10–15% is projected by 2100 due to increases in cloudiness over some northern high-latitude regions and over Antarctica.

3.2.8.2 AEROSOLS

The effect of atmospheric aerosols on surface UV radiation depends on their optical and microphysical properties and total atmospheric loading. While the tropospheric burden of sulfate aerosols is generally projected to decrease in the future, projections for black carbon (soot) are less certain (IPCC, 2007). Projections of aerosol properties have been aided by recent modeling studies (Kinne et al., 2006; Schulz et al., 2006). However, at present, despite general agreement on projections of annual mean aerosol optical thickness, the disparity of aerosol absorption in various models leads to large uncertainties in surface UV, precluding robust assessments of future aerosol effects on UV irradiance. There are also large uncertainties in the methods used to generate emissions scenarios as well as in assessing the present-day emissions, especially for black carbon and organic carbon (IPCC, 2007). Furthermore, it remains unresolved whether emissions of soil dust aerosols will increase or decrease in response to changes in the atmospheric state and circulation (Tegen et al., 2004). Differences in emission regulation strategies between countries result in large spatial variability in aerosol trends.

Climate model simulations project increases in aerosol optical thickness of ~1.4% by 2030 for the A1B scenario but decreases of ~5% for the SRES B1 scenario, a lower emission scenario (IPCC, 2000; Jacobson and Streets, 2009). Resultant changes in surface UV radiation are estimated to be smaller than –0.5% for the A1B scenario, and about 0.1–1.5% for the B1 scenario, depending on the aerosol properties and solar elevation.

3.2.8.3 SURFACE ALBEDO AND SEA ICE COVER

The effects of surface albedo on UV irradiance are well documented (WMO, 1999; WMO, 2003; WMO, 2007). Under clear-sky conditions, the presence of snow/ice may increase UV by up to 50%, while in overcast or close to overcast conditions with optically thick clouds, the UV increase due to high snow/ice surface albedo can reach several hundred percent because of effective multiple scattering. On the other hand, sea ice cover significantly reduces penetration of harmful UV-B irradiance in the underwater environment. As a result, possible climate warming-induced changes in snow and sea ice cover may affect both terrestrial and aquatic ecosystems.

Reductions in sea ice extent through the 21st century in both the Arctic and Antarctic have been projected by a number of models, albeit with a rather large range of model responses in the Northern Hemisphere sea ice extent, ranging from very little change to a strong and accelerating reduction over the 21st century (Zhang and Walsh, 2006). According to Overland and Wang (2007), the projected summer loss in sea ice extent would be greater than 40% by 2050 for the marginal seas of the Arctic basin. Stroeve et al. (2007) reported that sea ice in the Arctic is melting faster than projected in IPCC (2007) under all SRES emissions scenarios. The accelerated decrease in Arctic sea ice extent has also been documented in satellite data (Comiso et al., 2008). This sea ice melting is projected to decrease the surface albedo and increase UV irradiance in the underwater environment. In the 20th- and 21st-century simulations, Antarctic sea ice cover is projected to decrease more slowly than in the Arctic (Stroeve et al., 2007), particularly in the vicinity of the Ross Sea, where most models predict a local minimum in surface warming (Meehl et al., 2007).

It is well established that mountain glaciers and snow cover have declined on average in both hemispheres (IPCC, 2007). They are expected to continue declining in the future (Bradley et al., 2004). This would result in considerable local reductions in surface albedo and UV in the corresponding regions.

3.2.8.4 TROPOSPHERIC GASES

Several tropospheric gases, such as SO₂, NO₂, and ozone, can efficiently absorb UV-B radiation. Their influence depends mainly on their total column amount, which can be especially high over industrial areas and over areas influenced by forest fires. Their impact is also determined by the effectiveness of UV absorption discussed in Chapter 7 of WMO (2007) (Bais and Lubin et al., 2007). The average effect of increasing NO₂ on erythemal irradiance has been shown to be about –2% in industrial areas (Chubarova, 2008). However, on some days the influence can be much stronger. For example, in Tokyo the amount of NO₂ can be 20 times higher than the average, decreasing UV-B irradiance by about 15% (McKenzie et al., 2008). Similar effects from NO₂ have been observed during intense forest fires, when erythemal irradiance has been attenuated by 10–15% (Chubarova et al., 2009). SO₂ column amounts can easily reach 2 DU over areas affected by high volcanic activity or over regions close to coal burning industries, resulting in ~2% attenuation of erythemal irradiance. At some UV wavelengths, the reduction by SO₂ can exceed 20% (McKenzie et al., 2008).

The amounts of these gases in the troposphere depend strongly on their emissions. In industrialized regions, such as North America and Europe, emissions

of NO_x and volatile organic compounds are decreasing, while in regions dominated by developing countries, significant growth in emissions is observed (IPCC, 2007). Since 1980, SO₂ emissions in 25 countries in Europe have been reduced by more than a factor of 4, while in the USA they have been halved (IPCC, 2007). However, over the same period, SO₂ emissions from Asia and from developing countries in other regions have been increasing. There is a clear positive trend in tropospheric ozone concentrations projected by models under the A2p scenario, with increases between 11.4 and 20.5 DU by 2100 (Gauss et al., 2003). Taking into account that ozone absorbs UV radiation more effectively in the lower troposphere due to enhanced scattering, these increases in tropospheric ozone may result in approximately a 5–10% reduction in surface erythemal irradiance. The modeling study of Jacobson and Streets (2009) also projects by 2030 an increase in surface ozone of ~14% under the A1B scenario and ~4% under the B1 scenario.

3.3 PROJECTIONS OF OZONE THROUGH THE 21ST CENTURY

Since the 2006 Assessment (WMO, 2007), a new suite of 17 chemistry-climate model (CCM) simulations coordinated through the SPARC CCMVal activity has become available. These simulations, from the second phase of CCMVal (referred to as CCMVal-2), form the basis for this section and improve on the CCMVal-1 simulations reported in WMO (2007) by:

- Starting in 1960 rather than in 1980. In most regions of the atmosphere, ozone depletion occurs prior to 1980 in nearly all of the CCMs assessed here. By starting the simulations in 1960 at a time when ozone was not expected to be significantly affected by ODSs, and including sensitivity simulations, the CCMs can now be used to project the timing of the third stage of ozone recovery, i.e., the full recovery of ozone from the effects of ODSs. Stage-three ozone recovery was not reported on in WMO (2007). Furthermore, the availability of pre-1980 model data permits a more robust calculation of the 1980 ozone threshold and hence a more accurate determination of when ozone returns to 1980 levels.
- Having available almost all simulations from 1960 to 2100. In WMO (2007) only one CCM provided simulations beyond 2050. The extension to 2100 now permits more robust conclusions to be drawn regarding the expected evolution of ozone through the latter half of the 21st century.

- Applying a more rigorous statistical analysis. The larger number of models, the availability of continuous simulations from 1960 to 2100 by nearly all CCMs, and a new method for calculating and analyzing multi-model time series (described in Section 3.3.2.2) have allowed a more robust analysis than was presented in WMO (2007).
- Having available a number of sensitivity simulations with fixed forcings. In addition to the reference simulations as reported in WMO (2007), simulations where either surface concentrations of ODSs or GHGs are held fixed at their 1960 levels (Section 3.3.1) permit a more in-depth analysis of the factors affecting ozone through the 21st century than previously possible and allow the assessment of full ozone recovery from ODSs.
- Having available simulations based on different GHG emissions scenarios. WMO (2007) reported only on simulations based on the SRES A1B scenario.

3.3.1 Model Descriptions and Scenarios

In this chapter the focus is on “future” simulations to 2100, whereas the “past” simulations (from 1960 up to 2006) are discussed in Chapter 2. Ozone projections and the attribution of ozone changes to ODSs and GHGs are based on the recently completed CCMVal-2 multi-model ensemble. These simulations have been extensively analyzed in SPARC CCMVal (2010), as well as in a variety of individual model studies. In addition to this large ensemble of future reference simulations from 17 CCMs, in which realistic scenarios of ODSs and GHGs are used, several more specialized sensitivity simulations by a subset of CCMs (Vaughan et al., 2009; Eyring et al., 2010a; Eyring et al., 2010b; Charlton-Perez et al., 2010; Oman et al., 2010) are assessed here.

The CCM simulations are all transient simulations in which ozone responds interactively to the secular trends in GHGs, ODSs, and in other boundary conditions. They are commonly separated into “past” (or “historical”) transient reference simulations that are driven by observed forcing and “future” transient reference simulations that are forced by trace gas projections and generally use modeled sea surface temperatures (SSTs) and sea ice concentrations (SICs). The CCMVal-2 “past” reference simulation (REF-B1) is designed to reproduce ozone changes from 1960 to the recent past (2006) when global ozone observations are available. It includes solar and volcanic forcings, and SSTs/SICs from observations. It allows a detailed investigation of the role of natural variability and other atmospheric changes important for

ozone trends (see Chapter 2). The CCMVal-2 “future” reference simulation (REF-B2) is a self-consistent simulation from the past into the future. In this simulation the surface time series of halocarbons is based on the adjusted A1 halogen scenario (WMO, 2007; see also Section 3.2.1). The long-lived GHG concentrations are taken from the SRES A1B scenario (IPCC, 2000). SSTs and SICs are generally prescribed from coupled ocean model simulations. Of the 17 CCMs that provided ozone projections analyzed in this chapter, only CMAM was coupled to an interactive ocean model (see Table 3-1). Some CCMs generated an ensemble of future simulations with the same boundary conditions but different initial conditions (see Table 3-1). In general, the ozone variability between ensemble members from a single model is much smaller than the inter-model differences (Chapter 6, WMO, 2007; Austin et al., 2008).

Additional sensitivity simulations based on different emissions scenarios were also performed by some CCM groups to attribute the future evolution of stratospheric ozone to ODS and GHG forcings and to study the coupled chemistry-climate system under a variety of GHG scenarios (see Tables 3-1 and 3-2). These include sensitivity simulations with ODSs fixed at 1960 levels (fODS) to assess the milestone of full ozone recovery (Vaughn et al., 2009; Eyring et al., 2010a) (see Section 3.3.6). In addition, sensitivity simulations with GHGs fixed at 1960 levels (fGHG) were performed, for example, to address the issue of the linear additivity of the effects of GHGs and ODSs on ozone. By comparing the sum of the ozone responses in the fixed GHG and ODS simulations (each relative to the 1960 baseline) with the ozone response in the REF-B2 reference simulation, the linear additivity of the responses can be assessed (McLandress et al., 2010; Eyring et al., 2010a). A subset of four CCMs also provided future projections under GHG scenarios different to SRES A1B (Oman et al., 2010; Eyring et al., 2010b). These GHG sensitivity simulations (GHG-x) include simulations forced with the SRES A2 and B1 GHG scenario from IPCC (2000) and with the new Representative Concentration Pathways (RCPs; Moss et al., 2008) that form the basis for the climate simulations of the Coupled Model Intercomparison Project, Phase 5 (CMIP5, Taylor et al., 2009), in support of the Fifth IPCC Assessment Report. They are generated by integrated assessment models and harmonized with the historical emissions from Lamarque et al. (2010) in both amplitude and geographical distribution. The RCP simulations performed by CAM3.5 are RCP 8.5 (Riahi et al., 2007), RCP 4.5 (Clarke et al., 2007), and RCP 2.6 (van Vuuren et al., 2007), where the number after “RCP” indicates the radiative forcing in W/m^2 reached by 2100 in each scenario. By 2100, for example, CO_2 in the RCP 8.5 and SRES A2 scenarios is ~ 200 ppm and ~ 100 ppm higher than in SRES A1B, while in the

SRES B1/RCP 4.5 and RCP 2.6 scenario it is ~ 150 ppm and ~ 250 ppm lower, respectively. The different levels of GHGs lead to differences in ozone projections (see Section 3.2 on factors affecting future ozone).

3.3.2 Model Evaluation and Multi-Model Mean Analysis

3.3.2.1 MODEL EVALUATION

Confidence and guidance in interpreting CCM projections of future changes in atmospheric composition can be gained by first ensuring that the CCMs are able to reproduce key processes for stratospheric ozone (e.g., Eyring et al., 2005; SPARC CCMVal, 2010). Limitations and deficiencies in the models can be revealed through inter-model comparisons and through comparisons with observations. An improvement over the approach used in CCMVal-1 and WMO (2007) is that for the current Assessment, a more extensive set of ozone-related processes was evaluated in the CCMs (SPARC CCMVal, 2010). In this chapter the evolution of ozone and inorganic chlorine (Cl_y) is shown for individual CCMs in several figures to portray the full distribution of model simulations. However, the discussion and conclusions are based on the time series of the multi-model mean and associated statistical confidence and prediction intervals (see Section 3.3.2.2).

A detailed summary of the key findings of SPARC CCMVal (2010) on the evaluation of CCMs against observations is presented for chemical composition in Chapter 2, and for the Brewer-Dobson circulation (BDC) and temperature in Chapter 4. This section briefly summarizes relevant conclusions from these chapters, with a focus on processes and results that are important for long-term ozone projections.

- *BDC and Temperature.* Both are important drivers of the evolution of ozone. Most CCMs are capable of reproducing the amplitude and vertical structure of the observed trends in global-mean stratospheric temperatures, although the model spread is high in some regions. Tropical upwelling is well simulated in the lower stratosphere compared to meteorological analyses. Models consistently predict a strengthening of the BDC and hence a decrease in mean age of air as a result of climate change, but they disagree on the relative role of resolved and parameterized wave drag. This strengthening of the BDC is partly supported by several lines of observational evidence (see Section 4.2.2) but not by recent estimates of the age of air inferred from tracers observations in the northern midlatitude lower stratosphere, which indicate a statistically insignificant trend (Engel et al., 2009). However, the small model-simulated trends in the

BDC lie within the large uncertainties of the stratospheric age-of-air measurements.

- *Tropical and Midlatitude Ozone.* In the tropics, climate change and halogen loading influence total col-

umn ozone through dynamical processes in the lower stratosphere and chemical processes in the upper stratosphere. Over the historical period, the CCMs simulate negative trends in tropical upper stratospheric ozone, in agreement with observations (see Section 2.4.5.3). The

Table 3-1. A summary of the CCMs and the simulations used in this chapter. REF-B2 is the future reference simulation, fODS is a simulation with fixed ODSs, fGHG a simulation with fixed GHGs, and GHG-x are simulations with a GHG scenario different to SRES A1B; see details in Section 3.3.1 and Table 3-2. $N \times$ REF means that the group provided N realizations of this simulation. Further details on the models can be found in Morgenstern et al. (2010) and in Chapter 2 of SPARC CCMVal (2010) as well as in the references given below. EMAC-FUB and NIWA-SOCOL did not contribute a REF-B2 simulation for SPARC CCMVal (2010), but provided simulations later (Austin et al., 2010b; Eyring et al., 2010a).

CCM*	Group and Location**	Horizontal Resolution	Upper Level	Reference Simulation	fODS	fGHG	GHG-x	References
AMTRAC3	GFDL, USA	~200 km	0.017 hPa	REF-B2	---	---	---	Austin and Wilson (2010)
CAM3.5	NCAR, USA	$1.9^\circ \times 2.5^\circ$	3.5 hPa	REF-B2	---	---	RCP2.6 RCP4.5 RCP8.5	Lamarque et al. (2008)
CCSRNIES	NIES, Tokyo, Japan	T42	0.012 hPa	REF-B2	fODS	fGHG	SRESB1 SRESA2	Akiyoshi et al. (2009)
CMAM	MSC, Univ. of Toronto, York Univ., Canada	T31	0.00081 hPa	$3 \times$ REF-B2	$3 \times$ fODS	$3 \times$ fGHG	---	Scinocca et al. (2008); de Grandpré et al. (2000)
CNRM-ACM	Meteo-France, France	T63	0.07 hPa	REF-B2	---	---	---	Déqué (2007); Teyssède et al. (2007)
E39CA	DLR, Germany	T30	10 hPa	REF-B2 (with solar cycle and QBO)	---	fGHG	---	Stenke et al. (2009); Garny et al. (2009)
EMAC-FUB	FU Berlin, Germany	T42	0.01 hPa	REF-B2 (with solar cycle and QBO)	---	fGHG	---	Jöckel et al. (2006); Nissen et al. (2007)
GEOSCCM	NASA/GSFC, USA	$2^\circ \times 2.5^\circ$	0.015 hPa	REF-B2	fODS	---	SRESA2	Pawson et al. (2008)
LMDZrepro	IPSL, France	$2.5^\circ \times 3.75^\circ$	0.07 hPa	REF-B2	fODS	---	---	Jourdain et al. (2008)
MRI	MRI, Japan	T42	0.01 hPa	$2 \times$ REF-B2	fODS	fGHG	---	Shibata and Deushi (2008a; 2008b)
NIWA-SOCOL	NIWA, New Zealand	T30	0.01 hPa	REF-B2	---	---	---	Schraner et al. (2008); Egorova et al. (2005)

Table 3-1, continued.

SOCOL	PMOD/WRC; ETHZ, Switzerland	T30	0.01 hPa	3 × REF-B2	fODS	fGHG	---	Schraner et al. (2008); Egorova et al. (2005)
ULAQ	Univ. of L'Aquila, Italy	R6 / 11.5° × 22.5°	0.04 hPa	REF-B2	fODS	fGHG	---	Pitari et al. (2002); Eyring et al. (2006; 2007)
UMSLIMCAT	Univ. of Leeds, UK	2.5° × 3.75°	0.01 hPa	REF-B2	fODS	---	---	Tian and Chipperfield (2005); Tian et al. (2006)
UMUKCA-METO	MetOffice, UK	2.5° × 3.75°	84 km	REF-B2	---	---	---	Morgenstern et al. (2008; 2009)
UMUKCA-UCAM	Univ. of Cambridge, UK	2.5° × 3.75°	84 km	REF-B2	---	---	---	Morgenstern et al. (2008; 2009)
WACCM	NCAR, USA	1.9° × 2.5°	5.9603 × 10 ⁻⁶ hPa	3 × REF-B2	fODS	fGHG	SRESB1	Garcia et al. (2007)

* CCM acronyms are defined in Appendix B of this Assessment.

** GFDL, Geophysical Fluid Dynamics Laboratory (NOAA); NCAR, National Center for Atmospheric Research; NIES, National Institute for Environmental Studies; MSC, Meteorological Service of Canada; DLR, Deutschen Zentrum für Luft- und Raumfahrt; FU, Freie University; NASA, National Aeronautics and Space Administration; GSFC, Goddard Space Flight Center; IPSL, Institut Pierre-Simon Laplace; MRI, Meteorological Research Institute; NIWA, National Institute of Water and Atmospheric Research; PMOD, Physical-Meteorological Observatory-Davos; WRC, World Radiation Center; ETHZ, Swiss Federal Institute of Technology-Zürich.

Table 3-2. Summary of CCMVal-2 reference and sensitivity simulations used in this chapter.

Simulation Name	Period	GHGs	ODSs	SSTs/SICs	Background & Volcanic Aerosol	Solar Variability	QBO
REF-B2	Transient simulation 1960–2100	SRES A1B (medium) (from IPCC, 2000)	OBS + adjusted A1 scenario (WMO 2007, Table 8-5)	Modeled SSTs and SICs	OBS Background surface area density from 2000	No	Only internally generated
fODS Fixed ODSs	1960–2100	Same as in REF-B2	ODSs fixed at 1960 levels	Same as in REF-B2	Same as in REF-B2	Same as in REF-B2	Same as in REF-B2
fGHG Fixed GHGs	1960–2100	GHG fixed at 1960 levels	Same as in REF-B2	1955–1964 average of REF-B2, repeating each year	Same as in REF-B2	Same as in REF-B2	Same as in REF-B2
GHG-x (SRES A2 and B1, RCP 2.6, 4.5, and 8.5)	2000–2100	GHG scenario different from SRES A1B	Same as in REF-B2	SSTs/SICs distribution consistent with GHG scenario	Same as in REF-B2	Same as in REF-B2	Same as in REF-B2

multi-model mean over the historical period indicates a small negative trend in tropical total column ozone, with a rather large model range. This small negative modeled trend is difficult to verify against observations since their length is limited and natural variability is high. Over midlatitudes, the multi-model mean adequately reproduces the negative trends in total column ozone although there is significant model spread.

- *Polar Ozone.* Both models and observations indicate that Antarctic stratospheric ozone loss, together with increasing GHG concentrations, has led to a poleward shift and strengthening of the Southern Hemisphere westerly tropospheric jet during summer. Most CCMs adequately represent lower stratospheric Antarctic vortex isolation, although some have deficiencies with respect to specific chemical or dynamical polar processes. Overall, they tend to reproduce well the Antarctic ozone losses inferred from observations; however it should be noted that many models show a late final warming in the Southern Hemisphere. This will extend chemical ozone loss later into the Antarctic spring. In the Arctic, while a few models represent the chemical ozone loss observed over the past three decades, most underestimate the loss, mainly because they tend not to capture the low temperatures observed in the Arctic lower stratosphere.

The multi-model mean estimates of past ozone changes simulated by CCMs under the REF-B1 scenario are generally consistent with the observed changes (see Chapter 2 of SPARC CCMVal, 2010). Overall, there is sufficient agreement among the CCMs, and between CCMs and observations, on the underlying causes of the ozone changes so that general conclusions can be drawn and some confidence placed in the CCM projections.

3.3.2.2 ANALYSIS METHOD FOR MULTI-MODEL TIME SERIES

Chapter 9 of SPARC CCMVal (2010) introduced a time series additive model (TSAM) to analyze the CCMVal-2 multi-model projections. This method is used to calculate baseline-adjusted anomaly time series relative to the values at a particular reference year (here 1960 and 1980) for ozone and other species for each model simulation. The values at the reference year are obtained from a smooth fit to the model time series calculated with the TSAM method. This smooth fit is referred to as the individual model trend estimate. Note that the term “trend” does not denote the result of a linear regression analysis but rather refers to a smooth trajectory passing through the data. The multi-model trend estimate is the average of the individual model trend estimates. By definition, both the individual model trends and the multi-model trends pass

through zero at the specified reference year. Two types of uncertainty intervals are constructed. The first is the point-wise 95% confidence interval. This interval has a 95% chance of overlapping the true trend and represents the local uncertainty in the trend at each year. The second interval is the 95% prediction interval which, by construction, is larger than the confidence interval. The 95% prediction interval is a combination of the local uncertainty in the trend and uncertainty due to natural interannual variability about the trend; it gives a sense of where an ozone value for a given year might reasonably lie. Both the confidence and prediction intervals are time varying.

The credibility of simulated ozone projections is linked to a realistic representation of processes that drive stratospheric ozone. Process-based performance metrics have been used to assess the ability of CCMs to reproduce key processes for stratospheric ozone and its impact on climate (SPARC CCMVal, 2010). While it could be preferable to use metric-based weightings when calculating multi-model means, SPARC CCMVal (2010) concluded that more analysis is needed to assess the robustness and interpretation of performance metrics, and their possible use in assigning relative weights to ozone projections. For this reason, and to remain consistent with the multi-model mean time series presented in SPARC CCMVal (2010), the multi-model mean ozone projections from the CCMVal-2 simulations are shown here without applying weights. The robustness of the CCMVal-2 multi-model mean ozone projections and uncertainties is demonstrated by the fact that it is generally insensitive to whether outliers are included or not (Waugh and Eyring, 2008; Chapter 9 of SPARC CCMVal, 2010). Indeed, the multi-model means of total column ozone calculated from simulations of the four CCMs selected in Chapter 2 as the highest-scoring models are found to be very close to the multi-model means calculated from all 17 CCMs.

3.3.3 Tropical Ozone

3.3.3.1 LONG-TERM PROJECTIONS OF TROPICAL OZONE

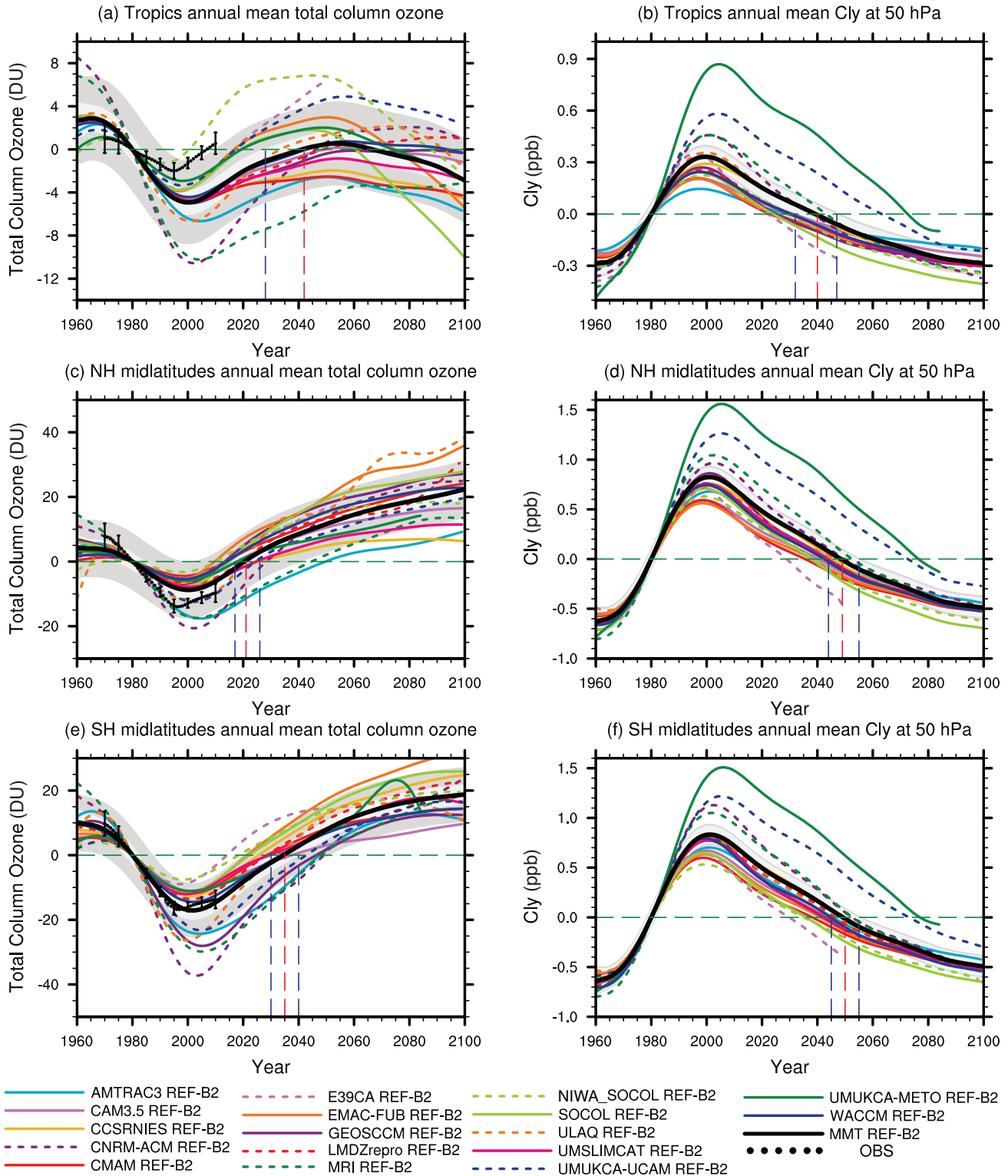
The 1960 to 2100 annual mean tropical (25°S–25°N) total column ozone time series are shown in Figure 3-6(a) for the REF-B2 simulations (Table 3-2). The simulated decrease in annual mean total column ozone of 8 DU from 1960 to 2000 is larger than observed. Following the simulated minimum in tropical ozone around 2000, by 2025 about 70% of the ozone lost since 1980 is projected to have been replenished and by 2050 ozone levels are projected to be at or very slightly above 1980 values (see Table 3-3). In the latter half of the 21st century, the annual mean tropical column ozone is projected to decline despite the projected

Table 3-3. Summary of the extent to which total column ozone is projected to have returned to 1960 and 1980 levels from its absolute minimum. A value of 0% denotes that ozone has not increased above the minimum, 50% denotes that ozone at this date is halfway between the simulated minimum and the 1960 or 1980 level, 100% denotes that ozone has returned to the 1960 or 1980 level, and >100% denotes that ozone exceeds the 1960 or 1980 level at this date. The reference year and the total column ozone in that year are listed in the second column. The year in which the minimum ozone occurred and the total column ozone at the minimum are listed in the 3rd column. In each of the cells in subsequent columns, the value obtained from the multi-model trend estimate is listed in boldface on the center line, with the 95% confidence intervals extracted from the TSAM statistics listed on the lines above and below. All ozone values have been rounded to the nearest DU and all percentage values to the nearest 5%.

Region	Reference Year; Total Column Ozone (DU)	Year When Minimum Occurs; Total Column Ozone (DU)	Difference to Reference Year, in 2025		Difference to Reference Year, in 2050		Difference to Reference Year, in 2075		Difference to Reference Year, in 2100	
			(DU)	(%)	(DU)	(%)	(DU)	(%)	(DU)	(%)
Unit			(DU)	(%)	(DU)	(%)	(DU)	(%)	(DU)	(%)
Global annual mean	1960 (312 DU)	2001 (296 DU)	-10	40%	-2	90%	1	105%	2	115%
			-8	50%	-1	95%	3	115%	4	125%
	-6		65%	1	105%	5	130%	6	140%	
	1980 (306 DU)	-4	60%	3	130%	7	170%	8	180%	
-2		80%	5	150%	8	180%	10	190%		
			0	100%	7	170%	10	200%	11	210%
Tropics annual mean	1960 (272 DU)	2000 (265 DU)	-5	30%	-3	55%	-4	45%	-7	0%
			-4	45%	-2	70%	-3	60%	-6	25%
	-3		55%	-1	85%	-2	70%	-4	45%	
	1980 (270 DU)	-3	40%	-1	80%	-2	60%	-4	20%	
-1		70%	0	110%	-1	90%	-3	40%		
			0	100%	2	140%	1	120%	-2	60%
Northern midlatitude annual mean	1960 (357 DU)	2000 (344 DU)	-4	70%	5	140%	11	185%	15	215%
			-2	85%	7	155%	14	205%	18	240%
	-1		90%	10	175%	16	225%	21	260%	
	1980 (353 DU)	0	100%	9	200%	15	265%	19	310%	
3		130%	11	230%	18	300%	22	355%		
			5	155%	14	255%	21	335%	25	380%
Southern midlatitude annual mean	1960 (349 DU)	2002 (322 DU)	-18	35%	-5	80%	3	110%	6	120%
			-15	45%	-2	90%	6	120%	9	130%
	-12		55%	1	105%	9	135%	12	145%	
	1980 (339 DU)	-8	55%	5	130%	13	175%	16	195%	
-5		70%	7	145%	16	190%	19	210%		
			-2	90%	11	165%	19	210%	22	230%
Antarctic October mean	1960 (374 DU)	2003 (244 DU)	-100	20%	-61	55%	-35	75%	-18	85%
			-95	30%	-53	60%	-26	80%	-9	95%
	-85		35%	-44	65%	-18	85%	1	100%	
	1980 (322 DU)	-50	35%	-10	85%	17	120%	33	140%	
-42		45%	-1	100%	25	130%	43	155%		
			-34	55%	8	110%	34	145%	52	165%
Arctic March mean	1960 (459 DU)	2002 (422 DU)	-19	50%	2	105%	18	150%	27	175%
			-15	60%	6	115%	22	160%	33	190%
	-10		75%	11	130%	27	175%	38	205%	
	1980 (445 DU)	-6	75%	15	165%	31	235%	41	290%	
-1		95%	20	185%	36	255%	46	300%		
			3	115%	24	205%	40	275%	52	325%

monotonic decline in 50 hPa tropical Cl_y through the 21st century (Figure 3-6(b)), with 1980 Cl_y values reached around 2040. Over the entire 1960 to 2100 period, secular variations in tropical column ozone are only ~10 DU.

Austin et al. (2010a; see also Chapter 9 of SPARC CCMVal, 2010) compared these future projections with those assessed in WMO (2007) and noted that there was little change, at least up to 2050. However, they found



reduced uncertainty in the projections, mainly because of a greater number of simulations covering the whole period from 1960 to 2100. Nonetheless, as with the CCM projections considered in WMO (2007), there was a wide spread among the tropical ozone amounts simulated by the individual models and these extended significantly above and below the observed values. Apart from two models, there were no notable changes in the model total column ozone biases in this region (Chapter 9 of SPARC CCMVal, 2010). WMO (2007) did not report on the projected behavior of tropical total column ozone after 2050, as only one CCM simulated that period (Bodeker and Waugh et al., 2007). On the other hand, the projections from that single model, shown in Figure 6-10 of WMO (2007), do not show the late 21st century decline in total column ozone found in the latest multi-model projections.

Oman et al. (2010) found that using the SRES A2 scenario rather than the SRES A1B in the GEOSCCM significantly increased the abundance of reactive nitrogen and hydrogen in the upper stratosphere. However, any increased chemical ozone destruction from the additional NO_y and HO_x was largely mitigated by the additional GHG cooling in the SRES A2 scenario, which slows gas-phase ozone destruction. As a result, the ozone evolution in the upper stratosphere was similar for both scenarios. Results from the CCSRNIES model confirm this finding (Eyring et al., 2010b). In general, Eyring et al. (2010b) found that the projected behavior of tropical total column ozone was not very sensitive to the range of different GHG scenarios (SRES A1B, A2, and B1; RCP 2.6, 4.5 and 8.5; see Section 3.3.1). By 2100 the differences among scenarios was only ~4 DU, which is small compared to the differences found in the extratropics (see Section 3.3.4).

3.3.3.2 PROCESSES DETERMINING FUTURE TROPICAL OZONE

Chapter 9 of SPARC CCMVal (2010) performed a multiple linear regression on the time series of tropical ozone in the current CCMs and found that between 2000 and 2100 the change in ozone was quite different above and below ~20 hPa (see Figure 3-2(b)). In the upper stratosphere ozone is projected to increase, with the largest increase of around 1.5 ppm occurring near 3 hPa for the multi-model mean. In contrast, lower stratospheric ozone is projected to decrease, consistent with earlier studies (WMO, 2007; Eyring et al., 2007). In both regions the rate of change in ozone is fairly constant through the 21st century (see for example Figure 9.4 of SPARC CCMVal, 2010). The projected increase in upper stratospheric ozone was found to be related mainly to a decrease in halogen concentrations (see Figures 3-2(c) and (d)) and GHG-induced cooling (see Figures 3-2(e) and (f)). These two mechanisms made roughly equal contributions to the ozone increase over the 21st century under the SRES A1B GHG and A1 adjusted halogen scenarios (Chapter 9 of SPARC CCMVal, 2010). In WMO (2007) and in the studies of Shepherd and Jonsson (2008), Jonsson et al. (2009), and Waugh et al. (2009), similar conclusions were reached based on single models. Figure 3-7 shows the results of a regression of global mean ozone concentration onto changes in ODS and CO₂ heating rates in simulations of the CMAM (Jonsson et al., 2009). Note that the change in ozone associated with future changes in GHG amounts is expected to be somewhat larger than that associated with future temperature changes, since some future GHG-induced cooling is balanced by ozone-induced warming (Shepherd and Jonsson, 2008). In the tropical lower stratosphere, the primary mechanism causing long-term changes in ozone is the increase in tropical upwelling through the 21st century, which is a robust feature in the CCM simulations (Chapters

Figure 3-6 (at left). 1980 baseline-adjusted multi-model trend estimates of annually averaged total column ozone (DU; left) and Cl_y at 50 hPa (ppb; right) for the tropics (25°S–25°N, upper row) and midlatitudes (middle row: 35°N–60°N, lower row: 35°S–60°S) (thick dark gray line) with 95% confidence and 95% prediction intervals appearing as light- and dark-gray shaded regions, respectively, about the trend (note the different vertical scale among the panels). The baseline-adjusted individual model trends are also plotted (colored lines). The red vertical dashed line indicates the year when the multi-model trend in total column ozone (left) and Cl_y at 50 hPa (right) returns to 1980 values and the blue vertical dashed lines indicate the uncertainty in these return dates. The black dotted lines in the left panels show observed total column ozone, where a linear least squares regression model was used to remove the effects of the quasi-biennial oscillation, solar cycle, El Niño-Southern Oscillation, and volcanoes from four observational data sets. 2σ uncertainties on the observations were derived by applying the regression model to 10,000 statistically equivalent time series obtained from Monte Carlo resampling of the regression model residuals. The observations include ground-based measurements (updated from Fioletov et al., 2002), merged satellite data (Stolarski and Frith, 2006), the National Institute of Water and Atmospheric Research (NIWA) combined total column ozone database (Bodeker et al., 2005), and Solar Backscatter Ultraviolet (SBUV, SBUV/2) retrievals (updated from Miller et al., 2002). The observational time series is shifted vertically so that it equals 0 in 1980. See Table 3-1 for model descriptions. Redrawn from Figures 9.2, 9.7, 9.8, and 9.9 of SPARC CCMVal (2010) and updated with two new CCM simulations.

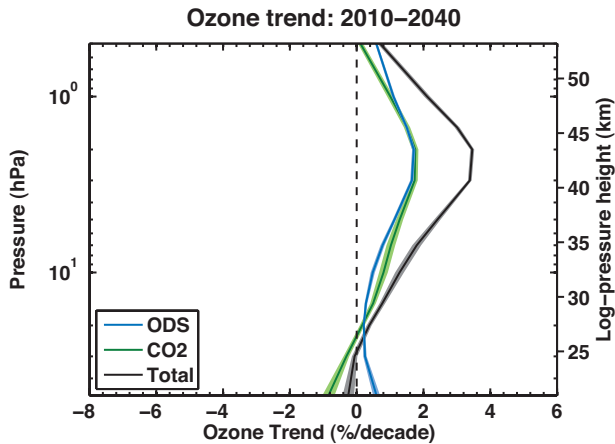


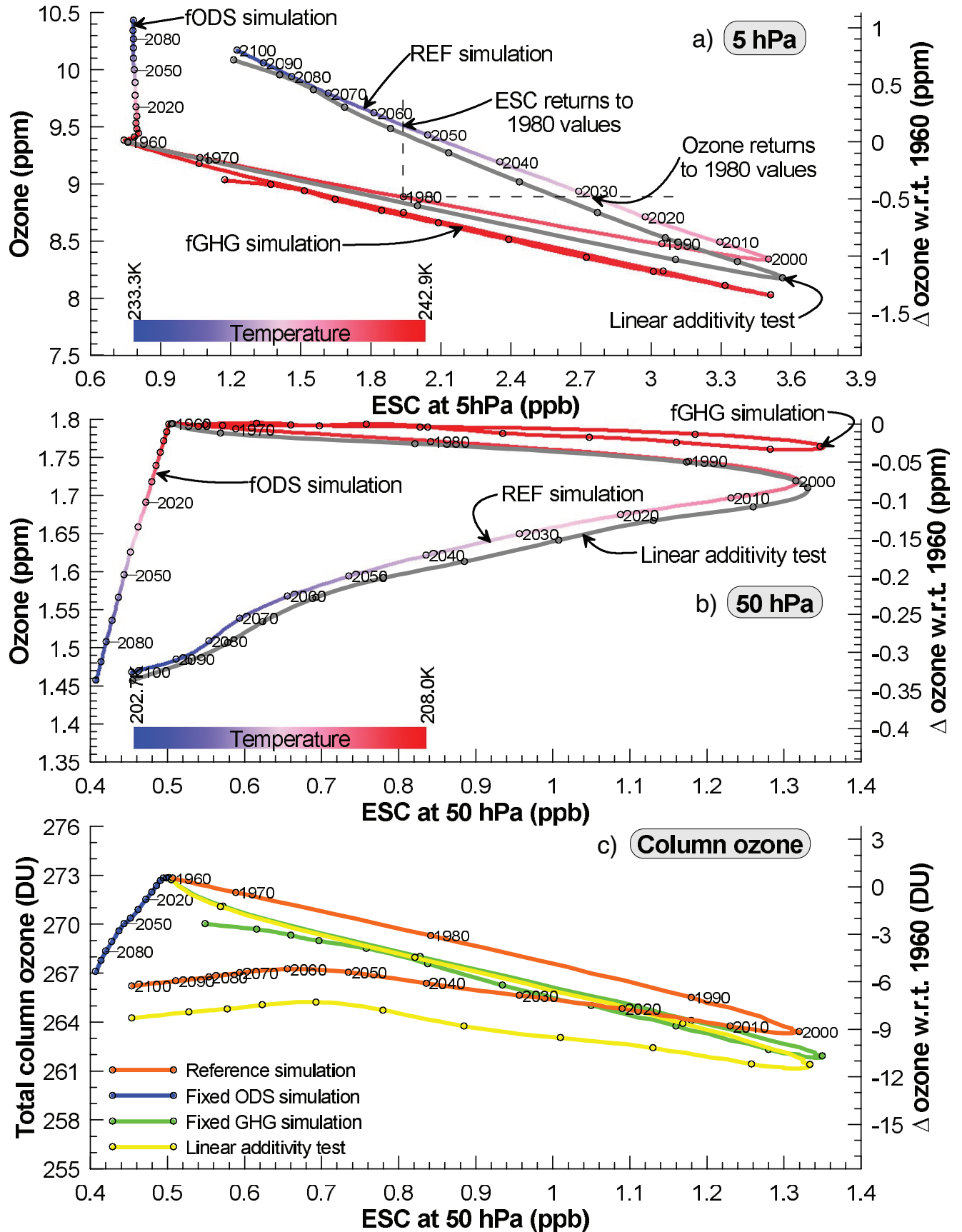
Figure 3-7. Attribution of future (2010–2040) global mean ozone changes over 50–0.5 hPa using simulations from the Canadian Middle Atmosphere Model (CMAM). The simulated ozone mixing ratio trend (%/decade) is shown in black while the contributions from CO₂ and ODSs changes to the ozone trend are shown in green and blue, respectively (note the ODS contribution is estimated from the upper stratospheric Cl_y). The gray shaded areas indicate the 99% confidence intervals for the linear fits to the ensemble average time series. The green and blue shaded regions indicate the uncertainty in the CO₂ and ODS attribution estimates, derived from the 99% confidence intervals for the fitted CO₂, ODS, ozone, and temperature linear trends. Adapted from Jonsson et al. (2009).

4 and 9 of SPARC CCMVal 2010; Eyring et al., 2010a). This increase in upwelling in the tropics ultimately leads to

a decrease in ozone levels in the tropical lower stratosphere, where ozone levels are mostly determined by a balance between the rate of ozone production and the ascent rate (see Section 3.2.4.1). Because GHG increases are projected to increase ozone in the tropical upper stratosphere, but decrease ozone in the tropical lower stratosphere, if or when ozone returns to historical levels (e.g., to the amounts of ozone observed in 1960 or 1980) will vary between these altitudes (see Section 3.3.6).

The attribution of ozone changes in the tropical upper and lower stratosphere, as well as in the total column, to changes in ODSs and GHGs from four CCMs analyzed by Eyring et al. (2010a) is shown in the correlative time series plots (i.e., plots showing the temporal evolution of the correlation between ozone and ESC) in Figure 3-8. The construction and evaluation methods for this figure and Figure 3-10 are described in Appendix 3A. The reference simulations show ozone decreasing from 1960 to 2000 in the upper stratosphere in response to increasing ESC. However, as ESC decreases from 2000 to 2100 ozone does not simply retrace the 1960 to 2000 path but is systematically elevated through the 21st century such that ozone returns to 1980 values in the late 2020s, well before ESC returns to its 1980 value in the mid-2050s. The elevated ozone through the 21st century results from GHG-induced stratospheric cooling (see Section 3.2.3) indicated by the red to blue transition from 1960 to 2100 in the reference trace in Figure 3-8(a), with a possible contribution from GHG-induced changes in transport. The fixed ODS simulation shows ozone in the upper stratosphere slowly increasing with time under the influence of GHG-induced stratospheric cooling. In contrast to the reference simulation, the fixed GHG simulation shows that the response of ozone to ESC through the 21st century is almost identical to that through the 20th century. In this simulation, because GHGs are fixed, temperatures show almost no

Figure 3-8 (at right). Correlative time series plots for 5 hPa, 50 hPa, and column ozone amounts (parts per million or Dobson units, left axis; ppm or DU change with respect to 1960, right axis) averaged between 25°S and 25°N as extracted from the CCM multi-model trend time series (see Appendix 3A-1). (a) Annual mean tropical ozone as a function of ESC = Cl_y + 5×Br_y (in parts per billion) at 5 hPa. (b) As in panel (a) but at 50 hPa and with ESC = Cl_y + 60×Br_y. In panels (a) and (b) the REF, fixed ODSs (fODS), and fixed GHGs (fGHG) simulations (see Table 3-2) are shown using traces colored according to the multi-model-mean temperature using the scale shown in the bottom left of each panel. The gray traces in these two panels show the additive effects of the fODS and fGHG simulations calculated from: Gray_{ESC}(*t*) = fGHG_{ESC}(*t*) + fODS_{ESC}(*t*) – fODS_{ESC}(1960) and Gray_{ozone}(*t*) = fGHG_{ozone}(*t*) + fODS_{ozone}(*t*) – fODS_{ozone}(1960). Differences between the gray and REF traces indicate a lack of linear additivity in the system. Panel (c), as in (b) but for total column ozone and without color coding by temperature. In this panel the linear additivity test trace is shown in yellow (yellow = blue + green). In all three panels, on each trace, reference years are shown every 10th data point with year labels shown for the REF and fODS simulations. The multi-model mean is derived from three CCMs in panel (a) (CCSRNIES, CMAM, and MRI) and four CCMs in panel (b) and (c) (CCSRNIES, CMAM, MRI, and WACCM). See Table 3-1 for model descriptions. From Eyring et al. (2010a), their Figure 4.



trend from 1960 to 2100. The close agreement between the REF and gray traces (the sum of the ozone changes due to only the effect of ODSs (fGHG) and due to only the effects of GHGs (fODS)) in Figure 3-8(a) indicates that the system is close to being linearly additive (i.e., the two effects can be considered separately). The system deviates most from linear additivity around the turn of the century when ODS abundances and ozone depletion are close to their maximum. This may result from the fact that the fODS simulations are forced by SSTs taken from coupled climate model simulations where the radiative forcing effects of the varying ODS levels were included. As a result, even though ODS levels are kept fixed at 1960 values in the fODS simulations, the radiative effects of the varying ODSs could be partly felt through the SSTs.

Eyring et al. (2010a) found that in the tropical lower stratosphere (Figure 3-8(b)), ozone shows little response to ESC through the 20th and 21st centuries, as seen from the fGHG trace. The ~25% decrease in ozone from 1960 to 2100 in the reference simulation results from GHG-induced changes to stratospheric dynamics as discussed above and confirmed by the fixed ODS simulation. Note also that in the fixed ODS simulation, ESC decreases with time in response to these circulation changes. As in the upper stratosphere, the response of ozone to ODSs and GHGs is again almost linearly additive as shown by the close agreement between the REF and gray traces in Figure 3-8(b). The ozone decreases simulated in the tropical lower stratosphere dominate the increases in the tropical upper stratosphere such that tropical total column ozone (Figure 3-8(c)) remains suppressed below what would be expected from changes in ESC from 2000 onwards. Interestingly, unlike ozone at 5 and 50 hPa in the tropics, total column ozone shows deviations away from linear additivity demonstrated by the lack of coincidence of the orange and yellow traces in Figure 3-8(c).

3.3.4 Midlatitude Ozone

3.3.4.1 LONG-TERM PROJECTIONS OF MIDLATITUDE OZONE

Figure 3-6 panels (c) to (f) show projections of 21st century midlatitude (35°N–60°N and 60°S–35°S) column ozone and Cl_y at 50 hPa (Austin et al., 2010a; Eyring et al., 2010a; Chapter 9 of SPARC CCMVal, 2010). The 50 hPa level was chosen as a representative level of future ozone changes in the lower stratosphere in the tropics, midlatitudes, and polar regions (see for example Figure 3-2(b) and Figure 3-9(b)). In the multi-model trend, in both hemispheres, minimum total column ozone is reached around the turn of the century, followed by a steady and significant increase. By 2025, northern (southern) midlatitude

total column ozone is projected to have regained 130% (70%) of the amount lost between 1980 and 2000 (2002) and 230% (145%) of this loss regained by 2050 (see Table 3-3). In other words, by 2050, midlatitude total column ozone in both hemispheres is projected to lie above 1980 levels. By 2100, the column ozone in the northern (southern) midlatitudes is projected to have increased by 22 DU (19 DU) compared to 1980 amounts (Table 3-3).

As noted by Austin et al. (2010a), the midlatitude column ozone broadly follows the behavior of Cl_y at 50 hPa (compare left and right panels of Figure 3-6) but with the ozone returning, on average, to 1980 levels 28⁺⁵ and 15 ± 5 years in advance of the chlorine for the northern and southern midlatitudes, respectively. For chlorine, there is, on average, no significant interhemispheric differences in the timing of the return to 1980 levels. Austin et al. (2010a) concluded that the earlier return of ozone to 1980 amounts in the Northern Hemisphere was mainly due to stronger transport from low latitudes, which was also noted in the independent studies of Shepherd (2008) and Li et al. (2009).

3.3.4.2 PROCESSES DETERMINING FUTURE MIDLATITUDE OZONE

Chapter 9 of SPARC CCMVal (2010) found in all simulations analyzed that the increase in the midlatitude total column ozone resulted from ozone increases throughout the stratosphere. The increase in the upper stratosphere peaks in volume mixing ratio at ~3 hPa in both hemispheres (see Figures 3-9(a) and (b)). This in turn was the result of the combined effects of (i) a decline in Cl_y (Figures 3-9(c) and (d); see also Figures 3-6(d) and (f)) and Br_y and, (ii) the GHG-induced cooling of the middle and upper stratosphere (Figures 3-9(e) and (f)). The relative importance of the factors affecting ozone can be different under a different GHG scenario (see Section 3.3.6). In a separate single model study, Waugh et al. (2009) also found that GHG-induced cooling of the middle and upper stratosphere was an important process for midlatitude ozone evolution in the 21st century under the SRES A1B scenario. For the northern midlatitudes, Li et al. (2009) estimated that by the 2060s stratospheric cooling, together with increased poleward transport by the BDC, increased the extratropical column ozone in the model analyzed by Waugh et al. (2009) by up to 6% compared to 1980 amounts. A smaller increase of 3% in the southern midlatitudes resulted from the smaller increase in transport in that hemisphere, consistent with the findings of Austin et al. (2010a). In both hemispheres the largest increase occurred at 60°. Chapter 9 of SPARC CCMVal (2010) found that the projected evolution of midlatitude middle and upper stratospheric ozone was very similar to that in the tropics in terms of the magnitude of the changes (compare Figures 3-2(b) and

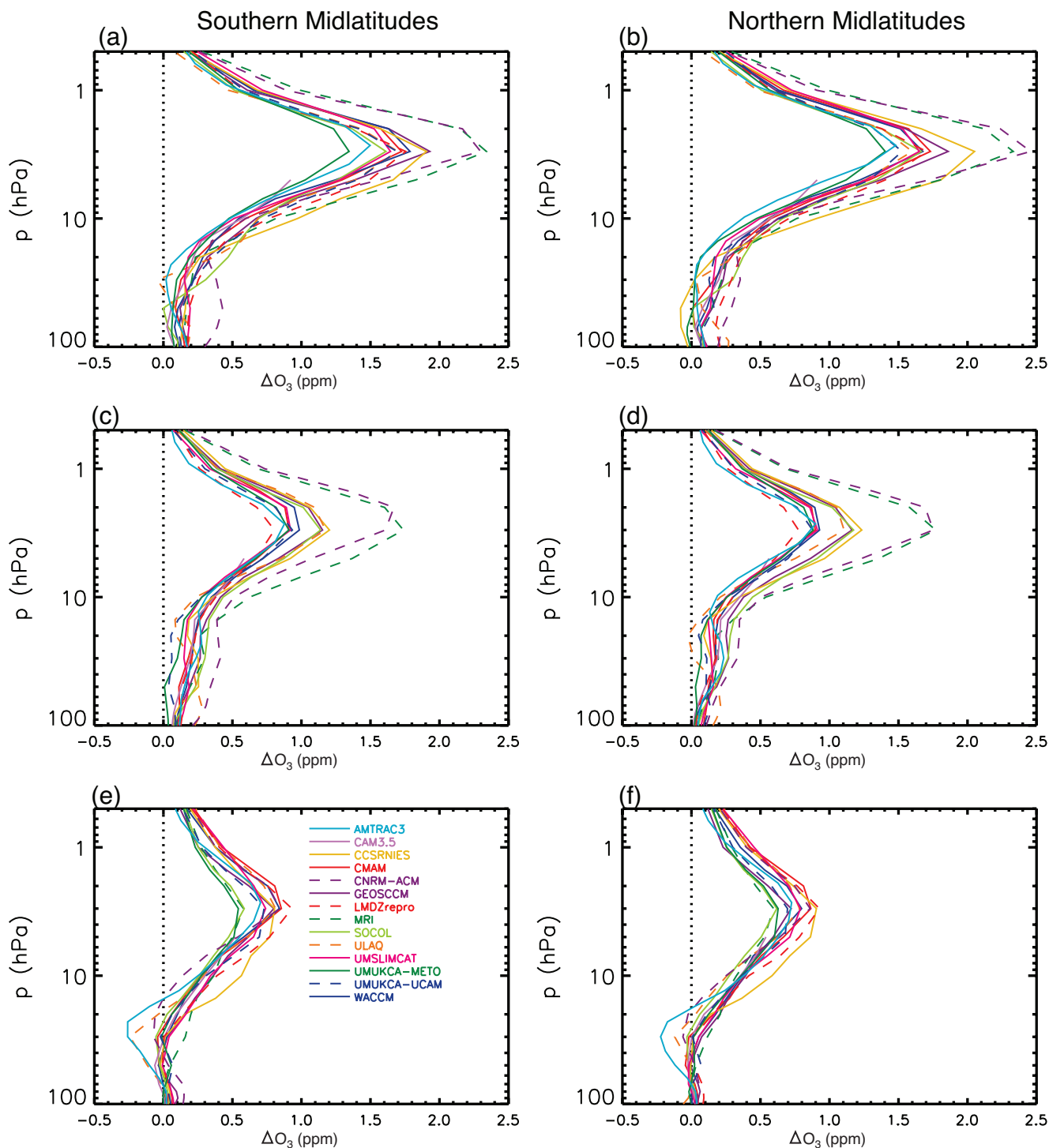


Figure 3-9. Vertical profiles of differences in midlatitude (30° – 50°) ozone (parts per million) over the 21st century based on a Multiple Linear Regression (MLR). Leftmost panels are for southern midlatitudes and rightmost panels for northern midlatitudes. (a) and (b) net change in the ozone profile from 2000 to 2100. (c) and (d) ozone changes congruent with changes in ESC. (e) and (f) ozone changes congruent with changes in temperature. See Table 3-1 for model descriptions. From Chapter 9 of SPARC CCMVal (2010), their Figure 9.10 (a)-(f).

3-9). In the lower stratosphere the evolution of midlatitude ozone differed from that in the tropics. However, in midlatitudes the increase in the residual meridional circulation leads to an increase in ozone rather than a decrease (Shepherd, 2008; Li et al., 2009).

An attribution of total column ozone changes in the northern and southern midlatitudes to changes in ODSs and GHGs from five CCMs analyzed by Eyring et al. (2010a) is shown in the correlative time series plot in panels (b) and (c) of Figure 3-10. The reference simulations show that total column ozone decreases from 1960 to 2000, but at a greater rate over southern midlatitudes than over northern midlatitudes. Over northern midlatitudes, ozone shows a -7 DU/ppb sensitivity to ESC over the 1960 to 2000 period, in general agreement with the results reported in Guillas et al. (2004). Over southern midlatitudes the sensitivity is -16 DU/ppb. The heightened sensitivity of total column ozone to ESC in the Southern Hemisphere most likely does not result from differences in the in situ contribution of ESC to southern midlatitude ozone destruction, but rather from the effects of export of ozone-depleted air from the Antarctic ozone hole. Because the multi-model trends shown in Figure 3-10 include fewer models than the multi-model trends displayed elsewhere, the quantitative values listed above are less certain than would be the case otherwise. A comparison of the reference and fixed GHG simulations for the midlatitudes shows that increasing GHGs have elevated ozone throughout the period. In both hemispheres, as ESC decreases, total column ozone does not simply retrace the 1960–2000 path, but shows systematically elevated ozone through the 21st century. As a result, over northern midlatitudes, total column ozone returns to 1980 values in the mid-2020s, well before ESC returns to its 1980 value around 2050. Similarly, over southern midlatitudes total column ozone returns to 1980 values in the mid-2030s (a decade later than in the northern midlatitudes), and well before ESC returns to its 1980 value around 2050. From the fixed ODS simulation (blue traces in Figure 3-10), it is clear that the elevated ozone through the 21st century results from GHG-induced stratospheric cooling and changes in transport, in particular changes in the strength of the BDC (see Figure 3-3). These simulations also show ESC decreasing with time even though ODSs are fixed at 1960 values. This likely results from the increasing strength of the BDC through the 21st century (Section 3.2.4.1) and a resultant decrease in the time available to photolyze ODSs. It is also clear from the reference and fixed ODS simulation traces in Figure 3-10 that by 2100, total column ozone over midlatitudes is still influenced by ESC. In both the northern and southern midlatitudes the effects of ODSs and GHGs on ozone are approximately additive (agreement of black and yellow traces in Figures 3-10(b) and (c) in the multi-model trend.

3.3.5 Polar Ozone

3.3.5.1 LONG-TERM PROJECTIONS OF POLAR OZONE

The largest ozone depletion seen in CCM simulations based on the SRES A1B GHG and A1 adjusted halogen scenarios occurs in the polar lower stratosphere, especially over Antarctica where large modeled ozone losses give rise to a springtime Antarctic ozone hole, consistent with observations. As a result, a major focus is the projected evolution of polar lower stratospheric ozone during spring.

Figure 3-11 shows the evolution of the individual model and multi-model trend estimates of total column ozone (left panels) and lower stratospheric inorganic chlorine (Cl_y) (right panels), for March in the Arctic (60°N – 90°N) and October in the Antarctic (60°S – 90°S) from the 17 CCMs analyzed by Eyring et al. (2010a). In both polar regions, the long-term evolution of total column ozone is qualitatively the same as in other regions. There is a broad minimum around 2000 followed by a slow increase until the end of the 21st century. There are, however, as in the extrapolar regions, significant quantitative differences among the models, including a wide spread in minimum values over Antarctica around 2000. Austin et al. (2010a) and Chapter 9 of SPARC CCMVal (2010) indicate that the spread between the individual model simulations of Antarctic total column ozone increased from CCMVal-1 to CCMVal-2, while no change was seen for the Arctic. However, when adjusting the raw data to a common 1980 baseline by removing the individual offset values with the TSAM method (Section 3.3.2.2), the model spread is considerably reduced.

In the Antarctic, the strongest ozone depletion in the October mean multi-model trend is simulated in 2003 (see Table 3-3). The minimum in the October multi-model trend total column ozone is about 80 DU lower than the 1980 value. For the Arctic, the largest total column ozone depletion simulated in March 2002 is $\sim 30\%$ of the Antarctic depletion simulated in October 2003 (Figure 3-11, left panels). Arctic spring ozone returns earlier to historical values than Antarctic spring ozone. Arctic total column ozone is projected to regain 95% (75–115%)¹ of the amount lost between 1980 and 2002 by 2025. Arctic column ozone is simulated to increase to 46 DU above 1980 values by the end of the 21st century, which is equivalent to an increase in column ozone of twice the amount lost between 1980 and 2002 (see Table 3-3). In Antarctica, 45% (35–55%) of the ozone lost since 1980 is projected to be replenished by 2025, and 100% (85–110%) by 2050. By the end of the 21st century, Antarctic October ozone

¹ All quoted ranges are 95% confidence intervals.

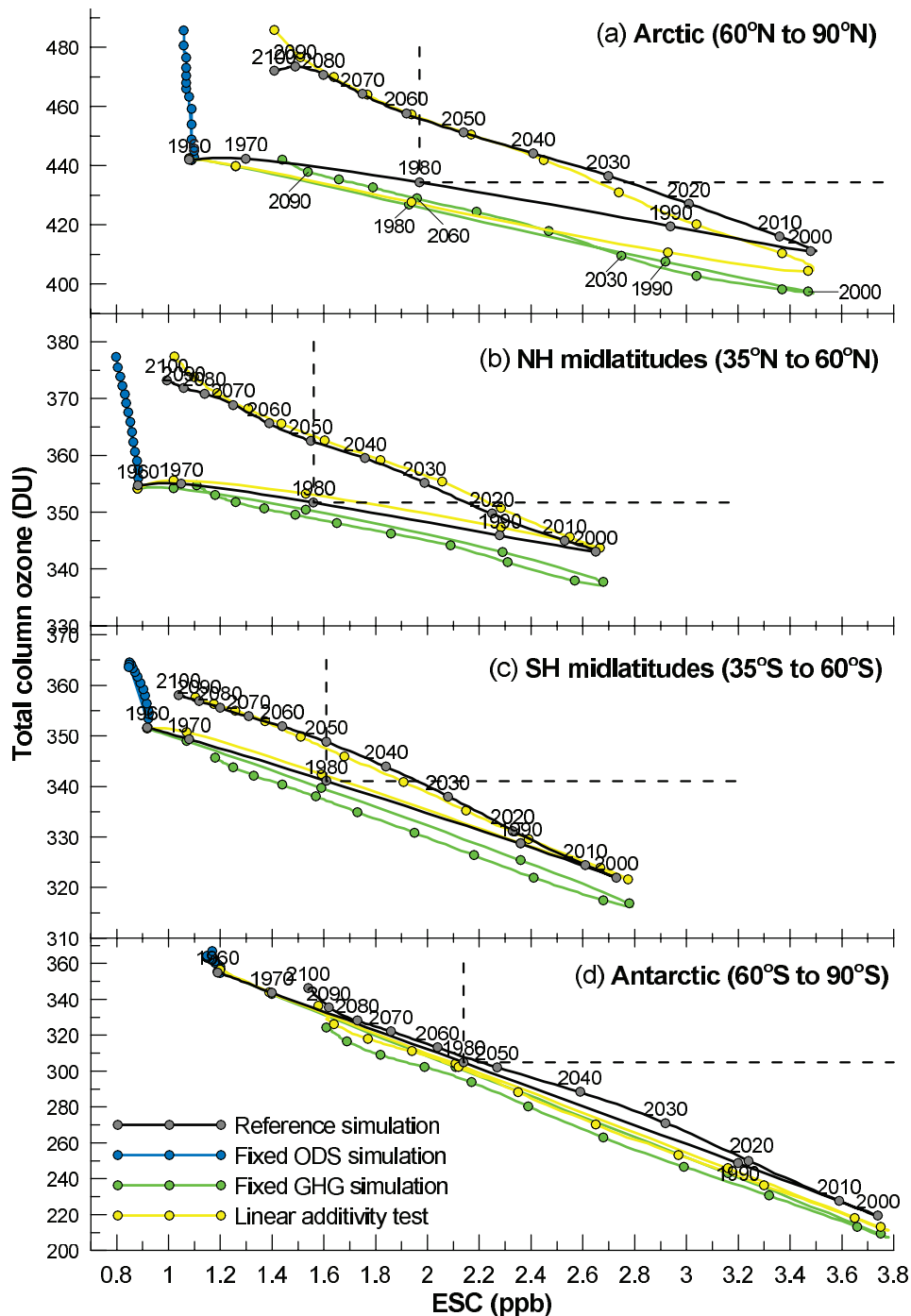


Figure 3-10. Correlative time series plots for total column ozone (Dobson units) averaged over different latitude ranges (Appendix 3A). (a) March means for the Arctic, (b) annual means for northern midlatitudes, (c) annual means for southern midlatitudes, and (d) October means for the Antarctic. ESC values are defined as $ESC = Cl_y + 60 \times Br_y$ at 50 hPa. The black trace shows the reference simulation with time-varying GHGs and ODSs with reference years shown every 10th data point. The blue trace shows results from a simulation where prescribed ODSs are fixed at 1960 values. The green trace shows results from a simulation where prescribed GHGs are fixed at 1960 values. The yellow traces show the additive effects of the fixed ODS and fixed GHG simulations (yellow = blue + green) as in Figure 3-8. Differences between the black and yellow traces indicate a lack of linearity in the system. The multi-model trend estimate is derived from five CCMs (CCSRNIES, CMAM, MRI, ULAQ, and WACCM; see Table 3-1). From Eyring et al. (2010a), their Figure 7.

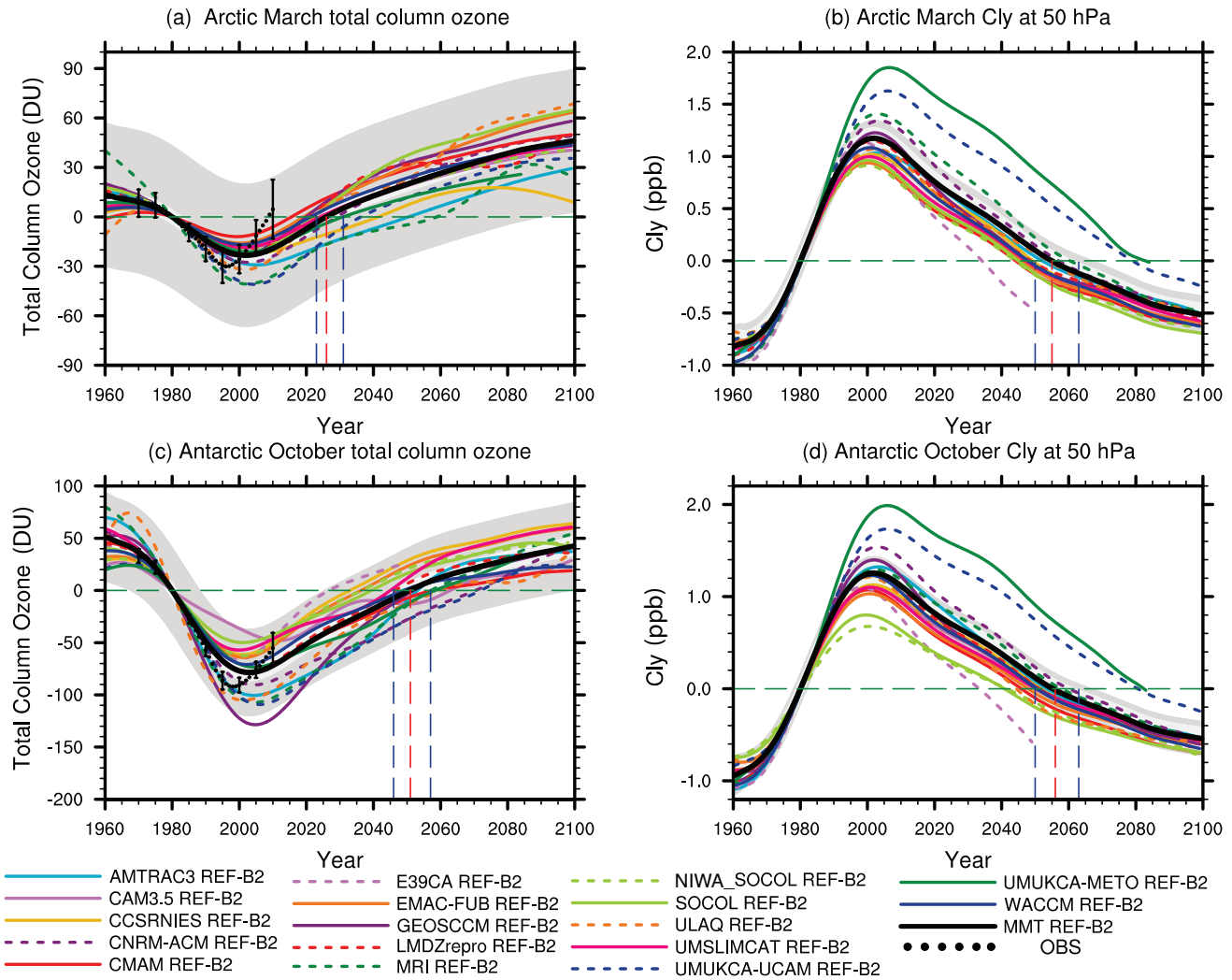


Figure 3-11. As in Figure 3-6, but for the latitude range 60°N – 90°N in March (upper row) and the latitude range 60°S – 90°S in October (lower row). The red vertical dashed line indicates the year when multi-model trend in total column ozone (DU; left) and Cl_y at 50 hPa (ppb; right) returns to 1980 values and the blue vertical dashed lines indicate the uncertainty in these return dates. Note the different vertical scale among the panels. Redrawn from Figures 9.11, 9.12, 9.13, and 9.14 of SPARC CCMVal (2010) and updated with two new CCM simulations.

is projected to be 43 DU above 1980 levels (compare to 78 DU decrease from 1980 to 2003). However, by 2100, October mean ozone is still projected to be 9 DU lower than in 1960 (95% of the 1960–2003 loss replenished) consistent with slightly enhanced ESC in 2100 compared to 1960.

Several different indices have been defined and applied in previous assessments to quantify variations in Antarctic ozone, in terms of the area of the ozone hole, the polar cap average ozone, the ozone mass deficit (Bodeker et al., 2005), or the daily minimum total column ozone in spring (WMO, 2007). Figure 3-12 (upper panel) shows the simulated and observed ozone hole areas, based on the

size of the area with column ozone less than 220 DU, from 17 CCMVal-2 simulations (Austin et al., 2010b; Chapter 9 of SPARC CCMVal, 2010). While a few models capture the observed size of the Antarctic ozone hole reasonably well, the models on average underestimate the observed ozone hole area by about 20% (Austin et al., 2010b). This value is similar to that found for the CCMVal-1 simulations (Eyring et al., 2006). It reveals that, although some of the CCMs have been improved since CCMVal-1, others have become worse, and no fundamental improvement was achieved for the majority of the models. The projected date when the Antarctic ozone hole will disappear varies from the 2020s in models with small ozone holes to

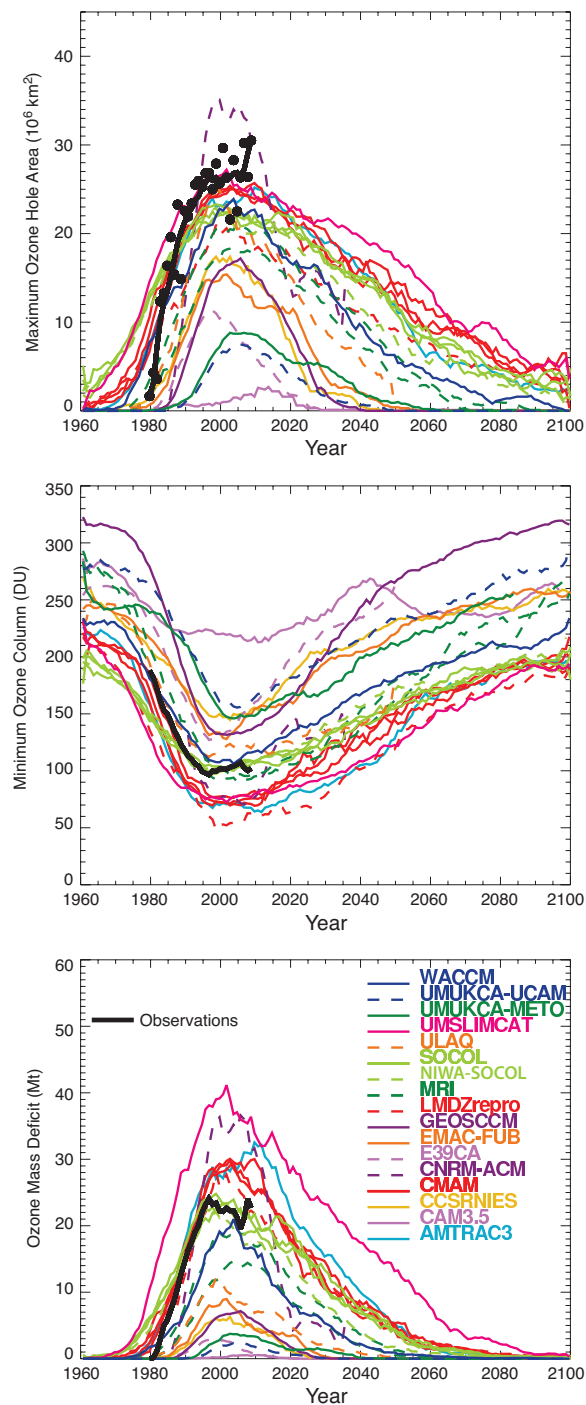


Figure 3-12. Simulated and observed ozone hole areas, based on a fixed 220 DU amount (upper panel), minimum Antarctic spring total ozone column (middle panel), and ozone mass deficit (lower panel) for the period 1960–2100, calculated from the CCMVal-2 REF-B2 simulations. The curves indicate 11-year running means of the data for individual years. See Table 3-1 for model descriptions. From Austin et al. (2010b), their Figures 4(a), 6, and 9.

the end of the simulation period in 2100 for those models that agree best with the observed ozone hole areas in the past. Even with some outliers removed, Antarctic spring ozone depletion below 220 DU is projected to still occur in a broad range between 2060 to 2100, or later. As discussed in Austin et al. (2010b), the representation of the ozone hole area in individual models depends on the definition used. For example, the use of an ozone isoline to define the ozone hole area (e.g., the 220 DU contour) in models that have a high or low ozone bias results in ozone hole areas that are systematically low or high, respectively, even if the models have realistic interannual and long-term variations. Calculating total column ozone changes relative to the 1960–1965 ozone mean leads to an improvement of the simulated ozone hole area in some models. These models have a general high ozone bias. Other models perform better when the steepest ozone gradient is used to define the edge of the ozone hole. This diagnostic identified some models where the simulated Antarctic polar vortices are too small in area compared to observations, which would also limit the size of their ozone holes (Bodeker et al., 2002). In general, most consistent results among the models are achieved when the steepest gradients are used. However, independent of the applied index for the ozone hole area, most CCMs have ozone holes that are significantly smaller than observed, by up to 30%. With the large spread between the individual CCM simulations of the Antarctic ozone hole and its likely dependence on the applied definition for the ozone hole, quantitative projections of the disappearance of the ozone hole remain uncertain.

The minimum spring ozone, calculated from Antarctic daily mean ozone from September to November (Figure 3-12, middle panel), shows a wide range of ozone values, from one model that does not fall below the 220 DU ozone hole threshold value to models with lower than observed ozone minima. Most models simulate the lowest ozone minima for the most recent years and suggest an increase of minimum ozone starting around 2010, which agrees well with projections in WMO (2007). Only models with a high ozone bias exceed the 220 DU limit by the end of the 21st century, while models that represent well or underestimate past ozone compared to observations, do not predict a return to minimum ozone values above 220 DU before 2100.

The ozone mass deficit, defined as the mass of ozone required to elevate column ozone everywhere over Antarctica to 220 DU, averaged over the months of September and October (Bodeker et al., 2005) (Figure 3-12, lower panel) is a sensitive diagnostic as it reflects how well the CCMs simulate the ozone hole area and the minimum ozone. Austin et al. (2010b) show that models that capture the observed size of the ozone hole area typically simulate lower than observed Antarctic ozone spring

minima, in contrast to models with smaller ozone holes that typically show higher than observed Antarctic ozone spring minima. Both errors contribute to a large spread in the ozone mass deficit of the models for the past and future. The models suggest that the ozone mass deficit should not increase any longer after about 2010; however, due to the sensitivity of this diagnostic, future projection of the ozone mass deficit is highly unreliable.

3.3.5.2 PROCESSES DETERMINING FUTURE POLAR OZONE

In both hemispheres, multi-model total column ozone in polar spring follows the evolution of Cl_y (Figure 3-11). Ozone starts to increase in the first decade of the 21st century at about the same time as the Cl_y abundances in the polar lower stratosphere have reached their maximum and begin to decline. Compared to CCMVal-1, the simulation of Cl_y , on average, has improved in the CCMVal-2 models due to improvements in individual CCMs (Austin et al., 2010a; Austin et al., 2010b; Chapter 9 of SPARC CCMVal, 2010); however, differences in Cl_y of up to 1 ppb in the polar lower stratosphere in October remain. These Cl_y differences, together with differences in the dynamical processes determining the strength of the stratospheric polar vortices and temperatures, cause the spread in simulated polar ozone.

The Cl_y concentrations in Figure 3-11 return to historical levels almost simultaneously in both hemispheres, while the ozone return dates show interhemispheric differences of more than two decades. As expected from the discussion in Section 3.2, this result implies that processes other than halogen chemistry affect the future evolution of polar ozone and that the relative impact of these processes varies with location. The relative contributions of ESC or increasing GHGs to the projected ozone change can be estimated by comparing the reference simulation with sensitivity simulations that use prescribed fixed historical abundances of GHGs or ODSs (Eyring et al., 2008). Waugh et al. (2009) compare a “climate change” simulation (i.e., using fixed ODS abundances for 1960) of the GEOSCCM with a reference simulation that accounts for GHG and ODS changes from 1960 to 2100. They find that in much of the stratosphere, the annual mean GHG-induced ozone increase from 1960–2100 is comparable to the ODS-induced ozone decrease for the period with highest ODS concentration (1995–2005). However, ozone in the Antarctic lower stratosphere is clearly dominated by ODS-induced destruction, and increases in GHG concentrations do not have a significant impact on Antarctic polar temperatures or ozone in their CCM. It should be noted that most studies of Antarctic ozone recovery focus on changes in October means. The effects of an extended polar vortex persistence, due to future GHG-induced cool-

ing and an associated seasonal delay of ozone recovery to November, on UV exposure has not been thoroughly assessed in multi-model studies.

Eyring et al. (2010a) found similar results in a multi-model framework using additional CCMVal-2 sensitivity simulations. As illustrated in Figure 3-10(d), reference simulations in the Antarctic show multi-model total column ozone decreasing from 1960 to 2000 with an average 53 DU/ppb sensitivity to ESC, leading to a 38% decrease in total column ozone over this period. Unlike the midlatitudes and Arctic, the total column ozone evolution over Antarctica in October shows almost no sensitivity to changes in GHGs, with the return path (21st century) closely tracking the outbound path (20th century). This is corroborated by the fixed ODS simulation, which shows almost no change in Antarctic ozone in October in response to increasing GHGs. If anything, increasing GHGs have slightly elevated Antarctic total column ozone in the model simulations. This updates earlier studies that predicted that increasing radiative cooling generated by increasing levels of GHGs or by GHG-induced stratospheric water vapor enhancements would worsen polar ozone depletion by increasing the likelihood for PSC formation, and might even create an ozone hole in the Arctic (Austin et al., 1992; Shindell et al., 1998; Kirk-Davidoff et al., 1999; Waibel et al., 1999). More recent research suggests that in the Arctic, GHG-induced changes in dynamics are expected to dominate the effects of GHG-induced radiative cooling on the formation of PSCs (Eyring et al., 2010a). In comparison, in the Antarctic, where the wintertime polar temperatures typically fall below the threshold for PSC formation, stratospheric cooling due to increasing GHGs does not strongly enhance October total column ozone depletion.

The multi-model trend of the reference simulations in the Arctic (Figure 3-10(a)) shows total column ozone decreasing from 1960 to 2000 with a -14 DU/ppb sensitivity to ESC, somewhat smaller than the -20 DU/ppb reported in observations (Dhomse et al., 2006). The increase in ESC from 1.1 ppb in 1960 to 3.5 ppb in 2000 leads to a 7.4% decrease in total column ozone over this period. In contrast to the Antarctic, total column ozone over the Arctic is elevated above what would be expected from changes in ESC. This most likely does not result from the effects of GHG-induced upper stratospheric cooling as in the tropics (Figure 3-8(a)) since, as discussed in Butchart et al. (2010), in the models the extra radiative cooling from increasing GHGs is approximately balanced by a concomitant increase in the adiabatic warming through increased polar downwelling. The net effect is a near-zero temperature trend in the Arctic winter lower stratosphere (Butchart et al., 2010; Figure 4.4 of SPARC CCMVal, 2010). The more likely cause is the strengthening of the BDC (Section 3.2.4.1), which more effectively advects ozone into

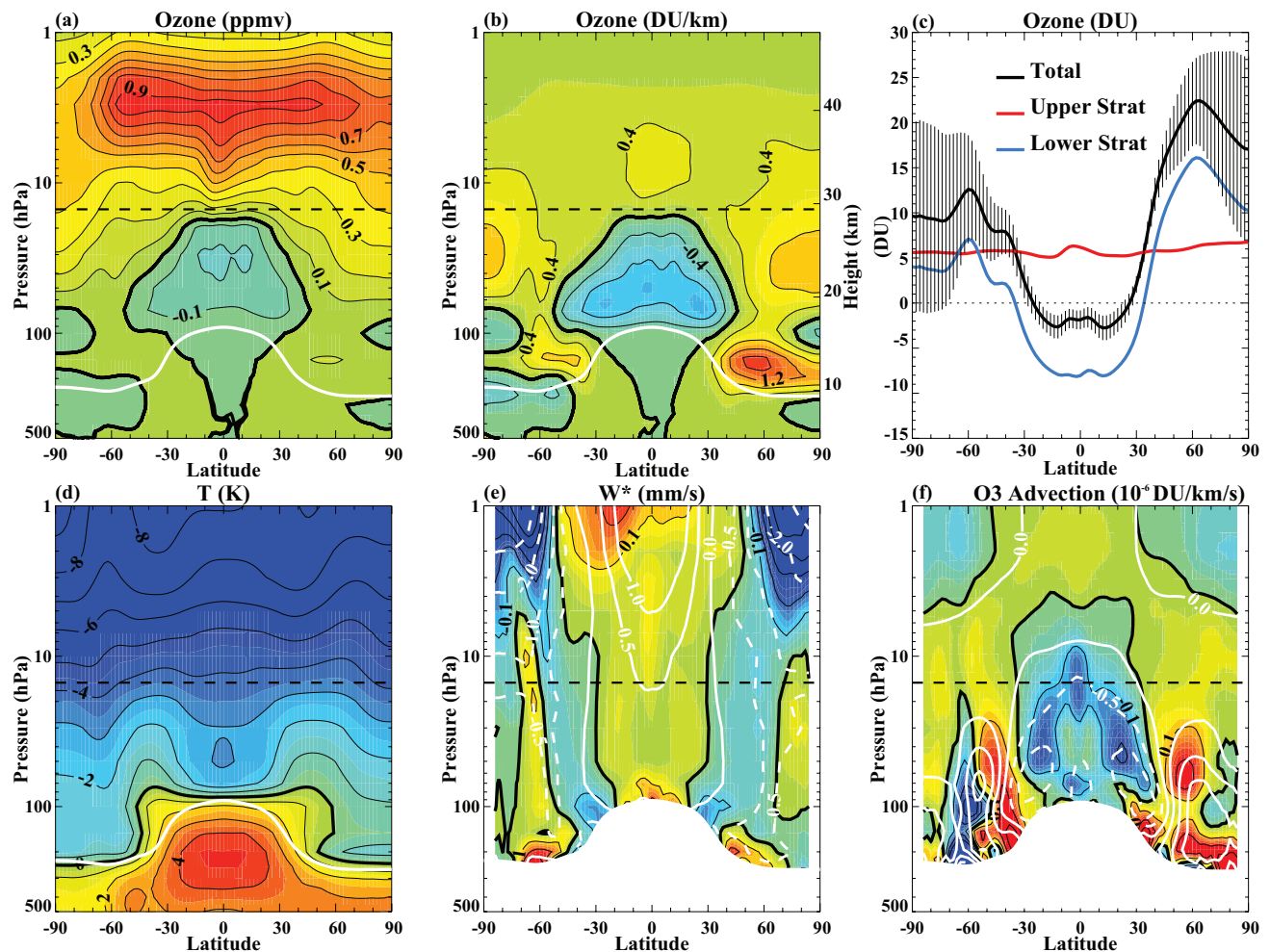


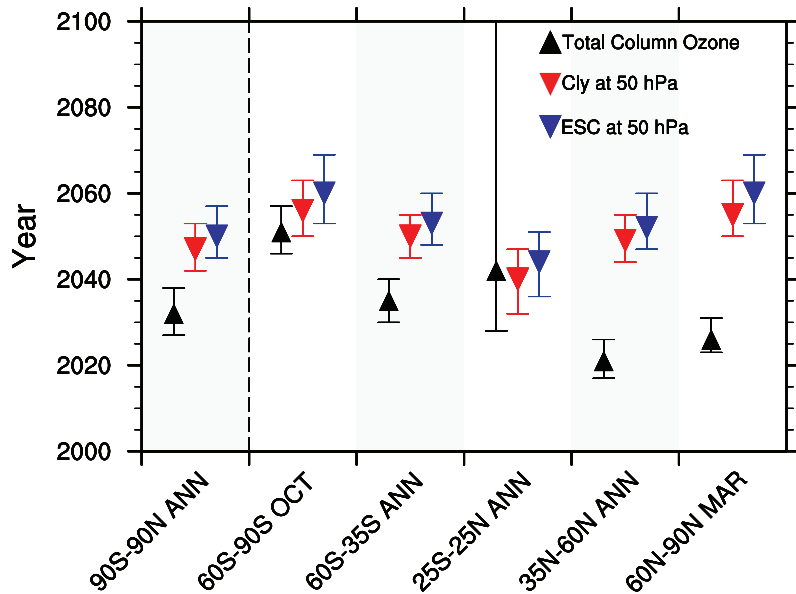
Figure 3-13. Annual mean, decadal differences between 2060–2069 and 1975–1984 from a simulation of the GEOS CCM with ODSs fixed at 1960 values. (a) Ozone concentrations in ppm, (b) ozone concentrations in DU/km, (c) total column ozone (DU) and contributions from the upper (above 15 hPa) and lower (below 15 hPa) stratosphere, (d) temperature (K) (e) Vertical residual velocity \bar{w}^* in mm/s, and (f) mean ozone advection (10^{-6} DU/km/s). From Li et al. (2009), their Figure 2.

the Arctic than the Antarctic stratosphere (Austin and Wilson, 2006; Shepherd, 2008). The effects of ODSs and GHGs on Arctic total column ozone appear to be largely independent and therefore add linearly as evidenced by the close agreement of the black and yellow traces in Figure 3-10(a).

Li et al. (2009) analyzed in more detail the effects of climate change on annual mean ozone by comparing the post-CFC era (2060–2069) with the period 1975–1984 in two simulations with the GEOS CCM. They found a uniform increase in ozone mixing ratio in the upper stratosphere (Figure 3-13(a)) that they ascribe to a slowing of photochemical ozone loss rates due to GHG-induced cooling (Figure 3-13(d)). However, the simulated changes in ozone column and their latitudinal structure are controlled

by changes in the lower stratosphere, where significant increases of column ozone are simulated at middle and high latitudes, specifically in the Northern Hemisphere (Figures 3-13(b) and (c)). They are associated with an acceleration of the Brewer-Dobson circulation in the model with increased tropical upwelling and extratropical downwelling (Figure 3-13(e)), leading to enhanced advective transport of ozone (Figure 3-13(f)). Although, in the annual mean, these dynamical effects are stronger at midlatitudes than at polar latitudes, the Li et al. (2009) study demonstrates that changes in ozone abundance and the mean advective transport have a qualitatively similar pattern in the lower stratosphere, and emphasizes the important role of changes in the mean advection for lower stratospheric ozone changes.

Figure 3-14. Date of return to 1980 total column ozone (black triangle and error bar), Cl_y at 50 hPa (red triangle and error bar), and ESC at 50 hPa (blue triangle and error bar) for the annual average (global, tropical, and midlatitude) and spring (polar) total ozone column derived from the multi-model trend of the CCMVal-2 reference simulations (17 CCMs) in each latitude band. The error bars on the multi-model trend estimate of return date are derived from the 95% confidence intervals. ESC is calculated as $Cl_y + 60 \times Br_y$ except for E39CA where Cl_y instead of ESC was used. While a few models project a return of tropical total column ozone to 1980 levels, most do not with the result that the 95% confidence interval extends from 2030 to beyond the end of the century which explains the large error bar in the tropical column ozone return dates. Redrawn from Figures 9.20 and 9.21 of SPARC CCMVal (2010) and updated with two new CCM simulations (from Eyring et al. (2010a), their Figure 10b).



3.3.6 Ozone Return Dates and Ozone Recovery

In this section, ozone return dates to levels typical of 1960 and 1980, derived from the CCM projections, are presented. These are complemented by quantitative statements about the expected date for full recovery of ozone from the effects of ODSs based on CCM simulations as described in Box 3-2. Specifically, a set of reference simulations and a set of fixed ODS simulations (as described in Section 3.3.1) are analyzed for the future date when the two sets of ozone projections are no longer statistically distinguishable within internal and inter-model variability (Eyring et al., 2010a). A Student t -test is applied to quantify the likelihood that, at some specified date, the ozone values taken from the two sets of simulations come from the same statistical population. The outcome of such tests is discussed using the terminology of the IPCC (see Box TS.1 of Solomon et al., 2007). For example a t -test result of >95% suggests that it is “extremely likely” that, within model variability, full ozone recovery from the effects of ODSs is projected to have occurred, if >90% it is “very likely,” while if >66% it is “likely” that it is projected to have occurred. For values between 33% and 66% probability, it is “about as likely as not” and for values <33% it is “unlikely” that full recovery of ozone is projected to have occurred.

The response to the question of when stratospheric ozone will return to undisturbed levels depends on the se-

lected target year. Figure 3-14 and Table 3-4 summarize 1960 and 1980 return dates of total column ozone in different latitude zones derived from the multi-model trend. Return dates generally occur later when referenced to 1960 and later at higher latitudes (Chapter 9 of SPARC CCMVal, 2010). However the increase is not symmetric about the equator, i.e., return dates are later in the Antarctic than in the Arctic.

CCM projections suggest that it is as likely as not that tropical total column ozone will return to 1980 values, since there is no consensus among the CCMs on a return to 1980 values by the end of the century (Austin et al., 2010a; Eyring et al., 2010a; Chapter 9 of SPARC CCMVal, 2010). Correspondingly, the uncertainty on tropical column ozone return dates derived from the 95% TSAM confidence interval extends from 2030 to beyond the end of the century in Figure 3-14. However, if instead of a return to 1980 values, a return to 1960 values is considered, models consistently predict that tropical total column ozone remains below values typical of 1960 due to the increase in tropical upwelling. In contrast, Cl_y and ESC (Table 3-5) in the tropics return to 1980 values faster than in all other regions with only minor differences between them. Full recovery of tropical column ozone from the effects of ODSs is not reached at the 95% confidence level by the end of the 21st century, while it is likely at the 65% level that total column ozone has fully recovered by ~2070 in the tropics (see Figure 3-15). In the tropical upper stratosphere, although ozone is influenced by ODSs throughout the 21st century, ozone returns to 1980 values

Table 3-4. Date of return to 1960 and 1980 total column ozone calculated from the multi-model trend estimate of the 17 CCMs' reference simulations.

Region	Date of Return	Year When Multi-Model Mean Total Column Ozone Returns	Year When Lower Bound of Error Bar Returns	Year When Upper Bound of Error Bar Returns
Global annual mean	1960	2053	2046	2064
	1980	2032	2027	2038
Tropics annual mean	1960	----	----	----
	1980	2042	2028	----
Northern midlatitude annual mean	1960	2029	2024	2036
	1980	2021	2017	2026
Southern midlatitude annual mean	1960	2055	2049	2064
	1980	2035	2030	2040
Antarctic October mean	1960	----	2100	---
	1980	2051	2046	2057
Arctic March mean	1960	2041	2036	2048
	1980	2026	2023	2031

in the late 2020s (Figure 3-8(a)), which is earlier than in other regions. Although ozone decreases continuously from 1960 to 2100 in the tropical lower stratosphere, together with the Arctic lower stratosphere, they are the only regions where ozone has very likely (i.e., more than 90% confidence level) fully recovered from the effects of ODSs by the end of the 21st century (Eyring et al., 2010a). How-

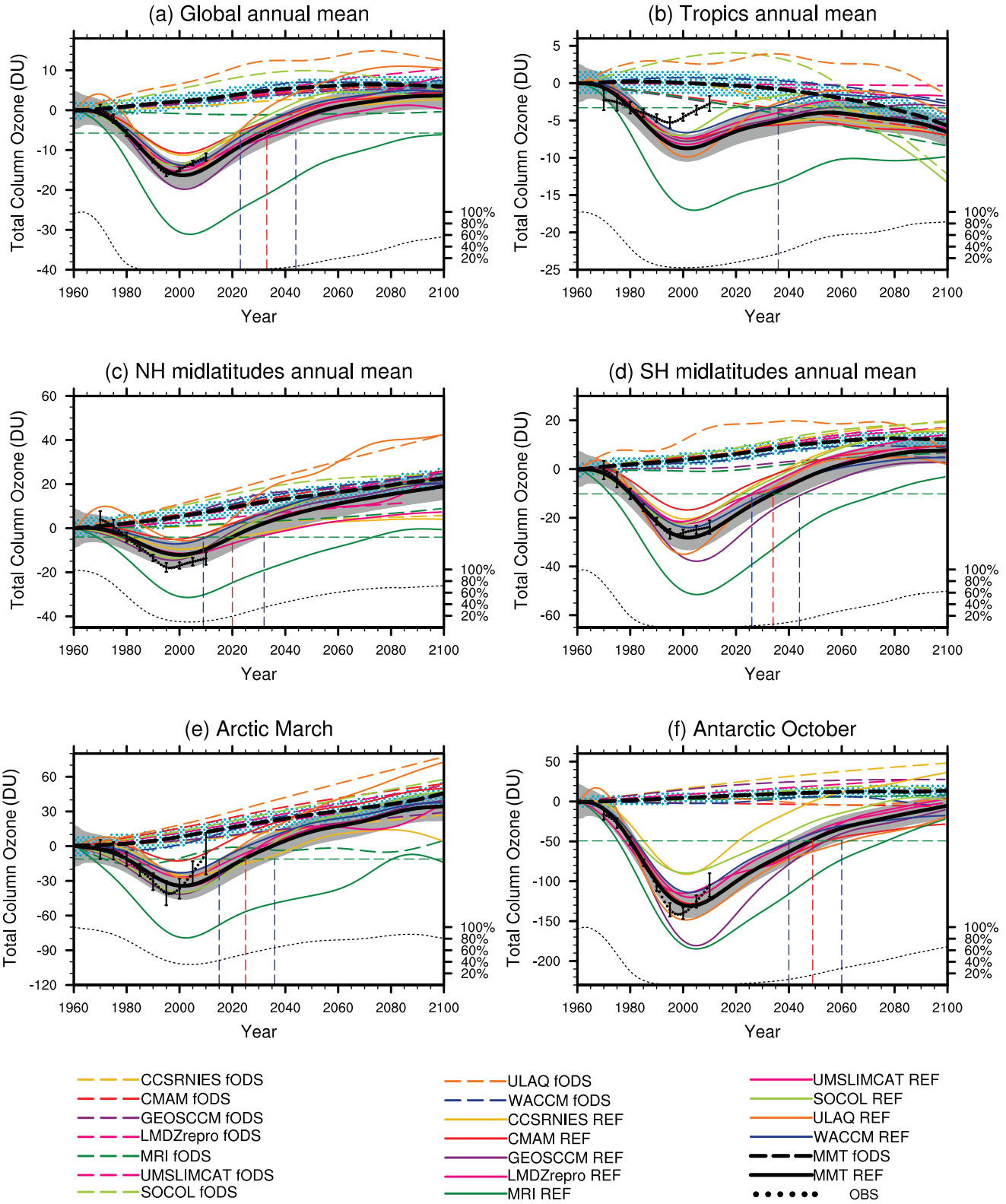
ever, in percentage terms, changes to the tropical ozone column over the 21st century are much smaller than those in other regions.

Of the five regions considered (see Table 3-4), total column ozone returns to 1980 values earliest over northern midlatitudes, around 2021 (2017–2026). While the total column ozone evolution is qualitatively similar

Table 3-5. Date of return to 1960 and 1980 ESC at 50 hPa calculated from the multi-model trend estimate of the 17 CCMs' reference simulations.

Region	Date of Return	Year When Multi-Model Mean ESC Returns	Year When Lower Bound of Error Bar Returns	Year When Upper Bound of Error Bar Returns
Global annual mean	1960	---	2092	---
	1980	2050	2045	2057
Tropics annual mean	1960	2087	2073	---
	1980	2044	2036	2051
Northern midlatitude annual mean	1960	---	---	---
	1980	2052	2047	2060
Southern midlatitude annual mean	1960	---	---	---
	1980	2053	2048	2060
Antarctic October mean	1960	---	---	---
	1980	2060	2053	2069
Arctic March mean	1960	---	---	---
	1980	2060	2053	2069

1960 Baseline-Adjusted Total Column Ozone (fODS)



over the midlatitudes of both hemispheres in the CCMs, southern midlatitude total column ozone returns to 1980 values later than over northern midlatitudes, i.e., around 2035 (2030–2040) (see Figure 3-14). The difference in the date of return to 1980 values appears to be due to interhemispheric differences in changes in transport. The increase in stratospheric circulation transports more ozone into the northern midlatitude lower stratosphere than into the southern midlatitudes (Shepherd, 2008). In addition, over southern midlatitudes, ozone is also influenced by ozone loss in the Antarctic, where the return to 1980 levels occurs much later. In all CCMs the return of ozone to 1980 values in the midlatitudes occurs 10 to 30 years earlier than that of Cl_y and ESC (around 2050 in both hemispheres). Nonetheless, by 2100 total column ozone over midlatitudes is still influenced by ODSs. Full recovery of total column ozone from ODSs has likely occurred in northern midlatitudes but not likely to have occurred over southern midlatitudes (Figure 3-15).

The Antarctic spring total column ozone evolution is dominated by the evolution of ODSs. Therefore, ozone, Cl_y , and ESC return dates are very similar in most models (Figure 3-14). The latest return of total column ozone to 1980 values is projected to occur over Antarctica which, for October means, occurs around 2051 (2046–2057), while 1960 values are not reached again before 2100 since Cl_y remains elevated above 1960 levels in 2100 (Figure 3-11(d)). In the Arctic, the sensitivity of the return date to the chosen baseline year (1960 or 1980) is small, with a return to 1980 ozone values around 2026 (2023–2031), and to 1960 values around 2041 (2036–2048). In contrast to the Antarctic, Arctic spring ozone returns earlier to 1980 values than Arctic chlorine, indicating that other effects such as changes in transport are more important for future ozone in the Arctic as is the case for northern midlatitudes

(Section 3.3.4.2). A return of stratospheric chlorine to the low values of 1960 does not happen in the polar regions before the end of the 21st century. It is unlikely that full ozone recovery from ODSs will be reached by the end of the 21st century over Antarctica, while it is likely that it will occur in the Arctic by ~2035 (Waugh et al., 2009; Eyring et al., 2010a) (see also Figure 3-15).

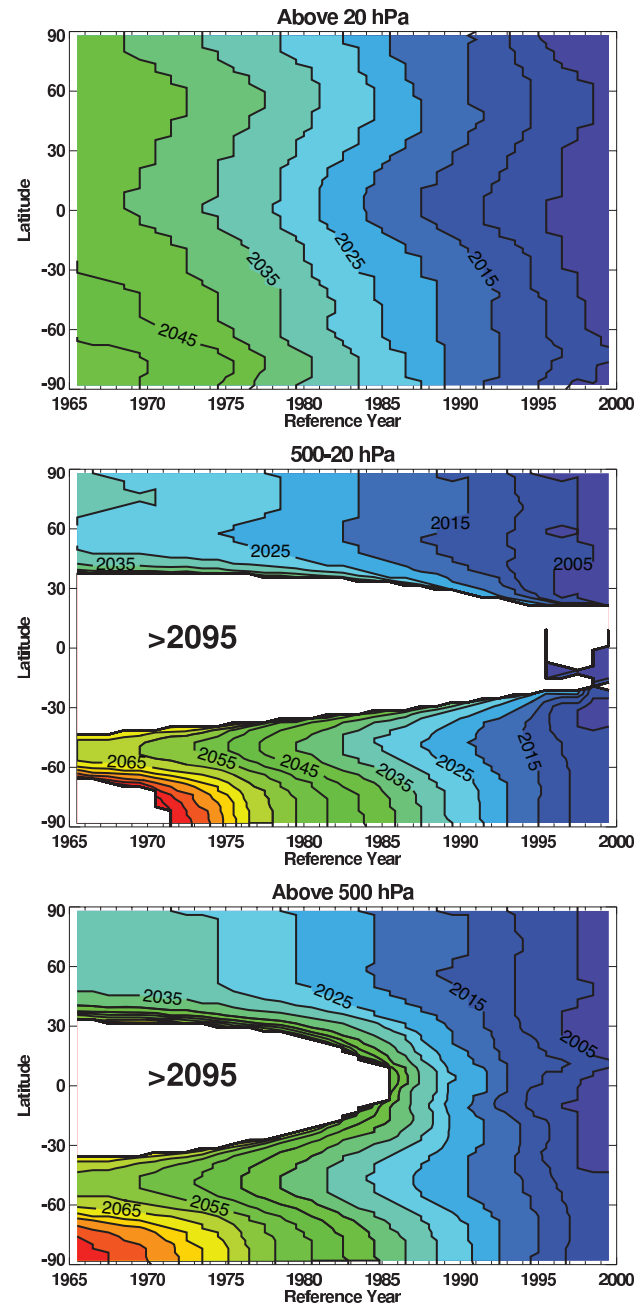
Global total column ozone is projected to return to its 1980 value around 2032 (2027–2038), which is 15 years earlier than when global Cl_y at 50 hPa returns to its 1980 value and 18 years earlier than when global ESC returns to its 1980 value. CCM projections suggest that this early return is primarily a result of GHG-induced cooling of the upper stratosphere, because the effects of circulation changes on tropical and extratropical ozone largely cancel in the global mean. Figure 3-16 summarizes return dates as a function of latitude for annual mean total column ozone to a value appropriate to reference years between 1965 and 2000 (Austin et al., 2010a; Chapter 9 of SPARC CCMVal, 2010). The figure shows results for the partial ozone column above 20 hPa (upper panel), the partial column between 500 and 20 hPa (middle panel) and for the combined column above 500 hPa. Tropospheric ozone below 500 hPa is excluded. Above 20 hPa, where changes in halogens and temperature dominate the ozone evolution, the return of ozone to historical levels is projected to occur steadily. In the lower stratosphere (Figure 3-16, middle panel) a return date could not be determined for the tropics due to the strengthening BDC which systematically decreases tropical ozone as the simulations proceed (Waugh et al., 2009). The results also show a strong hemispheric asymmetry, with Antarctic ozone returning to historical levels much later than Arctic ozone. Again, this is largely due to the increased BDC, which for the models, on average, has much more influence in the Northern Hemisphere

Figure 3-15 (at left). 1960 baseline-adjusted total column ozone projections in the reference simulations (thick black solid line) compared to the fixed halogen simulation (fODS, thick black dashed line): (a) global (90°S–90°N annual mean), (b) tropics (25°S–25°N annual mean), (c) northern midlatitudes (35°N–60°N annual mean), (d) southern midlatitudes (35°S–60°S annual mean), (e) Arctic (60°N–90°N March mean), and (f) Antarctic (60°S–90°S October mean). The colored lines show individual models for the subset that submitted fODS (see Table 3-1 for model descriptions). The horizontal green line shows the level of the multi-model trend estimate in 1980. The red vertical dashed line indicates the year when the multi-model trend estimate in the reference simulation returns to 1980 values and the blue vertical dashed lines indicate the uncertainty in these return dates. The black solid circles with vertical bars show the observations and their 2σ errors processed as in Figures 3-6 and 3-11. Nine CCMs are included in the multi-model mean (CCSRNIES, CMAM, GEOSCCM, LMDZrepro, MRI, SOCOL, UMSLIMCAT, ULAQ, and WACCM). In all regions except the tropics, the milestone of full ozone recovery occurs significantly later than when ozone returns to its 1980 values. The milestone of full ozone recovery is derived from the period when the fixed halogen simulation is not statistically distinguishable from the reference simulation (black dotted line in the bottom of each panel plotted against the percentage scale at the bottom right). For clarity, only the 95% confidence intervals are shown. Adapted from Eyring et al. (2010a), their Figure SM12.

Figure 3-16. Date of return of the annual mean column ozone to the value appropriate to the reference year indicated on the abscissa. The mean model result was smoothed with an 11-year running mean filter. Contour interval is 5 years; red values indicate later dates and blue values indicate earlier dates. Data prior to 1965 (which limits the definition of the reference year data) or after 2094 (which limits the data for the return year) do not exist because of the need for an accurate time-smoothed field. The white region in the figure indicates where the mean model ozone has not recovered by the end of the simulations (nominally 2094). Results are shown for the total column above 500 hPa (bottom panel), for the range 500–20 hPa (middle panel), and for the column above 20 hPa (top panel). From Chapter 9 of SPARC CCMVal (2010), their Figure 9.25.

than in the Southern Hemisphere (Austin and Wilson, 2006; Shepherd, 2008). The combination of the lower and upper stratospheric columns (Figure 3-16, lower panel) shows that in the tropics the total ozone column increases until about 2050 due to decreasing halogen amounts and stratospheric cooling, but thereafter ozone decreases due to the increasing BDC and does not return to pre-1985 values before the end of the simulations.

The ozone return dates discussed above apply to a single GHG scenario, the SRES A1B scenario. However, this scenario represents only one plausible future and it is therefore important to also assess the ozone return dates under different GHG evolutions. Ideally, all models that performed the reference simulations would have also performed all sensitivity simulations. However, the various GHG scenarios were only performed by a small subset of models (see GHG-x simulations in Table 3-1). Differences in stratospheric column ozone among six GHG scenarios (SRES A1B, A2, and B1; RCP 2.6, 4.5, and 8.5; see also Section 3.3.1) assessed from four CCMs by Eyring et al. (2010b) are found to be largest over northern midlatitudes and in the Arctic with divergence mainly in the second half of the 21st century. In the midlatitudes, the return of stratospheric column ozone to 1980 values varies by up to 10 years among the GHG scenarios, while in polar regions differences of 15–20 years are found. Overall, the differences of ozone return dates among the GHG scenarios simulated by the four individual models is of the same order as the uncertainty in ozone return dates derived from the multi-model mean of the 17 CCMs in Eyring et al. (2010a) in the midlatitudes, while it is smaller in the tropics and larger in the Arctic and Antarctic. The results



suggest that effects of GHG emissions on future stratospheric ozone should be considered in climate change mitigation policy, and ozone projections should be assessed under more than a single GHG scenario. However, more CCMs will need to perform the GHG sensitivity simulations to arrive at more robust conclusions. Furthermore, to assess full recovery of ozone from ODSs under different GHG scenarios, simulations with fixed ODSs under each scenario would be required.

3.3.7 Uncertainties in Model Projections and Open Questions

3.3.7.1 UNCERTAINTY IN FUTURE EMISSIONS SCENARIOS

Uncertainty in projections of stratospheric ozone can usefully be broken into four sources (Charlton-Perez et al. (2010) using an approach based on Hawkins and Sutton (2009)): (a) internal variability of the chemistry-climate system, (b) model uncertainty due to differences in the design and parameters of CCMs and missing or poorly represented processes in CCMs, (c) uncertainty in future emissions scenarios for GHGs, and (d) uncertainty in future emissions scenarios for ODSs, which is likely smaller than (a) to (c).

Figure 3-17 shows estimates of uncertainty in each of the three uncertainty components (a)–(c) for CCMVal-2 projections of total column ozone in six geographical regions of the globe. Note that the GHG scenario uncertainty was estimated using only a small subset of models. In total, four runs of three CCMs forced with SRES GHG scenarios (solid green lines) and three runs of a single CCM forced with RCP GHG scenarios (dashed green lines) provide the estimates shown (see Charlton-Perez et al. (2010) for more details).

In either case, it is clear that, for most geographical regions, model uncertainty is the dominant contributor to the total uncertainty in projections of future ozone column amount at least up to the mean estimate of ozone return to 1980 values. In the tropical band, internal variability is comparable in size to scenario uncertainty, but in other regions internal variability is generally a small contributor to total uncertainty in future ozone column amount. Charlton-Perez et al. (2010) therefore suggest that continued investment and development of CCMs could lead to a refinement of ozone projections for the period up to and including ozone return to 1980 values, assuming that CCM developments lead to a reduction in model uncertainty.

There remain other uncertainties associated with ozone prediction that are difficult to quantify, particularly the mean biases present in the ozone climatology of many of the CCMs (see Chapter 9 of SPARC CCMVal, 2010) and missing or poorly represented processes in the entire ensemble of CCMVal models (for example the quasi-biennial oscillation). The effects of solar variability were not considered in the CCM simulations assessed in this chapter. No CCM studies have yet assessed the effects of a long-term sustained change in solar output, such as the Maunder minimum, on stratospheric ozone. Other uncertainties, related to major changes in future human behavior

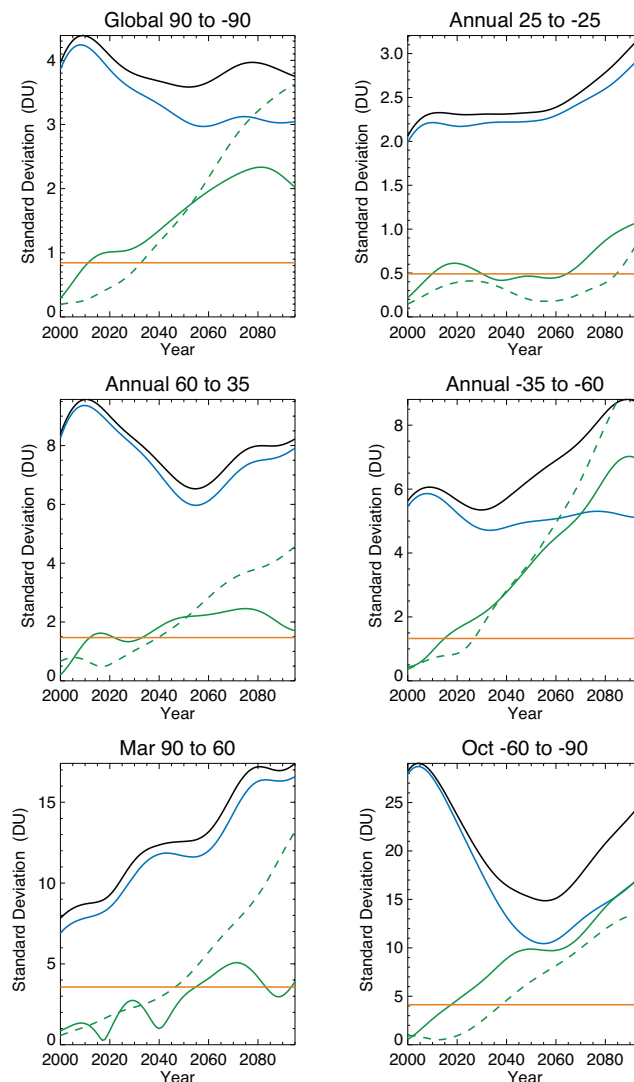


Figure 3-17. Uncertainty in the predicted total-column decadal-mean ozone amounts relative to 1980 values estimated for different geographic regions. Uncertainty is expressed as the one standard deviation estimate for internal variability (orange), model uncertainty (blue), and the total uncertainty (black) all shown in solid lines. Solid green lines show an estimate of the one standard deviation estimate for scenario uncertainty calculated from integrations of CCSRNIES, GEOSCCM, and WACCM forced with alternative SRES greenhouse gas scenarios. Dashed green lines show an alternative estimate of scenario uncertainty calculated using integrations of the CAM3.5 model forced with alternative RCP greenhouse gas scenarios. Total uncertainty estimates are derived from the SRES scenario integrations only. From Charlton-Perez et al. (2010), their Figure 3.

that are not considered in the scenarios used in this chapter, are discussed in Chapter 5 (Section 5.4) and include geoengineering of the climate system, increases in N₂O emissions from automotive biofuels, and enhanced emissions from aviation and rockets.

3.3.7.2 FUTURE CCM DEVELOPMENT

Following this Assessment, CCMs are likely to undergo significant further development that could have impacts on their projections of future ozone and could either increase or decrease the spread between models. The executive summary of SPARC CCMVal (2010) recommends that “Development should continue toward comprehensive troposphere-stratosphere CCMs, which include an interactive ocean, tropospheric chemistry, a naturally occurring QBO, spectrally resolved solar irradiance, and a fully resolved stratosphere.” The impact of some of these processes on ozone projections was partially assessed in multiple CCMs by CCMVal.

Other than in CMAM, sea surface temperatures and sea ice concentrations were prescribed in all other CCM simulations used in this chapter. Important couplings between the atmosphere, the oceans, and the cryosphere are currently not represented in CCMs. Inclusion of these couplings in the CCMs will lead to a more complete representation of the climate system and climate feedbacks, which could be important for simulations of stratospheric ozone and its impact on tropospheric climate. Several recent studies have shown that changes in global mean climate will have a significant, regionally dependent influence on future ozone concentrations and the correspondence between the return of ozone to pre-1960 or 1980 levels and the return of ESC amounts to pre-1960 or 1980 levels (Waugh et al., 2009; Shepherd and Jonsson, 2008). The impact of coupling CCMs to interactive ocean models remains to be assessed since the number of CCMs able to perform this coupling remains small.

Future assessments should also consider brominated very short-lived species (VSLS, see Section 3.2.1), as well as the uncertainty in how the organic halogen lower boundary condition is prescribed in CCMs. Currently, projections of future organic halogen loadings are based on projected emission rates and an estimate of the global atmospheric lifetime of each organic halogen. These factors are used to create time-dependent volume mixing ratio lower boundary conditions that are then used to force the CCMs. However, the destruction of each halogen in the CCMs is dependent on the tropical upwelling and meridional mixing (both linked to the strength and structure of the BDC), and chemical loss rates (e.g., photolysis rates). The CCM-derived halogen lifetimes can be very different from the lifetimes assumed for the given projection scenario. Some studies (Douglass et al., 2008) suggest that

the use of fixed mixing ratio lower boundary conditions provides an artificial constraint on model-derived ozone return dates. Furthermore, multi-model studies are necessary to fully evaluate the impact of ODS flux boundary conditions on ozone projections.

3.4 PROJECTIONS OF UV CHANGES RELATED TO OZONE CHANGES THROUGH THE 21ST CENTURY

Future changes in stratospheric ozone will cause changes of opposite sign in solar UV radiation received at the surface. However, UV radiation is also affected by a number of other factors (see Section 3.2.8), which are likely to change in the future. In this section only changes due to ozone are addressed. Simulations of future UV are based on ozone projections by CCMs, which take into account the effects of climate change on ozone (see Section 3.3). The effect of changes in ozone on erythemal irradiance can be quantified either with empirical relationships, such as the radiation amplification factor (RAF) concept (Booth and Madronich, 1994; Madronich, 2007), or, more accurately, with radiative transfer models.

3.4.1 Midlatitude and Tropical UV

Calculations with a radiative transfer model were used by Tourpali et al. (2009) to simulate the noontime erythemal solar irradiance received at the Earth’s surface under cloud-free conditions. These simulations were based only on total ozone columns, and vertical profiles of ozone and temperature, derived from 11 CCMs (CCMVal-1 models) simulating the evolution of stratospheric ozone (Eyring et al., 2006; Eyring et al., 2007). Following a peak between the late 1990s and early 2000s, erythemal irradiance was projected to decrease at all latitudes and in all seasons during the 21st century. Since erythemal irradiance changes were mostly driven by changes in total ozone, they tended to follow the pattern of the stratospheric ozone changes. The weakest changes, of the order of a few percent, were found in the tropics. At midlatitudes, the decreases ranged from 5–15% between 2000 and 2100, while at southern high latitudes the decrease was a factor two stronger because of the projected recovery of Antarctic ozone layer there.

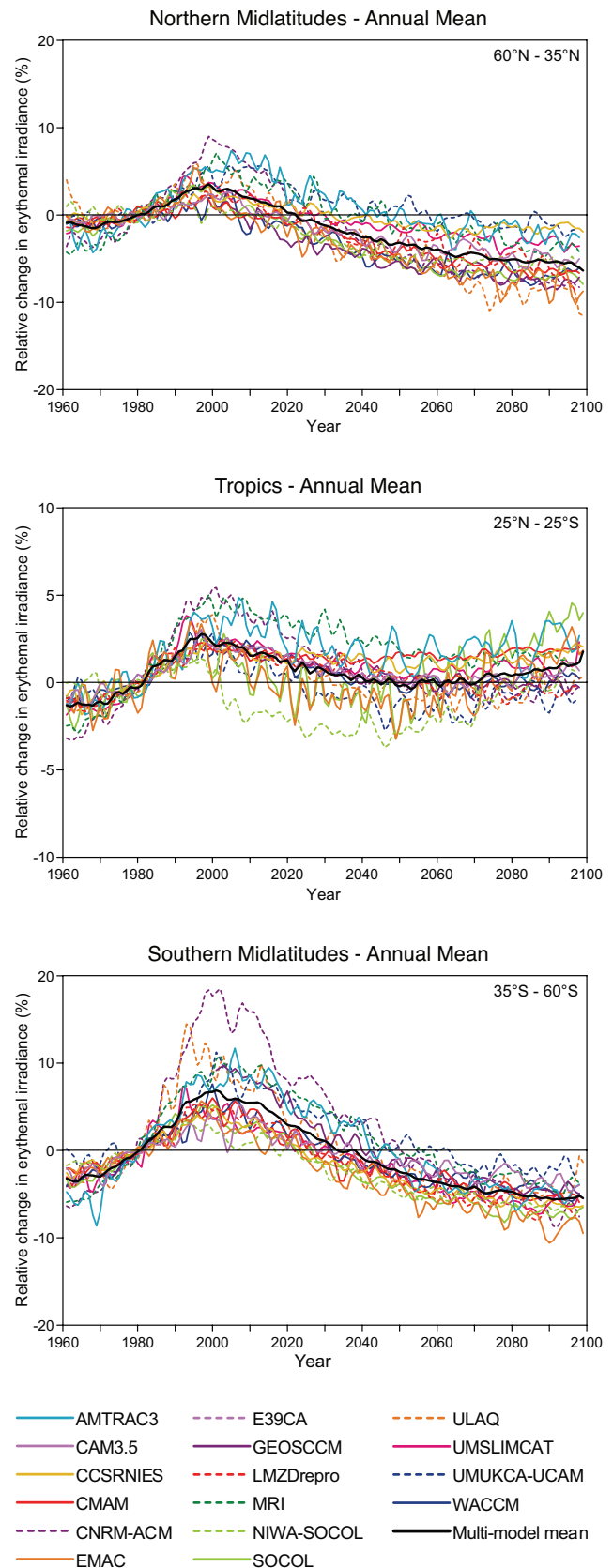
A follow-up study (Kazantzidis et al., 2010) provided quantitative estimates for the effect of the projected ozone changes on different biological weightings of UV irradiance (doses), such as DNA damage and vitamin D production, which have different sensitivities to ozone changes. For example, in some cases, changes in doses relevant to DNA damage can exceed those for erythema by a factor of two.

Ozone recovery will be affected by climate change (see also Section 3.2) and this will in turn affect the levels of UV radiation at the surface. Hegglin and Shepherd (2009) reported that the effects of a strengthened BDC on stratospheric ozone, which they entirely attributed to changes in GHG concentrations (assuming that the effect of ODSs on ozone were negligible in 1965 and 2095 in their simulations), would result in decreases in erythemal irradiance from 1965 to 2095 by about 9% at northern high latitudes. This change was found to be about three times larger than the change attributed to stratospheric ozone recovery from ODSs only, as estimated from the change in erythemal irradiance from 1965 to 2000.

More robust ozone projections can improve the accuracy of the estimated changes in surface UV irradiance. A new subset of simulations from 15 CCMs has become recently available through the CCMVal-2 activity of SPARC (see SPARC CCMVal (2010) and Section 3.3), and are used to repeat the erythemal irradiance calculations reported by Tourpali et al. (2009). More realistic and spatially varying climatological values for aerosols (Kinne et al., 2006) and surface reflectivity (Herman et al., 2001) are prescribed in the present calculations. Although cloud and aerosol fields are expected to change in the future (IPCC, 2007), they are kept constant here. For the period covered by the CCM simulations (1965–2100) and over a global grid of $10^\circ \times 15^\circ$ respectively, solar UV irradiance spectra (280–400 nm) at the surface are calculated with the radiative transfer model package libRadtran (Mayer and Kylling, 2005) for the 15th of each month.

These new simulations, shown in Figure 3-18, result in lower inter-model spread compared to the results of Tourpali et al. (2009), allowing a more robust estimation of the dates when erythemal irradiance is projected to return to 1980 values. At midlatitudes, erythemal irradiance is projected to decrease for all models throughout the 21st century. The return of the multi-model mean to

Figure 3-18. Annual means of surface erythemal irradiance changes (in %, relative to 1975–1985) under cloud-free conditions for three latitude belts representative for Northern Hemisphere midlatitudes (upper panel), tropics (middle panel), and Southern Hemisphere midlatitudes (lower panel), calculated with a radiative transfer model using projections of ozone and temperature from 15 CCMs. See Table 3-1 for model descriptions. For the models providing multiple runs, the average change of irradiance is shown. The black thick line represents the multi-model mean. All lines have been smoothed with a 1:2:1 filter. Note the different scale for the tropical belt. Updated from Tourpali et al. (2009) using projections from 15 CCMVal-2 models.



1980 values is projected to occur in 2023 for the Northern Hemisphere and in 2035 for the Southern Hemisphere; for individual models, the return date ranges from 2016 to 2055 and from 2038 to 2055, respectively. The large range on the erythemal irradiance return date reflects the large inter-model differences in total column ozone used as inputs in the surface UV calculations. The projected increases in column ozone above its levels in 1980 after the mid-21st century, especially in the Northern Hemisphere, result in decreases in erythemal irradiance of up to 5% below its levels in 1980 (Figure 3-18, upper panel), with important implications for ecosystems at high latitudes (UNEP, 2010). For example, such decreases may contribute to further deficiency in the vitamin D levels of humans (Edvardson et al., 2007; Kazantzidis et al., 2009; Kimlin et al., 2007; Webb and Engelsen, 2006), unless other factors, such as a possible decrease in cloudiness, would counteract these changes. In the event of increasing cloudiness due to climate change, or increasing aerosol load (likely over inhabited areas), the adverse effects concerning vitamin D production would be even larger.

The simulations for the tropics (Figure 3-18, middle panel) show a steady increase in surface erythemal irradiance up to the late 1990s and then a slow decrease until ~2050, when it reaches a minimum that is still higher than 1980 levels for most models. Thereafter, surface UV is projected to slowly increase toward the end of the 21st century, in response to the projected decreases in tropical column ozone due to the acceleration of the BDC. The tropical changes are small (at most 5% with respect to 1980 values) in comparison to the changes projected for the higher latitudes. This temporal behavior of tropical erythemal irradiance is common to most models and agrees with the simple estimates of Hegglin and Shepherd (2009). UV-B radiation in the tropics is high due to naturally occurring low total ozone columns and high solar elevation angles. Assuming no variations from other factors, if UV-B radiation remains above its values in 1980, the adverse effects on ecosystems from UV exposure might be enhanced in this region during the 21st century.

The uncertainty of the surface UV projections presented here could be much larger than the model range indicates. Indeed, more realistic projections of future UV radiation should include not only ozone, but also clouds, aerosols, and surface reflectivity. All these will likely be affected by climate change. In addition, anthropogenic tropospheric ozone and aerosols in the lower troposphere are likely to change as well (see Section 3.2.8). Clouds are the main modulator of UV radiation and current work shows that they may introduce considerable variability to the future UV time series and modify, or even reverse, the ozone-related trends in UV radiation. The evolution of these factors in the future, with patterns exhibiting

strong spatial variations (e.g., Trenberth and Fasullo, 2009), may modify accordingly the projected return date of UV irradiance to its 1980 levels.

3.4.2 Polar UV

In polar regions, the UV signatures of ozone reductions have been more pronounced compared to midlatitudes (see Chapter 2), resulting in measurable changes and, in some cases (e.g., in Antarctica), detectable increases in surface UV radiation (Bernhard et al., 2006).

In Tourpali et al. (2009), the ozone recovery projected by CCMs for the southern polar latitudes resulted in large reductions in erythemal irradiance under cloudless conditions of more than 30% between 2000 and 2095. When, instead of the annual mean, monthly means are considered, reductions of ~50% are found in the austral spring. The sign of the erythemal irradiance changes is reversed for polar regions, when its levels in the 1960s are taken as reference. Hegglin and Shepherd (2009) estimated increases in erythemal irradiance of up to 20% between 1965 and 2095 over the same region in late spring and early summer. This increase is nearly half of that generated by the Antarctic ozone hole from the increase in ODS levels since the 1960s. The increase is not so large in the new calculations, with the multi-model mean in 2100 being just above the 1960 level, though the range in the model estimates is large (see Figure 3-19). Some CCMs even report small decreases in erythemal irradiance for the same period.

The new UV simulations show that increases in clear-sky erythemal irradiance reach a rather broad maximum centered over the 2000s (Figure 3-19). The magnitude of this maximum varies between models, ranging, for the spring months, from ~5 to 15% in the Arctic, and from ~30 to 110% in Antarctica. This spread in the model estimates is a measure of the uncertainty of the simulations, which, together with their large year-to-year variability, makes it difficult to assess more accurately the magnitude and timing of the UV maximum. After the 2000–2010 decade, erythemal irradiance is projected to decrease at different rates for the two regions. In the Arctic, it is projected to return to its 1980 value between 2020 and 2030, while in Antarctica the return occurs only in the 2nd half of the 21st century. The rather slow decline in UV levels over Antarctica may have important biological consequences for Antarctic ecosystems, which will continue to be exposed to excess UV for most of the 21st century.

The expected increase in stratospheric ozone levels at southern polar latitudes is projected to accelerate surface warming over Antarctica (Son et al., 2009). This may accelerate ice and/or snow melting and, ultimately, may lead to exposure of organisms under the ice to UV

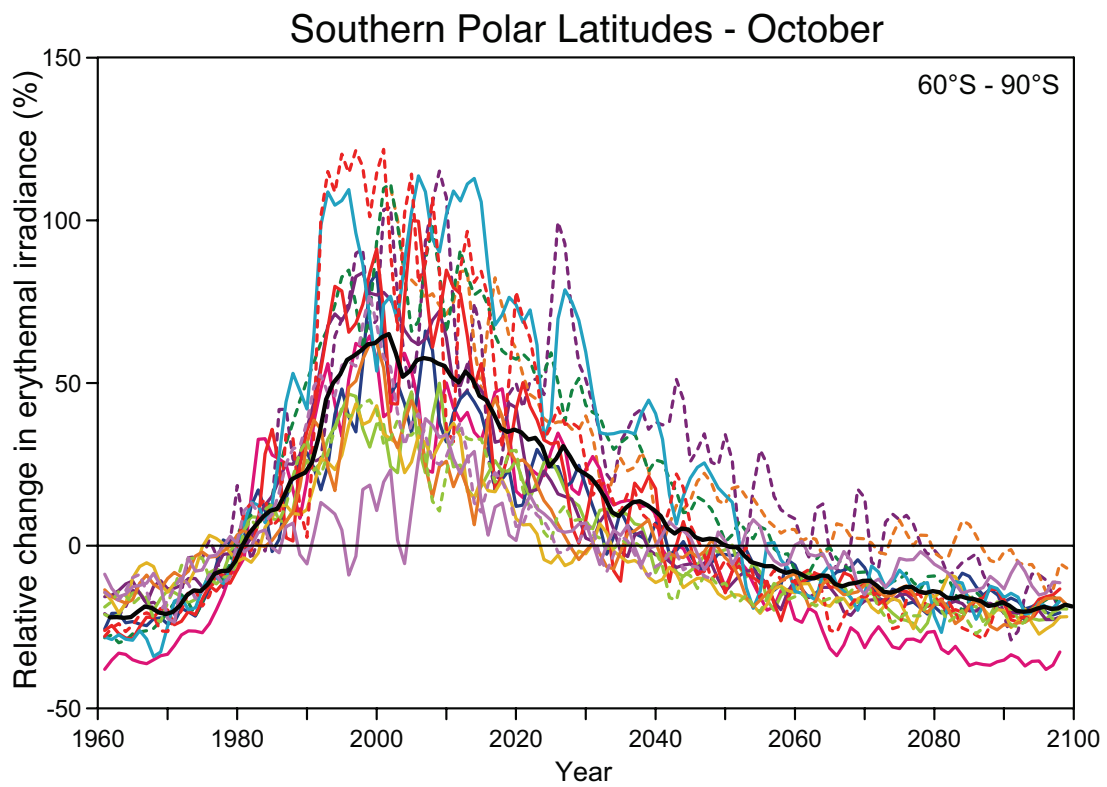
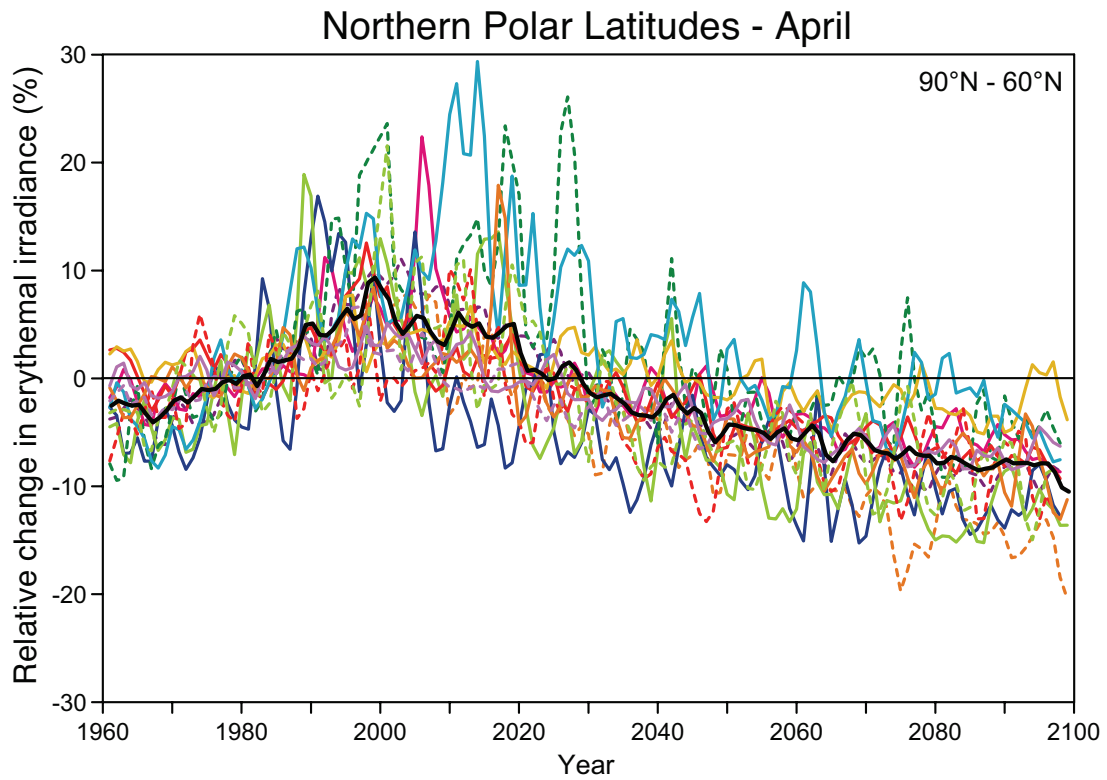


Figure 3-19. As in Figure 3-18 but for April in the Arctic (upper) and October in Antarctica (lower). The legend of Figure 3-18 applies also here. Note the different scales in the two panels. Updated from Tourpali et al. (2009) using projections from 15 CCMVal-2 models.

radiation and to a decrease of surface reflectivity. The reduction in surface reflectivity would reinforce the effect of rising stratospheric ozone levels by decreasing further surface UV irradiance over this region.

3.4.3 Link to UNEP Environmental Effects Panel Assessment

Changes in solar UV radiation at the surface are important due to the biological consequences—both negative and positive—for humans and for different ecosystems. The adverse effects of UV radiation on human health have dominated the public awareness during the last three decades because of ozone depletion. In recent years, though, much attention has been drawn to the benefits of solar UV radiation with respect to its involvement in the production of vitamin D, an important agent for human health (Edvardson et al., 2007; Kazantzidis et al., 2009; McKenzie et al., 2009; Webb et al., 1988). As the spectral characteristics of solar UV radiation at the surface depend on the changes in ozone, the recovery of the stratospheric ozone layer will reduce the harmful biological doses received by humans, but will reduce also the rate of production of vitamin D, especially in the winter months at high latitudes. Ozone depletion has also influenced other communities, terrestrial and marine, as well as biological and chemical processes in the environment (UNEP, 2007). Therefore, the recovery of stratospheric ozone and the timing of this recovery are important for both. The impacts of ozone depletion and recovery, and of the resulting changes in UV radiation on the environment and the ecosystems, will be focal points for discussion in the forthcoming assessment report of the Environmental Effects Assessment Panel (EEAP) of UNEP (UNEP, 2010).

Ozone depletion has shown seasonal and latitudinal variations. The projections of surface UV irradiance in the 21st century based on ozone changes projected by CCMs (as described in Section 3.4.1) reveal the importance of ozone variations in different regions. This can be seen in Figure 3-20, which shows the average change in daily erythemal irradiance between 1975–1985 and 2089–2099 for different seasons. Evidently there is a strong meridional gradient in the UV changes, which are small and positive in the tropics (up to 4%) and become negative with increasing magnitude at the middle and high latitudes. Although small in percentage, this increase in the tropics may be important for ecosystems living in this region, where irradiance levels are already high. As discussed above, the changes over Antarctica exceed –30% and are rather zonally symmetric. Such large decreases will have implications for the Antarctic ecosystems. Overall, the changes in UV radiation are fairly zonal over the middle and tropical latitudes and for all seasons, with longitudinal variations

of a few percent. In the winter/spring period of the Northern Hemisphere these longitudinal variations are slightly larger due to more regional changes in column ozone.

In the present report, the future UV radiation has been simulated only in terms of ozone variations. However, climate change may significantly impact surface UV levels either directly through changes in clouds, albedo, and aerosols, or indirectly through interaction with ozone, as discussed in Section 3.2.8. Clear-sky UV simulations, calculated from changes in ozone and changes in cloudiness and surface reflectivity taken from climate models, will be discussed in more detail in the forthcoming assessment report of the EEAP/UNEP (UNEP, 2010).

Because ozone depletion has been most severe in the southern high and polar latitudes, the effects on the ecosystems would likely be most pronounced and detectable over these regions. Antarctic communities have been exposed to alterations in the surface conditions of temperature, moisture, and ultraviolet radiation resulting from climate change and stratospheric ozone depletion (Solomon et al., 2005). After three decades of ozone depletion and enhanced UV exposure, communities may already be undergoing adaptation, species selection, and changes in species assemblages, communities, and distributions, with effects on ecosystem function (Wall, 2007). For the Antarctic terrestrial communities, the timing of exposure in early spring might be more important than the magnitude of UV-B exposure, since, in early spring, organisms may be in a physiologically inactive state and unaccustomed to these levels (Wall, 2007). Terrestrial organisms are also living under the snow cover that may provide protection from UV radiation (Cockell and Cordoba-Jabonero, 2004). Climate changes may result either in prolongation (through cooling) or in shrinking (through increases in sublimation and strengthening of katabatic winds) of periods with snow cover (Wall, 2007).

3.5 CONCLUSIONS

The focus of this chapter has been to assess and discuss projections of future ozone and its impact on surface UV. Future ozone will be mostly determined by changes in stratospheric halogen loading (ESC) and changes in climate parameters. Thus, the chronology of the third and last stage of ozone recovery from ODSs as defined in WMO (2007), and employed here, depends critically on the combination of these two factors. Separately evaluating the role of halogens in ozone depletion is of great interest because it is the primary concern of the Parties to the Montreal Protocol. Section 3.2 describes the primary factors controlling future ozone and surface UV. Stratospheric halogen loading has been the strongest influence on ozone in the last decades since the onset of the Antarctic ozone hole and midlatitude depletion. Stratospheric

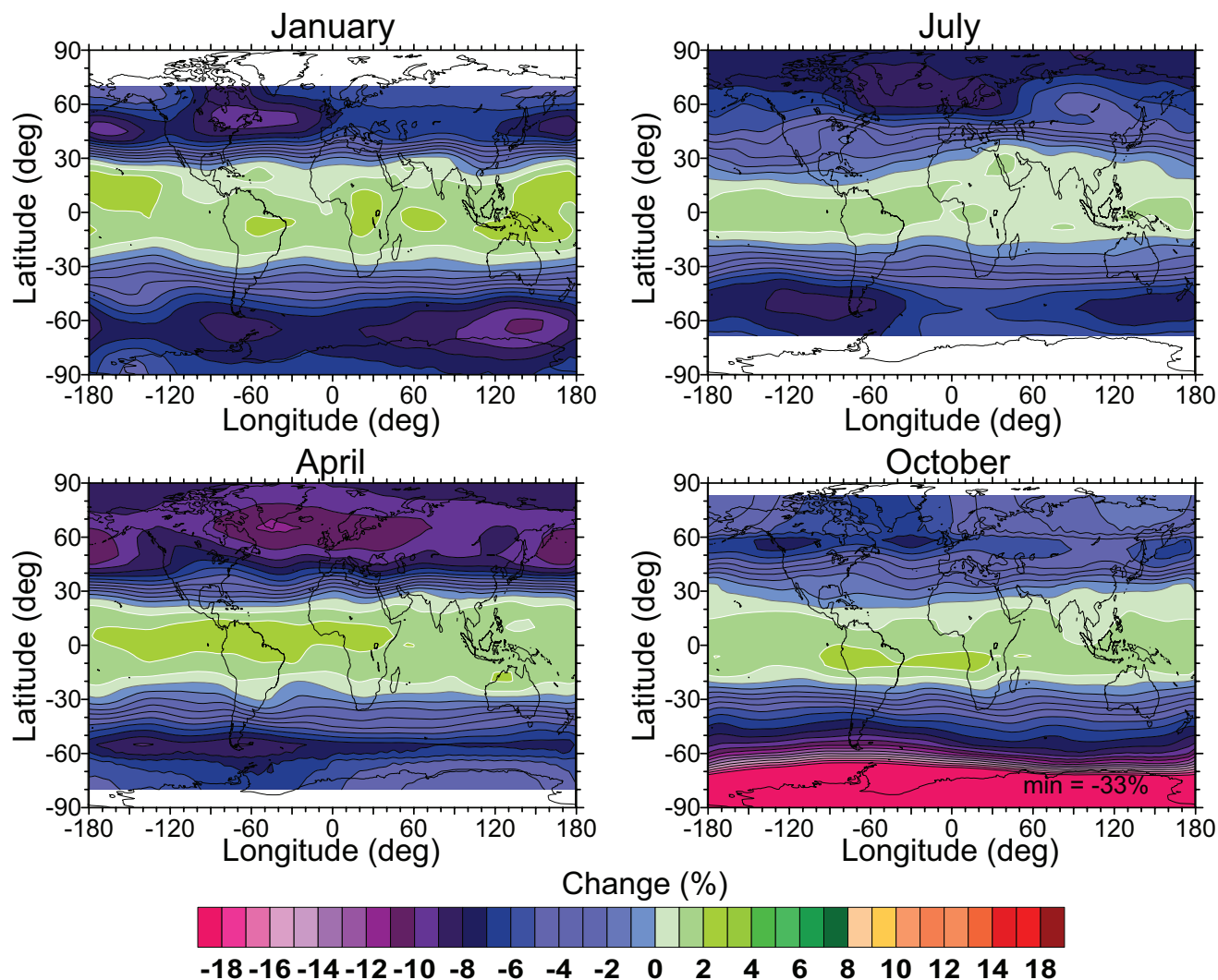


Figure 3-20. Multi-model average changes in surface erythemal irradiance between 2089–2099 and 1975–1985 under cloud-free conditions for four months, calculated with a radiative transfer model using projections of ozone and temperature from 15 CCMs. Updated from Tourpali et al. (2009) using projections from 15 CCMVal-2 models.

halogen loading has peaked in all regions of the stratosphere in the last two decades and is now diminishing at a rate primarily controlled by the atmospheric lifetimes of individual chlorine and bromine gases. Global and regional projections for the removal of halogens have very similar time dependences as shown in Figure 3-21 and indicate that the return of halogen amounts to 1960 values will not be achieved before 2100, except in the tropical lower stratosphere. A prominent feature of the halogen time series is that regional peak values are quite different. Because of the long average lifetimes of ODSs, the highest values are found in polar regions, where the average age of stratospheric air is greatest.

Other leading factors discussed in Section 3.2 are stratospheric levels of key ozone-destroying hydrogen and nitrogen species, stratospheric temperatures, the Brewer-Dobson circulation, dynamics of the polar vortex, and stratospheric aerosols. Many of these factors, which already influence ozone to some degree, are coupled such that the effects of an initial perturbation may be amplified to result in a larger effect on ozone than would have been the case otherwise. Links between components of the chemistry-climate system are indicated in Figure 3-22 with arrows representing chemistry, radiation, transport and other mechanisms. Many of these factors are influenced by anthropogenic emissions of GHGs and ODSs.

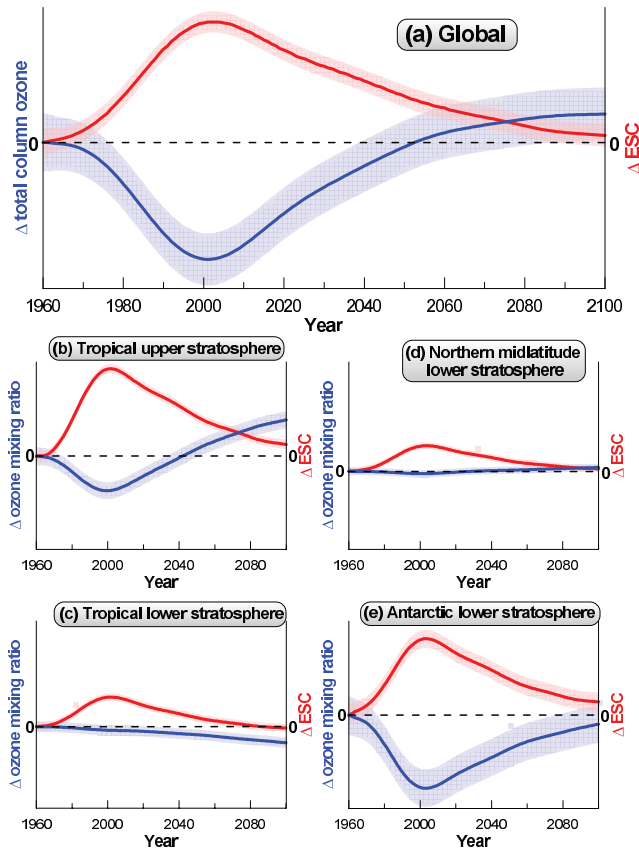


Figure 3-21. A schematic contrasting global and vertically resolved changes in ozone (blue) and ESC (red). In all cases changes with respect to the 1960 value are shown. Panel (a) shows the most common framework in which future projections of ozone are considered (compare to Figure 6-1 of WMO, 2007) while the other panels show the greater variety of responses of ozone to ESC in different regions of the atmosphere resulting from non-ESC drivers of ozone changes and their feedbacks and interactions (see Figure 3-22). The schematic is generated from multi-model means (solid lines) and 95% prediction intervals (shading) of REF-B2 simulations (Table 3-2) from the suite of CCMs used in this chapter.

For example, the increase in stratospheric CO_2 abundance is the main cause of the cooling trend in the stratosphere (see Section 4.2).

These multiple drivers of ozone changes and their interactions will create more diverse regional behavior in stratospheric ozone than would be expected from average global behavior or from the evolution of ODSs alone. This point is illustrated schematically in the time series shown in Figure 3-21, where an anticorrelation between the evolutions of ESC and total column ozone can be seen for the global average, for the Antarctic lower strato-

sphere, and for the tropical upper stratosphere. However, the influence of other drivers, in particular GHGs, is manifest in the global and tropical upper stratosphere, where ozone amounts return to 1960 levels in the middle of 21st century, although ODSs are still enhanced during this period. It is only in the Antarctic lower stratosphere, where the sensitivity of ozone to ESC maximizes, that ESC appears to remain the dominant driver until the end of the 21st century. In other regions, ozone changes are not well correlated with ESC. For example, in the tropical lower stratosphere, ozone amounts decrease steadily from 1960 to 2100 whereas in the northern midlatitude lower stratosphere, ozone shows a small negative response to ESC until 2020 before increasing throughout the 21st century. In these regions, GHG changes are the dominant driver of ozone changes.

The multiple interactions between the components of the chemistry-climate system (Figure 3-22) complicate a clean attribution of changes in ozone to changes in ODSs and other factors as required by the definition of full ozone recovery employed in this Assessment. For example, decreases in polar stratospheric ozone, resulting from increases in ESC, cool the stratosphere since heating from UV absorption by ozone is also reduced. This cooling in turn enhances the effectiveness of ESC by promoting the formation of polar stratospheric clouds. Increases in GHG concentrations drive additional radiative stratospheric cooling, but at the same time strengthen the BDC, which adiabatically warms the polar stratosphere and enhances mixing with lower latitudes. Sensitivity simulations using CCMs can be used to disentangle the effects of different drivers to ozone changes. Model results indicate that changes in ODSs and GHGs appear to affect ozone nearly independently.

The primary drivers of ozone changes, and their interactions, are largely described in the CCMs that have been used to make the ozone and UV projections presented in this chapter. To identify the causes of simulated future ozone changes, CCMs were also used to conduct sensitivity simulations in which one particular driver of ozone changes (e.g., ODSs or GHGs) was held constant. There are, however, processes that are not yet fully realized in models, such as potential changes in the quasi-biennial oscillation and coupling to the ocean. There are additional processes and associated potential feedbacks in the ocean-climate-stratosphere system (e.g., changes in marine biogenic emissions of halocarbons induced by changes in climate and surface UV) and in the terrestrial biosphere-climate-stratosphere system (e.g., emissions of ozone precursors) that are also currently absent in CCMs. Therefore, as progress is made toward the development of full Earth Systems Models that include a wider variety of processes and feedbacks, more comprehensive and robust future projections of ozone will become possible.

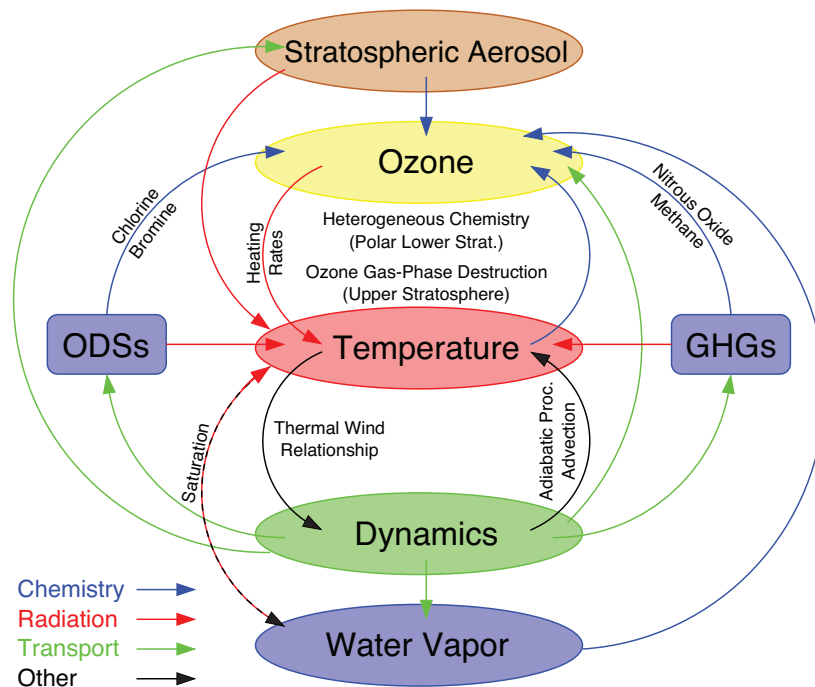


Figure 3-22. Schematic of ozone-focused stratospheric chemistry-climate interactions. Links between elements of the chemistry-climate system are indicated with arrows representing chemistry (blue), radiation (red), transport (green), and other mechanisms (black). Simple and more complex feedback cycles can be constructed following the linking mechanisms. A simple example is ozone depletion in the upper stratosphere leading to lower temperatures. Lower temperatures slow the gas-phase destruction of ozone, thereby reducing the amount of ozone depletion. The feedback loops involving stratospheric aerosol are currently not important, but they might become important again after a large volcanic eruption or in the context of some geoengineering proposals.

REFERENCES

- Akiyoshi, H., L.B. Zhou, Y. Yamashita, K. Sakamoto, M. Yoshiki, T. Nagashima, M. Takahashi, J. Kurokawa, M. Takigawa, and T. Imamura, A CCM simulation of the breakup of the Antarctic polar vortex in the years 1980-2004 under the CCMVal scenarios, *J. Geophys. Res.*, *114*, D03103, doi: 10.1029/2007JD009261, 2009.
- Austin, J., and R.J. Wilson, Ensemble simulations of the decline and recovery of stratospheric ozone, *J. Geophys. Res.*, *111*, D16314, doi: 10.1029/2005JD006907, 2006.
- Austin, J., and R.J. Wilson, Sensitivity of polar ozone to sea surface temperatures and halogen amounts, *J. Geophys. Res.*, *115*, D18303, doi: 10.1029/2009JD013292, 2010.
- Austin, J., N. Butchart, and K.P. Shine, Possibility of an Arctic ozone hole in a doubled- CO_2 climate, *Nature*, *360*, 221-225, doi: 10.1038/360221a0, 1992.
- Austin, J., J. Wilson, F. Li, and H. Vömel, Evolution of water vapor concentrations and stratospheric age of air in coupled chemistry-climate model simulations, *J. Atmos. Sci.*, *64*, 905-921, doi: 10.1175/JAS3866.1, 2007.
- Austin, J., K. Tourpali, E. Rozanov, H. Akiyoshi, S. Bekki, G. Bodeker, C. Brühl, N. Butchart, M. Chipperfield, M. Deushi, V. Fomichev, M. Giorgetta, L. Gray, K. Kodera, F. Lott, E. Manzini, D. Marsh, K. Matthes, T. Nagashima, K. Shibata, R.S. Stolarski, H. Struthers, and W. Tian, Coupled chemistry climate model simulations of the solar cycle in ozone and temperature, *J. Geophys. Res.*, *113*, D11306, doi: 10.1029/2007JD009391, 2008.
- Austin, J., J. Scinocca, D. Plummer, L. Oman, D. Waugh, H. Akiyoshi, S. Bekki, P. Braesicke, N. Butchart, M. Chipperfield, D. Cugnet, M. Dameris, S. Dhomse, V. Eyring, S. Frith, R.R. Garcia, H. Garny, A. Gettelman, S.C. Hardiman, D. Kinnison, J.F. Lamarque, E. Mancini, M. Marchand, M. Michou, O. Morgenstern, T. Nakamura, S. Pawson, G. Pitari, J. Pyle, E. Rozanov, T.G. Shepherd, K. Shibata, H. Teyssède, R.J. Wilson, and Y. Yamashita, Decline and recovery of total column ozone using a multi-model time series analysis, *J. Geophys. Res.*, *115*, D00M10, doi: 10.1029/2010JD013857, 2010a.
- Austin, J., H. Struthers, J. Scinocca, D.A. Plummer, H. Akiyoshi, A.J.G. Baumgaertner, S. Bekki, G.E. Bodeker, P. Braesicke, C. Brühl, N. Butchart, M.P. Chipperfield, D. Cugnet, M. Dameris, S. Dhomse, S. Frith, H. Garny, A. Gettelman, S.C. Hardiman, P. Jöckel, D. Kinnison, A. Kubin, J.F. Lamarque, U. Langematz, E. Mancini, M. Marchand, M. Michou, O. Morgenstern, T. Nakamura, J.E. Nielsen, G. Pitari, J. Pyle, E. Rozanov, T.G. Shepherd, K. Shibata, D. Smale, H. Teyssède, and Y. Yamashita, Chemistry-climate model simulations of spring Antarctic ozone, *J. Geophys. Res.*, *115*, D00M11,

- doi: 10.1029/2009JD013577, 2010b.
- Avallone, L.M., and M.J. Prather, Photochemical evolution of ozone in the lower tropical stratosphere, *J. Geophys. Res.*, *101* (D1), 1457-1461, 1996.
- Badosa, J., R.L. McKenzie, M. Kotkamp, J. Calbó, J.A. González, P.V. Johnston, M. O'Neill, and D.J. Anderson, Towards closure between measured and modelled UV under clear skies at four diverse sites, *Atmos. Chem. Phys.*, *7*, 2817-2837, 2007.
- Bais, A.F., and D. Lubin (Lead Authors), A. Arola, G. Bernhard, M. Blumthaler, N. Chubarova, C. Erlick, H.P. Gies, N. Krotkov, K. Lantz, B. Mayer, R.L. McKenzie, R.D. Piacentini, G. Seckmeyer, J.R. Slusser, and C.S. Zerefos, Surface ultraviolet radiation: Past, Present, and Future, Chapter 7 in *Scientific Assessment of Ozone Depletion: 2006*, Global Ozone Research and Monitoring Project—Report No. 50, 572 pp., World Meteorological Organization, Geneva, Switzerland, 2007.
- Baldwin, M., and M. Dameris (Lead Authors), J. Austin, S. Bekki, B. Bregman, N. Butchart, E. Cordero, N. Gillett, H.-F. Graf, C. Granier, D. Kinnison, S. Lal, T. Peter, W. Randel, J. Scinocca, D. Shindell, H. Struthers, M. Takahashi, and D. Thompson, Climate-ozone connections, Chapter 5 in *Scientific Assessment of Ozone Depletion: 2006*, Global Ozone Research and Monitoring Project—Report No. 50, 572 pp., World Meteorological Organization, Geneva, Switzerland, 2007.
- Bell, C.J., L.J. Gray, and J.E. Kettleborough, Changes in Northern Hemisphere stratospheric variability under increased CO₂ concentrations, *Quart. J. Roy. Meteorol. Soc.*, *136*, 1181-1190, doi: 10.1002/qj.633, 2010.
- Bernhard, G., C.R. Booth, J.C. Eghamjian, and S.E. Nichol, UV climatology at McMurdo Station, Antarctica, based on version 2 data of the National Science Foundation's Ultraviolet Radiation Monitoring Network, *J. Geophys. Res.*, *111*, D11201, doi: 10.1029/2005JD005857, 2006.
- Bodeker, G.E., and D.W. Waugh (Lead Authors), H. Akiyoshi, P. Braesicke, V. Eyring, D.W. Fahey, E. Manzini, M.J. Newchurch, R.W. Portmann, A. Robock, K.P. Shine, W. Steinbrecht, and E.C. Weatherhead, The ozone layer in the 21st century, Chapter 6 in *Scientific Assessment of Ozone Depletion: 2006*, Global Ozone Research and Monitoring Project—Report No. 50, 572 pp., World Meteorological Organization, Geneva, Switzerland, 2007.
- Bodeker, G.E., H. Struthers, and B.J. Connor, Dynamical containment of Antarctic ozone depletion, *Geophys. Res. Lett.*, *29* (7), 1098, doi: 10.1029/2001GL014206, 2002.
- Bodeker, G.E., H. Shiona, and H. Eskes, Indicators of Antarctic ozone depletion, *Atmos. Chem. Phys.*, *5*, 2603-2615, 2005.
- Booth, C.R., and S. Madronich, Radiation amplification factors: Improved formulations accounts for large increases in ultraviolet radiation associated with Antarctic ozone depletion, in *Ultraviolet Radiation in Antarctica: Measurements and Biological Effects*, AGU Antarctic Research Series, edited by C.S. Weiler and P.A. Penhale, 39-42, Washington, D.C., 1994.
- Bradley, R.S., F.T. Keimig, and H.F. Diaz, Projected temperature changes along the American cordillera and the planned GCOS network, *Geophys. Res. Lett.*, *31*, L16210, doi: 10.1029/2004GL020229, 2004.
- Braesicke, P., and J.A. Pyle, Changing ozone and changing circulation in northern mid-latitudes: Possible feedbacks?, *Geophys. Res. Lett.* *30* (2), 1059, doi: 10.1029/2002GL015973, 2003.
- Brühl, C., and P.J. Crutzen, On the disproportionate role of tropospheric ozone as a filter against solar UV-B radiation, *Geophys. Res. Lett.*, *16* (7), 703-706, 1989.
- Butchart, N., and A.A. Scaife, Removal of chlorofluorocarbons by increased mass exchange between the stratosphere and troposphere in a changing climate, *Nature*, *410* (6830), 799-802, 2001.
- Butchart, N., I. Cionni, V. Eyring, T.G. Shepherd, D.W. Waugh, H. Akiyoshi, J. Austin, C. Brühl, M.P. Chipperfield, E. Cordero, M. Dameris, R. Deckert, S. Dhomse, S.M. Frith, R.R. Garcia, A. Gettelman, M.A. Giorgetta, D.E. Kinnison, F. Li, E. Mancini, C. McLandress, S. Pawson, G. Pitari, D.A. Plummer, E. Rozanov, F. Sassi, J.F. Scinocca, K. Shibata, B. Steil, and W. Tian, Chemistry-climate model simulations of 21st century stratospheric climate and circulation changes, *J. Clim.*, *23* (20), 5349-5374, doi: 10.1175/2010JCLI3404.1, 2010.
- Caldeira, K., and L. Wood, Global and Arctic climate engineering: Numerical model studies, *Phil. Trans. Roy. Soc. A*, *366* (1882), 4039-4056, 2008.
- Charlton-Perez, A.J., L.M. Polvani, J. Austin, and F. Li, The frequency and dynamics of stratospheric sudden warmings in the 21st century, *J. Geophys. Res.*, *113*, D16116, doi: 10.1029/2007JD009571, 2008.
- Charlton-Perez, A.J., E. Hawkins, V. Eyring, I. Cionni, G.E. Bodeker, D.E. Kinnison, H. Akiyoshi, S.M. Frith, R. Garcia, A. Gettelman, J.F. Lamarque, T. Nakamura, S. Pawson, Y. Yamashita, S. Bekki, P. Braesicke, M.P. Chipperfield, S. Dhomse, M. Marchand, E. Mancini, O. Morgenstern, G. Pitari, D. Plummer, J.A. Pyle, E. Rozanov, J. Scinocca, K. Shibata, T.G. Shepherd, W. Tian, and D.W. Waugh, The potential to narrow uncertainty in projections of stratospheric ozone over the 21st century, *Atmos. Chem. Phys.*, *10*, 9473-9486, doi: 10.5194/acp-10-

- 9473-2010, 2010.
- Chipperfield, M.P., New version of the TOMCAT/SLIMCAT off-line chemical transport model: Intercomparison of stratospheric tracer experiments, *Quart. J. Roy. Meteorol. Soc.*, *132* (617), 1179-1203, doi: 10.1256/qj.05.51, 2006.
- Chipperfield, M.P., and W. Feng, Comment on: Stratospheric ozone depletion at northern mid-latitudes in the 21st century: The importance of future concentrations of greenhouse gases nitrous oxide and methane, *Geophys. Res. Lett.*, *30* (7), 1389, doi: 10.1029/2002GL016353, 2003.
- Chipperfield, M.P., and V.E. Fioletov (Lead Authors), B. Bregman, J. Burrows, B.J. Connor, J.D. Haigh, N.R.P. Harris, A. Hauchecorne, L.L. Hood, S.R. Kawa, J.W. Krzyścin, J.A. Logan, N.J. Muthama, L. Polvani, W.J. Randel, T. Sasaki, J. Stähelin, R.S. Stolarski, L.W. Thomason, and J.M. Zawodny, Global ozone: Past and Present, Chapter 3 in *Scientific Assessment of Ozone Depletion: 2006*, Global Ozone Research and Monitoring Project—Report No. 50, 572 pp., World Meteorological Organization, Geneva, Switzerland, 2007.
- Chubarova, N.Y., UV variability in Moscow according to long-term UV measurements and reconstruction model, *Atmos. Chem. Phys.*, *8*, 3025-3031, 2008.
- Chubarova, N.Y., Seasonal distribution of aerosol properties over Europe and their impact on UV irradiance, *Atmos. Meas. Tech.*, *2*, 593-608, doi: 10.5194/amt-2-593-2009, 2009.
- Chubarova, N.Y., N.G. Prilepsky, A.N. Rublev, and A.R. Riebau, A mega-fire event in central Russia: Fire weather, radiative, and optical properties of the atmosphere, and consequences for subboreal forest plants, in *Developments in Environmental Science*, Volume 8, edited by A. Bytnerowicz, M. Arbaugh, A. Riebau, and C. Andersen, 247-264, Elsevier B.V., Amsterdam, The Netherlands, available: http://www.fs.fed.us/psw/publications/4451/psw_2009_4451-001_247-264.pdf, 2009.
- CIE (Commission Internationale de l'Éclairage), Reference Action spectra for ultraviolet induced erythema and pigmentation of different human skin types, in *Technical Collection 103/3*, p.15-21, 1993.
- Clarke, L., J. Edmonds, H. Jacoby, H. Pitcher, J. Reilly, and R. Richels, *Scenarios of Greenhouse Gas Emissions and Atmospheric Concentrations*. Sub-report 2.1A of Synthesis and Assessment Product 2.1 by the U.S. Climate Change Science Program and the Subcommittee on Global Change Research. Department of Energy, Office of Biological & Environmental Research, Washington, D.C., U.S.A., 154 pp., 2007.
- Clement, A.C., R. Burgman, and J.R. Norris, Observational and model evidence for positive low-level cloud feedback, *Science*, *325* (5939), 460-464, doi: 10.1126/science.1171255, 2009.
- Cockell, C.S., and C. Córdoba-Jabonero, Coupling of climate change and biotic UV exposure through changing snow-ice covers in terrestrial habitats, *Photochem. Photobiol.*, *79* (1), 26-31, 2004.
- Comiso, J.C., C.L. Parkinson, R. Gersten, and L. Stock, Accelerated decline in the Arctic sea ice cover, *Geophys. Res. Lett.*, *35*, L01703, doi: 10.1029/2007GL0319, 2008.
- Crutzen, P.J., Albedo enhancement by stratospheric sulfur injections: A contribution to resolve a policy dilemma?, *Clim. Change*, *77* (3-4), 211-219, doi: 10.1007/s10584-006-9101-y, 2006.
- de Grandpré, J., S.R. Beagley, V.I. Fomichev, E. Griffioen, J.C. McConnell, A.S. Medvedev, and T.G. Shepherd, Ozone climatology using interactive chemistry: Results from the Canadian Middle Atmosphere Model, *J. Geophys. Res.*, *105* (D21), 26475-26491, 2000.
- Déqué, M., Frequency of precipitation and temperature extremes over France in an anthropogenic scenario: Model results and statistical correction according to observed values, *Global Planet. Change*, *57* (1-2), 16-26, doi: 10.1016/j.gloplacha.2006.11.030, 2007.
- Dhomse, S., M. Weber, I. Wohltmann, M. Rex, and J.P. Burrows, On the possible causes of recent increases in northern hemispheric total ozone from a statistical analysis of satellite data from 1979 to 2003, *Atmos. Chem. Phys.*, *6*, 1165-1180, 2006.
- Douglass, A.R., R.S. Stolarski, M.R. Schoeberl, C.H. Jackman, M.L. Gupta, P.A. Newman, J.E. Nielsen, and E.L. Fleming, Relationship of loss, mean age of air and the distribution of CFCs to stratospheric circulation and implications for atmospheric lifetimes, *J. Geophys. Res.*, *113*, D14309, doi: 10.1029/2007JD009575, 2008.
- Dufresne, J.L., and S. Bony, An assessment of the primary sources of spread of global warming estimates from coupled atmosphere-ocean models, *J. Clim.*, *21* (19), 5135-5144, doi: 10.1175/2008JCLI2239.1, 2008.
- Edvardsen, K., M. Brustad, O. Engelsen, and L. Aksnes, The solar UV radiation level needed for cutaneous production of vitamin D3 in the face. A study conducted among subjects living at a high latitude (68°N), *Photochem. Photobiol. Sci.*, *6*, 57-62, doi: 10.1039/b613263d, 2007.
- Egorova, T., E. Rozanov, V. Zubov, E. Manzini, W. Schmutz, and T. Peter, Chemistry-climate model SOCOL: A validation of the present-day climatology, *Atmos. Chem. Phys.*, *5*, 1557-1576, 2005.
- Engel, A., T. Möbius, H. Bönisch, U. Schmidt, R. Heinz, I. Levin, E. Atlas, S. Aoki, T. Nakazawa, S. Sug-

- awara, F. Moore, D. Hurst, J. Elkins, S. Schauffler, A. Andrews, and K. Boering, Age of stratospheric air unchanged within uncertainties over the past 30 years, *Nature Geoscience*, 2, 28-31, doi: 10.1038/ngeo388, 2009.
- Eyring, V., N.R.P. Harris, M. Rex, T.G. Shepherd, D.W. Fahey, G.T. Amanatidis, J. Austin, M.P. Chipperfield, M. Dameris, P.M. De F. Forster, A. Gettelman, H.F. Graf, T. Nagashima, P.A. Newman, S. Pawson, M.J. Prather, J.A. Pyle, R.J. Salawitch, B.D. Santer, and D.W. Waugh, A strategy for process-oriented validation of coupled chemistry-climate models, *Bull. Amer. Meteorol. Soc.*, 86 (8), 1117-1133, doi: 10.1175/BAMS-86-8-1117, 2005.
- Eyring, V., N. Butchart, D.W. Waugh, H. Akiyoshi, J. Austin, S. Bekki, G.E. Bodeker, B.A. Boville, C. Brühl, M.P. Chipperfield, E. Cordero, M. Dameris, M. Deushi, V.E. Fioletov, S.M. Frith, R.R. Garcia, A. Gettelman, M.A. Giorgetta, V. Grewe, L. Jourdain, D.E. Kinnison, E. Mancini, E. Manzini, M. Marchand, D.R. Marsh, T. Nagashima, P.A. Newman, J.E. Nielsen, S. Pawson, G. Pitari, D.A. Plummer, E. Rozanov, M. Schraner, T.G. Shepherd, K. Shibata, R.S. Stolarski, H. Struthers, W. Tian, and M. Yoshiki, Assessment of temperature, trace species, and ozone in chemistry-climate model simulations of the recent past, *J. Geophys. Res.*, 111, D22308, doi: 10.1029/2006JD007327, 2006.
- Eyring, V., D.W. Waugh, G.E. Bodeker, E. Cordero, H. Akiyoshi, J. Austin, S.R. Beagley, B.A. Boville, P. Braesicke, C. Brühl, N. Butchart, M.P. Chipperfield, M. Dameris, R. Deckert, M. Deushi, S.M. Frith, R.R. Garcia, A. Gettelman, M.A. Giorgetta, D.E. Kinnison, E. Mancini, E. Manzini, D.R. Marsh, S. Matthes, T. Nagashima, P.A. Newman, J.E. Nielsen, S. Pawson, G. Pitari, D.A. Plummer, E. Rozanov, M. Schraner, J.F. Scinocca, K. Semeniuk, T.G. Shepherd, K. Shibata, B. Steil, R.S. Stolarski, W. Tian, and M. Yoshiki, Multimodel projections of stratospheric ozone in the 21st century, *J. Geophys. Res.*, 112, D16303, doi: 10.1029/2006JD008332, 2007.
- Eyring, V., M.P. Chipperfield, M.A. Giorgetta, D.E. Kinnison, E. Manzini, K. Matthes, P.A. Newman, S. Pawson, T.G. Shepherd, and D.W. Waugh, Overview of the new CCMVal reference and sensitivity simulations in support of upcoming ozone and climate assessments and the planned SPARC CCMVal Report, *SPARC Newsletter No. 30*, 20-26, 2008.
- Eyring, V., I. Cionni, G.E. Bodeker, A.J. Charlton-Perez, D.E. Kinnison, J.F. Scinocca, D.W. Waugh, H. Akiyoshi, S. Bekki, M.P. Chipperfield, M. Dameris, S. Dhomse, S.M. Frith, H. Garny, A. Gettelman, A. Kubin, U. Langematz, E. Mancini, M. Marchand, T. Nakamura, L.D. Oman, S. Pawson, G. Pitari, D.A. Plummer, E. Rozanov, T.G. Shepherd, K. Shibata, W. Tian, P. Braesicke, S.C. Hardiman, J.F. Lamarque, O. Morgenstern, J.A. Pyle, D. Smale, and Y. Yamashita, Multi-model assessment of stratospheric ozone return dates and ozone recovery in CCMVal-2 models, *Atmos. Chem. Phys.*, 10, 9451-9472, doi: 10.5194/acp-10-9451-2010, 2010a.
- Eyring, V., I. Cionni, J.-F. Lamarque, H. Akiyoshi, G.E. Bodeker, A.J. Charlton-Perez, S.M. Frith, A. Gettelman, D.E. Kinnison, T. Nakamura, L.D. Oman, S. Pawson, and Y. Yamashita, Sensitivity of 21st century stratospheric ozone to greenhouse gas scenarios, *Geophys. Res. Lett.*, 37, L16807, doi: 10.1029/2010GL044443, 2010b.
- Fleming, E.L., C.H. Jackman, D.K. Weisenstein, and M.K.W. Ko, The impact of interannual variability on multi-decadal total ozone simulations, *J. Geophys. Res.*, 112, D10310, doi: 10.1029/2006JD007953, 2007.
- Fioletov, V.E., G.E. Bodeker, A.J. Miller, R.D. McPeters, and R. Stolarski, Global and zonal total ozone variations estimated from ground-based and satellite measurements: 1964-2000, *J. Geophys. Res.*, 107 (D22), 4647 doi: 10.1029/2001JD001350, 2002.
- Fomichev, V.I., W.E. Ward, S.R. Beagley, C. McLandress, J.C. McConnell, N.A. McFarlane, and T.G. Shepherd, Extended Canadian Middle Atmosphere Model: Zonal-mean climatology and physical parameterizations, *J. Geophys. Res.*, 107 (D10), 4087, doi: 10.1029/2001JD000479, 2002.
- Garcia, R.R., D.R. Marsh, D.E. Kinnison, B.A. Boville, and F. Sassi, Simulation of secular trends in the middle atmosphere, 1950-2003, *J. Geophys. Res.*, 112, D09301, doi: 10.1029/2006JD007485, 2007.
- Garny, H., G.E. Bodeker, and M. Dameris, Trends and variability in stratospheric mixing: 1979-2005, *Atmos. Chem. Phys.*, 7, 5611-5624, 2007.
- Garny, H., M. Dameris, and A. Stenke, Impact of prescribed SSTs on climatologies and long-term trends in CCM simulations, *Atmos. Chem. Phys.*, 9, 6017-6031, 2009.
- Gauss, M., G. Myhre, G. Pitari, M.J. Prather, I.S.A. Isaksson, T.K. Berntsen, G.P. Brasseur, F.J. Dentener, R.G. Derwent, D.A. Hauglustaine, L.W. Horowitz, D.J. Jacob, M. Johnson, K.S. Law, L.J. Mickley, J.-F. Müller, P.-H. Plantevin, J.A. Pyle, H.L. Rogers, D.S. Stevenson, J.K. Sundet, M. van Weele, and O. Wild, Radiative forcing in the 21st century due to ozone changes in the troposphere and the lower stratosphere, *J. Geophys. Res.*, 108 (D9), 4292, doi: 10.1029/2002JD002624, 2003.
- Gillett, N.P., H. Akiyoshi, S. Bekki, V. Eyring, R. Garcia, C.A. McLinden, A. Yu. Karpechko, D.A. Plummer, E. Rozanov, J. Scinocca, and K. Shibata, Attribution of observed changes in stratospheric ozone and tem-

- perature, *Atmos. Chem. Phys. Discuss.*, *10*, 17341-17367, doi: 10.5194/acpd-10-17341-2010, 2010.
- Guillas, S., M.L. Stein, D.J. Wuebbles, and J. Xia, Using chemistry transport modeling in statistical analysis of stratospheric ozone trends from observations, *J. Geophys. Res.*, *109*, D22303, doi: 10.1029/2004JD005049, 2004.
- Hadjinicolaou, P., and J.A. Pyle, The impact of Arctic ozone depletion on northern middle latitudes: Interannual variability and dynamical control, *J. Atmos. Chem.*, *47* (1), 25-43, 2004.
- Hadjinicolaou, P., J.A. Pyle, M.P. Chipperfield, and J.A. Kettleborough, Effect of interannual meteorological variability on mid-latitude O₃, *Geophys. Res. Lett.*, *24* (23), 2993-2996, 1997.
- Hawkins, E., and R. Sutton, The potential to narrow uncertainty in regional climate predictions, *Bull. Amer. Meteorol. Soc.*, *90* (8), 1095-1107, doi: 10.1175/2009BAMS2607, 2009.
- Heckendorn, P., D. Weisenstein, S. Fueglistaler, B.P. Luo, E. Rozanov, M. Schraner, L.W. Thomason, and T. Peter, Impact of geoengineering aerosols on stratospheric temperature and ozone, *Env. Res. Lett.*, *4* (4), 045108, doi: 10.1088/1748-9326/4/4/045108, 2009.
- Hegglin, M.I., and T.G. Shepherd, Large climate-induced changes in ultraviolet index and stratosphere-to-troposphere ozone flux, *Nature Geoscience*, *2*, 687-691 doi: 10.1038/ngeo604, 2009.
- Herman, J.R., D. Larko, E. Celarier, and J. Ziemke, Changes in the Earth's UV reflectivity from the surface, clouds and aerosols, *J. Geophys. Res.*, *106* (D6), 5353-5368, doi: 10.1029/2000JD900435, 2001.
- IPCC (Intergovernmental Panel on Climate Change), *Emissions Scenarios. A Special Report of Working Group III of the Intergovernmental Panel on Climate Change*, edited by N. Nakicenovic and R. Swart, 570 pp., Cambridge University Press, Cambridge, U.K., and New York, NY, U.S.A., 2000.
- IPCC (Intergovernmental Panel on Climate Change), *Climate Change 2007: The Physical Science Basis: Contribution of Working Group I to the Fourth Assessment Report of the Intergovernmental Panel on Climate Change*, edited by Solomon, S., D. Qin, M. Manning, Z. Chen, M. Marquis, K.B. Averyt, M. Tignor, and H.L. Miller, 996 pp., Cambridge University Press, Cambridge, U.K., and New York, NY, U.S.A., 2007.
- Jacobson, M.Z., and D.G. Streets, Influence of future anthropogenic emissions on climate, natural emissions, and air quality, *J. Geophys. Res.*, *114*, D08118, doi: 10.1029/2008JD011476, 2009.
- Jöckel, P., H. Tost, A. Pozzer, C. Brühl, J. Buchholz, L. Ganzeveld, P. Hoor, A. Kerkweg, M.G. Lawrence, R. Sander, B. Steil, G. Stiller, M. Tanarhte, D. Taraborrelli, J. van Aardenne, and J. Lelieveld, The atmospheric chemistry general circulation model ECHAM5/MESy1: Consistent simulation of ozone from the surface to the mesosphere, *Atmos. Chem. Phys.*, *6*, 5067-5104, doi: 10.5194/acp-6-5067-2006, 2006.
- Jonsson, A.I., V.I. Fomichev, and T.G. Shepherd, The effect of nonlinearity in CO₂ heating rates on the attribution of stratospheric ozone and temperature changes. *Atmos. Chem. Phys.*, *9*, 8447-8452, doi: 10.5194/acp-9-8447-2009, 2009.
- Jourdain, L., S. Bekki, F. Lott, and F. Lefèvre, The coupled chemistry-climate model LMDz-REPROBUS: Description and evaluation of a transient simulation of the period 1980–1999, *Ann. Geophys.*, *26*, 1391-1413, doi: 10.5194/angeo-26-1391-2008, 2008.
- Kazadzis, S., A. Bais, V. Amiridis, D. Balis, C. Meleti, N. Kouremeti, C.S. Zerefos, S. Rapsomanikis, M. Petrakakis, A. Kelesis, P. Tzoumaka, and K. Kelektsoglou, Nine years of UV aerosol optical depth measurements at Thessaloniki, Greece, *Atmos. Chem. Phys.*, *7*, 2091-2101, doi: 10.5194/acp-7-2091-2007, 2007.
- Kazantzidis, A., A.F. Bais, D.S. Balis, E. Kosmidis, and C.S. Zerefos, Sensitivity of solar UV radiation to ozone and temperature profiles at Thessaloniki (40.5°N, 23°E), Greece, *J. Atmos. Sol.-Terr. Phys.*, *67* (14), 1321-1330, doi: 10.1016/j.jastp.2005.05.003, 2005.
- Kazantzidis, A., A.F. Bais, M.M. Zempila, S. Kazadzis, P.N. den Outer, T. Koskela, and H. Slaper, Calculations of the human vitamin D exposure from UV spectral measurements at three European stations, *Photochem. Photobiol. Sci.*, *8*, 45-51, doi: 10.1039/b811216a, 2009.
- Kazantzidis, A., K. Tourpali, and A.F. Bais, Variability of cloud-free ultraviolet dose rates on global scale due to modeled scenarios of future ozone recovery, *Photochem. Photobiol.*, *86*, 117-122, doi: 10.1111/j.1751-1097.2009.00645.x, 2010.
- Kimlin, M.G., W.J. Olds, and M.R. Moore, Location and vitamin D synthesis: Is the hypothesis validated by geophysical data?, *J. Photochem. Photobiol. B: Biol.*, *86* (3), 234-239, doi: 10.1016/j.jphotobiol.2006.10.004, 2007.
- Kinne, S., M. Schulz, C. Textor, S. Guibert, Y. Balkanski, S.E. Bauer, T. Berntsen, T.F. Berglen, O. Boucher, M. Chin, W. Collins, F. Dentener, T. Diehl, R. Easter, J. Feichter, D. Fillmore, S. Ghan, P. Ginoux, S. Gong, A. Grini, J. Hendricks, M. Herzog, L. Horowitz, I. Isaksen, T. Iversen, A. Kirkavag, S. Kloster, D. Koch, J.E. Kristjansson, M. Krol, A. Lauer, J.-F. Lamarque, G. Lesins, X. Liu, U. Lohmann, V. Montanaro, G. Myhre, J. Penner, G. Pitari,

- S. Reddy, O. Seland, P. Stier, T. Takemura, and X. Tie, An AeroCom initial assessment – optical properties in aerosol component modules of global models, *Atmos. Chem. Phys.*, *6*, 1815-1834, doi: 10.5194/acp-6-1815-2006, 2006.
- Kinnison, D.E., K.E. Grant, P.S. Connell, D.A. Rotman, and D.J. Wuebbles, The chemical and radiative effects of the Mount Pinatubo eruption, *J. Geophys. Res.*, *99* (D12), 25705-25731, 1994.
- Kirk-Davidoff, D.B., E.J. Hints, J.G. Anderson, and D.W. Keith, The effect of climate change on ozone depletion through changes in stratospheric water vapour, *Nature*, *402*, 399-401, doi: 10.1038/46521, 1999.
- Konopka, P., J.-U. Groß, K.W. Hoppel, H.-M. Steinhilber, and R. Müller, Mixing and chemical ozone loss during and after the Antarctic polar vortex major warming in September 2002, *J. Atmos. Sci.*, *62* (3), 848-859, 2005.
- Lamarque, J.-F., D.E. Kinnison, P.G. Hess, and F.M. Vitt, Simulated lower stratospheric trends between 1970 and 2005: Identifying the role of climate and composition changes, *J. Geophys. Res.*, *113*, D12301, doi: 10.1029/2007JD009277, 2008.
- Lamarque, J.-F., T.C. Bond, V. Eyring, C. Granier, A. Heil, Z. Klimont, D. Lee, C. Liou, A. Mieville, B. Owen, M.G. Schultz, D. Shindell, S.J. Smith, E. Stehfest, J. Van Aardenne, O.R. Cooper, M. Kainuma, N. Mahowald, J.R. McConnell, V. Naik, K. Rami, and D.P. van Vuuren, Historical (1850–2000) gridded anthropogenic and biomass burning emissions of reactive gases and aerosols: Methodology and application, *Atmos. Chem. Phys.*, *10*, 7017-7039, doi: 10.5194/acp-10-7017-2010, 2010.
- Lapeta, B., O. Engelsen, Z. Litynska, B. Kois, and A. Kylling, Sensitivity of surface UV radiation and ozone column retrieval to ozone and temperature profiles, *J. Geophys. Res.*, *105* (D4), 5001-5007, 2000.
- Li, F., R.S. Stolarski, and P.A. Newman, Stratospheric ozone in the post-CFC era, *Atmos. Chem. Phys.*, *9*, 2207-2213, doi: 10.5194/acp-9-2207-2009, 2009.
- Lindfors, A., and A. Arola, On the wavelength-dependent attenuation of UV radiation by clouds, *Geophys. Res. Lett.*, *35*, L05806, doi: 10.1029/2007GL032571, 2008.
- Madronich, S., Analytic formula for the clear-sky UV index, *Photochem. Photobiol.*, *83* (6), 1537-1538, doi: 10.1111/j.1751-1097.2007.00200.x, 2007.
- Madronich, S., and S. Flocke: The role of solar radiation in atmospheric chemistry, in *The Handbook of Environmental Chemistry*, edited by P. Boule, 1-26, Springer-Verlag, Berlin Heidelberg, 1999.
- Madronich S., R.L. McKenzie, L.O. Björn, and M.M. Caldwell, Changes in biologically active ultraviolet radiation reaching the Earth's surface, *Photochem. Photobiol. B: Biology*, *46* (1-3), 5-19, doi: 10.1016/S1011-1344(98)00182-1, 1998.
- Matthews, H.D., and K. Caldeira, Transient climate-carbon simulations of planetary geoengineering, *Proc. Nat. Acad. Sci.*, *104* (24), 9949-9954, doi: 10.1073/pnas.0700419104, 2007.
- Mayer, B., and A. Kylling, Technical note: The libRadtran software package for radiative transfer calculations – description and examples of use, *Atmos. Chem. Phys.*, *5*, 1855-1877, doi: 10.5194/acp-5-1855-2005, 2005.
- McKenzie, R., D. Smale, G. Bodeker, and H. Claude, Ozone profile differences between Europe and New Zealand: Effects on surface UV irradiance and its estimation from satellite sensors, *J. Geophys. Res.*, *108* (D6), 4179, doi: 10.1029/2002JD002770, 2003.
- McKenzie, R.L., C. Weinreis, P.V. Johnston, B. Liley, H. Shiona, M. Kotkamp, D. Smale, N. Takegawa, and Y. Kondo, Effects of urban pollution on UV spectral irradiances, *Atmos. Chem. Phys.*, *8*, 5683-5697, doi: 10.5194/acp-8-5683-2008, 2008.
- McKenzie, R.L., J.B. Liley, and L.O. Björn, UV radiation: Balancing risks and benefits, *Photochem. Photobiol.*, *85* (1), 88-98, doi: 10.1111/j.1751-1097.2008.00400.x, 2009.
- McLandress, C., and T.G. Shepherd, Simulated anthropogenic changes in the Brewer-Dobson circulation, including its extension to high latitudes, *J. Clim.*, *22* (6), 1516-1540, doi: 10.1175/2008JCLI2679.1, 2009a.
- McLandress, C., and T.G. Shepherd, Impact of climate change on stratospheric sudden warmings as simulated by the Canadian Middle Atmosphere Model, *J. Clim.*, *22* (20), 5449-5463, 2009b.
- McLandress, C., A.I. Jonsson, D.A. Plummer, M.C. Reader, J.F. Scinocca, and T.G. Shepherd, Separating the dynamical effects of climate change and ozone depletion: Part 1. Southern Hemisphere stratosphere, *J. Clim.*, *23* (18), 5002-5020, doi: 10.1175/2010JCLI3586.1, 2010.
- Meehl, G.A., T.F. Stocker, W.D. Collins, P. Friedlingstein, A.T. Gaye, J.M. Gregory, A. Kitoh, R. Knutti, J.M. Murphy, A. Noda, S.C.B. Raper, I.G. Watterson, A.J. Weaver, and Z.-C. Zhao, Global climate projections, in *Climate Change 2007: The Physical Science Basis. Contribution of Working Group I to the Fourth Assessment Report of the Intergovernmental Panel on Climate Change*, edited by S. Solomon, D. Qin, M. Manning, Z. Chen, M. Marquis, K.B. Averyt, M. Tignor and H.L. Miller, 996 pp., Cambridge University Press, Cambridge, U.K., and New York, NY, U.S.A., 2007.
- Millard, G.A., T.A. Mather, D.M. Pyle, W.I. Rose, and B. Thornton, Halogen emissions from a small volcanic eruption: Modeling the peak concentrations,

- dispersion, and volcanically induced ozone loss in the stratosphere, *Geophys. Res. Lett.*, *33*, L19815, doi: 10.1029/2006GL026959, 2006.
- Miller, A.J., R.M. Nagatani, L.E. Flynn, S. Kondragunta, E. Beach, R. Stolarski, R.D. McPeters, P.K. Bhartia, M.T. DeLand, C.H. Jackman, D.J. Wuebbles, K.O. Patten, and R.P. Cebula, A cohesive total ozone data set from SBUV(2) satellite system, *J. Geophys. Res.*, *107*(D23), 4701, doi: 10.1029/2001JD000853, 2002.
- Morgenstern, O., P. Braesicke, M.M. Hurwitz, F.M. O'Connor, A.C. Bushell, C.E. Johnson, and J.A. Pyle, The world avoided by the Montreal Protocol, *Geophys. Res. Lett.*, *35*, L16811, doi: 10.1029/2008GL034590, 2008.
- Morgenstern, O., P. Braesicke, F.M. O'Connor, A.C. Bushell, C.E. Johnson, S.M. Osprey, and J.A. Pyle, Evaluation of the new UKCA climate-composition model - Part 1: The stratosphere, *Geosci. Model Dev.*, *2*, 43-57, doi: 10.5194/gmd-2-43-2009, 2009.
- Morgenstern, O., M.A. Giorgetta, K. Shibata, V. Eyring, D.W. Waugh, T.G. Shepherd, H. Akiyoshi, J. Austin, A.J.G. Baumgaertner, S. Bekki, P. Braesicke, C. Brühl, M.P. Chipperfield, D. Cugnet, M. Dameris, S. Dhomse, S.M. Frith, H. Garny, A. Gettelman, S.C. Hardiman, M.I. Hegglin, P. Jöckel, D.E. Kinnison, J.-F. Lamarque, E. Mancini, E. Manzini, M. Marchand, M. Michou, T. Nakamura, J.E. Nielsen, D. Olivieri, G. Pitari, D.A. Plummer, E. Rozanov, J.F. Scinocca, D. Smale, H. Teyssède, M. Toohey, W. Tian, and Y. Yamashita, Review of the formulation of present-generation stratospheric chemistry-climate models and associated external forcings, *J. Geophys. Res.*, *115*, D00M02, doi: 10.1029/2009JD013728, 2010.
- Moss, R., M. Babiker, S. Brinkman, E. Calvo, T. Carter, J. Edmonds, I. Elgizouli, S. Emori, L. Erda, K. Hibbard, R. Jones, M. Kainuma, J. Kelleher, J.-F. Lamarque, M. Manning, B. Matthews, J. Meehl, L. Meyer, J. Mitchell, N. Nakicenovic, B. O'Neill, R. Pichs, K. Riahi, S. Rose, P. Runci, R. Stouffer, D. van Vuuren, J. Weyant, T. Wilbanks, J.P. van Ypersele, and M. Zurek, *Towards New Scenarios for Analysis of Emissions, Climate Change, Impacts, and Response Strategies*, IPCC Expert Meeting Report, Intergovernmental Panel on Climate Change, Geneva, 132 pp., available: <http://www.aims.ucar.edu/docs/IPCC.meetingreport.final.pdf>, 2008.
- Newman, P.A., J.S. Daniel, D.W. Waugh, and E.R. Nash, A new formulation of equivalent effective stratospheric chlorine (EESC), *Atmos. Chem. Phys.*, *7*, 4537-4552, doi: 10.5194/acp-7-4537-2007, 2007.
- Nissen, K.M., K. Matthes, U. Langematz, and B. Mayer, Towards a better representation of the solar cycle in general circulation models, *Atmos. Chem. Phys.*, *7*, 5391-5400, doi: 10.5194/acp-7-5391-2007, 2007.
- Oman, L., D.W. Waugh, S. Pawson, R.S. Stolarski, and J.E. Nielsen, Understanding the changes of stratospheric water vapor in coupled chemistry-climate model simulations, *J. Atmos. Sci.*, *65* (10), 3278-3291, doi: 10.1175/2008JAS2696, 2008.
- Oman, L.D., D.W. Waugh, S.R. Kawa, R.S. Stolarski, A.R. Douglass, and P.A. Newman, Mechanisms and feedbacks causing changes in upper stratospheric ozone in the 21st century, *J. Geophys. Res.*, *115*, D05303, doi: 10.1029/2009JD012397, 2010.
- Overland, J.E., and M. Wang, Future regional Arctic sea ice declines, *Geophys. Res. Lett.*, *34*, L17705, doi: 10.1029/2007GL030808, 2007.
- Pawson, S., R.S. Stolarski, A.R. Douglass, P.A. Newman, J.E. Nielsen, S.M. Frith, and M.L. Gupta, Goddard Earth Observing System chemistry-climate model simulations of stratospheric ozone-temperature coupling between 1950 and 2005, *J. Geophys. Res.*, *113*, D12103, doi: 10.1029/2007JD009511, 2008.
- Pitari, G., E. Mancini, V. Rizi, and D.T. Shindell, Impact of future climate and emission changes on stratospheric aerosols and ozone, *J. Atmos. Sci.*, *59* (3), 414-440, 2002.
- Portmann, R.W., and S. Solomon, Indirect radiative forcing of the ozone layer during the 21st century, *Geophys. Res. Lett.*, *34*, L02813, doi: 10.1029/2006GL028252, 2007.
- Portmann, R.W., S. Solomon, R.R. Garcia, L.W. Thomason, L.R. Poole, and M.P. McCormick, Role of aerosol variations in anthropogenic ozone depletion in the polar regions, *J. Geophys. Res.*, *101* (D17), 22991-23006, 1996.
- Portmann, R.W., S.S. Brown, T. Gierczak, R.K. Talukdar, J.B. Burkholder, and A.R. Ravishankara, Role of nitrogen oxides in the stratosphere: A reevaluation based on laboratory studies, *Geophys. Res. Lett.*, *26* (15), 2387-2390, 1999.
- Randel, W.J., F. Wu, H. Vömel, G.E. Nedoluha, and P. Forster, Decreases in stratospheric water vapor after 2001: Links to changes in the tropical tropopause and the Brewer-Dobson circulation, *J. Geophys. Res.*, *111*, D12312, doi: 10.1029/2005JD006744, 2006.
- Randel, W.J., K.P. Shine, J. Austin, J. Barnett, C. Claud, N.P. Gillett, P. Keckhut, U. Langematz, R. Lin, C. Long, C. Mears, A. Miller, J. Nash, D.J. Seidel, D.W.J. Thompson, F. Wu, and S. Yoden, An update of observed stratospheric temperature trends, *J. Geophys. Res.*, *114*, D02107, doi: 10.1029/2008JD010421, 2009.
- Randeniya, L.K., P.F. Vohralik, and I.C. Plumb, Stratospheric ozone depletion at northern mid latitudes in the 21st century: The importance of future concentrations of greenhouse gases nitrous oxide and

- methane, *Geophys. Res. Lett.*, *29* (4), 1051, doi: 10.1029/2001GL014295, 2002.
- Rasch, P.J., S. Tilmes, R.P. Turco, A. Robock, L. Oman, C.-C. Chen, G.L. Stenchikov, and R.R. Garcia, An overview of geoengineering of climate using stratospheric sulphate aerosols, *Phil. Trans. R. Soc. A*, *366* (1882), 4007-4037, doi: 10.1098/rsta.2008.0131, 2008.
- Ravishankara, A.R., J.S. Daniel, and R.W. Portmann, Nitrous oxide (N₂O): The dominant ozone-depleting substance emitted in the 21st century, *Science*, *326* (5949), 123-125, doi: 10.1126/science.1176985, 2009.
- Riahi, K., A. Grübler, and N. Nakicenovic, Scenarios of long-term socio-economic and environmental development under climate stabilization, *Technological Forecasting and Social Change*, *74* (7), 887-935, doi: 10.1016/j.techfore.2006.05.026, 2007.
- Rieder, H.E., F. Holawe, S. Simic, M. Blumthaler, J.W. Krzyscin, J.E. Wagner, A.W. Schmalwieser, and P. Weihs, Reconstruction of erythemal UV-doses for two stations in Austria: A comparison between alpine and urban regions, *Atmos. Chem. Phys.*, *8*, 6309-6323, doi: 10.5194/acp-8-6309-2008, 2008.
- Rind, D., J. Lerner, J. Jonas, and C. McLinden, Effects of resolution and model physics on tracer transports in the NASA Goddard Institute for Space Studies general circulation models, *J. Geophys. Res.*, *112*, D09315, doi: 10.1029/2006JD007476, 2007.
- Robock, A., A. Marquardt, B. Kravitz, and G. Stenchikov, Benefits, risks, and costs of stratospheric geoengineering, *Geophys. Res. Lett.*, *36*, L19703, doi: 10.1029/2009GL039209, 2009.
- Rohs, S., C. Schiller, M. Riese, A. Engel, U. Schmidt, T. Wetter, I. Levin, T. Nakazawa, and S. Aoki, Long-term changes of methane and hydrogen in the stratosphere in the period 1978–2003 and their impact on the abundance of stratospheric water vapor, *J. Geophys. Res.*, *111*, D14315, doi: 10.1029/2005JD006877, 2006.
- Rosenfield, J.E., and A.R. Douglass, Doubled CO₂ effects on NO_y in a coupled 2D model, *Geophys. Res. Lett.*, *25* (23), 4381-4384, 1998.
- Royal Society, *Geoengineering the Climate: Science, Governance and Uncertainty*, Report 10/09, 98 pp., London GB, Royal Society, available: <http://royalsociety.org/geoengineering-the-climate/>, 2009.
- Schraner, M., E. Rozanov, C. Schnadt Poberaj, P. Kenzelmann, A.M. Fischer, V. Zubov, B.P. Luo, C.R. Hoyle, T. Egorova, S. Fueglistaler, S. Brönnimann, W. Schmutz, and T. Peter, Technical Note: Chemistry-climate model SOCOL: Version 2.0 with improved transport and chemistry/microphysics schemes, *Atmos. Chem. Phys.*, *8*, 5957-5974, doi: 10.5194/acp-8-5957-2008, 2008.
- Schulz, M., C. Textor, S. Kinne, Y. Balkanski, S. Bauer, T. Berntsen, T. Berglen, O. Boucher, F. Dentener, S. Guibert, I.S.A. Isaksen, T. Iversen, D. Koch, A. Kirkevåg, X. Liu, V. Montanaro, G. Myhre, J.E. Penner, G. Pitari, S. Reddy, Ø. Seland, P. Stier, and T. Takemura, Radiative forcing by aerosols as derived from the AeroCom present-day and pre-industrial simulations, *Atmos. Chem. Phys.*, *6*, 5225-5246, doi: 10.5194/acp-6-5225-2006, 2006.
- Schwander, H., P. Koepke, and A. Ruggaber, Uncertainties in modeled UV irradiances due to limited accuracy and availability of input data, *J. Geophys. Res.*, *102* (D8), 9419-9429, doi: 10.1029/97JD00244, 1997.
- Scinocca, J.F., N.A. McFarlane, M. Lazare, J. Li, and D. Plummer, Technical Note: The CCCma third generation AGCM and its extension into the middle atmosphere, *Atmos. Chem. Phys.*, *8*, 7055-7074, doi: 10.5194/acp-8-7055-2008, 2008.
- Shepherd, T.G., Dynamics, stratospheric ozone, and climate change, *Atmos.-Ocean*, *46* (1), 117-138, doi: 10.3137/ao.460106, 2008.
- Shepherd, T.G., and A.I. Jonsson, On the attribution of stratospheric ozone and temperature changes to changes in ozone-depleting substances and well-mixed greenhouse gases, *Atmos. Chem. Phys.*, *8*, 1435-1444, doi: 10.5194/acp-8-1435-2008, 2008.
- Shindell, D.T., D. Rind, and P. Lonergan, Increased polar stratospheric ozone losses and delayed eventual recovery owing to increasing greenhouse-gas concentrations, *Nature*, *392*, 589-592, doi: 10.1038/33385, 1998.
- Shibata, K., and M. Deushi, Long-term variations and trends in the simulation of the middle atmosphere 1980-2004 by the chemistry-climate model of the Meteorological Research Institute, *Ann. Geophys.*, *26*, 1299-1326, doi: 10.5194/angeo-26-1299-2008, 2008a.
- Shibata, K., and M. Deushi, Simulations of the stratospheric circulation and ozone during the recent past (1980-2004) with the MRI chemistry-climate model, *CGER's Supercomputer Monograph Report Vol.13*, Center for Global Environmental Research, National Institute for Environmental Studies, Japan, 154 pp., 2008b.
- Sinnhuber, B.-M., and I. Folkins, Estimating the contribution of bromoform to stratospheric bromine and its relation to dehydration in the tropical tropopause layer, *Atmos. Chem. Phys.*, *6*, 4755-4761, doi: 10.5194/acp-6-4755-2006, 2006.
- Sinnhuber, B.-M., N. Sheode, M. Sinnhuber, M.P. Chipperfield, and W. Feng, The contribution of anthropogenic bromine emissions to past stratospheric ozone trends: A modeling study, *Atmos. Chem. Phys.*, *9*, 2863-2871, doi: 10.5194/acp-9-2863-2009, 2009.

- Solomon, S., R.W. Portmann, R.R. Garcia, L.W. Thomason, L.R. Poole, and M.P. McCormick, The role of aerosol variations in anthropogenic ozone depletion at northern midlatitudes, *J. Geophys. Res.*, *101* (D3), 6713-6727, doi: 10.1029/95JD03353, 1996.
- Solomon, S., R.W. Portmann, T. Sasaki, D.J. Hofmann, and D.W.J. Thompson, Four decades of ozonesonde measurements over Antarctica, *J. Geophys. Res.*, *110*, D21311, doi: 10.1029/2005JD005917, 2005.
- Solomon, S., D. Qin, M. Manning, R.B. Alley, T. Bernsten, N.L. Bindoff, Z. Chen, A. Chidthaisong, J.M. Gregory, G.C. Hegerl, M. Heimann, B. Hewitson, B.J. Hoskins, F. Joos, J. Jouzel, V. Kattsov, U. Lohmann, T. Matsuno, M. Molina, N. Nicholls, J. Overpeck, G. Raga, V. Ramaswamy, J. Ren, M. Rusticucci, R. Somerville, T.F. Stocker, P. Whetton, R.A. Wood, and D. Wratt, Technical Summary. In: *Climate Change 2007: The Physical Science Basis. Contribution of Working Group I to the Fourth Assessment Report of the Intergovernmental Panel on Climate Change*, edited by S. Solomon, D. Qin, M. Manning, Z. Chen, M. Marquis, K.B. Averyt, M. Tignor and H.L. Miller, 996 pp., Cambridge University Press, Cambridge, U.K., and New York, NY, U.S.A., 2007.
- Son, S.-W., N.F. Tandon, L.M. Polvani, and D.W. Waugh, Ozone hole and Southern Hemisphere climate change, *Geophys. Res. Lett.*, *36*, L15705, doi: 10.1029/2009GL038671, 2009.
- SPARC (Stratospheric Processes And their Role in Climate), *Assessment of Stratospheric Aerosols Properties*, edited by L. Thomason and Th. Peter, SPARC Report No. 4, WCRP-124, WMO/TD- No. 1295, 2006.
- SPARC CCMVal, *SPARC CCMVal Report on the Evaluation of Chemistry-Climate Models*, edited by V. Eyring, T.G. Shepherd, D.W. Waugh, SPARC Report No. 5, WCRP-132, WMO/TD-No. 1526, available: http://www.atmosp.physics.utoronto.ca/SPARC/ccmval_final/index.php, 2010.
- Staiger, H., P.N. den Outer, A.F. Bais, U. Feister, B. Johnsen, and L. Vuilleumier, Hourly resolved cloud modification factors in the ultraviolet, *Atmos. Chem. Phys.*, *8*, 2493-2508, doi: 10.5194/acp-8-2493-2008, 2008.
- Stenke, A., V. Grewe, and M. Ponater, Lagrangian transport of water vapor and cloud water in the ECHAM4 GCM and its impact on the cold bias, *Clim. Dyn.*, *31* (5), 491-506, doi: 10.1007/s00382-007-0347-5, 2008.
- Stenke, A., M. Dameris, V. Grewe, and H. Garny, Implications of Lagrangian transport for simulations with a coupled chemistry-climate model, *Atmos. Chem. Phys.*, *9*, 5489-5504, doi: 10.5194/acp-9-5489-2009, 2009.
- Stolarski, R.S., and S. Frith, Search for evidence of trend slow-down in the long-term TOMS/SBUV total ozone data record: The importance of instrument drift uncertainty, *Atmos. Chem. Phys.*, *6*, 4057-4065, doi: 10.5194/acp-6-4057-2006, 2006.
- Strahan, S.E., and B.C. Polansky, Meteorological implementation issues in chemistry and transport models, *Atmos. Chem. Phys.*, *6*, 2895-2910, doi: 10.5194/acp-6-2895-2006, 2006.
- Stroeve, J., M.M. Holland, W. Meier, T. Scambos, and M. Serreze, Arctic sea ice decline: Faster than forecast, *Geophys. Res. Lett.*, *34*, L09501, doi: 10.1029/2007GL029703, 2007.
- Tanskanen, A., and T. Manninen, Effective UV surface albedo of seasonally snow-covered lands, *Atmos. Chem. Phys.*, *7*, 2759-2764, doi: 10.5194/acp-7-2759-2007, 2007.
- Taylor, K.E., R.J. Stouffer, and G.A. Meehl, A Summary of the CMIP5 Experiment Design, https://cmip.llnl.gov/cmip5/docs/Taylor_CMIP5_design.pdf, 2009.
- Tegen, I., M. Werner, S.P. Harrison, and K.E. Kohfeld, Relative importance of climate and land use in determining present and future global soil dust emission, *Geophys. Res. Lett.*, *31*, L05105, doi: 10.1029/2003GL019216, 2004.
- Telford, P., P. Braesicke, O. Morgenstern, and J. Pyle, Re-assessment of causes of ozone column variability following the eruption of Mount Pinatubo using a nudged CCM, *Atmos. Chem. Phys.*, *9*, 4251-4260, doi: 10.5194/acp-9-4251-2009, 2009.
- Teyssède, H., M. Michou, H.L. Clark, B. Josse, F. Karcher, D. Olivié, V.-H. Peuch, D. Saint-Martin, D. Cariolle, J.-L. Attié, P. Nédélec, P. Ricaud, V. Thouret, R.J. van der A, A. Volz-Thomas, and F. Chéroux, A new tropospheric and stratospheric Chemistry and Transport Model MOCAGE-Climat for multi-year studies: Evaluation of the present-day climatology and sensitivity to surface processes, *Atmos. Chem. Phys.*, *7*, 5815-5860, doi: 10.5194/acp-7-5815-2007, 2007.
- Tian, W., and M.P. Chipperfield, A new coupled chemistry-climate model for the stratosphere: The importance of coupling for future O₃-climate predictions, *Quart. J. Roy. Meteorol. Soc.*, *131* (605), 281-303, 2005.
- Tian, W., M.P. Chipperfield, L.J. Gray, and J.M. Zawodny, Quasi-biennial oscillation and tracer distributions in a coupled chemistry-climate model, *J. Geophys. Res.*, *111*, D20301, doi: 10.1029/2005JD006871, 2006.
- Tian, W., M.P. Chipperfield, and D. Lu, Impact of increasing stratospheric water vapor on ozone depletion and temperature change, *Adv. Atm. Sci.*, *26* (3), 423-437, doi: 10.1007/s00376-009-0423-3, 2009.

- Tie, X., and G. Brasseur, The response of stratospheric ozone to volcanic eruptions: Sensitivity to atmospheric chlorine loading, *Geophys. Res. Lett.*, 22 (22), 3035-3038, doi: 10.1029/95GL03057, 1995.
- Tilmes, S., R. Müller, and R. Salawitch, The sensitivity of polar ozone depletion to proposed geoengineering schemes, *Science*, 320 (5880), 1201-1204, doi: 10.1126/science.1153966, 2008a.
- Tilmes S., R. Müller, R.J. Salawitch, U. Schmidt, C.R. Webster, H. Oelhaf, C.C. Camy-Peyret, and J.M. Russell III, Chemical ozone loss in the Arctic winter 1991-1992, *Atmos. Chem. Phys.*, 8, 1897-1910, doi: 10.5194/acp-8-1897-2008, 2008b.
- Tilmes, S., R.R. Garcia, D.E. Kinnison, A. Gettelman, and P.J. Rasch, Impact of geoengineered aerosols on the troposphere and stratosphere, *J. Geophys. Res.*, 114, D12305, doi: 10.1029/2008JD011420, 2009.
- Tourpali K., A.F. Bais, A. Kazantzidis, C.S. Zerefos, H. Akiyoshi, J. Austin, C. Brühl, N. Butchart, M.P. Chipperfield, M. Dameris, M. Deushi, V. Eyring, M.A. Giorgetta, D.E. Kinnison, E. Mancini, D.R. Marsh, T. Nagashima, G. Pitari, D.A. Plummer, E. Rozanov, K. Shibata, and W. Tian, Clear sky UV simulations for the 21st century based on ozone and temperature projections from Chemistry-Climate Models, *Atmos. Chem. Phys.*, 9, 1165-1172, doi: 10.5194/acp-9-1165-2009, 2009.
- Trenberth, K.E., and J.T. Fasullo, Global warming due to increasing absorbed solar radiation, *Geophys. Res. Lett.*, 36, L07706, doi: 10.1029/2009GL037527, 2009.
- Tsay, S.-C., and K. Stamnes, Ultraviolet radiation in the Arctic: The impact of potential ozone depletions and cloud effects, *J. Geophys. Res.*, 97 (D8), 7829-7840, 1992.
- UNEP (United Nations Environment Programme), *Environmental Effects of Ozone Depletion and Its Interaction with Climate Change: 2006 Assessment*, Nairobi, 206 pp., 2007.
- UNEP (United Nations Environment Programme), *Environmental Effects of Ozone Depletion and Its Interactions with Climate Change: 2010 Assessment*, Nairobi, available: http://www.unep.ch/ozone/Assessment_Panels/EEAP/index.shtml, 2010.
- van Vuuren, D.P., M.G.J. den Elzen, P.L. Lucas, B. Eickhout, B.J. Strengers, B. van Ruijven, S. Wonink, and R. van Houdt, Stabilizing greenhouse gas concentrations at low levels: An assessment of reduction strategies and costs, *Clim. Change*, 81, 119-159, doi: 10.1007/s10584-006-9172-9, 2007.
- Waibel, A.E., Th. Peter, K.S. Carslaw, H. Oelhaf, G. Wetzel, P.J. Crutzen, U. Pöschl, A. Tsias, E. Reimer, and H. Fischer, Arctic ozone loss due to denitrification, *Science*, 283 (5410), 2064-2069, doi: 10.1126/science.283.5410.2064, 1999.
- Wall, D.H., Global change tipping points: Above- and below-ground biotic interactions in a low diversity ecosystem, *Phil. Trans. Roy. Soc. B*, 362 (1488), 2291-2306, doi: 10.1098/rstb.2006.1950, 2007.
- Waugh, D.W., and V. Eyring, Quantitative performance metrics for stratospheric-resolving chemistry-climate models, *Atmos. Chem. Phys.*, 8, 5699-5713, doi: 10.5194/acp-8-5699-2008, 2008.
- Waugh, D.W., L. Oman, S.R. Kawa, R.S. Stolarski, S. Pawson, A.R. Douglass, P.A. Newman, and J.E. Nielsen, Impacts of climate change on stratospheric ozone recovery, *Geophys. Res. Lett.*, 36, L03805, doi: 10.1029/2008GL036223, 2009.
- Webb, A.R., and O. Engelsen, Calculated ultraviolet exposure levels for a healthy vitamin D status, *Photochem. Photobiol.*, 82, 1697-1703, 2006.
- Webb, A.R., L. Kline, and M.F. Holick, Influence of season and latitude on the cutaneous synthesis of vitamin D3: Exposure to winter sunlight in Boston and Edmonton will not promote vitamin D3 synthesis in human skin, *J. Clin. Endocrin. Metabol.*, 67 (2), 373-378, doi: 10.1210/jcem-67-2-373, 1988.
- Wigley, T.M.L., A combined mitigation/geoengineering approach to climate stabilization, *Science*, 314 (5798), 452-454, doi: 10.1126/science.1131728, 2006.
- Wohltmann, I., R. Lehmann, M. Rex, D. Brunner, and J.A. Mäder, A process-oriented regression model for column ozone, *J. Geophys. Res.*, 112, D12304, 1-18, doi: 10.1029/2006JD007573, 2007.
- WMO (World Meteorological Organization), *Scientific Assessment of Ozone Depletion: 1998*, Global Ozone Research and Monitoring Project—Report No. 44, Geneva, Switzerland, 1999.
- WMO (World Meteorological Organization), *Scientific Assessment of Ozone Depletion: 2002*, Global Ozone Research and Monitoring Project—Report No. 47, 498 pp., Geneva, Switzerland, 2003.
- WMO (World Meteorological Organization), *Scientific Assessment of Ozone Depletion: 2006*, Global Ozone Research Monitoring Project—Report No. 50, 572 pp., Geneva, Switzerland, 2007.
- Zhang, X., and J.E. Walsh, Toward a seasonally ice-covered Arctic Ocean: Scenarios from the IPCC AR4 model simulations, *J. Clim.*, 19 (9), 1730-1747, doi: 10.1175/JCLI3767.1, 2006.

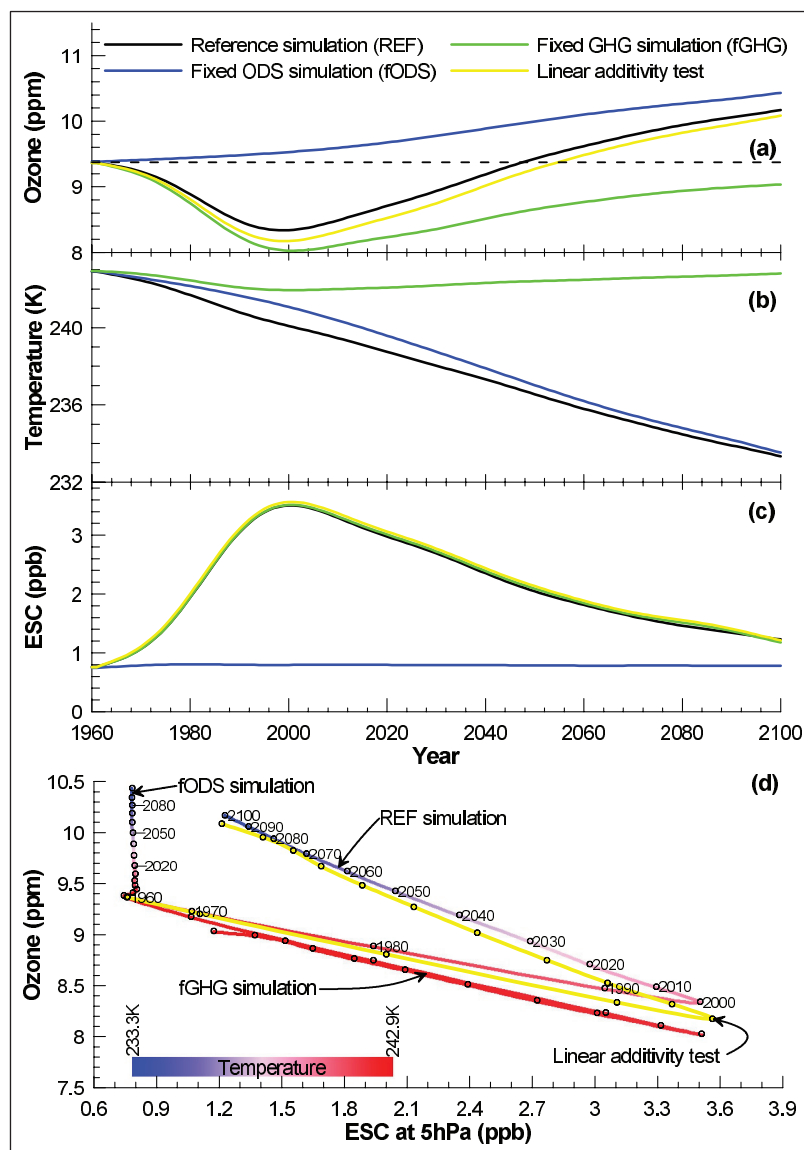
APPENDIX 3A Constructing Correlative Time Series Plots

The correlative time series plots shown in Figures 3-8 and 3-10 were constructed to illustrate how the rise and fall of ESC correlates with stratospheric ozone changes over multi-decadal time periods in scenarios that include and exclude the effects of GHGs and ODSs. This appendix describes how these plots are constructed and evaluated.

Calculated global or regional stratospheric ozone values typically are shown as time series and qualified by the corresponding time series of temperature and ESC because of the strong influence these parameters have in controlling ozone amounts. As an example, Figure 3A-1(a) shows multi-model area weighted ozone mixing ratios from 25°S to 25°N at 5 hPa from 1960 to 2100 for the reference (black), ODSs fixed at 1960 values (blue), and GHGs fixed at 1960 values (green) simulations (Table 3-2). The combination of the fixed ODS and fixed GHG simulations (detailed below), used to test for linear additivity, is shown in yellow. The CCSRNIES, MRI, and WACCM chemistry-climate models were used to form the multi-model trend and all time series were subjected to the TSAM smoothing described in Section 3.3.2.2. The results for temperature and ESC in the same model runs are shown in Figure 3A-1(b) and (c).

To test the linear additivity of the ozone responses to changes in ODSs and GHGs, the sum of the individual ozone responses in the fixed ODS and fixed GHG simulations was evaluated as a function of time (t) as

$$Ozone_{sum}(t) = fGHG_{ozone}(t) + fODS_{ozone}(t) - fODS_{ozone}(1960)$$



where $fODS_{ozone}(1960)$ is the ozone value in 1960 in all simulations (dashed line in Figure 3A-1(a)). This $Ozone_{sum}$ time series is shown as a yellow trace in Figure 3A-1(a) and (d). As for ozone, the linear additivity of the effects of changes in ODSs and GHGs on ESC is tested by calculating

$$ESC_{sum}(t) = fGHG_{ESC}(t) + fODS_{ESC}(t) - fODS_{ESC}(1960)$$

where the ESC terms correspond to those defined above for ozone and $fODS_{ESC}(1960)$ is the ESC value in 1960 in all simulations. The ESC_{sum} time series is shown as a yellow trace in Figure 3A-1(c) and (d). In the interests of clarity, the linear additivity of the effects of changes in ODSs and GHGs on temperature were not investigated and are therefore not shown in panel (b).

A correlative time series plot corresponding to the ozone, temperature,

Figure 3A-1. Time series for (a) ozone (ppm), (b) temperature (K), and (c) ESC (ppb) from CCM simulation results for 5 hPa between 25°S and 25°N (area-weighted) and corresponding correlative time series plot (d). The traces in (d) are color-coded by temperature, and decade year markers are shown with symbols and labels.

and ESC time series is shown in Figure 3A-1(d) with a separate line for each of the scenarios discussed above. Ozone is plotted on the ordinate and ESC on the abscissa because ESC is the expected main driver in the long-term ozone evolution. Symbols are used to mark decade years along each time series line and temperature is indicated with a color scale. A correlative time-series plot is of value because it highlights in a single panel the sensitivity and response of ozone to ESC and other variables in the CCMs over a multi-decadal period in a specific region or globally.

There are several important features of this plot type. For example, in this case, the fODS simulation appears in Figure 3A-1(d) as a nearly vertical line, the length of which indicates the overall effect of non-ODS factors on ozone. The fODS line may also deviate from the vertical indicating that non-ODS factors affect the conversion of ODSs to ESC. If the non-ODS factors had no influence on ozone and ESC, the fODS result would appear as a point on the plot. The temperature gradient along the line indicates a systematic change in this controlling factor. Apart from the fODS simulation, all simulations trace a broad path along the ESC axis from very low concentrations of ESC in 1960, through the peak in ESC around 2000 on the far right of the plot, and back to lower ESC concentrations by the end of the 21st century. In these cases, if ozone was controlled solely by ESC, the increasing and decreasing legs of this time series would trace the same path. Any deviation between the increasing and decreasing legs is indicative of a systematic influence of non-ODS factors. Finally, the separation at each point between the reference and linear additivity test traces indicates the degree to which the influence of ODS and GHG changes on ozone do not act independently, assuming that the uncertainties in these projections are small compared to this separation (McLandress et al., 2010). Thus, the time series displays and the correlative time series plot offer complementary views and insights into the evaluation of the CCM results.

CHAPTER 4

Stratospheric Changes and Climate

Coordinating Lead Authors:

P.M. Forster
D.W.J. Thompson

Lead Authors:

M.P. Baldwin
M.P. Chipperfield
M. Dameris
J.D. Haigh
D.J. Karoly
P.J. Kushner
W.J. Randel
K.H. Rosenlof
D.J. Seidel
S. Solomon

Coauthors:

G. Beig
P. Braesicke
N. Butchart
N.P. Gillett
K.M. Grise
D.R. Marsh
C. McLandress
T.N. Rao
S.-W. Son
G.L. Stenchikov
S. Yoden

Contributors:

E.C. Cordero
M.P. Free
A.I. Jonsson
J. Logan
D. Stevenson

CHAPTER 4

STRATOSPHERIC CHANGES AND CLIMATE

Contents

SCIENTIFIC SUMMARY	1
4.0 INTRODUCTION AND SCOPE	3
4.1 OBSERVED VARIATIONS IN STRATOSPHERIC CONSTITUENTS THAT RELATE TO CLIMATE.....	4
4.1.1 Long-Lived Greenhouse Gases and Ozone-Depleting Substances	4
4.1.2 Ozone.....	4
4.1.3 Stratospheric Water Vapor	4
Box 4-1. How Do Stratospheric Composition Changes Affect Stratospheric Climate?	5
4.1.4 Stratospheric Aerosols.....	8
4.2 OBSERVED VARIATIONS IN STRATOSPHERIC CLIMATE.....	10
4.2.1 Observations of Long-Term Changes in Stratospheric Temperature.....	10
4.2.2 Observations of Long-Term Changes in the Stratospheric Circulation	14
4.2.2.1 Stratospheric Zonal Flow.....	14
4.2.2.2 Brewer-Dobson Circulation.....	14
4.3 SIMULATIONS OF STRATOSPHERIC CLIMATE CHANGE.....	16
4.3.1 Simulation of Stratospheric Temperature Trends from Chemistry-Climate Models and Climate Models.....	16
4.3.2 Simulation of Brewer-Dobson Circulation Trends in Chemistry-Climate Models.....	22
4.4 EFFECTS OF VARIATIONS IN STRATOSPHERIC CLIMATE ON THE TROPOSPHERE AND SURFACE.....	25
4.4.1 Effects of Stratospheric Composition Changes on Global-Mean Surface Temperature and Tropospheric Temperature	25
4.4.2 Surface Climate Impacts of the Antarctic Ozone Hole	28
4.4.2.1 Effects on Winds, Storm Tracks, and Precipitation.....	30
4.4.2.2 Effects on Surface Temperatures and Sea Ice.....	31
4.4.2.3 Effects on Southern Ocean Temperatures and Circulation.....	32
4.4.2.4 Stratospheric Links to Southern Ocean Carbon.....	35
4.4.3 Stratospheric Variations and the Width of the Tropical Belt.....	37
4.4.4 Effects of Stratospheric Variations on Tropospheric Chemistry.....	38
4.4.5 Influence of the Stratosphere on the Impact of Solar Variability on Surface Climate.....	39
4.5 WHAT TO EXPECT IN THE FUTURE	41
4.5.1 Stratospheric Temperatures.....	41
4.5.2 Brewer-Dobson Circulation	42
4.5.3 Stratospheric Water Vapor	42
4.5.4 Tropopause Height and Width of the Tropical Belt.....	43
4.5.5 Radiative Effects and Surface Temperature.....	43
4.5.6 Tropospheric Annular Modes and Stratosphere-Troposphere Coupling	43
4.5.7 Tropospheric Chemistry	45
4.5.8 Solar and Volcanic Influences.....	45
REFERENCES	46

SCIENTIFIC SUMMARY

- **Stratospheric climate trends since 1980 are better understood and characterized than in previous Assessments and continue to show the clear influence of both human and natural factors.**
 - **New analyses of both satellite and radiosonde data give increased confidence relative to previous Assessments of the complex time/space evolution of stratospheric temperatures between 1980 and 2009.** The global-mean lower stratosphere cooled by 1–2 K and the upper stratosphere cooled by 4–6 K from 1980 to about 1995. There have been no significant long-term trends in global-mean lower-stratospheric temperatures since about 1995. The global-mean lower-stratospheric cooling did not occur linearly but was manifested as downward steps in temperature in the early 1980s and the early 1990s. The cooling of the lower stratosphere included the tropics and was not limited to extratropical regions as previously thought.
 - **The complex evolution of lower-stratospheric temperature is influenced by a combination of natural and human factors that has varied over time.** Ozone decreases dominate the lower-stratospheric cooling over the long term (since 1980). Major volcanic eruptions and solar activity have clear shorter-term effects. Since the mid-1990s, slowing ozone loss has contributed to the lack of temperature trend. Models that consider all of these factors are able to reproduce this complex temperature time history.
 - **The largest lower-stratospheric cooling continues to be found in the Antarctic ozone hole region during austral spring and early summer.** The cooling due to the ozone hole strengthened the Southern Hemisphere polar stratospheric vortex compared with the pre-ozone hole period during these seasons.
 - **Tropical lower-stratospheric water vapor amounts decreased by roughly 0.5 parts per million by volume (ppmv) around 2000 and remained low through 2009.** This followed an apparent but uncertain increase in stratospheric water vapor amounts from 1980–2000. The mechanisms driving long-term changes in stratospheric water vapor are not well understood.
 - **Stratospheric aerosol concentrations increased by between 4 to 7% per year, depending on location, from the late 1990s to 2009.** The reasons for the increases in aerosol are not yet clear, but small volcanic eruptions and increased coal burning are possible contributing factors.
- **There is new and stronger evidence for radiative and dynamical linkages between stratospheric change and specific changes in surface climate.**
 - **Changes in stratospheric ozone, water vapor, and aerosols all radiatively affect surface temperature.** The radiative forcing of climate in 2008 due to stratospheric ozone depletion (-0.05 ± 0.1 Watts per square meter (W/m^2)) is much smaller than the positive radiative forcing due to the chlorofluorocarbons (CFCs) and hydrochlorofluorocarbons (HCFCs) largely responsible for that depletion ($+0.31 \pm 0.03$ W/m^2). Radiative calculations and climate modeling studies suggest that the radiative effects of variability in stratospheric water vapor (roughly ± 0.1 W/m^2 per decade) can contribute to decadal variability in globally averaged surface temperature. Climate models and observations show that the negative radiative forcing from a major volcanic eruption such as Mt. Pinatubo in 1991 (roughly -3 W/m^2) can lead to a surface cooling that persists for about two years.
 - **Observations and model simulations show that the Antarctic ozone hole caused much of the observed southward shift of the Southern Hemisphere middle latitude jet in the troposphere during summer since 1980.** The horizontal structure, seasonality, and amplitude of the observed trends in the Southern Hemisphere tropospheric jet are only reproducible in climate models forced with Antarctic ozone depletion. The southward shift in the tropospheric jet extends to the surface of the Earth and is linked dynamically to the ozone hole-induced strengthening of the Southern Hemisphere stratospheric polar vortex.
 - **The southward shift of the Southern Hemisphere tropospheric jet due to the ozone hole has been linked to a range of observed climate trends over Southern Hemisphere mid and high latitudes during summer.**

Because of this shift, the ozone hole has contributed to robust summertime trends in surface winds, warming over the Antarctic Peninsula, and cooling over the high plateau. Other impacts of the ozone hole on surface climate have been investigated but have yet to be fully quantified. These include observed increases in sea ice area averaged around Antarctica; a southward shift of the Southern Hemisphere storm track and associated precipitation; warming of the subsurface Southern Ocean at depths up to several hundred meters; and decreases of carbon uptake over the Southern Ocean.

- **In the Northern Hemisphere, robust linkages between Arctic stratospheric ozone depletion and the tropospheric and surface circulation have not been established, consistent with the comparatively small ozone losses there.**
- **The influence of stratospheric changes on climate will continue during and after stratospheric ozone recovery.**
- **The global middle and upper stratosphere are expected to cool in the coming century, mainly due to carbon dioxide (CO₂) increases.** The cooling due to CO₂ will cause ozone levels to increase in the middle and upper stratosphere, which will slightly reduce the cooling. Stratospheric ozone recovery will also reduce the cooling. These ozone changes will contribute a positive radiative forcing of climate (roughly +0.1 W/m²) compared to 2009 levels, adding slightly to the positive forcing from continued increases in atmospheric CO₂ abundances. Future hydrofluorocarbon (HFC) abundances in the atmosphere are expected to warm the tropical lower stratosphere and tropopause region by roughly 0.3 K per part per billion (ppb) and provide a positive radiative forcing of climate.
- **Chemistry-climate models predict increases of stratospheric water vapor, but confidence in these predictions is low.** Confidence is low since these same models (1) have a poor representation of the seasonal cycle in tropical tropopause temperatures (which control global stratospheric water vapor abundances) and (2) cannot reproduce past changes in stratospheric water vapor abundances.
- **Future recovery of the Antarctic ozone hole and increases in greenhouse gases are expected to have opposite effects on the Southern Hemisphere tropospheric middle latitude jet.** Over the next 50 years, the recovery of the ozone hole is expected to reverse the recent southward shift of the Southern Hemisphere tropospheric jet during summer. However, future increases in greenhouse gases are expected to drive a southward shift in the Southern Hemisphere tropospheric jet during all seasons. The net effect of these two forcings on the jet during summer is uncertain.
- **Climate simulations forced with increasing greenhouse gases suggest a future acceleration of the stratospheric Brewer-Dobson circulation.** Such an acceleration would lead to decreases in column ozone in the tropics and increases in column ozone elsewhere by redistributing ozone within the stratosphere. The causal linkages between increasing greenhouse gases and the acceleration of the Brewer-Dobson circulation remain unclear.
- **Future stratospheric climate change will affect tropospheric ozone abundances.** In chemistry-climate models, the projected acceleration of the Brewer-Dobson circulation and ozone recovery act together to increase the transport of stratospheric ozone into the troposphere. Stratospheric ozone redistribution will also affect tropospheric ozone by changing the penetration of ultraviolet radiation into the troposphere, thus affecting photolysis rates.

4.0 INTRODUCTION AND SCOPE

Climate is changing at all levels in the atmosphere. This chapter considers changes in the stratosphere and the related aspects of troposphere and surface climate. While covering some of the same aspects presented in Chapter 5 (Baldwin and Dameris et al., 2007) of the previous Ozone Assessment (WMO, 2007), the current chapter is broader in scope and also addresses aspects of climate change beyond those associated with stratospheric ozone.

It is evident that the 1987 Montreal Protocol and its subsequent Amendments and Adjustments have led to reduced emissions of ozone-destroying halocarbons, many of which are greenhouse gases. The current chapter helps to place the Protocol's climate impact within a wider context by critically assessing the effect of stratospheric climate changes on the troposphere and surface climate, following a formal request for this information by the Parties to the Montreal Protocol. As requested, the current chapter also considers the effects on stratospheric climate of some emissions that are not addressed by the Montreal Protocol, but are included in the 1997 Kyoto Protocol. Hence, the chapter covers some of the issues assessed in past Intergovernmental Panel on Climate Change (IPCC) reports (IPCC,

2007; IPCC/TEAP, 2005). The current chapter is designed to provide useful input to future IPCC assessments.

The troposphere and surface climate are affected by many types of stratospheric change. Ozone plays a key role in such stratospheric climate change, but other physical factors play important roles as well. For this reason, we consider here the effects on the stratosphere of not only emissions of ozone-depleting substances (ODSs), but also of emissions of greenhouse gases, natural phenomena (e.g., solar variability and volcanic eruptions), and chemical, radiative, and dynamical stratosphere/troposphere coupling (Figure 4-1).

First, the chapter combines information about past trace gas emissions (from Chapter 1) and past ozone concentrations (from Chapter 2) with a new assessment of other relevant emissions (Section 4.1). It then draws on the assessed changes in emissions (Section 4.1) and observed stratospheric change (Section 4.2) to assess the nature and drivers of stratospheric climate change (Section 4.3). The chapter subsequently assesses the physical linkages between stratospheric climate change and climate change at Earth's surface (Section 4.4). The chapter closes with a discussion of future stratospheric climate change and its influence on the troposphere and surface climate (Section 4.5), which links to the Chapter 3 discussion of future

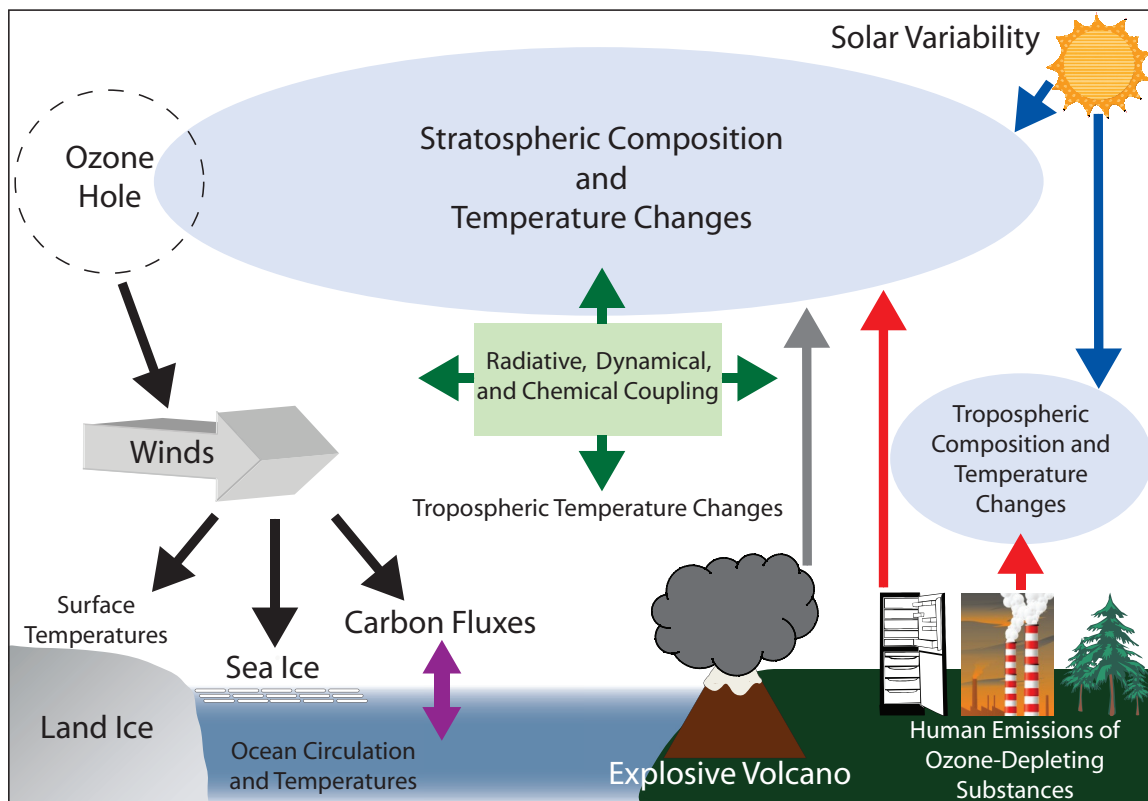


Figure 4-1. Schematic of the drivers and mechanisms considered in this chapter.

ozone trends. Section 4.5 also provides input into discussions of future scenarios in Chapter 5.

4.1 OBSERVED VARIATIONS IN STRATOSPHERIC CONSTITUENTS THAT RELATE TO CLIMATE

In this section we assess our current understanding of stratospheric composition changes. The mechanisms whereby such composition changes affect climate are reviewed briefly in Box 4-1.

4.1.1 Long-Lived Greenhouse Gases and Ozone-Depleting Substances

ODSs, carbon dioxide (CO₂), nitrous oxide (N₂O), and methane (CH₄) are all gases of tropospheric origin that impact climate and stratospheric ozone amounts. ODSs and N₂O directly impact ozone chemistry. Changes in atmospheric concentrations of CH₄ will lead to changes in stratospheric water vapor that in turn impact ozone chemistry and climate. Such gases also affect ozone indirectly via their effects on climate. Recent measurements and growth rates for these gases are covered in Chapter 1 of this report, with a summary of recent growth rates shown in Table 1-1 for the ODSs and Table 1-15 for other greenhouse gases. Atmospheric concentrations of CO₂, N₂O, CH₄, and ODS replacements are projected to increase in the future, as discussed in more detail in Section 4.5.

4.1.2 Ozone

Variations and trends in stratospheric ozone influence climate via direct radiative effects and the resulting temperature and circulation changes. Past changes in stratospheric ozone are reviewed in Chapter 2, and the key points are summarized here as they relate to climate.

Column ozone for the recent past (2006–2008) is approximately 2.5% and 3.5% lower than pre-1980 values for 60°N–60°S and the globe, respectively. Time series of global ozone anomalies show a relative minimum during the middle 1990s, followed by an increase and relatively constant values since 1999 (Chapter 2). Locally, the largest losses have occurred in the Antarctic ozone hole, which is associated with a near-total loss of ozone in the lower stratosphere (~15–22 km) during Southern Hemisphere spring. The Antarctic ozone hole has led to large changes in temperature and circulation in the Southern Hemisphere polar stratosphere, as assessed in WMO (2007) and Section 4.2 of this chapter. The ozone hole has also led to changes at the Southern Hemisphere surface, as assessed here in Section 4.4.2. In contrast to the Ant-

arctic, the Arctic is marked by smaller long-term trends and larger year-to-year variance in ozone during winter and spring (the variance is linked to meteorological variability). Observed changes in profile ozone (see Section 2.1.4.2 of Chapter 2) show relatively large percentage decreases across the globe in the upper stratosphere (~35–47 km), with net changes of over 10% between 1980 and 2009. For the same period, relatively small decreases of ozone concentrations have been observed for the altitude range ~24–32 km.

Significant long-term changes in ozone concentrations are found in the lower stratosphere (below 24 km), although the observational record in this region of the stratosphere is more uncertain due to the dearth of high-vertical resolution ozone measurements, including a lack of global long-term sampling from ozonesondes and continuous observations from high-vertical resolution satellite instruments. Despite this uncertainty, high-vertical resolution Stratospheric Aerosol and Gas Experiment (SAGE)-based ozone trends will be used in the climate simulations run for the IPCC Fifth Assessment Report. The long-term global observations from the SAGE I and II satellite data (covering 1979–2005) show net lower-stratospheric ozone concentration decreases of ~5–10% near 20 km, with the largest percentage decreases in the tropics (over 30°N–30°S) (Randel and Wu, 2007; see also Figure 2-27 in Chapter 2 of this Assessment). The decreases in lower tropical stratospheric ozone are uncertain (see discussion in Chapter 2), but are consistent with decreases in tropical stratospheric temperatures (Thompson and Solomon, 2005; Randel et al., 2009), and if robust provide possible observational evidence of increased upwelling in the lower tropical stratosphere (see Sections 4.2.2 and 4.3.2). Updated estimates of lower-stratospheric variations and trends are a topic of current research.

Changes in the amount of ozone since 1980 have caused a cooling of the lower and upper stratosphere (Section 4.3) and have likely contributed a negative radiative forcing of the surface climate (Section 4.4). They have also affected stratospheric circulation (Section 4.3) and caused significant changes to the surface-troposphere climate of the Southern Hemisphere (Section 4.4). Stratospheric ozone concentrations will continue to change in response to changes in ODSs and chemical feedbacks associated with stratospheric temperatures and composition, and these changes will continue to affect the climate of the stratosphere, troposphere, and surface (Section 4.5).

4.1.3 Stratospheric Water Vapor

Water vapor is the principal greenhouse gas and plays a key role in tropospheric and stratospheric chemistry. Throughout the atmosphere, water vapor plays both a radiative and chemical role. An increase in stratospheric

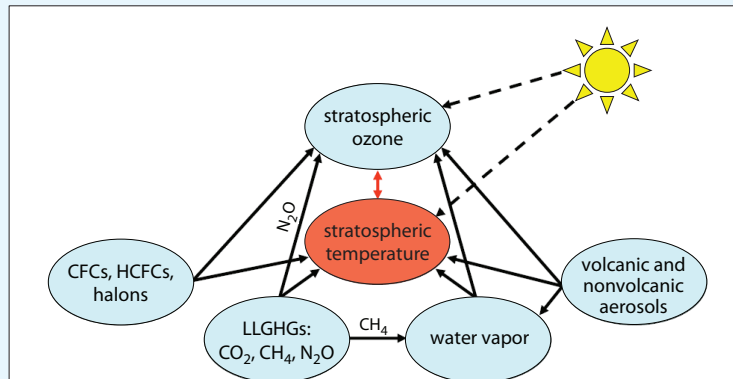
Box 4-1. How Do Stratospheric Composition Changes Affect Stratospheric Climate?

The vertical temperature structure of Earth's stratosphere is primarily driven by radiative processes (Figure 1). Solar radiation is principally absorbed by ozone, stratospheric aerosols, and molecular oxygen, and this absorption warms the stratosphere. Outgoing longwave (thermal infrared) radiation from the surface/troposphere is absorbed and re-emitted by greenhouse gases. Prime greenhouse gases in the atmosphere are water vapor (H_2O), ozone (O_3), carbon dioxide (CO_2), methane (CH_4), and nitrous oxide (N_2O). Additionally, halocarbons (i.e., chlorofluorocarbons (CFCs), hydrochlorofluorocarbons (HCFCs), and brominated chlorofluorocarbons (halons)) not only affect atmospheric chemistry, but are also significant greenhouse gases. Aerosols can also emit in the longwave range.

Whether a change of greenhouse gas concentration warms or cools the stratosphere depends on the strength of the absorption bands of the gas and the opacity of the troposphere at the wavelength of absorption (e.g., Clough and Iacono, 1995). In high opacity regions of the spectrum, where powerful greenhouse gases such as CO_2 and H_2O absorb, there is little transmission from the surface to the stratosphere. These gases in the stratosphere therefore receive upwelling radiation from the generally cooler tropopause region below and emit longwave radiation at the stratosphere's generally higher temperature. As this layer in the stratosphere emits more than it absorbed, the stratosphere cools if greenhouse gas concentrations are increasing. This is in contrast to their warming effect on the troposphere-surface region. CFCs, hydrofluorocarbons (HFCs), and other gases that absorb weakly in the "window" regions of the spectrum warm both the lower stratosphere and troposphere (e.g., Forster and Joshi, 2005) as they receive upwelling radiation from near the generally warmer surface and emit their radiation at a lower temperature. For strong absorbers the cooling effect in the stratosphere increases with altitude as these gases cool to space, maximizing at the stratopause near 50 km altitude where temperature is highest. For weaker absorbers their warming effect is maximized at the tropopause region, where the temperature contrast with the surface is largest.

The solar forcing of the Earth's atmosphere is modulated by the 11-year activity cycle of the sun that is reflected in fluctuations in the intensity of solar radiation at different wavelengths. 11-year solar UV irradiance variations have a direct impact on the radiation and ozone budget of the stratosphere (e.g., Haigh, 1994). During years with high solar activity the solar UV irradiance is clearly enhanced, leading to additional ozone production and heating in the stratosphere and above (e.g., Lee and Smith, 2003).

The feedbacks operating between temperature and ozone are determined not only by radiative processes but also by chemical processes (Figure 1). Stratospheric composition is intimately related to the absorption of incoming solar (shortwave) radiation. Solar ultraviolet (UV) radiation is involved in both the creation and destruction of ozone, resulting in a maximum ozone concentration near 25 km. The dominant ozone loss cycles in the middle and upper stratosphere (via the catalytic cycles of nitrogen oxides (NO_x), chlorine radicals (ClO_x), and odd hydrogen (HO_x)) slow with decreasing temperatures (e.g., Haigh and Pyle, 1982), leading to higher ozone concentrations. The situation is even more complicated in the polar lower stratosphere in late winter and spring. In addition to the gas-phase ozone loss cycles, as described above, there is an offset by chlorine- and bromine-containing reservoir species (Zeng and Pyle, 2003). These chemical substances are activated via heterogeneous processes on surfaces of polar stratospheric clouds. The rate of chlorine and bromine activation that determines the rate of ozone depletion is strongly dependent on stratospheric temperatures, increasing significantly below approximately 195 K due to enhanced particle formation. The amount of stratospheric ozone is also affected by heterogeneous chemical reactions acting on the surfaces of stratospheric aerosol particles. The injection of sulfate aerosols into the stratosphere leads to transformation of inactive chlorine compounds to active forms that destroy ozone.



Box 4-1, Figure 1. Schematic of ozone-temperature feedbacks due to changes in stratospheric chemical composition. Stratospheric temperature is determined directly by concentrations of radiatively active gases (e.g., long-lived greenhouse gases, LLGHGs) and aerosols (both emitted by explosive volcanic eruptions and human activities) via the absorption and emission of short- and longwave radiation. Moreover, the amount of stratospheric ozone is defined by transport via winds (i.e., dynamics) and chemical processes, which on its own part depends on concentrations of other greenhouse gases and aerosols. The picture is even more complex since stratospheric temperature influences net ozone production due to temperature-dependent reactions rates. The sun drives radiative, dynamical, and chemical processes affecting ozone and stratospheric temperature.

water vapor will radiatively cool the lower stratosphere and also affect the frequency of occurrence of polar stratospheric clouds, thereby impacting stratospheric ozone chemistry (Kirk-Davidoff et al., 1999; Feck et al., 2008). Enhanced levels of stratospheric water vapor strengthen ozone loss in the presence of ODSs. Hence, a climate with increased stratospheric water vapor will have a delayed ozone recovery even while ODSs are reduced (Shindell, 2001; Shindell and Grewe, 2002; Tian et al., 2009). Changes in stratospheric water vapor also can be a significant radiative forcing for surface climate (see Section 4.4.1).

The principal sources of stratospheric water vapor are entry through the tropical tropopause (Brewer, 1949) and oxidation of methane within the stratosphere (Jones et al., 1986; le Texier et al., 1988). Oxidation of molecular hydrogen (H_2) is another source of stratospheric water vapor, albeit currently small, but with the potential to grow in the future if hydrogen fuel cells come into common use (Tromp et al., 2003; Schultz et al., 2003).

Each source of stratospheric water vapor is associated with a distinct timescale. The input of water vapor into the stratosphere by an individual air parcel in the tropics is largely a function of the lowest temperature a parcel encounters on its transit into the stratosphere, as originally noted by Brewer (1949) and more recently discussed in Schiller et al. (2009). The actual trajectory a parcel takes does need to be considered (Fueglistaler et al., 2009), but a simple model of horizontal processing of air by passage through the Western Pacific cold point tropopause reasonably reproduces observed stratospheric humidity (Holton and Gettelman, 2001; Geller et al., 2002; Scaife et al., 2003). Variability in stratospheric water vapor on seasonal and interannual timescales has been well reproduced by climatological trajectory studies using saturation mixing ratios calculated from global temperature analyses (Jensen and Pfister, 2004; Fueglistaler and Haynes, 2005), demonstrating that to first order, variability in the entry of water vapor into the stratosphere is controlled by variability in tropical cold point temperatures. Convection overshooting into the stratosphere has been observed on limited occasions, and when it occurs likely hydrates the stratosphere locally (Khaykin et al., 2009; Nielsen et al., 2007). However, evidence for a global impact of this phenomenon is lacking at this time (Schiller et al., 2009). Because there is a relatively short turnover time for air in the lowermost stratosphere, on the order of months (Rosenlof and Holton, 1993), changes in the entry value of water vapor to the stratosphere due to tropical cold point temperature changes will be seen almost immediately throughout the lowermost stratosphere. However, there will be a time lag before the signal reaches the middle and upper stratosphere on the order of years. As noted in Engel et al. (2009) (and references therein), the mean age of air in the

middle stratosphere at northern midlatitudes (between 20 and 40 km) is approximately 4 years, hence the multiyear time lag before seeing a signal in the middle stratosphere.

Measurement of stratospheric water vapor concentrations is highly challenging and uncertain. There are significant discrepancies noted between coincident measurements of stratospheric water vapor concentrations using different in situ and satellite techniques (Vömel et al., 2007; Kley et al., 2000; Lambert et al., 2007; Weinstock et al., 2009). These discrepancies range from 10% to 50% or even greater in some cases and preclude combining data sets for trend analysis without extreme care. However, data quality is sufficient to examine annual and interannual variations of water vapor in the tropical lower stratosphere. Such variations have been noted to be in quantitative agreement with the idea that observed variations in tropical tropopause temperatures control the entry value of stratospheric water vapor (Randel et al., 2004; Fueglistaler and Haynes, 2005). Chapter 7 in SPARC CCMVal (2010) notes that most chemistry-climate models are able to reproduce the general sense of the annual cycle of water vapor in the tropical lower stratosphere with a minimum in Northern Hemisphere spring and a maximum in Northern Hemisphere fall and winter. There is a wide spread in the stratospheric entry value of water vapor in the models ranging from 2–6 parts per million by volume (ppmv). Kley et al. (2000) presented observationally based estimates ranging from 2.0–4.1 ppmv for the stratospheric entry value, and noted differences between measurement systems larger than the stated uncertainties for those instruments. Assessing the exact mechanism for the amount of dehydration of air entering the stratosphere requires better accuracy than currently exists. As concluded in Weinstock et al. (2009), the differences using coincident measurement noted between independent in situ instruments are sufficiently large that different conclusions can be reached with regard to the impact of convective processes in the tropical tropopause layer, and the degree of supersaturation that is plausible (Peter et al., 2006).

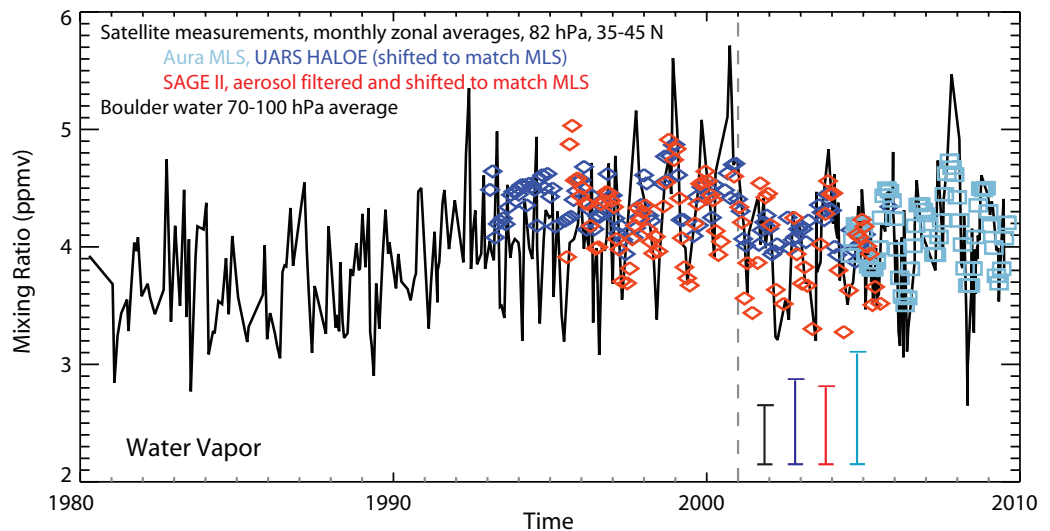
Global water vapor trend determination from the historical record is difficult. There are differences in trends noted between measurement systems covering the same time period (for example the Northern Hemisphere frost point balloon as compared with the Upper Atmosphere Research Satellite (UARS) Halogen Occultation Experiment (HALOE) satellite instrument, as noted in Randel et al., 2004). The multidecadal stratospheric water vapor record is limited to Northern Hemisphere midlatitudes. The longest continuous record of stratospheric water vapor data is from frost point balloon measurements taken at 40°N from Boulder, Colorado. At present, the longest satellite records are from SAGE II and HALOE instruments. Both of these instruments ceased operation in 2005, and there are a number of newer satellite instruments currently mea-

suring stratospheric water vapor concentrations, including Aura Microwave Limb Sounder (MLS), which has extensive spatial coverage. Using overlap periods between instruments, it may be possible to continue estimation of global trends; however, this is a current research endeavor and there is no relevant literature to assess at this time.

From the historic record of the amount of stratospheric water vapor, an increase based on midlatitude frost point balloon measurements below 30 km in Washington, D.C., and Boulder, Colorado, on the order of 0.05 ± 0.01 ppmv/yr for the period from 1964–2000 was reported by Oltmans et al. (2000). Corrections to the Boulder frost point data were reported by Scherer et al. (2008), which reduced the trend for the period from 1980–2000 to 0.03 ± 0.005 ppmv/yr. The time series of the revised Boulder data is shown in Figure 4-2 as well as the comparable time series from HALOE, SAGE II, and Aura MLS. Independent data from a variety of remote sounding and in situ sources show an average trend for the period from 1960–2000 of 0.045 ppmv/yr at Northern Hemisphere midlatitudes at levels below 30 kilometers (km) (Rosenlof et al., 2001). Analyses by Rohs et al. (2006) using in situ balloon measurements show that changes in methane mixing ratio can account for a midlatitude trend below 30 km of $.0132 \pm 0.002$ ppmv/yr of the Boulder increase. The exact mechanism for the remainder of the observed increase of water

vapor concentration for the period ending in 2000 is in question, with circulation changes postulated related to the width of the tropics (Zhou et al., 2001; Rosenlof, 2002), as well as changes in aerosol processes near the tropical tropopause (Notholt et al., 2005; Sherwood, 2002). As shown in Figure 4-2 (lower stratosphere midlatitudes) and Figure 4-3 (tropics), since the end of 2000, a decrease in the mixing ratio of water vapor entering the tropical stratosphere occurred (Randel et al., 2006; Rosenlof and Reid, 2008), coincident with a drop in tropical tropopause temperatures that has occurred during a period without an increase of methane concentration (Dlugokencky et al., 2009). The drop in tropical water vapor entry values estimated using HALOE data at 82 hPa is ~ 0.5 ppmv, or approximately 10% of average stratospheric water vapor values (Solomon et al., 2010), and 25% of the nominal maximum-to-minimum difference in the annual cycle of 82 hPa tropical water vapor as estimated from HALOE measurements. The drops in tropical tropopause temperature and entry of water vapor into the stratosphere at the end of 2000 appear to be associated with an increase in the rate of tropical upwelling (Randel et al., 2006; Rosenlof and Reid, 2008) and associated changes in eddy wave driving (Dhomse et al., 2008). There is not agreement in the literature as to the reason for the strengthening of tropical upwelling near the tropical tropopause; both tropical

Figure 4-2. Observed changes in stratospheric water vapor. Time series of stratospheric water vapor mixing ratio (ppmv) averaged from 70 to 100 hPa near Boulder Colorado (40°N, 105.25°W) from a balloonborne frost point hygrometer covering the period 1981 through 2009; satellite measurements are monthly averages, balloon data



plotted are from individual flights. Also plotted are zonally averaged satellite measurements in the 35°N–45°N latitude range at 82 hPa from the Aura MLS (turquoise squares), UARS HALOE (blue diamonds), and SAGE II instruments (red diamonds). The SAGE II and HALOE data have been adjusted to match MLS during the overlap period from mid-2004 to the end of 2005, as there are known biases (Lambert et al., 2007). Representative uncertainties are given by the colored bars; for the satellite data sets these show the uncertainty as indicated by the monthly standard deviations, while for the balloon dataset this is the estimated uncertainty provided in the Boulder data files. Figure adapted from Solomon et al. (2010).

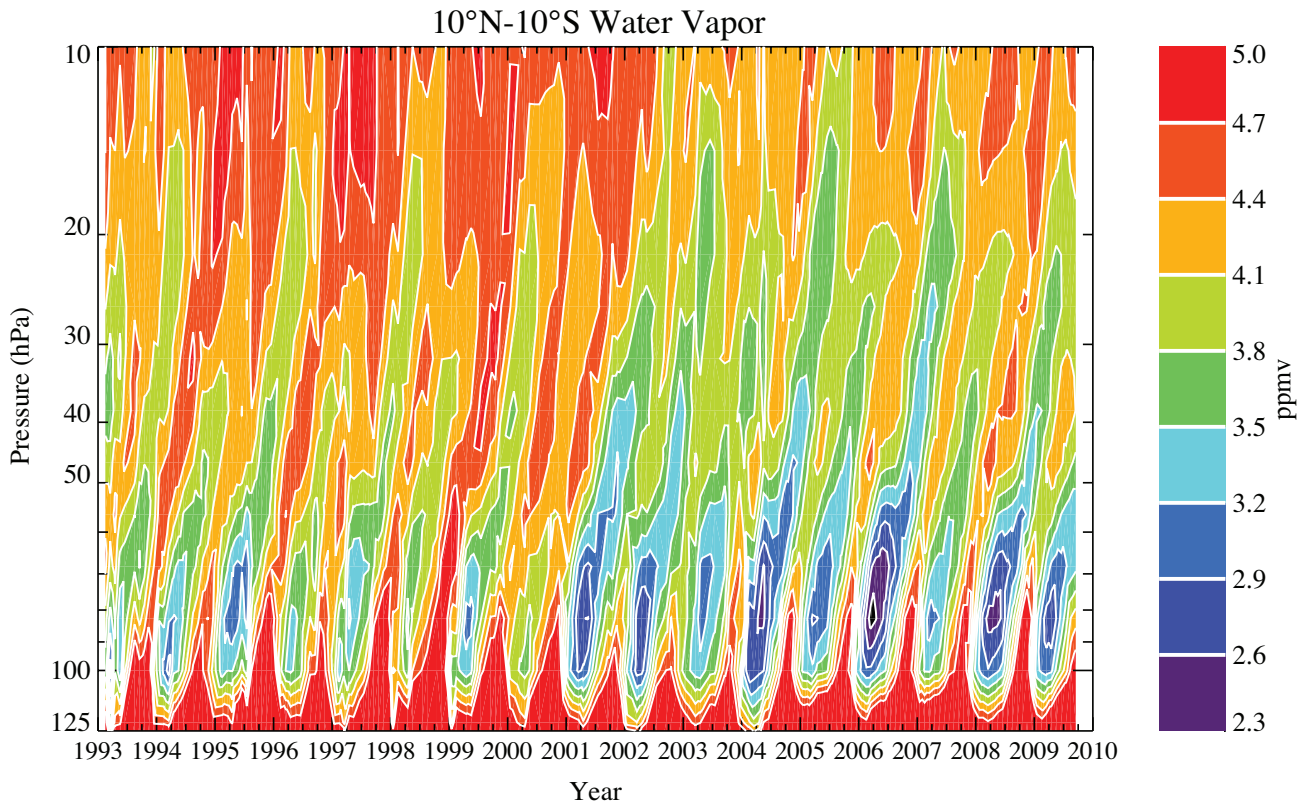


Figure 4-3. Tropical water vapor (ppmv, 10°N–10°S, monthly averages) plotted versus time, showing upward propagation of the water vapor tape recorder (Mote et al., 1996). This is a combination of UARS HALOE and Aura MLS measurements. During the period of data overlap (from mid-2004 through the end of 2005), differences were computed for matching profiles at each pressure level. That average shift was applied to the HALOE measurements at each level; for 82 hPa it is on the order of 0.5 ppmv. The key feature to note here is the change to lower values of the water vapor minimum (hygropause) at the end of 2000, and upward propagation of those lower values in subsequent years. Update of Figure 10 from Rosenlof and Reid (2008).

sea surface temperature changes (Deckert and Dameris, 2008) and changes in high-latitude wave forcing (Ueyama and Wallace, 2010) have been suggested.

There is a good understanding of the annual cycle of water vapor entering the stratosphere (Figure 4-3). The amplitude of the annual cycle is 50% to 60% of the mean and well explained by the known annual cycle in tropical tropopause temperatures (Reed and Vleck, 1969). In contrast, the trend in stratospheric water vapor is not well understood. Over the period 1950–2000 there was an increase in entry-level stratospheric water vapor on the order of 1%/yr (Rosenlof et al., 2001) during a period of increasing tropospheric methane and decreasing tropopause temperatures (Zhou et al., 2001). At the end of 2000 there was a decrease in stratospheric entry-level water vapor coincident with a step-like drop in tropical tropopause temperatures (Randel et al., 2006; Rosenlof and Reid, 2008). The observed long-term increase in stratospheric water vapor over the 1950–2000 period cannot be explained through

tropical tropopause temperature trends, although some aspects of interannual variability can be. The more recent decrease in stratospheric water vapor can be explained by tropical tropopause temperature changes, although the mechanism driving that temperature change is not well understood. Given the uncertainties in our understanding and modeling of past water vapor changes, it is difficult to predict changes expected in a future climate.

4.1.4 Stratospheric Aerosols

The stratospheric aerosol layer has often been characterized as a “background” punctuated by volcanic enhancements. The composition of these aerosols is largely sulfuric acid/water solutions, and hence is strongly dependent on sources of stratospheric sulfur. Carbonyl sulfide (OCS) is an important source of sulfur to the stratosphere (Crutzen, 1976). However, the observed abundance of background stratospheric aerosol is many times larger

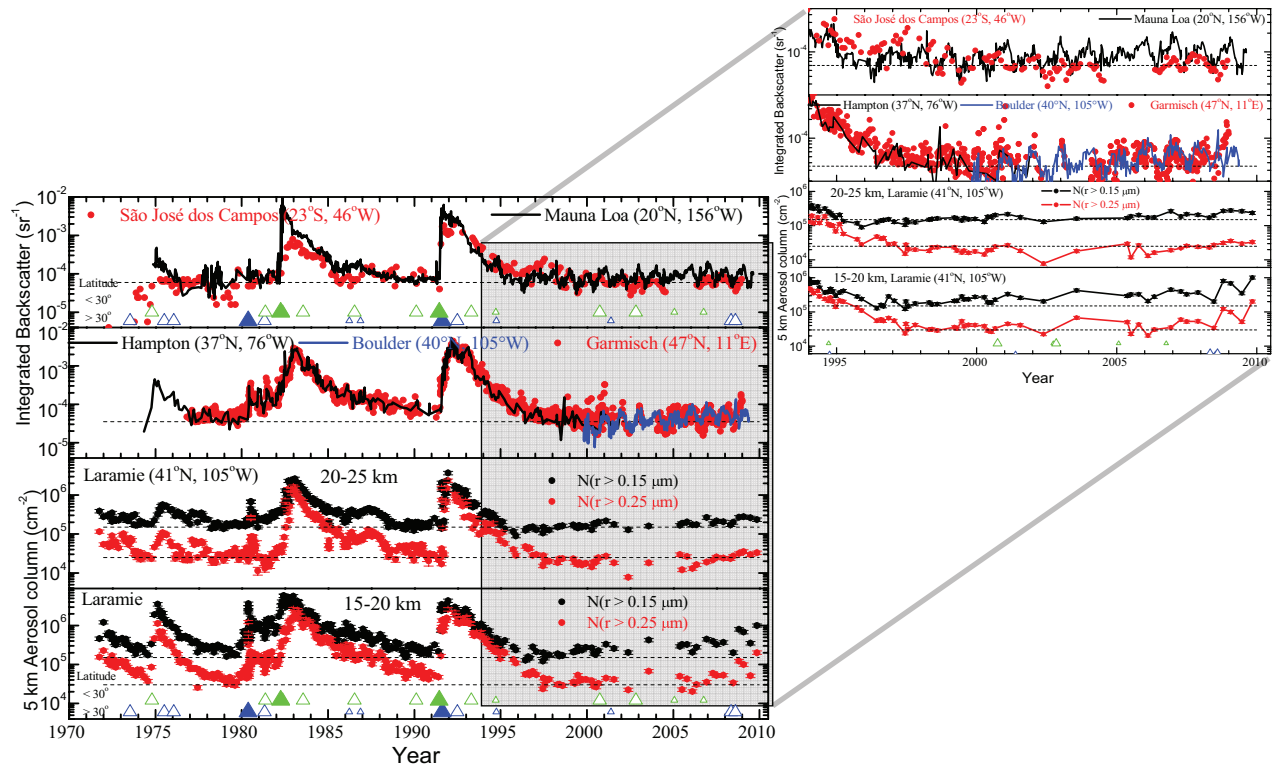


Figure 4-4. History of stratospheric integrated optical backscatter (sr^{-1}) at 694 nm from lidar measurements at five locations (top two panels) and 5 km aerosol column concentration (cm^{-2}) from in situ measurements over two altitude intervals above the tropopause at Laramie, Wyoming, USA (bottom two panels). Top panel shows measurements from São José dos Campos, Brazil, integration 17–35 km, and Mauna Loa, Hawaii, USA, integration 15.8–33 km. Second panel show measurements from Hampton, Virginia, USA, integration tropopause to 30 km, Boulder, Colorado, USA, integration 20–33 km, and Garmisch-Partenkirchen, Germany, integration tropopause +1 km - layer top. The measurements from São José dos Campos (589 nm), Boulder (532 nm), and Mauna Loa (532 nm since 1999) are scaled to 694 nm using a wavelength exponent of -1.4 . The times of volcanic eruptions are indicated in the top and bottom panels with triangles, separated into eruptions at latitudes less (green upper symbols) and greater (blue lower symbols) than 30 degrees. Eruptions with volcanic explosivity indices of 5 (large closed symbols), 4 (small open symbols), and 4 with some uncertainty (tiny open symbols) are shown. This figure extends that presented by Deshler (2008) and Hofmann et al. (2009). The Hampton measurements have been discontinued. Right multipanel plot is an expansion of the data since 1994.

than can be explained using OCS alone (Chin and Davis, 1995; Weisenstein et al., 1997; Pitari et al., 2002), which suggests an important role for other sources—such as sulfur dioxide (SO_2)—in pollution. Explosive volcanic eruptions that occurred in the past several decades include Mt. Pinatubo in 1991 and El Chichón in 1982, and these eruptions increased the integrated stratospheric aerosol abundance by more than a factor of ten, as shown in Figure 4-4. Volcanic aerosols directly affect stratospheric temperatures (as discussed in this chapter), as well as mid-latitude and polar surface chemistry and thus stratospheric ozone depletion (as discussed in Chapters 2 and 3). Large explosive eruptions also cause episodic cooling of global average surface temperatures for a few years and other

climate effects (see Section 4.4.1). There is presently no systematic global monitoring system to document long-term future changes in stratospheric aerosol that could affect ozone and climate.

Stratospheric aerosols have been measured at a few key sites using balloonborne optical counters and laser ranging (lidar) methods, beginning at some stations in the early to mid-1970s (e.g., Hofmann, 1990; Jäger, 2005; Deshler, 2008). Systematic global satellite measurements using visible spectroscopy (SAGE) began in the mid-1980s (Thomason et al., 1997) but were terminated in 2005. The data sets, methods used, their intercomparison, and the range of available records were recently reviewed under the auspices of SPARC (SPARC, 2006) and by Deshler (2008).

Hofmann (1990) noted an apparent increase in stratospheric aerosols between the late 1970s and the late 1980s, which are two periods with little volcanic influence (Figure 4-4); he suggested a positive trend in the nonvolcanic aerosol background of about 5%/yr over that decade. However, following the major eruption of Mt. Pinatubo in June 1991, stratospheric aerosol declined to the lowest values observed in at least two decades. Taken over the period 1970–2005, there has been no significant trend in background aerosols (Deshler, 2008), raising questions about the origin of the positive trend in the earlier data. However, while recent data remain close to that of the 1970s, they also reveal trends over limited time intervals. A closer look at the most recent data from numerous sites reveals increases of about 4%/yr to 7%/yr in backscatter from 20–30 km since the late 1990s (see Hofmann et al., 2009 and insets in Figure 4-4).

Hofmann et al. (2009) suggested that these recent increases could be linked to sulfur emissions from coal burning in China, which has dramatically increased in the past decade. Notholt et al. (2005) noted the importance of the Asian summer monsoon for transport of SO₂ to the tropical upper troposphere and for cross-tropopause transport, which they suggest could affect stratospheric water vapor transport. Such transport has the potential to influence the source of sulfur to the stratosphere as well. However, input from volcanoes, including from some less explosive eruptions previously thought to be small, may be more important than previously thought. For example, spaceborne laser ranging (lidar) observations at high resolution show evidence for substantial volcanic inputs to stratospheric aerosol associated with the eruption of Soufriere on Montserrat in mid-2006 (Vernier et al., 2009). The conclusion is that decadal variability in stratospheric aerosol is larger than previously anticipated. The relative contribution of recent anthropogenic versus natural emissions to changes in stratospheric aerosol loading remains an area of active research.

4.2 OBSERVED VARIATIONS IN STRATOSPHERIC CLIMATE

4.2.1 Observations of Long-Term Changes in Stratospheric Temperature

Substantial progress has been made since the 2006 Assessment (WMO, 2007) in the evaluation of past stratospheric temperature changes. As a result of this recent work, we have increased confidence relative to previous assessments of the magnitude and meridional structure of temperature trends in the lower stratosphere.

We also have a better understanding of the errors inherent in measurements of temperature changes in the middle and upper stratosphere. Three factors contribute to the changes in our understanding:

1. Improved knowledge of the inherent uncertainties in stratospheric data derived from spaceborne instruments (e.g., CCSP, 2006; Mears and Wentz, 2009; Shine et al., 2008) and radiosondes (e.g., Lanzante et al., 2003; Free et al., 2005; Sherwood et al., 2005; Thorne et al., 2005; CCSP, 2006; Free and Seidel, 2007; Randel et al., 2009), and in stratospheric products available from reanalysis products (e.g., Randel et al., 2009; Section 2.4 in Chapter 2 of this Assessment);
2. The emergence of several independent analyses of satellite and radiosonde data sets, with distinct approaches to homogeneity adjustments (e.g., Free et al., 2005; Haimberger, 2007; Haimberger et al., 2008; Thorne et al., 2005; Randel and Wu, 2006; Sherwood et al., 2008); and
3. The lengthening of data records with the passing of time.

There are now six global lower-stratospheric temperature data sets specifically developed for climate studies based on radiosonde data: RATPAC (Free et al., 2005); HadAT (Thorne et al., 2005); RATPAC-lite (an abridged version of the RATPAC data set; Randel and Wu, 2006); RAOBCORE (Haimberger, 2007); RICH (Haimberger et al., 2008); and IUK (Sherwood et al., 2008) (see Appendix B for definitions of these acronyms). The radiosonde data sets are not fully independent, but their different approaches to identifying and adjusting temporal inhomogeneities that can affect trends (particularly in the stratosphere) help us to characterize the overall uncertainty in estimates of long-term stratospheric temperature change since the late 1950s. There are now three lower-stratospheric temperature data sets derived from Microwave Sounding Unit (MSU) and Advanced MSU (AMSU) observations from polar-orbiting satellites since 1979 (University of Alabama-Huntsville (UAH), Christy et al., 2003; Remote Sensing Systems (RSS), Mears and Wentz, 2009; Center for Satellite Applications and Research (STAR), Zou et al., 2009). The lower-stratospheric MSU/AMSU temperature data are derived by blending MSU Channel 4 with AMSU Channel 9 data (see the discussion in Randel et al., 2009). The blended data are hereafter referred to simply as MSU4.

Figure 4-5 (from Thorne, 2009) presents time series of global-mean lower-stratospheric temperatures from five radiosonde and three MSU4 data sets. The radiosonde data have been vertically weighted as per the

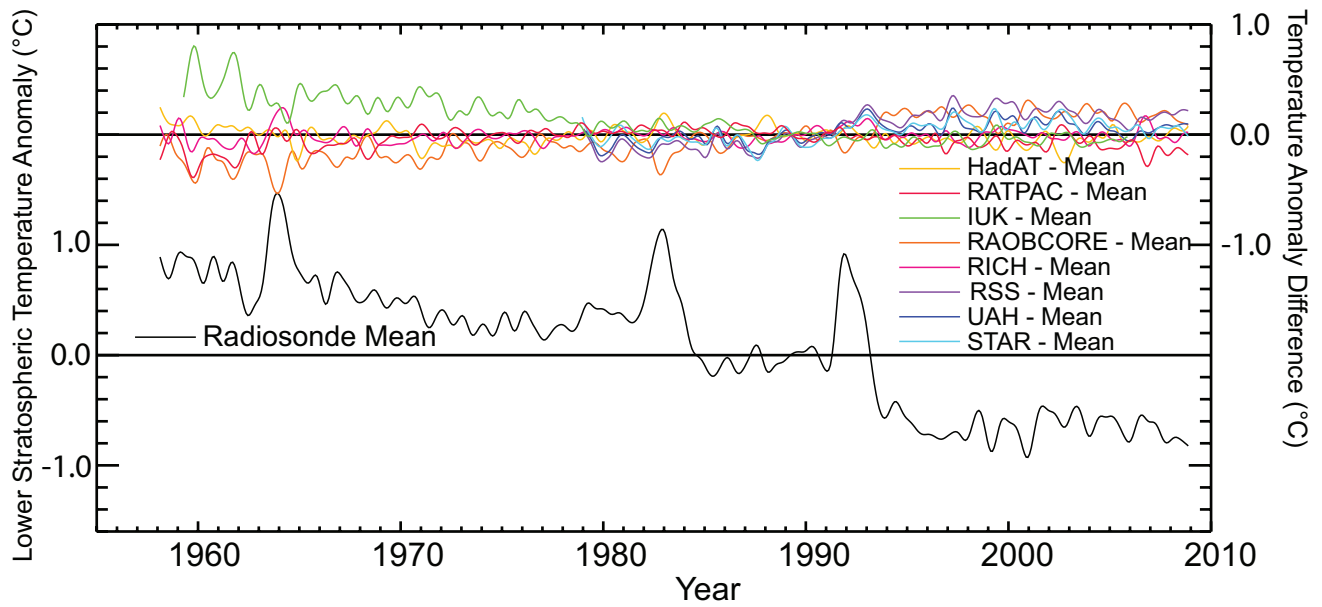


Figure 4-5. Global-mean lower-stratospheric temperature anomalies (1958–2008) from multiple data sets, including five radiosonde data sets (HadAT, IUK, RAOBCORE, RATPAC, and RICH) and three satellite MSU data sets (RSS, UAH, and STAR). Acronyms are defined in Appendix B of this Assessment. All time series are for the layer sampled by MSU channel 4, spanning 10–25 km in altitude, with a peak near 18 km. Black curve is the average of all available radiosonde data sets, and the colored curves show differences between individual data sets and this average. (Based on Thorne, 2009.)

MSU4 weighting function (the general time evolution of lower-stratospheric temperatures shown in Figure 4-5 is mirrored in time series based on global-mean radiosonde data at individual standard pressure levels between 100 and 30 hPa; not shown). The figure is an updated and extended version of the global-mean time series shown in, for example, Ramaswamy et al. (2001, 2006), Seidel and Lanzante (2004), CCSP (2006), and Thompson and Solomon (2009). Three key aspects of global-mean lower-stratospheric temperature changes are evidenced in all data sets:

1. In the global mean, the lower stratosphere has cooled by ~ 0.5 K/decade since 1980 (~ 0.35 K/decade in RAWinsonde OBServation (RAOB) data extended back to 1958). The robustness of the global-mean lower-stratospheric cooling has been documented in numerous recent studies (e.g., see the recent review by Randel et al., 2009), but varies slightly from data set to data set. For example, the cooling during 1980–2008 is 0.33 to 0.42 K/decade for the three MSU4 data sets but 0.50 ± 0.16 K/decade for the (vertically weighted) radiosonde data sets (Thorne, 2009; Figure 4-5).
2. The global-mean lower-stratospheric cooling has not occurred linearly but rather appears to be manifested as
3. two downward steps in temperature coincident with the end of the transient warming associated with explosive volcanic eruptions. The steps are most pronounced after the eruptions of El Chichón (1982) and Mt. Pinatubo (1991) and have been emphasized in numerous studies (Pawson et al., 1998; Seidel and Lanzante, 2004; Ramaswamy et al., 2006; Eyring et al., 2006; Free and Lanzante, 2009; Thompson and Solomon, 2009). Thompson and Solomon (2009) argue that the steps are consistent with the superposition of (i) long-term stratospheric cooling; (ii) transient warming due to volcanic aerosols loading; and (iii) transient cooling due to volcanically induced ozone depletion.

Another key aspect of recent stratospheric temperature trends is the near uniformity of the cooling at all latitudes outside of the polar regions since 1980. Trends based on lower-stratospheric data from multiple radiosonde data sets show cooling of ~ 0.4 K/decade (from RATPAC-lite data; Randel and Wu, 2006) to ~ 0.8

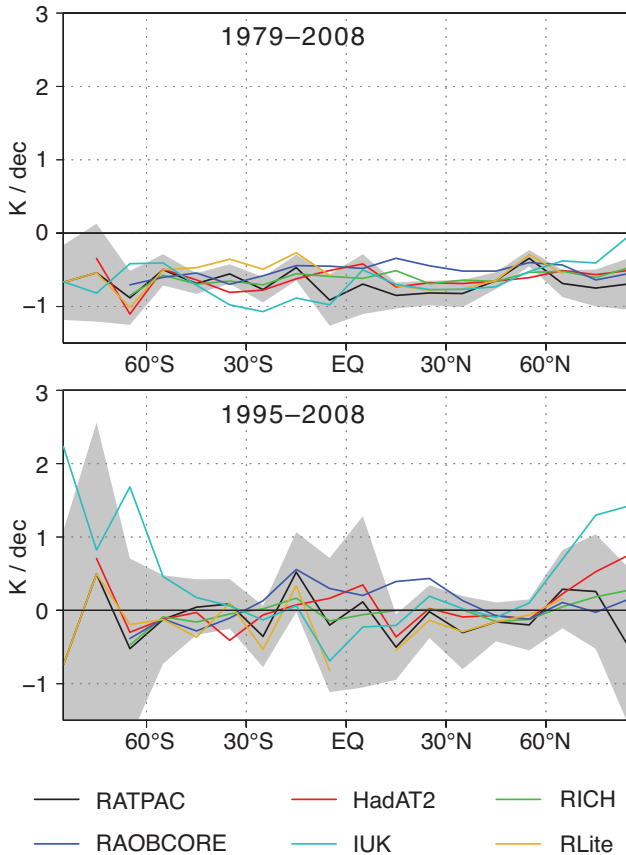


Figure 4-6. Zonal-mean temperature trends (K/decade) at 50 hPa from six adjusted radiosonde data sets for the periods 1979–2008 (top) and 1995–2008 (bottom). Gray shading indicates the 2-sigma trend confidence interval from the RATPAC data set (others are comparable). Trends are computed from temperature anomaly time series, omitting data for two years after the El Chichón and Mt. Pinatubo volcanic eruptions.

K/decade (from RATPAC data; Free et al., 2005) for 1980–2008 for zonal bands within about 45 degrees north and south of the equator (Figure 4-6 top; Thompson and Solomon, 2005; Free et al., 2005). The presence of significant lower-stratospheric cooling at tropical latitudes (Thompson and Solomon, 2005) has implications for the attribution of changes in stratospheric circulation, as discussed in Sections 4.2.2 and 4.3. The structure and amplitude of the lower-stratospheric cooling also has implications for the interpretation of tropospheric temperature trends estimated from the MSU2 satellite, since the MSU2 weighting function samples the lowermost stratosphere (e.g., Fu et al., 2004).

In the annual mean, the cooling of the tropical and middle latitudes since 1980 occurred primarily before 1995 (compare the top and bottom panels of Figure 4-6). Since

1995, annual-mean lower-stratospheric temperatures have remained steady over much of globe, albeit with significant rises over the polar regions in one but not all data sets (the IUK data; Figure 4-6 bottom). The drop in tropical tropopause temperatures circa 2001 highlighted in Section 4.1.3 is centered on a very narrow layer about the tropical tropopause (Randel et al., 2006) and is not apparent in trends at 50 hPa (which are shown in Figure 4-6 bottom).

Lower-stratospheric temperature trends also exhibit considerable seasonal variability. The top panel in Figure 4-7 (from Fu et al., 2010; see also Figure 11 in Randel et al., 2009) shows updated trends in the RSS MSU4 data as a function of latitude and calendar month. Regions of 90% significance are denoted by hatching. The bottom panel in Figure 4-7 shows time series of polar stratospheric temperatures averaged over the seasons indicated based on radiosonde data (from Randel et al., 2009). The tropical cooling evident in the annual-mean is largest between June and January (Figure 4-7, top). Between 1979 and 2007, the Southern Hemisphere polar regions are marked by significant (at the 90% level) cooling between November and March. During the same period, the Northern Hemisphere polar regions are marked by significant cooling during March/April and June–September. The polar warming in August–September in the Southern Hemisphere and December–January in the Northern Hemisphere are not statistically significant at the 90% level in the zonal mean (Figure 4-7, top).

Time series of 100 hPa polar temperature anomalies from radiosonde data confirm visually the following aspects of lower-stratospheric temperature trends (Figure 4-7, bottom): (1) the robust cooling of the polar regions during the spring and summer seasons in both hemispheres (with notably larger cooling observed in the Antarctic), and (2) the absence of significant temperature trends during the winter season in both hemispheres.

In contrast to the lower stratosphere, temperature changes in the middle and upper stratosphere are relatively uncertain due to the limited availability of long-term temperature data there. Radiosonde data are generally available only up to about 20 hPa, and the quality of radiosonde data diminishes with height. There is currently only one satellite data record (from the Stratospheric Sounding Unit) and one corresponding analysis (the analysis combines the available SSU zonal temperature anomaly data from ten separate satellites and is available through 2005; see Randel et al., 2009). Temperature trends based on lidar measurements have large sampling limitations and are only available at limited locations throughout the globe (see discussions in Randel et al., 2009, and Funatsu et al., 2008).

The Stratospheric Sounding Unit senses emissions from carbon dioxide and thus is sensitive to the increases in CO₂ over the past few decades (Shine et al., 2008). For this reason, trends derived from Stratospheric Sounding

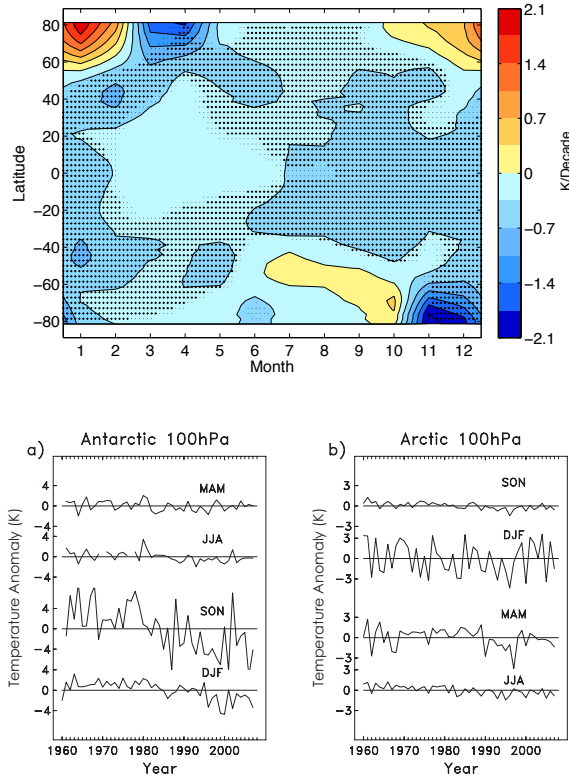


Figure 4-7. (top) Zonal-mean lower-stratospheric temperature trends (K/decade) for 1979–2007 for each calendar month from MSU4 observations (MSU4 spans roughly 10–25 km in altitude, with a peak near 18 km). The color contour interval is 0.35 K/decade. Warm colors indicate warming; cool colors indicate cooling. Hatching indicates where the trends are significant at the 90% confidence level. Results reproduced from Fu et al. (2010). (bottom) Time series of 100 hPa temperature anomalies (K) averaged over the polar regions based on radiosonde measurements (adapted from Randel et al., 2009).

Unit data that are not treated for the influence of increasing CO₂ (i.e., all Stratospheric Sounding Unit trends published prior to 2008) are affected by uncorrected changes in the retrieval weighting function. The principal effect of correcting the Stratospheric Sounding Unit weighting function for increasing CO₂ is to increase the cooling trends by as much as ~0.2–0.4 K/decade throughout much of the stratosphere (see Figure 4 in Shine et al., 2008). Recent analyses of Stratospheric Sounding Unit temperature data corrected for the increases in atmospheric CO₂ are summarized in Randel et al. (2009; compare Figures 18 and 19), and the updated figures of 60°S–60°N mean Stratospheric Sounding Unit temperatures are shown in Figure 4-8. The Stratospheric Sounding Unit temperature data suggest that (1) the middle and upper stratosphere cooled more rapidly

than the lower stratosphere (~1.5 K/decade for 1980–2005 for channels centered ~40–50 km) and (2) stratospheric temperatures remained steady from ~1995–2005 from the lower stratosphere up to ~1 hPa.

The outlook for evaluation of future changes in stratospheric temperature is mixed. It appears likely that multiple radiosonde and MSU/AMSU lower-stratospheric temperature analyses will continue to be available from several research teams. The recent initiation of a reference upper-air observing network (Seidel et al., 2009) bodes well for the eventual availability of high quality temperature (and water vapor and other) observations to calibrate and evaluate satellite and radiosonde data. Other data sets that will likely prove useful for future analyses of stratospheric temperatures include lidar deployed within the Network for the Detection of Atmospheric Composi-

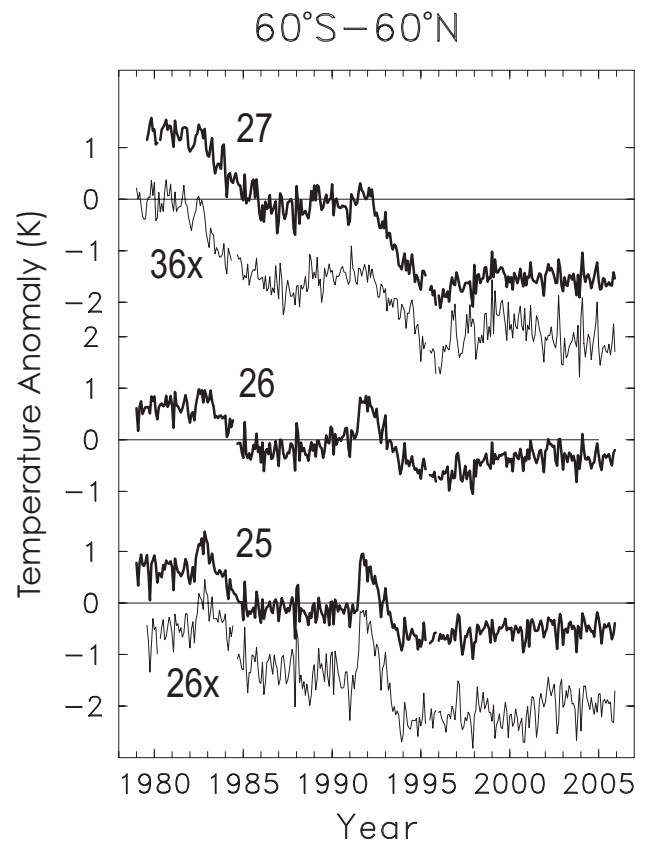


Figure 4-8. Time series of SSU temperature anomalies (K) for channels indicated (Figure 18 from Randel et al., 2009). Data for channels 26x and 36x are shifted for clarity. Exact weighting functions for the SSU satellite instrument can be found in Figure 1 of Randel et al. (2009). Channel 27 corresponds to ~34–52 km altitude, channel 36x to ~38–52 km, channel 26 to ~26–46 km, channel 25 to ~20–38 km, and channel 26x to ~21–39 km.

tion Change and the Global Positioning System radio occultation temperature profiles (the latter are available continuously starting in 2001). For the upper stratosphere, Stratospheric Sounding Unit data could be merged with AMSU observations to extend the record past 2005, but the lack of multiple analyses will continue to limit our understanding of temperature changes in the middle and upper stratosphere.

4.2.2 Observations of Long-Term Changes in the Stratospheric Circulation

4.2.2.1 STRATOSPHERIC ZONAL FLOW

Assessment of long-term trends in the stratospheric circulation is more difficult than it is for temperature because

1. Observations of horizontal stratospheric winds from rawinsondes are sparse and, in general, have not been homogenized for changes in instrumentation.
2. Estimates of the meridional overturning (i.e., the Brewer-Dobson) circulation based on chemical and age-of-air measurements are very noisy and have error bars that exceed the amplitude of the observed trends (Baldwin and Dameris et al., 2007; Engel et al., 2009).

Observed trends in the stratospheric horizontal wind field must be inferred indirectly from measurements of atmospheric temperature (derived from both radiosonde and spaceborne instruments) and atmospheric geopotential height (derived from radiosonde measurements through application of the hypsometric equation).

The trends in the Southern Hemisphere stratospheric vortex during austral spring are well established and were assessed in the 2006 Ozone Assessment (Baldwin and Dameris et al., 2007). They are revisited briefly here since they provide important context for the tropospheric trends assessed in Section 4.4.2. As assessed in the 2006 Assessment, temperatures and geopotential heights both dropped throughout the Southern Hemisphere polar stratosphere from ~1970 to the late 1990s (Thompson and Solomon, 2002). Figure 4-9 shows such trends extended to 2003 (from Thompson and Solomon, 2005). More recent updates of trends in polar geopotential height are not available. Since the trends in geopotential height are relatively small at middle latitudes (not shown), the polar trends in geopotential height shown in Figure 4-9 are consistent with an anomalous eastward acceleration of the Southern Hemisphere stratospheric polar vortex. The eastward acceleration of the Southern Hemisphere stratospheric vor-

tex between November and January is consistent with diabatic cooling associated with the Antarctic ozone hole (Vaugh et al., 1999; Thompson and Solomon, 2002) and is reflected in a delay in the dynamical breakdown of the Southern Hemisphere stratospheric vortex (Vaugh et al., 1999; Zhou et al., 2000; Karpetchko et al., 2005; Haigh and Roscoe, 2009).

The Northern Hemisphere polar stratosphere cooled markedly during winter and spring between the 1960s and the late 1990s (e.g., WMO, 2003), but exhibited a string of warm winters during the 2000s (Section 4.2.1; Randel et al., 2009). Hence, winter and springtime trends in Northern Hemisphere stratospheric zonal-flow are less significant and more difficult to interpret than those in the Southern Hemisphere. As evidenced in the time series in Figure 4-7 (bottom), the Northern Hemisphere polar stratospheric temperature trends are not significant during December–February. The statistically significant cooling and geopotential height decreases in the Northern Hemisphere polar stratosphere during summer (Figure 4-7; Figure 4-9) are not associated with marked meridional gradients, and thus do not imply changes in the stratospheric thermal wind.

4.2.2.2 BREWER-DOBSON CIRCULATION

The Brewer-Dobson circulation model is a simple circulation suggested by Brewer (1949) and Dobson (1956), and consists of three basic parts. The first part is the rising tropical motion of air from the troposphere into the stratosphere. The second part is poleward transport of air in the stratosphere. The third part is descending motion of air in both the stratospheric middle and polar latitudes. This seemingly simple picture leaves a number of possible ambiguities. For instance, the distribution of the tropical air rising through the tropical tropopause is important in that air rising in the inner tropics (near the equator) encounters lower tropopause temperatures than air rising in the outer tropics. The latitudinal distribution of the descending air is also important since middle latitude descending air is transported back into the troposphere (as a result of isentropic mixing), while the polar latitude descending air is transported into the polar lower stratosphere (via diabatic descent). The Brewer-Dobson circulation is driven primarily by the dissipation of Rossby and gravity waves that have propagated upward from the troposphere. Convective overshooting may also play a role in the vertical transport of trace species in the tropical lower stratosphere, but the role of convective overshooting is less understood than the role of stratospheric wave drag (e.g., Fueglistaler et al., 2009).

Measures of the Brewer-Dobson circulation include the upward flux of tropical air, but if this air descends elsewhere in the tropics, it should not be considered a part of the Brewer-Dobson circulation. The net upward mass

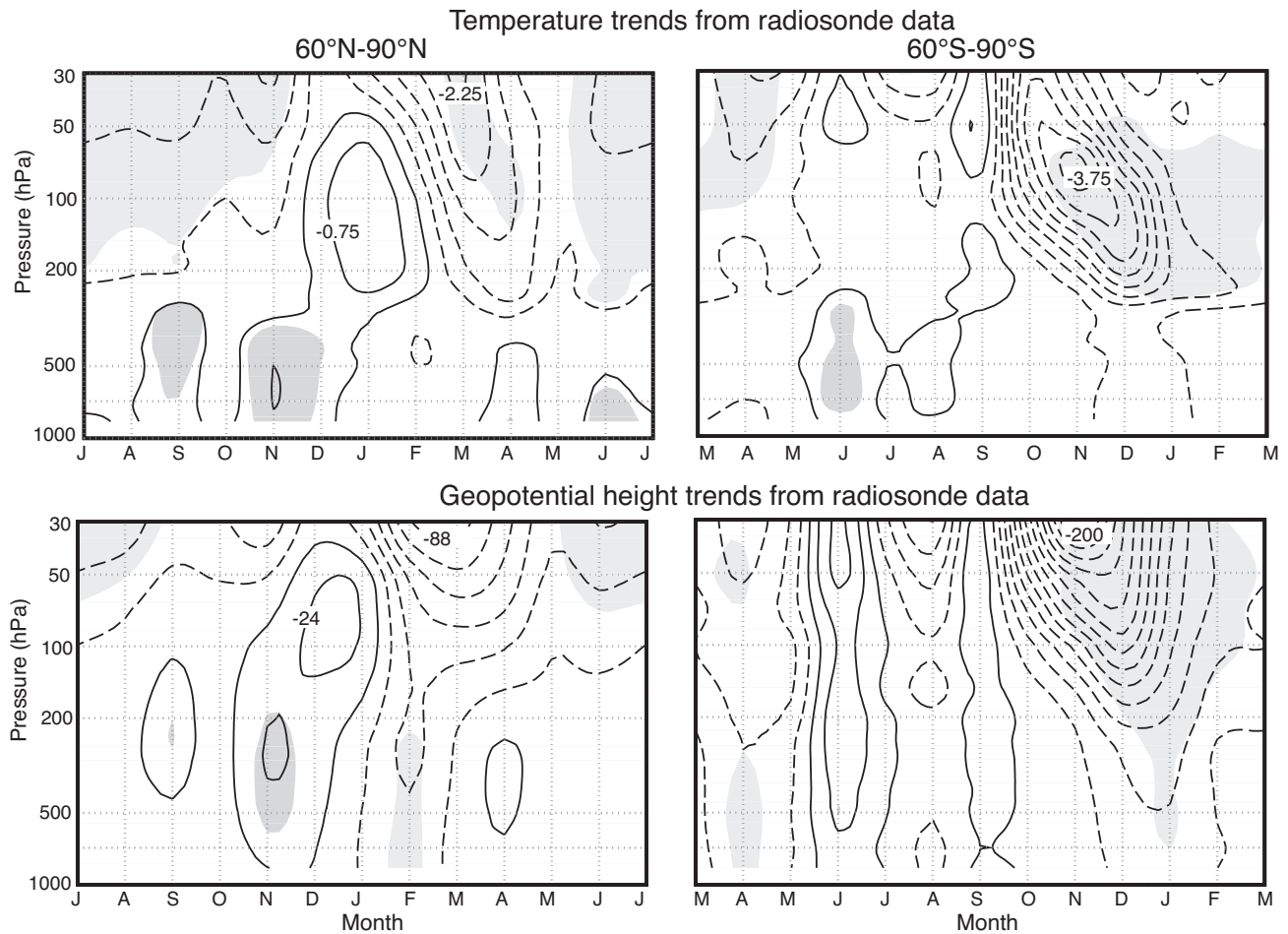


Figure 4-9. Trends in (top) temperature (K/decade) and (bottom) geopotential height (m/decade) averaged over (left) 60°N–90°N and (right) 60°S–90°S for 1979–2003. Trends are shown as a function of month and pressure level. Shading denotes trends that exceeded the 95% confidence level. Tick marks on the abscissa denote the center of the respective month. Note that the calendar months on the abscissa are shifted between the Northern and Southern Hemisphere. Trends based on radiosonde data from the Integrated Global Radiosonde Archive (IGRA). Units: K/decade (–0.25, 0.25, 0.75…) and m/decade (–8, 8, 24…). Based on Thompson and Solomon (2005).

flux of air into the tropical stratosphere is often taken as a measure of the Brewer-Dobson circulation, but this does not distinguish the latitudinal distribution of the rising tropical air, which can affect the ozone distribution differently. Theory (e.g., Plumb and Eluszkiewicz, 1999; Semeniuk and Shepherd, 2001; Zhou et al., 2006) indicates that for annually averaged upwelling at the equator to exist, wave Eliassen-Palm flux convergences must extend into the inner tropics (to about 12–15° latitude), and the distribution of the descending motions at middle and high latitudes depends on the distribution of Eliassen and Palm flux convergences there. However, the importance of tropical wave drag in driving the Brewer-Dobson circulation has recently been questioned by Ueyama and

Wallace (2010), on the basis of their observational analysis. Thus interpreting trends in the modeled and observed Brewer-Dobson circulation will require further research.

As discussed later in Section 4.3.2, climate model simulations consistently predict an acceleration of the Brewer-Dobson circulation in response to increasing greenhouse gases (e.g., Rind et al., 1998; Butchart and Scaife, 2001), amounting to an average increase of about 2%/decade in the annual mean net upward mass flux at 70 hPa through the 21st century (Butchart et al., 2006; McLandress and Shepherd, 2009; Butchart et al., 2010; Chapter 4 of SPARC CCMVal, 2010). Since the Brewer-Dobson circulation partially determines the distribution of stratospheric ozone, the simulated trends in the

Brewer-Dobson circulation link human emissions of CO₂ with the distribution of stratospheric ozone. The simulated trends have implications for stratospheric ozone and water vapor trends, and thus for the radiative forcing of the troposphere and surface climate (as discussed in Section 4.3.2).

The detection of trends in the Brewer-Dobson circulation in observations is complicated by two factors:

1. The trends in the Brewer-Dobson circulation are small through 2010, and only in the next few decades are predicted to depart from the natural variability (Section 4.3.2).
2. The Brewer-Dobson circulation is not a measurable quantity and hence trends in the Brewer-Dobson circulation cannot be directly observed, but rather are inferred from changes in the horizontal structure of lower-stratospheric temperature, constituent trends, and trends in the estimated age of air.

The three primary lines of observational evidence for increases in the strength of the lower-stratospheric meridional circulation include (1) cooling in the lower stratosphere that exceeds the cooling predicted by ozone depletion in the tropics but is less than the cooling predicted as a direct radiative response to ozone depletion (Thompson and Solomon, 2009); (2) out-of-phase temperature trends between polar and tropical latitudes during the Northern Hemisphere and Southern Hemisphere cold seasons, with largest cooling in the tropics (Thompson and Solomon, 2009; Fu et al., 2010); and (3) localized decreases in ozone in the lower tropical stratosphere in trends derived from the SAGE instruments (Chapter 2 and Figure 2-27). In general, the evidence for changes in the Brewer-Dobson circulation based on the structure of lower-stratospheric ozone and temperature trends is most robust in the tropics and less clear at middle and high latitudes.

There are two primary caveats associated with the above lines of evidence:

1. Stratospheric age-of-air estimates based on balloon-borne in situ measurement of sulfur hexafluoride (SF₆) and CO₂ do not indicate statistically significant trends in the Brewer-Dobson circulation (Engel et al., 2009), albeit age-of-air estimates do not uniquely reflect the Brewer-Dobson circulation, and the uncertainty bars on such estimates are very large (i.e., the modeled trends in the Brewer-Dobson circulation lie within the uncertainty estimates of the stratospheric age-of-air measurements in numerous climate change simulations).

2. Trends in tropical lower-stratospheric ozone from the SAGE data are subject to considerable uncertainty (Chapter 2).

4.3 SIMULATIONS OF STRATOSPHERIC CLIMATE CHANGE

4.3.1 Simulation of Stratospheric Temperature Trends from Chemistry-Climate Models and Climate Models

Multiyear observations of stratospheric temperature clearly indicate both large variability on multiple timescales and long-term changes (Section 4.2.1). The thermal structure of the stratosphere is influenced by natural as well as anthropogenic factors. An important task is to understand the impacts of natural forcing on the stratosphere to enable the identification and quantification of implications of human activities. Several studies have been performed to describe the evolution of stratospheric temperature, in particular the observed cooling (e.g., Ramaswamy et al., 2006; Dall'Amico et al., 2010a; Gillett et al., 2010; Randel et al., 2009; see Figures 4-5 and 4-9 for example time series of stratospheric temperature).

Attribution of stratospheric temperature variations and long-term changes can be undertaken through comparison of observed changes with simulations by a hierarchy of numerical models considering radiative, dynamical, and chemical processes in the atmosphere. Such numerical models can be binned into two general classes: (1) climate models, i.e., atmospheric general circulation models that are coupled to an ocean model, but mostly do not resolve the whole stratosphere; and (2) chemistry-climate models, i.e., atmospheric general circulation models that are interactively coupled to a detailed chemistry module, almost fully consider the stratosphere, but so far are generally not coupled to an ocean model. Both types of models can be used to assess both natural and anthropogenic forcings affecting the behavior of the atmosphere.

The prime natural forcings of stratospheric temperature fluctuations on interannual and decadal timescales are the solar activity cycle (with a timescale of 11 years), the El Niño-Southern Oscillation (with a timescale of ~3–5 years), and explosive volcanic eruptions (with sporadic timescales). The quasi-biennial oscillation in tropical stratospheric zonal winds is internally generated but can be considered as a forcing for extratropical stratospheric variability. Most climate models and chemistry-climate models consider the ~11-year activity cycle of the sun (i.e., solar variability is explicitly enforced by variation in radiative heating and photolysis rates) and the radiative and chemical effects of sporadic large volcanic

eruptions (i.e., changes in heating rates and heterogeneous chemistry due to an enhanced aerosol loading). Climate models predict ocean temperatures and to varying degrees are able to capture coupled air-sea variability associated with the El Niño-Southern Oscillation (e.g., AchutaRao and Sperber, 2006). In most chemistry-climate models, ocean surface temperatures are prescribed, using either historical measurements or values derived from climate model simulations. In the latter case, the realism of the El Niño-Southern Oscillation and its related variability is constrained by the realism of the prescribed (climate model-calculated) sea surface temperatures.

Atmospheric models reaching up into the mesosphere and with sufficient vertical resolution in the whole model domain (i.e., less than 1 km) are able to generate stratospheric quasi-biennial-like oscillations (e.g., Giorgetta et al., 2006; Punge and Giorgetta, 2008). Additionally, an adequate description of stratospheric quasi-biennial-like oscillations in stratosphere-resolving climate models requires small-scale gravity wave forcing (e.g., Takahashi, 1999; Scaife et al., 2000a) which is consistent with recent observational estimates (e.g., Ern and Preusse, 2009). Chemistry-climate models that do not generate a stratospheric quasi-biennial oscillation internally mostly have the observed behavior prescribed, i.e., by assimilating observed wind fields in the tropical lower stratosphere (see Morgenstern et al., 2010a).

In climate models and chemistry-climate models, the impact of human activities is generally considered as follows: long-lived greenhouse gases (i.e., CO₂, CH₄, and N₂O), anthropogenic aerosol loading, and ODSs (CFCs, HCFCs, and halons) are prescribed as either emissions or atmospheric concentrations. In chemistry-climate models, changes in the amount and distribution of water vapor and ozone are calculated in a self-consistent manner considering interactions of chemical, radiative, and dynamical (transport and mixing) processes, whereas in climate models, ozone fields are mostly prescribed without considering feedbacks; and effects of chemical processes on water vapor are neglected. Natural forcings such as changes in solar activity and explosive volcanic eruptions are also taken into account. Detailed summaries of suggested and used boundary conditions for recent chemistry-climate model simulations (see Chapter 3 of this report) have been given in Eyring et al. (2008), in Chapter 2 of the SPARC CCMVal report (2010), and in Morgenstern et al. (2010a)¹.

¹ The CCMVal project uses chemistry-climate models to simulate the atmosphere from 1960 to about 2100. CCMVal-2 is the second CCMVal project (SPARC CCMVal, 2010). The scenarios used in CCMVal-2 are outlined in Chapter 2 of the SPARC CCMVal (2010) report. REF-B1 (1960-2006) is defined as a transient run from 1960 (with a 10-year spin-up period) to the present (see Table 3-2 of this Assessment).

Figure 4-10 shows the time series of global-mean stratospheric temperature anomalies as derived from these chemistry-climate model simulations (colored lines) compared to satellite data (Microwave Sounding Unit/Stratospheric Sounding Unit) weighted over specific vertical levels (black lines). There is strong evidence for a large and significant cooling in most of the stratosphere during the last decades (Section 4.2.1; e.g., Randel et al., 2009; Randel, 2010; Thompson and Solomon, 2009). The observed stratospheric cooling has not evolved uniformly since the 1960s and the overall development is well reproduced by the majority of chemistry-climate models (see Figure 4-10).

Ramaswamy et al. (2006) noted that the observed cooling of the global lower stratosphere between 1979 and 2003 occurred in two distinct step-like transitions (see also Section 4.2.1). After a 2–3 year period of stratospheric warming due to enhanced aerosol loading of the stratosphere, these appeared subsequent to the two explosive volcanic eruptions, El Chichón (April 1982) and Mt. Pinatubo (June 1991), with each cooling transition being followed by a period of relatively steady temperatures. Ramaswamy et al. (2006) concluded that the anthropogenic factors forced the overall cooling and the natural factors modulated the temporal evolution of the cooling. Simulations performed with chemistry-climate models support these findings: the space-time structure of the observed cooling is largely attributable to the combined effect of stratospheric ozone depletion and increases in greenhouse gas concentrations, superimposed on effects due to solar irradiance variation and explosive volcanic eruptions (see Chapter 3 of SPARC CCMVal, 2010). Moreover, Thompson and Solomon (2009) provided observational analyses that indicate the step-like behavior of global mean stratospheric temperatures depends also on the temporal variability in global mean ozone following large volcanic eruptions. They argued that the warming and cooling pattern in global mean temperatures following major volcanic eruptions is consistent with the competing radiative and chemical effects of volcanic eruptions on stratospheric temperature and ozone. This conclusion was supported by a modeling exercise (Dall’Amico et al., 2010a) showing that if observed ozone values are prescribed in their model instead of the assumption of a “simple” linear ozone trend, the stepwise nature of the stratospheric cooling is better reproduced.

Thompson and Solomon (2009) also demonstrated that the contrasting latitudinal structures of recent stratospheric temperature (i.e., stronger cooling in the tropical lower stratosphere than in the extratropics) and ozone trends (i.e., enhanced ozone reduction in the tropical lower stratosphere) are consistent with the assumption of increases in the stratospheric overturning Brewer-Dobson circulation. The seasonality of tropical lower-stratospheric tem-

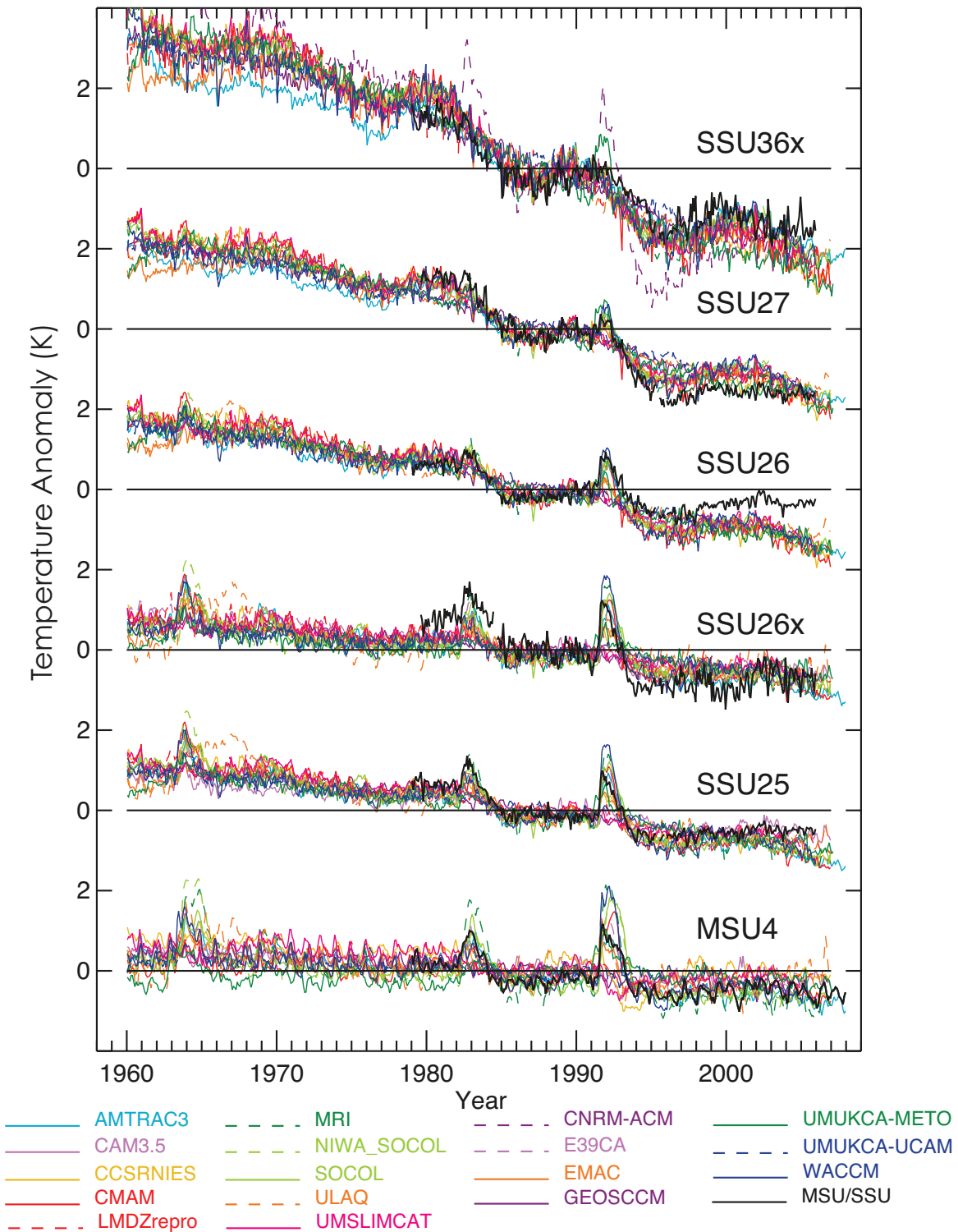


Figure 4-10. Global mean time series of satellite observed (Randel et al., 2009) and chemistry-climate model temperature anomalies (K) weighted for MSU/SSU weighting functions. The anomalies are calculated with respect to the period 1980–1994, as in the provided MSU/SSU anomalies. Exact weighting functions for the MSU/SSU satellite instruments can be found in Figure 1 of Randel et al. (2009). Channel 27 corresponds to ~34–52 km altitude, channel 36x to ~38–52 km, channel 26 to ~26–46 km, channel 25 to ~20–38 km, channel 26x to ~21–39 km, and channel MSU4 to ~13–22 km. See Table 3-1 in Chapter 3 of this Assessment for a description of the chemistry-climate models shown in the figure.

perature trends using the MSU4 (~13–22 km altitude) data (1979–2007) was examined by Fu et al. (2010). Evidence was given that the seasonality is a response to changes in the Brewer-Dobson circulation, as discussed further in Sections 4.2.2 and 4.3.2. Based on the same data set but focusing on the Southern Hemisphere, Lin et al. (2009) showed that the observed temperature patterns are characterized by cooling and warming regions of similar magnitudes, with strongest local trends occurring in austral spring. Canziani et al. (2008) found that the spring warming observed in the Southern Hemisphere stratosphere could be linked to an enhanced stationary planetary wavenumber 1 and increased total ozone associated with this wave at midlatitudes.

The results presented in Figure 4-10 show a better overall agreement between observations and chemistry-climate model results than in previous comparison studies (Eyring et al., 2006; WMO, 2007, Chapter 5). Global mean temperature anomalies, particularly the longer-term trend, derived from observations are reproduced well by most chemistry-climate model simulation results (Chapter 3 of SPARC CCMVal, 2010). On the one hand, this may be due to improved chemistry-climate models; on the other hand, this may be due to improvements in the retrievals of the observed temperature data. Nevertheless, there are still some differences in detail between observations and chemistry-climate model results in specific regions of the atmosphere, e.g., in the Arctic and Antarctic atmosphere (Austin et al., 2009). Since regional trends could be affected by various processes, possible reasons for such discrepancies can be manifold and need more specific investigations.

Figure 4-10 illustrates that many chemistry-climate models capture the leveling of the stratospheric temperature since the late 1990s. The impact of the prescribed sea surface temperatures is apparent as MSU4 temperatures (centered ~13–22 km) and chemistry-climate model temperatures are particularly well correlated compared to other levels. A disagreement between the models and observations is clearly seen in Stratospheric Sounding Unit channel 26 (SSU26; centered near ~26–46 km) over the last decade. SSU26 has a maximum weight at about 5 hPa and a considerable contribution from the lower stratosphere. Although the agreement is better in Stratospheric Sounding Unit channel 27 (SSU27; centered near ~34–52 km), which peaks at 2 hPa with less contribution from the lower stratosphere, the timing and duration of the flattening is quite different between models and observations. So far the reasons for these findings are not understood.

The corresponding vertical profiles of global temperature trends derived from MSU/Stratospheric Sounding Unit data and chemistry-climate models are shown in Figure 4-11. The observed stratospheric trend between 1980 and 2005 is connected with emissions of CO₂ and ODSs (Shepherd and Jonsson 2008; Gillett et al., 2010)

and is controlled radiatively by changes in CO₂, O₃, and H₂O concentrations (Shine et al., 2003). Jonsson et al. (2009) found that CO₂-induced cooling reduced upper-stratospheric ozone depletion by a factor of approximately 20% over the period from 1975–1995 (when the amount of stratospheric ODSs was increasing most rapidly) when compared with what would have been expected based on the ODS increases alone. This may not be true in the future as climate-ozone interaction becomes more important (see Section 4.5).

Nearly all chemistry-climate models successfully model the broad features of the observed temperature trend, with warming in the troposphere and cooling in

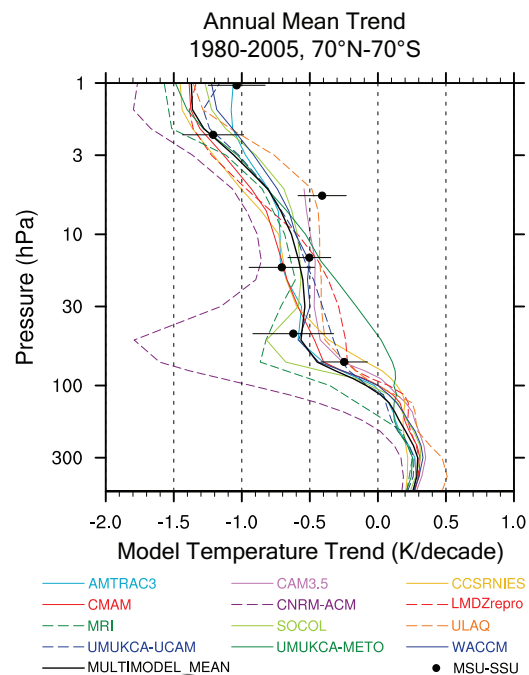


Figure 4-11. Near global (70°S–70°N) and annual mean trends for 1980-2005 (K/decade) for temperature of CCMVal REF-B1 model simulations. The figure includes satellite observed MSU/SSU trends and 95% confidence intervals. MSU/SSU data points include channels: MSU-4 (at 70 hPa), SSU25 (15 hPa), SSU26 (5 hPa), SSU27 (2 hPa), SSU15X (45 hPa), SSU26X (15 hPa), and SSU36X (1 hPa), where the specified pressure levels represent the approximate weighted mean heights derived from the MSU/SSU vertical weighting functions for each channel (see Randel et al., 2009). The solid black lines indicate the multi-model mean results. See Table 3-1 in Chapter 3 of this Assessment for a description of the chemistry-climate models shown in the figure. From Figure 3.2a from SPARC CCMVal (2010).

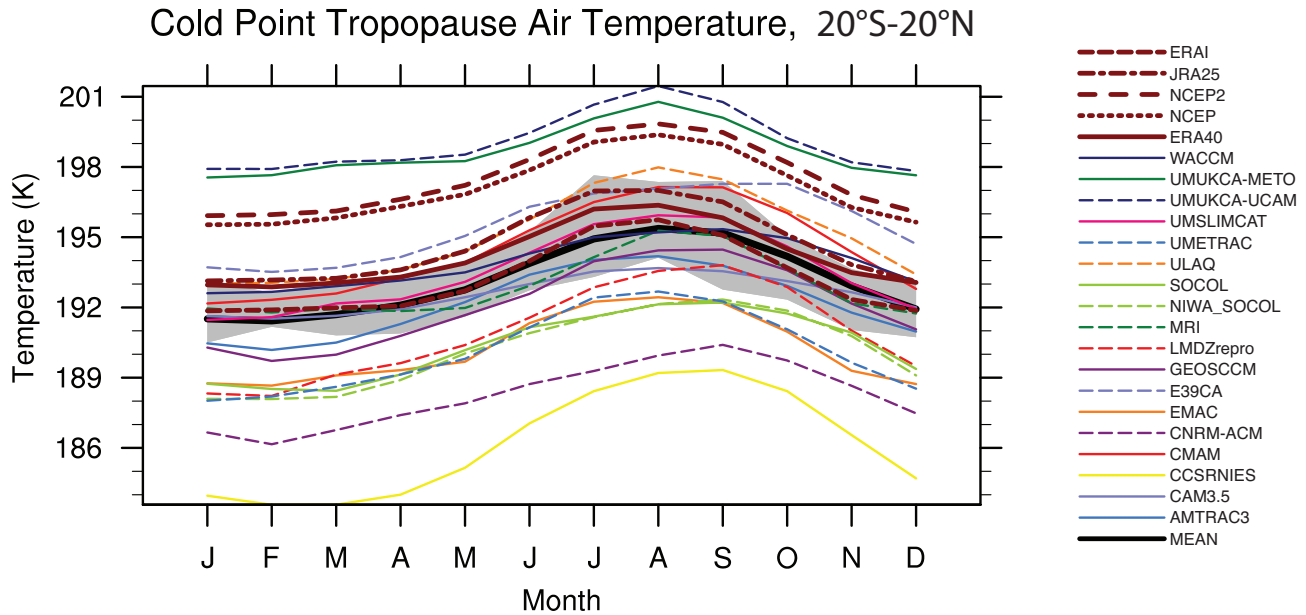


Figure 4-12. Annual cycle of tropical (20°S – 20°N) cold point tropopause temperature (K) from chemistry-climate models and observations. Model output and observations are from the period 1980–1999. Gray shaded region is 3σ variability from ERA40 analyses. Reanalysis systems in brown with different line styles: European Centre for Medium-Range Weather Forecasts (ECMWF) 40-year reanalysis (ERA40; solid), ECMWF Interim Re-Analysis (ERA-I; short dash), Japanese Re-Analysis (JRA25; dot dash), National Centers for Environmental Prediction (NCEP; dotted), and NCEP2 (long dashed). The multi-model mean (MEAN) is the thick black line. See Table 3-1 in Chapter 3 of this Assessment for a description of the chemistry-climate models shown in the figure. From Gettelman et al. (2010).

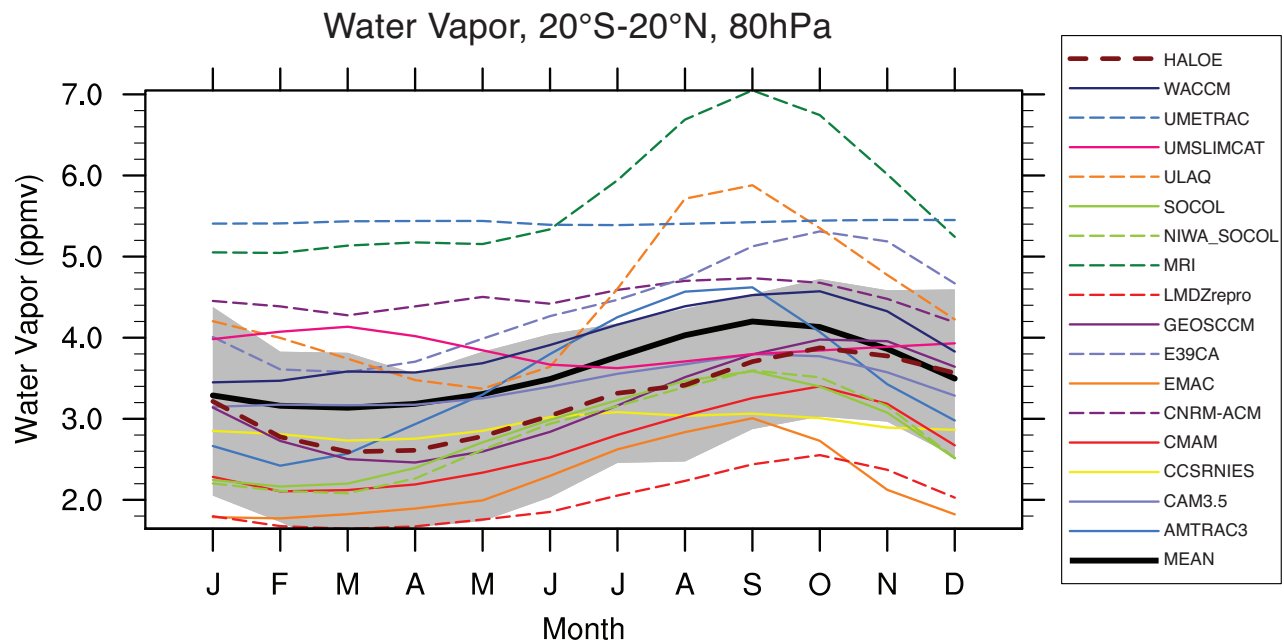


Figure 4-13. Annual cycle of tropical (20°S – 20°N) water vapor mixing ratio at 80 hPa from chemistry-climate models and observations. Model output from the period 1992–2004. Gray shaded region is 3σ variability from HALOE observations over 1992–2004 (thick brown dashed line). The multi-model mean (MEAN) is the thick black line. See Table 3-1 in Chapter 3 of this Assessment for a description of the chemistry-climate models shown in the figure. From Gettelman et al. (2010).

the stratosphere over this period. It should be noted that the tropospheric warming is by construction constrained towards observations because the historically observed sea surface temperatures are prescribed in most of the chemistry-climate models. In the stratosphere, most models capture the overall behavior of the vertical variations, with cooling maxima in the upper and lower stratosphere (Chapter 3 of SPARC CCMVal, 2010). This indicates that the natural and anthropogenic forcings considered in the chemistry-climate models seem to be sufficient to explain the global-mean temperature changes in the stratosphere over the last 50 years. Nevertheless, specific model results indicate that there are still several uncertainties.

For example, Gettelman et al. (2010) analyzed the annual cycle of the tropical cold point tropopause temperature, i.e., the region of lowest temperatures, comparing the results of chemistry-climate models (i.e., using the REF-B1 CCMVal-2 model fields; see footnote 1 in this section) with corresponding data derived from several reanalysis systems (Figure 4-12). Although almost all chemistry-climate models are able to reproduce the annual cycle, there are significant offsets between some models and observations. Interestingly, the multi-model mean is very close to ERA-40, and the model results presented in Figure 4-12 are generally in better agreement with observations than results from the chemistry-climate models used in the first set of CCMVal (CCMVal-1) experiments (Gettelman et al., 2009). The uncertainties in the chemistry-climate models' tropical cold point tropopause temperature affect the water vapor content of air entering the stratosphere (Figure 4-13), which is critical for the chemistry and the climate of the stratosphere (see also Section 4.1.3).

Other examples of model uncertainties were presented by Austin et al. (2008), who analyzed multidecadal simulations of chemistry-climate models concerning the presence of the 11-year solar activity cycle in ozone and temperature data, and compared it with respective satellite measurements. They showed that the currently available model systems have improved significantly compared to studies that were based on the previous generation of chemistry-climate models (e.g., Soukharev and Hood, 2006); model results and observations mostly agree, within stated uncertainties, with regard to the vertical structure of the ozone solar response, particularly in the tropics where a double vertical peak structure is now reproduced by chemistry-climate models with a minimum near 20 hPa, which is slightly below the minimum identified in observations (~10 hPa). The tropical temperature solar response calculated by the chemistry-climate models (Figure 4-14) also shows a “double peak,” whereas temperature data derived from satellite based measurements (Stratospheric Sounding Unit and MSU) do not indicate such a vertical response pattern. However, it is likely that the Stratospheric Sounding Unit has insufficient vertical

resolution to identify such a double peak structure (Gray et al., 2009).

Another uncertainty with regard to the impact of solar variability arises from recent measurements (April 2004–March 2008) of solar spectral irradiance acquired by the Solar Radiation and Climate Experiment satellite (Harder et al., 2009). While these observations show variations in total irradiance largely in line with previous solar activity cycles, they cast doubt on currently accepted models of the spectral composition of the irradiance variability. In particular they suggest much larger (by approximately a factor of six) differences at ultraviolet wavelengths, and negative changes (i.e., greater emissions at solar minimum relative to solar maximum) in the visible and near infrared. These measurements are currently available only over a four-year period during the final declining stages of the most recent solar cycle and therefore remain to be validated; however, if correct, they imply a much larger solar signal in stratospheric ozone (Haigh et al., 2010). The magnitudes of experimental uncertainties in both the irradiance and contemporaneous ozone data do not yet allow this to be tested.

Trends in stratospheric temperature could also be affected by changes in transport of radiatively active trace

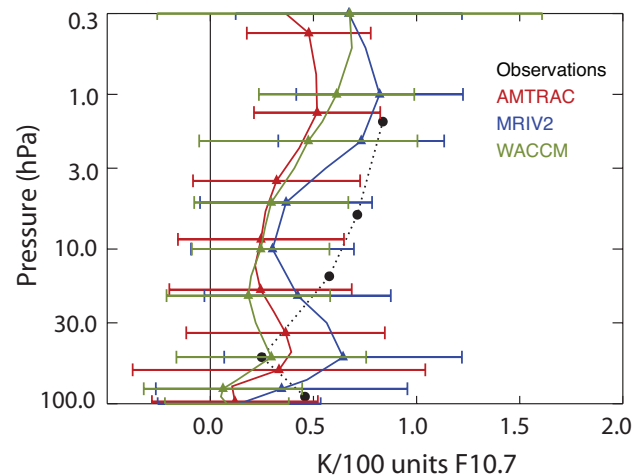


Figure 4-14. Temperature solar response averaged over the latitude range 25°S to 25°N. Units on x-axis in Kelvin per 100 units (in $10^{-22} \text{ W m}^{-2} \text{ Hz}^{-1}$) of the solar radio flux at 10.7 cm (F10.7). The figure shows the results from ensemble simulations for models that consider the 11-year solar activity cycle. The analyzed periods are: 1960–2004 (AMTRAC), 1980–2004 (MRI), and 1950–2003 (WACCM). The solar cycle derived from SSU and MSU data is indicated by the dotted black line. Data derived from observations (1979–1997) were reprocessed from Scaife et al. (2000b). (From Figure 12 of Austin et al., 2008.)

gases via changes in stratospheric circulation that might be induced by climate change (e.g., Cook and Roscoe, 2009). As noted in Section 4.3.2, the stratospheric Brewer-Dobson circulation is likely to be modified in the presence of enhanced greenhouse gas concentrations. Certainly any change in the strength of the Brewer-Dobson circulation would alter the thermal structure of the stratosphere. Moreover, it must be considered that an intensified Brewer-Dobson circulation would affect stratosphere-troposphere mass transport and lead to a quicker turnover time of stratospheric air, i.e., lower age of stratospheric air.

The simulated mean temperature changes (i.e., multi-model mean values) from 1979 to 2000 derived from a subset of the CMIP3² coupled ocean-atmosphere climate model simulations are dominated by zonally symmetric radiative cooling due to ozone depletion. Based on this result Lin et al. (2009) concluded that the climate models fail to simulate the warming in the southern polar stratosphere (see Figure 4-6), indicating a lack of the Brewer-Dobson circulation strengthening in these models. This interpretation contradicts the statements given above referring to chemistry-climate model results. A reason could be that most of the climate models used do not adequately resolve the stratosphere and therefore inadequately reproduce the Brewer-Dobson circulation and its changes. On the other hand it is still questionable if the recent (1995–2008) warming of the polar lower stratosphere is a robust and statistically significant feature. Gravity wave parameterizations within the climate models may also contribute to these differences.

The stratospheric temperature trends simulated by the large ensemble of climate models available from the CMIP3 experiments have been evaluated in the IPCC Fourth Assessment Report, although the main emphasis there was on attribution of climate variations in the troposphere (Hegerl et al., 2007 in IPCC, 2007). Those climate models do not generally include stratospheric chemical processes but some include specified changes in stratospheric ozone concentrations. For example, Schwarzkopf and Ramaswamy (2008) analyzed simulations of a CMIP3 climate model (GFDL-CM2.1) for the period from 1861 to 2003. They showed that the global-mean cooling in the stratosphere (mainly due to enhanced CO₂ concentrations) became significant as early as the first quarter of the 20th century. Thereafter the magnitude of stratospheric cooling by mid-20th century at ~20–50 hPa exceeded the magnitude of the warming near the surface. By the late 1970s, significant stratospheric ozone depletion had begun, enhancing the cooling.

The observed global mean temperature trends in the troposphere and lower stratosphere for recent decades are simulated well by most chemistry-climate models (e.g., Figure 4-10), but are not generally as well simulated by some CMIP3 climate models (Figure 4-15; from Cordero and Forster, 2006). The observed global mean cooling trend in the lower stratosphere is grossly underestimated by climate models that do not include specified decreases in stratospheric ozone over the last three decades. Even climate models that include specified ozone decreases slightly underestimate the observed cooling trend (for details see Cordero and Forster, 2006). In addition, climate models that include specified increases in stratospheric volcanic aerosols appear to overestimate the warming of the lower stratosphere after major volcanic eruptions (Figure 4-15), possibly because they neglect the ozone changes associated with the eruption and do not include the influence of the stratospheric quasi-biennial oscillation (Dall’Amico et al., 2010a). Moreover, Waugh et al. (2009) showed that the calculated cooling simulated in response to ozone depletion is larger in a model with interactive chemistry (i.e., a chemistry-climate model) than that determined by the same underlying atmospheric general circulation model that prescribes the identical zonal mean ozone forcing.

Climate models have also been used to show that tropopause height variations are a sensitive indicator of temperature changes in the upper troposphere and lower stratosphere. They have enabled attribution of observed trends in mean tropopause height over the last three decades of the last century to the combined influence of increasing concentrations of greenhouse gases and aerosols and decreasing amounts of stratospheric ozone (Santer et al., 2003). More recently, Son et al. (2009a) investigated results derived from six chemistry-climate models and found that historical changes (since 1960) in tropopause height are linked to ozone depletion.

4.3.2 Simulation of Brewer-Dobson Circulation Trends in Chemistry-Climate Models

The Brewer-Dobson circulation is the stratospheric wave-driven circulation that transports mass and constituents upward in the tropics and poleward and downward at higher latitudes (see Section 4.2.2 for a more detailed description). In the 2006 Assessment (WMO, 2007), chemistry-climate models were found to consistently predict an acceleration of the Brewer-Dobson circulation in response to increasing greenhouse gas concentrations, amounting to an average increase of about 2%/decade in the annual mean net upward mass flux at 70 hPa through the 21st century. Butchart et al. (2006) also found that over half of the annual mean trend was explained by changes

² CMIP3 refers to simulations of 20th and 21st century climate organized by the Coupled Model Intercomparison Project Phase 3 for use in IPCC experiments (Meehl et al., 2007).

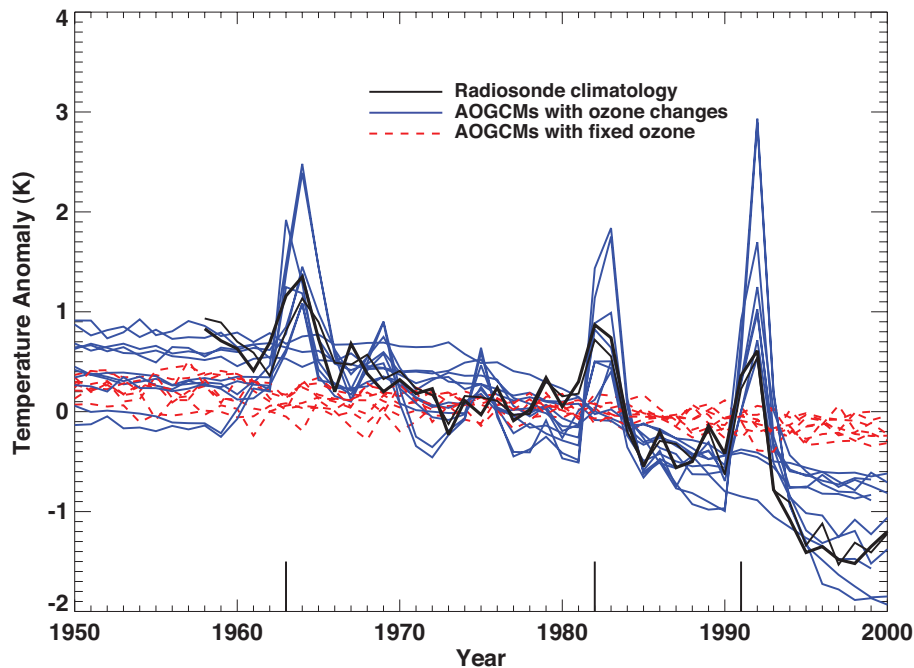


Figure 4-15. Time series of globally averaged annual temperature anomalies (K) at 50 hPa from radiosonde observations (black lines) and simulations of atmosphere-ocean general circulation models (AOGCMs; colored lines). Climate model simulations that included specified stratospheric ozone depletion, as well as increases in greenhouse gases and anthropogenic aerosols, are shown with blue lines, while model simulations that did not include stratospheric ozone depletion are shown with red dashed lines. Some, but not all, the models also include specified stratospheric volcanic aerosol amounts. Short vertical lines on the abscissa denote years of major volcanic eruptions. Figure modified from Cordeiro and Forster (2006).

in resolved wave drag, with the remainder assumed to be due to parameterized wave drag. They were unable to conclude whether changes in stratospheric ozone had any effect on the predicted trend in upward mass flux.

Subsequent to the previous Assessment (WMO, 2007) our understanding of the mechanisms driving the Brewer-Dobson circulation in simulations and its predicted future increase has advanced considerably. Chemistry-climate model intercomparison studies (Butchart et al., 2010; Chapter 4 of SPARC CCMVal, 2010) have shown that the $\sim 2\%$ /decade increase is a robust value for the lower stratosphere (Figure 4-16) in model simulations driven by comparable scenarios. Using a better set of model simulations (i.e., only transient simulations with common forcings using more mature models) and a more accurate calculation of the mass fluxes, Butchart et al. (2010) found that $\sim 70\%$ of the upward mass flux trend was due to parameterized orographic gravity wave drag, a value that was computed from only the subset of models that provided the gravity wave drag data. The importance of these waves in driving the acceleration of the Brewer-Dobson circulation has also been elucidated by a number of studies (Li et al., 2008; McLandress and Shepherd, 2009; Butchart et al., 2010). These studies have demonstrated that the predicted future increase in lower-stratospheric parameterized orographic gravity wave drag is a robust model

response to climate change, resulting from the eastward acceleration of the subtropical jets which increases the gravity wave momentum flux reaching the lower stratosphere. While the parameterized momentum fluxes are not well constrained by observations, they do respond in a physically consistent manner to changes in the large-scale circulation. It should also be noted that the similarity of the model results might be due in part to the similarity of the orographic gravity wave parameterizations.

Another advance has been our understanding of the role of resolved wave drag. However, due to a lack of the necessary diagnostic data available for model intercomparison studies, only individual model studies have been undertaken. In comparing these studies, some caution is required since different definitions are used to characterize tropical upwelling. Using the net upward mass flux at 70hPa, McLandress and Shepherd (2009) examined the contributions from different zonal wavenumbers. They found that 60% of the net upward mass flux trend due to resolved wave drag resulted from planetary waves, with the remainder coming from synoptic waves. On the other hand, Garcia and Randel (2008) and Calvo and Garcia (2009) employed a fixed latitude range that did not encompass the subtropics to define tropical upwelling. In the former study the trend in tropical upwelling resulted from changes in resolved wave drag in the subtropical

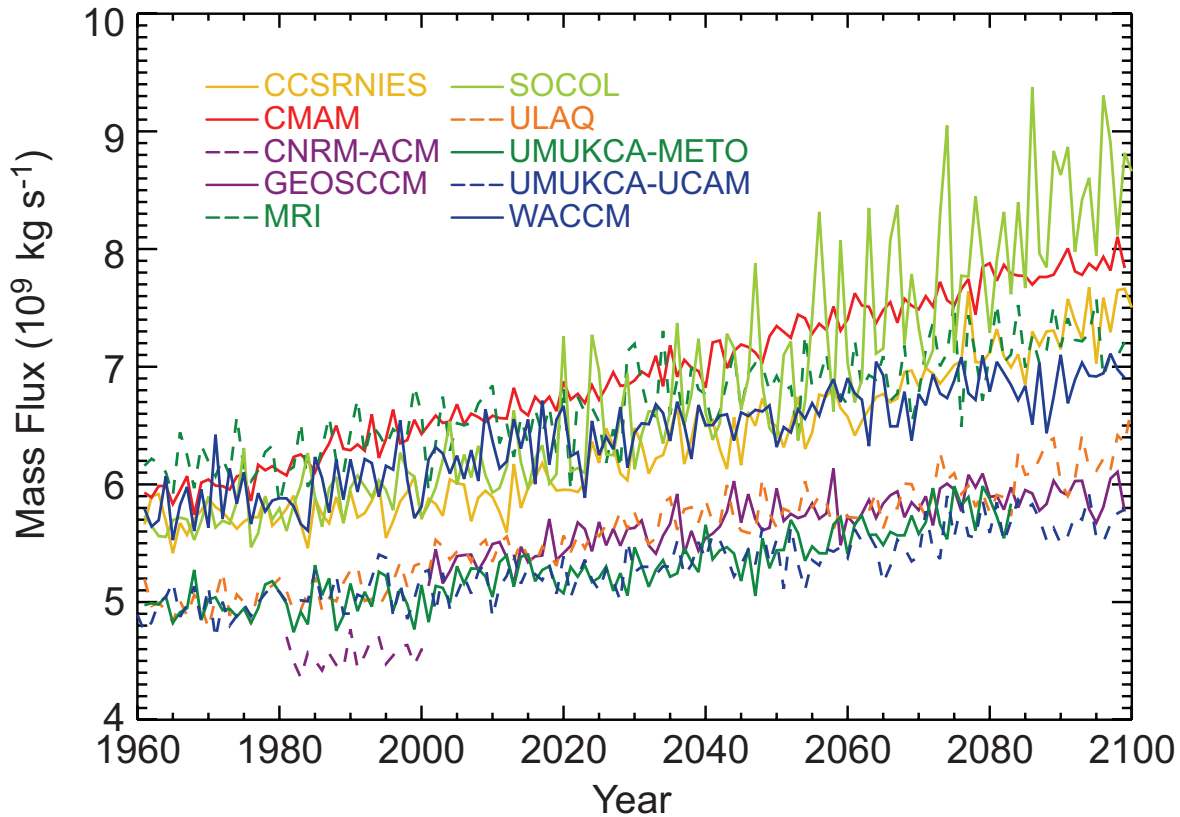


Figure 4-16. Annual mean upward mass flux (kg s^{-1}) at 70 hPa, calculated from residual mean vertical velocity between the turnaround latitudes of the Brewer-Dobson circulation, for the simulations prepared for the CCM-Val SPARC report. See Table 3-1 in Chapter 3 of this Assessment for a description of the chemistry-climate models shown in the figure. Figure from Chapter 4 of SPARC CCMVal (2010).

lower stratosphere, which in turn resulted from enhanced wave propagation due to changes in the zonal mean zonal winds. Calvo and Garcia (2009) concluded that enhanced dissipation of quasi-stationary planetary waves forced by increased tropical convection were responsible for the upwelling trends, at least in a fixed latitude band. A similar conclusion about the role of convectively forced stationary waves was made by Deckert and Dameris (2008), although they did not quantify the impact of those waves on upwelling trends.

Consistent with the predicted increase in net upward mass flux, the mean age of stratospheric air is predicted to decrease (Austin and Li, 2006; Garcia and Randel, 2008; Oman et al., 2009; Butchart et al., 2010). Oman et al. (2009) examined the impact of a number of different factors affecting mean age and concluded that their impact depended upon the time period examined. Over the past 40 years they found that ozone depletion was responsible for the simulated decrease in mean age, while later in this century after ozone has returned to 1980 levels, decreasing age was attributed to increasing greenhouse gas concentrations.

Another advance has been our understanding of the role of ozone depletion and recovery in the simulated net upward mass flux trends. Li et al. (2008) found that in the past nearly half of the trend in their simulations occurred in December–February. They attributed this to increased net downward mass flux in the Southern Hemisphere resulting from the delay in breakdown of the Antarctic polar vortex, which allowed Rossby waves to propagate higher into the summer stratosphere, thus driving the increased downwelling. The impact of ozone depletion (and recovery) on the upward mass flux trends was confirmed in McLandress et al. (2010) using a set of chemistry-climate model simulations in which greenhouse gas concentrations were held fixed in time and only ODSs were allowed to vary.

The role of parameterized orographic gravity wave drag in model simulations is better understood than in the previous Assessment (WMO, 2007). However, much more needs to be done to validate such parameterizations, particularly since they play a key role in the simulated accelerations of the Brewer-Dobson circulation.

Various prescriptions exist for parameterizing the influences of unresolved gravity waves, but they are based on specifications of certain parameters that are not well constrained by observations at the present time. As long as chemistry-climate models are strongly dependent on the parametrization of gravity waves, the simulated changes in the Brewer-Dobson circulation will remain similarly dependent on the model treatment of such unresolved physical processes.

The mechanisms responsible for the increased resolved wave drag are also unclear. As discussed in McLandress and Shepherd (2009), differences in the way tropical upwelling is computed have made it difficult to come to a clear consensus on which types of resolved waves are responsible for the increase in the Brewer-Dobson circulation. Quantifying whether the increased resolved wave driving of the Brewer-Dobson circulation results from changes in wave sources in the troposphere or wave propagation in the stratosphere is an outstanding issue.

4.4 EFFECTS OF VARIATIONS IN STRATOSPHERIC CLIMATE ON THE TROPOSPHERE AND SURFACE

In this section we assess the linkages between stratospheric variability and climate change in the troposphere and at the Earth's surface. The section includes an assessment of radiative, dynamical, and chemical coupling between the stratosphere and troposphere, but focuses primarily on the dynamical effects of the Antarctic ozone hole on surface climate. The evidence for a robust linkage between the Antarctic ozone hole and the surface flow in the Southern Hemisphere was assessed in Chapter 5 of WMO, 2007 (Baldwin and Dameris et al., 2007). Here we extend that assessment to include recent advances in our understanding of the linkages between the Antarctic ozone hole and surface climate change throughout the Southern Hemisphere. Key advances include a deeper understanding of the likely effects of Antarctic ozone depletion on surface weather, the circulation of the Southern Ocean, the distribution of Antarctic sea ice, and the Southern Hemisphere carbon cycle.

The primary novel effects of stratospheric climate variability on surface climate assessed in this section are summarized in Table 4-1. The text in Section 4.4 is organized into five components as follows:

- Section 4.4.1, stratospheric composition and global-mean surface temperatures
- Section 4.4.2, the Antarctic ozone hole and changes in Southern Hemisphere surface climate
- Section 4.4.3, stratospheric climate change and the tropical tropospheric circulation

Section 4.4.4, stratospheric variability and tropospheric chemistry

Section 4.4.5, solar-induced variability at stratospheric levels and tropospheric climate

4.4.1 Effects of Stratospheric Composition Changes on Global-Mean Surface Temperature and Tropospheric Temperature

Previous World Meteorological Organization (WMO) Ozone Assessments (e.g., WMO, 2007) and the recent IPCC Assessment (IPCC, 2007) have evaluated radiative forcings associated with changes in stratospheric climate. Radiative forcings give an indication of surface temperature change, whereby positive forcings enhance the global mean surface temperature and negative forcings tend to cool the surface. Stratospheric ozone was most recently assessed to give a net radiative forcing of $-0.05 \pm 0.1 \text{ W/m}^2$ between 1750 and 2005 (Forster et al., 2007a). Water vapor concentration changes associated with methane oxidation between 1750 and 2005 were assessed to contribute a forcing of $+0.07 \pm 0.05 \text{ W/m}^2$. The amount of stratospheric aerosol following volcanic eruptions can exert a strongly negative forcing on a short timescale, estimated to be roughly -3 W/m^2 following the eruption of Mt. Pinatubo. Note that volcanic eruptions can also have indirect forcings by affecting concentrations of ozone (see Chapter 3) and stratospheric water vapor (e.g., Joshi and Jones, 2009). The direct forcing of solar changes since 1750 is estimated to be small, although uncertainties exist in long-term trends in solar irradiance, in variations in its spectral composition, and also in its indirect effects on stratospheric ozone.

Figure 4-17 shows the ozone forcing since the 1970s evaluated from chemistry-climate models and observations using a single radiation model from Chapter 10 of SPARC CCMVal (2010). The 1970s-to-2004 radiative forcing is estimated to be $-0.03 \pm 0.2 \text{ W/m}^2$ (90% confidence range) from stratospheric ozone changes in 17 chemistry-climate model runs and $+0.03 \text{ W/m}^2$ employing Randel and Wu (2007) observations. Negative net radiative forcings arise from models with ozone decline in the lowermost stratosphere, particularly at or near the tropopause. This stratospheric ozone forcing is not entirely of anthropogenic origin, but includes components due to the indirect effect of volcanic eruptions and solar irradiance change. The large spread is possibly due to an incorrect ozone response to volcanic eruptions in certain chemistry-climate models (Chapter 10 of SPARC CCMVal, 2010). Including the uncertainty in radiative transfer modeling would be unlikely to increase the uncertainty range (Chapter 3 of SPARC CCMVal, 2010). As differences between

Table 4-1. Highlights of Section 4.4: How stratospheric climate variations affect the troposphere and surface.

Affected Tropospheric Climate Parameters	Currently Observed Effects	Currently Understood Causes	Level of Scientific Understanding
1. Global radiative balance affecting global mean surface temperature (Section 4.4.1)	<ul style="list-style-type: none"> Slight negative long-term radiative forcing from stratospheric ozone variations Slight positive long-term radiative forcing from stratospheric water vapor from methane oxidation Large decadal fluctuations in radiative forcing from stratospheric water vapor 	Stratospheric ozone trends, stratospheric water vapor trends, stratospheric aerosol trends, and other greenhouse gas trends affect stratospheric temperatures. These affect both the shortwave and long-wave components of the radiative budget.	Very Strong
2. Tropical tropospheric temperature (Section 4.4.1)	Tropical upper-tropospheric cooling trend	Reduced tropical stratospheric ozone cools stratospheric temperatures. This reduces longwave radiative flux into the tropical troposphere.	Medium
3. Antarctic tropospheric temperature (Section 4.4.1)	Late spring and summer Antarctic tropospheric cooling	ODS-induced stratospheric ozone loss cools Antarctic stratosphere. This reduces longwave radiative flux into the Antarctic troposphere.	Medium-Strong
4. Southern Annular Mode (SAM) (Section 4.4.2.1)	Trend to positive index of SAM in Southern Hemisphere summer. Evident as falls in geopotential height over the pole and an eastward acceleration of the surface winds over the Southern Ocean.	ODS-induced stratospheric ozone loss cools the Antarctic stratosphere. This induces a stratospheric dynamical response that couples to the tropospheric SAM.	Strong
5. Southern Hemisphere extratropical winds, storm tracks, and precipitation (Section 4.4.2.2)	<ul style="list-style-type: none"> Poleward shift of Southern Hemisphere extratropical jet in summer Reduced low pressure systems at low latitude and increased at high latitudes Poleward shift of Southern Hemisphere precipitation 	Effects 5–9 are all related to the summertime tropospheric SAM trend (climate parameter 4), which is caused by ODS-induced Antarctic stratospheric cooling.	Medium
6. Antarctic surface temperatures (Section 4.4.2.3)	<ul style="list-style-type: none"> Summertime warming of Antarctic Peninsula and cooling trend of East Antarctic High Plateau 		Medium-Strong
7. Antarctic sea ice (Section 4.4.2.3)	<ul style="list-style-type: none"> Increase in summertime Antarctic sea ice extent 		Medium
8. Southern Ocean temperatures and circulation (Section 4.4.2.4)	<ul style="list-style-type: none"> Warming of Southern Ocean subsurface and poleward shift of Southern Ocean density structure 		Low-Medium
9. Southern Ocean carbon cycle (Section 4.4.2.4)	<ul style="list-style-type: none"> Reduction in Southern Ocean carbon uptake 		Low-Medium
10. Width of tropical belt (Section 4.4.3)	Widening of tropical belt, with accompanying poleward shift of the jet streams, the downward branches of the Hadley Cell, and the region of high tropical tropopause	Attributed both to ODS-induced Antarctic ozone depletion and greenhouse warming.	Low

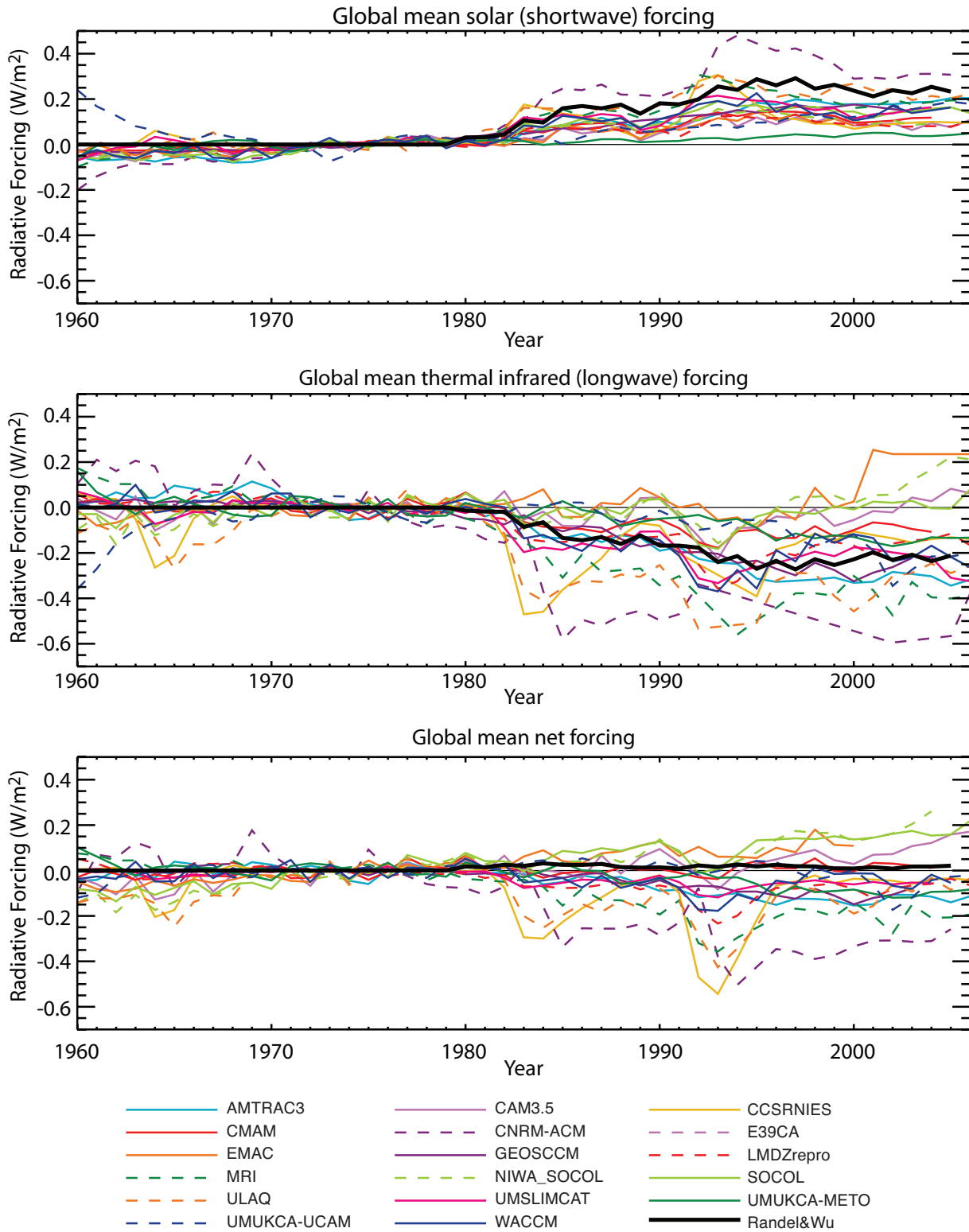


Figure 4-17. Stratospheric ozone global-mean radiative forcing (W/m^2) for shortwave (top), longwave (middle) and net (shortwave plus longwave) compared to the 1970s average, evaluated from the CCMVal REF-B1 scenario ozone fields (colored lines) and from the Randel and Wu (2007) observation-based data set (thick black line). See Table 3-1 in Chapter 3 of this Assessment for a description of the chemistry-climate models shown in the figure. Based on Chapter 10 of SPARC CCMVal (2010).

the SPARC CCMVal calculations and the IPCC assessment of the stratospheric ozone forcing are small, the IPCC assessment of this forcing is retained.

Decadal radiative effects of stratospheric composition changes are significant when compared to that from carbon dioxide, whose forcing increased by roughly 0.2 W/m^2 per decade since 1980 (Forster et al., 2007b). Solomon et al. (2010) estimated that the drop in stratospheric water vapor levels near the tropopause following 2000 (see Section 4.1.3) contributed a forcing of -0.1 W/m^2 . They show that decadal variation of stratospheric water vapor concentrations likely contributed to an enhanced rate of surface warming in the 1990s (see also Forster and Shine, 2002) and a reduced rate of surface warming in the 2000s (see Figure 4-18).

Volcanic aerosols directly affect surface climate by reflecting solar radiation to space. Major volcanic eruptions cool global average surface temperatures for a few years following an eruption (Hansen et al., 1992; Robock, 2000), and also influence the patterns of Northern Hemisphere surface climate through effects on the Northern Annular Mode (e.g., Shindell et al., 2004; Stenchikov et al., 2006). Several studies have underscored that a major volcanic eruption not only perturbs the atmosphere but also cools the oceans, thereby affecting ocean heat uptake, sea level, and climate for many decades (Church et al., 2005; Delworth et al., 2005; Gleckler et al., 2006; Domingues et al., 2008; Gregory et al., 2006; Stenchikov et al., 2009). Thus the timescale over which volcanic effects need to be considered in climate studies is much longer than the time over which the aerosols are present in the stratosphere, and is controlled by multiple factors, including not only the stratospheric timescales but also the slow transport time within the deep ocean.

Recent studies have shown that the changes in radiative forcing from changes in stratospheric composition manifest themselves by directly changing temperatures in the free troposphere. This is in addition to any surface-mediated temperature change. Parts of the observed tropospheric temperature trend in both the tropics and Southern Hemisphere polar regions have been linked to stratospheric ozone depletion and the associated stratospheric cooling trends (Forster et al., 2007b; Keeley et al., 2007; Grise et al., 2009).

In the tropics, observed cooling trends over 1985–2005 above 12 km in the upper troposphere do not appear to be linked to the local radiative impacts of ozone depletion in the upper troposphere but rather to the reduced downwelling longwave radiation associated with ozone depletion in the lower stratosphere (Forster et al., 2007b). The observed tropical upper-tropospheric temperature trends above 12 km are not well reproduced in climate model simulations, especially those with simple ozone prescriptions, suggesting the importance of properly prescribing tropical lower-stratospheric ozone in future

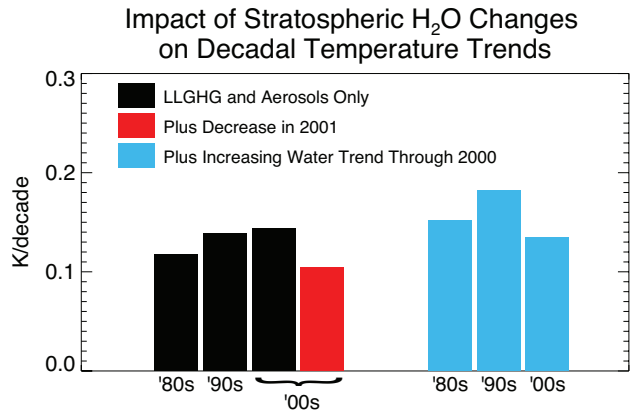


Figure 4-18. Decadal warming rates (K/decade) arising from (i) the long-lived greenhouse gases (LLGHG) and aerosols alone (black), as well as (ii) that obtained including the stratospheric water vapor decline after 2000 (red) and (iii) including both the stratospheric water vapor decline after 2000 and the increase in the 1980s and 1990s (cyan). Based on Solomon et al. (2010).

climate modeling studies of the tropical upper troposphere (Forster et al., 2007b; Allen and Sherwood, 2008).

Several recent studies have suggested that the observed summertime cooling trends in the Antarctic free troposphere are at least partially attributable to decreases in downwelling longwave radiation emitted from the Antarctic lower stratosphere (Keeley et al., 2007; Grise et al., 2009). The decreases in downwelling longwave radiation appear to be driven primarily by the stratospheric temperature changes associated with ozone depletion (Grise et al., 2009), particularly the ozone depletion above the lowermost stratosphere (Keeley et al., 2007). A caveat to the above studies is that they prescribe zonally symmetric stratospheric ozone concentrations for their radiative calculations. Zonal asymmetries in prescribed ozone concentrations at Southern Hemisphere high latitudes have been shown to cause additional cooling in the stratosphere and upper troposphere (e.g., Waugh et al., 2009; Gillett et al., 2009), but most of this additional cooling appears to be driven by dynamical rather than radiative processes (Crook et al., 2008). Dall'Amico et al. (2010b) also show the importance of representing global ozone variability including the stratospheric quasi-biennial oscillation for simulating ozone-climate effects.

4.4.2 Surface Climate Impacts of the Antarctic Ozone Hole

As discussed in Section 4.2 and in Chapter 5 of the previous Ozone Assessment (Baldwin and Dameris

et al., 2007), the robust stratospheric cooling in the Antarctic spring associated with the ozone hole is coincident with an anomalous eastward³ acceleration of the stratospheric polar vortex, and hence a delay in the springtime breakdown of the Southern Hemisphere stratospheric vortex. The trends in the Southern Hemisphere extratropical flow are not limited to stratospheric levels, but extend to Earth's surface during the spring/summer months of December and January, when the trends in the atmospheric flow are dominated by a poleward shift of the tropospheric zonal winds of the Southern Hemisphere (Thompson and Solomon, 2002; WMO, 2007). In WMO (2007), this tropospheric response was attributed to the Antarctic ozone hole, primarily based on the observational study of Thompson and Solomon (2002) and the modeling study of Gillett and Thompson (2003). In this section, we assess work since WMO (2007) on this stratosphere-troposphere connection and its implication for the surface climate of high southern latitudes.

In the stratosphere and troposphere, the spatial structure of the observed extratropical trends projects strongly upon the dominant and most persistent pattern of natural variability in the extratropical circulation: the Southern Annular Mode (Thompson and Wallace, 2000; Thompson and Solomon, 2002; Gillett and Thompson, 2003)⁴. In fact, the observational and modeling evidence outlined in Chapter 5 of the previous Ozone Assessment (Baldwin and Dameris et al., 2007) strongly suggests that the dynamical influence of the ozone hole on surface climate is manifested almost entirely in the structure of the Southern Annular Mode. However, we emphasize that the projection is clearest in the zonal mean and that the Southern Annular Mode does not account for all aspects of Southern Hemisphere climate trends: the trend in the

³ When used in the context of the wind, "eastward" (toward the east) is synonymous with "westerly" (from the west). We use the "eastward" terminology throughout this chapter since the term "westerly" has an ambiguous definition depending on what it is used to describe.

⁴ The Southern Annular Mode (SAM) is the dominant pattern of variability in the Southern Hemisphere extratropical circulation (e.g., see Thompson and Wallace 2000 and discussions in Chapter 5 of WMO, 2007). Typically, it is defined to be the leading empirical orthogonal function (EOF) of the Southern Hemisphere geopotential or zonal wind. For an EOF calculation using monthly mean time series and using all months of the year, the SAM based on (1) zonally varying 850 hPa geopotential, (2) zonal mean 1000-50 hPa geopotential, and (3) zonal mean 1000-50 hPa zonal wind respectively explains (1) 27%, (2) 47%, and (3) 45% of the variance (Table 2 of Thompson and Wallace, 2000). In the troposphere, SAM variability is characterized by meridional excursions of the tropospheric jet. During the Southern Hemisphere spring, the SAM also corresponds to variations in the strength of the polar vortex in the stratosphere. SAM dynamics is understood to reflect interactions between waves and the zonal mean flow (e.g., Limpasuvan and Hartmann, 2000).

annular mode is largest during summer (as noted below), it does not account for many zonally varying aspects of recent Southern Hemisphere climate change, and it may not fully account for zonally asymmetric forcing by ozone depletion (e.g., Crook et al., 2008).

That the response to the ozone hole is related to a persistent and dominant mode of internal variability like the Southern Annular Mode is expected based on general theoretical grounds (e.g., Leith, 1975; Gerber et al., 2008; Ring and Plumb, 2008) and also the fact that the annular mode dynamically connects the stratospheric and tropospheric circulations (Thompson and Wallace, 2000). The detailed dynamics of this stratosphere-to-troposphere link are still being explored; they have been linked to direct driving of the circulation by diabatic heating and changes to the eddy-induced stresses, to eddy mean-flow interactions in which the mean flow changes feed back onto the transient eddy driving field, to barotropic-mode dynamics, and to radiative driving (e.g., see Song and Robinson, 2004; Esler et al., 2006; Thompson et al., 2006; Simpson et al., 2009; Grise et al., 2009). But at this point, the precise dynamical mechanism(s) by which the tropospheric circulation responds to ozone depletion have not been fully elucidated.

Since WMO (2007), the robustness and seasonality of the tropospheric circulation response to Antarctic ozone depletion has been established in numerous climate simulations (e.g., Arblaster and Meehl, 2006; Miller et al., 2006; Cai and Cowan, 2007; Karpechko et al., 2008; Perlwitz et al., 2008; Fogt et al., 2009; Son et al., 2008, 2009b, 2010; Chapter 10 of SPARC CCMVal, 2010). Figure 4-19

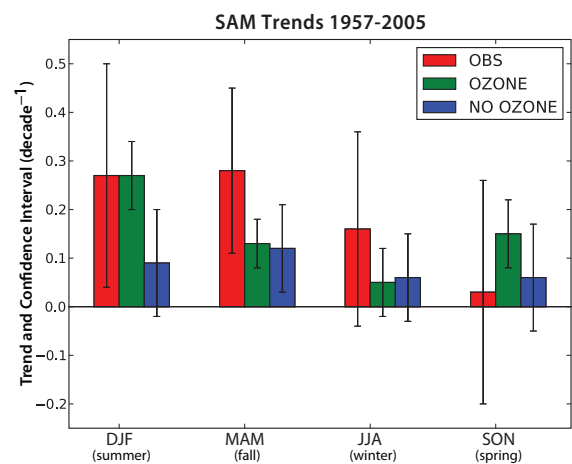


Figure 4-19. Seasonal trends over 1957–2005 in the SAM index (in units of decade⁻¹) from observations and the CMIP3 climate models with ("OZONE") and without ("NO OZONE") time-varying ozone forcing. The 95% confidence intervals reflect the number of time series involved in the trend analysis (see Fogt et al. 2009 for details). Data taken from Table 3 of Fogt et al. (2009).

(based on Table 3 of Fogt et al., 2009) provides an updated view of observed and simulated tropospheric circulation trends expressed in terms of the Southern Annular Mode. The positive trends in the Southern Annular Mode are most robust in observations and models during the austral summer and fall seasons (labeled DJF and MAM, respectively). During the austral summer season, a statistically significant positive Southern Annular Mode response is simulated only in those integrations that include the observed Antarctic ozone depletion (labeled “OZONE” in the figure). During the austral fall season, the simulated trends are half the observed value and occur whether or not ozone forcing is present. In the austral winter (labeled JJA), the observed and simulated trends are not significant. In the austral spring (labeled SON), there is a poorly understood discrepancy between the models and observations: the “OZONE” models produce a positive Southern Annular Mode trend when none is observed (Fogt et al., 2009).

The following caveat must be considered when interpreting the results in Figure 4-19: different models are included in the “OZONE” and “NO OZONE” sets in the figure, so it is difficult to cleanly attribute the Southern Annular Mode trend to ozone-related forcing in these simulations. We can begin to assess the separate effects of ozone and greenhouse gas forcing from a limited number of studies. For example, when ozone and greenhouse gas forcings are prescribed separately in the National Center for Atmospheric Research Community Climate System Model, it is clear that ozone forcing drives the primary Southern Annular Mode response in summer (Arblaster and Meehl, 2006). In addition, Sigmond et al. (2010) use timeslice integrations of the Canadian Middle Atmosphere Model to examine the effect of coupling to a dynamical ocean and sea ice model on the summertime Southern Annular Mode response to the ozone hole in the absence of greenhouse gas forcing. They find that the summertime Southern Annular Mode response is similar whether the ocean and sea ice state is prescribed or predicted. This implies that the ocean and sea ice response to the ozone hole have not caused further changes to the surface wind response to the ozone hole.

In the following subsections we assess our improved understanding of the surface climate impacts of the ozone-forced trends in the tropospheric circulation. We discuss how the trends in Figure 4-19 have affected the high-latitude climate of the Southern Hemisphere, including surface circulation and precipitation (Section 4.4.2.1), surface temperatures and sea ice (Section 4.4.2.2), Southern Ocean temperatures and circulation (Section 4.4.2.3), and the Southern Ocean’s contribution to the global carbon cycle (Section 4.4.2.4). Research in this area has advanced rapidly since the previous Assessment. In the absence of Arblaster and Meehl (2006)-type studies in which ozone and greenhouse gas forcing are separately applied

within coupled ocean-atmosphere climate models, we are not able to quantitatively assess the net impact of ozone forcing on the annual mean forcing of the Southern Annular Mode trends for the broader set of coupled climate models. There is an urgent need for such simulations to more precisely connect ODS-related ozone depletion to Southern Hemisphere climate change.

Climate impacts of Northern Hemisphere ozone depletion are not covered in this Assessment, since no definitive connection has been made between Northern Hemisphere ozone depletion and surface climate (e.g., Figure 4-9; Thompson and Solomon, 2005), despite the presence of pronounced stratosphere-troposphere coupling in association with dynamic variability in the stratospheric vortex (e.g., Baldwin and Dunkerton, 2001). The lack of an ozone-surface climate response in the Northern Hemisphere is consistent with the weak ozone losses observed there (Chapter 2; Solomon et al., 2007) and thus the weak radiative forcing and temperature trends in the Arctic stratosphere that are masked by relatively high natural variability in some seasons (Grise et al., 2009; Section 4.2).

4.4.2.1 EFFECTS ON WINDS, STORM TRACKS, AND PRECIPITATION

The austral summer trends in the Southern Annular Mode and strengthening of the eastward winds over the Southern Ocean are associated with a poleward shift of the extratropical jets in the Southern Hemisphere troposphere in summer (Gillett and Thompson, 2003; Archer and Caldeira, 2008). As would be expected from such a shift, observational studies reveal reductions in the number of low pressure systems and extratropical storms in Southern Hemisphere middle latitudes (e.g., Simmonds and Keay, 2000; Rao et al., 2003; Vera, 2003; Bengtsson et al., 2006; Pezza et al., 2007, 2008) and increases at high latitudes (e.g., Lynch et al., 2006). These changes in the storm tracks are apparent in both winter and summer. There are some suggestions of increases in the intensity of storms in the storm track (Simmonds and Keay, 2000) but a more recent analysis suggests that this result might be an artifact of changes in the available input data for the reanalyses considered (Bengtsson et al., 2006).

Onshore winds and extratropical weather systems are the causes of much of the precipitation over land in Southern Hemisphere middle latitudes. Hence, the changes in the Southern Annular Mode and the Southern Hemisphere storm track are expected to have led to changes in precipitation. Many recent studies have considered observed changes in regional precipitation over the past few decades and links to changes in Southern Hemisphere circulation. They have tried to separate the influences of the Southern Annular Mode from those due to decadal variations in El Niño-Southern Oscillation, the two major

factors affecting circulation variations in the Southern Hemisphere middle latitudes. No studies have directly attributed observed regional precipitation changes in summer to stratospheric ozone depletion yet, probably due to the large variability of regional precipitation and the sparse network of observing stations. However, a recent analysis of the CMIP3 ensemble of climate model simulations (CMIP3 is defined in Footnote 2 in Section 4.3.1) suggests a signal due to stratospheric ozone depletion in the multi-model average that includes increases in summer precipitation in the Southern Hemisphere high latitudes and decreases in middle latitudes due to stratospheric ozone depletion (Son et al., 2009b). This signal is likely to have contributed to observed changes in precipitation but might not be apparent relative to natural variability.

During the summer season, the positive polarity of the Southern Annular Mode is linked to increased precipitation in southeastern Australia (Gillett et al., 2006; Hendon et al., 2007; Meneghini et al., 2007) and South Africa (Gillett et al., 2006) and reduced precipitation in southwest New Zealand (Renwick and Thompson, 2006; Griffiths, 2006; Ummenhofer et al., 2009) and southwest South America (Gillett et al., 2006).

The increase in wind speeds over the Southern Ocean can generate more sea spray and lead to increases in natural cloud condensation nuclei for the formation of reflective low clouds in Southern Hemisphere summer (Korhonen et al., 2010). In a modeling study using observed wind trends input into a global aerosol model, Korhonen et al. (2010) find that the Southern Hemisphere wind trends since the 1980s give rise to a more than 20% increase in cloud condensation nuclei concentrations in the 50°S–65°S latitude band and a negative cloud radiative forcing of -0.7 W/m^2 . The latter, when added to the negative radiative forcing from stratospheric ozone loss, gives an ozone-related regional negative radiative forcing comparable to the positive radiative forcing from greenhouse gas increases over the same period.

4.4.2.2 EFFECTS ON SURFACE TEMPERATURES AND SEA ICE

The ozone hole-related summertime trends in the Southern Annular Mode are also linked to changes in Antarctic surface temperatures and sea ice. The Antarctic Peninsula region has experienced exceptional recent warming in austral summer (in excess of $1^\circ\text{C}/\text{decade}$ at some stations) since the late 1970s, greatly exceeding the global average and making it one of the fastest changing regions on Earth (e.g., Marshall et al., 2006; Zazulie et al., 2010). In contrast, a summer seasonal cooling trend has been noted at stations on the high plateau of east Antarctica (e.g., Thompson and Solomon, 2002; Turner et al., 2005), and these are linked to the previously noted cir-

ulation changes. The stronger eastward flow associated with the recent summertime trend in the Southern Annular Mode has reduced the effectiveness of blocking by the topography of the peninsula, allowing more maritime airmasses to penetrate across the peninsula and causing summer season warming on the east side of the peninsula that is three times stronger than that observed on the west side (Marshall et al., 2006). Thus both the spatial and seasonal patterns of the observed summertime surface climate changes in the past several decades support the identification of the Southern Annular Mode and ozone loss as a key factor in summertime climate change over much of Antarctica. The breakup of the Larsen-B ice shelf in 2002 was likely due at least in part to the remarkable warming in the Antarctic Peninsula region (Marshall et al., 2006).

The effect of changes in circulation on Antarctic sea ice has been probed using numerical analyses constrained by observed (reanalyzed) winds and temperatures (Goosse et al., 2009). This approach suggests that strengthening of the eastward winds has likely affected the spatial pattern of sea ice distributions, mainly through changes in sea ice advection (Goosse et al., 2009). The spatial pattern of satellite-observed recent changes in sea ice, with increased ice extent in the Ross Sea region and decreases near the peninsula, is well reproduced when atmospheric circulation and temperature changes are considered (as shown in Figure 4-20, taken from Goosse et al., 2009). Atmospheric circulation changes in response to ozone loss have been probed by several models, including, e.g., Gillett and Thompson (2003) and Turner et al. (2009). Natural variability in the Southern Annular Mode, the El Niño-Southern Oscillation, and/or the Pacific Decadal Oscillation may also contribute to recent trends in sea ice (Udagawa et al., 2009), as could other factors such as changes in precipitation or ocean heat transport (Zhang, 2007).

The very sparse spatial coverage of long-term Antarctic temperature records makes it difficult to derive trends averaged over the continent as a whole. Recently, reconstruction methods employing statistical approaches to data filling have been employed to derive trends averaged across Antarctica, drawing from composites using a range of station data, ice cores, and available automated weather stations (Chapman and Walsh, 2007; Monaghan et al., 2008; Steig et al., 2009). Strong warming has been derived for the west Antarctic region in some of these analyses (e.g., Steig et al., 2009), although this is heavily dependent on data from a single record (Byrd station). The most recent reconstruction suggests that Antarctica taken as a whole shows warming when the time period since 1957 is considered (Steig et al., 2009), although weaker warming is seen in some other reconstructions from 1960 (see Figure 4-21). Steig et al. (2009) and Gillett et al. (2008) suggest an important role for greenhouse gases in driving Antarctic temperatures especially prior

to onset of the ozone hole. This finding does not contradict the recent summer season cooling observed over east Antarctica since 1980 in association with the ozone hole; indeed those observations are included in the analysis (see Figure 4-21).

4.4.2.3 EFFECTS ON SOUTHERN OCEAN TEMPERATURES AND CIRCULATION

The summertime trend in the Southern Annular Mode implies an associated poleward shift and intensification of the surface zonal wind stress field and its curl (Oke and England, 2004; Cai and Cowan, 2007; Fyfe et al., 2007). In this subsection, we discuss the implications of the poleward intensification of the surface wind stress for the Southern Ocean temperature and circulation. Greenhouse gas forcing and ozone forcing both appear to affect the tropospheric surface winds, with the ozone-forced signal peaking in austral summer (e.g., Kushner et al., 2001; Thompson and Solomon, 2002; Gillett and Thompson, 2003; Miller et al., 2006; Arblaster and Meehl, 2006; Haigh and Roscoe, 2009). The following discussion is thus relevant to projections of Southern Ocean change under increasing greenhouse gases and ozone recovery (Section 4.5). However, we will focus on effects that can be plausibly linked to tropospheric impacts of stratospheric ozone depletion. Southern Ocean impacts also have implications for global climate and the Southern Ocean carbon cycle (Section 4.4.2.4).

Some of the influence of surface wind stress on the Southern Ocean can be understood by using surface wind

stress and its curl to diagnose Ekman transport and pumping (e.g., Fyfe and Saenko, 2006; Cai and Cowan, 2007). In the classical description, the surface eastward winds drive (1) the eastward Antarctic Circumpolar Current and (2) a meridional overturning circulation that consists of upwelling to the south of the Antarctic Circumpolar Current, northward flow at the surface at the latitude of the current, and downwelling to the north of the current. When ozone forcing results in a poleward intensification of the surface wind stress field, the Antarctic Circumpolar Current and wind-driven overturning circulation are expected to similarly undergo a poleward intensification. From the preindustrial period to the end of the 20th century, Fyfe and Saenko (2006) diagnose, on the basis of wind stress output from the CMIP3 models, a poleward shift of about 0.9 degrees latitude and a 5% strengthening of the Antarctic Circumpolar Current for the ensemble mean of the CMIP3 models. Cai and Cowan (2007) find that the ensemble mean of the CMIP3 “OZONE” simulations (which include ozone depletion) produce a zonal wind stress trend (expressed as a Southern Annular Mode trend) that is consistent with trends inferred from National Centers for Environmental Prediction/National Center for Atmospheric Research reanalyzed winds, and diagnose an accompanying change to the wind-driven ocean circulation in the subtropics and extratropics for these simulations. Consistent with Miller et al. (2006) and Son et al. (2009b), Cai and Cowan (2007) find that the “NO OZONE” simulations do not, on average, produce a realistic wind stress/Southern Annular Mode trend.

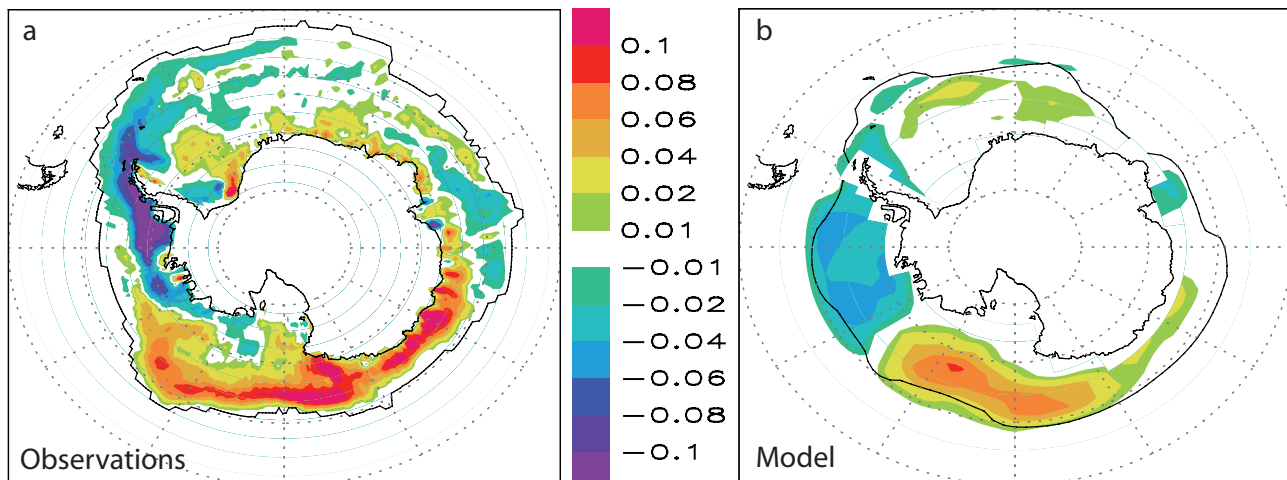


Figure 4-20. The trend of annual-mean sea ice concentration over the period 1980–2000 for (a) the observations (Rayner et al., 2003) and (b) for the model results averaged over the six simulations with data assimilation (units are the fractional change per decade). The black line represents the location of the climatological average September ice edge, as defined by an annual ice concentration equal to 15%, for the observations (a) and the model (b). Based on Goosse et al. (2009).

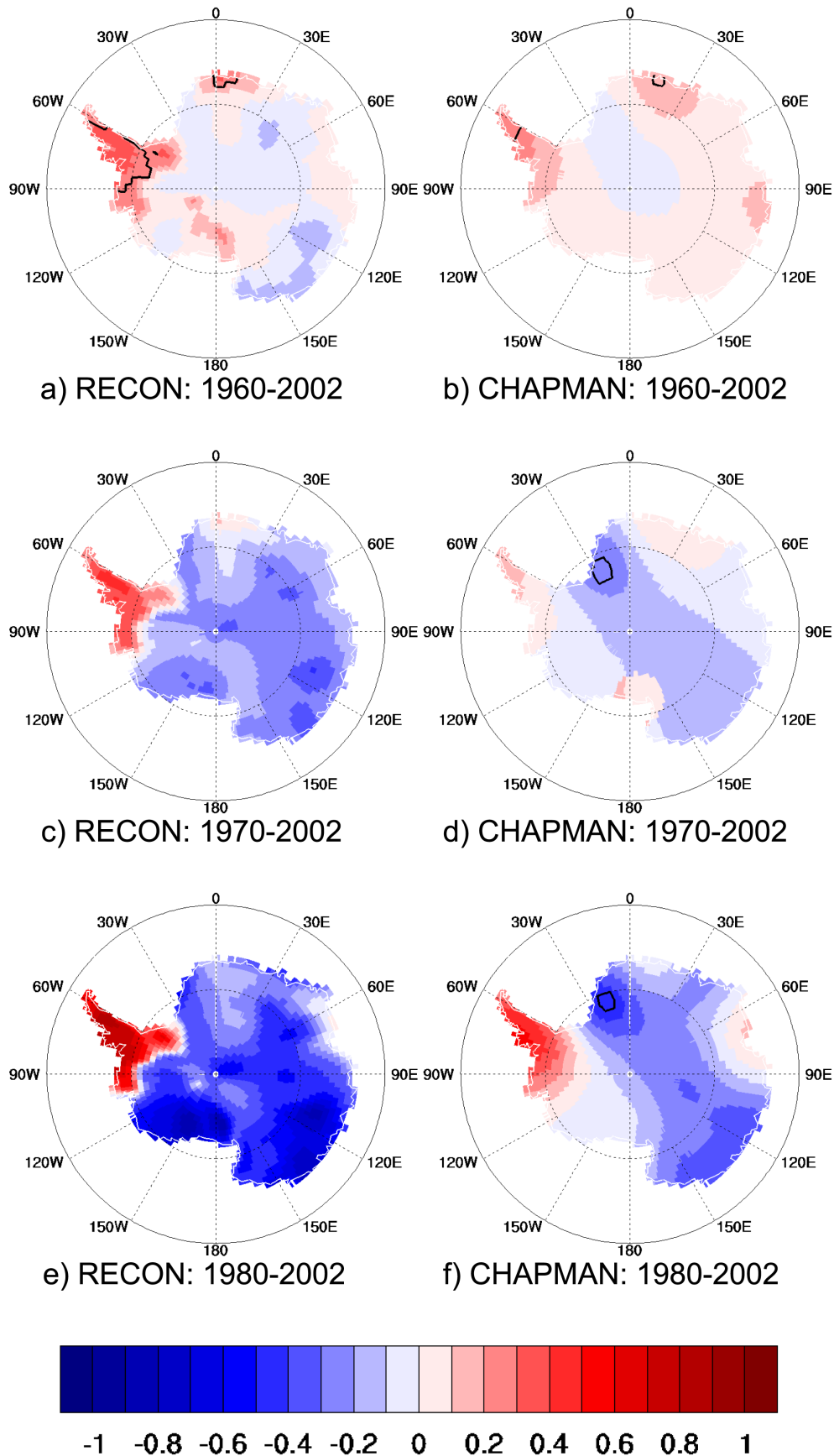


Figure 4-21. Spatial plots of the temporal trends (K/decade) of annual near-surface temperature for three different periods: (a and b) 1960–2002, (c and d) 1970–2002, and (e and f) 1980–2002. Figures a, c, and e are from the RECON temperature reconstruction, and Figures b, d, and f are from the CHAPMAN temperature reconstruction (figure from Monaghan et al., 2008; reconstructions described in that paper).

Key oceanographic observations⁵ and ocean model analysis support the viewpoint that the ocean circulation responds to the wind stress changes in a manner consistent with wind-driven ocean circulation theory. In particular, a significant temperature trend to depths up to 1200 m has been observed in the Antarctic Circumpolar Current (Gille, 2002, 2008; Aoki et al., 2003; Sprintall, 2008; Böning et al., 2008). Figure 4-22a shows observed oceanic temperature trends as a function of depth and dynamic height, which serves as a meridional coordinate, from Gille (2008). There is strong subsurface warming in the Antarctic Circumpolar Current, which is located in the 0.4–1.2 m dynamic height range. The subsurface warming is in large part consistent with a poleward shift of the ocean temperature structure by 1° latitude every 40 years (Figure 4-22b): 87% of the trend below 200m in the Antarctic Circumpolar Current region is explained by this construction. Important aspects of trends in the Antarctic Circumpolar Current region are reproduced in ocean models and in the CMIP3 coupled models, which allow a significant portion of the subsurface warming to be attributed to changes in the wind stress field (Oke and England, 2004; Fyfe, 2006; Fyfe et al., 2007; Gille, 2008). For example, Oke and England (2004), using an ocean model driven by prescribed atmospheric forcings, and Fyfe et al. (2007), using an ocean model coupled to a simplified atmospheric model, obtain intensified subsurface warming when realistic surface wind stress trends are imposed.

Since we can attribute much of the poleward shift in the surface wind stress to ozone forcing (Gillett and Thompson, 2003; Cai and Cowan, 2007; Son et al., 2009b; Fogt et al., 2009), we can infer that ozone forcing in the 1970–2000 period contributes to the observed subsurface warming in the Southern Ocean. That is, the stratospheric ozone-induced change in the Southern Ocean opposes the effects of global warming of the Earth’s surface; greenhouse gas forcing warms the ocean surface and increases high latitude precipitation, which stratifies the ocean surface and thereby reduces oceanic mixing of heat (and, by extension, the uptake of anthropogenic carbon dioxide). In the Geophysical Fluid Dynamics Laboratory coupled models CM2.0 and CM2.1, Russell et al. (2006) find that the enhanced Ekman transport signal associated with positive Southern Annular Mode-related wind trends counteracts this and contributes to an increased heat uptake. The implications of the circulation changes for the Southern Ocean carbon cycle are discussed in Section 4.4.2.4. Under ozone recovery (Section 4.5), the ozone-forced Southern Annular

⁵ It is outside the scope of this report to assess the calibration and sampling of long-term ocean observations; we will place more confidence in conclusions that have been repeatedly verified in the literature.

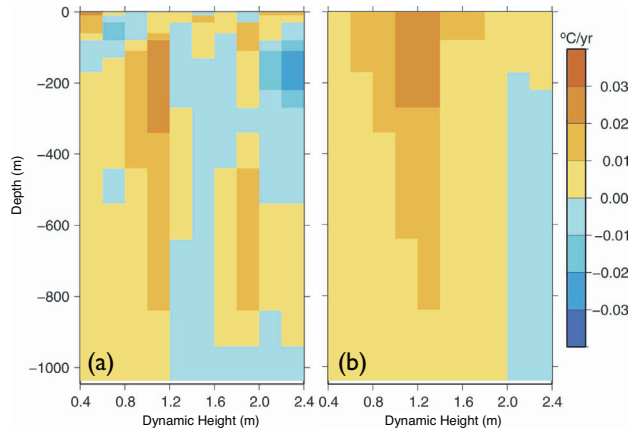


Figure 4-22. (a) Rate of change of ocean temperature (°C/yr) as a function of dynamic height (m), which serves as a meridional coordinate, from ship-based and autonomous float data. The Antarctic Circumpolar Current is in the range 0.4–1.2 m. (b) Effective rate of change of ocean temperature (°C/yr) that would result if ocean temperature structure were shifted poleward at a rate of 1° latitude per 40 years. Based on Gille (2008).

Mode trend in December, January, and February is expected to weaken or change sign (see Section 4.5); this effect would tend to reduce ocean heat uptake, but the net effect will depend on the combined effects of CO₂ increases and ozone recovery on the Southern Annular Mode.

Recent oceanographic literature provides some caveats about the straightforward connection between wind stress and Southern Ocean circulation. The complication relates to the effects of oceanic mesoscale (10 to 50 km scale) eddies, which are responsible for much of the transport of heat and constituents in the Southern Ocean. The CMIP3 generation ocean models cannot explicitly resolve mesoscale eddies and instead parameterize their effects with dynamically motivated mixing schemes (Gent and McWilliams, 1990). A developing body of work (e.g., Radko and Marshall, 2003; Hallberg and Gnanadesikan, 2006; Meredith and Hogg, 2006; Böning et al., 2008; Screen et al., 2009) shows that when they are explicitly resolved, mesoscale eddy effects could modify some of the conclusions presented above. In particular, for relatively fine ocean model resolution, the mesoscale eddy field can respond strongly to changes in wind stress and can counteract some of the changes to the Ekman circulation among other effects (e.g., Hallberg and Gnanadesikan, 2006; Meredith and Hogg, 2006; Screen et al., 2009). In a sensitivity test, Fyfe et al. (2007) impose this kind of effect in a coarse-resolution ocean model, but their approach has not been independently validated. Furthermore, not

all aspects of observed changes in the density structure in the Antarctic Circumpolar Current are represented by the wind-driven ocean circulation theory. In particular, intensification of the wind-driven Antarctic Circumpolar Current is associated with an increased slope (baroclinicity) of density surfaces. This increased slope is seen in CMIP3 class ocean models (e.g., Russell et al., 2006) but has not been detected in observations, which might be the result of mesoscale eddy effects (Böning et al., 2008). Solid conclusions will require a better understanding of uncertainties in trend analysis of multidecadal ocean observations. Nevertheless, since this recent work has implications for Southern Ocean circulation, density structure, temperatures, and carbon cycle, and connects to global climate issues, it appears that high-resolution ocean models will be required to fully evaluate the role of Antarctic ozone depletion in Southern Ocean climate change (see also Ito et al., 2010).

To summarize, the dynamical coupling between the stratosphere and troposphere in conjunction with forcing by the ozone hole suggests that the wind-driven Southern Ocean circulation should intensify as a result of polar stratospheric ozone depletion. This effect may contribute to observed subsurface warming in the Southern Hemisphere and has the potential to attenuate some of the surface global warming associated with greenhouse gas increases. Some predictions of the changes to the Antarctic Circumpolar Current and the Southern Hemisphere overturning could be dependent on ocean model resolution; thus, high-resolution ocean models will likely be required to assess with confidence how the Antarctic ozone hole and ozone recovery are likely to affect the Southern Ocean.

4.4.2.4 STRATOSPHERIC LINKS TO SOUTHERN OCEAN CARBON

The summertime trend in the Southern Annular Mode also provides a potential link between stratospheric ozone depletion and the flux of carbon at the Earth's surface: the ozone hole is linked to changes in the surface winds, and those changes in the surface winds are expected to affect the flux of carbon at the ocean surface. Our current understanding of these linkages is assessed below.

The primary anthropogenic driver of climate change is the emission of more than 9 gigatonnes of carbon (GtC) annually in the form of CO₂, mainly due to fossil fuel burning with smaller contributions from land use change (Forster et al., 2007a). Thus the processes that remove atmospheric carbon dioxide are critical to understanding current climate change.

The Southern Ocean plays a key role in the uptake of global carbon dioxide. As carbon dioxide increases, the net sink of CO₂ in the Southern Ocean would be expected to increase in the absence of other changes. However, re-

cent studies suggest that the Southern Ocean carbon sink has not strengthened over about the past two decades, and this behavior has been linked to changes in winds. Strong eastward winds drive a northward Ekman circulation in the Southern Ocean, which pushes surface waters away from the Antarctic continent and drives a strong ocean circulation that brings up water and dissolved carbon from the deep ocean.

As evidenced in Figure 4-23, the regions displaying broad reductions in carbon uptake correspond to those that underlie the largest tropospheric wind changes associated with the Southern Annular Mode, as obtained in a model driven by ozone depletion. Numerous studies have recently probed how changes in wind stress linked to the Southern Annular Mode have influenced carbon uptake in the Southern Ocean using a range of different approaches, some relying on global climate models, some on models forced by National Centers for Environmental Prediction/National Center for Atmospheric Research reanalyzed winds, some making use of inversion methods based on CO₂ observations, and some using station-based observations of atmospheric CO₂ (Wetzel et al., 2005; Butler et al., 2007; Le Quéré et al., 2007; Lenton and Matear, 2007; Lovenduski et al., 2008; Lenton et al., 2009; Khatiwala et al., 2009).

The observation-based inversion studies are subject to uncertainties in sampling and in the winds prescribed from reanalysis (Baker et al., 2006; Law et al., 2008; Le Quéré et al., 2007). Nevertheless these different types of analyses, including both models and inversion methods, support recent reductions in Southern Ocean carbon uptake. Taken together, this body of work suggests that the changes in wind stress over about the past three decades have reduced the net Southern Ocean carbon uptake by about 0.6–5 Gt (about 0.02–0.16 GtC/yr) compared to the trend that should be expected due to increasing atmospheric CO₂. One context for these numbers is provided by comparison to full compliance with the Kyoto Protocol, which corresponds to a reduction of global carbon emissions of about 0.5 GtC/yr by 2012 (see Velders et al., 2007, and Chapter 5 of this Assessment). The dominant mechanism for a reduction in carbon uptake is generally thought to be stronger upwelling and subsequent outgassing of natural carbon from the deep ocean induced by the wind stress changes (Le Quéré et al., 2007; Lovenduski et al., 2008; Hall and Visbeck, 2002). Note that both natural and anthropogenic carbon fluxes must be considered in assessing changes in the net carbon flux. Lenton et al. (2009) emphasized the dominant role of ozone depletion in driving the change in net carbon uptake in model simulations that explicitly tested the role of ozone versus other greenhouse gas forcings. Khatiwala et al. (2009) noted that only a small change (about 5%) in the ocean carbon sink is required to explain the observations.

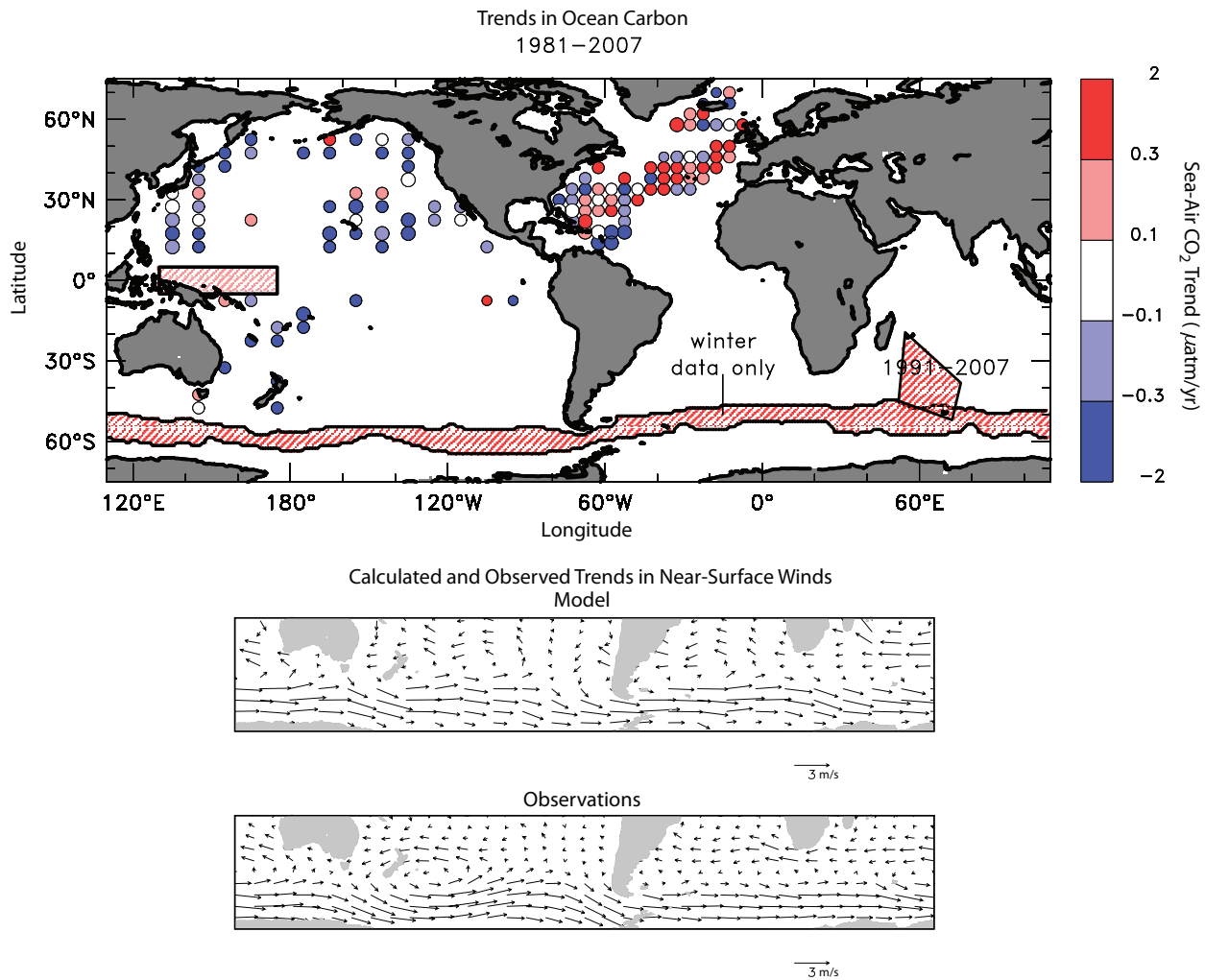


Figure 4-23. Top panel shows trends in the observed partial pressure of CO_2 for ocean minus air, for 1981–2007 ($\mu\text{atm}/\text{yr}$). The observed trends shown by the circles are calculated by fitting a linear trend to repeated measurements of surface-ocean and air CO_2 . Positive (red) values indicate regions where the partial pressure of CO_2 in the ocean is increasing faster than atmospheric CO_2 , indicating a weakening of the net ocean uptake (from Le Quéré et al., 2009). Large, medium, and small circles are plotted for trends with errors of <0.25 , 0.25 – 0.50 , and $>0.50 \mu\text{atm yr}^{-1}$, respectively. Trends are also shown for three broader areas where only a single estimate can be made (areas shown by hatching). As indicated on the figure, the trends in southern circumpolar waters were estimated from austral winter data only, whereas the trends in the South Indian Ocean were estimated for 1991–2007 only. No seasonal cycle was removed from the data in the western equatorial Pacific region. The amplitudes of the trends in the hatched regions are: equatorial Pacific warm pool (near Indonesia), $+0.3 \pm 2 \mu\text{atm}/\text{yr}$; Southern Ocean, $+0.5 \pm 0.6 \mu\text{atm}/\text{yr}$; South Indian Ocean, $+0.4 \pm 0.1 \mu\text{atm}/\text{yr}$. See Le Quéré et al. (2009) for details. The middle panel shows December–February calculated trends in near-surface winds at southern middle and high latitudes, from global model simulations forced by observed ozone depletion from 1979 to 1997, while the bottom panel shows observed December–May wind trends in the same region (based on Gillett and Thompson, 2003). Units on the bottom two panels are meters/second.

The downward transport of anthropogenic carbon by stronger overturning and the increasing thermal stratification of the Southern Ocean are also important to carbon and heat uptake, but analyses of the data suggest that these

effects have been overwhelmed by the effect of strengthening eastward flow on natural carbon fluxes (Le Quéré et al., 2007). Ito et al. (2010) suggest that higher spatial resolution may be needed to ensure accurate evaluation of

the oceanic processes that could contribute to the carbon uptake and its changes.

Future changes in the Southern Ocean carbon sink are subject to an uncertain combination of processes. As recovery of the ozone hole occurs, the circumpolar eastward wind changes related to ozone depletion should reverse (Section 4.5). However, the weakening of the circumpolar eastward flow due to ozone recovery is expected to be roughly compensated for by a strengthening of the circumpolar eastward flow due to increases in carbon dioxide and other greenhouse gases by late 21st century in summer (see Section 4.5). The effect of the eastward flow on the ocean carbon uptake this century will depend on the rate of increase of anthropogenic carbon in the surface ocean and the relative strength of the downward transport of anthropogenic carbon compared to the upward transport of natural carbon, which are both linked to changes in the ocean circulation (see, e.g., Zickfeld et al., 2008). Further, the extent to which the ocean circulation will adjust to altered stratification and winds over long timescales is uncertain.

4.4.3 Stratospheric Variations and the Width of the Tropical Belt

Changes in the tropical and extratropical tropopause layer, and their relation to changes in stratosphere/troposphere exchange of trace constituents, particularly water vapor, were addressed in the 2006 Ozone Assessment (Chapters 2 and 5: Law and Sturges et al., 2007, and Baldwin and Dameris et al., 2007). Since that Assessment, research has linked tropopause changes with changes in several other stratospheric and upper-tropospheric features. For example:

- the region of low column ozone values typical of the tropics has expanded in the Northern Hemisphere (Hudson et al., 2006);
- the jet streams have moved poleward in both hemispheres (Fu et al., 2006; Archer and Caldeira, 2008);
- the downward branches of the Hadley cell (where deep clouds are relatively rare compared with the upward branch) have moved poleward, as seen in outgoing longwave radiation, a surrogate for cloud top temperature (Hu and Fu, 2007). Mean meridional mass flux changes independently support this finding of Hadley cell expansion (Hu and Fu, 2007); and
- the region of high tropical tropopause expanded poleward in both hemispheres (Seidel and Randel, 2007).

The qualitative consistency of these observed changes in independent data sets suggests a widening of the tropical belt of between 2 and 5 degrees latitude between 1979 and 2005 (Figure 4-24), as summarized by Seidel et al. (2008) and Reichler (2009). Combined with an increase in the height of the tropical tropopause (Zhou et al., 2001; Santer et al., 2003; Seidel and Randel, 2006), the widening contributes to an increase in the volume of the tropical troposphere of ~5%.

Widening of the tropical belt (i.e., the region of globe with tropical characteristics), including poleward migration of the jet streams and associated migration of storm tracks, could be associated with changes in global precipitation patterns. Lu et al. (2007) found a significant correlation between expansion of the tropical belt, as determined by the location of the downward branches of the Hadley circulation, and the location of the subtropical dry zones in climate models. Poleward movement of precipitation patterns in climatically sensitive subtropical regions might be among the most significant surface climate impacts of tropical expansion, and may already have begun in North America (Seager et al., 2007). Zhou et al. (2001) also note that circulation changes related to tropical belt-widening impacting troposphere-to-stratosphere transport

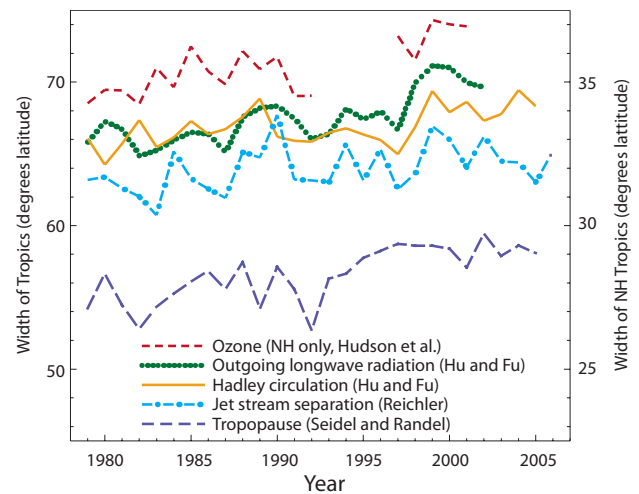


Figure 4-24. Changes in several estimates of the width of the tropical belt since 1979 (in degrees latitude). These include the width of the Hadley circulation, based on both outgoing longwave radiation and horizontal winds streamfunction (Hu and Fu, 2007); the separation of the Northern and Southern Hemisphere subtropical jet-stream cores (Reichler, 2009); the width of the region of frequent high tropopause levels (Seidel and Randel, 2007); and the width of the region with tropical column ozone levels (Northern Hemisphere only, right axis, Hudson et al., 2006). (Based on Seidel et al., 2008.)

may produce changes in the average stratospheric entry value of water vapor.

The cause(s) of these observed changes, their relation to changes in the lower troposphere and at the surface, and the likelihood that they will continue or be reversed in the future, are areas of active research. Insights into these issues have been obtained from two types of global climate models. One is coupled atmosphere-ocean global climate models, particularly the CMIP3 models, which consider ocean feedback but do not represent stratospheric processes in great detail. A second type is coupled chemistry-climate models, with more complete representation of the stratosphere but without an interactive ocean model. However, results to date from both CMIP3 and coupled chemistry-climate model simulations are uncertain because neither type of model includes all relevant processes and because the horizontal resolution of these global model systems is generally several degrees of latitude, which may make it difficult to resolve smaller but significant changes of the horizontal extent of the tropics.

Simulations of past climate change by CMIP3 models that include increases in greenhouse gas concentrations and stratospheric ozone depletion reveal changes in the width of the tropics as measured by changes in the region of high (tropical) tropopause heights (Lu et al., 2009), and modeled tropopause height changes have been linked to poleward migration of the jet streams (Lorenz and DeWeaver, 2007; Son et al., 2009b). More fundamentally, model simulations have linked imposed perturbations in heating of the stratosphere to tropospheric dynamical changes, including latitudinal shifts in jet streams (Simpson et al., 2009). But the widening simulated by CMIP3 models, for both the 20th and 21st centuries, is smaller than the observed widening over the last several decades (Johanson and Fu, 2009), suggesting both that the widening is not the result of natural variability alone (because it is not found in control simulations without anthropogenic forcing) and that the responsible mechanisms may not be well represented by those models.

The importance of stratospheric processes, particularly those related to ozone loss and recovery, is highlighted by comparison of CMIP3 and chemistry-climate model simulations (and projections) of tropopause height changes (Son et al., 2009a). Son et al. (2010) find that the increase in width of the Southern Hemisphere tropics in the CCMVal-2 models is linearly related to the simulated amount of ozone depletion. Lu et al. (2009) also show that widening of the tropics only occurs when they include the radiative impact of ozone depletion in their simulation. Different mechanisms may be responsible for different aspects of the observed changes in the width of the tropical zone, with halocarbons influencing ozone changes and tropopause height change at the subtropical edges of the tropical belt, and with sea surface temperatures and

CO₂ influencing tropopause changes within the tropical region (Deckert and Dameris, 2008; Lamarque and Solomon, 2010).

4.4.4 Effects of Stratospheric Variations on Tropospheric Chemistry

Changes in the stratosphere can also affect chemical processes in the troposphere in two principal ways. First, the return of air from the stratosphere at midlatitudes to high latitudes is the sink of many stratospheric chemical species. This stratosphere-troposphere transport is an important term in the overall budget of tropospheric ozone. Second, the overhead column of stratospheric ozone affects the penetration of UV radiation to the troposphere. Changes in column ozone are particularly important for modulating UV-B radiation (wavelength less than ~320 nanometers) which causes photolysis of O₃ to yield excited O(¹D) atoms. O(¹D) reacts with H₂O in the main formation reaction of tropospheric hydroxyl radicals (OH), the most important tropospheric oxidant. Any changes in the tropospheric circulation, which are driven from the stratosphere, can also change the distribution of tropospheric ozone.

The stratosphere can affect tropospheric chemistry through other mechanisms. For example, stratospheric radiative or circulation changes that contribute to different surface temperatures may impact emissions. However, these contributions will be very small compared to the large tropospheric climate changes induced by increasing atmospheric greenhouse gases. Therefore, this report concentrates on the impact of stratosphere-troposphere transport and column ozone changes. Isaksen et al. (2009) have recently reviewed tropospheric chemistry-climate interactions.

Tropospheric ozone levels are determined by the complex interaction between photochemistry and transport. The primary sources of tropospheric ozone are transport from the stratosphere and in situ photochemical production, and the main sinks are photochemistry and surface deposition. The net global tropospheric ozone burden is a small residual of these terms. Although it is recognized that input of ozone-rich air from the stratosphere (via stratosphere-troposphere transport) is an important term in this overall burden, there are significant variations in its quantification, which is usually done through diagnosing the stratosphere-troposphere transport term in global 3-D models (e.g., Stevenson et al., 2006). Wild (2007) and Wu et al. (2007) updated estimates of terms in the tropospheric ozone budget and investigated the causes of model-model differences from sensitivity runs of their own models. Wild (2007) concluded that some previous differences in modeled budgets could be reconciled by using updated

chemical mechanisms, but uncertainties in stratosphere-troposphere transport remained. Wu et al. (2007) found that the model-model differences were determined largely by differences in emissions and stratosphere-troposphere transport. The current best estimate of this term from observations is 550 ± 140 teragrams (Tg) per year (Olsen et al., 2001), which is in good agreement with model estimates of 550 ± 170 Tg/yr (Stevenson et al., 2006). The mean lifetime of ozone in the troposphere is around 25 days. Variations in the modeled tropospheric ozone burden, e.g., 340 ± 40 Tg (corresponding to a mean mixing ratio of approximately 45 ± 5 parts per billion by volume, ppbv) from Stevenson et al. (2006), are much smaller than variations in stratosphere-troposphere transport, although similar to variations in other ozone budget terms. Therefore, large variations in modeled flux from the stratosphere are not reflected in such large variations in the mean tropospheric ozone burden; the large photochemical and deposition terms damp out these variations.

Observations showed substantial declines in ozone throughout the troposphere in 1992–1993 following the eruption of Mt. Pinatubo (see Fusco and Logan, 2003) and a good correlation between trends in lower-tropospheric and lower-stratospheric ozone from 1992–2004 (Ordóñez et al., 2007). These declines were generally largest in the upper troposphere and linked to ozone loss in the lower stratosphere (which is discussed in Chapter 2). Terao et al. (2008) showed that stratospheric ozone contributes significantly (30–40% at midlatitudes to high latitudes) to the spring O₃ maximum at 500 hPa. The effects of past decreases in stratospheric ozone are not usually included in models used to estimate the tropospheric ozone budget. Fusco and Logan (2003) looked at the impact of decreases in lower-stratospheric ozone in their study of tropospheric ozone changes from 1970–1995. They found that decreases in lower stratosphere ozone might have reduced the stratospheric source by 30% over this time period. More recently, Hsu and Prather (2009) diagnosed the contribution of stratosphere-troposphere transport to the tropospheric ozone budget and included the effect of stratospheric ozone depletion from 1979 to 2004. They found a reduction of up to 10% in the stratosphere-troposphere transport ozone flux, but this caused only a small decrease in mean tropospheric ozone of 1 ppb (about 2%).

A number of older studies investigated how decreases in column ozone in the 1980s and 1990s affected tropospheric OH trends (e.g., Madronich and Granier, 1992; Bekki et al., 1994; Fuglestedt et al., 1994; Granier et al., 1996). More recently, Duncan and Logan (2008) used a three-dimensional (3-D) model to investigate the impact of various forcings, including changing overhead column ozone, on tropospheric OH and carbon monoxide (CO) from 1988–1997. During this relatively short period, overhead column ozone decreased due to the solar cycle

phase and eruption of Mt. Pinatubo, as well as the long-term trends in ozone-depleting substances. The decreased ozone column led to important year-round increases in OH, where a –3% change in the column caused a +4% change in OH. In spring/summer at higher latitudes, column ozone changes of –10% caused an increase in OH of about +8%. This contribution from stratospheric ozone variations makes an important contribution to the overall variability in tropospheric OH of $\pm 10\%$ over the past few decades inferred from methyl chloroform (Bousquet et al., 2005; Prinn et al., 2005). This contribution to increased OH made a small impact on the model CO trends, about 0.1–0.2 Tg/yr averaged over the period considered compared to a CO burden of about 500 Tg. However, this change was compensated for by an increase from oxidation of increasing CH₄, while changes in fossil fuel emissions had a much larger impact regionally.

Isaksen et al. (2005) studied the impact of decreased column ozone on tropospheric chemistry under different pollution conditions. They imposed a uniform global decrease in column ozone, affecting only their model's photolysis calculation, and studied the impact on surface ozone. They found that in polluted regions, i.e., regions of net tropospheric ozone production, the increased photochemical activity from faster photolysis led to more ozone production which in turn led to an additional 1 ppb surface ozone for the 10% column reduction over continental Europe in January. In contrast, in cleaner remote regions the enhanced photochemical activity increased the net sink of ozone. The largest effect was a decrease of 3 ppb at low latitudes to midlatitudes, but a change of 10% in the ozone column represents a large perturbation for these latitudes. Overall, these changes in surface ozone are therefore small.

4.4.5 Influence of the Stratosphere on the Impact of Solar Variability on Surface Climate

Changes in the stratosphere in response to solar variability have the potential to influence tropospheric climate by many of the radiative and dynamical processes outlined in Sections 4.4.1–4.4.4 above. Some specific linkages between solar variability, the stratosphere, and surface climate are assessed below. More detailed discussions of many of the issues related to the impact of solar variability on climate are presented by Gray et al. (2010).

The signals in stratospheric ozone and temperature produced by 11-year solar cycle variations in incoming radiation have been discussed in Section 2.4.3.2 of Chapter 2 and Section 4.3.1 of this chapter, respectively. While some details of the responses are not fully understood, a picture is emerging in the tropics in which the temperature

of the tropical upper stratosphere is warmer by 1.1–1.8 K and the lower stratosphere warmer by 0.5–0.8 K when the sun is more active, relative to when it is quiet (Randel et al., 2009; Gray et al., 2010). There is a related signal in zonal winds in a strengthening of the subtropical lower mesospheric jet in the winter hemisphere during high solar activity (Frame and Gray, 2010). A solar signal has also been detected in the stratospheric polar night jet in both hemispheres, and thus in the annular modes, (e.g., Kodera, 2002; Boberg and Lundstedt, 2002; Thejll et al., 2003; Kuroda and Kodera, 2004, 2005; Kuroda et al., 2007; Lee and Hameed, 2007; Barriopedro et al., 2008; Lee et al., 2008). Most of these studies, however, have used simple linear regression or confined their discussions to correlation coefficients. Hence they detect only the linear component of the response, and have not considered the impact of other potential forcing factors such as volcanic eruptions. Analyses using data sets that include the most recent solar maximum period, during which there was no major coincident volcanic activity, have now shown that a separation is indeed possible (Frame and Gray, 2010).

In a multiple regression analysis, Keckhut et al. (2005) find a temperature response in the tropics in rocketsonde and lidar data similar to that in the reanalysis studies. The response includes a seasonally varying out-of-phase signal in midlatitudes that Hampson et al. (2005) relate to the occurrence of stratospheric warmings. Haigh and Roscoe (2006) carried out a multiple regression analysis of time series of the Northern and Southern Annular Mode indices throughout the depth of the atmosphere. No significant response to the 11-year solar cycle was found if the solar and stratospheric quasi-biennial oscillation terms were included separately, but when they were combined into a single term (in which the phase of solar activity modulates the stratospheric quasi-biennial oscillation) to represent their interaction, a strongly significant result was found. This finding is consistent with the original results of Labitzke (1987), in which polar stratospheric height data were sorted by phase of the stratospheric quasi-biennial oscillation and level of solar activity.

Variations in incoming total solar irradiance of order 0.1% occur over the 11-year solar activity cycle (Fröhlich and Lean, 2004) resulting in a top-of-atmosphere radiative forcing of approximately 0.2 W/m^2 . On multidecadal timescales, underlying variations in total solar irradiance are less certain, but assessments suggest that there has been an overall increase in the range $1\text{--}4 \text{ W/m}^2$ since the year 1700, giving a top-of-atmosphere radiative forcing of $0.17\text{--}0.67 \text{ W/m}^2$ since that date (Gray et al., 2010). The amount of radiation reaching the tropopause, which provides a better indicator of climate radiative forcing, is dependent on the spectral composition of the radiation and the response of stratospheric ozone. This effect has been assessed to be a small addition to the radiative forcing value (Larkin et

al., 2000), but recent measurements from the Solar Radiation and Climate Experiment satellite (Harder et al., 2009) indicate that there may be compensating changes at UV and visible wavelengths which imply that solar radiative forcing at the tropopause would be out of phase with that at the top of the atmosphere due to absorption of the UV in the stratosphere (Haigh et al., 2010).

As well as direct radiative effects, variations in solar activity may produce a solar signal in the troposphere “top-down” from an initial response in the stratosphere. Early model studies of UV variations in the stratosphere (Haigh, 1996, 1999; Shindell et al., 1999; Balachandran et al., 1999; Larkin et al., 2000) obtained a response in the troposphere even though the near-surface in these model runs was constrained by imposed, seasonally varying, sea-surface temperatures. The main response to enhanced UV and stratospheric ozone in these models is (1) an expansion of the Hadley cell and (2) a poleward movement of the tropical convective maxima, the tropospheric jets, and the midlatitude storm tracks. The pattern of these anomalies was similar to the signal found in tropospheric zonal winds in reanalysis data (Haigh, 2003; Frame and Gray, 2010) and also in upper air temperatures and geopotential heights (Brönnimann et al., 2006) using a data set based on radiosonde and aircraft observations dating back to 1922. The amplitude of the modeled pattern depended on the magnitude of the ozone change but was generally about half the amplitude of that observed. The new Solar Radiation and Climate Experiment data, however, imply that the ozone response, and thus presumably the tropospheric response to the stratospheric warming, might be significantly larger.

This signal has the same spatial structure as, and thus presumably involves similar eddy-mean flow feedbacks to, the dominant pattern of atmospheric variability, i.e., the atmospheric annular modes. Feedback of the tropospheric zonal wind changes on the tropospheric eddy momentum fluxes appears to be important in establishing and maintaining the response to stratospheric forcing, as discussed in Section 4.4.2 (see also Polvani and Kushner, 2002; Kushner and Polvani, 2004, 2006; Song and Robinson, 2004). Coupling between the Hadley circulation and midlatitude eddies may also play a key part; in a mechanistic study focusing on the processes involved in a response to solar forcing, Haigh et al. (2005) obtained a zonal mean tropospheric response, qualitatively similar to the observed 11-year solar response, by imposing anomalous diabatic heating in the low-latitude lower stratosphere. Consistent with this result, the enhanced Hadley circulation response in the coupled chemistry-climate model simulations of Shindell et al. (2006) was linked to the additional condensational heating in the upper tropical troposphere and lower stratosphere relative to simulations with fixed ozone. Imposing a generic stratospheric heat-

ing in a simplified climate model, Simpson et al. (2009) have shown that it is the response of the eddy momentum fluxes to changes in structure of the tropopause region that drives the tropospheric response, so that details of the stratospheric response to solar variability may be important in determining the tropospheric signal.

Matthes et al. (2006), using a general circulation model with prescribed sea surface temperatures, found the response to UV variability in tropical vertical velocity was not uniformly distributed in longitude but was largest over the Indian and West Pacific Oceans—indicating an influence on the Walker circulation similar to that found in observations by Kodera (2004) and Kodera et al. (2007). The weakened ascent during solar maximum in the tropical troposphere of their model may result from the increased static stability in the tropopause region suppressing convection (Kodera and Shibata, 2006; Matthes et al., 2006).

Other studies have also identified solar influences on the strength and extent of the Walker circulation. van Loon et al. (2007) and Meehl et al. (2008) show a strengthening, at peak years of the 11-year solar cycle, which they identify as distinct from any El Niño-Southern Oscillation signal (van Loon and Meehl, 2008) although their approach has been questioned by Roy and Haigh (2010) and Zhou and Tung (2010). The associated sea surface temperature response at the peak years of the 11-year solar cycle is a cooler-than-normal equatorial eastern Pacific and poleward-shifted intertropical and South Pacific convergence zones with a warming following with a lag of a couple of years (Meehl et al., 2008; White and Liu, 2008).

The mechanisms invoked to explain this sea surface temperature response involve changes in the visible radiation absorbed by the tropical oceans, along with coupled air-sea interactions, and thus may be termed “bottom-up” rather than the “top-down” processes involving the stratosphere that are the focus of this report. Recent modeling studies (Rind et al., 2008; Meehl et al., 2009) have suggested that both pathways may combine to produce an amplified response to a small solar forcing. However, the responses probably depend on complex nonlinear interactions between different processes that have yet to be elaborated. Furthermore, all the mechanisms depend crucially on the spectral composition of the solar irradiance variability of which current understanding is currently being challenged by data from the Solar Radiation and Climate Experiment Spectra Irradiance Monitor (SIM) instrument (see the discussion in Section 4.3.1).

4.5 WHAT TO EXPECT IN THE FUTURE

The stratosphere is expected to change over the rest of this century in response to a range of forcing factors. Concentrations of the main anthropogenic greenhouse gases (CO₂, N₂O and CH₄, hydrofluorocarbons (HFCs),

and SF₆) are expected to continue to rise for at least several decades, but concentrations of halogenated ODSs have leveled off and are expected to decrease. Future stratospheric aerosol loading (especially from volcanoes) is unpredictable. Chapter 5 of this Assessment provides a number of possible scenarios of emissions and concentrations of anthropogenic greenhouse gases. These atmospheric concentration changes will affect both ozone concentrations and stratospheric climate in the future. The evolution of the future ozone layer is discussed extensively in Chapter 3. Here we briefly assess the predicted changes through 2100 in the stratospheric climate changes assessed in this chapter.

4.5.1 Stratospheric Temperatures

The evolution of stratospheric temperature is expected to depend on three main factors: the recovery of the ozone layer, increasing concentrations of most greenhouse gases, and the resulting changes to the mean overturning circulation in the stratosphere (the Brewer-Dobson circulation). At least one experiment predicts that changes in Arctic sea ice will drive changes in polar stratospheric wave forcing and thus temperatures (Scinocca et al., 2009). The recovery of the Antarctic ozone hole is expected to lead to higher temperatures in the Antarctic stratosphere during spring, and a reduction in the strength of the stratospheric polar vortex as the effects of ozone loss diminish. Outside the Antarctic stratosphere, future changes in stratospheric ozone are expected to lead to a reversal of the ozone-induced cooling observed in both the lowermost and upper stratosphere (Chapter 10 of SPARC CCMVal, 2010). However, in general the warming associated with ozone recovery will be outweighed by a larger cooling effect due to continued greenhouse gas increases (Chapter 5 of WMO, 2007; Chapter 10 of SPARC CCMVal, 2010; McLandress et al., 2010; Jonsson et al., 2009).

The projected evolution of stratospheric temperatures in the 21st century depends on both the choice of scenario and climate model used to project that scenario. All scenarios have CO₂ continuing to increase, with ODSs and stratospheric chlorine loading decreasing. An example of trends at 1 hPa is shown in Figure 4-25 for the NASA Goddard Space Flight Center (GSFC) Goddard Earth Observing System chemistry-climate model (GEOS) under the CCMVal REF-B2 scenario⁶. CO₂-induced cooling (including its effect on ozone) dominates the response, although ozone recovery reduces the rate of cooling over the next few decades. Under this scenario all the CCMVal models exhibit global cooling in the middle and upper

⁶ See SPARC CCMVal 2010, Chapter 2, for scenario details.

stratosphere by several degrees, with much smaller temperature changes of undetermined sign in the lower stratosphere (typically less than 0.5 K) (Chapter 3 of SPARC CCMVal, 2010).

Temperatures in the lower tropical stratosphere and tropopause region could be significantly affected if atmospheric concentrations of HFCs rise. At the one ppb level HFCs give an additional warming of 0.2–0.5 K to the lower tropical stratosphere region. This range depends on the spectral absorption characteristics of the HFC (Forster and Joshi, 2005). Note the HFCs with small atmospheric lifetimes are unlikely to reach high enough concentrations to have an appreciable effect (see Chapter 5 of this Assessment).

4.5.2 Brewer-Dobson Circulation

Atmospheric model simulations forced with increased greenhouse gas concentrations exhibit an acceleration of the Brewer-Dobson circulation (e.g., Rind et al., 1998; Butchart and Scaife, 2001; Butchart et al., 2010). This is an extremely robust response in the current generation of chemistry-climate models, as discussed in Section 4.3. The implications of a future increase in the Brewer-Dobson circulation are substantial. Such an increase would change the spatial distribution of stratospheric ozone, with increased total ozone at high latitudes and decreased total ozone in the tropics (see Figure 3-3 in Chapter 3 of this Assessment). It would also increase the stratosphere-to-troposphere ozone flux (Hegglin and Shepherd, 2009), and it would decrease the net age of stratospheric air (e.g., Austin and Li, 2006; Garcia and Randel, 2008; Oman et al., 2009; Butchart et al., 2010).

However, as noted in Section 4.2, the observational evidence for an increase in the Brewer-Dobson circulation is unclear. The observed decreases in tropical stratospheric temperatures are consistent with increased upwelling in the lower tropical stratosphere (e.g., Thompson and Solomon, 2005, 2009; Randel et al., 2009) as are the observed decreases in lower tropical stratospheric ozone (Randel and Wu, 2007; Chapter 2). But the reliability of the ozone and temperature data for assessing relatively small trends in this region of the atmosphere is still under investigation (e.g., Randel and Wu, 2006; Chapter 2). Estimates of long-term variations in age of air based on midlatitude balloon measurements of SF₆ and CO₂ over 1975–2005 have substantial uncertainties, but suggest no significant trends (Engel et al., 2009). Some effort has been made to use reanalyses to diagnose trends in the Brewer-Dobson circulation but without success due to inhomogeneities in the observational record and reanalyzed products (Iwasaki et al., 2009).

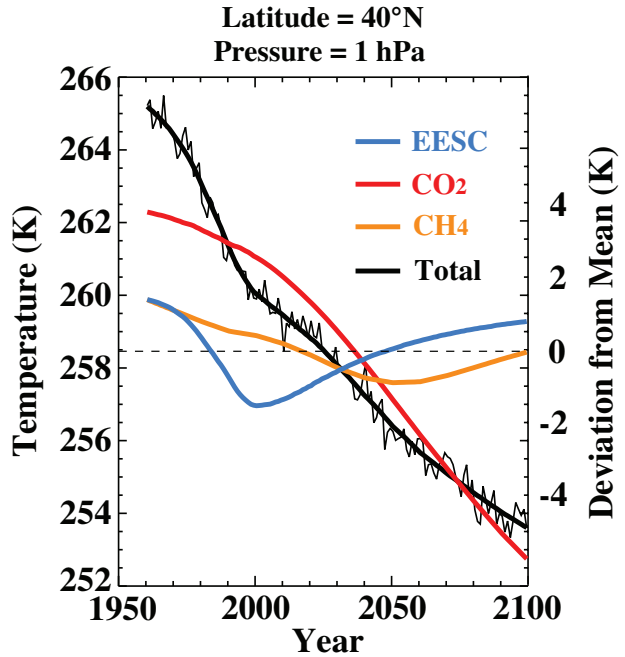


Figure 4-25. Time series of simulated temperatures (K) at 40°N and 1 hPa (thin black line), with the statistical fit as the heavy black line. Data are for the NASA GSFC GEOS chemistry-climate model under the CCMVal REF-B2 scenario. Scale on left shows temperatures for this time series. Scale on right shows deviations from the mean temperature due to changes in equivalent effective stratospheric chlorine (blue line), CO₂ (red line), and CH₄ (orange line). Based on Stolarski et al. (2010).

4.5.3 Stratospheric Water Vapor

Modeling studies of future greenhouse gas increases project that the tropical tropopause will warm and rise in altitude (Gettelman et al., 2009). One effect of a warmer tropical tropopause is an increase in stratospheric water vapor globally. Assumed increases in anthropogenic contributions to tropospheric methane, along with the possibility that natural sources of methane may increase in a warming climate, would also contribute to increases in stratospheric water vapor. Projected decreases in the net age of stratospheric air (Section 4.5.2) could lead to a slight decrease in stratospheric water vapor.

As presented in Gettelman et al. (2010), there is significant spread in chemistry-climate models' representation of both tropical cold point temperatures (Figure 4-12) and 80-hPa water vapor (used to represent stratospheric entry values), as shown in Figure 4-13. The trend in the historical record of tropical radiosonde cold point temperatures also does not agree with the multi-model

mean; the amplitude of the observed trend is more than an order of magnitude larger than the modeled trend (Gettelman et al., 2009). Given the discrepancies between modeled and measured tropical temperatures and lower-stratospheric water, we cannot provide any reliable prediction as to what the future evolution of stratospheric water vapor will be in a climate with increasing greenhouse gas concentrations.

4.5.4 Tropopause Height and Width of the Tropical Belt

Chemistry-climate models project that the tropopause height will continue to increase in the future, but with a trend weaker than that in the recent past (Son et al., 2009a; Gettelman et al., 2009). The reduced trend appears to be directly associated with stratospheric ozone recovery in the Southern Hemisphere in summer. With recovery of the ozone layer, chemistry-climate models also suggest that the observed trend toward widening of the tropics may weaken in the Southern Hemisphere in summer (Son et al., 2009a; Son et al., 2009b). However, our confidence in the magnitude of projected changes in the width of the tropics is limited by (1) discrepancies in such predictions derived from CMIP3 models and chemistry-climate models (Johanson and Fu, 2009; Son et al., 2009a) and (2) an incomplete understanding of the dynamics of the changes (Reichler, 2009).

4.5.5 Radiative Effects and Surface Temperature

By the middle of this century, global average concentrations of ozone-depleting substances may return to levels prior to 1960, but increasing concentrations of greenhouse gases are expected to alter stratospheric temperatures and circulation. Consequently, the ozone distribution will not simply return to its state prior to 1960. The altered ozone concentrations will continue to exert an anomalous radiative forcing on surface climate. Portmann and Solomon (2007) computed an ozone forcing at 2100 from CO₂, N₂O, and CH₄ changes under a range of IPCC Special Report on Emissions (i.e., SRES) scenarios. Although the induced ozone column changes were relatively large (up to a 5% change in the column, globally averaged) the overall radiative forcing since pre-1970 ranged between -0.1 W/m^2 and $+0.1 \text{ W/m}^2$. This small forcing is a result of most of the associated ozone change occurring in the upper stratosphere, where it only contributed a small radiative forcing (see Section 4.2.2 and Chapter 3).

4.5.6 Tropospheric Annular Modes and Stratosphere-Troposphere Coupling

As discussed in Section 4.4.2, only climate models that include observed changes in stratospheric ozone are able to reproduce the observed positive trend in the tropospheric Southern Annular Mode during austral summer over the past few decades. We infer that polar stratospheric ozone losses have been the dominant driver of the observed trend in the Southern Hemisphere surface circumpolar flow, as has been confirmed in those models that separately include ozone forcing with other radiative forcings held fixed (Gillett and Thompson, 2003; Shindell and Schmidt, 2004; Arblaster and Meehl, 2006).

In the absence of other forcings, stratospheric ozone recovery is expected to drive an equatorward shift in the Southern Hemisphere extratropical jet in the 21st century in austral summer that projects onto the negative polarity of the annular modes (e.g., Son et al., 2008). In contrast, future increases in atmospheric carbon dioxide concentrations are expected to lead to positive trends in the annular modes in both hemispheres (e.g., Fyfe et al., 1999; Kushner et al., 2001; Cai et al., 2003; Shindell and Schmidt, 2004; Brandefelt and Källén, 2004; Yin, 2005; Miller et al., 2006; Arblaster and Meehl, 2006; Lu et al., 2008), although the amplitudes of the greenhouse gas-induced trends vary from simulation to simulation (Yin, 2005; Miller et al., 2006). The effects of ozone recovery and increasing carbon dioxide on the Southern Annular Mode are expected to approximately cancel through the middle of the 20th century during austral summer, as evidenced in both CCMVal-2 simulations and CMIP3 simulations (e.g., Figure 4-26; SPARC CCMVal, 2010⁷). CMIP3 models without ozone recovery (Figure 4-26d) exhibit a weak positive Southern Annular Mode trend, which is presumably dominated by the greenhouse gas forcing.

There are several important caveats in the interpretation of annular mode trends. First, simulations of 20th century climate tend to place the Southern Hemisphere jet farther equatorward than is observed (Fyfe and Saenko, 2006; Son et al., 2010; Kidston and Gerber, 2010). The reasons for these biases are not well understood. But they seem to be important, as differences in the projected magnitude of the trend in the Southern Hemisphere are well correlated with biases in the latitude of the jet in the simulation of 20th century climate; models with a larger equatorward bias simulate a larger poleward shift in jet location, and vice versa (Son et al., 2010; Kidston and Gerber,

⁷ Note that the CCMVal-2 results shown in Figure 4-26 differ somewhat from those based on the previous generation CCMVal-1 models (Son et al., 2008; Perlwitz et al., 2008). Those runs indicate an equatorward shift of the jet at the surface in December, January, and February.

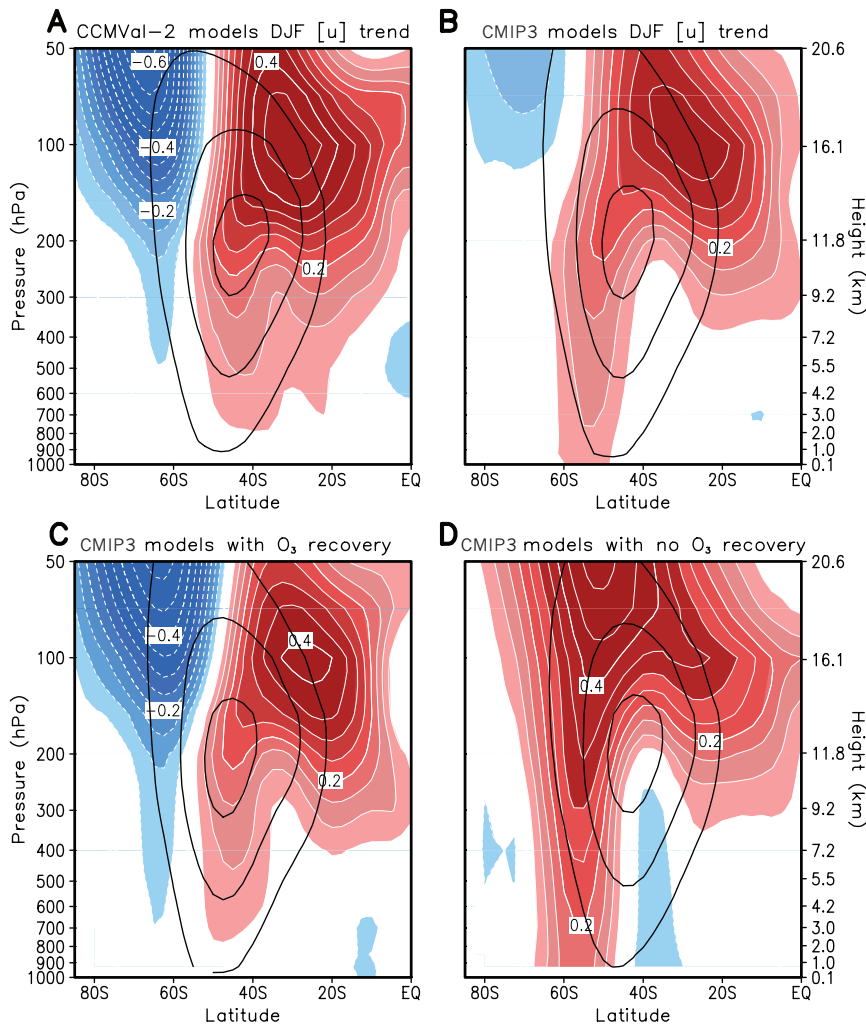


Figure 4-26. Trends in December-to-February (DJF) zonal-mean zonal wind. The multi-model mean trends between 2001 and 2050 are shown for the CCMVal-2 models (A), the CMIP3 models (B), the CMIP3 models with prescribed ozone recovery (C), and the CMIP3 models with no ozone recovery (D). Shading and contour intervals are $0.05 \text{ m s}^{-1} \text{ decade}^{-1}$. Deceleration and acceleration are indicated with blue and red colors, respectively, and trends weaker than $0.05 \text{ m s}^{-1} \text{ decade}^{-1}$ are omitted. Superimposed black solid lines are DJF zonal-mean zonal wind averaged from 2001 to 2010, with a contour interval of 10 m s^{-1} , starting at 10 m s^{-1} . From Son et al. (2008, 2010).

2010). This suggests that climate models may tend to overestimate the 21st century poleward shift in jet location (Kidston and Gerber, 2010).

An additional caveat involves the definition of the annular modes in the presence of a changing climate. Normally, the annular mode patterns are based on geopotential anomalies relative to a fixed climatology, such as for 1960–2010. In long model integrations including climate change, the future annular mode index is calculated by projecting anomalies (relative to 1960–2010) onto the annular mode patterns. However, the projected widespread warming of the troposphere will lift geopotential heights at all latitudes in the free troposphere, with the largest increases in the tropics. Because the annular mode patterns emphasize changes over the polar caps, much of the projected changes to geopotential will not be reflected in the annular mode index. Thus, the annular mode patterns are not a good proxy for long-term projected changes to hemispheric geopotential (e.g., Fyfe, 2003; Gerber et al., 2010). The zonal-mean response to anthropogenic forcing also appears to have a distinctive baroclinic signature

that is very different from the annular modes (Woollings, 2008). Shindell and Schmidt (2004) note a similar decoupling of the signatures of global warming and the Southern Annular Mode.

It is possible to modify the definition of the annular modes to compensate for the effects of tropospheric warming, but the resulting annular mode trends are not comparable to annular mode trends calculated using standard methodologies. For example, Morgenstern et al. (2010b) used a modified definition of the Northern Annular Mode (NAM) that partially accounts for the effects of tropospheric warming. With this modified definition, in the CCMVal-2 models, increasing CO_2 is generally associated with trends towards the negative polarity of the NAM in winter. An alternate methodology is to remove the slowly varying trend in geopotential heights from the climatology, resulting in annular mode indices that have no long-term trends (the geopotential height trends are contained in the slowly varying climatology). Using this method, Gerber et al. (2010) found that the structure and month-to-month variability of the annular modes remain

relatively robust over time in CMIP3 and CCMVal-2 model integrations of the 21st century (again, the trends in the mean of the annular mode indices are contained in the slowly varying climatology).

4.5.7 Tropospheric Chemistry

The future increases in stratospheric ozone will also impact tropospheric chemistry. The effects can be expected to be the reverse of the impacts of stratospheric ozone depletion over the past few decades discussed in Section 4.4.4. If stratospheric cooling leads to a thicker ozone layer than in the past (“super-recovery”) then future impacts may be larger. Decreasing UV radiation reaching the lower atmosphere is expected to decrease tropospheric OH. Duncan and Logan (2008) analyzed past CO trends. Based on their analysis, OH decreases due to ozone recovery would augment rather than cancel the positive impact of likely increasing CH₄ on CO trends. In any case, based on calculations during the period of ozone loss (Section 4.4.4), the impact is likely to be small but it remains to be quantified.

The flux of stratospheric ozone into the troposphere may also change in a future climate. Even with the same rate of mass transport, ozone increases in the lower stratosphere would lead to larger ozone transport into the troposphere. However, the stratosphere-troposphere transport mass flux may also change. Stevenson et al. (2006) studied the climate of 2030 using nine different models. They found ozone stratosphere-troposphere transport will increase by 0–19%. Zeng et al. (2008) investigated the impact of climate change on the tropospheric ozone budget using a 3-D chemistry-climate model with a relatively low lid and simple representation of stratospheric chemistry. For a 2100 atmosphere, they found that a doubling of CO₂ caused an 80% increase in ozone transport from the stratosphere, which led to increases in tropospheric ozone down to the surface. Similar studies using low-lid tropospheric chemistry models by Collins et al. (2003) and Sudo et al. (2003) showed large stratosphere-troposphere transport increases by 2100 of 40% and 130%, respectively.

Recently, Hegglin and Shepherd (2009) investigated the impact of climate change on ozone in the lower atmosphere in a model with full stratospheric chemistry. Under a moderate greenhouse gas emissions scenario they found the stratosphere-troposphere transport of ozone increased by 23% between 1965 and 2095 due to changes in the Brewer-Dobson circulation, i.e., a smaller value than the low-lid tropospheric models cited above, but for a different greenhouse gas scenario. Hegglin and Shepherd (2009) also investigated the impact of the changes in vertical and latitudinal distribution of ozone on surface UV. Between 1965 and 2095 they found surface clear-sky UV fluxes decreased by 9% at northern high latitudes, in-

creased by 4% in the tropics and increased by up to 20% at high southern latitudes. These changes in the clear-sky UV flux, due to circulation-induced changes in lower-stratospheric ozone, are different from those expected based on ozone recovery from halocarbon-induced depletion, and illustrate the importance of dynamics in controlling total ozone in the future as halocarbons decrease. Future UV levels will also be affected by changes in cloud cover (see Chapter 3, Section 3.4).

Future changes in the stratosphere-troposphere transport of ozone from ten chemistry-climate models have been assessed in Chapter 10 of SPARC CCMVal (2010). The report provided a comparison of the chemistry-climate model stratosphere-troposphere transport ozone flux with observations and other model studies for past and future time periods related to ozone depletion (1965–2000), ozone recovery (2000–2035), and climate change (1965–2095). The chemistry-climate model multi-model mean of the change in the stratosphere-troposphere transport ozone flux attributable to climate change (1965–2095) was slightly larger in the Northern Hemisphere (17%) than in the Southern Hemisphere (14%). The chemistry-climate model multi-model mean was generally consistent in terms of relative changes with the Canadian model results shown in Hegglin and Shepherd (2009), but showed a reduction in Northern Hemisphere stratosphere-troposphere transport ozone flux from 1965–2000 due to ozone depletion, as well as a weaker long-term increase in Northern Hemisphere stratosphere-troposphere transport ozone flux over 1965–2095 due to climate change. Over the period 2000–2030, the CCMVal-2 models showed increases in the global stratosphere-troposphere transport ozone flux of 10.3 (±2.0)% (see CCMVal, 2010, Chapter 10, Figure 10-22), which is toward the upper end of the range from tropospheric models reported by Stevenson et al. (2006).

4.5.8 Solar and Volcanic Influences

The existing observational record is short, and hence we do not fully understand the limits of natural variability in the stratosphere. Based on our current understanding, the influence of explosive volcanic eruptions on stratospheric ozone depletion is linked to heterogeneous chemistry on the surface of particles, and is very sensitive to the amount of chlorine loading (Section 3.2.5). Hence potential future volcanic eruptions are expected to be associated with increasingly less ozone depletion as chlorine declines, and are even expected to result in ozone increases by midcentury (Tie and Brasseur, 1995). On the other hand, the direct effects of major volcanic eruptions on climate (including surface cooling, stratospheric warming, winter season weather patterns, and changes in ocean heat content and sea level rise) are expected to continue to

occur in a manner that scales with the stratospheric aerosol abundance.

Future stratospheric temperatures and ozone levels will depend on variations in the solar radiation incident at the Earth. The sun is currently in an anomalously quiescent state (Fröhlich, 2009), which makes prediction of its future behavior and total solar irradiance highly uncertain. Furthermore, recent space-based measurements (Harder et al., 2009) have cast doubt on currently accepted models of the ozone response to solar variability. That said, while the impact of future variations in solar irradiance is highly uncertain, it is unlikely that solar variability will have more than a minor effect on ozone levels relative to the effects of the reduction in chlorine loading.

REFERENCES

- AchutaRao, K., and K.R. Sperber, ENSO simulation in coupled ocean-atmosphere models: Are the current models better?, *Clim. Dyn.*, 27, 1-15, doi: 10.1007/s00382-006-0119-7, 2006.
- Allen, R.J., and S.C. Sherwood, Warming maximum in the tropical upper troposphere deduced from thermal winds, *Nature Geosci.*, 1, 399-403, doi: 10.1038/ngeo208, 2008.
- Aoki, S., M. Yoritaka, and A. Masuyama, Multidecadal warming of subsurface temperature in the Indian sector of the Southern Ocean, *J. Geophys. Res.*, 108, 8081, doi: 10.1029/2000JC000307, 2003.
- Arblaster, J.M., and G.A. Meehl, Contributions of external forcings to Southern Annular Mode trends, *J. Clim.*, 19 (12), 2896-2905, doi: 10.1175/JCLI3774.1, 2006.
- Archer, C.L., and K. Caldeira, Historical trends in the jet streams, *Geophys. Res. Lett.*, 35, L08803, doi: 10.1029/2008GL033614, 2008.
- Austin, J., and F. Li, On the relationship between the strength of the Brewer–Dobson circulation and the age of stratospheric air, *Geophys. Res. Lett.*, 33, L17807, doi: 10.1029/2006GL026867, 2006.
- Austin, J., K. Tourpali, E. Rozanov, H. Akiyoshi, S. Bekki, G. Bodeker, C. Brühl, N. Butchart, M. Chipperfield, M. Deushi, V.I. Fomichev, M.A. Giorgetta, L. Gray, K. Kodera, F. Lott, E. Manzini, D. Marsh, K. Matthes, T. Nagashima, K. Shibata, R.S. Stolarski, H. Struthers, and W. Tian, Coupled chemistry-climate model simulations of the solar cycle in ozone and temperature, *J. Geophys. Res.*, 113, D11306, doi: 10.1029/2007JD009391, 2008.
- Austin, J., R.J. Wilson, H. Akiyoshi, S. Bekki, N. Butchart, C. Claud, V.I. Fomichev, P. Forster, R.R. Garcia, N.P. Gillett, P. Keckhut, U. Langematz, E. Manzini, T. Nagashima, W.J. Randel, E. Rozanov, K. Shibata, K.P. Shine, H. Struthers, D.W.J. Thompson, F. Wu, and S. Yoden, Coupled chemistry climate model simulations of stratospheric temperatures and their trends for the recent past, *J. Geophys. Res.*, 36, L13809, doi: 10.1029/2009GL038462, 2009.
- Baker, D.F., R.M. Law, K.R. Gurney, P. Rayner, P. Peylin, A.S. Denning, P. Bousquet, L. Bruhwiler, Y.-H. Chen, P. Ciais, I.Y. Fung, M. Heimann, J. John, T. Maki, S. Maksyutov, K. Masarie, M. Prather, B. Pak, S. Taguchi, and Z. Zhu, TransCom 3 inversion intercomparison: Impact of transport model errors on the interannual variability of regional CO₂ fluxes, 1988–2003, *Global Biogeochem. Cycles*, 20, GB1002, doi: 10.1029/2004GB002439, 2006.
- Balachandran N., D. Rind, P. Lonergan, and D. Shindell, Effects of solar cycle variability on the lower stratosphere and the troposphere, *J. Geophys. Res.*, 104, (D22) 27321-27339, 1999.
- Baldwin, M., and M. Dameris (Lead Authors), J. Austin, S. Bekki, B. Bregman, N. Butchart, E. Cordero, N. Gillett, H.-F. Graf, C. Granier, D. Kinnison, S. Lal, T. Peter, W. Randel, J. Scinocca, D. Shindell, H. Struthers, M. Takahashi, and D. Thompson, Climate-ozone connections, Chapter 5 in *Scientific Assessment of Ozone Depletion: 2006*, Global Ozone Research and Monitoring Project—Report No. 50, 572 pp., World Meteorological Organization, Geneva, Switzerland, 2007.
- Baldwin, M.P., and T.J. Dunkerton, Stratospheric harbingers of anomalous weather regimes, *Science*, 244 (5542), 581-584, 2001.
- Barriopedro, D., R. Garcia-Herrera, and R. Huth, Solar modulation of Northern Hemisphere winter blocking, *J. Geophys. Res.*, 113, D14118, doi: 10.1029/2008JD009789, 2008.
- Bekki, S., K.S. Law, and J.A. Pyle, Effect of ozone depletion on atmospheric CH₄ and CO concentrations, *Nature*, 371, 595-597, doi: 10.1038/371595a0, 1994.
- Bengtsson, L., K. Hodges, and E. Roeckner, Storm tracks and climate change, *J. Clim.*, 19 (15), 3518-3543, doi: 10.1175/JCLI3815.1, 2006.
- Boberg, F., and H. Lundstedt, Solar wind variations related to fluctuations of the North Atlantic oscillation, *Geophys. Res. Lett.*, 29, doi: 10.1029/2002GL014903, 2002.
- Böning, C.W., A. Dispert, M. Visbeck, S.R. Rintoul, and F.U. Schwarzkopf, The response of the Antarctic Circumpolar Current to recent climate change, *Nature Geosci.*, 1, 864-869, doi: 10.1038/ngeo362, 2008.
- Bousquet, P., D.A. Hauglustaine, P. Peylin, C. Carouge, and P. Ciais, Two decades of OH variability as inferred by an inversion of atmospheric transport and chemistry of methyl chloroform, *Atmos. Chem. Phys.*, 5, 2635-2656, doi: 10.5194/acp-5-2635-2005, 2005.
- Brandefelt, J., and E. Källén, The response of the Southern Hemisphere atmospheric circulation to an en-

- hanced greenhouse gas forcing, *J. Clim.*, *17* (22), 4425-4442, doi: 10.1175/3221.1, 2004.
- Brewer, A.W., Evidence for a world circulation provided by the measurements of helium and water vapour distribution in the stratosphere, *Quart. J. Roy. Meteorol. Soc.*, *75* (326), 351-363, doi: 10.1002/qj.49707532603, 1949.
- Brönnimann, S., T. Ewen, T. Griesser, and R. Jenne, Multidecadal signal of solar variability in the upper troposphere during the 20th century, *Space Sci. Rev.*, *125* (1-4), 305-315, doi: 10.1007/s11214-006-9065-2, 2006.
- Butchart, N., and A.A. Scaife, Removal of chlorofluorocarbons by increased mass exchange between the stratosphere and troposphere in a changing climate, *Nature*, *410*, 799-802, 2001.
- Butchart, N., A.A. Scaife, M. Bourqui, J. de Grandpré, S.H.E. Hare, J. Kettleborough, U. Langematz, E. Manzini, F. Sassi, K. Shibata, D. Shindell, and M. Sigmond, Simulations of anthropogenic change in the strength of the Brewer-Dobson circulation, *Clim. Dyn.*, *27* (7-8), 727-741, 2006.
- Butchart, N., I. Cionni, V. Eyring, T.G. Shepherd, D.W. Waugh, H. Akiyoshi, J. Austin, C. Brühl, M.P. Chipperfield, E. Cordero, M. Dameris, R. Deckert, S. Dhomse, S.M. Frith, R.R. Garcia, A. Gettelman, M.A. Giorgetta, D.E. Kinnison, F. Li, E. Mancini, C. McLandress, S. Pawson, G. Pitari, D.A. Plummer, E. Rozanov, F. Sassi, J.F. Scinocca, K. Shibata, B. Steil, and W. Tian, Chemistry-climate model simulations of 21st century stratospheric climate and circulation changes, *J. Clim.*, *23* (20), doi: 10.1175/2010JCLI3404.1, 2010.
- Butler, A.H., D.W.J. Thompson, and K.R. Gurney, Observed relationships between the Southern Annular Mode and atmospheric carbon dioxide, *Global Biogeochem. Cycles*, *21*, GB4014, doi: 10.1029/2006GB002796, 2007.
- Cai, W., and T. Cowan, Trends in Southern Hemisphere circulation in IPCC AR4 models over 1950–99: Ozone depletion versus greenhouse forcing, *J. Clim.*, *20* (4), 681-693, doi: 10.1175/JCLI4028.1, 2007.
- Cai, W., P.H. Whetton, and D.J. Karoly, The response of the Antarctic oscillation to increasing and stabilized atmospheric CO₂, *J. Clim.*, *16* (10), 1525-1538, 2003.
- Calvo, N., and R.R. Garcia, Wave forcing of the tropical upwelling in the lower stratosphere under increasing concentrations of greenhouse gases, *J. Atmos. Sci.*, *66* (10), 3184-3196, doi: 10.1175/2009JAS3085.1, 2009.
- Canziani, P.O., F.E. Malanca, and E.A. Agosta, Ozone and upper troposphere/lower stratosphere variability and change at southern midlatitudes 1980–2000: Decadal variations, *J. Geophys. Res.*, *113*, D20101, doi: 10.1029/2007JD009303, 2008.
- CCSP (U.S. Climate Change Science Program), *Temperature Trends in the Lower Atmosphere: Steps for Understanding and Reconciling Differences*, edited by T.R. Karl, S.J. Hassol, C.D. Miller, and W.L. Murray, Synthesis and Assessment Product 1.1, A Report by the Climate Change Science Program and the Subcommittee on Global Change Research, 164 pp., Washington, D.C., 2006.
- Chapman, W.L., and J.E. Walsh, A synthesis of Antarctic temperatures, *J. Clim.*, *20* (16), 4096-4117, doi: 10.1175/JCLI4236.1, 2007.
- Chin, M., and D. Davis, A reanalysis of carbonyl sulfide as a source of stratospheric background sulfur aerosol, *J. Geophys. Res.*, *100* (D5), 8993-9005, 1995.
- Christy, J.R., R.W. Spencer, W.B. Norris, W.D. Braswell, and D.E. Parker, Error estimates of version 5.0 of MSU-AMSU bulk atmospheric temperatures, *J. Atmos. Oceanic Technol.*, *20* (5), 613-629, 2003.
- Church, J. A., N.J. White, and J.M. Arblaster, Significant decadal-scale impact of volcanic eruptions on sea level and ocean heat content, *Nature*, *438*, 74-77, doi: 10.1038/nature04237, 2005.
- Clough, S., and M. Iacono, Line-by-line calculation of atmospheric fluxes and cooling rates. 2. Application to carbon dioxide, ozone, methane, nitrous oxide and the halocarbons, *J. Geophys. Res.*, *100* (D8), 16519-16535, 1995.
- Collins, W.J., R.G. Derwent, B. Garnier, C.E. Johnson, M.G. Sanderson, and D.S. Stevenson, Effect of stratosphere-troposphere exchange on the future tropospheric ozone trend, *J. Geophys. Res.*, *108* (D12), 8528, doi: 10.1029/2002JD002617, 2003.
- Cook, P.A., and H.K. Roscoe, Variability and trends in stratospheric NO₂ in Antarctic summer, and implications for stratospheric NO_y, *Atmos. Chem. Phys.*, *9*, 3601-3612, doi: 10.5194/acp-9-3601-2009, 2009.
- Cordero, E.C., and P.M.deF. Forster, Stratospheric variability and trends in models used for the IPCC AR4, *Atmos. Chem. Phys.*, *6*, 5369-5380, 2006.
- Crook, J.A., N.P. Gillett, and S.P.E. Keeley, Sensitivity of Southern Hemisphere climate to zonal asymmetry in ozone, *Geophys. Res. Lett.*, *35*, L07806, doi: 10.1029/2007GL032698, 2008.
- Crutzen, P.J., The possible importance of CSO for the sulfate layer of the stratosphere, *Geophys. Res. Lett.*, *3* (2), 73-76, 1976.
- Dall'Amico, M., L.J. Gray, K.H. Rosenlof, A.A. Scaife, K.P. Shine, and P.A. Stott, Stratospheric temperature trends: Impact of ozone variability and the QBO, *Clim. Dyn.*, *34* (2-3), doi: 10.1007/s00382-009-0604-x, 2010a.
- Dall'Amico, M., P.A. Stott, A.A. Scaife, L.J. Gray, K.H. Rosenlof, and, A.Y. Karpechko, Impact of stratospheric variability on tropospheric climate change,

- Clim. Dyn.*, 34(2-3), 399-417, doi: 10.1007/s00382-009-0580-1, 2010b.
- Deckert, R., and M. Dameris, Higher tropical SSTs strengthen the tropical upwelling via deep convection, *Geophys. Res. Lett.*, 35, L10813, doi: 10.1029/2008GL033719, 2008.
- Delworth, T.L., V. Ramaswamy, and G.L. Stenchikov, The impact of aerosols on simulated ocean temperature and heat content in the 20th century, *Geophys. Res. Lett.*, 32, L24709, doi: 10.1029/2005GL024457, 2005.
- Deshler, T., A review of global stratospheric aerosol: Measurements, importance, life cycle, and local stratospheric aerosol, *Atmos. Res.*, 90 (2-4), 223-232, doi: 10.1016/j.atmosres.2008.03.016, 2008.
- Dhomse, S., M. Weber, and J. Burrows, The relationship between tropospheric wave forcing and tropical lower stratospheric water vapor, *Atmos. Chem. Phys.*, 8, 471-480, 2008.
- Dlugokencky, E.J., L. Bruhwiler, J.W.C. White, L.K. Emons, P.C. Novelli, S.A. Montzka, K.A. Masarie, P.M. Lang, A.M. Crotwell, J.B. Miller, and L.V. Gatti, Observational constraints on recent increases in the atmospheric CH₄ burden, *Geophys. Res. Lett.*, 36, L18803, doi: 10.1029/2009GL039780, 2009.
- Dobson, G.M.B., Origin and distribution of the polyatomic molecules in the atmosphere, *Proc. Roy. Soc. London*, 236, 1205, 187-193, 1956.
- Domingues, C.M., J.A. Church, N.J. White, P.J. Gleckler, S.E. Wijffels, P.M. Barker, and J.R. Dunn, Improved estimates of upper-ocean warming and multi-decadal sea-level rise, *Nature*, 453, 1090-1093, doi: 10.1038/nature07080, 2008.
- Duncan, B.N., and J.A. Logan, Model analysis of the factors regulating the trends and variability of carbon monoxide between 1988 and 1997, *Atmos. Chem. Phys.*, 8, 7389-7403, 2008.
- Engel, A., T. Möbius, H. Bönisch, U. Schmidt, R. Heinz, I. Levin, E. Atlas, S. Aoki, T. Nakazawa, S. Sugawara, F. Moore, D. Hurst, J. Elkins, S. Schauffler, A. Andrews, and K. Boering, Age of stratospheric air unchanged within uncertainties over the past 30 years, *Nature Geosci.*, 2, 28-31, doi: 10.1038/ngeo388, 2009.
- Ern, M., and P. Preusse, Wave fluxes of equatorial Kelvin waves and QBO zonal wind forcing derived from SABER and ECMWF temperature space-time spectra, *Atmos. Chem. Phys.*, 9, 3957-3986, 2009.
- Esler, J.G., L.M. Polvani, and R.K. Scott, The Antarctic stratospheric sudden warming of 2002: A self-tuned resonance?, *Geophys. Res. Lett.*, 33, L12804, doi: 10.1029/2006GL026034, 2006.
- Eyring, V., N. Butchart, D.W. Waugh, H. Akiyoshi, J. Austin, S. Bekki, G.E. Bodeker, B.A. Boville, C. Brühl, M.P. Chipperfield, E. Cordero, M. Dameris, M. Deushi, V.E. Fioletov, S.M. Frith, R.R. Garcia, A. Gettelman, M.A. Giorgetta, V. Grewe, L. Jourdain, D.E. Kinnison, E. Mancini, E. Manzini, M. Marchand, D.R. Marsh, T. Nagashima, P.A. Newman, J.E. Nielsen, S. Pawson, G. Pitari, D.A. Plummer, E. Rozanov, M. Schraner, T.G. Shepherd, K. Shibata, R.S. Stolarski, H. Struthers, W. Tian, and M. Yoshiki, Assessment of temperature, trace species, and ozone in chemistry-climate model simulations of the recent past, *J. Geophys. Res.*, 111, D22308, doi: 10.1029/2006JD007327, 2006.
- Eyring, V., A. Gettelman, N.R.P. Harris, S. Pawson, T.G. Shepherd, D.W. Waugh, H. Akiyoshi, N. Butchart, M.P. Chipperfield, M. Dameris, D.W. Fahey, P.M.deF. Forster, P.A. Newman, M. Rex, R.J. Salawitch, and B.D. Santer, Report on the Third SPARC CCMVal Workshop, SPARC Newsletter No. 30, 17-19, available: <http://www.atmosph.physics.utoronto.ca/SPARC/Newsletter30Web/CCMVal.html>, 2008.
- Feck, T., J.-U. Groöß, and M. Riese, Sensitivity of Arctic ozone loss to stratospheric H₂O, *Geophys. Res. Lett.*, 35, L01803, doi: 10.1029/2007GL031334, 2008.
- Fogt, R.L., A.J. Monaghan, J. Perlwitz, D.H. Bromwich, J.M. Jones, and G.J. Marshall, Historical SAM variability. Part II: Twentieth-century variability and trends from reconstructions, observations, and the IPCC AR4 models, *J. Clim.*, 22 (20), 5346-5355, 2009.
- Forster, P.M.deF., and K.P. Shine, Assessing the climate impact of trends in stratospheric water vapor, *Geophys. Res. Lett.*, 29, doi: 10.1029/2001GL013909, 2002.
- Forster, P.M.deF., and M. Joshi, The role of halocarbons in the climate change of the troposphere and stratosphere, *Clim. Change*, 71 (1-2), 249-266, doi: 10.1007/s10584-005-5955-7, 2005.
- Forster, P., V. Ramaswamy, P. Artaxo, T. Berntsen, R. Betts, D.W. Fahey, J. Haywood, J. Lean, D.C. Lowe, G. Myhre, J. Nganga, R. Prinn, G. Raga, M. Schulz, and R. Van Dorland, Changes in atmospheric constituents and in radiative forcing, Chapter 2 in *Climate Change 2007: The Physical Science Basis. Contribution of Working Group I to the Fourth Assessment Report of the Intergovernmental Panel on Climate Change*, edited by S. Solomon, D. Qin, M. Manning, Z. Chen, M. Marquis, K.B. Averyt, M. Tignor, and H.L. Miller, 996 pp., Cambridge University Press, Cambridge, U.K. and New York, NY, U.S.A., 2007a.
- Forster, P.M., G. Bodeker, R. Schofield, S. Solomon, and D.W.J. Thompson, Effects of ozone cooling in the tropical lower stratosphere and upper troposphere, *Geophys. Res. Lett.*, 34, L23813, doi: 10.1029/2007GL031994, 2007b.
- Frame, T.H.A., and L.J. Gray, The 11-year solar cycle in

- ERA-40 data: An update to 2008, *J. Clim.*, 23 (8), doi: 10.1175/JCLI3150.1, 2213-2222, 2010.
- Free, M., and D.J. Seidel, Comments on "Biases in stratospheric and tropospheric temperature trends derived from historical radiosonde data," *J. Clim.*, 20 (14), 3704-3709, doi: 10.1175/JCLI4210.1, 2007.
- Free, M., and J. Lanzante, Effect of volcanic eruptions on the vertical temperature profile in radiosonde data and climate models, *J. Clim.*, 22 (11), 2925-2939, doi: 10.1175/2008JCLI2562.1, 2009.
- Free, M., S.J. Seidel, J.K. Angell, J. Lanzante, I. Durre, and T.C. Peterson, Radiosonde Atmospheric Temperature Products for Assessing Climate (RATPAC): A new data set of large-area anomaly time series, *J. Geophys. Res.*, 110, D22101, doi: 10.1029/2005JD006169, 2005.
- Fröhlich, C., Evidence of a long-term trend in solar irradiance, *Astron. Astrophys.*, 501 (3), L27-L30, doi: 10.1051/0004-6361/200912318, 2009.
- Fröhlich, C., and J. Lean, Solar radiative output and its variability: Evidence and mechanisms, *Astron Astrophys Rev* 12 (4), 273-320, doi: 10.1007/s00159-004-0024-1, 2004.
- Fu, Q., C.M. Johanson, S.G. Warren, and D.J. Seidel, Contribution of stratospheric cooling to satellite-inferred tropospheric temperature trends, *Nature*, 429, 55-58, doi: 10.1038/nature02524, 2004.
- Fu, Q., C.M. Johanson, J.M. Wallace, and T. Reichler, Enhanced mid-latitude tropospheric warming in satellite measurements, *Science*, 312 (5777), 1179-1179, doi: 10.1126/science.1125566, 2006.
- Fu, Q., S. Solomon, and P. Lin, On the seasonal dependence of tropical lower-stratospheric temperature trends, *Atmos. Chem. Phys.*, 10, 2643-2653, doi: 10.5194/acp-10-2643-2010, 2010.
- Fueglistaler, S., and P.H. Haynes, Control of interannual and longer-term variability of stratospheric water vapor, *J. Geophys. Res.*, 110, D24108, doi: 10.1029/2005JD006019, 2005.
- Fueglistaler, S., A.E. Dessler, T.J. Dunkerton, I. Folkins, Q. Fu, and P.W. Mote, Tropical tropopause layer, *Rev. Geophys.*, 47, RG1004, doi: 10.1029/2008RG000267, 2009.
- Fuglestad, J.S., J.E. Jonson, and I.S.A. Isaksen, Effects of reductions in stratospheric ozone on tropospheric chemistry through changes in photolysis rates, *Tellus*, 46B (3), 172-192, 1994.
- Funatsu, B., C. Claud, P. Keckhut, and A. Hauchecorne, Cross-validation of Advanced Microwave Sounding Unit and lidar for long-term upper-stratospheric temperature monitoring, *J. Geophys. Res.*, 113, D23108, doi: 10.1029/2008JD010743, 2008.
- Fusco, A.C., and J.A. Logan, Analysis of 1970-1995 trends in tropospheric ozone at Northern Hemisphere midlatitudes with the GEOS-CHEM model, *J. Geophys. Res.*, 108, 4449, doi: 10.1029/2002JD002742, 2003.
- Fyfe, J.C., Separating extratropical zonal wind variability and mean change, *J. Clim.*, 16 (5), 863-874, 2003.
- Fyfe, J.C., Southern Ocean warming due to human influence, *Geophys. Res. Lett.*, 33, L19701, doi: 10.1029/2006GL027247, 2006.
- Fyfe, J.C., and O.A. Saenko, Simulated changes in the extratropical Southern Hemisphere winds and currents, *Geophys. Res. Lett.*, 33, L06701, doi: 10.1029/2005GL025332, 2006.
- Fyfe, J.C., G.J. Boer, and G.M. Flato, The Arctic and Antarctic oscillations and their projected changes under global warming, *Geophys. Res. Lett.*, 26 (11), 1601-1604, 1999.
- Fyfe, J.C., O.A. Saenko, K. Zickfeld, M. Eby, and A.J. Weaver, The role of poleward-intensifying winds on Southern Ocean warming, *J. Clim.*, 20 (21), 5391-5400, doi: 10.1175/2007JCLI1764.1, 2007.
- Garcia, R.R., and W.J. Randel, Acceleration of the Brewer-Dobson circulation due to increases in greenhouse gases, *J. Atmos. Sci.*, 65 (8), 2731-2739, doi: 10.1175/2008JAS2712.1, 2008.
- Geller, M.A., X. Zhou, and M. Zhang, Simulations of the interannual variability of stratospheric water vapor, *J. Atmos. Sci.*, 59 (6), 1076-1085, 2002.
- Gent, P.R., and J.C. McWilliams, Isopycnal mixing in ocean circulation models, *J. Phys. Ocean.*, 20 (1), 150-155, 1990.
- Gerber, E.P., S. Voronin, and L.M. Polvani, Testing the annular mode autocorrelation timescale in simple atmospheric general circulation models, *Mon. Wea. Rev.*, 136, 1523-1536, doi: 10.1175/2007MWR2211.1, 2008.
- Gerber, E.P., M.P. Baldwin, H. Akiyoshi, J. Austin, S. Bekki, P. Braesicke, N. Buchart, M. Chipperfield, M. Dameris, S. Dhomse, S.M. Firth, R.R. Garcia, H. Garney, A. Gettelman, S.C. Hardiman, O. Morgenstern, J.E. Nielsen, S. Pawson, T. Peter, D.A. Plummer, J.A. Pyle, E. Rozanov, J.F. Scinocca, T.G. Shepherd, and D. Smale, Stratosphere-troposphere coupling and annular mode variability in chemistry-climate models, *J. Geophys. Res.*, 115, D00M06, doi: 10.1029/2009JD013770, 2010.
- Gettelman, A., T. Birner, V. Eyring, H. Akiyoshi, S. Bekki, C. Brühl, M. Dameris, D.E. Kinnison, F. Lefevre, F. Lott, E. Mancini, G. Pitari, D.A. Plummer, E. Rozanov, K. Shibata, A. Stenke, H. Struthers, and W. Tian, The tropical tropopause layer 1960-2100, *Atmos. Chem. Phys.*, 9, 1621-1637, 2009.
- Gettelman, A., M.I. Hegglin, S.-W. Son, J. Kim, M. Fujiwara, T. Birner, S. Kremser, M. Rex, J.A. Añel, H. Akiyoshi, J. Austin, S. Bekki, P. Braesicke, C.

- Brühl, N. Butchart, M. Chipperfield, M. Dameris, S. Dhomse, H. Garny, S.C. Hardiman, P. Jöckel, D.E. Kinnison, J.F. Lamarque, E. Mancini, M. Marchand, M. Michou, O. Morgenstern, S. Pawson, G. Pitari, D. Plummer, J.A. Pyle, E. Rozanov, J. Scinocca, T.G. Shepherd, K. Shibata, D. Smale, H. Teyssèdre, and W. Tian, Multimodel assessment of the upper troposphere and lower stratosphere: Tropics and global trends, *J. Geophys. Res.*, *115*, D00M08, doi: 10.1029/2009JD013638, 2010.
- Gille, S.T., Warming of the Southern Ocean since the 1950s, *Science*, *295* (5558), 1275-1277, doi: 10.1126/science.1065863, 2002.
- Gille, S.T., Decadal-scale temperature trends in the Southern Hemisphere ocean, *J. Clim.*, *21* (18), 4749-4765, doi: 10.1175/2008JCLI2131.1, 2008.
- Gillett, N.P., and D.W.J. Thompson, Simulation of recent Southern Hemisphere climate change, *Science*, *302* (5643), 273-275, 2003.
- Gillett, N.P., T.D. Kell, and P.D. Jones, Regional climate impacts of the Southern Annular Mode, *Geophys. Res. Lett.*, *33*, L23704, doi: 10.1029/2006GL027721, 2006.
- Gillett, N.P., D.A. Stone, P.A. Stott, T. Nozawa, A.Yu. Karpechko, G.C. Hegerl, M.F. Wehner, and P.D. Jones, Attribution of polar warming to human influence, *Nature Geosci.*, *1*, 750-754, doi: 10.1038/ngeo338, 2008.
- Gillett, N.P., J.F. Scinocca, D.A. Plummer, and M.C. Reader, Sensitivity of climate to dynamically-consistent zonal asymmetries in ozone, *Geophys. Res. Lett.*, *36*, L10809, doi: 10.1029/2009GL037246, 2009.
- Gillett, N.P., H. Akiyoshi, S. Bekki, V. Eyring, R. Garcia, C.A. McLinden, A. Yu. Karpechko, D.A. Plummer, E. Rozanov, J. Scinocca, and K. Shibata, Attribution of observed changes in stratospheric ozone and temperature, *Atmos. Chem. Phys. Discuss.*, *10*, 17341-17367, doi: 10.5194/acpd-10-17341-2010, 2010.
- Giorgetta, M.A., E. Manzini, E. Roeckner, M. Esch, and L. Bengtsson, Climatology and forcing of the quasi-biennial oscillation in the MAECHAM5 model, *J. Clim.*, *19* (16), 3882-3901, doi: 10.1175/JCLI3830.1, 2006.
- Gleckler, P.J., K. AchutaRao, J.M. Gregory, B.D. Santer, K.E. Taylor, and T.M.L. Wigley, Krakatoa lives: The effect of volcanic eruptions on ocean heat content and thermal expansion, *Geophys. Res. Lett.*, *33*, L17702, doi: 10.1029/2006GL026771, 2006.
- Goosse, H., W. Lefebvre, A. de Montety, E. Crespin, and A.H. Orsi, Consistent past half-century trends in the atmosphere, the sea ice, and the ocean at high southern latitudes, *Clim. Dyn.*, *33* (7-8), doi: 10.1007/s00382-008-0500-9, 2009.
- Granier, C., J.-F. Müller, S. Madronich, and G.P. Brasseur, Possible causes for the 1990-1993 decrease in the global tropospheric CO abundances: A three-dimensional sensitivity study, *Atmos. Env.*, *30* (10-11), 1673-1682, doi: 10.1016/1352-2310(95)00397-5, 1996.
- Gray, L.J., S.T. Rumbold, and K. Shine, Stratospheric temperature and radiative forcing response to 11-year solar cycle changes in irradiance and ozone, *J. Atmos. Sci.*, *66* (8), 2402-2417, doi: 10.1175/2009JAS2866.1, 2009.
- Gray, L.J., J. Beer, M. Geller, J.D. Haigh, M. Lockwood, K. Matthes, U. Cubasch, D. Fleitmann, R.G. Harrison, L. Hood, J. Luterbacher, G.A. Meehl, D. Shindell, B. van Geel, and W. White, Solar influence on climate, *Rev. Geophys.*, in press, 2010.
- Gregory, J.M., J.A. Lowe, and S.F.B. Tett, Simulated global-mean sea level change over the last half-millennium, *J. Clim.*, *19* (18), 4576-4591, doi: 10.1175/JCLI3881.1, 2006.
- Griffiths, G.M., Changes in New Zealand daily rainfall extremes 1930-2004, *Weather and Climate*, *26*, 3-46, 2006.
- Grise, K.M., D.W.J. Thompson, and P.M. Forster, On the role of radiative processes in stratosphere-troposphere coupling, *J. Clim.*, *22* (15), 4154-4161, doi: 10.1175/2009JCLI2756.1, 2009.
- Haigh, J.D., The role of stratospheric ozone in modulating the solar radiative forcing of climate, *Nature*, *370* (6490), 544-546, 1994.
- Haigh, J.D., The impact of solar variability on climate, *Science*, *272* (5264), 981-984, doi: 10.1126/science272.5264.981, 1996.
- Haigh, J.D., A GCM study of climate change in response to the 11-year solar cycle, *Quart. J. Roy. Meteorol. Soc.*, *125* (555), 871-892, 1999.
- Haigh, J.D., The effects of solar variability on the Earth's climate, *Phil. Trans. Roy. Soc. A*, *361* (1802), 95-111, 2003.
- Haigh, J.D., and J.A. Pyle, Ozone perturbation experiments in a two-dimensional circulation model, *Quart. J. Roy. Meteorol. Soc.*, *108*, 551-574, 1982.
- Haigh, J.D., and H.K. Roscoe, Solar influences on polar modes of variability, *Meteorol. Z.*, *15* (3), 371-378, 2006.
- Haigh, J.D., and H.K. Roscoe, The final warming date of the Antarctic polar vortex and influences on its interannual variability, *J. Clim.*, *22* (22), 5809-5819, 2009.
- Haigh, J.D., M. Blackburn, and R. Day, The response of tropospheric circulation to perturbations in lower-stratospheric temperature, *J. Clim.*, *18*, 3672-3685, 2005.
- Haigh, J.D., A.R. Winning, R. Toumi, and J.W. Harder, An influence of solar spectral variations on radiative forcing of climate, *Nature*, *467*, 696-699, doi:

- 10.1038/nature09426, 2010.
- Haimberger, L., Homogenization of radiosonde temperature time series using innovation statistics, *J. Clim.*, *20* (7), 1377-1403, doi: 10.1175/JCLI4050.1, 2007.
- Haimberger, L., C. Tavalato, and S. Sperka, Toward elimination of the warm bias in historic radiosonde temperature records—Some new results from a comprehensive intercomparison of upper-air data, *J. Clim.*, *21* (18), 4587-4606, doi: 10.1175/2008JCLI1929.1, 2008.
- Hall, A., and M. Visbeck, Synchronous variability in the Southern Hemisphere atmosphere, sea ice, and ocean resulting from the Annular Mode, *J. Clim.*, *15* (21), 3043-3057, doi: 10.1175/1520-0442(2002)015<3043:SVITSH>2.0.CO;2, 2002.
- Hallberg, R., and A. Gnanadesikan, The role of eddies in determining the structure and response of the wind-driven Southern Hemisphere overturning: Results from the Modeling Eddies in the Southern Ocean (MESO) project, *J. Phys. Ocean.*, *36* (12), 2232-2252, doi: 10.1175/JPO2980.1, 2006.
- Hampson J., P. Keckhut, A. Hauchecorne, and M.L. Chanin, The effect of the 11-year solar-cycle on the temperature in the upper-stratosphere and mesosphere: Part II: Numerical simulation and role of planetary waves, *J. Atmos. Sol. Terr. Phys.*, *67*, 948-958, 2005.
- Hansen, J., A. Lacis, R. Ruedy, and M. Sato, Potential climate impact of Mount Pinatubo eruption, *Geophys. Res. Lett.*, *19* (2), 215-218, doi: 10.1029/91GL02788, 1992.
- Harder, J.W., J.M. Fontenla, P. Pilewskie, E.C. Richard, and T.N. Woods, Trends in solar spectral irradiance variability in the visible and infrared, *Geophys. Res. Lett.*, *36*, L07801, doi: 10.1029/2008GL036797, 2009.
- Hegerl, G.C., F.W. Zwiers, P. Braconnot, N.P. Gillett, Y. Luo, J.A. Marengo Orsini, N. Nicholls, J.E. Penner, and P.A. Stott, Understanding and attributing climate change, Chapter 9 in *Climate Change 2007: The Physical Science Basis. Contribution of Working Group I to the Fourth Assessment Report of the Intergovernmental Panel on Climate Change*, edited by S. Solomon, D. Qin, M. Manning, Z. Chen, M. Marquis, K.B. Averyt, M. Tignor, and H.L. Miller, 996 pp., Cambridge University Press, Cambridge, U.K. and New York, NY, U.S.A., 2007.
- Hegglin, M.I., and T.G. Shepherd, Large climate-induced changes in ultraviolet index and stratosphere-to-troposphere ozone flux, *Nature Geosci.*, *2*, 687-691, doi: 10.1038/ngeo604, 2009.
- Hendon, H.H., D.W.J. Thompson, and M.C. Wheeler, Australian rainfall and surface temperature variations associated with the Southern Hemisphere Annular Mode, *J. Clim.*, *20* (11), 2452-2467, doi: 10.1175/JCLI4134.1, 2007.
- Hofmann, D.J., Increase in the stratospheric background sulfuric acid aerosol mass in the past 10 years, *Science*, *248* (4958), 996-1000, doi: 10.1126/science.248.4958.996, 1990.
- Hofmann, D.J., J. Barnes, M. O'Neill, M. Trudeau, and R. Neely, Increase in background stratospheric aerosol observed with lidar at Mauna Loa Observatory and Boulder, Colorado, *Geophys. Res. Lett.*, *36*, L15808, doi: 10.1029/2009GL039008, 2009.
- Holton, J.R., and A. Gettelman, Horizontal transport and the dehydration of the stratosphere, *Geophys. Res. Lett.*, *28* (14), 2799-2802, 2001.
- Hsu J., and M.J. Prather, Stratospheric variability and tropospheric ozone, *J. Geophys. Res.*, *114*, D06102, doi: 10.1029/2008JD010942, 2009.
- Hu, Y., and Q. Fu, Observed poleward expansion of the Hadley circulation since 1979, *Atmos. Chem. Phys.*, *7*, 5229-5236, 2007.
- Hudson, R.D., M.F. Andrade, M.B. Follette, and A.D. Frolov, The total ozone field separated into meteorological regimes—Part II: Northern Hemisphere mid-latitude total ozone trends, *Atmos. Chem. Phys.*, *6*, 5183-5191, 2006.
- IPCC, *Climate Change 2007: The Physical Science Basis. Contribution of Working Group I to the Fourth Assessment Report of the Intergovernmental Panel on Climate Change*, edited by S. Solomon, D. Qin, M. Manning, Z. Chen, M. Marquis, K.B. Averyt, M. Tignor, and H.L. Miller, 996 pp., Cambridge University Press, Cambridge, U.K. and New York, NY, U.S.A., 2007.
- IPCC/TEAP (Intergovernmental Panel on Climate Change/Technology and Economic Assessment Panel), *IPCC/TEAP Special Report on Safeguarding the Ozone Layer and the Global Climate System: Issues Related to Hydrofluorocarbons and Perfluorocarbons*, prepared by Working Groups I and III of the Intergovernmental Panel on Climate Change, and the Technical and Economic Assessment Panel, edited by B. Metz, L. Kuijpers, S. Solomon, S.O. Andersen, O. Davidson, J. Pons, D. de Jager, T. Kestin, M. Manning, and L. Meyer, 488 pp., Cambridge University Press, Cambridge, U.K. and New York, NY, U.S.A., 2005.
- Isaksen, I.S.A., C. Zerefos, K. Kourtidis, C. Meleti, S.B. Dalsøren, J.K. Sundet, A. Grini, P. Zanis, and D. Balis, Tropospheric ozone changes at unpolluted and semipolluted regions induced by stratospheric ozone changes, *J. Geophys. Res.*, *110*, D02302, doi: 10.1029/2004JD004618, 2005.
- Isaksen, I., C. Grainer, G. Myhre, T.K. Berntsen, S.B. Dal-

- seren, M. Gauss, Z. Klimont, R. Benestad, P. Bousquet, W. Collins, T. Cox, V. Eyring, D. Fowler, S. Fuzzi, P. Jöckel, P. Laj, U. Lohmann, M. Malone, P. Monks, A.S.H. Prevot, F. Raes, A. Richter, B. Rognerud, M. Schulz, D. Shindell, D.S. Stevenson, T. Storelvmo, W.-C. Wang, M. van Weele, M. Wild, and D. Wuebbles, Atmospheric composition change: Climate-Chemistry interactions, *Atmos. Env.*, *43* (33), 5138-5192, doi: 10.1016/j.atmosenv.2009.08.003, 2009.
- Ito, T., M. Woloszyn, and M. Mazloff, Anthropogenic carbon dioxide transport in the Southern Ocean driven by Ekman flow, *Nature*, *463*, 80-83, doi: 10.1038/nature08687, 2010.
- Iwasaki, T., H. Hamada, and K. Miyazaki, Comparisons of Brewer-Dobson circulations diagnosed from reanalyses, *J. Meteor. Soc. Jap.*, *87* (6), 997-1006, 2009.
- Jäger, H., Long-term record of lidar observations of the stratospheric aerosol layer at Garmisch-Partenkirchen, *J. Geophys. Res.*, *110*, D08106, doi: 10.1029/2004JD005506, 2005.
- Jensen, E., and L. Pfister, Transport and freeze-drying in the tropical tropopause layer, *J. Geophys. Res.*, *109*, D02207, doi: 10.1029/2003JD004022, 2004.
- Johanson, C.M., and M. Fu, Hadley cell widening: Model simulations versus observations, *J. Clim.*, *22* (10), 2713-2725, doi: 10.1175/2008JCLI2620.1, 2009.
- Jones, R.L., J.A. Pyle, J.E. Harries, A.M. Zavody, J.M. Russell III, and J.C. Gille, The water vapour budget of the stratosphere studied using LIMS and the SAMS satellite data, *Quart. J. Roy. Meteor. Soc.*, *112* (474), 1127-1143, doi: 10.1256/smsqj.47411, 1986.
- Jonsson, A.I., V.I. Fomichev, and T.G. Shepherd, The effect of nonlinearity in CO₂ heating rates on the attribution of stratospheric ozone and temperature changes, *Atmos. Chem. Phys.*, *9*, 8447-8452, 2009.
- Joshi, M.M., and G.S. Jones, The climatic effects of the direct injection of water vapour into the stratosphere by large volcanic eruptions, *Atmos. Chem. Phys.*, *9*, 6109-6118, 2009.
- Karpechko, A.Yu., N.P. Gillett, G.J. Marshall, and A.A. Scaife, Stratospheric influence on circulation changes in the Southern Hemisphere troposphere in coupled climate models, *Geophys. Res. Lett.*, *35*, L20806, doi: 10.1029/2008GL035354, 2008.
- Karpetchko, A., E. Kyrö, and B.M. Knudsen, Arctic and Antarctic polar vortices 1957-2002 as seen from the ERA-40 reanalyses, *J. Geophys. Res.*, *110*, D21109, doi: 10.1029/2005JD006113, 2005.
- Keckhut, P., C. Cagnazzo, M.-L. Chanin, C. Claud, and A. Hauchecorne, The 11-year solar-cycle effects on the temperature in the upper-stratosphere and mesosphere: Part I—Assessment of observations, *J. Atmos. Sol. Terr. Phys.*, *67*, 940-947, doi: 10.1016/j.jastp.2005.01.008, 2005.
- Keeley, S.P.E., N.P. Gillett, D.W.J. Thompson, S. Solomon, and P.M. Forster, Is Antarctic climate most sensitive to ozone depletion in the mid or lower stratosphere?, *Geophys. Res. Lett.*, *34*, L22812, doi: 10.1029/2007GL031238, 2007.
- Khatiwala, S., F. Primeau, and T. Hall, Reconstruction of the history of anthropogenic CO₂ concentrations in the ocean, *Nature*, *462*, 346-349, doi: 10.1038/nature08526, 2009.
- Khaykin, S., J.-P. Pommereau, L. Korshunov, V. Yushkov, J. Nielsen, N. Larsen, T. Christensen, A. Garnier, A. Lukyanov, and E. Williams, Hydration of the lower stratosphere by ice crystal geysers over land convective systems, *Atmos. Chem. Phys.*, *9*, 2275-2287, 2009.
- Kidston, J., and E.P. Gerber, Intermodel variability of the poleward shift of the austral jet stream in the CMIP3 integrations linked to biases in 20th century climatology, *Geophys. Res. Lett.*, *37*, L09708, doi: 10.1029/2010GL042873, 2010.
- Kirk-Davidoff, D.B., E.J. Hints, J.G. Anderson, and D.W. Keith, The effect of climate change on ozone depletion through changes in stratospheric water vapour, *Nature*, *402*, 399-401, doi: 10.1038/46521, 1999.
- Kley, D., J.M. Russell III, and C. Phillips, *SPARC Assessment of Upper Tropospheric and Stratospheric Water Vapor*, WCRP-No. 113, WMO/TD-No. 1043, SPARC Report No.2, 2000.
- Kodera, K., Solar cycle modulation of the North Atlantic Oscillation: Implication in the spatial structure of the NAO, *Geophys. Res. Lett.*, *29* (8), 1218, doi: 10.1029/2001GL014557, 2002.
- Kodera, K., Solar influence on the Indian Ocean Monsoon through dynamical processes, *Geophys. Res. Lett.*, *31*, L24209, doi: 10.1029/2004GL020928, 2004.
- Kodera, K., and K. Shibata, Solar influence on the tropical stratosphere and troposphere in the northern summer, *Geophys. Res. Lett.*, *33*, L19704, doi: 10.1029/2006GL026659, 2006.
- Kodera, K., K. Coughlin, and O. Arakawa, Possible modulation of the connection between the Pacific and Indian Ocean variability by the solar cycle, *Geophys. Res. Lett.*, *34*, L03710, doi: 10.1029/2006GL027827, 2007.
- Korhonen, H., K.S. Carslaw, P.M. Forster, S. Mikkonen, N.D. Gordon, and H. Kokkola, Aerosol climate feedback due to decadal increases in Southern Hemisphere wind speeds, *Geophys. Res. Lett.*, *37*, L02805, doi: 10.1029/2009GL041320, 2010.
- Kuroda, Y., and K. Kodera, Role of the Polar-night Jet Oscillation on the formation of the Arctic Oscillation in the Northern Hemisphere winter, *J. Geophys. Res.*, *109*, D11112, doi: 10.1029/2003JD004123, 2004.

- Kuroda, Y., and K. Kodera, Solar cycle modulation of the Southern Annular Mode, *Geophys. Res. Lett.*, *32*, L13802, doi: 10.1029/2005GL022516, 2005.
- Kuroda, Y., M. Deushi, and K. Shibata, Role of solar activity in the troposphere-stratosphere coupling in the Southern Hemisphere winter, *Geophys. Res. Lett.*, *34*, L21704, doi: 10.1029/2007GL030983, 2007.
- Kushner, P.J., and L.M. Polvani, Stratosphere-troposphere coupling in a relatively simple AGCM: The role of eddies, *J. Clim.*, *17* (3), 629-639, 2004.
- Kushner, P.J., and L.M. Polvani, Stratosphere-troposphere coupling in a relatively simple AGCM: Impact of the seasonal cycle, *J. Clim.*, *19* (21), 5721-5727, 2006.
- Kushner, P., I.M. Held, and T.L. Delworth, Southern Hemisphere atmospheric circulation response to global warming, *J. Clim.*, *14* (10), 2238-2249, 2001.
- Labitzke, K., Sunspots, the QBO and the stratospheric temperature in the north polar region, *Geophys. Res. Lett.*, *14* (5), 535-537, 1987.
- Lamarque, J.-F., and S. Solomon, Impact of changes in climate and halocarbons on recent lower stratosphere ozone and temperature trends, *J. Clim.*, *23* (10), 2599-2611, doi: 10.1175/2010JCLI3179.1, 2010.
- Lambert, A., W.G. Read, N.J. Livesey, M.L. Santee, G.L. Manney, L. Froidevaux, D.L. Wu, M.J. Schwartz, H.C. Pumphrey, C. Jimenez, G.E. Nedoluha, R.E. Cofield, D.T. Cuddy, W.H. Daffer, B.J. Drouin, R.A. Fuller, R.F. Jarnot, B.W. Knosp, H.M. Pickett, V.S. Perun, W.V. Snyder, P.C. Stek, R.P. Thurstans, P.A. Wagner, J.W. Waters, K.W. Jucks, G.C. Toon, R.A. Stachnik, P.F. Bernath, C.D. Boone, K.A. Walker, J. Urban, D. Murtagh, J.W. Elkins, and E. Atlas, Validation of the Aura Microwave Limb Sounder middle atmosphere water vapor and nitrous oxide measurements, *J. Geophys. Res.*, *112*, D24S36, doi: 10.1029/2007JD008724, 2007.
- Lanzante, J.R., S.A. Klein, and D.J. Seidel, Temporal homogenization of monthly radiosonde temperature data. Part I: Methodology, *J. Clim.*, *16* (2), 224-240, 2003.
- Larkin, A., J.D. Haigh, and S. Djavidnia, The effect of solar UV irradiance variations on the Earth's atmosphere, *Space Sci. Rev.*, *94* (1-2), 199-214, 2000.
- Law, K.S., and W.T. Sturges (Lead Authors), D.R. Blake, N.J. Blake, J.B. Burkholder, J.H. Butler, R.A. Cox, P.H. Haynes, M.K.W. Ko, K. Kreher, C. Mari, K. Pfeilsticker, J.M.C. Plane, R.J. Salawitch, C. Schiller, B.-M. Sinnhuber, R. von Glasow, N.J. Warwick, D.J. Wuebbles, and S.A. Yvon-Lewis, Halogenated very short-lived substances, Chapter 2 in *Scientific Assessment of Ozone Depletion: 2006*, Global Ozone Research and Monitoring Project—Report No. 50, 572 pp., World Meteorological Organization, Geneva, Switzerland, 2007.
- Law, R.M., R.J. Matear, and R.J. Francey, Comment On “Saturation of the southern ocean CO₂ sink due to recent climate change,” *Science*, *319* (5863), 570, 2008.
- Le Quéré, C., C. Rödenbeck, E.T. Buitenhuis, T.J. Conway, R. Langenfelds, A. Gomez, C. Labuschagne, M. Ramonet, T. Nakazawa, N. Metzl, N. Gillett, and M. Heimann, Saturation of the Southern Ocean CO₂ sink due to recent climate change, *Science*, *316* (5832), 1735-1738, doi: 10.1126/science.1136188, 2007.
- Le Quéré, C., M.R. Raupach, J.G. Canadell, and G. Marland, Trends in the sources and sinks of carbon dioxide, *Nature Geosci.*, *2*, 831-836, doi: 10.1038/ngeo689, 2009.
- le Texier, H., S. Solomon, and R.R. Garcia, The role of molecular hydrogen and methane oxidation in the water vapour budget of the stratosphere, *Quart. J. Roy. Meteorol. Soc.*, *114* (480), 281-295, doi: 10.1002/qj.49711448002, 1988.
- Lee, H., and A.K. Smith, Simulation of the combined effects of solar cycle, quasi-biennial oscillation, and volcanic forcing on stratospheric ozone changes in recent decades, *J. Geophys. Res.*, *108* (D2), 4049, doi: 10.1029/2001JD001503, 2003.
- Lee, J.N., and S. Hameed, Northern Hemisphere annular mode in summer: Its physical significance and its relation to solar activity variations, *J. Geophys. Res.*, *112*, D15111, doi: 10.1029/2007JD008394, 2007.
- Lee, J.N., S. Hameed, and D.T. Shindell, The northern annular mode in summer and its relation to solar activity variations in the GISS ModelE, *J. Atmos. Sol. Terr. Phys.*, *70* (5), 730-741, doi: 10.1016/j.jastp.2007.10.012, 2008.
- Leith, C.E., Climate response and fluctuation dissipation, *J. Atmos. Sci.*, *32*, 2022-2026, 1975.
- Lenton, A., and R.J. Matear, Role of the Southern Annular Mode (SAM) in Southern Ocean CO₂ uptake, *Global Biogeochem. Cycles*, *21*, GB2016, doi: 10.1029/2006GB002714, 2007.
- Lenton, A., F. Codron, L. Bopp, N. Metzl, P. Cadule, A. Tagliabue, and J. Le Sommer, Stratospheric ozone depletion reduces ocean carbon uptake and enhances ocean acidification, *Geophys. Res. Lett.*, *36*, L12606, doi: 10.1029/2009GL038227, 2009.
- Li, F., J. Austin, and J. Wilson, The strength of the Brewer-Dobson circulation in a changing climate: Coupled chemistry-climate model stimulation, *J. Clim.*, *21* (1), 40-57, doi: 10.1175/2007JCLI1663.1, 2008.
- Limpasuvan, V., and D.L. Hartmann, Wave-maintained annular modes of climate variability, *J. Clim.*, *13*, 4414-4429, 2000.
- Lin, P., Q. Fu, S. Solomon, and J.M. Wallace, Temperature trend patterns in Southern Hemisphere high

- latitudes: Novel indicators of stratospheric change, *J. Clim.*, 22 (23), 2009.
- Lorenz, D.J., and E.T. DeWeaver, Tropopause height and zonal wind response to global warming in the IPCC scenario integrations, *J. Geophys. Res.*, 112, D10119, doi: 10.1029/2006JD008087, 2007.
- Lovenduski, N.S., N. Gruber, and S.C. Doney, Toward a mechanistic understanding of the decadal trends in the Southern Ocean carbon sink, *Global Biogeochem. Cycles*, 22, GB3016, doi: 10.1029/2007GB003139, 2008.
- Lu, J., G.A. Vecchi, and T. Reichler, Expansion of the Hadley cell under global warming, *Geophys. Res. Lett.*, 34, L06805, doi: 10.1029/2006GL028443, 2007.
- Lu, J., G. Chen, and D.M.W. Frierson, Response of the zonal mean atmospheric circulation to El Niño versus global warming, *J. Clim.*, 21 (22), 5835-5851, doi: 10.1175/2008JCLI2200.1, 2008.
- Lu, J., C. Deser, and T. Reichler, Cause of the widening of the tropical belt since 1958, *Geophys. Res. Lett.*, 36, L03803, doi: 10.1029/2008GL036076, 2009.
- Lynch, A., P. Uotila, and J.J. Cassano, Changes in synoptic weather patterns in the polar regions in the twentieth and twenty-first centuries, Part 2: Antarctic, *Int. J. Climatol.*, 26 (9), 1181-1199, 2006.
- Madronich, S., and C. Granier, Impact of recent total ozone changes on tropospheric ozone photodissociation, hydroxyl radicals, and methane trends, *Geophys. Res. Lett.*, 19 (5), 465-467, 1992.
- Marshall, G.J., A. Orr, N.P.M. van Lipzig, and J.C. King, The impact of a changing Southern Hemisphere Annular Mode on Antarctic peninsula summer temperatures, *J. Clim.*, 19 (20), 5388-5404, doi: 10.1175/JCLI3844.1, 2006.
- Matthes, K., Y. Kuroda, K. Kodera, and U. Langematz, Transfer of the solar signal from the stratosphere to the troposphere: Northern winter, *J. Geophys. Res.*, 111, D06108, doi: 10.1029/2005JD006283, 2006.
- McLandress, C., and T.G. Shepherd, Simulated anthropogenic changes in the Brewer-Dobson circulation, including its extension to high latitudes, *J. Clim.*, 22 (6), 1516-1540, doi: 10.1175/2008JCLI2679.1, 2009.
- McLandress, C., A.I. Jonsson, D.A. Plummer, M.C. Reader, J.F. Scinocca, and T.G. Shepherd, Separating the dynamical effects of climate change and ozone depletion: Part 1. Southern Hemisphere stratosphere, *J. Clim.*, 23 (18), 5002-5020, doi: 10.1175/2010JCLI3586.1, 2010.
- Mears, C.A., and F.J. Wentz, Construction of the Remote Sensing Systems V3.2 atmospheric temperature records from the MSU and AMSU microwave sounders, *J. Atmos. Oceanic Technol.*, 26 (6), 1040-1056, doi: 10.1175/2008JTECHAI176.1, 2009.
- Meehl, G.A., C. Covey, T. Delworth, M. Latif, B. McAvaney, J.F.B. Mitchell, R.J. Stouffer, and K.E. Taylor, The WCRP CMIP3 multi-model dataset: A new era in climate change research, *Bull. Amer. Meteorol. Soc.*, 88 (9), 1383-1394, doi: 10.1175/BAMS-88-9-1383, 2007.
- Meehl, G.A., J.M. Arblaster, G. Branstator, and H. van Loon, A coupled air-sea response mechanism to solar forcing in the Pacific region, *J. Clim.*, 21 (12), 2883-2897, doi: 10.1175/2007JCLI1776.1, 2008.
- Meehl, G.A., J.M. Arblaster, K. Matthes, F. Sassi, and H. van Loon, Amplifying the Pacific climate system response to a small 11-year solar cycle forcing, *Science*, 325 (5944), 1114-1118, doi: 10.1126/science.1172872, 2009.
- Meneghini, B., I. Simmonds, and I.N. Smith, Association between Australian rainfall and the Southern Annular Mode, *Int. J. Climatol.*, 27, 109-121, doi: 10.1002/joc.1370, 2007.
- Meredith, M.P., and A.M. Hogg, Circumpolar response of the Southern Ocean eddy activity to a change in the Southern Annular Mode, *Geophys. Res. Lett.*, 33, L16608, doi: 10.1029/2006GL026499, 2006.
- Miller, R.L., G.A. Schmidt, and D.T. Shindell, Forced annular variations in the 20th century Intergovernmental Panel on Climate Change Fourth Assessment Report models, *J. Geophys. Res.*, 111, D18101, doi: 10.1029/2005JD006323, 2006.
- Monaghan, A.J., D.H. Bromwich, W. Chapman, and J.C. Comiso, Recent variability and trends of Antarctic near-surface temperature, *J. Geophys. Res.*, 113, D04105, doi: 10.1029/2007JD009094, 2008.
- Morgenstern, O., M.A. Giorgetta, K. Shibata, V. Eyring, D.W. Waugh, T.G. Shepherd, H. Akiyoshi, J. Austin, A.J.G. Baumgaertner, S. Bekki, P. Braesicke, C. Brühl, M.P. Chipperfield, D. Cugnet, M. Dameris, S. Dhomse, S.M. Frith, H. Garny, A. Gettelman, S.C. Hardiman, M.I. Hegglin, P. Jöckel, D.E. Kinnison, J.-F. Lamarque, E. Mancini, E. Manzini, M. Marchand, M. Michou, T. Nakamura, J.E. Nielsen, D. Olivie, G. Pitari, D.A. Plummer, E. Rozanov, J.F. Scinocca, D. Smale, H. Teyssède, M. Toohey, W. Tian, and Y. Yamashita, Review of the formulation of present-generation stratospheric chemistry-climate models and associated external forcings, *J. Geophys. Res.*, 115, D00M02, doi: 10.1029/2009JD013728, 2010a.
- Morgenstern, O., H. Akiyoshi, S. Bekki, P. Braesicke, N. Butchart, M.P. Chipperfield, D. Cugnet, M. Deushi, S.S. Dhomse, R.R. Garcia, A. Gettelman, N.P. Gillett, S.C. Hardiman, J. Jumelet, D.E. Kinnison, J.-F. Lamarque, F. Lott, M. Marchand, M. Michou, T. Nakamura, D. Olivie, T. Peter, D. Plummer, J.A.

- Pyle, E. Rozanov, D. Saint-Martin, J.F. Scinocca, K. Shibata, M. Sigmond, D. Smale, H. Teyssède, W. Tian, A. Voldoire, and Y. Yamashita, Anthropogenic forcing of the Northern Annular Mode in CC-MVal-2 models, *J. Geophys. Res.*, *115* (D00M03), doi: 10.1029/2009JD013347, 2010b.
- Mote, P.W., K.H. Rosenlof, M.E. McIntyre, E.S. Carr, J.C. Gille, J.R. Holton, J.S. Kinnerson, H.C. Pumphrey, J.M. Russell, and J.W. Waters, An atmospheric tape recorder: The imprint of tropical tropopause temperatures on stratospheric water vapor, *J. Geophys. Res.*, *101* (D2), 3989-4006, 1996.
- Nielsen, J.K., N. Larsen, F. Cairo, G. Di Donfrancesco, J.M. Rosen, G. Durré, G. Held, and J.P. Pomereau, Solid particles in the tropical lowest stratosphere, *Atmos. Chem. Phys.*, *7*, 685-695, 2007.
- Notholt, J., B.P. Luo, S. Füglistaler, D. Weisenstein, M. Rex, M.G. Lawrence, H. Bingemer, I. Wohltmann, T. Corti, T. Warneke, R. von Kuhlmann, and T. Peter, Influence of tropospheric SO₂ emissions on particle formation and the stratospheric humidity, *Geophys. Res. Lett.*, *32*, L07810, doi: 10.1029/2004GL022159, 2005.
- Oke, P.R., and M.H. England, Oceanic response to changes in the latitude of the Southern Hemisphere subpolar westerly winds, *J. Clim.*, *17* (5), 1040-1054, 2004.
- Olsen, S.C., C.A. McLinden, and M.J. Prather, Stratospheric N₂O-NO_y system: Testing uncertainties in a three-dimensional framework, *J. Geophys. Res.*, *106* (D22), 28771-28784, 2001.
- Oltmans, S.J., H. Vömel, D.J. Hofmann, K.H. Rosenlof, and D. Kley, The increase in stratospheric water vapor from balloonborne frostpoint hygrometer measurements at Washington D.C., and Boulder, Colorado, *Geophys. Res. Lett.*, *27* (21), 3453-3456, 2000.
- Oman, L., D.W. Waugh, S. Pawson, R.S. Stolarski, and P.A. Newman, On the influence of anthropogenic forcings on changes in the stratospheric mean age, *J. Geophys. Res.*, *114*, doi: 10.1029/2008JD010378, 2009.
- Ordóñez, C., D. Brunner, J. Staehelin, P. Hadjinicolaou, J.A. Pyle, M. Jonas, H. Wernli, and A.S.H. Prevot, Strong influence of lowermost stratospheric ozone on lower tropospheric background ozone changes over Europe, *Geophys. Res. Lett.*, *34*, L07805, doi: 10.1029/2006GL029113, 2007.
- Pawson, S., K. Labitzke, and S. Leder, Stepwise changes in stratospheric temperature, *Geophys. Res. Lett.*, *25* (12), 2157-2160, 1998.
- Perlwitz, J., S. Pawson, R.L. Fogt, J.E. Nielsen, and W.D. Neff, Impact of stratospheric ozone hole recovery on Antarctic climate, *Geophys. Res. Lett.*, *35*, L08714, doi: 10.1029/2008GL033317, 2008.
- Peter, T., C. Marcolli, P. Spichtinger, T. Corti, M.B. Baker, and T. Koop, When dry air is too humid, *Science*, *314* (5804), 1399-1402, doi: 10.1126/science.1135199, 2006.
- Pezza, A.B., I. Simmonds, and J.A. Renwick, Southern hemisphere cyclones and anticyclones: Recent trends and links with decadal variability in the Pacific Ocean, *Int. J. Climatol.*, *27* (11), 1403-1419, 2007.
- Pezza, A.B., T. Durrant, I. Simmonds, and I. Smith, Southern Hemisphere synoptic behavior in extreme phases of SAM, ENSO, sea ice extent, and southern Australia rainfall, *J. Clim.*, *21* (21), 5566-5584, doi: 10.1175/2008JCLI2128.1, 2008.
- Pitari, G., E. Mancini, V. Rizi, and D.T. Shindell, Impact of future climate and emission changes on stratospheric aerosols and ozone, *J. Atmos. Sci.*, *59* (3), 414-440, 2002.
- Plumb, R.A., and J. Eluszkiewicz, The Brewer-Dobson circulation: Dynamics of the tropical upwelling, *J. Atmos. Sci.*, *56*, 868-890, 1999.
- Polvani, L.M., and P.J. Kushner, Tropospheric response to stratospheric perturbations in a relatively simple general circulation model, *Geophys. Res. Lett.*, *29*, doi: 10.1029/2001GL014284, 2002.
- Portmann, R.W., and S. Solomon, Indirect radiative forcing of the ozone layer during the 21st century, *Geophys. Res. Lett.*, *34*, L02813, doi: 10.1029/2006GL028252, 2007.
- Prinn, R.G., J. Huang, R.F. Weiss, D.M. Cunnold, P.J. Fraser, P.G. Simmonds, A. McCulloch, C. Harth, S. Reimann, P. Salameh, S. O'Doherty, R.H.J. Wang, L.W. Porter, B.R. Miller, and P.B. Krummel, Evidence for variability of atmospheric hydroxyl radicals over the past quarter century, *Geophys. Res. Lett.*, *32*, L07809, doi: 10.1029/2004GL022228, 2005.
- Punge, H.J., and M.A. Giorgetta, Net effect of the QBO in a chemistry climate model, *Atmos. Chem. Phys.*, *8* (21), 6505-6525, 2008.
- Radko, T., and J. Marshall, Equilibration of a warm pumped lens on a β plane, *J. Phys. Oceanogr.*, *33* (4), 885-899, 2003.
- Ramaswamy, V., M.L. Chanin, J. Angell, J. Barnett, D. Gaffen, M. Gelman, P. Keckhut, Y. Koshelkov, K. Labitzke, J.J.R. Lin, A. O'Neill, J. Nash, W. Randel, R. Rood, K. Shine, M. Shiotani, and R. Swinbank, Stratospheric temperature trends: Observations and model simulations, *Rev. Geophys.*, *39* (1), 71-122, 2001.
- Ramaswamy, V., M.D. Schwarzkopf, W.J. Randel, B.D. Santer, B.J. Soden, and G.L. Stenchikov, Anthropogenic and natural influences in the evolution of lower stratospheric cooling, *Science*, *311* (5764), 1138-1141, 2006.

- Randel, W.J., Variability and trends in stratospheric temperature and water vapor, in *The Stratosphere: Dynamics, Transport and Chemistry*, A Festschrift to Celebrate Alan Plumb's 60th Birthday, American Geophysical Union, in press, 2010.
- Randel, W.J., and F. Wu, Biases in stratospheric and tropospheric temperature trends derived from historical radiosonde data, *J. Clim.*, *19* (10), 2094-2104, 2006.
- Randel, W.J., and F. Wu, A stratospheric ozone profile data set for 1979–2005: Variability, trends, and comparisons with column ozone data, *J. Geophys. Res.*, *112*, D06313, doi: 10.1029/2006JD007339, 2007.
- Randel, W.J., F. Wu, S.J. Oltmans, K. Rosenlof, and G.E. Nedoluha, Interannual changes of stratospheric water vapor and correlations with tropical tropopause temperatures, *J. Atmos. Sci.*, *61* (17), 2133-2148, 2004.
- Randel, W.J., F. Wu, H. Vömel, G.E. Nedoluha, and P. Forster, Decreases in stratospheric water vapor after 2001: Links to changes in the tropical tropopause and the Brewer-Dobson circulation, *J. Geophys. Res.*, *111*, D12312, doi: 10.1029/2005JD006744, 2006.
- Randel, W.J., K.P. Shine, J. Austin, J. Barnett, C. Claud, N.P. Gillett, P. Keckhut, U. Langematz, R. Lin, C. Long, C. Mears, A. Miller, J. Nash, D.J. Seidel, D.W.J. Thompson, F. Wu, and S. Yoden, An update of observed stratospheric temperature trends, *J. Geophys. Res.*, *114*, D02107, doi: 10.1029/2008JD010421, 2009.
- Rao, V.B., A.M.C. do Carmo, and S.H. Franchito, Interannual variations of storm tracks in the Southern Hemisphere and their connections with the Antarctic oscillation, *Int. J. Climatol.*, *23* (12), 1537-1545, doi: 10.1002/joc.948, 2003.
- Rayner, N.A., D.E. Parker, E.B. Horton, C.K. Folland, L.V. Alexander, D.P. Rowell, E.C. Kent, and A. Kaplan, Global analyses of sea surface temperature, sea ice, and night marine air temperature since the late nineteenth century, *J. Geophys. Res.*, *108*, 4407, doi: 10.1029/2002JD002670, 2003.
- Reed, R.J., and C.L. Vleck, The annual temperature variation in the lower tropical stratosphere, *J. Atmos. Sci.*, *26* (1), 163-167, 1969.
- Reichler, T., Changes in the atmospheric circulation as indicator of climate change, in *Climate Change: Observed Impacts on Planet Earth*, edited by T. M. Letcher, Elsevier BV, The Netherlands, ISBN: 978-0-444-53301-2, pp. 145-164, 2009.
- Renwick, J., and D. Thompson, The Southern Annular Mode and New Zealand climate, *Water Atmos.*, *14* (2), 24-25, 2006.
- Rind, D., D. Shindell, P. Lonergan, and N.K. Balachandran, Climate change and the middle atmosphere. Part III: The doubled CO₂ climate revisited, *J. Clim.*, *11* (5), 876-894, 1998.
- Rind, D., J. Lean, J. Lerner, P. Lonergan, and A. Leboisssitier, Exploring the stratospheric/tropospheric response to solar forcing, *J. Geophys. Res.*, *113*, D24103, doi: 10.1029/2008JD010114, 2008.
- Ring, M.J., and R.A. Plumb, The response of a simplified GCM to axisymmetric forcings: Applicability of the fluctuation–dissipation theorem, *J. Atmos. Sci.*, *65* (12), 3880-3898, 2008.
- Robock, A., Volcanic eruptions and climate, *Rev. Geophys.*, *38* (2), 191-219, 2000.
- Rohs, S., C. Schiller, M. Riese, A. Engel, U. Schmidt, T. Wetter, I. Levin, T. Nakazawa, and S. Aoki, Long-term changes of methane and hydrogen in the stratosphere in the period 1978-2003 and their impact on the abundance of stratospheric water vapor, *J. Geophys. Res.*, *111*, D14315, doi: 10.1029/2005JD006877, 2006.
- Rosenlof, K.H., Transport changes inferred from HALOE water and methane measurements, *J. Meteorol. Soc. Japan*, *80* (48), 831-848, 2002.
- Rosenlof, K.H., and J.R. Holton, Estimates of the stratospheric residual circulation using the downward control principle, *J. Geophys. Res.*, *98* (D6), 10465-10479, 1993.
- Rosenlof, K.H., and G.C. Reid, Trends in the temperature and water vapor content of the tropical lower stratosphere: Sea surface connection, *J. Geophys. Res.*, *113*, D06107, doi: 10.1029/2007JD009109, 2008.
- Rosenlof, K.H., S.J. Oltmans, D. Kley, J.M. Russell III, E.-W. Chiou, W.P. Chu, D.G. Johnson, K.K. Kelly, H.A. Michelsen, G.E. Nedoluha, E.E. Remsburg, G.C. Toon, and M.P. McCormick, Stratospheric water vapor increases over the past half-century, *Geophys. Res. Lett.*, *28* (7), 1195-1198, 2001.
- Roy, I., and J.D. Haigh, Solar cycle signals in sea level pressure and sea surface temperature, *Atmos. Chem. & Phys.*, *10*, 3147-3153, 2010.
- Russell, J.L., K.W. Dixon, A. Gnanadesikan, R.J. Stouffer, and J.R. Toggweiler, The Southern Hemisphere westerlies in a warming world: Propping open the door to the deep ocean, *J. Clim.*, *19* (24), 6382-6390, doi: 10.1175/JCLI3984.1, 2006.
- Santer, B.D., M.F. Wehner, T.M.L. Wigley, R. Sausen, G.A. Meehl, K.E. Taylor, C. Ammann, J. Arblaster, W.M. Washington, J.S. Boyle, and W. Brüggemann, Contributions of anthropogenic and natural forcing to recent tropopause height changes, *Science*, *301* (5632), 479-483, doi: 10.1126/science.1084123, 2003.
- Scaife, A.A., N. Butchart, C.D. Warner, D. Stainforth, W. Norton, and J. Austin, Realistic quasi-biennial

- oscillations in a simulation of the global climate, *Geophys. Res. Lett.*, *27* (21), 3481-3484, 2000a.
- Scaife, A.A., J. Austin, N. Butchart, S. Pawson, M. Keil, J. Nash, and I.N. James, Seasonal and interannual variability of the stratosphere diagnosed from UKMO TOVS analyses, *Quart. J. Roy. Meteorol. Soc.*, *126* (568), 2585-2604, 2000b.
- Scaife, A.A., N. Butchart, D.R. Jackson, and R. Swinbank, Can changes in ENSO activity help to explain increasing stratospheric water vapor?, *Geophys. Res. Lett.*, *30*, 1880, doi: 10.1029/2003GL017591, 2003.
- Scherer, M., H. Vömel, S. Fueglistaler, S.J. Oltmans, and J. Staehelin, Trends and variability of midlatitude stratospheric water vapour deduced from the re-evaluated Boulder balloon series and HALOE, *Atmos. Chem. Phys.*, *8*, 1391-1402, 2008.
- Schiller, C., J.-U. Groöb, P. Konopka, F. Plöger, F.H. Silva dos Santos, and N. Spelten, Hydration and dehydration at the tropical tropopause, *Atmos. Chem. Phys.*, *9*, 9647-9660, doi: 10.5194/acp-9-9647-2009, 2009.
- Schultz, M.G., T. Diehl, G.P. Brasseur, and W. Zittel, Air pollution and climate forcing impacts of a global hydrogen economy, *Science*, *302* (5645), 624-627, doi: 10.1126/science.1089527, 2003.
- Schwarzkopf, M.D., and V. Ramaswamy, Evolution of stratospheric temperature in the 20th century, *Geophys. Res. Lett.*, *35*, L03705, doi: 10.1029/2007GL032489, 2008.
- Scinocca, J.F., M.C. Reader, D.A. Plummer, M. Sigmond, P.J. Kushner, T.G. Shepherd, and A.R. Ravishankara, Impact of sudden Arctic sea-ice loss on stratospheric polar ozone recovery, *Geophys. Res. Lett.*, *36*, L24701, doi: 10.1029/2009GL041239, 2009.
- Screen, J.A., N.P. Gillett, D.P. Stevens, G.J. Marshall, and H.K. Roscoe, The role of eddies in the Southern Ocean temperature response to the Southern Annular Mode, *J. Clim.*, *22* (3), 806-818, doi: 10.1175/2008JCLI2416.1, 2009.
- Seager, R., M. Ting, I. Held, Y. Kushnir, J. Lu, G. Vecchi, H.P. Huang, N. Harnik, A. Leetmaa, N.C. Lau, C. Li, J. Velez and N. Naik, Model projections of an imminent transition to a more arid climate in Southwestern North America, *Science*, *316* (5828), 1181-1184, doi: 10.1126/science.1139601, 2007.
- Seidel, D.J., and J.R. Lanzante, An assessment of three alternatives to linear trends for characterizing global atmospheric temperature changes, *J. Geophys. Res.*, *109*, D14108, doi: 10.1029/2003JD004414, 2004.
- Seidel, D.J., and W.J. Randel, Variability and trends in the global tropopause estimated from radiosonde data, *J. Geophys. Res.*, *111*, D21101, doi: 10.1029/2006JD007363, 2006.
- Seidel, D.J., and W.J. Randel, Recent widening of the tropical belt: Evidence from tropopause observations, *J. Geophys. Res.*, *112*, D20113, doi: 10.1029/2007JD008861, 2007.
- Seidel, D.J., Q. Fu, W.J. Randel, and T.J. Reichler, Widening of the tropical belt in a changing climate, *Nature Geosci.*, *1*, 21-24, doi: 10.1038/nego.2007.38, 2008.
- Seidel, D.J., F.H. Berger, H.J. Diamond, J. Dykema, D. Goodrich, F. Immmler, W. Murray, T. Peterson, D. Sisterson, M. Sommer, P. Thorne, H. Vömel, and J. Wang, Reference upper-air observations for climate: Rationale, progress, and plans, *Bull. Amer. Meteorol. Soc.*, *90* (3), 361-369, doi: 10.1175/2008BAMS2540.1, 2009.
- Semeniuk, K., and T.G. Shepherd, Mechanism for tropical upwelling in the stratosphere, *J. Atmos. Sci.*, *58* (21), 3097-3115, 2001.
- Shepherd, T.G., and A.I. Jonsson, On the attribution of stratospheric ozone and temperature changes to changes in ozone-depleting substances and well mixed greenhouse gases, *Atmos. Chem. Phys.*, *8* (5), 1435-1444, 2008.
- Sherwood, S., A microphysical connection among biomass burning, cumulus clouds, and stratospheric moisture, *Science*, *295* (5558), 1272-1275, doi: 10.1126/science.1065080, 2002.
- Sherwood, S.C., J.R. Lanzante, and C. Meyer, Radiosonde daytime biases and late-20th century warming, *Science*, *309* (5740), 1556-1559, doi: 10.1126/science.1115640, 2005.
- Sherwood, S.C., C.L. Meyer, R.J. Allen, and H.A. Titchner, Robust tropospheric warming revealed by iteratively homogenized radiosonde data, *J. Clim.*, *21* (20), 5336-5352, doi: 10.1175/2008JCLI2320.1, 2008.
- Shindell, D.T., Climate and ozone response to increased stratospheric water vapor, *Geophys. Res. Lett.*, *28* (8), 1551-1554, 2001.
- Shindell, D.T., and V. Grewe, Separating the influence of halogen and climate changes on ozone recovery in the upper stratosphere, *J. Geophys. Res.*, *107*, doi: 10.1029/2001JD000420, 2002.
- Shindell, D., and G.A. Schmidt, Southern Hemisphere climate response to ozone changes and greenhouse gas increases, *Geophys. Res. Lett.*, *31*, L18209, doi: 10.1029/2004GL020724, 2004.
- Shindell, D.T., D. Rind, N. Balachandran, J. Lean, and P. Lonergan, Solar cycle variability, ozone, and climate, *Science*, *284* (5412), 305-308, 1999.
- Shindell, D.T., G.A. Schmidt, M.E. Mann, and G. Faluvegi, Dynamic winter climate response to large tropical volcanic eruptions since 1600, *J. Geophys. Res.*, *109*, D05104, doi: 10.1029/2003JD004151, 2004.
- Shindell, D.T., G. Faluvegi, R.L. Miller, G.A. Schmidt,

- J.E. Hansen, and S. Sun, Solar and anthropogenic forcing of tropical hydrology, *Geophys. Res. Lett.*, 33, L24706, doi: 10.1029/2006GL027468, 2006.
- Shine, K.P., M.S. Bourqui, P.M.F. Forster, S.H.E. Hare, U. Langematz, P. Braesicke, V. Grewe, M. Ponater, C. Schnadt, C.A. Smith, J.D. Haigh, J. Austin, N. Butchart, D.T. Shindell, W.J. Randel, T. Nagashima, R.W. Portmann, S. Solomon, D.J. Seidel, J. Lanzante, S. Klein, V. Ramaswamy, and M.D. Schwarzkopf, A comparison of model-simulated trends in stratospheric temperatures, *Quart. J. Roy. Meteorol. Soc.*, 129 (590), 1565-1588, 2003.
- Shine, K.P., J.J. Barnett, and W.J. Randel, Temperature trends derived from Stratospheric Sounding Unit radiances: The effect of increasing CO₂ on the weighting function, *Geophys. Res. Lett.*, 35, L02710, doi: 10.1029/2007GL032218, 2008.
- Sigmond, M., J.C. Fyfe, and J.F. Scinocca, Does the ocean impact the atmospheric response to stratospheric ozone depletion?, *Geophys. Res. Lett.*, 37, L12706, doi: 10.1029/2010GL043773, 2010.
- Simmonds, I., and K. Keay, Variability of Southern Hemisphere extratropical cyclone behavior, 1958–97, *J. Clim.*, 13 (3), 550-561, 2000.
- Simpson, I.R., M. Blackburn, and J.D. Haigh, The role of eddies in driving the tropospheric response to stratospheric heating perturbations, *J. Atmos. Sci.*, 66 (5), 1347-1365, doi: 10.1175/2008JAS2758.1, 2009.
- Solomon, S., R.W. Portmann, and D.W.J. Thompson, Contrasts between Antarctic and Arctic ozone depletion, *Proc. Natl. Acad. Sci.*, 104 (2), 445-449, doi: 10.1073/pnas.0604895104, 2007.
- Solomon, S., K.H. Rosenlof, R.W. Portmann, J.S. Daniel, S.M. Davis, T.J. Sanford, and G.-K. Plattner, Contributions of stratospheric water vapor to decadal changes in the rate of global warming, *Science*, 327 (5970), 1219-1223, doi: 10.1126/science.1182488, 2010.
- Son, S.-W., L.M. Polvani, D.W. Waugh, H. Akiyoshi, R. Garcia, D. Kinnison, S. Pawson, E. Rozanov, T.G. Shepherd, and K. Shibata, The impact of stratospheric ozone recovery on the Southern Hemisphere westerly jet, *Science*, 320 (5882), 1486-1489, doi: 10.1126/science.1155939, 2008.
- Son, S.-W., L.M. Polvani, D.W. Waugh, T. Birner, H. Akiyoshi, R.R. Garcia, A. Gettelman, D.A. Plummer, and E. Rozanov, The impact of stratospheric ozone recovery on tropopause height trends, *J. Clim.*, 22 (2), 429-445, doi: 10.1175/2008JCLI2215.1, 2009a.
- Son, S.-W., N.F. Tandon, L.M. Polvani, and D.W. Waugh, Ozone hole and Southern Hemisphere climate change, *Geophys. Res. Lett.*, 36, L15705, doi: 10.1029/2009GL038671, 2009b.
- Son, S.-W., E.P. Gerber, J. Perlwitz, L.M. Polvani, N.P. Gillett, K.-H. Seo, V. Eyring, T.G. Shepherd, D. Waugh, H. Akiyoshi, J. Austin, A. Baumgaertner, S. Bekki, P. Braesicke, C. Brühl, N. Butchart, M.P. Chipperfield, D. Cugnet, M. Dameris, S. Dhomse, S. Frith, H. Garny, R. Garcia, S.C. Hardiman, P. Jöckel, J.F. Lamarque, E. Mancini, M. Marchand, M. Michou, T. Nakamura, O. Morgenstern, G. Pitari, D.A. Plummer, J. Pyle, E. Rozanov, J.F. Scinocca, K. Shibata, D. Smale, H. Teyssède, W. Tian, and Y. Yamashita, Impact of stratospheric ozone on Southern Hemisphere circulation change: A multimodel assessment, *J. Geophys. Res.*, 115, D00M07, doi: 10.1029/2010JD014271, 2010.
- Song, Y., and W.A. Robinson, Dynamical mechanisms for stratospheric influences on the troposphere, *J. Atmos. Sci.*, 61 (14), 1711-1725, 2004.
- Soukharev, B.E., and L.L. Hood, Solar cycle variation of stratospheric ozone: Multiple regression analysis of long-term satellite data sets and comparisons with models, *J. Geophys. Res.*, 111, D20314, doi: 10.1029/2006JD007107, 2006.
- SPARC (Stratospheric Processes And their Role in Climate), *SPARC Assessment of Stratospheric Aerosol Properties*, edited by L. Thomason, and Th. Peter, World Climate Research Program Report 124, SPARC Report 4, WMO/TD-No. 1295, 346 pp., Verrières le Buisson, France, 2006.
- SPARC CCMVal, *SPARC Report on the Evaluation of Chemistry-Climate Models*, edited by V. Eyring, T.G. Shepherd, and D.W. Waugh, Stratospheric Processes And their Role in Climate (SPARC) Report No. 5, WCRP-132, WMO/TD-No. 1526, available: <http://www.atmosph.physics.utoronto.ca/SPARC>, 2010.
- Sprintall, J., Long-term trends and interannual variability of temperature in Drake Passage, *Prog. Ocean.*, 77 (4), 316-330, doi: 10.1016/j.pocean.2006.06.004, 2008.
- Steig, E.J., D.P. Schneider, S.D. Rutherford, M.E. Mann, J.C. Comiso, and D.T. Shindell, Warming of the Antarctic ice sheet surface since the 1957 International Geophysical Year, *Nature*, 457, 459-462, doi: 10.1038/nature07669, 2009.
- Stenchikov, G., K. Hamilton, R.J. Stouffer, A. Robock, V. Ramaswamy, B. Santer, and H.-F. Graf, Arctic Oscillation response to volcanic eruptions in the IPCC AR4 climate models, *J. Geophys. Res.*, 111, D07107, doi: 10.1029/2005JD006286, 2006.
- Stenchikov, G., T.L. Delworth, V. Ramaswamy, R.J. Stouffer, A. Wittenberg, and F. Zeng, Volcanic signals in oceans, *J. Geophys. Res.*, 114, D16104, doi: 10.1029/2008JD011673, 2009.
- Stevenson, D.S., F.J. Dentener, M.G. Schultz, K. Ellingsen, T.P.C. vanNoije, O. Wild, G. Zeng, M. Anann, C.S. Atherton, N. Bell, D.J. Bergmann, I. Bey,

- T. Butler, J. Cofala, W.J. Collins, R.G. Derwent, R.M. Doherty, J. Drevet, H.J. Eskes, A.F. Fiore, M. Gauss, D.A. Hauglustaine, L.W. Horowitz, I.S.A. Isaksen, M.C. Krol, J.-F. Lamarque, M.G. Lawrence, V. Montanaro, J.-F. Müller, G. Pitari, M.J. Prather, S.A. Pyle, S. Rast, J.M. Rodriguez, M.G. Sanderson, H.H. Savage, D.T. Shindell, S.E. Strahan, K. Sudo, and S. Szopa, Multi-model ensemble of present-day and near-future tropospheric ozone, *J. Geophys. Res.*, *111*, D8301, doi: 10.1029/2005JD006338, 2006.
- Stolarski, R.S., A.R. Douglass, P.A. Newman, S. Pawson, and M.R. Schoeberl, Relative contribution of greenhouse gases and ozone-depleting substances to temperature trends in the stratosphere: A chemistry-climate model study, *J. Clim.*, *23* (1), 28-42, doi: 10.1175/2009JCLI2955.1, 2010.
- Sudo, K., M. Takahashi, and H. Akimoto, Future changes in stratosphere-troposphere exchange and their impacts on future tropospheric ozone simulations, *Geophys. Res. Lett.*, *30* (24), 2256, doi: 10.1029/2003GL018526, 2003.
- Takahashi, M., Simulation of the Quasi-Biennial Oscillation in a general circulation model, *Geophys. Res. Lett.*, *26* (9), 1307-1310, 1999.
- Terao, Y., J.A. Logan, A.R. Douglass, and R.S. Stolarski, Contribution of stratospheric ozone to the interannual variability of tropospheric ozone in the northern extratropics, *J. Geophys. Res.*, *113*, D18309, doi: 10.1029/2008JD009854, 2008.
- Thejll, P., B. Christiansen, and H. Gleisner, On correlations between the North Atlantic Oscillation, geopotential heights, and geomagnetic activity, *Geophys. Res. Lett.*, *30*, 1347, doi: 10.1029/2002GL016598, 2003.
- Thomason, L., L.R. Poole, and T. Deshler, A global climatology of stratospheric aerosol surface area density deduced from Stratospheric Aerosol and Gas Experiment II measurements: 1984-1994, *J. Geophys. Res.*, *102* (D7), 8967-8976, 1997.
- Thompson, D.W.J., and J.M. Wallace, Annular modes in the extratropical circulation. Part I: Month-to-month variability, *J. Clim.*, *13* (5), 1000-1016, 2000.
- Thompson, D.W.J., and S. Solomon, Interpretation of recent Southern Hemisphere climate change, *Science*, *296* (5569), 895-899, 2002.
- Thompson, D.W.J., and S. Solomon, Recent stratospheric climate trends as evidenced in radiosonde data: Global structure and tropospheric linkages, *J. Clim.*, *18* (22), 4785-4795, 2005.
- Thompson, D.W.J., and S. Solomon, Understanding recent stratospheric climate change, *J. Clim.*, *22* (8), 1934-1943, doi: 10.1175/2008JCLI2482.1, 2009.
- Thompson, D.W.J., J.C. Furtado, and T.G. Shepherd, On the tropospheric response to anomalous stratospheric wave drag and radiative heating, *J. Atmos. Sci.*, *63* (10), 2616-2629, 2006.
- Thorne, P.W. (editor), Global climate, Chapter 2 in *State of the Climate 2008*, edited by T.C. Peterson and M.O. Baringer, Special Supplement to *Bull. Amer. Meteorol. Soc.*, *90* (8), 196 pp., 2009.
- Thorne, P.W., D.E. Parker, S.F.B. Tett, P.D. Jones, M. McCarthy, H. Coleman, and P. Brohan, Revisiting radiosonde upper air temperatures from 1958 to 2002, *J. Geophys. Res.*, *110*, D18105, doi: 10.1029/2004JD005753, 2005.
- Tian, W.S., M.P. Chipperfield, and D. Lu, Impact of increasing stratospheric water vapor on ozone depletion and temperature change, *Adv. Atmos. Sci.*, *26* (3), 423-437, doi: 10.1007/s00376-009-0423-3, 2009.
- Tie, X.X., and G. Brasseur, The response of stratospheric ozone to volcanic eruptions: Sensitivity to atmospheric chlorine loading, *Geophys. Res. Lett.*, *22* (22), 3035-3038, 1995.
- Tromp, T.K., R.-L. Shia, M. Allen, J.M. Eiler, and Y.L. Yung, Potential environmental impact of a hydrogen economy on the stratosphere, *Science*, *300* (5626), 1740-1742, doi: 10.1126/science.1085169, 2003.
- Turner, J., S.R. Colwell, G.J. Marshall, T.A. Lachlan-Cope, A.M. Carleton, P.D. Jones, V. Lagun, P.A. Reid, and S. Iagovkina, Antarctic climate change during the last 50 years, *Int. J. Climatol.*, *25* (3), 279-294, doi: 10.1002/joc.1130, 2005.
- Turner, J., J.C. Comiso, G.J. Marshall, T.A. Lachlan-Cope, T. Bracegirdle, T. Maksym, M.P. Meredith, Z. Wang, and A. Orr, Non-annular atmospheric circulation change induced by stratospheric ozone depletion and its role in the recent increase of Antarctic sea ice extent, *Geophys. Res. Lett.*, *36*, L08502, doi: 10.1029/2009GL037524, 2009.
- Udagawa, Y., Y. Tachibana, and K. Yamazaki, Modulation in interannual sea ice patterns in the Southern Ocean in association with large-scale atmospheric mode shift, *J. Geophys. Res.*, *114*, D21103, doi: 10.1029/2009JD011807, 2009.
- Ueyama, R., and J.M. Wallace, To what extent does high-latitude wave forcing drive tropical upwelling in the Brewer-Dobson Circulation?, *J. Atmos. Sci.*, *67* (4), 1232-1246, doi: 10.1175/2009JAS3216.1, 2010.
- Ummenhofer, C.C., A. Sen Gupta, and M.H. England, Causes of late twentieth-century trends in New Zealand precipitation, *J. Clim.*, *22* (1), 3-19, doi: 10.1175/2008JCLI2323.1, 2009.
- van Loon, H., and G.A. Meehl, The response in the Pacific to the sun's decadal peaks and contrasts to cold events in the Southern Oscillation, *J. Atmos. Solar Terr. Phys.*, *70* (7), 1046-1055, doi: 10.1016/j.jastp.2008.01.009, 2008.
- van Loon, H., G.A. Meehl, and D. Shea, Coupled air-sea

- response to solar forcing in the Pacific region during northern winter, *J. Geophys. Res.*, *112*, D02108, doi: 10.1029/2006JD007378, 2007.
- Velders, G.J.M., S.O. Andersen, J.S. Daniel, D.W. Fahey, and M. McFarland, The importance of the Montreal Protocol in protecting climate, *Proc. Natl. Acad. Sci.*, *104* (12), 4814-4819, doi: 10.1073/pnas.0610328104, 2007.
- Vera, C., Interannual and interdecadal variability of atmospheric synoptic-scale activity in the Southern Hemisphere, *J. Geophys. Res.*, *108*, 8077, doi: 10.1029/2000JC000406, 2003.
- Vernier, J.P., J.P. Pommereau, A. Garnier, J. Pelon, N. Larsen, J. Nielsen, T. Christensen, F. Cairo, L.W. Thomason, T. Leblanc, and I.S. McDerimid, Tropical stratospheric aerosol layer from CALIPSO lidar observations, *J. Geophys. Res.*, *114*, D00H10, doi: 10.1029/2009JD011946, 2009.
- Vömel, H., D.E. David, and K. Smith, Accuracy of tropospheric and stratospheric water vapor measurements by the cryogenic frost point hygrometer: Instrumental details and observations, *J. Geophys. Res.*, *112*, D08305, doi: 10.1029/2006JD007224, 2007.
- Waugh, D., W. Randel, S. Pawson, P. Newman, and E. Nash, Persistence of the lower stratospheric polar vortices, *J. Geophys. Res.*, *104* (D22), 27191-27201, 1999.
- Waugh, D.W., L. Oman, P.A. Newman, R.S. Stolarski, S. Pawson, J.E. Nielsen, and J. Perlwitz, Effect of zonal asymmetries in stratospheric ozone on simulated Southern Hemisphere climate trends, *Geophys. Res. Lett.*, *36*, L18701, doi: 10.1029/2009GL040419, 2009.
- Weinstock, E.M., J.B. Smith, D.S. Sayres, J.V. Pittman, J.R. Spackman, E.J. Hints, T.F. Hanisco, E.J. Moyer, J.M. St. Clair, M.R. Sargent, and J.G. Anderson, Validation of the Harvard Lyman- α in situ water vapor instrument: Implications for the mechanisms that control stratospheric water vapor, *J. Geophys. Res.*, *114*, D23301, doi: 10.1029/2009JD012427, 2009.
- Weissenstein, D., G. Yue, M. Ko, N.-D. Sze, J. Rodriguez, and C. Scott, A two-dimensional model of sulfur species and aerosols, *J. Geophys. Res.*, *102* (D11), 13019-13035, 1997.
- Wetzel, P., A. Winguth, and E. Maier-Reimer, Sea-to-air CO₂ flux from 1948 to 2003: A model study, *Global Biogeochem. Cycles*, *19*, GB2005, doi: 10.1029/2004GB002339, 2005.
- White W.B., and Z. Liu, Non-linear alignment of El Niño to the 11-yr solar cycle, *Geophys. Res. Lett.*, *35*, L19607, doi: 10.1029/2008GL034831, 2008.
- Wild, O., Modelling the global tropospheric ozone budget: Exploring the variability in current models, *Atmos. Chem. Phys.*, *7* (10), 2643-2660, doi: 10.5194/acp-7-2643-2007, 2007.
- Woollings, T., Vertical structure of anthropogenic zonal-mean atmospheric circulation change, *Geophys. Res. Lett.*, *35*, L19702, doi: 10.1029/2008GL034883, 2008.
- WMO (World Meteorological Organization), *Scientific Assessment of Ozone Depletion: 2002*, Global Ozone Research and Monitoring Project-Report No. 47, 498 pp., Geneva, Switzerland, 2003.
- WMO (World Meteorological Organization), *Scientific Assessment of Ozone Depletion: 2006*, Global Ozone Research and Monitoring Project-Report No. 50, 572 pp., Geneva, Switzerland, 2007.
- Wu, S., L.J. Mickley, D.J. Jacob, J.A. Logan, R.M. Yantosca, and D. Rind, Why are there large differences between models in global budgets of tropospheric ozone?, *J. Geophys. Res.*, *112*, D05302, doi: 10.1029/2006JD007801, 2007.
- Yin, J.H., A consistent poleward shift of the storm tracks in simulations of 21st century climate, *Geophys. Res. Lett.*, *32*, L18701, doi: 10.1029/2005GL023684, 2005.
- Zazulie, N., M. Rusticucci, and S. Solomon, Changes in climate at high southern latitudes: A unique daily record at Orcadas spanning 1903-2008, *J. Clim.*, *23*, 189-196, doi: 10.1175/2009JCLI3074.1, 2010.
- Zeng, G., and J.A. Pyle, Changes in tropospheric ozone between 2000 and 2100 modeled in a chemistry-climate model, *Geophys. Res. Lett.*, *30* (7), 1392, doi: 10.1029/2002GL016708, 2003.
- Zeng, G., J.A. Pyle, and P.J. Young, Impact of climate change on tropospheric ozone and its global budgets, *Atmos. Chem. Phys.*, *8*, 369-387, 2008.
- Zhang, J., Increasing Antarctic sea ice under warming atmospheric and oceanic conditions, *J. Clim.*, *20* (11), doi: 10.1175/JCLI4136.1, 2007.
- Zhou, J., and K.-K. Tung, Solar cycles in 150 years of global sea-surface temperature data, *J. Clim.*, *23* (12), 3234-3248, doi: 10.1175/2010JCLI3232.1, 2010.
- Zhou, S., M.E. Gelman, A.J. Miller, and J.P. McCormack, An inter-hemisphere comparison of the persistent stratospheric polar vortex, *Geophys. Res. Lett.*, *27* (8), 1123-1126, 2000.
- Zhou, T., M.A. Geller, and K. Hamilton, The roles of the Hadley Circulation and downward control in tropical upwelling, *J. Atmos. Sci.*, *63* (11), 2740-2757, 2006.
- Zhou, X.-L., M.A. Geller, and M. Zhang, Cooling trend of the tropical cold point tropopause temperatures and its implications, *J. Geophys. Res.*, *106* (D2), 1511-1522, 2001.
- Zickfeld, K., J.C. Fyfe, M. Eby, and A.J. Weaver, Comment on "Saturation of the southern ocean CO₂ sink due to recent climate change," *Science*, *319* (5863), 570, doi: 10.1126/science.1146886, 2008.
- Zou, C.-Z., M. Gao, and M.D. Goldberg, Error structure and atmospheric temperature trends in observations from the Microwave Sounding Unit, *J. Clim.*, *22* (7), 1661-1681, doi: 10.1175/2008JCLI2233.1, 2009.

CHAPTER 5

A Focus on Information and Options for Policymakers

Coordinating Lead Authors:

J.S. Daniel
G.J.M. Velders

Lead Authors:

O. Morgenstern
D.W. Toohy
T.J. Wallington
D.J. Wuebbles

Coauthors:

H. Akiyoshi
A.F. Bais
E.L. Fleming
C.H. Jackman
L.J.M. Kuijpers
M. McFarland
S.A. Montzka
M.N. Ross
S. Tilmes
M.B. Tully

Contributors:

S.O. Andersen
U. Langematz
P.M. Midgley

CHAPTER 5

A FOCUS ON INFORMATION AND OPTIONS FOR POLICYMAKERS

Contents

SCIENTIFIC SUMMARY	1
5.1 SUMMARY OF PREVIOUS ASSESSMENT AND KEY ISSUES TO BE ADDRESSED IN THE CURRENT ASSESSMENT	5
5.2 METRICS USED TO QUANTIFY OZONE AND CLIMATE IMPACTS	5
5.2.1 Background	5
5.2.2 Ozone Impacts: ODPs and EESC.....	7
5.2.2.1 Fractional Release Values and Global Lifetimes.....	7
5.2.2.2 Ozone Depletion Potentials.....	9
5.2.2.3 Equivalent Effective Stratospheric Chlorine	9
5.2.3 Climate Impacts: GWPs and Radiative Forcing.....	10
5.2.3.1 Lifetime Updates.....	11
5.2.3.2 Radiative Efficiency Updates	11
5.2.3.3 Updates to Indirect GWPs from Ozone Destruction.....	12
5.3 FUTURE BASELINE SCENARIOS	14
5.3.1 Chlorine- and Bromine-Containing Ozone-Depleting Substances	14
5.3.2 CO ₂ , CH ₄ , and N ₂ O	16
5.3.3 ODP- and GWP-Weighted Emissions, EESC, and Radiative Forcing	16
5.4 IMPACTS OF HUMAN ACTIVITIES RELEVANT TO OZONE POLICY	19
5.4.1 Background	19
5.4.2 Ozone Impacts.....	20
5.4.2.1 Chlorine- and Bromine-Containing ODSs.....	20
5.4.2.2 CO ₂ , CH ₄ , and N ₂ O	22
5.4.2.3 N ₂ O from Automotive Biofuels	22
5.4.2.4 Geoengineering: Enhancing Earth’s Albedo by Stratospheric Injection of Sulfur.....	23
5.4.2.5 Emissions from Aviation and Rockets.....	24
5.4.2.6 Summary.....	25
5.4.3 Climate Impacts.....	25
5.4.3.1 Major HFCs Used as Replacements for ODSs	25
5.4.3.2 Other Replacements for ODSs.....	30
5.4.4 Other Environmental Impacts	31
5.4.5 Impact of 2007 Accelerated HCFC Phase-Out	32
5.5 THE WORLD AVOIDED BY OZONE POLICY	33
5.5.1 ODS Production	33
5.5.2 Radiative Forcing	34
5.5.3 Climate and Ozone Impacts Avoided by the Montreal Protocol.....	35
5.5.4 UV Impacts of the Avoided Ozone Depletion	37
5.5.5 Summary	37
REFERENCES	38
APPENDIX 5A	
Table 5A-1. Direct Global Warming Potentials for selected gases.....	47

Table 5A-2. Assumptions made in obtaining production and emission estimates for the baseline (A1) scenario.....	50
Table 5A-3. Mixing ratios (ppt) of the ODSs considered in the baseline (A1) scenario.....	54
Table 5A-4. Halocarbon indirect GWPs from ozone depletion using the EESC-based method described in Daniel et al. (1995).....	56

SCIENTIFIC SUMMARY

Ozone Depletion Potentials (ODPs) and Global Warming Potentials (GWPs) are metrics frequently used to quantify the relative impacts of substances on ozone depletion and climate forcing. In Chapter 5, both ODPs and GWPs have been updated. The direct GWPs for some compounds presented here have not appeared previously in WMO/UNEP or Intergovernmental Panel on Climate Change (IPCC) assessments. Indirect GWPs have also been re-evaluated.

Information for Policymakers

- **The Montreal Protocol is working. It has protected the stratospheric ozone layer from much higher levels of depletion by phasing out production and consumption of ozone-depleting substances (ODSs).** Simulations show that unchecked growth in the emissions of ODSs would have led to ozone depletion globally in the coming decades much larger than has been observed. Solar ultraviolet-B (UV-B) radiation at the surface would also have increased substantially.
- **The Montreal Protocol and its Amendments and Adjustments have made large contributions toward reducing global greenhouse gas emissions.** Because many ODSs are potent greenhouse gases, the Montreal Protocol has successfully avoided larger climate forcing. In 2010, the decrease of annual ODS emissions under the Montreal Protocol is estimated to be about 10 gigatonnes (Gt) of carbon dioxide-equivalent (GtCO₂-eq) per year, which is about five times larger than the annual emissions reduction target for the first commitment period (2008–2012) of the Kyoto Protocol.
- **The accelerated hydrochlorofluorocarbon (HCFC) phase-out agreed to by the Parties to the Montreal Protocol in 2007 is projected to reduce cumulative HCFC emissions by 0.6–0.8 million ODP-tonnes between 2011 and 2050 and bring forward the year equivalent effective stratospheric chlorine (EESC) returns to 1980 levels by 4–5 years. In terms relevant to climate, the accelerated HCFC phase-out is projected to reduce emissions by 0.4–0.6 GtCO₂-eq per year averaged over 2011 through 2050.** The actual climate benefit will be determined, in part, by the climate impact of the compounds used to replace the HCFCs. In comparison, global anthropogenic emissions of CO₂ were greater than 30 Gt per year in 2008.
- **EESC at midlatitudes is projected to return to 1980 levels in 2046 for the baseline (A1) scenario, 2–3 years earlier than projected in the previous Assessment.** This revision is primarily due to an improved understanding of lower stratospheric chlorine and bromine release from ODSs, along with contributions from smaller projected HCFC emissions, and despite larger projected emissions of carbon tetrachloride (CCl₄) and a smaller 1980 mixing ratio of methyl bromide (CH₃Br).
- **EESC in the Antarctic vortex is projected to return to 1980 levels around 2073 for the baseline (A1) scenario, 7–8 years later than projected in the previous Assessment.** This is primarily due to an improved understanding of lower stratospheric chlorine and bromine release from ODSs, with smaller contributions from changes in the emissions of CCl₄ and HCFCs and a smaller 1980 mixing ratio of CH₃Br. The return to 1980 levels in the Antarctic vortex is about 26 years later than the return of midlatitude EESC to 1980 levels.
- **Due to the ongoing success of the Montreal Protocol and its Amendments and Adjustments in reducing the production, emissions, and abundances of controlled ODSs, other compounds and activities not controlled by the Montreal Protocol are becoming relatively more important to stratospheric ozone levels.**
- **Increasing abundances of radiatively important gases that are not controlled by the Montreal Protocol, especially CO₂, methane (CH₄), and nitrous oxide (N₂O), are expected to significantly affect future stratospheric ozone levels** (see also Chapter 3). Under many IPCC future scenarios, it is projected that these gases will cause globally averaged ozone changes larger than those resulting from any of the ODS reduction cases explored in this chapter.

- **A nitrous oxide (N₂O) ODP of 0.017 has been calculated. The anthropogenic ODP-weighted emission of N₂O is larger than that of any current halogenated ODS emission.** The ODP of N₂O is more uncertain than it is for halogenated substances, but it has been known since 1970 that N₂O depletes stratospheric ozone. Reductions in N₂O emissions would also reduce climate forcing.
- **Since the previous Assessment, new fluorocarbons have been suggested as possible replacements for potent HCFC and hydrofluorocarbon (HFC) greenhouse gases.** For example, HFC-1234yf (CF₃CF=CH₂) (ODP = 0; 100-year GWP = 4) is proposed to replace HFC-134a (CH₂FCF₃) (ODP = 0; 100-year GWP = 1370) in motor vehicle (mobile) air conditioning. Each new fluorocarbon proposed as a replacement will require an evaluation for ODP, GWP, atmospheric fate, safety, and toxicity for a thorough understanding of its potential environmental impact. Preliminary analyses of the atmospheric fate of HFC-1234yf indicate that global replacement of HFC-134a with HFC-1234yf at today's level of use is not expected to contribute significantly to tropospheric ozone formation or harmful levels of the degradation product TFA (trifluoroacetic acid). It is well established that TFA is a ubiquitous natural component of the hydrosphere, but uncertainties remain regarding its natural and anthropogenic sources, long-term fate, and abundances.

Options for Policymakers

A new baseline scenario for ODSs is presented in Chapter 5 that reflects our current understanding of atmospheric mixing ratios, production levels, and bank sizes. Elimination of future emissions, production, and banks of various ODSs are applied to this scenario to evaluate the maximum impacts of various hypothetical phase-outs (see Table S5-1). The year EESC returns to 1980 levels, and integrated EESC changes, are two metrics used in the evaluation. The calculations of the years when EESC returns to the 1980 level in these hypothetical cases do not consider other effects such as changing atmospheric transport and lifetimes. An elimination of anthropogenic N₂O emissions is also considered and compared to some ODS cases using globally averaged total ozone. In addition to the hypothetical cases discussed below, the impacts on stratospheric ozone of other activities, such as the use of automotive biofuels, commercial subsonic aircraft, and rocket launches, are considered in Chapter 5. These other activities are not expected to substantially affect stratospheric ozone now or in the near future.

- **Projections suggest that unmitigated HFC growth could result in GWP-weighted emissions up to 8.8 GtCO₂-eq per year by 2050, comparable to the GWP-weighted emissions of chlorofluorocarbons (CFCs) at their peak in 1988.** The highest of these projections assumes that developing countries use HFCs with GWPs comparable to those currently used in the same applications in developed countries. The projected radiative forcing in 2050 from these compounds (up to 0.4 W/m²) can be reduced by using compounds with lower GWPs.
- **Options available for limiting future halocarbon emissions will have less impact on future ozone levels than what has already been accomplished by the Montreal Protocol.**
- **Leakage of CFCs and leakage of halons from the banks are the largest sources of current ODP-weighted emissions of ODSs.** A delay of four years, from 2011 to 2015, in the capture and destruction of the estimated CFC banks is currently thought to reduce the potential ozone and climate benefits from these actions by about 30%. The percentage impact of a four-year delay in the capture and destruction of the halon banks is similar.
- **Elimination of future CCl₄ emissions is now projected to have a larger impact on integrated EESC than was projected in the previous Assessment.** Recent observed CCl₄ mixing ratios have declined more slowly than previously projected. Extrapolation of this trend leads to larger future projected emissions in the baseline scenario and thus to the increased projected impact of the elimination of emissions.
- **The estimated impact on integrated EESC resulting from elimination of future HCFC production is slightly smaller than in the previous Assessment.** The recent growth in reported HCFC production in developing countries was larger than projected in the previous Assessment. This alone would have resulted in a larger projected HCFC

Table S5-1. Summary of hypothetical cases for accelerating the recovery of the ozone layer and reducing carbon-equivalent emissions. The table below shows the reductions in integrated EESC and integrated CO₂-eq emissions relative to the baseline (A1) scenario that can be achieved in several hypothetical cases. The EESC excess above 1980 levels is integrated from 2011 until the time EESC returns to the 1980 level (before 2050). Any potential contribution from very short-lived substances is neglected.

Substance or Group of Substances	Reductions (%) in Integrated EESC (equivalent effective stratospheric chlorine)		Reduction in Cumulative GWP-Weighted Emissions from 2011 to 2050 (Gt of CO ₂ -equivalent)	
	2011	2015	2011	2015
<i>Bank capture and destruction in 2011 and 2015:</i>				
CFCs	11	7.0	7.9	5.5
Halons	14	9.1	0.4	0.3
HCFCs	4.8	5.3 ¹	4.9	5.5 ¹
<i>Production elimination after 2010:</i>				
HCFCs		8.8		13.2
CH ₃ Br for quarantine and pre-shipment		6.7		0.002
<i>Total emissions elimination after 2010:</i>				
CCl ₄ ²		7.6		0.9
CH ₃ CCl ₃		0.1		0.004
HFCs		0.0		Up to 170 ³

¹ The impact of a 2015 HCFC bank recovery is larger than a 2011 bank recovery because this calculation assumes destruction of the bank in only a single year, and because the bank in 2015 is larger than the bank in 2011 owing to continued annual production that is larger than the annual bank release.

² Banks are assumed to be zero. Emissions include uncertain sources such as possible fugitive emissions and unintended by-product emissions.

³ Strongly dependent on future projections and does not consider HFC-23 emissions. HFCs are not controlled by the Montreal Protocol, but are included in the basket of gases of the Kyoto Protocol.

production in the new baseline scenario compared to the previous Assessment, but is projected to be more than compensated for by the accelerated HCFC phase-out agreed to by the Parties to the Montreal Protocol in 2007. Projections suggest that total emissions of HCFCs will begin to decline in the coming decade due to measures already agreed to under the Montreal Protocol.

- **The elimination of all emissions of chlorine- and bromine-containing ODSs after 2010 would shift the year EESC reaches the 1980 level by about 13 years, from 2046 to 2033.** In terms relevant to climate, this would reduce emissions of these substances by about 0.7 GtCO₂-eq per year averaged over 2011 through 2050. Future production of HCFCs and the sum of the current banks of CFCs plus HCFCs contribute about equally to this number. In comparison, global anthropogenic emissions of CO₂ were greater than 30 Gt per year in 2008.
- **A phase-out of methyl bromide emissions from quarantine and pre-shipment (QPS) applications beginning in 2011 would shift the year EESC reaches the 1980 level earlier by 1.5 years compared to continued use at current levels.** Continuing critical-use exemptions (CUEs) indefinitely at the approved 2011 level would delay the return of EESC to 1980 levels by 0.2 years.
- **Elimination of anthropogenic emissions of very short-lived substances (VSLS) could shift the year EESC reaches the 1980 level earlier by almost 3 years,** if anthropogenic VSLS contribute 40 parts per trillion of EESC to the stratosphere. It remains unclear, however, how VSLS emissions reductions at different surface locations would affect their contribution to stratospheric chlorine. VSLS are not controlled by the Montreal Protocol.

5.1 SUMMARY OF PREVIOUS ASSESSMENT AND KEY ISSUES TO BE ADDRESSED IN THE CURRENT ASSESSMENT

The benefits of the Montreal Protocol and its Amendments and Adjustments to both stratospheric ozone and climate have been well documented. Controls on the production and consumption of ozone-depleting substances have been so successful, in fact, that remaining options for further reducing future emissions of ozone-depleting substances (ODSs) are not expected to be as effective in reducing future ozone depletion and climate forcing as what has already been accomplished. As the ability to make further ODS reductions becomes more limited and ODS emissions continue to decline, other processes and anthropogenic activities are expected to become relatively more important in affecting future ozone evolution.

The majority of this chapter is devoted to assessing the impacts of various ozone-relevant processes and activities on ozone depletion and climate forcing. It serves primarily as an update to Chapter 8 of the previous Assessment (Daniel and Velders et al., 2007). In that chapter, future equivalent effective stratospheric chlorine (EESC) projections were updated with the goal of providing a more accurate estimate of the time when the impact of ODSs on stratospheric ozone depletion would return to its 1980 level. The most significant updates resulted from improved bank estimates of chlorofluorocarbon-11 (CFC-11) and CFC-12. For the first time, bank estimates were available from a bottom-up method, leading to more reliable future projections. Before the previous Assessment, banks were estimated from the cumulative difference between production and emissions, a technique thought to be characterized by large uncertainties. The value for the relative effectiveness of bromine compared with chlorine was also increased to be consistent with the latest literature, making methyl bromide (CH_3Br) emissions and halon banks more important relative to the chlorine-containing ODSs than they would have been otherwise. Using the updated EESC projections, the impacts of eliminating future production, bank release, and emissions of several compound groups were quantified. It was found that the elimination of future hydrochlorofluorocarbon (HCFC) emissions could reduce future EESC more than the elimination of emissions of any other compound group. In 2007, the Parties to the Montreal Protocol decided to accelerate the production and consumption phase-out of the HCFCs. The previous Assessment was also the first assessment that presented dates for the return of EESC to 1980 levels relevant to both the midlatitude and Antarctic stratosphere.

In the current chapter, Ozone Depletion Potentials (ODPs) and Global Warming Potentials (GWPs) for ODSs and their replacements are updated. New scenarios are generated to explore the potential impacts of some current

hypothetical ODS and nitrous oxide (N_2O) emissions reductions on future ozone depletion and climate forcing. These new scenarios incorporate updated bottom-up bank estimates and the latest ODS mixing ratio observations. The impact of the 2007 HCFC accelerated phase-out is also quantified. This chapter assesses some additional processes and activities that are expected to affect future ozone levels through mechanisms that do not necessarily involve the emission of chlorine- and bromine-containing source gases. Some of these processes could affect future ozone levels more than future emissions of controlled ODSs. We also discuss the impact of the Montreal Protocol on climate forcing where appropriate. For example, in addition to the climate forcing of ODSs, we assess the impact of future hydrofluorocarbon (HFC) abundances on climate because these chemicals are commonly used as replacement compounds for ODSs. Finally, since the previous Assessment, additional work has been published that investigates the impact of the Montreal Protocol on both ozone and climate. These studies support our understanding that the Montreal Protocol and its Amendments and Adjustments have averted many profound changes to Earth and its atmosphere.

Uncertainties remain in our ability to evaluate the effects of human activities on future ozone levels. Where appropriate, we identify gaps in our understanding that inhibit a precise quantification of ozone impacts.

5.2 METRICS USED TO QUANTIFY OZONE AND CLIMATE IMPACTS

5.2.1 Background

Halocarbons and other long-lived gases released from Earth's surface become mixed in the lower atmosphere and are transported into the stratosphere by atmospheric dynamical processes. They are removed from the atmosphere by photolysis, reaction with excited-state oxygen atoms ($\text{O}(^1\text{D})$) and hydroxyl radicals (OH) (the latter typically only for unsaturated compounds or those containing C-H bonds), and for some compounds, uptake by the oceans and/or land (see Chapter 1). Halocarbons that are transported intact to the stratosphere can react or undergo photolysis and release their degradation products there directly. Some fraction of the degradation products from halocarbons that react before leaving the troposphere can also be transported to the stratosphere. The final degradation products are inorganic halogen species containing fluorine, chlorine, bromine, and iodine atoms. The fraction of the inorganic halogen present in the stratosphere as X atoms ($X = \text{Cl}, \text{Br}, \text{or I}$) and XO largely determines the efficiency of ozone destruction there. Fluorine atoms, for

example, exist as F and FO in very small relative quantities because fluorine species are rapidly converted into hydrogen fluoride (HF), a stable reservoir species that does not react with ozone. This prevents fluorine from contributing to ozone destruction to any significant degree (Ravishankara et al., 1994; Wallington et al., 1995). Iodine atoms participate in catalytic ozone destruction cycles, but rapid tropospheric loss of iodine-containing compounds reduces the amount of iodine reaching the stratosphere from surface emissions (see Chapter 1). Thus, it is primarily chlorine- and bromine-containing compounds that lead to ozone depletion. Halocarbons also absorb terrestrial radiation (long-wavelength infrared radiation emitted from Earth's surface and by the atmosphere) and contribute to the radiative forcing of climate.

Simple metrics have been widely used to quantify the contribution of individual compounds to stratospheric ozone depletion and climate change. ODPs and GWPs are the most established metrics and have been used in past climate and ozone assessments (IPCC, 1990, 1995, 1996, 2001, 2007; IPCC/TEAP, 2005; WMO, 1989, 1991, 1995, 1999, 2003, 2007). They have qualities that are particularly useful in policy discussions. Specifically, they are simple and transparent concepts that are straightforward to estimate and communicate. They approximate the integrated impact of the emission of a given gas relative to that for the emission of the same mass of a reference compound (generally CFC-11 for ODPs and carbon dioxide (CO₂) for GWPs). Some uncertainties in translating emissions into absolute environmental impacts tend to cancel, and the relative benefits of controlling emissions of different gases are highlighted when using such indices. ODPs and GWPs have found widespread use in international agreements such as the Montreal Protocol and Kyoto Protocol and in national regulatory discussions.

Both steady-state and time-dependent ODPs can provide valuable information about the potential for ozone destruction by a compound. **Steady-state ODPs are defined as the change in global ozone for a sustained unit mass emission of a specific compound relative to the change in global ozone for the sustained unit mass emission of CFC-11 (CFCl₃)** (Fisher et al., 1990; Solomon et al., 1992; Wuebbles, 1983). For compounds that are removed by linear processes, this is equivalent to assuming an emission pulse and integrating over the entire decay of the compound (Prather, 1996; 2002). CFC-11 was a widely used industrial compound in the 1970s and 1980s and so has been chosen as a convenient reference gas (Fisher et al., 1990; Wuebbles, 1981; Wuebbles, 1983). Steady-state ODPs have no time dependence and are frequently calculated using chemical transport models. The accuracy of the calculation depends on the model's ability to simulate the distribution of the considered compound and the associated ozone loss. However, because the ODPs are

defined relative to the ozone loss caused by CFC-11, it is generally expected that for chlorocarbon compounds ODPs demonstrate less sensitivity to photochemical modeling errors than do absolute ozone loss calculations. Steady-state ODPs are normally derived relative to a fixed atmosphere; there would be differences in some ODPs if calculations were made for a future atmosphere with different background composition. ODPs with some time horizon, referred to as time-dependent ODPs (Solomon and Albritton, 1992), are more analogous to GWPs and provide information regarding the different timescales over which the compound and reference gas (CFC-11) liberate chlorine and bromine into the stratosphere. Compounds that have shorter (longer) atmospheric lifetimes than CFC-11 have ODPs that decrease (increase) with increasing integration time. Semi-empirical ODPs have also been developed (Solomon et al., 1992) so steady-state and time-dependent ODPs could have an observational basis. Some semi-empirical steady-state values have been revised in this chapter to reflect updates to fractional release values and to some lifetimes. In previous assessments, the semi-empirical approach and model calculations have been shown to yield similar values for most gases.

The advantages and disadvantages of the ODP metric have been discussed in previous WMO/UNEP reports (WMO, 1989, 1991, 1995, 1999, 2003, 2007). The projected importance of non-halocarbon emissions to future ozone levels presents new challenges to the ODP concept and raises questions about their continued comprehensiveness. Emissions occurring in the stratosphere or upper troposphere from aviation and rockets present special challenges to the ODP concept, but may be able to be treated in a manner similar to how very-short-lived species are treated (as a function of where and when emissions occur). ODPs are discussed in more detail in Section 5.2.2 below.

Calculation of the GWP of a compound requires knowledge of its radiative efficiency and global lifetime. The change in net radiation at the tropopause caused by a given change in greenhouse gas concentration or mass is referred to as radiative efficiency. Radiative efficiency has units of Watts per square meter per part per billion (W m⁻² ppb⁻¹) or Watts per square meter per kilogram (W m⁻² kg⁻¹); it is calculated using radiative transfer models of the atmosphere and depends upon the strength and spectral position of a compound's absorption bands as well as atmospheric structure, surface temperature, and clouds. The Absolute Global Warming Potential (AGWP) for time horizon t' is defined as

$$\text{AGWP}_x(t') = \int_0^{t'} F_x \cdot x(t) dt \quad (5-1)$$

where F_x is the radiative efficiency of species x , $x(t)$ describes the decay with time of a unit pulse of compound x , and t' is the time horizon considered. F_x is given in terms

of $\text{W m}^{-2} \text{kg}^{-1}$ or in $\text{W m}^{-2} \text{ppb}^{-1}$. The AGWP usually has units of $\text{W m}^{-2} \text{kg}^{-1} \text{yr}$ and quantifies the future integrated radiative forcing over the time horizon of a unit mass pulse emission of a greenhouse gas. To compare the relative integrated effect of various compounds on climate, the GWP metric was developed. The GWP for time horizon t' (IPCC, 1990; 2001; 2007) can be defined as

$$\text{GWP}_x(t') = \frac{\text{AGWP}_x(t')}{\text{AGWP}_{\text{CO}_2}(t')} = \frac{\int_0^{t'} F_x \exp\left(-t/\tau_x\right) dt}{\int_0^{t'} F_{\text{CO}_2} R(t) dt} \quad (5-2)$$

where F_{CO_2} is the radiative efficiency of CO_2 , $R(t)$ is the response function that describes the decay of an instantaneous pulse of CO_2 , and the decay of the pulse of compound x has been rewritten assuming it obeys a simple exponential decay curve with a response time of τ_x . The pulse response terms lead to a dependence of GWPs on the integration time horizon; compounds that decay more quickly (slowly) than the reference (CO_2) have GWPs that decrease (increase) with increasing time horizon. As shown in equations (5-1) and (5-2), the most common definition of GWPs applies to pulsed emissions. However, GWPs have also been developed to evaluate the effect of sustained emissions (Berntsen et al., 2005; Johnson and Derwent, 1996).

We note that GWP is not the only metric available to compare the climatic impacts of different gases. The science of alternative metrics was considered by an Intergovernmental Panel on Climate Change (IPCC) expert panel recently (IPCC, 2009), which noted that metric design depends critically on the policy goal, and that “the GWP was not designed with a particular policy goal in mind.” Furthermore, the choice of time horizon used in calculating GWPs is not determined purely by climate science considerations. Rather, the choice often depends on what information is useful to decision makers, based in part on the time horizon of the impacts and on the values they consider most important. In an effort to account for the impact of the choice of time horizon, typically three time horizons have been considered (20, 100, and 500 years) when reporting GWPs.

The GWP index has three major advantages over most other indices used to measure the contribution of greenhouse gases to global warming: transparency, simplicity, and widespread acceptance. However, it also has several disadvantages (see, e.g., IPCC, 2009 and references therein). There is growing recognition of the limitations of the GWP metric especially when the impacts of short- and long-lived pollutants need to be considered together (Johansson et al., 2008; Tanaka et al., 2009; Fuglestvedt et al., 2010) and it has been argued that it is time to consider whether other metrics might be more useful (Shine, 2009). For example, there has been interest

in including the economics of emissions mitigation into a climate metric by applying cost-benefit and cost-effective approaches (e.g., Manne and Richels, 2001). Various alternatives have been presented to overcome some of the GWP limitations, but none has been widely accepted as a suitable replacement to date.

ODP and GWP metrics are often used to evaluate the relative integrated impacts arising from emissions, banks, production, etc., on ozone destruction and climate forcing. If time series of these potential impacts are desired, EESC and radiative forcing are used. These metrics are discussed in Sections 5.2.2 and 5.2.3.

5.2.2 Ozone Impacts: ODPs and EESC

5.2.2.1 FRACTIONAL RELEASE VALUES AND GLOBAL LIFETIMES

Fractional release values for various halocarbons are used both in the calculation of semi-empirical ODPs and in deriving EESC. The fractional release value at some location in the stratosphere quantifies the fraction of the source gas that has become photochemically degraded and has released its halogen atoms since it entered the stratosphere. The previous Assessment (Daniel and Velders et al., 2007) used fractional release values from earlier assessments, only updating CFC-114 to the value suggested by Schauffler et al. (2003). For this Assessment, we adopt most of the Newman et al. (2007) updated release values; these values are based on National Aeronautics and Space Administration (NASA) ER-2 field campaign observations using an approach similar to Schauffler et al. (2003). Douglass et al. (2008) showed that the lower stratospheric relationships between the fractional release of chlorine from CFC-11 and CFC-12 and the age of air (as discussed in Chapter 1) produced by simulations with realistic age-of-air values are in good agreement with relationships derived from aircraft observations (Schauffler et al., 2003). Another advantage of using the Newman et al. (2007) results is that they provide observationally based relationships between fractional release values and age-of-air values. This allows for more appropriate estimates of EESC that are relevant to various stratospheric locations, and in particular, polar regions. In the derivation of semi-empirical ODPs and of EESC presented in this chapter (see Table 5-1), we use the values of Newman et al. (2007) for all compounds in that study except for HCFC-141b and HCFC-142b. These two compounds were present in small abundances and had large temporal trends when the atmospheric measurements upon which these fractional release values are based were made, leading to large uncertainties. For this reason, we have retained the fractional release

Table 5-1. Lifetimes, fractional release values, and Ozone Depletion Potentials (ODPs) for long-lived halocarbons. ODPs recommended in this Assessment and ODPs adopted in the Montreal Protocol are included^a.

Halocarbon	Lifetime (years)	Fractional Release Value		Semi-Empirical ODP		ODP in Montreal Protocol
		WMO (2007) ^b	This Assessment ^c	WMO (2007)	This Assessment ^d	
Annex A-I						
CFC-11	45	0.47	0.47	1.0	1.0	1.0
CFC-12	100	0.28	0.23	1.0	0.82	1.0
CFC-113	85	0.35	0.29	1.0	0.85	0.8
CFC-114	190	0.13	0.12	1.0	0.58	1.0
CFC-115	1020		0.04	0.44 ^e	0.57	0.6
Annex A-II						
Halon-1301	65	0.29	0.28	16	15.9	10.0
Halon-1211	16	0.55	0.62	7.1	7.9	3.0
Halon-2402	20	0.57	0.65	11.5	13.0	6.0
Annex B-II						
CCl ₄	26	0.50	0.56	0.73	0.82	1.1
Annex B-III						
CH ₃ CCl ₃	5.0	0.51	0.67	0.12	0.16	0.1
Annex C-I						
HCFC-22	11.9	0.16	0.13	0.05	0.04	0.055
HCFC-123	1.3			0.02	0.01 ^f	0.02
HCFC-124	5.9			0.02		0.022
HCFC-141b	9.2	0.34	0.34 ^g	0.12	0.12	0.11
HCFC-142b	17.2	0.17	0.17 ^g	0.07	0.06	0.065
HCFC-225ca	1.9			0.02		0.025
HCFC-225cb	5.9			0.03		0.033
Annex E						
CH ₃ Br	0.8	0.53	0.60	0.51	0.66	0.6
Others						
Halon-1202	2.9		0.62	1.7		
CH ₃ Cl	1.0	0.38	0.44	0.02	0.02	

^a Ravishankara et al. (2009) have calculated an ODP for N₂O of 0.017.

^b In the previous Assessment, fractional release values relative to CFC-11 were used, with CFC-11 assumed to be 0.84. For this table, WMO (2007) values are scaled to a CFC-11 value of 0.47 to allow easy comparison with the current values.

^c From Newman et al. (2007), values for 3-year-old age of air.

^d Semi-empirical ODP values are not updated in this Assessment for halocarbons whose fractional release values were not estimated in Newman et al. (2007).

^e Model-derived value, WMO (2003).

^f From Wuebbles and Patten (2009) MOZART 3-D model calculation.

^g Values relative to CFC-11 are retained from WMO (2007) because of large uncertainties associated with the Newman et al. (2007) estimates for these compounds.

values relative to CFC-11 assumed in WMO (2007) for these two HCFCs, and we scale them to the appropriate CFC-11 fractional release value depending on the age of air considered. Additional information regarding the use of fractional release values can be found in Chapter 1. In calculating the 2010 ODP-weighted anthropogenic emissions for the A1 baseline scenario (Section 5.3.1), the most significant fractional release changes are for, in order of decreasing importance, CFC-12, HCFC-22, carbon tetrachloride (CCl_4), and halon-1211. A description of the sensitivity of EESC to fractional release and to other parameters can be found in Newman et al. (2007). We also use absolute fractional release values in this chapter, rather than normalizing all of the values as was done in previous assessments. We do this so the portion of EESC estimates attributable to chlorine and bromine source gases are representative of the actual amount of total inorganic chlorine (Cl_y) and total inorganic bromine (Br_y), respectively, in the regions of the stratosphere considered.

Global lifetimes are also used in the calculation of ODPs and EESC. As discussed in Chapter 1, lifetimes of CFC-114 and CFC-115 have been substantially revised since the previous Assessment. There have also been smaller revisions to several of the HCFCs that are included in Table 5-1. Douglass et al. (2008) also find, based on results from two-dimensional (2-D) and three-dimensional (3-D) models, that the range of atmospheric lifetime estimates for CFC-11 from models that best reproduce the observed relationship between age of air and fractional release is 56–64 years. The lifetime calculated for CFC-12 in this study was consistent with the value from the previous Assessment (100 years). Wuebbles et al. (2009) find consistent lifetimes for CFC-11, 54 years in the Model of Ozone and Related Tracers (MOZART) 3-D model (version 3.1) and 57 years in the current version of the University of Illinois Urbana-Champaign (UIUC) 2-D model, which includes an improved calculation of stratospheric age of air (Youn et al., 2010). In the previous three assessments (WMO, 1999, 2003, 2007), ODP derivations assumed an atmospheric lifetime for CFC-11 of 45 years based on analyses of observations (Cunnold et al., 1997; Volk et al., 1997) and older model results (Prinn and Zander, 1999). Because of the dearth of studies estimating ODS lifetimes with models that accurately calculate age of air, and because the Douglass et al. (2008) study only evaluated the lifetimes of CFC-11 and CFC-12, we continue to use a lifetime of 45 years for CFC-11; however, it should be recognized that in the future this lifetime may be assessed to be too small. The lack of comprehensive studies examining halocarbon lifetimes with models that accurately calculate age of air can be considered a gap in our current understanding. A full discussion of lifetime revisions can be found in Chapter 1.

5.2.2.2 OZONE DEPLETION POTENTIALS

An updated list of ODPs is provided in Table 5-1 for a number of long-lived halocarbons. The primary change from the previous Assessment (Daniel and Velders et al., 2007) is to update the semi-empirical ODPs by incorporating revised fractional release values and global lifetimes for some compounds. For ODP estimates in this chapter, fractional release values representative of air that has been in the stratosphere for 3 years are used. In the absence of new evidence, we continue to use a value of 60 for the relative effectiveness of bromine compared to chlorine for destroying ozone (α) at midlatitudes. For Antarctic calculations we continue to use a value of 65 (WMO, 2007). The semi-empirical ODP of CCl_4 is 10% higher than in the previous Assessment owing to a larger fractional release value (see Table 5-1 and Section 5.2.2.1). Although there are still significant gaps in our understanding of the CCl_4 budget, the recommended lifetime remains 26 years (see Chapter 1).

The ODP for HCFC-123 has been updated based on results from a three-dimensional model (Wuebbles and Patten, 2009). The calculated value of 0.0098 is similar to but smaller than the previous model-derived value of 0.014 based on 2-D model results (WMO, 2003). The ODPs for several short-lived compounds have also been discussed in Chapter 1.

Looking beyond the analyses of ODPs for halocarbons, Ravishankara et al. (2009) have calculated an ODP for nitrous oxide (N_2O) of 0.017 using a 2-D model. Although N_2O has a relatively small ODP, future changes in emissions and atmospheric concentrations of N_2O could have a significant effect on ozone compared with emissions of controlled ODSs because of the larger magnitude of N_2O 's anthropogenic emissions. The impact of N_2O emissions will be quantified in Section 5.4. The magnitude of past and future N_2O ODP-weighted emissions leads to concerns that include influences on the timing of the recovery of ozone, the “background” ozone level, the distribution of stratospheric ozone depletion, and the possibility of future decreases in ozone due to increasing N_2O (Ravishankara et al., 2009; Wuebbles, 2009).

5.2.2.3 EQUIVALENT EFFECTIVE STRATOSPHERIC CHLORINE

EESC has historically been used to relate measured surface mixing ratios of chlorine- and bromine-containing source gases to the stratospheric inorganic chlorine and bromine arising from these gases in key regions of the stratosphere and thus to the amount of ozone they will destroy (Daniel et al., 1995; WMO, 1995, 1999, 2003, 2007). It accounts for the fact that bromine is more

efficient than chlorine (on a per-atom basis) at destroying stratospheric ozone and that different source gases release their chlorine and bromine at different rates and locations. Both integrated EESC changes and the date when EESC returns to 1980 levels have been used in previous assessments to quantify the relative impacts of various hypothetical ODS emission cases. This approach has worked well because all the major anthropogenic sources of stratospheric chlorine and bromine are thought to be known, and they all have reasonably well-understood global lifetimes and stratospheric dissociation rates. Recently, EESC was reformulated so that it accounts for the age-of-air spectrum and the age-of-air dependent fractional release values (Newman et al., 2007). This reformulation allows EESC to represent the total Cl_y and Br_y in various regions of the stratosphere.

The concept of EESC does have limitations because of uncertainties in the transport time, uncertainties in the spatial and temporal dependencies of the bromine efficiency for ozone destruction versus chlorine (α) (generally considered a constant), the efficiency of stratospheric halogen release from the source gas, and possible temporal changes in transport times and source gas lifetimes (some effects described in Newman et al., 2006, 2007). It should be noted that the EESC concept also does not explicitly account for changing atmospheric emissions and concentration of other relevant constituents that can also affect ozone, such as CO_2 and methane (CH_4). Daniel et al. (2010) have recently provided a method to incorporate N_2O abundances into EESC. We will not adopt this method for the calculation of EESC in this Assessment because its publication was so recent, but we do show the impact of a hypothetical N_2O emission phase-out on globally averaged total column ozone that can be compared with the impact of other ODS phase-outs on ozone. By comparing 2-D model results with EESC, Daniel et al. (2010) showed that integrated EESC, despite its limitations, is proportional to the calculated integrated total ozone depletion reductions arising from various hypothetical ODS policy actions to within 30%.

The year 1980 is often taken as roughly representative of the time before the major stratospheric ozone losses occurred due to halocarbons. As a result, analyses are often based on the return of EESC to 1980 levels. If stratospheric ozone levels were affected by only halocarbons, the ozone layer would be expected to recover from human activities as anthropogenic ODSs are removed from the atmosphere. However, the actual picture of future levels of stratospheric ozone and the recovery from the past emissions of halocarbons is more complicated, making the use of a single date as a metric for total ozone recovery less meaningful. There are a number of activities and processes that are likely to substantially affect the future distribution and integrated amounts of ozone (see

Section 5.4 and Chapter 3). Some of these potential activities and processes include rocket launches, aviation, climate-related geoengineering actions, and emissions of CO_2 , CH_4 , and N_2O . So while the evolution of EESC in this chapter provides important information regarding the impact of certain human activities on stratospheric ozone, ozone is expected to recover at a different rate than this simple metric might imply.

The relative importance of the various future chlorine- and bromine-containing emissions, production, and banks are compared as in previous assessments using EESC in Section 5.4. New in this Assessment is that the impacts of some of these ODS cases are compared in terms of ozone depletion using the results of the Daniel et al. (2010) study (see Section 5.4.2). The intent of this approach is to provide information that can be used for determining which options are available and what their potential effects are on the future ozone layer. It will also allow us to compare the expected impacts of several potential ODS policy options with ozone changes from a broader range of activities, including expected future changes in greenhouse gases such as CO_2 , N_2O , and CH_4 .

5.2.3 Climate Impacts: GWPs and Radiative Forcing

Direct GWPs are tabulated in this chapter's Appendix 5A. The list of compounds evaluated in Appendix Table 5A-1 is intended to include potential replacements for the Montreal Protocol ODSs, but this list is not exhaustive. CO_2 and N_2O are also included in the table. Most source gases with atmospheric lifetimes of less than 6 months are not believed to contribute significantly to radiative forcing and are not included in Appendix Table 5A-1 (note that, in contrast to short-lived source gases, short-lived aerosols and tropospheric ozone are thought to contribute significantly to radiative forcing (IPCC, 2007)). Indirect GWPs are discussed later in this section and are also tabulated in Appendix 5A (Appendix Table 5A-4). The uncertainty associated with the direct GWPs listed in Appendix Table 5A-1 is estimated to be $\pm 35\%$ with 90% confidence (IPCC, 2007) reflecting uncertainties in the radiative efficiencies, lifetimes of the halocarbons, and uncertainties in our understanding of the carbon cycle (IPCC, 2001). It should be noted that because uncertainties in the carbon cycle make an important contribution to the total GWP uncertainty (IPCC, 2007), the relative climatic effects of different halocarbons (e.g., expressed as ratios of their GWPs) are likely accurate to much better than 35%.

We limit further discussion of GWPs to updates since the last Ozone Assessment. There are two reasons that updates have been made: (1) updates to the

atmospheric lifetimes and (2) new radiative efficiency recommendations. Although the atmospheric concentration of CO₂ continues to increase, its AGWPs were chosen to be the same as the IPCC (2007) Assessment so as to reduce confusion when comparing to values from that Assessment. The revisions to the lifetimes and radiative efficiencies discussed below affect GWP calculations and radiative forcing projections.

5.2.3.1 LIFETIME UPDATES

The lifetimes of several HCFCs and of most HFCs, including hydrofluoroethers (HFEs), have been updated from the previous Assessment. The lifetime for CH₃CH₂OCF₂CHF₂ (HFE-374pc2) of 5 years given in the previous Assessment was erroneous; the lifetime for this compound is actually rather short (approximately 2 months, see Chapter 1). Accordingly, this compound is now classified as a short-lived species. The lifetimes of CFC-114, CFC-115, and nitrogen trifluoride (NF₃) were also updated in response to work by Prather and Hsu (2008). A discussion of these lifetime updates and others, and the distinction between short- and long-lived species, can be found in Chapter 1.

5.2.3.2 RADIATIVE EFFICIENCY UPDATES

The radiative efficiency values used in the previous Assessment, the currently recommended values, and the values presented in the relevant references for the new and revised compounds are presented in Table 5-2. Since the last Assessment (WMO, 2007), additional radiative efficiency data have become available for HFE-43-10pccc124, HFC-365mfc, HFC-263fb, HFC-245eb,

HFC-245ea, and HFC-329p (all calculated assuming constant vertical profiles). Rajakumar et al. (2006) have provided the first measurements of the lifetimes and the radiative efficiencies for HFC-263fb, HFC-245eb, and HFC-245ea. These radiative efficiencies (Table 5-2) have been adopted in the calculation of the GWPs in the appendix (Appendix Table 5A-1). Inoue et al. (2008) report a radiative efficiency of 0.23 W m⁻² ppb⁻¹ for HFC-365mfc. This value is 10% larger than the value of 0.209 W m⁻² ppb⁻¹ reported by Barry et al. (1997) that was used in the previous Assessment (WMO, 2007). Inoue et al. (2008) concluded that the approximately 10% difference in the intensity of the infrared (IR) absorption spectrum was the origin of the different radiative efficiencies in the two studies. There being no obvious reason to prefer either study, an average of the results from Barry et al. (1997) and Inoue et al. (2008) was adopted in the current Assessment.

Sulfuryl fluoride (SO₂F₂) is being used increasingly as a replacement for methyl bromide (see Chapter 1, Section 1.5.2.2). It has an atmospheric lifetime of about 36 years and a substantial GWP. Papadimitriou et al. (2008a) and Sulbaek Andersen et al. (2009) measured the IR spectrum of SO₂F₂ and reported radiative efficiencies of 0.222 and 0.196 W m⁻² ppb⁻¹, respectively, for this molecule. The integrated absorption cross sections reported by Papadimitriou et al. (2008a) and Sulbaek Andersen et al. (2009) over the range 800–1540 cm⁻¹ are in excellent agreement (within approximately 1%) and both differ by only about 5% from that reported by Dillon et al. (2008). The approximately 10% difference in radiative efficiencies reported by Papadimitriou et al. (2008a) and Sulbaek Andersen et al. (2009) is probably due to the fact that Sulbaek Andersen et al. (2009) did not consider

Table 5-2. Radiative efficiency estimates (W m⁻² ppb⁻¹) for seven compounds whose recommended values have either changed since, or were not included in, the previous Assessment.

Chemical Formula	Common or Industrial Name	WMO (2007)	Recent Published Estimates	This Assessment
CHF ₂ OCF ₂ OC ₂ F ₄ OCHF ₂	HFE-43-10pccc124 ^a	1.37	1.02 (Wallington et al., 2009)	1.02
CH ₃ CF ₂ CH ₂ CF ₃	HFC-365mfc	0.21	0.23 (Inoue et al., 2008)	0.22
CHF ₂ CF ₂ CF ₂ CF ₃	HFC-329p	0.45	0.31 (Young et al., 2009)	0.31
CH ₃ CH ₂ CF ₃	HFC-263fb		0.13 (Rajakumar et al., 2006)	0.13
CH ₂ FCHF ₂ CF ₃	HFC-245eb		0.23 (Rajakumar et al., 2006)	0.23
CHF ₂ CHFCHF ₂	HFC-245ea		0.18 (Rajakumar et al., 2006)	0.18
SO ₂ F ₂	sulfuryl fluoride		0.222 (Papadimitriou et al., 2008a) 0.196 (Sulbaek Andersen et al., 2009)	0.22

^a Also referred to as H-Galden 1040x.

stratospheric adjustment (allowing the stratospheric temperatures to equilibrate to the greenhouse gas perturbation) in their radiative efficiency calculations. Sulbaek Andersen et al. (2009) used the estimation method described by Pinnock et al. (1995), which agrees to within $\pm 0.3\%$ with the global annual and annual cloudy-sky instantaneous radiative forcing calculations using the Reading narrowband model (Shine, 1991). Papadimitriou et al. (2008a) applied a line-by-line radiative transfer code, developed at the National Oceanic and Atmospheric Administration (NOAA), to a global-average cloudy-sky profile taking into account stratospheric adjustment. The effect of including stratospheric adjustment for a given gas depends on the position and intensity of its IR absorption features. Forster et al. (2005) have shown that inclusion of stratospheric adjustment increases the instantaneous radiative forcing of HFC-134a by approximately 10%. Pinnock et al. (1995) studied 19 halogenated alkanes and found that inclusion of stratospheric adjustment typically increased the instantaneous radiative efficiency by 5–10% (although in the case of HFC-41 there was actually a 7% decrease, see Table 4 in Pinnock et al. (1995)). Radiative forcing as defined by IPCC is based on the globally and annually averaged net downward irradiance change at the tropopause after allowing for stratospheric temperatures to adjust to radiative equilibrium. Hence, we adopt a value of $0.22 \text{ W m}^{-2} \text{ ppb}^{-1}$ from Papadimitriou et al. (2008a), which is consistent with the value reported by Sulbaek Andersen et al. (2009).

Wallington et al. (2009) revisited the IR spectrum of HFE-43-10pccc124, previously also referred to as H-Galden 1040x, and argued that the IR spectrum reported by Cavalli et al. (1998) used in previous WMO and IPCC reports is approximately 30% too strong. It was noted that use of the reference spectrum of Cavalli et al. (1998) would lead to carbon balances substantially greater than 100% in laboratory experiments of HFE-43-10pccc124 oxidation. The IR spectrum reported by Wallington et al. (2009) is in good agreement with that measured using the same experimental set-up 12 years earlier by Christidis et al. (1997). As discussed by Young et al. (2008), the radiative efficiency of HFE-43-10pccc124 in WMO (2007) is inconsistent with the expected trends based upon the database for other HFEs. The radiative efficiency reported by Wallington et al. (2009) is adopted here.

Young et al. (2009) reported the first measurements of the lifetime and radiative efficiency for $\text{CHF}_2\text{CF}_2\text{CF}_2\text{CF}_3$ (HFC-329p); these are used here.

As in all previous assessments, the atmospheric lifetime and radiative efficiency values used in the present Assessment can be traced to experimentally measured rate coefficients and IR spectra. Ab-initio quantum mechanical computational methods are available to calculate rate coefficients and IR spectra. Results from

ab-initio calculations have provided valuable fundamental insight into reaction mechanisms and the underlying processes giving rise to the IR spectra. However, such computational results have generally not been used directly to calculate GWPs. With advances in computational techniques, recent studies (e.g., Blowers and Hollingshead, 2009) suggest that atmospheric lifetimes and radiative efficiencies can now be calculated from first principles with accuracies comparable to those from experimental studies. This suggestion has yet to be fully investigated by the scientific community, and in the present Assessment we do not consider atmospheric lifetimes and radiative efficiencies that have been evaluated only by ab-initio methods.

5.2.3.3 UPDATES TO INDIRECT GWPs FROM OZONE DESTRUCTION

In addition to being greenhouse gases themselves, the ODSs play a significant role in the destruction of stratospheric ozone, another radiatively important gas. The distribution of ozone has important implications for Earth's climate system, not only because ozone absorbs solar radiation but also because it is a greenhouse gas that absorbs some of the infrared radiation emitted from Earth's surface and atmosphere. The change in ozone radiative forcing due to the addition of some ODS can be attributed to that ODS as an indirect radiative forcing. Stratospheric ozone losses are generally thought to cause a negative radiative forcing, canceling part of the increased radiative forcing arising from the direct influence of the halocarbons. The magnitude of the indirect effect is strongly dependent on the altitude profile of the halogen-induced ozone loss and will vary depending on the source gas considered. The latest estimate of radiative forcing from changes in stratospheric ozone since preindustrial times is $-0.05 \pm 0.10 \text{ W/m}^2$ (IPCC, 2007). However, there have not been recent studies that clearly estimate the amount of the ozone forcing attributable to halocarbon changes only.

In spite of the uncertainty associated with the radiative forcing from ozone loss caused by halocarbons, the indirect GWPs for various halocarbons have been included in previous Ozone Assessments using an approach similar to that described in Daniel et al. (1995) (e.g., see WMO, 2003, 2007). This approach is also used here to update indirect GWPs for selected halocarbons (Appendix Table 5A-4) and is based on the assumption of an approximate linear relationship between the change in EESC arising from a particular source gas and radiative forcing arising from stratospheric ozone loss. A complication that is ignored by this approach is that some of the observed ozone depletion, and its associated radiative forcing, is due to processes not related to ODSs. The previously published

indirect GWPs have primarily changed over time as a response to updates in the EESC scenarios, changes in the estimated efficiency of bromine relative to chlorine for destroying ozone, and changes in the estimates of the overall stratospheric ozone radiative forcing owing to halocarbon changes. These factors continue to represent important uncertainties in estimating the indirect GWPs using the EESC approach. This approach also cannot capture the source gas-dependent variations in the ozone loss profile and its resulting impact on radiative forcing. In past estimates of these indirect GWPs, the 1980 level of EESC has been assumed to represent a value below which no additional ozone loss occurs. This implied that the presence of an ODS after EESC fell below this level would lead to no additional ozone loss or negative radiative forcing due to that loss. No such threshold is adopted here, leading to slightly more negative indirect GWPs for the longer-lived ODSs in the absence of other changes. However, the change in stratospheric ozone from 1979 to 1998 is now estimated to be responsible for -0.05 W/m^2 forcing (IPCC, 2007). The adoption of this lower revised IPCC radiative forcing due to stratospheric ozone, compared with $-0.15 \pm 0.10 \text{ W/m}^2$ in WMO (2007), dominates the changes compared to the previous Assessment and makes the indirect effects less negative. The current calculations also incorporate the updated fractional release values for midlatitudes and polar regions (Newman et al., 2007). We continue to assume that radiative forcing due to polar

ozone loss is responsible for 40% of the -0.05 W/m^2 and that the polar depletion saturates at 1990 EESC levels (Daniel et al., 1995).

As a step toward obtaining indirect GWPs through a more fundamental approach, Youn et al. (2009) have explicitly evaluated the indirect radiative forcing for two of the halons, halon-1211 and halon-1301, using 2-D and 3-D atmospheric models. In Table 5-3, these values are compared with the direct and indirect GWPs found in WMO, 2007 (Daniel and Velders et al., 2007) and those updated for this Assessment using the approach discussed in the previous paragraph. The indirect GWP for halon-1211 derived by Youn et al. (2009) is much smaller (about 60%) than the WMO (2007) value, but does fall within a single standard deviation of it. The Youn et al. (2009) indirect GWP is larger in magnitude by about a factor of ten compared to its direct effect. The indirect effect of halon-1301 is about 25% smaller than previously reported but also agrees with the WMO (2007) value to within a single standard deviation. The updated indirect GWPs reported here for halon-1211 calculated using the EESC scaling approach is in much better agreement with the Youn et al. (2009) values than the WMO (2007) central estimate was. While the Youn et al. (2009) work represents a single study, these analyses suggest that more comprehensive atmospheric models have the potential to reduce our uncertainties in the halocarbon indirect GWPs.

Table 5-3. Direct and indirect Global Warming Potentials (mass basis) of halons. Youn et al. (2009) lifetimes are e-folding times based on an exponential curve fitted to the simulated atmospheric decay.

	Lifetimes (years)		Global Warming Potentials for 100-years Time Horizon					
			Direct GWP		Indirect GWP		Net GWP ^a	
	Halon-1211	Halon-1301	Halon-1211	Halon-1301	Halon-1211	Halon-1301	Halon-1211	Halon-1301
This Assessment	16	65	1890 ± 660	7140 ± 2500	-11,720 ± 23,430	-27,060 ± 54,130		
WMO (2007)	16	65	1890 ± 660	7140 ± 2500	-40,280 ± 27,120	-49,090 ± 34,280		
Youn et al. (2009) 2-D Model	14.4	72.4	1796	7122	-16,294	-36,247	-14,498	-29,127
Youn et al. (2009) 3-D Model	10.9	70.1	1699	6903	-17,050	-37,252	-15,351	-30,349

^a Concerns remain about the quantitative accuracy of adding the indirect forcing due to ozone changes to the direct forcing for the well-mixed halons. This addition was not performed in WMO (2007) or in this chapter, except for the results taken from Youn et al. (2009).

5.3 FUTURE BASELINE SCENARIOS

5.3.1 Chlorine- and Bromine-Containing Ozone-Depleting Substances

A new baseline scenario for the period 1950–2100 is developed for all ODSs along the same lines as in the previous Assessment (WMO, 2007), with future projections consistent with current controls imposed by the Montreal Protocol. Observed global average mixing ratios through the beginning of 2009 are used as a starting point for the projections, together with the production of ODSs through 2008 reported by the countries to the United Nations Environment Programme (UNEP, 2009), estimates of the bank sizes of ODSs for 2008 from the Technology and Economic Assessment Panel (TEAP, 2009), approved essential use exemptions for CFCs, critical-use exemptions for methyl bromide for 2008–2010, and production estimates of methyl bromide for quarantine and pre-shipment (QPS) use. Details of the baseline scenario are given in Appendix Table 5A-2. Calculated mixing ratios are tabulated in Appendix Table 5A-3 for each of the considered halocarbons from 1955 through 2100 (See also Figure 5-1). The years when observations are used are indicated in the table by the shaded regions. For those years, scenario mixing ratios are equal to the observations.

The mixing ratios in the new baseline scenario are similar to those in the previous Assessment (WMO, 2007) for most species. The larger future mixing ratios (2010–2050) for CFC-11 (+5 to 9 parts per trillion (ppt)) and CFC-12 (up to +9 ppt) are the result of slightly larger fractions of the bank emitted annually, based on 1999–2008 averages. The new baseline scenario has significantly larger future mixing ratios for CCl_4 (up to +12 ppt) than in WMO (2007) because of a different assumption regarding the decrease in future emissions (see Section 5.4.2.1). Emissions of each of the three considered HCFCs begin to decline at some time in the next decade in the baseline scenario due to existing Montreal Protocol controls. The projected future mixing ratios of HCFC-22 after about 2025 are lower than projected in the previous Assessment as a direct result of the accelerated HCFC phase-out (Montreal Protocol Adjustment of 2007, see Section 5.4.5). The initially larger mixing ratios in the period 2010–2020 are the result of an increase in reported production and a larger fraction of the bank emitted annually. The mixing ratios of HCFC-141b and HCFC-142b are larger than in the previous Assessment, by up to 8 ppt and 20 ppt, respectively, because of an increase in reported production and a different assumption regarding the future distribution of the total HCFC consumption over the three main HCFCs (see Appendix Table 5A-2). The mixing ratios of halon-1301 in the new baseline scenario

are somewhat different from those in the previous Assessment's baseline scenario. The older ones were based on a bank release calculation after 1995 because of large differences in observational records that existed at that time for the 1995–2005 period. Revised calibrations and measurements with new instruments using mass spectrometry (at NOAA) have led to an improved consistency between the labs (NOAA and Advanced Global Atmospheric Gases Experiment (AGAGE)) for the global mean mixing ratios and the rates of change in recent years (see Figure 1-1 of Chapter 1). Therefore, the mixing ratios here are taken as an average of the observations from those two networks in recent years and are derived using a consistent scaling to the NOAA data in years before AGAGE measured halon-1301 (before 2004).

The EESC corresponding to the baseline scenario is shown in Figure 5-2. The absolute values of EESC (right-hand axis) are substantially lower than presented in the previous Assessment because different fractional release values have been adopted and they are no longer scaled so the fractional release value of CFC-11 is 0.84. As stated in Section 5.2.2.1, this approach is taken because it allows the values now to provide meaningful estimates of Cl_y and Br_y abundances for 3-year-old air, a benefit that would be lost if the former scaling method were applied. Furthermore, since EESC is used in this chapter only as a relative measure, the absolute values are not important. If current EESC values are scaled so the peak value is the same as in the previous Assessment, the figure shows that the time series are quite similar. Differences appear because of the revised relative fractional release values and because of slightly revised emissions. In previous assessments, the year 1980 was taken as a benchmark year, representing a time before the major stratospheric ozone losses occurred due to halocarbons. Some ozone losses caused by human activities likely had already occurred due to, for example, halocarbon and N_2O emissions (see Chapter 3). Nevertheless, the year EESC returns to 1980 levels has been used as a measure for some degree of ozone layer recovery and to compare scenarios. Although we continue to recognize the limitations of this metric (see Section 5.2.2) it is used here to compare the new baseline scenario with the one in the previous Assessment and to compare the effects of hypothetical ODS emission reductions of chlorine- and bromine-containing ODSs (Table 5-4). In the new baseline scenario, including only Montreal Protocol-controlled ODSs, EESC returns to its 1980 levels in 2046 for mid-latitude conditions. This is 2–3 years earlier than in the previous Assessment (WMO, 2007) and is the result of two partially offsetting changes. First, future emissions of ODSs give a delay of 2–3 years, mainly as the net result of larger future emissions of CCl_4 , smaller future emissions of HCFCs owing to the accelerated HCFC phase-out (2007 Adjustment of the Montreal Protocol, see Section 5.4.5),

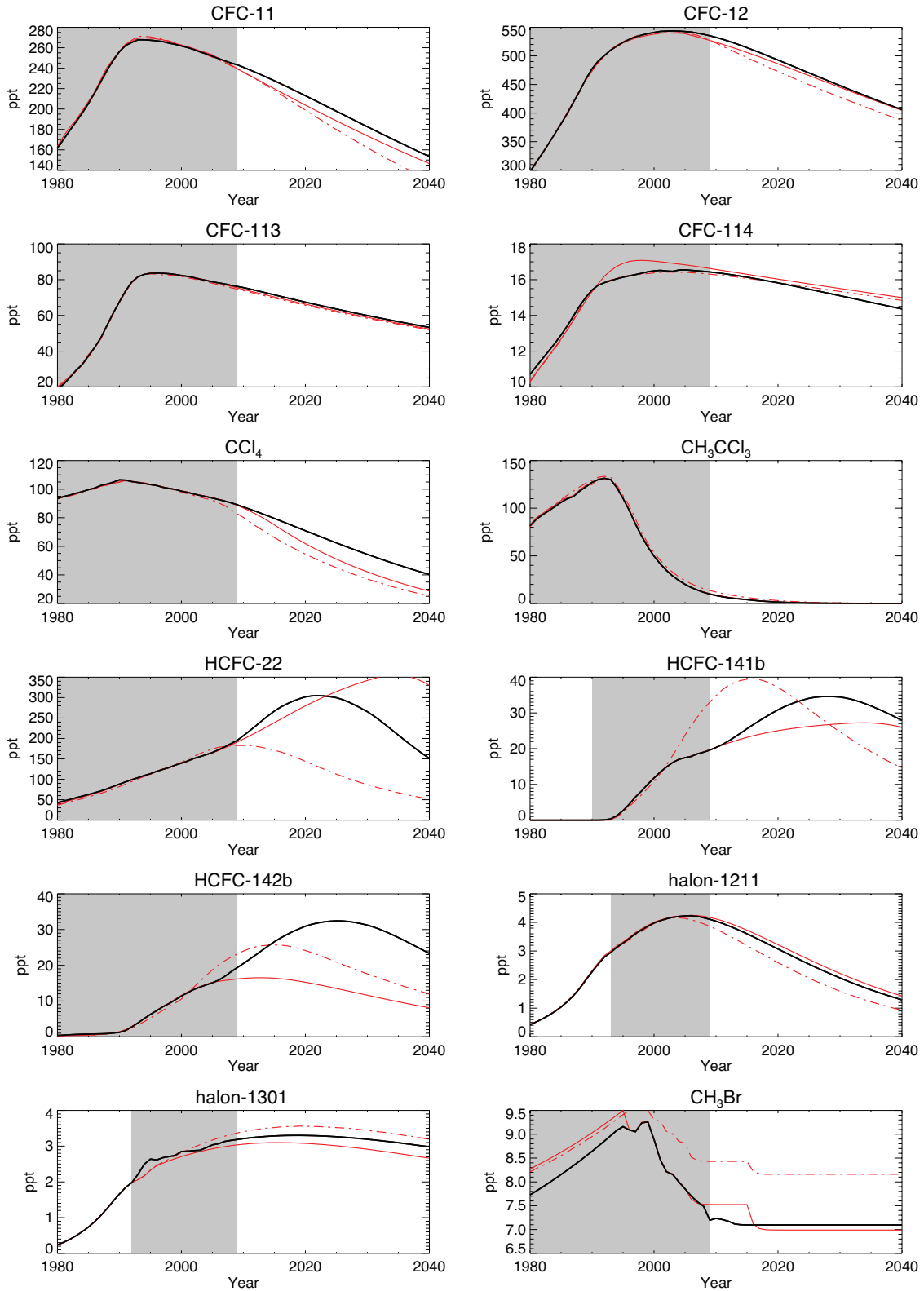
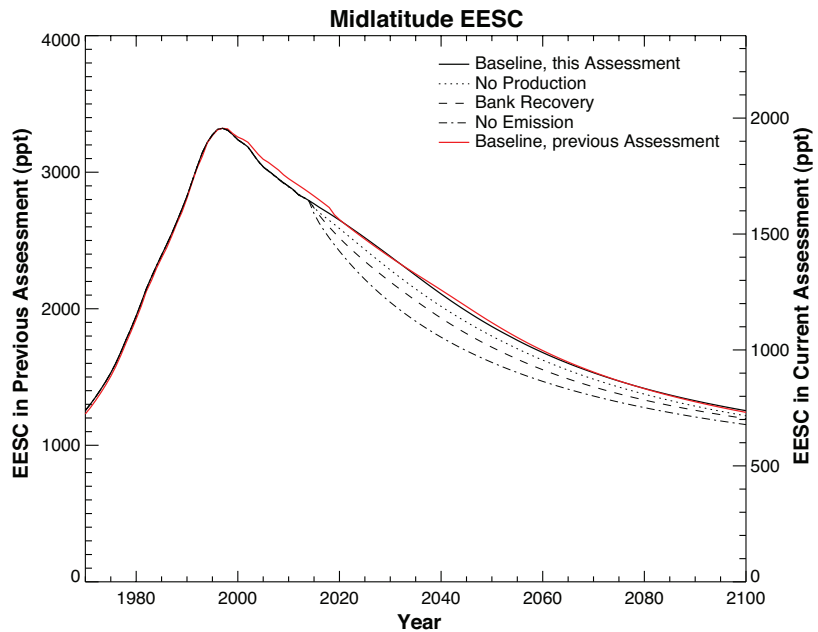


Figure 5-1. Historical and projected mixing ratios (in parts per trillion, ppt) of selected ODSs for the new baseline (A1) scenario (black) compared with the baseline scenarios of the previous Assessment (WMO, 2007) (solid red) and for WMO (2003) (dashed red). Shaded regions indicate years when mixing ratios are taken directly from observations (see Chapter 1).

Figure 5-2. Midlatitude EESC projections (in parts per trillion, ppt) calculated for the current baseline (A1) scenario (solid black) and three test cases: zero future production (dotted), full recovery and destruction of the 2010 bank (dashed), and zero future emission (dot-dashed) (all right-hand axis). EESC values for the baseline scenario of the previous Assessment are also shown (red, left-hand axis). For ease of comparison, the two ordinate axes are relatively scaled so the EESC peak of the current baseline scenario falls on top of the previous baseline scenario peak. Absolute EESC values are different in the two Assessments because in the previous Assessment, different relative halogen fractional release values were used, and the values were scaled so the CFC-11 absolute fractional release value was 0.84. No scaling was performed here so that EESC is more directly representative of Cl_y and Br_y .



and a smaller 1980 mixing ratio of CH_3Br (see Chapter 1, Section 1.2.1.6). Second, the use of revised fractional release values based on recent measurements brings forward the return to 1980 levels by 5–6 years. For Antarctic conditions EESC returns to its 1980 levels in the baseline in 2073. This is 7–8 years later than in the previous Assessment (WMO, 2007), mainly due to the use of fractional release values representative for Antarctic conditions (age of air = 5.5 years) and of a smaller 1980 mixing ratio of CH_3Br (Chapter 1, Section 1.2.1.6), with smaller contributions from the revisions in CCl_4 and HCFCs emissions.

5.3.2 CO_2 , CH_4 , and N_2O

The importance of non-ODS greenhouse gases to future ozone levels has been quantified in several published articles and is discussed in Chapter 3. In this chapter, IPCC Special Report on Emissions Scenarios (SRES)

(IPCC, 2000) scenario A1B is used to prescribe the future evolution of these three gases in the two 2-D model runs described in Daniel et al. (2010). The results of that study are used here to evaluate the impact of hypothetical future controls involving N_2O and the ODSs on globally averaged total column ozone against a backdrop of CO_2 and CH_4 changes and their associated impacts on ozone.

5.3.3 ODP- and GWP-Weighted Emissions, EESC, and Radiative Forcing

The contributions of ODSs to metrics relevant to ozone depletion and to climate change are shown in Figures 5-3 and 5-6. The panels of Figure 5-3 show the ODP-weighted emissions, GWP-weighted (100-year) emissions, EESC, and radiative forcing (RF) for the A1 baseline scenario from 1980–2100. In terms of EESC

Table 5-4 (at right). Comparison of scenarios and cases ^a: the year when EESC drops below the 1980 value for both midlatitude and Antarctic vortex cases, and integrated EESC differences (midlatitude case) relative to the baseline (A1) scenario ^b. Also shown are changes in integrated ODP- and GWP-weighted emissions and, for selected cases, changes in integrated ozone depletion from 2011–2050. Future projected changes in CH_4 and CO_2 are also expected to significantly alter ozone levels, perhaps by amounts larger than any of the cases considered in this table. However, their effects are not included here because changes in CH_4 and CO_2 that would decrease globally averaged ozone depletion would increase climate forcing. Values cited in chapter text calculated as differences between table entries may appear slightly inconsistent with table entries because of rounding.

Scenario and Cases ^a	Percent Difference in Integrated EESC Relative to Baseline Scenario for the Midlatitude Case		Year (x) When EESC is Expected to Drop Below 1980 Value ^b	Antarctic Vortex ^c	Change in ODP-Weighted Emission: 2011–2050	Change in GWP-Weighted Emission: 2011–2050	Percent Difference in Integrated O ₃ Depletion ^f : 2011–2050
	Midlatitude ^c				(Million tons CFC-11-eq)	(Billion tons CO ₂ -eq)	
	$\int_{1980}^x EESC dt$	$\int_{2011}^x EESC dt$					
Scenarios							
A1: Baseline scenario	-	-	2046.5	2072.7	-	-	-
Cases of zero production from 2011 onward of:							
P0: All ODSs	-5.4	-15	2043.0	2069.7	-0.70	-13.2	
CFCs	0.0	0.0	2043.0	2069.7	0	0	
Halons	0.0	0.0	2043.0	2069.7	0	0	
HCFCs	-3.2	-8.8	2044.5	2071.8	-0.45	-13.2	-0.15
CH ₃ Br for QPS	-2.4	-6.7	2044.9	2070.8	-0.26	-0.002	
Cases of zero emissions from 2011 onward of:							
E0: All ODSs (does not include N ₂ O)	-16	-43	2033.5	2059.4	-3.82	-27.2	-0.67
CFCs	-3.9	-11	2043.3	2068.5	-1.27	-7.9	
Halons	-5.0	-14	2043.3	2069.4	-1.09	-0.4	
HCFCs	-4.9	-13	2043.8	2071.4	-0.66	-18.1	
CCl ₄ ^g	-2.8	-7.6	2044.6	2071.6	-0.54	-0.9	
CH ₃ CCl ₃	0	-0.1	2046.5	2072.7	-0.004	-0.004	
CH ₃ Br for QPS	-2.4	-6.7	2044.9	2070.8	-0.26	-0.002	-0.09
Anthropogenic N ₂ O ^h					-6.0	-103	-0.35
Cases of full recovery of the 2011 banks of:							
B0: All ODSs	-10	-27	2039.3	2064.6	-2.57	-13.1	
CFCs	-3.9	-11	2043.3	2068.5	-1.27	-7.9	-0.13
Halons	-5.0	-14	2043.3	2069.4	-1.09	-0.4	-0.15
HCFCs	-1.8	-4.8	2045.8	2072.4	-0.22	-4.9	-0.07
Cases of full recovery of the 2015 banks of:							
B0: All ODSs	-7.1	20	2040.3	2065.7	-2.03	-11.3	
CFCs	-2.6	-7.0	2044.0	2069.4	-0.95	-5.5	
Halons	-3.3	-9.1	2043.8	2069.8	-0.83	-0.3	
HCFCs	-1.9	-5.3	2045.5	2072.2	-0.26	-5.5	
CH₃Br sensitivity:							
Same as A1, but critical-use exemptions continue at 2011 levels	+0.3	+0.8	2046.6	2073.0	+0.03	+0.0003	

^a Significance of ozone-depleting substances for future EESC were calculated in the hypothetical “cases” by setting production or emission to zero in 2011 and subsequent years or the bank of the ODSs to zero in the year 2011 or 2015.

^b When comparing to WMO (2007), revised fractional halogen release values have contributed to an earlier EESC recovery year for midlatitudes and a later one for the Antarctic vortex.

^c For midlatitude conditions, an age-of-air value of 3 years, corresponding fractional release values, and a value for α of 60 are used. For Antarctic vortex conditions, an age-of-air value of 5.5 years with corresponding fractional release values and a value for α of 65 are used.

^d Using semi-empirical ODPs from Table 5-1.

^e Using direct GWPs with 100-year time horizon (see Appendix Table 5A-1).

^f Integrated globally averaged total column ozone changes are taken from Daniel et al. (2010).

^g Banks are assumed to be zero. Emissions include uncertain sources such as possible fugitive emissions and unintended by-product emissions.

^h The integrated ODP- and GWP-weighted emissions correspond to the elimination of all anthropogenic N₂O emissions from 2011 onward in the A1B SRES scenario.

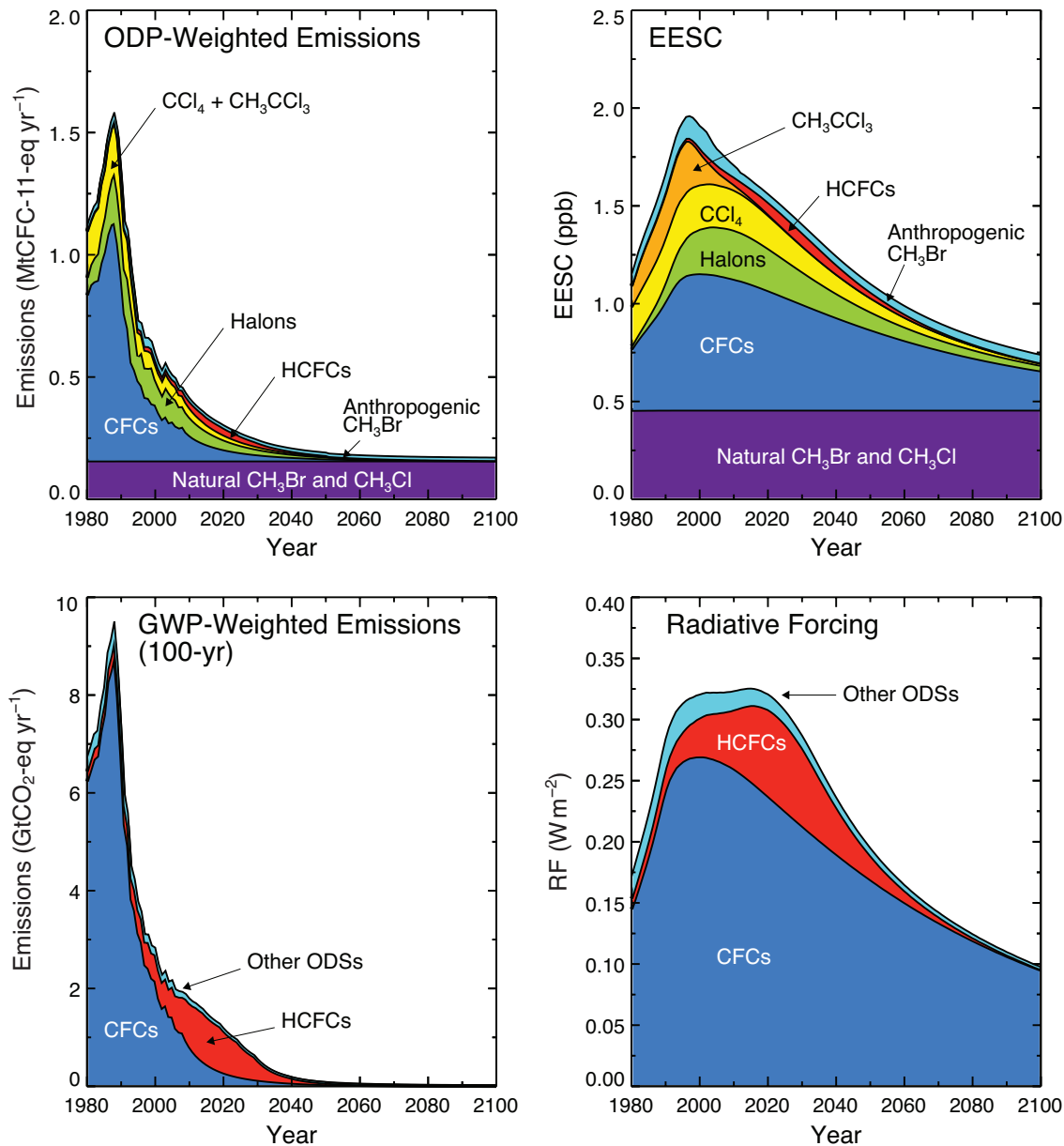


Figure 5-3. ODP- and GWP-weighted emissions, EESC, and radiative forcing of the chlorine- and bromine-containing ODSs of the baseline (A1) scenario. Only the direct GWP-weighted emissions and radiative forcing are considered here. Semi-empirical steady-state ODPs (Table 5-1) and 100-year GWPs (Appendix Table 5A-1) are used to weight emissions. The emissions and radiative forcing of the HFCs are not included in these graphs because of the large range in HFC scenarios. They are shown in Figure 5-5.

Figure 5-4 (at right). Banks of CFCs, HCFCs, and halons in 1995, 2008, and 2020 in megatonnes (Mt) and weighted by their ODPs and 100-year GWPs (direct term only). The 2008 bank is from TEAP (2009) for almost all compounds. The 1995 bank is derived by a backwards calculation using the historic emissions, UNEP production data, and the 2008 bank. The 2020 bank is calculated in the baseline scenario from estimates of future production and bank release rates. The pie slices show the sizes relative to those of the maximum values (1995 for the ODP- and GWP-weighted banks and 2008 for the bank in Mt) and therefore don't fill a full circle. The total bank size is given below each pie chart. For comparison, the HFC bank size has been estimated to have been 1.1 GtCO₂-eq in 2002 and 2.4 GtCO₂-eq in 2008, and has been projected to be 4.6 GtCO₂-eq in 2015 in a business-as-usual scenario (Velders et al., 2009).

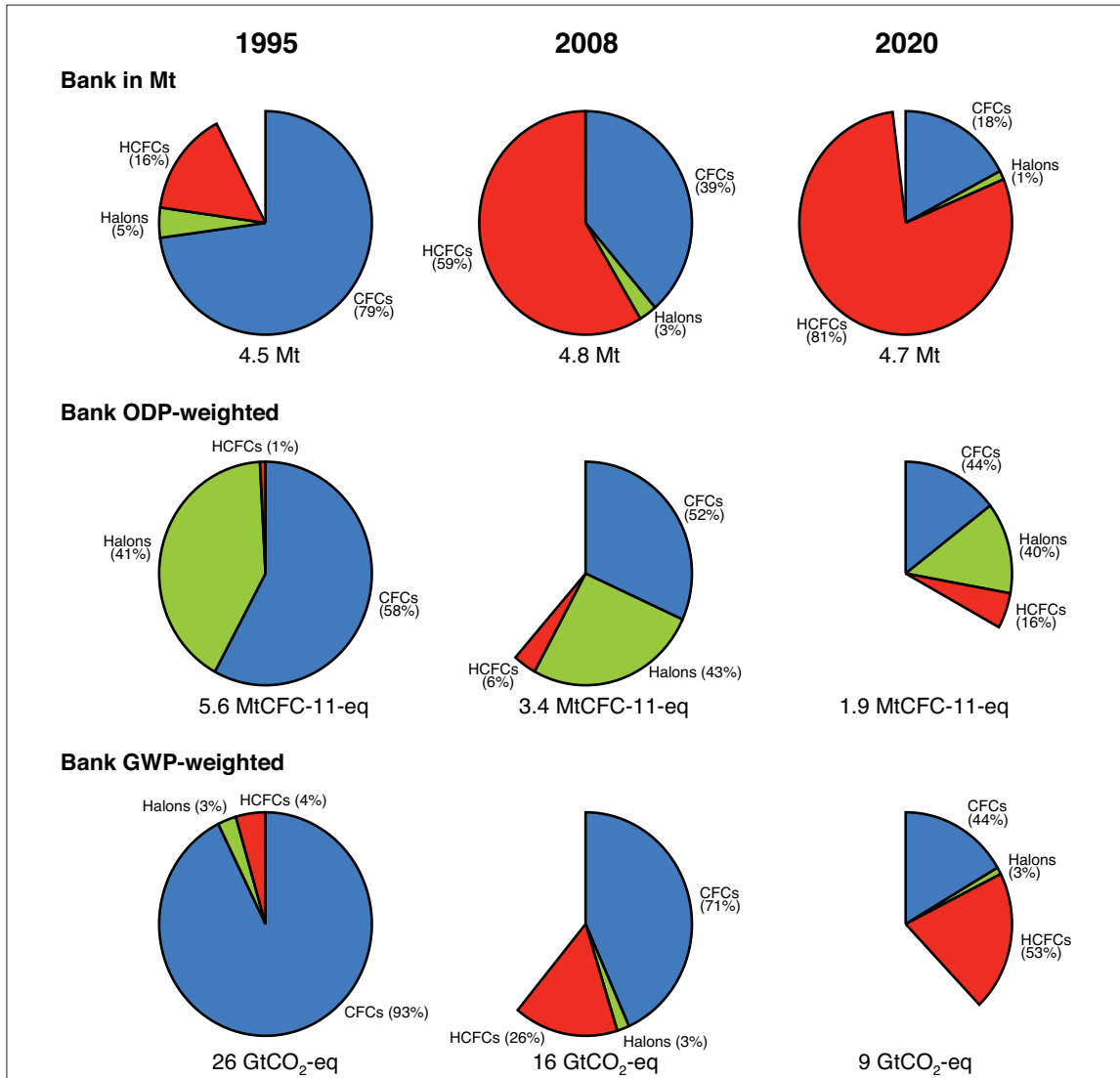
contribution, the largest contribution in the past and future comes from the CFCs and natural CH₃Cl and CH₃Br emissions. In terms of radiative forcing the CFCs are also the most important ODSs, but the HCFCs are projected to contribute more than 0.05 W/m² at their peak.

CFC, HCFC, and halon bank size estimates for 1995 and 2008 and projections for 2020 are shown in Figure 5-4. The contributions of the ODSs to the bank are compared by mass and when weighted by their ODPs and GWPs (100-year). The total size of the bank by mass remains more or less constant over time, but decreases significantly when considering their potential effect on depletion of the ozone layer (ODP-weighted) and on climate forcing (GWP-weighted). The decreasing contribution of the CFCs and increasing contribution of the HCFCs is particularly apparent when examining the banks by mass and when weighted by GWPs. The relative contributions of both the CFCs and halons remain the largest when considering the ODP-weighted banks.

5.4 IMPACTS OF HUMAN ACTIVITIES RELEVANT TO OZONE POLICY

5.4.1 Background

In this section, we assess the importance of various human activities that are relevant to ozone policy formulation. The focus is primarily on the extent to which future ozone depletion may be affected. We also discuss the potential effect of HFCs on climate forcing because the widespread use of HFCs has occurred directly as a result of ODS controls of the Montreal Protocol. We discuss geoengineering using atmospheric sulfur injections, and CO₂ and CH₄ emissions not because they necessarily have relevance for ozone policy decisions, but to assess their potential for inadvertent ozone impacts as a result of climate change policies or the absence of such policies.



5.4.2 Ozone Impacts

The Montreal Protocol and its Amendments and Adjustments have effectively controlled the emission of the most important ozone-depletion gases containing chlorine and bromine. It is a testament to the success of the Montreal Protocol that current potential policy options and activities that do not involve chlorine- or bromine-containing compounds are expected to have some of the greatest effects on future ozone levels. However, to maintain consistency with past reports and to address the relative importance of continued emissions of halogenated source gases, we provide in Section 5.4.2.1 an analysis of various hypothetical test cases using EESC as the comparison metric.

Chapter 8 of the previous Assessment (Daniel and Velders et al., 2007) focused strictly on the EESC index to quantify the potential effects of additional ODS controls on stratospheric ozone depletion. Here, results from 2-D model calculations in Daniel et al. (2010) are presented to augment the historical reliance on EESC and as a way to assess the ozone impact of several different assumptions of future emissions of halocarbons (e.g., CFCs, HCFCs, halons, CH₃Br) and N₂O (Section 5.4.2.2 and Chapter 3) (see Table 5-4). The phase-out and baseline scenarios assumed in Daniel et al. (2010) were similar to those in this chapter. However, that paper should be consulted for a consistent comparison of ozone changes with EESC changes. Estimates of ozone impacts from ODSs and N₂O future emission changes also allow for comparison with other activities and emissions, such as CO₂ and CH₄. The computational efficiency of 2-D models makes it possible now to perform multiple long-term simulations in a reasonable amount of time to examine the effects of various scenarios. The residual circulation framework used in 2-D models has been shown to provide realistic simulations of atmospheric transport on long timescales (>30 days). Recent studies have demonstrated good overall model agreement with a variety of observations in reproducing transport-sensitive features in the meridional plane (e.g., Fleming et al., 2007). These capabilities make these models useful tools for studying long-term ozone changes.

5.4.2.1 CHLORINE- AND BROMINE-CONTAINING ODSs

Alternative test cases, based on the baseline scenario of ODSs (Section 5.3.1), are constructed and used to examine the relative effects of reducing future emissions of groups of halocarbons on EESC and stratospheric ozone levels. These alternative cases fall into four categories: (1) “No future emission” cases; (2) “No future production” cases; (3) cases assuming the full capture and destruction of the 2011 bank; and (4) cases assuming full capture and destruction of the 2015 bank. For the bank

cases, the entire bank is considered, not just the portion that is estimated to be “accessible.” The 2015 bank recovery cases are run to quantify the impact of the implementation date of hypothetical bank emission controls; it should be recognized, however, that we do not have an estimate of the uncertainty in the future bank projections, on which these calculations are based. Full elimination of emissions, production, and banks are considered rather than some smaller fractional reduction because the intent is to provide policy-neutral cases that can be used to determine the impacts of other specific policy options. The impact of any option that involves a smaller reduction can be determined by simply scaling the results of Table 5-4. For example, if the “accessible” bank is estimated to be 30% of the total bank, the results in the table for that compound can be simply multiplied by 0.3 to determine the impact of capture and destruction of the accessible bank. The elimination of all future emissions represents the greatest possible reduction in future abundances that can be imparted by direct controls. The elimination of future production allows the ODSs currently residing in banks to continue to be released to the atmosphere as they would in the baseline scenario. The projections that consider the full capture and destruction of the 2011 bank complement the “No Production” scenarios in that the full 2011 bank is destroyed in a manner that releases no ODSs to the atmosphere; future production and the resulting future buildup of banks is allowed to continue, however. The expected future production is virtually zero for the CFCs and halons, but still significant for the HCFCs and possibly for CCl₄. The “No production” and “Full capture and destruction of the 2011 bank” cases are complementary in the sense that they may be combined to approximately estimate the “No emission” cases.

The effects of the alternative test cases are presented in Table 5-4 using metrics similar to those of previous assessments, i.e., the year EESC returns to its 1980 level for midlatitude and Antarctic vortex conditions, and the change in integrated EESC relative to the baseline scenario. These integrated values are dependent on the choice of the 1980 level. If a lower level were chosen, for example the 1975 level, the tendency is for the CFC options to gain in importance relative to the other ODS policy options. This results from the longer atmospheric lifetimes of the CFCs. Also in this table is the change in cumulative ODP- and GWP-weighted (direct contribution only) emissions. The latter gives an indication of the potential effects of the cases for climate forcing. In general, the various cases presented here lead to smaller integrated EESC differences (when integrated from 1980) and return year differences from the baseline scenario than the same test cases from WMO (2007). This is expected, as banks of most ODSs are smaller due to continued emission for 4 more years, and there are now fewer years to continue

to produce the various ODSs before the mandated phase-out. CCl_4 represents an exception to this. The increasing apparent importance of a CCl_4 production or consumption phase-out arises from projected CCl_4 emissions being larger in the current baseline scenario than in WMO (2007). The increased future emissions are based on an extrapolation of declining global emissions over the last 5 years (6%/year). This decline in CCl_4 emissions has not mirrored the strong decrease in reported production of CFC-11 and CFC-12 as it did in the 1980s and 1990s. This revised projection is thus not based on an improved understanding of the budget of CCl_4 , which still cannot be balanced nor can the interannual variability be explained with our current knowledge of CCl_4 sources and sinks (see Chapter 1). The incomplete understanding of the CCl_4 budget represents a significant gap.

Emissions of CFCs and halons from the banks are the largest sources of current ODP-weighted emissions of ODSs. An immediate phase-out of halon bank emission sources reduces future integrated EESC more than the elimination of emissions of any other compound or compound group, with slightly more of an impact than the elimination of future HCFC emissions. A delay of four years, from 2011 to 2015, in the capture and destruction of the estimated banks of CFCs and halons is currently thought to reduce the potential ozone and climate benefits by about 30% since ODSs continue to be emitted from these banks and production is thought to have essentially ceased.

A phase-out of methyl bromide emissions from quarantine and pre-shipment (QPS) applications beginning in 2011 would shift the year midlatitude EESC reaches the 1980 level earlier by 1.5 years compared to continued use at current levels. Continuing critical-use exemptions (CUE) at the approved 2011 level would delay the return of EESC to 1980 levels by 0.2 years.

The elimination of all emissions of chlorine- and bromine-containing ODSs after 2010 would shift the year midlatitude EESC reaches the 1980 level by about 13 years, from 2046 to 2033. In terms relevant to climate, this would reduce emissions of these compounds by about 0.7 gigatonnes (Gt) of CO_2 -equivalent ($\text{GtCO}_2\text{-eq}$) per year averaged over 2011 through 2050. Future production of HCFCs and the sum of the current banks of CFCs plus HCFCs contribute about equally to this number. In comparison, global anthropogenic emissions of CO_2 were greater than 30 Gt per year in 2008.

In past assessments, the potential impact of chlorine-containing VSLS has been neglected in the evaluation of hypothetical ODS emissions phase-outs. However, it is likely that their contribution is not negligible. As discussed in Chapter 1, anthropogenic VSLS are currently expected to contribute about 39 ppt chlorine to the

stratosphere with fairly large uncertainty. Because these likely release their chlorine quickly, this amount could contribute directly to EESC with a unit fractional release value. If included in EESC in this way, at midlatitudes, a phase-out of these compounds is expected to advance the return of EESC to 1980 levels by almost 3 years. The magnitude of this effect is significant compared to the long-lived ODS cases presented in Table 5-4. This impact depends strongly on the region of the stratosphere considered, with greater impacts in regions where less chlorine has been liberated from long-lived source gases, but where chemical ozone loss is still important. It is also unclear how VSLS emission reductions in specific locations and during different times of the year would quantitatively affect the abundance of stratospheric chlorine.

The uncertainties of the effects of the test cases presented in Table 5-4 have been estimated by varying several model parameters for each class of compounds (CFC, HCFCs, etc.) in the calculation: the size of the banks in 2008, the annual emission rate from the banks, the fractional release values, and the lifetimes of the compounds (Douglass et al., 2008; Martinerie et al., 2009). The lifetimes and annual emission rate from the banks are only varied for 2009–2100, since the data through 2008 is constrained by observations. A variation of 20% in the size of the 2008 banks of CFCs, HCFCs, and halons results in a variation of about 20% in the change in integrated EESC, for each class of compounds, in the case of a full recovery of the banks. The year EESC returns to the 1980 level varies by less than a year. Doubling the annual emission rate from the banks increases the change in integrated EESC by up to 15%, while reducing the annual emission rate by 50% decreases the changes in integrated EESC by up to 30%. Again, for most cases, the year EESC returns to the 1980 level varies by less than a year. Variations of 20% in the fractional release values per class of compound gives similar variations. Variations of up to ± 3 years occur in the year EESC returns to the 1980 level when varying the lifetimes of the CFCs by $\pm 20\%$. The effects of such a variation on the change in integrated EESC is less than $\pm 20\%$ for each compound group. These uncertainties have been applied to entire groups of compounds. These uncertainties are likely independent across compound groups for the size of the banks and annual emission rates from the banks, but perhaps not for the fractional release values and lifetimes.

The benefits of the Montreal Protocol that are calculated to have already been achieved are highlighted in Section 5.5. The cases considered here show that the options for limiting future halogenated ODS emissions are expected to have a much smaller impact on future ozone depletion and climate than what has already been accomplished by the Montreal Protocol.

5.4.2.2 CO₂, CH₄, AND N₂O

The increasing concentration of carbon dioxide (CO₂) in Earth's atmosphere warms the troposphere but cools the stratosphere. This cooling leads to slower gas-phase ozone loss reactions (Haigh and Pyle, 1979; Rosenfield et al., 2002), and thus to an increase in stratospheric ozone. Cooling of the polar lower stratosphere can also lead to enhanced polar stratospheric cloud (PSC) formation and more ozone destruction via more efficient heterogeneous chemistry (Chapter 3, Section 3.2.3). Increasing concentrations of methane and its effects on hydrogen oxides can enhance the destruction of ozone in the upper stratosphere. Increases in methane (CH₄) can also reduce the ozone loss in the stratosphere by converting chlorine from active species to the reservoir HCl, and can lead to NO_x-induced ozone production in the troposphere and lower stratosphere via the CH₄ oxidation cycle. Increases in methane and the subsequent oxidation to water vapor will also lead to weak stratospheric cooling. Future levels of CO₂ and CH₄ may be higher for some period of time compared with today. If they are, they would be expected to lead to higher levels of column ozone at midlatitudes (e.g., Li et al., 2009; Waugh et al., 2009; Hsu and Prather, 2010). Thus, there is the possibility of a "super-recovery," where the total amount of atmospheric ozone exceeds 1960 levels. Both 2-D (Rosenfield et al., 2002; Chipperfield and Feng, 2003; Portmann and Solomon, 2007; Daniel et al., 2010), and 3-D model (SPARC CCMVal, 2010) calculations suggest that increases in CO₂ and CH₄ will lead to total column ozone increases that are larger than what can be caused by decreases in future ODS or nitrous oxide (N₂O) emissions. Because increasing levels of CO₂ and CH₄ are expected to continue to lead to increased total ozone, but also increased climate forcing, we present this information as relevant for inadvertent ozone impacts due to climate policy choices. Further complicating the matter is that, for ozone, changes in circulation due to greenhouse gases are expected to be the dominant factor in the tropics, and this will lead to lower column ozone levels there. Additional discussion of the impacts of CO₂ and CH₄ on ozone can be found in Chapter 3.

N₂O emissions reductions, in contrast, would reduce climate forcing, and the resulting decrease in stratospheric nitrogen oxides would lead to higher ozone levels. Ravishankara et al. (2009) have shown that when ODS emissions are weighted by their steady-state ODPs, N₂O emissions represent the single most important anthropogenic emissions today for ozone depletion. Unmitigated, these emissions are also expected to remain the most significant throughout the 21st century. In the current atmosphere, CFCs lead to much more ozone depletion than does N₂O because of the large historic emissions and long lifetimes of the CFCs. The 2-D models used in Daniel et

al. (2010) suggest that N₂O causes an ozone depletion in the current atmosphere of about 3 Dobson units (DU) compared with the ODSs depleting about 18 DU. However, when the impact of phase-outs of future emissions are considered, an immediate phase-out of all anthropogenic N₂O emissions leads to a greater reduction in ozone depletion integrated through 2100 than the integrated ozone depletion reduction arising from an elimination of all future ODS emissions (Daniel et al., 2010). The climate forcing and ozone impacts of a hypothetical emissions phase-out beginning in 2011 of several ODSs and anthropogenic N₂O are compared in the final three columns of Table 5-4. These comparisons show the relative significance of these policy options using cumulative ODP- and GWP-weighted emissions and ozone integrated from 2011–2050. The significance of N₂O compared to the ODSs is not surprising given the higher current ODP-weighted emissions compared to the controlled ODSs. We emphasize that all the phase-outs considered are purely hypothetical with no consideration given to the economic or technological feasibility of implementing them.

5.4.2.3 N₂O FROM AUTOMOTIVE BIOFUELS

Anthropogenic emissions of N₂O total approximately 6.7 TgN yr⁻¹ (IPCC, 2007). Agriculture is responsible for 2.8 TgN yr⁻¹ and related emissions from rivers, estuaries and coastal zones add a further 1.7 TgN yr⁻¹. Emissions associated with fossil fuel combustion and industrial activities, biomass burning, atmospheric deposition, and human excreta combined account for the remaining 2.2 TgN yr⁻¹. The Greenhouse Gases, Regulated Emissions, and Energy Use in Transportation (GREET) model provides a life cycle assessment of biofuel production and uses, and includes allocation and differentiation of biofuels based on different agricultural practices (Wang, 2010). The GREET model provides N₂O emission factors for corn ethanol, sugarcane ethanol, and soy biodiesel in the United States of America (USA) of approximately 45, 25, and 17 g/MMBtu of fuel produced (MMBtu = million British thermal units, 1 MMBtu = 1.055 gigajoules (GJ)). The USA is the largest biofuel producer, and corn ethanol is the dominant biofuel produced in the USA and has the highest N₂O emissions per megajoule (MJ) of fuel produced. Combining 40 g N₂O/MMBtu with a production of 17.5 million tonnes of oil equivalent in 2008 (British Petroleum, 2009; 1 tonne of oil equivalent = 42 GJ) we estimate an emission of 0.018 TgN yr⁻¹ associated with production of corn ethanol in the USA. This is approximately 0.2% of the total anthropogenic emission of 6.7 TgN yr⁻¹ (IPCC, 2007). Crutzen et al. (2008) have argued that depending on N fertilizer uptake efficiency by plants, the formation of N₂O during the production of commonly used automotive biofuels, such as biodiesel from rapeseed

and bioethanol from corn (maize), can negate the CO₂ mitigation from fossil fuel savings. However, the analysis by Crutzen et al. (2008) does not consider allocation of emissions to the coproducts in the process (e.g., animal feed produced during corn ethanol production).

The contribution of automotive biofuels to global N₂O emissions is currently significantly below 1% and expected to remain so in the future. While global agricultural activities emit substantial amounts of N₂O, biofuel production itself is currently not a major contributor to N₂O emissions. Although current biofuel production represents a small fraction of total crude oil production, and increases in biofuel production appear likely, second generation biofuels (e.g., lignocellulosic ethanol) are anticipated to have substantially lower environmental impacts. Historical changes in the atmospheric concentrations of N₂O and emissions sources are discussed in Section 1.5.1.2 of Chapter 1.

5.4.2.4 GEOENGINEERING: ENHANCING EARTH'S ALBEDO BY STRATOSPHERIC INJECTION OF SULFUR

There is increasing concern that efforts to reduce global greenhouse gas emissions will not be sufficient to prevent Earth's climate from warming to levels that have never been experienced by modern societies. This has intensified the discussion about deliberate atmospheric modification schemes ("geoengineering") to counteract enhanced greenhouse warming due to industrial emissions (for example, see the review panel report on geoengineering (Royal Society, 2009)). Although fraught with uncertainties and side effects that have yet to be studied in detail (Keith et al., 2010), the notion of enhancing Earth's albedo by increasing particulate scattering of visible light in the stratosphere dates back many decades (e.g., Budyko, 1977; Dyson and Marland, 1979). It has been estimated that injection of particles designed for optimum scattering of shortwave radiation (e.g., sulfate or aluminum oxide) might be economically viable and would likely be the most cost-effective method of a class of geoengineering options called "solar radiation management" (Teller et al., 1997; Lenton et al., 2009; Royal Society, 2009). These studies also point out that the proposed solar radiation management techniques likely have the largest side effects of the geoengineering options considered. For example, changes in shortwave radiation would likely result in local temperature and precipitation changes, including increased prevalence of droughts (Hegerl and Solomon, 2009). Various possible side effects of geoengineering (e.g., Robock, 2008) besides the impact on ozone are not further discussed in this Assessment. Other methods that have been suggested for managing solar radiation

or taking up carbon dioxide (e.g., launching mirrors into space to harvest or block radiation; fertilizing the ocean to promote uptake of CO₂ by phytoplankton) could also impact stratospheric ozone, but are not considered here due to a lack of scientific investigations that would allow for an assessment of the impacts of these approaches.

Part of the reason injection of sulfate into the stratosphere has received considerable attention in recent years from the scientific community as an option for solar radiation management (Crutzen, 2006) is due to observations of modest cooling of the globe following major volcanic eruptions, which may be viewed a natural analog to this particular approach to manage Earth's radiation budget. The 1991 eruption of Mt. Pinatubo, for example, resulted in a decrease of global mean temperatures by 0.5°C for a few years (Soden et al., 2002). Observations from recent volcanic eruptions have shown that stratospheric ozone in middle and high latitudes is strongly influenced by the enhanced burden of liquid sulfate aerosols (e.g., Tabazadeh et al., 2002; Solomon et al., 1996; Portmann et al., 1996; Tilmes et al., 2008a). Recent model calculations have estimated a global temperature decrease of about one degree at Earth's surface could be achieved within about five years after the start of a hypothetical sulfate aerosol injection experiment (Robock et al., 2008; Tilmes et al., 2009). However, Heckendorn et al. (2009) have shown that the size distribution of aerosol particles is not fixed as assumed in earlier studies but strongly depends on different injection assumptions. The ability to achieve some amount of cooling that might be required to offset enhanced greenhouse-gas warming may be limited due to the coagulating and settling of aerosols. This process would also warm the tropical tropopause, perhaps resulting in enhanced abundances of stratospheric water vapor, which could accelerate ozone loss especially in the tropics and midlatitudes (Heckendorn et al., 2009). However, a significant increase of stratospheric water vapor was not observed after large volcanic eruptions.

Tilmes et al. (2008b, 2009) estimated the impact of an enhanced burden of stratospheric sulfur on the ozone layer during the period of time when stratospheric halogen loading is projected to slowly decline (Newman et al., 2007). Assuming an injection into the tropical stratosphere of a mass of volcanic-sized (submicron) sulfate aerosols large enough to counteract a doubling of CO₂ with respect to preindustrial values (Rasch et al., 2008a), ozone depletion in the Arctic polar vortex might be expected to double or triple (Tilmes et al., 2009). In addition, the expected recovery of the Antarctic ozone hole from the reduction in atmospheric halogen loading brought about by the Montreal Protocol might be delayed by between 30 and 70 years, depending on the assumed particle sizes (Tilmes et al., 2008b) (see Chapter 3). The

estimated impact on stratospheric ozone at low latitudes is expected to be smaller (about $\pm 3\%$) for 2050 chlorine conditions (Tilmes et al., 2009).

Studies to quantify the impact of geoengineering on ozone have so far assumed basic scenarios and idealized conditions, and they have focused entirely on sulfate aerosols. Particle size distributions are usually described in simple terms, with large uncertainties in the evolution of those distributions (Rasch et al., 2008b). More comprehensive microphysical models, such as the one described in Heckendorn et al. (2009), are necessary to describe the complete size-distributions for geoengineering experiments. Dynamical and chemical changes in the stratosphere as a result of geoengineering are still uncertain given our current modeling capabilities (Chapter 3).

Uncertainties also exist in the amount of sulfur necessary to counteract global warming, which in turn depends on the amount of aerosol deposition (e.g., Heckendorn et al., 2009) and on the strength of the stratospheric circulation in the models, whether assumed for present-day conditions, or for a future accelerated stratospheric circulation (Rasch et al., 2008a). To date there have been no investigations of the impact on ozone caused by a gradual ramp-up of the amount of SO_2 injected, with the purpose of keeping global average temperature nearly constant (Wigley, 2006). The amount of ozone that might be destroyed by deliberately increasing the aerosol loading of the stratosphere might also differ following a large volcanic eruption that further increases the amount of sulfur in the stratosphere (Tilmes et al., 2008b). Finally, there has been little study of an engineered stratospheric reflecting layer that uses materials other than sulfate (e.g., particles manufactured for maximum scattering of shortwave radiation and extended stratospheric lifetimes, as proposed by Teller et al., 1997).

These and other remaining gaps in our understanding of the full impacts of geoengineering on stratospheric ozone (and other aspects of the environment) are significant. The potential for significant risks to the ozone layer and the climate system, both known and unknown, from solar radiation management, as well as the fact that these approaches do not address other problems like ocean acidification as a result of increasing CO_2 levels, have been acknowledged (Royal Society, 2009).

5.4.2.5 EMISSIONS FROM AVIATION AND ROCKETS

Aviation

The importance of current aircraft emissions for ozone is well recognized (IPCC, 1999; WMO, 2003; Wuebbles et al., 2006; Maurice and Lee, 2009; Lee et al., 2009). Aircraft emissions, overall, are thought to increase globally averaged ozone columns by less than

0.5%, primarily due to photochemical production of ozone catalyzed by nitrogen oxides (NO_x), odd hydrogen (HO_x) (from H_2O), and hydrocarbon (HC) emissions. The production of ozone by emissions of NO_x and HCs is offset by the destruction of ozone that occurs when emissions of aerosols and water vapor enhance abundances of ozone-destroying active halogens. As a consequence, little or no impact on stratospheric ozone column abundances is expected from aircraft emissions transported into the lower stratosphere from the troposphere (WMO, 2003; Brasseur, 2008; Lee et al., 2009). New studies reinforce that there is a dual nature of aircraft emissions directly within the stratosphere or near the tropopause, with ozone production in some regions, and losses in others, and a strong dependence of the sign of net ozone changes on the latitude and altitude of those assumed emissions (Meilinger et al., 2005; Søvde et al., 2007; Pitari et al., 2008; Köhler et al., 2008; Cariolle et al., 2009).

Aviation-perturbed ozone can also affect the tropospheric oxidizing capacity, and thus levels of methane, a species that influences ozone chemistry in both the troposphere and stratosphere. Köhler et al. (2008) estimate that the increase in the oxidizing capacity of the troposphere due to aircraft emissions has reduced the lifetime of methane by 3.0%. Given that increases in methane are expected to increase stratospheric ozone (e.g., Section 5.4.2.2), this indirect change due to aircraft would be expected to have an offsetting effect on the increase in ozone columns.

Given that a large shift of worldwide aviation from subsonic to supersonic travel is unlikely in the foreseeable future, this Assessment assumes that aircraft emissions will be predominantly tropospheric. In this case, the net impact of those emissions will be ozone production, with some regional variation such as larger enhancements in heavily traveled flight corridors (e.g., Northern Hemisphere middle latitudes in summer). Ozone changes are expected to be smaller in the Southern Hemisphere, where there are fewer flights and emissions.

Rockets

A summary of the important processes that can contribute to ozone loss from rocket launches is found in Chapter 1. In the context of scientific and regulatory frameworks for protecting stratospheric ozone, the treatment of combustion emissions from rockets is somewhat complicated because ODP calculations involve some poorly understood processes, may be only regionally appropriate (not globally), and depend on many factors (e.g., propellant type, trajectory, latitude of launch site, etc.). In addition, the atmospheric lifetimes of rocket emissions (except for CO_2) are less than a few years, which are short compared to the lifetimes of most halocarbon source

gases. As is the case for aircraft, the impacts from rockets are due to primary and secondary products of combustion (e.g., H₂O, NO_x, hydrogen chloride (HCl), alumina, soot, and sulfate), and not to the fuels themselves. As with other processes presented in this chapter, the impact of rocket emissions on ozone may attract more attention in the coming decades if the space launch market grows (Ross et al., 2009).

Several new classes of rocket propellant are of particular concern even though they do not contain chlorine, because they could still have significant effects on ozone. The first, composed of aluminum and H₂O, has been proposed recently as an “environmentally friendly” solid rocket motor replacement. Because the emission from an Al/H₂O rocket is mainly composed of alumina particles (compared to 30% for conventional solid rocket motors), ozone losses from such a rocket could exceed those from conventional solid rocket motors for equal emission rates if there is an ample reservoir of chlorine in the stratosphere, which will be the case for at least a few decades. The second, a “hybrid” that uses N₂O and solid hydrocarbon as propellants, is being developed for widespread commercial spaceflight and could account for about one-third of all rocket emissions by 2020 (Seedhouse, 2008). Very little is known about the nature and magnitude of the emissions from this new hybrid rocket engine, though initial concerns for stratospheric ozone will focus on uncombusted N₂O and soot.

Given these uncertainties and the long lead times in space launch hardware engineering and development, the lack of metrics for addressing the global impacts of rocket emissions can be particularly problematic (Ross et al., 2009). Improved understanding of the processes involved in ozone depletion and development of suitable metrics can provide an important framework for launch industries to identify the factors responsible for the environmental impacts of rockets. This could allow, for example, for choice of propellant that best minimizes the environmental impacts.

5.4.2.6 SUMMARY

The ozone impacts of the processes discussed in Section 5.4.2 are qualitatively compared in Table 5-5. Our understanding of the ozone impact of activities directly relating to production and emissions of halocarbons and CO₂, CH₄, and N₂O is fairly advanced, while important gaps remain in our understanding of the impacts of other activities like aviation, space transport, and geoeengineering. Chlorine- and bromine-containing ODSs play the largest role in current ozone depletion while the enhancement of CO₂ and CH₄ above background levels has likely led to higher globally averaged ozone levels than otherwise would have occurred. However, because of the controls

already imposed by the Montreal Protocol on production and consumption of ODSs and the long atmospheric lifetimes of these compounds, the ability to further reduce future atmospheric ODS concentrations and thus ozone depletion through additional controls is more limited than before. Future ozone evolution is expected to be largely affected by activities and emissions not currently regulated by the Montreal Protocol, particularly by changes in CO₂, CH₄, and N₂O. Some of these activities and emissions will likely increase ozone and some will decrease it. Our ability to project future stratospheric ozone is becoming more complicated, in that activities controlled by the Montreal Protocol are likely no longer the most important ones for the future evolution of stratospheric ozone.

5.4.3 Climate Impacts

5.4.3.1 MAJOR HFCs USED AS REPLACEMENTS FOR ODSs

Global production and use of CFCs and halons have decreased significantly because of the phase-outs under the Montreal Protocol and its subsequent Amendments and Adjustments. As a direct result, the use of HCFCs and HFCs as replacements has increased in Article 5 and non-Article 5 countries (see Chapter 1). The HCFC increases occurred earlier and have been confirmed by long-term growth in observed atmospheric mixing ratios (Montzka et al., 2009; Stohl et al., 2009) (Chapter 1). Recent changes in northern-latitude mixing ratio observations are consistent with reduced use of HCFCs in non-Article 5 countries and increased use in Article 5 countries (Montzka et al., 2009). HCFCs have been used as low-ODP substitutes in many applications for high-ODP substances and were classified under the Protocol as “transitional substitutes” to be used during the time it took to commercialize new ozone-safe alternatives and replacements. In 2007 the Parties to the Montreal Protocol decided to accelerate the HCFC phase-out, in part to protect future climate. HCFC production and consumption in Article 5 countries will be frozen in 2013 and stepwise reduced, with a virtually complete phase-out in 2030. Non-Article 5 countries have agreed to a virtually complete phase-out in 2020. In adopting the accelerated HCFC phase-out, the Parties agreed to promote the use of HCFC alternatives that minimize the impact on climate.

With the global phase-out of HCFCs, much of the future application demand for refrigeration and air conditioning and heating is likely to met by HFCs, while the demand for thermal-insulating foam production is likely to be met by HFCs as well as hydrocarbons and not-in-kind thermal insulation such as fiberglass and mineral wool (IPCC/TEAP, 2005; Velders et al., 2009). HFCs

Table 5-5. Qualitative summary of anthropogenic processes affecting stratospheric ozone.

Activity	Mechanism	Effect on Ozone Layer		
		Ozone Column Increase or Decrease ^a	Understanding ^b	Approximate Maximum Impact ^c
Destruction of CFC banks	Ozone destruction by chlorine chemistry	+	High	Medium
Destruction of HCFC banks	Ozone destruction by chlorine chemistry	+	High	Small
Destruction of halon banks	Ozone destruction by chlorine and bromine chemistry	+	High	Medium
Eliminate HCFC production	Ozone destruction by chlorine chemistry	+	High	Medium
Eliminate CH ₃ Br production	Ozone destruction by bromine chemistry	+	Medium	Medium
Eliminate CCl ₄ production	Ozone destruction by chlorine chemistry	+	Medium-Low	Medium
Reduction in N ₂ O emissions ^d	Ozone destruction by NO _x	+	High	Medium
	Mitigation of ozone destruction by chlorine/bromine chemistry	-	Medium	Small
Reduction in CH ₄ emissions ^d	Ozone production	-	Medium	Large
	Ozone destruction by HO _x	+	Medium	Small
	Mitigation of ozone destruction by chlorine chemistry	-	Medium	Small
Reduction in CO ₂ emissions ^d	Middle- and upper-stratospheric temperature changes	-	High	Large
	Formation of PSCs	+	Medium	Large
	Circulation changes ^e	+ & -	Low	Large
Increased aviation emissions	Aerosols: heterogeneous ozone destruction by halogens	-	Medium	Depends on # of flights, altitudes, and locations
	Production of ozone by HC/HO _x /NO _x chemistry	+	Medium	"
	Contrail frequency	?	Low	"
	Activation of halogens	-	Low	"
Increased rocket / space-transport emissions	SRM ^f – ozone destruction by chlorine chemistry	-	High	Small at present launch rate
	SRM ^f – aerosols: Heterogeneous ozone destruction by halogens	-	Medium	"
	Water vapor	-	Low	"
	Soot	?	Low	"
	Ozone destruction by NO _x	-	Low	"
Geoengineering by sulfur injection	Heterogeneous ozone destruction by halogens	-	Medium-Low	Potentially large

Table 5-5, continued (notes).

Notes:

- ^a The “+” sign indicates more column ozone (i.e., less depletion) for the indicated policy option or activity; the “-” sign indicates less column ozone.
- ^b Understanding: “Low” indicates an inability to accurately quantify due to unknown or unquantifiable processes or emissions; “Medium” indicates remaining gaps in our understanding; “High” indicates that processes and values are believed to be well modeled and understood.
- ^c Approximate maximum impact: a relative scale that relates the various activities. This column is somewhat subjective and some of the entries depend strongly on the amount of future activity. Rocket emissions and aviation emissions have the potential to be important, given our current understanding, but specific information regarding flight altitude, number of flights, type of fuel, aerosol emissions, etc., needs to be specified before they can be usefully compared to the other ozone impacts.
- ^d The impacts of a reduction in N₂O, CH₄, and/or CO₂ emissions will depend on the sizes of the reductions. Therefore, the “Approximate maximum impact” is somewhat more subjective than for the ODS phase-outs.
- ^e Circulation changes are expected to decrease (increase) total column ozone in the tropics (extratropics). See discussion in Chapter 3.
- ^f SRM stands for solid rocket motor.

do not deplete the ozone layer but, along with CFCs and HCFCs, are greenhouse gases, which contribute to the radiative forcing of climate (IPCC/TEAP, 2005; Velders et al., 2009). Thus, the current transition away from CFCs in Article 5 countries and HCFCs in Article 5 and non-Article 5 countries has implications not only for the ozone layer, but also for future climate. HFCs are not controlled by the Montreal Protocol, but they are included in the basket of gases of the Kyoto Protocol.

The HFC emissions scenarios discussed here can be divided in two classes:

- One class consists of non-intervention scenarios based on growth rates in gross domestic product and population (IPCC, 2000) for the period up to the middle or end of the 21st century. In these scenarios, historical and current technological developments are extrapolated without intervention from political processes. Such scenarios were first developed for the IPCC–Special Report on Emissions Scenarios (SRES) (IPCC, 2000) during the time when HFCs had still very limited usage and when the transition from CFCs and HCFCs had just begun. New non-intervention HFC scenarios have been formulated by Velders et al. (2009) and by the German Federal Environment Agency (UBA, 2009). The scenarios in Velders et al. (2009) are based on assumptions similar to those of IPCC-SRES with respect to growth rates in gross domestic product and population, but have incorporated new current information on (1) reported recent increases in consumption of HCFCs in Article 5 countries of about 20% yr⁻¹ (through 2007), (2) replacement patterns of HCFCs by HFCs as reported in non-Article 5 countries, and (3) accelerated phase-out schedules of HCFCs in Article 5 and non-Article 5 countries (2007 Adjustment of the Montreal Protocol). The scenarios of UBA (2009) are based on more fundamental sector-specific growth rates and emissions factors for all relevant sectors in Article 5 and non-Article 5 countries and take into account the accelerated HCFC phase-out schedules.
- The other class of scenarios is based on projections of technological developments affected by policy incentives and can therefore be seen as intervention scenarios. The discussions by the Parties of the Montreal Protocol to promote the use of HCFC alternatives that minimize the impact on climate can also be considered an intervention. An intervention scenario was developed for IPCC/TEAP (2005) and recently updated (TEAP, 2009), covering short time periods up to 2015 and 2020, respectively. Others (Rao and Riahi, 2006; Ottinger Schaefer et al., 2006; van Vuuren et al., 2006) have reported HFC scenarios similar to those of SRES. Many of these latter scenarios have performed a relatively simple analysis to project future HFC emissions. Ottinger Schaefer et al. (2006) estimated HFC emissions through 2020 using a detailed sector analysis, but their analysis was performed before the 2007 accelerated HCFC phase-out was adopted, and their 2008 HFC emissions do not agree with the emissions derived from observations.

The new scenarios constructed for IPCC, the Representative Concentration Pathways (RCPs), also contain HFC emissions, but use relatively simple or older analyses for the HFCs (Riahi and Nakicenovic, 2007; Clarke et al., 2007; Smith and Wigley, 2006; Wise et al., 2009; van Vuuren et al., 2006, 2007).

In Figure 5-5 global HFC emissions and radiative forcing are shown for six of the scenarios described above. The scenarios do not contain emissions from HFC-23, which is a by-product from the production of HCFC-22 and is not significantly used as a replacement for ODSs. HFC-23 emissions are estimated to be 0.20 ± 0.03 GtCO₂-eq yr⁻¹ for 2006–2008 (Montzka et al., 2010), but are likely to decrease in the coming decade as a result of mitigation efforts for climate protection and because of projected decreases in HCFC-22 production. However, if mitigation is not successful, and unregulated production of HCFC-22 for use as a feedstock increases substantially, it is possible for HFC-23 emissions to increase in the future. The GWP-weighted HFC emissions are similar

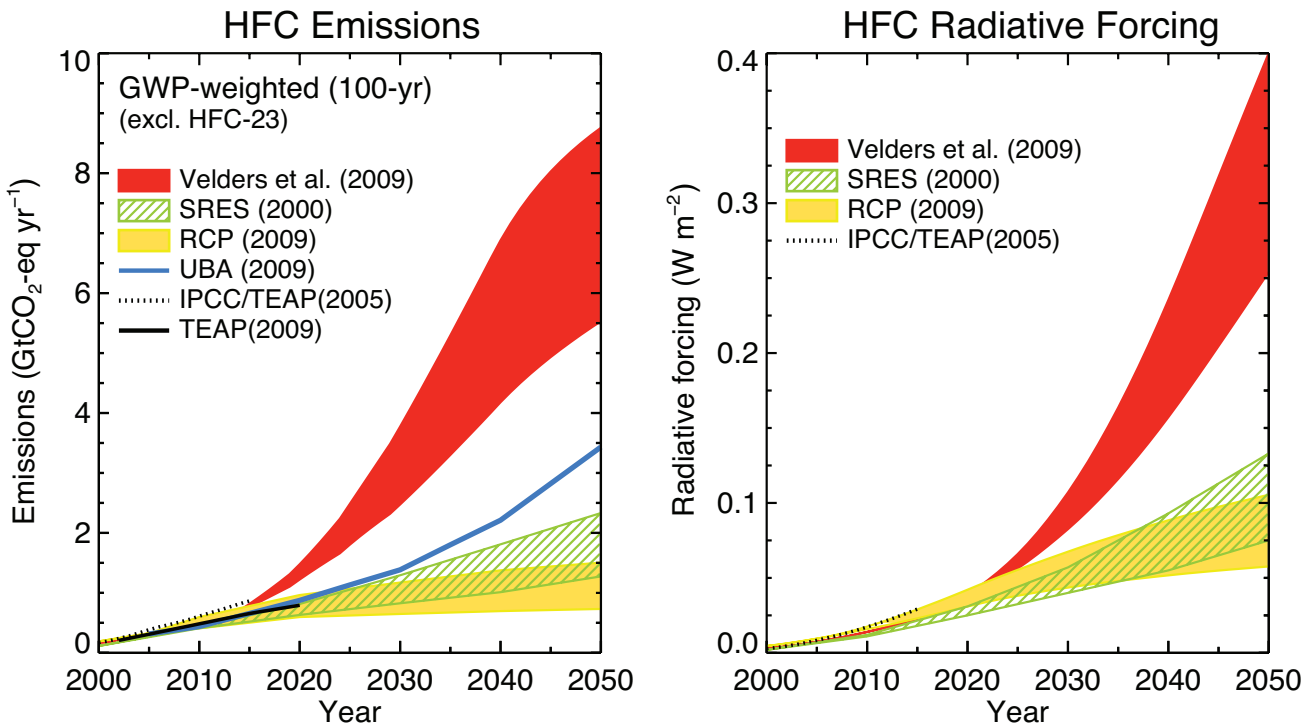
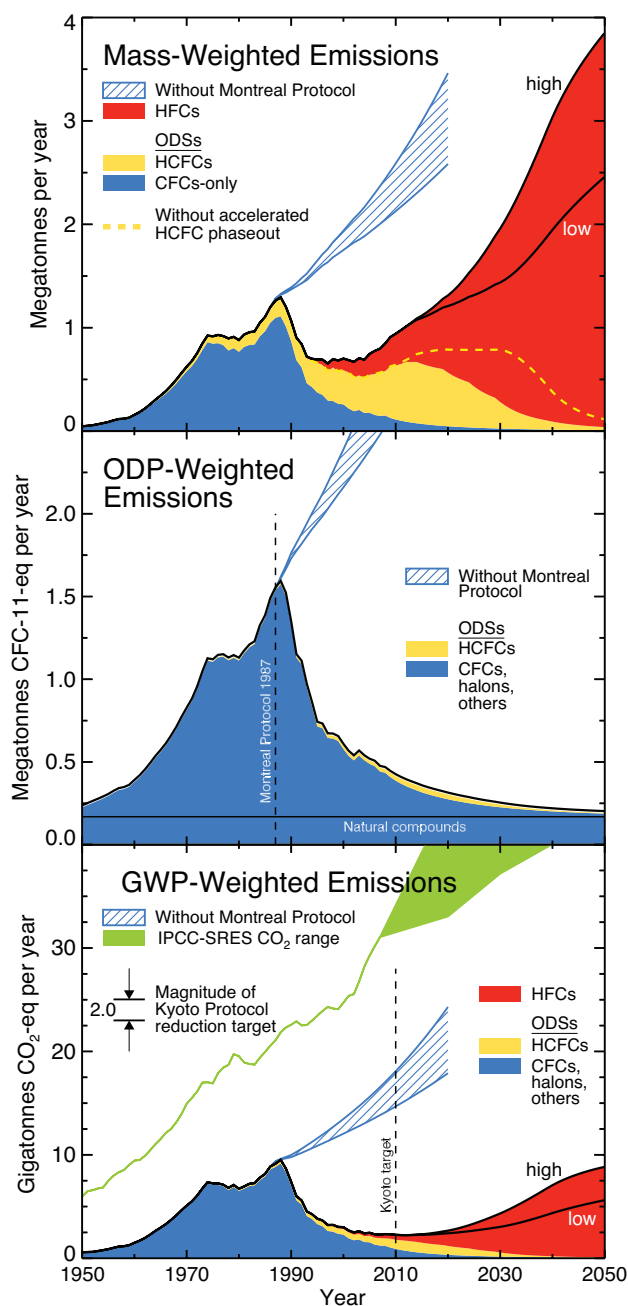


Figure 5-5. Global HFC emissions (left) and radiative forcing (right) in four long-term and two short-term scenarios. The long-term scenarios for the period 2000–2050 include the RCP scenarios and the non-intervention scenarios from Velders et al. (2009), UBA (2009), and SRES (IPCC, 2001). The short-term scenarios for the period 2000–2015/2020 include the IPCC-TEAP (2005) and TEAP (2009) scenarios. The RCP scenarios and the short-term scenarios assume intervention to mitigate climate forcing. Emissions of HFC-23, which is a by-product from the production of HCFC-22, are not included. HFC-23 emissions are estimated to be 0.20 ± 0.03 GtCO₂-eq yr⁻¹ for 2006–2008 (Montzka et al., 2010). The emission values are multiplied by their GWPs (100-year time horizon) to obtain annual equivalent GtCO₂ emissions. A GtCO₂-eq equals 1000 million metric tons carbon dioxide equivalent (MMTCO₂e). The color-shaded regions bound the upper and lower limits of the respective scenarios. Adapted from Velders et al. (2009).

through about 2015 for all six scenarios. However, while the emissions of TEAP (2009) increase linearly through 2020, the emissions of Velders et al. (2009) and UBA (2009) increase faster as a consequence of the growth rates in gross domestic product and the limits on consumption of HCFCs in Article 5 countries. By 2050, the total GWP-weighted HFC emissions are 5.5–8.8 GtCO₂-eq yr⁻¹ in Velders et al. (2009) and 3.5 GtCO₂-eq yr⁻¹ in UBA (2009); both are significantly larger than those of SRES (1.3–2.3 GtCO₂-eq yr⁻¹) (IPCC, 2000). The HFC emissions in Velders et al. (2009) are about four times larger than those of SRES in 2050 for two principal reasons. First, the starting points (2008) for consumption of HFCs by Velders et al. (2009) are substantially higher than assumed in SRES, based on higher reported consumption of HCFCs from 2000 to 2007 (UNEP, 2009) than was assumed in SRES. Second, in the Velders et al. (2009) study, the HFCs assumed to meet future demand (HFC-125 and HFC-143a) have larger GWPs than the HFCs

assumed in SRES (mostly HFC-134a). This follows from assuming that the future use of HFCs in applications in developing countries will follow the same trends already observed in developed countries. The current consumption values for HFC-125 and HFC-143a are supported by their emissions as estimated from observed atmospheric mixing ratios and account for approximately 80% of the CO₂-eq emission of HFCs in the year 2050. The lower emissions in the UBA (2009) scenarios compared with Velders et al. (2009) are the result of lower growth rates during 2020–2050 for the major HFC-consuming sectors and different replacement patterns for ODSs by HFCs and not-in-kind alternatives.

The current and expected future increased use of HFCs is largely the result of the phase-out of CFCs and HCFCs by the provisions of the Montreal Protocol, in combination with economic growth and an increase in living standards. As shown in Figure 5-6, total direct GWP-weighted emissions of ODSs peaked in 1988 at



9.4 GtCO₂-eq yr⁻¹ and decreased after that, whereas HFC emissions are projected to monotonically increase, primarily in Article 5 countries, exceeding those of ODSs after about 2020 in both Velders et al. (2009) and UBA (2009). In a business-as-usual scenario, starting in 1987, without Montreal Protocol regulations the GWP-weighted emissions of ODSs reach 15–18 GtCO₂-eq yr⁻¹ by 2010 (Velders et al., 2007). So, growth in HFC use and emissions would offset at least part of the climate benefits calculated to have been achieved by the Montreal Protocol.

Figure 5-6. Emissions of ODSs (CFCs, halons, HCFCs, and others) and their non-ozone-depleting substitutes (HFCs) from 1950 to 2050 (adapted from Velders et al., 2007, 2009). Emissions are the total from developing and developed countries. The legends identify the specific compound classes included in each panel. The high and low HFC labels identify the upper and lower limits, respectively, in global baseline scenarios from Velders et al. (2009). The blue hatched regions indicate the emissions that would have occurred, in the absence of the Montreal Protocol, with 2–3% annual production increases in ODSs. *Top panel:* Global mass-weighted emissions expressed in megatonnes per year. The yellow dashed line shows HCFC emissions calculated without the provisions of the accelerated HCFC phaseout under the 2007 Adjustment of the Montreal Protocol. *Middle panel:* Global ODP-weighted emissions expressed in megatonnes of CFC-11-equivalent per year. The emissions of individual gases are multiplied by their respective ODPs (CFC-11 = 1) to obtain aggregate, equivalent CFC-11 emissions. The dashed line marks 1987, the year of the Montreal Protocol signing. *Bottom panel:* Global GWP-weighted emissions expressed in gigatonnes of CO₂-equivalent per year. The emissions of individual gases are multiplied by their respective GWPs (direct, 100-year time horizon; CO₂ = 1) to obtain aggregate, equivalent CO₂ emissions. Shown for reference are emissions for the range of IPCC-SRES CO₂ scenarios (IPCC, 2000). The CO₂ emissions for 1950–2007 are from global fossil fuel and cement production. Beyond 2007, the shaded region for CO₂ reflects the range bracketed by the A1B and B2 SRES scenarios. The dashed line denotes 2010, the middle year of the first commitment period of the Kyoto Protocol. Also shown is the magnitude of the reduction target of the first commitment period of the Kyoto Protocol, which is based on a 1990–2010 projection of global greenhouse gas emission increases and the reduction target for participating countries.

The HFC scenario results are further put into context by comparing to projected global CO₂ emissions. Global annual HFC emissions in 2050 as projected by UBA (2009) and Velders et al. (2009) are equivalent (CO₂-eq basis) to 6–8% and 9–19%, respectively, of projected global CO₂ emissions in IPCC/SRES business-as-usual scenarios (A1B, A2, B1, and B2) (Figure 5-6).

In these HFC scenarios, only the direct contribution to climate forcing due to ODS and HFC emissions is considered. Indirect climate forcings associated with

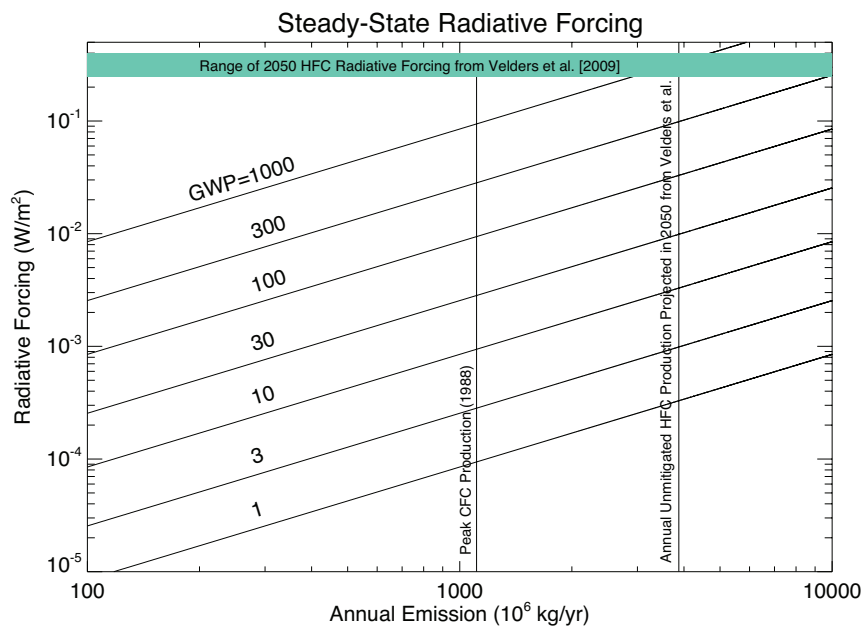


Figure 5-7. Relationship between annual emission rates and steady-state radiative forcing for compounds having seven different GWPs. Relationships are valid for compounds having lifetimes less than 20 years or so. For example, if 1 Tg/yr (10^9 kg/yr) were emitted of a gas with a GWP of 1, the steady-state radiative forcing would be slightly less than 10^{-4} W/m². For comparison, the 2008 estimated radiative forcing from CO₂, CH₄, and N₂O was 1.74, 0.5, and 0.17 W/m², respectively (<http://www.esrl.noaa.gov/gmd/aggi/>).

halocarbon usage arise from the energy used or saved during the application or product lifetime and energy required to manufacture the product, including the halocarbon used. For example, thermal insulating products in buildings and appliances reduce energy consumption, and refrigeration and AC systems consume energy over their lifetimes. A full evaluation of the total climate forcing resulting from the global transition away from CFCs and HCFCs toward HFCs requires consideration of both direct and indirect impacts over all associated halocarbon, non-halocarbon, and not-in-kind application lifecycles.

Three primary options are available to reduce the future climate impact of HFCs as demand continues to increase for products currently using HCFCs and HFCs: first is an increasing implementation of not-in-kind technologies (non-fluorocarbon based); second, use of HFCs that result in less energy used, because many products have significantly higher indirect climate impacts due to the energy used over the lifetime of the product than they do from emissions of the chemicals contained in the product; and third, lower-GWP HFC or other replacement chemicals could be used to satisfy demand. Figure 5-7 shows steady-state radiative forcing resulting from a given annual emission rate for seven representative GWP limits on replacements. If the total 2050 HFC production projected in Velders et al. (2009) were to be met, for example, by HFCs with an average GWP less than 10 or 100, and emissions are assumed to equal production, the steady-state globally averaged radiative forcing would be less than 0.003 or 0.03 W/m², respectively. These values are substantially smaller than the 0.25–0.4 W/m² range estimated in the unmitigated case in Velders et al. (2009). This analysis assumes that even very short-lived HFCs

can be considered to be well mixed. In reality, the global-mean lifetimes and radiative efficiencies of substances that are not well mixed will depend on the location of emission. There is currently not sufficient discussion of impacts of such short-lived substances on radiative forcing and climate in the literature to assess the significance of their inhomogeneous abundances on this type of analysis.

5.4.3.2 OTHER REPLACEMENTS FOR ODSs

Unsaturated HFCs (also known as hydrofluoroolefins, HFOs), hydrofluoroketones and perfluoroketones, hydrofluoroethers (HFEs), perfluoropolyethers, ammonia, hydrocarbons and CO₂ are either under consideration or in use as replacements for ODSs. The potential for these compounds to contribute to radiative forcing of climate is considered in this section (other potential environmental impacts are discussed in Section 5.4.4). Most of these compounds are short-lived, which limits their radiative forcing. See Chapter 1 for additional discussion of these compounds, and Tables 1-10 and 1-11 for a list of alternatives for ozone-depleting substances.

The reaction of hydroxyl radicals (OH) with unsaturated HFCs proceeds rapidly, and as a consequence, these unsaturated HFCs have atmospheric lifetimes that are in the range of 1–20 days. With such short lifetimes the contribution of unsaturated HFCs to radiative forcing will be small. For example, HFC-1234yf (CF₃CF=CH₂) has a GWP of approximately 4 (Nielsen et al., 2007; Papadimitriou et al., 2008b). HFC emissions are projected to be dominated by HFC-125 and HFC-143a and reach 3.5–8.8 GtCO₂-eq yr⁻¹ in 2050 (see Section 5.4.3.1). While substitution by unsaturated HFCs would reduce the

contribution of HFCs to radiative forcing, a full life cycle analysis (including emissions associated with the energy usage by appliances using the different compounds and including an analysis of the production of trifluoroacetic acid (TFA) and tropospheric ozone) would be needed to assess the total systemic environmental impact.

The atmospheric removal mechanism for HFEs is reaction with OH radicals. These rate coefficients decrease with increasing degree of fluorination of the ether. As seen from Appendix Table 5A-1, highly fluorinated HFEs (e.g., CHF_2OCF_3) can have substantial atmospheric lifetimes and large GWPs. Also, as evident from Appendix Table 5A-1 and discussed in Chapter 1, HFEs bearing several hydrogen atoms (e.g., $\text{C}_2\text{H}_5\text{OC}_4\text{F}_9$) have short atmospheric lifetimes and small GWPs. The GWPs for HFEs thus span a large range, and it is not possible to make any general statement regarding the benefit of the substitution of HFCs by HFEs. The benefits need to be assessed on a case-by-case basis. Perfluoropolyethers are not reactive toward OH radicals, or any other oxidant species in the atmosphere, have atmospheric lifetimes probably in excess of 800 years (Young et al., 2006), and will have large GWPs. The volatility and magnitude of possible emissions need to be considered when assessing the potential environmental impact of perfluoropolyethers. Finally, we note that the atmospheric oxidation products of unsaturated HFCs (HFOs), HFEs, hydrofluoroketones, perfluoroketones, and perfluoropolyethers are COF_2 , HC(O)F , HF, and fluorinated carboxylic acids (Calvert et al., 2008; D'Anna et al., 2005; Good and Francisco, 2003; Taniguchi et al., 2003; Wallington et al., 1994). These products have short atmospheric lifetimes and are not expected to contribute to radiative forcing.

As for the HFCs (Section 5.4.3.1), a full evaluation of the total environmental effects resulting from the global transition away from CFCs and HCFCs toward the compounds discussed in this section or other compounds requires consideration of both direct and indirect environmental impacts over all associated halocarbon, non-halocarbon, and not-in-kind application lifecycles.

5.4.4 Other Environmental Impacts

The potential exists for certain HCFCs, HFCs, HFEs, and unsaturated HFCs (HFOs) to contribute to tropospheric ozone formation, and degrade to give toxic compounds. The atmospheric degradation of HCFCs, HFCs, HFEs, and unsaturated HFCs is initiated by reaction with OH radicals leading to the formation of halogenated carbonyl compounds, which undergo further oxidation to HF, HCl, CO_2 , and, in some cases, trifluoroacetic acid (TFA) (see for example, IPCC/TEAP 2005; Calvert et al., 2008; Hurley et al., 2008; Nielsen et al., 2007; Papadimitriou et al., 2008b).

Hayman and Derwent (1997) assessed the potential contribution of HCFCs and HFCs to the formation of tropospheric ozone and concluded that these compounds do not have a large potential to contribute to ground-level ozone formation. As indicated from the lifetimes of the compounds listed in Appendix Table 5A-1, the reactivity of HFEs toward OH radicals is comparable to those of analogous HCFCs and HFCs. As with HCFCs and HFCs, HFEs are not expected to make a significant contribution to ground-level ozone formation. OH radicals react rapidly with $>\text{C}=\text{C}<$ double bonds, and unsaturated HFCs are typically much more reactive than HCFCs, saturated HFCs, and HFEs. The photochemical ozone creation potential (POCP) concept is a well-established method of ranking compounds by their ability to form ozone in the troposphere. POCP values are determined along an idealized straight-line trajectory using a photochemical trajectory model. Using the approach outlined by Derwent et al. (1998) and Jenkin (1998), Wallington et al. (2010) have estimated POCPs for representative unsaturated HFCs. The results are presented in Table 5-6 together with values for selected alkanes, alkenes, and HFCs. As seen from this table, the POCPs for unsaturated HFCs (HFOs) are much larger than those for longer-lived HFCs, much smaller than those for the parent alkenes, and for many compounds (including the commercially significant HFC-1234yf) lie between those of methane and ethane. Methane and ethane are oxidized sufficiently slowly that they do not contribute to any appreciable degree to local air quality issues and are generally exempt from air quality regulations. Luecken et al. (2010) conducted an atmospheric modeling study of the impact of replacing all HFC-134a currently used in vehicle air conditioning systems in the USA with HFC-1234yf. They concluded that such large-scale use of HFC-1234yf would result in a less than 0.01% increase in total ozone formed. Thus, this study provides further support for the expectation that unsaturated HFCs from mobile air conditioning will not make a significant contribution to tropospheric ozone formation in the near future.

The formation of hydrogen fluoride (HF) and hydrogen chloride (HCl) from the degradation of these source gases also should be addressed. Assuming that the combined global emissions of HCFCs, HFCs, HFEs, and unsaturated HFCs (HFOs) are of the order of 100 kilotonnes (Kt) per year, that they are uniformly distributed in the atmosphere, and an annual global precipitation of 4.9×10^{17} liters (Erchel, 1975), the concentrations of HF and HCl in precipitation from degradation of HCFCs, HFCs, HFEs, and HFOs will be of the order of 3×10^{-9} molar. Although HF and HCl are strong acids, the concentration of fluoride and chloride and the additional acidity in precipitation resulting from the atmospheric oxidation of HCFCs, HFCs (saturated and unsaturated), and HFEs would be minor.

Table 5-6. Photochemical ozone creation potentials (POCPs) for selected hydrofluoro-olefins and related alkanes, alkenes, and hydrofluoro-carbons.

Compound	Industrial or Common Name	POCP
CH ₂ =CH ₂	ethylene; ethene	100 ^a
CH ₂ =CF ₂	1,1 difluoroethylene; HFO-1132a	18.0 ^b
CF ₂ =CF ₂	Perfluoroethylene; HFO-1114	12.5 ^b
CH ₃ CH=CH ₂	propylene; propene	117 ^c
CH ₂ =CHCF ₃	HFO-1243zf	10.7 ^b
CH ₂ =CFCF ₃	HFO-1234yf	7.0 ^b
(Z)-CHF=CFCF ₃	HFO-1225ye(Z)	5.6 ^b
CF ₂ =CFCF ₃	Perfluoropropylene; HFO-1216	5.4 ^b
CH ₃ CH ₂ CH=CH ₂	1-butene	104 ^c
CH ₂ =CHCF ₂ CF ₃	HFO-1345czf	6.6 ^b
CH ₄	methane	0.6 ^d
CH ₂ F ₂	HFC-32	0.2 ^e
C ₂ H ₆	ethane	8 ^c
CH ₃ CHF ₂	HFC-152a	1.0 ^e
CH ₃ CF ₃	HFC-143a	0.0 ^e
CH ₂ FCF ₃	HFC-134a	0.1 ^e
C ₃ H ₈	propane	14 ^c
CH ₂ FCHF ₂ CF ₃	HFC-245eb	0.2 ^b
CHF ₂ CH ₂ CF ₃	HFC-236ea	0.0 ^b
CF ₃ CH ₂ CF ₃	HFC-227ea	0.0 ^e
<i>n</i> -C ₄ H ₁₀	butane	31 ^c

^a By definition.
^b Wallington et al. (2010).
^c Derwent et al. (2007).
^d Derwent et al. (1998).
^e Hayman and Derwent (1997).

TFA is a persistent, potentially toxic degradation product of some HCFCs (e.g., HCFC-123, -124), HFCs (e.g., HFC-134a, -227ea), and unsaturated HFCs (e.g., -1234yf, -1225ye (CF₃CF=CHF)). Its sources (natural and anthropogenic), sinks, and potential environmental effects have been reviewed by Tang et al. (1998), Solomon et al. (2003), and IPCC/TEAP (2005). In WMO (2007) it was concluded that “TFA from the degradation of HCFCs and HFCs will not result in environmental concentrations capable of significant ecosystem damage.” The available data suggest that the same conclusion is applicable to unsaturated HFCs and HFES. It has been shown that TFA is

ubiquitous in precipitation and ocean water even in remote areas (Berg et al., 2000; Frank et al., 2002; Scott et al., 2005; Scott et al., 2006; Von Sydow et al., 2000). Frank et al. (2002) estimated that the oceans contain 268 million tonnes of TFA. At a global level, the natural environmental loading of TFA greatly exceeds that expected from the atmospheric degradation of HCFCs, HFCs, and unsaturated HFCs (Kotamarthi et al., 1998). While Tromp et al. (1995) have argued that TFA will accumulate to high levels in seasonal wetlands, Boutonnet et al. (1999) showed that the assumptions made by Tromp et al. were highly improbable. Benesch et al. (2002) showed that TFA does not adversely affect the development of soil microbial communities and pool plant species in vernal ponds. Luecken et al. (2010) assessed the TFA concentrations following replacement of all HFC-134a currently used in vehicle air conditioning systems in the USA with HFC-1234yf. Their model predicted peak concentrations in rainfall of 1264 nanograms per liter. This level is similar to peak concentrations currently observed (Scott et al., 2006) and is approximately two orders of magnitude lower than the level considered safe for the most sensitive aquatic organisms (Luecken et al., 2010). See also Section 1.3.6.3 of Chapter 1 for a discussion on HFC-1234yf. Chapter 1 also discusses our current understanding of the sources of TFA. A current gap in our understanding is the lack of information concerning the natural sources and loss processes of TFA. This gap limits our ability to provide a precise assessment of the role of human activities in affecting local or regional abundances of TFA.

In summary, HCFCs, HFCs, HFES, and HFOs are not expected to contribute significantly to the formation of tropospheric ozone. In the concentrations expected in the environment in the near future, the degradation products of HCFCs, HFCs (saturated and unsaturated), and HFES are not expected to be toxic. However, for thorough understanding of the environmental impacts of replacements for CFCs, HCFCs, and long-lived HFCs, an evaluation of the ODPs, GWPs, atmospheric fate, safety, and toxicity is required for each replacement.

5.4.5 Impact of 2007 Accelerated HCFC Phase-Out

In 2007 the Parties to the Montreal Protocol adjusted the Protocol by accelerating the HCFC phase-out to protect the ozone layer and, in part, to further protect future climate. HCFC consumption in Article 5 countries will be frozen in 2013 and stepwise reduced, with a virtually complete phase-out in 2030. Before the 2007 Adjustment, a freeze in consumption was in place for Article 5 countries starting in 2016 with a complete phase-out in 2040. Non-Article 5 countries have agreed to a virtually

complete phase-out in 2020. The Adjustment also slightly changed the phase-out schedule for non-Article 5 countries, increasing the interim reduction during 2010 through 2014 from 65% to 75% below the baseline level.

The accelerated HCFC phase-out has beneficial implications for the ozone layer and does have the potential to reduce climate forcing. It is expected to cause a reduction in cumulative HCFC emissions, relative to the current baseline scenario of this chapter, of 11–14 megatonnes (Mt) for the period 2011–2050, or an ODP-weighted equivalence of 0.6–0.8 MtCFC-11-eq (Figure 5-6). Following the same methods of calculating mixing ratios and EESC as described in Section 5.2, this emission reduction accelerates the projected return of EESC to 1980 levels by 4–5 years. The resulting percentage reduction in EESC, integrated from 2011 until the 1980 level is reattained, is 10–12%, which is larger than any of the hypothetical zero-production cases discussed in Section 5.4.3.1.

In adopting the accelerated HCFC phase-out, the Parties agreed to promote the use of HCFC alternatives that minimize the impact on climate and other environmental effects. The evaluation of the impact of a replacement of HCFCs with HFCs and other compounds requires consideration of both direct and indirect impacts, such as due to changes in energy usage associated with a particular replacement, over all associated halocarbon and not-in-kind application lifecycles. However, estimating all indirect impacts is extremely difficult. If only direct contributions are considered, the HCFC cumulative emissions reduction attributable to the accelerated phase-out is, in terms of climate forcing and relative to the current baseline, estimated to be 0.4–0.6 GtCO₂-eq yr⁻¹ averaged over 2011 through 2050. In comparison, global anthropogenic emissions of CO₂ were greater than 30 Gt per year in 2008. Not-in-kind alternative technologies (such as Stirling cycles, mineral wool, thermoacoustic refrigeration) are expected to only play a minor replacement role for the HCFCs. Therefore, to realize most of this forcing reduction, the avoided HCFC consumption and emissions must be replaced by alternative compounds with small GWPs (e.g., ammonia, hydrocarbons, CO₂, low-GWP HFCs).

In addition to these potential benefits of the accelerated HCFC phase-out, there is also a climate benefit from the reduction in HFC-23 by-product emissions resulting from reduced HCFC-22 production.

5.5 THE WORLD AVOIDED BY OZONE POLICY

The success of the Montreal Protocol and its subsequent Amendments and Adjustments (Andersen and Sarma, 2002; UNEP, 2009) is evident from the large decreases in the production of ODSs since their peak at the end of the 1980s, from the large decreases in emissions, and from decreases in midlatitude EESC since the middle of

the 1990s that are expected to continue throughout the 21st century. The success becomes even more striking when comparing current projections of production, emissions, and mixing ratios of ODSs and of the ozone layer with what might have happened without the Montreal Protocol. Scenarios generated to explore what might have occurred in the absence of ozone mitigation policies have been sometimes referred to as the “road not taken” or “world avoided” scenarios. The studies discussed in Section 5.5.3, made possible by the recent progress in chemistry-climate modeling (CCM), demonstrate the considerable damage mankind could have inflicted upon the Earth System in the space of just a few decades, and the benefit of the Montreal Protocol for both the ozone layer and climate.

ODSs affect the climate system both as greenhouse gases and indirectly through their effect on ozone. Both mechanisms are discussed below, starting with a discussion of ODS emission scenarios in a “World Avoided” by the Montreal Protocol.

5.5.1 ODS Production

An assessment of how ODS mitigation policies have affected climate and the ozone layer first requires establishing alternative scenarios of ODS production and emission. These scenarios are based on various reasonable assumptions about what might have happened in the absence of a policy response to scientific advances regarding the environmental impact of halocarbons, and about rates of emissions growth in such non-intervention scenarios. For example, two of the different scenarios that have been considered follow from the assumptions that (1) early warnings of dangers posed by CFCs to the ozone layer (Molina and Rowland, 1974) would have been ignored or would not have existed (referred to here as the MR74 scenario), and (2) that the Montreal Protocol was not implemented (NMP87 scenario) (Velders et al., 2007). Although negotiations about limiting the emissions of ODSs had started prior to the discovery of the ozone hole (Farman et al., 1985; Chubachi and Kajiwara, 1986), a failure to detect polar ozone depletion or to link it to CFCs would likely have led to the adoption of weaker controls, particularly in subsequent negotiations that tightened the initial measures following dissemination of the results attributing the Antarctic losses to halocarbons (Parson, 2003). Prather et al. (1996) developed a scenario similar to MR74 assuming business-as-usual market-driven growth of CFC production after 1974. Under that scenario, although the ozone hole would have been detected, ozone science would have been delayed by around a decade. The mechanism of ozone depletion would have been established later, and emissions would have kept rising at 6% per year, with new uses for CFCs being introduced, until with a delay of 10 years ODS mitigation

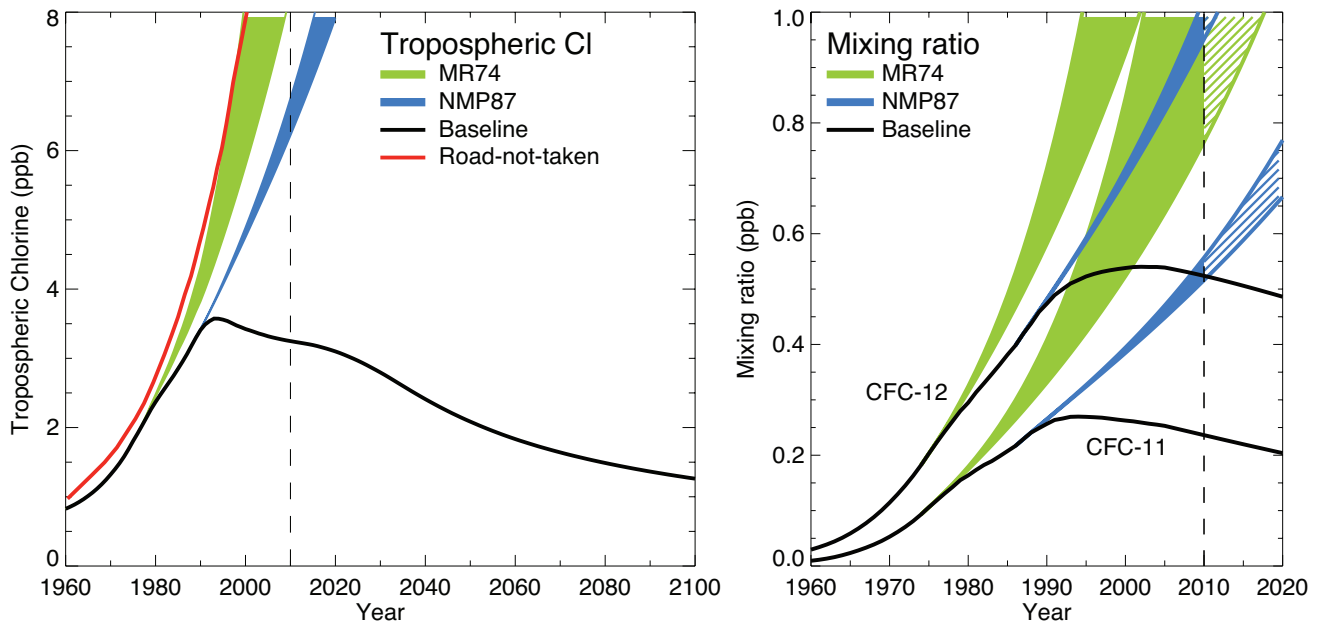


Figure 5-8. *Left panel:* Total chlorine from the baseline scenario (black) compared with three “World Avoided” scenarios. The “Road-not-taken” scenario is from Prather et al. (1996) and includes only the portion of the “Free Market” curve (described in that study) before controls were implemented. The MR74 and NMP87 scenarios are derived from Velders et al. (2007). *Right panel:* Tropospheric mixing ratios of the most significant CFCs under the MR74 (green) (no identification of the link between CFCs and ozone in 1974 by Molina and Rowland (1974)) and the NMP87 (blue) (no Montreal Protocol restrictions) scenarios; and as observed and assuming compliance with the fully amended and adjusted Montreal Protocol (black). (From Velders et al., 2007).

policies would have been introduced. In this scenario, the tropospheric abundance of total chlorine would rise to 9 parts per billion (ppb) by 2002 before mitigation policies took effect to reduce atmospheric abundances of chlorine. The Velders et al. (2007) MR74 scenario does not include mitigation. The second scenario from Velders et al. (2007), NMP87, is more conservative than MR74 and assumes CFC production would grow in proportion to the economy after 1987 (a characteristic of mature markets), with growth rates of 2–3%/year. Figure 5-8 summarizes the various World Avoided scenarios. Before 1987, NMP87 follows the observed chlorine abundance. Figure 5-6 shows the global emissions of ODSs and HFCs from 1950 to 2050 weighted by mass, ODPs, and GWPs for the baseline scenario and for the NMP87 scenario (Velders et al., 2007, 2009). Each of these scenarios results in a greatly enhanced stratospheric halogen loading compared to what has actually occurred.

5.5.2 Radiative Forcing

The radiative forcing (RF) potential of CFCs is well established, as was highlighted in WMO (1986). Velders et al. (2007) calculated the radiative forcing for the MR74 and NMP87 scenarios introduced above, and for the actual

and projected emissions of all ODSs (Table 5-7). For present-day abundances, the RF associated with halocarbons is around 0.3 W/m^2 or approximately 18% of that of CO_2 (IPCC, 2007). Under the MR74 scenario, by 2010 the radiative forcing due to all ODS would contribute 44% to 89% as much to global warming as CO_2 . Under NMP87, in 2010 the RF associated with ODSs would amount to about one-third of that of CO_2 . Even under this more conservative scenario, the RF increase due to ODSs between 1988 and 2010 would be at least 0.34 W/m^2 , which is substantial compared to the increase in RF due to CO_2 of 0.55 W/m^2 that has been experienced over that period.

The ODS forcing results should be adjusted for (a) the likely negative radiative forcings associated with ozone depletion caused by the ODS emissions (IPCC, 2007), and (b) the reduced emissions of replacement products that would not be needed without the mandated ODS reductions. HFCs are examples of replacement compounds; their usage is projected to grow sharply as a side effect of the Montreal Protocol (Figure 5-6), with potentially large increases in associated RF of up to 0.4 W/m^2 in non-intervention scenarios by 2050 (Velders et al., 2009). Although the ODS emissions under a no-Montreal Protocol scenario (NMP87) would have a considerably larger radiative forcing, continuing unmitigated emissions of high-GWP HFCs could

Table 5-7. Direct radiative forcing (W/m^2) of controlled ODSs and CO_2 (Velders et al., 2007; IPCC, 2001; IPCC, 2007). For comparison: in 2008, CH_4 and N_2O were responsible for a direct radiative forcing of 0.50, and 0.17 W/m^2 , respectively (www.esrl.noaa.gov/gmd/aggi/).

Scenario	1975	1988	2010
ODS Baseline	0.12	0.26	0.32
ODS MR74 ^a	0.12	0.30–0.34	0.8–1.6
ODS NMP87 ^b	0.12	0.26	0.60–0.65
CO_2	0.94	1.25	1.78–1.82

^a Scenario in which the early warnings of dangers posed by CFCs to the ozone layer (Molina and Rowland, 1974) were ignored or did not exist.

^b Scenario in which the Montreal Protocol was not implemented (“no Montreal Protocol”).

nonetheless substantially offset the effects of other greenhouse gas mitigation efforts. See Section 5.4.2.1 for more details regarding future HFC emissions. The combined effects of ozone depletion and enhanced HFC emissions are estimated to offset about 30% of the radiative forcing avoided by the ODSs phased out under the Montreal Protocol by 2010 (Velders et al., 2007).

In comparing the benefits of the Montreal and Kyoto Protocols for climate, one also needs to assume that if the Montreal Protocol did not exist, the ODSs would almost certainly have been included in the Kyoto Protocol because of the ODSs’ considerable GWPs. However, this would have likely resulted in a delay in implementing controls similar to the one described by Prather et al. (1996), and could have led to unmitigated growth of CFCs lasting longer than what actually occurred.

Even allowing for these offsetting effects, Velders et al. (2007) note that actions taken under the Montreal Protocol have been of considerably greater benefit to climate than the reduction target of the first commitment period (2008–2012) of the Kyoto Protocol (Figure 5-6). The annual ODS emission reduction resulting from the Montreal Protocol is estimated to be 10 to 12 $GtCO_2$ -eq yr^{-1} by 2010, or 5 to 6 times the Kyoto Protocol reduction target. In making this comparison, it is acknowledged that the Kyoto Protocol does not include anthropogenic halocarbons because these substances had previously been regulated by the Montreal Protocol. Also unlike the Kyoto Protocol, the Montreal Protocol has gone through a series of Amendments and Adjustments that have led to further emission reductions. The Kyoto Protocol has not yet gone through this process. The first commitment period aims for an overall reduction, relative to 1990 levels, of 5.2% of CO_2 -equivalent greenhouse gas emissions in Annex 1 countries. A proposed target for 2050 aims for 80% emission reductions, relative to 1990. Even compared to this

much more ambitious target, the climate benefit of the Montreal Protocol calculated to date is significant.

5.5.3 Climate and Ozone Impacts Avoided by the Montreal Protocol

Prather et al. (1996) also estimated the consequences to ozone of unmitigated halocarbon emissions growth. Using a 2-D model, they calculated a 10% loss of extrapolar, annual-mean ozone by 1998, relative to 1980. More recently, Morgenstern et al. (2008) and Newman et al. (2009) assessed the impact of a continuing increase of chlorine in the atmosphere on both ozone depletion and climate. By using comprehensive CCMs, these are the first studies to examine the atmospheric structural and dynamical response to highly elevated chlorine. Both studies demonstrate the substantial changes that would likely have occurred if it were not for the Montreal Protocol.

Morgenstern et al. (2008) compare climate under a 9 ppb total chlorine loading—the peak chlorine abundance projected in the Prather et al. (1996) scenario in about 2002—to the actual peak chlorine loading of around 3.5 ppb, which occurred in the late 1990s. In designing their calculations, they deliberately exclude the direct radiative effect of the CFC increases (the main topic of Velders et al., 2007) to focus exclusively on ozone changes and their climate impacts. The additional chlorine leads to a reduction of total ozone everywhere in their model (Morgenstern et al., 2009), with losses ranging from about 5% in the tropics to 20–30% in Arctic and over 50% in Antarctic spring; the average ozone loss between 60°S and 60°N in their model amounts to 8.3%. This is slightly less than estimated by Prather et al. (1996) for a somewhat lower chlorine abundance. The losses peak in three regions, namely in the chlorine layer around 40 km associated with gas-phase catalytic ozone destruction (Molina and Rowland, 1974), and at both high-latitude regions around 20 km, associated with heterogeneous polar processes. The ozone loss has a considerable impact on stratospheric temperatures, with the upper stratosphere cooling by up to 6 K, and a few degrees cooling in the lower stratosphere with warming above it associated with a change in upwelling of 9.6 μm radiation due to the ozone loss. Morgenstern et al. (2008) also find substantial extratropical near-surface regional climate change. At southern high latitudes, they find a surface warming of up to 3 K in spring in the lee of the Antarctic Peninsula, and cooling in parts of Western and Eastern Antarctica (Figure 5-9); these calculations are qualitatively consistent with observations in recent decades (leading for example to the collapse of the Larsen B ice shelf; MacAyeal et al., 2003). Morgenstern et al. (2008) associate the climate change found in their model simulations with a further strengthening of the Southern Annular

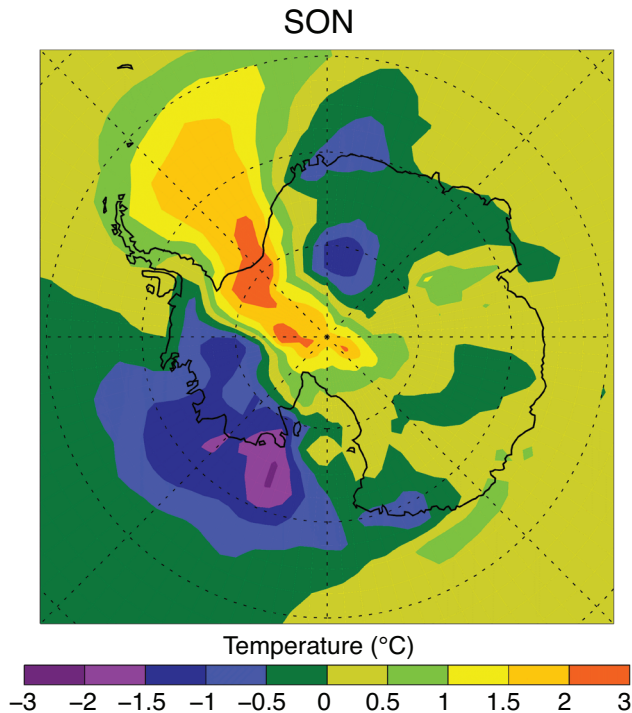


Figure 5-9. Difference between the 9 and 3.5 ppb total chlorine cases in Antarctic spring (September–November) temperature (°C) 20 m above the surface. (From Morgenstern et al., 2008).

Mode (SAM), the leading mode of variability of the southern extratropics, as has been observed during the period of historic ozone depletion (Thompson and Solomon, 2002; Fogt et al., 2009). For the Northern Hemisphere, their model produces substantial cooling in winter over Northern Asia and Western Europe, and warming over Northern North America and Greenland. Morgenstern et al. (2008) calculate a radiative forcing associated with the ozone depletion of -0.05 W/m^2 , which, in absolute terms, is at least an order of magnitude less than the direct radiative forcing associated with the increased ODSs (Velders et al., 2007). However, they note that regional climate change due to the additional ozone depletion, over Antarctica and the northern continents, is large compared to recent observed climate changes.

In assessing these regional climate impacts, one needs to consider that the skill of climate models in representing regional climate trends on decadal timescales is often low, particularly in the Northern Hemisphere (e.g., Figure TS.24 of IPCC, 2007). In the Northern Hemisphere, atmosphere-ocean global circulation models (AOGCMs) typically disagree on basic patterns of climate change, both among each other and compared with observations (e.g., Gillett, 2005). At southern high latitudes, climate models are somewhat more successful in representing patterns of climate change (e.g., Gillett and Thompson, 2003). The

projection by Morgenstern et al. (2008) appears plausible when comparing the patterns of the results to past climate changes in the Antarctic region. For the Northern Hemisphere, it is likely that ozone depletion would have led to substantial regional climate change, but the geographical pattern of change remains poorly understood.

Newman et al. (2009) perform and evaluate a transient simulation using the Goddard Earth Observing System Chemistry Climate Model (GEOSCCM) model (Pawson et al., 2008) in which EESC follows the MR74 scenario of Velders et al. (2007) with an assumed growth rate of 3% per year, leading to 9 ppb in 2019. They terminate their simulation in 2065 when EESC reaches 45 ppb. Other greenhouse gases follow the IPCC (2000) A1B scenario. In their simulation, such drastic increases of ODSs completely alter the structure of the stratosphere. Total global ozone drops by two-thirds during the course of the simulation; the loss is approximately linear in EESC. The ozone loss produced by Newman et al. (2009) is similar to that of Prather et al. (1996) for similar chlorine loading, although a strict comparison is complicated by Newman et al. (2009) displaying ozone loss as a function of equivalent effective chlorine and Prather et al. (1996) using actual chlorine. The changes found by Newman et al. (2009) are initially largely driven by high-latitude ozone loss (Figure 5-10). In around 2020 in the simulation, Arctic ozone in April drops below 220 Dobson units (DU) and would thus satisfy a common definition of an Arctic ozone hole. By 2060, Arctic ozone in the simulation drops below 100 DU in spring. There is a progressive deepening and lengthening of the lifetime of the Antarctic polar vortex in the simulation, eventually leading to a year-round ozone hole with westerlies in the southern mid- and high-latitude stratosphere. Newman et al. (2009) refer to this as the “perpetual winter.” At the end of the simulation, minimum ozone columns reach about 50 DU over Antarctica. After about 2045 in the simulation, enhanced upwelling cools the tropical lower stratosphere and triggers heterogeneous chemical processes similar to those currently observed in the Antarctic ozone hole. In the simulation, this leads to precipitous ozone depletion and nearly complete ozone loss in the tropical lower stratosphere by 2058. Newman et al. (2009) compare their results to complementary simulations assuming ODS abundances fixed at 1960 levels or following the A1 scenario (WMO, 2007) to demonstrate the effect of mitigating ODS emissions when the reference scenario has such dramatic chlorine increases.

Both Morgenstern et al. (2008) and Newman et al. (2009) exclude certain feedbacks that would have otherwise affected their results. In both studies, climate change due to ozone loss is not allowed to affect ocean conditions, which can have impacts that extend into the middle atmosphere (Kodama et al., 2007). In Newman et al. (2009), the direct RF due to the increasing ODSs (Velders et al., 2007)

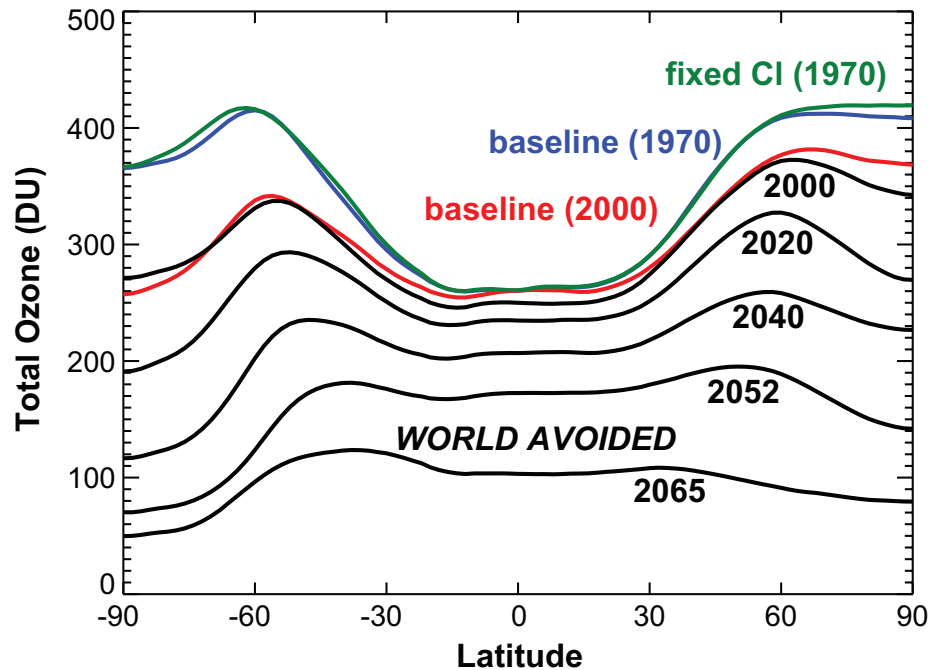


Figure 5-10. Zonal-mean total ozone in the World Avoided simulation (black), in 1970 for chlorine fixed at 1960 levels (green), and for a baseline scenario simulation in 1970 (blue) and 2000 (red). (Adapted from Newman et al., 2009).

is also not reflected in the ocean conditions; Morgenstern et al. (2008) exclude this effect by keeping the ODSs the same for radiation as in their reference simulation. Newman et al. (2009) prescribe tropospheric ozone and thus suppress feedback effects on tropospheric chemistry (e.g., tropospheric ozone production or loss caused by the increasing ultraviolet (UV) radiation). Morgenstern et al. (2008) use photolysis rates in the troposphere that do not reflect changes to the ozone column, thus also not allowing for such feedbacks. However, substantial decreases of tropospheric ozone do occur in Morgenstern et al. (2008) due to a decreased influx of stratospheric ozone. Further feedbacks not correctly treated in the simulations relate to a shortening of lifetimes of ODSs and long-lived greenhouse gases in the World Avoided simulations. Such shortening could occur from increased actinic fluxes and an acceleration of the Brewer-Dobson circulation, and would cause increasing emissions of ODSs to lead to less-than-proportional increases in their atmospheric abundances.

5.5.4 UV Impacts of the Avoided Ozone Depletion

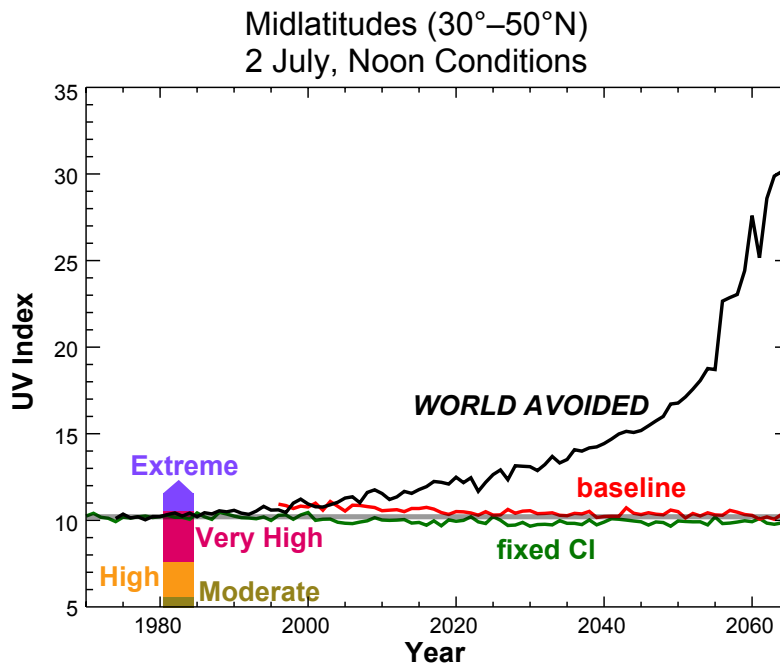
The decreases in ozone abundances in the World Avoided simulations (Prather et al., 1996; Morgenstern et al., 2008; Newman et al., 2009) would have led to an increase in solar ultraviolet radiation at Earth's surface. The magnitude of these increases varies with wavelength, depending on the absorption cross section of ozone, and with latitude, according to the latitudinal distribution

of ozone depletion. Newman et al. (2009) calculate the spectral changes in UV occurring in their simulation. At the shortest UV-B wavelengths, in relative terms, the calculated changes are extremely large; however, in absolute terms the surface irradiance at these wavelengths is weak. Regarding biologically relevant radiation, they show that decreases in stratospheric ozone due to increasing CFCs would have led to marked increases in erythemally weighted irradiance (which is proportional to the UV Index; Chapter 2), up to three times more in the summer of northern midlatitudes by 2065 (Figure 5-11), and with UV Index values in excess of 30 at midlatitudes of both hemispheres. The excess radiation would have had large impacts on the biosphere and on human health; for example, Northern Hemisphere midlatitude ozone losses would have led to a reduction of the sunburn time, at local noon for clear-sky midsummer conditions, from 15 to 5 minutes, and would increase DNA-damaging UV by approximately 550% between 1980 and 2065 (Newman et al., 2009).

5.5.5 Summary

“Road not taken” or “World Avoided” studies indicate that the Montreal Protocol has had considerable benefits for both the ozone layer and climate change. Total chlorine would have increased much beyond the observed peak of around 3.5 ppb. Consequences of uncontrolled growth in ODSs would have resulted both directly from the radiative forcing of the halocarbons, and indirectly from the ensuing ozone depletion. In 2010, the

Figure 5-11. Erythemally weighted UV radiation (expressed in terms of the UV Index) for noon conditions on 2 July at northern midlatitudes. Black: World Avoided. Red: A1 baseline scenario (WMO, 2007) for ODSs. Green: CI fixed at 1960 levels. Gray: 1975–1985 average of the fixed-CI simulation. The conventional color scale used in reporting the UV Index to the public is superimposed for reference showing the highest four divisions. (Adapted from Newman et al., 2009).



RF associated with unmitigated emissions of halocarbons could have reached 2 to 5 times what has actually occurred. The chemical consequences could have included a thinned ozone layer everywhere on the globe, the occurrence of an Arctic ozone hole, regional climate change in middle and high latitudes of both hemispheres, increased UV with associated biological and medical consequences, and changes in stratospheric circulation including, in an extreme case, year-round westerlies in the Southern-Hemisphere stratosphere (the “perpetual winter”). While many details associated with these calculated World Avoided impacts may have large uncertainties associated with them, there is no doubt that the Montreal Protocol and its Amendments and Adjustments have avoided additional profound changes to stratospheric ozone and climate.

REFERENCES

- Andersen, S.O., and K.M. Sarma, *Protecting the Ozone Layer — the Official UN History*, Earthscan, ISBN 1-85383-905-1, London, 2002.
- Barry, J., G. Locke, D. Scollard, H. Sidebottom, J. Treacy, C. Clerbaux, R. Colin, and J. Franklin, 1,1,1,3,3,-Pentafluorobutane (HFC-365mfc): Atmospheric degradation and contribution to radiative forcing, *Int. J. Chem. Kinet.*, 29 (8), 607-617, doi: 10.1002/(SICI)1097-4601(1997)29:8<607::AID-KIN6>3.0.CO;2-Y, 1997.
- Benesch, J.A., M.S. Gustin, G.R. Cramer, and T.M. Cahill, Investigation of effects of trifluoroacetate on vernal pool ecosystems, *Environ. Toxicol. Chem.*, 21 (3), 640-647, doi: 10.1002/etc.5620210325, 2002.
- Berg, M., S.R. Müller, J. Mühlemann, A. Wiedmer, and R.P. Schwarzenbach, Concentrations and mass fluxes of chloroacetic acids and trifluoroacetic acid in rain and natural waters in Switzerland, *Environ. Sci. Technol.*, 34, 2675-2683, doi: 10.1021/es990855f, 2000.
- Berntsen, T.K., J.S. Fuglestedt, M.M. Joshi, K.P. Shine, N. Stuber, M. Ponater, R. Sausen, D.A. Hauglustaine, and L. Li, Response of climate to regional emissions of ozone precursors: Sensitivities and warming potentials, *Tellus*, 57B (4), 283-304, 2005.
- Blowers, P., and K. Hollingshead, Estimations of global warming potentials from computational chemistry calculations for CH₂F₂ and other fluorinated methyl species verified by comparison to experiment, *J. Phys. Chem. A*, 113 (20), 5942-5950, doi: 10.1021/jp8114918, 2009.
- Boutonnet, J.C., P. Bingham, D. Calamari, C. de Rooij, J. Franklin, T. Kawano, J.-M. Libre, A. McCulloch, G. Malinverno, J.M. Odom, G.M. Rusch, K. Smythe, I. Sobolev, R. Thompson, and J.M. Tiedje, Environmental risk assessment of trifluoroacetic acid, *Hum. Ecol. Risk Assess.*, 5 (1), 59-124, 1999.
- Brasseur, G.P., *A Report on the Way Forward Based on the Review of Research Gaps and Priorities*, Aviation Climate Change Research Initiative, Federal Aviation Administration, 53 pp., available: http://www.faa.gov/about/office_org/headquarters_offices/aep/aviation_climate/media/ACCRI_Report_final.pdf,

- 2008.
- British Petroleum, *BP Statistical Review of World Energy June 2009*, Beacon Press, available: http://www.bp.com/liveassets/bp_internet/globalbp/globalbp_uk_english/reports_and_publications/statistical_energy_review_2008/STAGING/local_assets/2009_downloads/statistical_review_of_world_energy_full_report_2009.pdf, 2009.
- Budyko, M.I., Present-day climatic changes, *Tellus*, 29 (3), 193-204, doi: 10.1111/j.2153-3490.1977.tb00725.x, 1977.
- Calvert, J.G., R.G. Derwent, J.J. Orlando, G.S. Tyndall, and T.J. Wallington, *Mechanisms of Atmospheric Oxidation of the Alkanes*, 1008 pp., Oxford University Press, New York, NY, U.S.A., 2008.
- Cariolle D., D. Caro, R. Paoli, D.A. Hauglustaine, B. Cuénot, A. Cozic, and R. Paugam, Parameterization of plume chemistry into large-scale atmospheric models: Application to aircraft NO_x emissions, *J. Geophys. Res.*, 114, D19302, doi: 10.1029/2009JD011873, 2009.
- Cavalli, F., M. Glasius, J. Hjorth, B. Rindone, and N.R. Jensen, Atmospheric lifetimes, infrared spectra and degradation products of a series of hydrofluoroethers, *Atmos. Environ.*, 32 (21), 3767-3773, doi: 10.1016/S1352-2310(98)00106-X, 1998.
- Chipperfield, M.P., and W. Feng, Comment on: Stratospheric ozone depletion at northern mid-latitudes in the 21st century: The importance of future concentrations of greenhouse gases nitrous oxide and methane, *Geophys. Res. Lett.*, 30 (7), 1389, doi: 10.1029/2002GL016353, 2003.
- Christidis, N., M.D. Hurley, S. Pinnock, K.P. Shine, and T.J. Wallington, Radiative forcing of climate change by CFC-11 and possible CFC-replacements, *J. Geophys. Res.*, 102 (D16), 19597-19609, doi: 10.1029/97JD01137, 1997.
- Chubachi, S., and R. Kajiwara, Total ozone variations at Syowa, Antarctica, *Geophys. Res. Lett.*, 13 (12), 1197-1198, doi: 10.1029/GL013i012p01197, 1986.
- Clarke, L.E., J.A. Edmonds, H.D. Jacoby, H.M. Pitcher, J.M. Reilly, and R.G. Richels, *Scenarios of Greenhouse Gas Emissions and Atmospheric Concentrations*, Sub-report 2.1a of Synthesis and Assessment Product 2.1 by the U.S. Climate Change Science Program and the Subcommittee on Global Change Research, Department of Energy, Office of Biological & Environmental Research, Washington, D.C., U.S., 154 pp., 2007.
- Crutzen, P.J., Albedo enhancement by stratospheric sulfur injections: A contribution to resolve a policy dilemma?, *Clim. Change*, 77 (3-4), 211-220, doi: 10.1007/s10584-006-9101-y, 2006.
- Crutzen, P.J., A.R. Mosier, K.A. Smith, and W. Winiwarter, N₂O release from agro-biofuel production negates global warming reduction by replacing fossil fuels, *Atmos. Chem. Phys.*, 8 (2), 389-395, doi: 10.5194/acp-8-389-2008, 2008.
- Cunnold, D.M., R.F. Weiss, R.G. Prinn, D. Hartley, P.G. Simmonds, P.J. Fraser, B. Miller, F.N. Alyea, and L. Porter, GAGE/AGAGE measurements indicating reductions in global emissions of CCl₃F and CCl₂F₂ in 1992-1994, *J. Geophys. Res.*, 102 (D1), 1259-1269, 1997.
- Daniel, J.S, and G.J.M. Velders (Lead Authors), A.R. Douglass, P.M.D. Forster, D.A. Hauglustaine, I.S.A. Isaksen, L.J.M. Kuijpers, A. McCulloch, and T.J. Wallington, Halocarbon scenarios, ozone depletion potentials, and global warming potentials, Chapter 8 in *Scientific Assessment of Ozone Depletion: 2006*, Global Ozone Research and Monitoring Project—Report No. 50, World Meteorological Organization, Geneva, Switzerland, 2007.
- Daniel, J.S., S. Solomon, and D.L. Albritton, On the evaluation of halocarbon radiative forcing and global warming potentials, *J. Geophys. Res.*, 100 (D1), 1271-1285, 1995.
- Daniel, J.S., E.L. Fleming, R.W. Portmann, G.J.M. Velders, C.H. Jackman, and A.R. Ravishankara, Options to accelerate ozone recovery: Ozone and climate benefits, *Atmos. Chem. Phys.*, 10 (16), 7697-7707, doi: 10.5194/acp-10-7697-2010, 2010.
- D'Anna, B., S.R. Sellevåg, K. Wirtz, and C.J. Nielsen, Photolysis study of perfluoro-2-methyl-3-pentanone under natural sunlight conditions, *Environ. Sci. Technol.*, 39 (22), 8708-8711, doi: 10.1021/es048088u, 2005.
- Derwent, R.G., M.E. Jenkin, S.M. Saunders, and M.J. Pilling, Photochemical ozone creation potentials for organic compounds in Northwest Europe calculated with a master chemical mechanism, *Atmos. Environ.*, 32 (14-15), 2429-2441, 1998.
- Derwent, R.G., M.E. Jenkin, N.R. Passant, and M.J. Pilling, Reactivity-based strategies for photochemical ozone control in Europe, *Environ. Sci. Policy*, 10 (5), 445-453, doi: 10.1016/j.envsci.2007.01.005, 2007.
- Dillon, T.J., A. Horowitz, and J.N. Crowley, The atmospheric chemistry of sulphuryl fluoride, SO₂F₂, *Atmos. Chem. Phys.*, 8 (6), 1547-1557, doi: 10.5194/acp-8-1547-2008, 2008.
- Douglass, A.R., R.S. Stolarski, M.R. Schoeberl, C.H. Jackman, M.L. Gupta, P.A. Newman, J.E. Nielsen, and E.L. Fleming, Relationship of loss, mean age of air and the distribution of CFCs to stratospheric circulation and implications for atmospheric lifetimes, *J. Geophys. Res.*, 113, D14309, doi: 10.1029/2007JD009575, 2008.

- Dyson, F.J., and G. Marland, Technical fixes for the climate effects of CO₂, in *Workshop on the Global Effects of Carbon Dioxide from Fossil Fuels*, edited by W.P. Elliott and L. Machta, CONF-770385, U.S. Department of Energy, Washington, D.C., U.S., pp. 111-118, 1979.
- Erchel, E., *World Water Balance*, Elsevier, New York, NY, U.S.A., 1975.
- Farman, J.C., B.G. Gardiner, and J.D. Shanklin, Large losses of total ozone in Antarctica reveal seasonal ClO_x/NO_x interaction, *Nature*, *315*, 207-210, doi: 10.1038/315207a0, 1985.
- Fisher, D.A., C.H. Hales, D.L. Filkin, M.K.W. Ko, N.D. Sze, P.S. Connell, D.J. Wuebbles, I.S.A. Isaksen, and F. Stordal, Model calculations of the relative effects of CFCs and their replacements on stratospheric ozone, *Nature*, *344*, 508-512, doi: 10.1038/344508a0, 1990.
- Fleming, E.L., C.H. Jackman, D.K. Weisenstein, and M.K.W. Ko, The impact of interannual variability on multidecadal total ozone simulations, *J. Geophys. Res.*, *112*, D10310, doi: 10.1029/2006JD007953, 2007.
- Fogt, R.L., J. Perlwitz, S. Pawson, and M.A. Olsen, Inter-annual relationships between polar ozone and the SAM, *Geophys. Res. Lett.*, *36*, L04707, doi: 10.1029/2008GL036627, 2009.
- Forster, P.M. de F., J.B. Burkholder, C. Clerbaux, P.F. Coheur, M. Dutta, L.K. Gohar, M.D. Hurley, G. Myhre, R.W. Portmann, A. Ravishankara, K.P. Shine, T.J. Wallington, and D. Wuebbles, Resolution of the uncertainties in the radiative forcing of HFC-134a, *J. Quant. Spectrosc. Radiat. Transfer*, *93* (4), 447-460, doi: 10.1016/j.jqsrt.2004.08.038, 2005.
- Frank, H., E.H. Christoph, O. Holm-Hansen, and J.L. Bullister, Trifluoroacetate in ocean waters, *Environ. Sci. Technol.*, *36*, 12-15, doi: 10.1021/es0101532, 2002.
- Fuglestedt, J.S., K.P. Shine, T. Berntsen, J. Cook, D.S. Lee, A. Stenke, R.B. Skeie, G.J.M. Velders, and I.A. Waitz, Transport impacts on atmosphere and climate: Metrics, *Atmos. Environ.*, *44* (37), 4648-4677, doi: 10.1016/j.atmosenv.2009.04.044, 2010.
- Gillett, N.P., Northern Hemisphere circulation, *Nature*, *437* (7058), 496, doi: 10.1038/437496a, 2005.
- Gillett, N.P., and D.W.J. Thompson, Simulation of recent Southern Hemisphere climate change, *Science*, *302* (5643), 273-275, 2003.
- Good, D.A., and J.S. Francisco, Atmospheric chemistry of alternative fuels and alternative chlorofluorocarbons, *Chem. Rev.*, *103* (12), 4999-5024, doi: 10.1021/cr020654l, 2003.
- Haigh, J.D., and J.A. Pyle, A two-dimensional calculation including atmospheric carbon dioxide and stratospheric ozone, *Nature*, *279*, 222-224, doi: 10.1038/279222a0, 1979.
- Hayman, G.D., and R.G. Derwent, Atmospheric chemical reactivity and ozone-forming potentials of potential CFC replacements, *Environ. Sci. Technol.*, *31* (2), 327-336, 1997.
- Heckendorn, P., D. Weisenstein, S. Fueglistaler, B.P. Luo, E. Rozanov, M. Schraner, L.W. Thomason, and T. Peter, The impact of geoengineering aerosols on stratospheric temperature and ozone, *Env. Res. Lett.*, *4* (4), doi: 10.1088/1748-9326/4/4/045108, 2009.
- Hegerl, G.C., and S. Solomon, Risks of climate engineering, *Science*, *325* (5943), 955-956, doi: 10.1126/science.1178530, 2009.
- Hsu, J., and M.J. Prather, Global long-lived chemical modes excited in a 3-D chemistry transport model: Stratospheric N₂O, NO_y, O₃, and CH₄ chemistry, *Geophys. Res. Lett.*, *37*, L07805, doi: 10.1029/2009GL042243, 2010.
- Hurley, M.D., T.J. Wallington, M.S. Javadi, and O.J. Nielsen, Atmospheric chemistry of CF₃CF=CH₂: Products and mechanisms of Cl atom and OH radical initiated oxidation, *Chem. Phys. Lett.*, *450*, 263-267, doi: 10.1016/j.cplett.2007.11.051, 2008.
- Inoue, Y., M. Kawasaki, T.J. Wallington, and M.D. Hurley, Atmospheric chemistry of CF₃CH₂CF₂CH₃ (HFC-365mfc): Kinetics and mechanism of chlorine atom initiated oxidation, infrared spectrum, and global warming potential, *Chem. Phys. Lett.*, *462*, 164-168, doi: 10.1016/j.cplett.2008.07.054, 2008.
- IPCC (Intergovernmental Panel on Climate Change), *Climate Change: The IPCC Scientific Assessment*, edited by J.T. Houghton, G.J. Jenkins, and J.J. Ephraums, 364 pp., Cambridge University Press, Cambridge, U.K., 1990.
- IPCC (Intergovernmental Panel on Climate Change), *Climate Change, 1994: Radiative Forcing of Climate Change and an Evaluation of the IPCC IS92 Emission Scenarios*, edited by J.T. Houghton, L.G. Meira Filho, J. Bruce, H. Lee, B.A. Callander, E. Haites, N. Harris, and K. Maskell, 339 pp., Cambridge University Press, Cambridge, U.K., 1995.
- IPCC (Intergovernmental Panel on Climate Change), *Climate Change 1995: The Science of Climate Change*, edited by J.T. Houghton, L.G. Meira Filho, B.A. Callander, N. Harris, A. Kattenberg, and K. Maskell, 572 pp., Cambridge University Press, Cambridge, U.K., 1996.
- IPCC (Intergovernmental Panel on Climate Change), *Aviation and the Global Atmosphere, A Special Report of the Intergovernmental Panel on Climate Change*, edited by J.E. Penner, D. Lister, D.J. Griggs, D.J. Dokken, and M. McFarland, 373 pp.,

- Cambridge University Press, Cambridge, U.K., doi: 10.2277/0521664047, 1999.
- IPCC (Intergovernmental Panel on Climate Change), *Special Report on Emissions Scenarios*, Special Report of Working Group III of the Intergovernmental Panel on Climate Change, edited by N. Nakicenovic and R. Swart, 570 pp., Cambridge University Press, Cambridge, U.K. and New York, NY, U.S.A., 2000.
- IPCC (Intergovernmental Panel on Climate Change), *Climate Change 2001: The Scientific Basis, Contribution of Working Group I to the Third Assessment Report of the Intergovernmental Panel on Climate Change*, edited by J.T. Houghton, Y. Ding, D.J. Griggs, M. Noguer, P.J. van der Linden, X. Dai, K. Maskell, and C.A. Johnson, 881 pp., Cambridge University Press, Cambridge, U.K., 2001.
- IPCC (Intergovernmental Panel on Climate Change), *Climate Change 2007: The Physical Science Basis, Contribution of Working Group I to the Fourth Assessment Report of the Intergovernmental Panel on Climate Change*, edited by S. Solomon, D. Qin, M. Manning, Z. Chen, M. Marquis, K.B. Averyt, M. Tignor, and H.L. Miller, 996 pp., Cambridge University Press, Cambridge, U.K., and New York, NY, U.S.A., 2007.
- IPCC (Intergovernmental Panel on Climate Change), *Summary Report of the IPCC Expert Meeting on the Science of Alternative Metrics*, 18–20 March 2009, Oslo, Norway. IPCC-XXX/Doc.13 (31.III.2009), available: www.ipcc.ch/meetings/session30/doc13.pdf, 2009.
- IPCC/TEAP (Intergovernmental Panel on Climate Change/Technology and Economic Assessment Panel), *IPCC/TEAP Special Report on Safeguarding the Ozone Layer and the Global Climate System: Issues Related to Hydrofluorocarbons and Perfluorocarbons*, prepared by Working Groups I and III of the Intergovernmental Panel on Climate Change, and the Technical and Economic Assessment Panel, Cambridge University Press, Cambridge, U.K., and New York, NY, U.S.A., 2005.
- Jenkin, M.E., Photochemical ozone and PAN creation potentials: Rationalisation and methods of estimation, *AEA Technology plc*, Report AEAT-4182/20150/003, 1998.
- Johansson, D.J.A., U.M. Persson, and C. Azar, Uncertainty and learning: Implications for the trade-off between short-lived and long-lived greenhouse gases, *Clim. Change*, 88 (3-4), 293-308, doi: 10.1007/s10584-007-9381-x, 2008.
- Johnson, C.E., and R.G. Derwent, Relative radiative forcing consequences of global emissions of hydrocarbons, carbon monoxide and NO_x from human activities estimated with a zonally-averaged two-dimensional model, *Clim. Change*, 34 (3-4), 439-462, doi: 10.1007/BF00139301, 1996.
- Keith, D.W., E. Parson, and M.G. Morgan, Research on global sun block needed now, *Nature*, 463, 426-427, doi: 10.1038/463426a, 2010.
- Kodama, C., T. Iwasaki, K. Shibata, and S. Yukimoto, Changes in the stratospheric mean meridional circulation due to increased CO₂: Radiation- and sea surface temperature-induced effects, *J. Geophys. Res.*, 112, D16103, doi: 10.1029/2006JD008219, 2007.
- Köhler, M.O., G. Rädcl, O. Dessens, K.P. Shine, H.L. Rogers, O. Wild, and J.A. Pyle, Impact of perturbations to nitrogen oxide emissions from global aviation, *J. Geophys. Res.*, 113, D11305, doi: 10.1029/2007JD009140, 2008.
- Kotamarthi, V.R., J.M. Rodriguez, M.K.W. Ko, T.K. Tromp, N.D. Sze, and M.J. Prather, Trifluoroacetic acid from the degradation of HCFCs and HFCs: A three-dimensional modeling study, *J. Geophys. Res.*, 103 (D5), 5747-5758, 1998.
- Lee, D.S., G. Pitari, V. Grewe, K. Gierens, J.E. Penner, A. Petzold, M.J. Prather, U. Schumann, A. Bais, T. Berntsen, D. Iachetti, L.L. Lim, and R. Sausen, Transport impacts on atmosphere and climate: Aviation, *Atmos. Environ.*, 44 (37), doi: 10.1016/j.atmosenv.2009.06.005, 2009.
- Lenton, T.M., and N.E. Vaughan, The radiative forcing potential of different climate geoengineering options, *Atmos. Chem. Phys.*, 9 (15), 5539-5561, doi: 10.5194/acp-9-5539-2009, 2009.
- Li, F., R.S. Stolarski, and P.A. Newman, Stratospheric ozone in the post-CFC era, *Atmos. Chem. Phys.*, 9 (6), 2207-2213, doi: 10.5194/acp-9-2207-2009, 2009.
- Luecken, D.J., R.L. Waterland, S. Papasavva, K. Tadonno, W.T. Hutzell, J.P. Rugh, and S.O. Andersen, Ozone and TFA impacts in North America from degradation of 2,3,3,3-tetrafluoropropene (HFO-1234yf), a potential greenhouse gas replacement, *Environ. Sci. Technol.*, 44 (1), 343-348, doi: 10.1021/es902481f, 2010.
- MacAyeal, D.R., T.A. Scambos, C.L. Hulbe, and M.A. Fahnestock, Catastrophic ice-shelf break-up by an ice-shelf-fragment-capsize mechanism, *J. Glaciol.*, 49 (164), 22-36, 2003.
- Manne, A.S., and R.G. Richels, An alternative approach to establishing trade-offs among greenhouse gases, *Nature*, 410, 675-677, doi: 10.1038/35070541, 2001.
- Martinerie, P., E. Nourtier-Mazauric, J.-M. Barnola, W.T. Sturges, D.R. Worton, E. Atlas, L.K. Gohar, K.P. Shine, and G.P. Brasseur, Long-lived halocarbon

- trends and budgets from atmospheric chemistry modelling constrained with measurements in polar firm, *Atmos. Chem. Phys.*, 9 (12), 3911-3934, doi: 10.5194/acp-9-3911-2009, 2009.
- Maurice, L.Q., and D.S. Lee (eds.), *Assessing Current Scientific Knowledge, Uncertainties and Gaps in Quantifying Climate Change, Noise and Air Quality Aviation Impacts*, L.Q. Maurice, D.S. Lee, D.J. Wuebbles, I. Isaksen, L. Finegold, M. Vallet, M. Pilling, and J. Spengler, Final Report of the International Civil Aviation Organization (ICAO) Committee on Aviation and Environmental Protection (CAEP) Workshop, U.S. Federal Aviation Administration and Manchester Metropolitan University, Washington D.C. and Manchester, available: <http://web.mit.edu/aeroastro/partner/reports/caepimpac-treport.pdf>, 2009.
- Meilinger, S.K., B. Kärcher, and Th. Peter, Microphysics and heterogeneous chemistry in aircraft plumes – high sensitivity on local meteorology and atmospheric composition, *Atmos. Chem. Phys.*, 5 (2), 533-545, doi: 10.5194/acp-5-533-2005, 2005.
- Molina, M.J., and F.S. Rowland, Stratospheric sink for chlorofluoromethanes: Chlorine atom-catalysed destruction of ozone, *Nature*, 249, 5460, 810-812, doi: 10.1038/249810a0, 1974.
- Montzka, S.A., J.H. Butler, B.D. Hall, D.J. Mondeel, and J.W. Elkins, A decline in tropospheric organic bromine, *Geophys. Res. Lett.*, 30 (15), doi: 10.1029/2003GL017745, 2003.
- Montzka, S.A., B.D. Hall, and J.W. Elkins, Accelerated increases observed for hydrochlorofluorocarbons since 2004 in the global atmosphere, *Geophys. Res. Lett.*, 36, L03804, doi: 10.1029/2008GL036475, 2009.
- Montzka, S.A., L. Kuijpers, M.O. Battle, M. Aydin, K.R. Verhulst, E.S. Saltzman, and D.W. Fahey, Recent increase in global HFC-23 emissions, *Geophys. Res. Lett.*, 37, L02808, doi: 10.1029/2009GL041195, 2010.
- Morgenstern, O., P. Braesicke, M.M. Hurwitz, F.M. O'Connor, A.C. Bushell, C.E. Johnson, and J.A. Pyle, The world avoided by the Montreal Protocol, *Geophys. Res. Lett.*, 35, L16811, doi: 10.1029/2008GL034590, 2008.
- Morgenstern, O., P. Braesicke, F.M. O'Connor, A.C. Bushell, C.E. Johnson, S.M. Osprey, and J.A. Pyle, Evaluation of the new UKCA climate-composition model – part 1: The stratosphere, *Geosci. Model Dev.*, 2 (1), 43-57, doi: 10.5194/gmd-2-43-2009, 2009.
- Newman, P.A., E.R. Nash, S.R. Kawa, S.A. Montzka, and S.M. Schauffler, When will the Antarctic ozone hole recover?, *Geophys. Res. Lett.*, 33, L12814, doi: 10.1029/2005GL025232, 2006.
- Newman, P.A., J.S. Daniel, D.W. Waugh, and E.R. Nash, A new formulation of equivalent effective stratospheric chlorine (EESC), *Atmos. Chem. Phys.*, 7 (17), 4537-4552, doi: 10.5194/acp-7-4537-2007, 2007.
- Newman, P.A., L.D. Oman, A.R. Douglass, E.L. Fleming, S.M. Frith, M.M. Hurwitz, S.R. Kawa, C.H. Jackman, N.A. Krotkov, E.R. Nash, J.E. Nielsen, S. Pawson, R.S. Stolarski, and G.J.M. Velders, What would have happened to the ozone layer if chlorofluorocarbons (CFCs) had not been regulated?, *Atmos. Chem. Phys.*, 9 (6), 2113-2128, doi: 10.5194/acp-9-2113-2009, 2009.
- Nielsen, O.J., M.S. Javadi, M.P. Sulbaek Andersen, M.D. Hurley, T.J. Wallington, and R. Singh, Atmospheric chemistry of $\text{CF}_3\text{CF}=\text{CH}_2$: Kinetics and mechanisms of gas-phase reactions with Cl atoms, OH radicals, and O_3 , *Chem. Phys. Lett.*, 439, 18-22, doi: 10.1016/j.cplett.2007.03.053, 2007.
- Ottinger Schaefer, D., D. Godwin, and J. Harnisch, Estimating future emissions and potential reductions of HFCs, PFCs, and SF_6 , *Energy J. Special Issue 3*, 27, 63-68, in *Multi-Greenhouse Gas Mitigation and Climate Policy*, edited by F.C. de la Chesnaye and J.P. Weyant, International Association for Energy Economics, 2006.
- Papadimitriou, V.C., R.W. Portmann, D.W. Fahey, J. Mühle, R.F. Weiss, and J.B. Burkholder, Experimental and theoretical study of the atmospheric chemistry and global warming potential of SO_2F_2 , *J. Phys. Chem. A*, 112, 12657-12666, doi: 10.1021/jp806368u, 2008a.
- Papadimitriou, V.C., R.K. Talukdar, R.W. Portmann, A.R. Ravishankara, and J.B. Burkholder, $\text{CF}_3\text{CF}=\text{CH}_2$ and (Z)- $\text{CF}_3\text{CF}=\text{CHF}$: Temperature dependent OH rate coefficients and global warming potentials, *Phys. Chem. Chem. Phys.*, 10, 808-820, doi: 10.1039/b714382f, 2008b.
- Parson, E.A., *Protecting the Ozone Layer: Science and Strategy*, 396 pp., Oxford University Press, New York, NY, U.S.A., 2003.
- Pawson, S., R.S. Stolarski, A.R. Douglass, P.A. Newman, J.E. Nielsen, S.M. Frith, and M.L. Gupta, Goddard Earth Observing System chemistry-climate model simulations of stratospheric ozone-temperature coupling between 1950 and 2005, *J. Geophys. Res.*, 113, D12103, doi: 10.1029/2007JD009511, 2008.
- Pinnock, S., M.D. Hurley, K.P. Shine, T.J. Wallington, and T.J. Smyth, Radiative forcing of climate by hydrochlorofluorocarbons and hydrofluorocarbons, *J. Geophys. Res.*, 100 (D1), 23227-23238, doi: 10.1029/95JD02323, 1995.
- Pitari, G., D. Iachetti, E. Mancini, V. Montanaro, N. De

- Luca, C. Marizy, O. Dessens, H. Rogers, J. Pyle, V. Grewe, A. Stenke, and O.A. Søvde, Radiative forcing from particle emissions by future supersonic aircraft, *Atmos. Chem. Phys.*, 8 (14), 4069-4084, doi: 10.5194/acp-8-4069-2008, 2008.
- Portmann, R.W., and S. Solomon, Indirect radiative forcing of the ozone layer during the 21st century, *Geophys. Res. Lett.*, 34, L02813, doi: 10.1029/2006GL028252, 2007.
- Portmann, R.W., S. Solomon, R.R. Garcia, L.W. Thomason, L.R. Poole, and M.P. McCormick, Role of aerosol variations in anthropogenic ozone depletion in the polar regions, *J. Geophys. Res.*, 101 (D17), 22991-23006, 1996.
- Prather, M.J., Time scales in atmospheric chemistry: Theory, GWPs for CH₄ and CO, and runaway growth, *Geophys. Res. Lett.*, 23 (19), 2597-2600, 1996.
- Prather, M.J., Lifetimes of atmospheric species: Integrating environmental impacts, *Geophys. Res. Lett.*, 29 (22), 2063, doi: 10.1029/2002GL016299, 2002.
- Prather, M.J., and J. Hsu, NF₃, the greenhouse gas missing from Kyoto, *Geophys. Res. Lett.*, 35, L12810, doi: 10.1029/2008GL034542, 2008.
- Prather, M., P. Midgley, F. Sherwood Rowland, and R. Stolarski, The ozone layer: The road not taken, *Nature*, 381, 551-554, doi: 10.1038/381551a0, 1996.
- Prinn, R.G. and R. Zander (Lead Authors), D.M. Cunnold, J.W. Elkins, A. Engel, P.J. Fraser, M.R. Gunson, M.K.W. Ko, E. Mahieu, P.M. Midgley, J.M. Russell III, C.M. Volk, and R.F. Weiss, Long-lived ozone-related compounds, Chapter 1 in *Scientific Assessment of Ozone Depletion: 1998*, Global Ozone Research and Monitoring Project—Report No. 44, World Meteorological Organization, Geneva, Switzerland, 1999.
- Rajakumar, B., R.W. Portmann, J.B. Burkholder, and A.R. Ravishankara, Rate coefficients for the reactions of OH with CF₃CH₂CH₃ (HFC-263fb), CF₃CHFCH₂F (HFC-245eb), and CHF₂CHFCHF₂ (HFC-245ea) between 238 and 375 K, *J. Phys. Chem. A*, 110, 6724-6731, doi: 10.1021/jp056248y, 2006.
- Rao, S., and K. Riahi, The role of non-CO₂ greenhouse gases in climate change mitigation: Long-term scenarios for the 21st century, *Energy J. Special Issue 3*, 27, 177-200, in *Multi-Greenhouse Gas Mitigation and Climate Policy*, edited by F.C. de la Chesnaye, and J.P. Weyant, International Association for Energy Economics, 2006.
- Rasch, P.J., P.J. Crutzen, and D.B. Coleman, Exploring the geoengineering of climate using stratospheric sulfate aerosols: The role of particle size, *Geophys. Res. Lett.*, 35, L02809, doi: 10.1029/2007GL032179, 2008a.
- Rasch, P.J., S. Tilmes, R.P. Turco, A. Robock, L. Oman, C.-C. Chen, G.L. Stenchikov, and R.R. Garcia, An overview of geoengineering of climate using stratospheric sulphate aerosols, *Phil. Trans. Royal Soc. A*, 366 (1882), 4007-4037, doi: 10.1098/rsta.2008.0131, 2008b.
- Ravishankara, A.R., A.A. Turnipseed, N.R. Jensen, S. Barone, M. Mills, C.J. Howard, and S. Solomon, Do hydrofluorocarbons destroy stratospheric ozone?, *Science*, 263, 71-75, 1994.
- Ravishankara, A.R., J.S. Daniel, and R.W. Portmann, Nitrous oxide (N₂O): The dominant ozone-depleting substance emitted in the 21st century, *Science*, 326 (5949), 123-125, doi: 10.1126/science.1176985, 2009.
- Riahi, K., and N. Nakicenovic (eds.), Greenhouse Gases—Integrated Assessment, *Technol. Forecast. Soc. Change*, Special Issue, 74 (7), September 2007, 234 pp., ISSN 0040-1625, doi: 10.1016/S0040-1625(07)00140-0, 2007.
- Robock, A., 20 reasons why geoengineering may be a bad idea, *Bull. Atom. Sci.*, 64 (2), 14-18, doi: 10.2968/064002006, 2008.
- Robock, A., L. Oman, and G. Stenchikov, Regional climate responses to geoengineering with tropical and Arctic SO₂ injections, *J. Geophys. Res.*, 113, D16101, doi: 10.1029/2008JD010050, 2008.
- Rosenfield, J.E., A.R. Douglass, and D.B. Considine, The impact of increasing carbon dioxide on ozone recovery, *J. Geophys. Res.*, 107 (D6), 4049, doi: 10.1029/2001JD000824, 2002.
- Ross, M., D. Toohey, M. Peinemann, and P. Ross, Limits on the space launch market related to stratospheric ozone depletion, *Astropolitics*, 7, 50-82, doi: 10.1080/14777620902768867, 2009.
- Royal Society, *Geoengineering the Climate: Science, Governance and Uncertainty*, Report 10/09, London GB, The Royal Society, available: <http://royal-society.org/geoengineering-the-climate/>, 2009.
- Schauffler, S.M., E.L. Atlas, S.G. Donnelly, A. Andrews, S.A. Montzka, J.W. Elkins, D.F. Hurst, P.A. Romashkin, G.S. Dutton, and V. Stroud, Chlorine budget and partitioning during the Stratospheric Aerosol and Gas Experiment (SAGE) III Ozone Loss and Validation Experiment (SOLVE), *J. Geophys. Res.*, 108 (D5), 4173, doi: 10.1029/2001JD002040, 2003.
- Scott, B.F., R.W. Macdonald, K. Kannan, A. Fisk, A. Witter, N. Yamashita, L. Durham, C. Spencer, and D.C.G. Muir, Trifluoroacetate profiles in the Arctic, Atlantic, and Pacific Oceans, *Environ. Sci. Technol.*, 39 (17), 6555-6560, doi: 10.1021/es047975u, 2005.
- Scott, B.F., C.A. Moody, C. Spencer, J.M. Small, D.C.G. Muir, and S.A. Mabury, Analysis for

- perfluorocarboxylic acids/anions in surface waters and precipitation using GC-MS and analysis of PFOA from large-volume samples, *Environ. Sci. Technol.*, *40* (20), 6405-6410, doi: 10.1021/es061131o, 2006.
- Seedhouse, E., *Tourists in Space: A Practical Guide*, Springer Praxis Books, Chichester, U.K., doi: 10.1007/978-0-387-74644-9, 2008.
- Shine, K.P., On the cause of the relative greenhouse strength of gases such as the halocarbons, *J. Atmos. Sci.*, *48*, 1513-1518, doi: 10.1175/1520-0469(1991)048<1513:OTCOTR>2.0.CO;2, 1991.
- Shine K.P., The global warming potential—the need for an interdisciplinary retrieval, *Clim. Change*, *96*, 467-472, doi: 10.1007/s10584-009-9647-6, 2009.
- Smith, S.J., and T.M.L. Wigley, Multi-gas forcing stabilization with Minicam, *Energy J. Special Issue 3*, *27*, 373-392, in *Multi-Greenhouse Gas Mitigation and Climate Policy*, edited by F.C. de la Chesnaye and J.P. Weyant, International Association for Energy Economics, 2006.
- Soden, B.J., R.T. Wetherald, G.L. Stenchikov, and A. Robock, Global cooling after the eruption of Mount Pinatubo: A test of climate feedback by water vapor, *Science*, *296* (5568), 727-730, doi: 10.1126/science.296.5568.727, 2002.
- Solomon, S., and D.L. Albritton, Time-dependent ozone depletion potentials for short- and long-term forecasts, *Nature*, *357*, 33-37, doi: 10.1038/357033a0, 1992.
- Solomon, S., M. Mills, L.E. Heidt, W.H. Pollock, and A.F. Tuck, On the evaluation of ozone depletion potentials, *J. Geophys. Res.*, *97* (D1), 825-842, 1992.
- Solomon, S., R.W. Portmann, R.R. Garcia, L.W. Thomason, L.R. Poole, and M.P. McCormick, The role of aerosol variations in anthropogenic ozone depletion at northern midlatitudes, *J. Geophys. Res.*, *101* (D3), 6713-6727, 1996.
- Solomon, K.R., X. Tang, S.R. Wilson, P. Zanis, and A.F. Bais, Changes in tropospheric composition and air quality due to stratospheric ozone depletion, *Photochem. Photobiol. Sci.*, *2*, 62-67, doi: 10.1039/b211086e, 2003.
- Søvde, O.A., M. Gauss, I.S.A. Isaksen, G. Pitari, and C. Marizy, Aircraft pollution — a futuristic view, *Atmos. Chem. Phys.*, *7* (13), 3621-3632, doi: 10.5194/acp-7-3621-2007, 2007.
- SPARC CCMVal (Stratospheric Processes And their Role in Climate), *SPARC CCMVal Report on the Evaluation of Chemistry-Climate Models*, edited by V. Eyring, T.G. Shepherd, and D.W. Waugh, SPARC Report No. 5, WCRP-132, WMO/TD-No. 1526, available: http://www.atmosph.physics.utoronto.ca/SPARC/ccmval_final/index.php, 2010.
- Stohl, A., P. Seibert, J. Arduini, S. Eckhardt, P. Fraser, B.R. Grealley, C. Lunder, M. Maione, J. Mühle, S. O'Doherty, R.G. Prinn, S. Reimann, T. Saito, N. Schmidbauer, P.G. Simmonds, M.K. Vollmer, R.F. Weiss, and Y. Yokouchi, An analytical inversion method for determining regional and global emissions of greenhouse gases: Sensitivity studies and application to halocarbons, *Atmos. Chem. Phys.*, *9* (5), 1597-1620, doi: 10.5194/acp-9-1597-2009, 2009.
- Sulbaek Andersen, M.P., D.R. Blake, F.S. Rowland, M.D. Hurley, and T.J. Wallington, Atmospheric chemistry of sulfuranyl fluoride: Reaction with OH radicals, Cl atoms and O₃, atmospheric lifetime, IR spectrum, and global warming potential, *Environ. Sci. Technol.*, *43* (4), 1067-1070, doi: 10.1021/es802439f, 2009.
- Tabazadeh, A., K. Drdla, M.R. Schoeberl, P. Hamill, and O.B. Toon, Arctic “ozone hole” in a cold volcanic stratosphere, *Proc. Natl. Acad. Sci.*, *99* (5), 2609-2612, doi: 10.1073/pnas.052518199, 2002.
- Tanaka, K., B.C. O'Neill, D. Rokityanskiy, M. Obersteiner, and R.S.J. Tol, Evaluating global warming potentials with historical temperature, *Clim. Change*, *96*, 443-466, doi: 10.1007/s10584-009-9566-6, 2009.
- Tang, X., S. Madronich, T. Wallington, and D. Calamari, Changes in tropospheric composition and air quality, *J. Photochem. Photobiol. B: Biol.*, *46* (1-3), 83-95, doi: 10.1016/S1011-1344(98)00187-0, 1998.
- Taniguchi, N., T.J. Wallington, M.D. Hurley, A.G. Guschin, L.T. Molina, and M.J. Molina, Atmospheric chemistry of C₂F₅C(O)CF(CF₃)₂: Photolysis and reaction with Cl atoms, OH radicals, and ozone, *J. Phys. Chem. A*, *107* (15), 2674-2679, doi: 10.1021/jp0220332, 2003.
- TEAP (Technology and Economic Assessment Panel), *Task Force Decision XX/8 Report, Assessment of Alternatives to HCFCs and HFCs and Update of the TEAP 2005 Supplement Report Data*, coordinated by L. Kuijpers, and D. Verdonik, United Nations Environment Programme, Nairobi, Kenya, available: http://ozone.unep.org/teap/Reports/TEAP_Reports/teap-may-2009-decisionXX-8-task-force-report.pdf, 2009.
- Teller, E., L. Wood, and R. Hyde, Global warming and Ice Ages: I. Prospects for physics-based modulation of global change, *UCRL-JC-128715*, Lawrence Livermore National Laboratory, Livermore, California, U.S., 20 pp., 1997.
- Thompson, D.W.J., and S. Solomon, Interpretation of recent Southern Hemisphere climate change, *Science*, *296* (5569), 895-899, doi: 10.1126/

- science.1069270, 2002.
- Tilmes, S., R. Müller, R.J. Salawitch, U. Schmidt, C.R. Webster, H. Oelhaf, C.C. Camy-Peyret, and J.M. Russell III, Chemical ozone loss in the Arctic winter 1991–1992, *Atmos. Chem. Phys.*, *8* (7), 1897–1910, doi: 10.5194/acp-8-1897-2008, 2008a.
- Tilmes, S., R. Müller, and R. Salawitch, The sensitivity of polar ozone depletion to proposed geoengineering schemes, *Science*, *320* (5880), 1201–1204, doi: 10.1126/science.1153966, 2008b.
- Tilmes, S., R.R. Garcia, D.E. Kinnison, A. Gettelman, and P.J. Rasch, Impact of geo-engineered aerosols on troposphere and stratosphere, *J. Geophys. Res.*, *114*, D12305, doi: 10.1029/2008JD011420, 2009.
- Tromp, T.K., M.K.W. Ko, J.M. Rodriguez, and N.D. Sze, Potential accumulation of a CFC-replacement degradation product in seasonal wetlands, *Nature*, *376*, 327–330, doi: 10.1038/376327a0, 1995.
- UBA (Umweltbundesamt), *Projections of Global Emissions of Fluorinated Greenhouse Gases in 2050*, B. Gschrey and W. Schwarz, German Federal Environment Agency (Umweltbundesamt), Report-no. UBA-FB 001318, available: <http://www.umwelt-daten.de/publikationen/fpdf-l/3866.pdf>, 2009.
- UNEP (United Nations Environment Programme), data on production and consumption of ozone depleting substances under the Montreal Protocol, downloaded from <http://www.unep.org/ozone>, Nairobi, Kenya, 2009.
- van Vuuren, D.P., B. Eickhout, P.L. Lucas, and M.D.G. Den Elzen, Long-term multi-gas scenarios to stabilise radiative forcing, *Energy J. Special Issue 3*, *27*, 201–233, in *Multi-Greenhouse Gas Mitigation and Climate Policy*, edited by F.C. de la Chesnaye and J.P. Weyant, International Association for Energy Economics, 2006.
- van Vuuren, D.P., M.G.J. den Elzen, P.L. Lucas, B. Eickhout, B.J. Strengers, B. van Ruijven, S. Wonink, and R. van Houdt, Stabilizing greenhouse gas concentrations at low levels: An assessment of reduction strategies and costs, *Clim. Change*, *81* (2), 119–159, doi: 10.1007/s10584-006-9172-9, 2007.
- Velders, G.J.M., S.O. Andersen, J.S. Daniel, D.W. Fahey, and M. McFarland, The importance of the Montreal Protocol in protecting climate, *Proc. Natl. Acad. Sci.*, *104* (12), 4814–4819, doi: 10.1073/pnas.0610328104, 2007.
- Velders, G.J.M., D.W. Fahey, J.S. Daniel, M. McFarland, and S.O. Andersen, The large contribution of projected HFC emissions to future climate forcing, *Proc. Natl. Acad. Sci.*, *106* (27), 10949–10954, doi: 10.1073/pnas.0902817106, 2009.
- Volk, C.M., J.W. Elkins, D.W. Fahey, G.S. Dutton, J.M. Gilligan, M. Loewenstein, J.R. Podolske, K.R. Chan, and M.R. Gunson, Evaluation of source gas lifetimes from stratospheric observations, *J. Geophys. Res.*, *102* (D21), 25543–25564, 1997.
- Von Sydow, L.M., A.B. Grimvall, H.B. Borén, K. Laniewski, and A.T. Nielsen, Natural background levels of trifluoroacetate in rain and snow, *Environ. Sci. Technol.*, *34*, 3115–3118, doi: 10.1021/es9913683, 2000.
- Wallington, T.J., W.F. Schneider, D.R. Worsnop, O.J. Nielsen, J. Sehested, W. DeBruyn, and J.A. Shorter, Environmental impact of CFC replacements — HFCs and HCFCs, *Environ. Sci. Technol.*, *28* (7), 320A–326A, 1994.
- Wallington, T.J., W.F. Schneider, J. Sehested, and O.J. Nielsen, Hydrofluorocarbons and stratospheric ozone, *Faraday Discuss.*, *100*, 55–64, 1995.
- Wallington, T.J., M.D. Hurley, and O.J. Nielsen, The radiative efficiency of HCF₂OCF₂OCF₂CF₂OCF₂H (H-Galden 1040x) revisited, *Atmos. Environ.*, *43*, 4247–4249, doi: 10.1016/j.atmosenv.2009.05.046, 2009.
- Wallington, T.J., M.P. Sulbaek Andersen, and O.J. Nielsen, Estimated photochemical ozone creation potentials (POCPs) of CF₃CF=CH₂ (HFO-1234yf) and related hydrofluoroolefins (HFOs), *Atmos. Environ.*, *44* (11), 1478–1481, doi: 10.1016/j.atmosenv.2010.01.040, 2010.
- Wang, M., Greenhouse Gases, Regulated Emissions, and Energy Use in Transportation (GREET) Model, Version 1.8d.1, downloaded August 27, 2010, available: http://www.transportation.anl.gov/modeling_simulation/GREET/, 2010.
- Waugh, D.W., L. Oman, S.R. Kawa, R.S. Stolarski, S. Pawson, A.R. Douglass, P.A. Newman, and J.E. Nielsen, Impacts of climate change on stratospheric ozone recovery, *Geophys. Res. Lett.*, *36*, L03805, doi: 10.1029/2008GL036223, 2009.
- Wigley, T.M.L., A combined mitigation/geoengineering approach to climate stabilization, *Science*, *314* (5798), 452–454, doi: 10.1126/science.1131728, 2006.
- Wise, M., K. Calvin, A. Thomson, L. Clarke, B. Bond-Lamberty, R. Sands, S.J. Smith, and A. Janetos, J. Edmonds, Implications of limiting CO₂ concentrations for land use and energy, *Science*, *324* (5931), 1183–1186, doi: 10.1126/science.1168475, 2009.
- WMO (World Meteorological Organization), *Atmospheric Ozone 1985: Assessment of Our Understanding of the Processes Controlling its Present Distribution and Change* (3 volumes), Global Ozone Research and Monitoring Project—Report No. 16, Geneva, Switzerland, 1986.
- WMO (World Meteorological Organization), *Scientific Assessment of Stratospheric Ozone: 1989, Volume*

- I, Global Ozone Research and Monitoring Project—Report No. 20, Geneva, Switzerland, 1989.
- WMO (World Meteorological Organization), *Scientific Assessment of Ozone Depletion: 1991*, Global Ozone Research and Monitoring Project—Report No. 25, Geneva, Switzerland, 1991.
- WMO (World Meteorological Organization), *Scientific Assessment of Ozone Depletion: 1994*, Global Ozone Research and Monitoring Project—Report No. 37, Geneva, Switzerland, 1995.
- WMO (World Meteorological Organization), *Scientific Assessment of Ozone Depletion: 1998*, Global Ozone Research and Monitoring Project—Report No. 44, Geneva, Switzerland, 1999.
- WMO (World Meteorological Organization), *Scientific Assessment of Ozone Depletion: 2002*, Global Ozone Research and Monitoring Project—Report No. 47, Geneva, Switzerland, 2003.
- WMO (World Meteorological Organization), *Scientific Assessment of Ozone Depletion: 2006*, Global Ozone Research and Monitoring Project—Report 50, Geneva, Switzerland, 2007.
- Wuebbles, D.J., *The Relative Efficiency of a Number of Halocarbons for Destroying Stratospheric Ozone*, 11 pp., Lawrence Livermore National Laboratory, Livermore, CA, 1981.
- Wuebbles, D.J., Chlorocarbon emission scenarios: Potential impact on stratospheric ozone, *Geophys. Res. Lett.*, *88* (C2), 1433-1443, 1983.
- Wuebbles, D.J., Nitrous oxide: No laughing matter, *Science*, *326* (5949), 56-57, doi: 10.1126/science.1179571, 2009.
- Wuebbles, D.J., and K.O. Patten, Three-dimensional modeling of HCFC-123 in the atmosphere: Assessing its potential environmental impacts and rationale for continued use, *Environ. Sci. Technol.*, *43* (9), 3208-3213, doi: 10.1021/es802308m, 2009.
- Wuebbles, D.J., A. Douglass, B. Kärcher, W.-C. Wang, S. Baughcum, R.P. d'Entremont, A. Dessler, P. Ginoux, R. Herman, A. Heymsfield, I. Isaksen, D. Jacob, S. Lele, J. Logan, J. McConnell, R. Mialy, P. Minnis, D. Mitchell, D. Murphy, L. Pan, J. Penner, M. Prather, J. Rodriguez, K. Rosenlof, K. Sassen, R. Sausen, K. Shine, A. Tabazadeh, I. Waitz, P. Yang, and F. Yu, *Workshop on the Impacts of Aviation on Climate Change: A Report of Findings and Recommendations*, Partnership for Air Transportation Noise and Emissions Reduction, Report No. PARTNER-COE-2006-004, available: <http://web.mit.edu/aeroastro/partner/reports/climatewrksp-rpt-0806.pdf>, 2006.
- Wuebbles, D.J., D. Youn, K. Patten, D. Wang, and M. Martínez-Avilés, Metrics for ozone and climate: Three-dimensional modeling studies of ozone depletion potentials and indirect global warming potentials, in *Twenty Years of Ozone Decline. Proceedings of the Symposium for the 20th Anniversary of the Montreal Protocol*, edited by C. Zerefos, G. Contopoulos, and G. Skalkeas, 297-326, Springer Publishing, Dordrecht, The Netherlands, doi: 10.1007/978-90-481-2469-5, 2009.
- Youn, D., K.O. Patten, J.-T. Lin, and D.J. Wuebbles, Explicit calculation of indirect global warming potentials for halons using atmospheric models, *Atmos. Chem. Phys.*, *9* (22), 8719-8733, doi: 10.5194/acp-9-8719-2009, 2009.
- Youn, D., K.O. Patten, D.J. Wuebbles, H. Lee, and C.-W. So, Potential impact of iodinated replacement compounds CF₃I and CH₃I on atmospheric ozone: A three-dimensional modeling study, *Atmos. Chem. Phys.*, *10* (20), 10129-10144, doi: 10.5194/acp-10-10129-2010, 2010.
- Young, C.J., M.D. Hurley, T.J. Wallington, and S.A. Mabury, Atmospheric lifetime and global warming potential of a perfluoropolyether, *Environ. Sci. Technol.*, *40*, 2242-2246, doi: 10.1021/es052077z, 2006.
- Young, C.J., M.D. Hurley, T.J. Wallington, and S.A. Mabury, Molecular structure and radiative efficiency of fluorinated ethers: A structure-activity relationship, *J. Geophys. Res.*, *113*, D24301 doi: 10.1029/2008JD010178, 2008.
- Young, C.J., M.D. Hurley, T.J. Wallington, and S.A. Mabury, Atmospheric chemistry of CF₃CF₂H and CF₃CF₂CF₂H: Kinetics and products of gas-phase reactions with Cl atoms and OH radicals, infrared spectra, and formation of perfluorocarboxylic acids, *Chem. Phys. Lett.*, *473*, 251-256, doi: 10.1016/j.cplett.2009.04.001, 2009.
- Yvon-Lewis, S.A., E.S. Saltzman, and S.A. Montzka, Recent trends in atmospheric methyl bromide: Analysis of post-Montreal Protocol variability, *Atmos. Chem. Phys.*, *9* (16), 5963-5974, doi: 10.5194/acp-9-5963-2009, 2009.

APPENDIX 5A

TABLES

Table 5A-1. Direct Global Warming Potentials for selected gases.

Industrial Designation or Common Name	Chemical Formula	Radiative Efficiency ^a (W m ⁻² ppb ⁻¹)	Lifetime ^b (years)	Global Warming Potential for Given Time Horizon		
				20 years	100 years	500 years
Carbon dioxide	CO ₂	1.38×10 ^{-5 c}		1	1	1
Nitrous oxide	N ₂ O	3.03×10 ⁻³	114	289	298	153
Chlorofluorocarbons						
CFC-11	CCl ₃ F	0.25	45	6,730	4,750	1,620
CFC-12	CCl ₂ F ₂	0.32	100	11,000	10,900	5,200
CFC-13	CCIF ₃	0.25	640	10,800	14,400	16,400
CFC-113	CCl ₂ FCCIF ₂	0.30	85	6,540	6,130	2,690
CFC-114	CCIF ₂ CCIF ₂	0.31	190	7,890	9,180	6,330
CFC-115	CCIF ₂ CF ₃	0.18	1,020	5,290	7,230	9,120
Hydrochlorofluorocarbons						
HCFC-21	CHCl ₂ F	0.14	1.7	530	151	46
HCFC-22	CHClF ₂	0.20	11.9	5,130	1,790	545
HCFC-123	CHCl ₂ CF ₃	0.14	1.3	273	77	24
HCFC-124	CHClFCF ₃	0.22	5.9	2,110	619	188
HCFC-141b	CH ₃ CCl ₂ F	0.14	9.2	2,240	717	218
HCFC-142b	CH ₃ CCIF ₂	0.20	17.2	5,390	2,220	678
HCFC-225ca	CHCl ₂ CF ₂ CF ₃	0.20	1.9	429	122	37
HCFC-225cb	CHClFCF ₂ CCIF ₂	0.32	5.9	2,060	606	184
Hydrofluorocarbons						
HFC-23	CHF ₃	0.19	222	11,900	14,200	10,700
HFC-32	CH ₂ F ₂	0.11	5.2	2,470	716	218
HFC-41	CH ₃ F	0.02	2.8	377	107	33
HFC-125	CHF ₂ CF ₃	0.23	28.2	6,290	3,420	1,070
HFC-134	CHF ₂ CHF ₂	0.18	9.7	3,420	1,110	339
HFC-134a	CH ₂ FCF ₃	0.16	13.4	3,730	1,370	416
HFC-143	CH ₂ FCHF ₂	0.13	3.5	1,240	352	107
HFC-143a	CH ₃ CF ₃	0.13	47.1	5,780	4,180	1,440
HFC-152a	CH ₃ CHF ₂	0.09	1.5	468	133	40
HFC-227ea	CF ₃ CHFCF ₃	0.26	38.9	5,480	3,580	1,180
HFC-236cb	CH ₂ FCF ₂ CF ₃	0.23	13.1	3,560	1,290	392

Table 5A-1, continued.

Industrial Designation or Common Name	Chemical Formula	Radiative Efficiency ^a (W m ⁻² ppb ⁻¹)	Lifetime ^b (years)	Global Warming Potential for Given Time Horizon		
				20 years	100 years	500 years
HFC-236ea	CHF ₂ CHF ₂ CF ₃	0.30	11	4,170	1,410	430
HFC-236fa	CF ₃ CH ₂ CF ₃	0.28	242	8,100	9,820	7,710
HFC-245ca	CH ₂ FCF ₂ CHF ₂	0.23	6.5	2,440	726	221
HFC-245ea	CHF ₂ CHFCHF ₂	0.18 ^d	3.2	983	280	85
HFC-245eb	CH ₂ FCHF ₂ CF ₃	0.23 ^d	3.1	1,220	346	105
HFC-245fa	CHF ₂ CH ₂ CF ₃	0.28	7.7	3,410	1,050	318
HFC-263fb	CH ₃ CH ₂ CF ₃	0.13 ^d	1.2	365	104	31
HFC-329p	CHF ₂ CF ₂ CF ₂ CF ₃	0.31 ^d	28.4	4,640	2,530	792
HFC-365mfc	CH ₃ CF ₂ CH ₂ CF ₃	0.22 ^d	8.7	2,670	842	256
HFC-43-10mee	CF ₃ CHFCHF ₂ CF ₃	0.40	16.1	4,170	1,660	506
Chlorocarbons						
Methyl chloroform	CH ₃ CCl ₃	0.06	5.0	506	146	45
Carbon tetrachloride	CCl ₄	0.13	26	2,700	1,400	435
Methyl chloride	CH ₃ Cl	0.01	1.0	45	13	4
Bromocarbons and Halons						
Methyl bromide	CH ₃ Br	0.01	0.8	19	5	2
Bromodifluoromethane	CHBrF ₂	0.14	5.2	1,250	362	110
Halon-1211	CBrClF ₂	0.30	16	4,750	1,890	575
Halon-1301	CBrF ₃	0.32	65	8,480	7,140	2,760
Halon-2402	CBrF ₂ CBrF ₂	0.33	20	3,680	1,640	503
Fully Fluorinated Species						
Nitrogen trifluoride	NF ₃	0.21	500	13,300	17,500	18,500
Sulfur hexafluoride	SF ₆	0.52	3,200	16,300	22,800	32,600
Trifluoromethylsulfur-pentafluoride	SF ₅ CF ₃	0.57	800 ^e	13,200	17,800	21,400
Perfluoromethane	CF ₄	0.10	50,000	5,210	7,390	11,200
Perfluoroethane	C ₂ F ₆	0.26	10,000	8,630	12,200	18,200
Perfluoropropane	C ₃ F ₈	0.26	2,600	6,310	8,830	12,500
Perfluorocyclopropane	c-C ₃ F ₆	0.42	~3,000	12,800	17,900	25,500
Perfluorobutane	C ₄ F ₁₀	0.33	2,600	6,330	8,850	12,500
Perfluorocyclobutane	c-C ₄ F ₈	0.32	3,200	7,310	10,300	14,700
Perfluoropentane	C ₅ F ₁₂	0.41	4,100	6,510	9,150	13,300
Perfluorohexane	C ₆ F ₁₄	0.49	3,100	6,620	9,290	13,300
Perfluorodecalin	C ₁₀ F ₁₈	0.56	~2,000	5,530	7,700	10,600

Table 5A-1, continued.

Industrial Designation or Common Name	Chemical Formula	Radiative Efficiency ^a (W m ⁻² ppb ⁻¹)	Lifetime ^b (years)	Global Warming Potential for Given Time Horizon		
				20 years	100 years	500 years
Halogenated Alcohols and Ethers						
HFE-125	CHF ₂ OCF ₃	0.44	119	13,700	14,200	7,510
HFE-134	CHF ₂ OCHF ₂	0.45	24.4	11,930	5,960	1,840
HFE-143a	CH ₃ OCF ₃	0.27	4.8	2,920	840	256
HFE-227ea	CF ₃ OCHFCF ₃	0.40	51.6	8,170	6,180	2,200
HFCE-235da2 (isoflurane)	CHF ₂ OCHClCF ₃	0.38	3.5	1,650	470	143
HFE-236ea2 (desflurane)	CHF ₂ OCHFCF ₃	0.44	10.8	5,460	1,840	560
HFE-236fa	CF ₃ OCH ₂ CF ₃	0.34	7.5	3,240	988	300
HFE-245cb2	CH ₃ OCF ₂ CF ₃	0.32	4.9	2,350	680	207
HFE-245fa1	CF ₃ OCH ₂ CHF ₂	0.30	6.6	2,880	859	261
HFE-245fa2	CHF ₂ OCH ₂ CF ₃	0.31	5.5	2,540	740	225
HFE-254cb2	CH ₃ OCF ₂ CHF ₂	0.28	2.5	1,210	345	105
HFE-329mcc2	CF ₃ CF ₂ OCF ₂ CHF ₂	0.49	22.5	6,300	3,000	925
HFE-338mcf2	CF ₃ CF ₂ OCH ₂ CF ₃	0.43	7.5	3,150	963	293
HFE-347mcc3	CF ₃ CF ₂ CF ₂ OCH ₃	0.34	5.0	1,910	553	168
HFE-347mcf2	CF ₃ CF ₂ OCH ₂ CHF ₂	0.41	6.6	2,950	881	268
HFE-356mec3	CF ₃ CHFCF ₂ OCH ₃	0.30	3.8	1,430	408	124
HFE-356pcf2	CHF ₂ CF ₂ OCH ₂ CHF ₂	0.37	5.7	2,580	754	229
HFE-356pcf3	CHF ₂ CF ₂ CH ₂ OCHF ₂	0.39	3.5	1,710	488	148
HFE-356pcc3	CHF ₂ CF ₂ CF ₂ OCH ₃	0.33	3.8	1,570	448	136
	(CF ₃) ₂ CHOCHF ₂	0.41	21.2	5,580	2,570	789
	(CF ₃) ₂ CFOCH ₃	0.31	3.7	1,310	373	114
HFE-43-10pccc124	CHF ₂ OCF ₂ OC ₂ F ₄ OCHF ₂	1.02 ^d	13.5	8,130	2,990	909
HFE-7100 (HFE-449 blend)	C ₄ F ₉ OCH ₃	0.31	4.7	1,320	379	115
HFE-7200 (HFE-569 blend)	C ₄ F ₉ OC ₂ H ₅	0.30	0.8	208	59	18
HFE-236ca12	CHF ₂ OCF ₂ OCHF ₂	0.66	25	11,320	5,730	1,770
HFE-338pcc13	CHF ₂ OCF ₂ CF ₂ OCHF ₂	0.87	12.9	8,660	3,120	949
	(CF ₃) ₂ CHOH	0.28	1.9	726	206	63
Miscellaneous						
Sulfuryl fluoride	SO ₂ F ₂	0.22 ^d	36	7,580	4,740	1,540

^a Taken from WMO (2007), unless stated otherwise.

^b Taken from Chapter 1, unless stated otherwise.

^c Assumes CO₂ mixing ratio is 378 parts per million (ppm).

^d See Table 5-2.

^e Midpoint of range given in Chapter 1.

Table 5A-2. Assumptions made in obtaining production and emission estimates for the baseline (A1) scenario.

General Approach for All Species	
<p>Production: For the years when production is reported to UNEP, reported values (or best estimates of production values for cases in which reporting is incomplete) are used. Before this, WMO (2007) production values are generally used. In the future, annual figures are determined from the lesser of the Protocol limitations and the most recent annual estimates.</p> <p>Emission: For the years when mixing ratio observations are available, emissions are calculated using the box model described in Daniel and Velders et al. (2007) with the lifetimes of Appendix Table 5A-1. Emissions before this are usually consistent with WMO (2007) but are also forced to yield mixing ratios that meld smoothly into the measurement record. Future emissions are determined using a fixed annual bank release fraction, calculated as the average ratio over the past 10 years between the annual emissions and estimated bank plus production.</p> <p>Bank: The bank assumed to be in place at the start of the measurement record is set at such a value that the IPCC (2009) bank for 2008 is attained. The bank at the end of each year is equal to the bank at the beginning of the year plus production during that year minus emissions during that year.</p>	
Approach for Specific Species	
Species	Description
CFC-11	<p>Production: 1950–1985: WMO (2007) 1986, 1989–2008: UNEP (2009)^a, 1987–1988 interpolated from 1986 and 1989 values 2009–2010: Approved critical-use exemptions for non-Article 5(1) countries 2010: Approved critical-use exemptions for Article 5(1) countries, 2009 value interpolated from 2008 and 2010 values. All critical-use exemptions for CFCs are assumed to be CFC-11 After 2010: No production</p> <p>Emission: 1979–2008: Emissions calculated from observed global abundance trends 2009–2100: Annual emissions are a constant fraction of 0.05 of the bank, extrapolated from the previous years</p> <p>Bank: 1979 bank set to 1,705 Kt to attain a 2008 bank of 1,420 Kt (TEAP, 2009). The bank projected for 2008 in the previous Assessment was 1,380 Kt.</p>
CFC-12	<p>Same as CFC-11, except: Annual emissions from 2009–2100 are a constant fraction of 0.15 of the bank</p> <p>Bank: 1979 bank set to 941 Kt to attain a 2008 bank of 394 Kt (TEAP, 2009). The bank projected for 2008 in the previous Assessment was 499 Kt.</p>
CFC-113	<p>Same formalism as for CFC-11, except: Annual emissions from 2009–2100 are a constant fraction of 0.5 of the estimated bank. (Although our scenario has a non-zero bank in 2010, according to TEAP (2009) the bank has been zero since 2002.)</p>
CFC-114	<p>Same formalism as for CFC-11 except: Bank calculated based on historic production and emission data Annual emission from 2009–2100 is a constant fraction of 0.1 of the estimated bank</p>
CFC-115	<p>Same as CFC-11, except: Emissions from 2009–2100 are a constant fraction of 0.02 of the bank</p> <p>Bank: 2008 bank of 16 Kt (TEAP, 2009)</p>

Table 5A-2, continued.

Approach for Specific Species	
CCl ₄	<p>Production and bank not considered due to gaps in our understanding of the origin of much of the global emission</p> <p>Emission:</p> <p>1951–1979: WMO (2003)</p> <p>1980–2008: Emissions calculated from observed global abundance trends</p> <p>2009–2050: Emissions decrease by 6% per year (average derived from observations and a 26-year lifetime during 2004 to 2008)</p> <p>2051–2100: No emission</p>
CH ₃ CCl ₃	<p>Production not explicitly considered</p> <p>Emission:</p> <p>1950–1978: WMO (2003)</p> <p>1979–2008: Emissions calculated from observed global abundance trends</p> <p>2009–2014: Emission equal to the 2004–2008 average</p> <p>2015–2100: No emission</p>
HCFC-22	<p>Production:</p> <p>1950–1988: WMO (2003)</p> <p>1989, 1992–2008: UNEP (2009)^a, 1990–1991 interpolated from 1989 and 1992 values</p> <p>Non-Article 5(1) countries: 2009 production is 2004–2008 average; 2010–2013 Montreal Protocol phase-out schedule applied</p> <p>The base level HCFC consumption in non-Article 5(1) countries is calculated as the consumption in 1989 + 2.8% of the 1989 CFC consumption (ODP-weighted). In WMO (2007), the 2.8% of the CFC consumption was assigned completely to HCFC-22. In this Assessment it is distributed over the three main HCFCs based on their historic production. This results in larger future emissions of HCFC-141b and HCFC-142b.</p> <p>Article 5(1) countries: 2009–2012 is linearly extrapolated from 2004–2008; 2013–2040 Montreal Protocol phase-out schedule applied</p> <p>Emission:</p> <p>1950–1992: Emissions calculated to yield mixing ratios consistent with WMO (2007)</p> <p>1993–2008: Emissions calculated from observed global abundance trends</p> <p>2009–2100: Assume an annual bank release fraction of 0.18 (average of 2002–2008)</p> <p>Bank:</p> <p>1993 bank set to 302 Kt to attain a 2008 bank of 1,618 Kt (TEAP, 2009). The bank projected for 2008 in the previous Assessment was 2,083 Kt.</p>
HCFC-141b	<p>Production as in HCFC-22</p> <p>Emission:</p> <p>1990–2008: Emissions calculated from observed global abundance trends</p> <p>2009–2100: Annual emissions calculated assuming a bank release fraction of 0.05 (average of 2003–2008)</p> <p>Bank:</p> <p>1994 bank set to 115 Kt to attain a 2008 bank of 941 Kt (TEAP, 2009). The bank projected for 2008 in the previous Assessment was 961 Kt.</p>
HCFC-142b	<p>Production as in HCFC-22</p> <p>Emission:</p> <p>1979–2008: Emissions calculated from observed global abundance trends</p> <p>2009–2100: Annual emissions calculated assuming a bank release fraction of 0.11 (average of 1999–2008)</p> <p>Bank:</p> <p>1993 bank set to 95 Kt to attain a 2008 bank of 273 Kt (TEAP, 2009). The bank projected for 2008 in the previous Assessment was 211 Kt.</p>

Table 5A-2, continued.

Approach for Specific Species	
Halon-1211	<p>Production:</p> <p>1986, 1989–2008: UNEP (2009), 1987–1988 interpolated from 1986 and 1989 values non-Article 5(1) countries: zero production from 2009–2100 Article 5(1) countries: 2009 production is 2006–2008 average; zero from 2010–2100</p> <p>Emission:</p> <p>1950–1992: WMO (2007) 1993–2008: Emissions calculated from observed global abundance trends 2009–2100: Annual emissions calculated assuming a bank release fraction of 0.075 (average of 1999–2008)</p> <p>Bank:</p> <p>1993 bank is set to 128 Kt to attain a 2008 bank of 74 Kt (TEAP, 2009). The bank projected for 2008 in the previous Assessment was 86 Kt.</p>
Halon-1301	<p>Production as in halon-1211</p> <p>Emission:</p> <p>1950–1992: WMO (2007) 1992–2008: Emissions calculated from observed global abundance trends 2009–2100: Annual emissions calculated assuming a bank release fraction of 0.04 (average of 1999–2008)</p> <p>Bank:</p> <p>1992 bank is set to 74 Kt to attain a 2008 bank of 47 Kt (TEAP, 2009). The bank projected for 2008 in the previous Assessment was 31 Kt.</p>
Halon-1202	Same as WMO (2007)
Halon-2402	<p>Production as in halon-1211</p> <p>Emission:</p> <p>1970–2003: based on WMO (2007), but adjusted to meld smoothly into the measurement record 2004–2008: Emissions calculated from observed global abundance trends 2009–2100: Annual emissions calculated assume a bank release fraction of 0.08 (average of 2004–2008)</p> <p>Bank:</p> <p>1995 bank is set to 20 Kt to allow the emissions meld smoothly into the emissions derived from observations. The corresponding 2008 bank of 9.1 Kt is much larger than from TEAP (2009) of 1.3 Kt. A bank of 1.3 Kt would result in emissions a factor of 8 smaller than derived from observations for 2004–2008. The bank projected for 2008 in the previous Assessment was 1.8 Kt.</p>
CH ₃ Br	<p>Production/emissions from Yvon-Lewis et al. (2009): natural production/emission (102 Kt), gasoline (5.7 Kt), biomass (11.3 Kt), biofuel (6.1 Kt), non QPS-fumigation. Parenthetical values for anthropogenic sources are emission estimates for 1996 and 2007 (Yvon-Lewis et al., 2009 and references therein) and are held constant into the future.</p> <p>QPS production from 1995–2008 from UNEP (2009), held constant at 11.2 Kt (2004–2008 average) for 2009–2100</p> <p>Approved critical-use exemptions (CUE) for 2009–2011 (no CUE after 2011)</p> <p>Emissions:</p> <p>1950–2008: Emissions calculated from surface observations and derived from South Pole firm measurements (using a global lifetime of 0.75 years to be consistent with Yvon-Lewis et al., 2009)</p> <p>2009–2100: Fumigation emissions equal 0.6 times production for fumigation. The combination of anthropogenic and natural emissions, constrained by the total emissions derived from observations of concentrations, leads to an anthropogenic fraction of total emissions of 0.30</p>

Table 5A-2, continued.

Approach for Specific Species	
(CH ₃ Br, continued)	Bank: in 1992, in agreement with Montzka et al. (2003) (see also Chapter 1). No bank considered
CH ₃ Cl	Emission: 1950–1995: Global emissions derived from firn measurements at the South Pole 1996–2100: Emissions held constant at 1995 levels, as in WMO (2003) and WMO (2007)

^a Estimated in cases in which reporting is not complete or reporting is made in compound classes rather than individually. The production data for each species in each year is obtained from UNEP (2009) and is consistent with the totals for each group of species as usually reported by UNEP.

Table 5A-3. Mixing ratios (ppt) of the ODSs considered in the baseline (A1) scenario¹. Values are for the beginning of the corresponding year. Potentially important short-lived gases that may currently contribute 3–8 ppt of stratospheric bromine and 40–130 ppt of stratospheric chlorine (see Chapter 1) are not shown in the table.

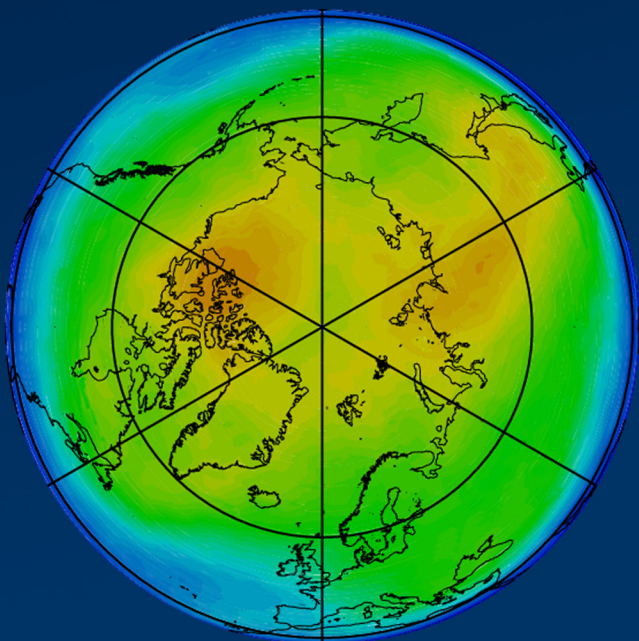
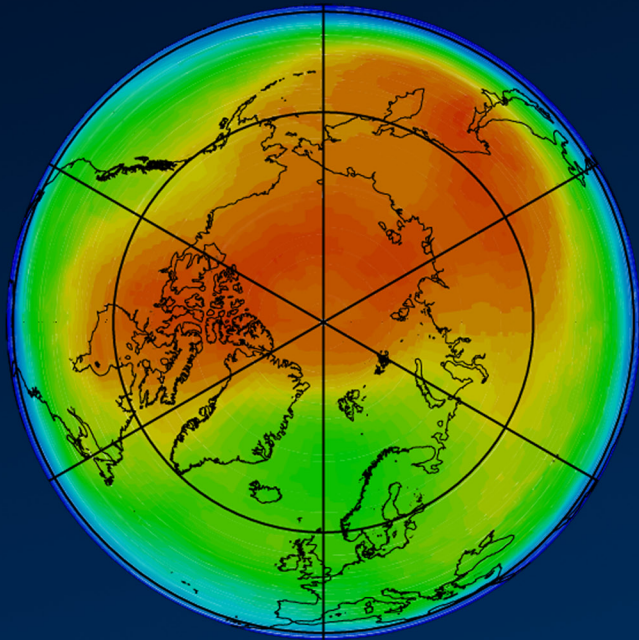
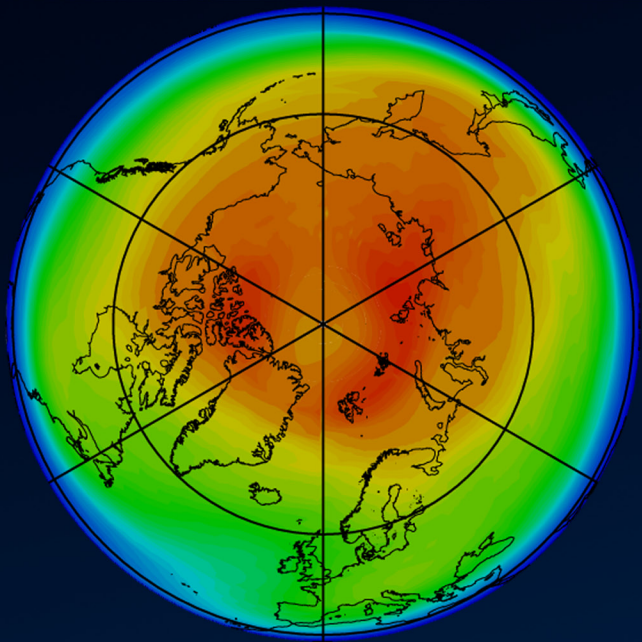
	CFC-11		CFC-113		CFC-115		CH ₃ CCl ₃		HCFC-22		HCFC-141b		Halon-1211		Halon-1202		Halon-1301		Halon-2402		CH ₃ Br	CH ₃ Cl
	CFC-11	CFC-12	CFC-113	CFC-114	CFC-115	CCl ₄	CH ₃ CCl ₃	HCFC-22	HCFC-141b	HCFC-142b	Halon-1211	Halon-1202	Halon-1301	Halon-2402	CH ₃ Br	CH ₃ Cl						
1955	3.3	14.3	1.2	2.6	0.0	42.3	0.1	1.0	0.0	0.0	0.0	0.0	0.0	0.0	0.0	0.0	0.0	0.0	0.0	6.3	491.3	
1960	9.5	29.5	1.9	3.8	0.0	52.1	1.5	2.1	0.0	0.0	0.0	0.0	0.0	0.0	0.0	0.0	0.0	0.0	0.0	6.5	510.3	
1965	23.5	58.8	3.1	5.0	0.0	64.4	4.7	4.9	0.0	0.0	0.0	0.0	0.0	0.0	0.0	0.0	0.0	0.0	0.0	6.7	528.1	
1970	52.8	114.3	5.5	6.5	0.2	75.9	16.2	12.1	0.0	0.0	0.0	0.0	0.0	0.0	0.0	0.0	0.0	0.0	0.0	7.0	539.9	
1975	106.1	203.1	10.4	8.3	0.6	85.5	40.0	23.8	0.0	0.2	0.12	0.01	0.04	0.06	0.01	0.04	0.06	0.01	0.04	7.4	545.8	
1980	161.9	297.4	19.0	10.7	1.3	93.3	81.6	42.5	0.0	0.4	0.42	0.01	0.24	0.15	0.01	0.24	0.15	0.01	0.24	7.7	548.3	
1981	170.3	313.9	21.5	11.1	1.5	94.8	88.3	46.6	0.0	0.5	0.52	0.01	0.31	0.17	0.01	0.31	0.17	0.01	0.31	7.8	548.6	
1982	179.2	329.9	25.3	11.6	1.8	95.8	93.0	50.7	0.0	0.5	0.63	0.02	0.39	0.19	0.02	0.39	0.19	0.02	0.39	7.9	548.9	
1983	187.4	346.7	29.2	12.0	2.1	97.1	97.2	54.8	0.0	0.6	0.75	0.02	0.49	0.21	0.02	0.49	0.21	0.02	0.49	8.0	549.1	
1984	196.0	363.9	32.5	12.4	2.4	98.2	101.7	58.8	0.0	0.7	0.88	0.02	0.61	0.24	0.02	0.61	0.24	0.02	0.61	8.1	549.3	
1985	205.4	381.2	37.3	12.9	2.8	99.6	106.1	62.7	0.0	0.7	1.04	0.02	0.74	0.26	0.02	0.74	0.26	0.02	0.74	8.2	549.4	
1986	215.8	399.3	42.0	13.4	3.1	100.8	110.0	66.9	0.0	0.8	1.22	0.02	0.89	0.29	0.02	0.89	0.29	0.02	0.89	8.2	549.5	
1987	227.0	419.2	47.4	14.0	3.5	102.5	112.3	71.5	0.0	0.8	1.44	0.02	1.06	0.32	0.02	1.06	0.32	0.02	1.06	8.3	549.6	
1988	238.0	438.4	54.4	14.5	3.9	103.6	118.0	76.7	0.0	0.9	1.69	0.03	1.25	0.35	0.03	1.25	0.35	0.03	1.25	8.4	549.7	
1989	247.7	459.6	61.3	15.0	4.3	104.9	122.5	82.5	0.0	1.0	1.98	0.03	1.46	0.38	0.03	1.46	0.38	0.03	1.46	8.5	549.8	
1990	256.2	477.5	67.6	15.4	4.7	106.5	127.2	88.2	0.0	1.2	2.27	0.03	1.66	0.41	0.03	1.66	0.41	0.03	1.66	8.6	549.8	
1991	262.2	491.0	73.8	15.7	5.1	106.3	130.0	93.7	0.0	1.8	2.54	0.03	1.84	0.44	0.03	1.84	0.44	0.03	1.84	8.7	549.9	
1992	265.2	500.7	78.7	15.8	5.6	105.3	131.4	99.1	0.1	2.8	2.79	0.03	1.97	0.46	0.03	1.97	0.46	0.03	1.97	8.9	549.9	
1993	267.8	510.1	81.6	15.9	6.0	104.7	130.1	103.9	0.3	3.9	3.02	0.04	2.20	0.49	0.04	2.20	0.49	0.04	2.20	9.0	549.9	
1994	267.8	517.1	83.0	16.0	6.4	104.0	121.5	109.2	1.2	5.1	3.20	0.04	2.48	0.51	0.04	2.48	0.51	0.04	2.48	9.1	549.9	
1995	267.4	523.8	83.6	16.1	6.8	103.2	110.3	113.6	2.7	6.3	3.34	0.04	2.63	0.52	0.04	2.63	0.52	0.04	2.63	9.2	550.0	
1996	266.8	528.9	83.7	16.2	7.1	102.5	97.8	119.4	4.5	7.3	3.50	0.05	2.60	0.51	0.05	2.60	0.51	0.05	2.60	9.1	550.0	
1997	266.0	533.5	83.6	16.3	7.4	101.3	83.4	124.2	6.4	8.4	3.66	0.05	2.67	0.51	0.05	2.67	0.51	0.05	2.67	9.1	550.0	
1998	264.5	536.4	83.3	16.4	7.6	100.5	70.6	128.7	8.2	9.3	3.80	0.05	2.70	0.51	0.05	2.70	0.51	0.05	2.70	9.2	550.0	
1999	263.3	539.0	82.9	16.4	7.7	99.8	59.3	134.7	10.1	10.3	3.92	0.05	2.73	0.51	0.05	2.73	0.51	0.05	2.73	9.3	550.0	
2000	261.7	541.0	82.3	16.5	7.9	98.6	49.7	139.5	11.8	11.4	4.02	0.04	2.84	0.50	0.04	2.84	0.50	0.04	2.84	8.9	550.0	
2001	260.1	542.8	81.8	16.5	8.0	97.7	41.6	144.7	13.5	12.4	4.11	0.04	2.85	0.50	0.04	2.85	0.50	0.04	2.85	8.5	550.0	
2002	258.3	543.4	81.1	16.5	8.0	96.6	34.6	150.9	14.8	13.2	4.17	0.03	2.87	0.50	0.03	2.87	0.50	0.03	2.87	8.2	550.0	
2003	255.9	543.5	80.3	16.5	8.1	95.6	28.9	155.4	16.1	13.9	4.22	0.03	2.88	0.49	0.03	2.88	0.49	0.03	2.88	8.2	550.0	
2004	253.9	543.4	79.6	16.5	8.2	94.7	24.1	160.3	17.0	14.5	4.25	0.02	2.95	0.49	0.02	2.95	0.49	0.02	2.95	8.0	550.0	

	CFC-11		CFC-113		CFC-115		CH ₃ CCl ₃		HCFC-22		HCFC-141b		Halon-1211		Halon-1301		CH ₃ Br	
	CFC-114	CFC-114	CFC-114	CCl ₄	CH ₃ CCl ₃	HCFC-22	HCFC-141b	HCFC-142b	Halon-1202	Halon-1301	Halon-2402	CH ₃ Cl						
2005	251.6	542.7	78.8	16.6	8.3	8.3	93.7	20.1	165.5	17.5	15.1	4.26	0.02	3.03	0.48	7.9	550.0	550.0
2006	249.4	541.8	78.2	16.5	8.3	8.3	92.7	16.7	172.2	17.8	15.8	4.27	0.01	3.06	0.48	7.7	550.0	550.0
2007	247.2	539.8	77.6	16.5	8.4	8.4	91.6	14.1	179.3	18.6	16.9	4.24	0.01	3.12	0.48	7.6	550.0	550.0
2008	245.1	537.7	76.8	16.5	8.4	8.4	90.4	11.7	187.3	19.0	18.2	4.19	0.01	3.15	0.47	7.5	550.0	550.0
2009	243.3	535.3	76.2	16.4	8.4	8.4	89.0	9.8	195.2	19.6	19.3	4.14	0.00	3.18	0.47	7.2	550.0	550.0
2010	240.9	532.5	75.6	16.4	8.4	8.4	87.6	8.3	206.8	20.3	20.5	4.07	0.00	3.20	0.46	7.2	550.0	550.0
2011	238.4	529.4	74.8	16.3	8.4	8.4	86.0	7.1	218.6	21.1	21.7	3.99	0.00	3.22	0.46	7.2	550.0	550.0
2012	235.8	525.9	74.0	16.3	8.4	8.4	84.5	6.1	230.9	22.1	22.9	3.91	0.00	3.24	0.45	7.2	550.0	550.0
2013	233.1	522.3	73.2	16.2	8.4	8.4	82.8	5.3	243.6	23.2	24.2	3.82	0.00	3.26	0.44	7.1	550.0	550.0
2014	230.4	518.4	72.3	16.2	8.4	8.4	81.2	4.6	255.7	24.4	25.4	3.72	0.00	3.27	0.44	7.1	550.0	550.0
2015	227.6	514.4	71.5	16.1	8.4	8.4	79.5	4.1	267.1	25.6	26.6	3.62	0.00	3.28	0.43	7.1	550.0	550.0
2020	213.0	492.8	67.4	15.8	8.4	8.4	70.9	1.5	301.8	30.9	30.9	3.08	0.00	3.29	0.38	7.1	550.0	550.0
2025	197.8	470.3	63.6	15.5	8.4	8.4	62.4	0.5	299.8	34.1	32.4	2.55	0.00	3.26	0.32	7.1	550.0	550.0
2030	182.6	448.0	59.9	15.1	8.4	8.4	54.4	0.2	265.4	34.4	31.2	2.06	0.00	3.19	0.27	7.1	550.0	550.0
2035	167.7	426.5	56.5	14.7	8.4	8.4	47.0	0.1	208.0	31.9	27.8	1.65	0.00	3.09	0.22	7.1	550.0	550.0
2040	153.5	405.8	53.3	14.4	8.4	8.4	40.3	0.0	151.0	27.9	23.3	1.30	0.00	2.97	0.18	7.1	550.0	550.0
2045	139.9	386.1	50.2	14.0	8.4	8.4	34.4	0.0	105.0	23.5	18.9	1.01	0.00	2.85	0.15	7.1	550.0	550.0
2050	127.2	367.3	47.4	13.6	8.4	8.4	29.2	0.0	71.1	19.3	14.9	0.78	0.00	2.71	0.12	7.1	550.0	550.0
2055	115.4	349.4	44.7	13.3	8.4	8.4	24.2	0.0	47.5	15.6	11.6	0.60	0.00	2.57	0.09	7.1	550.0	550.0
2060	104.4	332.4	42.1	12.9	8.3	8.3	20.0	0.0	31.5	12.4	9.0	0.46	0.00	2.43	0.07	7.1	550.0	550.0
2065	94.4	316.2	39.7	12.6	8.3	8.3	16.5	0.0	20.8	9.8	6.8	0.35	0.00	2.29	0.06	7.1	550.0	550.0
2070	85.2	300.7	37.4	12.3	8.3	8.3	13.6	0.0	13.7	7.7	5.2	0.26	0.00	2.16	0.05	7.1	550.0	550.0
2075	76.8	286.1	35.3	12.0	8.3	8.3	11.2	0.0	9.0	6.1	3.9	0.20	0.00	2.02	0.04	7.1	550.0	550.0
2080	69.1	272.1	33.3	11.6	8.2	8.2	9.3	0.0	5.9	4.7	3.0	0.15	0.00	1.90	0.03	7.1	550.0	550.0
2085	62.2	258.8	31.4	11.3	8.2	8.2	7.6	0.0	3.9	3.7	2.2	0.11	0.00	1.77	0.02	7.1	550.0	550.0
2090	55.9	246.2	29.6	11.1	8.2	8.2	6.3	0.0	2.6	2.9	1.7	0.08	0.00	1.66	0.02	7.1	550.0	550.0
2095	50.2	234.2	27.9	10.8	8.2	8.2	5.2	0.0	1.7	2.2	1.3	0.06	0.00	1.55	0.01	7.1	550.0	550.0
2100	45.1	222.8	26.3	10.5	8.1	8.1	4.3	0.0	1.1	1.7	0.9	0.05	0.00	1.44	0.01	7.1	550.0	550.0

¹Note: Areas are shaded for compounds in years when mixing ratio values are forced to equal global estimates inferred from observations. The pre-1995 global mixing ratio trend for CH₃Br was derived from SH firm data by including a time-varying hemispheric ratio that increased linearly from 1.0 in 1940 to 1.3 in 1995 (see Section 1.2.1.6 of Chapter 1). This is based on the concurrent decline in the measured hemispheric difference and industrially averaged emissions since 1998, and suggests a mean hemispheric mixing ratio difference close to 0 ppt for CH₃Br in preindustrial times. Previously, a constant hemispheric ratio had been used. CH₃Cl mixing ratios before 1995 were also derived from South Pole firm data (Butler et al., 1999). From 1995 onward, global means of CH₃Br are based on surface observations, while global means of CH₃Cl are held constant (Chapter 1). All other shaded areas are from atmospheric observations from one or more measurement networks (Chapter 1).

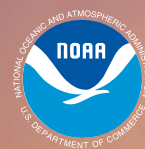
Table 5A-4. Halocarbon indirect GWPs from ozone depletion using the EESC-based method described in Daniel et al. (1995). Values have been updated for the new scenarios and fractional release values. Indirect forcing from ozone depletion is also now assumed to continue even after EESC drops below the 1980 level, consistent with our understanding that this level does not represent a threshold value for ozone depletion. Uncertainties in direct GWPs represent 35% of the direct value; uncertainties in the indirect GWPs reflect the uncertainty in stratospheric ozone radiative forcing quoted in IPCC (-0.05 ± 0.10 W/m²) even though that forcing is not attributed to only halocarbons.

Gas	Direct GWP			Indirect GWP		
CFC-11	4,750	±	1,660	-1,630	±	3,250
CFC-12	10,900	±	3,810	-1,270	±	2,540
CFC-113	6,130	±	2,150	-1,310	±	2,630
CFC-114	9,180	±	3,210	-562	±	1,120
CFC-115	7,230	±	2,530	-137	±	275
HCFC-22	1,790	±	630	-58	±	116
HCFC-123	77	±	27	-25	±	50
HCFC-124	619	±	217	-30	±	60
HCFC-141b	717	±	252	-158	±	316
HCFC-142b	2,220	±	780	-97	±	193
HCFC-225ca	122	±	42	-27	±	54
HCFC-225cb	606	±	214	-39	±	78
CH ₃ CCl ₃	146	±	53	-212	±	424
CCl ₄	1,400	±	490	-1,300	±	2,600
CH ₃ Br	5	±	2	-851	±	1,700
Halon-1211	1,890	±	660	-11,720	±	23,430
Halon-1301	7,140	±	2,500	-27,060	±	54,130
Halon-2402	1,640	±	570	-19,780	±	39,570



Twenty Questions and Answers About the Ozone Layer: 2010 Update

*Scientific Assessment of
Ozone Depletion: 2010*



World Meteorological Organization
United Nations Environment Programme
National Oceanic and Atmospheric Administration
National Aeronautics and Space Administration
European Commission

TWENTY QUESTIONS AND ANSWERS ABOUT THE OZONE LAYER: 2010 UPDATE

Coordinating Lead Authors:

David W. Fahey
Michaela I. Hegglin

The update of this component of the Assessment was discussed by the 74 scientists who attended the Panel Review Meeting for the 2010 Ozone Assessment (Les Diablerets, Switzerland, 28 June–2 July 2010). In addition, subsequent contributions, reviews, or comments were provided by the following individuals: Ross J. Salawitch (Special Recognition), Stephen A. Montzka (Special Recognition), Stephen O. Andersen (Special Recognition), Pieter J. Aucamp, Alkiviadis F. Bais, Peter F. Bernath, Gregory E. Bodeker, Janet F. Bornman, Geir O. Braathen, Peter Braesicke, Irene Cionni, Martin Dameris, John S. Daniel, Susana B. Diaz, Ellsworth G. Dutton, James W. Elkins, Christine A. Ennis, Veronika Eyring, Vitali E. Fioletov, Marvin A. Geller, Sophie Godin-Beekmann, Malcolm K.W. Ko, Kirstin Krüger, Lambert Kuijpers, Michael J. Kurylo, Igor Larin, Gloria L. Manney, C. Thomas McElroy, Rolf Müller, Eric R. Nash, Paul A. Newman, Samuel J. Oltmans, Nigel D. Paul, Judith Perlwitz, Jean-Pierre Pommereau, Claire E. Reeves, Stefan Reimann, Alan Robock, Michelle L. Santee, Dian J. Seidel, Theodore G. Shepherd, Peter Simmonds, Anne K. Smith, Richard S. Stolarski, Matthew B. Tully, Guus J.M. Velders, Elizabeth C. Weatherhead, Ann R. Webb, Ray F. Weiss, and Durwood Zaelke.

Twenty Questions and Answers About the Ozone Layer: 2010 Update

Contents

INTRODUCTION	Q.1
Section I: OZONE IN OUR ATMOSPHERE	
Q1: What is ozone and where is it in the atmosphere?	Q.4
Q2: How is ozone formed in the atmosphere?	Q.6
Q3: Why do we care about atmospheric ozone?	Q.8
Q4: How is total ozone distributed over the globe?	Q.10
Q5: How is ozone measured in the atmosphere?	Q.12
Section II: THE OZONE DEPLETION PROCESS	
Q6: What are the principal steps in stratospheric ozone depletion caused by human activities?	Q.14
Q7: What emissions from human activities lead to ozone depletion?	Q.16
Q8: What are the reactive halogen gases that destroy stratospheric ozone?	Q.20
Q9: What are the chlorine and bromine reactions that destroy stratospheric ozone?	Q.24
Q10: Why has an “ozone hole” appeared over Antarctica when ozone-depleting substances are present throughout the stratosphere?	Q.27
Section III: STRATOSPHERIC OZONE DEPLETION	
Q11: How severe is the depletion of the Antarctic ozone layer?	Q.31
Q12: Is there depletion of the Arctic ozone layer?	Q.36
Q13: How large is the depletion of the global ozone layer?	Q.40
Q14: Do changes in the Sun and volcanic eruptions affect the ozone layer?	Q.42
Section IV: CONTROLLING OZONE-DEPLETING SUBSTANCES	
Q15: Are there controls on the production of ozone-depleting substances?	Q.45
Q16: Has the Montreal Protocol been successful in reducing ozone-depleting substances in the atmosphere?	Q.48
Section V: IMPLICATIONS OF OZONE DEPLETION AND THE MONTREAL PROTOCOL	
Q17: Does depletion of the ozone layer increase ground-level ultraviolet radiation?	Q.52
Q18: Is depletion of the ozone layer the principal cause of climate change?	Q.55
Q19: Have reductions of ozone-depleting substances under the Montreal Protocol also protected Earth’s climate?	Q.60
Section VI: STRATOSPHERIC OZONE IN THE FUTURE	
Q20: How is ozone expected to change in the coming decades?	Q.64
Additional Topics	
• Global Ozone Network	Q.13
• Understanding Stratospheric Ozone Depletion	Q.15
• Heavier-Than-Air CFCs	Q.19
• Replacing Lost Ozone in the Stratosphere	Q.26
• The Discovery of the Antarctic Ozone Hole	Q.30
• The 2002 Antarctic Ozone Hole	Q.35

INTRODUCTION

Ozone is present only in small amounts in Earth's atmosphere. Nevertheless, it is vital to human well-being and ecosystem health.

Most ozone resides in the upper part of the atmosphere. This region, called the stratosphere, is more than 10 kilometers (6 miles) above Earth's surface. There, about 90% of atmospheric ozone is contained in the "ozone layer," which shields us from harmful ultraviolet radiation from the Sun.

It was discovered in the mid-1970s that some human-produced chemicals could lead to depletion of the ozone layer. The resulting increase in ultraviolet radiation at Earth's surface would likely increase the incidences of skin cancer and eye cataracts, and also adversely affect plants, crops, and ocean plankton.

Following the discovery of this environmental issue, researchers sought a better understanding of this threat to the ozone layer. Monitoring stations showed that the abundances of the ozone-depleting substances (ODSs) were steadily increasing in the atmosphere. These trends were linked to growing production and use of chemicals like chlorofluorocarbons (CFCs) for refrigeration and air conditioning, foam blowing, and industrial cleaning. Measurements in the laboratory and in the atmosphere characterized the chemical reactions that were involved in ozone destruction. Computer models of the atmosphere employing this information were used to predict how much ozone depletion was occurring and how much more might occur in the future.

Observations of the ozone layer showed that depletion was indeed occurring. The most severe and most surprising ozone loss was discovered to be recurring in springtime over Antarctica. The loss in this region is commonly called the "ozone hole" because the ozone depletion is so large and localized. A thinning of the ozone layer also has been observed over other regions of the globe, such as the Arctic and northern and southern midlatitudes.

The work of many scientists throughout the world has provided a basis for building a broad and solid scientific understanding of the ozone depletion process. With this understanding, we know that ozone depletion is indeed occurring and why. Most important, we know that if the most potent ODSs were to continue to be emitted and increase in the atmosphere, the result would be more depletion of the ozone layer.

In response to the prospect of increasing ozone depletion,

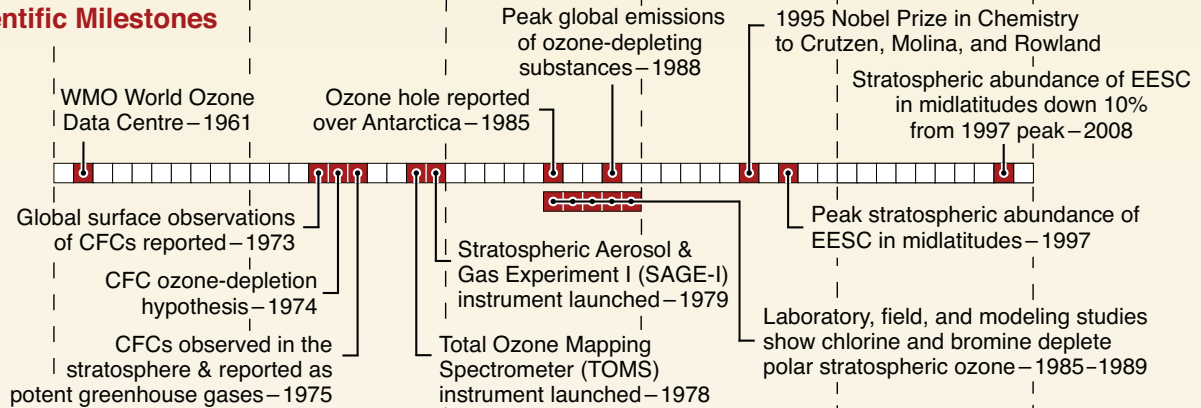
the governments of the world crafted the 1987 United Nations Montreal Protocol as an international means to address this global issue. As a result of the broad compliance with the Protocol and its Amendments and Adjustments and, of great significance, industry's development of "ozone-friendly" substitutes for the now-controlled chemicals, the total global accumulation of ODSs has slowed and begun to decrease. In response, global ozone depletion is no longer increasing. Now, with continued compliance, we expect substantial recovery of the ozone layer by the late 21st century. The day the Montreal Protocol was agreed upon, 16 September, is now celebrated as the International Day for the Preservation of the Ozone Layer.

This is a story of notable achievements: discovery, understanding, decisions, actions, and verification. It is a story written by many: scientists, technologists, economists, legal experts, and policymakers, in which continuous dialogue has been a key ingredient. A timeline of milestones associated with stratospheric ozone depletion is illustrated in Figure Q0-1. The milestones relate to stratospheric ozone science, international scientific assessments, and the Montreal Protocol.

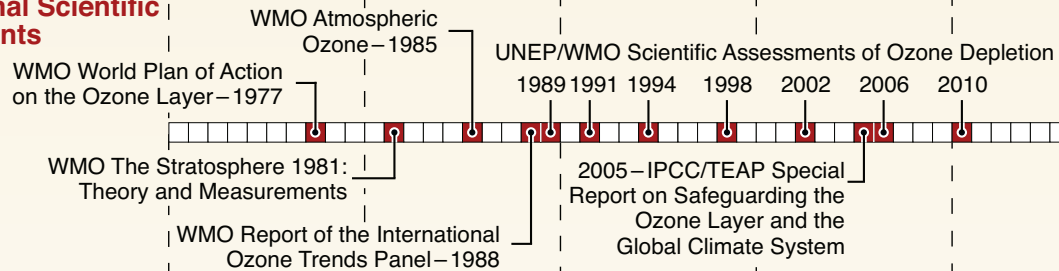
To help maintain a broad understanding of the relationship between ozone depletion, ODSs, and the Montreal Protocol, this component of the *Scientific Assessment of Ozone Depletion: 2010* presents 20 questions and answers about the often-complex science of ozone depletion. Most questions and answers are updates of those presented in previous Ozone Assessments, while others have been added or expanded to address newly emerging issues. The questions address the nature of atmospheric ozone, the chemicals that cause ozone depletion, how global and polar ozone depletion occur, the success of the Montreal Protocol, and what could lie ahead for the ozone layer. Computer models project that the influence on global ozone of greenhouse gases and changes in climate will grow significantly in the coming decades and exceed the importance of ODSs in most atmospheric regions by the end of this century. Ozone and climate are indirectly linked because both ODSs and their substitutes contribute to climate change. A brief answer to each question is first given in italics; an expanded answer then follows. The answers are based on the information presented in the 2010 and earlier Assessment reports as well as other international scientific assessments. These reports and the answers provided here were prepared and reviewed by a large international group of scientists¹.

Milestones in the History of Stratospheric Ozone Depletion

Scientific Milestones



International Scientific Assessments



Montreal Protocol Milestones

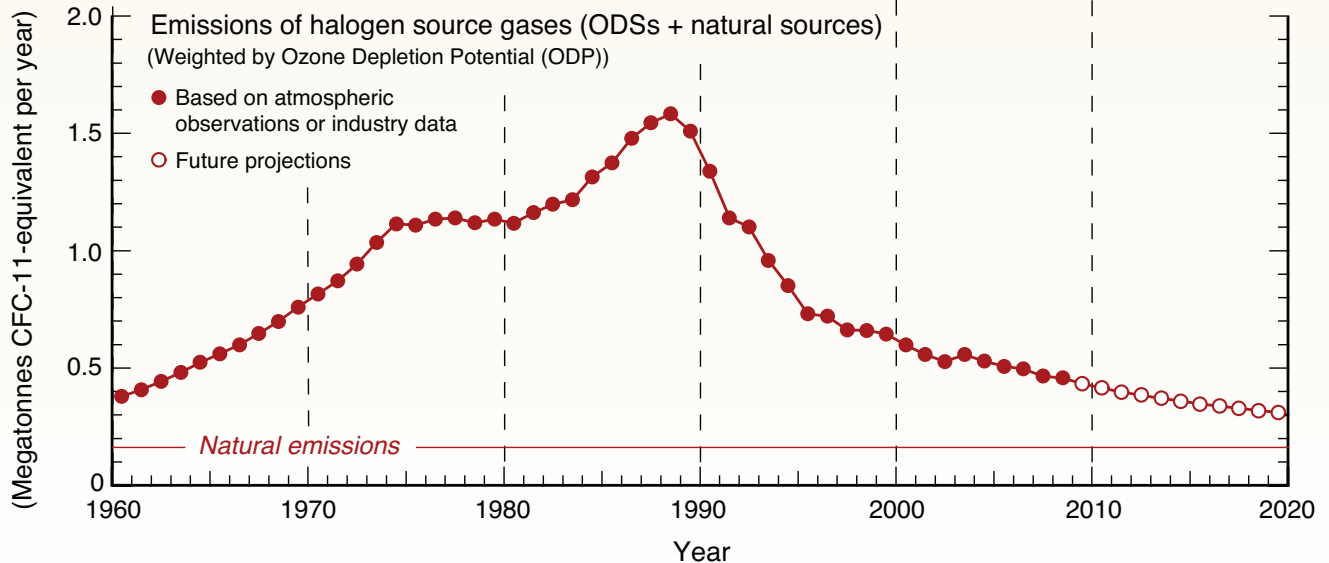
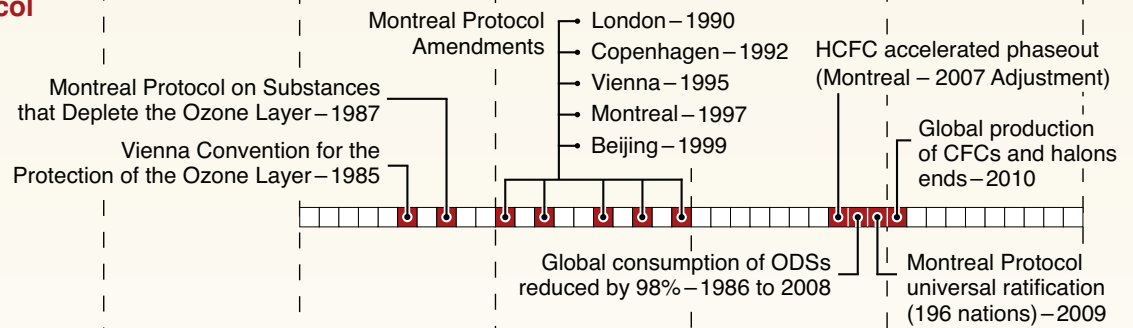


Figure Q0-1. Stratospheric ozone depletion milestones. This timeline highlights milestones related to the history of ozone depletion. Events represent the occurrence of important scientific findings, the completion of international scientific assessments, and highlights of the Montreal Protocol. The graph shows the history and near future of annual total emissions of ozone-depleting substances (ODSs) combined with natural emissions of halogen source gases. ODSs are halogen source gases controlled under the Montreal Protocol. The emissions, when weighted by their potential to destroy ozone, peaked near 1990 after several decades of steady increases (see Q19). Between 1990 and the present, emissions have decreased substantially as a result of the Montreal Protocol and its subsequent Amendments and Adjustments coming into force (see Q15). The Protocol began with the Vienna Convention for the Protection of the Ozone Layer in 1985. The provisions of the Protocol and its Amendments and Adjustments decisions have depended on information embodied in international scientific assessments of ozone depletion that have been produced periodically since 1989 under the auspices of UNEP and WMO. Atmospheric observations of ozone, CFCs, and other ODSs have increased substantially since the early 1970s. For example, the SAGE and TOMS satellite instruments have provided essential global views of stratospheric ozone for several decades. The Nobel Prize in Chemistry in 1995 was awarded for research that identified the threat to ozone posed by CFCs and that described key reactive processes in the stratosphere. By 2008, stratospheric chlorine abundances in the stratosphere were 10% lower than their peak values reached in the late 1990s and were continuing to decrease. January 2010 marked the end of global production of CFCs and halons under the Protocol. (A megatonne = 1 billion (10^9) kilograms.)

EESC: Equivalent effective stratospheric chlorine

ODS: Ozone-depleting substance

WMO: World Meteorological Organization

IPCC: Intergovernmental Panel on Climate Change

TEAP: Technology and Economic Assessment Panel
of the Montreal Protocol

UNEP: United Nations Environment Programme

¹ The update of this component of the Assessment was discussed by the 74 scientists who attended the Panel Review Meeting for the 2010 Ozone Assessment (Les Diablerets, Switzerland, 28 June–2 July 2010). In addition, subsequent contributions, reviews, or comments were provided by the following individuals: Ross J. Salawitch (Special Recognition), Stephen A. Montzka (Special Recognition), Stephen O. Andersen (Special Recognition), Pieter J. Aucamp, Alkiviadis F. Bais, Peter F. Bernath, Gregory E. Bodeker, Janet F. Bornman, Geir O. Braathen, Peter Braesicke, Irene Cionni, Martin Dameris, John S. Daniel, Susana B. Diaz, Ellsworth G. Dutton, James W. Elkins, Christine A. Ennis, Veronika Eyring, Vitali E. Fioletov, Marvin A. Geller, Sophie Godin-Beekmann, Malcolm K.W. Ko, Kirstin Krüger, Lambert Kuijpers, Michael J. Kurylo, Igor Larin, Gloria L. Manney, C. Thomas McElroy, Rolf Müller, Eric R. Nash, Paul A. Newman, Samuel J. Oltmans, Nigel D. Paul, Judith Perlwitz, Jean-Pierre Pommereau, Claire E. Reeves, Stefan Reimann, Alan Robock, Michelle L. Santee, Dian J. Seidel, Theodore G. Shepherd, Peter Simmonds, Anne K. Smith, Richard S. Stolarski, Matthew B. Tully, Guus J.M. Velders, Elizabeth C. Weatherhead, Ann R. Webb, Ray F. Weiss, and Durwood Zaelke.

Q1

What is ozone and where is it in the atmosphere?

Ozone is a gas that is naturally present in our atmosphere. Each ozone molecule contains three atoms of oxygen and is denoted chemically as O₃. Ozone is found primarily in two regions of the atmosphere. About 10% of atmospheric ozone is in the troposphere, the region closest to Earth (from the surface to about 10–16 kilometers (6–10 miles)). The remaining ozone (about 90%) resides in the stratosphere between the top of the troposphere and about 50 kilometers (31 miles) altitude. The large amount of ozone in the stratosphere is often referred to as the “ozone layer.”

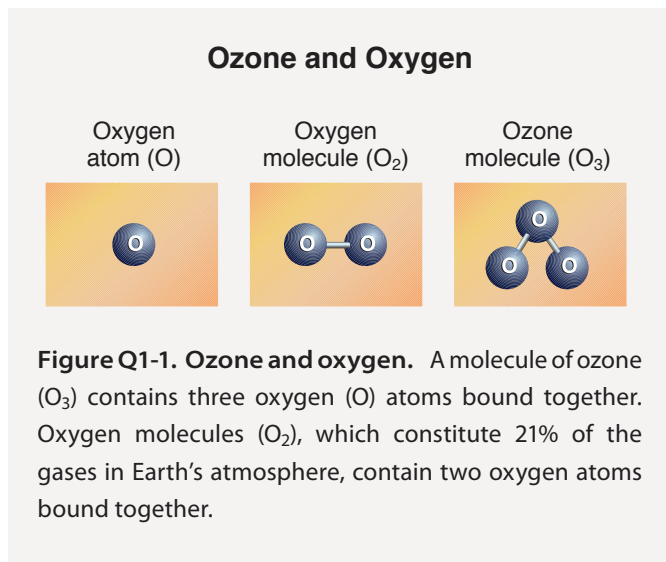
Ozone is a gas that is naturally present in our atmosphere. Ozone has the chemical formula O₃ because an ozone molecule contains three oxygen atoms (see Figure Q1-1). Ozone was discovered in laboratory experiments in the mid-1800s. Ozone’s presence in the atmosphere was later discovered using chemical and optical measurement methods. The word ozone is derived from the Greek word *ὄζειν* (*ozein*), meaning “to smell.” Ozone has a pungent odor that allows it to be detected even at very low amounts. Ozone reacts rapidly with many chemical compounds and is explosive in concentrated amounts. Electrical discharges are generally used to produce ozone for industrial processes such as air and water purification and bleaching of textiles and food products.

Ozone location. Most ozone (about 90%) is found in the stratosphere, which begins about 10–16 kilometers (6–10 miles) above Earth’s surface and extends up to about 50 kilometers (31 miles) altitude. The stratospheric region with the highest ozone concentration is commonly known as the “ozone layer” (see Figure Q1-2). The ozone layer extends over the entire globe with some variation in altitude and thickness. The remaining ozone, about 10%, is found in the troposphere, which is the lowest region of the atmosphere, between Earth’s surface and the stratosphere.

Ozone abundance. Ozone molecules have a low relative abundance in the atmosphere. In the stratosphere near the peak concentration of the ozone layer, there are typically a few thousand ozone molecules for every *billion* air molecules (1 billion = 1,000 million). Most air molecules are either oxygen (O₂) or nitrogen (N₂) molecules. In the troposphere near

Earth’s surface, ozone is even less abundant, with a typical range of 20 to 100 ozone molecules for each billion air molecules. The highest surface values result when ozone is formed in air polluted by human activities.

As an illustration of the low relative abundance of ozone in our atmosphere, one can imagine bringing all the ozone molecules in the troposphere and stratosphere down to Earth’s surface and uniformly distributing these molecules into a layer of gas extending over the globe. The resulting layer of pure ozone would have an average thickness of about three millimeters (about one-tenth inch) (see Q4). Nonetheless, this extremely small fraction of the atmosphere plays a vital role in protecting life on Earth (see Q3).



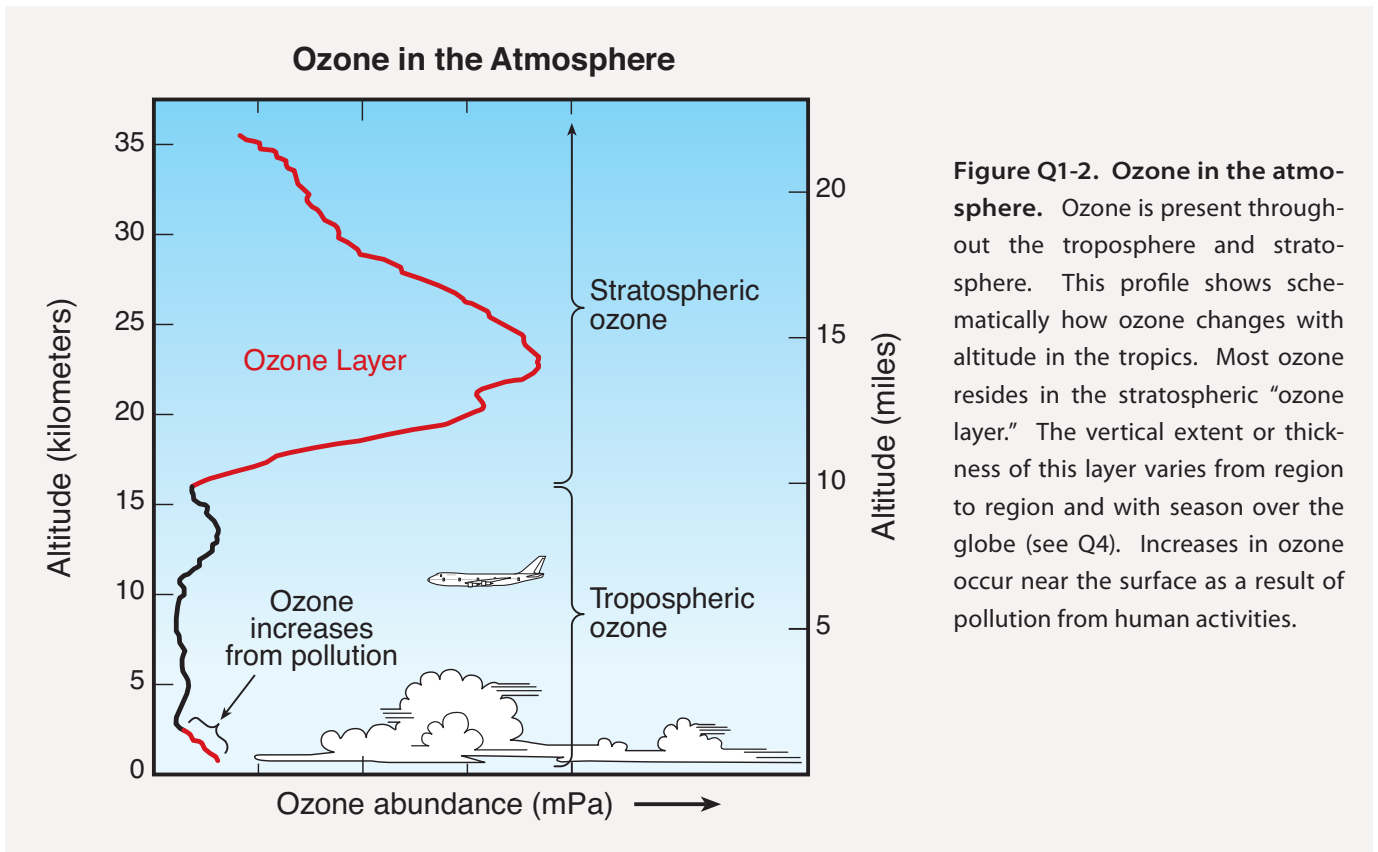


Figure Q1-2. Ozone in the atmosphere. Ozone is present throughout the troposphere and stratosphere. This profile shows schematically how ozone changes with altitude in the tropics. Most ozone resides in the stratospheric “ozone layer.” The vertical extent or thickness of this layer varies from region to region and with season over the globe (see Q4). Increases in ozone occur near the surface as a result of pollution from human activities.

Q2

How is ozone formed in the atmosphere?

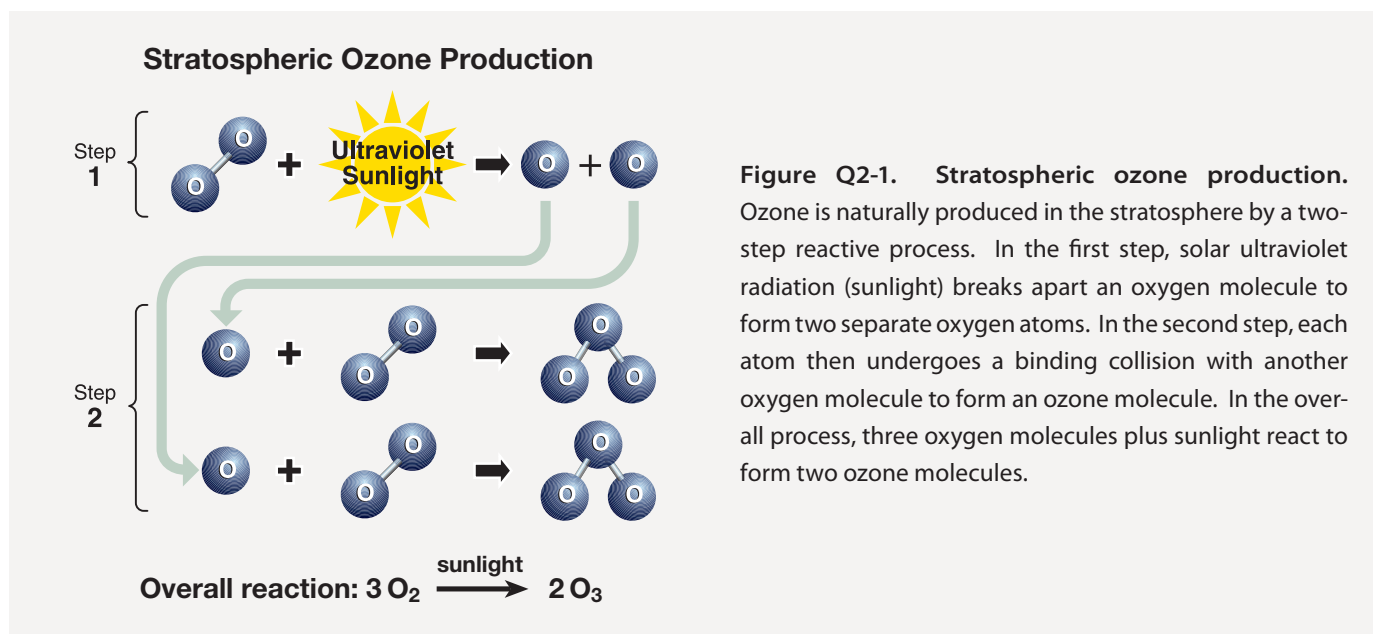
Ozone is formed throughout the atmosphere in multistep chemical processes that require sunlight. In the stratosphere, the process begins with an oxygen molecule (O_2) being broken apart by ultraviolet radiation from the Sun. In the lower atmosphere (troposphere), ozone is formed by a different set of chemical reactions that involve naturally occurring gases and those from pollution sources.

Stratospheric ozone. Stratospheric ozone is formed naturally by chemical reactions involving solar ultraviolet radiation (sunlight) and oxygen molecules, which make up 21% of the atmosphere. In the first step, solar ultraviolet radiation breaks apart one oxygen molecule (O_2) to produce two oxygen atoms (2 O) (see Figure Q2-1). In the second step, each of these highly reactive atoms combines with an oxygen molecule to produce an ozone molecule (O_3). These reactions occur continually whenever solar ultraviolet radiation is present in the stratosphere. As a result, the largest ozone production occurs in the tropical stratosphere.

The production of stratospheric ozone is balanced by its destruction in chemical reactions. Ozone reacts continually with sunlight and a wide variety of natural and human-produced chemicals in the stratosphere. In each reaction, an ozone molecule is lost and other chemical compounds are produced. Important reactive gases that destroy ozone are hydrogen and nitrogen oxides and those containing chlorine and bromine (see Q8).

Some stratospheric ozone is regularly transported down into the troposphere and can occasionally influence ozone amounts at Earth's surface, particularly in remote, unpolluted regions of the globe.

Tropospheric ozone. Near Earth's surface, ozone is produced by chemical reactions involving naturally occurring gases and gases from pollution sources. Ozone production reactions primarily involve hydrocarbon and nitrogen oxide gases, as well as ozone itself, and all require sunlight for completion. Fossil fuel combustion is a primary source of pollutant gases that lead to tropospheric ozone production. The production of ozone near the surface does not significantly contribute to the abundance of stratospheric ozone. The amount of surface ozone is too small in comparison and the transport of surface air to the stratosphere is not effective enough. As in the stratosphere, ozone in the troposphere is destroyed by naturally occurring chemical reactions and by reactions involving human-produced chemicals. Tropospheric ozone can also be destroyed when ozone reacts with a



variety of surfaces, such as those of soils and plants.

Balance of chemical processes. Ozone abundances in the stratosphere and troposphere are determined by the *balance* between chemical processes that produce and destroy ozone. The balance is determined by the amounts of reactive gases and how the rate or effectiveness of the various reactions varies with sunlight intensity, location in the atmosphere, temperature, and other factors. As atmospheric conditions change to favor ozone-producing reactions in a certain loca-

tion, ozone abundances increase. Similarly, if conditions change to favor other reactions that destroy ozone, abundances decrease. The balance of production and loss reactions combined with atmospheric air motions determines the global distribution of ozone on timescales of days to many months. Global ozone has decreased during the past several decades because the amounts of reactive gases containing chlorine and bromine have increased in the stratosphere (see Q13) due to human activities.

Q3

Why do we care about atmospheric ozone?

Ozone in the stratosphere absorbs a large part of the Sun's biologically harmful ultraviolet radiation. Stratospheric ozone is considered "good" ozone because of this beneficial role. In contrast, ozone formed at Earth's surface in excess of natural amounts is considered "bad" ozone because it is harmful to humans, plants, and animals. Natural ozone near the surface and in the lower atmosphere plays an important beneficial role in chemically removing pollutants from the atmosphere.

Good ozone. Stratospheric ozone is considered good for humans and other life forms because it absorbs ultraviolet-B (UV-B) radiation from the Sun (see Figure Q3-1). If not absorbed, UV-B radiation would reach Earth's surface in amounts that are harmful to a variety of life forms. In humans, increased exposure to UV-B radiation increases the risks of skin cancer, cataracts, and a suppressed immune system. UV-B radiation exposure before adulthood and cumulative exposure are both important health risk factors. Excessive UV-B exposure also can damage terrestrial plant life, single-cell organisms, and aquatic ecosystems. Other UV radiation, UV-A, which is not absorbed significantly by ozone, causes premature aging of the skin.

Protecting good ozone. In the mid-1970s, it was discovered that gases containing chlorine and bromine atoms

released by human activities could cause stratospheric ozone depletion (see Q6). These gases, referred to as halogen source gases, and as ozone-depleting substances (ODSs), chemically release their chlorine and bromine atoms after they reach the stratosphere. Ozone depletion increases surface UV-B radiation above naturally occurring amounts. International efforts have been successful in protecting the ozone layer through controls on ODS production and consumption (see Q15 and Q16).

Bad ozone. Ozone near Earth's surface in excess of natural amounts is considered bad ozone. It is formed by reactions involving human-made pollutant gases. Increasing surface ozone above natural levels is harmful to humans, plants, and other living systems because ozone reacts strongly to destroy or alter many biological molecules. High ozone exposure reduces crop yields and forest growth. In humans, expo-

UV Protection by the Ozone Layer

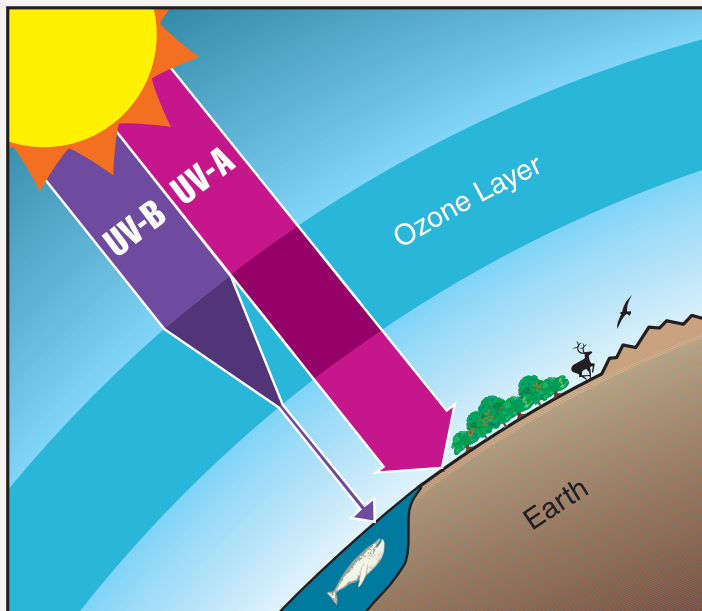


Figure Q3-1. UV protection by the ozone layer. The ozone layer resides in the stratosphere and surrounds the entire Earth. UV-B radiation (280- to 315-nanometer (nm) wavelength) from the Sun is strongly absorbed in this layer. As a result, the amount of UV-B reaching Earth's surface is greatly reduced. UV-A (315- to 400-nm wavelength), visible light, and other solar radiation are not strongly absorbed by the ozone layer. Human exposure to UV-B radiation increases the risks of skin cancer, cataracts, and a suppressed immune system. UV-B radiation exposure can also damage terrestrial plant life, single-cell organisms, and aquatic ecosystems.

sure to high levels of ozone can reduce lung capacity; cause chest pains, throat irritation, and coughing; and worsen pre-existing health conditions related to the heart and lungs. In addition, increases in tropospheric ozone lead to a warming of Earth's surface because ozone is a greenhouse gas (see Q18). The negative effects of excess tropospheric ozone contrast sharply with the protection from harmful UV-B radiation afforded by an abundance of stratospheric ozone.

Reducing bad ozone. Limiting the emission of certain common pollutants reduces the production of excess ozone in the air surrounding humans, plants, and animals. Natural emissions from the biosphere, mainly from trees, also participate in reactions that produce ozone. Major sources of pollutants include large cities where fossil fuel consumption and industrial activities are greatest. Many programs around the globe have already been successful in reducing or limiting the

emission of pollutants that cause production of excess ozone near Earth's surface.

Natural ozone. In the absence of human activities, ozone would still be present near Earth's surface and throughout the troposphere and stratosphere because ozone is a natural component of the clean atmosphere. Ozone plays important roles in the atmosphere beyond absorbing UV radiation. For example, ozone initiates the chemical removal of many pollutants, such as carbon monoxide (CO) and nitrogen oxides (NO_x), as well as some greenhouse gases, such as methane (CH₄). In addition, the absorption of UV-B radiation by ozone is a natural source of heat in the stratosphere, causing temperatures to increase with altitude. Stratospheric temperatures affect the balance of ozone production and destruction processes (see Q2) and air motions that redistribute ozone throughout the stratosphere.

Q4

How is total ozone distributed over the globe?

The distribution of total ozone over the Earth varies with location on timescales that range from daily to seasonal. The variations are caused by large-scale movements of stratospheric air and the chemical production and destruction of ozone. Total ozone is generally lowest at the equator and highest in polar regions.

Total ozone. Total ozone at any location on the globe is defined as the sum of all the ozone in the atmosphere directly above that location. Most ozone resides in the stratospheric ozone layer and a small percentage (about 10%) is distributed throughout the troposphere (see Q1). Total ozone values are often reported in *Dobson units* denoted as “DU.” Typical values vary between 200 and 500 DU over the globe (see Figure Q4-1). The ozone molecules required for total ozone to be 500 DU around the globe, for example, could also form a layer of pure ozone gas at Earth’s surface having a thickness of only 5 millimeters (0.2 inches) (see Q1).

Global distribution. Total ozone varies strongly with latitude over the globe, with the largest values occurring at middle and high latitudes during all seasons (see Figure Q4-1). This is the result of ozone production rates from solar ultraviolet radiation that are highest on average in the tropics, and the large-scale air circulation in the stratosphere that slowly transports tropical ozone toward the poles. Ozone accumulates at middle and high latitudes, increasing the thickness (or vertical extent) of the ozone layer and, at the same time, total ozone. In contrast, the values of total ozone are the lowest in the tropics in all seasons (except in the ozone hole) because the *thickness* of the ozone layer is smallest there.

Seasonal distribution. Total ozone also varies with season, as is shown in Figure Q4-1 using two-week averages of ozone taken from 2009 satellite observations. March and September plots represent the early spring and fall seasons in the Northern and Southern Hemispheres. June and December plots similarly represent the early summer and winter seasons. Total ozone shows a maximum at high latitudes during spring as a result of increased transport of ozone from its source region in the tropics toward the polar regions during late fall and winter. This ozone transport is much weaker during the summer and early fall periods and is weaker overall in the Southern Hemisphere. An important feature of seasonal ozone changes is the natural chemical destruction that occurs when daylight is continuous in the summer polar stratosphere, which causes total ozone to decrease gradually

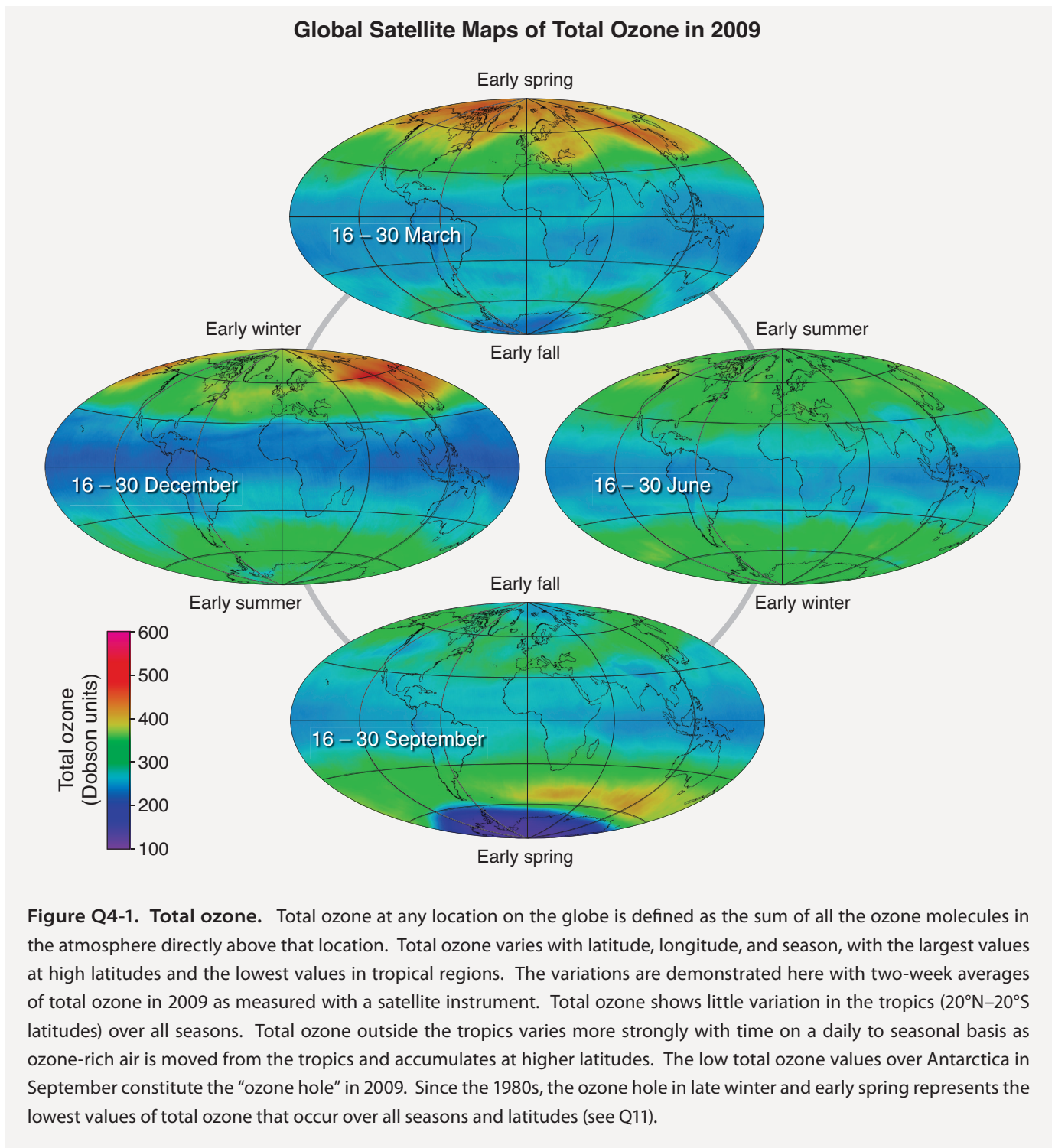
toward its lowest values in early fall.

This natural seasonal cycle can be observed clearly in the Northern Hemisphere as shown in Figure Q4-1, with increasing values in Arctic total ozone during winter, a clear maximum in spring, and decreasing values from summer to fall. In the Antarctic, however, a pronounced minimum in total ozone is observed during spring. The minimum is a consequence of the “ozone hole,” which describes the widespread chemical destruction of ozone by ozone-depleting substances (see Q6 and Q11) in spring. In the late 1970s, before the ozone hole appeared each year, much higher ozone values were found in Antarctic spring (see Q11). Now, the lowest values of total ozone across the globe and all seasons are found every spring in the Antarctic as shown in Figure Q4-1. After spring, these low values disappear from total ozone maps as polar air mixes with lower-latitude air containing much higher ozone values.

In the tropics, the total ozone changes through the spring-summer-fall-winter progression of the seasons are much smaller than in the polar regions. This is because seasonal changes in both sunlight and ozone transport are smaller in the tropics than in the polar regions.

Natural variations. Total ozone varies strongly with latitude and longitude within the seasonal plots in Figure Q4-1. These patterns, which change on daily to weekly timescales, come about for two reasons. First, natural air motions mix and blend air between regions of the stratosphere that have high ozone values and those that have low ozone values. Tropospheric weather systems can temporarily change the thickness of the ozone layer in a region, and thereby change total ozone. The geographical variation in these air motions in turn causes variations in the distribution of total ozone.

Second, ozone variations occur as a result of changes in the balance of chemical production and loss processes as air moves to and from different locations over the globe. This balance, for example, is very sensitive to the amount of sunlight in a region.



There is a good understanding of how chemistry and air motions work together to cause the observed large-scale features in total ozone, such as those seen in Figure Q4-1. Ozone changes are routinely monitored by a large group of investiga-

tors using satellite, airborne, and ground-based instruments. The continued analysis of these observations provides an important basis to quantify the contribution of human activities to ozone depletion.

Q5

How is ozone measured in the atmosphere?

The amount of ozone in the atmosphere is measured by instruments on the ground and carried aloft on balloons, aircraft, and satellites. Some instruments measure ozone locally by continuously drawing air samples into a small detection chamber. Other instruments measure ozone remotely over long distances by using ozone's unique optical absorption or emission properties.

The abundance of ozone in the atmosphere is measured by a variety of techniques (see Figure Q5-1). The techniques make use of ozone's unique optical and chemical properties. There are two principal categories of measurement techniques: *local* and *remote*. Ozone measurements by these techniques have been essential in monitoring changes in the ozone layer and in developing our understanding of the processes that control ozone abundances.

Local measurements. Local measurements of atmospheric ozone abundance are those that require air to be drawn directly into an instrument. Once inside an instrument's detection chamber, ozone is measured by its absorption of ultraviolet (UV) light or by the electrical current or light produced in a chemical reaction involving ozone. The last approach is used in the construction of "ozonesondes," which are lightweight, ozone-measuring modules suitable for launching on small balloons. The balloons ascend far enough in the atmosphere to measure ozone in the stratospheric ozone layer. Ozonesondes are launched regularly at many locations around the world. Local ozone-measuring instruments using optical or chemical detection schemes are also used routinely on research aircraft to measure the distribution of ozone in the troposphere and lower stratosphere. High-altitude research aircraft can reach the ozone layer at most locations over the globe and can reach farthest into the layer at high latitudes. Ozone measurements are also being made routinely on some commercial aircraft flights.

Remote measurements. Remote measurements of total ozone amounts and the altitude distributions of ozone are obtained by detecting ozone at large distances from the instrument. Most remote measurements of ozone rely on its unique absorption of UV radiation. Sources of UV radiation that can be used are the Sun, lasers, and starlight. For example, satellites use the absorption of solar UV radiation by the atmosphere or the absorption of sunlight scattered from the surface of Earth to measure ozone over nearly the entire globe on a daily basis. Lasers are routinely deployed at ground

sites and on research aircraft to detect ozone over a distance of many kilometers along the laser light path. A network of ground-based detectors measures ozone by detecting small changes in the amount of the Sun's UV radiation that reaches Earth's surface. Other instruments measure ozone using its absorption of infrared or visible radiation or its emission of

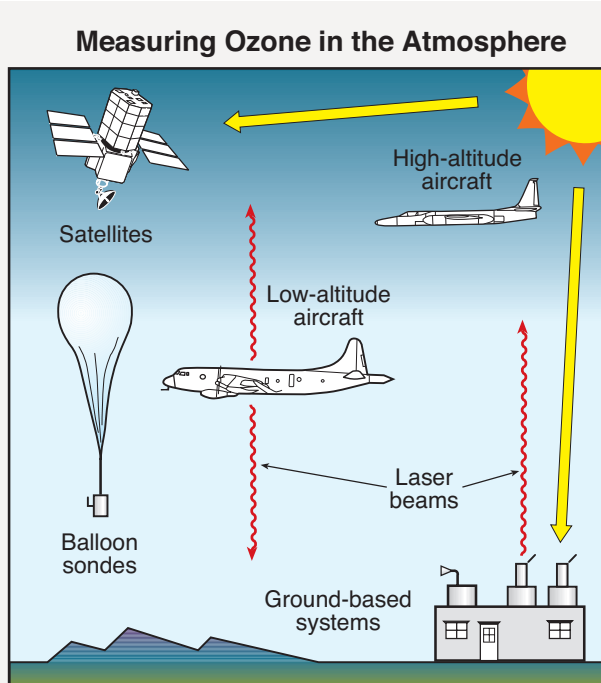


Figure Q5-1. Ozone measurements. Ozone is measured throughout the atmosphere with instruments on the ground, aircraft, high-altitude balloons, and satellites. Some instruments measure ozone locally in sampled air and others measure ozone remotely some distance away from the instrument. Instruments use optical techniques, with the Sun and lasers as light sources; detect the microwave emissions from ozone; or use chemical reactions that are unique to ozone. At many locations over the globe, regular measurements are made to monitor total ozone amounts and their variations over time.

microwave or infrared radiation. Emission measurements at night, which is particularly valuable for sampling polar regions in continuous darkness. have the advantage of providing remote ozone measurements

Global Ozone Network

The first instrument for routinely monitoring total ozone was developed by Gordon M.B. Dobson in the United Kingdom in the 1920s. The instrument, called a Féry spectrometer, made its measurements by examining the wavelength spectrum of solar ultraviolet radiation (sunlight) using a photographic plate. A small network of instruments distributed around Europe allowed Dobson to make important discoveries about how total ozone varies with location and time. In the 1930s a new instrument was developed by Dobson, now called a Dobson spectrophotometer, which precisely measures the intensity of sunlight at two ultraviolet wavelengths: one that is strongly absorbed by ozone and one that is weakly absorbed. The difference in light intensity at the two wavelengths provides a measure of total ozone above the instrument location.

A global network of total-ozone observing stations was established in 1957 as part of the International Geophysical Year. Today, there are about 100 sites located around the world ranging from South Pole, Antarctica (90°S), to Ellesmere Island, Canada (83°N), that routinely measure total ozone. The accuracy of these observations is maintained by regular instrument calibrations and intercomparisons. Data from the network have been essential for understanding the effects of chlorofluorocarbons (CFCs) and other ozone-depleting substances on the global ozone layer, starting before the launch of space-based ozone-measuring instruments and continuing to the present day. Ground-based instruments with excellent long-term stability and accuracy are now routinely used to help calibrate space-based observations of total ozone.

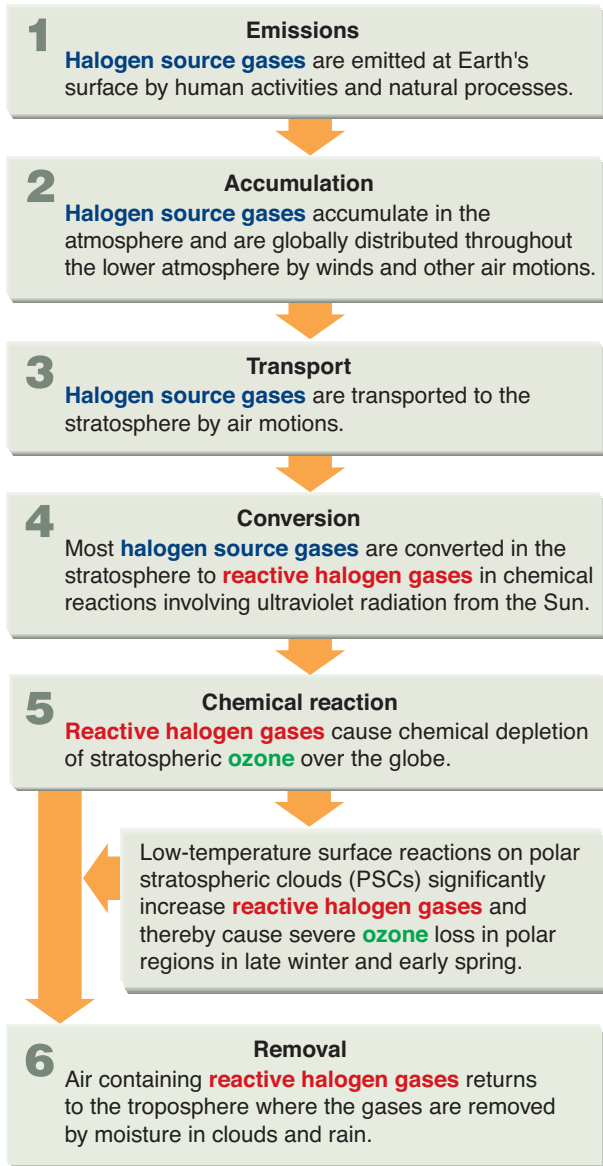
Pioneering scientists have traditionally been honored by having units of measure named after them. Accordingly, the unit of measure for total ozone is called the "Dobson unit" (see Q4).

Q6

What are the principal steps in stratospheric ozone depletion caused by human activities?

The initial step in the depletion of stratospheric ozone by human activities is the emission, at Earth's surface, of gases containing chlorine and bromine. Most of these gases accumulate in the lower atmosphere because they are unreactive and do not dissolve readily in rain or snow. Natural air motions transport these accumulated gases to the stratosphere, where they are converted to more reactive gases. Some of these gases then participate in reactions that destroy ozone. Finally, when air returns to the lower atmosphere, these reactive chlorine and bromine gases are removed from Earth's atmosphere by rain and snow.

Principal Steps in the Depletion of Stratospheric Ozone



Emission, accumulation, and transport. The principal steps in stratospheric ozone depletion caused by human activities are shown in Figure Q6-1. The process begins with the *emission*, at Earth's surface, of source gases containing the halogens chlorine and bromine (see Q7). The halogen source gases, often referred to as ozone-depleting substances (ODSs), include manufactured chemicals released to the atmosphere in a variety of applications, such as refrigeration, air conditioning, and foam blowing. Chlorofluorocarbons (CFCs) are an important example of chlorine-containing gases. Emitted source gases *accumulate* in the lower atmosphere (troposphere) and are *transported* to the stratosphere by natural air motions. The accumulation occurs because most source gases are highly unreactive in the lower atmosphere. Small amounts of these gases dissolve in ocean waters. The low reactivity of these manufactured halogenated gases is one property that makes them well suited for specialized applications such as refrigeration.

Some halogen gases are emitted in substantial quantities from natural sources (see Q7). These emissions also accumulate in the troposphere, are transported to the stratosphere, and participate in ozone destruction reactions. These naturally emitted gases are part of the natural balance of ozone production and destruction that predates the large release of manufactured halogenated gases.

Figure Q6-1. Principal steps in stratospheric ozone depletion. The stratospheric ozone depletion process begins with the emission of halogen source gases by human activities and natural processes. Those emitted by human activities are also called ozone-depleting substances (ODSs). Subsequent steps are accumulation, transport, conversion, chemical reaction, and removal. Ozone depletion by halogen source gases occurs globally. Large seasonal ozone losses occur in polar regions as a result of reactions involving polar stratospheric clouds (PSCs). Ozone depletion ends when reactive halogen gases are removed by rain and snow in the troposphere and deposited on Earth's surface.

Conversion, reaction, and removal. Halogen source gases do not react directly with ozone. Once in the stratosphere, halogen source gases are chemically *converted* to reactive halogen gases by ultraviolet radiation from the Sun (see Q8). The rate of conversion is related to the atmospheric lifetime of a gas (see Q7). Gases with longer lifetimes have slower conversion rates and survive longer in the atmosphere after emission. Lifetimes of the principal ODSs vary from 1 to 100 years (see Q7). Emitted gas molecules with atmospheric lifetimes greater than a few years circulate between the troposphere and stratosphere multiple times, on average, before conversion occurs.

The reactive gases formed from halogen source gases *react* chemically to destroy ozone in the stratosphere (see Q9). The average depletion of total ozone attributed to reactive gases is smallest in the tropics and largest at high latitudes (see Q13). In polar regions, surface reactions that occur at low temperatures on polar stratospheric clouds (PSCs) greatly increase the abundance of the most reactive chlorine gas, chlorine monoxide (ClO) (see Q10). This results in substantial ozone

destruction in polar regions in late winter and early spring (see Q11 and Q12).

After a few years, air in the stratosphere returns to the troposphere, bringing along reactive halogen gases. These gases are then *removed* from the atmosphere by rain and other precipitation or deposited on Earth's land or ocean surfaces. This removal brings to an end the destruction of ozone by chlorine and bromine atoms that were first released to the atmosphere as components of halogen source gas molecules.

Tropospheric conversion. Halogen source gases with short lifetimes (less than 1 year) undergo significant chemical conversion in the troposphere, producing reactive halogen gases and other compounds. Source gas molecules that are not converted are transported to the stratosphere. Only small portions of reactive halogen gases produced in the troposphere are transported to the stratosphere because most are removed by precipitation. Important examples of halogen gases that undergo some tropospheric removal are the hydrochlorofluorocarbons (HCFCs), methyl bromide (CH₃Br), and gases containing iodine (see Q7).

Understanding Stratospheric Ozone Depletion

Our understanding of stratospheric ozone depletion has been obtained through a combination of laboratory studies, computer models, and atmospheric observations. The wide variety of chemical reactions that occur in the stratosphere have been discovered and studied in *laboratory studies*. Chemical reactions between two gases follow well-defined physical rules. Some of these reactions occur on the surfaces of polar stratospheric clouds (PSCs) formed in the winter stratosphere. Reactions have been studied that involve many different molecules containing chlorine, bromine, fluorine, and iodine and other atmospheric constituents such as carbon, oxygen, nitrogen, and hydrogen. These studies have shown that several reactions involving chlorine and bromine directly or indirectly destroy ozone in the stratosphere.

Computer models have been used to examine the combined effect of the large group of known reactions that occur in the stratosphere. These models simulate the stratosphere by including representative chemical abundances, winds, air temperatures, and the daily and seasonal changes in sunlight. These analyses show that under certain conditions chlorine and bromine react in catalytic cycles in which one chlorine or bromine atom destroys many thousands of ozone molecules. Models are also used to simulate ozone amounts observed in previous years as a strong test of our understanding of atmospheric processes and to evaluate the importance of new reactions found in laboratory studies. The responses of ozone to possible future changes in the abundances of trace gases, temperatures, and other atmospheric parameters have been extensively explored with specialized computer models (see Q20).

Atmospheric *observations* have shown what gases are present in different regions of the stratosphere and how their abundances vary. Gas and particle abundances have been monitored over time periods spanning a daily cycle to decades. Observations show that halogen source gases and reactive halogen gases are present in the stratosphere at the amounts required to cause observed ozone depletion. Ozone and chlorine monoxide (ClO), for example, have been observed extensively with a variety of instruments. ClO is a highly reactive gas that is involved in catalytic ozone destruction cycles throughout the stratosphere (see Q9). Instruments on the ground and on satellites, balloons, and aircraft now routinely detect ozone and ClO remotely using optical and microwave signals. High-altitude aircraft and balloon instruments are also used to detect both gases locally in the stratosphere (see Q5). The observations of ozone and reactive gases made in past decades are used extensively in comparisons with computer models in order to increase confidence in our understanding of stratospheric ozone depletion.

Q7

What emissions from human activities lead to ozone depletion?

Certain industrial processes and consumer products result in the emission of ozone-depleting substances (ODSs) to the atmosphere. ODSs are manufactured halogen source gases that are controlled worldwide by the Montreal Protocol. These gases bring chlorine and bromine atoms to the stratosphere, where they destroy ozone in chemical reactions. Important examples are the chlorofluorocarbons (CFCs), once used in almost all refrigeration and air conditioning systems, and the halons, which were used in fire extinguishers. Current ODS abundances in the atmosphere are known directly from air sample measurements.

Halogen source gases versus ODSs. Those halogen source gases emitted by human activities and controlled by the Montreal Protocol are referred to as ODSs within the Montreal Protocol, by the media, and in the scientific literature. The Montreal Protocol now controls the global production and consumption of ODSs (see Q15). Halogen source gases that have only natural sources are not classified as ODSs. The contributions of ODSs and natural halogen source gases to chlorine and bromine entering the stratosphere in 2008 are shown in Figure Q7-1.

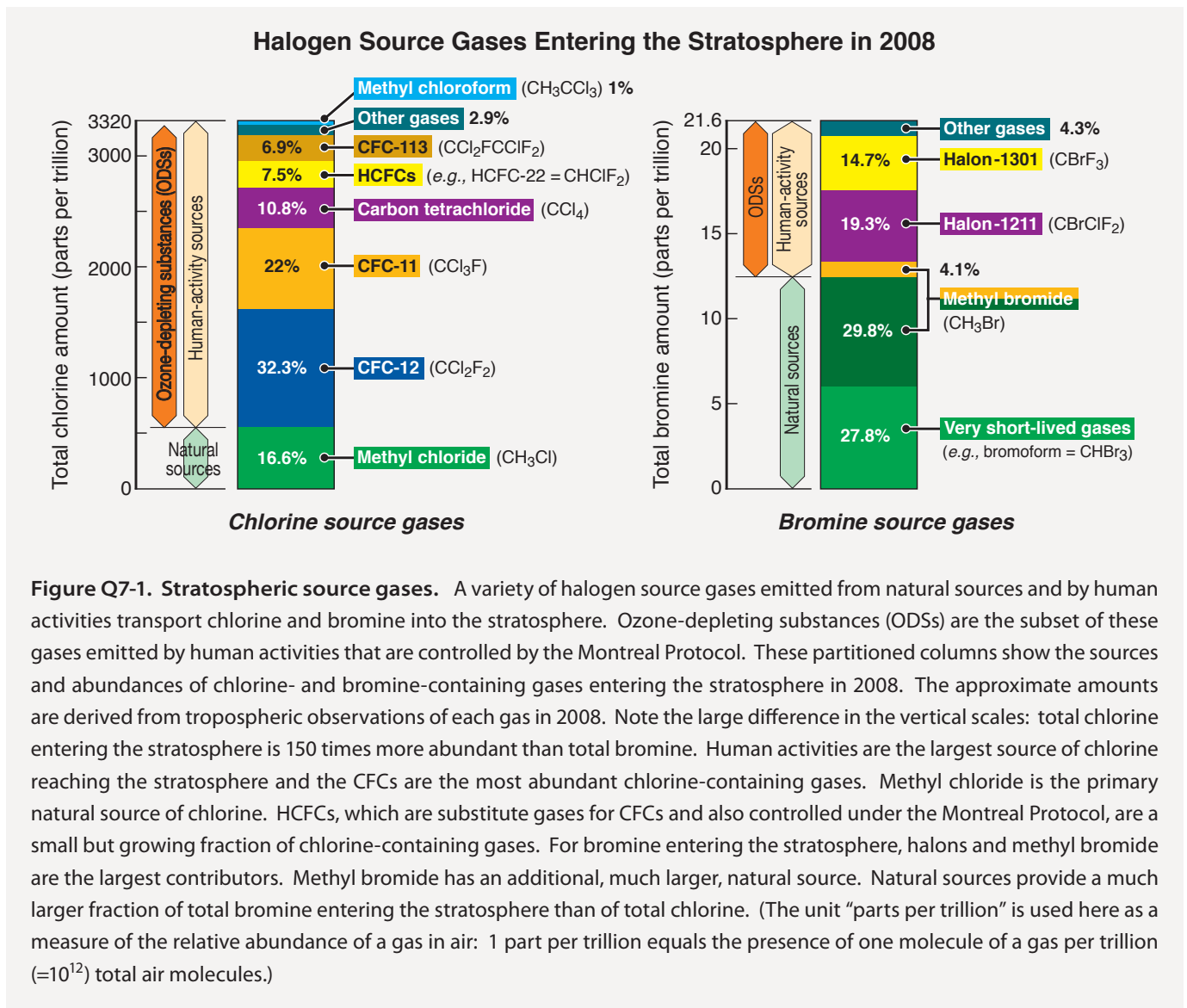
Ozone-depleting substances (ODSs). ODSs are manufactured for specific industrial uses or consumer products, most of which result in the eventual emission of these gases to the atmosphere. ODS emissions have increased substantially from the middle to the late 20th century, reached a peak in the late 1980s, and are now in decline (see Figure Q0-1). A large fraction of ODS emissions reach the stratosphere and lead to ozone depletion because chlorine and bromine atoms react to destroy ozone. ODSs that contain only carbon, chlorine, and fluorine are called *chlorofluorocarbons*, usually abbreviated as CFCs. CFCs, along with carbon tetrachloride (CCl₄) and methyl chloroform (CH₃CCl₃), historically have been the most important chlorine-containing halogen source gases emitted by human activities. These and other chlorine-containing ODSs have been used in many applications, including refrigeration, air conditioning, foam blowing, aerosol propellants, and cleaning of metals and electronic components.

Another category of ODSs contains bromine. The most important of these gases are the halons and methyl bromide (CH₃Br). Halons are halocarbon gases originally developed to extinguish fires. Halons were widely used to protect large computer installations, military hardware, and commercial aircraft engines. As a consequence, halons are often released directly into the atmosphere upon use. Halon-1211 and halon-1301 are the most abundant halons emitted by human

activities (see Figure Q7-1). Methyl bromide is used primarily as an agricultural and pre-shipping fumigant.

Natural sources of chlorine and bromine. There are a few halogen source gases present in the stratosphere that have large natural sources. These include methyl chloride (CH₃Cl) and methyl bromide (CH₃Br), both of which are emitted by oceanic and terrestrial ecosystems. Natural sources of these two gases contributed about 17% of the chlorine in the stratosphere in 2008 and about 30% of the bromine (see Figure Q7-1). Very short-lived source gases containing bromine, such as bromoform (CHBr₃), are also released to the atmosphere primarily from biological activity in the oceans. Only a fraction of these emissions reaches the stratosphere, because these gases are rapidly removed in the lower atmosphere. The contribution of these very short-lived gases to stratospheric bromine is estimated to be about 28%, but this has a large uncertainty. The contribution to stratospheric chlorine of short-lived chlorinated gases from natural and human sources is much smaller (less than 3%) and is included in *Other gases* in Figure Q7-1. The amounts of chlorine and bromine in the stratosphere from natural sources are believed to have been fairly constant since the middle of the 20th century and, therefore, cannot be the cause of ozone depletion as observed since the 1980s.

Other human sources of chlorine and bromine. Other chlorine- and bromine-containing gases are released regularly from human activities. Common examples are the use of chlorine gases to disinfect swimming pools and wastewater, fossil fuel burning, biomass burning, and various industrial processes. These emissions do not contribute significantly to stratospheric amounts of chlorine and bromine because either the global source is small, or the emitted gases and their degradation products are short-lived (very reactive or highly soluble). As a consequence, the chlorine and bromine content of these gases is prevented from reaching the stratosphere in significant amounts.



Lifetimes and emissions. After emission, halogen source gases are either naturally removed from the atmosphere or undergo chemical conversion in the troposphere or stratosphere. The time to remove or convert about 60% of a gas is often called its atmospheric lifetime. Lifetimes vary from less than 1 year to 100 years for the principal chlorine- and bromine-containing gases (see Table Q7-1). The long-lived gases are primarily destroyed in the stratosphere and essentially all of the emitted halogen is available to participate in the destruction of stratospheric ozone. Gases with the short lifetimes (e.g., the HCFCs, methyl bromide, methyl chloride, and the very short-lived gases) are substantially destroyed in the troposphere and, therefore, only a fraction of the emitted halogen contributes to ozone depletion in the stratosphere.

The amount of an emitted gas that is present in the atmo-

sphere represents a balance between the emission rate and the lifetime of the gas. Emission rates and atmospheric lifetimes vary greatly for the source gases, as indicated in Table Q7-1. For example, the atmospheric abundances of most of the principal CFCs and halons have decreased since 1990 while those of the leading substitute gases, the hydrochlorofluorocarbons (HCFCs), continue to increase under the provisions of the Montreal Protocol (see Q16). In the coming decades, the emissions and atmospheric abundances of all controlled gases are expected to decrease under these provisions.

Ozone Depletion Potential (ODP). Halogen source gases are compared in their effectiveness to destroy stratospheric ozone using the ODP, as listed in Table Q7-1 (see Q18). A gas with a larger ODP destroys more ozone over its atmospheric lifetime. The ODP is calculated relative to CFC-11,

Table Q7-1. Atmospheric lifetimes, global emissions, Ozone Depletion Potentials, and Global Warming Potentials of some halogen source gases and HFC substitute gases.

Gas	Atmospheric Lifetime (years)	Global Emissions in 2008 (Kt/yr) ^a	Ozone Depletion Potential (ODP) ^c	Global Warming Potential (GWP) ^c
Halogen source gases				
Chlorine gases				
CFC-11	45	52–91	1	4750
CFC-12	100	41–99	0.82	10900
CFC-113	85	3–8	0.85	6130
Carbon tetrachloride (CCl ₄)	26	40–80	0.82	1400
HCFCs	1–17	385–481	0.01–0.12	77–2220
Methyl chloroform (CH ₃ CCl ₃)	5	Less than 10	0.16	146
Methyl chloride (CH ₃ Cl)	1	3600–4600	0.02	13
Bromine gases				
Halon-1301	65	1–3	15.9	7140
Halon-1211	16	4–7	7.9	1890
Methyl bromide (CH ₃ Br)	0.8	110–150	0.66	5
Very short-lived gases (e.g., CHBr ₃)	Less than 0.5	^b	^b very low	^b very low
Hydrofluorocarbons (HFCs)				
HFC-134a	13.4	149 ± 27	0	1370
HFC-23	222	12	0	14200
HFC-143a	47.1	17	0	4180
HFC-125	28.2	22	0	3420
HFC-152a	1.5	50	0	133
HFC-32	5.2	8.9	0	716

^a Includes both human activities (production and banks) and natural sources. Emissions are in units of kilotonnes per year (1 kilotonne = 1000 metric tons = 1 gigagram = 10⁹ grams).

^b Estimates are very uncertain for most species.

^c 100-year GWPs. ODPs and GWPs are discussed in Q18. Values are calculated for emissions of an equal mass of each gas.

which has an ODP defined to be 1. The calculations, which require the use of computer models of the atmosphere, use as the basis of comparison the ozone depletion from an equal mass of each gas emitted to the atmosphere. Halon-1211 and halon-1301 have ODPs significantly larger than CFC-11 and most other emitted gases because bromine is much more effective overall (about 60 times) on a per-atom basis than chlorine in chemical reactions that destroy ozone. The gases with small ODP values generally have short atmospheric lifetimes or contain fewer chlorine and bromine atoms.

Fluorine and iodine. Fluorine and iodine are also halogen atoms. Many of the source gases in Figure Q7-1 also con-

tain fluorine atoms in addition to chlorine or bromine. After the source gases undergo conversion in the stratosphere (see Q6), the fluorine content of these gases is left in chemical forms that do not cause ozone depletion. As a consequence, halogen source gases that contain fluorine and no other halogens are not classified as ODSs. An important category is the hydrofluorocarbons (HFCs), which are included in Table Q7-1 because they are ODS substitute gases with ODPs of zero (see Q18).

Iodine is a component of several gases that are naturally emitted from the oceans. Although iodine can participate in ozone destruction reactions, these iodine-containing source gases generally have very short lifetimes and, as a result, only

a very small fraction reaches the stratosphere. There are large uncertainties in how these emissions vary with season and geographical region.

Other non-halogen gases. Other non-halogen gases that influence stratospheric ozone abundances have also increased in the stratosphere as a result of emissions from human activities. Important examples are methane (CH_4) and nitrous oxide (N_2O), which react in the stratosphere to form water vapor and reactive hydrogen, and nitrogen oxides, respectively. These reactive products participate in

the destruction of stratospheric ozone (see Q2). Increasing abundances of N_2O and CH_4 , as well as CO_2 , are expected to significantly affect future stratospheric ozone through combined effects on temperature, winds, and chemistry (see Q20). Although all of these gases are part of the Kyoto Protocol (see Q15) because they are climate gases, they are not classified as ODSs under the Montreal Protocol. Although past emissions of ODSs still dominate global ozone depletion, the *current* emissions of N_2O from human activities will destroy more stratospheric ozone than the *current* emissions of any ODS.

Heavier-Than-Air CFCs

CFCs and other ozone-depleting substances reach the stratosphere despite the fact that they are “heavier than air.” For example, molecules of CFC-11 (CCl_3F) and CFC-12 (CCl_2F_2) are approximately 4–5 times heavier than the average molecule of air, since air is composed primarily of oxygen and nitrogen. The emissions of long-lived gases accumulate in the lower atmosphere (troposphere). The distribution of these gases in the troposphere and stratosphere is not controlled by the molecular weight of each gas because air is in continual motion in these regions as a result of winds and convection. Continual air motions ensure that new emissions of long-lived gases are horizontally and vertically well mixed throughout the troposphere within a few months. It is this well-mixed air that enters the lower stratosphere from upward air motions in tropical regions, bringing with it ozone-depleting substances emitted from any location on Earth’s surface.

Atmospheric measurements confirm that ozone-depleting substances with long atmospheric lifetimes are well mixed in the troposphere and are present in the stratosphere (see Figure Q8-2). The amounts found in these regions are generally consistent with the emission estimates reported by industries and governments. Measurements also show that gases that are “lighter than air,” such as hydrogen (H_2) and methane (CH_4), are also well mixed in the troposphere, as expected, and not found only in the upper atmosphere. Noble gases from very light helium to very heavy xenon, which all have very long atmospheric lifetimes, are also uniformly distributed throughout the troposphere and stratosphere. Only at altitudes well above the troposphere and stratosphere (above 85 kilometers (53 miles)), where much less air is present, does the influence of winds and convection diminish to the point where heavy gases begin to separate from lighter gases as a result of gravity.

Q8

What are the reactive halogen gases that destroy stratospheric ozone?

Emissions from human activities and natural processes represent a large source of chlorine- and bromine-containing gases that enter the stratosphere. When exposed to ultraviolet radiation from the Sun, these halogen source gases are converted to more reactive gases containing chlorine and bromine. Some reactive gases act as chemical reservoirs that convert to form the most reactive gases, namely chlorine monoxide (ClO) and bromine monoxide (BrO). The most reactive gases participate in catalytic reactions that efficiently destroy ozone. Most volcanoes emit some reactive halogen gases that readily dissolve in water and are usually washed out of the atmosphere before they can reach the stratosphere.

Reactive gases containing the halogens chlorine and bromine lead to the chemical destruction of stratospheric ozone. Halogen-containing gases present in the stratosphere can be divided into two groups: *halogen source gases* and *reactive halogen gases* (Figure Q8-1). The source gases, which include ozone-depleting substances (ODSs), are emitted at Earth's surface by natural processes and by human activities (see Q7). Once in the stratosphere, the halogen source gases chemically convert at different rates to form the reactive halogen gases. The conversion occurs in the stratosphere for most gases instead of the troposphere because solar ultraviolet radiation (sunlight) is more intense in the stratosphere.

Reactive halogen gases. The chemical conversion of halogen source gases, which involves solar ultraviolet radiation (sunlight) and other chemical reactions, produces a number of reactive halogen gases. These reactive gases contain all of the chlorine and bromine atoms originally present in the source gases. The most important reactive chlorine- and bromine-containing gases that form in the stratosphere are shown in Figure Q8-1. Throughout the stratosphere, the most abundant are typically hydrogen chloride (HCl) and chlorine nitrate (ClONO₂). These two gases are considered important *reservoir* gases because, while they don't react directly with ozone, they can be converted to the *most reactive* forms that

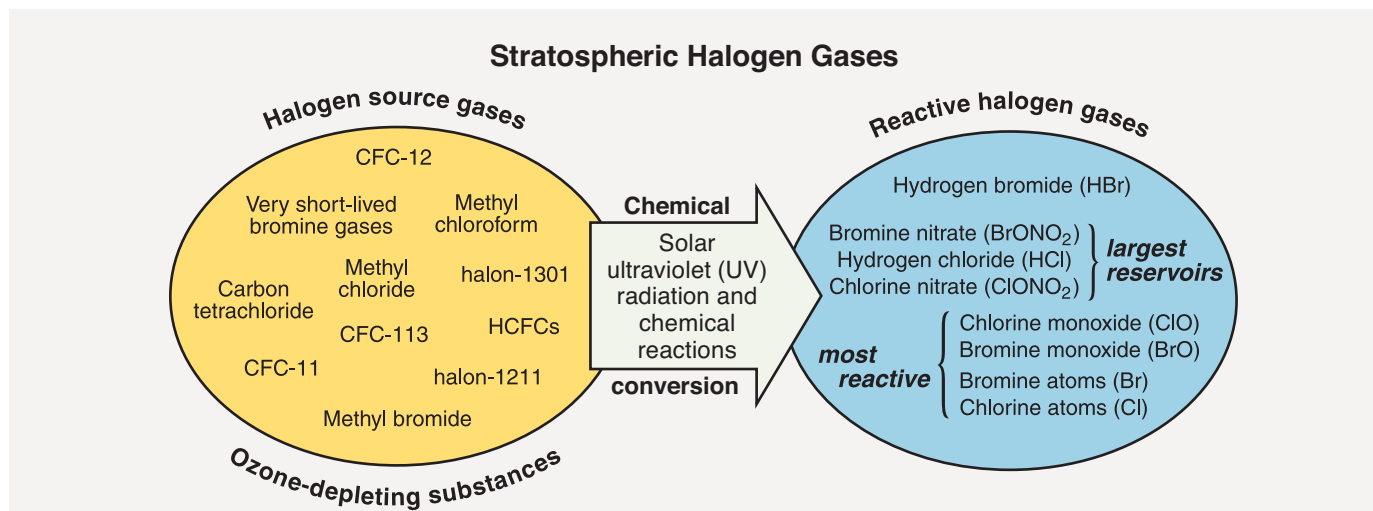


Figure Q8-1. Conversion of halogen source gases. Halogen source gases containing chlorine and bromine are chemically converted to reactive halogen gases primarily in the stratosphere. The conversion requires solar ultraviolet radiation and a few chemical reactions. The shorter-lived gases undergo some conversion in the troposphere. The reactive halogen gases contain all the chlorine and bromine originally present in the source gases before conversion. The reactive gases can be grouped into the reservoir gases, which do not directly destroy ozone, and the most reactive gases, which participate in ozone destruction cycles (see Q9). A principal reactive gas, ClO, is formed by reactions of the reservoir gases HCl and ClONO₂ that occur on the surfaces of liquid and solid polar stratospheric clouds (PSCs) (see Q10).

do chemically destroy ozone. The most reactive forms are chlorine monoxide (ClO) and bromine monoxide (BrO), and chlorine and bromine atoms (Cl and Br). A large fraction of available reactive bromine is generally in the form of BrO, whereas usually only a small fraction of reactive chlorine is in the form of ClO. The special conditions that occur in the polar regions in winter cause the reservoir gases ClONO₂ and HCl to undergo nearly complete conversion to ClO in reactions on polar stratospheric clouds (PSCs) (see Q10).

Reactive chlorine at midlatitudes. Reactive chlorine gases have been observed extensively in the stratosphere with both local and remote measurement techniques. The measurements from space displayed in Figure Q8-2 are representative of how the amounts of chlorine-containing gases change between the surface and the upper stratosphere at midlatitudes. Available chlorine (see red line in Figure Q8-2) is the sum of chlorine contained in halogen source gases and the reactive gases (e.g., HCl, ClONO₂, ClO). Available chlorine is constant to within about 15 percent from the surface to 47 kilometers (31 miles) altitude. In the troposphere, available chlorine is contained almost entirely in the source gases described in Figure Q7-1. At higher altitudes, the source gases become a smaller fraction of available chlorine as they are converted to

the reactive chlorine gases. At the highest altitudes, available chlorine is all in the form of the reactive chlorine gases.

In the altitude range of the ozone layer at midlatitudes, as shown in Figure Q8-2, the reactive reservoir gases HCl and ClONO₂ account for most of the available chlorine. ClO, the most reactive gas in ozone depletion, is a small fraction of available chlorine. The low abundance of ClO limits the amount of ozone destruction that occurs outside of polar regions.

Reactive chlorine in polar regions. Reactive chlorine gases in polar regions undergo large changes between the fall and late winter. Meteorological and chemical conditions in both polar regions are now routinely observed from space in all seasons. Fall and winter conditions over the Antarctic are contrasted in Figure Q8-3 using seasonal observations made near the center of the ozone layer (about 18 km (11.3 miles)) (see Figure Q12-3).

In fall (May), ozone values are high over the entire Antarctic continent and beyond. Temperatures are mid-range, HCl and nitric acid (HNO₃) are high, and ClO is very low. High HCl indicates that substantial conversion of halogen source gases has occurred in the stratosphere. In the past decades, HCl and ClONO₂ reactive reservoir gases have increased substantially in the stratosphere following increased emissions of halogen source gases. HNO₃ is an abundant, naturally

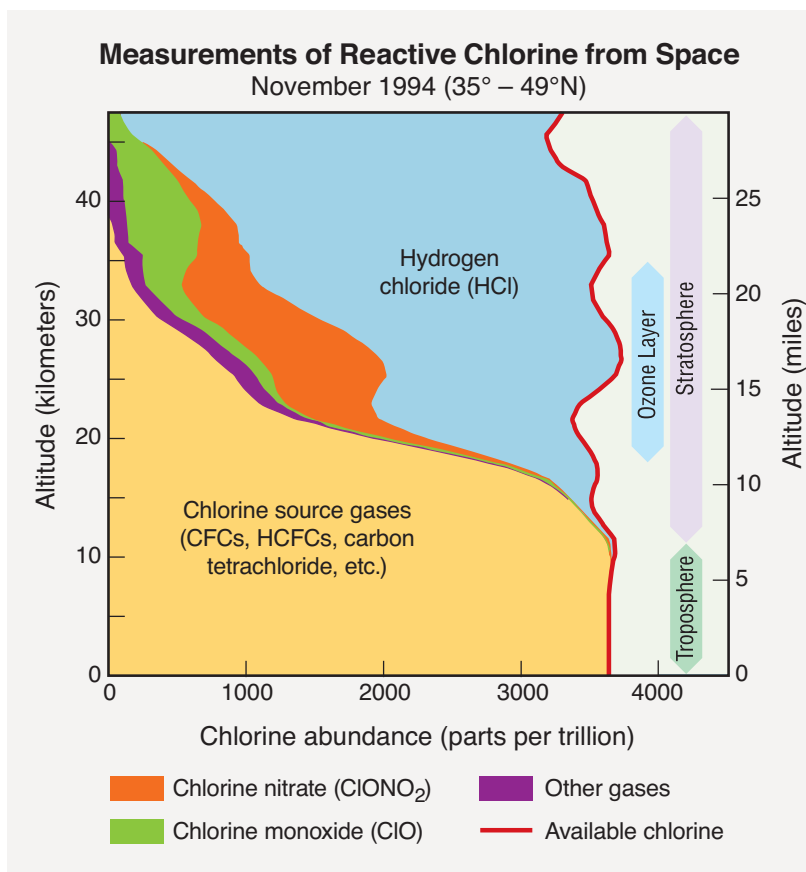
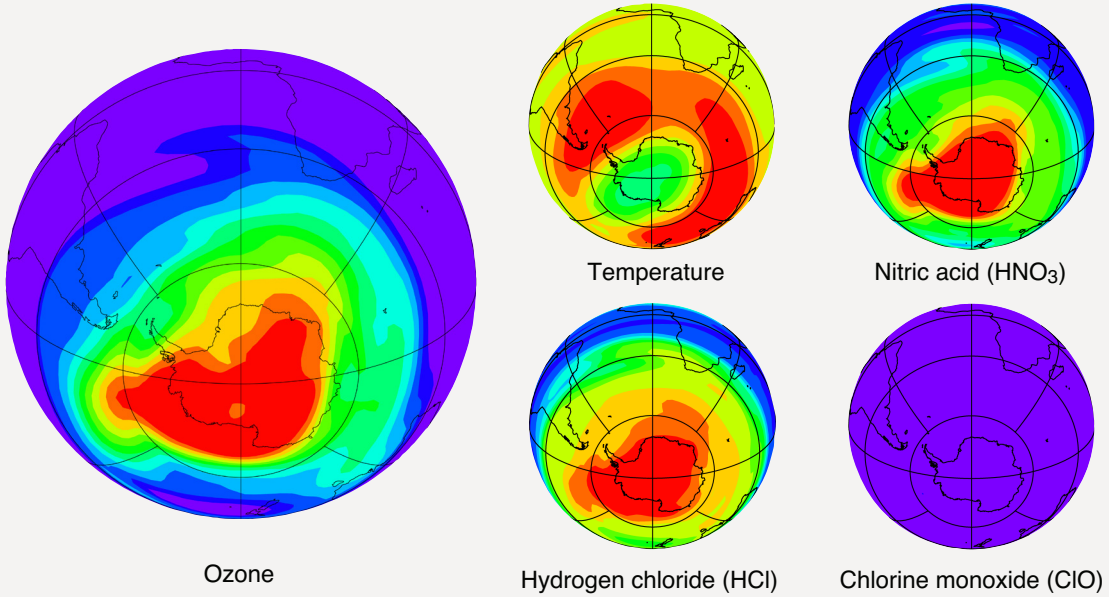


Figure Q8-2. Reactive chlorine gas observations.

The abundances of chlorine source gases and reactive chlorine gases as measured from space in 1994 are displayed with altitude for a midlatitude location. In the troposphere (below about 10 kilometers), all chlorine is contained in the source gases. In the stratosphere, the abundances of reactive chlorine gases increase with altitude as the amounts of chlorine source gases decline. This is a consequence of chemical reactions initiated by solar ultraviolet radiation that convert source gases to reactive gases (see Figure Q8-1). The principal reactive chlorine gases formed are HCl, ClONO₂, and ClO. Summing the source gases with the reactive gases gives "Available chlorine," which is nearly constant with altitude up to 47 km. In the ozone layer (18–35 km), chlorine source gases are still present and HCl and ClONO₂ are the most abundant reactive chlorine gases. (The unit "parts per trillion" is defined in the caption of Figure Q7-1.)

Chemical Conditions Observed in the Ozone Layer Over Antarctica

Normal ozone amounts in fall (1 May 2008) at 18-km altitude



Large ozone depletion in late winter (15 September 2008) at 18-km altitude

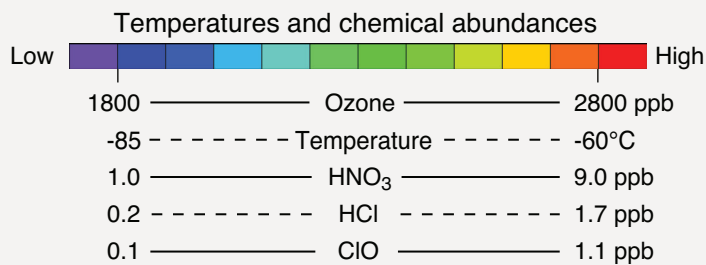
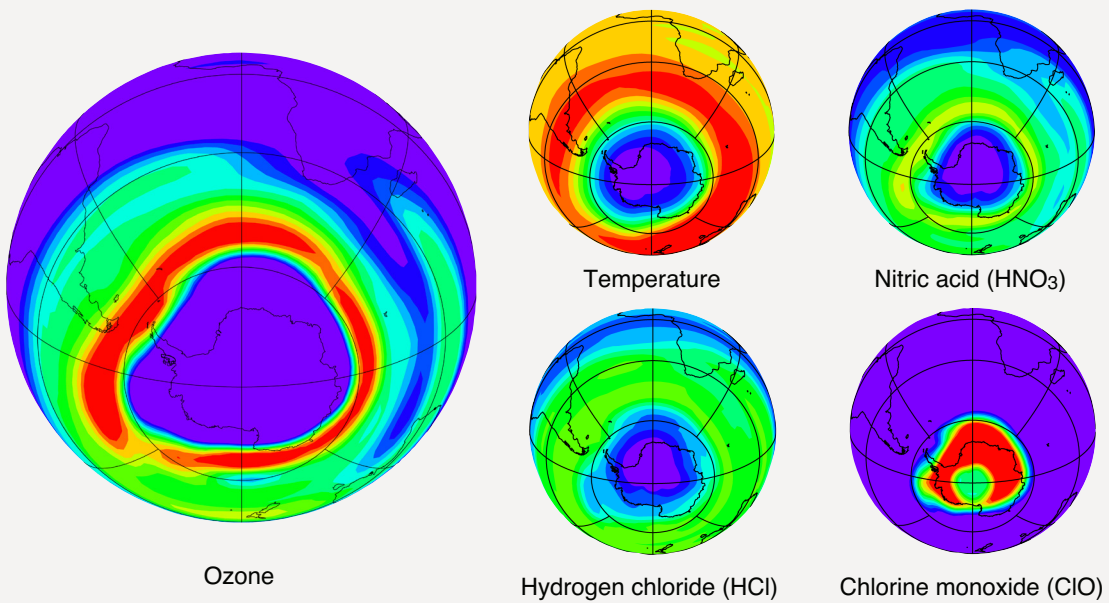


Figure Q8-3. Chemical conditions in the ozone layer over Antarctica. Observations of the chemical conditions in the Antarctic region highlight the changes associated with severe ozone depletion that forms the ozone hole. Satellite instruments now routinely monitor ozone, reactive chlorine gases, and temperatures in the global stratosphere. Results are shown here for fall (May) and late winter (September) seasons in Antarctic winter for a narrow altitude region near 18 kilometers (11.2 miles) within the ozone layer (see Figure Q12-3). Ozone has normal high values in fall before the onset of ozone destruction reactions causes wide spread depletion by late winter. High ozone is accompanied by moderate temperatures, normal high values of HCl and HNO₃, and normal very low ClO amounts. When ClO is not enhanced, significant ozone destruction from ozone-depleting substances does not occur. Chemical conditions are quite different in late winter when ozone undergoes severe depletion. Temperatures are much lower, HCl has been converted to ClO, the most reactive chlorine gas, and HNO₃ has been removed by the gravitational settling of PSC particles. ClO values closely surrounding the South Pole are low in September because ClO formation requires sunlight, which is still gradually returning to the highest latitudes. The high ClO values in late winter last for 1 to 2 months, cover an area that at times exceeds that of the Antarctic continent, and efficiently destroy ozone in sunlit regions in late winter/early spring. Ozone typically reaches its minimum values in early to mid-October (see Q12). Note that the first and last colors in the color bar represent values outside the indicated range of values. (The unit “parts per billion,” abbreviated “ppb,” is used here as a measure of the relative abundance of a gas in air: 1 part per billion equals the presence of one molecule of a gas per billion (=10⁹) total air molecules (compare to ppt in Figure Q7-1)).

occurring stratospheric compound that moderates ozone destruction chemistry and also condenses to help form polar stratospheric clouds (PSCs) (see Q10). Low ClO indicates that little conversion of the reactive reservoirs occurs in the fall, thereby limiting catalytic ozone destruction.

By late winter (September), ozone amounts reflect substantial depletion at 18-km altitude over an area larger than the Antarctic continent. Depletion throughout much of the altitude range of the ozone layer created the 2008 ozone hole shown in Figure Q11-3 (see altitude profile in Figure Q12-3). The associated meteorological and chemical conditions in late winter are very different from those found in fall: very low temperatures, very low HCl and HNO₃, and very high ClO. Low stratospheric temperatures are characteristic of winter when solar heating is reduced. Low HCl and high ClO reflect the conversion of the reactive halogen reservoir compounds, HCl and ClONO₂, to the most reactive chlorine form, ClO. This conversion occurs selectively in winter on PSCs and other stratospheric particles, which form at the very low temperatures (see Q10). Low HNO₃ is indicative of its condensation to form PSCs, some of which subsequently move to lower altitudes through gravitational settling. High ClO abundances generally cause ozone depletion to continue in the Antarctic region until mid-October (spring), when the lowest ozone values usually are observed (see Q11). As temperatures rise at the end of the winter, halting further PSC formation, ClO is converted back into the reactive reservoir species HCl and ClONO₂ (see Q10), and ozone destruction is curtailed.

Similar though less dramatic changes in meteorological and chemical conditions are also observed between fall and winter in the Arctic, where winter ozone depletion is less severe than in the Antarctic.

Reactive bromine observations. Fewer measurements are available for reactive bromine gases in the lower stratosphere than for reactive chlorine, in part because of the lower abundance of bromine. The most widely observed bromine gas is bromine monoxide (BrO), which can be observed from space. Estimates of reactive bromine abundances in the stratosphere are larger than expected from the conversion of the halons and methyl bromide source gases, suggesting that the contribution of the very short-lived bromine-containing gases to reactive bromine must also be significant (see Q7).

Other sources. Other emission sources of reactive halogen gases exist that are associated with natural processes and human activities. Most emissions become trapped in the lower atmosphere when dissolved in water, and ultimately are returned to Earth's surface before they can reach the stratosphere. Volcanoes are an important episodic source of reactive halogen gases (e.g., HCl) that do not reach the stratosphere in appreciable quantities (see Q14). Other examples include reactive chlorine produced by evaporation of ocean spray. Sea salt products dissolve in water and are removed in the lower atmosphere. Solid rocket motors, such as those used on the Space Shuttle, release reactive chlorine gases directly into the troposphere and stratosphere. At current launch rates, the emitted quantities are very small in comparison with halogen emissions from other human activities.

Q9

What are the chlorine and bromine reactions that destroy stratospheric ozone?

Reactive gases containing chlorine and bromine destroy stratospheric ozone in “catalytic” cycles made up of two or more separate reactions. As a result, a single chlorine or bromine atom can destroy many thousands of ozone molecules before it leaves the stratosphere. In this way, a small amount of reactive chlorine or bromine has a large impact on the ozone layer. A special situation develops in polar regions in the late winter/early spring season where large enhancements in the abundance of the most reactive gas, chlorine monoxide, leads to severe ozone depletion.

Stratospheric ozone is destroyed by reactions involving **reactive halogen gases**, which are produced in the chemical conversion of *halogen source gases* (see Figure Q8-1). The most reactive of these gases are chlorine monoxide (ClO), bromine monoxide (BrO), and chlorine and bromine atoms (Cl and Br). These gases participate in three principal reaction cycles that destroy ozone.

Cycle 1. Ozone destruction Cycle 1 is illustrated in Figure Q9-1. The cycle is made up of two basic reactions: $\text{Cl} + \text{O}_3$ and $\text{ClO} + \text{O}$. The net result of Cycle 1 is to convert one ozone molecule and one oxygen atom into two oxygen molecules. In each cycle, chlorine acts as a *catalyst* because ClO and Cl react and are re-formed. In this way, one Cl atom participates in many cycles, destroying many ozone molecules. For typical stratospheric conditions at middle or low latitudes, a single chlorine atom can destroy hundreds of ozone molecules

before it happens to react with another gas, breaking the catalytic cycle, and up to tens of thousands of ozone molecules during the total time of its stay in the stratosphere.

Polar Cycles 2 and 3. The abundance of ClO is greatly increased in polar regions during winter as a result of reactions on the surfaces of polar stratospheric clouds (PSCs) (see Q8 and Q10). Cycles 2 and 3 (see Figure Q9-2) become the dominant reaction mechanisms for polar ozone loss because of the high abundances of ClO and the relatively low abundance of atomic oxygen (which limits the rate of ozone loss by Cycle 1). Cycle 2 begins with the self-reaction of ClO. Cycle 3, which begins with the reaction of ClO with BrO, has two reaction pathways to produce either Cl and Br or BrCl. The net result of both cycles is to destroy two ozone molecules and create three oxygen molecules. Cycles 2 and 3 account for most of the ozone loss observed in the Arctic and Antarctic stratospheres

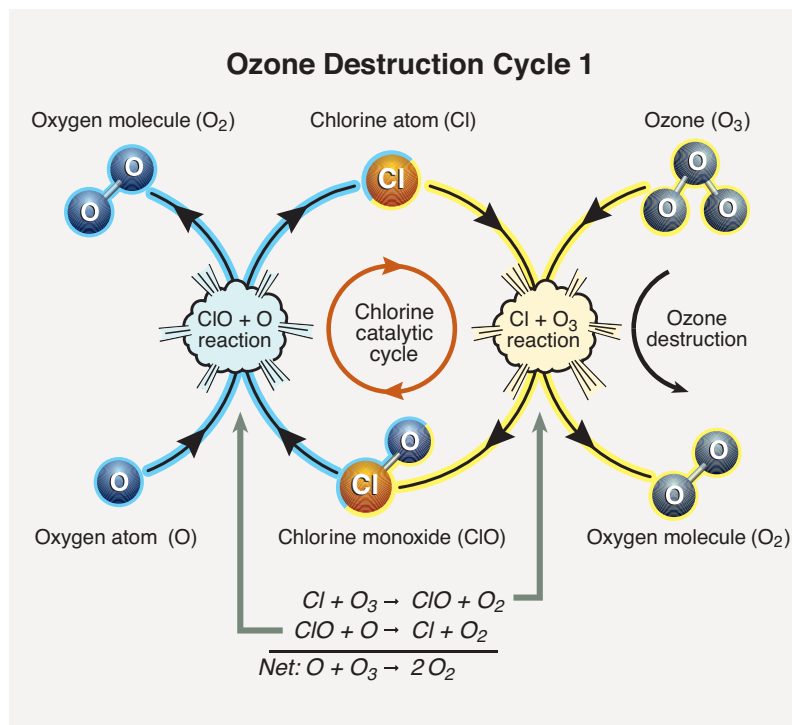


Figure Q9-1. Ozone destruction Cycle 1. The destruction of ozone in Cycle 1 involves two separate chemical reactions. The net or overall reaction is that of atomic oxygen with ozone, forming two oxygen molecules. The cycle can be considered to begin with either ClO or Cl. When starting with ClO, the first reaction is ClO with O to form Cl. Then, Cl reacts with ozone and re-forms ClO, consuming ozone in the process. The cycle then begins again with another reaction of ClO with O. Chlorine is considered a catalyst for ozone destruction because Cl and ClO are re-formed each time the reaction cycle is completed, and ozone is simply removed. Atomic oxygen (O) is formed when solar ultraviolet radiation (sunlight) reacts with ozone and oxygen molecules. Cycle 1 is most important in the stratosphere at tropical and middle latitudes, where solar ultraviolet radiation is most intense.

Ozone Destruction Cycles in Polar Regions

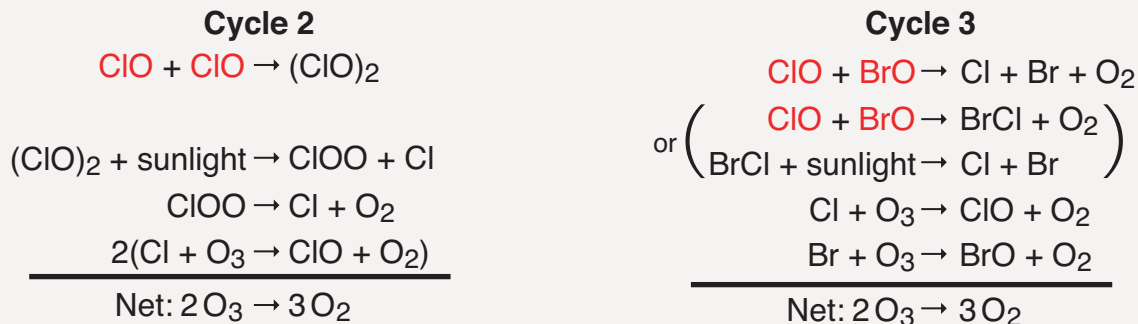


Figure Q9-2. Polar ozone destruction Cycles 2 and 3. Significant destruction of ozone occurs in polar regions because ClO abundances reach large values. In this case, the cycles initiated by the reaction of ClO with another ClO (Cycle 2) or the reaction of ClO with BrO (Cycle 3) efficiently destroy ozone. The net reaction in both cases is two ozone molecules forming three oxygen molecules. The reaction of ClO with BrO has two pathways to form the Cl and Br product gases. Ozone destruction Cycles 2 and 3 are catalytic, as illustrated for Cycle 1 in Figure Q9-1, because chlorine and bromine gases react and are re-formed each time the reaction cycle is completed. Visible sunlight is required to complete each cycle and to help form and maintain ClO abundances. During polar night and other periods of darkness, ozone cannot be destroyed by these reactions.

in the late winter/early spring season (see Q11 and Q12). At high ClO abundances, the rate of polar ozone destruction can reach 2 to 3% per day in late winter/early spring.

Sunlight requirement. Sunlight is required to complete and maintain Cycles 1 through 3. Cycle 1 requires sunlight because atomic oxygen is formed only with solar ultraviolet radiation. Cycle 1 is most important in the stratosphere at tropical and middle latitudes, where solar ultraviolet radiation (sunlight) is most intense.

Cycles 2 and 3 require visible sunlight to complete the reaction cycles and to maintain ClO abundances. In the continuous darkness of winter in the polar stratosphere, reaction Cycles 2 and 3 cannot occur. It is only in late winter/early spring when sunlight returns to the polar regions that these cycles can occur. Therefore, the greatest destruction of ozone occurs in the partially to fully sunlit periods after midwinter in the polar stratosphere. The visible sunlight needed in Cycles 2 and 3 is not sufficient to form ozone because this process requires solar ultraviolet radiation (see Q1). In the stratosphere in the late winter/early spring period, solar ultra-

violet radiation is weak at low Sun angles. As a result, ozone destruction by Cycles 2 and 3 in the sunlit winter stratosphere greatly exceeds ozone production.

Other reactions. Global ozone abundances are controlled by many reactions that both produce and destroy ozone (see Q2). Chlorine and bromine catalytic reactions are but one group of ozone destruction reactions. Reactive hydrogen and reactive nitrogen gases, for example, are involved in other catalytic ozone-destruction cycles that also occur in the stratosphere. These reactions occur naturally in the stratosphere and their importance has not been as strongly influenced by human activities as have reactions involving halogens. The sources of reactive hydrogen and nitrogen gases are the naturally occurring gases methane (CH_4) and nitrous oxide (N_2O), respectively. The importance of reactive hydrogen and nitrogen gases relative to reactive halogen gases is expected to increase in the future, because the atmospheric abundances of the reactive halogen gases are decreasing as a result of the Montreal Protocol, while CH_4 and N_2O abundances are projected to increase substantially due to human activities.

Replacing Lost Ozone in the Stratosphere

The idea is sometimes put forth that humans could compensate for lost global stratospheric ozone by replacing it. Ozone could be manufactured, stored, transported to the stratosphere, and released in depleted regions. Unfortunately, the idea has substantial practical limitations.

Ozone amounts in the stratosphere reflect a continual *balance* between chemical production and destruction (see Q2). The addition of chlorine and bromine to the stratosphere from human activities has changed the natural balance by increasing ozone destruction and, thereby, lowering stratospheric ozone amounts. Chlorine and bromine destroy ozone in catalytic reactions that allow each atom to destroy many thousands of ozone molecules (see Q9). A one-time injection of manufactured ozone to the stratosphere would not restore the natural balance because the added ozone would be destroyed in the same chemical reactions with chlorine and bromine within about a year. Thus, ozone additions would need to be large and continuous as long as stratospheric chlorine and bromine amounts remained enhanced above natural amounts, a condition expected to persist for several decades (see Q16). Continuous replacement for decades would pose unprecedented technical and resource challenges that will likely be unacceptable to decision makers in the international community.

Specific technical difficulties in replacing stratospheric ozone are the large amounts of ozone required and the delivery method. The total amount of atmospheric ozone is approximately 3,000 megatons (1 megaton = 1 billion kilograms) with most residing in the stratosphere. Compensating for the average global ozone loss, currently about 3%, would require 90 megatons of ozone to be distributed regularly throughout the stratosphere many kilometers above Earth's surface. The energy required to produce this amount of ozone would be a significant fraction of the electrical power generated annually in the United States, for example, which is now approximately 4 trillion kilowatt hours. Processing and storing requirements for ozone, which is explosive and toxic in large quantities, would increase the energy requirement. In addition, methods suitable to deliver and distribute large amounts of ozone to the stratosphere have not been developed. Concerns for a global delivery system would include further significant energy use and unforeseen environmental consequences.

Q10

Why has an “ozone hole” appeared over Antarctica when ozone-depleting substances are present throughout the stratosphere?

Ozone-depleting substances are present throughout the stratospheric ozone layer because they are transported great distances by atmospheric air motions. The severe depletion of the Antarctic ozone layer known as the “ozone hole” occurs because of the special atmospheric and chemical conditions that exist there and nowhere else on the globe. The very low winter temperatures in the Antarctic stratosphere cause polar stratospheric clouds (PSCs) to form. Special reactions that occur on PSCs, combined with the relative isolation of polar stratospheric air, allow chlorine and bromine reactions to produce the ozone hole in Antarctic springtime.

The severe depletion of stratospheric ozone in late winter and early spring in the Antarctic is known as the “ozone hole” (see Q11). The ozone hole first appeared over Antarctica because atmospheric and chemical conditions unique to this region increase the effectiveness of ozone destruction by reactive halogen gases (see Q8). In addition to an abundance

of these reactive gases, the formation of the Antarctic ozone hole requires temperatures low enough to form polar stratospheric clouds (PSCs), isolation from air in other stratospheric regions, and sunlight.

Distributing halogen gases. Halogen source gases emitted at Earth’s surface are present in comparable abundances

Minimum Air Temperatures in the Polar Stratosphere

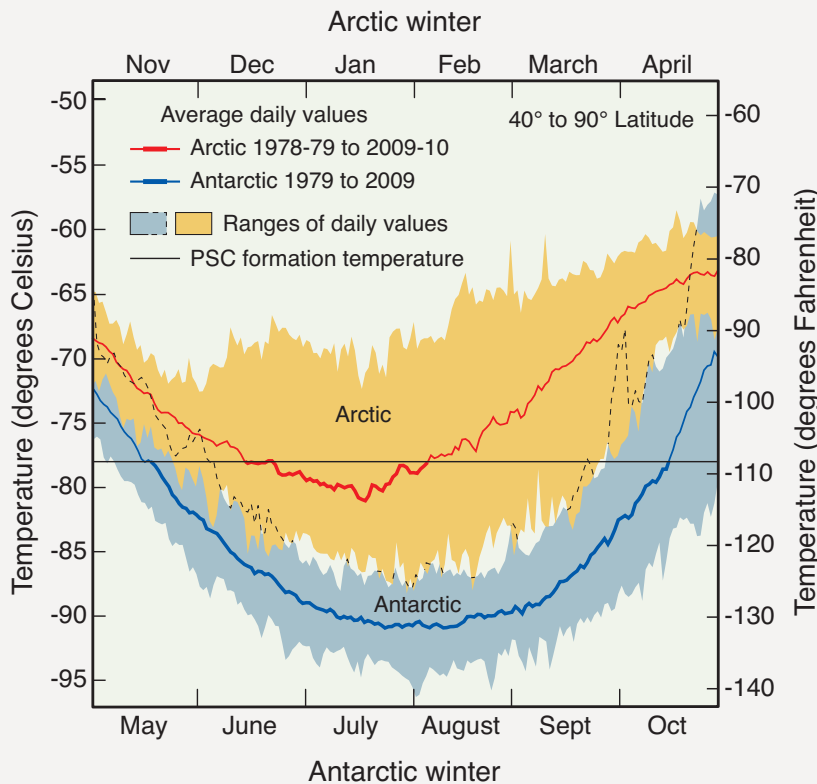


Figure Q10-1. Arctic and Antarctic temperatures.

Air temperatures in both polar regions reach minimum values in the lower stratosphere in the winter season. Average daily minimum values over Antarctica are as low as -90°C in July and August in a typical year. Over the Arctic, average minimum values are near -80°C in late December and January. Polar stratospheric clouds (PSCs) are formed in the polar ozone layer when winter minimum temperatures fall below the formation temperature of about -78°C . This occurs on average for 1 to 2 months over the Arctic and 5 to 6 months over Antarctica (see heavy red and blue lines). Reactions on liquid and solid PSC particles cause the highly reactive chlorine gas ClO to be formed, which catalytically destroys ozone (see Q9). The range of winter minimum temperatures found in the Arctic is much greater than in the Antarctic. In some years, PSC formation temperatures are not reached in the Arctic, and significant ozone

depletion does not occur. In contrast, PSC formation temperatures are always present for many months somewhere in the Antarctic, and severe ozone depletion now occurs in each winter season (see Q11). (Note that the dashed black lines denote the upper limits of the Antarctic temperature range where they overlap with the Arctic temperature range.)

throughout the stratosphere in both hemispheres even though most of the emissions occur in the Northern Hemisphere. The abundances are comparable because most source gases have no significant natural removal processes in the lower atmosphere and because winds and convection redistribute and mix air efficiently throughout the troposphere on the time-scale of weeks to months. Halogen gases (in the form of source gases and some reactive products) enter the stratosphere primarily from the tropical upper troposphere. Stratospheric air motions then transport these gases upward and toward the pole in both hemispheres.

Low polar temperatures. The severe ozone destruction represented by the ozone hole requires that low temperatures be present over a range of stratospheric altitudes, over large geographical regions, and for extended time periods. Low temperatures are important because they allow liquid and solid PSCs to form. Reactions on the surfaces of these PSCs initiate a remarkable increase in the most reactive chlorine gas, chlorine monoxide (ClO) (see below and Q8). Stratospheric temperatures are lowest in both polar regions in winter. In the Antarctic winter, minimum daily temperatures are generally much lower and less variable than in the Arctic winter (see Figure Q10-1). Antarctic temperatures also remain below the PSC formation temperature for much longer periods during winter. These and other meteorological differences occur because of the unequal distribution among land, ocean, and mountains between the hemispheres at middle and high latitudes. The winter temperatures are low enough for PSCs to form somewhere in the Antarctic for nearly the entire winter (about 5 months) and in the Arctic for only limited periods (10–60 days) in most winters.

Isolated conditions. Stratospheric air in the polar regions is relatively isolated from other stratospheric regions for long periods in the winter months. The isolation comes about because of strong winds that encircle the poles, forming a polar vortex, which prevents substantial motion of air into or out of the polar stratosphere. This circulation strengthens in winter as stratospheric temperatures decrease, with the result that the isolation of air in the vortex is much more effective in the Antarctic than the Arctic. Once chemical changes occur in polar regions from reactions on PSCs, the isolation preserves those changes for many weeks to months.

Polar stratospheric clouds (PSCs). Reactions on the surfaces of liquid and solid PSCs can substantially increase the relative abundances of the most reactive chlorine gases. These reactions convert the reservoir forms of reactive chlorine gases, chlorine nitrate (ClONO₂) and hydrogen chloride

(HCl), to the most reactive form, ClO (see Figure Q8-1). ClO increases from a small fraction of available reactive chlorine to comprise nearly all chlorine that is available. With increased ClO, additional catalytic cycles involving ClO and BrO become active in the chemical destruction of ozone whenever sunlight is available (see Q9).

Different types of liquid and solid PSC particles form when stratospheric temperatures fall below about -78°C (-108°F) in polar regions (see Figure Q10-1). As a result, PSCs are often found over large areas of the winter polar regions and over significant altitude ranges. With a temperature threshold of

Arctic Polar Stratospheric Clouds (PSCs)



Figure Q10-2. Polar stratospheric clouds. This photograph of an Arctic polar stratospheric cloud (PSC) was taken from the ground at Kiruna, Sweden (67°N), on 27 January 2000. PSCs form in the ozone layer during winters in the Arctic and Antarctic stratospheres wherever low temperatures occur (see Figure Q10-1). The particles grow from the condensation of water and nitric acid (HNO_3). The clouds often can be seen with the human eye when the Sun is near the horizon. Reactions on PSCs cause the highly reactive chlorine gas ClO to be formed, which is very effective in the chemical destruction of ozone (see Q9).

-78°C , PSCs exist in larger regions and for longer time periods in the Antarctic than the Arctic. The most common type of PSC forms from nitric acid (HNO_3) and water condensing on pre-existing liquid sulfuric acid-containing particles. Some of these particles freeze to form reactive solid particles. At even lower temperatures (-85°C or -121°F), water condenses to form ice particles. PSC particles grow large enough and are numerous enough that cloud-like features can be observed from the ground under certain conditions, particularly when the Sun is near the horizon (see Figure Q10-2). PSCs are often found near mountain ranges in polar regions because the motion of air over the mountains can cause local cooling of stratospheric air, which increases condensation of water and HNO_3 .

When average temperatures begin increasing by late winter, PSCs form less frequently and their surface conversion reactions produce less ClO. Without continued ClO production, ClO amounts decrease and other chemical reactions re-form the reactive reservoirs, ClONO_2 and HCl. When PSC temperatures no longer occur, on average, either by late January to early February in the Arctic or by mid-October in the Antarctic, the most intense period of ozone depletion ends.

Nitric acid and water removal. Once formed, PSC particles fall to lower altitudes because of gravity. The largest particles can descend several kilometers or more in the stratosphere during the low-temperature winter/spring period that lasts several months in Antarctica. Because PSCs often contain a significant fraction of available HNO_3 , their descent removes HNO_3 from regions of the ozone layer. This process is called *denitrification* of the stratosphere. With less HNO_3 , the highly reactive chlorine gas ClO remains chemically active for a longer period, thereby increasing chemical ozone destruction. Significant denitrification occurs each

winter in the Antarctic and in some, but not all, Arctic winters, because PSC formation temperatures must be sustained over an extensive altitude region and time period to effect denitrification (see Figure Q10-1).

Ice particles form when temperatures are a few degrees lower than PSC formation temperatures. If ice temperatures persist for weeks to months over extensive altitude regions, ice particles will also fall several kilometers due to gravity. As a result, a significant fraction of water vapor can also be removed from regions of the ozone layer. This process is called *dehydration* of the stratosphere. With the low temperatures required to form ice, dehydration is common in the Antarctic and rare in the Arctic winters. The removal of water vapor does not directly affect the catalytic reactions that destroy ozone. Dehydration indirectly affects ozone destruction by suppressing PSC formation, which reduces ClO production in PSC reactions.

Discovering the role of PSCs. Ground-based observations of PSCs, and knowledge of their formation processes, were available many years before the role of PSCs in polar ozone destruction was recognized. The geographical and altitude extent of PSCs in both polar regions was not known fully until PSCs were observed by a satellite instrument in the late 1970s. The role of PSC particles in converting reactive chlorine gases to ClO was not understood until after the discovery of the Antarctic ozone hole in 1985. Our understanding of the chemical role of PSC particles developed from laboratory studies of their surface reactivity, computer modeling studies of polar stratospheric chemistry, and measurements that directly sampled particles and reactive chlorine gases, such as ClO, in the polar stratosphere.

The Discovery of the Antarctic Ozone Hole

The first decreases in Antarctic total ozone were observed in the early 1980s over research stations located on the Antarctic continent. The measurements were made with ground-based Dobson spectrophotometers (see box in Q5). The observations showed unusually low total ozone during the late winter/early spring months of September, October, and November. Total ozone was lower in these months compared with previous observations made as early as 1957. The early published reports came from the Japan Meteorological Agency and the British Antarctic Survey. The results became widely known to the world after three scientists from the British Antarctic Survey published their observations in the scientific journal *Nature* in 1985 and speculated that CFCs were the cause. Soon after, satellite measurements confirmed the spring ozone depletion and further showed that in each late winter/early spring season starting in the early 1980s, the depletion extended over a large region centered near the South Pole. The term “ozone hole” came about as a description of the very low total ozone values that encircled the Antarctic continent in satellite images for many weeks (see Q11). Currently, the formation and severity of the Antarctic ozone hole are documented each year by a combination of satellite, ground-based, and balloon observations of ozone.

Very early Antarctic ozone measurements. The first total ozone measurements made in Antarctica with Dobson spectrophotometers occurred in the 1950s following extensive measurements in the Northern Hemisphere and Arctic region. Total ozone values found in spring were around 300 DU, surprisingly lower than in the Arctic spring, because the assumption then was that the two polar regions would have similar values. We now know that these Antarctic values were not anomalous; indeed they are similar to those observed there in the 1970s before the ozone hole appeared (see Figure Q11-3). We also now know that Antarctic total ozone values, in comparison with Arctic values, are systematically lower in the early spring because the polar vortex is much stronger and, therefore, much more effective in reducing the transport of ozone-rich air from midlatitudes to the pole (compare Figures Q11-3 and Q12-2).

In 1958, measurements of total ozone were made at the Dumont d’Urville station (66.7°S, 140°E) in Antarctica using a photographic plate method to analyze solar ultraviolet radiation after it passed through the ozone layer. The reported measurements were anomalously low, reaching 110–120 DU in September and October. These values are similar to minimum ozone hole values now routinely observed over Antarctica in the same months (see Figure Q11-2). Some have speculated that these limited observations provide evidence that an ozone hole existed before ODS emissions were large enough to cause the depletion. However, analyses of the more extensive Dobson spectrophotometer measurements made at several other Antarctic locations in 1958 did not confirm the low total ozone values. These measurements indicate that the photographic plate determinations were not a reliable source of total ozone values at the Dumont d’Urville station in 1958.

Q11

How severe is the depletion of the Antarctic ozone layer?

Severe depletion of the Antarctic ozone layer was first reported in the mid-1980s. Antarctic ozone depletion is seasonal, occurring primarily in late winter and early spring (August–November). Peak depletion occurs in early October when ozone is often completely destroyed over a range of altitudes, thereby reducing total ozone by as much as two-thirds at some locations. This severe depletion creates the “ozone hole” apparent in images of Antarctic total ozone made using satellite observations. In most years the maximum area of the ozone hole far exceeds the size of the Antarctic continent.

The severe depletion of Antarctic ozone, known as the “ozone hole,” was first reported in the mid-1980s. The depletion is attributable to chemical destruction by reactive halogen gases that increased in the stratosphere in the latter half of the 20th century (see Q16). Conditions in the Antarctic winter and early spring stratosphere are highly suitable for ozone depletion because of (1) the long periods of extremely low temperatures, which cause polar stratospheric clouds (PSCs) to form; (2) the large abundance of reactive halogen gases produced in reactions on PSCs; and (3) the isolation of stratospheric air, which allows time for chemical destruction processes to occur. The severity of Antarctic ozone depletion

can be seen using satellite observations of total ozone, ozone altitude profiles, and long-term changes in total ozone.

Antarctic ozone hole. The most widely used images of Antarctic ozone depletion are derived from measurements of total ozone made with satellite instruments. A map of Antarctic early spring measurements shows a large region centered near the South Pole in which total ozone is highly depleted (see Figure Q11-1). This region has come to be called the “ozone hole” because of the near-circular contours of low ozone values in the maps. The area of the ozone hole is defined here as the geographical region contained within the 220-Dobson unit (DU) contour in total ozone maps (see white line in Figure

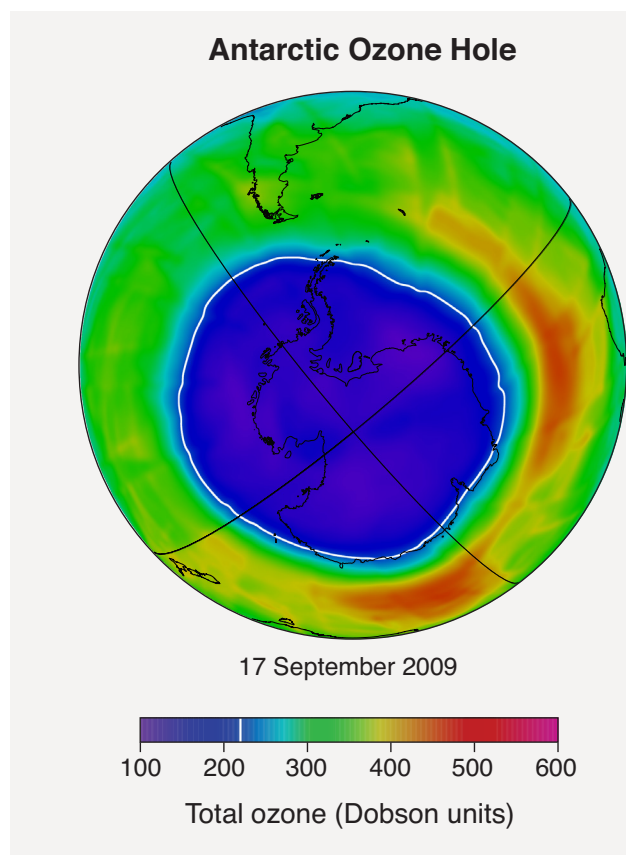


Figure Q11-1. Antarctic ozone hole. Total ozone values are shown for high southern latitudes on 17 September 2009 as measured by a satellite instrument. The dark blue and purple regions over the Antarctic continent show the severe ozone depletion or “ozone hole” now found during every spring. Minimum values of total ozone inside the ozone hole are close to 100 Dobson units (DU) compared with normal Antarctic springtime values of about 350 DU (see Figure Q11-3). The ozone hole area is usually defined as the geographical area within the 220-DU contour (see white line) on total ozone maps. In late spring or early summer (November–December) the ozone hole disappears in satellite images as ozone-depleted air is displaced and mixed with ozone-rich air transported toward the pole from outside the ozone hole. Note that maximum total ozone values in the Southern Hemisphere in this late winter period are generally located in a crescent-shaped region surrounding the ozone hole.

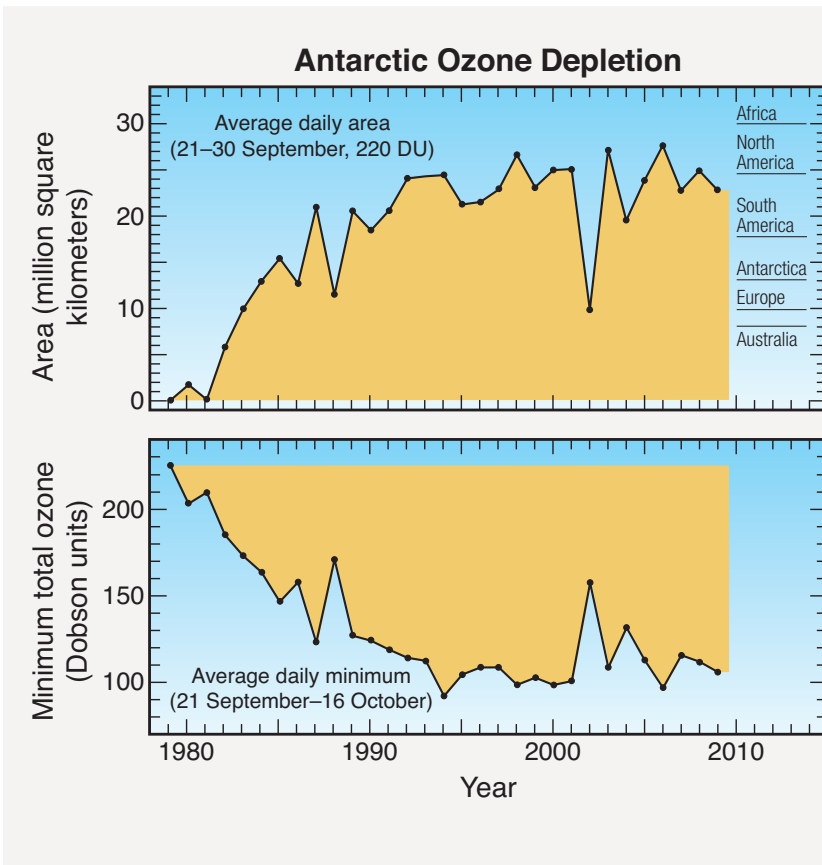


Figure Q11-2. Antarctic ozone hole features. Long-term changes are shown for key aspects of the Antarctic ozone hole: the area enclosed by the 220-DU contour on maps of total ozone (upper panel) and the minimum total ozone amount within the 220-DU contour (lower panel). The values are derived from satellite observations and averaged for each year at a time near the peak of ozone depletion, as defined by the dates shown in each panel. The areas of continents are included for reference in the upper panel. The magnitude of ozone depletion gradually increased beginning in 1980. In the 1990s, the depletion reached steady year-to-year values, except for the unusually low depletion in 2002 (see Figure Q11-4 and following box). The magnitude of Antarctic ozone depletion will decrease as ODSs are removed from the atmosphere (see Figure Q16-1). The return of Antarctic total ozone to 1980 values is not expected to occur before 2050 (see Q20).

Q11-1). The maximum area has reached 25 million square kilometers (about 10 million square miles) in recent years, which is nearly twice the area of the Antarctic continent (see Figure Q11-2). Minimum values of total ozone inside the ozone hole averaged in late September to mid-October are near 100 DU, which is two-thirds below normal springtime values of about 350 DU (see Figures Q11-3 and Q12-1). Low total ozone inside the ozone hole contrasts strongly with the distribution of much larger values *outside* the ozone hole. This common feature can also be seen in Figure Q11-1, where a crescent-shaped region with maximum values of about 500 DU surrounds a large portion of the ozone hole in September 2009.

Altitude profiles of Antarctic ozone. The low total ozone values within the ozone hole are caused by nearly complete removal of ozone in the lower stratosphere. Balloonborne instruments (see Q5) demonstrate that this depletion occurs within the ozone layer, the altitude region that normally contains the highest ozone abundances. At geographic locations with the lowest total ozone values, balloon measurements show that the chemical destruction of ozone is complete over an altitude region of several kilometers. For example, in the ozone profile over South Pole, Antarctica, on 9 October 2006 (see Figure Q12-3), ozone abundances are essentially zero over

the altitude region of 14 to 21 kilometers. The lowest winter temperatures and highest reactive chlorine (ClO) abundances occur in this altitude region (see Figure Q8-3). The differences in the average South Pole ozone profiles between the decades 1962–1971 and 1990–2009 in Figure Q12-3 show how reactive halogen gases have dramatically altered the ozone layer. In the 1960s, a normal ozone layer is clearly evident in the October average profile with a peak near 16 kilometers altitude. In the 1990–2009 average profile, a broad minimum centered near 16 kilometers now occurs with ozone values reduced by up to 90% of normal values.

Long-term total ozone changes. The significant springtime ozone depletion represented by the ozone hole has only been observed since the early 1980s even though low winter temperatures and isolated conditions occur each year in the Antarctic stratosphere. Prior to 1980, the amounts of reactive halogen gases in the stratosphere were insufficient to cause significant depletion. Satellite observations can be used in multiple ways to examine how ozone depletion has changed in the Antarctic region over the last 30–40 years:

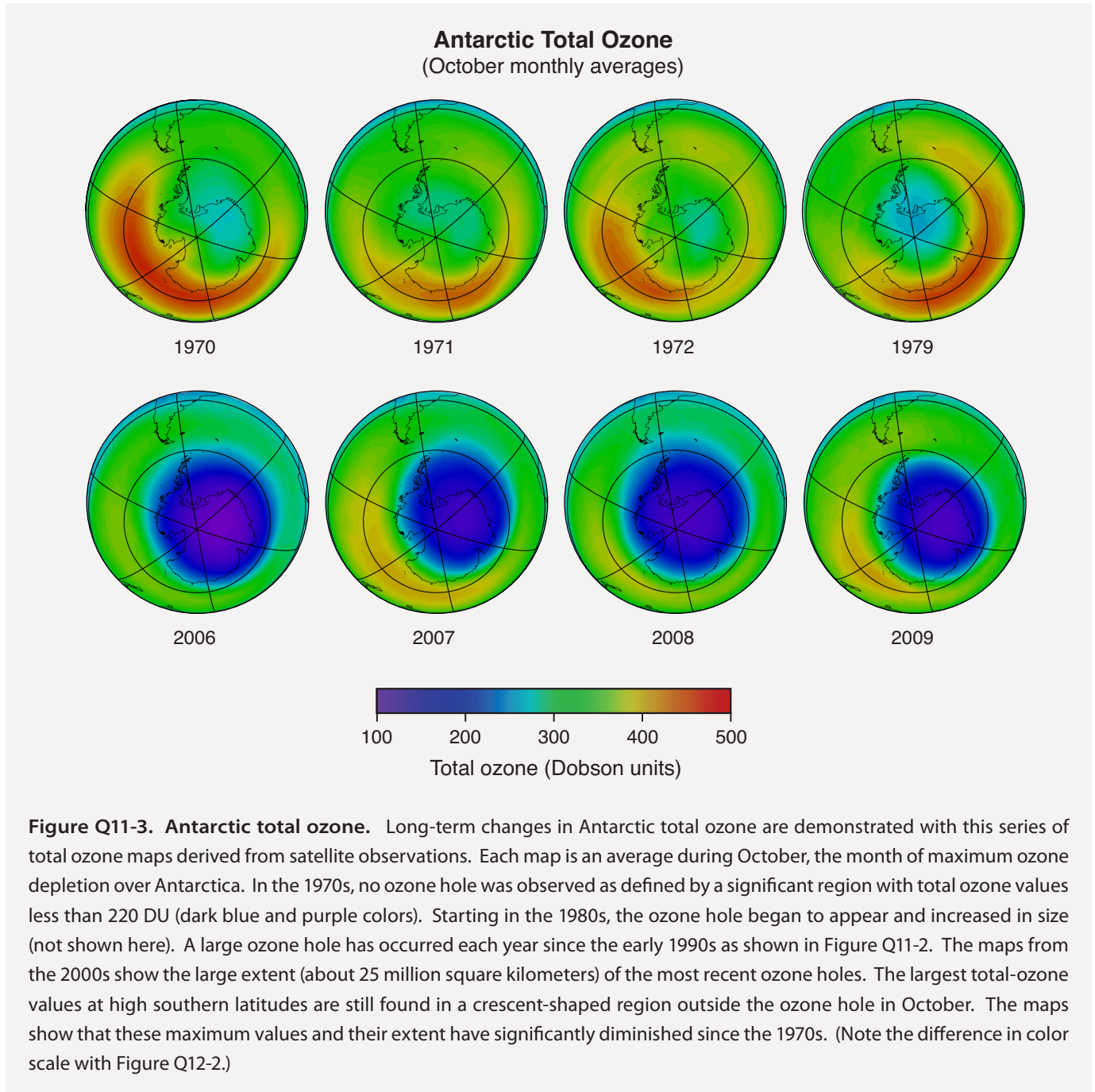
- First, *ozone hole areas* displayed in Figure Q11-2 show that depletion has increased since 1980 to become fairly stable in the 1990s and early 2000s near a value of 25 million

square kilometers. The exception is the unexpected low depletion in 2002, which is explained in the box at the end of this Question. The ozone-hole area is defined here as the geographical area inside the 220-DU contour on total ozone maps (see Figure Q11-1).

- ▶ Second, *minimum Antarctic ozone* amounts displayed in Figure Q11-2 show that the severity of the depletion has increased beginning around 1980 along with the ozone hole area. Fairly constant minimum values near 100 DU

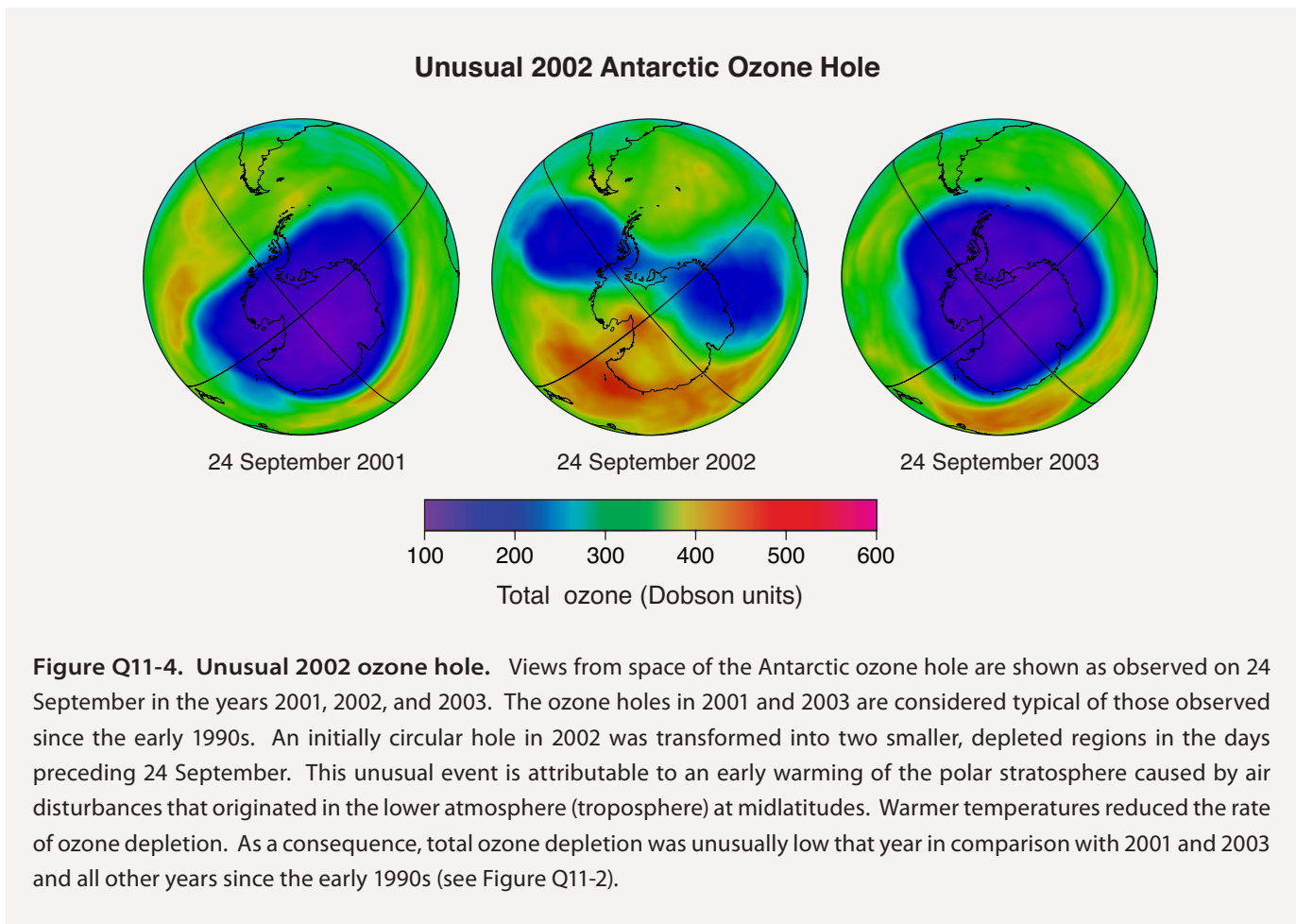
were observed in the 1990s and 2000s with 2002 being an exception.

- ▶ Third, *total ozone maps* over the Antarctic and surrounding regions show how the ozone hole has developed over time (see Figure Q11-3). October averages of total ozone confirm the absence of an ozone hole in the 1970s and its persistent occurrence in the late 2000s.
- ▶ Fourth, values of *total ozone poleward of 63°S* averaged for each October show how total ozone has changed when



averaged over the ozone hole and its surrounding areas (see Figure Q12-1). The values decrease strongly starting from those found in the 1970s and now are approximately 37% less than in pre-ozone-hole years (1970–1982). The average values show a larger year-to-year variability than found for the other ozone measures noted above because the average includes areas outside the ozone hole where the distribution of total ozone varies in response to meteorological conditions. The maps in Q11-3 show also how the maximum in total ozone surrounding the ozone hole each year has diminished over the last three decades, adding to the decreases noted in Figure Q12-1.

Disappearance of the ozone hole in spring. The severe depletion of Antarctic ozone occurs in the late winter/early spring season. In spring, temperatures in the polar lower stratosphere increase (see Figure Q10-1), ending PSC formation and reactions on aerosols and, consequently, the most effective chemical cycles that destroy ozone. Winter-time isolation of high-latitude air ends during this time with increasing exchange of air between the Antarctic stratosphere and lower latitudes. This allows substantial amounts of ozone-rich air to be transported poleward, where it displaces or mixes with air depleted in ozone. As a result of these large-scale transport and mixing processes, the ozone hole disappears by December.



The 2002 Antarctic Ozone Hole

The 2002 Antarctic ozone hole showed features that looked surprising at the time (see Figure Q11-4). It had much less ozone depletion as measured by the area of the ozone hole or minimum total-ozone amounts in comparison with the 2001 ozone hole. The 2002 values now stand out clearly in the year-to-year changes in these quantities displayed in Figure Q11-2. There were no forecasts of an ozone hole with unusual features in 2002 because the chemical and meteorological conditions required to deplete ozone, namely low temperatures and available reactive halogen gases, were present that year and did not differ substantially from previous years. The ozone hole initially formed as expected in August and early September 2002. Later, during the last week of September, an unexpected and surprisingly strong meteorological event occurred that dramatically reshaped the ozone hole into two separate depleted regions. As a result of this disturbance, the combined area of these two regions in late September and early October was significantly less than that observed for the previous or subsequent ozone holes.

The unexpected meteorological influence in 2002 resulted from specific atmospheric air motions that sometimes occur in polar regions. Meteorological analyses of the Antarctic stratosphere show that it was warmed by very strong, large-scale weather systems that originated in the lower atmosphere (troposphere) at midlatitudes in late September. At that time, Antarctic temperatures are generally very low (see Q10) and ozone destruction rates are near their peak values. The influence of these tropospheric systems extended poleward and upward into the stratosphere, disturbing the normal circumpolar wind flow (polar vortex) and warming the lower stratosphere where ozone depletion was ongoing. Higher temperatures reduced the rate of ozone depletion and led to the higher minimum values observed for total ozone in Figure Q11-2. The higher-than-normal impact of these weather disturbances during the critical time period for ozone loss reduced the total loss of ozone in 2002.

The strong influence of the 2002 warming event is unique in the many decades of Antarctic meteorological observations. Another warming event occurred in 1988 causing smaller changes in the ozone hole features in Figure Q11-2. Large warming events are difficult to predict because of the complex conditions leading to their formation.

In 2003 through 2009, ozone hole features returned to values observed from the mid-1990s to 2001 (see Figure Q11-2). The high ozone depletion found since the mid-1990s, with the exception of 2002, is expected to be typical of coming years. A significant, sustained reduction of Antarctic ozone depletion, leading to full recovery of total ozone, requires comparable, sustained reductions of ODSs in the stratosphere. Even with the source gas reductions already underway (see Q16), the return of Antarctic total ozone to 1980 values is not expected to occur before 2050.

Q12

Is there depletion of the Arctic ozone layer?

Yes, significant depletion of the Arctic ozone layer now occurs in most years in the late winter/early spring period (January–March). However, the maximum depletion is less severe than that observed in the Antarctic and is more variable from year to year. A large and recurrent “ozone hole,” as found in the Antarctic stratosphere, does not occur in the Arctic.

Significant depletion of total ozone has been observed in the Arctic stratosphere in recent decades. The depletion is attributable to chemical destruction by reactive halogen gases, which increased in the stratosphere in the latter half of the 20th century (see Q16). Arctic depletion also occurs in the late winter/early spring period (January–March) over a somewhat shorter period than in the Antarctic (July–October). Similar to the Antarctic (see Q11), Arctic depletion occurs because of (1) the periods of extremely low temperatures, which cause polar stratospheric clouds (PSCs) to form; (2) the large abundance of reactive halogen gases produced in reactions on PSCs; and (3) the isolation of stratospheric air, which allows time for chemical destruction processes to occur.

Arctic ozone depletion is much less than that observed each Antarctic winter/spring season. Large and recurrent ozone holes as found in the Antarctic stratosphere do not occur in the Arctic. Depletion is limited because, in comparison to Antarctic conditions, Arctic average temperatures are always significantly higher (see Figure Q10-1) and the isolation of stratospheric air is less effective. Temperature and other meteorological differences occur because northern polar latitudes have more land and mountainous regions than southern polar latitudes (compare Figures Q11-3 and Q12-2). In a few Arctic winters, for example, PSCs did not form because temperatures never reached low enough values. These differences cause the extent and timing of Arctic ozone depletion to vary considerably from year to year. Depletion in some winter/spring seasons occurs over many weeks; in others only for brief early or late periods; and in some not at all.

Long-term total ozone changes. Satellite observations can be used in two important ways to examine the average total ozone abundances in the Arctic region for the last 30–40 years and to contrast these values with Antarctic abundances:

- First, *total ozone poleward of 63°N* averaged for each March shows quantitatively how total ozone has changed in the Arctic (see Figure Q12-1). The seasonal poleward and downward transport of ozone-rich air is naturally stron-

ger in the Northern Hemisphere. As a result, total ozone values at the *beginning* of each winter season in the Arctic are considerably higher than in the Antarctic. Before depletion sets in, normal Arctic values are close to 450 DU and Antarctic values near 330 DU. Decreases from pre-ozone-hole average values (1970–1982) were observed in the Arctic by the mid-1980s, when larger changes were already occurring in the Antarctic. The decreases in total ozone have reached a maximum of about 30% and generally remain smaller than those found in the Antarctic. The low value of Arctic total ozone in March 1997 relative to 1970–1982 observations is the most comparable to Antarctic depletion. In the 1996/1997 Arctic winter, low temperatures facilitated large amounts of chemical depletion, while meteorological conditions kept ozone transport to high latitudes below average values.

Overall, the Arctic values tend to show larger year-to-year variability than in the Antarctic. Ozone differences from the 1970-to-1982 average value are due to a combination of chemical destruction by ODSs and meteorological (natural) variations. In the last two decades, these two aspects have contributed about equally to observed ozone changes. The amount of chemical destruction depends in large part on stratospheric temperatures. Meteorological conditions determine how well Arctic stratospheric air is isolated from ozone-rich air at lower latitudes and influence the extent of low temperatures.

- Second, *total ozone maps* over the Arctic and surrounding regions (see Figure Q12-2) show year-to-year changes in March total ozone. In the 1970s, total ozone values were near 450 DU when averaged over the Arctic region in March. Beginning in the 1990s and continuing into the late 2000s, values above 450 DU were increasingly absent from the March average maps. A comparison of the 1971 and 2009 maps, for example, shows a striking reduction of total ozone throughout the Arctic region. The large geographical extent of low total ozone in the map of March 1997 is rare in

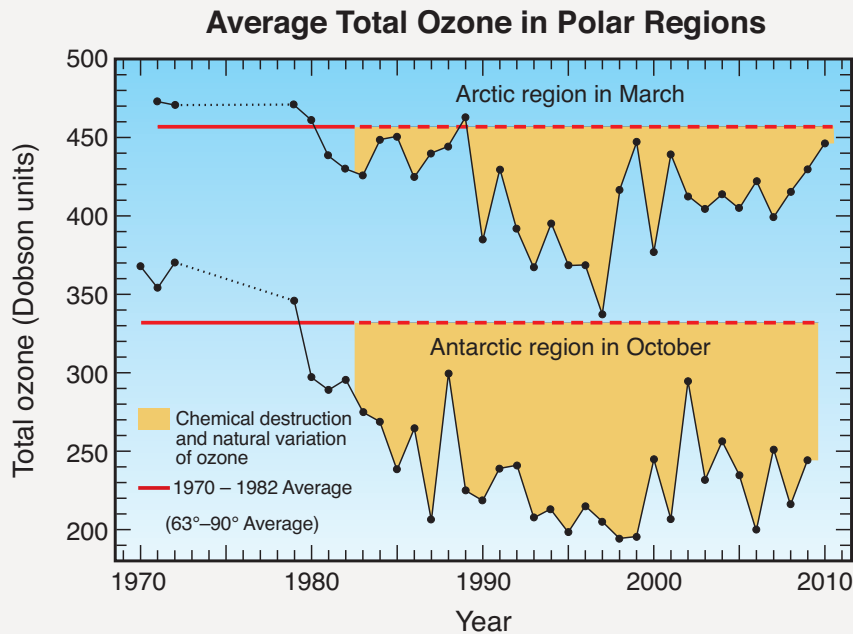


Figure Q12-1. Average total ozone in polar regions. Long-term changes in average total ozone are shown for the Antarctic and Arctic for the respective regions defined by latitudes between 63° and 90°. Total ozone is measured with satellite instruments. The reference values (red lines) are averages of springtime total ozone values available from observations between 1970 and 1982. Each point represents a monthly average for October in the Antarctic or March in the Arctic. After 1982, significant ozone depletion is found in most years in the Arctic and all years in the Antarctic. The largest average depletions have occurred in the Antarctic

since 1990. The ozone changes are the combination of chemical destruction and natural variations. Variations in meteorological conditions influence the year-to-year changes in ozone, particularly in the Arctic. Essentially all of the decrease in the Antarctic and usually about 50% of the decrease in the Arctic each year are attributable to chemical destruction by reactive halogen gases. In the Arctic, the other 50% is attributable to natural variations in the amounts of ozone transported to polar regions before and during winter. Average total ozone values over the Arctic are naturally larger at the beginning of each winter season because, in the preceding months, more ozone is transported poleward in the Northern Hemisphere than in the Southern Hemisphere.

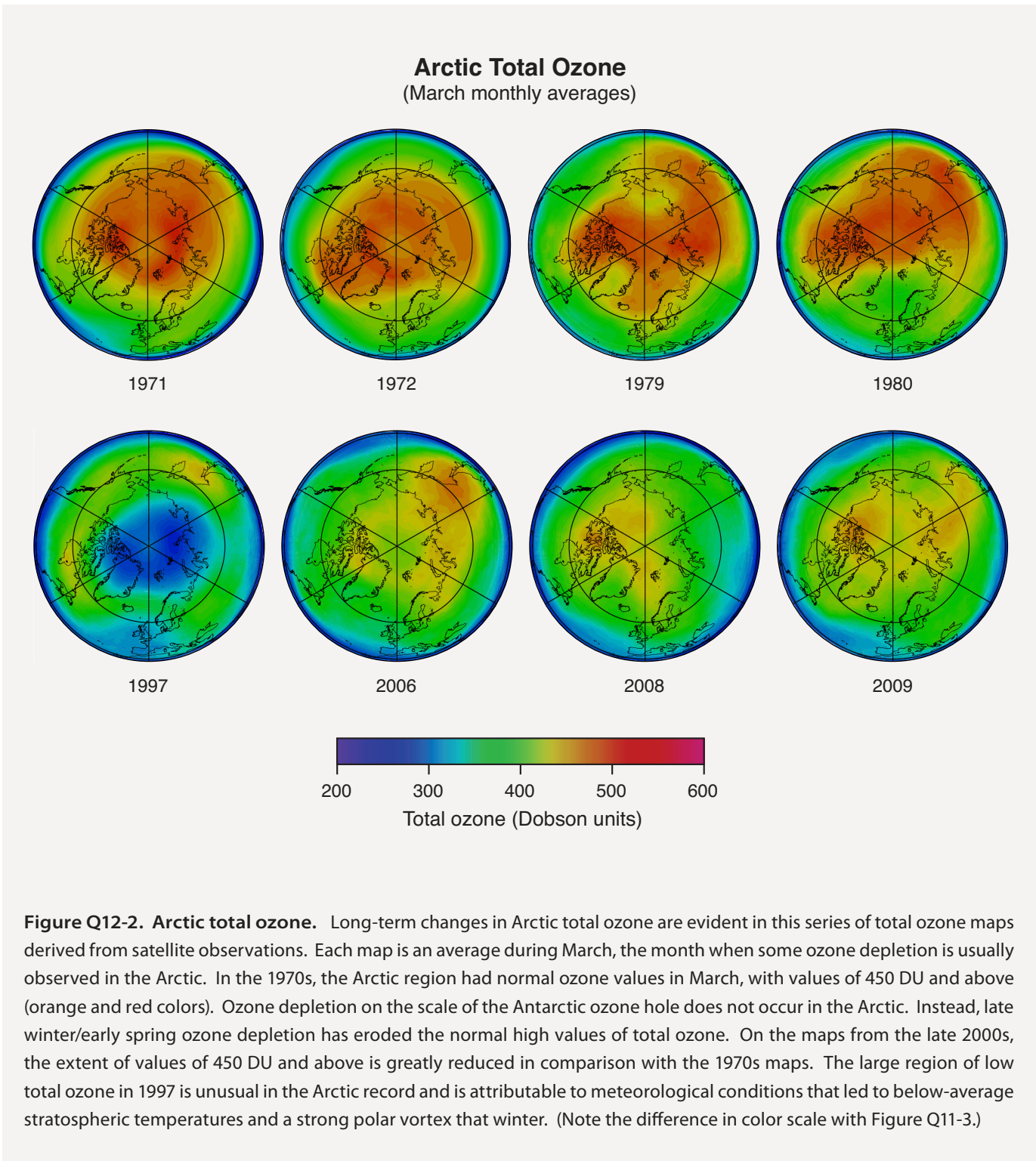
the Arctic observational record of the last three decades as noted above in the discussion of Figure Q12-1.

Altitude profiles of Arctic ozone. Arctic ozone is measured using a variety of instruments (see Q5), as in the Antarctic, to document daily to seasonal changes within the ozone layer. Spring Arctic and Antarctic balloonborne measurements are contrasted in Figure Q12-3 using Arctic profiles from the Ny-Ålesund research station at 79°N. For 1991–2009, the March average reveals a substantial ozone layer and total ozone of 382 DU, contrasting sharply with the severely depleted Antarctic ozone layer in the October average for these years. This further demonstrates how higher stratospheric temperatures and meteorological variability have protected the Arctic ozone layer from the greater ozone losses that occur in the Antarctic, despite similar reactive halogen abundances in the two regions.

The separate Arctic profile shown for 29 March 1996 is one of the most severely depleted in the two-decade record from Ny-Ålesund. Although significant, this depletion is modest in

comparison to that routinely observed in the Antarctic, such as in the profile from 9 October 2006. The near-complete depletion of ozone over many kilometers in altitude, as is now common in the Antarctic stratosphere, has never been observed in the Arctic.

Restoring ozone in spring. As in the Antarctic, ozone depletion in the Arctic is confined to the late winter/early spring season. In spring, temperatures in the polar lower stratosphere increase (see Figure Q10-1), ending PSC formation and reactions on aerosols, as well as the most effective chemical cycles that destroy ozone. Wintertime isolation of high-latitude air ends during this time with increasing exchange of air between the Arctic stratosphere and lower latitudes. This allows more ozone-rich air to be transported poleward, where it displaces or mixes with air in which ozone may have been depleted. As a result of this large-scale transport and mixing processes, any ozone depletion disappears by April or earlier.



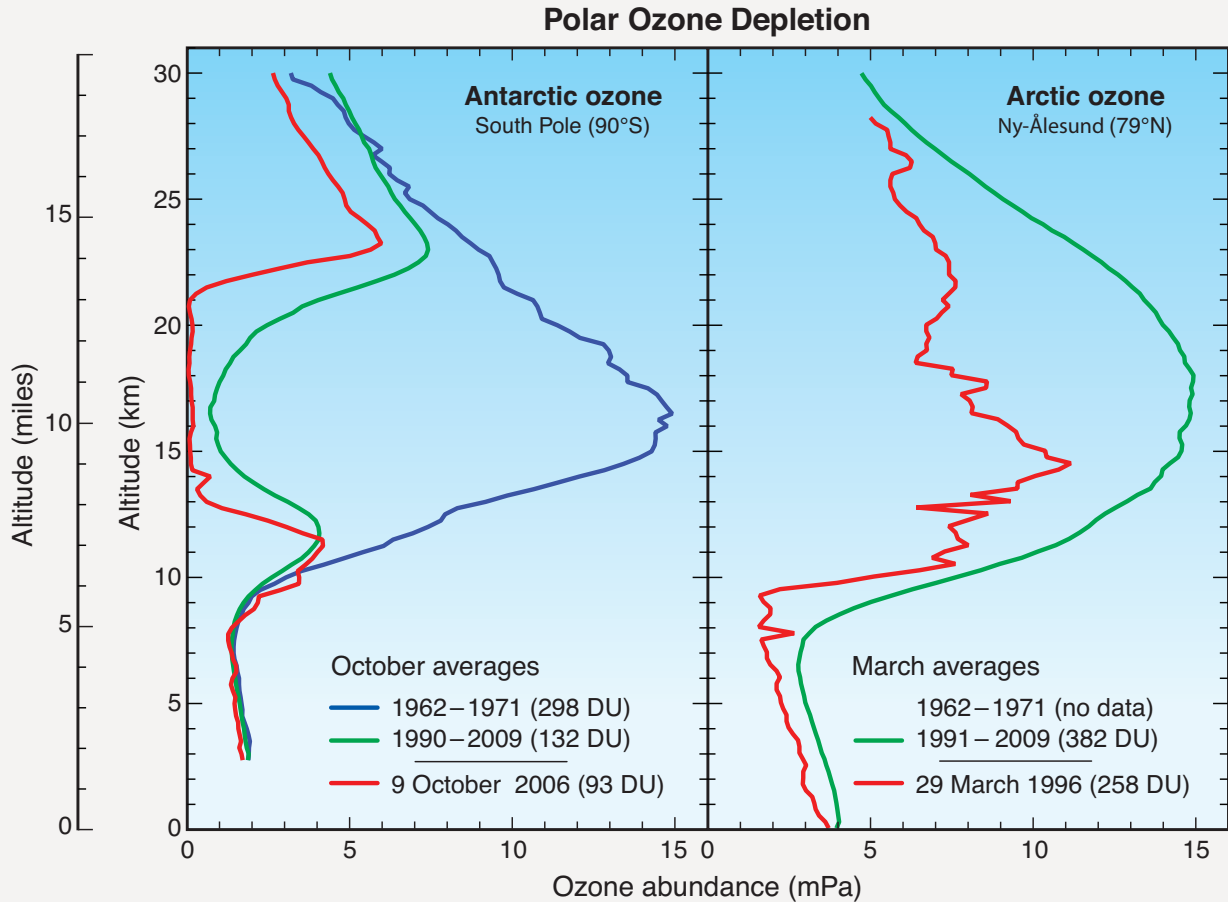


Figure Q12-3. Vertical distribution of Arctic and Antarctic ozone. Most stratospheric ozone resides between about 10 and 30 kilometers (6 to 19 miles) above Earth’s surface. Long-term observations of the ozone layer with balloonborne instruments allow winter ozone altitude profiles to be compared between the Antarctic and Arctic regions. In the Antarctic at the South Pole (left panel), a normal ozone layer was observed to be present between 1962 and 1971. In more recent years, as shown here for 9 October 2006, ozone is almost completely destroyed between 14 and 21 kilometers (9 to 13 miles) in the Antarctic in spring. Average October values in the last decades (1990–2009) are 90% lower than pre-1980 values at the peak altitude of the ozone layer (16 kilometers). In contrast, the Arctic ozone layer is still present in spring as shown by the average March profile for 1991–2009 obtained over the Ny-Ålesund site (right panel). No Ny-Ålesund data are available for the 1962–1971 period before significant ODS destruction began. Some March profiles do reveal significant depletion, as shown here for 29 March 1996. In such years, winter minimum temperatures are generally lower than normal, allowing PSC formation for longer periods. Arctic profiles with depletion similar to that shown for 9 October 2006 at the South Pole have never been observed. The number in parentheses for each profile is the total ozone value in Dobson units (DU). Ozone abundances are shown here as the pressure of ozone at each altitude using the unit “milli-Pascals” (mPa) (100 million mPa = atmospheric sea-level pressure).

Q13

How large is the depletion of the global ozone layer?

Depletion of the global ozone layer began gradually in the 1980s and reached a maximum of about 5% in the early 1990s. The depletion has lessened since then and now is about 3.5% averaged over the globe. The average depletion exceeds the natural year-to-year variations of global total ozone. The ozone loss is very small near the equator and increases with latitude toward the poles. The larger polar depletion is attributed to the late winter/early spring ozone destruction that occurs there each year.

Global total ozone has decreased beginning in the 1980s (see Figure Q13-1). The decreases have occurred in the stratospheric ozone layer where most ozone resides (see Figure Q1-2). In the early 1990s, the depletion of global total ozone reached a maximum of about 5% below the 1964–1980 average. The depletion has lessened since then and now averages about 3.5% for 2006–2009. The observations shown in Figure Q13-1 have been smoothed to remove regular ozone changes that are due to natural seasonal and solar effects (see Q14). The depleted amounts are larger than the remaining natural variations in global total ozone amounts.

The observed global ozone depletion in the last three decades is attributable to increases in reactive halogen gases in the stratosphere. The lowest global total ozone values since 1980 have occurred in the years following the eruption of Mt. Pinatubo in 1991, which temporarily increased the number of sulfuric acid-containing particles throughout the stratosphere. These particles significantly increased the effectiveness of reactive halogen gases in destroying ozone (see Q14) and, thereby, increased global ozone depletion by 1–2% for several years following the eruption.

Polar regions. Observed total ozone depletion varies significantly with latitude on the globe (see Figure Q13-1). The largest reductions have occurred at high southern latitudes as a result of the severe ozone loss over Antarctica each late winter/early spring period. The next largest losses are observed in the high latitudes of the Northern Hemisphere, caused in part by winter losses over the Arctic. Although the depletion in polar regions is larger than at lower latitudes, the influence of polar regions on global ozone is limited by their small geographical area. Latitudes above 60° account for only about 13% of Earth's surface.

Midlatitude regions. Ozone depletion is also observed at the midlatitudes spanning the region between equatorial and polar latitudes. In comparison with the 1964–1980 averages, total ozone averaged for 2005–2009 is about 3.5% lower

in northern midlatitudes (35°N–60°N) and about 6% lower at southern midlatitudes (35°S–60°S). Midlatitude depletion has two contributing factors. First, ozone-depleted air over both polar regions is dispersed away from the poles during and after each winter/spring period, thereby reducing average ozone at nonpolar latitudes. Second, chemical destruction occurring at midlatitudes contributes to observed depletion in these regions. This contribution is much smaller than in polar regions because the amounts of reactive halogen gases are lower and a seasonal increase of the most reactive halogen gases, such as the increase in ClO in Antarctic late winter (see Figure Q8-3), does not occur in midlatitude regions.

Tropical region. There has been little or no depletion of total ozone in the tropics (20°N–20°S latitude). In this region of the lower stratosphere, air has only recently (less than 18 months) been transported from the lower atmosphere (troposphere). As a result, the conversion of ozone-depleting substances (ODSs) to reactive halogen gases is very small. With so little reactive halogen amounts, total ozone depletion in this region is also very small. In addition, ozone production is high in the tropical stratosphere because average solar ultraviolet radiation is highest in the tropics. In contrast, stratospheric air in polar regions has been in the stratosphere for an average of 4 to 7 years, allowing time for significant conversion of ODSs to reactive halogen gases. The systematic differences in the age of stratospheric air are a well-understood consequence of the large-scale atmospheric transport: air enters the stratosphere in the tropics, moves poleward into both hemispheres, and then descends and ultimately returns to the lower atmosphere.

Recovery of global ozone. Global ozone is no longer declining as it was in the 1980s and early 1990s because ODSs are no longer increasing in the atmosphere (see Q16). During recovery from ODSs, global total ozone is expected to reach 1980 and earlier values in the coming decades. The recovery process depends on the slow removal of ODSs from

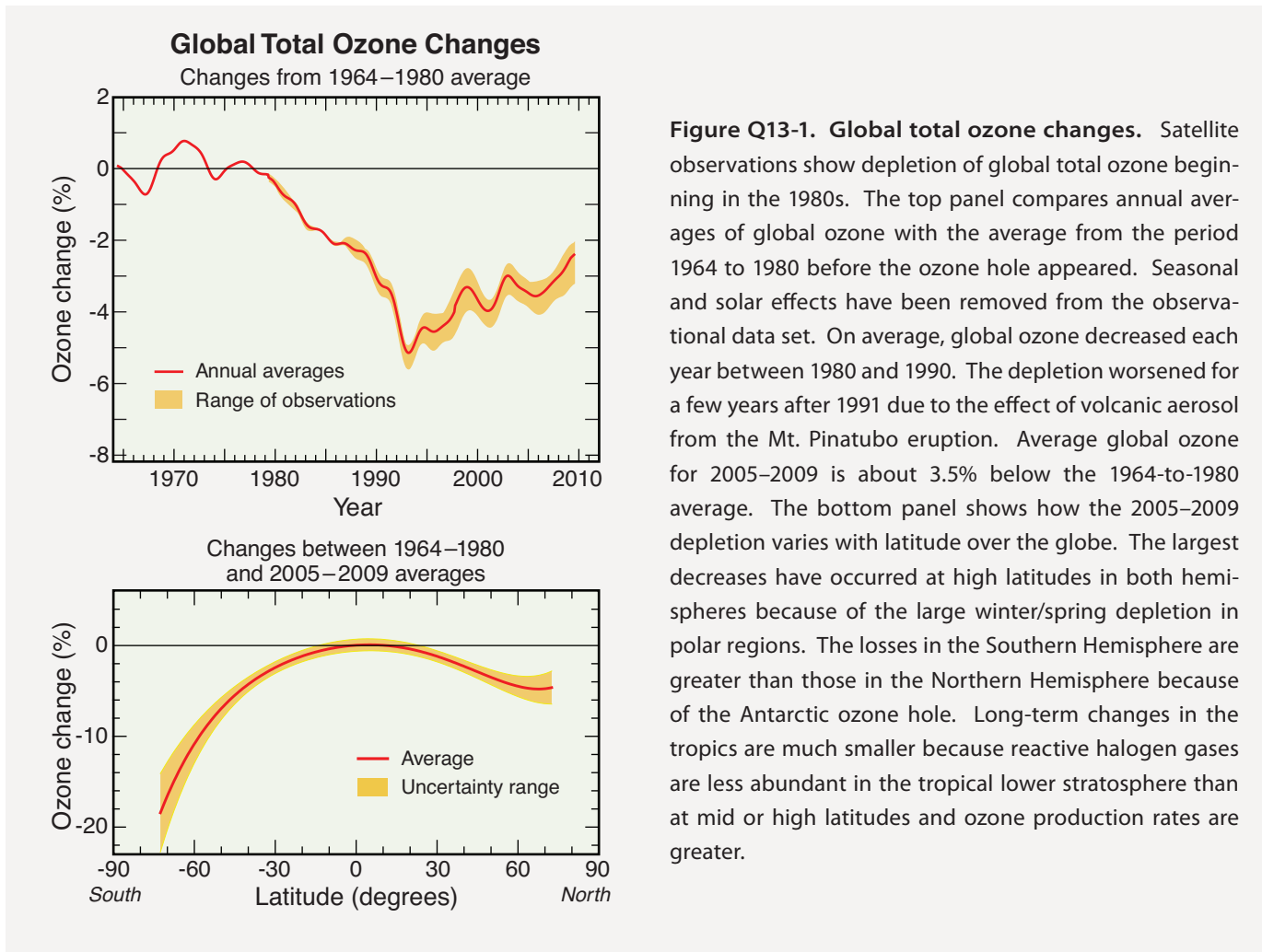


Figure Q13-1. Global total ozone changes. Satellite observations show depletion of global total ozone beginning in the 1980s. The top panel compares annual averages of global ozone with the average from the period 1964 to 1980 before the ozone hole appeared. Seasonal and solar effects have been removed from the observational data set. On average, global ozone decreased each year between 1980 and 1990. The depletion worsened for a few years after 1991 due to the effect of volcanic aerosol from the Mt. Pinatubo eruption. Average global ozone for 2005–2009 is about 3.5% below the 1964-to-1980 average. The bottom panel shows how the 2005–2009 depletion varies with latitude over the globe. The largest decreases have occurred at high latitudes in both hemispheres because of the large winter/spring depletion in polar regions. The losses in the Southern Hemisphere are greater than those in the Northern Hemisphere because of the Antarctic ozone hole. Long-term changes in the tropics are much smaller because reactive halogen gases are less abundant in the tropical lower stratosphere than at mid or high latitudes and ozone production rates are greater.

the stratosphere following emission reductions. Future changes in climate parameters will also influence ozone. The global ozone increases observed in the last 20 years cannot be attributed solely to reductions in ODSs that began in the

1990s, because global ozone also responded strongly to the Mt. Pinatubo eruption. The projections of long-term changes in total ozone for different regions of the globe are described in Q20.

Q14

Do changes in the Sun and volcanic eruptions affect the ozone layer?

Yes, factors such as changes in solar radiation, as well as the formation of stratospheric particles after volcanic eruptions, do influence the ozone layer. However, neither factor can explain the average decreases observed in global total ozone over the last three decades. If large volcanic eruptions occur in the coming decades, ozone depletion will increase for several years afterwards.

Changes in solar radiation and increases in stratospheric particles from volcanic eruptions both affect the abundance of stratospheric ozone. Over the last three decades, global total ozone has decreased over the globe and is now about 3.5% below pre-1980 values (see Q13). The depletion is attributed to changes in reactive halogen gases, which are represented by changes in *equivalent effective stratospheric chlorine* (EESC). EESC values account for stratospheric chlorine and bromine abundances and their different effectiveness in destroying ozone (see definition in Q16). A comparison of the smooth year-to-year changes in ozone and EESC shows that the quantities are inversely related to each other, with ozone first decreasing while EESC increases (see Figure Q14-1). After the mid-1990s, the annual changes in both quantities are sharply reduced. Changes in solar output and volcanic activity do not show such smooth long-term changes, as discussed below, and therefore are not considered to be the cause of long-term global ozone depletion.

Total ozone and solar changes. The formation of stratospheric ozone is initiated by ultraviolet (UV) radiation coming from the Sun (see Figure Q2-1). As a result, an increase in the Sun's radiation output increases the amount of ozone in Earth's atmosphere. The Sun's radiation output and sunspot number vary over the well-documented 11-year solar cycle. Observations over several solar cycles since the 1960s show that global total ozone levels vary by 1 to 2% between the maximum and minimum of a typical cycle. Changes in incoming solar radiation at a wavelength of 10.7 cm are often used as a surrogate for changes in solar output at UV wavelengths. The long-term changes in the 10.7-cm output in Figure Q14-1 clearly show alternating periods of maximum and minimum values in total solar output separated by about 5–6 years. If changes in solar output were the cause of global ozone depletion, a gradually decreasing output would have been observed around 1980 or earlier, slowing sharply in the mid-1990s. Since such a decrease was not observed, nor is expected based on longer-term solar observations, the long-

term decreases in global ozone cannot result from changes in solar output alone. Most analyses presented in this and previous international scientific assessments quantitatively account for the influence of the 11-year solar cycle on long-term variations in ozone.

Total ozone and past volcanoes. Explosive volcanic eruptions inject sulfur gases directly into the stratosphere, causing new sulfate particles to be formed. The particles initially form in the stratosphere downwind of the volcano and then spread throughout the hemisphere or globally as air is transported by stratospheric winds. One method of detecting the presence of volcanic particles in the stratosphere uses observations of the transmission of solar radiation through the atmosphere (see Figure Q14-1). When large amounts of new particles are formed in the stratosphere over an extensive region, solar transmission is measurably reduced. The eruptions of Mt. Agung (1963), El Chichón (1982), and Mt. Pinatubo (1991) are the most recent examples of sulfur injections that temporarily reduced solar transmission.

Laboratory measurements and stratospheric observations have shown that chemical reactions on the surfaces of volcanically produced particles can increase ozone destruction by increasing the amounts of the highly reactive chlorine gas chlorine monoxide (ClO). The ozone response depends on the total abundance of EESC after the eruption (see Q16). At times of relatively low EESC, such as the early 1980s, ozone is not very sensitive to stratospheric injection of volcanic sulfate particles. At times of higher EESC amounts, such as from 1980 to the present, global ozone is expected to decrease significantly following large explosive eruptions. The most recent large eruption was that of Mt. Pinatubo, which resulted in up to a 10-fold increase in the number of particles available for surface reactions. Both El Chichón and Mt. Pinatubo increased global ozone depletion for a few years (see Figure Q14-1). EESC was too low for ozone depletion to occur after the Mt. Agung eruption in 1963. The effect on ozone diminishes during the years following an eruption as volcanic particles are gradually

The Solar Cycle, Volcanic Eruptions, Global Ozone, and Equivalent Effective Stratospheric Chlorine

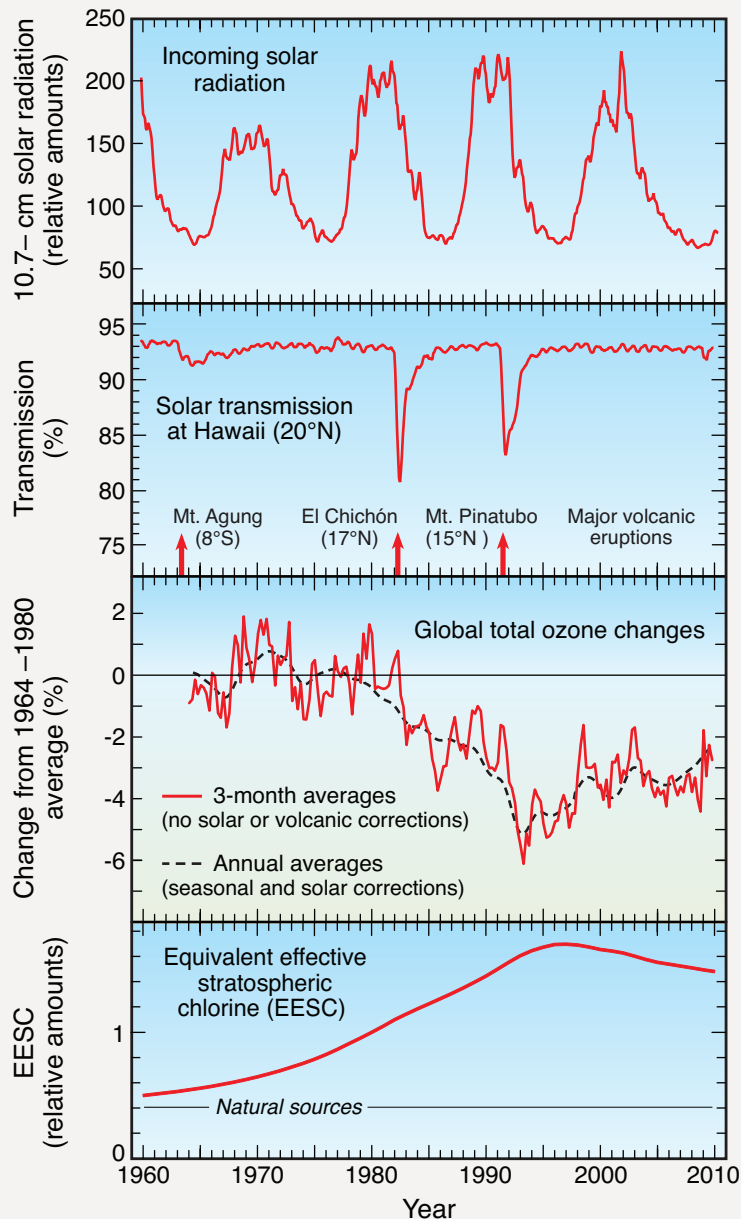


Figure Q14-1. Solar changes and volcanoes.

Global total ozone values have decreased beginning in the early 1980s. Ozone values shown are the 3-month averages without corrections for solar or volcanic effects and annual averages corrected for seasonal and solar effects (from Figure Q13-1). These long-term ozone *decreases* are primarily attributable to equivalent effective stratospheric chlorine (EESC), which has *increased* over the same time period. Since the mid-1990s, changes in both quantities have slowed. Incoming solar radiation varies on a well-recognized 11-year cycle related to sunspot activity. The amount of incoming solar radiation at a wavelength of 10.7 cm is often used as a surrogate for incoming solar radiation at UV wavelengths that produce stratospheric ozone. The 10.7-cm radiation values clearly show the recent periods of solar maximum and minimum. A comparison of the solar radiation and ozone changes strongly indicates that the cyclic changes in solar output alone cannot account for the long-term decrease in total ozone. Following large volcanic eruptions, transmission of solar radiation to Earth's surface is reduced by the large number of new sulfur-containing particles formed in the stratosphere. The three large volcanic eruptions that occurred between 1960 and 2010 temporarily decreased solar transmission as measured in Hawaii. Volcanic particles increase ozone depletion only for a few years before they are removed from the stratosphere by natural processes. As a consequence, the two most recent volcanic eruptions cannot be the cause of the continuous long-term decrease found in global total ozone.

removed from the stratosphere by natural air circulation. As particles are removed, solar transmission is restored. Based on the short residence time of volcanic particles in the stratosphere, the two large eruptions in the past three decades cannot account directly for the continuous long-term decreases in global total ozone observed over the same period.

Reactive chlorine from volcanoes. Explosive volcanic plumes generally contain large quantities of reactive chlorine

in the form of hydrogen chloride (HCl). HCl is a reactive halogen gas that can be converted to ClO, which rapidly destroys ozone (see Figure Q8-3). The plumes also contain a considerable amount of water vapor, which forms rainwater and ice in the rising fresh plume. Rainwater and ice efficiently scavenge and remove HCl while it is still in the lower atmosphere (troposphere). As a result, most of the HCl in explosive volcanic plumes does not enter the stratosphere. After recent explosive

eruptions, observations of HCl in the stratosphere have confirmed that increases are small compared with the total amount of chlorine in the stratosphere from other sources.

Antarctic volcanoes. Volcanoes on the Antarctic continent are of special interest due to their proximity to the Antarctic ozone hole. An explosive eruption could in principle inject volcanic aerosol and small amounts of HCl directly into the stratosphere over Antarctica, which could lead to ozone depletion. However, to be a possible cause of the annually recurring ozone hole beginning in the early 1980s, explosive Antarctic eruptions would need to have occurred at least every few years to maintain volcanic emissions in the stratosphere. This is not the case. Only the Mt. Erebus volcano is currently active in Antarctica. No explosive eruptions of Mt. Erebus or any other Antarctic volcano have occurred since 1980. Therefore, explosive volcanic eruptions in the last three decades have not caused the Antarctic ozone hole and, as noted above, have not been sufficient to cause the long-term depletion of global total ozone.

Total ozone and future volcanoes. Observations and atmospheric models indicate that the record-low ozone levels observed in 1992–1993 resulted from the large number of particles produced by the Mt. Pinatubo eruption, combined with the relatively large amounts of EESC present in the stratosphere in the early 1990s. If the Mt. Pinatubo eruption had occurred before 1980, changes to global ozone would have been much smaller than observed in 1992–1993 because EESC values were much lower. EESC values will remain substantial in the early decades of the 21st century even as ODSs decline globally, with 1980 values reached by about 2050 (see Figures Q16-1 and Q20-2). Large volcanic eruptions in the intervening years will cause more ozone depletion. If an explosive eruption larger than Mt. Pinatubo were to occur, peak ozone losses could be larger than previously observed and substantial ozone losses could persist for longer time periods. As halogen gas abundances gradually decline to 1980 values, the effect of volcanic eruptions on ozone will lessen.

Q15

Are there controls on the production of ozone-depleting substances?

Yes, the production and consumption of ozone-depleting substances are controlled under a 1987 international agreement known as the “Montreal Protocol on Substances that Deplete the Ozone Layer” and by its subsequent Amendments and Adjustments. The Protocol, now ratified by all 196 United Nations members, establishes legally binding controls on national production and consumption of ozone-depleting substances (ODSs). Production and consumption of all principal ODSs by developed and developing nations will be almost completely phased out before the middle of the 21st century.

Montreal Protocol. In 1985, a treaty called the *Vienna Convention for the Protection of the Ozone Layer* was signed by 20 nations in Vienna. The signing nations agreed to take appropriate measures to protect the ozone layer from human activities. The Vienna Convention was a framework agreement that supported research, exchange of information, and future protocols. In response to growing concern, the *Montreal Protocol on Substances that Deplete the Ozone Layer* was signed in 1987 and, following sufficient country ratification, entered into force in 1989. The Protocol has been successful in establishing legally binding controls for developed and developing nations on the production and consumption of halogen source gases known to cause ozone depletion. Halogen source gases containing chlorine and bromine controlled under the Montreal Protocol are referred to as ozone-depleting substances (ODSs). National consumption of an ODS is defined as the amount that production and imports of the substance exceed its export to other nations. The Protocol provisions are structured for developed countries to act first and for developing countries to follow with some financial assistance. In 2010, the Montreal Protocol became the first international treaty to achieve universal ratification by all 196 United Nations members.

Amendments and Adjustments. As the scientific basis of ozone depletion became more certain after 1987 and substitutes and alternatives became available to replace ODSs, the Montreal Protocol was strengthened with Amendments and Adjustments. Each Amendment is named after the city in which the meeting of the Parties to the Montreal Protocol took place and by the year of the meeting. The timeline in Figure Q0-1 shows some of the major decisions that have been adopted in the last two decades. These decisions have put additional ODSs under control, accelerated existing control measures, and prescribed phase-out dates for the production and consumption of certain gases. The initial Protocol called

for a 50% reduction in chlorofluorocarbon (CFC) production and a freeze on halon production. The 1990 London Amendment called for a phase-out of the production and consumption of the most damaging ODSs in developed nations by 2000 and in developing nations by 2010. The 1992 Copenhagen Amendment accelerated the phase-out date to 1996 in developed nations. Further controls on ODSs were agreed upon in later meetings in Vienna (1995), Montreal (1997, 2007), and Beijing (1999).

Influence of the Montreal Protocol. Montreal Protocol controls are based on several factors that are considered separately for each ODS. The factors include (1) the effectiveness in depleting ozone in comparison with other substances (see Ozone Depletion Potential (ODP) in Q18), (2) the availability of suitable substitutes for domestic and industrial use, and (3) the potential impact of controls on developing nations. The influence of Montreal Protocol provisions on stratospheric ODS abundances can be demonstrated with long-term changes in *equivalent effective stratospheric chlorine* (EESC). Calculations of EESC combine the amounts of chlorine and bromine present in surface air to form a measure of the potential for ozone destruction in a particular stratospheric region on an annual basis (see definition in Q16). The long-term changes in EESC at midlatitudes are shown in Figure Q15-1 for several cases:

► **No Protocol.** Without the Montreal Protocol the production, use, and emissions of CFCs and other ozone-depleting substances is expected to have increased after 1987 with an annual growth rate of about 3% (business-as-usual scenario). As a result, EESC is projected to have increased nearly 10-fold by the mid-2050s compared with the 1980 value. Computer models of the atmosphere indicate that such high EESC values would have at least doubled global total ozone depletion between 1990 and 2010 and increased it far beyond that by midcentury. As a result,

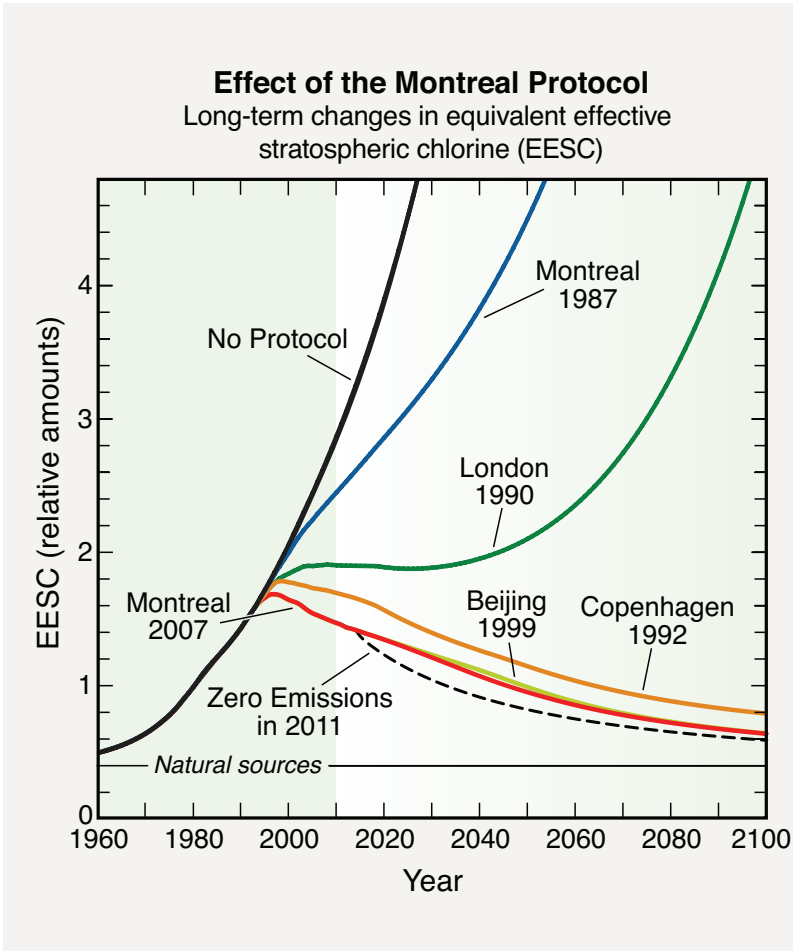


Figure Q15-1. Effect of the Montreal Protocol. The objective of the Montreal Protocol is the protection of the ozone layer through control of the global production and consumption of ODSs. Projections of the future abundances of ODSs expressed as equivalent effective stratospheric chlorine (EESC) values (see Q16) are shown separately for the midlatitude stratosphere for (1) no Protocol provisions, (2) the provisions of the original 1987 Montreal Protocol and some of its subsequent Amendments and Adjustments, and (3) zero emissions of ODSs starting in 2011. The city names and years indicate where and when changes to the original 1987 Protocol provisions were agreed upon (see Figure Q0-1). EESC is a relative measure of the potential for stratospheric ozone depletion that combines the contributions of chlorine and bromine from ODS surface observations (see Q16). Without the Protocol, EESC values are projected to have increased significantly in the 21st century. Only with the Copenhagen (1992) and subsequent Amendments and Adjustments did projected EESC values show a long-term decrease.

harmful UV-B radiation would have increased substantially at Earth's surface, causing a global rise in skin cancer and cataract cases (see Q17).

- ▶ **Montreal Protocol provisions.** International compliance with only the 1987 provisions of the Montreal Protocol and the later 1990 London Amendment would have substantially slowed the projected growth of EESC. Not until the 1992 Copenhagen Amendments and Adjustments did the Protocol projections show a *decrease* in future EESC values. The provisions became more stringent with the Amendments and Adjustments adopted in Beijing in 1999 and Montreal in 1997 and 2007. Now, with full compliance to the Protocol, most ODSs will be almost completely phased out, with some exemptions for critical uses (see Q16). Global EESC is slowly decaying from its peak value in the late 1990s and is expected to reach 1980 values in the mid-21st century. The success of the Montreal Protocol to date is demonstrated by the decline in ODP-weighted *emissions* of ODSs shown in Figure Q0-1. Total emissions peaked in 1988 at values about 10-fold higher than natural

emissions. Between 1988 and 2010, ODS emissions from human activities have decreased by over 80%.

- ▶ **Zero emissions.** EESC values in the coming decades will be influenced by (1) the slow natural removal of ODSs still present in the atmosphere, (2) emissions from continued production and use of ODSs, and (3) emissions from currently existing *banks* containing a variety of ODSs. ODS banks are associated with applications that involve long-term containment of halogen gases. Examples are CFCs in refrigeration equipment and insulating foams, and halons in fire-fighting equipment. New emissions are projected based on continued production and consumption of ODSs, particularly in developing nations, under existing Protocol provisions.

The zero-emissions case demonstrates the EESC values that would occur if it were possible to set all ODS emissions to zero beginning in 2011. This would eliminate the contributions from new production and bank emissions. Significant differences from the Montreal 2007 projections are evident in the first decades following 2011 because the

phase-out of all ODS production under the Protocol is not yet complete and bank emissions are substantial. Zero emissions would bring forward the return of EESC to 1980 levels by about 13 years.

HCFC substitute gases. The Montreal Protocol provides for the use of hydrochlorofluorocarbons (HCFCs) as transitional, short-term substitute compounds for ODSs with higher ODPs, such as CFC-12. HCFCs are used for refrigeration, in making insulating foams, and as solvents, all of which were primary uses of CFCs. HCFCs are generally more reactive in the troposphere than other ODSs because they contain hydrogen (H) in addition to chlorine, fluorine, and carbon. HCFCs are 88 to 98% *less effective* than CFC-12 in depleting stratospheric ozone because their chemical removal occurs primarily in the troposphere (see ODPs in Table Q7-1). This removal protects stratospheric ozone from most of the halogen content of HCFC emissions. In contrast, CFCs and many other ODSs release all of their halogen content in the stratosphere because they are chemically inert in the troposphere (see Q6).

Under the provisions of the Montreal Protocol, developed and developing countries may continue to use HCFCs as ODS substitutes in the coming decades before they are ultimately phased out. In the most recent Adjustment to the Protocol (Montreal 2007), the phase-out of HCFCs for all Parties was accelerated so that it will be complete in 2030, a decade earlier than in previous provisions. In adopting this decision, the

Parties reduced the contribution of HCFC emissions to both long-term ozone depletion and future climate forcing (see Q18 and Q19).

HFC substitute gases. Hydrofluorocarbons (HFCs) are used as long-term substitute compounds for CFCs, HCFCs, and other ODSs. HFCs contain hydrogen, fluorine, and carbon. HFCs do not contribute to ozone depletion because they contain no chlorine, bromine, or iodine. As a consequence, HFCs are not ODSs and are not subject to the provisions of the Montreal Protocol. HFCs and all ODSs are radiatively active gases that contribute to human-induced climate change based on their accumulation in the atmosphere (see Q18). HFCs are included in the *basket of gases* being controlled by the Kyoto Protocol of the United Nations Framework Convention on Climate Change (UNFCCC). The Kyoto Protocol is an international treaty designed to protect climate by controlling *emissions* of HFCs, carbon dioxide (CO₂), methane (CH₄), nitrous oxide (N₂O), perfluorocarbons (PFCs), and sulfur hexafluoride (SF₆). HFC emissions are expected to grow substantially in coming decades as the demand for their use as substitute gases and in new applications increases in developed and developing countries. The climate change contribution from future HFC emissions will be minimized if HFCs with very low Global Warming Potentials (GWPs) (less than 100) are chosen to meet the growing demand (see Q18).

Q16

Has the Montreal Protocol been successful in reducing ozone-depleting substances in the atmosphere?

Yes, as a result of the Montreal Protocol, the overall abundance of ozone-depleting substances (ODSs) in the atmosphere has been decreasing for about a decade. If the nations of the world continue to comply with the provisions of the Montreal Protocol, the decrease will continue throughout the 21st century. Those gases that are still increasing in the atmosphere, such as halon-1301 and HCFC-22, will begin to decrease in the coming decades if compliance with the Protocol continues. Only after midcentury will the effective abundance of ODSs fall to values that were present before the Antarctic ozone hole was observed in the early 1980s.

The Montreal Protocol and its Amendments and Adjustments have been very successful in reducing the atmospheric abundance of ozone-depleting substances (ODSs). ODSs are halogen source gases released by human activities. Under the Protocol, the production and consumption of individual ODSs are now controlled in all 196 nations that are Parties to the Protocol (see Q15). The success of the Montreal Protocol controls is documented by (1) observed changes and future projections of the atmospheric abundance of the principal ODSs and (2) long-term values of *equivalent effective stratospheric chlorine* (EESC).

Individual ODS reductions. The reduction in the atmospheric abundance of an ODS in response to controls on production and consumption depends principally on two factors: (1) how rapidly an ODS is used and released to the atmosphere after being produced and (2) the lifetime for the removal of the ODS from the atmosphere (see Table Q7-1). For example, the abundances of ODSs with short lifetimes respond quickly to emission reductions. Long-term changes in ODS abundances are constructed from (1) estimates of historical emissions and bank quantities using industry reports, (2) abundances measured in air trapped for years in accumulated snow (firn) in polar regions, (3) observed atmospheric abundances using ground-based measurements, and (4) projections of future abundances based on compliance with Montreal Protocol provisions and patterns of use in developed and developing countries. The results for individual ODSs and the natural chlorine source gas, methyl chloride (CH₃Cl), are shown in Figure Q16-1 and described as follows:

► **CFCs.** Chlorofluorocarbons (CFCs) include some of the most destructive chlorine-containing ODSs. CFC-11 and CFC-12, each with an Ozone Depletion Potential (ODP) near 1, are the most abundant ODSs in the atmosphere owing to large historical emissions and long atmospheric lifetimes (45–100 years). Production and consumption of

CFCs in developed countries ended in 1996 and that in developing countries ended by January 2010. As a consequence, CFC-11 and CFC-113 abundances have peaked in the atmosphere and have been declining for more than a decade. In contrast, CFC-12 abundances have only recently shown a decrease, owing to its longer lifetime (100 years) and continuing emissions from CFC-12 banks, namely, refrigeration and air conditioning equipment and thermal insulating foams. With no further global production of the principal CFCs allowed except for limited exempted uses and with some continuing emissions from banks, CFC abundances are projected to decline steadily throughout this century.

► **Halons.** Halons are the most destructive bromine-containing ODSs. The most abundant in the atmosphere, halon-1211 and halon-1301, have abundances about 100 times less than CFC-11 and CFC-12 and account for a significant fraction of bromine from all ODSs (see Figure Q7-1). Production and consumption of halons in developed countries ended in 1994 and that in developing countries ended by January 2010. In the 2005–2008 period, atmospheric abundances of halon-1211 showed a significant decrease for the first time. Halon-2402 abundances have been decreasing for a few years while those of halon-1301 continue to increase. The increase is likely due to substantial banks in fire-extinguishing and other equipment that gradually release halon-1301 to the atmosphere. The abundance of halon-1301 is expected to remain high well into the 21st century because of its long lifetime (65 years) and continued release.

► **Methyl chloroform.** The largest reduction to date in the abundance of an ODS (about 90% from its peak value) has been observed for methyl chloroform. Production and consumption of methyl chloroform in developed countries ended in January 1996 and that in developing countries

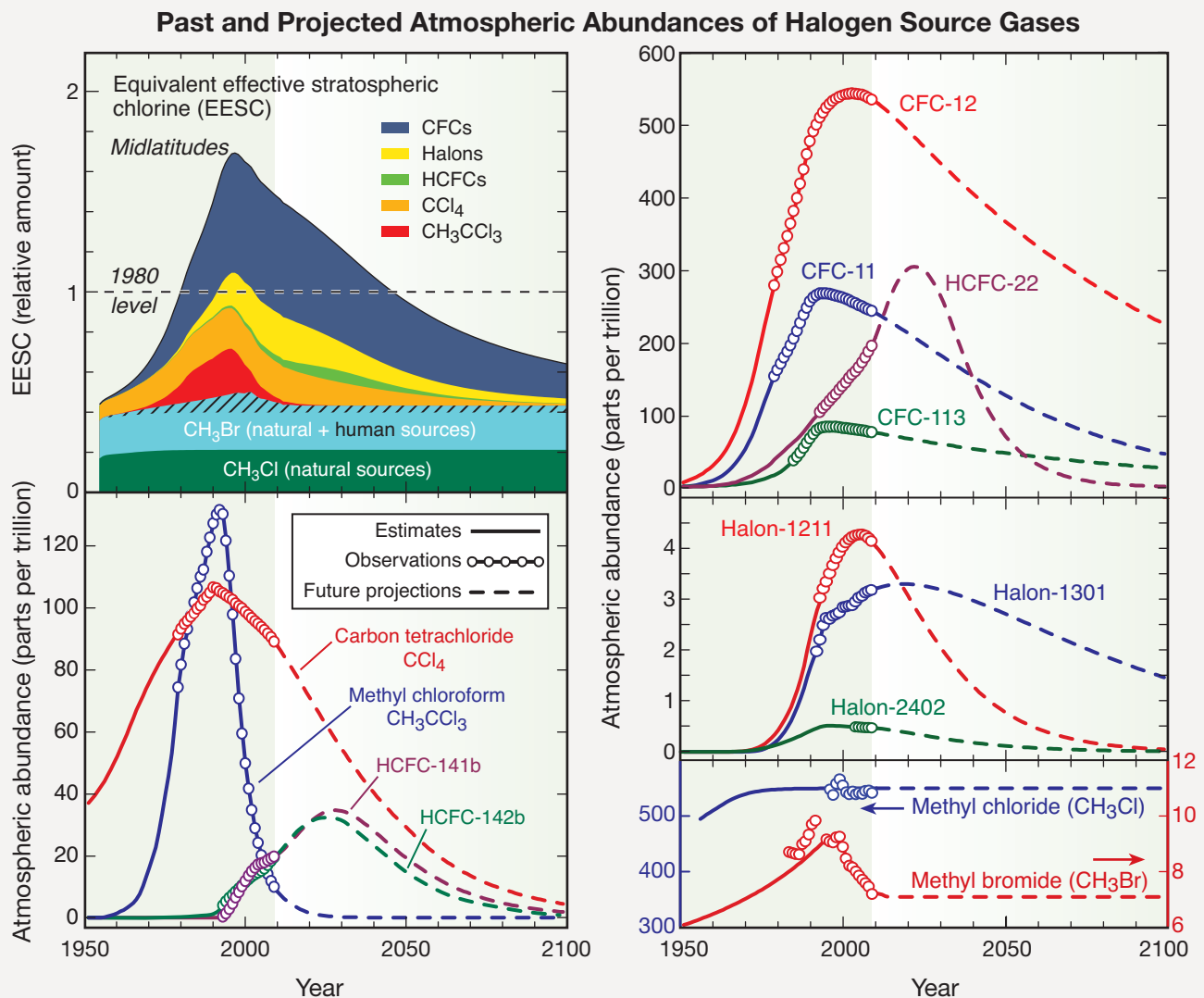


Figure Q16-1. Halogen source gas changes. The atmospheric abundances of individual ozone-depleting substances (ODSs) at Earth's surface were obtained using a combination of direct atmospheric measurements, estimates of historical abundance, and future projections of abundance. The gases shown are all ODSs except for methyl chloride. The past increases of CFCs, along with those of carbon tetrachloride, methyl chloroform, and halon-1211, have slowed and reversed in the last two decades. HCFCs, which are used as transitional substances to replace CFCs, will likely continue to increase in the coming decades before a complete phase-out. Halon-1301 abundances will also likely continue to grow in the next decade while current halon banks are depleted. Future decreases in methyl bromide are expected to be small. Abundances of methyl chloride, which is not controlled under the Montreal Protocol and has large natural sources, are projected to be constant in the future.

The rise in equivalent effective stratospheric chlorine (EESC) values in the 20th century has slowed and reversed in the last decade (top left panel). EESC is a measure of the potential for ozone depletion in the stratosphere derived from surface measurements of chlorine and bromine gases (see Q16). EESC values are reduced as ODS emissions decrease. EESC, as shown here for the stratosphere at midlatitudes, returns to 1980 values around 2050. In polar regions, the return to 1980 values occurs almost 10 years later. International compliance with the Montreal Protocol provisions will ensure that EESC values will continue to decrease as projected (see Q15). (The unit "parts per trillion" is defined in the caption of Figure Q7-1.)

is scheduled to end by January 2015. Atmospheric abundances responded rapidly to the reduced emissions starting in the mid-1990s because methyl chloroform has a short atmospheric lifetime (about 5 years). Methyl chloroform is used mainly as a solvent and has no significant long-term storage following production. It will approach complete removal from the atmosphere after the phase-out in developing countries is complete.

- ▶ **HCFC substitute gases.** The Montreal Protocol allows for the use of hydrochlorofluorocarbons (HCFCs) as short-term, transitional substitutes for CFCs and in other specific applications. As a result, the abundances of HCFC-22, HCFC-141b, and HCFC-142b continue to grow in the atmosphere with rates that have remained constant or increased in recent years in response to greater application demand. HCFCs pose a lesser threat to the ozone layer than CFCs because they have low ODP values (less than 0.12). The most recent Adjustment to the Montreal Protocol (Montreal 2007) accelerated the phase-out of HCFCs by a decade for both developed (2020) and developing countries (2030) (see Q15). Even with the accelerated phase-out, future projections show HCFC abundances that continue to increase, reach peak values before the mid-21st century, and steadily decrease thereafter. The response of atmospheric abundances to decreasing emissions will be relatively rapid because of short atmospheric lifetimes of HCFCs (less than 20 years).
- ▶ **Carbon tetrachloride.** Carbon tetrachloride has been phased out in both developed countries (January 1996) and developing countries (January 2010). As a result, atmospheric abundances of carbon tetrachloride have been decreasing for two decades. The decline is somewhat less rapid than expected, suggesting that actual emissions are larger than reported or the atmospheric lifetime is greater than current estimates. Production of carbon tetrachloride for use as raw material (feedstock) to make other chemicals is exempted under the Protocol because emission to the atmosphere does not occur in this case.
- ▶ **Methyl chloride and methyl bromide.** Both methyl chloride and methyl bromide are distinct among halogen source gases because substantial fractions of their emissions are associated with natural processes (see Q7). Methyl chloride is not an ODS under the Montreal Protocol because it is not manufactured or used in appreciable quantities. Its abundance in the atmosphere has remained fairly constant throughout the last 60 years and will remain constant if the balance of its natural production and loss processes

remains unchanged. Methyl bromide is controlled under the Protocol because it is manufactured for use as a fumigant. Developed country production and consumption of methyl bromide ended in January 2005 and that in developing countries is scheduled to end by January 2015. The Protocol currently provides exemptions for some methyl bromide production and use as an agricultural and pre-shipment fumigant. Atmospheric abundances of methyl bromide responded rapidly to the reduced emissions starting in 1999 because its atmospheric removal lifetime is less than 1 year. Future projections show only small changes in methyl bromide abundances based on the assumptions of unchanged contributions from natural sources and small use in developing countries. An important uncertainty in these projections is the future amounts that will be produced and emitted under Montreal Protocol use exemptions.

Equivalent effective stratospheric chlorine (EESC). Important measures of the success of the Montreal Protocol are the past and projected changes in the values of equivalent effective stratospheric chlorine (EESC), which was introduced in Figures Q14-1 and Q15-1. EESC is designed as one measure of the potential for ozone depletion in the stratosphere that can be calculated from atmospheric *surface abundances* of ODSs and natural chlorine and bromine gases. All gases used in the calculation are shown in Figure Q7-1. For both past and future EESC values, the required atmospheric abundances are derived from measurements, historical estimates, or future projections based on compliance with Montreal Protocol provisions.

EESC is expressed as a hypothetical amount of chlorine available in the stratosphere to deplete ozone. The term *equivalent* indicates that bromine gases, scaled by their greater per-atom effectiveness in depleting ozone, are included in EESC. The term *effective* indicates that only the estimated fraction of ODSs that are currently in the form of reactive halogen gases in the stratosphere is included in an EESC value (see Q8). Although chlorine is much more abundant in the stratosphere than bromine (about 150-fold) (see Figure Q7-1), bromine atoms are about 60 times more effective than chlorine atoms in chemically destroying ozone in the lower stratosphere. EESC generally depends on the year and latitude region in the stratosphere being considered.

Another quantitative measure of the potential for ozone depletion in the stratosphere that is highly related to EESC is *effective stratospheric chlorine* (ESC). ESC, as defined in Q20, is calculated with chemistry-climate models rather than directly from ODS observations.

Long-term changes in EESC. In the latter half of the 20th century up until the 1990s, EESC values steadily increased (see Figure Q16-1), causing global ozone depletion. As a result of the Montreal Protocol regulations, the long-term increase in EESC slowed, values reached a peak, and EESC began to decrease in the 1990s. The initial decrease came primarily from the substantial, rapid reductions in emissions of methyl chloroform, which has a lifetime of only 5 years. The decrease is continuing with declining emissions of CFCs and other long-lived ODSs. Decreasing EESC means that the potential

for stratospheric ozone depletion is now lessening each year as a result of the Montreal Protocol. Decreases in EESC are projected to continue throughout the 21st century if all nations continue to comply with the provisions of the Protocol. The decrease will continue because as emissions are reduced, natural processes continue to gradually remove halogen-containing gases from the global atmosphere. Reduction of EESC values to 1980 values or lower will require several more decades because the most abundant ODS molecules now in the atmosphere have lifetimes ranging from 10 to 100 years.

Q17

Does depletion of the ozone layer increase ground-level ultraviolet radiation?

Yes, ultraviolet radiation at Earth's surface increases as the amount of overhead total ozone decreases, because ozone absorbs ultraviolet radiation from the Sun. Measurements by ground-based instruments and estimates made using satellite data provide evidence that surface ultraviolet radiation has increased in large geographic regions in response to ozone depletion.

The depletion of stratospheric ozone leads to an increase in solar ultraviolet radiation at Earth's surface. The increase occurs primarily in the ultraviolet-B (UV-B) component of the Sun's radiation. UV-B is defined as radiation in the wavelength range of 280 to 315 nanometers, which is invisible to the human eye. Long-term changes in UV-B radiation reaching the surface have been measured directly and can be estimated from total ozone changes.

UV-B radiation can harm humans, other life forms, and materials (see Q3). Most of the effects of sunlight on the human body are caused by UV-B exposure. A principal effect is skin erythema, which leads to sunburning. Excess exposure may lead to skin cancers. Erythema radiation is regularly reported to the public in many countries in the form of the "UV Index." The long-term changes in surface UV-B radiation are important to study because of its potential harmful effects and relationship to ozone depletion.

Surface UV-B radiation. The amount of UV-B radiation reaching Earth's surface at a particular location depends in large part on total ozone at that location. Ozone molecules in the stratosphere and in the troposphere absorb UV-B radiation, thereby significantly reducing the amount that reaches Earth's surface (see Q3). If conditions occur that reduce the abundance of ozone molecules somewhere in the troposphere or stratosphere, total ozone is reduced and the amount of UV-B radiation reaching Earth's surface below is increased proportionately. This relationship between total ozone and surface UV-B radiation has been confirmed at a variety of locations with direct measurements of both quantities.

Additional causes of UV changes. The actual amount of UV-B radiation reaching the Earth's surface at a specific location and time depends on a number of factors in addition to total ozone. The primary additional factor is the position of the Sun in the sky, which changes with daily and seasonal cycles. Other factors include local cloudiness, the altitude of the location, the amount of ice or snow cover, and the amounts of atmospheric particles (aerosols) in the atmosphere above the location. Changes in clouds and aerosols are partially related

to air pollution and greenhouse gas emissions from human activities. Measurements indicate that both increases and decreases in UV radiation at certain locations have resulted from changes in one or more of these factors. Estimating the impact of changes in these factors is complex. For example, an increase in cloud cover usually results in a reduction of UV radiation below the clouds and could at the same time increase surface radiation in any nearby mountainous regions above the clouds.

Long-term surface UV changes. Long-term changes in UV-B radiation have been estimated from measurements made with special UV monitoring instruments at several surface locations since about 1990. For example, as a consequence of Antarctic ozone depletion, the average UV-B measured at the South Pole during spring between 1991 and 2006 was 55–85% larger than estimated for the years 1963–1980. In addition, satellite observations of ozone changes have been used to estimate changes in surface UV-B radiation that have occurred over the past three decades. With satellite observations, the UV-B radiation changes can be separately attributed to changes in ozone and clouds. The results show that erythema radiation has increased by up to 6% between 1979 and 2008 over a wide range of latitudes outside the tropics (see lower panel of Figure Q17-1). The largest percentage increases have occurred at high polar latitudes in both hemispheres, where the largest annual decreases in total ozone are observed (see Figure Q13-1). Over this time period the UV increases due to ozone depletion are partially offset by changes in cloudiness, primarily in the high latitudes of the Southern Hemisphere (see top panel in Figure Q17-1). Without changes in cloudiness, the increases in erythema radiation at these latitudes would have reached a maximum close to 9%. The smallest changes in erythema UV have been in the tropics, where long-term changes in total ozone are smallest (see Q13). In the tropics and in the Northern Hemisphere the average changes in clouds during this period were very small. As a result, the net increases in erythema radiation in these regions are determined primarily by ozone depletion.

UV Index changes. The UV Index is a measure of the erythemal radiation that occurs at a particular surface location and time. The index is used internationally to increase public awareness about the detrimental effects of UV on human health and to guide the need for personal protective measures. The maximum daily UV Index varies with location and season, as shown for three sites in Figure Q17-2. The UV Index increases when moving from high to low latitudes and is highest in summer when the midday Sun is closest to overhead. UV Index values in San Diego, California, at 32°N, for example, are generally higher than those in Barrow, Alaska, at 71°N. At all latitudes, UV Index values increase in mountainous regions and over snow- or ice-covered regions. The UV Index is zero during periods of continuous darkness in winter at high-latitude locations.

The UV Index over Antarctica has increased dramatically due to ozone depletion, as illustrated in Figure Q17-2.

Normal index values for Palmer, Antarctica, at 64°S in spring were estimated from satellite measurements made during the period 1978–1980, before the appearance of the ozone hole over Antarctica. In the period from 1991 to 2006, the severe and persistent ozone depletion that occurred in late winter and early spring over Antarctica increased the average UV Index well above normal values for several months. Now, the spring UV Index measured in Palmer, Antarctica, routinely equals or exceeds spring and summer values measured in San Diego, California, located at a much lower latitude (32°N).

UV changes and human health. Over the past several decades, depletion of the stratospheric ozone layer together with societal changes in lifestyle have increased UV-B radiation exposure for many people. Increased exposure has adverse health effects, primarily associated with eye and skin disorders. UV radiation is a recognized risk factor for some types of cataracts. For the skin, the most common threat is

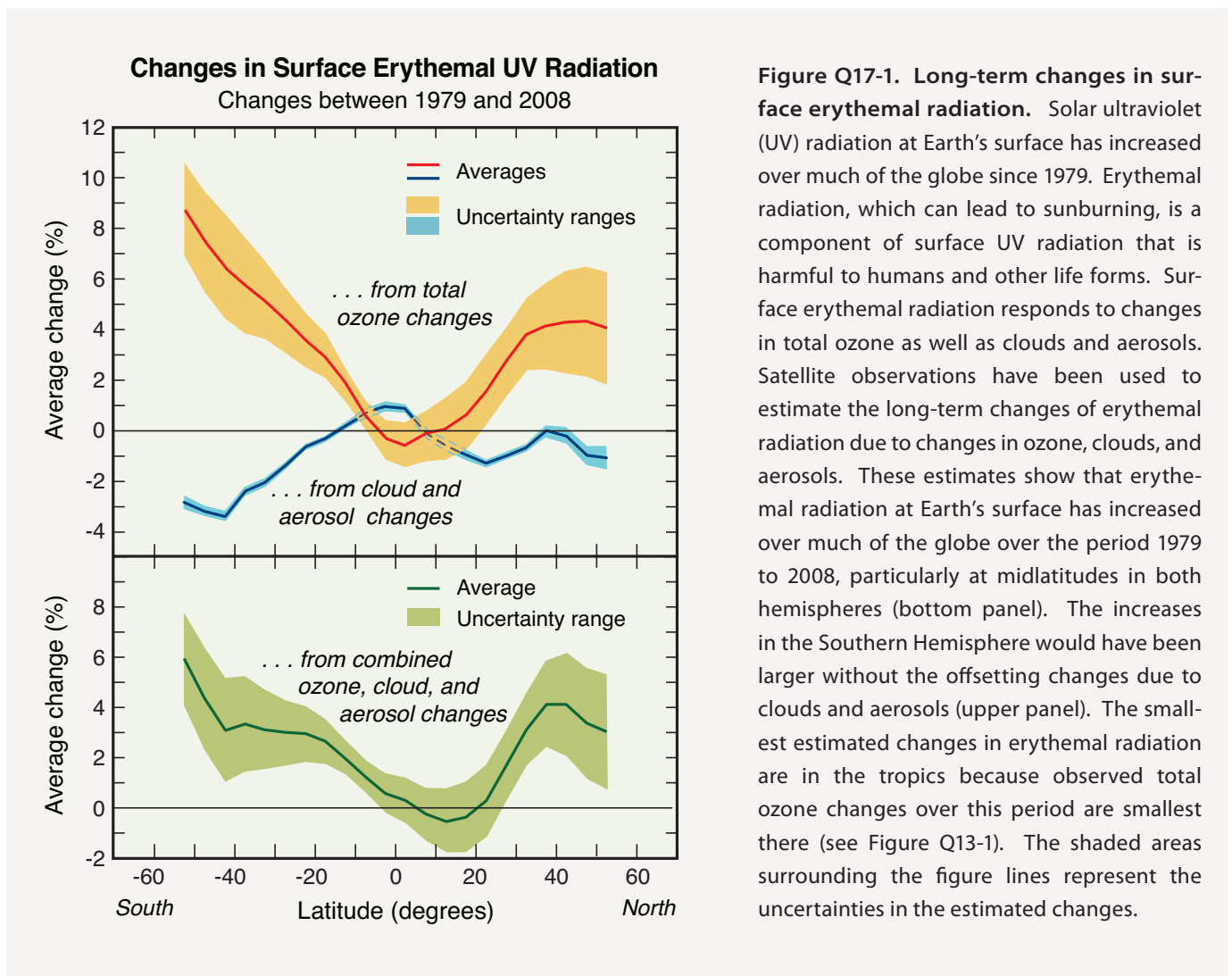
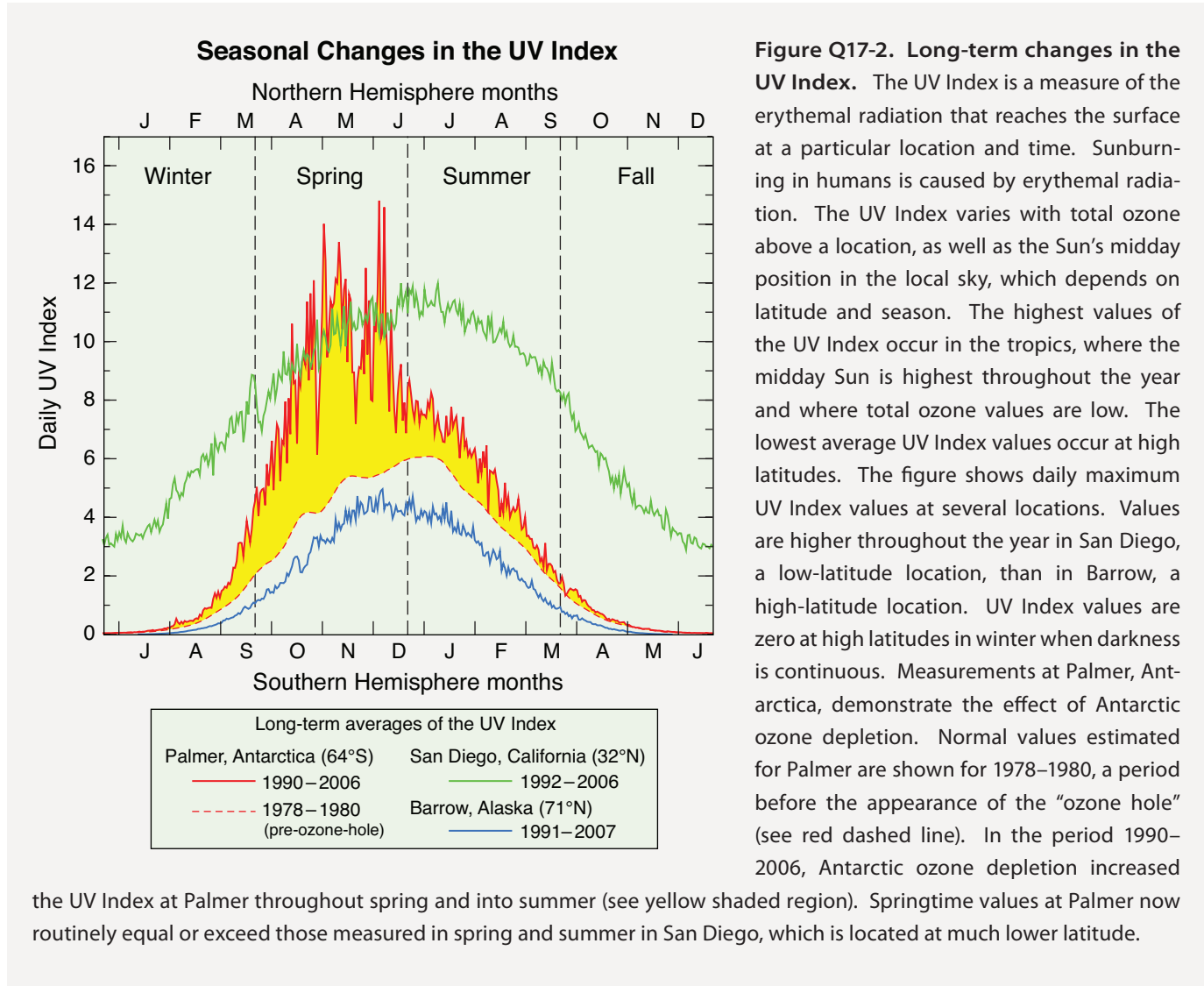


Figure Q17-1. Long-term changes in surface erythemal radiation. Solar ultraviolet (UV) radiation at Earth’s surface has increased over much of the globe since 1979. Erythemal radiation, which can lead to sunburning, is a component of surface UV radiation that is harmful to humans and other life forms. Surface erythemal radiation responds to changes in total ozone as well as clouds and aerosols. Satellite observations have been used to estimate the long-term changes of erythemal radiation due to changes in ozone, clouds, and aerosols. These estimates show that erythemal radiation at Earth’s surface has increased over much of the globe over the period 1979 to 2008, particularly at midlatitudes in both hemispheres (bottom panel). The increases in the Southern Hemisphere would have been larger without the offsetting changes due to clouds and aerosols (upper panel). The smallest estimated changes in erythemal radiation are in the tropics because observed total ozone changes over this period are smallest there (see Figure Q13-1). The shaded areas surrounding the figure lines represent the uncertainties in the estimated changes.

skin cancer. Over the past decades, the incidence of several types of skin tumors has risen significantly among people of all skin types. Skin cancer in humans occurs long after exposure to sunburning UV. With current Montreal Protocol provisions, projections of additional skin cancer cases associated with ozone depletion are largest in the early to middle decades of the 21st century and represent a significant global health

issue. An important human health benefit of UV-B radiation exposure is the production of vitamin D, which plays a significant role in bone metabolism and the immune system. Human exposure to solar UV-B radiation requires a careful balance to maintain adequate vitamin D levels while minimizing long-term risks of skin and eye disorders.



Q18

Is depletion of the ozone layer the principal cause of climate change?

No, ozone depletion itself is not the principal cause of climate change. Changes in ozone and climate are directly linked because ozone absorbs solar radiation and is also a greenhouse gas. Stratospheric ozone depletion and increases in global tropospheric ozone that have occurred in recent decades have opposing contributions to climate change. The ozone-depletion contribution, while leading to surface cooling, is small compared with the contribution from all other greenhouse gas increases, which leads to surface warming. The total forcing from these other greenhouse gases is the principal cause of observed and projected climate change. Ozone depletion and climate change are indirectly linked because both ozone-depleting substances and their substitutes are greenhouse gases.

While stratospheric ozone depletion is not the principal cause of climate change, aspects of ozone depletion and climate change are closely linked. Both processes involve gases released to the atmosphere by human activities. The links are best understood by examining the contribution to climate change of the gases involved: ozone; ozone-depleting substances (ODSs) (or halogen source gases) and their substitutes; and other leading greenhouse gases.

Greenhouse gases and the radiative forcing of climate. The warming of the Earth by the Sun is enhanced by the presence of natural *greenhouse gases*, of which water vapor is an important example. Without this natural greenhouse effect, the Earth's surface would be much colder. Human activities since the preindustrial era have led to long-term increases in the atmospheric abundances of a number of long-lived and short-lived greenhouse gases. This group

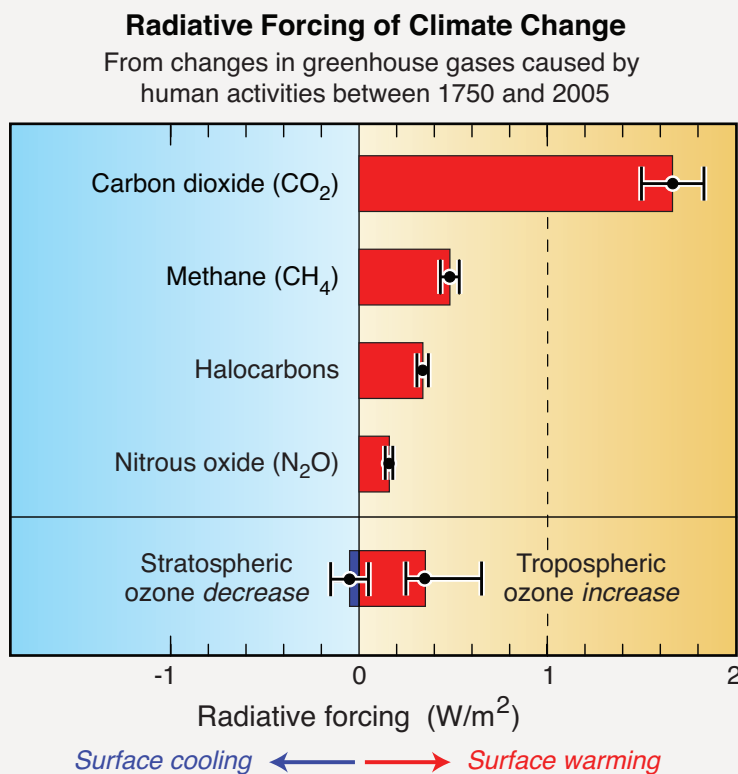


Figure Q18-1. Radiative forcing of greenhouse gases. Human activities since the start of the Industrial Era (around 1750) have caused increases in the abundances of several short-lived and long-lived gases, known as greenhouse gases, that all contribute to the radiative forcing of climate, also known as climate forcing. Radiative forcing is expressed in units of *watts per square meter (W/m²)*. As shown in the figure, the largest forcings are those of carbon dioxide (CO₂), followed by methane (CH₄), tropospheric ozone, halocarbon gases, and nitrous oxide (N₂O). The black whiskers on each bar show uncertainties in the values. Tropospheric ozone increases result from the emission of pollutant gases and create a positive ozone forcing. Positive forcings lead to a warming of Earth's surface. In contrast, stratospheric ozone depletion represents a small negative forcing, which leads to cooling of Earth's surface. Halocarbons include all ODSs, their substitutes, and a few

other gases (see Figure Q18-2). In the coming decades, ODS abundances and stratospheric ozone depletion are expected to be reduced, along with their associated radiative forcings.

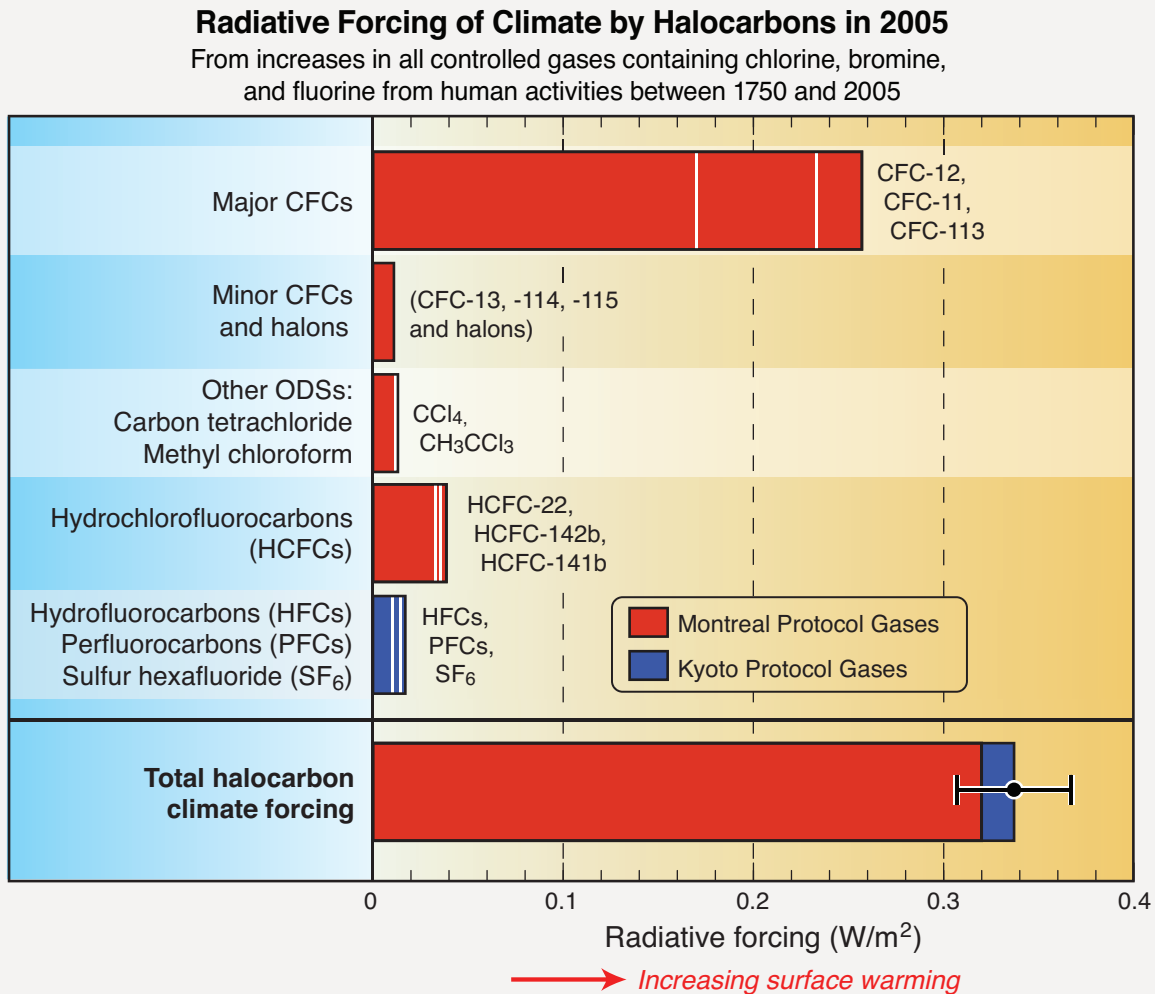


Figure Q18-2. Halocarbons and radiative forcing of climate change. Halocarbon gases in the atmosphere represent an important contribution to the radiative forcing of climate between 2005 and the preindustrial era (see Figure Q18-1). Halocarbons are all gases containing chlorine, bromine, or fluorine atoms that are now controlled as ozone-depleting substances (ODSs) by the Montreal Protocol or as climate change gases by the Kyoto Protocol (see color shading). Shown in the figure are the separate contributions of each gas or group of gases, as estimated using atmospheric abundance histories and Global Warming Potentials (GWPs) (see Figure Q18-3). The gases listed in the right hand labels begin with the largest contribution in each group, except for CFC-13, CFC-114, CFC-115, and halons, which are shown as one total value. The individual forcing terms add together to form the bottom bar representing the total halocarbon forcing. The forcings of CFC-11 and CFC-12, the largest halocarbon contributions, are already decreasing and will continue to decrease as CFCs are gradually removed from the atmosphere (see Figure Q16-1). In contrast, the contributions of the intermediate-term ODS substitute gases, HCFCs, are projected to grow for another two decades before decreasing. The future contributions of the long-term ODS substitute gases, HFCs, are also expected to increase. In this case, the total contribution will depend strongly on which HFCs are used because the GWPs of individual HFCs vary widely (see Figure Q18-3).

includes stratospheric and tropospheric ozone, halocarbons, carbon dioxide (CO₂), methane (CH₄), and nitrous oxide (N₂O). ODSs and their substitutes make up a large fraction of the halocarbons in today's atmosphere. The natural abundances of these gases in Earth's atmosphere change the balance between incoming solar radiation and outgoing infrared radiation, warming the atmosphere and surface. Increases in the abundance of these gases from human activities cause more outgoing radiation to be absorbed, which further warms the atmosphere and surface. This change in Earth's radiative balance caused by human activities is called a *radiative forcing of climate* or, more simply, a *climate forcing*. The magnitude of this *energy imbalance* is usually evaluated at the top of the troposphere (tropopause) and is expressed using units of *watts per square meter* (W/m²). The potential for climate change increases as this radiative forcing increases.

A summary of radiative forcings in 2005 resulting from the increases in the principal long-lived and short-lived greenhouse gases during the Industrial Era is shown in Figure Q18-1. All forcings shown relate to human activities. Positive forcings generally lead to *warming* and negative forcings lead to *cooling* of Earth's surface. Climate forcings also lead to other changes, such as in precipitation patterns and extreme weather events. International climate assessments conclude that much of the observed surface warming and changes in other climate parameters over the last decades is due to increases in the abundance of carbon dioxide and other greenhouse gases caused by human activities.

Stratospheric and tropospheric ozone. Stratospheric and tropospheric ozone both absorb infrared radiation emitted by Earth's surface, trapping heat in the atmosphere. Stratospheric ozone also significantly absorbs solar radiation. As a result, increases or decreases in stratospheric or tropospheric ozone induce a climate forcing and, therefore, represent direct links between ozone and climate. In recent decades, global stratospheric ozone has *decreased* due to rising reactive chlorine and bromine amounts in the atmosphere, while global tropospheric ozone in the Industrial Era has *increased* due to pollution from human activities (see Q3). Stratospheric ozone depletion has caused a small *negative* radiative forcing since preindustrial times, while increases in tropospheric ozone have caused a *positive* radiative forcing (see Figure Q18-1). Summing the positive forcing due to tropospheric ozone increases with the smaller negative forcing from stratospheric ozone depletion yields a net positive radiative forcing. The large uncertainty in tropospheric ozone forcing reflects the difficulty in quantifying tropospheric ozone trends and in

modeling the complex production and loss processes that control its abundance. The negative radiative forcing from stratospheric ozone depletion will diminish in the coming decades as ODSs are gradually removed from the atmosphere.

Stratospheric ozone depletion cannot be a principal cause of present-day global climate change for two reasons: first, the climate forcing from ozone depletion is negative, which leads to surface cooling. Second, the total forcing from other long-lived and short-lived gases in Figure Q18-1 is positive and far larger. The total forcing from these other gases is the principal cause of observed and projected climate change.

Carbon dioxide, methane, and nitrous oxide. The accumulation of carbon dioxide during the Industrial Era represents the largest climate forcing related to human activities. Carbon dioxide concentrations continue to increase in the atmosphere primarily as the result of burning fossil fuels (coal, oil, and natural gas) for energy and transportation, as well as from cement manufacturing. The atmospheric abundance of carbon dioxide in 2005 was about 36% above what it was 260 years ago in preindustrial times. Carbon dioxide is considered a *long-lived* gas, since a significant fraction remains in the atmosphere 100–1000 years after emission.

Methane is a *short-lived* climate gas (atmospheric lifetime of about 10 years) that has both human and natural sources. Human sources include livestock, rice agriculture, and landfills. Natural sources include wetlands, oceans, and forests.

Nitrous oxide is a *long-lived* climate gas (atmospheric lifetime of about 110 years) that also has both human and natural sources. The largest human source is agricultural activities, especially related to fertilization. Microbial processes in soils that are part of natural biogeochemical cycles represent the largest natural source. In the stratosphere, nitrous oxide is the principal source of reactive nitrogen species, which participate in ozone destruction cycles (see Q2 and Q7).

Halocarbons. Halocarbons in the atmosphere contribute to both ozone depletion and climate change. As used here, halocarbons represent those gases containing chlorine, bromine, or fluorine atoms that are now controlled substances under the Montreal Protocol or the Kyoto Protocol. ODSs are the halocarbons controlled under the Montreal Protocol. HFC substitute gases, perfluorocarbons (PFCs), and sulfur hexafluoride (SF₆) are controlled under the Kyoto Protocol. In 2005, the halocarbon contribution to climate forcing was 0.34 W/m², which is the third or fourth largest following carbon dioxide and methane (see Figure Q18-1). The contributions of individual halocarbon gases are highlighted in Figure Q18-2. Within the halocarbons, CFCs contribute the largest percentage (80%) to the 2005 climate

Evaluation of Selected Ozone-Depleting Substances and Substitute Gases Relative importance of equal mass emissions for ozone depletion and climate change

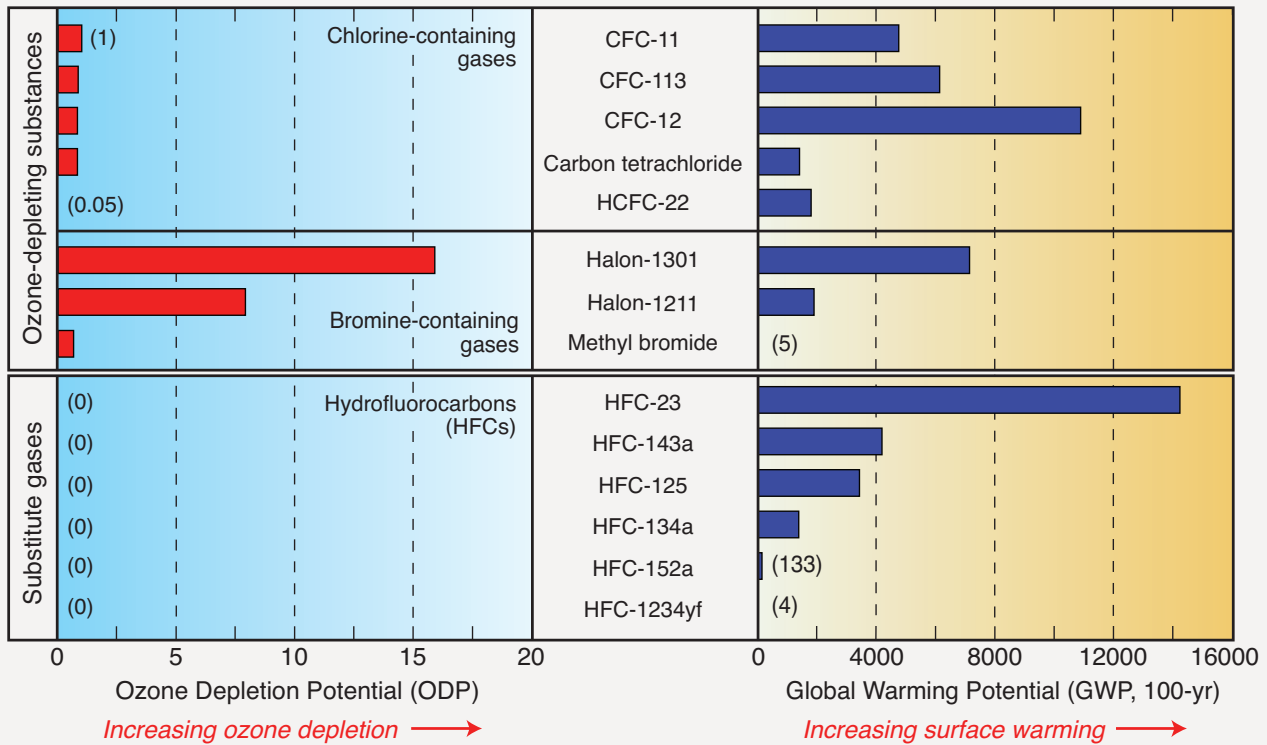


Figure Q18-3. ODPs and GWPs. ODSs and their substitutes can be compared via their Ozone Depletion Potentials (ODPs) and Global Warming Potentials (GWPs) (see Table Q7-1). Larger ODPs or GWPs indicate greater potential for ozone depletion or climate warming, respectively, when a gas is emitted to the atmosphere. The ODP and GWP values are derived assuming an equal mass of each gas is emitted. The GWPs shown here are evaluated for a 100-year time interval after emission. The ODP of CFC-11 and the GWP of CO₂ are assigned reference values of 1.0. The CFCs, halons, and HCFCs are ozone-depleting substances (see Q7) while HFCs, used as ODS substitutes, do not destroy ozone (ODPs equal 0). The ODPs of the halons far exceed those of the CFCs. All ODSs and their substitutes shown here have a non-zero GWP, with values spanning the wide range of 4 to 14,000.

forcing. HCFCs, the intermediate-term ODS substitutes, make the next largest contribution (12%). The atmospheric abundance of HFCs, the longer-term ODS substitutes, contributes only 3% to the 2005 halocarbon climate forcing.

The large contribution of the CFCs is expected to gradually decrease following the projected decline in their atmospheric abundance (see Figure Q16-1). Based on their long lifetimes, CFCs will still make a significant contribution, and most likely the largest ODS contribution, to halocarbon climate forcing at the end of the 21st century. Halocarbons controlled under the Kyoto Protocol (HFCs, PFCs, and SF₆) represent about 5% of halocarbon climate forcing in 2005. With the projected growth of HFC production and consumption in

developing nations, this percentage contribution is expected to increase substantially in the coming decades.

Ozone Depletion Potentials and Global Warming Potentials. An important way of comparing the influence of individual halocarbons on ozone depletion and climate change is to use Ozone Depletion Potentials (ODPs) and Global Warming Potentials (GWPs). The ODP and GWP of a gas quantify its effectiveness in causing ozone depletion and climate forcing, respectively (see Table Q7-1). The principal halocarbon gases are contrasted with each other in Figure Q18-3. The ODP of CFC-11 and the GWP of carbon dioxide are assigned reference values of 1. The CFCs and carbon tetrachloride all have ODPs near 1, indicating comparable

effectiveness in causing ozone depletion. The principal halons have ODPs greater than 7, making them the most effective ozone-depleting substances. HFCs have ODPs of zero since they cause no ozone depletion (see Q7).

All halocarbons have non-zero GWPs and, therefore, contribute to climate forcing. The GWP does not correspond strongly with the ODP of a gas because these quantities depend on different chemical and physical properties. For example, while HFC-134a does not destroy ozone (ODP equal 0), each gram emitted is 1,370 times more effective than a gram of carbon dioxide in causing climate forcing. The future selection of specific HFCs as ODS substitutes or for use in new global applications will have important consequences for climate forcing. When these HFCs are eventually released to the atmosphere, the contribution to climate forcing will depend on their GWPs, which could vary over a wide range (4 to 14,000).

Montreal Protocol regulations have led to reductions in CFC emissions and increases in HCFC emissions (see Q16). As a result of these actions, the total radiative forcing from ODSs is slowly decreasing (see Q19). Overall halocarbon radiative forcing, however, is slowly increasing because of growing contributions from HFCs, PFCs, and SF₆. It is important to note that, despite having a GWP that is small in

comparison to many other halocarbons and other greenhouse gases, carbon dioxide is the most important greenhouse gas related to human activities because its emissions are large and its atmospheric abundance is far greater than the abundances of other emitted gases.

Impact of climate change on ozone. Certain changes in Earth's climate could affect the future of the ozone layer. Stratospheric ozone is influenced by changes in temperatures and winds in the stratosphere. For example, lower temperatures and stronger polar winds could both increase the extent and severity of winter polar ozone depletion. While the Earth's surface is expected to continue warming in response to the net positive radiative forcing from greenhouse gas increases, the stratosphere is expected to continue cooling. A cooler stratosphere would extend the time period over which polar stratospheric clouds (PSCs) are present in winter and early spring and, as a result, might increase polar ozone depletion. In the upper stratosphere at altitudes above PSC formation regions, a cooler stratosphere is expected to increase ozone amounts because lower temperatures decrease the effectiveness of ozone loss reactions. Furthermore, climate change may alter the strength of the stratospheric circulation and with it the distribution of ozone in the stratosphere (see Q20).

Q19

Have reductions of ozone-depleting substances under the Montreal Protocol also protected Earth's climate?

Yes. All ozone-depleting substances are also greenhouse gases that contribute to climate forcing when they accumulate in the atmosphere. Montreal Protocol controls have led to a substantial reduction in the emissions of ozone-depleting substances (ODSs) over the last two decades. These reductions have provided the added benefit of reducing the human contribution to climate change while protecting the ozone layer. Without Montreal Protocol controls, the climate forcing contribution from annual ODS emissions could now be 10-fold larger than its present value, which would be a significant fraction of the climate forcing from current carbon dioxide (CO₂) emissions.

The success of the Montreal Protocol in controlling the production and consumption of ozone-depleting substances (ODSs) has protected the ozone layer (see Q15). The resulting reductions in atmospheric abundances of ODSs also reduced the human influence on climate because all ODSs are greenhouse gases (see Q18). By protecting both ozone and climate, the Montreal Protocol has provided a *dual benefit* to society and Earth's ecosystems. In the following, the dual benefit of the Montreal Protocol is highlighted by considering long-term baseline and world-avoided scenarios of ODS emissions that use Ozone Depletion Potentials (ODPs), Global Warming Potentials (GWPs), equivalent effective stratospheric chlorine (EESC), and the radiative forcing of climate change.

Baseline ODS scenarios. The baseline scenarios of past and future ODS emissions presented here include the emissions of principal halogen source gases. They are constructed from (1) historical annual production and consumption of individual ODSs reported to the Montreal Protocol, (2) projected annual production and consumption of ODSs

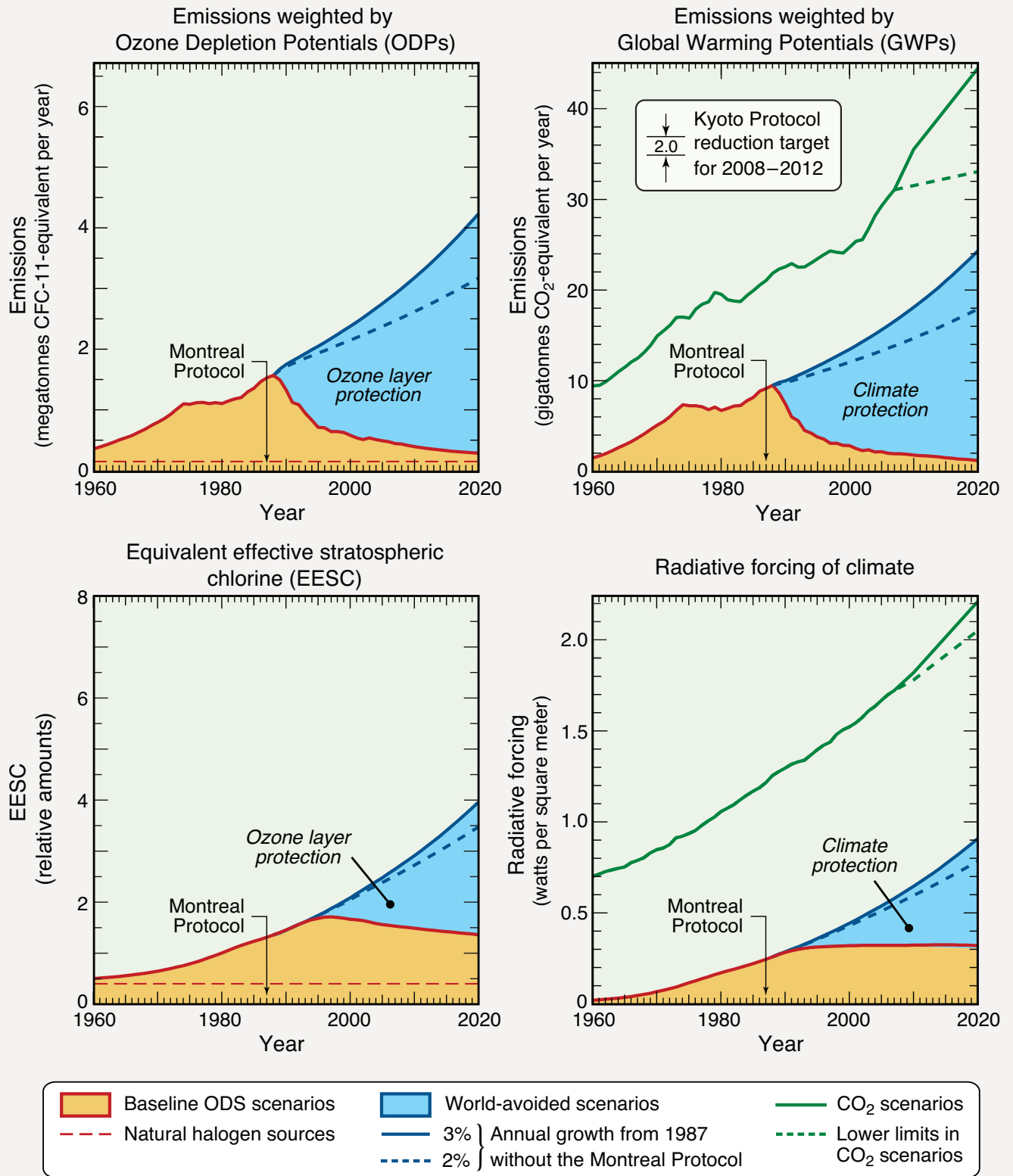
for future years based on provisions of the Protocol, (3) estimates of ODS banks, (4) atmospheric observations of ODSs and some naturally occurring halogen source gases, such as methyl chloride (CH₃Cl), and (5) weighting factors related to ozone depletion and climate change.

In forming two of the baseline scenarios shown in Figure Q19-1 (upper panels), the emissions of each gas are added together after being *weighted* (multiplied) by the Ozone Depletion Potential (ODP) or the Global Warming Potential (GWP) of the respective gas (see Q18 and Table Q7-1). In the ODP-weighted scenario, the emission sum is expressed as *CFC-11-equivalent* emissions because CFC-11 is the reference gas with an assigned ODP value of 1. For example, in the sum, 1 kg of halon-1211 emissions is added as 7.9 kg of CFC-11-equivalent emissions because the ODP of halon-1211 is 7.9. Similarly, the GWP-weighted sum is expressed as *CO₂-equivalent* emissions because CO₂ is the reference gas with an assigned GWP of 1. For example, in the sum, 1 kg of carbon tetrachloride emissions is added as 1400 kg of CO₂-equivalent emissions

Figure Q19-1. Montreal Protocol protection of ozone and climate. The provisions of the Montreal Protocol have substantially reduced ozone-depleting substances (ODSs) in the atmosphere. This has protected the ozone layer and also reduced the potential for climate change because ODSs are greenhouse gases. The scenarios and comparisons shown here demonstrate this dual benefit of the Montreal Protocol. Baseline scenarios for ODS emissions include all principal gases weighted by their Ozone Depletion Potentials (ODPs) or Global Warming Potentials (GWPs) (top panels). With these weightings, emissions are expressed as CFC-11-equivalent or CO₂-equivalent mass per year. The lower panels show EESC and radiative forcing of climate as derived from the respective ODP- and GWP-weighted scenarios. The world-avoided emission scenarios assume ODS emission growth of 2 or 3% per year beyond 1987 abundances. Shown for reference are the emissions and radiative forcing of CO₂, and the emissions reduction target of the first commitment period of the Kyoto Protocol. The contributions of natural halogen source gases are shown in the ODP-weighted and EESC scenarios (red dashed lines) and are negligible in the GWP-weighted and radiative forcing scenarios. The magnitude of the dual benefit has increased since about 1987 as shown by differences between the world-avoided and baseline scenarios (blue shaded regions in each panel). For completeness, these differences can be adjusted by offsets due to additional ozone depletion and HFC emissions (see text). (A megatonne = 1 billion (10⁹) kilograms. A gigatonne = 1 trillion (10¹²) kilograms.)

The Montreal Protocol Protection of Ozone and Climate

From global emissions of all ozone-depleting substances (ODSs) and CO₂



because the GWP of carbon tetrachloride is 1400.

World-avoided ODS scenarios. The baseline scenario of ODS emissions can be contrasted with a scenario of ODS emissions that the world has *avoided* by agreeing to the Montreal Protocol (see Figure Q19-1). These world-avoided emissions are estimated by assuming that emissions of ODSs in the baseline scenario increase beyond 1987 values with a 2 or 3% annual growth rate. These growth rates are consistent with the strong market for ODSs in the late 1980s that included a wide variety of current and potential applications and that had potential for substantial new growth in developing countries.

CO₂ emission scenarios. Long-term CO₂ emission scenarios are also shown for comparison, as derived from past and projected CO₂ emissions, because CO₂ is the principal greenhouse gas related to human activities. The projected CO₂ emissions have high and low scenarios that are derived using different basic assumptions about future economies, technical progress, and societal decisions.

ODP-weighted emissions scenarios. The ODP-weighted emissions in the ODS baseline scenario are a measure of the overall threat to stratospheric ozone from ODSs (see Figure Q19-1, upper left panel). When ODP-weighted emissions increase (decrease) in a given year, more (less) ozone will be destroyed in future years. ODP-weighted emissions increased substantially in the baseline scenario between 1960 and 1987, the year the Montreal Protocol was signed (see Figure Q19-1 and Q0-1). After 1987, ODP-weighted emissions began a long and steady decline to present-day values. The decline in emissions is expected to continue, causing the atmospheric abundances of individual ODSs to decrease (see Figure Q16-1). The reduction in ODP-weighted emissions from the 1987 value is a conservative measure of the annual emissions avoided by the Montreal Protocol since 1987 and, hence, of the success of the Montreal Protocol in protecting the ozone layer.

Annual ODP-weighted emissions in the world-avoided scenario are about double the 1987 values by 2020. The annual differences between the world-avoided emissions and the baseline scenario (blue shaded region in Figure Q19-1) provide reasonable upper-limits to the ODP-weighted emissions avoided by the Montreal Protocol each year since 1987.

GWP-weighted emissions scenarios. The GWP-weighted emissions in the ODS baseline scenario are a measure of the overall threat to climate from ODSs (see Figure Q19-1, upper right panel). As ODS emissions accumulate in the atmosphere, their climate forcing contribution increases. The long-term changes in the GWP-weighted scenario are

very similar to those in the ODP-weighted scenario. Both show an increase before 1987 and decrease afterwards. The similarity follows from the predominant role that CFC-11 and CFC-12 emissions play in ozone depletion and climate forcing from ODSs. The reduction in GWP-weighted emissions since 1987 is a conservative measure of the substantial success of the Montreal Protocol in reducing the potential for climate change from human activities. The annual differences since 1987 between the world-avoided emissions and the baseline scenario (blue shaded region in Figure Q19-1) provide reasonable upper-limits to the GWP-weighted emissions avoided by the Montreal Protocol each year since 1987.

The climate protection calculated using differences between world-avoided emissions and the baseline scenario has two offsetting effects. The first is the additional ozone depletion that would be caused by world-avoided ODS emissions. Ozone depletion offsets ODS climate forcing because a greenhouse gas (ozone) is being removed from the atmosphere in response to ODS emissions (see Q18). The second effect is the increase in emissions of HFC substitute gases that occurred in response to ODS reductions from Montreal Protocol controls. More HFCs in the atmosphere offset the gain in climate protection from ODS reductions because HFCs are also greenhouse gases (see Q18).

The combined magnitude of these offsets in 2010, for example, is about 30% of the difference between the baseline and world-avoided scenarios. The resulting net GWP-weighted emission reduction in 2010 is about 9.7–12.5 gigatonnes CO₂-equivalent per year. In contrast, the annual emissions reduction target adopted by the Kyoto Protocol during its first commitment period (2008–2012) is estimated as 2 gigatonnes CO₂-equivalent per year (see Figure Q19-1). The reductions are expected to result from controlling the Kyoto Protocol basket of gases that includes HFCs and does not include ODSs (see Q18). As a result, the upper limit for the net reduction in annual GWP-weighted emissions achieved by the Montreal Protocol in 2010 is *5- to 6-fold larger* than the Kyoto Protocol target.

Annual GWP-weighted emissions of ODSs were a large percentage (about 20–40%) of CO₂-baseline emissions between 1960 and 1989 (see Figure Q19-1). Thereafter, this percentage has steadily decreased and is projected to reach 2–3% by 2020. This projection stands in sharp contrast to the world-avoided scenario, in which the percentage increases to 40–75% of CO₂-baseline emissions by 2020.

EESC scenarios. The EESC scenario in Figure Q19-1 (lower left panel) provides a measure of the year-to-year potential of the atmospheric abundances of ODSs to destroy

stratospheric ozone. Changes in historical and projected atmospheric *emissions* of ODSs cause changes in their atmospheric *abundances*. The derivation of EESC from ODS atmospheric abundances is discussed in Q16 and similar EESC baseline scenarios are shown in Figures Q14-1, Q15-1, and Q16-1 for different time intervals. An *increase* in ODP-weighted emissions always leads to some increase in EESC in the years following the emissions. When ODS-weighted emissions *decreased* after 1987, EESC did not proportionally decrease because of the long atmospheric lifetimes of the principal ODSs. In Figure Q19-1, for example, EESC reached its peak nearly a decade after the peak in ODP-weighted emissions, and by 2010 the decrease in EESC from its peak value was only about 10%, compared to the 70% decrease in ODP-weighted emissions achieved by 2010.

Radiative forcing of climate change scenarios. The radiative forcing derived for the ODS baseline scenario in Figure Q19-1 (lower right panel) provides a measure of the year-to-year contribution to climate forcing from atmospheric ODS abundances. The radiative forcing of an ODS is proportional to its radiative efficiency and the net increase in its atmospheric abundance during the Industrial Era. Increases in abundance up to the present are derived from atmospheric observations. Future abundances rely on projected emissions and atmospheric lifetimes of each gas. In Figure Q19-1, radiative forcing due to ODSs increases smoothly from 1960 onward, peaks in 2003 and decreases very gradually in subsequent years. Radiative forcing responds to ODS emission reductions in a manner similar to EESC, with the current slow decline attributable to the two principal contributing gases, CFC-11 and CFC-12, and their long atmospheric lifetimes (45–100 years).

The differences in ODS climate forcing between the world-avoided and baseline scenarios are offset by additional ozone depletion and HFC emissions in a manner similar to that noted above for differences in GWP-weighted emissions. After accounting for these two offsets, the climate forcing due to ODSs in the world-avoided scenario is approximately 70% higher than that in the baseline scenario in 2010 and approximately 30% of that due to CO₂.

The considerable contributions that ODSs could have made to climate forcing, if not controlled by the Montreal Proto-

col, attests to their potency as greenhouse gases. ODSs had negligible atmospheric abundances 50–60 years ago and, as a group, represent chlorine amounts that currently are about 100,000 times less abundant in the atmosphere than CO₂.

The future. Fewer control options are available to increase the dual benefit of the Montreal Protocol beyond 2020 because the most effective and abundant ODSs have already been phased out under Montreal Protocol provisions (see Q16). The most recent Montreal Protocol action increased ozone and climate protection by accelerating the phase-out of HCFCs (Montreal in 2007) (see Q15). This provision is expected to reduce total GWP-weighted emissions of HCFCs by about 50% between 2010 and 2050, corresponding to about 18 gigatonnes of CO₂-equivalent emissions. The accelerated HCFC phase-out protects ozone by advancing the date that EESC returns to 1980 values by 4–5 years.

Ozone and climate protection could be further enhanced with Montreal Protocol provisions that increase the effectiveness of capturing and destroying ODSs contained in banks, namely, those ODSs currently being used in refrigeration, air conditioning, and fire protection equipment, or stockpiled for servicing long-term applications.

Future projections suggest that growth in HFC production and consumption could result in GWP-weighted emissions of up to 8.8 gigatonnes CO₂-equivalent per year by 2050, primarily in developing nations. The 2050 value is comparable to the peak in GWP-weighted ODS emissions in 1988 (see Figure Q19-1). The estimate assumes that HFC application demand would be met using the same suite of HFCs currently used in developed countries. If future HFC demand is met instead with lower-GWP substances, the 2050 estimate would be substantially reduced. International proposals have been put forth for the Montreal Protocol to expand its production and consumption controls to include HFCs. The expansion would occur in collaboration with the Kyoto Protocol, which currently includes HFCs in its basket of gases. If the proposals are successful, the Montreal Protocol would have the opportunity to guide the transition from ODSs to HFCs in a manner that would optimize the protection of the ozone layer and climate while minimizing the burden on participating nations.

Q20

How is ozone expected to change in the coming decades?

Substantial recovery of the ozone layer from the effects of ozone-depleting substances (ODSs) is expected near the middle of the 21st century, assuming global compliance with the Montreal Protocol. Recovery will occur as ODSs and reactive halogen gases in the stratosphere decrease in the coming decades. In addition to responding to ODSs, future ozone amounts will increasingly be influenced by expected changes in climate. The resulting changes in stratospheric ozone will depend strongly on the geographic region. During the long recovery period, large volcanic eruptions could temporarily reduce global ozone amounts for several years.

Substantial recovery from the depletion of global and polar ozone caused by ODSs is expected in the later decades of this century. The recovery follows on the success of the Montreal Protocol in reducing the global production and consumption of ODSs. Now, the atmospheric abundances of most major ODSs and the associated values of equivalent effective stratospheric chlorine (EESC) are in decline (see Q16). In contrast to the diminishing role of ODSs, changes in climate are expected to have an increasing influence on future ozone. Important aspects are the projected growth of greenhouse gas abundances and the resulting changes in stratospheric temperatures and the stratospheric circulation. Chemistry-climate models can be used to project how ozone is expected to respond to changes in ODSs and climate in different geographical regions during the recovery period. Global events, such as major volcanic eruptions and geoengineering actions, may also influence future total ozone amounts.

Using chemistry-climate models. Projections of total ozone presented here are based on the results from a group of chemistry-climate models that take into account the influences of changes in ODSs and climate. These models show how changes in ozone are expected to vary across global regions by evaluating the complex interaction of the processes that control ozone and climate involving radiation, chemistry, and transport. Required model inputs include, for example, historical and projected emissions of ODSs, carbon dioxide (CO₂), methane (CH₄), and nitrous oxide (N₂O), and changes in sea surface temperatures. The results from chemistry-climate model simulations are used to identify aspects of the models that are particularly important for future ozone abundances. For example, model projections for the coming decades show a strengthening in the atmospheric circulation that brings air to the stratosphere in the tropics, moves air poleward into both hemispheres, and then returns it to the troposphere at middle to high latitudes. These circu-

lation changes will significantly alter the global distribution of ozone and the atmospheric lifetimes of ODSs and other long-lived gases.

Simulating recent ozone changes. Comparisons of model results with observations help confirm the causes of ozone depletion and increase confidence in model projections of future ozone amounts. Two important measures of ozone, global total ozone and minimum total ozone values in the Antarctic, are compared to the group of chemistry-climate model simulations in Figure Q20-1. Both ozone measures show substantial depletion since 1980. The average model value follows the observed decline in both ozone measures, indicating that the main processes involved in ozone depletion are reasonably well represented by the models. Some differences between the simulations and observations can be explained by unusual meteorological conditions, volcanic eruptions, changes in solar activity, or other natural influences, which are not all fully accounted for in the various models used here. In Figure Q20-1, global total ozone has increased in the last 20 years, while Antarctic minimum ozone values have been relatively constant. The global total ozone increases cannot be attributed solely to reductions in ODSs that began in the 1990s, because total ozone has also recovered from additional depletion caused by the 1991 Mt. Pinatubo eruption (see Q14).

Equivalent stratospheric chlorine (ESC) projections. Equivalent stratospheric chlorine (ESC) values are also projected in chemistry-climate models to represent how the potential for reactive halogen gases (see Q8) to destroy ozone varies over time. ESC is similar to equivalent effective stratospheric chlorine (EESC) (see Q16) in that both represent a weighted sum of reactive chlorine and bromine gases in the stratosphere. The weighting in each accounts for the greater effectiveness of bromine atoms in destroying ozone. ESC can be calculated more precisely and comprehensively

than EESC because the chemistry-climate models can derive ESC as a function of altitude, latitude, longitude, and time. The ESC calculations are based on the history and projections of ODS surface abundances and the chemical and transport processes that control (1) the conversion of ODSs to reactive halogen gases, (2) the distribution of reactive halogen gases in the global stratosphere and (3) their ultimate removal from the stratosphere.

The long-term changes in ESC in the global and regional analyses shown in Figure Q20-2 are highly similar. In all regions, changes in ESC from 1960 values increase smoothly with time, reach a peak near the end of the 20th century, and decrease gradually until the end of the 21st century. Values at the end of the 21st century are approaching those in 1960, indicating that ODSs are largely removed from the stratosphere by that time. ESC returns to 1980 values several decades sooner than to 1960 values because of the slow rate of decline.

Peak ESC values around the year 2000 are highest in polar regions and lowest in the tropics. In the tropics, stratospheric air has only recently been transported from the troposphere, with the result that only a small fraction of ODSs has undergone conversion to reactive halogen gases (see Q8). In polar

regions, the fraction is much larger because stratospheric air requires several years on average to journey from its entry point in the tropics to the polar lower stratosphere. During this time, a much larger fraction of ODSs undergoes conversion to reactive halogen gases.

Long-term total ozone projections. Total ozone changes derived from chemistry-climate models, as referenced to 1960 values, are shown in Figure Q20-2. The range of values from the group of models is included in the figure as one measure of the uncertainty in the model projections. Total ozone changes in the different regions are described as follows:

► **Antarctic.** Total ozone changes are largest in the Antarctic region in springtime (October). Chemistry-climate models show that ODSs are the predominant factor in Antarctic ozone depletion in the past and in the coming decades. Changes in climate parameters have a smaller role. As a result, total ozone changes closely *mirror* changes in ESC: as ESC increases, ozone proportionately decreases; as ESC decreases, ozone proportionately increases. Antarctic total ozone is projected to return to 1980 levels after midcentury and later than in any other region. Meteorological variability in polar regions in late

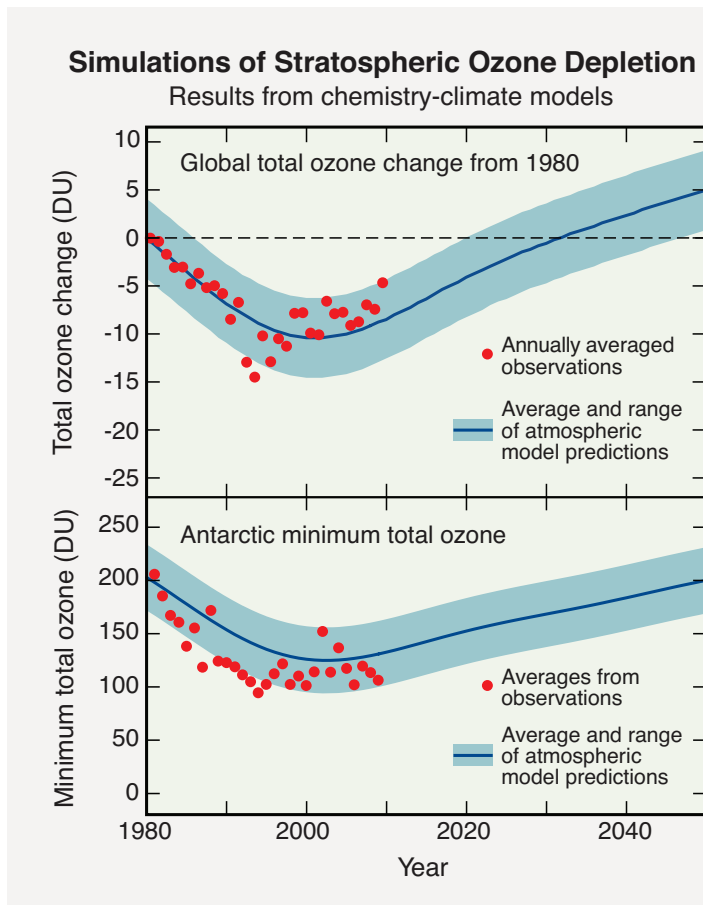
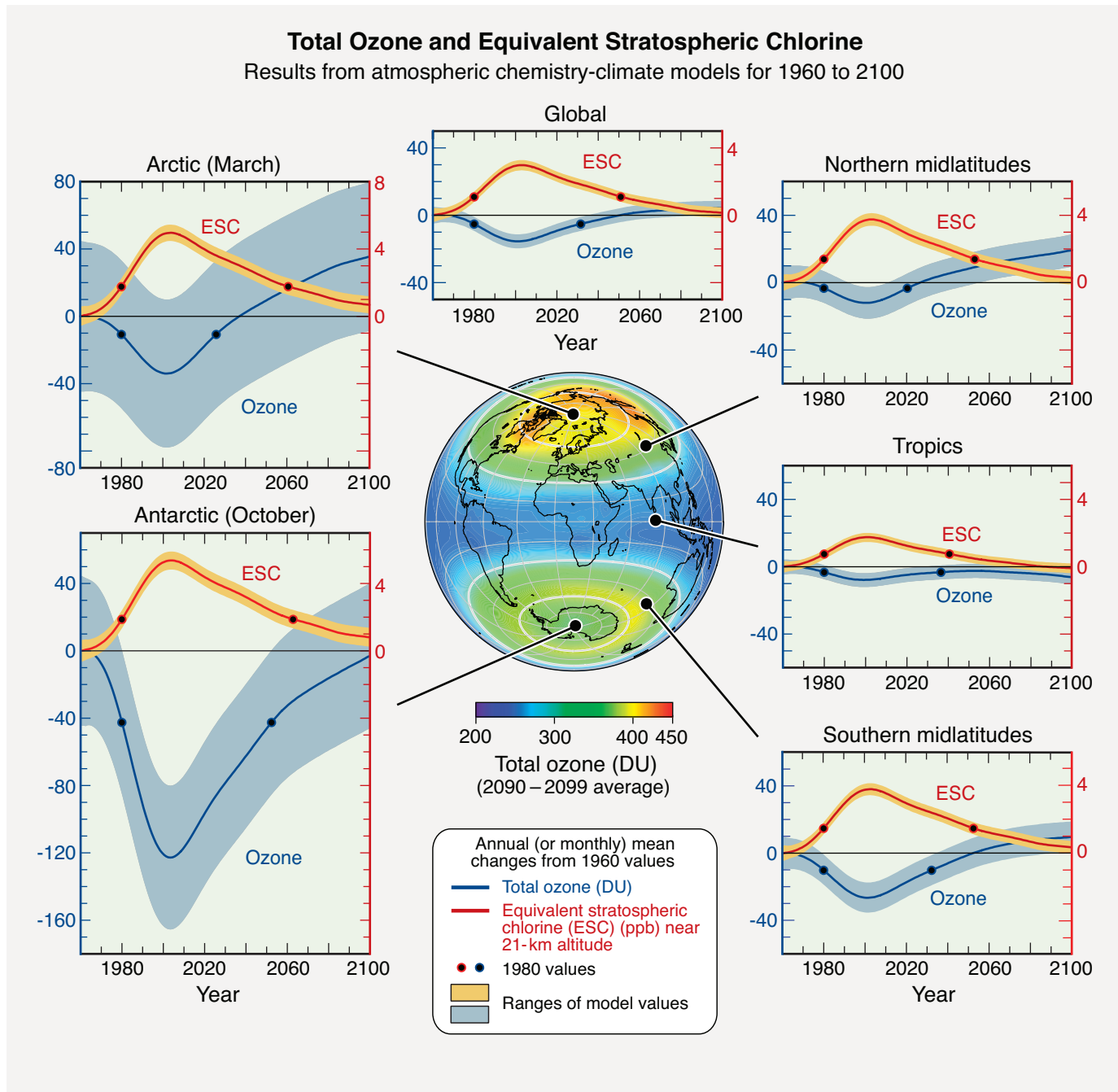


Figure Q20-1. Simulations of ozone depletion.

Chemistry-climate models of the atmosphere that account for changes in ozone-depleting substances (ODSs) and climate parameters are widely used to assess past ozone changes and project future ozone. Agreement in comparisons of model results with observations increases confidence in the model projections and our understanding of the processes leading to ozone depletion. Observed values of global total ozone (top panel) and minimum total ozone values over Antarctica (bottom panel) decreased beginning in the early 1980s (red points). Ozone is no longer decreasing in either region. The observations lie mostly within the range of projections derived from a group of chemistry-climate models (blue shading). Differences between models and observations can occur due to unusual meteorological conditions, volcanic eruptions, changes in solar activity, or other influences, which are not fully accounted for in the different models. As ODS abundances decrease in the 21st century, chemistry-climate models project global total ozone to increase steadily and exceed 1980 values, and Antarctic minimum ozone to return to 1980 values.



winter/early spring when ozone depletion occurs causes a large range in the model projections.

► **Arctic.** Total ozone changes in the Arctic region in springtime (March) are considerably smaller than in the Antarctic. In contrast to the Antarctic, ozone changes do not closely mirror changes in ESC. After midcentury, Arctic total ozone increases to values above those that would be expected from ESC reductions alone because of the strengthening of the atmospheric circulation and the enhanced stratospheric cooling associated with increases

in CO₂. By 2100 Arctic total ozone is projected to be well above both 1960 and 1980 values. The large range in projections compared to other nonpolar regions is due to greater meteorological variability as noted for the Antarctic. Arctic total ozone is projected to return to 1980 levels between 2020 and 2035, which is two to three decades before ESC returns to 1980 levels, and to continue to increase until the end of the century.

► **Northern and southern midlatitudes.** The annual averages of total ozone changes in midlatitudes are much

Figure Q20-2. Long-term changes in ozone and equivalent stratospheric chlorine (ESC). Chemistry-climate models are used to make projections of total ozone amounts that account for the effects of ozone-depleting substances (ODSs) and climate change. Regional and global projections are shown for total ozone and ESC for the period 1960–2100, referenced to 1960 values. The globe in the center shows average total ozone projections for the last decade of the 21st century. Total ozone depletion increased after 1960 as ESC values steadily increased throughout the stratosphere. ESC values have peaked and are now in a slow decline. All the projections show maximum total ozone depletion around 2000, coincident with the highest abundances of ESC. Thereafter, total ozone increases, except in the tropics, as ESC slowly declines. In all the projections except the Antarctic and the tropics, total ozone returns to 1960 values by midcentury, which is earlier than expected from the decrease in ESC alone. The earlier returns are attributable to climate change, which influences total ozone through changes in stratospheric transport and temperatures. In the tropics, in contrast, climate change causes total ozone to remain below 1960 values throughout the century. In the Antarctic, the effect of climate change is smaller than in other regions. As a result, Antarctic total ozone in springtime mirrors the changes in ESC, with both closely approaching 1960 values at century's end. The dots on each curve mark the occurrences of 1980 values of total ozone and ESC. Note that the equal vertical scales in each panel allow direct comparisons of ozone and ESC changes between regions.

smaller than the springtime losses in polar regions. Both midlatitude regions resemble the Arctic with total ozone returning to 1960 and 1980 values much sooner than ESC. In the northern midlatitudes, the models predict a return to 1960 values in 2030 whereas ESC requires the full century to return close to 1960 values. Total ozone in southern midlatitudes changes in a manner similar to the northern midlatitudes. Differences are that in southern midlatitudes the 1960 return date for total ozone is somewhat later (2055) and the maximum ozone depletion observed near 2000 is greater. Both aspects reflect the influence of Antarctic stratospheric air, depleted in ozone, being routinely transported to southern midlatitudes in spring (see Q11). The more rapid return of total ozone in both regions compared with ESC derives again from the influence of climate-induced changes in transport and upper stratospheric temperatures in the model projections. The model range is significantly less in midlatitude annual averages than in the polar springtime averages. After returning to either 1960 or 1980 values, total ozone continues to increase in both hemispheres and significantly exceeds those values by 2100.

- ▶ **Tropics.** Total ozone changes in the tropics are smaller than in any other region. Ozone is less sensitive to ESC in the tropical stratosphere because of the dominant roles of production and transport in controlling ozone. In contrast to other regions, chemistry-climate models project total ozone to remain below 1960 values throughout the 21st century. Total ozone gradually returns to 1980 values in 2040, peaks around 2060 and decreases again until the end of the century. The different total ozone behavior in the tropics

is due to the changing balance between ozone increases in the upper stratosphere and decreases in the lower stratosphere. The ozone increases in the upper stratosphere occur from declining ODS abundances and decreases in temperatures caused by increasing greenhouse gases, primarily CO₂. In the lower stratosphere, ozone is reduced because the strengthening of the stratospheric circulation reduces the time for ozone production before air leaves the tropics. These circulation changes also influence the Arctic and midlatitude regions as noted above.

- ▶ **The globe.** The annual averages of global total ozone are projected to return to 1960 levels around the middle of the century (2040 to 2080) while ESC returns to 1960 values near century's end. The comparable return dates for 1980 values are substantially earlier. Chemistry-climate model analysis suggests that this early return of total ozone is primarily a result of upper stratosphere cooling and a strengthened circulation as noted for midlatitude ozone. The larger total ozone changes shown for polar regions in springtime do not significantly influence global total ozone values because these values are annual averages and polar regions are a small geographical fraction of the globe.

Future ultraviolet radiation. Projections of long-term changes in total ozone can be used to estimate long-term changes in solar ultraviolet radiation reaching Earth's surface (see Q17). The UV-B component of ultraviolet radiation increases as total ozone decreases. Based on the global total ozone projections, clear-sky UV-B radiation is expected to *decrease* below 1960 values by the end of the century because ozone is above 1960 values in the later decades. The latitude

regions likely to have some *increase* in ultraviolet radiation are the Antarctic and the tropics, where total ozone remains lower than 1960 values until the end of the century. Large increases or decreases in surface erythemal radiation away from 1960 values are expected to lead to adverse effects on human and ecosystem health.

Volcanoes and geoengineering. Other factors not included in chemistry-climate models can potentially affect future total ozone amounts. Explosive volcanic eruptions have temporarily reduced global total ozone in the past (see Q14). Similar eruptions, especially in the early decades of this century when ESC values are highest, are also expected to reduce total ozone for a few years. Volcanic eruptions are

an additional source of uncertainty not included in the ozone projections in Figure Q20-2.

Several *geoengineering* methods have been proposed to reduce climate forcing from human activities. A widely discussed proposal is the enhancement of sulfate aerosols in the stratosphere from direct injections of sulfur or sulfuric acid. The expected response is a cooling of the climate system from increased aerosol scattering of sunlight, similar to that observed after some explosive volcanic eruptions. The required injections, if sustained over many years, are likely to have unintended consequences such as reductions in total ozone amounts and changes in stratospheric temperatures and circulation.

APPENDICES

APPENDIX A

List of International Authors, Contributors, and Reviewers

APPENDIX B

Major Acronyms and Abbreviations

APPENDIX C

Major Chemical Formulae and Nomenclature
from this Assessment

APPENDIX A

LIST OF INTERNATIONAL AUTHORS, CONTRIBUTORS, AND REVIEWERS

COCHAIRS

Ayité-Lô Nohende Ajavon	Université de Lomé	Togo
Paul A. Newman	NASA Goddard Space Flight Center	USA
John A. Pyle	University of Cambridge, National Centre for Atmospheric Science	UK
A.R. Ravishankara	NOAA ESRL Chemical Sciences Division	USA

AUTHORS AND CONTRIBUTORS

CHAPTER 1 OZONE-DEPLETING SUBSTANCES (ODSs) AND RELATED CHEMICALS

Coordinating Lead Authors

Stephen A. Montzka	NOAA ESRL Global Monitoring Division	USA
Stefan Reimann	Swiss Federal Laboratories for Materials Science and Technology (Empa)	Germany

Lead Authors

Andreas Engel	Goethe University, Frankfurt am Main	Germany
Kirstin Krüger	IFM-GEOMAR / Leibniz-Institute of Marine Sciences at Kiel University	Germany
Simon O'Doherty	University of Bristol	UK
William T. Sturges	University of East Anglia	UK

Coauthors

Donald R. Blake	University of California, Irvine	USA
Marcel Dorf	University of Heidelberg	Germany
Paul J. Fraser	CSIRO Division of Marine and Atmospheric Research	Australia
Lucien Froidevaux	Jet Propulsion Laboratory, California Institute of Technology	USA
Kenneth Jucks	NASA Headquarters	USA
Karin Kreher	National Institute of Water and Atmospheric Research (NIWA)	New Zealand
Michael J. Kurylo	Goddard Earth Sciences and Technology Center / University of Maryland Baltimore County	USA
Abdelwahid Mellouki	Institut de Combustion Aérothermique Réactivité et Environnement (ICARE), CNRS	France
John Miller	CIRES-University of Colorado / NOAA ESRL Global Monitoring Division	USA
Ole John Nielsen	University of Copenhagen	Denmark
Vladimir L. Orkin	National Institute of Standards and Technology	USA
Ronald G. Prinn	Massachusetts Institute of Technology, Center for Global Change Science	USA
Robert Rhew	University of California, Berkeley	USA
Michelle L. Santee	Jet Propulsion Laboratory, California Institute of Technology	USA
Andreas Stohl	Norwegian Institute for Air Research (NILU)	Norway
Daniel P. Verdonik	Hughes Associates, Inc.	USA

Contributors

Elliot Atlas	University of Miami	USA
Peter F. Bernath	University of York	UK
Thomas Blumenstock	Karlsruhe Institute of Technology	Germany
James H. Butler	NOAA ESRL Global Monitoring Division	USA
André Butz	Netherlands Institute for Space Research (SRON)	The Netherlands
Brian J. Connor	BC Consulting Limited	New Zealand
Pierre Duchatelet	University of Liège	Belgium
Geoffrey S. Dutton	CIRES-University of Colorado / NOAA ESRL Global Monitoring Division	USA
François Hendrick	Belgian Institute for Space Aeronomy	Belgium
Paul B. Krummel	Centre for Australian Weather & Climate Research / CSIRO Marine & Atmospheric Research	Australia
Lambert Kuijpers	Technical University, Eindhoven Center for Sustainability	The Netherlands
Emmanuel Mahieu	University of Liège	Belgium
Alistair J. Manning	Met Office	UK
Jens Mühle	Scripps Institution of Oceanography, University of California, San Diego	USA
Klaus Pfeilsticker	University of Heidelberg	Germany
Birgit Quack	IFM-GEOMAR / Leibniz-Institute of Marine Sciences at Kiel University	Germany
Martin N. Ross	The Aerospace Corporation	USA
Ross J. Salawitch	University of Maryland	USA
Sue Schauffler	National Center for Atmospheric Research, Atmospheric Chemistry Division	USA
Isobel J. Simpson	University of California, Irvine	USA
Darin W. Toohey	University of Colorado	USA
Martin K. Vollmer	Swiss Federal Laboratories for Materials Science and Technology (Empa)	Switzerland
Timothy J. Wallington	Ford Motor Company	USA
Hsiang J. (Ray) Wang	Georgia Institute of Technology	USA
Ray F. Weiss	Scripps Institution of Oceanography, University of California, San Diego	USA
Masaaki Yamabe	National Institute of Advanced Industrial Science and Technology; TEAP	Japan
Yoko Yokouchi	National Institute for Environmental Studies	Japan
Shari A. Yvon-Lewis	Texas A&M University	USA

CHAPTER 2

STRATOSPHERIC OZONE AND SUFACE ULTRAVIOLET RADIATION

Coordinating Lead Authors

Anne Douglass	NASA Goddard Space Flight Center	USA
Vitali Fioletov	Environment Canada	Canada

Lead Authors

Sophie Godin-Beekmann	Laboratoire Atmosphères, Milieux, Observations Spatiales (LATMOS)/UPMC, CNRS	France
Rolf Müller	Forschungszentrum Jülich	Germany
Richard S. Stolarski	NASA Goddard Space Flight Center	USA
Ann R. Webb	University of Manchester, School of Earth, Atmospheric, and Environmental Sciences	UK

Coauthors

Antti Arola	Finnish Meteorological Institute	Finland
James B. Burkholder	NOAA ESRL Chemical Sciences Division	USA
John P. Burrows	University of Bremen, Institute of Environmental Physics	Germany/UK
Martyn P. Chipperfield	University of Leeds	UK
Raul Cordero	Universidad de Santiago de Chile	Chile
Christine David	Laboratoire Atmosphères, Milieux, Observations Spatiales (LATMOS)/UPMC, CNRS	France

Peter N. den Outer	National Institute for Public Health and the Environment	The Netherlands
Susana B. Diaz	INGEBI / CADIC / Consejo Nacional de Investigaciones Cientificas	Argentina
Lawrence E. Flynn	NOAA National Environmental Satellite, Data, and Information Service	USA
Michaela I. Hegglin	University of Toronto	Canada
Jay R. Herman	University of Maryland-JCET / Goddard Space Flight Center	USA
Petra Huck	National Institute of Water and Atmospheric Research (NIWA)	New Zealand
Serm Janjai	Silpakorn University	Thailand
Imre M. Jánosi	Eötvös Loránd University, Budapest	Hungary
Janusz W. Krzyściński	Polish Academy of Sciences	Poland
Yi Liu	Chinese Academy of Sciences, Institute of Atmospheric Physics	China
Jennifer Logan	Harvard University	USA
Katja Matthes	Helmholtz Centre Potsdam (GFZ) / Freie Universität Berlin	Germany
Richard L. McKenzie	National Institute of Water and Atmospheric Research (NIWA)	New Zealand
Nzioka John Muthama	University of Nairobi	Kenya
Irina Petropavlovskikh	CIRES-University of Colorado / NOAA ESRL Global Monitoring Division	USA
Michael Pitts	NASA Langley Research Center	USA
S. Ramachandran	Physical Research Laboratory	India
Markus Rex	Alfred Wegener Institute for Polar and Marine Research, Potsdam	Germany
Ross J. Salawitch	University of Maryland	USA
Björn-Martin Sinnhuber	University of Bremen	Germany
Johannes Staehelin	Swiss Federal Institute of Technology – Zurich	Switzerland
Susan Strahan	NASA Goddard Space Flight Center	USA
Kleareti Tourpali	Aristotle University of Thessaloniki	Greece
Jéssica Valverde-Canossa	Universidad Nacional	Costa Rica
Corinne Vigouroux	Belgian Institute for Space Aeronomy	Belgium

Contributors

Gregory E. Bodeker	Bodeker Scientific	New Zealand
Timothy Canty	University of Maryland	USA
Hugo De Backer	Royal Meteorological Institute of Belgium	Belgium
Philippe Demoulin	University of Liège	Belgium
Uwe Feister	Deutscher Wetterdienst	Germany
Stacey M. Frith	Science Systems and Applications, Inc.	USA
Jens-Uwe Grooß	Forschungszentrum Jülich	Germany
Frank Hase	Karlsruhe Institute of Technology	Germany
Jon Klyft	Chalmers University of Technology	Sweden
Takashi Koide	Japan Meteorological Agency	Japan
Michael J. Kurylo	Goddard Earth Sciences and Technology Center / University of Maryland Baltimore County	USA
Diego Loyola	Deutsches Zentrum für Luft- und Raumfahrt, Institut für Methodik der Fernerkundung	Germany
Chris A. McLinden	Environment Canada	Canada
Inna A. Megretskaya	Harvard University	USA
Prijitha J. Nair	Laboratoire Atmosphères, Milieux, Observations Spatiales (LATMOS)/UPMC, CNRS	France
Mathias Palm	University of Bremen	Germany
Dimitrios Papanastasiou	CIRES-University of Colorado / NOAA ESRL Chemical Sciences Division	USA
Lamont R. Poole	Science Systems and Applications, Inc.	USA
Matthias Schneider	Karlsruhe Institute of Technology	Germany
Robyn Schofield	Alfred Wegener Institute for Polar and Marine Research, Potsdam	Germany
Harry Slaper	National Institute for Public Health and the Environment	The Netherlands
Wolfgang Steinbrecht	Deutscher Wetterdienst	Germany
Susann Tegtmeier	IFM-GEOMAR / Leibniz-Institute for Marine Sciences at Kiel University	Germany
Yukio Terao	National Institute for Environmental Studies	Japan

Simone Tilmes	National Center for Atmospheric Research	USA
Dmitry I. Vyushin	University of Toronto	Canada
Mark Weber	University of Bremen, Institute of Environmental Physics	Germany
Eun-Su Yang	University of Alabama in Huntsville	USA

CHAPTER 3 FUTURE OZONE AND ITS IMPACT ON SURFACE UV

Coordinating Lead Authors

Slimane Bekki	Laboratoire Atmosphères, Milieux, Observations Spatiales (LATMOS)/IPSL, CNRS	France
Gregory E. Bodeker	Bodeker Scientific	New Zealand

Lead Authors

Alkiviadis F. Bais	Aristotle University of Thessaloniki	Greece
Neal Butchart	Met Office Hadley Centre	UK
Veronika Eyring	Deutsches Zentrum für Luft- und Raumfahrt, Institut für Physik der Atmosphäre	Germany
David W. Fahey	NOAA ESRL Chemical Sciences Division	USA
Douglas E. Kinnison	National Center for Atmospheric Research, Atmospheric Chemistry Division	USA
Ulrike Langematz	Freie Universität Berlin	Germany
Bernhard Mayer	Ludwig-Maximilians-University Munich	Germany
Robert W. Portmann	NOAA ESRL Chemical Sciences Division	USA
Eugene Rozanov	World Radiation Center/Institute for Atmospheric and Climate Science-Zürich (ETHZ)	Switzerland

Coauthors

Peter Braesicke	University of Cambridge, National Centre for Atmospheric Science	UK
Andrew J. Charlton-Perez	University of Reading	UK
Natalia E. Chubarova	Moscow State University	Russia
Irene Cionni	Deutsches Zentrum für Luft- und Raumfahrt, Institut für Physik der Atmosphäre	Germany
Susana B. Diaz	INGEBI / CADIC / Consejo Nacional de Investigaciones Cientificas	Argentina
Nathan P. Gillett	Environment Canada, Canadian Centre for Climate Modelling and Analysis	Canada
Marco A. Giorgetta	Max-Planck-Institut für Meteorologie – Hamburg	Germany
Ninong Komala	National Institute of Aeronautics and Space	Indonesia
Franck Lefèvre	Laboratoire Atmosphères, Milieux, Observations Spatiales (LATMOS)/IPSL, CNRS	France
Charles McLandress	University of Toronto	Canada
Judith Perlwitz	CIRES-University of Colorado / NOAA ESRL Physical Sciences Division	USA
Thomas Peter	Swiss Federal Institute of Technology, Institute for Atmospheric and Climate Science	Switzerland
Kiyotaka Shibata	Meteorological Research Institute	Japan

Contributors

Hideharu Akiyoshi	National Institute for Environmental Studies	Japan
John Austin	University Corporation for Atmospheric Research / NOAA Geophysical Fluid Dynamics Laboratory	USA
Martyn P. Chipperfield	University of Leeds	UK
Martin Dameris	Deutsches Zentrum für Luft- und Raumfahrt, Institut für Physik der Atmosphäre	Germany
Sandip Dhomse	University of Leeds	UK
Stacey M. Frith	Science Systems and Applications, Inc.	USA
Rolando R. Garcia	National Center for Atmospheric Research, Atmospheric Chemistry Division	USA

Hella Garny	Deutsches Zentrum für Luft- und Raumfahrt, Institut für Physik der Atmosphäre	Germany Germany
Andrew Gettelman	National Center for Atmospheric Research, Atmospheric Chemistry Division	USA
Steven C. Hardiman	Met Office Hadley Centre	UK
Patrick Jöckel	Max Planck Institute for Chemistry, Mainz; now at DLR-IPA	Germany
Andreas I. Jonsson	University of Toronto	Canada
Andreas Kazantzidis	University of Patras	Greece
Anne Kubin	Freie Universität Berlin	Germany
Jean-François Lamarque	National Center for Atmospheric Research, Atmospheric Chemistry Division	USA
Eva Mancini	Università degli Studi di L'Aquila, Dipartimento di Fisica	Italy
Marion Marchand	Laboratoire Atmosphères, Milieux, Observations Spatiales (LATMOS)/IPSL, CNRS	France
Martine Michou	GAME-CNRM/Météo-France, CNRS	France
Olaf Morgenstern	National Institute of Water and Atmospheric Research (NIWA)	New Zealand
Luke D. Oman	NASA Goddard Space Flight Center	USA
Steven Pawson	NASA Goddard Space Flight Center	USA
Giovanni Pitari	Università degli Studi di L'Aquila, Dipartimento di Fisica	Italy
David Plummer	Environment Canada, Canadian Centre for Climate Modelling and Analysis	Canada
John A. Pyle	University of Cambridge, National Centre for Atmospheric Science	UK
David Saint-Martin	GAME-CNRM/Météo-France, CNRS	France
John F. Scinocca	Environment Canada, Canadian Centre for Climate Modelling and Analysis	Canada
Theodore G. Shepherd	University of Toronto	Canada
Dan Smale	National Institute of Water and Atmospheric Research (NIWA)	New Zealand
Richard S. Stolarski	NASA Goddard Space Flight Center	USA
Hubert Teysse�re	GAME-CNRM/Météo-France, CNRS	France
Simone Tilmes	National Center for Atmospheric Research, Climate and Global Dynamics Division	USA

**CHAPTER 4
STRATOSPHERIC CHANGES AND CLIMATE**

Coordinating Lead Authors

Piers M. Forster	University of Reading	UK
David W.J. Thompson	Colorado State University	USA

Lead Authors

Mark P. Baldwin	Northwest Research Associates	USA
Martyn P. Chipperfield	University of Leeds	UK
Martin Dameris	Deutsches Zentrum für Luft- und Raumfahrt, Institut für Physik der Atmosphäre	Germany
Joanna D. Haigh	Imperial College London	UK
David J. Karoly	University of Melbourne	Australia
Paul J. Kushner	University of Toronto, Department of Physics	Canada
William J. Randel	National Center for Atmospheric Research, Atmospheric Chemistry Division	USA
Karen H. Rosenlof	NOAA ESRL Chemical Sciences Division	USA
Dian J. Seidel	NOAA Air Resources Laboratory	USA
Susan Solomon	NOAA ESRL Chemical Sciences Division	USA

Coauthors

Gufran Beig	Indian Institute of Tropical Meteorology	India
Peter Braesicke	University of Cambridge, National Centre for Atmospheric Science	UK
Neal Butchart	Met Office Hadley Centre	UK
Nathan P. Gillett	Environment Canada, Canadian Centre for Climate Modelling and Analysis	Canada
Kevin M. Grise	Colorado State University	USA

Daniel R. Marsh	National Center for Atmospheric Research, Atmospheric Chemistry Division	USA
Charles McLandress	University of Toronto	Canada
T. Narayan Rao	National Atmospheric Research Laboratory	India
Seok-Woo Son	McGill University	Canada
Georgiy L. Stenchikov	King Abdullah University of Science and Technology	Saudi Arabia
Shigeo Yoden	Kyoto University	Japan

Contributors

Eugene C. Cordero	San Jose State University	USA
Melissa P. Free	NOAA Air Resources Laboratory	USA
Andreas I. Jonsson	University of Toronto	Canada
Jennifer Logan	Harvard University	USA
David Stevenson	University of Edinburgh	UK

CHAPTER 5

A FOCUS ON INFORMATION AND OPTIONS FOR POLICYMAKERS

Coordinating Lead Authors

John S. Daniel	NOAA ESRL Chemical Sciences Division	USA
Guus J.M. Velders	Netherlands Environmental Assessment Agency (PBL)	The Netherlands

Lead Authors

Olaf Morgenstern	National Institute of Water and Atmospheric Research (NIWA)	New Zealand
Darin W. Toohey	University of Colorado	USA
Timothy J. Wallington	Ford Motor Company	USA
Donald J. Wuebbles	University of Illinois	USA

Coauthors

Hideharu Akiyoshi	National Institute for Environmental Studies	Japan
Alkiviadis F. Bais	Aristotle University of Thessaloniki	Greece
Eric L. Fleming	Science Systems and Applications, Inc.	USA
Charles H. Jackman	NASA Goddard Space Flight Center	USA
Lambert Kuijpers	Technical University, Eindhoven Center for Sustainability	The Netherlands
Mack McFarland	DuPont Chemicals and Fluoroproducts	USA
Stephen A. Montzka	NOAA ESRL Global Monitoring Division	USA
Martin N. Ross	The Aerospace Corporation	USA
Simone Tilmes	National Center for Atmospheric Research, Climate and Global Dynamics Division	USA
Matthew B. Tully	Australian Bureau of Meteorology	Australia

Contributors

Stephen O. Andersen	Co-Chair, Montreal Protocol Technology and Economic Assessment Panel (TEAP)	USA
Ulrike Langematz	Freie Universität Berlin	Germany
Pauline M. Midgley	University of Bern	Switzerland

TWENTY QUESTIONS AND ANSWERS ABOUT THE OZONE LAYER: 2010 UPDATE

Coordinating Lead Authors

David W. Fahey	NOAA ESRL Chemical Sciences Division	USA
Michaela I. Hegglin	University of Toronto	Canada

CHAPTER EDITORIAL CONTRIBUTORS

CHAPTER 1: OZONE-DEPLETING SUBSTANCES (ODSs) AND RELATED CHEMICALS

Nada Derek CSIRO Division of Atmospheric Research Australia

CHAPTER 3: FUTURE OZONE AND ITS IMPACT ON SURFACE UV

Stefanie Kremser Bodeker Scientific New Zealand

TWENTY QUESTIONS AND ANSWERS ABOUT THE OZONE LAYER: 2010 UPDATE

Jennifer Fox NOAA ESRL Chemical Sciences Division USA

SCIENTIFIC REVIEW AND ADISORY GROUP

Malcolm K.W. Ko NASA Langley Research Center USA
 Theodore G. Shepherd University of Toronto Canada
 Susan Solomon NOAA ESRL Chemical Sciences Division USA

REVIEWERS

Patricio Aceituno Universidad de Chile Chile
 Ayité-Lô Nohende Ajavon Université de Lomé Togo
 Hideharu Akiyoshi National Institute for Environmental Studies Japan
 Daniel L. Albritton NOAA ESRL Chemical Sciences Division (retired) USA
 Taofiki Aminou Université Nationale du Bénin Département de Chimie/FAST Benin
 Stephen O. Andersen Co-Chair, Montreal Protocol Technology and
 Economic Assessment Panel (TEAP) USA
 Julie M. Arblaster Australian Bureau of Meteorology /
 National Center for Atmospheric Research Australia/USA
 Ghassem Asrar World Climate Research Programme / World Meteorological Organization Switzerland
 Pieter J. Aucamp Ptersa South Africa
 John Austin University Corporation for Atmospheric Research /
 NOAA Geophysical Fluid Dynamics Laboratory USA
 Alkiviadis F. Bais Aristotle University of Thessaloniki Greece
 Mark P. Baldwin Northwest Research Associates USA
 Dimitris Balis Aristotle University of Thessaloniki Greece
 Slimane Bekki Laboratoire Atmosphères, Milieux, Observations Spatiales
 (LATMOS)/IPSL, CNRS France
 Peter F. Bernath University of York UK
 Gregory E. Bodeker Bodeker Scientific New Zealand
 Rumén D. Bojkov University of Dresden Germany
 Janet F. Bornman University of Waikato New Zealand
 Geir O. Braathen World Meteorological Organization Switzerland
 Peter Braesicke University of Cambridge, National Centre for Atmospheric Science UK
 Christoph Brühl Max Planck Institute for Chemistry, Mainz Germany
 Claus Brünig European Commission Belgium

Dominik Brunner	Swiss Federal Laboratories for Materials Science and Technology (Empa)	Switzerland
John P. Burrows	University of Bremen, Institute of Environmental Physics	Germany/UK
Pablo O. Canziani	Pontificia Universidad Católica Argentina / CONICET	Argentina
Bruno Carli	Consiglio Nazionale delle Ricerche, Institute of Applied Physics	Italy
Lucy Carpenter	University of York	UK
Ken Carslaw	University of Leeds, School of Earth and Environment	UK
Marie-Lise Chanin	Laboratoire Atmosphères, Milieux, Observations Spatiales (LATMOS)/IPSL/UVSQ, CNRS	France
Martyn P. Chipperfield	University of Leeds	UK
Natalia E. Chubarova	Moscow State University	Russia
Irene Cionni	Deutsches Zentrum für Luft- und Raumfahrt, Institut für Physik der Atmosphäre	Germany
Hans Claude	Deutscher Wetterdienst	Germany
Cathy Clerbaux	Laboratoire Atmosphères, Milieux, Observations Spatiales (LATMOS)/IPSL, CNRS-INSU	France
Gerrie Coetzee	South African Weather Service	South Africa
William J. Collins	Met Office Hadley Centre	UK
Derek M. Cunnold	Georgia Institute of Technology	USA
Martin Dameris	Deutsches Zentrum für Luft- und Raumfahrt, Institut für Physik der Atmosphäre	Germany
John S. Daniel	NOAA ESRL Chemical Sciences Division	USA
Martine De Mazière	Belgian Institute for Space Aeronomy	Belgium
Dick Derwent	rdscientific	UK
Panuganti Devara	Indian Institute of Tropical Meteorology	India
Roseanne Diab	Academy of Science of South Africa	South Africa
Susana B. Diaz	INGEBI / CADIC / Consejo Nacional de Investigaciones Cientificas	Argentina
Anne R. Douglass	NASA Goddard Space Flight Center	USA
Ellsworth G. Dutton	NOAA ESRL Global Monitoring Division	USA
Kalju Eerme	Tartu Observatory	Estonia
James William Elkins	NOAA ESRL Global Monitoring Division	USA
Andreas Engel	Goethe University, Frankfurt am Main	Germany
Christine A. Ennis	CIRES-University of Colorado / NOAA ESRL Chemical Sciences Division	USA
Veronika Eyring	Deutsches Zentrum für Luft- und Raumfahrt, Institut für Physik der Atmosphäre	Germany
David W. Fahey	NOAA ESRL Chemical Sciences Division	USA
Vitali E. Fioletov	Environment Canada	Canada
Ian Folkins	Dalhousie University	Canada
Piers M. Forster	University of Leeds	UK
James Franklin	CLF-Chem Consulting	Belgium
John C. Fyfe	Environment Canada, Canadian Centre for Climate Modeling and Analysis	Canada
Annie Gabriel	Department of the Environment, Water, Heritage and the Arts	Australia
Rolando R. Garcia	National Center for Atmospheric Research, Atmospheric Chemistry Division	USA
Marvin A. Geller	Stony Brook University	USA
Andrew Gettelman	National Center for Atmospheric Research, Atmospheric Chemistry Division	USA
Manuel Gil	Instituto Nacional de Técnica Aeroespacial	Spain
Sophie Godin-Beekmann	Laboratoire Atmosphères, Milieux, Observations Spatiales (LATMOS)/UPMC, CNRS	France
Marco González	United Nations Environment Programme, Ozone Secretariat	Kenya
Hans-F Graf	University of Cambridge, National Centre for Atmospheric Science	UK
Lesley Gray	Reading University, National Centre for Atmospheric Science	UK

Ebrahim Hajizadeh	Department of Environment	Iran
Neil R.P. Harris	University of Cambridge, European Ozone Research Coordinating Unit	UK
Dennis L. Hartmann	University of Washington, Department of Atmospheric Sciences	USA
Birgit Hassler	CIRES-University of Colorado / NOAA ESRL Chemical Sciences Division	USA
Michaela I. Hegglin	University of Toronto	Canada
Ernest Hilsenrath	University of Maryland Baltimore County	USA
David J. Hofmann	NOAA ESRL Global Monitoring Division	USA
Paul Horwitz	United Nations Environment Programme, Ozone Secretariat	USA
Robert D. Hudson	University of Maryland, Department of Atmospheric and Oceanic Science	USA
Mohammad Ilyas	Albiruni Environment and Science Development Centre (EnviSC)	Malaysia
Takashi Imamura	National Institute for Environmental Studies	Japan
Ivar S.A. Isaksen	University of Oslo	Norway
Kenneth Jucks	NASA Headquarters	USA
David J. Karoly	University of Melbourne	Australia
Philippe Keckhut	Laboratoire Atmosphères, Milieux, Observations Spatiales (LATMOS)/IPSL/UVSQ, CNRS	France
Douglas E. Kinnison	National Center for Atmospheric Research, Atmospheric Chemistry Division	USA
Malcolm K.W. Ko	NASA Langley Research Center	USA
Kunihiko Kodera	Nagoya University / Meteorological Research Institute, Japan Meteorological Agency	Japan
Takashi Koide	Japan Meteorological Agency	Japan
Ninong Komala	National Institute of Aeronautics and Space	Indonesia
Yutaka Kondo	University of Tokyo	Japan
Karin Kreher	National Institute of Water and Atmospheric Research (NIWA)	New Zealand
Mark Kroon	Royal Netherlands Meteorological Institute (KNMI)	The Netherlands
Kirstin Krüger	IFM-GEOMAR / Leibniz-Institute of Marine Sciences at Kiel University	Germany
Lambert Kuijpers	Technical University, Eindhoven Center for Sustainability	The Netherlands
Michael J. Kurylo	Goddard Earth Sciences and Technology Center / University of Maryland Baltimore County	USA
Paul J. Kushner	University of Toronto, Department of Physics	Canada
Esko Kyrö	Finnish Meteorological Institute	Finland
Shyam Lal	Physical Research Laboratory	India
Tom Land	U.S. Environmental Protection Agency	USA
Igor Larin	Russian Academy of Sciences	Russia
Katharine Law	Laboratoire Atmosphères, Milieux, Observations Spatiales (LATMOS)/UPMC/UVSQ, CNRS	France
Jos Lelieveld	Max Planck Institute for Chemistry, Mainz	Germany
Sasha Madronich	National Center for Atmospheric Research, Atmospheric Chemistry Division	USA
Gloria L. Manney	Jet Propulsion Laboratory, California Institute of Technology / New Mexico Institute of Mining and Technology	USA
Alistair J. Manning	Met Office	UK
Elisa Manzini	Max-Planck-Institut für Meteorologie – Hamburg	Germany
John C. McConnell	York University, Department of Earth and Space Science and Engineering	Canada
C. Thomas McElroy	Environment Canada	Canada
Mack McFarland	DuPont Chemicals and Fluoroproducts	USA
Norman McFarlane	SPARC International Project Office	Canada
Danny McKenna	Oak Ridge National Laboratory	USA
Richard L. McKenzie	National Institute of Water and Atmospheric Research (NIWA)	New Zealand
Charles McLandress	University of Toronto	Canada

Mario J. Molina	University of California, San Diego and Mario Molina Center for Strategic Studies in Energy and the Environment	USA/Mexico
Stephen A. Montzka	NOAA ESRL Global Monitoring Division	USA
Rolf Müller	Forschungszentrum Jülich	Germany
Cathrine Lund Myhre	Norwegian Institute for Air Research (NILU)	Norway
Hideaki Nakane	National Institute for Environmental Studies	Japan
Eric R. Nash	Science Systems and Applications, Inc.	USA
Cindy Newberg	U.S. Environmental Protection Agency	USA
Mike Newchurch	University of Alabama in Huntsville	USA
Paul A. Newman	NASA Goddard Space Flight Center	USA
Ole John Nielsen	University of Copenhagen	Denmark
Alan O'Neill	National Centre for Earth Observation / University of Reading	UK
Samuel J. Oltmans	NOAA ESRL Global Monitoring Division	USA
Luke D. Oman	NASA Goddard Space Flight Center	USA
Edward A. Parson	University of Michigan	USA
Nigel D. Paul	Lancaster University	UK
Stuart A. Penkett	University of East Anglia, Norwich	UK
Judith Perlwitz	CIRES-University of Colorado / NOAA ESRL Physical Sciences Division	USA
Thomas Peter	Swiss Federal Institute of Technology, Institute for Atmospheric and Climate Science	Switzerland
Giovanni Pitari	Università degli Studi di L'Aquila, Dipartimento di Fisica	Italy
R. Alan Plumb	Massachusetts Institute of Technology	USA
David Plummer	Environment Canada, Canadian Centre for Climate Modelling and Analysis	Canada
Jean-Pierre Pommereau	Laboratoire Atmosphères, Milieux, Observations Spatiales (LATMOS), CNRS	France
Michael Ponater	Deutsches Zentrum für Luft- und Raumfahrt, Institut für Physik der Atmosphäre	Germany
Lamont R. Poole	Science Systems and Applications, Inc.	USA
Robert W. Portmann	NOAA ESRL Chemical Sciences Division	USA
Michael J. Prather	University of California, Irvine / Earth System Science Department	USA
Ronald G. Prinn	Massachusetts Institute of Technology, Center for Global Change Science	USA
John A. Pyle	University of Cambridge, National Centre for Atmospheric Science	UK
V. Ramaswamy	NOAA Geophysical Fluid Dynamics Laboratory	USA
William J. Randel	National Center for Atmospheric Research, Atmospheric Chemistry Division	USA
A.R. Ravishankara	NOAA ESRL Chemical Sciences Division	USA
Claire E. Reeves	University of East Anglia / National Centre for Atmospheric Sciences	UK
Stefan Reimann	Swiss Federal Laboratories for Materials Science and Technology (Empa)	Switzerland
Markus Rex	Alfred Wegener Institute for Polar and Marine Research, Potsdam	Germany
Martin Riese	Research Centre Jülich, Institute for Chemistry and Dynamics of the Geosphere	Germany
Vincenzo Rizi	Università degli Studi di L'Aquila	Italy
Alan Robock	Rutgers University	USA
Howard K. Roscoe	British Antarctic Survey	UK
Vladimir Ryabinin	World Climate Research Programme/World Meteorological Organization	Switzerland
Ross J. Salawitch	University of Maryland	USA
Michelle L. Santee	Jet Propulsion Laboratory, California Institute of Technology	USA
K. Madhava Sarma	Consultant	India
Robert Sausen	Deutsches Zentrum für Luft- und Raumfahrt, Institut für Physik der Atmosphäre	Germany
Adam A. Scaife	Met Office Hadley Centre	UK

Ulrich Schmidt	Goethe University, Institute for Atmosphere and Environment	Germany
Ulrich Schumann	Deutsches Zentrum für Luft- und Raumfahrt, Institut für Physik der Atmosphäre	Germany
Dian J. Seidel	NOAA Air Resources Laboratory	USA
Megumi Seki	United Nations Environment Programme, Ozone Secretariat	Kenya
Jonathan Shanklin	British Antarctic Survey	UK
Wafik M. Sharobiem	Egyptian Meteorological Authority, Scientific Research Department	Egypt
Theodore G. Shepherd	University of Toronto	Canada
Keith P. Shine	University of Reading, Department of Meteorology	UK
Masato Shiotani	Kyoto University, Research Institute for Sustainable Humanosphere	Japan
Michael Sigmond	University of Toronto	Canada
Peter Simmonds	University of Bristol, School of Chemistry	UK
Anne Smith	National Center for Atmospheric Research, Atmospheric Chemistry Division	USA
Susan Solomon	NOAA ESRL Chemical Sciences Division	USA
Johannes Staehelin	Swiss Federal Institute of Technology – Zurich	Switzerland
Wolfgang Steinbrecht	Deutscher Wetterdienst	Germany
Georgiy L. Stenchikov	King Abdullah University of Science and Technology	Saudi Arabia
Richard S. Stolarski	NASA Goddard Space Flight Center	USA
Frode Stordal	University of Oslo, Department of Geosciences	Norway
Fred Stroh	Forschungszentrum Jülich GmbH, Institute for Chemistry and Dynamics of the Geosphere	Germany
William T. Sturges	University of East Anglia	UK
Kenshi Takahashi	Kyoto University	Japan
David W. Tarasick	Environment Canada, Air Quality Research Division	Canada
Said Ali Thaoubane	Université des Comores	Comores
David W.J. Thompson	Colorado State University	USA
Simone Tilmes	National Center for Atmospheric Research, Climate and Global Dynamics Division	USA
Matthew B. Tully	Australian Bureau of Meteorology	Australia
Ronald Van der A	Royal Netherlands Meteorological Institute (KNMI)	The Netherlands
Karel Vanicek	Czech Hydrometeorological Institute	Czech Republic
Guus J.M. Velders	Netherlands Environmental Assessment Agency (PBL)	The Netherlands
Marc von Hobe	Forschungszentrum Jülich	Germany
Darryn W. Waugh	Johns Hopkins University	USA
Elizabeth C. Weatherhead	CIRES-University of Colorado / NOAA ESRL Global Systems Division	USA
Ann R. Webb	University of Manchester, School of Earth, Atmospheric, and Environmental Sciences	UK
Mark Weber	University of Bremen, Institute of Environmental Physics	Germany
Ray F. Weiss	Scripps Institution of Oceanography, University of California, San Diego	USA
Donald J. Wuebbles	University of Illinois	USA
Shigeo Yoden	Kyoto University	Japan
Yoko Yokouchi	National Institute for Environmental Studies	Japan
Durwood Zaelke	Institute for Governance and Sustainable Development	USA
Rodolphe Zander	University of Liège	Belgium
Christos S. Zerefos	International Ozone Commission; Academy of Athens	Greece
Lingxi Zhou	Chinese Meteorological Administration, Chinese Academy of Meteorological Sciences	China

OZONE PEER-REVIEW MEETING

*Les Diablerets, Switzerland
28 June – 2 July 2010*



by Jean-Pierre Pommerau, June 2010

Patricio Aceituno Chile	Universidad de Chile	
Ayité-Lô Nohende Ajavon Stephen O. Andersen	Université de Lomé Co-Chair, Montreal Protocol Technology and Economic Assessment Panel (TEAP)	Togo USA
Pieter J. Aucamp Alkiviadis F. Bais Slimane Bekki	Ptersa Aristotle University of Thessaloniki Laboratoire Atmosphères, Milieux, Observations Spatiales (LATMOS)/IPSL, CNRS	South Africa Greece France
Peter F. Bernath Gregory E. Bodeker Janet F. Bornman Geir O. Braathen Peter Braesicke John P. Burrows Lucy Carpenter Martyn P. Chipperfield Martin Dameris	University of York Bodeker Scientific University of Waikato World Meteorological Organization University of Cambridge, National Centre for Atmospheric Science University of Bremen, Institute of Environmental Physics University of York University of Leeds Deutsches Zentrum für Luft- und Raumfahrt, Institut für Physik der Atmosphäre	UK New Zealand New Zealand Switzerland UK Germany/UK UK UK Germany
John S. Daniel Susana B. Diaz Anne R. Douglass Andreas Engel Christine A. Ennis Veronika Eyring	NOAA ESRL Chemical Sciences Division INGEBI / CADIC / Consejo Nacional de Investigaciones Cientificas NASA Goddard Space Flight Center Goethe University, Frankfurt am Main CIRES-University of Colorado / NOAA ESRL Chemical Sciences Division Deutsches Zentrum für Luft- und Raumfahrt, Institut für Physik der Atmosphäre	USA Argentina USA Germany USA Germany
David W. Fahey Vitali E. Fioletov Piers M. Forster Marvin A. Geller Sophie Godin-Beekmann	NOAA ESRL Chemical Sciences Division Environment Canada University of Leeds Stony Brook University Laboratoire Atmosphères, Milieux, Observations Spatiales (LATMOS)/UPMC, CNRS	USA Canada UK USA France
Marco González Neil R.P. Harris	United Nations Environment Programme, Ozone Secretariat University of Cambridge, European Ozone Research Coordinating Unit	Kenya UK

Michaela I. Hegglin	University of Toronto	Canada
Kenneth Jucks	NASA Headquarters	USA
David J. Karoly	University of Melbourne	Australia
Malcolm K.W. Ko	NASA Langley Research Center	USA
Takashi Koide	Japan Meteorological Agency	Japan
Kirstin Krüger	IFM-GEOMAR / Leibniz-Institute of Marine Sciences at Kiel University	Germany
Lambert Kuijpers	Technical University, Eindhoven Center for Sustainability	The Netherlands
Michael J. Kurylo	Goddard Earth Sciences and Technology Center / University of Maryland Baltimore County	USA
Paul J. Kushner	University of Toronto, Department of Physics	Canada
Igor Larin	Russian Academy of Sciences	Russia
Elisa Manzini	Max-Planck-Institut für Meteorologie – Hamburg	Germany
Mack McFarland	DuPont Chemicals and Fluoroproducts	USA
Stephen A. Montzka	NOAA ESRL Global Monitoring Division	USA
Rolf Müller	Forschungszentrum Jülich	Germany
Hideaki Nakane	National Institute for Environmental Studies	Japan
Paul A. Newman	NASA Goddard Space Flight Center	USA
Alan O’Neill	National Centre for Earth Observation / University of Reading	UK
Judith Perlwitz	CIRES-University of Colorado / NOAA ESRL Physical Sciences Division	USA
Thomas Peter	Swiss Federal Institute of Technology, Institute for Atmospheric and Climate Science	Switzerland
Jean-Pierre Pommereau	Laboratoire Atmosphères, Milieux, Observations Spatiales (LATMOS), CNRS	France
Robert W. Portmann	NOAA ESRL Chemical Sciences Division	USA
Michael J. Prather	University of California, Irvine / Earth System Science Department	USA
John A. Pyle	University of Cambridge, National Centre for Atmospheric Science	UK
V. Ramaswamy	NOAA Geophysical Fluid Dynamics Laboratory	USA
A.R. Ravishankara	NOAA ESRL Chemical Sciences Division	USA
Claire E. Reeves	University of East Anglia / National Centre for Atmospheric Sciences	UK
Stefan Reimann	Swiss Federal Laboratories for Materials Science and Technology (Empa)	Switzerland
Ross J. Salawitch	University of Maryland	USA
Dian J. Seidel	NOAA Air Resources Laboratory	USA
Wafik M. Sharobiem	Egyptian Meteorological Authority, Scientific Research Department	Egypt
Theodore G. Shepherd	University of Toronto	Canada
Peter Simmonds	University of Bristol, School of Chemistry	UK
Anne Smith	National Center for Atmospheric Research, Atmospheric Chemistry Division	USA
Susan Solomon	NOAA ESRL Chemical Sciences Division	USA
Georgiy L. Stenchikov	King Abdullah University of Science and Technology	Saudi Arabia
Richard S. Stolarski	NASA Goddard Space Flight Center	USA
William T. Sturges	University of East Anglia	UK
Said Ali Thaoubane	Université des Comores	Comores
David W.J. Thompson	Colorado State University	USA
Matthew B. Tully	Australian Bureau of Meteorology	Australia
Guus J.M. Velders	Netherlands Environmental Assessment Agency (PBL)	The Netherlands
Darryn W. Waugh	Johns Hopkins University	USA
Ann R. Webb	University of Manchester, School of Earth, Atmospheric, and Environmental Sciences	UK
Ray F. Weiss	Scripps Institution of Oceanography, University of California, San Diego	USA
Donald J. Wuebbles	University of Illinois	USA
Lingxi Zhou	Chinese Meteorological Administration, Chinese Academy of Meteorological Sciences	China

Sponsoring Organizations Liaisons

Geir O. Braathen World Meteorological Organization Switzerland
Marco González United Nations Environment Programme Kenya
A.R. Ravishankara National Oceanic and Atmospheric Administration USA
Kenneth Jucks National Aeronautics and Space Administration USA
Claus Brüning European Commission Belgium

Assessment Coordinator and Technical Editor

Christine A. Ennis CIRES/NOAA ESRL Chemical Sciences Division USA

Publication/Graphics Design and Layout

Debra Dailey-Fisher (*Publication, Design, Layout, & Graphics Lead*) NOAA ESRL CSD USA
Dennis Dickerson (*Graphics & Layout Design, "Twenty Questions"*) Respond Grafiks USA
Albert D. Romero (*Consulting and Support*) NOAA Boulder Facilities Operations Division USA

Editorial Assistance

Debra Dailey-Fisher NOAA ESRL Chemical Sciences Division USA
Jessica N. Lucas NOAA Earth System Research Laboratory USA

Reference Research and Editing

Barbara Keppler NOAA ESRL Chemical Sciences Division USA
Jessica N. Lucas NOAA Earth System Research Laboratory USA
Debra R. Wilson NOAA ESRL Chemical Sciences Division USA
Kristen McCormack Boulder High School USA
Mary Gutierrez NOAA ESRL Chemical Sciences Division USA
Debra Dailey-Fisher NOAA ESRL Chemical Sciences Division USA
William L. Fisher Fisher Enterprises USA
Christine A. Ennis CIRES/NOAA ESRL Chemical Sciences Division USA

Conference Coordination and Documentation

Christine A. Ennis CIRES/NOAA ESRL Chemical Sciences Division USA
Geir O. Braathen World Meteorological Organization Switzerland
Debra Dailey-Fisher NOAA ESRL Chemical Sciences Division USA
John A. Pyle University of Cambridge UK
Norman McFarlane SPARC International Project Office Canada
Theodore G. Shepherd University of Toronto Canada

Conference Support

Jeanne S. Waters NOAA ESRL Chemical Sciences Division USA
Kathy A. Thompson CSC USA
Debra Dailey-Fisher NOAA ESRL Chemical Sciences Division USA
Jennifer Fox CIRES/NOAA ESRL Chemical Sciences Division USA
Chantal Renaudot World Meteorological Organization Switzerland
Rose M. Kendall CSC USA
Ruth Batten UNEP Ozone Secretariat Kenya
Ann Gachingiri UNEP Ozone Secretariat Kenya
Peter Braesicke University of Cambridge UK
Tina Jost University of Cambridge UK
Victoria De Luca SPARC International Project Office UK
David Dokken IPCC Working Group II Technical Support Unit USA
Kyle Terran University Corporation for Atmospheric Research USA
Eric Kissel IPCC Working Group II Technical Support Unit USA

Computing and Networking Support

Richard J. Tisinai and Jennifer Fox CIRES/NOAA ESRL Chemical Sciences Division USA

Document Distribution

Jeanne S. Waters NOAA ESRL Chemical Sciences Division USA
Debra Dailey-Fisher NOAA ESRL Chemical Sciences Division USA
Chantal Renaudot World Meteorological Organization Switzerland
Ruth Batten UNEP Ozone Secretariat Kenya

APPENDIX B

MAJOR ACRONYMS AND ABBREVIATIONS

A1	baseline (or most likely) halocarbon scenario of the 2006 Ozone Assessment
A1B	scenario of the IPCC Special Report on Emissions Scenarios (SRES)
A5	Article 5 countries of the Montreal Protocol
AAE	Absorption Angstrom Exponent
AASE	Airborne Arctic Stratospheric Expedition (NASA)
Ab	baseline halocarbon scenario of the 2002 Ozone Assessment
ACE-FTS	Atmospheric Chemistry Experiment Fourier Transform Spectrometer
AERONET	AERosol RObotic NETwork
AGAGE	Advanced Global Atmospheric Gases Experiment
AGWP	Absolute Global Warming Potential
AMA	average mean age
AMSU	Advanced Microwave Sounding Unit
AMTRAC	Atmospheric Model with TRansport and Chemistry (Table 3-1)
AO	Arctic Oscillation
AOGCM	atmosphere-ocean general circulation model
AOT	aerosol optical thickness
AR4	IPCC Fourth Assessment Report
ARCTAS	Arctic Research of the Composition of the Troposphere from Aircraft and Satellites
ARCPAC	Aerosol, Radiation, and Cloud Processes affecting Arctic Climate
ATLAS	Atmospheric Laboratory for Applications and Science
ATMOS	Atmospheric Trace Molecule Spectroscopy
AVE	Aura Validation Experiment
B1	a lower-emissions scenario of the IPCC Special Report on Emissions Scenarios (SRES)
B2	scenario of the IPCC Special Report on Emissions Scenarios (SRES)
BC	black carbon
BCE	Before the Common Era
BDC	Brewer-Dobson circulation
BL	boundary layer
BP	British Petroleum
BUV	Backscatter (or Backscattered) Ultraviolet (spectrometer)
C	Celsius (unit of temperature)
CADIC	Centro Austral de Investigaciones Cientificas (Argentina)
CALIOP	Cloud-Aerosol Lidar with Orthogonal Polarization
CALIPSO	Cloud-Aerosol Lidar and Infrared Pathfinder Satellite Observation
CAM	Community Atmosphere Model (Table 3-1)
CATO	Candidoz Assimilated Three-dimensional Ozone
CCM	chemistry-climate model
CCMVal	Chemistry-Climate Model (CCM) Validation Activity
CCSP	Climate Change Science Program (United States)
CCSR-NIES	Center for Climate-Systems Research – National Institute for Environmental Studies CCM (Table 3-1)
CDM	Clean Development Mechanism
CE	Common Era

CFC	chlorofluorocarbon
CHAMP	Challenging Minisatellite Payload
CIE	Commission Internationale de l'Éclairage (France)
CIRES	Cooperative Institute for Research in Environmental Sciences (United States)
cm	centimeters (unit of length)
CMAM	Canadian Middle Atmosphere Model (Table 3-1)
CMF	cloud modification factor
CMIP	Coupled Model Intercomparison Project
CNRM	Centre National de Recherches Météorologiques (France)
CNRM-ACM	CNRM ARPEGE-Climate model (Table 3-1)
CNRS	Centre National de la Recherche Scientifique (France)
CONICET	Consejo de Investigaciones Científicas y Técnicas (Argentina)
CO ₂ -eq	carbon dioxide equivalents
COS	carbonyl sulfide (also OCS)
CPT	cold point tropopause
CR-AVE	Costa Rica-Aura Validation Experiment
CSIRO	Commonwealth Scientific and Industrial Research Organisation (Australia)
CTM	chemistry and transport model
CUE	critical-use exemption
CUSUM	Cumulative Sum of Residuals
DFA	difluoroacetic acid
DIAL	differential absorption lidar
DJF	December-January-February
DLR	Deutschen Zentrum für Luft- und Raumfahrt (Germany)
DMS	dimethyl sulfide
DNA	deoxyribonucleic acid
DOAS	Differential Optical Absorption Spectroscopy
DU	Dobson unit
E39CA	a coupled chemistry-climate model of DLR (Table 3-1)
EC	European Commission
ECl	equivalent chlorine
ECMWF	European Centre for Medium-Range Weather Forecasts (United Kingdom)
EEAP	Environmental Effects Assessment Panel
EECl	equivalent effective chlorine
EESC	equivalent effective stratospheric chlorine
EMAC	ECHAM/MESSy Atmospheric Chemistry model of FUB (Table 3-1)
ENSO	El Niño-Southern Oscillation
Envisat	Environmental Satellite
EP	Eliassen-Palm
EPA	Environmental Protection Agency (United States)
ER-2	Earth Resources-2 (aircraft)
ERA	ECMWF Re-Analysis
ERA-40	ECMWF 40-year reanalysis
ERA1	ECMWF Interim Re-Analysis
ERS	European Remote Sensing Satellite
ESC	equivalent stratospheric chlorine
ESRL	Earth System Research Laboratory (NOAA)
EU	European Union
EUPLEX	European Polar Stratospheric Cloud and Lee Wave Experiment

fGHG	sensitivity simulation with fixed greenhouse gas levels (see Chapter 3 and Table 3-2)
fODS	sensitivity simulation with fixed ozone-depleting substance levels (see Chapter 3 and Table 3-2)
FT	free troposphere
FTIR	Fourier transform infrared
FUB	Freie Universität Berlin (Germany)
GCM	general circulation model
GEOS	Goddard Earth Observing System
GEOSCCM	Goddard Earth Observing System Chemistry-Climate Model (Table 3-1)
GFDL	Geophysical Fluid Dynamics Laboratory (NOAA)
Gg	Gigagrams (10^9 grams) (unit of mass)
GHG	greenhouse gas
GHG-x	a greenhouse gas sensitivity simulation (see Chapter 3 and Table 3-2)
GISS	Goddard Institute for Space Studies (NASA)
GJ	gigajoule (10^9 joules) (unit of energy)
GMD	Global Monitoring Division (NOAA/ESRL)
GOME	Global Ozone Monitoring Experiment
GREET	Greenhouse Gases, Regulated Emissions, and Energy Use in Transportation (model)
GSFC	Goddard Space Flight Center (NASA)
Gt	gigatonnes
GtCO ₂ -eq	gigatonnes of carbon dioxide equivalents
GWP	Global Warming Potential
HadAT	Hadley Centre radiosonde temperature product
HALOE	Halogen Occultation Experiment
HAMMONIA	HAMBURG Model of the Neutral and Ionized Atmosphere
HC	hydrocarbon
HCFC	hydrochlorofluorocarbon
HFC	hydrofluorocarbon
HFE	hydrofluorinated ether or hydrofluoroether
HFO	hydrofluoro-olefin
hPa	hectoPascal (10^2 Pascal) (unit of pressure)
IGRA	Integrated Global Radiosonde Archive (NOAA)
INGEBI	Instituto de Investigaciones en Ingeniería Genética y Biología Molecular (Argentina)
IPA	Institut für Physik der Atmosphäre (DLR) (Germany)
IPCC	Intergovernmental Panel on Climate Change
IPSL	Institut Pierre-Simon Laplace (France)
IR	infrared
IUK	Iterative Universal Kriging
IUP	Institute of Environmental Physics, University of Bremen (Germany)
IUPAC	International Union of Pure and Applied Chemistry
J	joule (unit of energy)
JCET	Joint Center for Earth Systems Technology (United States)
JJA	June-July-August
JMA	Japan Meteorological Agency (Japan)
JPL	Jet Propulsion Laboratory (NASA)
JRA25	Japanese 25-year Reanalysis Project

K	Kelvin (unit of temperature)
kcal	kilocalories (10^3 calories) (unit of energy)
kg	kilogram (10^3 grams) (unit of mass)
km	kilometer (10^3 meters) (unit of length)
Kt	kilotons (10^3 tons) (unit of mass)
LLGHG	long-lived greenhouse gases
LMDZrepro	general circulation model of the Laboratory of Dynamic Meteorology (IPSL) (Table 3-1)
LMS	lowermost stratosphere
LS	lower stratosphere
LZRH	level of zero clear-sky radiative heating
m	meter (unit of length)
MAC	mobile air conditioning
MAM	March-April-May
MATCH	Model for Atmospheric Transport and Chemistry
MBL	marine boundary layer
MetOp	Meteorological Operational satellite
MFA	monofluoroacetic acid
MFRSR	Multi-Filter Rotating Shadowband Radiometer
mg	milligram (10^{-3} grams) (unit of mass)
MILAGRO	Megacity Initiative: Local and Global Research Observations
MIPAS	Michelson Interferometer for Passive Atmospheric Sounding
MIT	Massachusetts Institute of Technology
MLD	mixed layer depth
MJ	megajoule (10^6 joules) (unit of energy)
MLR	multiple linear regression
MLS	Microwave Limb Sounder
mm	millimeters (10^{-3} meters) (unit of length)
μm	micrometer; micron (10^{-6} meters) (unit of length)
MMBtu	million British thermal units (1MMBtu = 1.055 gigajoules)
MOD	merged ozone data set
MODIS	Moderate Resolution Imaging Spectroradiometer
mol	mole (unit, amount of substance)
molec	molecule
MOZAIC	Measurement of Ozone and Water Vapor by Airbus In-Service Aircraft
MOZART	Model for Ozone and Related Chemical Tracers
MRI	Meteorological Research Institute chemistry-climate model (Japan) (Table 3-1)
MSG	Meteosat Second Generation
MSU	Microwave Sounding Unit
MtCFC-11-eq	megatonnes of CFC-11 equivalents
Mt	megatonne
mW	milliWatt (10^{-3} Watts)
NAM	Northern Annular Mode
NAO	North Atlantic Oscillation
NASA	National Aeronautics and Space Administration (United States)
NAT	nitric acid trihydrate
NCAR	National Center for Atmospheric Research (United States)
NCEP	National Centers for Environmental Prediction (United States)
ng	nanogram (10^{-9} grams) (unit of mass)

NH	Northern Hemisphere
NIES	National Institute for Environmental Studies (Japan)
NIWA	National Institute of Water and Atmospheric Research (New Zealand)
nm	nanometers (10^{-9} meters) (unit of length)
NOAA	National Oceanic and Atmospheric Administration (United States)
NPLS	nonparametric least-squares fit
1-D	one-dimensional
OCS	carbonyl sulfide (also COS)
ODP	Ozone Depletion Potential
ODS	ozone-depleting substance
OMI	Ozone Monitoring Instrument
OSIRIS	Optical Spectrograph and InfraRed Imager System
PBL	planetary boundary layer
PEM	Pacific Exploratory Mission
PFC	perfluorocarbon
Pg	petagram (10^{15} grams) (unit of mass)
PG	product gas
PGI	product gas injection
PhotoComp	photolysis intercomparison
POAM	Polar Ozone and Aerosol Measurement
POCP	Photochemical Ozone Creation Potential
ppb	part per billion
ppbv	part per billion by volume
ppm	part per million
ppmv	part per million by volume
ppt	part per trillion
pptv	part per trillion by volume
PSC	polar stratospheric cloud
PSS	photochemical steady state
PTFE	polytetrafluoroethylene
PWLT	piecewise linear trend
QBO	quasi-biennial oscillation
QPS	quarantine and pre-shipment
RAF	radiation amplification factor
RAOB	RAwinsonde OBServation
RAOBCORE	Radiosonde Observation Correction using Reanalyses
RATPAC	Radiosonde Atmospheric Temperature Products for Assessing Climate
RCP	Representative Concentration Pathway
RECON	a near-surface temperature reconstruction
REF-B2	reference “future” simulation of SPARC CCMVal-2 (see Table 3-2)
RF	radiative forcing
RICH	Radiosonde Innovation Composite Homogenization
RO	radio occultation
RSS	Remote Sensing Systems Inc.

s	second
SAD	surface area density
SAGE	Stratospheric Aerosol and Gas Experiment
SAM	Southern Annular Mode
SAM II	Stratospheric Aerosol Measurement II
SAOZ	Système d'Analyse par Observation Zénithale
SAP	Scientific Assessment Panel
SBUV/SBUV2	Solar Backscatter (or Backscattered) Ultraviolet (spectrometer)
SCIAMACHY	Scanning Imaging Absorption Spectrometer for Atmospheric Chartography
SCISAT	a Canadian satellite also known as Atmospheric Chemistry Experiment (ACE)
SE	southeast
SG	source gas
SGI	source gas injection
SH	Southern Hemisphere
SIC	sea ice concentration
SLIMCAT	Single-Layer Isentropic Model of Chemistry and Transport
SOCOL	modeling tool for studies of Solar-Climate-Ozone Links (Table 3-1)
SOGE	System for Observation of Halogenated Greenhouse Gases in Europe
SOLVE	SAGEIII (Stratospheric Aerosol and Gas Experiment III) Ozone Loss and Validation Experiment (NASA)
SON	September-October-November
SPARC	Stratospheric Processes and Their Role in Climate (WCRP)
sr	steradian (unit of solid angle)
SRES	Special Report on Emissions Scenarios (IPCC)
SRM	solid rocket motor
SSA	stratospheric sulfate aerosol
SSA	single scattering albedo
SST	sea surface temperature
SSU	Stratospheric Sounding Unit
SSW	sudden stratospheric warming
STAR	System for Transfer of Atmospheric Radiation
STE	stratosphere-troposphere exchange
STS	supercooled ternary solution
SZA	solar zenith angle
2-D	two-dimensional
3-D	three-dimensional
TC4	Tropical Composition, Cloud and Climate Coupling mission
TCO	tropospheric column ozone
TEAP	Technology and Economic Assessment Panel (UNEP)
TFA	trifluoroacetic acid
Tg	teragrams (10^{12} grams) (unit of mass; equivalent to megatonne)
THESEO	Third European Stratospheric Experiment on Ozone
T-M	tropical-midlatitude
TOMCAT	Toulouse Off-line Model of Chemistry and Transport
TOMS	Total Ozone Mapping Spectrometer
TSAM	time series additive model
TST	troposphere-to-stratosphere transport
TTL	tropical tropopause layer
TUV	Tropospheric Ultraviolet-Visible model

UAH	University of Alabama–Huntsville
UARS	Upper Atmosphere Research Satellite
UBA	Umweltbundesamt (Germany Federal Environment Agency)
UCI	University of California, Irvine
UDMH	unsymmetrical dimethylhydrazine
UEA	University of East Anglia (United Kingdom)
UIUC	University of Illinois at Urbana-Champaign
UK	United Kingdom
UKCA	U.K. Chemistry and Aerosols chemistry-climate model (Table 3-1)
ULAQ	University of L'Aquila chemistry-climate model (Italy) (Table 3-1)
UMSLIMCAT	Unified Model Single-Layer Isentropic Model of Chemistry and Transport CCM (Table 3-1)
UNEP	United Nations Environment Programme
UNFCCC	United Nations Framework Convention on Climate Change
UPMC	Université Pierre et Marie Curie (France)
US, USA	United States of America
USDA	United States Department of Agriculture
UT	upper troposphere
UTLS	upper troposphere/lower stratosphere
UV	ultraviolet
UV-A	ultraviolet-A (315–400 nm)
UV-B	ultraviolet-B (280–315 nm)
UVSQ	Université Versailles Saint-Quentin (France)
VSL	very short-lived
VSLs	very short-lived substance
W	Watt (unit of energy)
WACCM	Whole-Atmosphere Community Climate Model (Table 3-1)
WCRP	World Climate Research Programme
WFDOAS	Weighting Function Differential Optical Absorption Spectroscopy
WMO	World Meteorological Organization

APPENDIX C

MAJOR CHEMICAL FORMULAE AND NOMENCLATURE FROM THIS ASSESSMENT

HALOGEN-CONTAINING SPECIES

Cl	atomic chlorine	Br	atomic bromine
Cl _y	total inorganic chlorine	Br _y	total inorganic bromine
CCl _y	organic chlorine	CBr _y	organic bromine
Cl ₂	molecular chlorine	Br ₂	molecular bromine
ClO	chlorine monoxide	BrO	bromine monoxide
Cl ₂ O	dichlorine monoxide	Br ₂ O	dibromine monoxide
ClO _x	chlorine radicals ([ClO] + 2×[ClOOCl])	BrO _x	bromine radicals
OCIO	chlorine dioxide		
ClOO	chloroperoxy radical		
Cl ₂ O ₂ , ClOOCl	dichlorine peroxide (ClO dimer)		
ClONO ₂ , ClNO ₃	chlorine nitrate	BrONO ₂ , BrNO ₃	bromine nitrate
HCl	hydrogen chloride (hydrochloric acid)	HBr	hydrogen bromide
HOCl	hypochlorous acid	HOBr	hypobromous acid
F	atomic fluorine	I	atomic iodine
F ₂	molecular fluorine	I ₂	molecular iodine
F _y	total inorganic fluorine	I _y	total inorganic iodine
HF	hydrogen fluoride (hydrofluoric acid)	IO	iodine monoxide
		IO _x	iodine radicals
		OIO	iodine dioxide
		HOI	hypoiodous acid
SF ₆	sulfur hexafluoride		
SO ₂ F ₂	sulfuryl fluoride		
NF ₃	nitrogen trifluoride		
PBr ₃	phosphorus tribromide		

HALOCARBONS**CHLOROFLUOROCARBONS (CFCs)**

CFC-11	CCl_3F
CFC-12	CCl_2F_2
CFC-13	CClF_3
CFC-113	$\text{CCl}_2\text{FCClF}_2$
CFC-113a	CCl_3CF_3
CFC-114	$\text{CClF}_2\text{CClF}_2$
CFC-114a	CCl_2FCF_3
CFC-115	CClF_2CF_3

HALONS

halon-1202	CBr_2F_2
halon-1211	CBrClF_2
halon-1301	CBrF_3
halon-2402	$\text{CBrF}_2\text{CBrF}_2$
halon-2311	CHBrClCF_3
(Halothane)	

HYDROFLUOROCARBONS (HFCs)

HFC-23	CHF_3
HFC-32	CH_2F_2
HFC-41	CH_3F
HFC-125	CHF_2CF_3
HFC-134	CHF_2CHF_2
HFC-134a	CH_2FCF_3
HFC-143	CH_2FCHF_2
HFC-143a	CH_3CF_3
HFC-152	$\text{CH}_2\text{FCH}_2\text{F}$
HFC-152a	CH_3CHF_2
HFC-161	$\text{CH}_3\text{CH}_2\text{F}$
HFC-227ea	$\text{CF}_3\text{CHF}_2\text{CF}_3$
HFC-236cb	$\text{CH}_2\text{FCF}_2\text{CF}_3$
HFC-236ea	$\text{CHF}_2\text{CHF}_2\text{CF}_3$
HFC-236fa	$\text{CF}_3\text{CH}_2\text{CF}_3$

CHLOROCARBONS

CH_3Cl	methyl chloride, chloromethane
CH_2Cl_2	methylene chloride, dichloromethane
CHCl_3	chloroform, trichloromethane
CCl_4	carbon tetrachloride
CHClCCl_2	trichloroethylene, trichloroethene
CCl_2CCl_2	tetrachloroethene, perchloroethene
$\text{CH}_3\text{CH}_2\text{Cl}$, $\text{C}_2\text{H}_5\text{Cl}$	ethyl chloride, chloroethane
$\text{CH}_2\text{ClCH}_2\text{Cl}$	1,2 dichloroethane
CH_3CCl_3	methyl chloroform
$\text{CH}_3\text{CHClCH}_3$	isopropylchloride, 2-chloropropane
$\text{CH}_3\text{CH}_2\text{CH}_2\text{Cl}$	n-propyl chloride, 1-chloropropane
COCl_2 , $\text{Cl}_2\text{C}(\text{O})$	phosgene, carbonyl chloride

HYDROCHLOROFLUOROCARBONS (HCFCs)

HCFC-21	CHCl_2F
HCFC-22	CHClF_2
HCFC-31	CH_2ClF
HCFC-123	CHCl_2CF_3
HCFC-123a	$\text{CHClF}_2\text{CF}_2\text{Cl}$
HCFC-123b	$\text{CHF}_2\text{CCl}_2\text{F}$
HCFC-124	$\text{CHClF}_2\text{CF}_3$
HCFC-124a	$\text{CHF}_2\text{CClF}_2$
HCFC-133a	CH_2ClCF_3
HCFC-141b	$\text{CH}_3\text{CCl}_2\text{F}$
HCFC-142b	CH_3CClF_2
HCFC-225ca	$\text{CHCl}_2\text{CF}_2\text{CF}_3$
HCFC-225cb	$\text{CHClF}_2\text{CF}_2\text{CClF}_2$
HCFC-234fb	$\text{CF}_3\text{CH}_2\text{CCl}_2\text{F}$
HCFC-243cc	$\text{CH}_3\text{CF}_2\text{CCl}_2\text{F}$

HFC-245cb	$\text{CH}_3\text{CF}_2\text{CF}_3$
HFC-245ca	$\text{CH}_2\text{FCF}_2\text{CHF}_2$
HFC-245ea	$\text{CHF}_2\text{CHFCHF}_2$
HFC-245eb	$\text{CH}_2\text{FCH}_2\text{CF}_3$
HFC-245fa	$\text{CHF}_2\text{CH}_2\text{CF}_3$
HFC-263fb	$\text{CH}_3\text{CH}_2\text{CF}_3$
HFC-272ca	$\text{CH}_3\text{CF}_2\text{CH}_3$
HFC-281ea	$\text{CH}_3\text{CHFCH}_3$
HFC-365mfc	$\text{CH}_3\text{CF}_2\text{CH}_2\text{CF}_3$
HFC-356mcf	$\text{CH}_2\text{FCH}_2\text{CF}_2\text{CF}_3$
HFC-356mff	$\text{CF}_3\text{CH}_2\text{CH}_2\text{CF}_3$
HFC-338pcc	$\text{CHF}_2\text{CF}_2\text{CF}_2\text{CHF}_2$
HFC-43-10mee	$\text{CF}_3\text{CHFCH}_2\text{CF}_2\text{CF}_3$
HFC-458mfcf	$\text{CF}_3\text{CH}_2\text{CF}_2\text{CH}_2\text{CF}_3$
HFC-55-10mcf	$\text{CF}_3\text{CF}_2\text{CH}_2\text{CH}_2\text{CF}_2\text{CF}_3$

BROMOCARBONS

CH_3Br	methyl bromide, bromomethane
CH_2Br_2	methylene bromide, dibromomethane
CHBr_3	bromoform, tribromomethane
$\text{CH}_3\text{CH}_2\text{Br}$, $\text{C}_2\text{H}_5\text{Br}$	ethyl bromide, bromoethane
$\text{CH}_2\text{BrCH}_2\text{Br}$	1,2 dibromoethane
$\text{CH}_3\text{CH}_2\text{CH}_2\text{Br}$, $\text{n-C}_3\text{H}_7\text{Br}$	n-propyl bromide, n-PB, 1-bromopropane
COBr_2	carbonyl bromide

IODOCARBONS

CH ₃ I	methyl iodide, iodomethane
CH ₂ I ₂	diiodomethane
CH ₃ CH ₂ I, C ₂ H ₅ I	ethyl iodide, iodoethane
CH ₃ CHICH ₃	isopropyl iodide, 2-iodopropane
CH ₃ CH ₂ CH ₂ I, n-C ₃ H ₇ I	n-propyl iodide, 1-iodopropane

OTHERS

CHBr ₂ Cl	dibromochloromethane
CH ₂ BrCl	bromochloromethane
CHBrCl ₂	bromodichloromethane
CH ₂ BrI	bromoiodomethane
CHBrF ₂	bromodifluoromethane
CH ₂ ClI	chloroiodomethane
CF ₃ I	trifluoroiodomethane
CF ₃ CF ₂ CF ₂ I	1-iodo-heptafluoropropane
COClF	chlorofluorocarbonyl
SF ₅ CF ₃	trifluoromethylsulfurpentafluoride

FLUOROCARBONS

CF ₄ (PFC-14)	perfluoromethane, carbon tetrafluoride
C ₂ F ₆ , CF ₃ CF ₃ (PFC-116)	perfluoroethane
C ₃ F ₈ , CF ₃ CF ₂ CF ₃ (PFC-218)	perfluoropropane
c-C ₃ F ₆ (PFC-C216)	perfluorocyclopropane
C ₄ F ₁₀ (PFC-31-10)	perfluorobutane
c-C ₄ F ₈ (PFC-C318)	perfluorocyclobutane
C ₅ F ₁₂ (PFC-41-12)	perfluoropentane
C ₆ F ₁₄ (PFC-51-14)	perfluorohexane
C ₇ H ₁₆ (PFC-61-16)	perfluoroheptane
C ₁₀ F ₁₈	perfluorodecalin
COF ₂	carbonyl fluoride
CH ₂ FC(O)OH	monofluoroacetic acid (MFA)
CHF ₂ C(O)OH	difluoroacetic acid (DFA)
CF ₃ C(O)OH	trifluoroacetic acid (TFA)

OTHER CHEMICAL SPECIES

O	atomic oxygen	H	atomic hydrogen
O(³ P)	atomic oxygen (ground state)	H ₂	molecular hydrogen
O(¹ D)	atomic oxygen (first excited state)	OH	hydroxyl radical
O ₂	molecular oxygen	HO ₂	hydroperoxyl radical
O ₃	ozone	H ₂ O	water
O _x	odd oxygen (O, O(¹ D), O ₃) or oxidant (O ₃ + NO ₂)	HO _x	odd hydrogen (H, OH, HO ₂ , H ₂ O ₂)
N	atomic nitrogen	HNO ₂ , HONO	nitrous acid
N ₂	molecular nitrogen	HOONO	pernitrous acid
N ₂ O	nitrous oxide	HNO ₃	nitric acid
NO	nitric oxide	NH ₃	ammonia
NO ₂	nitrogen dioxide	NH ₄ NO ₃	ammonium nitrate
NO ₃	nitrogen trioxide, nitrate radical		
N ₂ O ₅	dinitrogen pentoxide		
NO _x	nitrogen oxides (NO + NO ₂)		
NO _y	total reactive nitrogen (usually includes NO, NO ₂ , NO ₃ , N ₂ O ₅ , ClONO ₂ , HNO ₄ , HNO ₃)		
S	atomic sulfur	H ₂ S	hydrogen sulfide
SO ₂	sulfur dioxide	CS ₂	carbon disulfide
H ₂ SO ₄	sulfuric acid	COS, OCS	carbonyl sulfide
CH ₃ SCH ₃	DMS, dimethyl sulfide		
C	carbon atom	CO ₂	carbon dioxide
CO	carbon monoxide		
CH ₄	methane	CH ₃ OH	methyl alcohol, methanol
CH ₃ CH ₃	ethane		
CH ₃ CH ₂ CH ₃	propane		